IEEE/CAA Journal of Automatica Sinica

published FOSC papers (2015-2017)

Contents

Guest editorials:

The remaining papers (online):

Paper download links

Guest Editorial for Special Issue on Fractional Order Systems and Controls

YangQuan Chen, *Senior Member, IEEE*, Dingyü Xue, and Antonio Visioli, *Senior Member, IEEE*

I. INTRODUCTION

FRACTIONAL calculus is about differentiation and integration of non-integer orders. Using integer-order models and controllers for complex natural or man-made systems is simply for our *own* convenience while the nature runs in a fractional order dynamical way. Using integer order traditional tools for modelling and control of dynamic systems may result in suboptimum performance, that is, using fractional order calculus tools, we could be "*more* optimal" as already documented in the literature. An interesting remark is that, using integer order traditional tools, more and more "anomalous" phenomena are being reported or perhaps complained but in applied fractional calculus community, it is now more widely accepted that "*Anomalous is normal*" in nature. We believe, beneficial uses of fractional calculus from an engineering point of view are possible and important. We also hope that fractional calculus might become an enabler for new science discoveries. Bruce J. West just finished a new book entitled "*The Fractional Dynamic View of Complexity - Tomorrow's Science*" (CRC Press, 2015). We resonate that, with this special issue, "Fractional Order Systems and Controls" will one day enable "tomorrow's sciences".

Since 2012, several special issues were published in some leading journals which showcase the active interference of fractional calculus to control engineering. Clearly, there is a strong need to have a special issue in an emerging leading control journal such as *IEEE/CAA Journal of Automatica Sinica (JAS)*. This focused special issue on control theory and applications is yet another effort to bring forward the latest updates from the applied fractional calculus community. For that we feel very excited and we hope the readers will feel the same.

The aim of this special issue is to show the control engineering research community the usefulness of the fractional order tools from signals to systems to controls. It is our sincere hope that this special issue will become a milestone of a significant trend in the future development of classical and modern control theory. The contributions may stimulate future industrial applications of the fractional order control leading to simpler, more economical, more energy efficient, more reliable and versatile systems with increasing complexities.

Citation: YangQuan Chen, Dingyü Xue, Antonio Visioli. Guest editorial for special issue on fractional order systems and controls. *IEEE/CAA Journal of Automatica Sinica*, 2016, **3**(3): 255−256

YangQuan Chen is with the Mechatronics, Embedded Systems and Automation (MESA) Lab, School of Engineering, University of California, Merced, 5200 North Lake Road, Merced, CA 95343, USA (e-mail: yqchen@ieee.org).

Dingyü Xue is with the School of Information Sciences and Engineering, Northeastern University, Shenyang 110004, China (e-mail: xuedingyu@ise.neu.edu.cn).

Antonio Visioli is with the Department of Mechanical and Industrial Engineering,University of Brescia, Via Branze 38, I-25123 Brescia, Italy (e-mail: antonio.visioli@ing.unibs.it).

II. SCANNING THE ISSUE

This issue is a fractional amount of accepted papers grouped in two parts. Other accepted papers will be published in the upcoming issues.

A. Fractional Order Modeling

Complexity calls for fractional order modeling. The paper by West and Turalska is on the fractional Landau model. The extension is not mathematically but physically motivated by recent experiments showing a dependence of the decay of fluctuations on memory where in the model the exponential is replaced by an inverse power law. This transition is explained herein as being due to critical slowing down. The fractional calculus is used to model this memory and to relate the index of the inverse power law decay to that of the fractional derivative in time. This sets an important example of extension of integer order model to fractional order model that should be physics based.

The next paper by Cao, Chen, and Stuart is on a fractional micro-macro model for crowds of pedestrians based on fractional mean field games. Obviously, the considered system involving human is complex that calls for fractional order models. The same is true for the paper by Huang, Chen, Li, and Shi on fractional order modeling of human operator behavior with second order controlled plant and experiment research.

Ma, Zhou, Li, and Chen presented an interesting study on fractional modeling and state-of-charge (SOC) estimation of Lithium-ion battery. Chen, Li, Wilson, Huang discussed fractional modeling for the coupled MR damper and its damping system analysis based on fractional calculus. In common, we can observe that the human individual in crowds, the individual ion in Li-ion battery, the individual magnetic particle in MR fluid, collectively form complex systems with complex behaviors due to complex interactions of individuals and complex environments. Thus fractional order modeling is called to better service.

In the paper by Zhou, Zhang, Gao, Wang, and Ma, parameter estimation and topology identification of uncertain general fractional-order complex dynamical networks with time delay is developed to get a fractional model.

These papers were included in this issue to showcase the usefulness of the idea of fractional calculus in complex systems modeling.

B. Fractional Order Control

Using fractional order controller has been an intensely studied topic in recent years. We selected five papers to include in this special issue due to page budget limit.

The paper by Wang, Li, and Chen is about H_∞ output feedback control of linear time-invariant fractional-order systems over finite frequency range. It is the first result in fractional order control considering finite frequency range in H_∞ setting. The paper by Chen, Lu, and Li presented a rigorous study of the ellipsoidal invariant set of fractional order systems subject to actuator saturation when the uncertainties are in the convex combination form.

Naderi Soorki and Tavazoei showed how to achieve constrained swarm stabilization of fractional order linear time invariant swarm systems, while the paper by Aguila-Camacho and Duarte-Mermoud focused on how to improving the control energy in model reference adaptive controllers using fractional adaptive laws. This issue ends with a paper by Rojas-Moreno on an approach to design MIMO fractional order controllers for unstable nonlinear plants.

ACKNOWLEDGEMENTS

The guest editors wish to thank Professor Fei-Yue Wang, the Editor-in-Chief of *IEEE/CAA JAS*, for the initial idea, and Dr. Yan Ou for offering significant amount of help in the whole peer review process and the special issue scheduling given the amount of submissions and workload. Thanks go to all the authors, for their submissions, and the large number of reviewers, who carefully and timely evaluated and commented the papers submitted.

YangQuan Chen (M'95–SM'98) earned his Ph. D. degree in advanced control and instrumentation from Nanyang Technological University, Singapore, in 1998. Dr. Chen was on the faculty of Electrical and Computer Engineering at Utah State University before he joined the School of Engineering, University of California, Merced in 2012 where he teaches "Mechatronics" for juniors and "Fractional Order Mechanics" for graduates. His current research interests include mechatronics for sustainability, cognitive process control and hybrid lighting control, multi-UAV based cooperative multi-spectral "personal remote sensing" and applications, applied fractional calculus in controls, signal processing and energy informatics; distributed measurement and distributed control of distributed parameter systems using mobile actuator and sensor networks.

Dingyü Xue received his BSc, MSc and D Phil from Shenyang University of Technology in 1985, Northeastern University, China in 1988 and Sussex University, UK in 1992, respectively. He has been a professor in the School of Information Science and Engineering, Northeastern University since 1997. He is the author of several books on control system computer-aided design, system simulation and scientific computation. His major research interest covers the areas of fractional calculus and fractional-order systems, CACSD, systems simulation, system modelling and identification.

Antonio Visioli was born in Parma, Italy, in 1970. He received the Laurea degree in Electronic Engineering from the University of Parma in 1995 and the Ph. D. degree in Applied Mechanics from the University of Brescia in 1999. Currently he holds a professor position in Automatic Control at the Department of Mechanical and Industrial Engineering of the University of Brescia. He is a senior member of IEEE and a member of the TC on Education of IFAC, of the IEEE Control Systems Society TC on Control Education and of the IEEE Industrial Electronics Society TC on Factory Automation Subcommittees on Event-Based Control & Signal and on Industrial Automated Systems and Control, and of the national board of Anipla (Italian Association for Automation). His research interests include industrial robot control and trajectory planning, dynamic inversion based control, industrial control, and fractional control. He is the author or co-author or editor of four international book, one textbook and of more than 200 papers in international journals and conference proceedings.

Guest Editorial for Special Issue on Fractional Order Systems and Controls

YangQuan Chen, *Senior Member, IEEE*, Dingyü Xue, and Antonio Visioli, *Senior Member, IEEE*

I. Introduction

FRACTIONAL calculus has been applied in all MAD (modeling, analysis and design) aspects of control systems engineering since Shunji Manabe's pioneering work in early 1960s.

The 2016 International Conference on Fractional Differentiation and Its Applications (ICFDA) was held in Novi Sad, Serbia, July 18-20. Quoting from the website http://www.icfda16.com/ "*Fractional Calculus (FC for short) is a modern and expanding domain of mathematical analysis. The notion of fractional differentiation, or more appropriately the differentiation of arbitrary real order, means an operation analogous to standard differentiation which will take into account, memory effects if the independent variable is time, or nonlocal effects in the case of spatial independent variables. The order of the derivative may also be variable, distributed or complex. Basically, FC includes more information in the model than offered by the classical integer order calculus. Besides an essential mathematical interest, its overall goal is general improvement of the physical world models for the purpose of computer simulation, analysis, design and control in practical applications ...*", one has a clear impression that "fractional calculus" is "*application oriented*". The conference had two interesting plenary roundtable panel discussions:

1) Fractional Calculus: D'où venons-nous? Que sommes-nous? Où allons-nous? (Where do We Come From? What are We? Where are We Going?)
2) How to Improve Image and Impact of Fractional Calculus Research Community

The consensus of the community is to move forward with impacts in mind while seeking new frontiers. The Steering Committee chaired by one of the Guest Editors (Y. Q. Chen) decided to have 2018 ICFDA in Jordan and 2020 in Poland.

The aim of this special issue is to show the control engineering research community the usefulness of the fractional order tools from signals to systems to controls. It is our sincere hope that you can find something fractionally delicious in this fractional special issue.

Citation: YangQuan Chen, Dingyü Xue, Antonio Visioli. Guest Editorial for Special Issue on Fractional Order Systems and Controls. *IEEE/CAA Journal of Automatica Sinica*, 2016, **3**(4): 398−399

YangQuan Chen is with the Mechatronics, Embedded Systems and Automation (MESA) Lab, School of Engineering, University of California, Merced, 5200 North Lake Road, Merced, CA 95343, USA (e-mail: yqchen@ieee.org, or, yangquan.chen@ucmerced.edu).

Dingyü Xue is with the School of Information Sciences and Engineering, Northeastern University, Shenyang 110004, China (e-mail: xuedingyu@ise.neu.edu.cn).

Antonio Visioli is with the Department of Mechanical and Industrial Engineering, University of Brescia, Via Branze 38, I-25123 Brescia, Italy (e-mail: antonio.visioli@unibs.it).

II. Scanning the Issue

A fractional number of papers was published in the previous issue (vol. 3, no. 3) which already covered two parts (Fractional Order Modeling and Fractional Order Control) within which another fractional number of published papers was selected to produce video abstracts for a better dissemination.

This issue is still a fractional amount of accepted papers grouped in two parts. Other accepted papers will be published in the upcoming issues.

A. Fractional Order Control Analysis

Control systems engineering goes in the cycles of modeling, analysis and design (MAD). This section included 4 papers. Sathiyaraj and Balasubramaniam studied the controllability properties of fractional order stochastic differential inclusions with fractional Brownian motion in finite dimensional space. It is in an abstract setting but the topic is important because controllability is the first issue to be investigated in control analysis. Fractional order stochastic differential inclusions appear to be an emerging topic in advanced fractional order systems. Alagoz presented a note on robust stability analysis of fractional order interval systems by minimum argument vertex and edge polynomials. The presented results are more advanced and sharpened compared to the existing results. It is interesting to note that the stability checking of interval fractional order LTI systems was included in Chapter 53, in V. D. Blondel and A. Megretski (Editors). "*Unsolved problems in the mathematics of systems and control*" Princeton University Press in July 2004. The 3rd paper is single-authored by M. S. Tavazoei entitled "Criteria for Response Monotonicity Preserving in Approximation of Fractional Order Systems." It offered a new angle and perhaps a new needed constraint when performing finite dimensional FOS (fractional order systems) approximation. It is interesting to note this contribution over the previous two criteria: frequency-domain response fitting as well as time domain impulse response fitting. H. Chen and Y. Q. Chen's paper entitled "Fractional-order Generalized Principle of Self-support (FOG PSS) in Control Systems Design" is perhaps among the few that contains cartoons. The idea is quite interesting and useful. The PSS by late Z. Novakovic in 1992 was almost neglected or forgotten in the control community although he presented convincing amount of experimental results in his book to illustrate his control systems design framework. The key message is: The control signal contains the real dynamics of the system under control.

FOG PSS brings fractional order error dynamic model into PSS which opens a chance to achieve a better performance that the best achievable using the original PSS.

These four papers were included in this fractional issue to showcase the diverse ideas of beneficial use of fractional calculus in control systems analysis.

B. Fractional Order Control Design

Being able to analyze is only the beginning. Being able to design or synthesize based on available information on model, performance and constraints, is a step closer to real applications. Thus "control design" is as interesting as, if not more interesting than, "control analysis". This section includes 5 papers related to "Fractional Order Control Design".

Cheng, Wang, Wei, Liang and Wang presented a very nice tutorial review type of work entitled "Study on Four Disturbance Observers for FO-LTI Systems" with the authors' own developments on new schemes and comparisons. Disturbance observer (DOB) based control has been a very active research topic due to its effectiveness in many real world applications. It is interesting to note that there is a dedicated WeChat group on "Anti-disturbance Control and Applications" with over 100 members mostly in Chinese. Padula and Visioli suggested a set-point filter design for a two-degree-of-freedom fractional control system. Set-point filter can be considered as command filter to condition the final closed-loop transfer function. For fractional order systems, this 2DOF design is original and practically useful. Nie, Wang, Liu and Lan's paper is titled "Identification and PID Control for a Class of Delay Fractional-order Systems" that gives the readers the tool for control engineering practice when starting from a reaction curve test. The final two papers are on nonlinear fractional order systems. Hua, Zhang, Li and Guan's paper is on robust output feedback control for fractional order nonlinear systems with time-varying delays while Zhao, Wang, and Li's paper is about state feedback control for a class of fractional order nonlinear systems.

III. ACKNOWLEDGEMENTS

The guest editors wish to thank Professor Fei-Yue Wang, the Editor-in-Chief of IEEE/CAA JAS, for the initial idea, and Dr. Yan Ou for offering significant amount of help in the whole peer review process and the special issue scheduling given the amount of submissions and workload. Thanks go to all the authors, for their submissions, and the large number of reviewers, who carefully and timely evaluated and commented the papers submitted.

YangQuan Chen (M'95–SM'98) earned his Ph.D. degree in advanced control and instrumentation from Nanyang Technological University, Singapore, in 1998. Dr. Chen was on the faculty of Electrical and Computer Engineering at Utah State University before he joined the School of Engineering, University of California, Merced in 2012 where he teaches "Mechatronics" and "Unmanned Aerial Systems" for undergraduates and "Fractional Order Mechanics" and "Nonlinear Control" for graduates. His current research interests include mechatronics for sustainability, cognitive process control and hybrid lighting control, multi-UAV based cooperative multi-spectral "personal remote sensing" and applications, applied fractional calculus in controls, signal processing and energy informatics; distributed measurement and distributed control of distributed parameter systems using mobile actuator and sensor networks.

Dingyü Xue received his BSc, MSc and D Phil from Shenyang University of Technology in 1985, Northeastern University, China in 1988 and Sussex University, UK in 1992, respectively. He has been a professor in the School of Information Science and Engineering, Northeastern University since 1997. He is the author of several books on control system computer-aided design, system simulation and scientific computation. His major research interest covers the areas of fractional calculus and fractional-order systems, CACSD, systems simulation, system modelling and identification.

Antonio Visioli was born in Parma, Italy, in 1970. He received the Laurea degree in Electronic Engineering from the University of Parma in 1995 and the Ph.D. degree in Applied Mechanics from the University of Brescia in 1999. Currently he holds a professor position in Automatic Control at the Department of Mechanical and Industrial Engineering of the University of Brescia. He is a senior member of IEEE and a member of the TC on Education of IFAC, of the IEEE Control Systems Society TC on Control Education and of the IEEE Industrial Electronics Society TC on Factory Automation Subcommittees on Event-Based Control & Signal and on Industrial Automated Systems and Control, and of the national board of Anipla (Italian Association for Automation). His research interests include industrial robot control and trajectory planning, dynamic inversion based control, industrial control, and fractional control. He is the author or co-author or editor of four international books, one textbook and of more than 200 papers in international journals and conference proceedings.

Cyber-Physical Systems as General Distributed Parameter Systems: Three Types of Fractional Order Models and Emerging Research Opportunities

Fudong Ge, YangQuan Chen, *Senior Member, IEEE*, and Chunhai Kou

***Abstract*—Cyber-physical systems (CPSs) are man-made complex systems coupled with natural processes that, as a whole, should be described by distributed parameter systems (DPSs) in general forms. This paper presents three such general models for generalized DPSs that can be used to characterize complex CPSs. These three different types of fractional operators based DPS models are: fractional Laplacian operator, fractional power of operator or fractional derivative. This research investigation is motivated by many fractional order models describing natural, physical, and anomalous phenomena, such as sub-diffusion process or super-diffusion process. The relationships among these three different operators are explored and explained. Several potential future research opportunities are then articulated followed by some conclusions and remarks.**

***Index Terms*—Cyber-physical systems (CPSs), generalized distributed parameter systems (DPSs), fractional Laplacian operator, fractional power of operator, fractional derivative.**

I. INTRODUCTION

It is well known that the cyber-physical systems (CPSs) with integrated computational and physical processes can be regarded as a new generation of control systems and can interact with humans through many new modalities[1]. The objective of CPS is to develop new science and engineering methods in which cyber and physical designs are compatible, synergistic, and integrated at all scales. Besides, as we all know, the distributed parameter systems (DPSs) can be used to well characterize those cyber-physical process[2−3] and the actions and measurements of the system studied are better described by utilizing the actuators and sensors, which was first introduced by El Jai and Pritchard in [4] and mainly focused on the locations, number and spatial distributions of the actuators and sensors.

Moreover, in the past several decades, fractional calculus has shown great potential in science and engineering applications and some phenomena such as self-similarity, non-stationary, non-Gaussian process and short or long memory process are all closely related to fractional calculus[5−7]. It is now widely believed that, using fractional calculus in modeling can better capture the complex dynamics of natural and man-made systems, and fractional order controls can offer better performance not achievable before using integer order controls[8−9].

Motivated by the above arguments, in this paper, let Ω be an open bounded subset of $\mathbf{R}^n$ with smooth boundary $\partial\Omega$ and we consider the following fractional DPSs:

$$z_t(x,t) + Az(x,t) = u(x,t) \quad \text{in } \Omega \times [0,b], \tag{1}$$

where $b > 0$ is a given constant, u is the control input depending on the number and the structure of actuators and A may be a fractional Laplacian operator, a fractional power of operator or a fractional derivative.

The contribution of this present paper is to analyze the relationship among the fractional Laplacian operator, fractional power of operator and fractional derivative and try to explore the opportunities and research challenges related to the fractional order DPSs emerging at the same time. To the best of our knowledge, no result is available on this topic. We hope that the results here could provide some insights into the control theory of this field and be used in real-life applications.

The rest of the paper is organized as follows. The relationship among fractional Laplacian operator, fractional power of operator and fractional derivative are explored in Section II. In Section III, the emerging research opportunities of the fractional order DPSs with those three operators are discussed. Several conclusions and remarks of this paper are given in the last section.

II. THREE DIFFERENT TYPES OF OPERATORS

In this section, we shall introduce some basic relationships among the fractional Laplacian operator, fractional power of operator and fractional derivative. For further information, we refer the readers to papers from [10] to [36] in the reference section of the present paper and the references cited therein.

A. Fractional Laplacian Operator and Fractional Power of Operator

This subsection is devoted to the difference between the fractional Laplacian operator and fractional power of operator. For more details, please see [10−15] and their cited references.

Manuscript received August 25, 2015, accepted September 7, 2015. This work was supported by Chinese Universities Scientific Fund (CUSF-DH-D-2014061) and Natural Science Foundation of Shanghai (15ZR1400800). Recommended by Associate Editor Antonio Visioli.

Citation: Fudong Ge, YangQuan Chen, Chunhai Kou. Cyber-physical systems as general distributed parameter systems: three types of fractional order models and emerging research opportunities. *IEEE/CAA Journal of Automatica Sinica*, 2015, **2**(4): 353−357

Fudong Ge is with the College of Information Science and Technology, Donghua University, Shanghai 201620, China (e-mail: gefd2011@gmail.com).

YangQuan Chen is with the Mechatronics, Embedded Systems and Automation Lab, University of California, Merced, CA 95343, USA (e-mail: ychen53@ucmerced.edu).

Chunhai Kou is with the Department of Applied Mathematics, Donghua University, Shanghai 201620, China (e-mail: kouchunhai@dhu.edu.cn).

Let us denote $(-\triangle)^{\alpha/2}$ the nonlocal operator (also called the fractional Laplacian operator) defined pointwise by the following Cauchy principal value integral

$$(-\triangle)^{\alpha/2}f(x)=C_\alpha P.V.\int_{\mathbf{R}}\frac{f(x)-f(y)}{|x-y|^{1+\alpha}}\mathrm{d}y,\ 0<\alpha<2, \quad (2)$$

where $C_\alpha=\frac{2^\alpha\Gamma(1/2+\alpha/2)}{\sqrt{\pi}|\Gamma(-\alpha/2)|}$ is a constant dependent on the order α. Obviously, we see that the fractional Laplacian $(-\triangle)^{\alpha/2}$ is a nonlocal operator which depends on the parameter α and recovers the usual Laplacian as $\alpha\to 2$. For more information about the fractional Laplacian operator, see [16−20] and the references cited therein. Now we have the following result.

Theorem 1[21]**.** Suppose that $(-\triangle)^{\alpha/2}$ is defined in $L^2(0,l)$ for $\alpha\in(0,2)$. Then, the eigenvalues of the following spectral problem

$$(-\triangle)^{\alpha/2}\xi(x)=\lambda\xi(x),\quad x\in(0,l), \quad (3)$$

where $\xi\in L^2(0,l)$ is extended to all $\mathbf{R}$ by 0 is

$$\lambda_n=\left(\frac{n\pi}{l}-\frac{(2-\alpha)\pi}{4l}\right)^\alpha+O\left(\frac{1}{n}\right) \quad (4)$$

satisfying

$$0<\lambda_1<\lambda_2\le\cdots\le\lambda_i\le\cdots.$$

Moreover, the corresponding eigenfunctions ξ_n of λ_n, after normalization, form a complete orthonormal basis in $L^2(0,l)$.

Note that the constant in the error term $O\left(\frac{1}{n}\right)$ tends to zero when α approaches 2 and in the particular case, when $\alpha=2$, we see that $\lambda_n=(n\pi/l)^2$ without the error term.

However, for a positive operator A on bounded domain $[0,l]$, suppose $0<\lambda_1\le\lambda_2\le\cdots\le\lambda_n\le\cdots$ are the eigenvalues of A, $\{\xi_1,\xi_2,\dots,\xi_n,\dots\}$ are the corresponding eigenfunctions and ξ_n $(i=1,2,\dots)$ form an orthonormal basis of $L^2(0,l)$. Let $(\cdot,\cdot)$ be the inner product of $L^2(0,l)$. We define the fractional power of operator A as follows:

$$A^\beta f(x)=\sum_{n=1}^{\infty}\lambda_n^\beta(\xi_n,f)\xi_n(x),\quad f\in L^2(0,l). \quad (5)$$

Then λ_n^β $(i=1,2,\dots)$ are the eigenvalues of A^β. This implies that the two operators are different.

Moreover, the work spaces of the two operators (fractional Laplacian operator and fractional power of operator A) are different. Before stating our main results, we first introduce two Banach spaces, which are specified in [11, 13, 14, 16].

For $\Omega\subseteq\mathbf{R}^n$ is a bounded domain, $s\in(0,1)$ and $p\in[1,\infty)$, we define the classical Sobolev space $W^{s,p}(\Omega)$ as follows[13]:

$$W^{s,p}(\Omega):=\left\{f\in L^p(\Omega):\frac{f(x)-f(y)}{|x-y|^{\frac{n}{p}+s}}\in L^p(\Omega\times\Omega)\right\} \quad (6)$$

endowed with the natural norm

$$\|f\|_{W^{s,p}(\Omega)} := \left(\int_\Omega|f(x)|^p\mathrm{d}x+\int_\Omega\int_\Omega\frac{|f(x)-f(y)|^p}{|x-y|^{n+sp}}\mathrm{d}x\mathrm{d}y\right)^{1/p}$$

is an intermediary Banach space between $L^p(\Omega)$ and $W^{1,p}(\Omega)$. When a non-integer $s>1$, let $s=m+\sigma$ with $m\in\mathbf{N}$ and $\sigma\in(0,1)$. In this case, let $D^\beta f$ with $|\beta|=m$ be the distributed derivative of f, then the classical Sobolev space $W^{s,p}(\Omega)$ defined by

$$W^{s,p}(\Omega):=\left\{\begin{array}{r} f\in W^{m,p}(\Omega):D^\beta f\in W^{\sigma,p}(\Omega)\ \text{for}\\ \text{all }\beta\text{ such that }|\beta|=m\end{array}\right\} \quad (7)$$

with respect to the norm

$$\|f\|_{W^{s,p}(\Omega)}:=\left(\|f\|^p_{W^{m,p}(\Omega)}+\|D^\beta f\|^p_{W^{\sigma,p}(\Omega)}\right)^{1/p} \quad (8)$$

is a Banach space. Clearly, if $s=m$ is an integer, the space $W^{s,p}(\Omega)$ coincides with the Sobolev space $W^{m,p}(\Omega)$.

Besides, let $\rho(x)\sim\frac{1}{\delta^\alpha(x)}$ with $\delta(x)=\mathrm{dist}(x,\Omega^c)$. Define another space as follows:

$$W^{s,p}_\rho(\Omega):=\{f\in W^{s,p}(\Omega):\rho(x)f(x)\in L^p(\Omega)\} \quad (9)$$

with the norm

$$\|f\|_{W^{s,p}_\rho(\Omega)} := \left(\int_\Omega|\rho(x)f(x)|^p\mathrm{d}x+\int_\Omega\int_\Omega\frac{|f(x)-f(y)|^p}{|x-y|^{n+sp}}\mathrm{d}x\mathrm{d}y\right)^{1/p}. \quad (10)$$

Actually, $W^{s,p}_\rho(\Omega)$ is called nonlocal Sobolev space and we have $W^{s,p}_\rho(\Omega)\subseteq W^{s,p}(\Omega)$[14, 16].

By the Remark 2.1 in [11], for the fractional power of operator, we take the classical fractional Sobolev space as its work space. But for fractional Laplacian operator, we must take the nonlocal Sobolev space as its work space, which can be regarded as the weighted fractional Sobolev space. More precisely, for any element $f\in W^{s,p}(\Omega)$, since $-\triangle$ is a local operator and we do not know how $f(x)$ approaches 0 when $x\to\partial\Omega$. Even if considering the space $W^{s,p}_0(\Omega);=\{f\in W^{s,p}(\Omega):f|_{\partial\Omega}=0\}$, we only know that the function $f=0$ on the boundary and we do not know how f approaches 0. However, for the fractional Laplacian operator, it is a nonlocal operator and it is defined in the whole space. So, it provides information about how f approaches 0 as $x\to\partial\Omega$. In fact, from the definition of nonlocal Sobolev space, we know that $\frac{f(x)}{\delta^\alpha(x)}\to 0$ as $x\to\partial\Omega$, which dictates how f approaches 0 near boundary. It coincides with the result of the Theorem 1.2 in [22]. Thus, this is a significant difference between the fractional power of operator $A=-\triangle$ and the fractional Laplacian operator.

Besides, it is well known that

$$\|\triangle f\|_{W^{s,p}(\Omega)}=\|f\|_{W^{s+2,p}(\Omega)}.$$

But for the fractional Laplacian operator $(-\triangle)^\alpha$,

$$\|(-\triangle)^\alpha f\|_{W^{s,p}(\Omega)}=\|f\|_{W^{s+2\alpha,p}(\Omega)}$$

will not hold. By using Fourier transform, we have

$$\|(-\triangle)^\alpha f\|_{W^{s,p}_\rho(\Omega)}=\|f\|_{W^{s+2\alpha,p}_\rho(\Omega)}.$$

Finally, by [15], let X be a rotationally invariant stable process of index $\alpha\in(0,1)$. Its symbol is given by $\eta(f)=-|f|^\alpha$ for all $f\in\mathbf{R}^n$. It is instructive to accept that η is the symbol for a legitimate differential operator; then, using the usual correspondence $f_j\to -i\partial_j$ for $1\le j\le n$, we would write

$$A=\eta(\Omega)=-\left(\sqrt{-\partial_1^2-\cdots-\partial_n^2}\right)^\alpha=-(-\triangle)^{\alpha/2}. \quad (11)$$

In fact, it is very useful to interpret $\eta(\Omega)$ as a fractional power of the operator $-\triangle$. However, for the fractional Laplacian operator, it can be defined as the generator of α-stable Lévy processes. More precisely, if X_t is the isotropic α-stable Lévy processes starting at zero and f is a smooth function, then

$$(-\triangle)^{\alpha/2}f(x)=\lim_{h\to0^+}\frac{\mathrm{E}[f(x)-f(x+X_h)]}{h}. \tag{12}$$

This also indicates that the fractional power of operator $-\triangle$ and the fractional Laplacian operator are different.

B. Fractional Laplacian Operator and Fractional Derivative

This subsection is focused on the relationship between the fractional Laplacian operator and the Riesz fractional derivative.

Definition 1[23]**.** The Riesz fractional operator for $n-1<\alpha\leq n$ on a finite interval $0\leq x\leq l$ is defined as

$$\frac{\partial^\alpha}{\partial|x|^\alpha}f(x)=\frac{-1}{2\cos(\frac{\alpha\pi}{2})}\left[{}_0D_x^\alpha+{}_xD_l^\alpha\right]f(x), \tag{13}$$

where

$$0D_x^\alpha f(x)=\frac{1}{\Gamma(n-\alpha)}\frac{\partial^n}{\partial x^n}\int_0^x(x-\eta)^{-\alpha-1+n}f(\eta)\mathrm{d}\eta$$

and

$$xD_l^\alpha f(x)=\frac{(-1)^n}{\Gamma(n-\alpha)}\frac{\partial^n}{\partial x^n}\int_x^l(\eta-x)^{-\alpha-1+n}f(\eta)\mathrm{d}\eta$$

are the left-sided and right-sided Riemann-Liouville fractional derivative, respectively.

Moreover, according to [24], the fractional Laplacian is the operator with symbol $|x|^\alpha$. In other words, the following formula holds:

$$(-\triangle)^{\alpha/2}f(x)=\mathcal{F}^{-1}|x|^\alpha\mathcal{F}f(x), \tag{14}$$

where $\mathcal{F}$ and $\mathcal{F}^{-1}$ denote the Fourier transform and inverse Fourier transform of $f(x)$, respectively. We refer the readers to [25] for a detailed proof of the equivalence between the two definitions (1) and (2) of fractional Laplacian operator.

By using Luchko's theorem in [26], we obtain the following result on the equivalent relationship between the Riesz fractional derivative $\frac{\partial^\alpha}{\partial|x|^\alpha}$ and the fractional Laplacian operator $-(-\triangle)^{\alpha/2}$.

Lemma 1[27]**.** For a function $f(x)$ defined on the finite domain $[0,l]$, and $f(0)=f(l)=0$, the following equality holds:

$$\begin{aligned}-\left(-\triangle\right)^{\alpha/2}f(x)&=\frac{-1}{2\cos(\frac{\alpha\pi}{2})}\left[{}_0D_x^\alpha f(x)+{}_xD_l^\alpha f(x)\right]\\&=\frac{\partial^\alpha}{\partial|x|^\alpha}f(x),\end{aligned}$$

where $\alpha\in(1,2)$ and the space fractional derivative $\frac{\partial^\alpha}{\partial|x|^\alpha}$ is a Riesz fractional derivative.

For more information on the analytical solution of the generalized multi-term time and space fractional partial differential equations with Dirichlet nonhomogeneous boundary conditions, we refer the readers to [27]. For more information on the numerical solution of fractional partial differential equation with Riesz space fractional derivatives on a finite domain, consult [28−29].

C. Fractional Derivative and Fractional Power of Operator

In this part, we first show the following definition of the positive operator.

Definition 2[30]**.** The operator A is said to be positive if its spectrum $\sigma(A)$ lies in the interior of the sector of angle $\varphi\in(0,\pi)$, symmetric with respect to the real axis, and if on the edges of this sector, $S_1=\{\rho\mathrm{e}^{\mathrm{i}\varphi}:0\leq\rho<\infty\}$ and $S_2=\{\rho\mathrm{e}^{-\mathrm{i}\varphi}:0\leq\rho<\infty\}$, and outside it the resolvent $(\lambda I-A)^{-1}$ is subject to the bound

$$\left\|(\lambda I-A)^{-1}\right\|\leq\frac{M(\varphi)}{1+|\lambda|}. \tag{15}$$

Moreover, for a positive operator A, any $\alpha>0$, one can define the negative fractional power of operator A by the following formula[31]:

$$A^{-\alpha}=\frac{1}{2\pi\mathrm{i}}\int_\Gamma\lambda^{-\alpha}R(\lambda)\mathrm{d}\lambda,\left(\begin{array}{l}R(\lambda)=(A-\lambda I)^{-1},\\ \Gamma=S_1\cup S_2\end{array}\right). \tag{16}$$

It is then quite easy to see that $A^{-\alpha}$ is a bounded operator, which is an entire function of α, satisfying $A^{-\alpha}=A^{-n}$ if α is an integer n, and $A^{-(\alpha+\beta)}=A^{-\alpha}A^{-\beta}$ for all $\alpha,\beta\in\mathbf{C}$. Using (16), we have

$$A^{-\alpha}=\frac{1}{2\pi\mathrm{i}}\int_{-\infty}^0\lambda^{-\alpha}R(\lambda)\mathrm{d}\lambda+\frac{1}{2\pi\mathrm{i}}\int_0^{-\infty}\lambda^{-\alpha}R(\lambda)\mathrm{d}\lambda. \tag{17}$$

Then taking the integration along the lower and upper sides of the cut respectively: $\lambda=s\mathrm{e}^{-\pi\mathrm{i}}$ and $\lambda=s\mathrm{e}^{\pi\mathrm{i}}$, it follows that

$$\begin{aligned}A^{-\alpha}&=\frac{\mathrm{e}^{\alpha\pi\mathrm{i}}}{2\pi\mathrm{i}}\int_0^\infty s^{-\alpha}R(-s)\mathrm{d}s-\frac{\mathrm{e}^{-\alpha\pi\mathrm{i}}}{2\pi\mathrm{i}}\int_0^\infty s^{-\alpha}R(-s)\mathrm{d}s\\&=\frac{\cos(\alpha\pi)+\mathrm{i}\sin(\alpha\pi)}{2\pi\mathrm{i}}\int_0^\infty s^{-\alpha}R(-s)\mathrm{d}s\\&\quad-\frac{\cos(\alpha\pi)-\mathrm{i}\sin(\alpha\pi)}{2\pi\mathrm{i}}\int_0^\infty s^{-\alpha}R(-s)\mathrm{d}s\\&=\frac{\sin(\alpha\pi)}{\pi}\int_0^\infty s^{-\alpha}R(-s)\mathrm{d}s\\&=\frac{1}{\Gamma(\alpha)\Gamma(1-\alpha)}\int_0^\infty s^{-\alpha}R(-s)\mathrm{d}s.\end{aligned}$$

Moreover, for any $\alpha\in(n-1,n)$, we get that

$$A^\alpha f=A^{\alpha-n}A^nf=\frac{\int_0^\infty s^{\alpha-n}R(-s)A^nf\mathrm{d}s}{\Gamma(n-\alpha)\Gamma(1+\alpha-n)}. \tag{18}$$

and for more properties on the fractional power of a positive operator, please see [32−35] and the references cited therein.

Now we are ready to state the following results on the connection of fractional derivative and integral with fractional power of positive operator.

Theorem 2. Let the absolutely space

$$AC^n[0,l]:=\{f:f^{(n-1)}(x)\in C[0,l],\ f^{(n)}(x)\in L^2[0,l]\}$$

and let A be the operator defined by the formula $Af(x)=f'(x)$ with the domain

$$\{f:f\in AC^n[0,l],\ f^{(n)}(0)=0\}.$$

Then A is a positive operator in the Banach space $AC^n[0,l]$ and

$$A^\alpha f(x)={}_0D_x^\alpha f(x),\quad n-1<\alpha<n \tag{19}$$

for all $f(x) \in D(A)$.

Proof. By [36], the operator $A + sI$ $(s \geq 0)$ has a bounded inverse and the resolvent of A is given by

$$\left((A+sI)^{-1} f\right)(x) = \int_0^x \mathrm{e}^{-s(x-y)} f(y)\mathrm{d}y. \tag{20}$$

Then the operator A is a positive operator in $AC^n[0,l]$ and (17) gives

$$\begin{aligned} A^\alpha f(x) &= \frac{\int_0^\infty s^{\alpha-n} R(-s) A^n f(x)\mathrm{d}s}{\Gamma(n-\alpha)\Gamma(1+\alpha-n)} \\ &= \frac{\int_0^\infty s^{\alpha-n} (A+sI)^{-1} f^{(n)}(x)\mathrm{d}s}{\Gamma(n-\alpha)\Gamma(1+\alpha-n)} \\ &= \frac{\int_0^\infty s^{\alpha-n} \int_0^x \mathrm{e}^{-s(x-y)} f^{(n)}(y)\mathrm{d}y\mathrm{d}s}{\Gamma(n-\alpha)\Gamma(1+\alpha-n)} \\ &= \frac{\int_0^x \left[\int_0^\infty s^{\alpha-n}\mathrm{e}^{-s(x-y)}\mathrm{d}s\right] f^{(n)}(y)\mathrm{d}y}{\Gamma(n-\alpha)\Gamma(1+\alpha-n)}. \end{aligned}$$

Let $s(x-y) = \lambda$, we get that

$$\begin{aligned} \int_0^\infty s^{\alpha-n}\mathrm{e}^{-s(x-y)}\mathrm{d}s &= (x-y)^{n-\alpha-1}\int_0^\infty \lambda^{\alpha-n}\mathrm{e}^{-\lambda}\mathrm{d}\lambda \\ &= (x-y)^{n-\alpha-1}\Gamma(\alpha-n+1). \end{aligned}$$

Then

$$\begin{aligned} A^\alpha f(x) &= \frac{\int_0^x (x-y)^{n-\alpha-1}\Gamma(\alpha-n+1) f^{(n)}(y)\mathrm{d}y}{\Gamma(n-\alpha)\Gamma(1+\alpha-n)} \\ &= \frac{1}{\Gamma(n-\alpha)}\int_0^x (x-y)^{n-\alpha-1} f^{(n)}(y)\mathrm{d}y \\ &= {}_0D_x^\alpha f(x). \end{aligned}$$

□

III. THE EMERGING RESEARCH OPPORTUNITIES

Recent advances in modeling and control of fractional diffusion systems, fractional reaction-diffusion systems and fractional reaction-diffusion-advection systems have been reviewed in the framework of CPSs. The fractional order DPSs have now been found wide applications for describing many physical phenomena, such as sub-diffusion or super-diffusion processes. At the same time, to our best knowledge, many problems are still open calling for research cooperation of multi-disciplines such as mathematical modelling, engineering applications, and information sciences.

First, it is worth noting that in the more recent monograph[37], the theory of pseudo-differential operators with singular symbols, and the connections between them and those three types of operators are explored. See [38−40] for more knowledge on pseudo-differential operator. Moreover, we claim that those equivalences between fractional Laplacian operator and fractional derivative, fractional order of operator and fractional derivative discussed in this paper can introduce new mathematical vehicles to study fractional order generalized DPSs. For example, when we study a fractional DPSs with Riesz fractional derivative, by Lemma 1 in Section II-B, the spectral representation methods can be used to characterize the solution of the dynamic system. Then we can study the existence of solutions, stability, controllability and observability of the system under consideration.

Potential topics such as modeling the sub-diffusion or super-diffusion processes with consideration of the networked mobile actuators and mobile sensors, the communication among the actuators and sensors, collocated or non-collocated actuators and sensors, their robustness and optimality problems are all interesting and worthy much more efforts in future. Another interesting and important topic concerns the time-space fractional DPSs where the traditional first order derivative is replaced by a fractional order derivative with respect to the time t.

Furthermore, in the case of diffusion systems, it is worth mentioning that, in general, not all the states can be reached in the whole domain of interest[4, 41−42] and it would be more challenging in nature since the dynamics of the real-life control problem is always hybrid continuous and discrete. Due to the spatial-temporal sampling and discrete nature of decision and control, the notions of regional analysis should be introduced, i.e., we can consider the regional stability, regional controllability, regional observability etc. of the system under consideration. In addition, as stated in [43], from an application point of view, some plain questions such as "How many actuators/sensors are sufficient and how to best configure them for a fractional DPSs control process?", "Given the desirable zone shape, is it possible to control or contain the fractional diffusion process within the given zone?", if not, "How to quantify the controllability/observability of the actuators/sensors" and etc. might be asked, which in fact raises some important theoretical challenges and open new opportunities for further research.

IV. CONCLUSION

This paper is concerned with the fractional order DPSs with three different operators: fractional Laplacian operator, fractional power of operator and fractional derivative. The relationship among the three operators and the emerging research opportunities are introduced. We hope that the results here could provided some insight into the control theory analysis of fractional order DPSs in particular and CPSs in general. The results presented here can also be extended to complex fractional order DPSs and various open questions are still pending. For instance, the problem of regional optimal control of fractional order DPSs with more complicated sensing and actuation configurations are of great interest.

REFERENCES

[1] Lee E A. Cyber physical systems: design challenges. In: Proceedings of the 11th IEEE International Symposium on Object Oriented Real-Time Distributed Computing (ISORC). Orlando, FL: IEEE, 2008. 363−369
[2] Song Z, Chen Y Q, Sastry C R, Tas N C. *Optimal Observation for Cyber-physical Systems: a Fisher-information-matrix-based Approach*. London: Springer, 2009.
[3] Tricaud C, Chen Y Q. *Optimal Mobile Sensing and Actuation Policies in Cyber-physical Systems*. London: Springer, 2012.
[4] El Jai A, Pritchard A J. *Sensors and Controls in the Analysis of Distributed Systems*. New York: Halsted Press, 1988.
[5] Podlubny I. *Fractional Differential Equations*, Vol. 198. New York: Academic Press, 1999.
[6] Kilbas A A, Srivastava H M, Trujillo J J. *Theory and Applications of Fractional Differential Equations*. Amsterdam, Netherlands: Elsevier Science, 2006.
[7] Klimek M. *On Solutions of Linear Fractional Differential Equations of a Variational Type*. Czestochowa: Publishing Office of Czestochowa University of Technology, 2009.

[8] Torvik P J, Bagley R L. On the appearance of the fractional derivative in the behavior of real materials. *Journal of Applied Mechanics*, 1984, **51**(2): 294−298

[9] Mandelbrot B B. *The Fractal Geometry of Nature*, Vol. 173. San Francisco: W. H. Freeman, 1983.

[10] Lv G Y, Duan J Q, He J C. Nonlocal elliptic equations involving measures. *Journal of Mathematical Analysis and Applications*, 2015, **432**(2): 1106−1118

[11] Lv G Y, Duan J Q. Martingale and weak solutions for a stochastic nonlocal Burgers equation on bounded intervals. arXiv preprint arXiv: 1410.7691 [math. P R], October 28, 2014.

[12] He J C, Duan J Q, Gao H J. Global solutions for a nonlocal Ginzberg-Landau equation and a nonlocal Fokker-Plank equation. arXiv preprint arXiv: 1312. 5836 [math. A P], December 20, 2013.

[13] Di Nezza E, Palatucci G, Valdinoci E. Hitchhiker's guide to the fractional Sobolev spaces. *Bulletin des Sciences Mathématiques*, 2012, **136**(5): 521−573

[14] Du Q, Gunzburger M, Lehoucq R B, Zhou K. A nonlocal vector calculus, nonlocal volume-constrained problems, and nonlocal balance laws. *Mathematical Models and Methods in Applied Sciences*, 2013, **23**(3): 493−540

[15] Applebaum D. *Lévy Processes and Stochastic Calculus* (Second edition). Cambridge: Cambridge University Press, 2009.

[16] Du Q, Gunzburger M, Lehoucq R B, Zhou K. Analysis and approximation of nonlocal diffusion problems with volume constraints. *SIAM Review*, 2012, **54**(4): 667−696

[17] Choi W, Kim S, Lee K A. Asymptotic behavior of solutions for nonlinear elliptic problems with the fractional Laplacian. *Journal of Functional Analysis*, 2014, **266**(11): 6531−6598

[18] Barrios B, Colorado E, De Pablo A, Sánchez U. On some critical problems for the fractional Laplacian operator. *Journal of Differential Equations*, 2012, **252**(11): 6133−6162

[19] Micu S, Zuazua E. On the controllability of a fractional order parabolic equation. *SIAM Journal on Control and Optimization*, 2006, **44**(6): 1950−1972

[20] Fattorini H O, Russell D L. Exact controllability theorems for linear parabolic equations in one space dimension. *Archive for Rational Mechanics and Analysis*, 1971, **43**(4): 272−292

[21] Kwaśnicki M. Eigenvalues of the fractional Laplace operator in the interval. *Journal of Functional Analysis*, 2012, **262**(5): 2379−2402

[22] Ros-Oton X, Serra J. The dirichlet problem for the fractional Laplacian: regularity up to the boundary. *Journal de Mathématiques Pures et Appliquées*, 2014, **101**(3): 275−302

[23] Gorenflo R, Mainardi F. Random walk models for space-fractional diffusion processes. *Fractional Calculus and Applied Analysis*, 1998, **1**(2): 167−191

[24] Samko S G, Kilbas A A, Marichev O I. *Fractional Integrals and Derivatives: Theory and Applications*. New York: Gordon and Breach Science Publishers, 1993.

[25] Landkof N S, Doohovskoy A P. *Foundations of Modern Potential Theory (Grundlehren der mathematischen Wissenschaften)*. New York: Springer, 1972.

[26] Luchko Y, Gorenflo R. An operational method for solving fractional differential equations with the Caputo derivatives. *Acta Mathematica Vietnamica*, 1999, **24**(2): 207−233

[27] Jiang H, Liu F, Turner I, Burrage K. Analytical solutions for the multi-term time-space Caputo-Riesz fractional advection-diffusion equations on a finite domain. *Journal of Mathematical Analysis and Applications*, 2012, **389**(2): 1117−1127

[28] Yang Q, Liu F, Turner I. Numerical methods for fractional partial differential equations with Riesz space fractional derivatives. *Applied Mathematical Modelling*, 2010, **34**(1): 200−218

[29] Liu F, Anh V, Turner I. Numerical solution of the space fractional Fokker-Planck equation. *Journal of Computational and Applied Mathematics*, 2004, **166**(1): 209−219

[30] Ashyralyev A. A note on fractional derivatives and fractional powers of operators. *Journal of Mathematical Analysis and Applications*, 2009, **357**(1): 232−236

[31] Komatsu H. Fractional powers of operators. *Pacific Journal of Mathematics*, 1966, **19**(2): 285−346

[32] Komatsu H. Fractional powers of operators, II. Interpolation spaces. *Pacific Journal of Mathematics*, 1967, **21**(1): 89−111

[33] Komatsu H. Fractional powers of operators, III. Negative powers. *Journal of the Mathematical Society of Japan*, 1969, **21**(2): 205−220

[34] Carracedo C M, Alix M S. *The Theory of Fractional Powers of Operators*. Amsterdam: Elsevier, 2001.

[35] Balakrishnan A V. Fractional powers of closed operators and the semigroups generated by them. *Pacific Journal of Mathematics*, 1960, **10**(2): 419−439

[36] Faris W G. Methods of applied mathematics second semester lecture notes [Online], available: http://math.arizona.edu/ faris/methbweb/methlecb.pdf, January 2, 2015.

[37] Umarov S. *Introduction to Fractional and Pseudo-differential Equations with Singular Symbols*, Vol. 41. Switzerland: Springer, 2015.

[38] Hahn M, Kobayashi K, Umarov S. SDEs driven by a time-changed Lévy process and their associated time-fractional order pseudo-differential equations. *Journal of Theoretical Probability*, 2012, **25**(1): 262−279

[39] Umarov S. Algebra of pseudo-differential operators with variable analytic symbols and propriety of the corresponding equations. *Differential Equations*, 1991, **27**(6): 753−759

[40] Hahn M, Umarov S. Fractional Fokker-Planck-Kolmogorov type equations and their associated stochastic differential equations. *Fractional Calculus and Applied Analysis*, 2011, **14**(1): 56−79

[41] Afifi L, Chafia A, El Jai A. Regionally efficient and strategic actuators. *International Journal of Systems Science*, 2002, **33**(1): 1−12

[42] Ge F D, Chen Y Q, Kou C H. Regional controllability of anomalous diffusion generated by the time fractional diffusion equations. In: Proceedings of the 2015 ASME International Design Engineering Technical Conferences (ASME IDETC/CIE 2015), Boston, 2015, DETC2015-46697. See also: arXiv preprint arXiv: 1508. 00047

[43] Chen Y Q, Moore K L, Song Z. Diffusion boundary determination and zone control via mobile actuator-sensor networks (MAS-net): challenges and opportunities. In: Proceedinds of SPIE, Intelligent Computing: Theory and Applications II. Orlando, FL: SPIE, 2004, 5421: 102−113

Fudong Ge Ph. D. candidate in the College of Information Science and Technology of Donghua University, China. He joined the MESA Lab of the University of California, Merced in October, 2014 as an exchange Ph. D. student hosted by Prof. YangQuan Chen. His research interests include existence, stability of solutions for fractional differential equations, continuous time random walks and anomalous diffusion systems, distributed measurement and distributed control problems in general distributed parameter systems or cyber-physical systems in general form.

YangQuan Chen earned his Ph. D. degree in advanced control and instrumentation from Nanyang Technological University, Singapore, in 1998. Dr. Chen was on the Faculty of Electrical and Computer Engineering at Utah State University before he joined the School of Engineering, University of California, Merced in 2012 where he teaches "Mechatronics" for juniors and "Fractional Order Mechanics" for graduates. His current research interests include mechatronics for sustainability, cognitive process control and hybrid lighting control, multi-UAV based cooperative multi-spectral "personal remote sensing" and applications, applied fractional calculus in controls, signal processing and energy informatics, distributed measurement and distributed control of distributed parameter systems using mobile actuator and sensor networks. Corresponding author of this paper.

Chunhai Kou received his Ph. D. degree from Shanghai Jiao Tong University, Shanghai, China, in 2002. He joined the Department of Science, Donghua University in 2004 where he teaches "Stability Analysis of Nonlinear Differential Equations", "Theory and Applications of Fractional Differential Equations" and "Mathematical Analysis". His current research interests include stability analysis of differential equations based on the Lyapunov theory, basic theory of differential inclusions, applied fractional calculus in controls, existence, stability of solutions for the fractional differential equations.

The Fractional Landau Model

Bruce J. West and Malgorzata Turalska

***Abstract*—Herein the Landau model of the transition from laminar to turbulent fluid flow is generalized to include the effect of memory. The original Landau model is quadratically nonlinear and memoryless, with turbulent fluctuations decaying exponentially. However, recent experiments show a dependence of the decay of fluctuations on memory, with the exponential being replaced by an inverse power law. This transition is explained herein as being due to critical slowing down. The fractional calculus is used to model this memory and to relate the index of the inverse power law decay to that of the fractional derivative in time.**

***Index Terms*—Fluid dynamics, turbulence, fractional calculus, partial differential equations, nonlinear equations.**

I. INTRODUCTION

NONLINEAR dynamics blossomed in the decades of the 1980's and 1990's, subsequently becoming foundational, not only in the description of mechanical systems[1], but in non-equilibrium statistical physics, as well[2]. Much of that analysis bypassed the contributions made by Koopman[3] and von Neumann[4−5], in which they formulated classical mechanics using linear operators to represent physical observables, providing a Hilbert space for the theory of nonlinear dynamic systems. The mathematics of this latter theory was carried to maturity by Kowalski[6]. Herein we apply a version of these techniques to the solution of fractional nonlinear rate equations.

The strategy we adopt herein is to introduce the new technique to examine Landau's theory of the critical instability leading to turbulent fluid flow. In this application we demonstrate how nonlinear systems can be solved using a generalization of normal modes from linear to nonlinear dynamic systems. It cannot be stressed too strongly that this method yields non-perturbative solutions, not linearized approximate solutions to the nonlinear dynamic equations. This is a straight-forward application of the Koopman-von Neumann approach to the solution of an initial value problem.

Memory effects appear as integro-differential equation in the study of open systems interacting with the environment in the form of generalized Langevin equations[7]. It has been shown that the fractional calculus very often results from these integral expressions and have proven to be useful for modeling systems with memory, as demonstrated in viscoelastic materials[8], biological processes[9−10], wave propagation in porous media[11], instability in fluid dynamics[12], and a general perspective on the utility of the fractional calculus is presented in [13−14]. The normal mode technique is generalized to include the effect of memory modeled using a fractional time derivative. This occurs generically when there is no time-scale separation between the microscopic and macroscopic levels of description, that is, the non-differentiable nature of the microscopic dynamics (non-integrable Hamiltonian dynamics) is transmitted to the macroscopic level[15].

In Section II, the Landau theory of the transition from laminar to turbulent fluid flow is briefly presented. The nonlinear rate equation is solved using the spectral decomposition method of Koopman and von Neumann to obtain the analytic solution. At early times this solution is shown to undergo an inverse power law decay, characteristic of critical slowing near a critical point. Section III generalizes the Landau theory of the transition to turbulence to include memory using the fractional calculus. The resulting fractional nonlinear rate equation is solved and the power law index for the critical slowing down at early time is shown to be the same as the fractional derivative index. We draw some conclusions in Section IV.

II. LANDAU TRANSITION THEORY

Historically the fluctuations in turbulent fluid flow have been modeled to be memoryless and often with Gaussian statistics[16], using Langevin equations for the dynamics[7]. More recent experiments/observations have shown that Lévy statistics more accurately model turbulent fluctuations and that they contain memory[14]. The transition from laminar to turbulent fluid flow is described by Landau as a critical phase transition, with the essential features of the flow given in terms of simple models. Consider the nonlinear rate equation for the model of the onset of a critical instability of fluid flow introduced by Landau[16−17]:

$$\frac{\mathrm{d}u}{\mathrm{d}t} = 2\gamma u - \alpha u^2, \tag{1}$$

which is valid for times on the time scale $1/\gamma$; α is the Landau parameter; $u(t) = |A(t)|^2$, and $A(t)$ is the time-dependent amplitude of the fluid velocity.

Near the critical point, where the flow becomes unstable and transitions to turbulence, the linear coefficient can be expressed as the difference in Reynolds number $\gamma \propto (R - R_c)$ and subsequently vanishes at criticality where $R = R_c$[18]. Consequently, the dynamics are dominated by the nonlinear interaction in the transition region, but that need not concern us here.

Manuscript received September 8, 2015; accepted January 18, 2016. Recommended by Associate Editor YangQuan Chen.

Citation: Bruce J. West, Malgorzata Turalska. The fractional Landau model. *IEEE/CAA Journal of Automatica Sinica*, 2016, **3**(3): 257−260

Bruce J. West is with the Information Science Directorate, Army Research Office, Research Triangle Park, NC 27708, USA (e-mail: bruce.j.west@att.net).

Malgorzata Turalska is with the Department of Physics, Duke University, Durham, NC 27708, USA (e-mail: mat51@phy.duke.edu).

Color versions of one or more of the figures in this paper are available online at http://ieeexplore.ieee.org.

A. Exact Solution

The exact solution to (1) can be obtained by introducing the operator $\mathcal{O}$ such that (1) takes the form

$$\frac{\mathrm{d}u}{\mathrm{d}t} = \mathcal{O}u \tag{2}$$

and the eigenfunction/eigenvalue expansion of the solution is

$$u(t) = \sum_{k=0}^{\infty} v_k \phi_k(u_0) \chi_k(t), \tag{3}$$

where $\chi_k(t)\,\phi_k(u_0)$ is the eigenfunction, factored into a piece determined by the eigenvalue and the piece determined by the initial condition $u(0) = u_0$ for the nonlinear dynamics. The set of coefficients $\{v_k\}$ is determined by the initial condition.

Inserting (3) into (2), yields for the time dependence of the eigenfunctions

$$\frac{\mathrm{d}\chi_k(t)}{\mathrm{d}t} = \lambda_k \chi_k(t) \Rightarrow \chi_k(t) = \mathrm{e}^{\lambda_k t}. \tag{4}$$

Correspondingly, the eigenvalue equations are determined by

$$\begin{aligned}\mathcal{O}_0\phi_k(u_0) &= \left[2\gamma u_0 - \alpha u_0^2\right]\frac{\mathrm{d}\phi_k(u_0)}{\mathrm{d}u_0}\\ &= \lambda_k u_0.\end{aligned} \tag{5}$$

Integrating this equation yields

$$\phi_k(u_0) = \left(\frac{u_0}{u_0 - \frac{\alpha}{2\gamma}}\right)^{\frac{\lambda_k}{2\gamma}} \tag{6}$$

for which the eigenvalue are determined to be $\lambda_k = -2\gamma k$ by equating coefficients of the time-dependent terms obtained by inserting (3) into (1). The expansion coefficients are chosen such that the series solution satisfies the initial condition, resulting in

$$\left(-\frac{\alpha}{2\gamma}\right)^k v_k = \frac{2\gamma}{\alpha}. \tag{7}$$

In this way the eigenfunction expansion (3) reduces to

$$u(t) = \frac{2\gamma}{\alpha}\sum_{k=0}^{\infty}\left(\frac{u_0 - \frac{2\gamma}{\alpha}}{u_0}\right)^k \mathrm{e}^{-2\gamma k t}, \tag{8}$$

$$= \frac{2\gamma}{\alpha}\frac{u_0 \mathrm{e}^{2\gamma t}}{(\mathrm{e}^{2\gamma t} - 1)\,u_0 + \frac{2\gamma}{\alpha}}. \tag{9}$$

The asymptotic form of the solution is given by

$$\lim_{t\to\infty} u(t) = \frac{2\gamma}{\alpha}. \tag{10}$$

Consequently, the maximum amplitude of the fluid velocity scales with the deviation of the Reynolds number from its critical value $\sqrt{(R - R_c)}$. Note that the asymptotic time scale is still much smaller than the period of oscillation of $A(t)$[18]. It is also of interest to consider the $\gamma \to 0$ limit as the system approaches criticality

$$\lim_{\gamma\to 0} u(t) = \frac{u_0}{1 + \alpha u_0 t}, \tag{11}$$

which is the phenomenon of critical slowing down, that is, the decay of any fluctuation in the velocity field slows as turbulence (the critical point) is approached.

In the Kolmogorov picture of turbulence the random formation and breakup of eddies rapidly erase memory, but this equilibrium argument is difficult to realize in nature[19]. Turbulence with memory is certainly an unorthodox notion theoretically, but this seems to be the conclusion entailed by observations. The most recent experiments [19] suggest that Landau's theory for the transition to turbulence might be better modeled using a fractional rate equation.

III. GENERALIZED LANDAU THEORY

We suggest a fractional Landau equation (FLE) as the lowest-order model that includes the memory effect

$$\partial_\tau^\beta[u] = 2\gamma u - \alpha u^2, \tag{12}$$

where all the parameters retain their original interpretation and $\partial_\tau^\beta[\cdot]$ is the Caputo derivative[20] in the "time" τ having units of $(\sec)^{1/\beta}$. The index of the fractional derivative determines the strength of the memory in the phenomena of interest, with no memory at the integer value $\beta = 1$ and increasing memory as β recedes to zero. Consequently, for the moment, we consider the fractional equation with $0 < \beta < 1$.

The fractional Landau model (FLM) can be written formally as, using the operator introduced in the integer-value equation,

$$\partial_\tau^\beta[u] = \mathcal{O}u, \tag{13}$$

whose solution can be expressed in terms of the eigenfunction expansion given by (3)[21]. Inserting the eigenfunction expansion into the fractional equation and separating terms yields

$$\partial_\tau^\beta[\chi_k(\tau)] = \lambda_k \chi_k(\tau). \tag{14}$$

The solution to this linear fractional rate equation is the Mittag-Leffler function (MLF)[20, 22]:

$$\chi_k(\tau) = E_\beta\left(\lambda_k \tau^\beta\right), \tag{15}$$

which has the series form

$$E_\beta(z) = \sum_{k=0}^{\infty}\frac{z^k}{\Gamma(k\beta + 1)}. \tag{16}$$

The eigenvalue spectrum is again determined by the solution to (5), using the early time stretched exponential form of the MLF. The expansion coefficients in turn are determined by the initial condition and results in the solution for the FLM being given by[23]

$$u(\tau) = \frac{2\gamma}{\alpha}\sum_{k=0}^{\infty}\left(\frac{u_0 - \frac{2\gamma}{\alpha}}{u_0}\right)^k E_\beta\left(-2k\gamma\tau^\beta\right). \tag{17}$$

Consequently, the Landau model with long-term memory has been decomposed into nonlinear modes, with eigenfunctions and eigenvalues that map over from the memoryless model. It is clear that since

$$\lim_{\beta\to 1} E_\alpha\left(-2k\gamma\tau^\beta\right) = \mathrm{e}^{-2\gamma k\tau}$$

the solution equation (17) reduces to (8) at $\beta = 1$, as it should. However, the solution to the FLM has not been published previously and in Fig. 1 we present a comparison of the analytic solution with the solution obtained from a numerical integration of the FLE. The numerical integration was performed with the help of Adams-Bashforth-Moulton predictor-corrector technique, developed by Diethelm et al.[18]. The two calculations differ by 2 % at most and this deviation is discussed elsewhere[23].

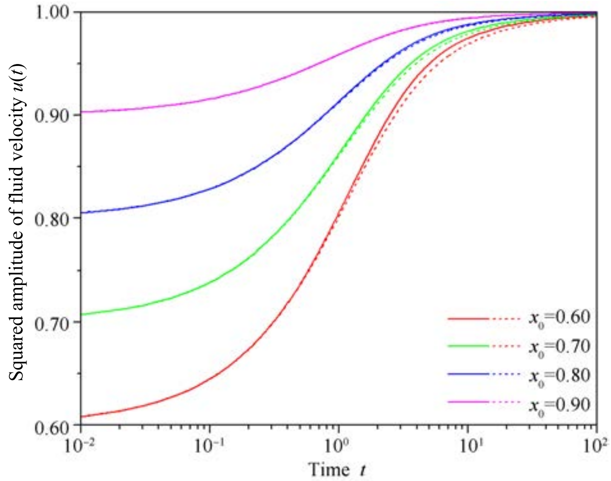

Fig. 1. The solid lines are the analytic solutions to the FLM and the dashed curves are from the numerical integration of the FLE. The four different sets of curves are for the initial conditions indicated. The time scale parameter is $\gamma = 0.5$ and the Landau parameter is $\alpha = 1.0$. The step of numerical integration is $h = 10^{-3}$.

The rapidly decaying exponential function in the Landau model is replaced with the slowly decaying MLF in the FLM, since the MLF has the scale-free property in the asymptotic limit

$$\lim_{\tau\to\infty} E_\beta\left(-2k\gamma\tau^\beta\right) \propto \frac{1}{\tau^\beta}. \tag{18}$$

In the $\gamma \to 0$ limit of criticality the MLF can be replaced with the exponential:

$$\lim_{\gamma\to 0} E_\beta\left(-2k\gamma\tau^\beta\right) \propto \exp\left(-2k\gamma\tau^\beta\right),$$

and (17) simplifies to

$$\lim_{\gamma,\tau\to 0} u(\tau) = \frac{u_0}{1+\alpha u_0\tau^\beta}, \tag{19}$$

so that with memory and $0 < \beta < 1$, the transition to turbulence is slower than in the memoryless case, since asymptotically $\tau > \tau^\beta$ for $\beta < 1$.

The solution given by (19) predicts that the energy of the turbulent flow field, at a point in space, asymptotically decays as an inverse power law in time. Numerical calculations of the Euler equations using the "t-model" in 2D and 3D yield inverse power-law decay with $\beta = 1.84$[24]. The solution to the fractional Landau model must therefore be generalized to $1 < \beta < 2$. This can be done by expressing the solution in terms of its initial value u_0, taking the initial time derivative $\dot{u}_0 = 0$ and noting that as $\gamma \to 0$ the critical slowing down maintains the asymptotic form $1/\tau^\beta$, although now $\tau^\beta > \tau$, asymptotically, since $\beta > 1$. The decay of turbulent fluctuations is faster than in the memoryless case, but certainly much slower than the pre-critical exponential case.

IV. Conclusion

In summary the spectral decomposition of the solution to a nonlinear dynamic equations can be generalized to fractional nonlinear rate equations and subsequently solved without approximation[21, 23]. In considering the Landau model for the transition to turbulence we used a phenomenological argument to motivate replacing the first-order with a fractional-order time derivative, but that need not be done. Stanislavsky[25] used subordination theory to develop a fractional Hamiltonian formalism, in which Hamilton's equations are given in terms of fractional derivatives. Memory is entailed by the dynamics of systems so described. He observed that space and time in these complex systems are not the continuous featureless processes first assumed by Newton[14], and turbulence certainly qualifies as being complex.

Acknowledgment

The authors would like to thank the U.S. Army Research Office for supporting this research.

References

[1] Arnold V I. *Mathematical Methods of Classical Mechanics(Second Edition)*. New York: Springer-Verlag, 1989.

[2] Lichtenberg A J, Lieberman M A. *Regular and Stochastic Motion*. New York: Springer-Verlag, 1983.

[3] Koopman B O. Hamiltonian systems and transformation in Hilbert space. *Proceedings of the National Academy of Sciences of the United States of America*, 1931, **17**: 315−318

[4] von Neumann J. Zur Operatorenmethode in der klassischen Mechanik. *Annals of Mathematics*, 1932, **33**: 587−642

[5] von Neumann J. Züsatze zur Arbeit zur Operatorenmethode. *Annals of Mathematics*, 1932, **33**: 789−791

[6] Kowalski K. *Methods of Hilbert Spaces in the Theory of Nonlinear Dynamical Systems*. Singapore: World Scientific, 1994.

[7] Lindenberg K, West B J. *The Nonequilibrium Statistical Mechanics of Open and Closed Systems*. New York: Wiley-VCH, 1990.

[8] Stiassnie M. On the application of fractional calculus for the formulation of viscoelastic models. *Applied Mathematical Modelling*, 1979, **3**(4): 300−302

[9] Magin R L. Fractional calculus models of complex dynamics in biological tissues. *Computers & Mathematics with Applications*, 2010, **59**(5): 1586−1593

[10] Henry B I, Langlands T A M, Wearne S L. Fractional cable models for spiny neuronal dendrites. *Physical Review Letters*, 2008, **100**(12): 128103

[11] Garra R. Fractional-calculus model for temperature and pressure waves in fluid-saturated porous rocks. *Physical Review E*, 2011, **84**(3): 036605

[12] Prajapati J C, Patel A D, Pathak K N, Shukla A K. Fractional calculus approach in the study of instability phenomenon in fluid dynamics. *Palestine Journal of Mathematics*, 2012, **1**(2): 95−103

[13] West B J. Colloquium: fractional calculus view of complexity: a tutorial. *Reviews of Modern Physics*, 2014, **86**(4): 1169−1186

[14] West B J. *Fractional Calculus View of Complexity: Tomorrow's Science*. New York: CRC Press, 2015.

[15] Grigolini P, Rocco A, West B J. Fractional calculus as a macroscopic manifestation of randomness. *Physical Review E*, 1999, **59**(3): 2603−2613

[16] Monin A S, Yaglom A M, Lumley J L. *Statistical Fluid Mechanics. Vol. 1: Mechanics of Turbulence*. Cambridge, MA: The MIT Press, 1971.

[17] Landau L D, Lifshitz E M. *Fluid Mechanics (Second Edition). Vol. 6. Course of Theoretical Physics*. U.S.A.: Butterworth-Heinemann, 1987.

[18] Diethelm K, Ford N J, Freed A D, Luchko Y. Algorithms for the fractional calculus: a selection of numerical methods. *Computer Methods in Applied Mechanics and Engineering*, 2005, **194**(6−8): 743−773

[19] Cooper N G. Putting design into turbulence. 1663, Los Alamos Science & Technology Magazine. 2009. 10−15

[20] Podlubny I. *Fractional Differential Equations*. New York: Academic Press, 1999.

[21] Svenkeson A, Glaz B, Stanton S, West B J. Spectral decomposition of nonlinear systems with memory. to be published

[22] West B J, Bologna M, Grigolini P. *Physics of Fractal Operators*. New York: Springer, 2003.

[23] Turalska M, West B J. A search for a spectral technique to solve nonlinear fractional differential equations. to be published

[24] Hald O H, Stinis P. Optimal prediction and the rate of decay for solutions of the Euler equations in two and three dimensions. *Proceedings of the National Academy of Sciences of the United States of America*, 2007, **104**: 6527−6532

[25] Stanislavsky A A. Hamiltonian formalism of fractional systems. *The European Physical Journal B*, 2006, **49**(1): 93−101

Bruce J. West received received the B. A. in physics at SUNY Buffalo in 1965; an M. S. and Ph. D. degrees in physics at the University of Rochester, in 1967 and 1970, respectively. From 1983 to 1989, he was Director of the Division of Applied Nonlinear Science, La Jolla Institute, CA, USA. In 1989 he become a Professor of Physics at the University of North Texas. He was Chair of the Department of Physics at UNT in years 1989-1999. Since 1999 he is Chief Scientist in the Mathematical and Information Sciences Directorate at the Army Research Office, Research Triangle Park, NC. He is a member of the New York Academy of Sciences, the American Physiological Society, the American Geophysical Union, and the American Association for the Advancement of Science. Additionally, he is a Fellow of the American Physical Society, the American Association for the Advancement of Science, and the Army Research Laboratory. His research interests concentrate on the application of nonlinear dynamics, systems theory, and complexity theory to biomedical and social phenomena. Corresponding author of this paper.

Malgorzata Turalska is currently a postdoctoral researcher in Department of Physics at Duke University. She received her M. S. in biomedical engineering from the Wroclaw University of Technology, Poland in 2006, and her Ph. D. in physics from the University of North Texas in 2011. Her research interests are the broad area of network science, nonlinear dynamics and complex systems.

A Fractional Micro-Macro Model for Crowds of Pedestrians Based on Fractional Mean Field Games

Kecai Cao, YangQuan Chen, *Senior Member, IEEE*, Daniel Stuart

***Abstract*—Modeling a crowd of pedestrians has been considered in this paper from different aspects. Based on fractional microscopic model that may be much more close to reality, a fractional macroscopic model has been proposed using conservation law of mass. Then in order to characterize the competitive and cooperative interactions among pedestrians, fractional mean field games are utilized in the modeling problem when the number of pedestrians goes to infinity and fractional dynamic model composed of fractional backward and fractional forward equations are constructed in macro scale. Fractional micro-macro model for crowds of pedestrians are obtained in the end. Simulation results are also included to illustrate the proposed fractional microscopic model and fractional macroscopic model, respectively.**

***Index Terms*—Fractional mean field games, microscopic model, macroscopic model, micro-macro model, fractional calculus.**

I. INTRODUCTION

METHODOLOGY for modeling of crowds of pedestrians has been categorized as micro scale, macro scale and meso scale in previous research. It is reasonable to choose different models in different scenarios as "All models are wrong but some of them are useful" (George E. P. Box)[1]. Thus, no models are perfect for all scenarios.

A. Short Review of Mathematical Model for Crowds of Pedestrians

A lot of work has been done for developing microscopic model since Dirk Helbing's work of [2−3] because the framework of social forces are similar to the framework of Newton's principle and it is not difficult to understand. Another reason for the widespread use of this social force model lies in that heterogeneity of each pedestrian such as mobilities or reactions can be considered explicitly. Thus not only theoretical work but also simulation results have gained a lot of attention such as [4−7] and [8]. One thing should be pointed out is that the burden of computation in micro scale has imposed great challenges when the number of pedestrians goes to infinity and some effects such as pedestrian's memory, long range interactions or other statistical characteristics have been seldom considered in previous work. The burden of computation in microscopic model have been successfully removed in macroscopic model as all pedestrians are treated as uniform physical particles. Thus different kinds of macroscopic models have been published based on the conservation law of mass and momentum such as [9−12], high order macroscopic model in [13], nonlinear macroscopic model in [14] and coupled macroscopic-microscopic model in [15]. Although the burden of computation in macroscopic model has been reduced greatly compared with that in microscopic model, main disadvantages of macroscopic model are that individual characteristics of each pedestrian have been ignored and heterogeneity of different pedestrians cannot be characterized in the macro scale.

The authors believe that something important (as mentioned below) has been neglected in previous research and its effects should be included in the problem of modeling and control of crowds so that obtained results are close to reality.

1) Consideration of fractal time

Movement of human beings is the result of complex interactions of physical part, psychological part and some other factors that cannot be explained easily. Inter-event time has been proved to have an important role in characterizing people's movement as shown in [1]. The fact is that the distribution of inter-event time in our real life satisfies one form of power law in most cases while distribution of exponential form has been always assumed in previous research using calculus of integer order. Thus fractional order of time scale should be considered in characterizing movement and decision process of human beings.

2) Consideration of fractal space

Another important thing should be pointed out is that in previous research, the time scale of each pedestrian is assumed to be uniform and the dimensions of space are restricted to 1D, 2D and 3D. But these assumptions are only reasonable if the crowds of pedestrians can fill space like particles of gases or fluids while it is not the case usually. Thus only normal diffusive process has been considered in previous research and there are few results which have been obtained under sub-diffusive process or super-diffusive process characterized by

Manuscript received September 6, 2015; accepted January 6, 2016. This work was supported by National Natural Science Foundation of China (61374055), Natural Science Foundation of Jiangsu Province (BK20131381), China Postdoctoral Science Foundation funded project (2013M541663), Jiangsu Planned Projects for Postdoctoral Research Funds (1202015C), Scientific Research Foundation for the Returned Overseas Chinese Scholars, State Education Ministry (BJ213022), Scientific Research Foundation of Nanjing University of Posts and Telecommunications (NY214075, XJKY14004). Recommended by Associate Editor Antonio Visioli.

Citation: Kecai Cao, YangQuan Chen, Daniel Stuart. A fractional micro-macro model for crowds of pedestrians based on fractional mean field games. *IEEE/CAA Journal of Automatica sinica*, 2016, **3**(3): 261−270

Kecai Cao is with College of Automation, Nanjing University of Posts and Telecommunications, Nanjing 210023, China (e-mail: caokecai@gmail.com).

YangQuan Chen is with Mechatronics Embedded Systems and Automation Lab, School of Engineering, University of California, Merced, CA 95343, USA (e-mail: ychen53@ucmerced.edu).

Daniel Stuart is with Department of Electrical and Computer Engineering, Utah State University, Logan, UT 84322, USA (e-mail: idahoeinstein@gmail.com).

Color versions of one or more of the figures in this paper are available online at http://ieeexplore.ieee.org.

fractal space.

3) Consideration of interactions

Long range interactions have been considered in the schooling of fish, flocking of birds and control of multi-agent systems and effects of long range interactions that dominate system's phase transition have received a lot of attention recently. Based on obtained results in [16], we can say that long range interactions in micro scale are connected with the fractional dynamics in macro scale.

B. Modeling and Control Based on Mean Field

For crowds of pedestrians with large numbers, it is impossible and not necessary to consider all the interactions one by one. In previous research, methods based on mean field have been proposed to approximate the mass effects of these interactions for physical system, financial system and social dynamic system and the readers are referred to [17−20]. The basic idea of mean field framework is replacing all the interactions with an average interaction in "mean-field" form to relieve the burden of computation on each agent.

Mean field theory has been applied to control of multi-agent systems in [21−23] where decentralized consensus protocols and decentralized optimizing algorithms are considered using the philosophy of mean field. Mean field theory has also been applied to the modeling problem of crowds of pedestrians in recent years. For example, coupled dynamic model composed of backward Hamilton-Jacobi-Bellman equations and forward Fokker-Planck equations have been presented using mean-field limit approach in [20]; Phenomenons that are occurring in two-population's interactions such as congestion and aversion have been modeled using the method of mean field games in [24] where coupled dynamic model composed of backward Hamilton-Jacobi-Bellman equations and forward Fokker-Planck equations are obtained; The mean field games theory has also been used to construct traffic model in macro scale based on interactions in micro scale in [25] while fractional dynamic games have been used in [26] to construct dynamic models for crowds of pedestrians.

With the help of calculus of fractional order, in this paper we try to include the fractal time, fractal space and statistical characteristics that have been neglected in previous research on the modeling of crowds so that obtained models could be much more close to reality. Based on our previous work on fractional modeling of crowds[27−29], fractional mean field games theory has been investigated in this paper to describe the competitive and cooperative interactions among pedestrians. The rest of the paper is organized as follows. Fractional microscopic model, fractional macroscopic model and fractional dynamic model based on mean-field games are presented in Section III. Simulation results for the proposed fractional macroscopic model and fractional microscopic model have been shown in Section IV.

II. PRELIMINARIES

The definitions of fractal derivative and lemmas that will be used in the following are firstly presented for the easy of reading.

Definition 1[30]**.** For a set $F \subset \mathbf{R}$ and a subdivision $P_{[a,b]}$, $a<b$, the mass function $\gamma^\alpha(F,a,b,)$ is given by

$$\gamma^\alpha(F,a,b)=\lim_{\delta\to 0}\inf_{\{P_{[a,b]}:|P|<\delta\}}\sum_{i=0}^{n-1}\frac{(x_{i+1}-x_i)^\alpha}{\Gamma(\alpha+1)}\theta(F,[x_i,x_{i+1}]),$$

where $\theta(F,[x_i,x_{i+1}])=1$ if $F\cap[x_i,x_{i+1}]$ is non-empty, and zero otherwise, $P_{[a,b]}$ is a subdivision of the interval $[a,b]$ and

$$|P|=\max_{0\leq i\leq n-1}(x_{i+1}-x_i),$$

the infimum being taken over all subdivisions P of $[a,b]$ such that $|P|<\delta$.

Definition 2[30]**.** Let a_0 be an arbitrary but fixed real number. The integral staircase function $S_F^\alpha(x)$ of order α for a set F is given by

$$S_F^\alpha(x)=\begin{cases}\gamma^\alpha(F,a_0,x), & \text{if} \quad x\geq a_0,\\ -\gamma^\alpha(F,a,x_0), & \text{otherwise.}\end{cases}$$

Definition 3[30]**.** The fractal derivative for F^α-derivative of f at x is

$$D_F^\alpha(f(x))=F-\lim_{y\to x}\frac{f(y)-f(x)}{S_F^\alpha(y)-S_F^\alpha(x)}, \tag{1}$$

if the limit exists.

From Definition 1 to Definition 3 listed above, it is easy to see that the definition of integer order can be treated as one special case of fractal derivative when $\alpha=1$. Thus the fractional calculus offers us much more freedom in modeling dynamic behaviors where ordinary differential equations and methods of calculus of integer order are inadequate.

III. MAIN RESULTS

A. Fractional Microscopic Model

The following dynamic model of integer order has been extensively used in previous research of particles, human beings or some other agents in micro scale

$$\begin{cases}\dfrac{\mathrm{d}x_i}{\mathrm{d}t}=v_i,\\ m_i\dfrac{\mathrm{d}v_i}{\mathrm{d}t}=f_i^S+\sum\limits_{j=1}^{n}f_{ij}^N+\sum f_k^W,\end{cases} \tag{2}$$

where x_i is the position and v_i is the velocity. One common assumption has been made that movement of each pedestrian is continuous and differentiable everywhere. That is the case if we observe the movement of each pedestrian with a very large scale such as in macro scale. However the condition of differentiable everywhere is hard to be satisfied in reality. So, will the $\frac{\mathrm{d}x}{\mathrm{d}t}$ give the true picture of pedestrian's movement in micro scale or will the $\frac{\mathrm{d}^\alpha x}{\mathrm{d}t^\alpha}$ be much closer to reality when only continuous condition is satisfied, are the questions to be explored. Related research on this fractional aspect has been shown in [31] to characterize the zigzag phenomenon that is unfolded in traffic control system. For each pedestrian, continuous but not differential trajectory is also very common due to interactions with its neighbors as shown in Fig. 1. Another fact that has been neglected in lots of previous research is that memory of human beings has been seldom considered. This is another proof that $\frac{\mathrm{d}^\alpha x}{\mathrm{d}t^\alpha}$ is the much better choice than $\frac{\mathrm{d}x}{\mathrm{d}t}$ in characterizing the movement of each pedestrian.

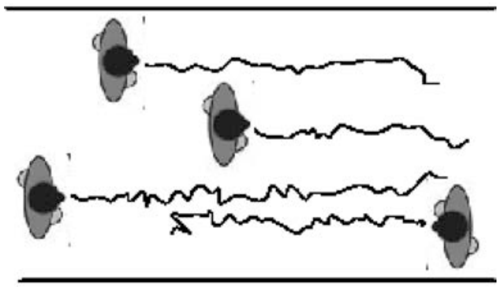

Fig. 1. Zig-zag phenomenon in movement of each pedestrian.

Dynamic model of integer order that was brought out by Dirk Helbing in [2−3] has been extended to the following dynamic model of fractional order for each pedestrian

$$\begin{cases} \dfrac{\mathrm{d}^\alpha x_i}{\mathrm{d}t^\alpha} = v_i, \\ m_i \dfrac{\mathrm{d}^\alpha v_i}{\mathrm{d}t^\alpha} = f_i^S + \sum\limits_{j=1}^{n} f_{ij}^N + \sum f_k^W, \end{cases} \tag{3}$$

where x_i and v_i are position and velocity of each pedestrian (2) respectively, f_i^S is the self-driven force towards some desired velocity, f_{ij}^N is the interaction between agent i and its neighbor j and f_k^W represents the interactions with environment such as walls or corridors.

B. Fractional Macroscopic Model

As fractal time and fractal space have been neglected in previous models of crowds, only macroscopic models of integer order have been obtained in previous research. Some statistical phenomenons observed in recent years have forced people to reconsider the effectiveness of obtained dynamic model of integer order.

1) Distribution of inter-event time that is dominating or affecting movement of each pedestrian can be better approximated by power law rather than exponential distribution[1]. Thus dynamic models of integer order where exponential distribution has been assumed are no longer effective when confronted with the distribution of power law. As the hidden dynamics behind distribution of power law is connected with dynamics of fractional order, it is much preferable to model crowds of pedestrians using calculus of fractional order;

2) Different from particles of gases or fluids, pedestrians do not fill the 2D or 3D space and distribution of the pedestrians is not uniform in the entire space. Thus space of integer order is not enough to describe the distribution of pedestrians and fractal space of fractional order should be included in modeling of crowds of pedestrians.

Based on [9] where modeling of traffic system has been considered using calculus of integer order, we try to model crowds of pedestrians using calculus of fractional order in the following.

Denote $\rho(x,t)$ as the density of crowds as shown in Fig. 2, then mass of pedestrians between $x = x_1$ to $x = x_2$ at time t can be computed as

$$\text{mass in}[x_1,x_2] \text{ at time} t := \int_{x_1}^{x_2} \rho(x,t)\mathrm{d}x^\beta. \tag{4}$$

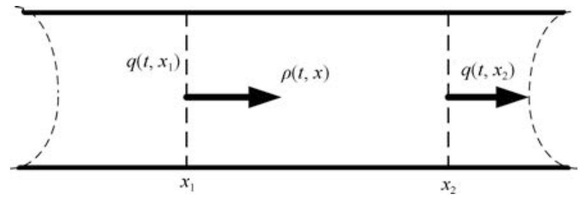

Fig. 2. Conservation of mass.

For $t \in [t_1,t_2]$, the total mass that enters this domain from the left boundary at $x = x_1$ is given by

$$\text{inflow at } x_1 \text{ from } t_1 \text{ to } t_2 := \int_{t_1}^{t_2} \rho(x_1,t)v(t,x_1)\mathrm{d}t^\alpha \tag{5}$$

Similarly, the total mass that leaves this domain from the right boundary at $x = x_2$ for $t \in [t_1,t_2]$ is given by

$$\text{outflow at } x_2 \text{ from } t_1 \text{ to } t_2 := \int_{t_1}^{t_2} \rho(x_2,t)v(t,x_2)\mathrm{d}t^\alpha \tag{6}$$

The change of people in the area between x_1 and x_2 is caused by crossing of people at the boundary of x_1 and x_2. Assuming no pedestrians are created or destroyed, then the change of mass of pedestrians in space $[x_1,x_2]$ in time interval $[t_1,t_2]$ is equal to the mass that is entering at x_1 minus that exiting from x_2. This conservation can be described using

$$\begin{aligned} &\int_{x_1}^{x_2} \rho(x,t_2)\mathrm{d}x^\beta - \int_{x_1}^{x_2} \rho(x,t_1)\mathrm{d}x^\beta \\ &\quad = \int_{t_1}^{t_2} \rho(x_1,t)v(t,x_1)dt^\alpha - \int_{t_1}^{t_2} \rho(x_2,t)v(t,x_2)\mathrm{d}t^\alpha. \end{aligned}$$

The above equation can also be written as the following double integral form

$$\int_{x_1}^{x_2} \int_{t_1}^{t_2} \left\{ \frac{\partial}{\partial t^\alpha}\rho(x,t) + \frac{\partial}{\partial x^\beta}[\rho(x,t)v(t,x)] \right\} \mathrm{d}t^\alpha \mathrm{d}x^\beta = 0. \tag{7}$$

Since equation (7) should be satisfied for any t and any x, the following fractional order model for crowds of pedestrians in one dimensional space

$$\frac{\partial}{\partial t^\alpha}\rho(x,t) + \frac{\partial}{\partial x^\beta}[\rho(x,t)v(t,x)] = 0, \tag{8}$$

can be derived where fractal time and fractal space have been included in (8).

Remark 1. Part of the results of fractional model in macro scale has been firstly brought out in [27] and is listed here to guarantee the completeness.

Remark 2. Similar results are also obtained in [32] where fractional model for traffic flow has been derived using fractional conservation law. Different from the work of [32] where dimension of time is α, dimension of surface is 2α and dimension of volume is 3α, there are no such restrictions in our fractional model (8).

C. Fractional Micro-macro Model

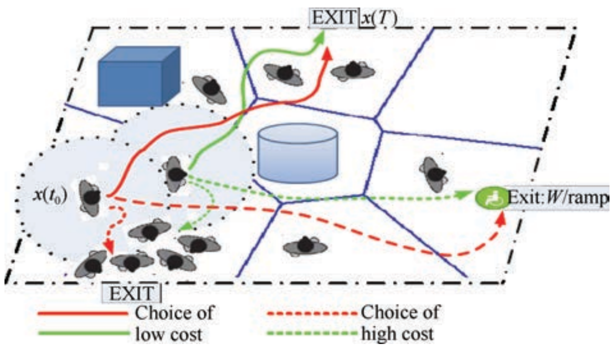

Fig. 3. Movement of pedestrians based on fractional mean field games.

1) Fractional Hamilton-Jacobi-Bellman Equation

For each pedestrian i, we assume the following cost function to be minimized in his/her movement between initial starting point $x(t_0)=x_0$ and desired location $x(T)$ as shown in Fig. 3.

$$J(t_0,x_0)=\inf_{v(\cdot)}\int_{t_0}^{T} f(t,x(t),v(t))\mathrm{d}t^{\alpha}+h(T,x(T)), \tag{9}$$

where convex function $h(T,x(T))$ is the terminal cost, convex even function $f(t,x(t),v(t))$ describes some different kinds of running cost between the initial point and destination.

Remark 3. A typical quadratic cost function that is independent of position of pedestrians' can be selected as $\frac{1}{2}|v|^2$ to penalize pedestrians that are moving too fast; Much more generalized running cost functions that depend on time, position and velocity have been adopted in the following derivation of fractional Hamilton-Jacobi-Bellman equation.

Similar to the derivation of Hamilton-Jacobi-Bellman equation of integer order in optimal control, the fractional Hamilton-Jacobi-Bellman equation will be discussed firstly and then optimal velocity will be prescribed for each pedestrian at each time step. Suppose after an infinitesimal time interval $\mathrm{d}t^{\alpha}$, the pedestrian will arrive at one new place $x_0+v\mathrm{d}t^{\alpha}$ and thus incurring a travel cost of $f(v)\mathrm{d}t^{\alpha}$ where new cost function for the remaining journey is described by $J(t_0+\mathrm{d}t^{\alpha},x_0+v\mathrm{d}t^{\alpha})$. The above analysis leads to the following relationship between $J(t_0,x_0)$ and $J(t_0+\mathrm{d}t^{\alpha},x_0+v\mathrm{d}t^{\alpha})$

$$J(t_0,x_0)=J(t_0+\mathrm{d}t^{\alpha},x_0+v\mathrm{d}t^{\alpha})+f(v)\mathrm{d}t^{\alpha}. \tag{10}$$

Based on Taylor expansion, Equation (10) can be rewritten as

$$\begin{aligned}J(t_0,x_0)=J(t_0,x_0)+dt^{\alpha}[&\frac{\partial^{\alpha}}{\partial t^{\alpha}}J(t_0,x_0)\\&+v\cdot\frac{\partial^{\beta}}{\partial x^{\beta}}J(t_0,x_0)+f(v)],\end{aligned} \tag{11}$$

and the optimal problem (9) is now transformed into finding proper v to minimize

$$v\cdot\frac{\partial^{\beta}}{\partial x^{\beta}}J(t_0,x_0)+f(v).$$

Considering the fact that $f(\cdot)$ is an even function, the above minimization problem is equivalent to the maximization problem of

$$v\cdot\frac{\partial^{\beta}}{\partial x^{\beta}}J(t_0,x_0)-f(v). \tag{12}$$

Based on the Legendre transformation $H:R^d\rightarrow R$ of $f:R^d\rightarrow R$ by

$$H(p):=\sup_{v(\cdot)} v\cdot p-f(v) \tag{13}$$

whose maximum value are functions of p. For the maximization problem of (12), we can see that the maximum value is obtained as $H(\frac{\partial^{\beta}}{\partial x^{\beta}}J(t_0,x_0))$ for some v. Then substituting the minimum value $-H(\frac{\partial^{\beta}}{\partial x^{\beta}}J(t_0,x_0))$ into (11), the following equation

$$J(t_0,x_0)=J(t_0,x_0)+\mathrm{d}t^{\alpha}[\frac{\partial^{\alpha}}{\partial t^{\alpha}}J(t_0,x_0)-H(\frac{\partial^{\beta}}{\partial x^{\beta}}J(t_0,x_0))]$$

will be satisfied for any t_0 and any x_0. Then the fractional Hamilton-Jacobi-Bellman equation is derived as

$$-\frac{\partial^{\alpha}}{\partial t^{\alpha}}J(t_0,x_0)+H(\frac{\partial^{\beta}}{\partial x^{\beta}}J(t_0,x_0))=0. \tag{14}$$

From the above discussions, we know that there is one v that minimize the following expression

$$v\cdot\frac{\partial^{\beta}}{\partial x^{\beta}}J(t_0,x_0)+f(v),$$

and $\widetilde{v}=-v$ maximize the following expression

$$v\cdot\frac{\partial^{\beta}}{\partial x^{\beta}}J(t_0,x_0)-f(v).$$

As seen from (13), $\widetilde{v}$ as a function of p should satisfy that

$$\frac{\partial}{\partial\widetilde{v}}(\widetilde{v}\cdot p-f(\widetilde{v}))=0.$$

On the other hand, the derivative of $H(p)$ can be obtained as follows

$$\frac{d}{dp}H(p)=\frac{\partial H}{\partial\widetilde{v}}\frac{\partial\widetilde{v}}{\partial p}+\frac{\partial H}{\partial p}=\widetilde{v},$$

using chain rule and then the velocity for each pedestrian to move in the next step is derived as

$$v=-H'(\frac{\partial^{\beta}}{\partial x^{\beta}}J(t_0,x_0)).$$

2) Fractional Macro Model Based on Fractional Mean Field Games

Based on inspiration of [25] on traffic system, we assume the following utility function for the i-th pedestrian

$$f_i^N(x_i,v_i)=v_i(1-F(\frac{1}{N}\sum\omega(x_j-x_i))),$$

where the first term v_i means that the i-th pedestrian tries to arrive his destination as fast as possible; the second term means that the i-th pedestrian adapts his velocity according to pedestrians around him. Bounded non-negative anticipating function $\omega(\cdot)$ has been introduced to weigh different impacts of pedestrians in the neighborhood of the i-th pedestrian according to their distances. Thus for the i-th pedestrian, cooperative and competitive interacting with other pedestrians are manifested through choosing velocity in the next step.

First, we show that the following expression is satisfied

$$\lim_{N\to\infty}\frac{1}{N}\sum\omega(x_j-x_i)\to\int_0^\infty\rho_t(y)\omega(y-x)\mathrm{d}y^\beta,$$

where N is the number of interacting pedestrians, $\rho_t(y)$ is the number of pedestrians in interval $[x,x+dx^\beta]$ and $\omega(\cdot)$ is the anticipating function mentioned above.

Denote $\Gamma_t^N(x)=\frac{1}{N}\sum 1_{\{x_j<x\}}$ as the empirical distribution function for the crowds composed of N pedestrians. Then based on the Lebesgue-Stieltjes integral it can be concluded that

$$\frac{1}{N}\sum\omega(x_j-x_i)=\int_0^\infty\omega(y-x)\mathrm{d}\Gamma_t^N(y).$$

If there is one non-decreasing right-continuous function $\Gamma_t(x)$ such that the following expression is satisfied

$$\int_0^\infty\omega(y-x)\mathrm{d}\Gamma_t^N(y)\to\int_0^\infty\omega(y-x)\mathrm{d}\Gamma_t(y)(N\to\infty).$$

Then

$$\frac{1}{N}\sum\omega(x_j-x_i)\to\int_0^\infty\rho_t(y)\omega(y-x)\mathrm{d}y^\beta(N\to\infty)$$

will be satisfied. As $\rho_t(y)$ is the number of pedestrians in interval $[x,x+\mathrm{d}x^\beta]$, existence of non-decreasing right-continuous function $\Gamma_t(x)$ can be guaranteed from $\mathrm{d}\Gamma_t(x)=\rho_t(x)\mathrm{d}x^\beta$. Thus we can impose the following mean field payoff function

$$J(t_0,x_0,\rho_t(x))=\sup_{v(\cdot)}\int_{t_0}^T v(1-F(\int_0^\infty\rho_t(y)\omega(y-x)\mathrm{d}y^\beta))\mathrm{d}t^\alpha +h(T,x(T))$$

for pedestrians that are competitively and cooperatively interacting with other pedestrians.

Based on similar derivations shown in Section III-C-1, the following fractional Hamilton-Jacobi-Bellman equation

$$-\frac{\partial^\alpha}{\partial t^\alpha}J(t_0,x_0)+H(\frac{\partial^\beta}{\partial x^\beta}J(t_0,x_0,\rho_t(x)))=0$$

can also be obtained for modeling cooperative and competitive crowds using mean field game theory when the number of pedestrians goes to infinity.

Remark 4. Differences from previous work are listed as following:

a) Only functions of Dirac type and exponential type for $\omega(x_j-x_i)$ have been considered in [25]. Anticipating function of inverse power form

$$f_i^N(x_i,v_i)=v_i[1-F(\frac{1}{N}\sum(|x_j-x_i|+1)^{-2})]$$

can be included in this paper considering the long range effects in interacting of multiple pedestrians, where $\frac{1}{N}$ has been introduced to normalize the effects of other pedestrians on the i-th pedestrian.

b) Mean field games theory is also utilized in [20] for modeling crowds of pedestrians. But obtained results of [20] are only restricted to the framework of calculus of integer order and many statistical characteristics are not considered such as power law in distribution of crowds, power law in distribution of inter-event time and long range interactions among pedestrians.

3) Fractional Micro-macro Model

As shown in Fig. 4, the fractional micro-macro model for crowds of pedestrians using fractional mean field games can be described as the following backward-forward PDE systems

$$\begin{cases}-\frac{\partial^\alpha}{\partial t^\alpha}J(t_0,x_0,\rho_t(x))+H(\frac{\partial^\beta}{\partial x^\beta}J(t_0,x_0,\rho_t(x)))=0,\\ \frac{\partial}{\partial t^\alpha}\rho(t,x)+\frac{\partial}{\partial x^\beta}[\rho(t,x)v(t,x)]=0,\end{cases}\tag{15}$$

and

$$\begin{cases}\frac{\mathrm{d}^\alpha x_i}{\mathrm{d}t^\alpha}=v_i,\\ m_i\frac{\mathrm{d}^\alpha v_i}{\mathrm{d}t^\alpha}=f_i^S+\sum_{j=1}^n f_{ij}^N+\sum f_k^W.\end{cases}\tag{16}$$

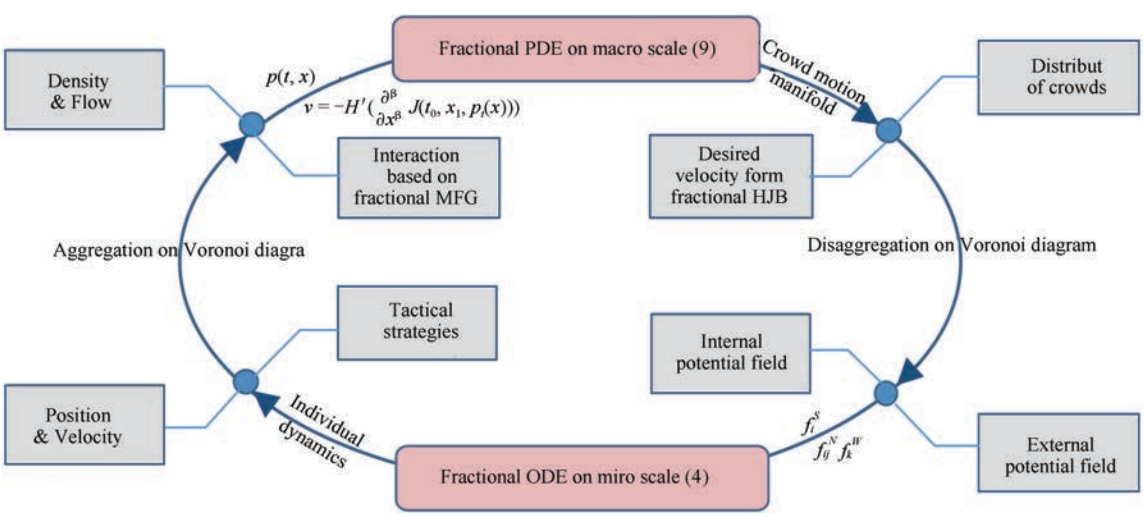

Fig. 4. Fractional micro-macro model of crowds of pedestrians.

The fractional microscopic model and fractional macroscopic model are connected through aggregation and disaggregation on Voronoi Diagram. From Fig. 4, the following can be observed.

1) Movements of each microscopic model are determined by not only internal potential fields such as the self-driven force towards some desired velocity described using f_i^S in (16) but also external interactions from neighbors and environments which are described using f_{ij}^N and f_k^W. Some other elements such as deviations from optimal movement of the whole crowds are also playing an important role in the movement of each individual pedestrian. All these information are generated from the dynamic model in macro scale;

2) Density and velocity that are needed in macroscopic model are derived from aggregation of individual's position and velocity. When the number of pedestrians goes to infinity, the crowds of pedestrians are treated as some intelligent flows that are described with the help of fractional MFG as shown in (15). For the backward part, v can be solved from the first line of (15) under initial condition on $J(T,X_T)$ and initial distribution of $\rho_0(x)$; Then substitute the obtained v:

$$v=-H'(\frac{\partial^\beta}{\partial x^\beta}J(t_0,x_0,\rho_t(x)))$$

into the forward part and $\rho(t,x)$ will be obtained from the second line of equation (15) under initial condition $\rho_0(x)$.

Due to the complexity of crowds of pedestrians, fractional microscopic model and fractional macroscopic model that interacted with each other have been constructed in this paper. Fractional mean field games have also been utilized in describing the macroscopic model when the number of pedestrians goes to infinity.

Remark 5. To the author's knowledge, the paper is one of the first works applying fractional mean field games to fractional macroscopic and microscopic model for competitive and cooperative crowds of pedestrians. Although some theoretical results have been obtained, a lot of work is waiting for further efforts such as existence and uniqueness of solution, rate of convergence and stability of desired equilibrium.

IV. Simulation Results

Considering unexpected or dangerous events in real-life experiment, only some initial simulation results are conducted to show the differences between model of fractional order and model of integer order in macro scale and micro scale. Due to the difficulties caused when the number of pedestrians goes to infinity, simulation results in macro scale and micro scale are separated in the following subsections. All we want to show is that calculus of fractional order has offered us much more freedom in describing complex phenomenon or dynamics such as crowds of pedestrians. It is much preferable to choose different model according to different scenarios and there are a lot of interesting problems needing to be considered in future.

A. Fractional Macroscopic Model

1) Simulation in Closed and Square Area Without Exit: Simulations on fractional macroscopic model (8) are firstly conducted where $\beta=1$ is imposed for simplicity. Lax-Friedrichs scheme has been used to approximate the spatial derivatives in solving the nonlinear partial differential equations due to its efficiency in computation. Based on Lax-Friedrichs scheme, the following PDE on 2D plane

$$\frac{\partial}{\partial t^\alpha}\rho(t,x,y)+\frac{\partial}{\partial x}[\rho(t,x,y)v(t,x,y)] + \frac{\partial}{\partial y}[\rho(t,x,y)v(t,x,y)]=0,$$

has been transformed into

$$\frac{\partial}{\partial t^\alpha}\rho(t,x,y)+\frac{1}{2Dx}[\rho(t,x+1,y)v(t,x+1,y) - \rho(t,x-1,y)v(t,x-1,y)]+\frac{1}{2Dy}[\rho(t,x,y+1)v(t,x,y+1) - \rho(t,x,y-1)v(t,x,y-1)]=0$$

in this simulation and the following Gaussian distribution

$$\rho(x,y,0)=C\exp(-(x-a)^2-(y-b)^2),$$

has been selected as the initial distribution of density where $C=1$ is the density value and (a,b) determines the center of this initial distribution. Average speed of free flow has been chosen to be $v_x=v_y=1.36\,\mathrm{ms}^{-1}$as done in many previous studies for pedestrians. Pedestrians have also been assumed to move freely within a square area with no obstacles and no exits in the first simulations.

Simulation results for $\alpha=0.6$ and $\alpha=1$ are shown in Figs. 5-6 and Figs. 7-8, respectively. From Fig. 5 and Fig. 7, it can be concluded that pedestrians described using fractional model are much scattered in the closed square area than that described using model of integer order. Same conclusions can also be obtained from comparisons of Fig. 6 and Fig. 8. Other fractional orders can also be tested using the methods proposed in this paper but data from reality are much preferable to find the proper orders for modeling the crowds of pedestrians in macro scale.

2) Simulation in Closed and Square Area with one Exit

Based on results obtained in Section IV-A-1, the following dynamic model has been simulated for pedestrians in closed and square area with one exit

$$\begin{cases}\frac{\partial}{\partial t^\alpha}\rho(t,x,y)+\frac{\partial}{\partial x}[\rho(t,x,y)v(t,x,y)] \\ \quad +\frac{\partial}{\partial y}[\rho(t,x,y)v(t,x,y)]=0,\\ v_t+vv_x \;=\frac{V-v}{\tau}-\frac{C_0^2}{\rho}\rho_x,\\ u_t+uu_y \;=\frac{U-u}{\tau}-\frac{C_0^2}{\rho}\rho_y,\end{cases}$$

where $C_0=0.8$ is the anticipation term that describes the response of pedestrians to density of people and V and U are some desired velocity that are obtained for the crowds. In order to lead the crowd moving toward the exit, the desired velocity V and U are selected as done in [33]

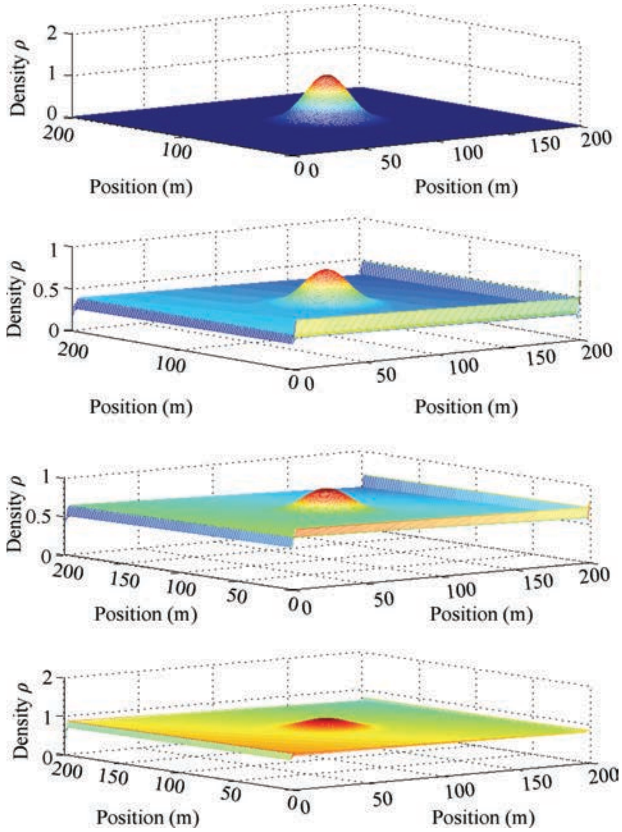

Fig. 5. Density response for crowds of pedestrians with $\alpha = 0.6$ using Lax-Friedrichs scheme.

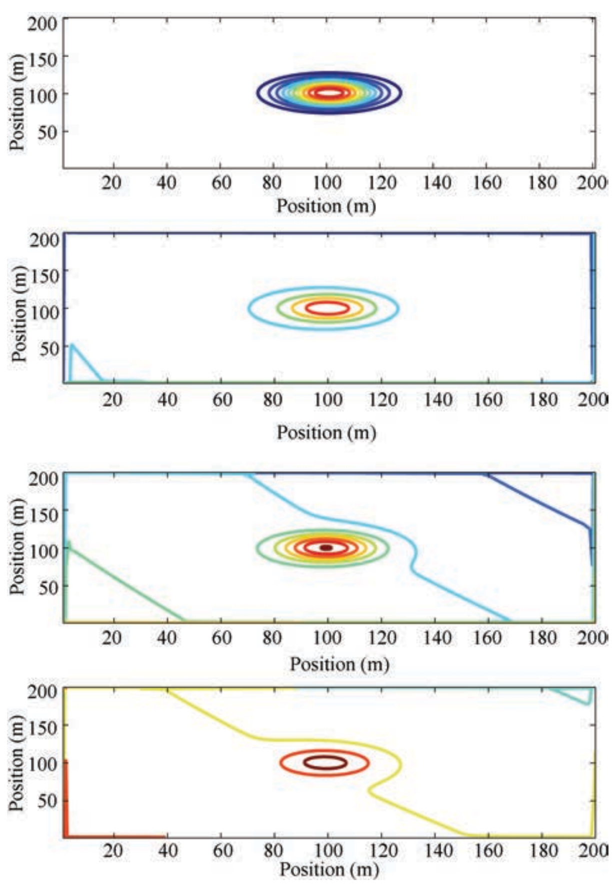

Fig. 6. Contour of the density response for crowds of pedestrians with $\alpha = 0.6$ using Lax-Friedrichs scheme.

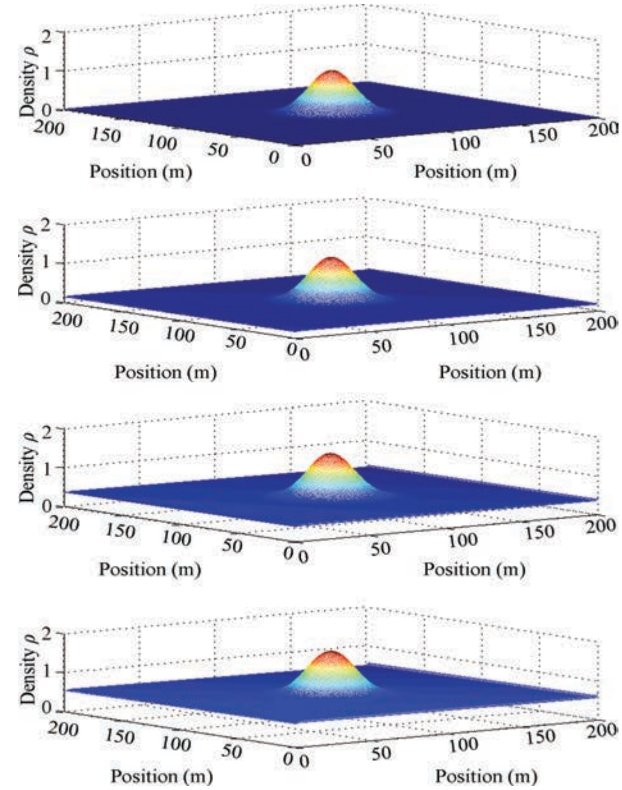

Fig. 7. Density response for crowds of pedestrians of integer order using Lax-Friedrichs scheme.

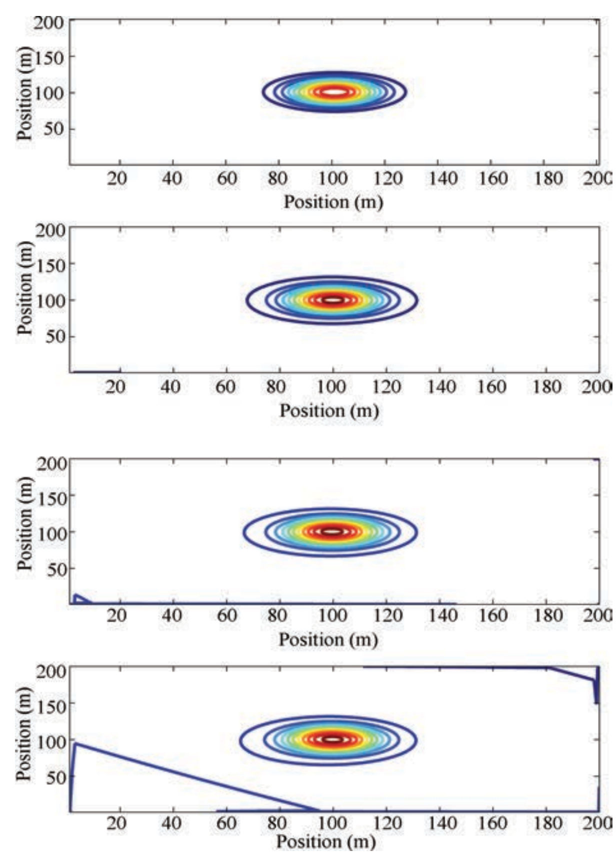

Fig. 8. Contour of the density response for crowds of pedestrians of integer order using Lax-Friedrichs scheme.

$$\begin{cases} V = & V(\rho)\frac{x_e - x_i}{\sqrt{(x_e-x_i)^2+(y_e-y_i)^2}}, \\ U = & U(\rho)\frac{y_e - y_i}{\sqrt{(x_e-x_i)^2+(y_e-y_i)^2}}, \end{cases}$$

where $V(\rho)$ and $U(\rho)$ are the flux-density relationship for Greenshield's model.

Simulation results are shown in Figs. 9-10 where dynamic model with fractional orders 0.85 and 1 are used. Simulation results show that the density of pedestrians around the exit is much lower in model of fractional order than that obtained using model of integer order. In simulations, the authors found that the final density of pedestrians is depending on the fractional order selected in the simulation and how to choose the best order to model the dynamics of crowds is an interesting problem that is worthy of further consideration in future research.

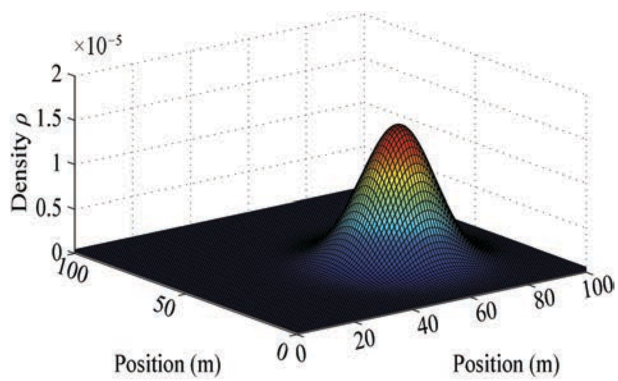

Fig. 9. Density response for crowds of pedestrians with $\alpha = 0.85$ using Lax-Friedrichs scheme.

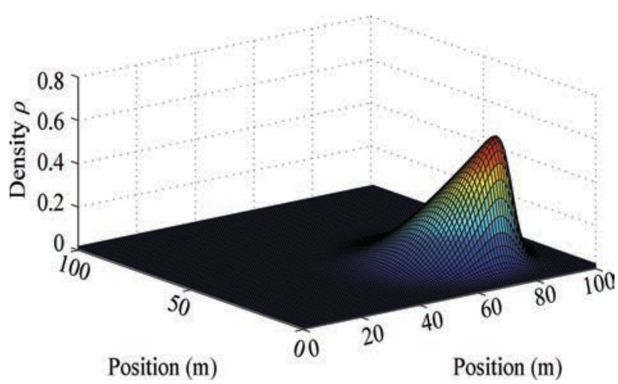

Fig. 10. Contour of the density response for crowds of pedestrians with $\alpha = 1$ using Lax-Friedrichs scheme.

B. Fractional Microscopic Model

In this section, six pedestrians with fractional order $\alpha \in (0,1)$, $\alpha = 1$ and $\alpha \in (1,2)$ are employed respectively to show their effects on pedestrian's evacuation process. Simulations of crowds of pedestrians with fractional order $\alpha = 0.6$, $\alpha = 1$ and $\alpha = 1.3$ are shown in Figs. 11-13 respectively. Results show that all agents firstly reach consensus through interacting with their neighbors without games. But parts of them change their desired value and fragmentation phenomenon are observed through these simulations after some penalty terms are injected into the simulations. Obtained simulation results have shown that pedestrians with different orders have different performance. Thus fractional calculus has provided us much more freedom in analysis and control of this kind of complex system. How to quantitatively characterize the relationship between order of fractional model, fractional controller and fractional games are interesting topics to be considered by the authors.

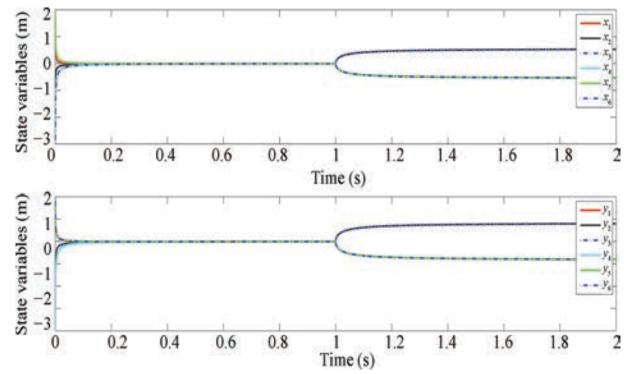

Fig. 11. Responses of six pedestrians with $\alpha = 0.6$.

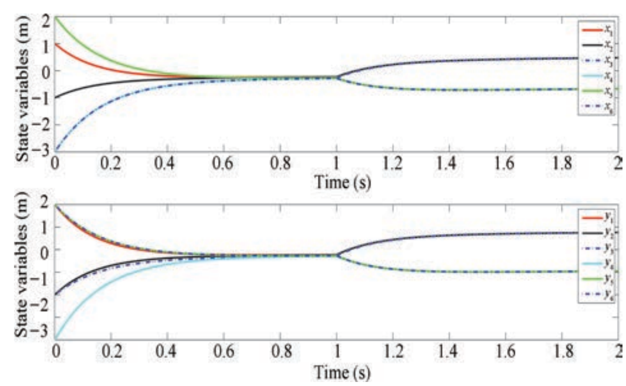

Fig. 12. Responses of six pedestrians with $\alpha = 1$.

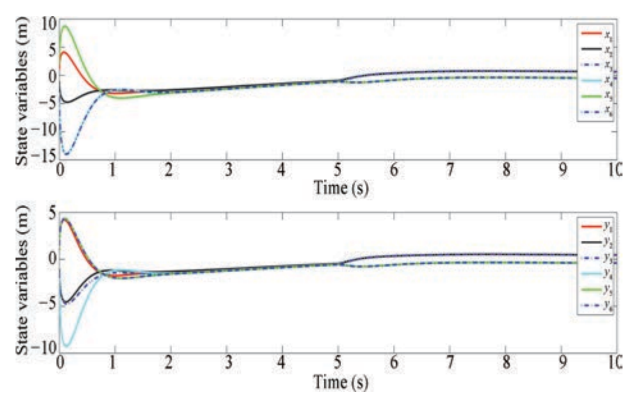

Fig. 13. Responses of six pedestrians with $\alpha = 1.3$.

V. Conclusions

Modeling of crowds of pedestrians have been considered in this paper from the view of fractional calculus. Not only fractional microscopic models but also fractional macroscopic models have been proposed in this paper. Fractional mean field games theory has been introduced in the modeling of crowds of pedestrians and coupled PDEs composed of fractional backward part and fractional forward part have been investigated. Although some theoretical results and some initial simulations are presented in this paper, there is much more work unexplored along this topic, such as solution of fractal MFG systems, stability of the fractal MFG system and performance of this fractal system, controller design based on mean field, performance evaluation of dynamic crowds and security problems related to control of crowds.

REFERENCES

[1] West B J, Turalska M, Grigolini P. *Networks of Echoes: Imitation, Innovation and Invisible Leaders*. Switzerland: Springer International Publishing, 2014.

[2] Helbing D, Molnar P. Social force model for pedestrian dynamics. *Physical Review E*, 1995, **51**(5): 4282−4286

[3] Helbing D, Farkas I, Vicsek T. Simulating dynamical features of escape panic. *Nature*, 2000, **407**(6803): 487−490

[4] Bellomo N, Bianca C, Coscia V. On the modeling of crowd dynamics: an overview and research perspectives. *SeMA Journal*, 2011, **54**(1): 25−46

[5] Couzin I D, Krause J, Franks N R, Levin S A. Effective leadership and decision-making in animal groups on the move. *Nature*, 2005, **433**(7025): 513−516

[6] Couzin I D. Collective cognition in animal groups. *Trends in Cognitive Sciences*, 2009, **13**(1): 36−43

[7] Song W G, Xu X, Wang B H, Ni S J. Simulation of evacuation processes using a multi-grid model for pedestrian dynamics. *Physica A*, 2006, **363**(2): 492−500

[8] Shiwakoti N, Sarvi M, Rose G, Burd M. Animal dynamics based approach for modeling pedestrian crowd egress under panic conditions. *Transportation Research, Part B: Methodological*, 2011, **45**(9): 1433−1449

[9] Kachroo P. *Pedestrian Dynamics: Mathematical Theory and Evacuation Control*. Boca Raton: CRC Press, 2009.

[10] Helbing D. A fluid dynamic model for the movement of pedestrians. *Complex Systems*, 1992, **6**: 391−415

[11] Hughes R L. A continuum theory for the flow of pedestrians. *Transportation Research, Part B: Methodological*, 2002, **36**(6): 507−535

[12] Hughes R L. The flow of human crowds. *Annual Review of Fluid Mechanics*, 2003, **35**: 169−182

[13] Jiang Y Q, Zhang P, Wong S C, Liu R X. A higher-order macroscopic model for pedestrian flows. *Physica A: Statistical Mechanics and its Applications*, 2010, **389**(21): 4623−4635

[14] Al-nasur S J. New Models for Crowd Dynamics and Control [Ph. D. dissertation], Virginia Polytechnic Institute and State University, Virginia, 2006.

[15] Lattanzio C, Maurizi A, Piccoli B. Moving bottlenecks in car traffic flow: a PDE-ODE coupled model. *SIAM Journal on Mathematical Analysis*, 2011, **43**(1): 50−67

[16] Ishiwata R, Sugiyama Y. Relationships between power-law long-range interactions and fractional mechanics. *Physica A*, 2012, **391**(23): 5827−5838

[17] Achdou Y, Camilli F, Capuzzo-Dolcetta I. Mean field games: numerical methods for the planning problem. *SIAM Journal on Control and Optimization*, 2012, **50**(1): 77−109

[18] Caines P E. Mean field stochastic control. In: Proceedings of the 48th Conference on Decision and Control and the 28th Chinese Control Conference. Shanghai, China: IEEE, 2009.

[19] Gueant. A reference case for mean field games models. *Journal de Mathematiques Pures et Appliquees*, 2009, **92**(3): 276−294

[20] Dogbe C. Modeling crowd dynamics by the mean-field limit approach. *Mathematical and Computer Modelling*, 2010, **52**(9−10): 1506−1520

[21] Nourian M, Malhame R P, Huang M Y, Caines P E. Mean field (NCE) formulation of estimation based leader-follower collective dynamics. *International Journal of Robotics & Automation*, 2011, **26**(1): 120−129

[22] Nourian M, Caines P E, Malhame R P, Huang M Y. Mean field LQG control in leader-follower stochastic multi-agent systems: likelihood ratio based adaptation. *IEEE Transactions on Automatic Control*, 2012, **57**(11): 2801−2816

[23] Nourian M, Caines P E, Malhame R P, Huang M Y. Nash, social and centralized solutions to consensus problems via mean field control theory. *IEEE Transactions on Automatic Control*, 2013, **58**(3): 639−653

[24] Lachapelle A, Wolfram M T. On a mean field game approach modeling congestion and aversion in pedestrian crowds. *Transportation Research, Part B: Methodological*, 2011, **45**(10): 1572−1589

[25] Chevalier G, Le Ny J, Malhame R. A micro-macro traffic model based on mean-field games. In: Proceedings of the 2015 American Control Conference. Chicago, IL, USA: IEEE, 2015. 1983−1988

[26] Bogdan P, Marculescu R. A fractional calculus approach to modeling fractal dynamic games. In: Proceedings of the 50th IEEE Conference on Decision and Control and European Control Conference. Orlando, FL: IEEE, 2011. 255−260

[27] Cao K C, Zeng C B, Stuart D, Chen Y Q. Fractional order dynamic modeling of crowd pedestrians. In: Proceedings of the 5th Symposium on Fractional Differentiation and its Applications. 2012.

[28] Cao K C, Chen Z Q, Stuart D, Yue D. Cyber-physical modeling and control of crowd of pedestrians: a review and new framework. *IEEE/CAA Journal of Automatica Sinica*, 2015, **2**(3): 334−344

[29] Cao K C, Chen Y Q, Stuart D. A new fractional order dynamic model for human crowd stampede system. In: Proceedings of the ASME 2015 International Design Engineering Technical Conferences and Computers and Information in Engineering Conference. Boston, USA: ASME, 2015.

[30] Parvate A, Gangal A D. Fractal differential equations and fractal-time dynamical systems. *Pramana*, 2005, **64**(3): 389−409

[31] Das S. *Functional Fractional Calculus*. Berlin Heidelberg: Springer-Verlag, 2011.

[32] Wang L F, Yang X J, Baleanu D, Cattani C, Zhao Y. Fractal dynamical model of vehicular traffic flow within the local fractional conservation laws. *Abstract and Applied Analysis*, 2014, **2014**(2014): Article ID 635760

[33] Kachroo P, Al-Nasur S J, Wadoo S A, Shende A. *Pedestrian Dynamics: Feedback Control of Crowd Evacuation*. Berlin Heidelberg: Springer-Verlag, 2008.

Kecai Cao obtained his Ph. D. degree from Southeast University in 2007 and his bachelor degree from University of Electronic Science and Technology of China in 2003. He is interested in finding the true interaction rules among natural systems such as flocking of birds, swarming of fishes and grouping of human beings and some man-made systems such as multiple vehicles on the ground or in the air. He is currently engaged in fractional order modeling and control of crowd pedestrian systems, distributed control of multiple dynamic systems such as non-holonomic robots, underactuated rigid systems. Corresponding author of this paper.

YangQuan Chen earned his Ph. D. from Nanyang Technological University, Singapore, in 1998. He was a faculty of Electrical Engineering at Utah State University from 2000-2012. He joined the School of Engineering, University of California, Merced in 2012 teaching "Mechatronics", "Engineering Service Learning" and "Unmanned Aerial Systems" for undergraduates and "Fractional Order Mechanics" and "Nonlinear Controls" for graduates. His current research interests include mechatronics for sustainability, cognitive process control, small multi-UAV based cooperative multi-spectral "personal remote sensing" and applications, applied fractional calculus in controls, modeling and complex signal processing; distributed measurement and distributed control of distributed parameter systems using mobile actuator and sensor networks. He has been the Co-Chair for IEEE RAS Technical Committee (TC) on Unmanned Aerial Vehicle and Aerial Robotics (2012-2018). He was the Mechatronics and Embedded Systems Applications (MESA) TC Chair for ASME Design Engineering Division in 2009-2010 and served as an Associated Editor for ASME Journal of Dynamics Systems, Measurements and Control (2009-2015). Currently, he serves as the Topic Editor-in-Chief of *International Journal of Advanced Robotic Systems* (Field Robotics) and a Senior Editor for *International Journal of Intelligent Robotic Systems*. He is an Associate Editor for *Fractional Calculus and Applied Analysis*, *IEEE Transactions on Control Systems Technology*, *Mechatronics*, *Control Engineering Practice*, *IET Control Theory and Applications*, and *ISA Transactions*. Dr. Chen serves as the Steering Committee Chair for International Conference on Fractional Derivatives and Applications, a program chair for 2016 International Conference on Unmanned Aircraft Systems (ICUAS), and a member of the IEEE-USA's Committee on Transportation and Aerospace Policy (CTAP). His most recent books include "Modeling, Analysis and Design of Control Systems in Matlab and Simulink" (with Dingyü Xue, World Scientific 2014) and "Scientific Computing with MATLAB, 2nd Ed." (with Dingyü Xue, CRC Press 2016). He is a member of IEEE, ASME, AIAA, ASPRS, AUVSI and AMA.

Daniel Stuart earned his Ph. D. at Utah State University, Logan, Utah (2016). He has been a researcher and instructor there covering courses in mobile robotics as well as research in controls and crowd dynamics. He has a background in multi-agent consensus, collective motion, and pedestrian tracking systems. His current research interests include study of individuals with disabilities and how they interact within a crowd, gaining understanding on how different groups of disabilities differ in their impact and ability in emergency evacuation, and applications of fractional calculus and fractional potential fields in the modeling of various interaction aspects of individuals with disabilities.

Fractional Order Modeling of Human Operator Behavior with Second Order Controlled Plant and Experiment Research

Jiacai Huang, YangQuan Chen, *Senior Member, IEEE,* Haibin Li, and Xinxin Shi

***Abstract*—Modeling human operator's dynamics plays a very important role in the manual closed-loop control system, and it is an active research area for several decades. Based on the characteristics of human brain and behavior, a new kind of fractional order mathematical model for human operator in single-input single-output (SISO) systems is proposed. Compared with the traditional models based on the commonly used quasi-linear transfer function method or the optimal control theory method, the proposed fractional order model has simpler structure with only few parameters, and each parameter has explicit physical meanings. The actual data and experiment results with the second-order controlled plant illustrate the effectiveness of the proposed method.**

***Index Terms*—Fractional order modeling, fractional calculus, human operator, human in the loop, second order controlled plant.**

I. Introduction

THE modeling of human operator is still an open problem. In manual closed-loop control system, an accurate mathematical model of human operator is very important and provides criteria to the controller design of the manual control system. The human operator is a very complex system whose behavior range includes not only skilled control tasks, but also instinctive and emotional reactions, such as those resulting from pain or fear.

For decades, modeling human operator's dynamics has been an active research area. The earliest study that considered the human operator as a linear servomechanism is Tustin in 1947[1], who proposed that the main part of the operator's behavior might be described by an "appropriate linear law", despite the amplitude' nonlinear variations and haphazard fluctuations. In 1948, Reference [2] studied the human operator as an engineering system, and proposed the following theory of the human operator in control system: the human operator behaves basically as an intermittent correction servo consisting of ballistic movement, moreover there are some counteracting processing tending to make controls seem continuous. In 1959, Mcruer considered the role of human elements in certain closed loop control systems and proposed a quasi-linear mathematical model for the human operator, which is composed of two components — a describing function and remnant[3]. In [4], the rms-error performance of a human operator in a simple closed-loop control system was measured and compared with the performance of an "optimum" linear controller, the comparison results showed that the human operator performs almost as well as a highly constrained optimum linear controller. In [5] the human operators were considered as a monitor and controller of multidegree of freedom system, and the experiment results showed that the human operators are in fact random sampling device and nearly ideal observers, meanwhile individual operator may have fixed patterns of scanning for a short period and change the patterns from time to time, and different human operators have different patterns.

In 1965, Mcruer[6] studied the human pilot dynamics in compensatory system and proposed human pilot models with different controlled element, and the experiments results validated the proposed models. In 1967, Mcruer summarized the current state of the quasi-linear pilot models, including experimental data and equations of describing function models for compensatory, pursuit, periodic, and multiloop control situations[7]. In [8], the deficiencies of the existing quasi-linear pilot models have been analyzed and then some new analytical approaches from automatic control theory have been proposed to estimate pilot response characteristics for novel situations.

In [9], based on the assumption that the operator behaves as an optimal controller and information processor subject to the operators inherent physical limitations, a mathematical model of the instrument-monitoring behavior of the human operator was developed. In [10], an adaptive model with variable structure was presented to describe the behavior of the human operator in response to sudden changes in plant dynamics and transient disturbances. In [11], a pilot model based on Kalman filtering and optimal control was given which provides for estimation of the plant state variables, the forcing functions, the time delay, and the neuromuscular lag. The remnant which is an important component of the quasi-linear model for the human operator was discussed in [12],

Manuscript received September 8, 2015; accepted January 13, 2016. This work was supported by National Natural Science Foundation of China (61104085, 51505213), Natural Science Foundation of Jiangsu Province (BK20151463, BK20130744), Innovation Foundation of NJIT (CKJA201409, CKJB201209) sponsored by Jiangsu Qing Lan Project, and the Jiangsu Government Scholarship for Overseas Studies (JS-2012-051). Recommended by Associate Editor Antonio Visioli.

Citation: Jiacai Huang, YangQuan Chen, Haibin Li, Xinxin Shi. Fractional order modeling of human operator behavior with second order controlled plant and experiment research. *IEEE/CAA Journal of Automatica Sinica*, 2016, **3**(3): 271−280

Jiacai Huang, Haibin Li, and Xinxin Shi are with the School of Automation, Nanjing Institute of Technology, Nanjing 211167, China (e-mail: huangjiacai@126.com; 924066146@qq.com; sxx@njit.edu.cn).

YangQuan Chen is with the School of Engineering, University of California, CA 95343, USA (e-mail: ychen53@ucmerced.edu).

Color versions of one or more of the figures in this paper are available online at http://ieeexplore.ieee.org.

and a model for remnant was postulated in which remnant is considered to arise from an equivalent observation noise vector whose components are linearly independent white noise processes. In [13] and [14], a mathematical model of the human as a feedback controller was developed using optimal control and estimation theory.

From 70s to the early 21st century, the problem of human operator modeling has been widely studied and a lot of new achievements emerged[15−28].

In recent years, with the new situation and different application, the modeling of human operator's dynamics is still an active research area. In [29], a two-step method using wavelets and a windowed maximum likelihood estimation method was proposed for the estimation of a time-varying pilot model parameters. In [30], the human control model in teleoperation rendezvous on the basis of human information processing was studied, and the longitudinal and lateral control models for the human operator were presented based on phase plane control method and fuzzy control method. In [31], a review of pilot model used for flight control system design that focuses specifically on physiological and manual control aspects was presented.

For a human-in-the-loop system in safety-critical application, the correctness of such systems depends not only on the autonomous controller, but also on the actions of the human controller. In [32], a formalism for human-in-the-loop control systems was presented which focuses on the problem of synthesizing a semi-autonomous controller from high-level temporal specification that expects occasional human intervention for correct operation. In [33], the three different approaches (engineering, physiology, and applied experimental psychology) to the study of human operator have been discussed, and the importance of the studying the human operator has been pointed out. In [34], the accurate control of human arm movement in machine-human cooperative control of GAS tungsten arc welding (GTAW) process was studied and an adaptive neuro-fuzzy inference system (ANFIS) model was proposed to model the intrinsic nonlinear and time-varying characteristic of the human welder response, at last the human control experimental results verified that the proposed controller was able to track varying set-points and is robust under measurement and input disturbances.

The existing models for human operator are complicated and established by integer order calculus. In this paper, based on the characteristics of human brain and behavior, the fractional order human operator model is proposed and validated by the actual data.

II. FRACTIONAL ORDER CALCULUS

Fractional calculus has been known since the development of the integer order calculus, but for a long time it has been considered as a sole mathematical problem. In recent decades, fractional calculus has become an interesting topic among system analysis and control fields due to its long memory characteristic[35−40].

Fractional calculus is a generalization of integer order integration and differentiation to non-integer order ones. Let symbol ${}_aD_t^\lambda$ denote the fractional order fundamental operator, defined as follows[35]:

$$ {}_aD_t^\lambda \triangleq D^\lambda = \begin{cases} \frac{\mathrm{d}^\lambda}{\mathrm{d}t^\lambda}, & R(\lambda) > 0, \\ 1, & R(\lambda) = 0, \\ \int_a^t (\mathrm{d}\tau)^{-\lambda}, & R(\lambda) < 0, \end{cases} \tag{1} $$

where a and t are the limits of the operation, λ is the order of the operation, and generally $\lambda \in \mathbf{R}$ and λ can be a complex number.

The three most used definitions for the general fractional differentiation and integration are the Grunwald-Letnikov (GL) definition[36], the Riemann-Liouville (RL) definition and the Caputo definition[37].

The GL definition is given as

$$ {}_aD_t^\lambda f(t) = \lim_{h\to 0} h^{-\lambda} \sum_{j=0}^{\left[\frac{t-a}{h}\right]} (-1)^j \begin{pmatrix} \lambda \\ j \end{pmatrix} f(t-jh), \tag{2} $$

where $[\cdot]$ means the integer part, h is the calculus step, and $\begin{pmatrix} \lambda \\ j \end{pmatrix} = \frac{\lambda!}{j!(\lambda-j)!}$ is the binomial coefficient.

The RL definition is given as

$$ {}_aD_t^\lambda f(t) = \frac{1}{\Gamma(n-\lambda)} \frac{\mathrm{d}^n}{\mathrm{d}t^n} \int_a^t \frac{f(\tau)}{(t-\tau)^{\lambda-n+1}} \mathrm{d}\tau, \tag{3} $$

where $n-1 < \lambda < n$ and $\Gamma(\cdot)$ is the Gamma function.

The Caputo definition is given as

$$ {}_aD_t^\lambda f(t) = \frac{1}{\Gamma(n-\lambda)} \int_a^t \frac{f^n(\tau)}{(t-\tau)^{\lambda-n+1}} \mathrm{d}\tau, \tag{4} $$

where $n-1 < \lambda < n$.

Having zero initial conditions, the Laplace transformation of the RL definition for a fractional order λ is given by $L\left\{{}_aD_t^\lambda f(t)\right\} = s^\lambda F(s)$, where $F(s)$ is Laplace transformation of $f(t)$.

III. REVIEW OF THE QUASI-LINEAR MODELS FOR HUMAN OPERATOR

The quasi-linear transfer function is an effective method for the modeling of human operator, and the quasi-linear models have been found to be useful for the analysis of closed loop compensatory behavior in the manual control system. For a simple compensatory manual control system, the functional block diagram is shown as Fig. 1, where $i(t)$ is the system input, $e(t)$ is the system error, $c(t)$ is the human operator output, $m(t)$ is the system output.

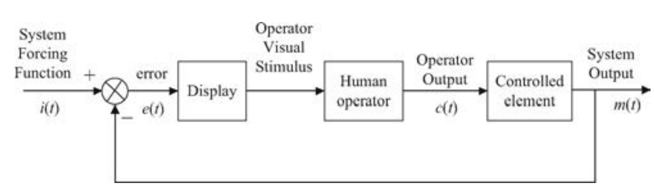

Fig. 1. Functional block diagram of the manual control system.

For the above compensatory manual control system, the generalized form of the quasi-linear model for human operator was proposed as follows[3, 6−8]:

$$Y_{P1}(s)=\frac{C(s)}{E(s)}=K_p\frac{\tau_L s+1}{\tau_I s+1}\frac{\mathrm{e}^{-Ls}}{\tau_N s+1},\tag{5}$$

where $C(s)$ and $E(s)$ are the Laplace transforms of $c(t)$ and $e(t)$ respectively, τ_L and τ_I represent the equalisation characteristics of human operator, L and τ_N represent the reaction time and neuromuscular delay of human operator respectively, K_p represents the human operator's gain which is dependant on the task and the operator's adaptive ability. The parameters in the above transfer function are adjustable as needed to make the system output follow the forcing function, i.e., the parameters, as adjusted, reflect the operator's efforts to make the overall system (including himself) stable and the error small. The quasi-linear model of (5) has been widely quoted in the literature.

Based on the human operator model described by (5), the mathematical model of the manual control system is shown in Fig. 2.

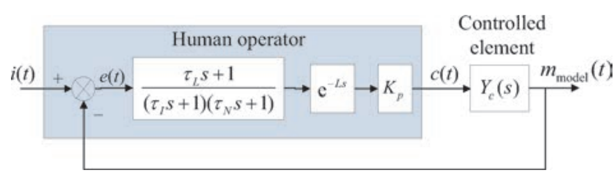

Fig. 2. The mathematical model of the manual control system.

In [15], a detailed research was made on the compensatory manual control system which is shown in Fig. 1, in which the forcing function (i.e., the system input) $i(t)$ is a random appearing signal, and in the human operating process, the error $e(t)$ and human output $c(t)$ can be obtained. By studying the relationship between the error $e(t)$ and human output $c(t)$, the mathematical models for human operator with respect to controlled plants were proposed in [15].

Because the second order controlled plant is representative and classic in application, in this paper we take it as an example, which is described as follows:

$$Y_c(s)=\frac{K_c}{s(Ts+1)},\qquad T=\frac{1}{3},K_c=1,\tag{6}$$

then the system input $i(t)$, the system output $m(t)$, the system error $e(t)$, the human operator output $c(t)$ and the lag of the operator output $\frac{C(s)}{s+3}$ were recorded as Figs. 3(a)-3(e).

From the above experiment result, when the lag of the operator output $c(t)$ (i.e., Fig. 3(d)) is compared with the system error $e(t)$, a great similarity can be seen, so the following transfer function between $c(t)$ and $e(t)$ was proposed in [15]:

$$Y_{P2}(s)=\frac{C(s)}{E(s)}=K_p(s+\frac{1}{T})\mathrm{e}^{-Ls}=K_p(s+3)\mathrm{e}^{-Ls},\tag{7}$$

where K_p is the human operator's gain; L is the time delay of human operator, which is about $L=0.16\,\mathrm{s}$.

Based on the human operator model described by (7), the mathematical model of the manual control system is shown in Fig. 4.

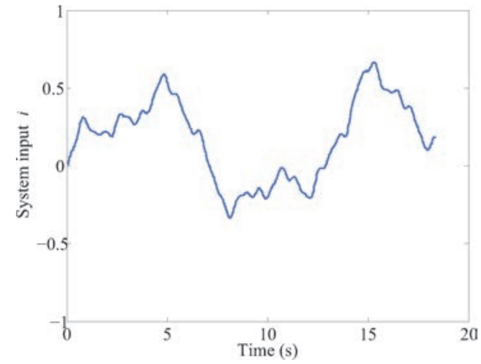

(a) System input $i(t)$

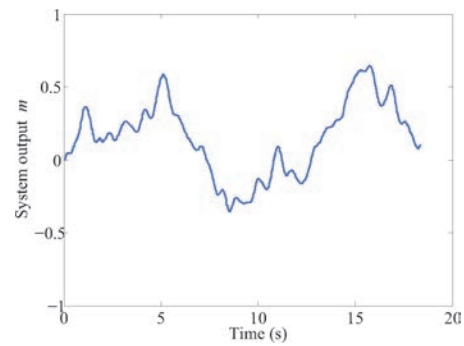

(b) System output $m(t)$

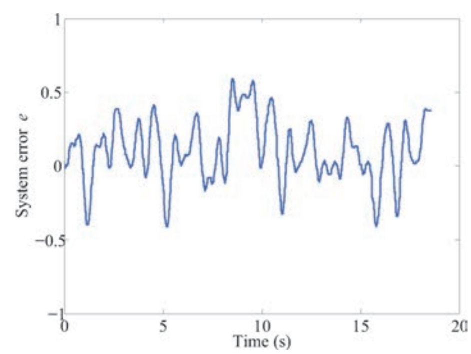

(c) System error $e(t)$

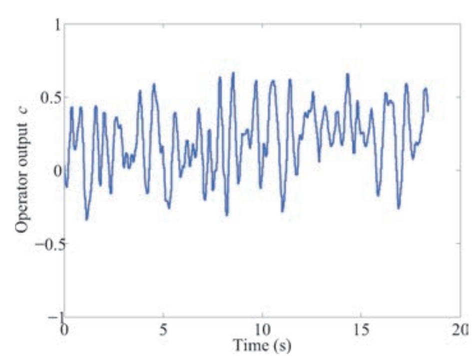

(d) Human operator output $c(t)$

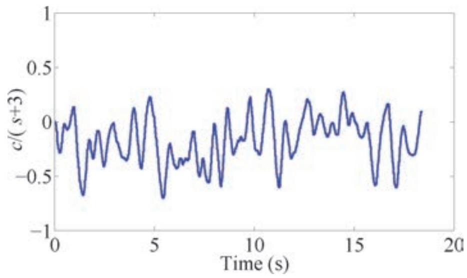

(e) The lag of operator output, i.e., $\frac{c}{s+3}$

Fig. 3. Manual control system response, $Y_c(s) = \frac{K_c}{s(Ts+1)}$, with $T = \frac{1}{3}$, $K_c = 1$.

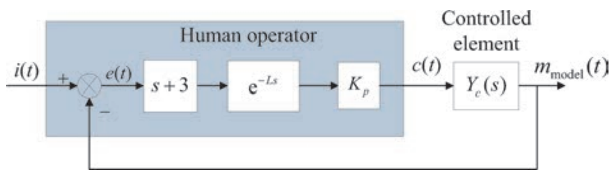

Fig. 4. The mathematical model of the manual control system.

IV. Fractional Order Mathematical Model For Human Operator Behavior

In the existing research, the human operator models are established based on the integer order calculus. In fact, the human body is a highly nonlinear servomechanism, the control task is completed through the cooperation of the eyes, the brain nervous, the muscles and the hands, as shown in Fig. 5.

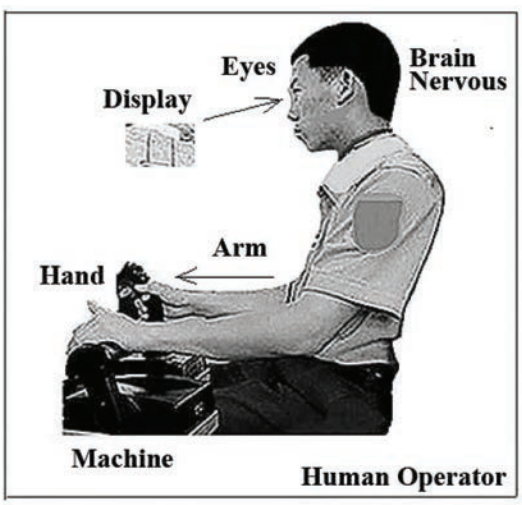

Fig. 5. The control structure of a human operator.

Let us consider the manual control system shown in Fig. 1, in which the human operator is shown in Fig. 3. In this system, the human operator controls the machine by hands to follow the target. The eyes act as a sensor, the brain acts as controller and sends the nervous system signal to the arm and hand to follow the target. The muscles of the arm and hand are employed as power actuators. Meanwhile the human has the following characteristic[1, 32]:

1) For human brain, the later the thing happens, the clearer the memory is. On the contrary, the earlier, the poorer. In other words, the human brain has higher memory level for the newer things, and lower memory level for the older things.

2) During the human action, there exists dead-time in the nervous system, including the dead-time from the retina to the brain, and the dead time from the brain to the muscle.

3) The human muscle has the viscoelastic property.

From the above facts, it can be concluded that the dynamics of the human operator's brain is mostly like a kind of fractional order integral or derivative which exhibits a long memory characteristics, and so the human operator can be seen as a fractional order controller with time delay, then in this paper the fractional order model for human operator in single-input single-output (SISO) systems is proposed as follow:

$$Y_{P3}(s) = \frac{C(s)}{E(s)} = \frac{K_p \mathrm{e}^{-Ls}}{s^{\alpha}},\ \alpha \in \mathbf{R}, \tag{8}$$

where α is the fractional order which describes the dynamics of the human operator, and α can be positive or negative; K_p is the human operator's gain; L is the total time delay of human operator, including the dead-time in the nervous system from the retina to the brain, and the dead time in the nervous system from the brain to the muscle. In real system, the α and other parameters can be obtained by online or off-line identification.

Based on fractional order model of the human operator described by (8), the mathematical model of the manual control system is shown in Fig. 6.

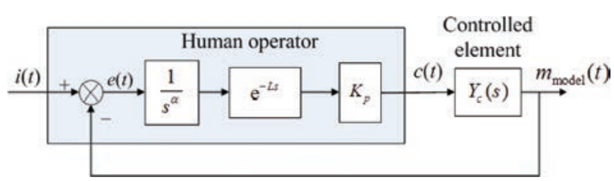

Fig. 6. The mathematical model of the manual control system.

In the following section, the effectiveness of the proposed fractional order model for human operator will be validated.

V. Model Validation with Actual Data

In this section, the off-line verification and comparison will be done using the traditional mathematical models described by (5) and (7), and the new proposed fractional order model described by (8). In the model verification process, the $best\_fit$ parameters for the above three models have been obtained by the $fminsearch$ function with actual data taken from [15], and the following cost function, i.e., the root mean square error (RMSE) is used:

$$J = \sqrt{\frac{\int_0^T (m_{\text{model}}(t) - m(t))^2}{T}}, \tag{9}$$

where $m(t)$ is the actual output of the manual control system, $m_{\text{model}}(t)$ is the model output of the manual control system by using the human operator model and the actual input (i.e., as shown in Fig. 2, Fig. 4, and Fig. 6, T is the operating time period of human operator.

In order to get the $best\_fit$ parameters of each model, the following searching criteria is adopted.

Case 1. When the human operator model is described by (8), i.e., the proposed fractional order model, the searching criteria is

$$\{\alpha^*, K_p^*, L^*\}_{best\_fit} = \min_{\alpha\in\mathbf{R};K_p,L\in\mathbf{R}^+}(J). \tag{10}$$

In this case, the fractional order differentiation/integration symbol $\frac{1}{s^\alpha}$ is implemented by the Grunwald-Letnikov (GL) definition described as (2).

Case 2. When the human operator model is described as (7), i.e., the traditional model, the searching criteria is

$$\{K_p^*, L^*\}_{best\_fit} = \min_{K_p,L\in\mathbf{R}^+}(J). \tag{11}$$

Case 3. When the human operator model is described as (5), i.e. another traditional model proposed in [3, 6-8], the searching criteria is

$$\{T_L^*, T_I^*, T_N^*, K_p^*, L^*\}_{best\_fit} = \min_{T_L,T_I,T_N,K_p,L\in\mathbf{R}^+}(J). \tag{12}$$

A. The Minimum RMSE and best_fit Parameters for Each Model

Using the above searching criteria (10)-(12), the minimum RMSE and the corresponding $best\_fit$ parameters value for each model are obtained as shown in Table I. From Table I, it is obvious that the proposed fractional order model described by (8) has the smallest RMSE, and the corresponding order of the model is $\alpha = -0.4101$. This means that compared with the traditional model, the proposed fractional order model described by (8) is the $best\_fit$ model for describing the human operator behavior, in other word, the human operator is a fractional order system.

B. The RMSE of the Proposed Fractional Order Model for Different α and L

In this section, the RMSE of the proposed model described by (8) for different α, L and K_p will be scanned. Because the time delay and gain of human operator have finite range, so in this scanning process, the time delay L gets some fixed value between 0 to 0.4, and the gain K_p gets the fixed value of 1, 3 and 5. For each K_p and L, the α is varied from -0.95 to -0.05 with 0.05 step length. The scan results are shown in Figs. 7-11.

1) When the gain of the human operator is $K_p = 1$, the RMSE scan result for each L is shown in Fig. 7, and the 3-D RMSE scan result for different α and L is shown in Fig. 8. From Fig. 7 and Fig. 8 it is clear that: a) the corresponding α for the minimum RMSE is fractional; b) when the time delay L gets bigger value, the corresponding minimum RMSE is also bigger.

2) When the gain of the human operator is $K_p = 3$, the RMSE scan result for each L is shown in Fig. 9, from which it can be seen that: a) the corresponding α for the minimum RMSE is fractional; b) when the time delay L gets smaller value, the corresponding minimum RMSE is bigger, this is because the gain of the human operator gets the bigger value in this case.

3) When the gain of the human operator gets the value $K_p = 5$ or $K_p = 7$, the RMSE scan results for each L are shown in Fig. 10 and Fig. 11 respectively. From the figures it can be seen that the corresponding α for the minimum RMSE is fractional. Meanwhile as the K_p gets the big value in these two cases, Fig. 10 and Fig. 11 only show the RMSE for $L = 0.05$, and the RMSE for other L (which is greater than 0.05 s) is too large to be shown in the figures.

TABLE I
$best\_fit$ PARAMETERS VALUE AND RMSE FOR EACH MODEL

Model	Parameter	Value
$Y_{P3}(s)=\frac{K_p\mathrm{e}^{-Ls}}{s^\alpha}$	RMSE	0.0012
	α^*	-0.4101
	K_p^*	4.403
	L^*(s)	0.117
$Y_{P2}(s)=K_p(s+3)\mathrm{e}^{-Ls}$	RMSE	0.0018
	K_p^*	7.994
	L^*(s)	0.014
$Y_{P1}(s)=\frac{K_p(T_Ls+1)\mathrm{e}^{-Ls}}{(T_Is+1)(T_Ns+1)}$	RMSE	0.0024
	K_p^*	1.7298
	T_L^*	1.8146
	T_I^*	0.162
	T_N^*	0.162
	L^*(s)	0.006

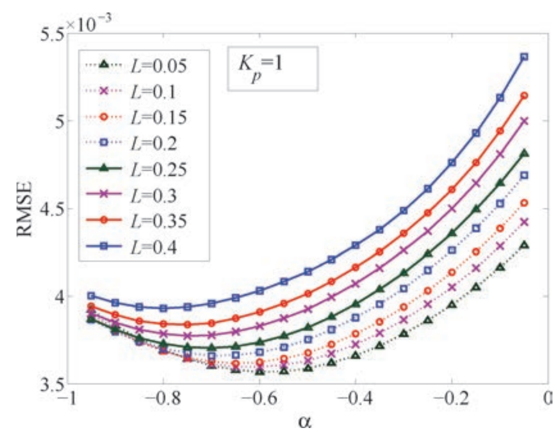

Fig. 7. The RMSE scan result for different α with fixed L, and $K_p = 1$.

VI. EXPERIMENT RESEARCH

In this section, the human-in-the-loop control experiment will be done based on the Quanser SRV02 Rotary Servo Base unit. The experiment platform is shown in Fig. 12, which is composed of a human operator, a steering wheel, a torque sensor, a motor, a computer installed with Quanser/Matlab real time software and QPIDe data acquisition card. The steering wheel is fixed with the torque sensor which is mounted on the desk. The voltage output of the torque sensor is power

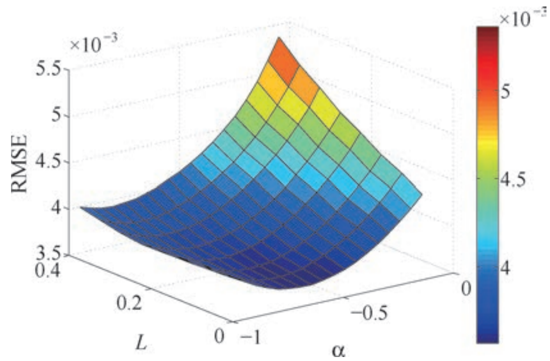

Fig. 8. The 3-D RMSE scan result for different α and L, and $K_p = 1$.

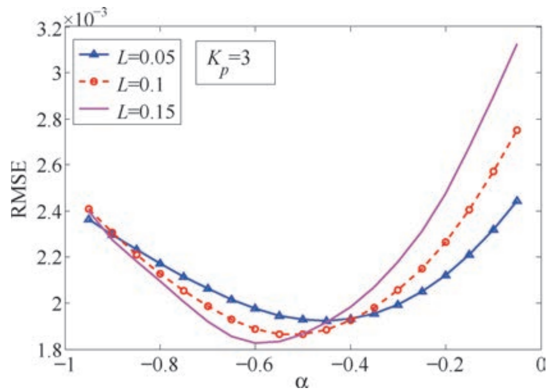

Fig. 9. The RMSE scan result for different α with fixed L, and $K_p = 3$.

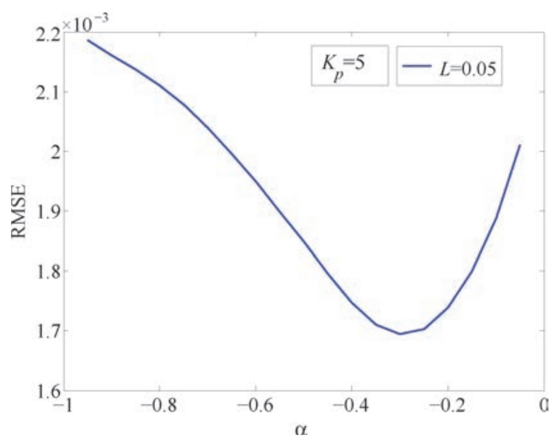

Fig. 10. The RMSE scan result for different α with fixed L, and $K_p = 5$.

amplified and transferred to the motor. The motor works on voltage to position control mode, and the encoder on the motor offers a high resolution of 4096 counts per revolution in quadrature mode (1024 lines per revolution). The QPIDe card samples the voltage output of the torque sensor together with the encoder output. In the experiment, the system input, output and error information are all shown on the display screen of the computer, and the human operator observes the system error and applies a force around the steering wheel, and so controls

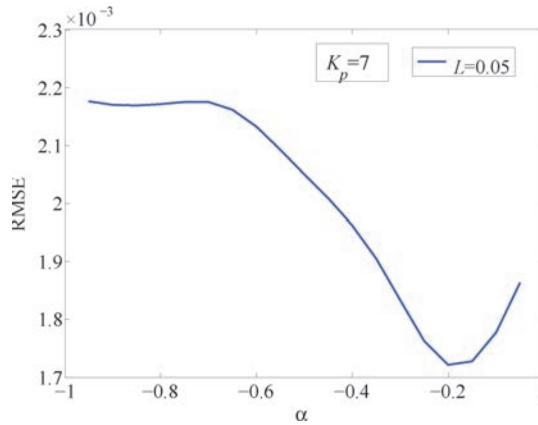

Fig. 11. The RMSE scan result for different α with fixed L, and $K_p = 7$.

the motor's position to follow the system input. The block diagram of the human-in-the-loop control system is shown in Fig. 13.

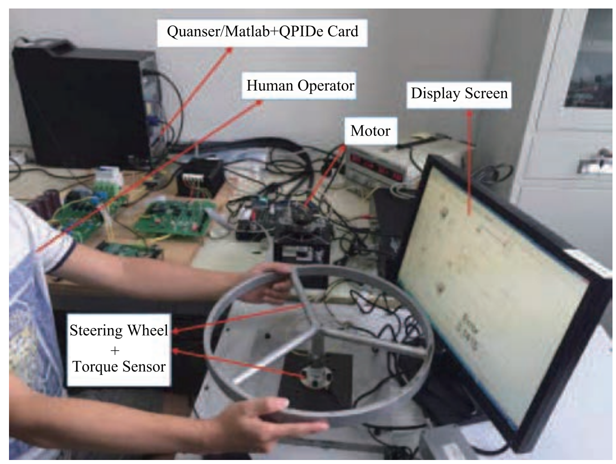

Fig. 12. The human-in-the-loop control experiment platform.

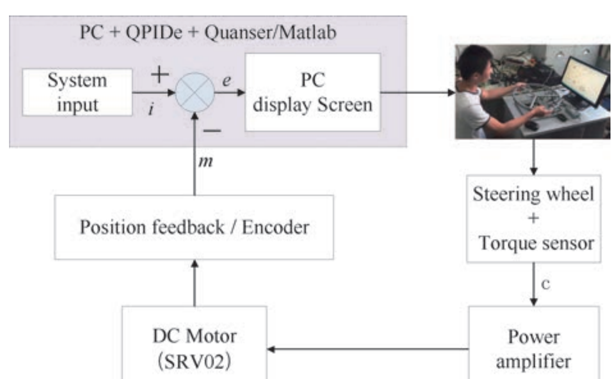

Fig. 13. The block diagram of the human-in-the-loop control experiment.

In the experiment, the motor works in position control mode, in this case it is a second order system and its transfer function is described as follows:

$$Y_c(\mathrm{s}) = \frac{K}{s(\tau s+1)} = \frac{60.2362}{s(s+39.37)}, \tag{13}$$

where $K = 1.53$ rad/s/V, $\tau = 0.0254$ s. In this experiment, the time delay of the human operator is tested at about $L = 0.3$ s, and the system input $i(t)$, system output $m(t)$, system error $e(t)$ and operator output $c(t)$ are real time recorded as shown in Figs. 14-17.

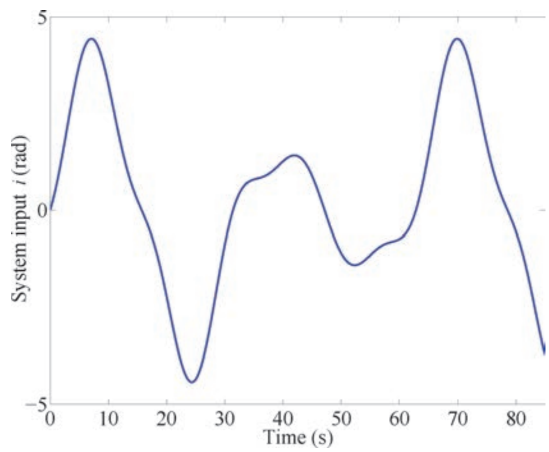

Fig. 14. The system input of the human-in-the-loop control experiment.

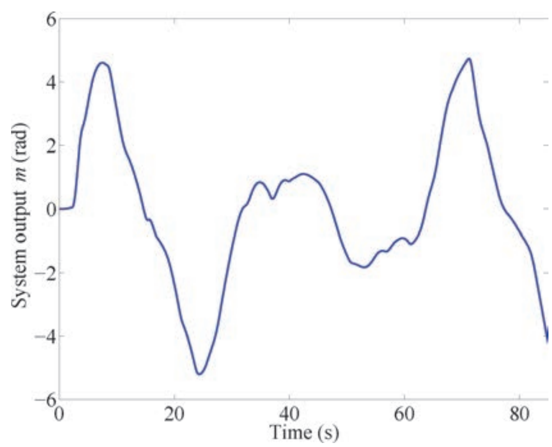

Fig. 15. The system output of the human-in-the-loop control experiment.

A. The Minimum RMSE and $best\_fit$ Parameters for Each Model

Using the experiment data and the searching criteria (10)-(12), the minimum RMSE and the corresponding $best\_fit$ parameters value for each model are obtained as shown in Table II. From Table II, it is obvious that the proposed fractional order model described by (8) has the smallest RMSE, and the corresponding order of the model is $\alpha = -0.3873$. This means that compared with the traditional model, the proposed fractional order model described by (8) is the $best\_fit$ model for describing the human operator behavior, in other words,

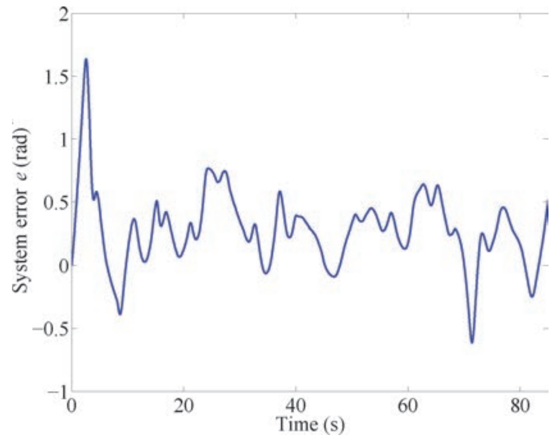

Fig. 16. The system error of the human-in-the-loop control experiment.

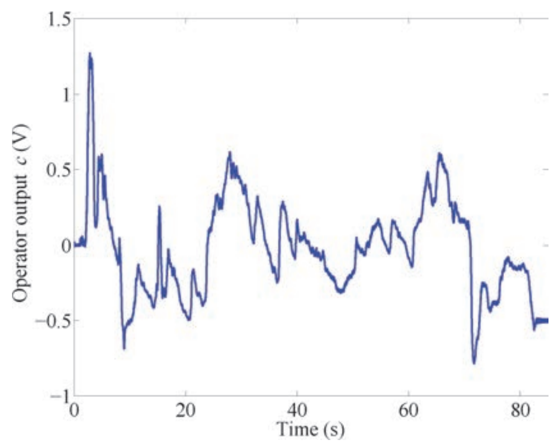

Fig. 17. The human operator output (1 V = 4 N· m).

the human operator is a fractional order system. This result is consistent with the result obtained in Section IV.

B. The Models Parameters for Different L

In general, the time delay of human operator varies in small range, so in this section the proposed fractional order model described by (8) and the conventional model described by (5) will be considered, and the models' parameters distribution for different human time delay L will be scanned. As the time delay of human operator has finite range, so in this scanning process the time delay L varies from 0.01 to 0.6 with 0.01 step length. The scan results are shown in Figs. 18-21.

Fig. 18 and Fig. 19 show that the distributions of α and K_p of the proposed fraction order model are smooth, meanwhile as the time delay L decreases, the fractional order α tends to increase negatively. Fig. 20 and Fig. 21 show that the parameters K_p, T_L, T_I and T_N of the conventional model described by (5) fluctuate in large scale. From this point of view, the proposed fractional order model described by (8) is suitable to describe the human operator behavior.

TABLE II
$best\_fit$ PARAMETERS VALUE AND RMSE FOR EACH MODEL ($L = 0.3\,\mathrm{s}$)

Model	Parameter	Value
$Y_{P3}(s)=\frac{K_p\mathrm{e}^{-Ls}}{s^{\alpha}}$	RMSE	3.751×10^{-3}
	α^*	-0.3873
	K_p^*	0.7643
$Y_{P2}(s)=K_p(s+39.37)\mathrm{e}^{-Ls}$	RMSE	4.172×10^{-3}
	K_p^*	0.6099
$Y_{P1}(s)=\frac{K_p(T_Ls+1)\mathrm{e}^{-Ls}}{(T_Is+1)(T_Ns+1)}$	RMSE	4.036×10^{-3}
	K_p^*	1.078
	T_L^*	0.1481
	T_I^*	0.0001
	T_N^*	0.7804

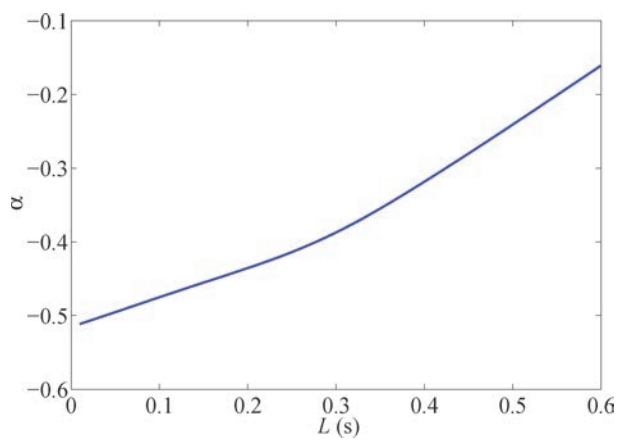

Fig. 18. The fractional order α distribution of human operator for different L using the proposed model described by (8).

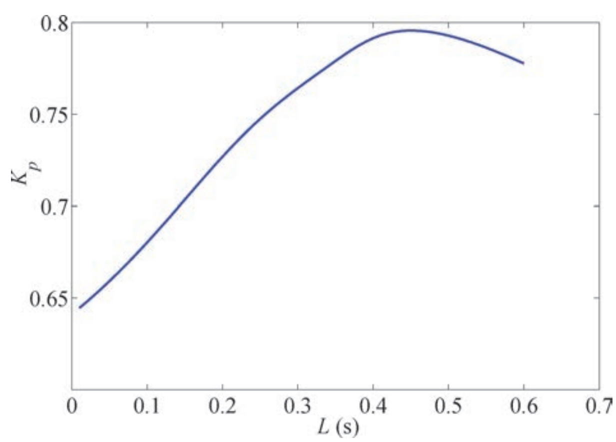

Fig. 19. The gain K_p distribution of human operator for different L using the proposed model described by (8).

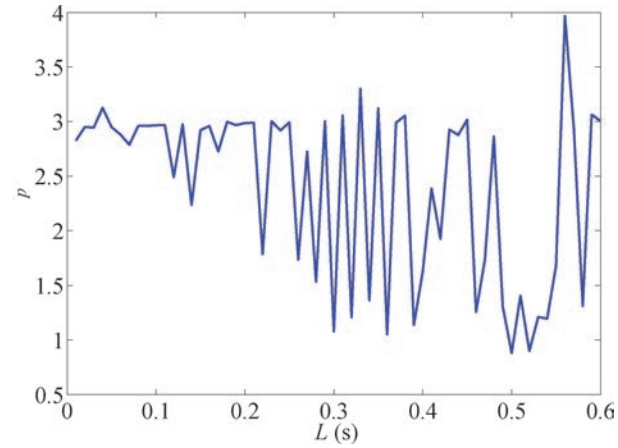

Fig. 20. The gain K_p distribution of human operator for different L using the conventional model described by (5).

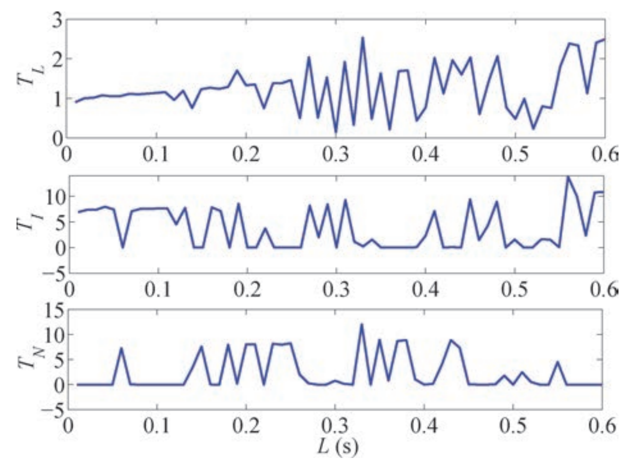

Fig. 21. The T_L, T_I, T_N distributions of human operator for different L using the conventional model described by (5).

VII. Conclusion

In this paper, based on the characteristics of human brain and behavior, the fractional order mathematical model for human operator is proposed. Based on the actual data, the models verifications have been done, and the $best\_fit$ parameters for the proposed model and the traditional models have been obtained. The verification results show that the proposed fractional order model is the $best\_fit$ model for describing the human operator behavior, in other words, the human operator is a fractional order system in such a system. The experiment results also provide the correctness of the above conclusion.

The proposed fractional order model described by (8) for human operator behavior not only has small RMSE, but also has a simple structure with only few parameters, and each parameter has definite physical meaning.

In the future work, we will research the model for human operator considering other types of controlled plant.

Acknowledgment

The authors would like to thank the graduate student Cui Lei who helped in digitizing the old data.

References

[1] Tustin A. The nature of the operator's response in manual control, and its implications for controller design. *Journal of the Institution of Electrical*

Engineers, Part II A: Automatic Regulators and Servo Mechanisms, 1947, **94**(2): 190−206

[2] Craik K J W. Theory of the human operator in control systems. *British Journal of Psychology, General Section*, 1948, **38**(3): 142−148

[3] McRuer D T, Krendel E S. The human operator as a servo system element. *Journal of the Franklin Institute*, 1959, **267**(6): 511−536

[4] Roig R W. A comparison between human operator and optimum linear controller RMS-error performance. *IRE Transactions on Human Factors in Electronics*, 1962, **HFE-3**(1): 18−21

[5] Senders J W. The human operator as a monitor and controller of multidegree of freedom systems. *IEEE Transactions on Human Factors in Electronics*, 1964, **HFE-5**(1): 2−5

[6] McRuer D T. Human operator dynamics in compensatory systems. Systems Technology Inc Hawthorne Ca, 1965.

[7] McRuer D T, Jex H R. A review of quasi-linear pilot models. *IEEE Transactions on Human Factors in Electronics*, 1967, **HFE-8**(3): 231−249

[8] McRuer D T, Hofmann L G, Jex H R, Moore G P, Phatak A V. New approaches to human-pilot/vehicle dynamic analysis. Systems Technology Inc Hawthorne Ca, 1968.

[9] Baron S, Kleinman D L. The human as an optimal controller and information processor. *IEEE Transactions on Man-Machine Systems*, 1969, **10**(1): 9−17

[10] Phatak A V, Bekey G A. Model of the adaptive behavior of the human operator in response to a sudden change in the control situation. *IEEE Transactions on Man-Machine Systems*, 1969, **10**(3): 72−80

[11] Wierenga R D. An evaluation of a pilot model based on Kalman filtering and optimal control. *IEEE Transactions on Man-Machine Systems*, 1969, **10**(4): 108−117

[12] Levison W H, Baron S, Kleinman D L. A model for human controller remnant. *IEEE Transactions on Man-Machine Systems*, 1969, **10**(4): 101−108

[13] Kleinman D L, Baron S, Levison W H. An optimal control model of human response, part I: theory and validation. *Automatica*, 1970, **6**(3): 357−369

[14] Baron S, Kleinman D L, Levison W H. An optimal control model of human response, part II: prediction of human performance in a complex task. *Automatica*, 1970, **6**(3): 371−383

[15] McRuer D T, Krendel E S. Mathematical models of human pilot behavior. Advisory Group for Aerospace Research and Development. NATO Science and Technology Organization, 1974.

[16] Tomizuka M, Whitney D E. The human operator in manual preview tracking (an experiment and its modeling via optimal control). *Journal of Dynamic Systems, Measurement, and Control*, 1976, **98**(4): 407−413

[17] Phatak A, Weinert H, Segall I, Day C N. Identification of a modified optimal control model for the human operator. *Automatica*, 1976, **12**(1): 31−41

[18] Gabay E, Merhav S J. Identification of a parametric model of the human operator in closed-loop control tasks. *IEEE Transactions on Systems, Man, and Cybernetics*, 1977, **7**(4): 284−292

[19] McRuer D. Human dynamics in man-machine systems. *Automatica*, 1980, **16**(3): 237−253

[20] Govindaraj T, Ward S L, Poturalski R J, Vikmanis M M. An experiment and a model for the human operator in a time-constrained competing-task environment. *IEEE Transactions on Systems, Man, and Cybernetics*, 1985, **SMC-15**(4): 496−503

[21] Sworder D D, Haaland K S. A hypothesis evaluation model for human operators. *IEEE Transactions on Systems, Man, and Cybernetics*, 1989, **19**(5): 1091−1100

[22] Boer E R, Kenyon R V. Estimation of time-varying delay time in nonstationary linear systems: an approach to monitor human operator adaptation in manual tracking tasks. *IEEE Transactions on Systems, Man, and Cybernetics, Part A: Systems and Humans*, 1998, **28**(1): 89−99

[23] Phillips C A, Repperger D W. An informatic model of human operator control. In: Proceedings of the 1st Joint [Engineering in Medicine and Biology, 1999. 21st Annual Conference and the 1999 Annual Fall Meetring of the Biomedical Engineering Society] BMES/EMBS Conference, 1999. Atlanta, GA: IEEE, 1999.

[24] Doman D B, Anderson M R. A fixed-order optimal control model of human operator response. *Automatica*, 2000, **36**(3): 409−418

[25] Macadam C C. Understanding and modeling the human driver. *Vehicle System Dynamics*, 2003, **40**(1−3): 101−134

[26] Kovacevic D, Pribacic N, Jovic M, Antonic R, Kovacevic A. Modeling human operator controlling process in different environments. In: Proceedings of the 19th International Conference on Artificial Neural Networks. Berlin Heidelberg: Springer, 2009. 475−484

[27] Celik O, Ertugrul S. Predictive human operator model to be utilized as a controller using linear, neuro-fuzzy and fuzzy-ARX modeling techniques. *Engineering Applications of Artificial Intelligence*, 2010, **23**(4): 595−603

[28] Tervo K. Discrete data-based state feedback model of human operator. In: Proceedings of the 2010 IEEE/ASME International Conference on Mechatronics and Embedded Systems and Applications (MESA). Qingdao, China: IEEE, 2010. 202−207

[29] Zaal P M T, Sweet B T. Estimation of time-varying pilot model parameters. In: Proceedings of the 2011 AIAA Modeling and Simulation Technologies Conference. Portland, Oregon: AIAA, 2011.

[30] Zhang B, Li H Y, Tang G J. Human control model in teleoperation rendezvous. *Science China Information Sciences*, 2014, **57**(11): 1−11

[31] Lone M, Cooke A. Review of pilot models used in aircraft flight dynamics. *Aerospace Science and Technology*, 2014, **34**: 55−74

[32] Li W C, Sadigh D, Sastry S S, Seshia S A. Synthesis for human-in-the-loop control systems. *Tools and Algorithms for the Construction and Analysis of Systems*. Berlin Heidelberg: Springer, 2014. 470−484

[33] Rao M S P. The human operator in man-machine systems. *Defence Science Journal*, 2014, **6**(3): 182−190

[34] Liu Y K, Zhang Y M. Control of human arm movement in machine-human cooperative welding process. *Control Engineering Practice*, 2014, **32**: 161−171

[35] Chen Y Q, Petráš I, Xue D Y. Fractional order control — a tutorial. In: Proceedings of the 2009 American Control Conference 2009. St. Louis, MO: IEEE, 1397−1411

[36] Li Y, Chen Y Q, Podlubny I. Stability of fractional-order nonlinear dynamic systems: Lyapunov direct method and generalized Mittag-Leffler stability. *Computers & Mathematics with Applications*, 2010, **59**(5): 1810−1821

[37] Oldham K B, Spanier J. *The Fractional Calculus*. New York: Academic Press, 1974.

[38] Podlubny I. Fractional-order systems and $PI^{\lambda}D^{\mu}$-controllers. *IEEE Transactions on Automatic Control*, 1999, **44**(1): 208−214

[39] Li H S, Luo Y, Chen Y Q. A fractional order proportional and derivative (FOPD) motion controller: tuning rule and experiments. *IEEE Transactions on Control Systems Technology*, 2010, **18**(2): 516−520

[40] Podlubny I. *Fractional Differential Equations. Vol. 198*. San Diego: Academic Press, 1999.

Jiacai Huang graduated from Jilin University (JLU), China, in 2000. He received the M. Eng. and Ph. D. degrees in Automation School from JLU in 2003 and 2006, respectively. He is currently a professor at the School of Automation, Nanjing Institute of Technology, China. His research interests include human-in-the-loop control, fractional-order motion control, and vision-guided robotics. Corresponding author of this paper.

YangQuan Chen earned his Ph. D. from Nanyang Technological University, Singapore, in 1998. He was a faculty of Electrical Engineering at Utah State University from 2000-2012. He joined the School of Engineering, University of California, Merced in 2012 teaching "Mechatronics", "Engineering Service Learning" and "Unmanned Aerial Systems" for undergraduates and "Fractional Order Mechanics" and "Nonlinear Controls" for graduates. His current research interests include mechatronics for sustainability, cognitive process control, small multi-UAV based cooperative multi-spectral "personal remote sensing" and applications, applied fractional calculus in controls, modeling and complex signal processing; distributed measurement and distributed control of distributed parameter systems using mobile actuator and sensor networks. He has been the Co-Chair for IEEE RAS Technical Committee (TC) on Unmanned Aerial Vehicle and Aerial Robotics (2012-2018). He was the Mechatronics and Embedded Systems Applications (MESA) TC Chair for ASME Design Engineering Division in 2009-2010 and served as an Associated Editor for *ASME Journal of Dynamics Systems, Measurements and Control* (2009-2015). Currently, he serves as the Topic Editor-in-Chief of *International Journal of Advanced Robotic Systems* (Field Robotics) and a Senior Editor for International Journal of Intelligent Robotic Systems. He is an Associate Editor for *Fractional Calculus and Applied Analysis*, *IEEE Transactions on Control Systems Technology*, *Mechatronics*, *Control Engineering Practice*, *IET Control Theory and Applications*, and *ISA Transactions*. Dr. Chen serves as the Steering Committee Chair for International Conference on Fractional Derivatives and Applications, a program chair for 2016 International Conference on Unmanned Aircraft Systems (ICUAS), and a member of the IEEE-USA's Committee on Transportation and Aerospace Policy (CTAP). His most recent books include "*Modeling, Analysis and Design of Control Systems in Matlab and Simulink*" (with Dingyü Xue, World Scientific 2014) and "*Scientific Computing with MATLAB*, 2^{nd} *Ed*." (with Dingyü Xue, CRC Press 2016). He is a member of IEEE, ASME, AIAA, ASPRS, AUVSI and AMA.

Haibin Li graduated from Suqian College, China, in 2015. He is currently a master student at Nanjing Institute of Technology, China. His main research interest is human-in-the-loop control.

Xinxin Shi graduated from Nanjing University of Science and Technology (NJUST), China, in 2007. She received the Ph. D. degree in mechatronic control engineering from NJUST in 2012. She is currently an associate professor at the School of Automation, Nanjing Institute of Technology, Nanjing, China. Her research interests include fractional-order control, precision motion control of linear motor, active disturbance rejection control, and robotics.

Fractional Modeling and SOC Estimation of Lithium-ion Battery

Yan Ma, Xiuwen Zhou, Bingsi Li, and Hong Chen, *Senior Member, IEEE*

***Abstract*—This paper proposes a state of charge (SOC) estimator of Lithium-ion battery based on a fractional order impedance spectra model. Firstly, a battery fractional order impedance model is derived on the grounds of the characteristics of Warburg element and constant phase element (CPE) over a wide range of frequency domain. Secondly, a frequency fitting method and parameter identification algorithm based on output error are presented to identify parameters of the fractional order model of Lithium-ion battery. Finally, the fractional order Kalman filter approach is introduced to estimate the SOC of the lithium-ion battery based on the fractional order model. The simulation results show that the fractional-order model can ensure an acceptable accuracy of the SOC estimation, and the error of estimation reaches maximally up to 0.5 % SOC.**

***Index Terms*—Lithium-ion battery, fractional order model, electrochemical impedance spectra, fractional Kalman filter.**

I. INTRODUCTION

GENERALLY, the electrochemical reactions inside lithium-ion battery are complicated in the running electric vehicle (EV), which is a highly nonlinear dynamic system. State of charge (SOC)[1] is defined as the percentage of the amount of left energy to the rated capacity of a battery, which cannot be measured directly, it only can be estimated by measured variables such as current and terminal voltage. The accurate estimation of SOC is the key problem in the field of power battery.

The methods of SOC estimation are categorized into direct experiment measurement methods and estimation methods based on battery models. Coulomb counting method and current integration method are the most popular experiment measurement methods, which are simple to obtain SOC. However, these methods result in high errors caused by the accumulation of errors in numerical integration in current measurement. State observer[2−3], Kalman filter (KF)[4−5] and particle filter (PF)[6−7] are used to estimate SOC based on the model of Lithium-ion battery. The SOC estimation error of each method is summarized in [8], which shows that the existing integer order battery SOC estimation methods mainly have estimation error larger than 1 %, which may be because the models which are obtained through the external characteristics of the power battery cannot show the precise internal characteristics. The dynamics of the battery is described by a set of integer order calculus equations. But complex electrochemical reactions are described by the fractional order function.

The fractional order calculus (FOC) is a natural extension of the classical integral order calculus. References [9−11] have shown that most phenomena, such as damping, friction, mechanical vibration, dynamic backlash, sound diffusion, etc., have fractional order properties. Thus, FOC is widely used in modeling, kinetics estimation, etc. FOC is also used to develop the electrochemical models of the super capacitors and so on.

When it comes to FOC battery modeling and SOC estimation, [12] uses FOC model obtained by system identification to estimate crankability of battery, [13] proposes lead acid battery state of charge estimation with FOC, and [14] deals with a fractional order state space model for the lithium-ion battery and its time domain system identification method. The existing FOC modeling for battery meets the same problem, the estimation accuracy in not high enough for battery management system.

The electrochemical impedance spectroscopy (EIS) method is one of the most accurate methods to model the electrochemical Li-ion batteries. There are many studies which have tried to utilize the impedance spectra directly to estimate SOC, but EIS method is too complicated to be used directly. EIS method is mainly used with equivalent circuit model at present[15−16].

The remainder of the paper is organized as follows. Section II discusses the battery fractional-order modeling based on impedance spectra; Section III discusses how to obtain characteristic curve between open circuit voltage (OCV) and SOC, states order identification with frequency method and parameters identification according to the output error identification algorithm; Section IV presents fractional order Kalman filter for SOC estimation; Section V draws conclusions from the preceding work and offers suggestion for further study.

II. FRACTIONAL MODELLING OF BATTERY

The impedance spectra curve of the Lithium-ion battery can be got through Electrochemical workstation and is shown in

Manuscript received August 31, 2015; accepted December 21, 2015. This work was supported by National Natural Science Foundation of China (615 20106008, U1564207, 61503149), High Technology Research and Development Program of Jilin (20130204021GX), Specialized Research Fund for Graduate Course Identification System Program (Jilin University) of China (450060523183), and Graduate Innovation Fund of Jilin University (20151 48). Recommended by Associate Editor YangQuan Chen.

Citation: Yan Ma, Xiuwen Zhou, Bingsi Li, Hong Chen. Fractional modeling and SOC estimation of Lithium-ion battery. *IEEE/CAA Journal of Automatica Sinica*, 2016, **3**(3): 281−287

Yan Ma is with the State Key Laboratory of Automotive Simulation and Control, Jilin University, China, and also with the Department of Control Science and Engineering, Jilin University (Campus Nanling), Changchun 1300 25, China (e-mail: yma@jlu.edu.cn).

Xiuwen Zhou and Bingsi Li are with Jilin University, Changchun 130012, China (e-mail: zhou_xiuwen@126.com; lbsmichelle@163.com).

Hong Chen is with the State Key Laboratory of Automotive Simulation and Control, Jilin University, Changchun 130012, China, and with the Department of Control Science and Engineering, Jilin University (Campus Nanling), Changchun 130025, China (e-mail: chenh98cn@126.com).

Color versions of one or more of the figures in this paper are available online at http://ieeexplore.ieee.org.

Fig. 1. As shown in the figure, the impedance spectra can be divided into three sections: the high frequency section, the mid frequency section and the low frequency section.

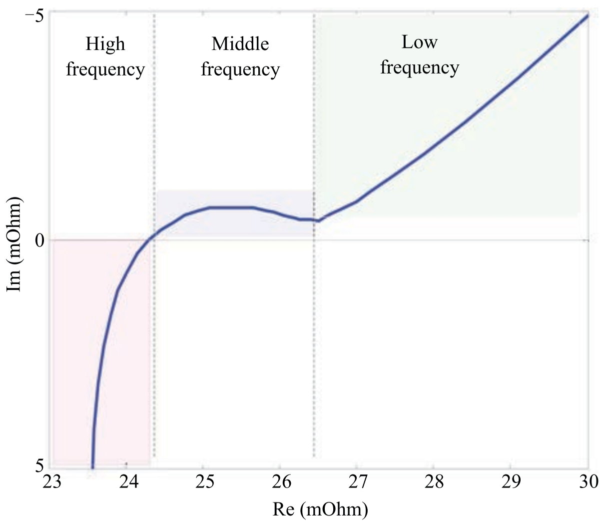

Fig. 1. Impedance spectra of a Li-ion battery.

In the high frequency section, the impedance spectra curve intersects with the real axis and the intersection point could be represented by an Ohmic resistance.

In the low frequency section, the impedance spectra curve is a straight line with a constant slope, and has the same impedance spectroscopy characteristic with constant phase element (CPE) which is usually referred to as a Warburg element.

The middle frequency section forms a depressed semicircle, which is a well-known phenomenon in electrochemistry. Such a depressed semicircle could be modeled by paralleling a Warburg element or CPE with a resistance, which is referred to as a ZARC element (it yields an arc in the Z plane)[17].

From the analysis above, the equivalent circuit model can be described as Fig. 2. V_{oc} denotes open circuit voltage (OCV), and V_o denotes battery terminal voltage which can be directly measured; $R_1 \in \mathbf{R}$ denotes the value of Ohmic resistance, I denotes the current, and V_1 denotes the voltage of R_1; $C_2 \in \mathbf{R}$ is the coefficient of CPE in ZARC element, $R_2 \in \mathbf{R}$ denotes the value of Ohmic resistance in ZARC element, and V_2 denotes the terminal voltage of ZARC element; $W \in \mathbf{R}$ is the coefficient of Warburg element, and V_3 denotes the voltage of Warburg element.

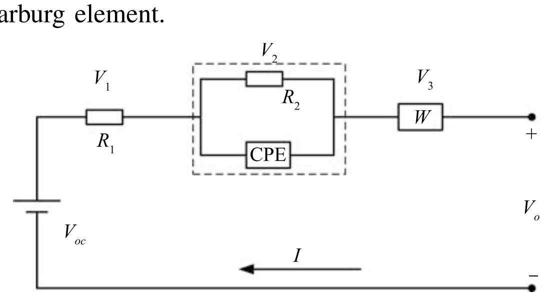

Fig. 2. Fractional equivalent circuit model.

From the above description, the battery can be described by a fractional model. To simplify the FOC equation, we define the denotation as follows:

$$\Delta^r = \begin{cases} \frac{\mathrm{d}^r}{\mathrm{d}t^r}, & r > 0, \\ 1, & r = 0, \\ \int (\mathrm{d}\tau)^r, & r < 0. \end{cases}$$

The mathematical model in high frequency can be described as (1).

$$V_1 = R_1 I, \tag{1}$$

where $R_1 \in \mathbf{R}$ denotes the value of Ohmic resistance, I denotes the current, and V_1 denotes the voltage of R_1.

The mathematical model in middle frequency can be described as (2).

$$\Delta^\beta V_2 = -\frac{1}{R_2 C_2} V_2 - \frac{1}{C_2} I, \tag{2}$$

where $C_2 \in \mathbf{R}$ is the coefficient of CPE, $\beta \in \mathbf{R}$, $-1 < \beta < 1$ denotes the fractional order of CPE, $R_2 \in \mathbf{R}$ denotes the value of Ohmic resistance in ZARC element, I denotes the current across the ZARC element, and V_2 denotes the terminal voltage of ZARC element.

The mathematical model of Warburg element in low frequency can be described as (3).

$$\Delta^\alpha V_3 = -\frac{1}{W} I, \tag{3}$$

where $W \in \mathbf{R}$ is the coefficient, Δ^α denotes α order of the fractional element, $\alpha \in \mathbf{R}$, $-1 < \alpha < 1$ is the fractional order of Warburg element, V_3 denotes the voltage of Warburg element, and I denotes the current across the Warburg element.

For the determined relationship of OCV and SOC, SOC can be regarded as a system state, which can be presented as follows:

$$\Delta^1 S_{oc} = -\frac{1}{Q_n} I, \tag{4}$$

where Q_n denotes the nominal capacity (Ah) of battery.

The relationship between SOC and OCV is nonlinear and it is not easy to draw a mathematical interpretation for it. It is easy to find that when SOC is between 20 % and 80 % the relationship is considered to be linear and can be written as follows:

$$V_{oc} = k \cdot S_{oc} + d, \tag{5}$$

where k and d are the coefficients which can be calculated from the curve fitting.

Set the system state vector as $x = \begin{bmatrix} V_2 & V_3 & S_{oc} \end{bmatrix}^{\mathrm{T}}$, the system input as $u = I$, and the system output as $y = V_o - d$. The continuous fractional state space function can be written as (6).

$$\begin{cases} \Delta^N x = Ax + Bu, \\ y = Cx + Du, \end{cases} \tag{6}$$

where $A = \begin{bmatrix} -\frac{1}{R_2 C_2} & 0 & 0 \\ 0 & 0 & 0 \\ 0 & 0 & 0 \end{bmatrix}$, $B = \begin{bmatrix} -\frac{1}{C_2} \\ -\frac{1}{W} \\ -\frac{1}{Q_n} \end{bmatrix}$, $C = \begin{bmatrix} 1 & 1 & k \end{bmatrix}$, $D = -R_1$, $N = \begin{bmatrix} \beta \\ \alpha \\ 1 \end{bmatrix}$.

According to the stochastic theory, the discrete state space function is obtained as follows:

$$\begin{cases}\Delta^N x_{k+1} = Ax_k + Bu_k,\\ y_k = Cx_k + Du_k,\end{cases} \tag{7}$$

where $x_k \in \mathbf{R}^3$ denotes the system state vector, $y_k \in \mathbf{R}$ denotes the system output, and $u_k \in \mathbf{R}$ denotes the system input, all at the time instant k.

The fractional order Grünwald-Letnikov definition is given as

$$\Delta^N x_k = \frac{1}{T_s^N}\sum_{j=0}^{k}(-1)^j \left(\begin{array}{c} N \\ j \end{array}\right) x_{k-j}, \tag{8}$$

where T_s is the sample interval, and k is the number of samples for which the derivative is calculated,

$$\left(\begin{array}{c} N \\ j \end{array}\right) = \begin{cases}1, & j=0,\\ \frac{N(N-1)\cdots(N-j+1)}{j!}, & j>0.\end{cases}$$

Equation (9) can be derived from (8).

$$\begin{aligned} x_{k+1} = {} & T_s^N \Delta^N x_{k+1} - \left(\begin{array}{c} N \\ 1 \end{array}\right) x_k \\ & + \sum_{j=2}^{k+1}(-1)^j \left(\begin{array}{c} N \\ j \end{array}\right) x_{k-j+1}. \end{aligned} \tag{9}$$

The discrete state space function of the battery can be written as (10).

$$\begin{cases} x_{k+1} = T_s^N(A+NE)x_k + T_s^N Bu_k - \sum\limits_{j=2}^{k+1}\gamma_j x_{k-j+1},\\ y_k = Cx_k + Du_k,\end{cases} \tag{10}$$

where $\gamma_j = \mathrm{diag}\left\{\left(\begin{array}{c} \beta \\ j \end{array}\right)\left(\begin{array}{c} \alpha \\ j \end{array}\right)\left(\begin{array}{c} 1 \\ j \end{array}\right)\right\}$.

Let $A_d = T_s^N(A+NE)$, $B_d = T_s^N B$, $C_d = C$, $D_d = D$, and E be unit matrix. Considering the process noise and output noise, the discrete state space function of the system can be written as

$$\begin{cases} x_{k+1} = A_d x_k + B_d u_k + w_k - \sum\limits_{j=2}^{k+1}\gamma_j x_{k-j+1},\\ y_k = C_d x_k + D_d u_k + v_k,\end{cases} \tag{11}$$

where $w_k \in \mathbf{R}^3$ is process noise, representing the modeling uncertainty and unknown input, $v_k \in \mathbf{R}$ is output noise, on behalf of the measurement disturbance, w_k and v_k are assumed to be independent, zero mean Gaussian noise processes with the covariance matrices $\mathrm{E}[w_k w_j^{\mathrm{T}}] = Q_k\delta_{kj}$, $\mathrm{E}[v_k v_j^{\mathrm{T}}] = R_k\delta_{kj}$, and δ_{kj} is Kronecker function.

III. PARAMETER IDENTIFICATION

Parameter identification of battery model can be divided into two sections, curve fitting of relationship between OCV and SOC and parameter identification in battery model. We will describe the two parts separately as following.

A. Curve Fitting Between OCV and SOC

OCV is obtained by fitting average value of charging and discharging terminal voltages which are measured by applying constant pulse current for each time 10 % SOC to battery in both of charging and discharging modes.

Through the above test, the unknown parameters k and d in (5) can be obtained by curve fitting.

The specific test procedure is as follows:

1) Discharge the battery till it reaches the minimum discharging voltage (2 V in our case) at room temperature, and keep it idle for 12 hours.

2) Charge the battery with a constant current of 0.2 C (0.5 A) till terminal voltage reaches 3.7 V. During the procedure, idle the battery for 2 minutes after each 10 % SOC charging. Record every minimum voltage, as shown in Table I.

TABLE I
MINIMUM POINTS OF EVERY SOC WHILE CHARGING

SOC (%)	Voltage (mV)
1	2664
11	3140
21	3233
31	3278
41	3304
51	3318
61	3322
71	3341
81	3382
91	3408
100	3702

3) Idle the battery for 12 hours.

4) Discharge the battery with a constant current of 0.2 C (0.5 A) till terminal voltage reaches 2 V. During the procedure, idle the battery for 2 minutes after each 10 % SOC discharging. Record every maximum voltage, as shown in Table II.

TABLE II
MAXIMUM POINTS OF EVERY SOC WHILE DISCHARGING

SOC (%)	Voltage (mV)
99	3434
89	3284
79	3274
69	3266
59	3360
49	3240
39	3222
29	3192
19	3147
9	2812
0	2431

5) Fit minimum points and maximum points that we collected in prior experiments respectively and average the two curves, which are shown in Fig. 3.

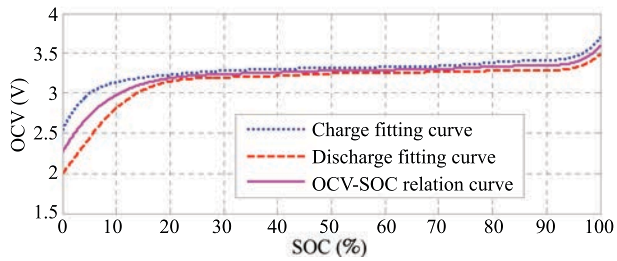

Fig. 3. OCV measurement during charging and discharging.

Fitting the OCV-SOC relationship from 20 % SOC to 80 % SOC as shown in Fig. 4, we can get the values $k = 0.002086$ and $d = 3.166$.

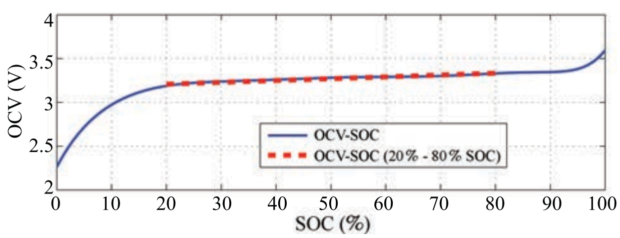

Fig. 4. OCV-SOC curves between 20 % and 80 % SOC.

B. Parameter Identification of Model

Identify unknown parameters in (6) with time domain and frequency domain method separately.

1) Identify the order of states using frequency fitting method in frequency domain: This impedance spectra curve of the Warburg element has the slope of $\alpha\pi/2$. The slope of the low-frequency part of the impedance spectra is nearly $\pi/4$, so parameter α is equal to 0.5.

The impedance spectra curve of the loop consisting of a CPE and a resistance is shaped like a semicircle. The regression rate of the semicircle will be changed with β. The bigger β is, the bigger the curve radian is. When $\beta = 0.65$, the measured impedance spectra will be matched well, shown in Fig. 5.

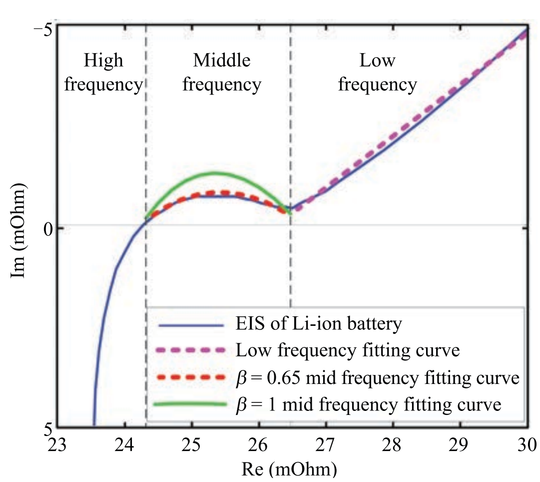

Fig. 5. System state order fitting curve.

Fig. 5 shows that the impedance spectra curve obtained by the order of state identification can match the measured impedance spectra well, which means that the fractional-order model can express the characteristic of Lithium-ion battery well.

2) Unknown parameter identification: Unknown parameters are identified via output error identification algorithm in time domain[18−19]. The output error approach is diagrammed in Fig. 6.

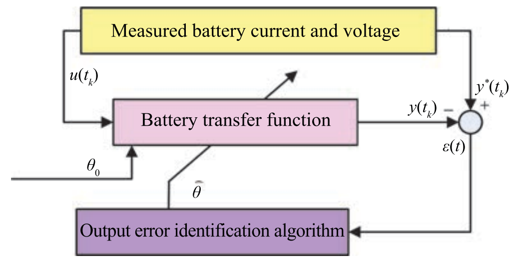

Fig. 6. Parameter identification of battery by output error approach.

The transfer function of fractional order equivalent circuit model shown in Fig. 1 can be written as

$$\begin{aligned} H(s) &= \frac{V(s)}{I(s)} = \frac{1}{Ws^{\alpha}} \cdot R_1 \cdot \frac{R_2(\frac{1}{C_2 s^{\beta}})}{R_2 + (\frac{1}{C_2 s^{\beta}})} \\ &= \frac{R_1 R_2}{Ws^{\alpha}(1 + C_2 R_2 s^{\beta})}, \end{aligned} \tag{12}$$

where $V = V_o - V_{oc}$.

Equation (12) can be written as (13).

$$V(s)Ws^{\alpha}(1 + C_2 R_2 s^{\beta}) = I(s)R_1 R_2. \tag{13}$$

Applying of inverse Laplace transform algorithm, we have

$$W\frac{\mathrm{d}^{\alpha}}{\mathrm{d}t}V(t) + C_2 R_2 W \frac{\mathrm{d}^{\alpha+\beta}}{\mathrm{d}t}V(t) = R_1 R_2 I(t). \tag{14}$$

Let $a = R_1 R_2$, $b = W$, $c = C_2 R_2 W$, $\theta = \begin{bmatrix} a \\ b \\ c \end{bmatrix}$, $p = \dfrac{\mathrm{d}}{\mathrm{d}t}$.

Equation (14) is written as

$$G(p) = \frac{V(t)}{I(t)} = \frac{a}{bp^{\alpha} + cp^{\alpha+\beta}} = \frac{B(\theta)}{A(p,\theta)}. \tag{15}$$

The noise-free output $y(t_k)$ is supposed to be corrupted by an additive white measurement noise $v(t_k)$ which is normally distributed with a zero mean and R variance, considered at discrete instants. The complete equation can be written in the form

$$\begin{cases} y(t_k) = G(p) \cdot u(t_k), \\ y^*(t_k) = y(t_k) + v(t_k), \end{cases} \tag{16}$$

where $y^*(t_k)$ is the measured output of the system.

Assume that an error function $\varepsilon(t)$ is given by the output error, i.e.,

$$\begin{aligned} \varepsilon(t) &= y^*(t_k,\theta) - \frac{B(\theta)}{A(p,\theta)}u(t) \\ &= A(p,\theta)\left(\frac{y^*(t_k,\theta)}{A(p,\theta)}\right) - B(\theta)\left(\frac{u(t)}{A(p,\theta)}\right) \\ &= A(p,\theta)y_f^*(t) - B(\theta)u_f(t), \end{aligned} \tag{17}$$

where $y_f^*(t) = y^*(t,\theta)/A(p,\theta)$ and $u_f(t) = u(t)/A(p,\theta)$. Hence, a linear low-pass filter is applied to the measured input part and output part separately instead of a direct differentiation of the input variable and output variable. As shown in (17), the filter converts the output error into an equation error[20].

Let $F^n(p) = 1/A(p,\theta^n)$, $n = 1,2,\dots$ stands for the iteration number. In practical cases, $A(p,\theta)$ being unknown, an estimation $F^n(p) = 1/\hat{A}(p,\hat{\theta}^n)$ is computed iteratively.

The noise-free output variable is obtained through an auxiliary model, i.e.,

$$y^n(t) = \frac{\hat{B}(\hat{\theta}^n)}{\hat{A}(p,\hat{\theta}^n)}u(t). \tag{18}$$

The filtered input, output, and measured output are computed respectively with

$$\begin{aligned} u_f(t) &= F^n(p)u(t), \\ p^\alpha y_f(t) &= p^\alpha F^n(p)y(t), \\ p^\alpha y_f^*(t) &= p^\alpha F^n(p)y^*(t). \end{aligned}$$

And they are gathered in the regression vectors as

$$\begin{aligned} \varphi_f(k) &= \begin{bmatrix} u_f(k) & -p^\alpha y_f^*(k) & -p^{\alpha+\beta} y_f^*(k) \end{bmatrix}^{\mathrm{T}}, \\ \varphi_f^n(k) &= \begin{bmatrix} u_f(k) & -p^\alpha y_f(k) & -p^{\alpha+\beta} y_f(k) \end{bmatrix}^{\mathrm{T}}. \end{aligned}$$

Thus, we have

$$\begin{aligned} \Phi_f^n &= \begin{bmatrix} \varphi_f^n(0) & \dots & \varphi_f^n(T_{\text{final}}) \end{bmatrix}, \\ \Phi_f &= \begin{bmatrix} \varphi_f(0) & \dots & \varphi_f(T_{\text{final}}) \end{bmatrix}, \\ Y_f^* &= \begin{bmatrix} y_f^*(0) & \dots & y_f^*(T_{\text{final}}) \end{bmatrix}. \end{aligned} \tag{19}$$

The optimization problem of the parameter identification can be stated as

$$\hat{\theta}_k = \arg\min_\theta \left\| [\Phi_f^n \Phi_f^{\mathrm{T}}]\theta - [\Phi_f^n Y_f^*] \right\|^2. \tag{20}$$

The solution is given by

$$\hat{\theta}_k = (\Phi_f^n \Phi_f^{\mathrm{T}})^{-1} \Phi_f^n Y_f^*, \tag{21}$$

and the algorithm is iterated until convergence, when $\max\left|\frac{\hat{\theta}_k - \hat{\theta}_{k-1}}{\hat{\theta}_k}\right| < \varepsilon$, where ε is chosen by the accuracy of modeling.

Specific identification process can be described as:

1) $k = 0$, initialize the parameters with $\theta_0 = \begin{bmatrix} 0 & 0 & 0 \end{bmatrix}^{\mathrm{T}}$.

2) $k = 1,2,3,\dots$, calculate noise-free output $y(k)$ according to θ_{k-1} and (16).

3) Filter the current, the terminal voltage, and the noise-free terminal voltage based on (18).

4) Determine variables based on (19).

5) Update the identified parameters $\hat{\theta}_k$ by (21).

6) Calculate the relative error of $\left|\frac{\hat{\theta}_k - \hat{\theta}_{k-1}}{\hat{\theta}_k}\right|$ from 2) to 5) until the error is less than 0.05.

After the identification process, the value of every element can be gotten as $R_2 = \frac{a}{R_1}$, $W = b$, $C_2 = \frac{c}{R_2 W}$ in (6), $Q_n = C_n \times 3600$ where C_n is the nominal capacity, i.e., $R_2 = 2.1\,\text{m}\Omega$, $W = 26.5$, $C_2 = 11\,\text{mF}$.

The intersection of impedance spectra with real axis in high frequency shows the value of resistance. From the impedance spectra curve we can get $R_1 = 24.3\,\text{m}\Omega$.

Bring the above parameters into (6), the discrete fractional model can be written as

$$\begin{cases} x_{k+1} = A_d x_k + B_d u_k + w_k - \sum\limits_{j=2}^{k+1} \gamma_j x_{k-j+1}, \\ y_k = C_d x_k + D_d u_k + v_k, \end{cases} \tag{22}$$

where

$$A_d = \begin{bmatrix} \beta - \frac{1}{R_2 C_2} & 0 & 0 \\ 0 & \alpha & 0 \\ 0 & 0 & 1 \end{bmatrix} = \begin{bmatrix} -43289.39 & 0 & 0 \\ 0 & 0.5 & 0 \\ 0 & 0 & 1 \end{bmatrix},$$

$$B_d = \begin{bmatrix} \frac{-1}{C_2} \\ \frac{-1}{W} \\ \frac{-1}{Q_n} \end{bmatrix} = \begin{bmatrix} -90.9 \\ -0.038 \\ -0.00011 \end{bmatrix}, \quad N = \begin{bmatrix} 0.65 \\ 0.5 \\ 1 \end{bmatrix},$$

$$C_d = \begin{bmatrix} 1 & 1 & k \end{bmatrix} = \begin{bmatrix} 1 & 1 & 0.21 \end{bmatrix}, \quad D_d = -R_1 = -0.0243.$$

C. Model Validation

The current profile consists of many charge/discharge pulses, at different current levels. Economic Commission for Europe (ECE) 15 urban driving cycle which is used on electric vehicles is selected to simulate a typical driving pattern. The current profile shown in Fig. 7 repeats the ECE 15 urban driving cycle 3 times, and each circle is running for 400 s.

The voltage curve, shown in Fig. 8, includes the two curves. One is the output of the identified model and the other is the measured voltage of the battery. And Fig. 9 shows the error of the two voltage curves at different time. It is easy to find that almost all the voltage errors are within 20 mV. When the input

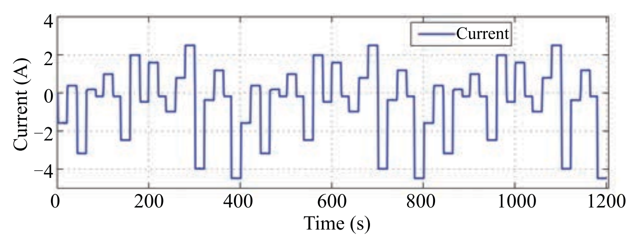

Fig. 7. Current profile for model validation.

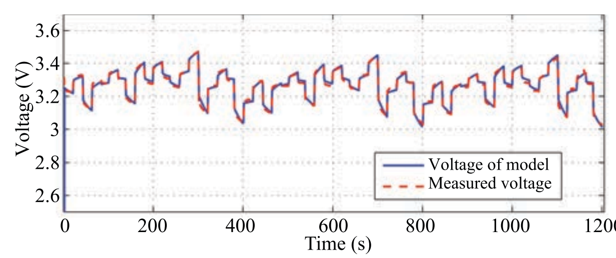

Fig. 8. Voltage profile for model validation.

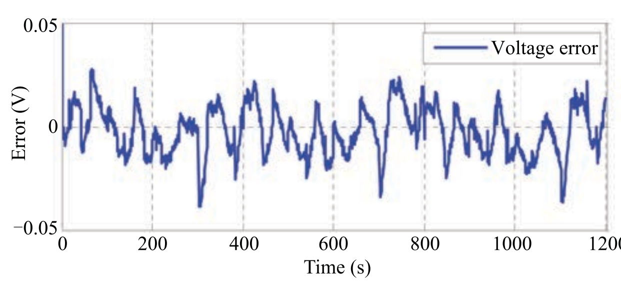

Fig. 9. Voltage error for model validation.

charging current or discharging current switches largely, the error is reaches to 40 mV.

Thus the identified fractional order model is accurate.

IV. SOC ESTIMATION BASED ON FRACTIONAL ORDER MODEL

The work described in this paper was undertaken using 26 650 Lithium-ion batteries manufactured by A123 (2.5 Ah, 3.3 V batteries) which are shown in Fig. 10, and the battery test machine is shown in Fig. 11.

Fig. 10. A123 cell.

Fig. 11. Battery test equipment.

A fractional order estimator is designed to estimate SOC of the battery.

For the common integer order system, Kalman filter approach is widely used to estimate the parameters of the system.

Hence, fractional order Kalman filter (FKF)[21] is selected to estimate the SOC of the battery.

The process can be described as:

1) $k = 0$

The Kalman filter is initialized with the best available information of state and error covariance. The initialized value of state estimation and error covariance are expressed as: the covariance matrices of process noise Q, the covariance matrices of measurement noise R, the initialized system state $\hat{x}_0$, and the covariance matrices of initialized system state $P_0 = E[(\hat{x}_0 - x_0)(\hat{x}_0 - x_0)^{\mathrm{T}}]$.

2) $k = 1, 2, \ldots$

State estimation propagation

$$\tilde{x}_k = A_d x_{k-1} + B_d I_k - \sum_{j=1}^{k} \gamma_j \begin{pmatrix} N \\ j \end{pmatrix} x_{k-j}. \quad (23)$$

Error covariance propagation

$$\tilde{P}_k = (A_d + N_1)P_{k-1} + Q_{k-1} + \sum_{j=2}^{k} N_j P_{k-j} N_j^{\mathrm{T}}. \quad (24)$$

Kalman gain update

$$K_k = \tilde{P}_k C^{\mathrm{T}} (C \tilde{P}_k C^{\mathrm{T}} + R_k). \quad (25)$$

State estimation update

$$\hat{x}_k = \tilde{x}_k + K_k(y_k - C\tilde{x}_k). \quad (26)$$

Error covariance update

$$P_k = (1 - K_k C)\tilde{P}_k. \quad (27)$$

3) Save the estimated state and covariance for further iteration.

4) Separate the system state, and we will get SOC timely.

The current profile shown in Fig. 12 is employed as validation scenario. Under this condition, fractional Kalman filter and Kalman filter (KF) are used to estimate terminal voltage and SOC of battery. Both the measured terminal voltage and model terminal voltage are shown in Fig. 13. From Fig. 13, we can see the battery is tested in full SOC range (i.e., terminal voltage from 2.0 V to 3.6 V), and both the terminal voltage estimated by FKF and KF can trace the measured terminal voltage well, but the FKF results are more precise than the KF ones.

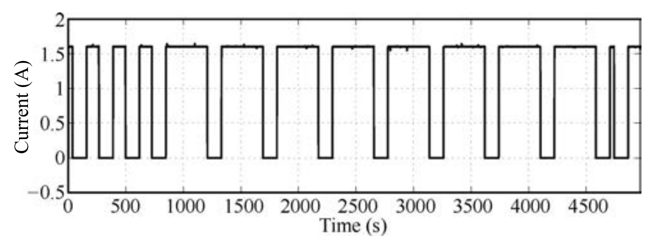

Fig. 12. Current profile for SOC estimation.

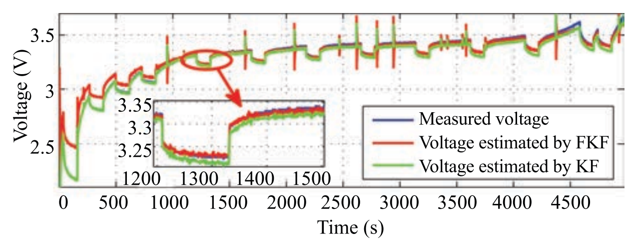

Fig. 13. Terminal voltage profile for SOC estimation.

SOC estimation and SOC estimation error curves are shown in Fig. 14 and Fig. 15, respectively. From Fig. 15 we will see, at the beginning of battery charging, the FKF estimation error is almost the same as KF estimation error. And with further charging of battery, precision of FKF will rise gradually while precision of KF gets worse. At the late charging period, both the FKF and KF error are increasing, but the FKF estimation error is always smaller than the KF one. In the whole test, the error of FKF can be reduced up to max 0.5 % SOC, while the error of KF reaches 3 %.

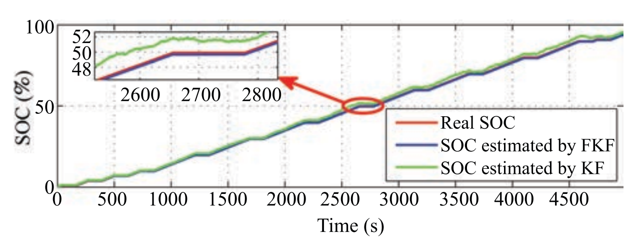

Fig. 14. SOC estimation.

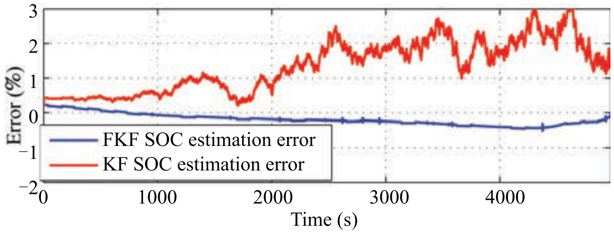

Fig. 15. SOC estimation error.

V. CONCLUSION

Based on the analysis of the impedance spectra, a simplified battery fractional-order model is derived. A new identification method is presented to identify the orders of the states and parameters based on the fractional-order system. The fractional Kalman filter is utilized to estimate the SOC of the lithium-ion battery based on the fractional-order model. The simulation results show the SOC estimation with fractional Kalman filter is consistent with expectations. However just one battery is tested in the paper, battery pack will be tested in further study.

REFERENCES

[1] Wang Y, Zhang C, Chen Z. A method for joint estimation of state-of-charge and available energy of LiFePO_4 batteries. *Applied Energy*, 2014, **135**: 81−87

[2] Kim D, Koo K, Jeong J J, Goh T, Sang W K. Second-order discrete-time sliding mode observer for state of charge determination based on a dynamic resistance Li-ion battery model. *Energies*, 2013, **6**(10): 5538−5551

[3] Chen X, Shen W X, Cao Z, Kapoor A. Sliding mode observer for state of charge estimation based on battery equivalent circuit in electric vehicles. *Australian Journal of Electrical and Electronics Engineering*, 2012, **9**(3): 225−234

[4] Li D, Ouyang J, Li H, Wan J F. State of charge estimation for LiMn_2O_4 power battery based on strong tracking sigma point Kalman filter. *Journal of Power Sources*, 2015, **279**: 439−449

[5] He Ling-Na, Wang Yun-Hong. SOC estimation based on improved sampling point Kalman filter for mine-used battery. *Journal of Mechanical and Electrical Engineering*, 2014, **31**(9): 1213−1217 (in Chinese)

[6] Wang Y J, Zhang C B, Chen Z H. A method for state-of-charge estimation of LiFePO_4 batteries at dynamic currents and temperatures using particle filter. *Journal of Power Sources*, 2015, **279**: 306−311

[7] Li J H, Barillas J K, Guenther C, Danzer M A. Multicell state estimation using variation based sequential Monte Carlo filter for automotive battery packs. *Journal of Power Sources*, 2015, **277**: 95−103

[8] Lu L G, Han X B, Li J Q, Hua J F, Ouyang M G. A review on the key issues for Lithium-ion battery management in electric vehicles. *Journal of Power Sources*, 2013, **226**: 272−288

[9] Deng Li-Wei, Song Shen-Min. Synchronization of fractional order hyperchaotic systems based on output feedback sliding mode control. *Acta Automatica Sinica*, 2014, **40**(11): 2420−2427 (in Chinese)

[10] Sadli I, Urbain M, Hinaje M, Martin J P, Raël S, Davat B. Contributions of fractional differentiation to the modelling of electric double layer capacitance. *Energy Conversion and Management*, 2010, **51**(12): 2993−2999

[11] Fairweather A J, Foster M P, Stone D A. Battery parameter identification with pseudo random binary sequence excitation (PRBS). *Journal of Power Sources*, 2011, **196**(22): 9398−9406

[12] Sabatier J, Cugnet M, Laruelle S, Grugeon S, Sahut B, Oustaloup A, Tarascon J M. A fractional order model for lead-acid battery crankability estimation. *Communications in Nonlinear Science and Numerical Simulation*, 2010, **15**(5): 1308−1317

[13] Sabatier J, Aoun M, Oustaloup A, Grégoire G, Ragot F, Roy P. Fractional system identification for lead acid battery state of charge estimation. *Signal Processing*, 2006, **86**(10): 2645−2657

[14] Wu H J, Yuan S F, Yin C L. A Lithium-Ion battery fractional order state space model and its time domain system identification. In: Proceedings of the 2012 FISITA World Automotive Congress. Berlin Heidelberg: Springer, 2013, **192**: 795−805

[15] Luo Y F, Gong C S A, Chang L X, Liu Y H. AC impedance technique for dynamic and static state of charge analysis for Li-ion battery. In: Proceedings of the 17th IEEE International Symposium on Consumer Electronics (ISCE). Hsinchu, China: IEEE, 2013: 9−10

[16] Eddahech A, Briat O, Bertrand N, Delétage J Y, Vinassa J M. Behavior and state-of-health monitoring of Li-ion batteries using impedance spectroscopy and recurrent neural networks. *International Journal of Electrical Power and Energy Systems*, 2012, **42**(1): 487−494

[17] Barsoukov E, Macdonald J R. *Impedance Spectroscopy: Theory, Experiment, and Applications* (2nd edition). Hoboken, NJ: Wiley-Interscience, 2005.

[18] Guermah S, Djennoune S, Bettayeb M. Discrete-time fractional-order systems: modeling and stability issues. *Advances in Discrete Time Systems*. INTECH Open Access Publisher, 2012.

[19] Guermah S, Djennoune S, Bettayeb M. Controllability and observability of linear discrete-time fractional-order systems. *International Journal of Applied Mathematics and Computer Science*, 2008, **18**(2): 213−222

[20] Victor S, Malti R, Garnier H, Oustaloup A. Parameter and differentiation order estimation in fractional models. *Automatica*, 2013, **49**(4): 926−935

[21] Sierociuk D, Dzieliński A. Fractional Kalman filter algorithm for the states, parameters and order of fractional system estimation. *International Journal of Applied Mathematics and Computer Science*, 2006, **16**(1): 129−140

Yan Ma received the B. S. degree in the Automatica Department from Harbin Engineering University, China, in 1992, M. S. and Ph. D. degrees in the Department of Control Science and Engineering from Jilin University, China, in 1995 and 2006. In 1995, she joined former Jilin University of Technology. She has been a post doctor at Poly University, Hong Kong. Since 2009, she has been a professor at Jilin University. Her current research interests include nonlinear estimation methods and applications in power management system of EV, and robust filter methods.

Xiuwen Zhou graduated from Jilin University, China, in 2013. She is currently a master student in the Department of Control Science and Engineering, Jilin University, China. Her research interests include battery management system of EV.

Bingsi Li graduated from Jilin University, China, in 2014. She is currently a master student in the Department of Control Science and Engineering, Jilin University, China. Her research interests include battery management system of EV.

Hong Chen received the B. S. and M. S. degrees in process control from Zhejiang University, China, in 1983 and 1986, respectively, and Ph. D. degree from the University of Stuttgart, Germany, in 1997. In 1986, she joined Jilin University of Technology, China. From 1993 to 1997, she was a "Wissenschaftlicher Mitarbeiter" at the Institut Fuer Systemdynamik und Regelungstechnik, University of Stuttgart. Since 1999, she has been a professor at Jilin University, where she serves currently as Tang Aoqing Professor. Her current research interests include model predictive control, optimal and robust control, nonlinear control and applications in process engineering and mechatronic systems. Corresponding author of this paper.

Fractional Modeling and Analysis of Coupled MR Damping System

Bingsan Chen, Chunyu Li, Benjamin Wilson, and Yijian Huang

***Abstract*—The coupled magnetorheological (MR) damping system addressed in this paper contains rubber spring and magnetorheological damper. The device inherits the damping merits of both the rubber spring and the magnetorheological damper. Here a fractional-order constitutive equation is introduced to study the viscoelasticity of the combined damper. An introduction to the definitions of fractional calculus, and the transfer function representation of a fractional-order system are given. The fractional-order system model of a magnetorheological vibration platform is set up using fractional calculus, and the function of displacement is presented. It is indicated that the fractional-order constitutive equation and the transfer function are feasible and effective means for investigating of magnetorheological vibration device.**

***Index Terms*—Fractional calculus, magnetorheological (MR) fluid, fractional-order constitutive equation, fractional-order system, system modeling.**

I. INTRODUCTION

MAGNETORHEOLOGICAL (MR) fluids are particulate suspensions whose rheological properties are dramatically altered by magnetic fields. In shear flow, an applied magnetic field can increase the apparent viscosity by several orders of magnitude. This phenomenon is currently being exploited in commercial applications.

MR dampers are a new research development in the field of semi-active control. The mechanical model of an MR fluid is a key way to reach the ideal control effect of the device. In fact, the mechanical properties of MR fluids and their dampers are also influenced by many factors including the vibration displacement, the acceleration, the vibration frequency among other factors. The dynamics of an MR damper can be described through both theoretical and empirical relationships. Stanway[1−2] established a rational mechanics model based on MR fluids viscosity. The Stanway model contains Coulomb friction and viscous damping, but the elastic characteristic of the MR fluids is not included; Zhou and Qu[3] modified the Bingham model based on a constitutive relation for MR fluids, the precise calculation of mechanical characteristics is given, but the model is inconvenient due to its many parameters; Gamota and Filisko[4] also proposed a similar viscoelastic-plastic mechanical model.

In this paper, the viscoelastic model of the MR damper is established by fractional calculus. As the physical meaning of fractional calculus is not clear, not achieving its genetic characteristics and infinite memory function, so its practical engineering application is latter than the integer order calculus, although they were present almost at the same time. Fractional calculus has been introduced into rheology by Slonimsky[5] and Friedrich[6], et al., to study the nonlinear constitutive relation. Considerable progress has been made in using fractional calculus to study nonlinear viscoelasticity. Bagley and Torvik[7] used fractional calculus to study the three- dimensional constitutive relation as well as find limits of the model parameters caused by the thermodynamic effects. Paggi et al.[8] modeled the thermoviscoelastic rheological behavior of ethylene vinyl acetate (EVA) to assess the deformation and the stress state of photovoltaic (PV) modules and their durability; Jóźwiak et al.[9] studied the dynamic behavior of biopolymer materials with fractional Maxwell and Kelvin-Voigt rheological models. Fractional calculus has been a breakthrough in the theory and application of the constitutive equation, and emerged as a new principle and method for the constitutive equation of viscoelastic materials. Therefore, the constitutive equation applying fractional calculus theory of viscoelastic materials is always one key research field.

In this paper, the fractional calculus is introduced to explore the viscoelastic properties of the composite MR-rubber damper, and the mechanical properties of the composite are also studied. The dynamic characteristics of the composite damper are verified by experiments, which provide the practical basis for verification of the theoretical results on MR shock absorber.

II. MODEL ESTABLISHMENT

A. Fractional Order Model

The fractional order derivative rheological model is based on the spring, dashpot and friction element.

Manuscript received September 21, 2015; accepted February 1, 2016. This work was supported by National Natural Science Foundation of China (51305079), Natural Science Foundation of Fijian Province (2015J01180), Outstanding Young Talent Support Program of Fijian Provincial Education Department (JA14208, JA14216), and the China Scholarship Council. Recommended by Associate Editor YangQuan Chen.

Citation: Bingsan Chen, Chunyu Li, Benjamin Wilson, Yijian Huang. Fractional modeling and analysis of coupled MR damping system. *IEEE/CAA Journal of Automatica Sinica*, 2016, **3**(3): 288−294

Bingsan Chen is with the School of Mechanical and Automotive Engineering, Fujian University of Technology, Fuzhou 350118, China and the Department of Chemical and Biological Engineering, University of Wisconsin, Madison, WI 53705, USA (e-mail: bschen126@163.com).

Chunyu Li and Yijian Huang are with the School of Mechanical and Automotive Engineering, Fujian University of Technology, Fuzhou 350118, China (e-mail: chunyuli_0023@163.com; yjhuang@hqu.edu.cn).

Benjamin Wilson is with the Department of Chemical and Biological Engineering, University of Wisconsin, Madison, WI 53705, USA (e-mail: wilsonbt1@gmail.com).

Color versions of one or more of the figures in this paper are available online at http://ieeexplore.ieee.org.

As shown in Fig. 1 (a), for $a = 0$, the model is a typical Hook theorem, given by (1).

$$\sigma(t) = \tau^0 E D_t^0 \varepsilon(t), \tag{1}$$

where $\sigma(t)$ represents applied stress, E is the elastic modulus, $D_t^0\varepsilon(t)$ is the 0 order time derivative with respect to t of the strain $\varepsilon(t)$.

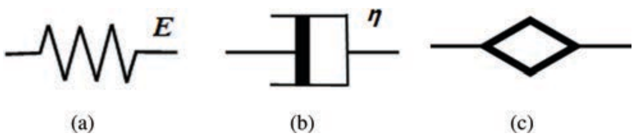

Fig. 1. Elastic coefficient and viscosity: (a) Hookinan spring, $a = 0$; (b) Newtonian dashpot, $a = 1$; (c) Abel sticky pot, $0 < a < 1$.

When $a = 1$ shown as Fig. 1 (b), the behavior obeys the laws of Newtonian fluid, and the constitutive equation is given by (2).

$$\sigma(t) = \tau^1 \eta D_t^1 \varepsilon(t), \tag{2}$$

where $\tau^1 = \eta/E$ is the relaxation time for the dashpot, η is dynamic viscosity, and E represents the elasticity modulus of the dashpot, and $D_t^1\varepsilon(t)$ is the first time derivative of strain with respect to time t.

In practical application of some materials or devices, the fluid behaves viscoelastically and the mechanical properties exhibit both spring and dashpot characteristics. We can use Fig. 1 (c) to describe the Abel sticky pot.

$$\sigma(t) = \tau^\alpha E D_t^\alpha \varepsilon(t), \tag{3}$$

where $D_t^\alpha\varepsilon(t)$ is the fractional derivative of α order of the strain with respect to time with evidently $0 \le \alpha \le 1$.

B. Definition of Fractional Derivative

The most common definition of Riemann-Liouville (R-L) fractional integral is given by[10]

$$ {}_{a_0}D_t^q f(t) = \frac{1}{\Gamma(n-q)} \frac{\mathrm{d}^n}{\mathrm{d}x^n} \int_{a_0}^t (t-\xi)^{(n-q)-1} f(\xi)\mathrm{d}\xi, \quad n-1 \le q < n, \tag{4}$$

where $\Gamma(\cdot)$ is gamma function, q is a non-integer order, a_0 is the iterative initial value. In addition, the Caputo definition is often adopted in engineering applications, given by the following equation:

$$ {}_a^C D_t^q f(t) = \frac{1}{\Gamma(n-q)} \int_a^t (t-\xi)^{(n-q)-1} f^{(n)}(\xi)\mathrm{d}\xi, \quad n-1 < q \le n, \tag{5}$$

In order to distinguish Caputo definition from R-L fractional calculus definition, we decorate it with the additional apex C. The fractional calculus definitions given by R-L and Caputo are all defined in time domain as a function $f(t)$. The Laplace transformation of the R-L definitions is related to the initial value of the fractional differential and fractional calculus. Although the solutions can be found, a reasonable physical interpretation to these solutions is difficult to understand[6]. The advantage of the Caputo fractional calculus definition is that the physical meaning of the initial value is the same as integer order calculus.

So for an arbitrary real number p, the definition of fractional calculus is given by

$$D_t^p f(t) = \frac{\mathrm{d}^n}{\mathrm{d}t^n}(D_t^{p-n} f(t)), \quad 0 < n - p < 1, \tag{6}$$

Equation (6) can also be simplified to

$$D_t^q f(t) = \frac{\mathrm{d}^q}{\mathrm{d}t^q}. \tag{7}$$

C. Fractional Order Model of MR Damper

In Fig. 2, the shock absorber is composed of an MR damper and a rubber damper, which possesses the advantages of the rubber and the MR damper. The damping force can be adjusted rapidly with little control energy requirement. In view of the structural characteristics of the coupled shock absorber, a typical standard linear solid model is presented, also called the Zener model[10], as shown in Fig. 2 (b). The fractional order Zener model can be obtained by replacing the traditional Newton dashpot with the Abel dashpot. The constitutive relation can be written as[10]:

$$\sigma + \tau^\alpha D^\alpha \sigma(t) = E_2 \tau^\alpha D^\alpha \varepsilon(t) + E_1 \varepsilon(t), \quad 0 \le \alpha < 1, \tag{8}$$

where E_1 is the relaxed modulus, E_2 is the unrelaxed modulus shown in Fig. 2. When a sinusoidal pressure is applied, the storage modulus (E') and loss modulus (E'') can be got from (8)

$$E' = \frac{E_2(\omega\tau)^{2\alpha} + (\omega\tau)^\alpha (E_1+E_2)\cos\left(\alpha\frac{\pi}{2}\right) + E_1}{\left[1+(\omega\tau)^\alpha \cos\left(\alpha\frac{\pi}{2}\right)\right]^2 + \left[(\omega\tau)^\alpha \sin\left(\alpha\frac{\pi}{2}\right)\right]^2}, \tag{9}$$

$$E'' = \frac{(E_2-E_1)(\omega\tau)^\alpha \sin\left(\alpha\frac{\pi}{2}\right)}{\left[1+(\omega\tau)^\alpha \cos\left(\alpha\frac{\pi}{2}\right)\right]^2 + \left[(\omega\tau)^\alpha \sin\left(\alpha\frac{\pi}{2}\right)\right]^2}, \tag{10}$$

where in both (9) and (10), ω is angular frequency (rad/s), $\omega = 2\pi f$, and f is frequency (Hz).

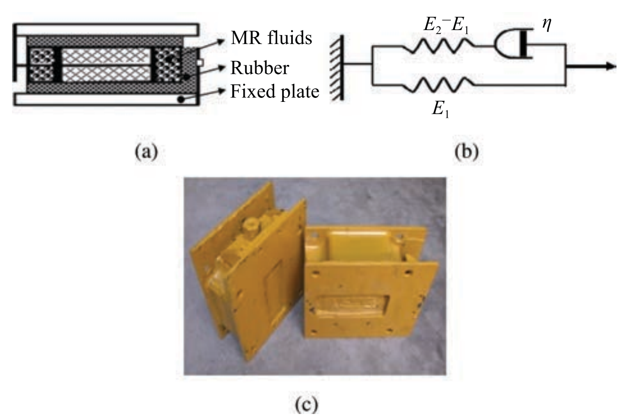

Fig. 2. The principle of the damper and the simplified model: (a) The schematic diagram of the shock absorber; (b) Simplified model; (c) The shock absorber.

Substituting the structure parameters obtained from the coupled shock absorber into the (9) and (10), the storage modulus (E') and loss modulus (E'') can be calculated, shown in Figs. 3 and 4. The storage modulus E' increases as a function of the system frequency, while the loss modulus E'' is nonlinear. Using verified parameters and changing the order of the Abel dashpot from 0.2 to 1, E' and E'' exhibit different characteristics. When the frequency is less than 10 Hz, E' decreases with the increase of the order α. When the frequency is larger than 10 Hz, the law is opposite, showing that the smaller α produces larger elastic properties of the shock absorber. When $0 < \alpha < 1$, the E'' increases with the increase of the order α, showing an increase in the viscous behavior. When $\alpha = 1$, the E'' has a fast drop when the frequency is larger than 10 Hz, when the frequency increases beyond a certain value, the loss modulus is smaller than a small α, as the Fig. 4 showing, the loss modulus in $\alpha = 1$ is smaller than $\alpha = 0.8$ when the frequency is larger than 32 Hz.

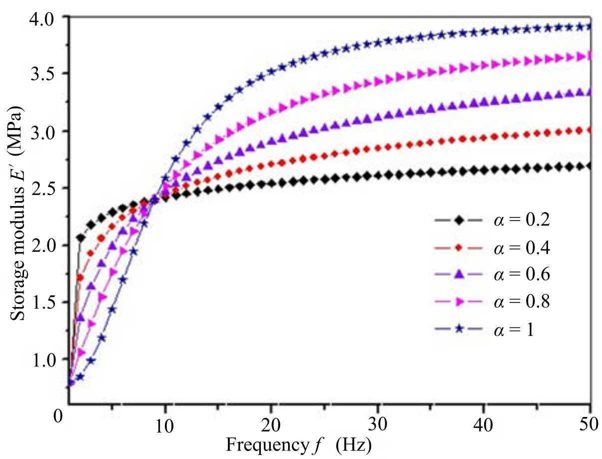

Fig. 3. The storage modulus of Zener model E'.

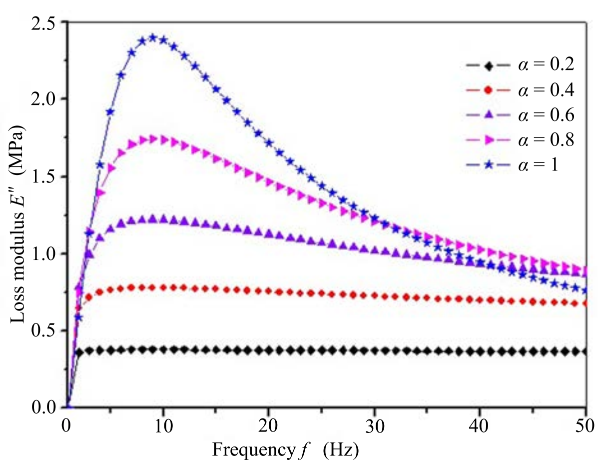

Fig. 4. The loss modulus of Zener model E''.

When the applied magnetic field is manipulated according to the damping part of the coupled MR damper, the viscoelastic properties of the entire shock absorber can be changed dramatically. The magnetic field can be manipulated by changing the current, I, of the system. In Fig. 5, the storage modulus is plotted as a function of frequency for two different values of α. In Fig. 5 (a), as I is increased, the storage modulus asymptote increases. Also as I is increased, the storage modulus approaches the asymptote more rapidly. In Fig. 5 (b) the asymptotic value of each current is larger than the corresponding current in Fig. 5 (a). Similar to Fig. 6 (a), the storage modulus gradually approaches the asymptote as frequency is increased. As I is increased, the storage modulus approaches the asymptote much more rapidly.

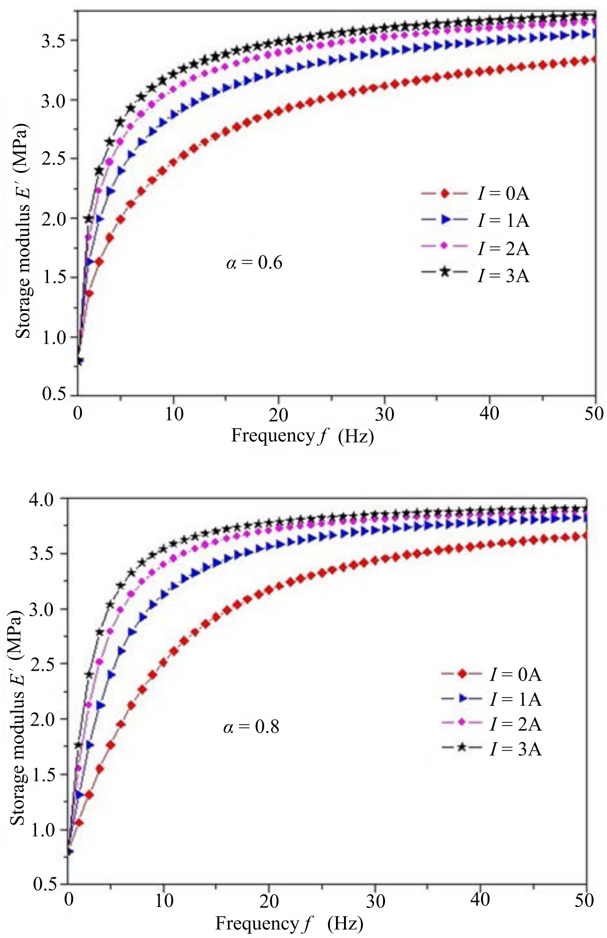

Fig. 5. The storage modulus E' of the Zener model with different currents.

In Fig. 6, the loss modulus is plotted as a function of frequency. In Fig. 6 (a), for $I = 0$, the loss modulus reaches a maximum for $f = 8$. As frequency is increased, the loss modulus gradually decreases. For $I > 0$, the modulus rapidly increases and reaches a maximum value for $f = 4$. The maximums for all values of I are all very similar in magnitude. However, as frequency is increased, larger currents possess a smaller loss modulus. In Fig. 6 (b), for $I = 0$, the maximum in loss modulus occurs at $f = 8$. The loss modulus then gradually decreases. For $I > 0$, the maximum occurs for $f = 4$. Furthermore, the decrease in loss modulus is much more rapid than what we observed in Fig. 6 (a) for $\alpha = 0.6$. In addition, the maximum for all values of I is larger than the maximums observed in Fig. 6 (a). The viscous characteristics of the coupled MR damper are reflected in the low working frequency. At large frequency the viscous performance of the damper is decreased, which is directly related to the working magnetic field.

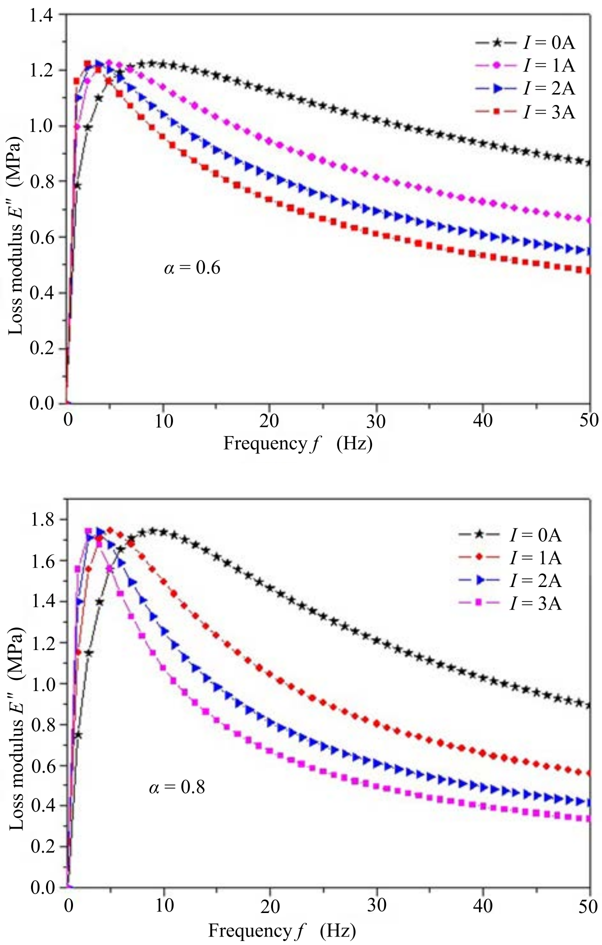

Fig. 6. The loss modulus E'' of the Zener model with different currents.

III. Experimental Platform

From the above analysis, it can be seen that the fractional order model can accurately describe the viscoelasticity of the shock absorber. In order to further the study and analyze the dynamic performance of the damper, equivalent viscous damping is introduced[11]. The equivalent viscous damping is used to replace the complex damping machine.

A. Experiment Platform and Model Analysis

From (8), the resistance, $f(t)$, is provided, and the direction is opposite to the speed of the mass, m. The force applied to the system is $F\sin\omega t$, as shown in Fig. 7 (a), the two-order mode for a single degree of freedom dynamic system is defined as:

$$m\ddot{x}(t)+c\dot{x}(t)+kx(t)=F\sin\omega t, \tag{11}$$

where k is the stiffness of the damper, c is the damping coefficient. Here, some characteristic parameters of the vibration system are introduced: natural frequency of the system $\omega_n = \sqrt{k/m}$, critical damping coefficient $c_c = 2\sqrt{km}$, and the damping factor $\mu = c/c_c$. So (11) can also be written as

$$\ddot{x}(t)+2\mu\omega_n^2\dot{x}(t)+\omega_n^2x(t)=\frac{F\sin\omega t}{m}, \tag{12}$$

and the two order vibration system in fractional order form can be given as:

$$D^2x(t)+2\mu\omega_nD^\beta x(t)+\omega_n^2x(t)=P(t),\quad 0<\beta\leq 1. \tag{13}$$

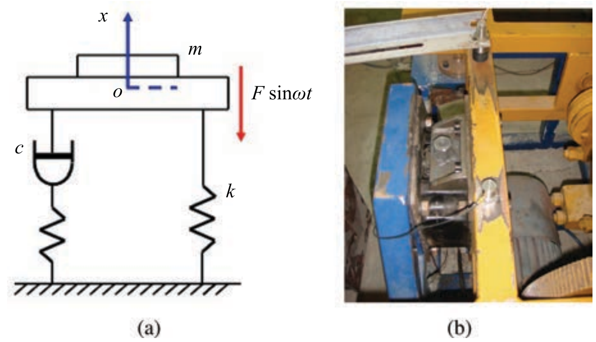

Fig. 7. The simplified model and the real experimental platform: (a) The simplified model of the experimental platform; (b) The real experimental platform.

In order to simplify (13), here $A_1 = \mu\omega_n$, $A_2 = w_n^2$, so (13) can be written as follows:

$$D^2x(t)+A_1D^\beta x(t)+A_2x(t)=F(t). \tag{14}$$

Laplace transform was applied on the fractional differential (14) to get:

$$s^2X(s)+A_1s^\beta X(s)+A_2X(s)=F(s). \tag{15}$$

The Caputo fractional derivative operator can also be used with initial values $x(0^+)=c_0$, $\dot{x}(0^+)=c_1$, this is called the composite fractional vibration equation. The transfer function for the fractional order system can be obtained by using the Laplace transform[12−13]:

$$G(s)=\frac{1}{s^2+\mu^\beta\omega_n^\beta s^\beta+\omega_n^2},\quad 0<\beta<2. \tag{16}$$

For the differential equation (11), the Grünwald-Letnikov (G-L) definition is used to solve the differential equation. The Grünwald-Letnikov method is the direct numerical method for solving fractional calculus.

The G-L definition of fractional calculus is as follows:

$$\begin{aligned}{}_aD_t^{\beta_i}x(t)&=\frac{1}{h^{\beta_i}}\sum_{j=0}^{\frac{t-a}{h}}w_j^{(\beta_i)}x_{t-jh}\\&=\frac{1}{h^{\beta_i}}\left[x_t+\sum_{j=1}^{\frac{t-a}{h}}w_j^{(\beta_i)}x_{t-jh}\right].\end{aligned} \tag{17}$$

In (17), a is the initial value for the numerical calculation, and to meet $0<a<1$, h is the calculation step size, $w_j^{(\beta_i)}$ is the coefficient of a polynomial $(1+z)^{\beta_j}$, which can be derived from the following recursive formula[14]:

$$w_0^{\beta_i}=1,\ w_j^{(\beta_i)}=\left(1-\frac{\beta_i+1}{j}\right)w_{j-1}^{(\beta_i)},\quad j=1,2,\ldots. \tag{18}$$

Equation (18) is substituted into (17), the numerical solution of (17) can be directly derived from differential equation:

$$x_t = \frac{1}{\sum_{i=0}^{n} \frac{a_i}{h^{\beta_i}}} \left[P(t) - \sum_{i=0}^{n} \frac{a_i}{h^{\beta_i}} \sum_{j=1}^{\frac{t-a}{h}} w_j^{(\beta_i)} x_{t-jh} \right], \quad (19)$$

where x_t is the sampled displacement data. $P(t)$ is the controllable input external force, and a_i denotes the iterative value during the process of calculation.

The numerical solution and the analytical solution for the trinomial model (i.e., $\alpha_2 = 2$, $\alpha_1 = \alpha$, $\alpha_0 = 0$) excited by unit step function are shown in Fig. 8. The solutions are calculated based on (15) and by the method of Adomian decomposition, respectively. In Fig. 8, the displacement is plotted as a function of time. From Fig. 8, both the numerical and analytical solutions exhibit similar displacement for all values of time considered. Therefore, the numerical solution of G-L can be applied to engineering analysis. In this paper, the fractional order model and the integer order model are analyzed using the numerical solution.

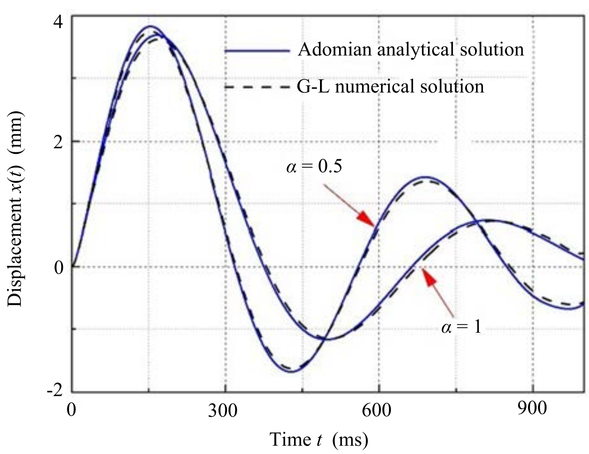

Fig. 8. Adomian decomposition method solution vs G-L definition numerical solution.

B. Measurement and Control Device

The measurement and control system of MR damper is shown in Fig. 7. In the MR damper, the sensor collects the signals of vibration, displacement and acceleration. LabVIEW is used to process, analyze, and display the collected data. Then, based on the specific vibration control requirements and other related parameters (system structure, magnetorheological material characteristics, etc.), the required control current is calculated using the GBIP mode in LabVIEW. Through LabVIEW, the vibrational damping force can be controlled. The changes to the vibrational parameters of the experimental platform can be observed, and the output current can be adjusted to achieve a more desirable vibrational damping effect. The response of the shock absorber is of the order of several tens of milliseconds. A high signal sampling rate is required in order to meet the required vibrational reduction.

The system consists of temperature, acceleration, and displacement sensors, as well as a data acquisition card of virtual instrument system, data acquisition terminal, software system using LabVIEW7.0 version, programmable current source, etc.

IV. Experiment Analysis

The dynamic characteristics in the MR fluids are considered with changing mass percent of carbonyl iron. In Figs. 9 and 10, the mass percentages of carbonyl considered are 74 % and 78 %. The eccentricity is large for vibration frequencies of 10 Hz and 11 Hz. The dynamic parameters of the system model are described in Tables I and II.

TABLE I
$f = 10$ Hz, THE PARAMETERS A_1, A_2, β, $D(e)$ OF THE MODEL IN DIFFERENT WORKING FLUIDS

MRF (%)	I (A)	A_1 (s^{-2})	A_2 (s^{-1})	β	$\sum D(e)$
74	1	28.625	28.723	0.6800	35.624
		20.122	22.980	1	189.356
78	1	42.389	42.436	0.6890	36.234
		38.452	39.015	1	195.236
74	3	58.963	58.967	0.8400	32.149
		51.273	51.519	1	128.265
78	3	64.398	64.386	0.8410	34.572
		59.581	59.815	1	168.426

TABLE II
$f = 11$ Hz, THE PARAMETERS A_1, A_2, β, $D(e)$ OF THE MODEL UNDER DIFFERENT WORKING FLUIDS

MRF (%)	I (A)	A_1 (s^{-2})	A_2 (s^{-1})	β	$\sum D(e)$
74	1	30.058	29.264	0.6800	38.605
		23.612	24.532	1	249.437
78	1	62.424	61.426	0.6950	40.096
		100.000	100.000	1	258.812
74	3	63.912	62.117	0.8400	35.012
		100.000	100.000	1	244.707
78	3	69.046	66.084	0.8430	37.155
		100.000	100.000	1	234.314

1) The order β of fractional order model is related to the vibration damping performance of MR fluids. With the same control current and the nonmagnetic saturation situation, the damping capacity and the model order β increase with the increase of the mass fraction of the carbonyl iron powder. As shown in Fig. 9, at $f = 10$ Hz, $I = 1$ A, the fractional order β increases from 0.68 to 0.689 as mass fraction M increased from 74 % to 78 % accordingly. Similar situation can be seen from Fig. 10, at $f = 11$ Hz, $I = 1$ A, the fractional order β increases from 0.68 to 0.695 as mass fraction M adjusted from 74 % to 78 %. From the results we can find that the order number is changed with the different working fluids.

2) The viscoelastic characteristics of the system with higher iron content is stronger: such as, $f = 10$ Hz, $I = 1$ A, when $M = 74$ %, 78 % respectively, the viscosity coefficients of A_1 are 28.625, 42.389, which shows a significant increase; viscoelastic ratio ξ is respectively 0.9965 and 0.9988, which is also increased weakly, so can also be viewed unchanged.

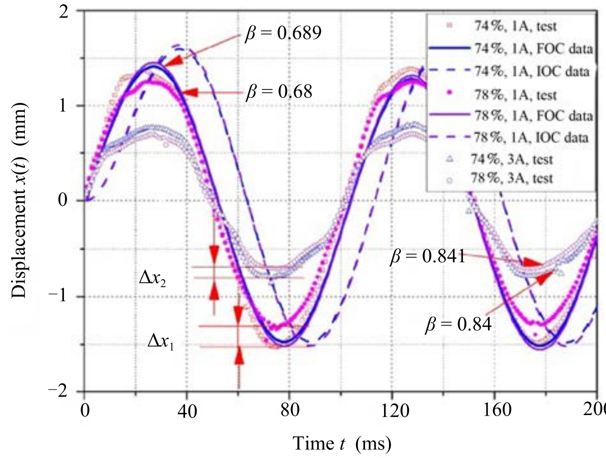

Fig. 9. $f = 10\,\mathrm{Hz}$, the displacements and the fractional order in different working fluids.

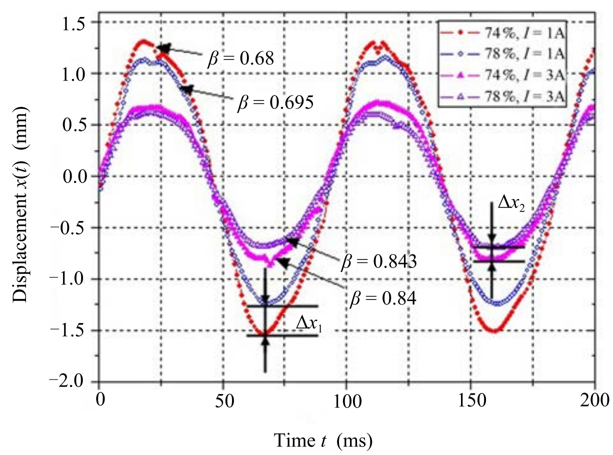

Fig. 10. $f = 11\,\mathrm{Hz}$, the vibration displacements and the fractional order in different working fluids.

3) Δx_1 and Δx_2 represent the variation displacement of the two working fluids in 1 A, 3 A respectively, it can be seen that $\Delta x_1 > \Delta x_2$, and under the working current of 3 A, the changes of MR fluids damping characteristics are reducing.

4) The displacement of the theoretical fractional model and the integer order model are given in Figs. 9 and 10. It can be seen that the fitting curve of fractional order model is more close to the sampled displacement curve than that of the integer order model, and the results are in agreement with the computed results of Tables I and II. Based on the same sampled signal, the residual sum of squares $\sum D(e)$ obtained by fitting the fractional order models is less than that of the integer order models obtained by fitting the integer model, indicating that the fractional order system model is more accurate than the integer order system model.

The effect of working fluids on the vibrational energy of the system is analyzed quantitatively by using the variance analysis. As shown in Table III, taking $I = 1\,\mathrm{A}$ in Fig. 9 for example, σ_1^2 is the variance at $M = 74\,\%$, and σ_2^2 is variance at $M = 78\,\%$, σ_1^2/σ_2^2 denotes the energy coefficient, we can find that the replacement of the working fluids has great influence on the dynamic energy coefficient, whose average value is 1.148, indicating that different MR liquids of the system have certain influence on the system.

TABLE III
$I = 1\,\mathrm{A}$, THE VARIANCE OF THE SAMPLED DATA SEGMENTS WITH DIFFERENT CURRENTS

No.	Sampled data	74 %, $\sigma_1^2\,(\mathrm{mm}^2)$	78 %, $\sigma_2^2\,(\mathrm{mm}^2)$	σ_1^2/σ_2^2
1	6000-6500	0.0313	0.0270	1.159
2	6500-7000	0.0316	0.0267	1.184
3	7000-7500	0.0313	0.0268	1.168
4	7500-8000	0.0313	0.0274	1.142
5	8000-8500	0.0308	0.0277	1.112
6	8500-9000	0.0306	0.0270	1.133
7	9000-9500	0.0307	0.0269	1.141
Average value				8.039/7 = 1.148

V. Conclusions

The above analysis shows the mechanical properties of the coupled MR damper using viscous and elastic characteristics, presenting the properties of an elastic solid and a viscous fluid, and through the experiment, we have shown that:

1) the constitutive equation with fractional derivative method is derived from a strict formula, which has definite physical meaning;

2) the viscoelastic constitutive equation with the fractional derivative can be used to describe the mechanical vibration performance of the coupled MR damper with great accuracy than the integer order model;

3) the dynamic characteristics of the system are related to the order number of the fractional order model: under the same operating frequency, with the increase of the control current, the order of the fractional model is increased, and the viscoelastic properties of the shock absorber are enhanced.

References

[1] Stanway R, Sproston J L, Stevens N G. Non-linear modelling of an electro-rheological vibration damper. *Journal of Electrostatics*, 1987, **20**(2): 167−184

[2] Spencer B F Jr, Dyke S J, Sain M K, Carlson J D. Phenomenological model for magnetorheological damper. *Journal of Engineering Mechanics*, 1997, **123**(3): 230−238

[3] Zhou Qiang, Qu Wei-Lian. Two mechanic models for magnetorheological damper and corresponding test verification. *Earthquake Engineering and Engineering Vibration*, 2002, **22**(4): 144−150 (in Chinese)

[4] Gamota D R, Filisko F E. Dynamic mechanical studies of electrorheological materials: moderate frequencies. *Journal of Rheology*, 1991, **35**(3): 399−425

[5] Slonimsky G L. Laws of mechanical relaxation processes in polymers. *Journal of Polymer Science Part C: Polymer Symposia* , 1967, **16**(3): 1667−1672

[6] Friedrich C. Relaxation and retardation functions of the maxwell model with fractional derivatives. *Rheologica Acta*, 1991, **30**(2): 151−158

[7] Bagley R L, Torvik P J. On the fractional calculus model of viscoelastic behavior. *Journal of Rheology*, 1986, **30**(1): 133−155

[8] Paggi M, Sapora A. An accurate thermoviscoelastic rheological model for ethylene vinyl acetate based on fractional calculus. *International Journal of Photoenergy*, 2015, **2015**: Article ID 252740

[9] Jóźwiak B, Orczykowska M, Dziubiński M. Fractional generalizations of maxwell and kelvin-voigt models for biopolymer characterization. *PLoS One*, 2015, **10**(11): e0143090

[10] Alcoutlabi M, Martinez-Vega J J. Application of fractional calculus to viscoelastic behaviour modelling and to the physical ageing phenomenon in glassy amorphous polymers. *Polymer*, 1998, **39**(25): 6269−6277

[11] Li Zhuo, Xu Bing-Ye. Equivalent viscous damping system for viscoelastic fractional derivative model. *Journal of Tsinghua University (Science and Technology)*, 2000, **40**(11): 27−29 (in Chinese)

[12] Wang Zhen-Bin, Cao Guang-Yi, Zhu Xin-Jian. Application of fractional calculus in system modeling. *Journal of Shanghai Jiaotong University*, 2004, **38**(5): 802−805 (in Chinese)

[13] Wang Zhen-Bin, Cao Guang-Yi. Two system modeling methods using fractional calculus. *Journal of System Simulation*, 2004, **16**(4): 810−812 (in Chinese)

[14] Xue D Y, Chen Y Q. *Solving Applied Mathematical Problems with Matlab*. Boca Raton: CRC Press, 2008.

Bingsan Chen Associate professor at Fujian University of Technology, Fuzhou, China. He received the B. Sc. degree in mechanical engineering from Beihua University, Jilin, China, in 2004. He received the Ph. D. degree in mechanical manufacture from Huaqiao University, Xiamen, China, in 2009. His research interests include smart materials and signal processing of the mechanical system. Corresponding author of this paper.

Chunyu Li Engineer at Fujian University of Technology, Fuzhou, China. She received the B. Sc. degree in mechanical engineering from Beihua University, Jilin, China, in 2004. Her research interests include smart materials and laser cladding.

Benjamin Wilson Research assistant at University of Wisconsin-Madison. He received the B. S. degree from Purdue University in Chemical Engineering, USA. He received the Ph. D. degree in January 2016, also from Purdue University in Chemical Engineering, USA. His research interests include magnetorheological (MR) fluids.

Yijian Huang Professor at Huaqiao University, Xiamen, China. He received the B. Sc. degree in physics from Xiamen University, Xiamen, China, in 1968. He received the M. Sc. degree in fluid drive and control from Zhejiang University, Hangzhou, China, in 1981. His research interests include smart materials and signal processing of the mechanical system.

Parameter Estimation and Topology Identification of Uncertain General Fractional-order Complex Dynamical Networks with Time Delay

Xiaojuan Chen, Jun Zhang, and Tiedong Ma

***Abstract*—Complex networks have attracted much attention from various fields of sciences and engineering in recent years. However, many complex networks have various uncertain information, such as unknown or uncertain system parameters and topological structure, which greatly affects the system dynamics. Thus, the parameter estimation and structure identification problem has theoretical and practical importance for uncertain complex dynamical networks. This paper investigates identification of unknown system parameters and network topologies in uncertain fractional-order complex network with time delays (including coupling delay and node delay). Based on the stability theorem of fractional-order differential system and the adaptive control technique, a novel and general method is proposed to address this challenge. Finally two representative examples are given to verify the effectiveness of the proposed approach.**

***Index Terms*—Complex networks, fractional-order, parameter estimation, structure identification, time delay.**

I. INTRODUCTION

COMPLEX networks widely exist in the world, from Internet to World Wide Web, from communication networks to social network, etc.. All the above networks can be represented in terms of nodes and edges, where edges indicate connections between nodes. Due to the tremendous potentials in real applications, the research of complex networks has become a hot topic in modern scientific research[1−4]. In recent years, synchronization in complex network, as collective behavior, has received increasing attention and been extensively investigated due to its potential applications in many fields, including secure communization, image processing, neural networks, information science, etc.[5−9]. However, there exists much uncertain information in real-world complex networks[10−11], such as the unknown or uncertain topological structure and node dynamics, as it is often difficult to exactly know all system parameters beforehand in many practical applications. Moreover, the uncertainty would greatly affect the modeling, understanding and controlling of the complex networks. Therefore, the issue of network structure and parameter identification is of theoretical and practical importance for uncertain complex dynamical networks. However, due to the nonlinear, complex, and high dimensional nature of the practical complex networks, it is very difficult to exactly identify its topological structure and system parameters by using the traditional approaches. Recently, some researchers have made great effort to address this problem and some valuable results have been obtained[12−14]. Wu[12] proposed an adaptive feedback control method to identify the exact topology of weighted general complex dynamical networks with time delay. Zhou et al.[13] investigated the topology identification of weighted complex dynamical networks. Liu et al.[14] proposed a novel adaptive feedback control approach to simultaneously identify the unknown or uncertain network topological structure and system parameters of uncertain delayed general complex dynamical networks. It is noted that the mentioned references [12−14] mainly contribute to the control or identification of networks with nodes of conventional integer-order dynamics.

On the other hand, the study of complex network with fractional-order dynamic nodes also begins to attract increasing interest among the researchers. It is well known that the fractional calculus is a classical mathematical notion, and is a generalization of ordinary differentiation and integration to arbitrary order[15]. However, the fractional calculus did not attract much attention for a long time due to lack of application background. Nowadays, many known systems can be described by fractional-order systems, such as viscoelastic system, dielectric polarization, electromagnetic waves[16−18]. Compared with the classical integer-order models, fractional-order derivatives provide an excellent instrument for the description of memory and hereditary properties of various materials and processes. Therefore, it may be more accurate to model by fractional-order derivatives than integer-order ones. It is demonstrated that many fractional-order differential systems behave chaotically or hyperchaotically, such as the fractional-order Chua circuit[19], the fractional-order Lorenz system[20], the fractional-order chaotic and hyperchaotic Rössler system[21], etc.. Following these findings, synchronization of chaotic fractional-order differential systems becomes a challenging and interesting problem due to the potential applications in secure communication and control processing.

Not surprisingly, a complex network with nodes modeled by fractional-order differential systems has currently been one of the most promising research topics. However, due to the limited theories for the coupled fractional-order dynamical

Manuscript received August 31, 2015; accepted December 3, 2015. This work was supported by the Basic and Frontier Research Project of Chongqing (cstc2013jcyjA70006, cstc2015jcyjA40038). Recommended by Associate Editor Antonio Visioli.

Citation: Xiaojuan Chen, Jun Zhang, Tiedong Ma. Parameter estimation and topology identification of uncertain general fractional-order complex dynamical networks with time delay. *IEEE/CAA Journal of Automatica Sinica*, 2016, **3**(3): 295−303

Xiaojuan Chen is with the Department of Automobile Engineering, Chongqing College of Electronic Engineering, Chongqing 401331, China (e-mail: chenyuhanjuan@outlook.com).

Jun Zhang and Tiedong Ma are with the College of Automation, Chongqing University, Chongqing 400044, China (e-mail: lahmz@outlook.com; tdma@cqu.edu.cn).

systems, the synchronization between fractional-order complex networks is still a challenging research topic. Compared with integer-order complex networks, the fractional-order complex networks related studies are still few[22−29]. For example, Chai et al.[22] investigated synchronization of general fractional-order complex dynamical networks by adaptive pinning method. In [23−25], the authors discussed the cluster synchronization in fractional-order complex networks. Wu and Lu[26] investigated outer synchronization between two different fractional-order general complex networks. The above mentioned literatures concentrated on the research of fractional-order network with known system parameters and network structures. So far, there are very few studies on the parameter estimation and topology identification of uncertain fractional-order complex networks.

Time delay is ubiquitous in many physical systems due to the finite switching speed of amplifiers, the finite signal propagation time in biological networks, traffic congestions and so forth. Time delay in the interaction may influence the dynamical behavior of the system. Si et al.[27] has investigated the identification of fractional-order complex network with unknown system parameters and network topologies. Yang and Jiang[28] has discussed the drive-response fractional-order complex dynamical network with uncertainty. Unfortunately, time delay is ignored. Although Ma et al.[29] discussed parameter identification and synchronization problem of fractional-order neural networks with time delays, but only the case of state variables $x \in \mathbf{R}$ is discussed, and the case for state vector $x \in \mathbf{R}^n$ has not been investigated.

Motivated by the above discussion, in this paper, we will study the identification of unknown system parameters and network topologies in uncertain fractional-order complex network with coupling delay and node delay. The paper is organized as follows. In Section II, some fractional-order definitions and lemmas are given. Sections III and VI study the parameter estimation and topology identification method for delayed fractional-order complex networks with different nodes. In Section V, two representative examples are given to demonstrate the effectiveness of the proposed method. Finally, some concluding remarks are given in Section VI.

Throughout this paper, the following notations are used. $\|\cdot\|$ is the Euclidean norm of a vector. A^{T} means the transpose of the matrix A. I_n denotes the identity matrix with dimension n. $\otimes$ represents the Kronecker product of two matrices.

II. PRELIMINARIES AND NOTATIONS

A. The Definition of Fractional Calculus

The fractional-order integer-differential operator is the generalized concept of an integer-order integer-differential operator, which is denoted by a fundamental operator as follows:

$$
{}_aD_t^q = \begin{cases} \dfrac{\mathrm{d}^q}{\mathrm{d}t^q}, & R(q) > 0, \\ 1, & R(q) = 0, \\ \int_a^t (\mathrm{d}\tau)^{-q}, & R(q) < 0, \end{cases} \tag{1}
$$

where q is the fractional-order calculus operator which can be a complex number, a and t are the limits of the operation. The commonly used definitions are Grunwald-Letnikov (GL), Riemann-Liouville (RL), and Caputo (C) definitions. In the rest of this paper, the notation $\dfrac{\mathrm{d}^q}{\mathrm{d}t^q}$ is chosen as the Caputo fractional derivation operator.

Definition 1. The Caputo fractional derivative is defined as follows

$$
D^q x(t) \doteq {}_a^cD_t^q x(t) = \begin{cases} \frac{1}{\Gamma(n-q)} \int_a^t (t-\tau)^{n-q-1} x^{(n)}(\tau)\mathrm{d}\tau, \\ \qquad\qquad\qquad n-1 < q < n, \\ \dfrac{\mathrm{d}^n}{\mathrm{d}t^n} x(t), \qquad\qquad q = n, \end{cases} \tag{2}
$$

where $\Gamma(\cdot)$ is the Gamma function which is defined by $\Gamma(z) = \int_0^\infty \mathrm{e}^{-z} t^{z-1} \mathrm{d}t$.

It should be noted that the advantage of the Caputo approach is that the initial conditions for fractional differential equations with Caputo derivatives take on the same form as those for integer-order ones, which have well understood physical meaning. Therefore, in the rest of this paper, the notation $\dfrac{\mathrm{d}^q}{\mathrm{d}t^q}$ is chosen as the Caputo fractional derivation operator.

B. Mathematical Preliminaries

Consider uncertain dynamical systems

$$
D^q x_i(t) = \bar{f}_i(t, x_i(t), \alpha_i), \tag{3}
$$

or rewrite systems (3) in the following form:

$$
D^q x_i(t) = f_i(t, x_i(t)) + F_i(t, x_i(t))\alpha_i, \tag{4}
$$

where $x_i(t) \in \mathbf{R}^n$ are state vectors, $\alpha_i \in \mathbf{R}^{m_i}$ are unknown system parameter vectors for $i = 1, 2, \ldots, N$, in which m_i are positive integers. $f_i(t, x_i(t)) \in \mathbf{R}^n$ is a continuous vector function and $F_i(t, x_i(t)) \in \mathbf{R}^{n \times m_i}$ is a continuous matrix function.

Assumption 1 (A1). Suppose that there exist positive constants L_i such that

$$
\left\|\bar{f}_i(t, x(t), \alpha_i) - \bar{f}_i(t, y(t), \alpha_i)\right\| \le L_i \|x(t) - y(t)\|, \tag{5}
$$

where $x(t), y(t) \in \mathbf{R}^n$ are time-varying vectors, and α_i is the parameter vector of function $\bar{f}_i(\cdot)$.

Assumption 2 (A2). Denote $F_i(t, x_i(t)) = (F_i^{(1)}(t, x_i(t)), F_i^{(2)}(t, x_i(t)), \ldots, F_i^{(m_i)}(t, x_i(t)))$. Suppose that $F_i^{(j)}(t, x_i(t)) \in \mathbf{R}^n$ for $j = 1, 2, \ldots, m_i$, and $\{\{F_i^{(j)}(t, x_i(t))\}_{j=1}^{m_i}, \{Ax_j(t-\tau)\}_{j=1}^N\}$ are linearly independent on the orbit $\{x_i(t), x_i(t-\tau)\}_{i=1}^N$ of synchronization manifold.

If time delay τ is considered, similar to (3) and (4), we can get the following delayed uncertain dynamical systems:

$$
D^q x_i(t) = \bar{g}_i(t, x_i(t), x_i(t-\tau), \beta_i), \quad i = 1, 2, \ldots, N, \tag{6}
$$

or

$$
\begin{aligned} D^q x_i(t) &= \bar{g}_i(t, x_i(t), x_i(t-\tau), \beta_i) \\ &= g_i(t, x_i(t), x_i(t-\tau)) \\ &\quad + G_i(t, x_i(t), x_i(t-\tau))\beta_i, \end{aligned} \tag{7}
$$

where $x_i(t)$, $x_i(t-\tau) \in \mathbf{R}^n$ are the state vectors, $\beta_i \in \mathbf{R}^{q_i}$ are the unknown parameter vector. $g_i(t, x_i(t), x_i(t-\tau)) \in \mathbf{R}^n$ is a continuous vector function and $G_i(t, x_i(t), x_i(t-\tau)) \in \mathbf{R}^{n \times q_i}$ is a continuous matrix function.

Assumption 3 (A3). Assume that there exists a nonnegative constant M satisfying

$$\|\bar{g}_i(t,x(t),x(t-\tau),\beta_i)-\bar{g}_i(t,y(t),y(t-\tau),\beta_i)\| \leq \sqrt{M}\left(\|x(t)-y(t)\|^2+\|x(t-\tau)-y(t-\tau)\|^2\right)^{\frac{1}{2}}. \tag{8}$$

Assumption 4 (A4). Denote $G_i(t,x_i(t),x_i(t-\tau)) = (G_i^{(1)}(t,x_i(t),x_i(t-\tau)), G_i^{(2)}(t,x_i(t),x_i(t-\tau)), \cdots, G_i^{(q_i)}(t, x_i(t), x_i(t-\tau)))$. Assume that $G_i^{(j)}(t,x_i(t),x_i(t-\tau)) \in \mathbf{R}^n$ for $j=1,2,\cdots,q_i$, and $\{\{G_i^{(j)}(t,x_i(t),x_i(t-\tau))\}_{j=1}^{q_i}, \{Ax_j(t)\}_{j=1}^N\}$ are linearly independent on the orbit $\{x_i(t), x_i(t-\tau)\}_{j=1}^N$ of synchronization manifold.

Lemma 1[30]**.** Consider a delayed fractional order system:

$$D^q x(t) = f(x(t),x(t-\tau)), \tag{9}$$

where fractional order $0<q\leq 1$, $x(t)=(x_1,x_2,\dots,x_n)^{\rm T}\in\mathbf{R}^n$ is the state vector. $f(x(t),x(t-\tau)) = (f_1(x(t),x(t-\tau_1)), f_2(x(t),x(t-\tau_2)),\dots,f_n(x(t),x(t-\tau_n)))^{\rm T}$ is nonlinear vector function satisfying Lipschitz condition and the delay time $\tau=(\tau_1,\tau_2,\dots,\tau_n)^{\rm T}\in\mathbf{R}^n$. If there exist a positive definite matrix P and a semi positive definite matrix Q such that

$$x^{\rm T}(t)PD^q x(t) + x^{\rm T}(t)Qx(t) - x^{\rm T}(t-\tau)Qx(t-\tau)\leq 0, \tag{10}$$

then the delayed fractional system (9) is Lyapunov stable.

Lemma 2[26]**.** For any vector x, $y\in\mathbf{R}^n$, the inequality $2x^{\rm T}y\leq x^{\rm T}x+y^{\rm T}y$ holds.

III. Structure Identification of Uncertain General Fractional-Order Complex Dynamical Networks with Coupling Delay

Consider a complex dynamical network with time-varying coupling delay and N different nodes, which is described by

$$D^q x_i(t) = \bar{f}_i(t,x_i(t),\alpha_i) + \sum_{j=1}^N c_{ij}Ax_j(t-\tau), \tag{11}$$

or it can be rewritten in the following form:

$$D^q x_i(t) = f_i(t,x_i(t)) + F_i(t,x_i(t))\alpha_i + \sum_{j=1}^N c_{ij}Ax_j(t-\tau), \tag{12}$$

where $x_i(t)=(x_{i1}(t),x_{i2}(t),\dots,x_{in}(t))^{\rm T}\in\mathbf{R}^n$ is the state vector of the ith node, $i=1,\dots,N$, τ is the constant time delay. $C=(c_{ij})_{N\times N}\in\mathbf{R}^{N\times N}$ is an unknown or uncertain coupling configuration matrix, and c_{ij} is the weight or coupling strength. If there exists a link from nodes i to j ($j\neq i$), then $c_{ij}\neq 0$, otherwise, $c_{ij}=0$. $A\in\mathbf{R}^{n\times n}$ is an inner-coupling matrix which determines the interaction variables.

Hereafter, the coupling configuration matrix C need not be symmetric, irreducible, or diffusive. Of course, it is necessary to ensure the boundedness of complex dynamical networks in this paper. The main goal is to identify these unknown or uncertain coupling strengths, namely the network topological structure, and all unknown system parameter vectors α_i of the complex dynamical networks.

Consider another complex dynamical network which will be referred to as the response network with coupling delay as follows:

$$D^q\hat{x}_i(t) = f_i(t,\hat{x}_i(t)) + F_i(t,\hat{x}_i(t))\hat{\alpha}_i + \sum_{j=1}^N \hat{c}_{ij}A\hat{x}_j(t-\tau)+u_i, \tag{13}$$

where $\hat{x}_i(t)=(\hat{x}_{i1}(t),\hat{x}_{i2}(t),\dots,\hat{x}_{in}(t))^{\rm T}\in\mathbf{R}^n$ is the response state vector of the i-th node, $u_i\in\mathbf{R}^n$ is its controller, $\hat{c}_{ij}$ is the estimated value of weight c_{ij}, and vector $\hat{\alpha}_i$ is the estimated value of the unknown parameter vector α_i.

Denote $\tilde{x}_i=\hat{x}_i-x_i$, $\tilde{c}_{ij}=\hat{c}_{ij}-c_{ij}$, $\tilde{\alpha}_i=\hat{\alpha}_i-\alpha_i$. The systems (12) and (13) achieve synchronization if $\tilde{x}_i\to 0$ as $t\to\infty$. Then the error system is given by

$$\begin{aligned}\tilde{x}_i(t) = {} & f_i(t,\hat{x}_i(t))+F_i(t,\hat{x}_i(t))\hat{\alpha}_i - f_i(t,x_i(t)) \\ & - F_i(t,x_i(t))\alpha_i + \sum_{j=1}^N \hat{c}_{ij}A\hat{x}_j(t-\tau) \\ & - \sum_{j=1}^N c_{ij}Ax_j(t-\tau)+u_i.\end{aligned} \tag{14}$$

That is,

$$\begin{aligned}D^q\tilde{x}_i(t) = {} & \bar{f}_i(t,\hat{x}_i(t),\alpha_i) - \bar{f}_i(t,x_i(t),\alpha_i) \\ & + F_i(t,\hat{x}_i(t))\tilde{\alpha}_i + \sum_{j=1}^N \tilde{c}_{ij}A\hat{x}_j(t-\tau) \\ & - \sum_{j=1}^N c_{ij}A\tilde{x}_j(t-\tau)+u_i.\end{aligned} \tag{15}$$

Theorem 1. Suppose that Assumptions A1 and A2 hold. Then the uncertain coupling configuration matrix C and parameter vectors α_i of uncertain general delayed complex dynamical network (12) can be identified by the estimated values $\hat{C}$ and $\hat{\alpha}_i$ via the response network

$$\begin{cases} D^q\hat{x}_i = f_i(t,\hat{x}_i(t)) + F_i(t,\hat{x}_i(t))\hat{\alpha}_i \\ \qquad + \sum\limits_{j=1}^N \hat{c}_{ij}A\hat{x}_j(t-\tau)+u_i, \\ u_i = -k_i\tilde{x}_i(t), \\ D^q k_i = d_i\|\tilde{x}_i\|^2, \\ D^q\hat{\alpha}_i = -F_i^{\rm T}(t,\hat{x}_i(t))\tilde{x}_i(t), \\ D^q\hat{c}_{ij} = -\delta_{ij}\tilde{x}_i(t)^{\rm T}A\hat{x}_j(t-\tau), \end{cases} \tag{16}$$

where i, $j\in\{1,2,\dots,N\}$ and d_i, δ_{ij} are any positive constants.

Proof. Denote $\tilde{k}_i=k_i-k_i^*$, and k_i^* is a positive constant. Further denote $X=(\tilde{X}^{\rm T},\tilde{\alpha}^{\rm T},\tilde{c}^{\rm T},\tilde{k}^{\rm T})^{\rm T}$, where

$$\begin{cases} \tilde{X} = \left(\tilde{x}_1^{\rm T},\tilde{x}_2^{\rm T},\dots,\tilde{x}_N^{\rm T}\right)^{\rm T}, \quad \tilde{x}_i=(\tilde{x}_{i1},\tilde{x}_{i2},\dots,\tilde{x}_{in})^{\rm T}, \\ \tilde{\alpha} = \left(\tilde{\alpha}_1^{\rm T},\tilde{\alpha}_2^{\rm T},\dots,\tilde{\alpha}_N^{\rm T}\right)^{\rm T}, \quad \tilde{\alpha}_i=(\tilde{\alpha}_{i1},\tilde{\alpha}_{i2},\dots,\tilde{\alpha}_{im_i})^{\rm T}, \\ \tilde{c} = \left(\tilde{c}_1^{\rm T},\tilde{c}_2^{\rm T},\dots,\tilde{c}_N^{\rm T}\right)^{\rm T}, \quad \tilde{c}_i=(\tilde{c}_{i1},\tilde{c}_{i2},\dots,\tilde{c}_{iN})^{\rm T}, \\ \tilde{k} = \left(\tilde{k}_1,\tilde{k}_2,\dots,\tilde{k}_N\right)^{\rm T}. \end{cases} \tag{17}$$

Choose the real symmetric positive definite matrix P as

$$P = \mathrm{diag}\left\{ \underbrace{1,\ldots,1}_{nN+\sum_{i=1}^{N} m_i}, \frac{1}{\delta_{11}},\ldots,\frac{1}{\delta_{NN}},\frac{1}{d_1},\ldots,\frac{1}{d_N} \right\}, \quad (18)$$

$$Q = \mathrm{diag}\left\{ \underbrace{1,\ldots,1}_{nN}, \underbrace{0,\ldots,0}_{\sum_{i=1}^{N} m_i+N^2+N} \right\}. \quad (19)$$

Then we have

$$\begin{aligned}
J =& X^{\mathrm{T}}(t)PD^qX(t) + X^{\mathrm{T}}(t)QX(t) \\
&- X^{\mathrm{T}}(t-\tau)QX(t-\tau) \\
=& \sum_{i=1}^{N} \tilde{x}_i^{\mathrm{T}}(t)D^q\tilde{x}_i(t) + \sum_{i=1}^{N}\tilde{\alpha}_i^{\mathrm{T}}D^q\tilde{\alpha}_i \\
&+ \sum_{i=1}^{N}\sum_{j=1}^{N}\frac{1}{\delta_{ij}}\tilde{c}_{ij}D^q\tilde{c}_{ij} + \sum_{i=1}^{N}\frac{1}{d_i}\tilde{k}_iD^q\tilde{k}_i \\
&+ \sum_{i=1}^{N}\tilde{x}_i^{\mathrm{T}}(t)\tilde{x}_i(t) - \sum_{i=1}^{N}\tilde{x}_i^{\mathrm{T}}(t-\tau)\tilde{x}_i(t-\tau) \\
=& \sum_{i=1}^{N}\tilde{x}_i^{\mathrm{T}}(t)\left\{\bar{f}_i(t,\hat{x}_i(t),\alpha_i) - \bar{f}_i(t,x_i(t),\alpha_i)\right\} \\
&+ \sum_{i=1}^{N}\tilde{x}_i^{\mathrm{T}}(t)F_i(t,\hat{x}_i(t))\tilde{\alpha}_i \\
&+ \sum_{i=1}^{N}\sum_{j=1}^{N}c_{ij}\tilde{x}_i^{\mathrm{T}}(t)A\tilde{x}_j(t-\tau) - \sum_{i=1}^{N}k_i\|\tilde{x}_i(t)\|^2 \\
&+ \sum_{i=1}^{N}\sum_{j=1}^{N}\tilde{c}_{ij}\tilde{x}_i^{\mathrm{T}}(t)A\hat{x}_j(t-\tau) \\
&+ \sum_{i=1}^{N}\tilde{\alpha}_i^{\mathrm{T}}D^q\tilde{\alpha}_i + \sum_{i=1}^{N}\sum_{j=1}^{N}\frac{1}{\delta_{ij}}\tilde{c}_{ij}D^q\tilde{c}_{ij} \\
&+ \sum_{i=1}^{N}(k_i-k^*)\|\tilde{x}_i(t)\|^2 \\
&+ \sum_{i=1}^{N}\tilde{x}_i^{\mathrm{T}}(t)\tilde{x}_i(t) - \sum_{i=1}^{N}\tilde{x}_i^{\mathrm{T}}(t-\tau)\tilde{x}_i(t-\tau) \\
\le& \sum_{i=1}^{N}L_i\tilde{x}_i^{\mathrm{T}}(t)\tilde{x}_i(t) \\
&+ \sum_{i=1}^{N}\tilde{x}_i(t)F_i(t,\hat{x}_i(t))\tilde{\alpha}_i + \sum_{i=1}^{N}\tilde{\alpha}_i^{\mathrm{T}}D^q\tilde{\alpha}_i \\
&+ \sum_{i=1}^{N}\sum_{j=1}^{N}\tilde{c}_{ij}\tilde{x}_i^{\mathrm{T}}(t)A\hat{x}_j(t-\tau) \\
&+ \sum_{i=1}^{N}\sum_{j=1}^{N}\frac{1}{\delta_{ij}}\tilde{c}_{ij}D^q\tilde{c}_{ij} \\
&+ \sum_{i=1}^{N}\sum_{j=1}^{N}c_{ij}\tilde{x}_i^{\mathrm{T}}(t)A\tilde{x}_j(t-\tau) - \sum_{i=1}^{N}k^*\|\tilde{x}_i(t)\|^2 \\
&+ \sum_{i=1}^{N}\tilde{x}_i^{\mathrm{T}}(t)\tilde{x}_i(t) - \sum_{i=1}^{N}\tilde{x}_i^{\mathrm{T}}(t-\tau)\tilde{x}_i(t-\tau) \\
\le& \sum_{i=1}^{N}\tilde{x}_i^{\mathrm{T}}(t)\tilde{x}_i(t) + \sum_{i=1}^{N}\sum_{j=1}^{N}c_{ij}\tilde{x}_i(t)A\tilde{x}_j(t-\tau) \\
&- \sum_{i=1}^{N}k^*\|\tilde{x}_i(t)\|^2 + \sum_{i=1}^{N}\tilde{x}_i^{\mathrm{T}}(t)\tilde{x}_i(t) \\
&- \sum_{i=1}^{N}\tilde{x}_i^{\mathrm{T}}(t-\tau)\tilde{x}_i(t-\tau), \\
\le& L\tilde{X}^{\mathrm{T}}(t)\tilde{X}(t) + \tilde{X}^{\mathrm{T}}(t)(C\otimes A)\tilde{X}(t-\tau) \\
&- k^*\tilde{X}^{\mathrm{T}}(t)\tilde{X}(t) + \tilde{X}^{\mathrm{T}}(t)\tilde{X}(t) \\
&- \tilde{X}^{\mathrm{T}}(t-\tau)\tilde{X}(t-\tau) \\
\le& L\tilde{X}^{\mathrm{T}}(t)\tilde{X}(t) + \frac{1}{2}\tilde{X}^{\mathrm{T}}(t)(CC^{\mathrm{T}}\otimes AA^{\mathrm{T}})\tilde{X}(t) \\
&+ \frac{1}{2}\tilde{X}^{\mathrm{T}}(t-\tau)\tilde{X}(t-\tau) - k^*\tilde{X}^{\mathrm{T}}(t)\tilde{X}(t) \\
&+ \tilde{X}^{\mathrm{T}}(t)\tilde{X}(t) - \tilde{X}^{\mathrm{T}}(t-\tau)\tilde{X}(t-\tau) \\
=& \left(L - k^* + 1 + \frac{1}{2}\lambda_{\max}(CC^{\mathrm{T}}\otimes AA^{\mathrm{T}})\right)\tilde{X}^{\mathrm{T}}(t)\tilde{X}(t) \\
&- \frac{1}{2}\tilde{X}^{\mathrm{T}}(t-\tau)\tilde{X}(t-\tau),
\end{aligned} \quad (20)$$

where $L = \max\{L_i | 1 \le i \le N.\}$. Lemma 2 is used in the last inequality of (20). It is obvious that there exists sufficiently large positive constant k^* such that J is negative definite. Namely, $X^{\mathrm{T}}(t)PD^qX(t)+X^{\mathrm{T}}(t)QX(t)-X^{\mathrm{T}}(t-\tau)QX(t-\tau) \le 0$ holds, which implies the Lyapunov stability of error system (14) or (15) by Lemma 1. □

Remark 1. It should be especially pointed out that the coupling configuration matrix C need not be symmetric, irreducible, even diffusive.

Remark 2. The positive constants δ_{ij}, d_i in the updating laws D^qk_i and $D^q\hat{c}_{ij}$ can control the convergence speed of the synchronization and identification.

Remark 3. Assumption A2 is a very essential condition for guaranteeing the success of identification. Without this condition, it may cause false identification result. Similarly, Assumption A4 guarantees the identification of the next section.

IV. Structure Identification of an Uncertain General Complex Dynamical Network with Node Delay

Consider an uncertain general complex dynamical network consisting of N different nodes with time delay τ, called the drive network, which is described by

$$D^qx_i(t) = \bar{g}_i(t,x_i(t),x_i(t-\tau),\beta_i) + \sum_{j=1}^{N}c_{ij}Ax_j(t), \quad (21)$$

where the node dynamics can be rewritten as follows

$$\begin{aligned}&\bar{g}_i\left(t, x_i(t), x_i\left(t-\tau\right), \beta_i\right)\\&\quad= g_i\left(t, x_i\left(t\right), x_i\left(t-\tau\right)\right) + G_i\left(t, x_i\left(t\right), x_i\left(t-\tau\right)\right)\beta_i,\end{aligned} \tag{22}$$

and β_i $(i=1,2,\ldots,N)$ are unknown or uncertain system parameter vectors.

Construct another controlled general fractional-order complex network, called response network, which is given by

$$D^q\hat{x}_i = \bar{g}_i\left(t, \hat{x}_i(t), \hat{x}_i\left(t-\tau\right), \hat{\beta}_i\right) + \sum_{j=1}^{N}\hat{c}_{ij}A\hat{x}_j(t) + u_i, \tag{23}$$

where $\hat{x}_i(t) = (\hat{x}_{i1}(t), \hat{x}_{i2}(t), \ldots, \hat{x}_{in}(t))^{\mathrm{T}} \in \mathbf{R}^n$ is the response state vector of the i-th node, $u_i \in \mathbf{R}^n$ is its control input, $\hat{c}_{ij}$ and $\hat{\beta}_i$ are the estimated values of c_{ij} and β_i, respectively. Denote $\tilde{x}_i = \hat{x}_i - x_i$, $\tilde{c}_{ij} = \hat{c}_{ij} - c_{ij}$, $\tilde{\beta}_i = \hat{\beta}_i - \beta_i$. Thus the error system is described by

$$\begin{aligned}D^q\tilde{x}_i\left(t\right) &= \bar{g}_i\left(t, \hat{x}_i\left(t\right), \hat{x}_i\left(t-\tau\right), \beta_i\right)\\&\quad - \bar{g}_i\left(t, x_i\left(t\right), x_i\left(t-\tau\right), \beta_i\right)\\&\quad + G_i\left(t, \hat{x}_i\left(t\right), \hat{x}_i\left(t-\tau\right)\right)\tilde{\beta}_i\\&\quad + \sum_{j=1}^{N}\tilde{c}_{ij}A\hat{x}_j\left(t\right) + \sum_{j=1}^{N}c_{ij}A\tilde{x}_j\left(t\right) + u_i.\end{aligned} \tag{24}$$

Theorem 2. Suppose that Assumptions A3 and A4 hold. Then uncertain coupling configuration matrix C and system parameter vectors β_i can be identified by using the estimated values $\hat{C}$ and $\hat{\beta}_i$ via the response network

$$\begin{cases}D^q\hat{x}_i\left(t\right) = g_i\left(t, \hat{x}_i\left(t\right), \hat{x}_i\left(t-\tau\right)\right)\\\qquad + G_i\left(t, \hat{x}_i\left(t\right), \hat{x}_i\left(t-\tau\right)\right)\hat{\beta}_i + \sum\limits_{j=1}^{N}\hat{c}_{ij}A\hat{x}_j\left(t\right) + u_i,\\u_i = -k_i\tilde{x}_i\left(t\right),\\D^q k_i = d_i\left\|\tilde{x}_i\left(t\right)\right\|^2,\\D^q\hat{\beta}_i = -G_i^{\mathrm{T}}\left(t, \hat{x}_i\left(t\right), \hat{x}_i\left(t-\tau\right)\right)\tilde{x}_i\left(t\right),\\D^q\hat{c}_{ij} = -\delta_{ij}\tilde{x}_i^{\mathrm{T}}\left(t\right)A\hat{x}_j\left(t\right),\end{cases} \tag{25}$$

where i, $j \in \{1, 2, \ldots, N\}$, d_i, δ_{ij} are any positive constants.

Proof. Denote $\tilde{k}_i = k_i - k_i^*$, k_i^* is a positive constant. Further denote $X = (\tilde{X}^{\mathrm{T}}, \tilde{\beta}^{\mathrm{T}}, \tilde{c}^{\mathrm{T}}, \tilde{k}^{\mathrm{T}})^{\mathrm{T}}$, where

$$\begin{cases}\tilde{X} = \left(\tilde{x}_1^{\mathrm{T}}, \tilde{x}_2^{\mathrm{T}}, \ldots, \tilde{x}_N^{\mathrm{T}}\right)^{\mathrm{T}}, & \tilde{x}_i = \left(\tilde{x}_{i1}, \tilde{x}_{i2}, \ldots, \tilde{x}_{in}\right)^{\mathrm{T}},\\\tilde{\beta} = \left(\tilde{\beta}_1^{\mathrm{T}}, \tilde{\beta}_2^{\mathrm{T}}, \ldots, \tilde{\beta}_N^{\mathrm{T}}\right)^{\mathrm{T}}, & \tilde{\beta}_i = \left(\tilde{\beta}_{i1}, \tilde{\beta}_{i2}, \ldots, \tilde{\beta}_{im_i}\right)^{\mathrm{T}},\\\tilde{c} = \left(\tilde{c}_1^{\mathrm{T}}, \tilde{c}_2^{\mathrm{T}}, \ldots, \tilde{c}_N^{\mathrm{T}}\right)^{\mathrm{T}}, & \tilde{c}_i = \left(\tilde{c}_{i1}, \tilde{c}_{i2}, \ldots, \tilde{c}_{iN}\right)^{\mathrm{T}},\\\tilde{k} = \left(\tilde{k}_1, \tilde{k}_2, \ldots, \tilde{k}_N\right)^{\mathrm{T}}.\end{cases} \tag{26}$$

Choose the real symmetric positive definite matrix P as

$$P = \mathrm{diag}\left(\underbrace{1, \ldots, 1}_{nN + \sum_{i=1}^{N} m_i}, \frac{1}{\delta_{11}}, \ldots, \frac{1}{\delta_{NN}}, \frac{1}{d_1}, \ldots, \frac{1}{d_N}\right), \tag{27}$$

$$Q = \mathrm{diag}\left(\underbrace{\frac{M}{2}, \ldots, \frac{M}{2}}_{nN}, \underbrace{0, \ldots, 0}_{\sum_{i=1}^{N} m_i + N^2 + N}\right). \tag{28}$$

Then, we have

$$\begin{aligned}J &= X^{\mathrm{T}}(t)PD^qX(t) + X^{\mathrm{T}}\left(t\right)QX\left(t\right)\\&\quad - X^{\mathrm{T}}\left(t-\tau\right)QX\left(t-\tau\right)\\&= \sum_{i=1}^{N}\tilde{x}_i^{\mathrm{T}}\left(t\right)D^q\tilde{x}_i\left(t\right) + \sum_{i=1}^{N}\tilde{\beta}_i^{\mathrm{T}}D^q\tilde{\beta}_i\\&\quad + \sum_{i=1}^{N}\sum_{j=1}^{N}\frac{1}{\delta_{ij}}\tilde{c}_{ij}D^q\tilde{c}_{ij} + \sum_{i=1}^{N}\frac{1}{d_i}\tilde{k}_iD^qk_i\\&\quad + \sum_{i=1}^{N}\frac{M}{2}\tilde{x}_i^{\mathrm{T}}\left(t\right)\tilde{x}_i\left(t\right) - \sum_{i=1}^{N}\frac{M}{2}\tilde{x}_i^{\mathrm{T}}\left(t-\tau\right)\tilde{x}_i\left(t-\tau\right)\\&= \sum_{i=1}^{N}\tilde{x}_i^{\mathrm{T}}\left(t\right)\left(\bar{g}_i\left(t, \hat{x}_i\left(t\right), \hat{x}_i\left(t-\tau\right), \beta_i\right)\right.\\&\quad - \bar{g}_i\left(t, x_i\left(t\right), x_i\left(t-\tau\right), \beta_i\right)\\&\quad + G_i\left(t, \hat{x}_i\left(t\right), \hat{x}_i\left(t-\tau\right)\right)\tilde{\beta}_i\\&\quad \left.+ \sum_{j=1}^{N}\tilde{c}_{ij}A\hat{x}_j\left(t\right) + \sum_{j=1}^{N}c_{ij}A\tilde{x}_j\left(t\right) - k_i\tilde{x}_i\left(t\right)\right)\\&\quad - \sum_{i=1}^{N}\tilde{\beta}_i^{\mathrm{T}}G_i^{\mathrm{T}}\left(t, \hat{x}_i\left(t\right), \hat{x}_i\left(t-\tau\right)\right)\tilde{x}_i\left(t\right)\\&\quad - \sum_{i=1}^{N}\sum_{j=1}^{N}\tilde{c}_{ij}\tilde{x}_i^{\mathrm{T}}\left(t\right)A\hat{x}_j\left(t\right) + \sum_{i=1}^{N}\left(k_i - k^*\right)\left\|\tilde{x}_i^{\mathrm{T}}\left(t\right)\right\|^2\\&\quad + \sum_{i=1}^{N}\frac{M}{2}\tilde{x}_i^{\mathrm{T}}\left(t\right)\tilde{x}_i\left(t\right) - \sum_{i=1}^{N}\frac{M}{2}\tilde{x}_i^{\mathrm{T}}\left(t-\tau\right)\tilde{x}_i\left(t-\tau\right)\\&= \sum_{i=1}^{N}\tilde{x}_i^{\mathrm{T}}(t)(\bar{g}_i(t, \hat{x}_i(t), \hat{x}_i(t-\tau), \beta_i)\\&\quad - \bar{g}_i(t, x_i(t), x_i(t-\tau), \beta_i))\\&\quad + \sum_{i=1}^{N}\sum_{j=1}^{N}\tilde{x}_i^{\mathrm{T}}\left(t\right)c_{ij}A\tilde{x}_j\left(t\right) - k^*\sum_{j=1}^{N}\left\|\tilde{x}_i\left(t\right)\right\|^2\\&\quad + \sum_{i=1}^{N}\frac{M}{2}\tilde{x}_i^{\mathrm{T}}\left(t\right)\tilde{x}_i\left(t\right) - \sum_{i=1}^{N}\frac{M}{2}\tilde{x}_i^{\mathrm{T}}\left(t-\tau\right)\tilde{x}_i\left(t-\tau\right)\\&\le \frac{1}{2}\sum_{i=1}^{N}\tilde{x}_i^{\mathrm{T}}(t)\tilde{x}_i(t) + \frac{1}{2}\|\bar{g}_i(t, \hat{x}_i(t), \hat{x}_i(t-\tau), \beta_i)\\&\quad - \bar{g}_i(t, x_i(t), x_i(t-\tau), \beta_i)\|^2\\&\quad + \sum_{i=1}^{N}\sum_{j=1}^{N}\tilde{x}_i^{\mathrm{T}}\left(t\right)c_{ij}A\tilde{x}_j\left(t\right) - k^*\sum_{j=1}^{N}\left\|\tilde{x}_i\left(t\right)\right\|^2\\&\quad + \sum_{i=1}^{N}\frac{M}{2}\tilde{x}_i^{\mathrm{T}}\left(t\right)\tilde{x}_i\left(t\right) - \sum_{i=1}^{N}\frac{M}{2}\tilde{x}_i^{\mathrm{T}}\left(t-\tau\right)\tilde{x}_i\left(t-\tau\right)\\&\le \frac{1}{2}\sum_{i=1}^{N}\tilde{x}_i^{\mathrm{T}}\left(t\right)\tilde{x}_i\left(t\right) + \frac{M}{2}\left(\left\|\tilde{x}_i\left(t\right)\right\|^2 + \left\|\tilde{x}_i\left(t-\tau\right)\right\|^2\right)\end{aligned}$$

$$
\begin{aligned}
&+\sum_{i=1}^{N}\sum_{j=1}^{N}\tilde{x}_i^{\mathrm{T}}(t)\,c_{ij}A\tilde{x}_j(t)-k^*\sum_{j=1}^{N}\|\tilde{x}_i(t)\|^2\\
&+\sum_{i=1}^{N}\frac{M}{2}\tilde{x}_i^{\mathrm{T}}(t)\,\tilde{x}_i(t)-\sum_{i=1}^{N}\frac{M}{2}\tilde{x}_i^{\mathrm{T}}(t-\tau)\,\tilde{x}_i(t-\tau)\\
=&\left(\frac{1}{2}+M-k^*\right)\tilde{X}^{\mathrm{T}}(t)\,\tilde{X}(t)+\tilde{X}^{\mathrm{T}}(t)\,(C\otimes A)\,\tilde{X}(t)\\
\le&\left(\frac{1}{2}+M-k^*+\lambda_{\max}(C\otimes A)\right)\tilde{X}^{\mathrm{T}}(t)\tilde{X}(t). \qquad (29)
\end{aligned}
$$

It is obvious that there exists sufficiently large positive constant k^* such that J is negative definite. Namely, $X^{\mathrm{T}}(t)P \times D^qX(t)+X^{\mathrm{T}}(t)QX(t)-X^{\mathrm{T}}(t-\tau)QX(t-\tau)\le 0$ holds, which implies the Lyapunov stability of error system (24) by Lemma 1. □

V. NUMERICAL SIMULATIONS

In this section, two representative examples are given to verify the effectiveness of the proposed parameters estimation and structure identification approaches.

A. Identification with Coupling Time Delay

The well-known Lü system with fractional order derivative is used as the node dynamics in the uncertain network, which is described as

$$D^qx_i(t)=f_i\,(t,x_i\,(t))+F_i\,(t,x_i(t))\,\alpha_i, \qquad (30)$$

where $q=0.9$, $x_i(t)=(x_{i1}(t),x_{i2}(t),x_{i3}(t))^{\mathrm{T}}$ is state vector, $f_i(t,x_i(t)) = (0,-x_{i1}(t)x_{i3}(t),x_{i1}(t)x_{i2}(t))^{\mathrm{T}}$, $F_i(t,x_i(t)) = \mathrm{diag}\{x_{i2}(t)-x_{i1}(t),x_{i2}(t),-x_{i3}(t)\}$, and $\alpha_i=(\alpha_{i1},\alpha_{i2},\alpha_{i3})^{\mathrm{T}}$, $i=1,\ldots,4$. Fig. 1 shows the chaotic attractor of fractional-order Lü system.

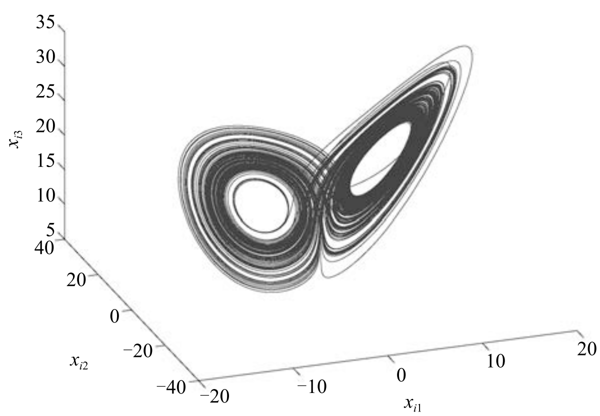

Fig. 1. Chaotic attractor of fractional-order Lü system.

The weight configuration matrix is set as

$$C=\begin{pmatrix}-5&1&4&0\\3&-4&1&0\\0&1&-3&2\\1&3&0&-4\end{pmatrix}. \qquad (31)$$

Let $\alpha_i=(\alpha_{i1},\alpha_{i2},\alpha_{i3})^{\mathrm{T}}=(36,\ 20+i,\ 3)^{\mathrm{T}}$ for $i=1,\ldots,4$. $\tau=0.2$, and networks inner-coupling matrix $A=\mathrm{diag}\{1,\ 1,\ 1\}$.

According to Theorem 1, the coupling configuration matrix C and system parameter vectors α_i of complex networks (12) can be identified by using adaptive control laws (16). Fig. 2 shows the identification of the uncertain system parameters, while Fig. 3 illustrates the identification of the unknown network topology.

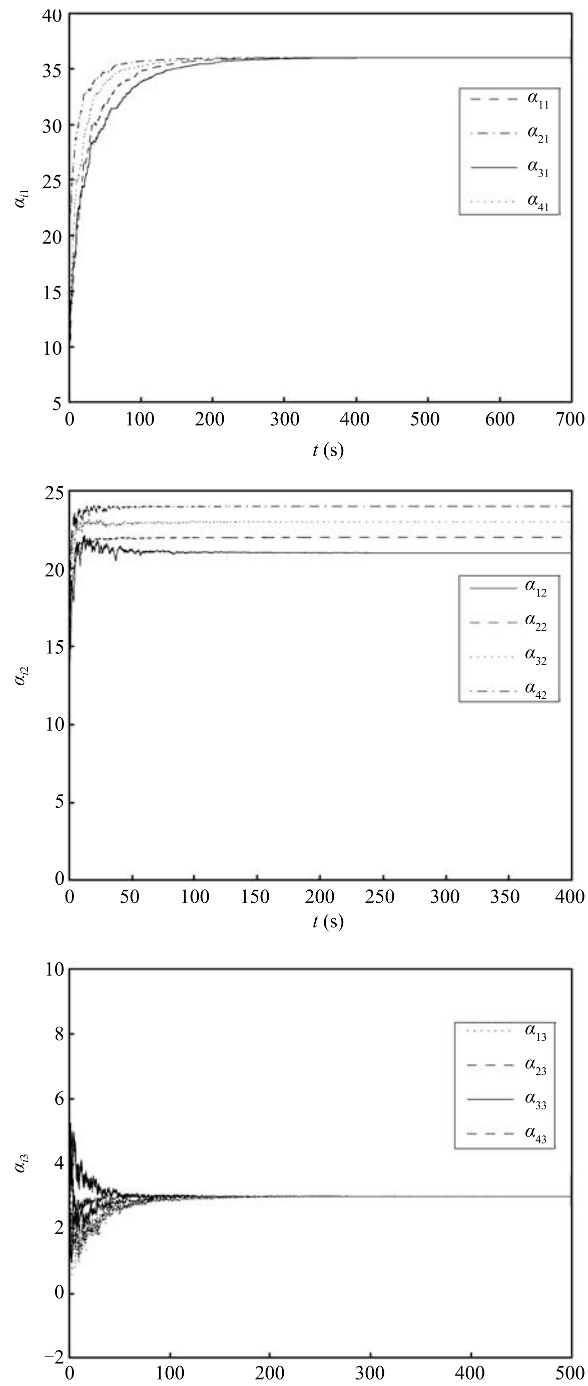

Fig. 2. Identification of uncertain parameters.

B. Identification with Node Time Delay

In this subsection, we consider the uncertain network (21) with four nonidentical delayed Lü systems, and the single delayed Lü system is described as

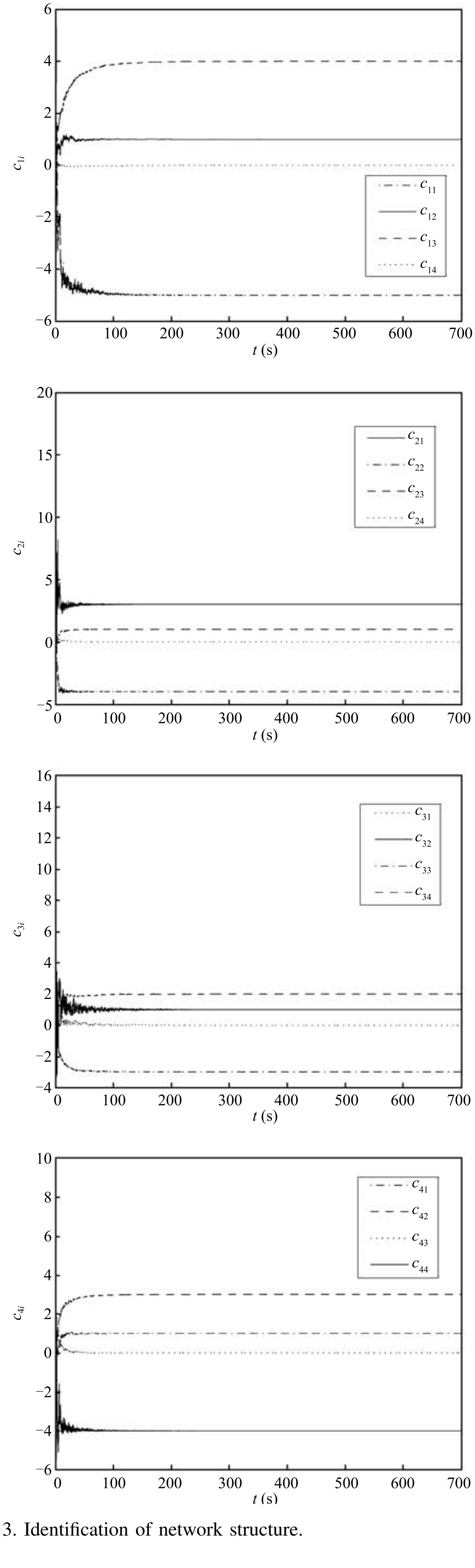

Fig. 3. Identification of network structure.

$$\begin{cases} D^q x_{i1}(t) = \beta_{i1}\left(x_{i2}(t-\tau) - x_{i1}(t-\tau)\right), \\ D^q x_{i2}(t) = -x_{i1}(t-\tau)\, x_{i3}(t-\tau) + \beta_{i2} x_{i2}(t-\tau), \\ D^q x_{i3}(t) = x_{i1}(t-\tau)\, x_{i2}(t-\tau) - \beta_{i3} x_{i3}(t-\tau), \end{cases} \tag{32}$$

where $q = 0.9$, $\beta_i = (\beta_{i1}, \beta_{i2}, \beta_{i3})^{\mathrm{T}} = (36,\ 20+i,\ 3)^{\mathrm{T}}$ for $i = 1, \ldots, 4$. Let $A = \mathrm{diag}\{1, 1, 1\}$ and $\tau = 0.002$. Here, the coupling configuration matrix C is also defined as (31). The chaotic attractor of delayed fractional-order Lü system (32) is shown in Fig. 4. According to Theorem 2, the unknown or uncertain coupling configuration matrix C and system parameter vector β_i can be estimated by using $\hat{C}$ and $\hat{\beta}_i$, respectively. Fig. 5 shows the identification of the uncertain

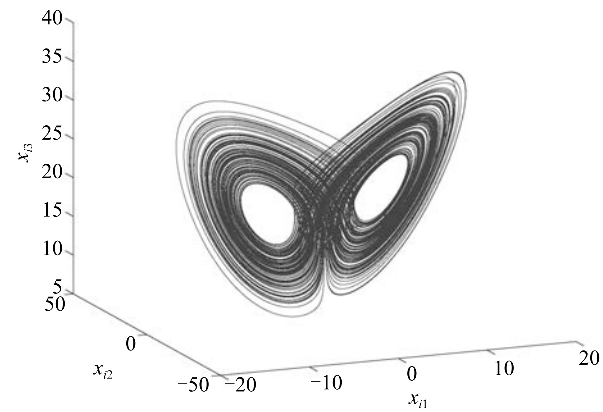

Fig. 4. Chaotic attractor of delayed fractional-order Lü system.

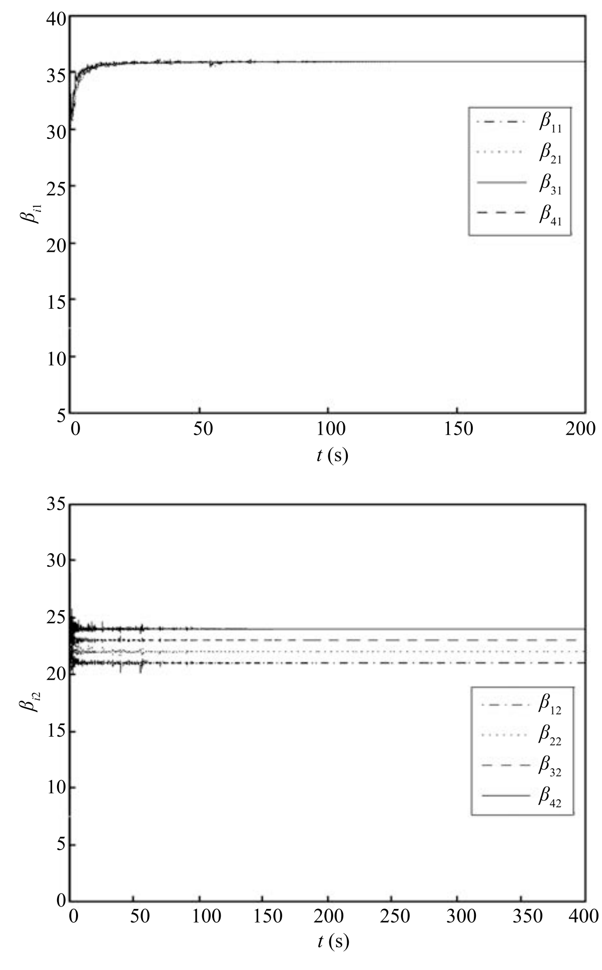

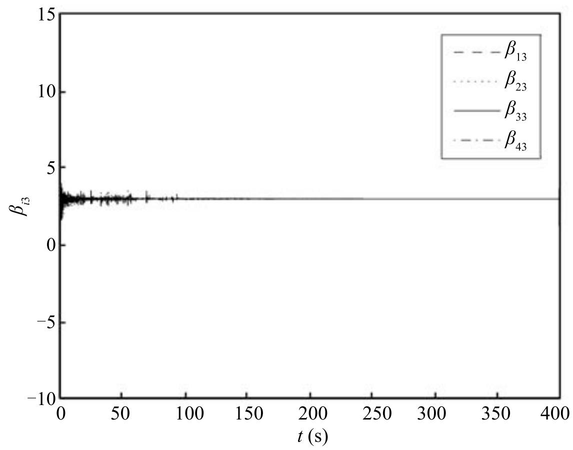

Fig. 5. Identification of uncertain parameters.

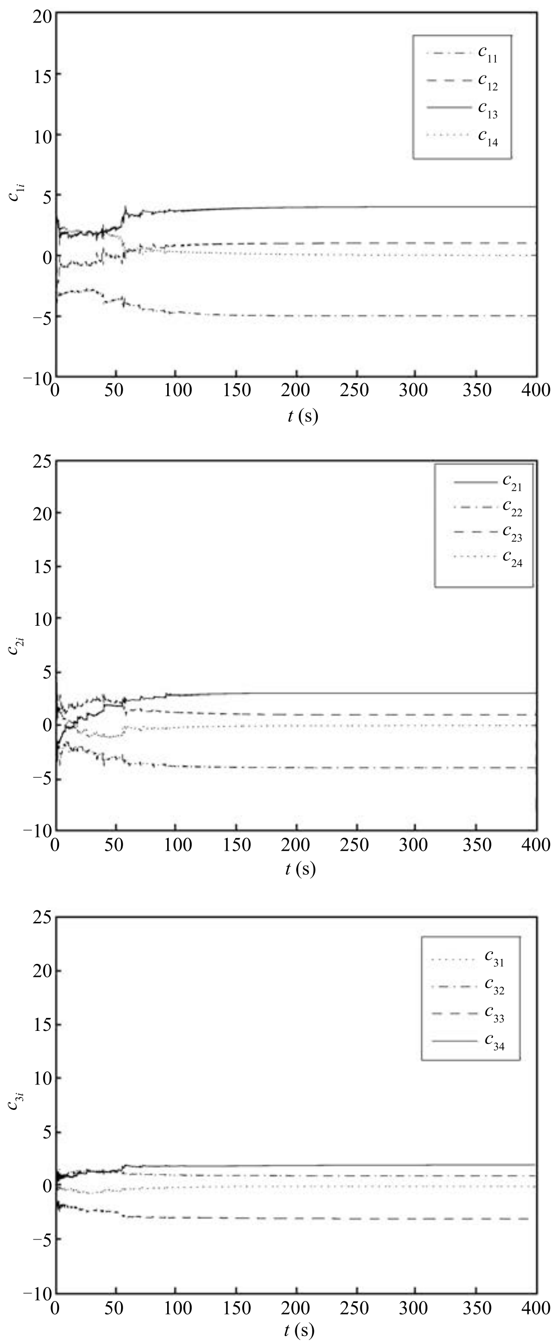

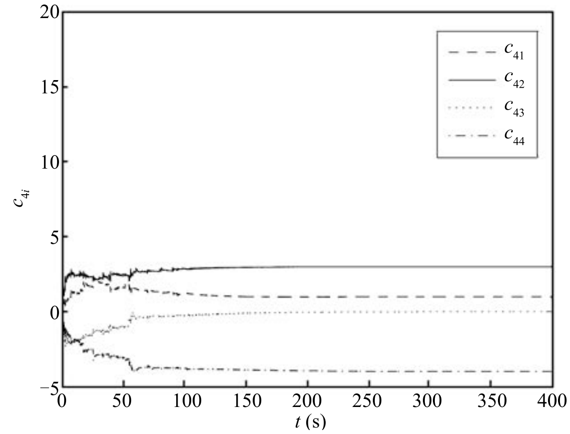

Fig. 6 Identification of network structure.

system parameters, and Fig. 6 illustrates the identification of the unknown network topology.

VI. Conclusion

In this paper, a novel and feasible approach to identify the parameters and network topology of fractional-order complex network with time delay is proposed. Based on the stability theorem of fractional-order differential system and the adaptive control technique, two useful identification criteria are derived. Illustrative simulations are provided to verify the correctness and effectiveness of the proposed methods.

References

[1] Strogatz S H. Exploring complex networks. *Nature*, 2001, **410**(6825): 268−276

[2] Wang X F, Chen G R. Complex networks: small-world, scale-free and beyond. *IEEE Circuits and Systems Magazine*, 2003, **3**(1): 6−20

[3] Boccaletti S, Latora V, Moreno Y, Chavez M, Hwang D U. Complex networks: structure and dynamics. *Physics Reports*, 2006, **424**(4−5): 175−308

[4] Albert R, Barabási A L. Statistical mechanics of complex networks. *Reviews of Modern Physics*, 2002, **74**(1): 47−97

[5] Chen G R, Dong X N. *From Chaos to Order: Methodologies, Perspectives and Applications*. Singapore: World Scientific, 1998.

[6] Xie Q X, Chen G R, Bollt E M. Hybrid chaos synchronization and its application in information processing. *Mathematical and Computer Modelling*, 2002, **35**(1−2): 145−163

[7] Li X, Wang X F, Chen G R. Pinning a complex dynamical network to its equilibrium. *IEEE Transactions on Circuits and Systems I: Regular Papers*, 2004, **51**(10): 2074−2087

[8] Arenas A, Díaz-Guilera A, Kurths J, Moreno Y, Zhou C S. Synchronization in complex networks. *Physics Reports*, 2008, **469**(3): 93−153

[9] Wu X J, Lu H T. Hybrid synchronization of the general delayed and non-delayed complex dynamical networks via pinning control. *Neurocomputing*, 2012, **89**: 168−177

[10] Lu J Q, Cao J D. adaptive complete synchronization of two identical or different chaotic (hyperchaotic) systems with fully unknown parameters. *Chaos*, 2005, **15**(4): 043901

[11] Yu D C, Righero M, Kocarev L. Estimating topology of networks. *Physical Review Letters*, 2006, **97**(18): 188701

[12] Wu X Q. Synchronization-based topology identification of weighted general complex dynamical networks with time-varying coupling delay. *Physica A: Statistical Mechanics and Its Applications*, 2008, **387**(4): 997−1008

[13] Zhou J, Lu J A. Topology identification of weighted complex dynamical networks. *Physica A: Statistical Mechanics and Its Applications*, 2007, **386**(1): 481−491

[14] Liu H, Lu J A, Lü J H, Hill D J. Structure identification of uncertain general complex dynamical networks with time delay. *Automatica*, 2009, **45**(8): 1799−1807

[15] Nagih A, Plateau G. Problémes fractionnaires: tour d'horizon sur les applications et méthodes de résolution. *RAIRO-Operations Research*, 1999, **33**(4): 383−419

[16] Koeller R C. Applications of fractional calculus to the theory of viscoelasticity. *Journal of Applied Mechanics*, 1984, **51**(2): 299−307

[17] Heaviside O. *Electromagnetic Theory*. New York: Chelsea, 1971.

[18] Podlubny I. *Fractional Differential Equations*. San Diego: Academic Press, 1999.

[19] Hartley T T, Lorenzo C F, Qammer H K. Chaos in a fractional order Chua's system. *IEEE Transactions on Circuits and Systems I: Fundamental Theory and Applications*, 1995, **42**(8): 485−490

[20] Grigorenko I, Grigorenko E. Chaotic dynamics of the fractional Lorenz system. *Physical Review Letters*, 2003, **91**(3): 034101

[21] Li C G, Chen G R. Chaos and hyperchaos in the fractional-order Rössler equations. *Physica A: Statistical Mechanics and Its Applications*, 2004, **341**: 55−61

[22] Chai Y, Chen L P, Wu R C, Sun J. Adaptive pinning synchronization in fractional-order complex dynamical networks. *Physica A: Statistical Mechanics and Its Applications*, 2012, **391**(22): 5746−5758

[23] Chen L P, Chai Y, Wu R C, Sun J, Ma T D. Cluster synchronization in fractional-order complex dynamical networks. *Physics Letters A*, 2012, **376**(35): 2381−2388

[24] Yang L X, He W S, Zhang F D, Jia J P. Cluster projective synchronization of fractional-order complex network via pinning control. *Abstract and Applied Analysis*, 2014, **2014**: Article ID 314742

[25] Wang G S, Xiao J W, Wang Y W, Yi J W. Adaptive pinning cluster synchronization of fractional-order complex dynamical networks. *Applied Mathematics and Computation*, 2014, **231**: 347−356

[26] Wu X J, Lu H T. Outer synchronization between two different fractional-order general complex dynamical networks. *Chinese Physics B*, 2010, **19**(7): 070511

[27] Si G Q, Sun Z Y, Zhang H Y, Zhang Y B. Parameter estimation and topology identification of uncertain fractional order complex networks. *Communications in Nonlinear Science and Numerical Simulation*, 2012, **17**(12): 5158−5171

[28] Yang L X, Jiang J. Adaptive synchronization of drive-response fractional-order complex dynamical networks with uncertain parameters. *Communications in Nonlinear Science and Numerical Simulation*, 2014, **19**(5): 1496−1506

[29] Ma W Y, Li C P, Wu Y J, Wu Y Q. Adaptive synchronization of fractional neural networks with unknown parameters and time delays. *Entropy*, 2014, **16**(12): 6286−6299

[30] Hu J B, Lu G P, Zhang S B, Zhang L D. Lyapunov stability theorem about fractional system without and with delay. *Communications in Nonlinear Science and Numerical Simulation*, 2015, **20**(3): 905−913

Xiaojuan Chen received the B. S. degree in automation from the College of Electronic Information and Automation, Chongqing University of Technology, Chongqing, China, in 2004 and the M. S. degree in automation in control theory and control engineering from the College of Automation, Chongqing University, Chongqing, China, in 2007. She is currently working as a lecturer in the Department of Automobile Engineering, Chongqing College of Electronic Engineering, Chongqing, China. Her research interests include both fundamental investigations and practical engineering applications in embedded technology, wireless power supply and automatics.

Jun Zhang received the bachelor's degree from the College of Mobile Telecommunications, Chongqing University of Posts and Telecommunications, Chongqing, China, in 2013. He is currently a master student in the College of Automation, Chongqing University, China. His research interests include synchronization of complex networks and fractional-order system.

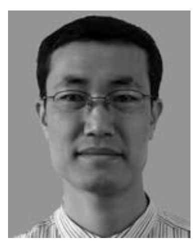

Tiedong Ma received the Ph. D. degree in control theory and control engineering from Northeastern University, Shenyang, China, in 2009. He is currently an associate professor of the College of Automation, Chongqing University, Chongqing, China. His research interests include cooperative control of multi-agent systems, impulsive control and synchronization of complex networks. Corresponding author of this paper.

H_∞ Output Feedback Control of Linear Time-invariant Fractional-order Systems over Finite Frequency Range

Cuihong Wang, Huanhuan Li, and YangQuan Chen, *Senior Member, IEEE*

***Abstract*—This paper focuses on the H_∞ output feedback control problem of linear time-invariant fractional-order systems over finite frequency range. Based on the generalized Kalman-Yakubovic-Popov (KYP) Lemma and a key projection lemma, a necessary and sufficient condition is established to ensure the existence of the H_∞ output feedback controller over finite frequency range, a desirable property in control engineering practice. By using the matrix congruence transformation, the feedback control gain matrix is decoupled and further parameterized by a scalar matrix. Two iterative linear matrix inequality algorithms are developed to solve this problem. Finally, numerical examples are provided to illustrate the effectiveness of the proposed method.**

***Index Terms*—Fractional-order system, Kalman-Yakubovic-Popov (KYP) Lemma, finite frequency range, H_∞ control.**

I. INTRODUCTION

FRACTIONAL-ORDER dynamic system has received a growing interest due to the fact that many real-world physical systems can be well characterized by fractional-order state equations and modeling various physical phenomena involves less parameters than traditional integer-order system[1]. Many useful analysis and synthesis results about fractional-order systems have emerged, such as stability[2−4] and Mittag-Leffler stability analysis[5], robust stability[6−7], H_∞ performance analysis[8], H_∞ feedback control[9−11], and so on.

On the other hand, the Kalman-Yakubovich-Popov (KYP) Lemma has been proved to be a very strong tool to convert frequency domain inequalities (FDIs) to linear matrix inequalities (LMIs)[12]. Many control methods have been developed with the help of KYP Lemma[13−15]. However, KYP Lemma just only characterizes FDIs in entire frequency range and does not deal with the multiple FDIs in finite range. The generalized Kalman-Yakubovich-Popov (GKYP) Lemma provided in [16] extends the standard KYP Lemma to present the LMI characterization of FDIs in finite frequency range. It has been shown that the GKYP Lemma is profitable for system dissipative analysis and control synthesis problems which can be exactly converted to semidefinite programming or convex optimization problems. Based on GKYP Lemma, H_∞ model reduction[17] and static output feedback control[18] problem for integer-order systems have been investigated over finite frequency. Furthermore, the H_∞ performance analysis and H_∞ control synthesis for fractional-order systems have been also considered in [8−10]. But these results are presented over the entire frequency range. It is worth noting that the H_∞ synthesis problems over a finite frequency range is essentially different from the entire frequency range case this is because even the state feedback control problem cannot be completely solved via convex optimization[17].

In this paper, we will investigate the problem of H_∞ static output feedback (SOF) controller synthesis for linear time-invariant fractional-order systems subject to finite frequency range. Based on the GKYP Lemma and a key projection lemma, necessary and sufficient condition is firstly established for the existence of a SOF controller that ensures the fractional order system is asymptotically stable and satisfies the prescribed H_∞ performance index over a finite frequency range. Then, by using matrix congruence transformation, the feedback gain matrix is decoupled from matrix variables and parameterized by a scalar matrix. Moreover, two iterative algorithms are developed to solve this problem. Finally, numerical examples are given to demonstrate the effectiveness of our proposed method.

Notations. For a matrix M, its transpose and complex conjugate transpose are denoted by $M^{\rm T}$, M^*, respectively. The symbol H_n stands for the set of $n\times n$ Hermitian matrices. For a matrix $M\in \mathbf{H}_n$, inequalities $M>0$ (≥ 0) and $M<0$ (≤ 0) denote positive (semi) definiteness and negative (semi) definiteness, respectively. For matrices Φ and P, $\Phi\otimes P$ means the Kronecker product. All the matrices are assumed to be of compatible dimensions and $*$ is used to denote the Hermitian part. For any matrix $M\in\mathbf{C}^{n\times n}$, ${\rm Her}(X)=X+X^*$. ${\rm Re}(M)$ represents the real parts of the complex matrix M. For $G\in\mathbf{C}^{n\times m}$ and $\Pi\in\mathbf{H}_{n+m}$, a function $\sigma:\mathbf{C}^{n\times m}\times\mathbf{H}_{n+m}\rightarrow\mathbf{H}_m$ is defined by

$$\sigma(G,\Pi):=\left[\begin{array}{c}G\\ I_m\end{array}\right]^*\Pi\left[\begin{array}{c}G\\ I_m\end{array}\right].$$

j denotes the imaginary unit.

II. PRELIMINARIES

In this paper, taking the physical meaning into consideration, the Caputo fractional-order derivative is used and defined

Manuscript received October 14, 2015; accepted January 19, 2016. Recommended by Associate Editor Dingyü Xue.

Citation: Cuihong Wang, Huanhuan Li, YangQuan Chen. H_∞ output feedback control of linear time-invariant fractional-order systems over finite frequency range. *IEEE/CAA Journal of Automatica Sinica*, 2016, **3**(3): 304−310

Cuihong Wang and Huanhuan Li are with the Department of Mathematics and Computer Science, Shanxi Normal University, Linfen 041004, China (e-mail: wcjhlove@gmail.com; huanhuanli9582@163.com).

YangQuan Chen is with the School of Engineering, University of California, Merced, CA 95343, USA (e-mail: yqchen@ieee.org).

as follows:

$$D^\alpha f(t) = \frac{\mathrm{d}^\alpha f(t)}{\mathrm{d}t^\alpha} = \frac{1}{\Gamma(m-\alpha)}\int_0^t \frac{f^{(m)}(\tau)}{(t-\tau)^{\alpha+1-m}}\mathrm{d}\tau,$$

where $f(t)$ is a time-dependent function, α represents the order of the derivative ($m-1 \le \alpha < m$, m is an integer).

Consider the following linear time-invariant fractional-order system admitting a pseudo state space representation of the form

$$\begin{cases} D^\alpha x(t) = Ax(t) + B_1 u(t) + Bw(t), \\ z(t) = Cx(t) + Dw(t), \\ y(t) = C_y x(t), \end{cases} \tag{1}$$

where α is the fractional order and $\alpha \in (0,\ 2)$. $x(t) \in \mathbf{R}^n$ is system state, $u(t) \in \mathbf{R}^m$ is control input, $w(t) \in \mathbf{R}^q$ is disturbance input, $z(t) \in \mathbf{R}^s$ is control output, $y(t) \in \mathbf{R}^l$ is measured output. $A \in \mathbf{R}^{n\times n}$, $B_1 \in \mathbf{R}^{n\times m}$, $B \in \mathbf{R}^{n\times q}$, $C \in \mathbf{R}^{s\times n}$, $C_y \in \mathbf{R}^{l\times n}$, and $D \in \mathbf{R}^{s\times q}$ are known matrices.

In general, the frequency ranges can be visualized as the following set of complex numbers that represents certain curves on the complex plane:

$$\Lambda(\Phi,\Psi) := \{\lambda \in \mathbf{C} | \sigma(\lambda,\Phi) = 0, \sigma(\lambda,\Psi) \ge 0\}, \tag{2}$$

where Φ, $\Psi \in \mathbf{H}_2$.

Define $\bar{\Lambda}(\Phi,\Psi) = \Lambda(\Phi,\Psi) \cup \{\infty\}$ if Λ is bounded, otherwise $\bar{\Lambda}(\Phi,\Psi) = \Lambda(\Phi,\Psi)$.

By choosing appropriate Φ and Ψ in (2), the set $\Lambda(\Phi,\Psi)$ can be specified to define a certain range of the frequency curve. For fractional-order system, we can choose

$$\Phi = \begin{bmatrix} 0 & r \\ * & 0 \end{bmatrix}$$

to represent the curve $\Lambda = \{(\mathrm{j}\omega)^\alpha | \omega \in \Omega\}$, where $r = \mathrm{e}^{\mathrm{j}\theta}$, $\theta = (\alpha-1)\pi/2$, Ω is a subset of real numbers specified by appropriate choice of Ψ, Table I shows an example.

TABLE I
CHOICE OF Ψ FOR DIFFERENT FREQUENCY RANGES

	HF	MF	LF
Ω	$\omega \ge \omega_h$	$\omega_l \le \omega \le \omega_h$	$\omega \le \omega_l$
Ψ	$\begin{bmatrix} 1 & 0 \\ * & -\omega_h^{2\alpha} \end{bmatrix}$	$\begin{bmatrix} -1 & \mathrm{j}r\omega_c \\ * & -\omega_l^\alpha\omega_h^\alpha \end{bmatrix}$	$\begin{bmatrix} -1 & 0 \\ * & \omega_l^{2\alpha} \end{bmatrix}$

In Table I, $\omega_c := (\omega_l^\alpha + \omega_h^\alpha)/2$, $\omega_h \ge 0$, $\omega_l \ge 0$, and HF, MF and LF denote high, middle and low frequency ranges, respectively.

In this paper, we focus on the static output feedback controller in the following form:

$$u(t) = Ky(t), \tag{3}$$

then, we have the following closed-loop system

$$\begin{cases} D^\alpha x(t) = \hat{A}x(t) + B\omega(t), \\ z(t) = Cx(t) + D\omega(t), \end{cases} \tag{4}$$

where $\hat{A} = A + B_1 K C_y$.

Therefore, the finite frequency H_∞ static output feedback control problem can be formulated as follows.

Problem FF-H_∞-SOFC (Finite frequency H_∞ static output feedback control). For a pre-specified frequency range $\Lambda(\Phi,\Psi)$ and a given performance index $\gamma > 0$, The problem of the H_∞ static output feedback control over frequency range $\Lambda(\Phi,\Psi)$ is to find a static output feedback controller (2) such that:

1) The closed-loop system (3) is asymptotically stable.

2) The transfer function $G(s)$ of closed-loop system (3) satisfies the finite frequency H_∞ performance $\sup_{\omega\in\Lambda(\Phi,\Psi)} \bar{\sigma}(G(\mathrm{j}\omega)) < \gamma$, where $G(s) = C(s^\alpha I - \hat{A})^{-1}B + D$, $\bar{\sigma}$ denotes the maximum singular value of a matrix.

The following lemma is very useful in the proofs of the main results of this paper.

Lemma 1[11]**.** Let $A \in \mathbf{R}^{n\times n}$, the linear time-invariant system $D^\alpha x(t) = Ax(t)$ with $\alpha \in (0,1)$ is asymptotically stable if and only if there exists Hermitian matrix $H > 0$ such that $(\mathrm{Re}(rH))^{\mathrm{T}} A^{\mathrm{T}} + A(\mathrm{Re}(rH)) < 0$.

Lemma 2[11]**.** Let $A \in \mathbf{R}^{n\times n}$, the linear time-invariant system $D^\alpha x(t) = Ax(t)$ with $\alpha \in (1,2)$ is asymptotically stable if and only if there exists Hermitian matrix $H > 0$ such that $rHA^{\mathrm{T}} + \bar{r}AH < 0$.

Lemma 3 (GKYP Lemma)[16, 19]**.** Given real matrices A, B, C, D, a real symmetric matrix Π, and Φ, Ψ, $\in \mathbf{H}_2$, let $G(\lambda) = C(\lambda I - A)^{-1}B + D$. Then the frequency range inequality

$$\begin{bmatrix} G(\lambda) \\ I \end{bmatrix}^* \Pi \begin{bmatrix} G(\lambda) \\ I \end{bmatrix} < 0$$

holds for all $\lambda \in \bar{\Lambda}(\Phi,\Psi)$ if and only if there exist Hermitian matrices P and $Q > 0$ such that

$$\begin{bmatrix} A & I \\ C & 0 \end{bmatrix} (\Phi \otimes P + \Psi \otimes Q) \begin{bmatrix} A & I \\ C & 0 \end{bmatrix}^{\mathrm{T}} + \begin{bmatrix} B & 0 \\ D & I \end{bmatrix} \Pi \begin{bmatrix} B & 0 \\ D & I \end{bmatrix}^{\mathrm{T}} < 0.$$

Remark 1. Let

$$\Pi = \begin{bmatrix} I & 0 \\ 0 & \gamma^2 I \end{bmatrix}$$

or

$$\Pi = \begin{bmatrix} 0 & -I \\ -I & 0 \end{bmatrix},$$

the characterization of Lemma 3 turns into the bounded real lemma and positive real lemma.

Lemma 4 (Projection Lemma)[20]**.** Given a symmetric matrix $\Xi \in \mathbf{R}^{m\times m}$ and two matrices P, Q of column dimension m, consider the problem of finding some matrix Θ of compatible dimensions such that

$$\Xi + P^{\mathrm{T}}\Theta^{\mathrm{T}}Q + Q^{\mathrm{T}}\Theta P < 0. \tag{5}$$

Denote by $\aleph_P$, $\aleph_Q$ any matrices whose columns form basis of the null space of P and Q, respectively. Then (5) is solvable for Θ if and only if

$$\begin{cases} \aleph_P^{\mathrm{T}} \Xi \aleph_P < 0, \\ \aleph_Q^{\mathrm{T}} \Xi \aleph_Q < 0. \end{cases}$$

III. MAIN RESULTS

In this section, we will firstly investigate the H_∞ static output feedback control for fractional-order systems over middle frequency ranges. Based on the GKYP Lemma and the projection lemma, we will give the necessary and sufficient condition that the problem of FF-H_∞-SOFC is solvable.

Theorem 1. Given performance index $\gamma > 0$, fractional order $\alpha \in (0,1)$, system matrices A, B_1, B, C, D, C_y, a feedback gain K and finite frequency range $\Lambda_{MF} = \{\omega \in \mathbf{R} : \omega_l \leq \omega \leq \omega_h, \omega_l, \omega_h \geq 0\}$. Problem FF-$H_\infty$-SOFC is solvable if and only if there exist Hermitian matrices $H > 0$, $Q > 0$, P, and real matrix $E = [E_1,\ E_2]$ such that the following matrix inequalities hold:

$$\Xi = \mathrm{Her}(\hat{A}(\mathrm{Re}(rH))) < 0, \tag{6}$$

and

$$\Sigma = \begin{bmatrix} -Q & \Sigma_{12} & -E_2 & 0 \\ * & \Sigma_{22} & \Sigma_{23} & B \\ * & * & \Sigma_{33} & D \\ * & * & * & -I \end{bmatrix} < 0, \tag{7}$$

where $r = \mathrm{e}^{\mathrm{j}\theta}$, $\theta = (\alpha - 1)\pi/2$, $\hat{A} = A + B_1 K C_y$, and

$$\begin{aligned} \Sigma_{12} =& rP + \mathrm{j}r\omega_c Q - E_1, \\ \Sigma_{22} =& -\omega_l^\alpha \omega_h^\alpha Q + \mathrm{Her}(\hat{A}E_1), \\ \Sigma_{23} =& \hat{A}E_2 + E_1^{\mathrm{T}} C^{\mathrm{T}}, \\ \Sigma_{33} =& -\gamma^2 I + \mathrm{Her}(CE_2). \end{aligned}$$

Proof. (Necessity). It follows from Lemma 1 and Lemma 3 that the problem of FF-H_∞-SOFC is solvable if and only if there exist Hermitian matrices $H > 0$, $Q > 0$ and P such that the following matrix inequalities hold. That is,

$$\Xi = \mathrm{Her}(\hat{A}(\mathrm{Re}(rH))) < 0,$$

and

$$\begin{aligned} &\begin{bmatrix} \hat{A} & I \\ C & 0 \end{bmatrix} \begin{bmatrix} -Q & rP + \mathrm{j}r\omega_c Q \\ \bar{r}P - \mathrm{j}\omega_c Q & -\omega_l^\alpha \omega_h^\alpha Q \end{bmatrix} \begin{bmatrix} \hat{A} & I \\ C & 0 \end{bmatrix}^{\mathrm{T}} \\ &\quad + \begin{bmatrix} B & 0 \\ D & I \end{bmatrix} \begin{bmatrix} I & 0 \\ 0 & -\gamma^2 I \end{bmatrix} \begin{bmatrix} B & 0 \\ D & I \end{bmatrix}^{\mathrm{T}} \\ &\quad = \begin{bmatrix} \hat{A} & I & 0 \\ C & 0 & I \end{bmatrix} \Theta \begin{bmatrix} \hat{A} & I & 0 \\ C & 0 & I \end{bmatrix}^{\mathrm{T}} < 0, \end{aligned}$$

where

$$\Theta = \begin{bmatrix} -Q & rP + \mathrm{j}r\omega_c Q & 0 \\ * & -\omega_l^\alpha \omega_h^\alpha Q + BB^{\mathrm{T}} & BD^{\mathrm{T}} \\ * & * & DD^{\mathrm{T}} - \gamma^2 I \end{bmatrix}.$$

Note that

$$\begin{bmatrix} I & 0 & 0 \end{bmatrix} \Theta \begin{bmatrix} I & 0 & 0 \end{bmatrix}^{\mathrm{T}} = -Q < 0,$$

and denote that

$$\Gamma = \begin{bmatrix} -I & \hat{A}^{\mathrm{T}} & C^{\mathrm{T}} \end{bmatrix}, \quad \Lambda = \begin{bmatrix} 0 & I & 0 \\ 0 & 0 & I \end{bmatrix},$$

then, we can obtain

$$\aleph_\Gamma = \begin{bmatrix} \hat{A}^{\mathrm{T}} & C \\ I & 0 \\ 0 & I \end{bmatrix}, \quad \aleph_\Lambda = \begin{bmatrix} I & 0 & 0 \end{bmatrix}^{\mathrm{T}},$$

and

$$\aleph_\Gamma^{\mathrm{T}} \Theta \aleph_\Gamma < 0, \quad \aleph_\Lambda^{\mathrm{T}} \Theta \aleph_\Lambda < 0.$$

It follows from the projection lemma that there exists a real matrix $E = [E_1\ E_2]$ such that

$$\Theta + \Gamma^{\mathrm{T}} E \Lambda + \Lambda^{\mathrm{T}} E^{\mathrm{T}} \Gamma < 0,$$

which implies $\Sigma < 0$ holds by Schur complement lemma.

(Sufficiency). It follows from Schur complement lemma that $\Xi_2 < 0$ is equivalent to $\Theta + \Gamma^{\mathrm{T}} E \Lambda + \Lambda^{\mathrm{T}} E^{\mathrm{T}} \Gamma < 0$. Using the projection lemma, $\aleph_\Gamma^{\mathrm{T}} \Theta \aleph_\Gamma < 0$ holds. Therefore, the sufficiency is trivially true. □

Remark 2. In the above theorem, the feedback gain K is coupled with matrix variables and is intrinsically non convex. In the following theorem, the feedback gain matrix K will be decoupled from matrices H, E_1, and E_2, simultaneously, and will be parameterized by a positive scalar matrix.

Theorem 2. Given performance index $\gamma > 0$, fractional order $\alpha \in (0,1)$, system matrices A, B_1, B, C, D and C_y, and the finite frequency range $\Lambda_{MF} = \{\omega \in \mathbf{R} : \omega_l \leq \omega \leq \omega_h,\ \omega_l, \omega_h \geq 0\}$. Problem FF-$H_\infty$-SOFC is solvable if and only if there exist Hermitian matrices $H > 0$, $Q > 0$, P, real matrices $E = [E_1,\ E_2]$, U, and a scalar $\epsilon > 0$, such that the following matrix inequalities hold

$$\bar{\Xi} = \begin{bmatrix} \bar{\Xi}_{11} & -(\mathrm{Re}(rH))^{\mathrm{T}} - B_1 L C_y \\ * & -\epsilon I \end{bmatrix} < 0, \tag{8}$$

and

$$\bar{\Sigma} = \begin{bmatrix} -Q & \bar{\Sigma}_{12} & -E_2 & 0 & 0 \\ * & \bar{\Sigma}_{22} & \bar{\Sigma}_{23} & B & \bar{\Sigma}_{25} \\ * & * & \bar{\Sigma}_{33} & D & -E_2^{\mathrm{T}} \\ * & * & * & -I & 0 \\ * & * & * & * & -\epsilon I \end{bmatrix} < 0, \tag{9}$$

where $r = \mathrm{e}^{\mathrm{j}\theta}$, $\theta = (\alpha - 1)\pi/2$, and

$$\begin{aligned} \bar{\Xi}_{11} =& \mathrm{Her}\left(A(\mathrm{Re}(rH)) - B_1 L C_y U^{\mathrm{T}} B_1^{\mathrm{T}}\right) \\ &+ \epsilon B_1 U U^{\mathrm{T}} B_1^{\mathrm{T}}, \\ \bar{\Sigma}_{12} =& rP + \mathrm{j}r\omega_c Q - E_1, \\ \bar{\Sigma}_{22} =& -\omega_l^\alpha \omega_h^\alpha Q + \mathrm{Her}(AE_1 - B_1 L C_y U^{\mathrm{T}} B_1^{\mathrm{T}}) \\ &+ \epsilon B_1 U U^{\mathrm{T}} B_1^{\mathrm{T}}, \\ \bar{\Sigma}_{23} =& AE_2 + E_1^{\mathrm{T}} C^{\mathrm{T}}, \\ \bar{\Sigma}_{33} =& -\gamma^2 I + \mathrm{Her}(CE_2), \\ \bar{\Sigma}_{25} =& -E_1^{\mathrm{T}} - B_1 L C_y. \end{aligned}$$

Moreover, the static output feedback control gain is designed as $K = \epsilon^{-1} L$.

Proof. (Necessity). It follows from Theorem 1 that problem FF-H_∞-SOFC is solvable if and only if there exist Hermitian matrices $H > 0$, $Q > 0$, P and real matrix $E = [E_1, E_2]$ such that (6) and (7) hold. It is always possible to find a sufficiently large scalar ϵ such that

$$\begin{bmatrix} \mathrm{Her}(\hat{A}(\mathrm{Re}(rH))) & -\mathrm{Re}(rH)^{\mathrm{T}} \\ * & -\epsilon I \end{bmatrix} < 0,$$

and

$$\begin{bmatrix} \Xi_2 & \Upsilon^{\mathrm{T}} \\ * & -\epsilon I \end{bmatrix} < 0,$$

where $\Upsilon = [0 \ \ -E_1 \ \ -E_2 \ \ 0]$.

Taking congruence transformation yields

$$\Gamma_1^{\mathrm{T}} \begin{bmatrix} \mathrm{Her}(\hat{A}(\mathrm{Re}(rH))) & -(\mathrm{Re}(rH))^{\mathrm{T}} \\ * & -\epsilon I \end{bmatrix} \Gamma_1 = \begin{bmatrix} \Phi_{11} & \Phi_{12} \\ * & -\epsilon I \end{bmatrix} < 0. \tag{10}$$

with

$$\Gamma_1 = \begin{bmatrix} I & 0 \\ (B_1KC_y)^{\mathrm{T}} & I \end{bmatrix},$$
$$\Phi_{11} = \mathrm{Her}(A(\mathrm{Re}(rH)) - \epsilon(B_1KC_y)(B_1KC_y)^{\mathrm{T}},$$
$$\Phi_{12} = -(\mathrm{Re}(rH))^{\mathrm{T}} - \epsilon B_1KC_y.$$

Let $\epsilon K = L$ and note that

$$B_1(LC_y - \epsilon U)\epsilon^{-1}(LC_y - \epsilon U)^{\mathrm{T}} B_1^{\mathrm{T}} \geq 0$$

holds for any real matrix U. Expanding this inequality, one has

$$-(B_1LC_y)\epsilon^{-1}(B_1LC_y)^{\mathrm{T}} \leq -B_1LC_yU^{\mathrm{T}}B_1^{\mathrm{T}} - B_1U(LC_y)^{\mathrm{T}}B_1^{\mathrm{T}} + \epsilon B_1UU^{\mathrm{T}}B_1^{\mathrm{T}}. \tag{11}$$

Using above inequality and combining (10), we get (8). In the same way, taking congruence transformation, we have

$$\Gamma_2^{\mathrm{T}} \begin{bmatrix} \Xi_2 & \Upsilon^{\mathrm{T}} \\ * & -\epsilon I \end{bmatrix} \Gamma_2 < 0,$$

with

$$\Gamma_2 = \begin{bmatrix} I & 0 & 0 & 0 & 0 \\ 0 & I & 0 & 0 & 0 \\ 0 & 0 & I & 0 & 0 \\ 0 & 0 & 0 & I & 0 \\ 0 & (B_1KC_y)^{\mathrm{T}} & 0 & 0 & I \end{bmatrix}.$$

Let $\epsilon K = L$ and use inequality (11), we get (9).

(Sufficiency). Suppose that there exist Hermitian matrices $H > 0$, $Q > 0$, P, real matrices $E = [E_1, \ \ E_2]$, U and a scalar $\epsilon > 0$ such that (8) and (9) hold. From (11), (8) implies that

$$\begin{bmatrix} \tilde{\Phi}_{11} & -(\mathrm{Re}(rH))^{\mathrm{T}} - B_1LC_y \\ * & -\epsilon I \end{bmatrix} < 0,$$

where

$$\tilde{\Phi}_{11} = \mathrm{Her}(A(\mathrm{Re}(rH)) - (B_1LC_y)\epsilon^{-1}(LC_y)^{\mathrm{T}}B_1^{\mathrm{T}},$$

choosing $U = \epsilon^{-1}LC_y$ yields

$$\begin{bmatrix} \bar{\Phi}_{11} & -(\mathrm{Re}(rH))^{\mathrm{T}} - \epsilon B_1 U \\ * & -\epsilon I \end{bmatrix} < 0,$$

where, $\bar{\Phi}_{11} = \mathrm{Her}(A(\mathrm{Re}(rH)) - \epsilon B_1UU^{\mathrm{T}}B_1^{\mathrm{T}}$.

Therefore, using congruence transformation and letting $\epsilon^{-1}L = K$, we can conclude that

$$\begin{bmatrix} \mathrm{Her}(\hat{A}(\mathrm{Re}(rH))) & -(\mathrm{Re}(rH))^{\mathrm{T}} \\ * & -\epsilon I \end{bmatrix} < 0,$$

and $\mathrm{Her}(\hat{A}(\mathrm{Re}(rH))) < 0$. Similarly, one can deduce that (9) implies (7). □

Remark 3. Based on congruence transformation, the feedback gain K can be decoupled from H, E_1 and E_2 simultaneously, and parameterized by a positive scalar ϵ. Note that the matrix inequalities in (8) and (9) are still bilinear, however, we can fix U to make them linear. Using the method provided in [21−22], we defined $\eta \in \mathbf{R}$ satisfying that

$$\begin{cases} \bar{\Xi} - \mathrm{diag}\{\eta I, 0\} < 0, \\ \bar{\Sigma} - \mathrm{diag}\{0, \eta I, 0, 0, 0\} < 0. \end{cases}$$

It is easily known from the proof of Theorem 1 that η achieves its minimum when $U = \epsilon^{-1}LC_y$, which naturally leads to an iterative LMI (ILMI) algorithm.

Algorithm 1 (ILMI algorithm).

Step 1. Set $j = 1$. For a given H_∞ performance level $\gamma > 0$, and the finite frequency range $\Lambda_{FF} = \{\omega \in \mathbf{R} : \omega_l \leq \omega \leq \omega_h, \ \omega_l, \omega_h \geq 0\}$. Solve the following relaxed LMIs

$$\mathrm{Her}(A(\mathrm{Re}(rH)) + B_1W_1) < 0, \tag{12}$$

and

$$\begin{bmatrix} -Q & \hat{\Phi}_{12} & -E_2 & 0 \\ * & \hat{\Phi}_{22} & \hat{\Phi}_{23} & B \\ * & * & \hat{\Phi}_{33} & D \\ * & * & * & -I \end{bmatrix} < 0. \tag{13}$$

where

$$\hat{\Phi}_{12} = rP + \mathrm{j}r\omega_c Q - E_1,$$
$$\hat{\Phi}_{22} = -\omega_l^\alpha \omega_h^\alpha Q + \mathrm{Her}(AE_1 + B_1W_2),$$
$$\hat{\Phi}_{23} = AE_2 + B_1W_3 + E_1^{\mathrm{T}}C^{\mathrm{T}},$$
$$\hat{\Phi}_{33} = -\gamma^2 I + Her(CE_2),$$

with variables in $S \triangleq \{$Hermitian matrices $H > 0$, $Q > 0$, P, and real matrices, E_1, E_2, W_1, W_2 and $W_3\}$.

The initial value U_1 is obtained as

$$U_1 = W_1(\mathrm{Re}(rH))^{-1}.$$

Step 2. For fixed U_j, solve the following minimization problem for matrix variables in the set $S \triangleq \{$Hermitian matrices $H > 0$, $Q > 0$, P, real matrices $E = [E_1, E_2]$, U and a scalar $\epsilon > 0\}$

$$\min \ \eta,$$
$$\text{s.t.} \begin{cases} \bar{\Xi} - \mathrm{diag}\{\eta I, 0\} < 0, \\ \bar{\Sigma} - \mathrm{diag}\{0, \eta I, 0, 0, 0\} < 0, \end{cases} \tag{14}$$

where $\bar{\Xi}$ and $\bar{\Sigma}$ are defined in (8) and (9) respectively. Denote the obtained η as η_j.

Step 3. If $\eta_j < 0$, then a desired feedback gain is obtained as $K = \epsilon^{-1}L$.

Step 4. Fix $\eta = \eta_j$, minimize ϵ such that LMIs (14) hold, denote the obtained ϵ and L as ϵ_j and L_j.

Step 5. If $|\eta_j - \eta_{j-1}|/\eta_{j-1} < \tau$, where τ is a prescribed tolerance, then this algorithm fails to find the desired feedback gain K, stop; If not, update η_{j+1} as $U_{j+1} = \epsilon_j^{-1}L_jC_y$. Set $j := j + 1$ and go to Step 2.

Before employing the ILMI algorithm, it is suggested to find some initial value which is "close" to the desired solution. We adopt the following initial optimization algorithm provided in [11]. Denote $\bar{W} = [W_1,\ W_2,\ W_3]$ and $\bar{E} = [\mathrm{Re}(rH),\ E_1,\ E_2]$.

Algorithm 2 (Initial optimisation).

Step 1. Set $j = 1$. For a given H_∞ performance level $\gamma > 0$, and the finite frequency range $\Lambda_{FF} = \{\omega \in \mathbf{R} : \omega_l \le \omega \le \omega_h, \omega_l, \omega_h \ge 0\}$, find Hermitian matrices $H > 0$, $Q > 0$, P, and real matrices W_1, W_2, W_3 such that LMIs (12) and (13) hold. Denote the feasible solution $\bar{E}$ and $\bar{W}$ as $\bar{E}_j$ and $\bar{W}_j$.

Step 2. Fix $\bar{E} = \bar{E}_j$, minimize $\delta = \|\bar{W} - N \otimes \bar{E}\|_2$, such that LMIs (12) and (13) hold, where N is a real matrix variable. Denote the obtained N as N_j.

Step 3. Fix $N = N_j$, minimize $\delta = \|\bar{W} - N \otimes \bar{H}\|_2$, such that LMIs (12) and (13) hold. Denote the minimized δ as δ_j.

Step 4. Set $j := j + 1$, and repeat Step 2 and Step 3. If $|\delta_j - \delta_{j-1}|/\delta_{j-1} \le \mu$, where μ is a prescribed tolerance, then stop. The initial value U_1 is given by $U_1 = W_1(\mathrm{Re}(rH))^{-1}$.

Follow the similar line, we can give the condition that the problem of FF-H_∞-SOFC is solvable over low frequency range as follows.

Theorem 3. Given performance index $\gamma > 0$, fractional order $\alpha \in (0, 1)$, system matrices A, B_1, B, C, D, C_y, a feedback gain K and finite frequency range $\Lambda_{LF} = \{\omega \in \mathbf{R} : \omega \le \omega_l,\ \omega_l \ge 0\}$. Problem FF-$H_\infty$-SOFC is solvable if and only if there exist Hermitian matrices $H > 0$, P and $Q > 0$, real matrix U, $E = [E_1,\ E_2]$ and real scalar ϵ such that the following matrix inequalities hold

$$\tilde{\Xi} = \begin{bmatrix} \tilde{\Xi}_{11} & -(\mathrm{Re}(rH))^{\mathrm{T}} - B_1 L C_y \\ * & -\epsilon I \end{bmatrix} < 0,$$

and

$$\tilde{\Sigma} = \begin{bmatrix} -Q & rP - E_1 & -E_2 & 0 & 0 \\ * & \tilde{\Sigma}_{22} & \tilde{\Sigma}_{23} & B & \tilde{\Sigma}_{25} \\ * & * & \tilde{\Sigma}_{33} & D & -E_2^{\mathrm{T}} \\ * & * & * & -I & 0 \\ * & * & * & * & \epsilon I \end{bmatrix} < 0,$$

where $r = \mathrm{e}^{\mathrm{j}\theta}$, $\theta = (\alpha - 1)\pi/2$, and

$$\begin{aligned} \tilde{\Xi}_{11} &= \mathrm{Her}\left(A(\mathrm{Re}(rH)) - B_1 L C_y U^{\mathrm{T}} B_1^{\mathrm{T}}\right) \\ &\quad + \epsilon B_1 U U^{\mathrm{T}} B_1^{\mathrm{T}}, \\ \tilde{\Sigma}_{23} &= A E_2 + E_1^{\mathrm{T}} C^{\mathrm{T}}, \\ \tilde{\Sigma}_{22} &= \omega_l^{2\alpha} Q + \mathrm{Her}(A E_1 - B_1 L C_y U^{\mathrm{T}} B_1^{\mathrm{T}}) \\ &\quad + \epsilon B_1 U U^{\mathrm{T}} B_1^{\mathrm{T}}, \\ \tilde{\Sigma}_{25} &= -E_1^{\mathrm{T}} - B_1 L C_y, \\ \tilde{\Sigma}_{33} &= -\gamma^2 I + \mathrm{Her}(C E_2). \end{aligned}$$

Moreover, the static output feedback control gain is designed as $K = \epsilon^{-1} L$.

For highest frequency case, we can refer to the designed method in [17] and use the following condition.

Theorem 4. Given performance index $\gamma > 0$, fractional order $\alpha \in (0, 1)$, system matrices A, B_1, B, C, D and C_y, and the finite frequency range $\Lambda_{HF} = \{\omega \in \mathbf{R} : \omega \ge \omega_h, \omega_h \ge 0\}$. Problem FF-$H_\infty$-SOFC is solvable if and only if there exist Hermitian matrices $H > 0$, P, and $Q > 0$, real matrix U, and a scalar $\epsilon > 0$, such that the following matrix inequalities hold

$$\hat{\Xi} = \begin{bmatrix} \hat{\Xi}_{11} & -(\mathrm{Re}(rH))^{\mathrm{T}} - B_1 L C_y \\ * & -\epsilon I \end{bmatrix} < 0,$$

and

$$\hat{\Sigma} = \begin{bmatrix} \hat{\Sigma}_{11} & \bar{r} P C^{\mathrm{T}} & AQ & B & P + r B_1 L C_y \\ * & -\gamma^2 I & CQ & D & 0 \\ * & * & -Q & 0 & rQ \\ * & * & * & -I & 0 \\ * & * & * & * & -\epsilon I \end{bmatrix} < 0,$$

where $r = \mathrm{e}^{\mathrm{j}\theta}$, $\theta = (\alpha - 1)\pi/2$, and

$$\begin{aligned} \hat{\Xi}_{11} &= \mathrm{Her}\left(A(\mathrm{Re}(rH)) - B_1 L C_y U^{\mathrm{T}} B_1^{\mathrm{T}}\right) \\ &\quad + \epsilon B_1 U U^{\mathrm{T}} B_1^{\mathrm{T}}, \\ \hat{\Sigma}_{11} &= \mathrm{Her}(rAP - B_1 L C_y U^{\mathrm{T}} B_1^{\mathrm{T}}) - \omega_h^{2\alpha} Q \\ &\quad + \epsilon B_1 U U^{\mathrm{T}} B_1^{\mathrm{T}}. \end{aligned}$$

Moreover, the static output feedback control gain is designed as $K = \epsilon^{-1} L$.

Remark 4. The designed algorithms of H_∞ static output feedback controller for fractional order system over high frequency and low frequency ranges can refer to the middle frequency case and hence is omitted for brevity.

Remark 5. When the problem of FF-H_∞-SOFC for system with the fractional order $\alpha \in [1, 2)$ case is considered, we just need to replace the stability condition based on Lemma 2. For example, we just replace LMI (8) by

$$\begin{bmatrix} \Psi_{11} & -H - \bar{r} B_1 L C_y \\ * & -\epsilon I \end{bmatrix} < 0,$$

where $\Psi_{11} = \mathrm{Her}\left(\bar{r} A H - B_1 L C_y U^{\mathrm{T}} B_1^{\mathrm{T}}\right) + \epsilon B_1 U U^{\mathrm{T}} B_1^{\mathrm{T}}$.

IV. Numerical Example

Example 1. Consider the system (1) with the following parameters:

$$\begin{aligned} &A = \begin{bmatrix} -8 & -0.8 \\ -2 & 0.5 \end{bmatrix}, \quad B_1 = \begin{bmatrix} -0.6 \\ 2 \end{bmatrix}, \quad B = \begin{bmatrix} 1 \\ 0.1 \end{bmatrix}, \\ &C = \begin{bmatrix} 1.2 & 2 \end{bmatrix}, \quad C_y = \begin{bmatrix} 1 & -130 \end{bmatrix}, \quad D = 0.1, \\ &\alpha = 0.8, \quad \omega_l = 0.2, \quad \omega_h = 4. \end{aligned}$$

The eigenvalues of A are $\lambda_1 = -8.1842$, $\lambda_2 = 0.6842$, which implies the open-loop system is unstable. Using Algorithm 2, the initial value U_1 is obtained as

$$U_1 = \begin{bmatrix} -5.0654 & -1.4742 \end{bmatrix},$$

and using Algorithm 1, the desired static output feedback gain matrix is obtained as $K = 0.1370$. We can easily compute and find that closed-loop system has the stable eigenvalues $\lambda_1 = -8.7288$, $\lambda_2 = -34.4677$. In addition, with the designed controller, Fig. 1 shows the H_∞ norm of the closed-loop system is smaller than thant of open-loop system.

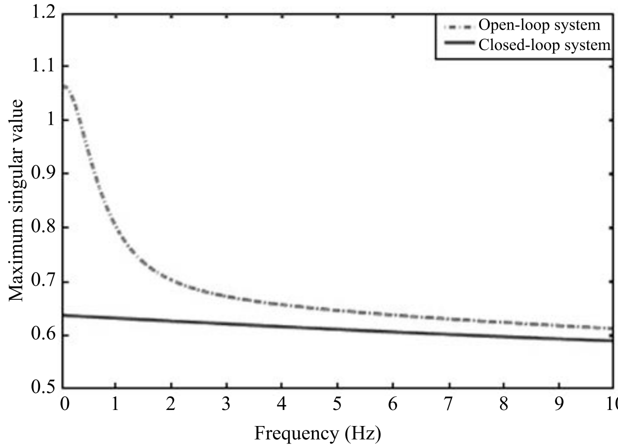

Fig. 1. Maximum singular value comparison, open-loop vs. closed-loop systems.

Example 2. Consider the system (1) with the following parameters:

$$A=\left[\begin{array}{cc}-2.01 & 0\\ 0 & -5.3\end{array}\right],\quad B_1=\left[\begin{array}{c}-5\\ 0.5\end{array}\right],$$

$$B=\left[\begin{array}{c}0.2\\ 0.5\end{array}\right],\quad C=\left[\begin{array}{cc}0.99 & 1.01\end{array}\right],$$

$$C_y=\left[\begin{array}{cc}1.01 & 1.89\end{array}\right],\quad D=0.58,\quad \alpha=1.2.$$

When $w(t)=0$, it is easy to see such system is asymptotically stable. Thus, in the following setting, we mainly make the comparison of H_∞ norm of closed loop system over different frequency ranges. Firstly, for different frequency ranges, we adopt same initial matrix $U=[-0.2923\ 0.1175]$ which can be obtained by solving LMI (12). Then we can design the different desired static output feedback controller using ILMI algorithm over three kinds of frequency ranges. After that, the norm values of the transfer function of the open-loop system and the closed-loop systems over three kinds of frequency ranges, are compared in Fig. 2, and the H_∞ norm comparison are presented in Table II. From Fig. 2, we can see that controllers over three kinds of frequency ranges yield the smaller H_∞ norm compared with the open loop system. From Table II, we can see the least H_∞ norm are generated by controller over the frequency range $[0.2\ 0.5]$, which exactly is the range that the supremum point of maximum singular value of open loop system belongs to. Therefore, if the disturbance has a finite frequency, the minimization on the entire frequency range may not give the optimal solution. In order to achieve a better result in the optimization, it is meaningful to investigate the finite frequency H_∞ control.

V. CONCLUSIONS

In this paper, the H_∞ output feedback control problem of fractional-order systems over finite frequency range has been investigated. Based on the GKYP Lemma and the Projection Lemma, we have established the existence conditions of the desired static output feedback controller. By matrix congruence transformation, the feedback gain matrix is decoupled with three matrix variables simultaneously, and further parameterized by a scalar matrix. Two iterative LMI algorithms have been presented to obtain the desired results. Furthermore, the existence conditions of desired controller have been extended to the high frequency and low frequency cases. Moreover, the design method is feasible for the fractional order $\alpha \in (1,2)$ case. Finally, numerical examples are given to show the effectiveness of our design method.

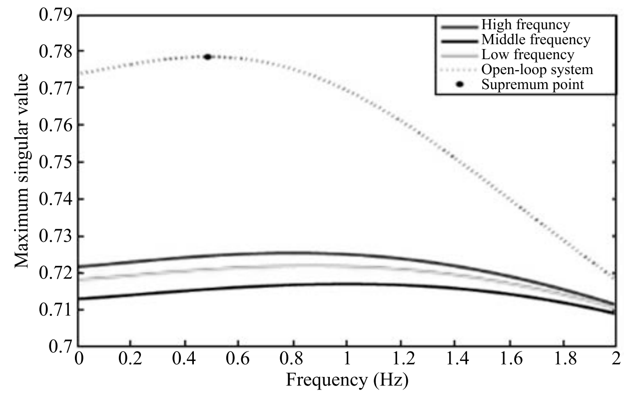

Fig. 2. Comparison of different frequency ranges.

TABLE II
H_∞ NORM COMPARISON OVER DIFFERENT FREQUENCY RANGES

Open-loop	$\omega > 0$	$0.2 \le \omega \le 0.5$	$\omega \le 0.7$
0.7784	0.7255	0.7171	0.7220

REFERENCES

[1] Podlubny I. *Fractional Differential Equations*. New York: Academic Press, 1999.

[2] Matignon D. Stability results for fractional differential equations with applications to control processing. In: Proceedings of the 1996 IMACS-SMC, Vol. 2. 1996. 963−968

[3] Sabatier J, Farges C, Trigeassou J C. A stability test for non-commensurate fractional order systems. *Systems and Control Letters*, 2013, **62**(9): 739−746

[4] Sabatier J, Moze M, Farges C. LMI stability conditions for fractional order systems. *Computers and Mathematics with Applications*, 2010, **59**(5): 1594−1609

[5] Li Y, Chen Y Q, Podlubny I. Mittag-Leffler stability of fractional order nonlinear dynamic systems. *Automatica*, 2009, **45**(8): 1965−1969

[6] Ahn H S, Chen Y Q. Necessary and sufficient stability condition of fractional-order interval linear systems. *Automatica*, 2008, **44**(11): 2985−2988

[7] Ma Y D, Lu J G, Chen W D. Robust stability and stabilization of fractional order linear systems with positive real uncertainty. *ISA Transactions*, 2014, **53**(2): 199−209

[8] Liang S, Wei Y H, Pan J W, Gao Q, Wang Y. Bounded real lemmas for fractional order systems. *International Journal of Automation and Computing*, 2015, **12**(2): 192−198

[9] Farges C, Fadiga L, Sabatier J. H_∞ analysis and control of commensurate fractional order systems. *Mechatronics*, 2013, **23**(7): 772−780

[10] Fadiga L, Farges C, Sabatier J, Santugini K. H_∞ output feedback control of commensurate fractional order systems. In: Proceedings of the

2013 European Control Conference (ECC). Zurich: IEEE, 2013. 4538−4543

[11] Shen J, Lam J. State feedback H_∞ control of commensurate fractional-order systems. *International Journal of Systems Science*, 2014, **45**(3): 363 −372

[12] Rantzer A. On the Kalman-Yakubovich-Popov lemma. *Systems and Control Letters*, 1996, **28**(1): 7−10

[13] Najson F. On the Kalman-Yakubovich-Popov lemma for discrete-time positive linear systems: a novel simple proof and some related results. *International Journal of Control*, 2013, **86**(10): 1813−1823

[14] Sreeram V, Sahlan S. Improved results on frequency-weighted balanced truncation and error bounds. *International Journal of Robust and Nonlinear Control*, 2012, **22**(11): 1195−1211

[15] Stefanovski J. Kalman-Yakubovich-Popov lemma for descriptor systems. *Systems and Control Letters*, 2014, **74**: 8−13

[16] Iwasaki T, Hara S. Generalized KYP lemma: unified frequency domain inequalities with design applications. *IEEE Transactions on Automatic Control*, 2005, **50**(1): 41−59

[17] Shen J, Lam J. Improved results on H_∞ model reduction for continuous-time linear systems over finite frequency ranges. *Automatica*, 2015, **53**: 79−84

[18] Li X W, Gao H J. A heuristic approach to static output-feedback controller synthesis with restricted frequency-range specifications. *IEEE Transactions on Automatic Control*, 2014, **59**(4): 1008−1014

[19] Pipeleer G, Vandenberghe L. Generalized KYP lemma with real data. *IEEE Transactions on Automatic Control*, 2011, **56**(12): 2942−2946

[20] Gahinet P, Apkarian P. A linear matrix inequality approach to H_∞ control. *International Journal of Robust and Nonlinear Control*, 1994, **4**(4): 421−448

[21] Cao Y Y, Lam J, Sun Y X. Static output feedback stabilization: an ILMI approach. *Automatica*, 1998, **34**(12): 1641−1645

[22] Shu Z, Lam J. An augmented system approach to static output-feedback stabilization with H_∞ performance for continuous-time plants. *International Journal of Robust and Nonlinear Control*, 2009, **19**(7): 768−785

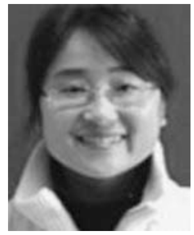

Cuihong Wang received the M. Sc. and Ph. D. degrees from Southwest Jiaotong University, Chengdu, China, in 2005 and 2008, respectively. She is currently an associate professor at Shanxi Normal University, Linfen, China. Her research interests include singular systems, time delay systems, fractional system, stability analysis, model reduction, and robust control. Corresponding author of this paper.

Huanhuan Li Master student at Shanxi Normal University, Linfen, China. Her current research interests include fractional order systems, model reduction and robust control.

YangQuan Chen received the Ph. D. degree in advanced control and instrumentation from Nanyang Technological University, Singapore, in 1998. Dr. Chen was at the Faculty of Electrical and Computer Engineering, Utah State University before he joined the School of Engineering, University of California, Merced in 2012 where he teaches "Mechatronics" for juniors and "Fractional order mechanics" for graduates. His current research interests include mechatronics for sustainability, cognitive process control and hybrid lighting control, multi-UAV based cooperative multi-spectral "personal remote sensing" and applications, applied fractional calculus in controls, signal processing and energy informatics; distributed measurement and distributed control of distributed parameter systems using mobile actuator and sensor networks.

The Ellipsoidal Invariant Set of Fractional Order Systems Subject to Actuator Saturation: The Convex Combination Form

Kai Chen, Junguo Lu, and Chuang Li

***Abstract*—The domain of attraction of a class of fractional order systems subject to saturating actuators is investigated in this paper. We show the domain of attraction is the convex hull of a set of ellipsoids. In this paper, the Lyapunov direct approach and fractional order inequality are applied to estimating the domain of attraction for fractional order systems subject to actuator saturation. We demonstrate that the convex hull of ellipsoids can be made invariant for saturating actuators if each ellipsoid with a bounded control of the saturating actuators is invariant. The estimation on the contractively invariant ellipsoid and construction of the continuous feedback law are derived in terms of linear matrix inequalities (LMIs). Two numerical examples illustrate the effectiveness of the developed method.**

***Index Terms*—Fractional order, saturation, convex hull, invariant set, ellipsoid, domain of attraction.**

I. INTRODUCTION

IN this paper, we focus on the domain of attraction of the original for a class of fractional order systems with saturating actuators. Fractional order systems, which are based on fractional calculus, have attracted much attentions in recent decades. Fractional calculus has a long history over 300 years, and it is a branch of mathematical analysis that deals with the possibility of taking real number or complex number powers of differentiation and integration operators[1]. In recent years, considerable interest in fractional calculus has been stimulated by the applications that this calculus found in numerical analysis and different areas of physics and engineering, possibly including fractal phenomena[2]. Especially in some special areas, such as viscoelastic materials[3] and electro-chemical systems[4], the application of fractional-order models is more adequate and elegant than integer-order models for the investigation of dynamic behavior. The most significant reason is that the fractional differential equations (FDEs) have the ability of revealing inherent memory and inherited character of various materials and processes in real physical world.

In control engineering field, the fractional order $PI^{\lambda}D^{\mu}$ (FOPID) controller is an active topic for its excellent control performance and the tuning method for FOPID controller has attract more attentions. In the past decades, a number of tuning methods for fractional order controllers are proposed in the literatures, such as [5-7]. However, most of obtained results are derived in the frequency domain, and it is hard to handle nonlinearities, e.g., actuator saturation, of the considered systems.

The stability and stabilization problems of integer order state space model have been widely investigated. In [8], a method for estimating the domain of attraction of the origin for a system under a saturated linear feedback is proposed. And in [9], the stability and stabilization problems of a class of continuous-time and discrete-time Markovian jump linear systems with partly unknown transition probabilities are investigated. The robust stochastic stability problem for discrete-time uncertain singular Markov jump systems with actuator saturation is considered in [10]. As the extension of integer order systems, the stability and stabilization problems of fractional order state space model also have attracted great attractions. Control problems of fractional order systems have achieved tremendous attention in recent years due to the inherent memory advantage of fractional derivatives.

Iterative learning control is one of important robust linear control methods for fractional order linear systems. In [11], Chen investigated the classical Arimoto D-type iterative learning control (ILC) updating law uses the first order derivative (with transfer functions) of tracking error. The convergence of the iterative process for fractional order linear systems was first discussed in time domain in [12], which is a meaningful work, and the fractional order iterative learning control for time-varying systems in convolution form are analyzed. In [13], Li discussed the convergence of the iterative process for fractional order linear time invariant (LTI) system, and proved that the convergence conditions of the fractional order and integer order iterative learning schemes are equivalent for $D = 0$.

Another important issue is the robust stability and stabilization problems of fractional order systems. In [14], the problems of robust stability and stabilization for a class of fractional order linear time invariant systems with convex polytopic uncertainties were considered. Several methods to

Manuscript received September 1, 2015; accepted December 21, 2015. This work was supported by Natural Science Foundation of Hainan Province (20156218) and National Natural Science Foundation of China (61374030). Recommended by Associate Editor YangQuan Chen.

Citation: Kai Chen, Junguo Lu, Chuang Li. The ellipsoidal invariant set of fractional order systems subject to actuator saturation: the convex combination form. *IEEE/CAA Journal of Automatica Sinica*, 2016, **3**(3): 311−319

Kai Chen and Chuang Li are with the School of Mechanical and Electrical Engineering, Hainan University, Haikou 570228, China (e-mail: 374550635@qq.com; lc@hainu.edu.cn).

Junguo Lu is with the Department of Automation, Shanghai JiaoTong University, and also with the Key Laboratory of System Control and Information Processing, Ministry of Education of China, Shanghai 200240, China (e-mail: jglu@sjtu.edu.cn).

Color versions of one or more of the figures in this paper are available online at http://ieeexplore.ieee.org.

investigate the stability and stabilization of fractional order linear systems are proposed in [15] and [16] which are based on the conclusion in [14]. In this years, the control synthesis of fractional order system was wide investigated. Reference [17] investigated the robust stability of uncertain parameters FO-LTI interval systems, which have deterministic linear coupling relationship between fractional order and other model parameters. The robust stability for uncertain fractional-order systems of two types of order $\alpha \in (0,1)$ are investigated in [18].

In engineering practice, it is important to consider the input saturation. The performance of the closed-loop system may be severely degraded or be unstable when the actuator is under saturation. The actuator saturation for the integer order systems has received great attention in the past decades. However, in the stability analysis of fractional order systems, it is still an open topic. In this paper, we consider the control of fractional order linear systems subject to actuator saturation $D^{\alpha}x(t) = Ax(t) + BSat(u(t))$. To ensure the stabilization of this fractional order linear system, we first concern with the closed-loop stability under a given linear state feedback $u = Fx$. The Lyapunov approach is the mostly fundamental approach to deal with the stability issues of integer order systems. However, it is still an open topic to choose proper Lyapunov function candidates for fractional order systems. Several works have been dedicated to this problem.

For stable fractional order systems, the decay rate of solution is in the sense of Mittag-Leffler function rather than exponential function, which motivates the concept of Mittag-Leffler stability of fractional order systems. Mittag-Leffler stabilities were firstly proposed in [19] and [20] for the commensurate case and incommensurate case, respectively. Even though the generalization of classical Lyapunov direct approach to the fractional order case is proposed, the commonly used quadratic Lyapunov function candidate is not valid for fractional order systems since the fractional derivative of composite function is an infinite series. To the best of our knowledge, stability analysis of fractional order systems based on the Lyapunov direct approach is still an open problem, and only a few works are dedicated to this topic. By the equivalent transformation between the solution of FDEs with that of ODEs, the Lyapunov direct approach was adopted to investigate the stability of fractional order nonlinear systems[21].

Only few works are related to the estimation of domain of attraction for fractional order systems. Such as, in [22], the sector bounded condition of saturation nonlinearity and Gronwall-Bellman inequality were adopted to derive estimation algorithm of attraction in terms of bilinear matrix inequality.

Our contributions of this paper include:

1) Propose a method to obtain the domain of attraction for fractional order systems through a set of ellipsoids.

2) Demonstrate that the convex hull of ellipsoids can be made invariant for fractional order linear systems subject to actuator saturation if each ellipsoid in a set with a bounded control of the saturating actuators is invariant.

By comparing our paper with the previous conclusions, it could be observed that less conservative results were obtained through the proposed method.

The rest of this paper is organized as follows: In Section II, some necessary preliminaries and the problem statement are introduced. The domain of attraction under a given saturated linear feedback is discussed in Section III. To obtain the feedback matrix, the construction of continuous feedback laws are introduced in Section IV. To show the effectiveness of this method, two numerical examples are shown in Section V. Finally, Section VI draws the conclusion.

Notations. $\mathbf{R}^n$ is the set of real n dimensional vectors, and $\mathbf{R}^{n\times m}$ is the set of real $n \times m$ dimensional matrices. $Sat(\cdot)$ stands for the standard saturation function. For a $P \in \mathbf{R}^{n\times n}$, $P > 0$ and $\rho \in (0, \infty)$, an ellipsoid is denoted as $\Psi(P, \rho) := \{x \in \mathbf{R}^n : x^{\mathrm{T}}Px \leq \rho\}$ where P is a positive-definite matrix. Especially, we use $\Psi(P)$ to denote $\Psi(P, 1)$. In this paper, we are interested in a convex function determined by a set of positive-definite matrices $P_1, P_2, P_3, \ldots, P_N \in \mathbf{R}^{n\times n}$ to obtain the maximum estimation on the invariance of the considered fractional order systems.

II. Problem Statement and Necessary Preliminaries

A. Preliminaries

Definition 1[23]**.** A quadratic function can be defined as follows:

$$V_c(x) = x^{\mathrm{T}}Px,$$

where $P \in \mathbf{R}^{n\times n}$ is a positive-definite matrix. For a positive number ρ, a level set of $V_c(\cdot)$, denoted by $L_{V_c}(\rho)$, is

$$L_{V_c}(\rho) := \{x \in \mathbf{R}^n; V_c(x) \leq \rho\} = \Psi(P, \rho).$$

Definition 2. The α-th ($\alpha > 0$) order fractional integral of a fractional calculus function $f(t)$ is defined as

$$\mathcal{I}^{\alpha}f(t) = D^{-\alpha}f(t) = \frac{1}{\Gamma(\alpha)}\int_0^t \frac{f(\tau)}{(t-\tau)^{1-\alpha}}\mathrm{d}\tau.$$

Definition 3. The α-th ($\alpha > 0$) order fractional derivative of an integrable and differentiable function $f(t)$ is introduced as

$$D^{\alpha}f(t) = \frac{1}{\Gamma(m-\alpha)}\int_0^t \frac{f^{(m)}(\tau)}{(t-\tau)^{1+\alpha-m}}\mathrm{d}\tau,$$

where m is an integer satisfying $m - 1 < \alpha < m$. $f^{(m)}(\cdot)$ is the m-th derivative of function $f(\cdot)$ and $\Gamma(\cdot)$ is the Euler-Gamma function.

Lemma 1[23]**.** For a set of positive-definite matrices $P_1, P_2, P_3, \ldots, P_N \in \mathbf{R}^{n\times n}$, Let $P(\gamma) := \sum_{j=1}^{N}\gamma_j P_j$, Then,

$$L_{V_c}(\rho) = co\{\Psi(P_j, \rho), j \in I[1, N]\} = \bigcup_{\gamma\in\Gamma}\Psi(P(\gamma), \rho),$$

where $\gamma \in \mathbf{R}^N$, N is a positive integer number, and $co\{\cdot\}$ stands for the convex hull.

Lemma 2[24]**.** Let $x(t) \in \mathbf{R}^n$ be a vector of differentiable functions. Then, for any time instant $t \geq 0$, the following relationship holds

$$D^{\beta}(x^{\mathrm{T}}(t)Px(t)) \leq 2x^{\mathrm{T}}(t)P(D^{\beta}x(t)),$$

where $P \in \mathbf{R}^{n\times n}$ is a constant symmetric positive-definite matrix.

Lemma 3[25]**.** Define $\Phi(F) = \{x \in \mathbf{R}^n : |f_i x| \le 1, i \in [1, m]\}$, and f_i is the i-th row of the matrix F. Let $P \in \mathbf{R}^{n\times n}$ be a positive-definite matrix. Suppose that $\rho > 0$. An ellipsoid $\Omega(P, \rho) = \{x \in \mathbf{R}^n : x^{\mathrm{T}} P x \le \rho\}$ is included in $\Phi(F)$ if and only if,

$$f_i^{\mathrm{T}} P f_i \le \rho.$$

Let Ξ denote the set of $m \times m$ diagonal matrices whose diagonal elements are either 0 or 1. Then, there are 2^m elements in Ξ. Suppose that elements of Ξ are labeled as E_i with $i \in [1, 2^m]$. Then, $E_i^- = I_m - E_i$ is also an element of Ξ, where I_m is the $m \times m$ dimensional identity matrix.

Lemma 4[25]**.** Given $F, H \in \mathbf{R}^{m\times n}$. Suppose that $| h_j x |\le 1$, then we have

$$Sat(Fx) \in co\{E_i F x + E_i^- H x, i \in [1, 2^m]\},$$

where h_j is the j-th row of the matrix H.

Lemma 5[19]**.** Let $x = 0$ be an equilibrium point for the non-autonomous fractional order system $D^\alpha x(t) = f(t, x)$. Assume that there exists a Lyapunov functin $V(t, x)$ and three class-K functions $\beta_i, i = 1, 2, 3$ satisfying

$$\beta_1(\|x\|) \le V(t, x) \le \beta_2(\|x\|),$$
$$D^\beta V(t, x) \le -\beta_3(\|x\|),$$

where $\beta \in (0, 1)$. Then the equilibrium point of system $D^\alpha x(t) = f(t, x)$ is asymptotically Mittag-Leffler stable.

Lemma 6[26]**.** Considering an ellipsoid $\Psi(P)$, if there exists an $H \in \mathbf{R}^{m\times n}$ such that

$$\begin{aligned}&(A + BE_i F + E_i^- H)^{\mathrm{T}} P + P(A + BE_i F\\&+ E_i^- H) < 0, \forall i \in I[1, 2^m],\end{aligned}$$

and $\Psi(P, \rho) \subset \Phi(F)$, then $\Psi(P, \rho)$ is an invariant set of fractional order system $D^\alpha x(t) = Ax(t) + BSat(Fx)$.

B. Problem Statement

Considering the open-loop fractional order linear system subject to actuator saturation:

$$D^\alpha x(t) = Ax(t) + BSat(u), \tag{1}$$

where the fractional order $0 < \alpha < 1$. $x \in \mathbf{R}^n$, $u \in \mathbf{R}^m$ are the state and input, respectively. $A \in \mathbf{R}^{n\times n}$, $B \in \mathbf{R}^{n\times m}$ are constant system matrices. $Sat(\cdot) : \mathbf{R}^m \to \mathbf{R}^m$ is the standard saturation function, and $Sat(u) = [Sat(u_1)\ \ Sat(u_2)\ \ \ldots\ \ Sat(u_m)]^{\mathrm{T}}$, where $Sat(u_i) = \mathrm{Sign}(u_i)\min\{1, |u_i|\}$.

The objective of this paper is to obtain an estimation of the domain of attraction for system (1) and obtain a feedback law $u = Sat(Fx)$, under which the closed-loop system,

$$D^\alpha x(t) = Ax(t) + BSat(Fx), \tag{2}$$

is asymptotically stable, where $F \in \mathbf{R}^{m\times n}$ is the feedback matrix. Then the input control is linear with respect to state x in the domain of the state space $\Phi(F)$.

Remark 1. Lyapunov stability method is an important tool for stability analysis of nonlinear systems. There are two methods to explore the stability of nonlinear systems: the Lyapunov indirect approach and the Lyapunov direct approach. In previous work [27], we utilized the Lyapunov indirect approach and Gronwall-Bellman inequality to analyse the decay law of solution. It is an effective way to investigate the global asymptotic stability and controller synthesis of fractional order systems with nonlinearity. However, we are interested in the invariance of considered systems in this study, which means we are more concerned about the local asymptotic stability than the global asymptotic stability. Therefore, the method in [27] is not enough to handle the invariance estimation problem of fractional order systems with actuator saturation.

The Lyapunov direct approach introduce an energy function to analysis the stability of the nonlinear system directly. It is an efficient way to investigate the invariance of nonlinear system. In this paper, we primarily consider Mittag-Leffler stability of the closed-loop systems with the state feedback law using Lyapunov direct approach.

Remark 2. From Definition 1 and [18], one can obtain that the quadratic function $V_c(x) = x^{\mathrm{T}} P x$ is the most popular Lyapunov function candidate to investigate the stability and control method of integer order systems. However, for fractional order systems, it is not suitable to use this function directly. The main reason for this problem is that the quadratic Lyapunov function is not valid since the fractional derivative of composite function is an infinite series. Lemma 2 provides a direct way to adopt this quadratic Lyapunov function for the fractional order systems. Thus the quadratic Lyapunov function can be used to analyze the stability and stabilization of fractional order system by expressing a linear feedback law subject to saturation into a convex hull of a group of auxiliary linear feedback matrices.

The objective of this paper is to obtain a series of feedback functions to reduce the conservatism of the domain of attraction. To that end, we are interested in a function determined by a set of positive-definite matrices $P_1, P_2, P_3, ldots, P_N \in \mathbf{R}^{n\times n}$. Let $Q_j = P_j^{-1}$, $j \in I[1, N]$. For a vector $\gamma \in \mathbf{R}^N$, define

$$Q(\gamma) := \sum_{j=1}^{N} \gamma_j Q_j, \qquad P(\gamma) := Q^{-1}(\gamma),$$

where $\gamma \in \mathbf{R}^N : \sum_{j=1}^{N} \gamma_j = 1$, $\gamma \in \Gamma$. Thus we change the quadratic function as,

$$V_c(x) = x^{\mathrm{T}} P(\gamma) x.$$

From Lemmas 2-4 and Definition 1, the ellipsoid $\Psi(P, \rho) := \{x \in \mathbf{R}^n : x^{\mathrm{T}} P x \le \rho\}$ is said to be contractively invariant if $D^\alpha(x^{\mathrm{T}} P(\gamma) x) < 0$ for all $x \in \Psi(P, \rho) \setminus \{0\}$. Obviously, $\Psi(P, \rho)$ is inside the domain of attraction.

III. Domain Of Attraction Under a Given Saturated Linear Feedback

In this section, we consider the calculation problems corresponding to the quadratic function and apply it to fractional order linear systems. And then the estimation of the domain of attraction is illustrated.

A. Calculation Problems

From [26] and Remark 2, we know different reference polyhedrons will result in different ellipsoid set. Obviously, a single ellipsoid will result in much conservation. To deal with this situation and reduce the conservatism of the estimation, in this paper, a set of reference polyhedrons is used to produce multiple ellipsoids. Thus, these ellipsoids will combined to a convex hull and it can extend the domain of the invariant set $\Psi(P,\rho)$. One convex hull which is combined by three ellipsoids is shown in Fig. 1. We denote the convex hull of the ellipsoids

$$co\{\Psi(P_j,\rho), j\in I[1,N] := \{\sum_{j=1}^{N}\gamma_j x_j : x_j\in\Psi(P_j,\rho),\gamma\in\Gamma\}.$$

There are various ways to define the composite quadratic function with a set of matrices $P_1, P_2, \ldots, P_N > 0$. For the convenience of analysis, we define this function as follows,

$$V_c(x) := \max_{\gamma\in\Gamma} x^{\mathrm{T}}\left(\sum_{j=1}^{N}\gamma_j P_j\right)x,\quad \sum_{j=1}^{N}\gamma_j = 1.$$

For convenience, only two ellipsoids are considered in this paper. Thus,

$$\begin{aligned} V_c(x) &= \max_{\gamma\in\Gamma} x^{\mathrm{T}}\left(\sum_{j=1}^{N}\gamma_j P_j\right)x \\ &= \max_{\lambda\in[0,1]} x^{\mathrm{T}}\left(\lambda Q_1 + (1-\lambda))Q_2\right)^{-1}x, \end{aligned} \tag{3}$$

where $N = 2$, and λ is a real number. Denote $\Psi(P,\rho)$ as a bounded convex set, it can be easily translated into the following form by Schur complement,

$$\sup_{\gamma\in\Gamma}\delta, \tag{4}$$

$$\text{s.t.}\begin{bmatrix}\delta & x^{\mathrm{T}}\\ x & \sum\limits_{j=1}^{N}\gamma_j Q_j\end{bmatrix}\geq 0,\quad \sum_{j=1}^{N}\gamma_j = 1, \tag{5}$$

$$\Rightarrow \text{s.t.}\begin{bmatrix}\delta & x_i^{\mathrm{T}}\\ x_i & \lambda Q_1 + (1-\lambda)Q_2\end{bmatrix}\geq 0.$$

Fig. 1 shows a two dimensional level set which is the convex hull of three ellipsoids.

Remark 3. In order to calculate the optimal value of $\gamma = \gamma^*(x)$, the LMI problem (5) needs to be solved. However, the calculation is a time-consuming process. Reference [23] provides a simplified way to get $\gamma^*(x)$.

Denote that $\alpha(\lambda,x) = x^{\mathrm{T}}\left(\lambda Q_1 + (1-\lambda))Q_2\right)^{-1}x$. Then, let $x\in\mathbf{R}^n$ and $Q_1, Q_2 > 0$ be given. Assume that $Q_1 - Q_2$ is nonsingular. Let $U\in\mathbf{R}^{n\times n}$ be such that $U^{\mathrm{T}}U = UU^{\mathrm{T}} = I$ and $U^{\mathrm{T}}xx^{\mathrm{T}}U = \mathrm{diag}\{x^{\mathrm{T}}x, 0,\ldots,0\}$. Let $\hat{Q}_1 = U^{\mathrm{T}}Q_1U, \hat{Q}_2 = U^{\mathrm{T}}Q_2U$ and partition $\hat{Q}_1$ and $\hat{Q}_2$ as

$$\hat{Q}_1 = [\hat{q}_1, \hat{Q}_{12}], \hat{Q}_2 = [\hat{q}_2\quad \hat{Q}_{22}], \hat{q}_1, \hat{q}_2\in\mathbf{R}^{n\times 1}.$$

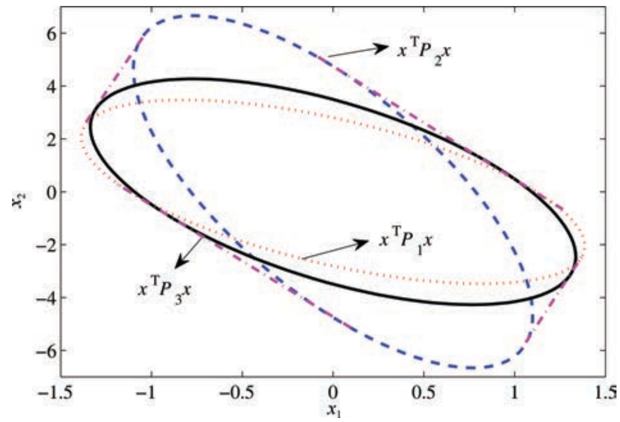

Fig. 1. The invariant set which is the convex hull of three ellipsoids (See the magenta dash-dotted outer curve).

Then $\frac{\partial\alpha}{\partial\lambda} = 0$ at $\lambda\in[0,1]$ if and only if

$$\det\begin{bmatrix}\lambda(\hat{Q}_{12}-\hat{Q}_{22})+\hat{Q}_{22} & \hat{Q}_1-\hat{Q}_2\\ 0_{(n-1)\times(n-1)} & \lambda(\hat{Q}_{12}-\hat{Q}_{22}^{\mathrm{T}})^{\mathrm{T}}+\hat{Q}_{22}^{\mathrm{T}}\end{bmatrix} = 0. \tag{6}$$

Using this method requires less time than solving the LMI problem.

Remark 4. In this section, only two ellipsoids are used in (3). For this case, $Q_1 - Q_2$ is nonsingular and $\gamma^*(x)$ can be easily calculated by the technology in Remark 3. Obviously, using more ellipsoids will make the conservatism less. However, for the case where $N > 2$, $\gamma^*(x)$ could be non unique in some special condition. Such as, the case that one of Q_j might be the combined convex hull of other matrices, which may be considered as degenerated. Although, one can assume that there is no this kind of condition, it is hard to keep the uniqueness and continuity of $\gamma^*(x)$. Thus, for $N > 2$ case, it is difficult to compute the $\gamma^*(x)$ and needs further study.

B. Analysis of Attraction Domain

Assume the set of ellipsoid $\Psi(P_j,\rho_j), j\in I[1,N]$ is given, the fractional order system can be invariant with a corresponding saturated linear feedback Fx. For simplicity and reducing the conservatism of the domain of attraction, a set of invariant ellipsoids $\Psi(P_j,\rho_j), j\in I[1,N]$ was considered with $\rho_j = 1$.

Theorem 1. Suppose that the state feedback law F and an ellipsoid $\Psi(P_j), j\in I[1,N]$ are given. If there exists a matrix $H_j\in\mathbf{R}^{m\times n}$ satisfying

$$\begin{aligned}&(A+B(E_iF+E_i^-H_j))^{\mathrm{T}}P_j + P_j(A+B(E_iF+E_i^-H_j))\\ &\quad\leq 0,\quad \forall i\in I[1,2^m], j\in I[1,N]\end{aligned} \tag{7}$$

and $\Psi(P_j)\subset\Phi(H_j)$, then $co\{\Psi(P_j), j\in I[1,N]\}$ is an invariant set of closed-loop system (2).

Proof. From Lemma 5 we know, the following inequality needs to be proved to ensure the asymptotic Mittag-Leffler stability of the fractional order linear system (2) corresponding the quadratic function (1),

$$D^{\alpha}V(t,x) = D^{\alpha}(x^{\mathrm{T}}P_jx) < 0, \forall x\in\Psi(P_j,\rho)\setminus\{0\}, \tag{8}$$

applying fractional inequality in Lemma 2 and Lemma 4 to inequality (8), gives

$$\begin{aligned}D^\alpha(x^{\mathrm{T}}P_jx) &\le 2x^{\mathrm{T}}P_j(D^\alpha(x))\\ &= 2x^{\mathrm{T}}P_j(Ax+BSat(Fx))\\ &= 2x^{\mathrm{T}}A^{\mathrm{T}}P_jx + 2x^{\mathrm{T}}P_jB\sum_{i=1}^{2^m}\eta_i(E_iFx+E_i^-H_jx),\end{aligned}$$

where $0 \le \eta_i \le 1$ and $\sum_{i=1}^{2^m}\eta_i = 1$.

From Theorem 1, one can obtain that $D^\alpha(x^{\mathrm{T}}P_jx) < 0$ for all $x \in \Psi(P_j,\rho)\backslash\{0\}$. And it is easy to notice that $Sat(Fx)$ is a convex hull of $E_iFx + E_i^-H_jx$ for all $i \in [1,2^m], j \in I[1,N]$ in (9). Thus, the Mittag-Leffler stability of the fractional order linear closed-loop system $D^\alpha x(t) = Ax(t) + BSat(Fx)$ is ensured.

The condition of $\Psi(P_j) \subset \Phi(H_j)$ is equivalent to $\rho h_{ji}P_j^{-1}h_{ji}^{\mathrm{T}} \le 1$, then it can be written as follows by Schur complement,

$$\begin{bmatrix}1 & h_{ji}(\frac{P_j}{\rho})^{-1}\\ (\frac{P_j}{\rho})^{-1}h_{ji}^{\mathrm{T}} & (\frac{P_j}{\rho})^{-1}\end{bmatrix} \ge 0, \tag{9}$$

for all $i \in [1,m]$.

Denote $Q_j = (\frac{P_j}{\rho})^{-1}$. Let $G_j = H_j(\frac{P_j}{\rho})^{-1}$ and the i-th row of matrix G_j be g_{ji}, i.e., $g_{ji} = h_{ji}(\frac{P_j}{\rho})^{-1}$. Hence, the condition $\Psi(P_j,\rho) \subset \Phi(H_j), j \in I[1,N]$ can be formulated as,

$$\begin{bmatrix}1 & g_{ji}\\ g_{ji}^{\mathrm{T}} & Q_j\end{bmatrix} \ge 0, \text{ for } i \in [1,m], j \in I[1,N], \tag{10}$$

where $Q_j \in \mathbf{R}^{n\times n}$, $G_j \in \mathbf{R}^{m\times n}$. Due to the fact that $x_0 \in co\{\Psi(P_j, j \in I[1,N])\}$, there exists $x_j \in \Psi(P_j)$ and $\gamma_j \ge 0, j \in I[1,N]$, such that $\gamma_1+\gamma_2+\cdots+\gamma_N = 1$ and $x_0 = \gamma_1x_1+\gamma_2x_2+\cdots+\gamma_Nx_N$. Denote $Q = \gamma_1Q_1+\gamma_2Q_2+\cdots+\gamma_NQ_N$ and $P = Q^{-1}$. Then from Lemma 1, one can obtain that $\Psi(P) \subset co\{\Psi(P_j), j \in I[1,N]\}$.

Let $G = \gamma_1G_1+\gamma_2G_2+\cdots+\gamma_NG_N$ and g_i be the ith row of G, combining inequality (7) and inequality (10), gives

$$\begin{aligned}&Q(A{+}BE_iF)^{\mathrm{T}} + (A+BE_iF)Q\\ &\quad + G^{\mathrm{T}}E_i^-B^{\mathrm{T}} + BE_i^-G \le 0, \forall i \in [1,2^m],\end{aligned}\tag{11}$$

and

$$\begin{bmatrix}1 & g_i\\ g_i^{\mathrm{T}} & Q\end{bmatrix} \ge 0, \text{ for } i \in [1,m]. \tag{12}$$

Denote $H = GQ^{-1}$, then one can obtain

$$\begin{aligned}&(A+B(E_iF+E_i^-H))^{\mathrm{T}}P + P(A+B(E_iF+E_i^-H))\\ &\quad \le 0, \forall i \in I[1,2^m],\end{aligned}\tag{13}$$

and

$$\begin{aligned}&\begin{bmatrix}1 & h_k(\frac{P}{\rho})^{-1}\\ (\frac{P}{\rho})^{-1}h_k^{\mathrm{T}} & (\frac{P}{\rho})^{-1}\end{bmatrix} \ge 0, k \in I[1,m]\\ &\quad \Leftrightarrow \Psi(P) \subset \Phi(H).\end{aligned}\tag{14}$$

From the above fact, one can easily derive the conclusion that $\Psi(P)$ is invariant, which means that a trajectory starting from x_0 will stay inside of $\Psi(P_j)$ and it is a subset of $co\{\Psi(P_j), j \in I[1,N]\}$. Since that x_0 is a random point inside $co\{\Psi(P_j), j \in I[1,N]\}$, then one can obtain that the convex hull is an invariant set. If "$<$" holds for all the inequalities, then the state trajectory will converge to the origin for all the initial states. □

Theorem 1 shows that if each $\Psi(P_j)$ is invariant, then, their convex hull, $co\{\Psi(P_j), j \in I[1,N]\}$ is also invariant. This theorem provides the sufficient condition for an ellipsoid to be inside the domain of attraction. To maximize the cross-section of the ellipsoid in the state-space $\mathbf{R}^n$, the following type of convex set is considered in this paper:

$$X_R = co\{x_1, x_2, \ldots, x_l\},$$

where X_R represents polyhedrons. Then the problem that how to choose the ellipsoid $\Psi(P^*,\rho)$ with the largest volume from all the ellipsoids $\Psi(P,\rho)$ which satisfies the Theorem 1 is considered. It can be concerned with the maximum quantity of $\lambda_R(\Psi(P,\rho))$ and then it is formulated as

$$\sup_{P_j>0,\rho,H_j} \lambda, \tag{15}$$

$$\text{s.t. } \lambda X_R \subset \Psi(P_j,\rho), \tag{16}$$

$$\begin{aligned}&(A+BE_iF+E_i^-H_j)^{\mathrm{T}}P_j\\ &\quad + P_j(A+BE_iF+E_i^-H_j) < 0, \text{ for } i \in [1,2^m],\end{aligned}\tag{17}$$

where $P_j \in \mathbf{R}^{n\times n}$, $H_j \in \mathbf{R}^{m\times n}, j \in I[1,N], \rho = 1$. Inequalities (15)-(17) can be formulated as follows:

$$\inf_{Q_j>0,G} \Lambda, \tag{18}$$

$$\begin{bmatrix}\Lambda & x_{ji}^{\mathrm{T}}\\ x_{ji} & Q_j\end{bmatrix} \ge 0, \text{ for } i \in [1,l], j \in I[1,N], \tag{19}$$

$$\begin{aligned}&Q_jA^{\mathrm{T}} + AQ_j + BE_i^{-1}G_j + G_j^{\mathrm{T}}(BE_i^{-1})^{\mathrm{T}}\\ &\quad + Q_j(BE_iF)^{\mathrm{T}} + (BE_iF)Q_j, \text{ for } i \in [1,2^m],\end{aligned}\tag{20}$$

where $\Lambda = \frac{1}{\lambda^2}$, $Q_j = (\frac{P_j}{\rho})^{-1}$, $G_j = H_j(\frac{P_j}{\rho})^{-1}$.

IV. Controller Synthesis

In this section, the possibility that a level set can get invariant with controls subject to actuator saturation is investigated. Then, a continuous feedback law that guarantees the invariance of the convex hull of ellipsoids $co\{\Psi(P_j), j \in I[1,N]\} = L_{V_c}(1)$ is constructed.

Considering the fractional order system $D^\alpha(x) = Ax + BSat(u)$, where $0 < \alpha < 1$. Only the initial condition needs to be specified. For x_0, the state trajectory of system (2) is defined as $\psi(t,x_0)$. Then the *domain of attraction* of the origin is

$$\mathit{\Psi} := \{x_0 \in \mathbf{R}^n : \lim_{t\to\infty}\psi(t,x_0) = 0\}.$$

Denote $P \in \mathbf{R}^{n\times n}$ be a positive-definite matrix and $V_c(x) = x^{\mathrm{T}}Px$ as Lyapunov function of fractional order system (2). Then, the ellipsoid $\Psi(P,\rho) = \{x \in \mathbf{R}^n : x^{\mathrm{T}}Px \le \rho\}$ is said to be *(contractively) invariant* if $D^\alpha V(x) < 0$ for all $x \in \Psi(P,\rho)\backslash\{0\}$, and then ellipsoid $\Psi(P^*,\rho)$ is called the *invariant set* of fractional order systems (2). Let $\rho = 1$, hence, if the ellipsoid $\Psi(P)$ is contractive invariant set, it is inside the domain of attraction.

Fact 1[25]**.** For a raw vector $f_0 \in \mathbf{R}^{1\times n}$ and matrix $P > 0$, $\Psi(P) \subset \Phi(f_0)$ if and only if,

$$f_0 P^{-1} f_0^{\mathrm{T}} \leq 1 \Leftrightarrow \begin{bmatrix} 1 & f_0 P^{-1} \\ P^{-1} f_0^{\mathrm{T}} & P^{-1} \end{bmatrix} \geq 0.$$

The equality $f_0 P^{-1} f_0^{\mathrm{T}} = 1$ holds if and only if the ellipsoid $\Psi(P)$ touches the hyperplane $f_0 x = 1$ at $x_0 = P^{-1} f_0^{\mathrm{T}}$ (the only intersection), namely,

$$1 = f_0 x_0 > f_0 x \quad \forall x \in \Psi(P) \backslash \{x_0\},$$

the ellipsoid $\Psi(P)$ lies strictly between the hyperplane $f_0 x = 1$ and $f_0 x = -1$ without touching them.

Theorem 2. Assuming that each of ellipsoids $\Psi(P_j), j \in I[1, N]$ is contractively invariant. Then, as a result, the level set $L_{V_c}(1)$ is also contractively invariant.

Proof. The proof of invariance is as follows. Let $V_j(x) = x^{\mathrm{T}} P_j x$. Assuming there exists a $u_j \in \mathbf{R}^m, |u_j|_\infty \leq 1$ such that

$$D^\alpha(x_j^{\mathrm{T}} P_j x_j) \leq 2x_j^{\mathrm{T}} P_j (Ax_j + BSat(u_j)) \leq 0. \tag{21}$$

As the fact that if $D^\alpha V_j(x) < 0$ for all $x \in \Psi(P_j)\backslash\{0\}$, and then ellipsoid $\Psi(P_j)$ is said to be invariant. From Lemma 2, we know,

$$D^\alpha(X_j^{\mathrm{T}} P_j x_j) \leq 2x_j^{\mathrm{T}} P_j D^\alpha(x_j),$$

and if the inequality

$$2x_j^{\mathrm{T}} P_j D^\alpha(x_j) \leq 0,$$

is specified, the ellipsoid $\Psi(P_j), j \in I[1, N]$ is contractively invariant. Let $r_0 = (P_0 x_0)^{\mathrm{T}}$, $x_0 \in \mathcal{L}_{V_c}(1)$, where $\mathcal{L}_{V_c}(1)$ is the edge of $L_{V_c}(1)$. Then we get $r_0 x_0 = x_0^{\mathrm{T}} P(\gamma^*(x_0)) x_0 = 1$, which means the hyperplane $r_0 x = 1$ is tangential to the convex set $L_{V_c}(1)$ at x_0. Then the level set $L_{V_c}(1)$ lies between $r_0 x = 1$ and $r_0 x = -1$, therefore

$$\Psi(P_j) \subset \Phi(r_0) \forall j \in I[1, N_0],$$

and

$$1 = r_0 x_0 \geq r_0 x_j.$$

In fact, the $r_0 x_j = 1$ is established for all $r_j \in I[1, N]$. It can be proved as follows: suppose that $r_0 x_j < 1$ for some j, such as $r_0 x_1 < 1$, then

$$\begin{aligned} 1 &= r_0 x_0 = \xi_1 r_0 x_1 + \sum_{j=2}^{N_0} \xi_j r_0 x_j \\ &\leq \xi_1 r_0 x_1 + \sum_{j=2}^{N_0} \xi_j \leq \sum_{j=1}^{N_0} \xi_j = 1, \end{aligned}$$

which is a contradiction. Similarly, the $r_0 x_j = 1$ implies that $\Psi(P_j)$ touches the hyperplane $r_0 x = 1$ at $x = x_j$. Then, the hyperplane $r_0 x = 1$ is tangential to $\Psi(P_j)$ at x_j for every $j \in I[1, N_0]$. One can obtain from Fact 1 that

$$r_0^{\mathrm{T}} = P_j x_j \quad \forall j \in I[1, N_0].$$

By inequality (21) and the assumption we know, there exists a $u_j \in \mathbf{R}^m, |u_j|_\infty < 1$ such that inequality (21) is satisfied. Let $u_0 = \sum_{j=1}^{N_0} \xi_j u_j$. Then, by $|u_0|_\infty \leq 1$ and by the convexity,

$$D^\alpha(x_0^{\mathrm{T}} P_0 x_0) \leq 2r_0(Ax_0 + BSat(u_0)) \leq 0.$$

Due to the fact that x_0 is a random point in $L_{V_c}(1)$, hence, the level set $L_{V_c}(1)$ is contractively invariant. □

Theorem 3. Consider ellipsoid $\Psi(P_j)$ and feedback matrices $F_j \in \mathbf{R}^{m\times n}$. For the closed-loop fractional order system (2), if the ellipsoid type convex set X_R is considered, then the state feedback matrix $F_j \in \mathbf{R}^{m\times n}$ can be obtained as $F_j = Y_j Q_j^{-1}$, where Y_j, Q_j are solutions of the following optimization problem:

$$\inf_{Q_j > 0, Y_j, G_j} \Lambda, \tag{22}$$

$$\text{s.t. } (10), (19), \text{ and}$$

$$\begin{aligned} &Q_j A^{\mathrm{T}} + AQ_j + BE_i^{-1} G_j + G_j^{\mathrm{T}} (BE_i^{-1})^{\mathrm{T}} \\ &\quad + Y_j^{\mathrm{T}} E_i^{\mathrm{T}} B^{\mathrm{T}} + BE_i Y_j \leq 0, \text{ for } i \in [1, 2^m], j \in [1, N]. \end{aligned} \tag{23}$$

Let $\gamma^*(x)$ be such that $x^{\mathrm{T}} P(\gamma^*(x)) x = V_c(x)$, define,

$$Y(\gamma) = \sum_{j=1}^{N} \gamma_j Y_j, \quad Q(\gamma) = \sum_{j=1}^{N} \gamma_j Q_j, \tag{24}$$

then the fractional order linear closed-loop system is invariant under the feedback $u = Sat(F((\gamma^*(x)x))$, which is continuous while the vector function $\gamma^*(\cdot)$ is continuous.

Proof. Let $G_j = Q_j H_j$, $G(\gamma) = \sum_{j=1}^{N} \gamma_j G_j$ and $H(\gamma) = G(\gamma) Q^{-1}(\gamma)$, give

$$\begin{aligned} &Q(\gamma) A^{\mathrm{T}} + AQ(\gamma) + BE_i^{-1} G(\gamma) + G(\gamma)^{\mathrm{T}} (BE_i^{-1})^{\mathrm{T}} \\ &\quad + Y(\gamma)^{\mathrm{T}} E_i^{\mathrm{T}} B^{\mathrm{T}} + BE_i Y(\gamma) \leq 0, \end{aligned} \tag{25}$$

for all $i \in [1, 2^m]$ and $\gamma \in \Gamma$. The previous inequality can be formulated as follows:

$$\begin{aligned} &(A + B(E_i F(\gamma) + D_i^- H(\gamma)))^{\mathrm{T}} P(\gamma) \\ &\quad + P(\gamma)(A + B(E_i F(\gamma) + D_i^- H(\gamma))) \\ &\quad \leq 0, \forall i \in I[1, 2^m]. \end{aligned} \tag{26}$$

By Lemma 6, $\Psi(P(\gamma)) \subset \Phi(F(\gamma))$ and inequality (26) can make sure that the ellipsoid set $\Psi(P(\gamma))$ is invariant under the control of $u = sat(F(\gamma)x)$. Thus, by Theorem 2, one can get the level set $L_{V_c}(1)$ is invariant under the control of $u = Sat(F(\gamma^*(x)))x$. □

V. Numerical Examples

A. Example 1. Comparative Example

We use an example of [22] to illustrate the effectiveness of our method. For fractional order linear systems (2), let $\alpha = 0.7$, and

$$A = \begin{bmatrix} 0.7 & -1.4 \\ -0.2 & 1.5 \end{bmatrix}, B = \begin{bmatrix} 1 & 0 \\ 0 & 1 \end{bmatrix}.$$

The following reference polyhedrons is chosen as the prescribed convex set:

$$X_R = co\{x, -x\},$$

where $x_1 = [1 \quad 0]^{\mathrm{T}}, x_2 = [0 \quad 1]^{\mathrm{T}}$. Then, according the approach we proposed in [21], the following two ellipsoids can be obtained

$$P_1 = \begin{bmatrix} 4.7515 & -0.3347 \\ -0.3347 & 2.2345 \end{bmatrix}, P_2 = \begin{bmatrix} 0.2985 & -0.5538 \\ -0.5538 & 2.9894 \end{bmatrix}.$$

The boundaries of the two ellipsoids are plotted in red solid curves, while the dotted curves are the boundaries of $\Psi(P(\gamma))$ as γ varies in the set Γ. The shape of $L_{V_c}(1) = \bigcup_{\gamma\in\Gamma} \Psi(P(\gamma))$ can be obtained by those blue dotted curves in Fig. 2. To illustrate the effectiveness of the proposed method, the following closed-ball $B_\epsilon := \{x \in \mathbf{R}^n : x^{\mathrm{T}}x \le 0.4326\}$, who is proposed in [22] is also demonstrated in Fig. 2.

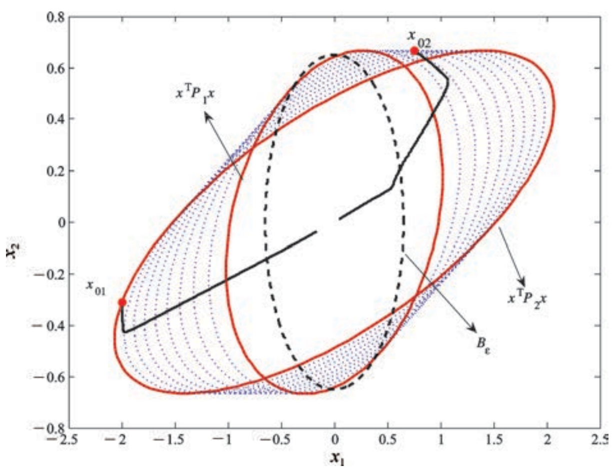

Fig. 2. Comparison between proposed method and existing method[22].

The convex combination of P_1 and P_2 in Fig. 2 shows that the proposed method provides a satisfactory estimation on the domain of attraction and also can obtain better estimation that the approach in [22].

Remark 5. From Fig. 2 we know, the closed-ball B_ϵ which proposed in [22] is almost contained in the convex hull of the proposed method. Two state trajectories started from initial points $x_{01} = [-2 \ -0.3127], x_{02} = [0.750.6665]$ on the boundary of $L_{V_c(1)}$ shows that, the trajectories are convergent to origin , and the proposed method provides better estimation on the domain of attraction than method in [22]. This method extend the domain of attraction. The control signals $u_1(t)$, $u_2(t)$ and the Lyapunov function $V_c(x(t))$ of example 1 are illustrated in Fig. 3. Comparative example indicates that the proposed method is less conservative than [22].

B. Example 2. Continuous State Feedback Control Law Synthesis

In this paper, we consider the fractional order system with

$$\alpha = 0.9, A = \begin{bmatrix} 1.6 & -0.5 \\ -0.6 & 0.6 \end{bmatrix}, B = \begin{bmatrix} 5 \\ -5 \end{bmatrix}.$$

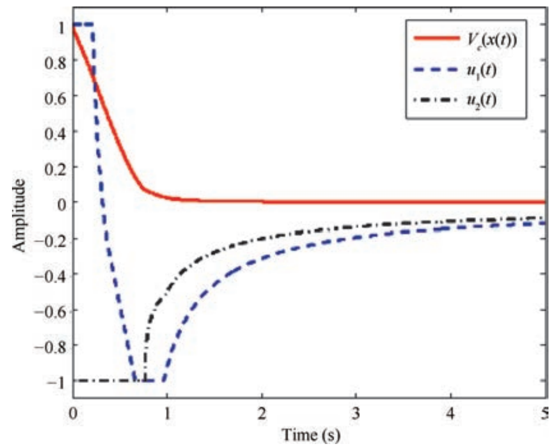

Fig. 3. Signals $u_1(t)$, $u_2(t)$ and the Lyapunov function $V_c(x(t))$.

For this example, we choose the following reference polyhedrons as the prescribed convex set:

$$X_R = co\{x_i, -x_i\}, \ i = 1, 2,$$

where $x_1 = [1 \quad 0]^{\mathrm{T}}, x_2 = [0 \quad 1]^{\mathrm{T}}$, then respectively, the following two feedback matrices can be designed with the approach proposed in [21],

$$F_1 = [-0.0414 \quad -0.2897], \quad F_2 = [0.2161 \quad -0.3540],$$

along with two ellipsoids $\Psi(P_1)$ and $\Psi(P_2)$, where,

$$P_1 = \begin{bmatrix} 0.7985 & 0.1881 \\ 0.1881 & 0.1270 \end{bmatrix},$$

$$P_2 = \begin{bmatrix} 1.6258 & 0.1881 \\ 0.1881 & 0.0443 \end{bmatrix}.$$

The matrix P_1 and F_1 are designed such that the closed-loop system (2) is locally Mittag-Leffler stable and the estimated ellipsoid invariant set is maximized with respect to the bounded convex set X_R. Similarly, the matrix P_2 and F_2 are designed such that $\lambda X_R \subset \Psi(P)$. The boundaries of the two ellipsoids are plotted in red solid curves, while the dotted curves are the boundaries of $\Psi(P(\gamma))$ as γ varies in the set Γ. The shape of $L_{V_c}(1) = \bigcup_{\gamma\in\Gamma} \Psi(P(\gamma))$ can be obtained by those blue dotted curves in Fig. 4. The $\gamma^*(x)$ can be obtained by computing the optimization problem (4) or the formula in (6).

From Theorem 2. we know,

$$F(\gamma^*) = (\gamma^* Y_1 + (1-\gamma^*)Y_2)(\gamma^* Q_1 + (1-\gamma^*)Q_2)^{-1},$$

$$Y_1 = \begin{bmatrix} -0.9000 & 1.7921 \end{bmatrix}, Y_2 = \begin{bmatrix} -0.9000 & 5.9397 \end{bmatrix},$$

and

$$Q_1 = \begin{bmatrix} 1.9228 & -2.8469 \\ -2.8469 & 12.0873 \end{bmatrix}, Q_2 = \begin{bmatrix} 1.2087 & -5.1320 \\ -5.1320 & 44.3652 \end{bmatrix}.$$

Fig. 5 shows that the state trajectories with different initial conditions. Obviously, the closed-loop system (2) is asymptotically Mittag-Leffler stable. To obtain the control signal and the composite quadratic function, the state trajectory from initial point $x_{01} = [1.2300 \ -3.9533]$ and $x_{02} = [-1.200 \ 4.2699]$

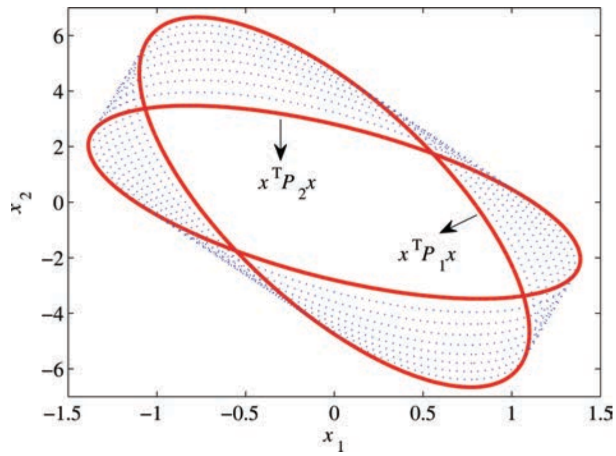

Fig. 4. Convex hull of two provided ellipsoids.

started from the boundary of level set $L_{V_c}(1)$ is illustrated in Fig. 5. The control signal $u(t)$ and the Lyapunov function $V_c(x(t))$ of trajectory started from x_{01} are demonstrated in Fig. 6, and the value of $\gamma^*(x)$ is plotted in Fig. 7 as $x(t)$ varies along the time.

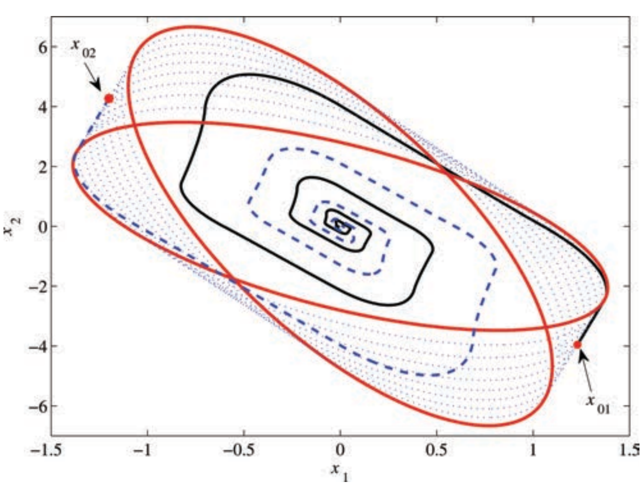

Fig. 5. State trajectory with different initial conditions.

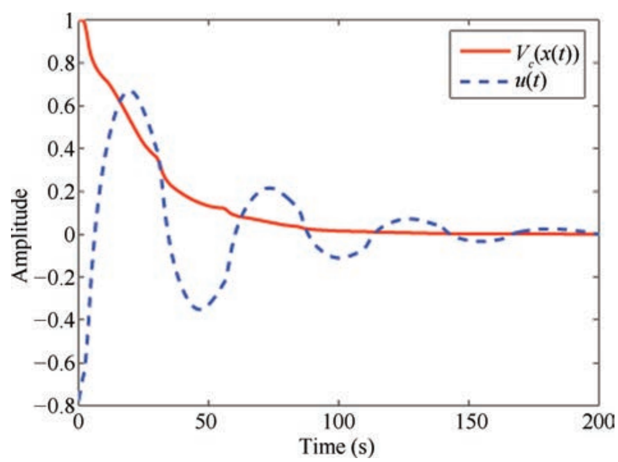

Fig. 6. Control signal $u(t)$ and the Lyapunov function $V_c(x(t))$.

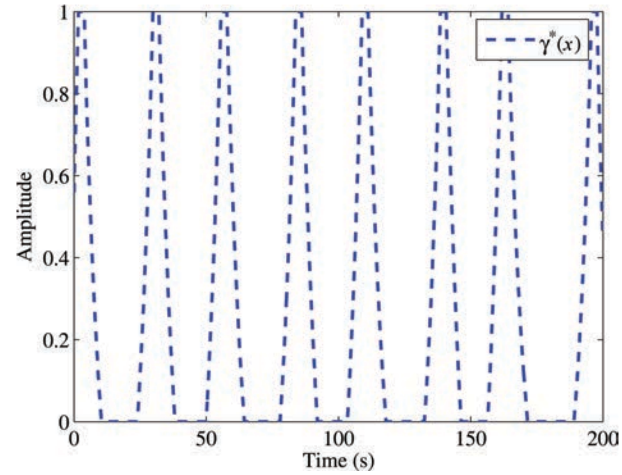

Fig. 7. $\gamma^*(x)$ varies in $[0, 1]$.

VI. Conclusion

This paper provides a method for the estimation of the domain of attraction and state feedback synthesis utiize the convex combination form for fractional order systems subject to actuator saturation with the fractional order $0 < \alpha < 1$. The ellipsoidal invariant set of fractional order systems subject to actuator saturation is investigated by convex hull form for the first time. Then we demonstrate that the convex hull of ellipsoids can be made invariant for fractional order linear systems subject to actuator saturation if each ellipsoid in a set with a bounded control of the saturating actuators is invariant. The results show that the proposed method is effective to handle saturation nonlinearity. The composite quadratic Lyapunov function and Lyapunov direct approach are applied in this paper to estimate the invariant ellipsoids for fractional order systems. In particular, by using a set of feedback laws to make the convex hull of a set of ellipsoid invariant, one proper method is proposed to construct a continuous feedback law.

In order to facilitate analysis, the case $N = 2$ is chosen in this paper. A more effective way needs to be specified to compute the condition $N > 2$. Nevertheless, the stability analysis problem for fractional order system subject to actuator saturation with the fractional order $1 < \alpha < 2$ is still unsolved. The stability conditions for fractional order systems is concerned with the fractional order, thus our future work is related to the problem of order-dependent estimation on the domain of attraction.

References

[1] Sabatier J, Agrawal O P, Machado J A T. *Advances in Fractional Calculus*. Netherlands: Springer, 2007.

[2] Mainardi F. Fractional calculus. *Fractals and Fractional Calculus in Continuum Mechanics*. Vienna: Springer, 1997. 291−348

[3] Meral F C, Royston T J, Magin R. Fractional calculus in viscoelasticity: an experimental study. *Communications in Nonlinear Science and Numerical Simulation*, 2010, **15**(4): 939−945

[4] Baleanu D, Golmankhaneh A K, Golmankhaneh A K, Baleanu M C. Fractional electromagnetic equations using fractional forms. *International Journal of Theoretical Physics*, 2009, **48**(11): 3114−3123

[5] Luo Y, Chen Y Q. Fractional order [proportional derivative] controller for a class of fractional order systems. *Automatica*, 2009, **45**(10): 2446−2450
[6] Luo Y, Chen Y Q. Stabilizing and robust fractional order PI controller synthesis for first order plus time delay systems. *Automatica*, 2012, **48**(9): 2159−2167
[7] Kheirizad I, Jalali A A, Khandani K. Stabilization of all-pole unstable delay systems by fractional-order [PI] and [PD] controllers. *Transactions of the Institute of Measurement and Control*, 2013, **35**(3): 257−266
[8] Hu T S, Lin Z L, Chen B M. An analysis and design method for linear systems subject to actuator saturation and disturbance. *Automatica*, 2002, **38**(2): 351−359
[9] Zhang L X, Boukas E K. Stability and stabilization of Markovian jump linear systems with partly unknown transition probabilities. *Automatica*, 2009, **45**(2): 463−468
[10] Ma S, Zhang C, Zhu S. Robust stability for discrete-time uncertain singular Markov jump systems with actuator saturation. *IET Control Theory & Applications*, 2011, **5**(2): 255−262
[11] Chen Y Q, Moore K L. On $D\alpha$-type iterative learning control. In: Proceedings of the 40th IEEE Conference on Decision and Control. Orlando, FL: IEEE, 2001. 4451−4456
[12] Li Y, Chen Y, Ahn H S. Fractional order iterative learning control. In: Proceedings of the ICCAS-SICE 2009. Fukuoka, Japan: IEEE, 2009. 3106−3110
[13] Li Y, Chen Y Q, Ahn H S. Fractional-order iterative learning control for fractional-order linear systems. *Asian Journal of Control*, 2011, **13**(1): 54−63
[14] Lu J G, Chen Y Q. Stability and stabilization of fractional-order linear systems with convex polytopic uncertainties. *Fractional Calculus and Applied Analysis*, 2013, **16**(1): 142−157
[15] Li C, Wang J C. Robust stability and stabilization of fractional order interval systems with coupling relationships: the $0 < \alpha < 1$ case. *Journal of the Franklin Institute*, 2012, **349**(7): 2406−2419
[16] Lu J G, Ma Y D, Chen W D. Maximal perturbation bounds for robust stabilizability of fractional-order systems with norm bounded perturbations. *Journal of the Franklin Institute*, 2013, **350**(10): 3365−3383
[17] Liao Z, Peng C, Li W, Wang Y. Robust stability analysis for a class of fractional order systems with uncertain parameters. *Journal of the Franklin Institute*, 2011, **348**(6): 1101−1113
[18] Jiao Z, Zhong Y S. Robust stability for fractional-order systems with structured and unstructured uncertainties. *Computers & Mathematics with Applications*, 2012, **64**(10): 3258−3266
[19] Li Y, Chen Y Q, Podlubny I. Mittag-Leffler stability of fractional order nonlinear dynamic systems. *Automatica*, 2009, **45**(8): 1965−1969
[20] Yu J M, Hu H, Zhou S B, Lin X R. Generalized Mittag-Leffler stability of multi-variables fractional order nonlinear systems. *Automatica*, 2013, **49**(6): 1798−1803
[21] Li C, Wang J, Lu J. Observer-based robust stabilisation of a class of non-linear fractional-order uncertain systems: an linear matrix inequalitie approach. *IET Control Theory & Applications*, 2012, **6**(18): 2757−2764
[22] Lim Y H, Oh K K, Ahn H S. Stability and stabilization of fractional-order linear systems subject to input saturation. *IEEE Transactions on Automatic Control*, 2013, **58**(4): 1062−1067
[23] Hu T S, Lin Z L. Composite quadratic Lyapunov functions for constrained control systems. *IEEE Transactions on Automatic Control*, 2003, **48**(3): 440−450
[24] Duarte-Mermoud M A, Aguila-Camacho N, Gallegos J A, Castro-Linares R. Using general quadratic Lyapunov functions to prove Lyapunov uniform stability for fractional order systems. *Communications in Nonlinear Science and Numerical Simulation*, 2015, **22**(1−3): 650−659
[25] Hu T S, Lin Z L. *Control Systems with Actuator Saturation: Analysis and Design*. Basel: Birkhäuser, 2001.
[26] Li C, Lu J G. On the ellipsoidal invariant set of fractional order systems subject to actuator saturation. In: Proceedings of the 34th Chinese Control Conference. Hangzhou, China: IEEE, 2015. 800−805
[27] Li C, Wang J C, Lu J G, Ge Y. Observer-based stabilisation of a class of fractional order non-linear systems for $0 < \alpha < 2$ case. *IET Control Theory & Applications*, 2014, **8**(13): 1238−1246

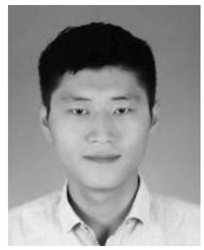

Kai Chen received the B. S. degree from Hainan University in 2015. He is now a postgraduate student in Hainan University. His research interests include robust control, fractional order control, and pattern recognition.

Junguo Lu received the B. S. and Ph. D. degrees from Nanjing University of Science and Technology, China, in 1997 and 2002, respectively. He is a former senior research associate and research fellow in City University of Hong Kong, China and is now professor in Shanghai Jiao Tong University, China. His research interests include intelligent robotics, fractional order control theory, and complex networks.

Chuang Li received his B. S. and M. S. degrees from Naval University of Engineering in 2004 and from Guangxi University in 2009, respectively. He received his Ph. D. degree from Shanghai Jiao Tong University in 2013. He is now a lecturer in Hainan University. His research interests include robust control, fractional order control theory, and model predictive control. Corresponding author of this paper.

Constrained Swarm Stabilization of Fractional Order Linear Time Invariant Swarm Systems

Mojtaba Naderi Soorki and Mohammad Saleh Tavazoei, *Member, IEEE*

***Abstract*—This paper deals with asymptotic swarm stabilization of fractional order linear time invariant swarm systems in the presence of two constraints: the input saturation constraint and the restriction on distance of the agents from final destination which should be less than a desired value. A feedback control law is proposed for asymptotic swarm stabilization of fractional order swarm systems which guarantees satisfying the above-mentioned constraints. Numerical simulation results are given to confirm the efficiency of the proposed control method.**

***Index Terms*— Fractional order system, swarm system, swarm stability, input saturation, constraint stabilization.**

I. INTRODUCTION

COORDINATION of multi-agent swarm systems has attracted great interest in recent years. Coordinated movement of fish and formation of birds are two examples of coordination of multi-agent swarm systems in nature. Also, it is known that the swarm behavior of networks of agents has potential applications in various areas (for example in formation control[1−2], flocking[3] and sensor networks[4]). Asymptotic swarm stability, as a general form of consensus, is one of the interesting behaviors in swarm systems. Till now, different studies have been done in this regard[5−9]. The dynamic model of agents in most of these studies has been considered in a classical integer order form, whereas the dynamic model of many real-world systems can be better described by fractional order dynamical equations[10−11]. Considering this point, study on fractional order swarm systems has attracted much interest in recent years[12−20]. For example, these studies include obtaining conditions for coordination in the networked fractional order systems[12], time response behavior analysis of agents in asymptotically swarm stable fractional order swarm systems[16], controller design for enforcing the agents in uncertain fractional order systems to track a desired trajectory while achieving consensus[18], and deriving consensus conditions in the presence of communication time-delays[14,19−20].

In practice, we are faced with different constraints in coordination of multi-agent swarm systems (for example, measurement constraints[21], dealing with agents having nonlinear dynamics[22], communication constraints[23], uncertainty in the dynamical models of the agents[24], and time-varying communication links[25]). One of the major challenges in the swarm systems is to control the agents when they are exposed to input saturation constraint[26−29]. In real-world swarm systems, this constraint is commonly due to physical limitations of the actuators. In this paper, the aim is asymptotic swarm stabilization of fractional order linear time invariant swarm systems subject to input constraints. To clarify the motivation of the paper, let us give an example. Consider a multi-robot system composed of a large number of cooperative mobile robots[18]. Assume that the aim of coordination is consensus in such a system[30−31]. In some situations, it is more accurate and realistic to model these robots with fractional order differential equations[32−33] (for example, when the friction is modeled by the fractional order equations[34−35], or when the robots are driven on the sandy or muddy road[12]). In these situations, we face a multi-agent system with a fractional order swarm model. Also due to the physical constraints, in these cases the input torque that should be applied to the wheels of the robot for changing the velocity or the orientation is limited. Generally speaking, in the mentioned example the control objective is to achieve consensus in a multi-robot system as a fractional order swarm system where the control inputs are subjected to input constraints. This example clearly verifies the importance of controller design in the presence of control input constraints for achieving consensus in a fractional order swarm system.

Considering input saturation constraints, consensus in networked multi-agent systems has been studied in [26−29]. But, the dynamics of each agent in these papers is in classical integer order form. Recently, [36] has considered input saturation in stability and stabilization of fractional order linear systems. In the present paper, the results of[36] are used for proposing a control law for asymptotic swarm stabilization of fractional order swarm systems in the presence of input saturation constraints. Another constraint is also considered in this paper. More precisely, the other constraint is an assumption that during achieving consensus, all the agents will be inside a specified region and the distance of agents from the final destination is less than a desired value. To reveal the motivation for considering such a constraint in this paper, we again recall the above-mentioned example on consensus in a multi-robot system. In this swarm system, due to the communication and environmental limitations, it may be desirable that the distance between the robots and their final distention is less than a specified value during the reaching consensus. This control objective can be satisfied by considering the second constraint in the controller design

Manuscript received August 31, 2015; accepted January 1, 2016. This work was supported by the Research Council of Sharif University of Technology under Grant (G930720). Recommended by Associate Editor YangQuan Chen.

Citation: Mojtaba Naderi Soorki, Mohammad Saleh Tavazoei. Constrained swarm stabilization of fractional order linear time invariant swarm systems. *IEEE/CAA Journal of Automatica Sinica*, 2016, **3**(3): 320−331

Mojtaba Naderi Soorki and Mohammad Saleh Tavazoei are with Electrical Engineering Department, Sharif University of Technology, Azadi Ave, Tehran 11365-9363, Iran (email: mojtabanaderi@aut.ac.ir; tavazoei@sharif.edu).

Color versions of one or more of the figures in this paper are available online at http://ieeexplore.ieee.org.

procedure. In summary, the main contribution of the paper is to propose a feedback controller for asymptotic swarm stabilization of fractional order linear time invariant swarm systems in the presence of the aforementioned constraints.

This paper is organized as follows: The problem formulation and some preliminaries are given in Section II. Section III presents some properties on linear transformations appeared in our study. The control law for the asymptotic swarm stabilization of fractional order swarm systems with input constraint is obtained in Section IV. Simulation results in Section V are given to confirm the analytical results. Finally, conclusions in Section VI close the paper.

II. Preliminaries

A. Notations

The notations used in this paper are fairly standard. $\mathbf{R}^+$ denotes the set of positive real numbers. sgn$(\cdot)$ and *sat*$(\cdot)$ respectively indicate the sign and saturation functions. $sym\{X\}$, where X is a real square matrix, denotes the symmetric matrix $X^{\mathrm{T}}+X$. diag $\{c_1, c_2, \dots, c_n\}$ specifies a diagonal matrix with diagonal entries c_1, c_2, $\dots$, and c_n. If $z \in \mathbf{C}$, $arg(z)$ denotes the argument of z. Also, I_m and $\otimes$ respectively indicate the $m \times m$ identity matrix and the kronecker product operator. $eig(A)$ denotes eigenvalue of the square matrix A. $Nu(M)$ and $Ra(M)$ are respectively the null space and the range space of matrix M. $\|\cdot\|$ and $\|\cdot\|_\infty$ specify respectively 2-norm and infinity-norm functions. The distance between vector $e = [e_1, e_2, \dots, e_n] \in \mathbf{R}^n$ and the non-empty set S is defined by $D(e, S) := inf_{s \in S} ||e - s||$. Moreover, $A_{(i)}$ denotes the i-th row of matrix $A \in \mathbf{R}^{m\times n}$. Finally for the vectors $A_1, A_2, A_3 \in \mathbf{R}^n$, the vector inequality $A_1 \le A_2 \le A_3$ means $A_{1_{(i)}} \le A_{2_{(i)}} \le A_{3_{(i)}}, i = 1, \dots n$.

B. Fractional Order Linear Time Invariant Swarm Systems

A fractional order linear time invariant swarm system of N agents can be described by[16]

$$D_t^\alpha x_i = Ax_i + F\sum_{j=1}^{N} w_{ij}(x_j - x_i) + Bu_i, \quad i = 1, 2, \dots, N. \tag{1}$$

where $A \in \mathbf{R}^{d\times d}$, $F \in \mathbf{R}^{d\times d}, B \in \mathbf{R}^{d\times m}$, $x_i \in \mathbf{R}^d$, $u_i \in \mathbf{R}^m$, $w_{ij} \ge 0$, and $\alpha \in (0, 1]$. Also, in (1) D_t^α denotes the Caputo fractional derivative operator defined as follows[37].

$$D_t^\alpha f(t) = \frac{1}{\Gamma(\lceil\alpha\rceil - \alpha)} \int_0^{\mathrm{T}} \frac{f^{(\lceil\alpha\rceil)}(\tau)}{(t-\tau)^{\alpha - \lceil\alpha\rceil + 1}} \mathrm{d}\tau, \quad 0 < \alpha \notin \mathbf{Z}. \tag{2}$$

In this swarm system, the communication among agents is described by a weighted graph of order N, denoted by G, such that each agent is corresponding to a vertex of G. This graph may either be directed or undirected. w_{ij} in (1) indicates the weight of the edge between i-th and j-th agents and can be considered as a measure of data transmission between these two agents[38]. The adjacency matrix of graph G is as follows:

$$W_G = \begin{bmatrix} w_{11} & \dots & w_{1N} \\ \vdots & \ddots & \vdots \\ w_{N1} & \cdots & w_{NN} \end{bmatrix}$$

The concept of asymptotic swarm stability in a swarm system is defined on the basis of the relative distances between the agents[38].

Definition 1 (Asymptotic swarm stability)[38]. The fractional order linear time invariant swarm system in (1) is asymptotically swarm stable if for each $\bar{\varepsilon} > 0$ there exists $\bar{T} > 0$ such that $\|x_i(t) - x_j(t)\| < \bar{\varepsilon}$ for all $i, j \in \{1, 2, \dots, N\}$ and $t > \bar{T}$.

Considering the pseudo state vector of agents as $x = [x_1^{\mathrm{T}}, \dots, x_N^{\mathrm{T}}]^{\mathrm{T}}$, the swarm system in (1) can be rewritten as[38]

$$D_t^\alpha x = (I_N \otimes A - L \otimes F)x + (I_N \otimes B)U, \tag{3}$$

where $U = [u_1^{\mathrm{T}}, \dots, u_N^{\mathrm{T}}]^{\mathrm{T}}$ is the input vector and $L = L(G)$ is the Laplacian matrix of graph G[39]. In this paper, the following assumption is considered on communication graph G.

Assumption 1. Graph G in swarm system (1) is in one of the following forms:

1) G is an undirected connected graph.

2) G is a directed graph which includes a spanning tree and the eigenvalues of its Laplacian matrix are real numbers.

Let $\lambda_1 = 0$, $\lambda_2, \dots, \lambda_N \in \mathbf{R}^+$ be the eigenvalues of the Laplacian matrix L of fractional order linear time invariant swarm system in (1) (Considering Assumption 1, the Laplacian matrix L has exactly one zero eigenvalue and its other eigenvalues are positive real[5]). Also, assume that the Jordan canonical form of L is denoted by J. This means that there exists a non-singular matrix T such that

$$J = TLT^{-1} = \begin{bmatrix} 0 & 0 & 0 & \cdots & 0 \\ 0 & \lambda_2 & * & \cdots & 0 \\ \vdots & \vdots & \vdots & \ddots & \vdots \\ 0 & 0 & \dots & \dots & * \\ 0 & 0 & \cdots & 0 & \lambda_N \end{bmatrix},$$

where "$*$" may either be 1 or 0. By defining $\tilde{x} = [\tilde{x}_1^{\mathrm{T}}, \tilde{x}_2^{\mathrm{T}}, \dots, \tilde{x}_N^{\mathrm{T}}]^{\mathrm{T}} = (T \otimes I_d)x$ and $\tilde{U} = [\tilde{u}_1^{\mathrm{T}}, \tilde{u}_2^{\mathrm{T}}, \dots, \tilde{u}_N^{\mathrm{T}}]^{\mathrm{T}} = (T \otimes I_m)U$, the swarm system in (3) is rewritten as

$$D_t^\alpha \tilde{x} = (I_N \otimes A - J \otimes F)\tilde{x} + (I_N \otimes B)\tilde{U}, \tag{4}$$

where matrix $I_N \otimes A - J \otimes F$ is of the form

$$I_N \otimes A - J \otimes F = \begin{bmatrix} A & 0 & 0 & \cdots & 0 \\ 0 & A - \lambda_2 F & \times & \cdots & 0 \\ 0 & \vdots & \vdots & \ddots & \vdots \\ \vdots & 0 & \cdots & \cdots & \times \\ 0 & 0 & \cdots & 0 & A - \lambda_N F \end{bmatrix} \in \mathbf{R}^{Nd \times Nd}, \tag{5}$$

and each "$\times$" represents a block in $\mathbf{R}^{d\times d}$ that may either be $-F$ or 0[16, 38]. Also, matrix $I_N \otimes B$ in (4) is expressed as follows.

$$I_N \otimes B = \begin{bmatrix} B & 0 & 0 & \cdots & 0 \\ 0 & B & 0 & \cdots & 0 \\ \vdots & \vdots & \vdots & \ddots & \vdots \\ 0 & 0 & \cdots & \cdots & 0 \\ 0 & 0 & \cdots & 0 & B \end{bmatrix} \in \mathbf{R}^{Nd\times Nm}. \tag{6}$$

The following lemma presents the necessary and sufficient conditions for asymptotic swarm stability of the fractional order swarm system (1) by checking the asymptotic stability of a fractional order linear time invariant system.

Lemma 1[38]**.** The fractional order linear time invariant swarm system (1) with Assumption 1 is asymptotically swarm stable if and only if the following system

$$D_t^{\alpha}\hat{x} = \hat{A}\hat{x} + \hat{B}\hat{U}, \tag{7}$$

is asymptotically stable where $\hat{x} = [\tilde{x}_2^{\mathrm{T}}, \tilde{x}_3^{\mathrm{T}}, \ldots, \tilde{x}_N^{\mathrm{T}}]^{\mathrm{T}} \in \mathbf{R}^{(N-1)d}$, $\hat{U} = [\tilde{u}_2^{\mathrm{T}}, \tilde{u}_3^{\mathrm{T}}, \ldots, \tilde{u}_N^{\mathrm{T}}]^{\mathrm{T}} \in \mathbf{R}^{(N-1)m}$ and matrices $\hat{A}$ and $\hat{B}$ are defined as follows:

$$\hat{A} = \begin{bmatrix} A-\lambda_2 F & \times & 0 & \cdots & 0 \\ 0 & A-\lambda_3 F & \times & \cdots & 0 \\ 0 & \vdots & \vdots & \ddots & \vdots \\ \vdots & 0 & \cdots & \cdots & \times \\ 0 & 0 & \cdots & 0 & A-\lambda_N F \end{bmatrix} \in \mathbf{R}^{(N-1)d\times(N-1)d} \tag{8}$$

$$\hat{B} = \begin{bmatrix} B & 0 & 0 & \cdots & 0 \\ 0 & B & 0 & \cdots & 0 \\ \vdots & \vdots & \vdots & \ddots & \vdots \\ 0 & 0 & \cdots & \cdots & 0 \\ 0 & 0 & \cdots & 0 & B \end{bmatrix} \in \mathbf{R}^{(N-1)d\times(N-1)m}$$

Although Lemma 1 has been presented in [38] for integer order case (i.e. where $\alpha = 1$), its proof can be easily extended to the fractional order case[16]. On the other hand, system (7) is asymptotically stable (or equivalently the swarm system (1) with Assumption 1 is asymptotically swarm stable) if and only if the condition $|arg(\lambda)| > \alpha\pi/2$ is satisfied for each eigenvalue λ of matrix $\hat{A}$[40]. In such a case, matrix $\hat{A}$ is called an α-Hurwitz matrix

C. Problem Statement

In this paper, the aim is asymptotic swarm stabilization of fractional order linear time invariant swarm system (1) under the following constraints:

Constraint 1. The control inputs $u_i, i = 1, 2, \ldots, N$, in (1) should be bounded as $|u_{i(l)}| \le \bar{u}_{i(l)}$, $i = 1, 2, \ldots, N, l = 1, 2, \ldots m$, where $\bar{u}_{i(l)} \in \mathbf{R}^+$ denotes the allowable upper bound for the l-th control input of i-th agent.

Constraint 2. The distance between $x(t) = [x_1^{\mathrm{T}}(t), \ldots, x_N^{\mathrm{T}}(t)]^{\mathrm{T}} \in \mathbf{R}^{Nd}$ and the set $\{x \in \mathbf{R}^{Nd} | x = [x_1^{\mathrm{T}}, \ldots, x_N^{\mathrm{T}}]^{\mathrm{T}},\ x_1 = x_2 = \cdots = x_N,\ x_i \in \mathbf{R}^d\,(i = 1, \ldots, N)\}$ in the Nd-dimensional space should be less than $\mu \in \mathbf{R}^+$ for each $t \ge 0$.

Constraint 1 specifies the input saturation constraints in the fractional order swarm system (1). Actually, this constraint will bound the input signals in (1) similar to the virtual saturation function $sat(u_i) : \mathbf{R}^m \to \mathbf{R}^m$ where

$$sat(u_i) = [sat(u_{i(1)}), sat(u_{i(2)}), \ldots, sat(u_{i(m)})]^{\mathrm{T}} \tag{9}$$

and $sat(u_{i(l)}), i = 1, 2, \ldots, N,\ l = 1, 2, \ldots, m$ is defined as follows[36].

$$sat(u_{i(l)}) = \mathrm{sgn}(u_{i(l)})\min(\bar{u}_{i(l)}, |u_{i(l)}|). \tag{10}$$

Also, Constraint 2 states that during reaching consensus the pseudo state vector of agents $(x(t))$ should be inside a specified region. Note that the line $x_1 = x_2 = \cdots = x_N$ expresses a situation in which the pseudo states of all agents are the same. This situation can be interpreted as the "final destination" in the problem of swarm stabilization. In fact, Constraint 2 enforces that during reaching consensus, the distance between agents and this final destination is less than a desired value specified by μ.

III. Some Properties of $x \to (QT \otimes I_d)x$

According to the definitions of pseudo-state variables $x = [x_1^{\mathrm{T}}, \ldots, x_N^{\mathrm{T}}]^{\mathrm{T}} \in \mathbf{R}^{Nd}$, $\tilde{x} = [\tilde{x}_1^{\mathrm{T}}, \tilde{x}_2^{\mathrm{T}}, \ldots, \tilde{x}_N^{\mathrm{T}}]^{\mathrm{T}} = (T \otimes I_d)x$, and $\hat{x} = [\tilde{x}_2^{\mathrm{T}}, \tilde{x}_3^{\mathrm{T}}, \ldots, \tilde{x}_N^{\mathrm{T}}]^{\mathrm{T}} \in \mathbf{R}^{(N-1)d}$ in the previous section, one can easily obtain the vector $\hat{x}$

$$\hat{x} = (Q \otimes I_d)(T \otimes I_d)x = (QT \otimes I_d)x, \tag{11}$$

where

$$Q = \begin{bmatrix} 0 & 1 & 0 & \cdots & 0 \\ \vdots & 0 & \vdots & \ddots & \vdots \\ 0 & \vdots & \vdots & \cdots & 0 \\ 0 & 0 & \cdots & 0 & 1 \end{bmatrix}_{(N-1)\times N.} \tag{12}$$

In this section, the linear transformation $x \in \mathbf{R}^{Nd} \to \hat{x} = (QT \otimes I_d)x \in \mathbf{R}^{(N-1)d}$ is studied from the viewpoint of geometric properties. We will use these geometric properties to solve the main problem in the next section. At first, consider the following lemma.

Lemma 2. By the linear transformation $x \to \hat{x} = Px$, where $P = QT \otimes I_d$, T is the transition matrix introduced in Section II-B and Q is defined as in (12), the closed ball $\beta_\varepsilon := \{\hat{x} \in \mathbf{R}^{(N-1)d} | \hat{x}^{\mathrm{T}}\hat{x} \le \varepsilon\}$ transforms to the region $\beta'_\varepsilon := \{x \in \mathbf{R}^{Nd} | x^{\mathrm{T}}zx \le \varepsilon\}$ with $z = P^{\mathrm{T}}P$.

Proof. By substituting $\hat{x}$ from (11) in the definition of the closed ball β_ε, the region β'_ε is easily obtained. □

It is clear that the center of the closed ball β_ε in Lemma 2 is the origin. According to Lemma 2, the set $\{x \in \mathbf{R}^{Nd} | x^{\mathrm{T}}zx = 0\}$ specifies all the vectors which are transformed by the aforementioned transformation to the origin. The geometric interpretation of this set is revealed in Lemma 3.

Lemma 3. If $P = QT \otimes I_d$, $z = P^{\mathrm{T}}P$, and matrices T and Q are as in Lemma 2, then $\{x \in \mathbf{R}^{Nd} | x_1 = x_2 = \cdots = x_N\} = \{x \in \mathbf{R}^{Nd} | x^{\mathrm{T}}zx = 0\}$.

Proof. To prove this lemma, we show that the set $\{x \in \mathbf{R}^{Nd} | x_1 = x_2 = \cdots = x_N\}$ is the only solution of the equation $x^{\mathrm{T}}zx=0$. The equation $x^{\mathrm{T}}zx=0$ can be written as

$$x^{\mathrm{T}}zx=x^{\mathrm{T}}P^{\mathrm{T}}Px=\|Px\|^2=0, \tag{13}$$

which is equivalent to

$$Px=(QT\otimes I_d)x=0. \tag{14}$$

For simplicity, assume that $d=1$ which results in $I_d=1$ (The proof can be easily extended for $d>1$). Assuming $I_d=1$ and using(12), (14) can be written as

$$QTx=\begin{bmatrix} t_{2,1} & \cdots & t_{2,N} \\ \vdots & \ddots & \vdots \\ t_{N,1} & \cdots & t_{N,N}\end{bmatrix}\begin{bmatrix} x_1 \\ x_2 \\ \vdots \\ x_N\end{bmatrix}=0, \tag{15}$$

where $t_{i,k}$ $(i=2,3,\ldots,N, k=1,2,\ldots,N)$ denotes the elements of similarity matrix T. On the other hand,

$$T\begin{bmatrix} \hat{t}_{11} \\ \hat{t}_{11} \\ \vdots \\ \hat{t}_{11}\end{bmatrix}=\begin{bmatrix} 1 \\ 0 \\ \vdots \\ 0\end{bmatrix}, \tag{16}$$

where $[\hat{t}_{11},\ldots,\hat{t}_{11}]^{\mathrm{T}}$ is the first column of matrix T^{-1}[16, 18]. Equation (16) means that the sum of all entries in each row (except the first row) of matrix T is zero, i.e. $\sum_{k=1}^{N} t_{i,k}=0, \mathrm{i}=2,3,\ldots,N$. As a result, according to (15), it is easy to conclude that each member of the set $\{x\in\mathbf{R}^{Nd}|x_1=x_2=\cdots=x_N\}$ is a solution for equation (13). Also, according to the independent linearity of the rows of the matrix T, the rank of matrix QT in (15) is $N-1$. So, the set $\{x\in\mathbf{R}^{Nd}|x_1=x_2=\cdots=x_N\}$ specifies all of the solutions of equation (13). □

To express a geometric property for the region β'_ε introduced in Lemma 2, some preliminary lemmas are needed. These lemmas (Lemmas 4-6) are as follows.

Lemma 4[41]**.** Let $\bar{G}\in\mathbf{R}^{n\times n}$ and $\bar{H}\in\mathbf{R}^{m\times m}$ be two arbitrary matrices and have singular values (eigenvalues) $\sigma_i, i=1,2,\ldots,n$ and μ_j, $j=1,2,\ldots,m$ respectively. Then, the mn singular values (eigenvalues) of matrix $\bar{G}\otimes\bar{H}$ are as follows.

$$\sigma_1\mu_1,\ldots,\sigma_1\mu_m,\ \sigma_2\mu_1,\ldots,\sigma_2\mu_m,\ \ldots\ ,\sigma_n\mu_1,\ldots,\sigma_n\mu_m. \tag{17}$$

Lemma 5. If $S:=S'\otimes I_d$, where matrix S' is defined as

$$S'=\begin{bmatrix} N-1 & -1 & \cdots & -1 \\ -1 & N-1 & \ddots & \vdots \\ \vdots & \vdots & \cdots & -1 \\ -1 & \cdots & -1 & N-1\end{bmatrix}\in\mathbf{R}^{N\times N}, \tag{18}$$

then

$$\|S\|=N. \tag{19}$$

Proof. It can be verified that the characteristic polynomial of matrix S' is

$$\det(\lambda I-S')=\lambda(\lambda-N)^{N-1}. \tag{20}$$

From (20), S' has one zero eigenvalue, and the other eigenvalues of this matrix are equal to N. Therefore, the maximum singular value of real symmetric matrix S' or equivalently its 2-norm is N. □

Lemma 6. Let $\rho_{\min}$ denote the minimum singular value of matrix QT where T is the transition matrix introduced in Section II-B and Q is defined by (12). In this case,

$$\|Sx\|\le\frac{N}{\rho_{\min}}\|Px\|,\quad \forall x\in\mathbf{R}^{Nd}, \tag{21}$$

where matrices P and S are respectively defined in Lemmas 2 and 5.

Proof. In the proof of Lemma 3, it is verified that $Nu(P)=\{x\in\mathbf{R}^{Nd}|x_1=x_2=\cdots=x_N\}$. On the other hand, by considering the structure of matrix S' in (18) and noting $S=S'\otimes I_d$ it is deduced that $Nu(S)=\{x\in\mathbf{R}^{Nd}|x_1=x_2=\cdots=x_N\}$. Therefore, subspaces $Nu(S)$ and $Nu(P)$ are identical, and consequently, the orthogonal complements of these subspaces (i.e., $Ra(S^{\mathrm{T}})$ and $Ra(P^{\mathrm{T}})$) are also identical. Now, by the range-null space decomposition of $\mathbf{R}^{Nd}$[42], each $x\in\mathbf{R}^{Nd}$ can be uniquely written as $x=x_{Nu}+x_{Ra}$ where $x_{Nu}\in Nu(S)=Nu(P)=\{x\in\mathbf{R}^{Nd}|x_1=x_2=\cdots=x_N\}$ and $x_{Ra}\in Ra(S^{\mathrm{T}})=Ra(P^{\mathrm{T}})$. Since $Sx_{Nu}=0$, for each $x\in\mathbf{R}^{Nd}$ decomposed in the form $x=x_{Nu}+x_{Ra}$ we have

$$\|Sx\|=\|Sx_{Ra}\|. \tag{22}$$

Let us define the new matrix $\hat{P}$ as follows:

$$\hat{P}=(Q^{\mathrm{T}}QT)\otimes I_d. \tag{23}$$

Considering the structures of matrices Q and QT from (12) and (15), it is deduced that matrix $Q^{\mathrm{T}}QT$ is in the form

$$Q^{\mathrm{T}}QT=\begin{bmatrix} 0 & \cdots & 0 \\ t_{2,1} & \cdots & t_{2,N} \\ \vdots & \ddots & \vdots \\ t_{N,1} & \cdots & t_{N,N}\end{bmatrix}. \tag{24}$$

As discussed in the proof of Lemma 3, we know that $\sum_{k=1}^{N} t_{i,k}=0,\ i=2,3,\ldots,N$. According to this equality, nonsingularity of matrix T, and structure of matrix $Q^{\mathrm{T}}QT$ in (24), it is found that $\hat{P}x_{Nu}=0$ if and only if $x_{Nu}\in\{x\in\mathbf{R}^{Nd}|x_1=x_2=\cdots=x_N\}$. Hence, $Nu(\hat{P})=Nu(S)=Nu(P)$, $Ra(\hat{P})=Ra(S)=Ra(P)$, and for each $x\in\mathbf{R}^{Nd}$ decomposed as $x=x_{Nu}+x_{Ra}$, we have

$$\left\|\hat{P}x\right\|=\left\|\hat{P}x_{Ra}\right\|. \tag{25}$$

It can be easily verified that matrix Q in (12) has the property $Q^{\mathrm{T}}Q=\left(Q^{\mathrm{T}}Q\right)^2$. This property enforces that $x^{\mathrm{T}}P^{\mathrm{T}}Px=x^{\mathrm{T}}\hat{P}^{\mathrm{T}}\hat{P}x$, for each $x\in\mathbf{R}^{Nd}$, and consequently $\|Px\|=\left\|\hat{P}x\right\|$. From this equality and (25),

$$\|Px\|=\left\|\hat{P}x_{Ra}\right\|. \tag{26}$$

Since T is an invertible matrix, the rank of matrix $Q^{\mathrm{T}}QT$ equals $N-1$. This means that matrix $Q^{\mathrm{T}}QT$ has one zero singular value (namely $\rho_1=0$) and $N-1$ nonzero singular values denoted by $\rho_2, \rho_3, \ldots, \rho_N$. Hence, according to Lemma 4 the singular values of matrix $\hat{P}$ are

$$\underbrace{0, \ldots, 0}_{d \text{ times}}, \underbrace{\rho_2, \ldots, \rho_2}_{d \text{ times}}, \underbrace{\rho_3, \ldots, \rho_3}_{d \text{ times}}, \ldots, \underbrace{\rho_N, \ldots, \rho_N}_{d \text{ times}}. \tag{27}$$

Now, consider the following two matrix inequalities

$$\|Sx_{Ra}\| \leq \|S\| \, \|x_{Ra}\|, \tag{28}$$

and

$$\rho_{\min} \|x_{Ra}\| \leq \left\|\hat{P}x_{Ra}\right\|, \tag{29}$$

for each $x_{Ra} \in Ra(\hat{P}) = Ra(S) = Ra(P)$, where $\rho_{\min}$ indicates the minimum nonzero singular value of matrix $\hat{P}$. From (15) and (24), it is found that the only difference between matrices $Q^{\mathrm{T}}QT$ and QT is an extra zero row. Hence, these two matrices have the same nonzero singular values (i.e. $\rho_2, \rho_3, \ldots, \rho_N$). This means that $\rho_{\min}$ is the minimum singular value of matrix QT. According to (28) and (29), it is obtained that

$$\|Sx_{Ra}\| \leq \|S\| \frac{\left\|\hat{P}x_{Ra}\right\|}{\rho_{\min}}. \tag{30}$$

By substituting $\|Sx_{Ra}\|$ and $\left\|\hat{P}x_{Ra}\right\|$ respectively from (22) and (26) in (30), and noting that $\|S\| = N$ (Lemma 5), inequality (21) is deduced. □

Finally, a geometric property for the region β'_ε is revealed in the following lemma. Actually this lemma helps us to satisfy Constraint 2 in the controller design procedure of the next section.

Lemma 7. Define the set in Lemma 3 as $\bar{M} := \{x \in \mathbf{R}^{Nd} | x_1 = x_2 = \cdots = x_N\}$. Also, assume that the positive constant ε satisfies the condition

$$\varepsilon \leq \mu^2 \rho^2_{\min}, \tag{31}$$

where $\mu \in \mathbf{R}^+$, $\rho_{\min}$ is the minimum singular value of matrix QT, T is the transition matrix introduced in Section II. B and Q is defined by (12). In this case $D(x, \bar{M}) \leq \mu$, $\forall x \in \beta'_\varepsilon = \{x \in \mathbf{R}^{Nd} | x^{\mathrm{T}} zx \leq \varepsilon\}$.

Proof. Consider $\bar{m} = [\hat{m}, \hat{m}, \ldots, \hat{m}]^{\mathrm{T}} \in \mathbf{R}^{Nd}$ as a member of the set $\bar{M}$. Then for each $x \in \beta'_\varepsilon$, $D(x, \bar{M})$ is defined as

$$\begin{aligned} D(x, \bar{M}) &= \inf_{\bar{m} \in \bar{M}} \|x - \bar{m}\| \\ &= \inf_{\hat{m} \in \mathbf{R}^d} \sqrt{\|x_1 - \hat{m}\|^2 + \|x_2 - \hat{m}\|^2 + \cdots + \|x_N - \hat{m}\|^2} \end{aligned} \tag{32}$$

By setting the gradient of $\|x_1 - \hat{m}\|^2 + \|x_2 - \hat{m}\|^2 + \ldots + \|x_N - \hat{m}\|^2$ with respect to $\hat{m}$ equal to zero, it is found that the minimum of this function occurs at $\hat{m} = \hat{m}^*$ where

$$\hat{m}^* = \frac{1}{N} \sum_{i=1}^{N} x_i. \tag{33}$$

Hence, the distance of x from $\bar{M}$ is equal to $\|x - \bar{m}^*\|$ where $\bar{m}^* = [\hat{m}^*, \hat{m}^*, \ldots, \hat{m}^*]^{\mathrm{T}}$. Consequently, (34) is concluded.

$$D(x, \bar{M}) = \frac{\sqrt{\|(N-1)x_1 - x_2 - \cdots - x_N\|^2 + \cdots + \|(N-1)x_N - x_1 - \cdots - x_{N-1}\|^2}}{N}. \tag{34}$$

According to the definition of matrix S in Lemma 5, (34) can be written as

$$D(x, \bar{M}) = \frac{\|Sx\|}{N}. \tag{35}$$

As we know, the set $\beta'_\varepsilon = \{x \in \mathbf{R}^{Nd} | x^{\mathrm{T}} zx \leq \varepsilon\}$ indicates all the points placed inside the surface $x^{\mathrm{T}} zx = \varepsilon$. According to the definition of z, i.e. $z = P^{\mathrm{T}} P$, we have

$$\|Px\|^2 \leq \varepsilon, \tag{36}$$

for each x in the set $\beta'_\varepsilon = \{x \in \mathbf{R}^{Nd} | x^{\mathrm{T}} zx \leq \varepsilon\}$. Inequalities (31) and (36) result in

$$\|Px\| \leq \mu \rho_{\min}. \tag{37}$$

Finally, (21) and (37) yield in the following inequality for the distance indicated by (35).

$$D(x, \bar{M}) = \frac{\|Sx\|}{N} \leq \mu \tag{38}$$

□

IV. Design of the Stabilizing Controller

In this section, the aim is to design a controller for the swarm system (1) such that asymptotic swarm stability is guaranteed and the Constraints 1 and 2 are simultaneously met. To this end, at first in Section IV-A two useful theorems from [36] have been restated. Then, the control law is proposed in Section IV-B.

A. Two Useful Theorems

At first, let us restate a theorem related to the asymptotic stability of fractional order linear time invariant systems subject to input saturation.

Theorem 1[36]**.** Consider the following fractional order linear time invariant system

$$D_t^\alpha x(t) = \bar{A}x(t) + \bar{B} sat(u(t)), \; x(0) = x_0, \tag{39}$$

where $0 < \alpha < 1$, $x(t) \in \mathbf{R}^n$, $u(t) \in \mathbf{R}^m$, $\bar{A} \in \mathbf{R}^{n \times n}$, $\bar{B} \in \mathbf{R}^{n \times m}$ and the saturation function $sat(u(t)) : \mathbf{R}^m \to \mathbf{R}^m$ is of the form

$$sat(u(t)) = [sat(u(t)_{(1)}), sat(u(t)_{(2)}), \ldots, sat(u(t)_{(m)})]^{\mathrm{T}}, \tag{40}$$

where $sat(u(t)_{(l)}), l = 1, 2, \ldots, m$ is defined as follows.

$$sat(u(t)_{(l)}) = \operatorname{sgn}(u(t)_{(l)}) \min(\bar{u}(t)_{(l)}, |u(t)_{(l)}|). \tag{41}$$

Also, assume that $u(t) = Kx(t)$, where $K \in \mathbf{R}^{m\times n}$. If there exists a diagonal matrix $\gamma = \operatorname{diag}\{\gamma_1, \gamma_2, \dots, \gamma_m\}$ such that $0 < \gamma_i \leq 1$ for all $i = 1, \dots, m$ and $\left|\arg(eig(\bar{A} + \bar{B}\gamma K))\right| > \alpha\pi/2$, then there exists a sufficiently small closed ball, denoted by $\beta_\delta := \{x \in \mathbf{R}^n | \, \|x\| \leq \delta\}$, such that system (39) is asymptotically stable for any $x_0 \in \beta_\delta \subset S(\gamma K, u_0)$, where $u_o = [u_{o(1)}, u_{o(1)}, \dots, u_{o(m)}]^{\mathrm{T}}$, $u_{o(i)} \in \mathbf{R}^+$ denotes the saturation level for the i-th input $(i = 1, \dots, m)$, and $S(\gamma K, u_0)$ is defined by

$$S(\gamma K, u_0) = \{x(t) \in \mathbf{R}^n | - u_0 \leq \gamma K x(t) \leq u_0\}. \quad (42)$$

As mentioned in [36], asymptotic stability of (39) means that for every $\varepsilon > 0$, there exists $\delta > 0$ such that for every initial condition $x_0 \in \beta_\delta = \{x_0 \in \mathbf{R}^n | \, \|x_0\| \leq \delta\}$ the solution $x(t, x_0)$ remains in the closed ball $\beta_\varepsilon := \{x \in \mathbf{R}^n | \, \|x\| \leq \varepsilon\}$. In [36], it has been shown that the region β_ε, can be used to estimate $S(\gamma K, u_0)$ in (42). Also, the following theorem has been proved which presents a procedure to determine the state feedback control gain K.

Theorem 2[36]**.** Consider system (39) with the state feedback controller $u(t) = Kx(t)$, $K \in \mathbf{R}^{m\times n}$. If there exists matrix $X \in \mathbf{R}^{m\times n}$, symmetric positive definite matrix $H \in \mathbf{R}^{n\times n}$, diagonal matrix $\gamma = \operatorname{diag}\{\gamma_1, \gamma_2, \dots, \gamma_m\}$ $(0 < \gamma_i \leq 1$ for all $i = 1, \dots, m)$, and positive constant ε such that

$$\sum_{i=1}^{2} sym\{\Theta_{i1} \otimes (\bar{A}H + \bar{B}X)\} < 0, \quad (43)$$

$$\sum_{i=1}^{2} sym\{\Theta_{i1} \otimes (\bar{A}H + \bar{B}\gamma X)\} < 0, \quad (44)$$

$$\begin{bmatrix} 2H - \varepsilon I & \gamma_i X_{(i)}^{\mathrm{T}} \\ \gamma_i X_{(i)} & u_{0(i)}^2 \end{bmatrix} \geq 0, \quad (45)$$

where

$$\Theta_{11} = \Theta_{21}^{\mathrm{T}} = \begin{bmatrix} \sin(\frac{\alpha\pi}{2}) & -\cos(\frac{\alpha\pi}{2}) \\ \cos(\frac{\alpha\pi}{2}) & \sin(\frac{\alpha\pi}{2}) \end{bmatrix}, \quad (46)$$

then the fractional order system (39) is asymptotically stabilizable for any $x_0 \in \beta_\delta$ by using the state feedback controller $u(t) = Kx(t)$ with the state feedback control gain $K = XH^{-1}$. Also, the trajectory $x(t, x_0)$ is placed in the closed ball $\beta_\varepsilon = \{x \in \mathbf{R}^n | \, \|x\| \leq \varepsilon\}$.

B. Constraint Swarm Stabilization

In this subsection, a controller for swarm stabilization of fractional order linear time invariant swarm systems is proposed which simultaneously satisfies Constraints 1 and 2. Before presenting this control law, consider the following assumption that is necessary for designing the swarm stabilizing controller in this subsection. It is assumed that the swarm system (1) satisfies the following assumption.

Assumption 2. In the fractional order linear time invariant swarm system (1), all the pairs of matrices $(A - \lambda_i F, B)$ for all $i = 2, \dots, N$ are stabilizable, where $\lambda_2, \dots, \lambda_N \in \mathbf{R}^+$ denote the nonzero eigenvalues of the Laplacian matrix L.

Now, the proposed swarm stabilizing controller is presented in the following theorem which simultaneously satisfies Constraints 1 and 2.

Theorem 3. Consider the fractional order linear time invariant swarm system (1) which satisfies Assumptions 1 and 2. Also, assume that the positive constant ε satisfies condition (31). Let $U = [u_1^{\mathrm{T}}, \dots, u_N^{\mathrm{T}}]^{\mathrm{T}}$ be given by

$$U = (T^{-1}Q^{\mathrm{T}} \otimes I_m) sat(\hat{K}(QT \otimes I_d)x), \quad (47)$$

where the matrix $\hat{K} = XH^{-1} \in \mathbf{R}^{(N-1)m\times(N-1)d}$ is chosen such that the following matrix inequalities

$$\sum_{i=1}^{2} sym\{\Theta_{i1} \otimes (\hat{A}H + \hat{B}X)\} < 0, \quad (48)$$

and

$$\begin{bmatrix} 2H - \varepsilon I & X_{(i)}^{\mathrm{T}} \\ X_{(i)} & u_{0(i)}^2 \end{bmatrix} \geq 0, \quad (49)$$

are satisfied for matrix $X \in \mathbf{R}^{(N-1)m\times(N-1)d}$ and symmetric positive definite matrix $H \in \mathbf{R}^{(N-1)d\times(N-1)d}$, and $u_{o\ i(l)} = \bar{u}_{i(l)} / \left\|T^{-1}\right\|_\infty$, $i = 1, 2, \dots, N$, $l = 1, 2, \dots, m$ where $u_{o\ i(j)} \in \mathbf{R}^+$ denotes the saturation level for the saturation function used in (47) and T is the transition matrix introduced in Section II-B. In this case, there is a region $\beta'_\delta := \{x_0 \in \mathbf{R}^{Nd} | x_0^{\mathrm{T}} z x_0 \leq \delta\} \subset \hat{S}(\hat{K}, \bar{u})$ $(\delta > 0)$ such that the aforementioned swarm system is asymptotically swarm stable for any $x_0 \in \beta'_\delta$, where $\bar{u} = [\bar{u}_{(1)}, \bar{u}_{(2)}, \dots, \bar{u}_{(N)}]^{\mathrm{T}}$, $\bar{u}_{(i)} = [\bar{u}_{i\ (1)}, \bar{u}_{i\ (2)}, \dots, \bar{u}_{i\ (m)}]^{\mathrm{T}}$ $(i = 1, 2, \dots N)$, and the region $\hat{S}(\hat{K}, \bar{u})$ is defined by

$$\hat{S}(\hat{K}, \bar{u}) = \\ \{x(t) \in \mathbf{R}^{Nd} | - \bar{u} \leq \left\|T^{-1}\right\|_\infty \hat{K}(QT \otimes I_d)x(t) \leq \bar{u}\}. \quad (50)$$

Also, in such a case the Constraints 1 and 2 are simultaneously satisfied for all $x_0 \in \beta'_\delta$.

Proof. Consider the system

$$D_t^\alpha \hat{x} = \hat{A}\hat{x} + \hat{B} sat(\hat{U}), \quad (51)$$

which is a fractional order linear time invariant system subject to input saturation. Also, assume that matrices $\hat{A}$ and $\hat{B}$ in system (51) are in the forms introduced in (8). According to Theorem 1, if there exists diagonal matrix $\gamma = \operatorname{diag}\{\gamma_1, \gamma_2, \dots, \gamma_{(N-1)m}\}$ such that $0 < \gamma_i \leq 1$ for all $i = 1, \dots, (N-1)m$ and $\left|\arg(eig(\hat{A} + \hat{B}\gamma\hat{K}))\right| > \alpha\pi/2$ for some $\hat{K} \in \mathbf{R}^{(N-1)d\times(N-1)m}$, then by using $\hat{U} = \hat{K}\hat{x}$ the system in (51) is asymptotically stable for any $\hat{x}_0 \in \beta_\delta \subset S(\gamma\hat{K}, u_o)$, where $u_o \in \mathbf{R}^{(N-1)m}$ denotes the saturation level vector for the control input and $S(\gamma\hat{K}, u_0)$ is defined as

$$S(\gamma\hat{K}, u_0) = \{\hat{x}(t) \in \mathbf{R}^{(N-1)m} | - u_0 \leq \gamma\hat{K}\hat{x}(t) \leq u_0\}. \quad (52)$$

Consider matrix γ as an identity matrix, i.e. $\gamma = I_{(N-1)m\times(N-1)m}$. Hence, the condition $\left|\arg(eig(\hat{A} + \hat{B}\gamma\hat{K}))\right| > \alpha\pi/2$ can be written as

$$\left|\arg(eig(\hat{A} + \hat{B}\hat{K}))\right| > \alpha\frac{\pi}{2}. \quad (53)$$

$\hat{K}$ can be found for satisfying condition (53) if the pair $(\hat{A},\hat{B})$ is stabilizable. According to the block diagonal form of matrices $\hat{A}$ and $\hat{B}$ (See (8)), the stabilizability of the pair $(\hat{A},\hat{B})$ is deduced from the stabilizability of the pair matrices $(A-\lambda_i F, B)$ for all $i=2,\ldots,N$. This means that if Assumption 2 holds, $\hat{K}$ can be found for satisfying condition (53). On the other hand, based on Theorem 2 and considering matrix γ as an identity matrix, Equations (48) and (49) can be used to find $\hat{K}$ in order to guarantee the asymptotic stability of system (51). Asymptotic stability of this system results in $\lim_{t\to\infty}\hat{x}(t)=0$, which is equivalent to asymptotic swarm stability of system (1) provided that Assumption 1 holds (Lemma 1).

Now, we are faced with four problems that need to be answered for completing the proof. First, obtaining the control signal $U\in\mathbf{R}^{Nm}$ in the form (47) to guarantee asymptotic stability of swarm system (1) according to the above-described control signal $\hat{U}=\hat{K}\hat{x}\in\mathbf{R}^{(N-1)m}$. Second, finding the upper bound of input controls in (3) (i.e., $\bar{u}$) according to the saturation level of the saturation function in (47) (i.e., u_o) in order to show that Constraint 1 is met by using control signal (47). Third, obtaining the region $\hat{S}(\hat{K},\bar{u})$ based on the region $S(\gamma\hat{K},u_0)$, and fourth, finding the positive constant ε such that Constraint 2 is satisfied. The latter problem has been answered in Lemma 7. According to this lemma, to achieve the Constraint 2 the positive constant ε in the region β'_ε should satisfy (31).

The other issues will be answered in the following parts:

1) Finding the control signal $U\in\mathbf{R}^{Nm}$: Note that $U=[u_1^{\rm T},\ldots,u_N^{\rm T}]^{\rm T}\in\mathbf{R}^{Nm}$, $\tilde{U}=[\tilde{u}_1^{\rm T},\tilde{u}_2^{\rm T},\ldots,\tilde{u}_N^{\rm T}]^{\rm T}\in\mathbf{R}^{Nm}$and $\hat{U}=[\tilde{u}_2^{\rm T},\tilde{u}_3^{\rm T},\ldots,\tilde{u}_N^{\rm T}]^{\rm T}\in\mathbf{R}^{(N-1)m}$. According to the relation $\tilde{U}=(T\otimes I_m)U$, we have

$$U=(T^{-1}\otimes I_m)\tilde{U}, \tag{54}$$

where $\tilde{U}=[\tilde{u}_1^{\rm T},\hat{U}^{\rm T}]^{\rm T}$. Assuming $\hat{U}=\hat{K}\hat{x}$ and considering the saturation function on $\hat{U}$ results in

$$U=(T^{-1}\otimes I_m)\left[\begin{array}{c}\tilde{u}_1\\ sat(\hat{K}\hat{x})\end{array}\right]. \tag{55}$$

Matrix $(T^{-1}\otimes I_m)$ is in the following form [16,18]

$$(T^{-1}\otimes I_m)=\left[\begin{array}{cc}\hat{t}_{11}I_m & \cdots\\ \hat{t}_{11}I_m & \cdots\\ \vdots & \ddots\\ \hat{t}_{11}I_m & \cdots\end{array}\right]. \tag{56}$$

By substituting $\hat{x}$ from (11) and $(T^{-1}\otimes I_m)$ from (56) into (55), it is Obtained that

$$\begin{aligned}U&=\left[\begin{array}{cc}\hat{t}_{11}I_m & \cdots\\ \hat{t}_{11}I_m & \cdots\\ \vdots & \ddots\\ \hat{t}_{11}I_d & \cdots\end{array}\right]\left[\begin{array}{c}\tilde{u}_1\\ sat(\hat{K}(QT\otimes I_d)x)\end{array}\right]\\ &=(1_N\otimes(\hat{t}_{11}\tilde{u}_1))+(T^{-1}Q^{\rm T}\otimes I_m)sat(\hat{K}(QT\otimes I_d)x),\end{aligned} \tag{57}$$

where $1_N=[\underbrace{1,1,\ldots,1}_{N}]^{\rm T}\in\mathbf{R}^{N\times 1}$ and $\tilde{u}_1\in\mathbf{R}^m$ is an arbitrary input vector. By considering $\tilde{u}_1$ as a zero vector, the input control (47) is achieved which yields asymptotic swarm stability in swarm system (1).

2) Finding the upper bound of control signal i.e. $\bar{u}$: By substituting $\tilde{U}$ with $sat(\tilde{U})$ in (54) and defining $M=[m_{i,j}]:=(T^{-1}\otimes I_m)\in\mathbf{R}^{Nm\times Nm}$, one can obtain (58).

For simplicity, we redefine $U=[u_1^*,u_2^*,\ldots,u_{Nm}^*]^{\rm T}$ and $\tilde{U}=[\tilde{u}_1^*,\tilde{u}_2^*,\ldots,\tilde{u}_{Nm}^*]^{\rm T}$. Hence, (58) can be rewritten as (59).

$$\left[\begin{array}{c}\left[\begin{array}{c}u_{1,1}\\ \vdots\\ u_{1,m}\end{array}\right]\\ \left[\begin{array}{c}u_{2,1}\\ \vdots\\ u_{2,m}\end{array}\right]\\ \vdots\\ \left[\begin{array}{c}u_{N,1}\\ \vdots\\ u_{N,m}\end{array}\right]\end{array}\right]=\left[\begin{array}{cccc}m_{1,1} & m_{1,2} & \cdots & m_{1,Nm}\\ m_{2,1} & \cdots & \cdots & m_{2,Nm}\\ \vdots & \vdots & \ddots & \vdots\\ m_{Nm,1} & m_{Nm,2} & \cdots & m_{Nm,Nm}\end{array}\right]\left[\begin{array}{c}\left[\begin{array}{c}sat(\tilde{u}_{1,1})\\ \vdots\\ sat(\tilde{u}_{1,m})\end{array}\right]\\ \left[\begin{array}{c}sat(\tilde{u}_{2,1})\\ \vdots\\ sat(\tilde{u}_{2,m})\end{array}\right]\\ \vdots\\ \left[\begin{array}{c}sat(u_{N,1})\\ \vdots\\ sat(u_{N,m})\end{array}\right]\end{array}\right]. \tag{58}$$

$$\left[\begin{array}{c}u_1^*\\ u_2^*\\ \vdots\\ u_{Nm}^*\end{array}\right]=\left[\begin{array}{cccc}m_{1,1} & m_{1,2} & \cdots & m_{1,Nm}\\ m_{2,1} & \cdots & \cdots & m_{2,Nm}\\ \vdots & \vdots & \ddots & \vdots\\ m_{Nm,1} & m_{Nm,2} & \cdots & m_{Nm,Nm}\end{array}\right]\left[\begin{array}{c}sat(\tilde{u}_1^*)\\ sat(\tilde{u}_2^*)\\ \vdots\\ sat(\tilde{u}_{Nm}^*)\end{array}\right]. \tag{59}$$

From (59),

$$u_i^* = \sum_{j=1}^{Nm} m_{i,j} sat(\tilde{u}_j^*), \; i = 1, 2, \ldots, Nm. \tag{60}$$

Hence, the upper bound of control input u_i^* is obtained as follows.

$$|u_i^*| \le u_{o(i)} \sum_{j=1}^{Nm} m_{i,j} \le u_{o(i)} \sum_{j=1}^{Nm} |m_{i,j}|, \; i = 1, 2, \ldots, Nm. \tag{61}$$

According to the definition of infinity matrix norm, we have

$$\|M\|_\infty = \max_{i=1,2,\ldots,Nm} \sum_{j=1}^{Nm} |m_{i,j}| \; . \tag{62}$$

Finally, (61) and (62) result in

$$|u_i^*| \le u_{o(i)} \|M\|_\infty \;\; i = 1, 2, \ldots, Nm. \tag{63}$$

Now, from the properties of infinity matrix norm, the matrix norm $\|M\|_\infty$ in (63) can be written as

$$\|M\|_\infty = \left\|T^{-1} \otimes I_d\right\|_\infty = \left\|T^{-1}\right\|_\infty. \tag{64}$$

Hence, (63) is written as

$$|u_i^*| \le u_{o(i)} \left\|T^{-1}\right\|_\infty, \; i = 1, 2, \ldots, Nm. \tag{65}$$

Choosing $u_{o(i)}$, $i = 1, 2, \ldots, Nm$ as

$$u_{o(i)} = \frac{\bar{u}_i}{\|T^{-1}\|_\infty} \tag{66}$$

results in the following saturation level as the upper bound for the i-th control input of input vector U in (47).

$$|u_i^*| \le \bar{u}_i, \; i = 1, 2, \ldots, Nm. \tag{67}$$

Consequently, if $\bar{u}_{i(l)} = \left\|T^{-1}\right\|_\infty u_{o\ i(l)} \in \mathbf{R}^+$, $i = 1, 2, \ldots, N$, $l = 1, 2, \ldots, m$ Constraint 1 is satisfied by using control signal (47).

3) Obtaining the region $\hat{S}(\hat{K}, \bar{u})$: According to (66),

$$u_o = \frac{\bar{u}}{\|T^{-1}\|_\infty}, \tag{68}$$

where $u_o \in \mathbf{R}^{(N-1)m}$ and $\bar{u} \in \mathbf{R}^{Nm}$. By substituting (11) and (68) into (52) and considering the assumption $\gamma = I_{(N-1)m \times (N-1)m}$, the region $\hat{S}(\hat{K}, \bar{u})$ in (48) is obtained. □

V. Numerical Simulations

In this section, the results of the previous section are verified by two numerical examples. Numerical simulations of this section have been done by using the Adams-type predictor-corrector method introduced in [43] for solving fractional order differential equations.

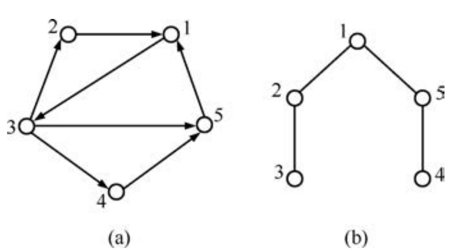

Fig. 1. (a) Graph G_a in Example 1; (b) Graph G_b in Example 2.

Example 1. Consider the following fractional order linear time invariant swarm system:

$$D_t^{0.8} x_i = A x_i + F \sum_{j=1}^{5} w_{ij}(x_j - x_i) + B u_i, \quad i = 1, \ldots, 5, \tag{69}$$

where

$$A = \begin{bmatrix} 1.6 & -0.9 \\ 3 & 1.2 \end{bmatrix}, \; F = \begin{bmatrix} 3.2 & -3 \\ 4 & 5 \end{bmatrix}, \; B = \begin{bmatrix} 1 \\ 0 \end{bmatrix}. \tag{70}$$

Graph G_a expressing the communication among these agents is shown in Fig. 1(a). Also, the adjacency matrix of this graph is considered as

$$W_{G_a} = \begin{bmatrix} 0 & 0.4 & 0 & 0 & 0.7 \\ 0 & 0 & 0.2 & 0 & 0 \\ 0.3 & 0 & 0 & 0 & 0 \\ 0 & 0 & 0.6 & 0 & 0 \\ 0 & 0 & 1.2 & 0.8 & 0 \end{bmatrix}.$$

In this case, the eigenvalues of the Laplacian matrix for the mentioned graph are $\lambda(G_a) = \{0,\ 0.2776,\ 0.8856,\ 1.1811,\ 1.8557\}$. According to (8), matrices $\hat{A}$ and $\hat{B}$ are in the following forms:

$$\hat{A} = \begin{bmatrix} A - \lambda_2 F & 0 & 0 & \cdots & 0 \\ 0 & A - \lambda_3 F & 0 & \cdots & 0 \\ 0 & \vdots & \vdots & \ddots & \vdots \\ \vdots & 0 & \cdots & \cdots & 0 \\ 0 & 0 & \cdots & 0 & A - \lambda_5 F \end{bmatrix} \in \mathbf{R}^{8 \times 8}$$

where

$$A - \lambda_2 F = \begin{bmatrix} 0.7118 & -0.0673 \\ 1.8897 & -0.187 \end{bmatrix},$$
$$A - \lambda_3 F = \begin{bmatrix} -1.2341 & 1.7569 \\ -0.5426 & -3.2282 \end{bmatrix},$$
$$A - \lambda_4 F = \begin{bmatrix} -2.1794 & 2.6432 \\ -1.7243 & -4.7053 \end{bmatrix},$$
$$A - \lambda_5 F = \begin{bmatrix} -4.3383 & 4.6671 \\ -4.4228 & -8.0786 \end{bmatrix},$$

and

$$\hat{B} = \begin{bmatrix} 1 & 0 & 0 & 0 & 0 & 0 & 0 & 0 \\ 0 & 0 & 1 & 0 & 0 & 0 & 0 & 0 \\ 0 & 0 & 0 & 0 & 1 & 0 & 0 & 0 \\ 0 & 0 & 0 & 0 & 0 & 0 & 1 & 0 \end{bmatrix}^{\mathrm{T}}.$$

It is worth noting that matrix $\hat{A}$ is not α-Hurwitz with $\alpha = 0.8$. In this example, the aim is asymptotic swarm stabilization of the above-described swarm system in the presence of Constraint 1 with saturation level $\bar{u} = [2; 2; 2; 2; 2]^{\mathrm{T}}$ and Constraint 2 with $\mu = 1.8$. To achieve this aim, from Theorem 3 the control can be chosen as

$$U = (T^{-1} Q^{\mathrm{T}} \otimes I_1) sat(\hat{K}(QT \otimes I_2) x), \tag{71}$$

where the matrices T and Q have the following forms:

$$T=\begin{bmatrix} 0.2988 & 0.5976 & 1.0956 & 0.1394 & 0.1046 \\ 0.1977 & -1.0194 & 0.5420 & 0.1994 & 0.0803 \\ -1.3072 & 0.7626 & -0.9340 & 2.2997 & -0.8211 \\ 2.1783 & -0.8881 & -0.5886 & -2.5635 & 1.8620 \\ 0.3645 & -0.0881 & -0.9182 & -1.1266 & 1.7683 \end{bmatrix},$$

$$Q=\begin{bmatrix} 0 & 1 & 0 & 0 & 0 \\ 0 & 0 & 1 & 0 & 0 \\ 0 & 0 & 0 & 1 & 0 \\ 0 & 0 & 0 & 0 & 1 \end{bmatrix}_{4\times 5}.$$

Considering $\left\|T^{-1}\right\|_{\infty}=2.657$, the saturation level is chosen as $u_0=\ 0.7527$ (See (68)). Moreover since $\mu=1.8$ and $\rho_{\min}=0.6819$, one can choose $\varepsilon=1.5$ to satisfy (31). Solving the matrix inequalities in (48) and (49) with $\varepsilon=1.5$ results in the matrix $\hat{K}$ as follows.

$$\hat{K}=[\hat{K}_1\ \hat{K}_2]\in\mathbf{R}^{4\times 8}, \tag{72}$$

where

$$\hat{K}_1=\begin{bmatrix} -7.6211 & -2.6937 & 0 & 0 \\ 0 & 0 & -1.1352 & -1.2980 \\ 0 & 0 & 0 & 0 \\ 0 & 0 & 0 & 0 \end{bmatrix}\in\mathbf{R}^{4\times 4}$$

$$\hat{K}_2=\begin{bmatrix} 0 & 0 & 0 & 0 \\ 0 & 0 & 0 & 0 \\ -1.1076 & -2.2546 & 0 & 0 \\ 0 & 0 & -2.3234 & -4.5966 \end{bmatrix}\in\mathbf{R}^{4\times 4}$$

As shown in Fig. 2, the considered aim is achieved by applying the control law (71). More precisely, Fig. 2 (a) confirms that asymptotic swarm stability is achieved. Also, Figs. 2 (b) and 2 (c) respectively reveal that Constraint 1 with saturation level $\bar{u}=[2;2;2;2;2]^{\mathrm{T}}$ and Constraint 2 with $\mu=1.8$ are satisfied.

Example 2. Consider the following fractional order linear time invariant swarm system with five agents

$$D_t^{0.8}x_i=Ax_i+F\sum_{j=1}^{5}w_{ij}(x_j-x_i)+Bu_i\ ,\ i=1,\ldots,5. \tag{73}$$

$$A=\begin{bmatrix} -0.1 & 0.7 \\ -5.2 & 1.8 \end{bmatrix},\ F=\begin{bmatrix} 2 & -10 \\ 4 & -6 \end{bmatrix},\ B=\begin{bmatrix} 2 & 0 \\ 0 & 1 \end{bmatrix}. \tag{74}$$

The undirected graph G_b describing the communication among these agents is shown in Fig. 1 (b). Also, the adjacency matrix of this graph is considered as

$$W_{G_b}=\begin{bmatrix} 0 & 1.2 & 0 & 0 & 0.8 \\ 1.2 & 0 & 0.4 & 0 & 0 \\ 0 & 0.4 & 0 & 0 & 0 \\ 0 & 0 & 0 & 0 & 0.9 \\ 0.8 & 0 & 0 & 0.9 & 0 \end{bmatrix}.$$

The eigenvalues of the Laplacian matrix for the mentioned graph are as follows:

$$\lambda(G_b)=\{0,\ 0.2935,\ 0.8222,\ 2.1424,\ 3.3419\}$$

The matrices $\hat{A}$ and $\hat{B}$ in this example are

$$\hat{A}=\begin{bmatrix} A-\lambda_2F & 0 & 0 & \cdots & 0 \\ 0 & A-\lambda_3F & 0 & \cdots & 0 \\ 0 & \vdots & \vdots & \ddots & \vdots \\ \vdots & 0 & \cdots & \cdots & 0 \\ 0 & 0 & \cdots & 0 & A-\lambda_5F \end{bmatrix}\in\mathbf{R}^{8\times 8}$$

where

$$A-\lambda_2F=\begin{bmatrix} -0.6871 & 3.6354 \\ -6.3742 & 3.5613 \end{bmatrix},$$

$$A-\lambda_3F=\begin{bmatrix} -1.7444 & 8.9222 \\ -8.4889 & 6.7333 \end{bmatrix},$$

$$A-\lambda_4F=\begin{bmatrix} -4.3848 & 22.1239 \\ -13.7695 & 14.6543 \end{bmatrix},$$

$$A-\lambda_5F=\begin{bmatrix} -6.7837 & 34.1185 \\ -18.5674 & 21.8511 \end{bmatrix},$$

and

$$\hat{B}=\mathrm{diag}\{2,1,2,1,2,1,2,1\}.$$

Matrix $\hat{A}$ is not α-Hurwitz with $\alpha=0.8$. In this case, matrices T and Q have the following forms:

$$T=\begin{bmatrix} -0.447 & -0.447 & -0.447 & -0.447 & -0.447 \\ -0.032 & 0.196 & 0.736 & -0.537 & -0.362 \\ 0.501 & 0.519 & -0.492 & -0.486 & -0.042 \\ 0.181 & -0.481 & 0.110 & -0.499 & 0.689 \\ -0.718 & 0.511 & -0.069 & -0.162 & 0.439 \end{bmatrix}$$

$$Q=\begin{bmatrix} 0 & 1 & 0 & 0 & 0 \\ 0 & 0 & 1 & 0 & 0 \\ 0 & 0 & 0 & 1 & 0 \\ 0 & 0 & 0 & 0 & 1 \end{bmatrix}_{4\times 5}$$

Suppose that all the input control signals are subjected to constraint with upper bound 4, i.e. $\bar{u}=[4;4;4;4;4;4;4;4;4]^{\mathrm{T}}$ in Constraint 1. Moreover, the aim is to achieve asymptotic swarm stability in the considered swam system while Constraint 2 with $\mu=1.5$ is satisfied. To achieve asymptotic swarm stability with considering the mentioned constraints, according to Theorem 3 the control law is chosen in the following form

$$U=(T^{-1}Q^{\mathrm{T}}\otimes I_2)sat(\hat{K}(QT\otimes I_2)x). \tag{75}$$

From equality $\left\|T^{-1}\right\|_{\infty}=2.1538$, the saturation level is obtained as $u_0=1.8572$. Also since $\rho_{\min}=1$, we choose $\varepsilon=1$ to satisfy (31). Solving the matrix inequalities (48) and (49) with $\varepsilon=1$ yields

$$\hat{K}=\mathrm{diag}\{\hat{K}_1,\hat{K}_2,\hat{K}_3,\hat{K}_4\}\in\mathbf{R}^{8\times 8}, \tag{76}$$

where

$$\hat{K}_1=\begin{bmatrix} -4.8508 & 2.3989 \\ 6.8251 & -7.6845 \end{bmatrix},\hat{K}_2=\begin{bmatrix} -5.6536 & 2.2859 \\ 9.8021 & -16.0606 \end{bmatrix},$$

$$\hat{K}_3=\begin{bmatrix} -9.2684 & 5.0800 \\ 19.4285 & -44.1909 \end{bmatrix},\hat{K}_4=\begin{bmatrix} -16.9353 & 21.5528 \\ 41.1281 & -108.9224 \end{bmatrix}.$$

Numerical simulation results presented in Fig. 3 (a) confirm that asymptotic swarm stability is achieved by applying the control law (75) with the obtained specifications. Moreover, Figs. 3 (b) and 3 (c) verify that the aforementioned constraints are also satisfied in this case. For a comparison, simulation results of the swarm system in (73) by applying control law (75) and without considering saturation function in this law (unsaturated control inputs) have been presented in Fig. 4. By comparing the simulation results of Figs. 3 and 4, it can be seen that without considering the input constraint, the convergence rate of the agents to reach consensus increases. But in this case, as a negative point the values of control inputs at the beginning of the motion are too large which can cause practical problems due to physical constraints of the actuators in the real-world applications. This means that involving Constraint 1 in design procedure can yield in more applicable control signals.

As it is confirmed by the above-mentioned numerical examples, by using the feedback control law (47) asymptotic swarm stability is achieved in fractional order linear time invariant swarm system (1) with a directed/undirected topology graph satisfying Assumption 1. Applying this control law, the distance of the agents from the final destination is less than a desired value. In addition, the input signals do not exceed a predetermined value.

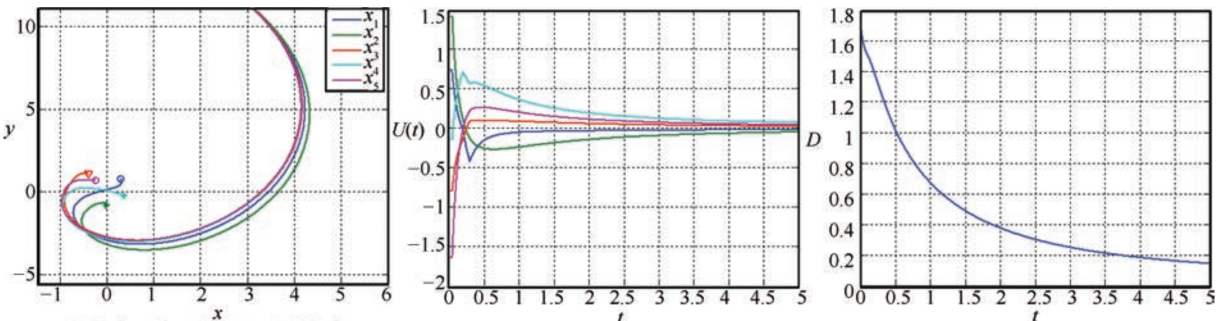

(a) Trajectories of agents (Achieving asymptoticswarm stability) (b) Control inputs (Satisfying Constraint 1) (c) Distance from the finaldestination (It is seen that this distance ($D(x(t), \bar{M})$)does not exceed μ =1.8 and tends to zero)

Fig. 2. Numerical simulation results of Example 1 where $x_0 = [[0.3, 0.8], [-0.01, -0.8], [-0.4, 1.1], [0.36, -0.22], [-0.23, 0.7]]^{\mathrm{T}}$.

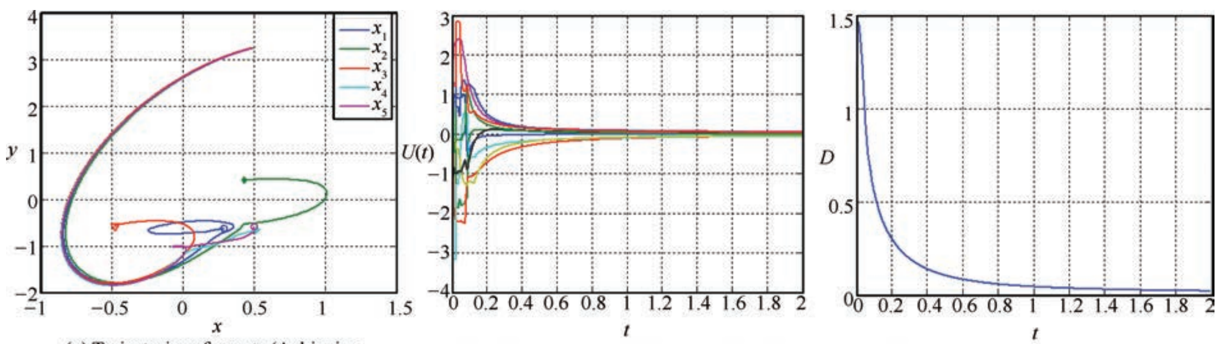

(a) Trajectories of agents (Achieving asymptoticswarm stability) (b) Control inputs (Satisfying Constraint1) (c) Distance from the finaldestination (It is seen that this distance ($D(x(t), \bar{M})$) does not exceed μ =1.5 and tends to zero)

Fig. 3. Numerical simulation results of Example 2 where $x_0 = [[0.29, -0.63], [0.43, 0.41], [-0.48, -0.59], [0.52, -0.65], [0.50, -0.58]]^{\mathrm{T}}$.

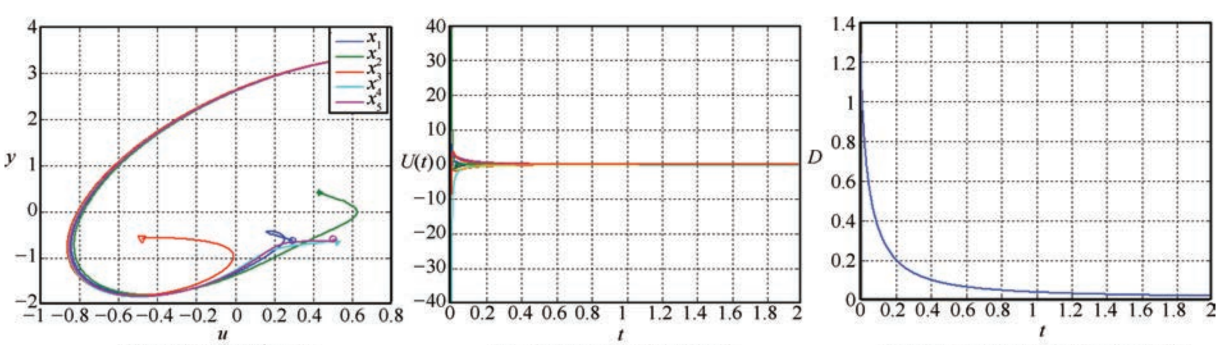

(a) Trajectories of agents (b) Unsaturated control inputs (c) Distance from the final destination

Fig. 4. Numerical simulation results of Example 2 without considering input saturation constraint.

VI. CONCLUSION

Constrained swarm stabilization of fractional order linear time invariant swarm systems is studied in this paper. In this study, a bounded state-feedback control law is proposed to ensure asymptotic swarm stability in fractional order swarm systems. This law enforces that the distance of agents from the final destination is less than a desired value. Numerical simulation results demonstrated the effectiveness of the proposed control law.

REFERENCES

[1] Zou A M, Kumar K D. Distributed attitude coordination control for spacecraft formation flying. *IEEE Transactions on Aerospace and Electronic Systems*, 2012, **48**(2): 1329−1346

[2] Olfati-Saber R, Murray R M. Distributed cooperative control of multiple vehicle formations using structural potential functions. In: Proceedings of the 15th IFAC World Congress. Barcelona, Spain: IFAC, 2002. 242

[3] Su H S, Wang X F, Lin Z L. Flocking of multi-agents with a virtual leader. *IEEE Transactions on Automatic Control*, 2009, **54**(2): 293−307

[4] Cortés J, Bullo F. Coordination and geometric optimization via distributed dynamical systems. *SIAM Journal on Control and Optimization*, 2005, **44**(5): 1543−1574

[5] Olfati-Saber R, Murray R M. Consensus problems in networks of agents with switching topology and time-delays. *IEEE Transactions on Automatic Control*, 2004, **49**(9): 1520−1533

[6] Tang Z J, Huang T Z, Shao J L, Hu J P. Consensus of second-order multi-agent systems with nonuniform time-varying delays. *Neurocomputing*, 2012, **97**: 410−414

[7] Tian Y P, Zhang Y. High-order consensus of heterogeneous multi-agent systems with unknown communication delays. *Automatica*, 2012, **48**(6): 1205−1212

[8] Ren W. Consensus tracking under directed interaction topologies: algorithms and experiments. *IEEE Transactions on Control Systems Technology*, 2010, **18**(1): 230−237

[9] Xi J X, Shi Z Y, Zhong Y S. Consensus analysis and design for high-order linear swarm systems with time-varying delays. *Physica A: Statistical Mechanics and its Applications*, 2011, **390**(23−24): 4114−4123

[10] Magin R L. Fractional calculus models of complex dynamics in biological tissues. *Computers and Mathematics with Applications*, 2010, **59**(5): 1586−1593

[11] Cafagna D. Fractional calculus: a mathematical tool from the past for present engineers. *IEEE Industrial Electronics Magazine*, 2007, **1**(2): 35−40

[12] Cao Y, Li Y, Ren W, Chen Y Q. Distributed coordination of networked fractional-order systems. *IEEE Transactions on Systems, Man, and Cybernetics, Part B, Cybernetics*, 2010, **40**(2): 362−370

[13] Song C, Cao J. Consensus of fractional-order linear systems. In: Proceedings of the 2013 9th Asian Control Conference. Istanbul, Turkey: IEEE, 2013. 1−4

[14] Lu J Q, Shen J, Cao J D, Kurths J. Consensus of networked multi-agent systems with delays and fractional-order dynamics. *Consensus and Synchronization in Complex Networks*. Berlin Heidelberg: Springer, 2013. 69−110

[15] Yin X X, Yue D, Hu S L. Consensus of fractional-order heterogeneous multi-agent systems. *IET Control Theory and Applications*, 2013, **7**(2): 314−322

[16] Naderi Soorki M, Tavazoei M S. Fractional-order linear time invariant swarm systems: asymptotic swarm stability and time response analysis. *Central European Journal of Physics*, 2013, **11**(6): 845−854

[17] Sun W, Li Y, Li C P, Chen Y Q. Convergence speed of a fractional order consensus algorithm over undirected scale-free networks. *Asian Journal of Control*, 2011, **13**(6): 936−946

[18] Naderi Soorki M, Tavazoei M S. Adaptive consensus tracking for fractional-order linear time invariant swarm systems. *Journal of Computational and Nonlinear Dynamics*, 2014, **9**(3): 031012

[19] Shen J, Cao J, Lu J. Consensus of fractional-order systems with non-uniform input and communication delays. *Proceedings of the Institution of Mechanical Engineers, Part I: Journal of Systems and Control Engineering*, 2012, **226**(2): 271−283

[20] Shen J, Cao J D. Necessary and sufficient conditions for consensus of delayed fractional-order systems. *Asian Journal of Control*, 2012, **14**(6): 1690−1697

[21] Zheng Y S, Wang L. Finite-time consensus of heterogeneous multi-agent systems with and without velocity measurements. *Systems and Control Letters*, 2012, **61**(8): 871−878

[22] Yu W, Chen G, Cao M, Kurths J. Second-order consensus for multiagent systems with directed topologies and nonlinear dynamics. *IEEE Transactions on Systems, Man, and Cybernetics, Part B: Cybernetics*, 2010, **40**(3): 881−891

[23] Wen G H, Duan Z S, Yu W W, Chen G R. Consensus in multi-agent systems with communication constraints. *International Journal of Robust and Nonlinear Control*, 2012, **22**(2): 170−182

[24] Han D K, Chesi G. Robust consensus for uncertain multi-agent systems with discrete-time dynamics. *International Journal of Robust and Nonlinear Control*, 2014, **24**(13): 1858−1872

[25] Li T, Zhang J F. Consensus conditions of multi-agent systems with time-varying topologies and stochastic communication noises. *IEEE Transactions on Automatic Control*, 2010, **55**(9): 2043−2057

[26] Li Y, Xiang J, Wei W. Consensus problems for linear time-invariant multi-agent systems with saturation constraints. *IET Control Theory and Applications*, 2011, **5**(6): 823−829

[27] Meng Z Y, Zhao Z, Lin Z. On global consensus of linear multi-agent systems subject to input saturation. In: Proceedings of the 2012 American Control Conference (ACC). Montreal, Canada: IEEE, 2012. 4516−4521

[28] Geng H, Chen Z Q, Liu Z X, Zhang Q. Consensus of a heterogeneous multi-agent system with input saturation. *Neurocomputing*, 2015, **166**: 382−388

[29] Fan M C, Zhang H T, Li Z L. Distributed semiglobal consensus with relative output feedback and input saturation under directed switching networks. *IEEE Transactions on Circuits and Systems II: Express Briefs*, 2015, **62**(8): 796−800

[30] Wang Z Y, Gu D B, Meng T, Zhao Y Z. Consensus target tracking in multi-robot systems. *Intelligent Robotics and Applications*. Berlin Heidelberg: Springer, 2010. 724−735

[31] Khoo S, Xie L, Man Z. Robust finite-time consensus tracking algorithm for multirobot systems. *IEEE/ASME Transactions on Mechatronics*, 2009, **14**(2): 219−228

[32] David S A, Balthazar J M, Julio B H S, Oliveira C. The fractional-nonlinear robotic manipulator: modeling and dynamic simulations. *AIP Conference Proceedings*, 2012, **1493**(1): 298−305

[33] Jezierski E, Ostalczyk P. Fractional-order mathematical model of pneumatic muscle drive for robotic applications. *Robot Motion and Control 2009*. London: Springer, 2009. 113−122

[34] Sjöberg M, Kari L. Nonlinear isolator dynamics at finite deformations: an effective hyperelastic, fractional derivative, generalized friction model. *Nonlinear Dynamics*, 2003, **33**(3): 323−336

[35] Mendes R V, Vázquez L. The dynamical nature of a backlash system with and without fluid friction. *Nonlinear Dynamics*, 2007, **47**(4): 363−366

[36] Lim Y H, Oh K K, Ahn H S. Stability and stabilization of fractional-order linear systems subject to input saturation. *IEEE Transactions on Automatic Control*, 2013, **58**(4): 1062−1067

[37] Podlubny I. *Fractional Differential Equations*. San Diego, CA: Academic Press, 1999.

[38] Cai N, Xi J X, Zhong Y S. Swarm stability of high-order linear time-invariant swarm systems. *IET Control Theory and Applications*, 20011, **5**(2): 402−408

[39] Godsil C, Royle G F. *Algebraic Graph Theory*. New York: Springer, 2001.

[40] Caponetto R, Dongola G, Fortuna L, Petras I. *Fractional Order Systems: Modeling and Control Applications*. Hackensack, NJ: World Scientific, 2010.

[41] Laub A J. *Matrix Analysis for Scientists & Engineers*. Philadelphia, PA, USA: Society for Industrial and Applied Mathematics (SIAM), 2004.

[42] Meyer C D. *Matrix Analysis and Applied Linear Algebra*. Philadelphia, PA, USA: Society for Industrial and Applied Mathematics (SIAM), 2000.

[43] Diethelm K, Ford N J, Freed A D. A predictor-corrector approach for the numerical solution of fractional differential equations. *Nonlinear Dynamics*, 2002, **29**(1−4): 3−22

Mojtaba Naderi Soorki received the bachelor and master degrees in electrical engineering from Amirkabir University of Technology, Tehran, Iran, in 2008 and 2010, respectively. Currently he is a Ph. D. candidate in electrical engineering at Sharif University of Technology, Tehran, Iran. His research interests include fractional order systems, multi-agent systems, swarm stability and consensus in swarm systems.

Mohammad Saleh Tavazoei received the bachelor, master, and Ph. D. degrees in electrical engineering from the Sharif University of Technology, Tehran, Iran, in 2003, 2005, and 2008, respectively. He is currently an associate professor with the Department of Electrical Engineering, Sharif University of Technology. His current research interests include dynamical behavior analysis of fractional order systems and applications of these systems in control system design. Dr. Tavazoei is the recipient of the Young Investigator Award of IEEE Iran Section in 2012.

Improving the Control Energy in Model Reference Adaptive Controllers Using Fractional Adaptive Laws

Norelys Aguila-Camacho and Manuel A. Duarte-Mermoud, *Senior Member, IEEE*

***Abstract*—This paper presents the analysis of the control energy consumed in model reference adaptive control (MRAC) schemes using fractional adaptive laws, through simulation studies. The analysis is focused on the energy spent in the control signal represented by means of the integral of the squared control input (ISI). Also, the behavior of the integral of the squared control error (ISE) is included in the analysis.**

The orders of the adaptive laws were selected by particle swarm optimization (PSO), using an objective function including the ISI and the ISE, with different weighting factors. The results show that, when ISI index is taken into account in the optimization process to determine the orders of adaptive laws, the resulting values are fractional, indicating that control energy of the scheme might be better managed if fractional adaptive laws are used.

***Index Terms*—Control energy, fractional adaptive laws, model reference adaptive control.**

I. INTRODUCTION

The main idea behind direct model reference adaptive control (direct MRAC) technique is to create a closed loop system with adjustable parameters, such that the application of the resulting control signal to the plant makes the output of the plant to follow the output of a given reference model. Adaptive laws for adjusting controller parameters have been synthesized using several techniques, where the most commonly used is the gradient approach, in which the estimated parameter is the result of a differential equation of integer order, moving in the negative direction of the gradient of the criterion function to be minimized[1].

The fractional calculus, that is calculus of integrals and derivatives of real or complex orders[2], has been increasingly used in many fields of science and engineering, and the control techniques are not the exception. Since the paper by Vinagre et al.[3], which as far as we know is the first paper proposing the inclusion of fractional operators in MRAC schemes, many works have been published including fractional operators not only in MRAC schemes (see for example [4−9]) but also in some other adaptive schemes[10−11]. Some researchers have mentioned advantages of using fractional operators in MRAC schemes such as better management of noise[10], better behavior under disturbances[4−5, 9] and improvements in transient responses[3, 9], among others.

However, there is still a reticence in the adaptive control community about using these fractional operators inside adaptive schemes because of their complexity. In [9] it has been mentioned that the use of fractional adaptive laws in a MRAC scheme for an automatic voltage regulator leads to a smoother control signal, which is a very interesting fact. This behavior could be seen as a better management of the energy used in the control scheme, and this could be a point in favor of the fractional operators, at least in MRAC schemes, since energy efficiency is a trending topic nowadays due to the increasing cost of energy worldwide.

This paper makes a preliminary analysis of the behavior of control signals in a MRAC scheme, when fractional adaptive laws are used to adjust control parameters. The analysis is made empirically, since it follows from simulation studies, but we believe this could be the first step to a more detailed study on this topic. The results show that the introduction of fractional adaptive laws in the MRAC schemes analyzed leads to smoother control signals, with a lower integral of the squared control, which can be seen as a better management of the energy spent in the control scheme. The simulations also show that there could exist a trade-off between the control energy and the convergence speed of the control error, which suggests the use of optimization techniques to select the suitable orders to be used in adaptive laws.

The paper is organized as follows. Section II presents some basic concepts about fractional calculus. Section III introduces the MRAC scheme that is analyzed in the paper, with the corresponding fractional adaptive laws. Section IV presents the simulation and analysis of the results for the MRAC scheme, implemented for three different plants: one stable, one marginally stable and one unstable. Finally, Section V presents the conclusions of the study.

II. BASIC CONCEPTS

This section presents some basic concepts of fractional calculus, which are used in this paper.

Manuscript received September 1, 2015; accepted January 25, 2016. This work was supported by CONICYT-Chile, under the Basal Financing Program (FB0809), Advanced Mining Technology Center, FONDECYT Project (1150488), Fractional Error Models in Adaptive Control and Applications, FONDECYT (3150007), and Postdoctoral Program 2015. Recommended by Associate Editor Antonio Visioli.

Citation: Norelys Aguila-Camacho and Manuel A. Duarte-Mermoud. Improving the control energy in model reference adaptive controllers using fractional adaptive laws. *IEEE/CAA Journal of Automatica Sinica*, 2016, **3**(3): 332−337

Norelys Aguila-Camacho, Manuel A. Duarte-Mermoud are with the Department of Electrical Engineering and the Advanced Mining Technology Center, University of Chile, Chile (e-mail: naguila@ing.uchile.cl; mduartem@ing.uchile.cl).

Color versions of one or more of the figures in this paper are available online at http://ieeexplore.ieee.org.

A. Fractional Calculus

Fractional calculus studies integrals and derivatives of real or complex orders[2]. The Riemann-Liouville fractional integral is one of the main concepts of fractional calculus, and is presented in Definition 1.

Definition 1 (Riemann-Liouville fractional integral)[2].

$$I_{a+}^{\alpha} f(t) = \frac{1}{\Gamma(\alpha)} \int_a^t \frac{f(\tau)}{(t-\tau)^{1-\alpha}} \mathrm{d}\tau, \quad t > a,\ R(\alpha) > 0, \tag{1}$$

where $\Gamma(\alpha)$ corresponds to the Gamma Function, given by Equation (2).

$$\Gamma(\alpha) = \int_0^{\infty} t^{\alpha-1} \mathrm{e}^{-t} \mathrm{d}t. \tag{2}$$

There are several definitions regarding fractional derivatives. Definition 2 corresponds to the fractional derivative according to Caputo, and is the one used in this paper for implementing fractional adaptive laws.

Definition 2 (Caputo fractional derivative)[2].

$${}_{t_0}^{C}D_t^{\alpha} x(t) = \frac{1}{\Gamma(n-\alpha)} \int_a^t \frac{f^{(n)}(\tau)}{(t-\tau)^{\alpha-n+1}} \mathrm{d}\tau, \tag{3}$$

where $t > a, \quad n-1 < \alpha < n, \quad n \in \mathbf{Z}^{+}$.

III. Model Reference Adaptive Control Scheme

In this section, we present the structure of the MRAC scheme analyzed in this work. Since this adaptive scheme has been very well studied in [1], for the sake of space we only present here the equations needed for its implementation. For more specific details, the reader is referred to [1], Chapter 5.

A. MRAC Scheme for Plants with Only the Output Accessible

Usually, the whole state of a plant is not accessible, because some variables cannot be physically measured or because there is no instrumentation available to do it. In these cases, the designer has access only to the input and output of the plant, and the control scheme must be designed under these constraints.

Let us consider a single-input single-output linear time invariant plant of n-th order described by the vector differential equation

$$\begin{aligned} \dot{x}_p(t) &= A_p x_p(t) + b_p u(t), \\ y_p(t) &= h_p^{\mathrm{T}} x_p(t), \end{aligned} \tag{4}$$

where $A_p \in \mathbf{R}^{n\times n}$, $b_p, h_p \in \mathbf{R}^n$ are completely unknown. $x_p \in \mathbf{R}^n$ is the state vector, which is not accessible, and $u, y_p \in \mathbf{R}$ are the input and the output of the system. The plant is assumed to be controllable and observable.

An asymptotically stable reference model is specified by the linear time-invariant system described by

$$\begin{aligned} \dot{x}_m(t) &= A_m x_m(t) + b_m r(t), \\ y_m(t) &= h_m^{\mathrm{T}} x_m(t), \end{aligned} \tag{5}$$

where $A_m \in \mathbf{R}^{n\times n}$ is a known asymptotically stable matrix and $b_m, h_m \in \mathbf{R}^n$ are known vectors. The reference model is assumed to be controllable and observable. $y_m \in \mathbf{R}$ is the output of the reference model and $r \in \mathbf{R}$ is a bounded reference input. It is assumed that $y_m(t)$, for all $t \geq t_0$, represents the desired trajectory for $y_p(t)$.

The transfer function of the plant (4) can be represented as

$$W_p(s) = h_p^{\mathrm{T}} (sI - A_p)^{-1} b_p = k_p \frac{Z_p(s)}{R_p(s)} \tag{6}$$

where k_p is the high frequency gain and $Z_p(s), R_p(s)$ are monic polynomials with unknown parameters. It is assumed that $Z_p(s)$ is a Hurwitz polynomial and that the sign of k_p is known. The control goal here is to keep bounded all the signals of the scheme and that $\lim_{t\to\infty} (y_p(t) - y_m(t)) = 0$.

As we may expect, having no access to the plant state implies that a more complex control scheme has to be used in the problem to synthesize stable adaptive laws, compared to the case when the whole state $x_p(t)$ is accessible (see [1], Chapter 3). For this kind of scheme and with no loss of generality, it is assumed that the transfer function of the reference model is strictly positive real (SPR). The transfer function of the reference model is represented as

$$W_m(s) = h_m^{\mathrm{T}} (sI - A_m)^{-1} b_m = k_m \frac{Z_m(s)}{R_m(s)}, \tag{7}$$

where k_m is the high frequency gain and $Z_m(s), R_m(s)$ are monic coprime and Hurwitz polynomials with all the parameters known. Note that since the reference model is chosen by the designer, then all these conditions can be fulfilled.

This control problem has to be solved in a different way for plants with relative degree $n^* = 1$ and for plants with relative degree $n^* \geq 2$[1]. For the sake of simplicity, let us consider that the plant under study has relative degree $n^* = 1$. Then, the control input to the plant is chosen as

$$u(t) = \theta^{\mathrm{T}}(t)\, \omega(t), \tag{8}$$

where $\theta(t) \in \mathbf{R}^{2n}$ is a vector of adjustable parameters and $\omega(t) \in \mathbf{R}^{2n}$ is a vector of known signals. Specifically

$$\begin{aligned} \theta(t) &= \begin{bmatrix} k(t) & \theta_1^{\mathrm{T}}(t) & \theta_0(t) & \theta_2^{\mathrm{T}}(t) \end{bmatrix}^{\mathrm{T}}, \\ \omega(t) &= \begin{bmatrix} r(t) & \omega_1^{\mathrm{T}}(t) & y_p(t) & \omega_2^{\mathrm{T}}(t) \end{bmatrix}^{\mathrm{T}}, \end{aligned} \tag{9}$$

with $k, \theta_0 : \mathbf{R}^+ \to \mathbf{R}; \theta_1, \omega_1 : \mathbf{R}^+ \to \mathbf{R}^{n-1}; \theta_2, \omega_2 : \mathbf{R}^+ \to \mathbf{R}^{n-1}$.

The auxiliary signals $\omega_1(t) \in \mathbf{R}^{n-1}, \omega_2(t) \in \mathbf{R}^{n-1}$ are obtained by filtering the input and the output, respectively,

$$\begin{aligned} \dot{\omega}_1(t) &= \Lambda \omega_1(t) + l\, u(t), \\ \dot{\omega}_2(t) &= \Lambda \omega_2(t) + l\, y_p(t), \end{aligned} \tag{10}$$

where $\Lambda \in \mathbf{R}^{(n-1)\times(n-1)}$ and $l \in \mathbf{R}^{n-1}$ must be chosen such that $\det(sI - \Lambda) = Z_m(s)$ and the pair (Λ, l) is controllable and asymptotically stable.

Defining the control error as

$$e(t) = y_p(t) - y_m(t), \tag{11}$$

then for the classic integer order MRAC (IOMRAC) the stable adaptive laws for the parameters are generated as

$$\begin{aligned} \dot{k}(t) &= -\gamma \operatorname{sgn}(k_p)\, e(t)\, r(t), \\ \dot{\theta}_0(t) &= -\gamma \operatorname{sgn}(k_p)\, e(t)\, y_p(t), \\ \dot{\theta}_1(t) &= -\gamma \operatorname{sgn}(k_p)\, e(t)\, \omega_1(t), \\ \dot{\theta}_2(t) &= -\gamma \operatorname{sgn}(k_p)\, e(t)\, \omega_2(t), \end{aligned} \tag{12}$$

where $\gamma \in \mathbf{R}^+$ corresponds to the adaptive gain[1].

In this work we are going to use the same structure already explained for the IOMRAC scheme, but using fractional adaptive laws (FOMRAC) given by

$$\begin{aligned} {}^C D_{t_0}^{\alpha_k} k(t) &= -\gamma \operatorname{sgn}(k_p)\, e(t)\, r(t), \\ {}^C D_{t_0}^{\alpha_0} \theta_0(t) &= -\gamma \operatorname{sgn}(k_p)\, e(t)\, y_p(t), \\ {}^C D_{t_0}^{\alpha_1} \theta_1(t) &= -\gamma \operatorname{sgn}(k_p)\, e(t)\, \omega_1(t), \\ {}^C D_{t_0}^{\alpha_2} \theta_2(t) &= -\gamma \operatorname{sgn}(k_p)\, e(t)\, \omega_2(t), \end{aligned} \tag{13}$$

where α_k, α_0 and each component of α_1, α_2 belong to the interval $(0, 1]$. It is important to have in mind that these fractional orders can be different for every component of the adaptive laws.

It should also be noted that, although some advances have been made regarding the stability analysis of fractional adaptive schemes[12], the stability of this particular case has not been proved yet. Nevertheless, since the main idea of this work is obtaining some empirical conclusions from simulation studies on the control effort, we will focus only on this topic. The reader will observe, however, that in simulation studies the fractional case remains stable as well.

IV. SIMULATIONS STUDIES

In this section we will study the control of three second order plants, using the controller presented in Section III, through simulations. The plants under control have the same vectors b_p, h_p specified in (14), and only the matrix A_p changes from one plant to another.

In the first case we study an unstable plant ($a_{11} = 4,\ a_{12} = -1,\ a_{21} = 5,\ a_{22} = -3$) with poles $p_1 = 3.1926$ and $p_2 = -2.1926$. The second case corresponds to a marginally stable plant ($a_{11} = -5,\ a_{12} = 1,\ a_{21} = 0,\ a_{22} = 0$), with poles $p_1 = 0$ and $p_2 = -5$. Finally, the third case corresponds to a stable plant ($a_{11} = -5,\ a_{12} = 3,\ a_{21} = -15,\ a_{22} = 1$) with complex conjugate poles $p_{1,2} = -2 \pm 6i$. The reference model is asymptotically stable, as detailed in (14).

$$\begin{aligned} A_p &= \begin{bmatrix} a_{11} & a_{12} \\ a_{21} & a_{22} \end{bmatrix},\ A_m = \begin{bmatrix} -1 & 0 \\ 0 & -2 \end{bmatrix}, \\ b_p &= b_m = \begin{bmatrix} 1 \\ 1 \end{bmatrix},\ h_p = h_m = \begin{bmatrix} 1 \\ 0 \end{bmatrix}. \end{aligned} \tag{14}$$

The initial conditions used in simulations are $x_p(0) = [0\ \ 1]^{\mathrm{T}}$ and $x_m(0) = [1\ \ 5]^{\mathrm{T}}$.

It can be checked that the transfer function of the reference model is SPR and the relative degree is $n^* = 1$ for the three plants, so that conditions for designing MRAC are fulfilled. Since the numerator of the reference model transfer function is $Z_m(s) = s + 2$, the design parameters Λ, l were chosen as $\Lambda = -2$ and $l = 1$.

For the three plants to be controlled, the initial conditions of the four estimated parameters were chosen as $\theta(0) = [5\ \ 4\ \ -8\ \ -5]^{\mathrm{T}}$, the simulation time was set to $T = 500\,\mathrm{s}$, $\gamma = 1$ and the reference input $r(t)$ used is a unit step.

As we mentioned at the beginning of this paper, we will focus on analyzing how the management of control energy can be improved using fractional adaptive laws. To that extent, we use the integral of the squared input (ISI) as an indicator of the control energy, calculated using the following expression

$$ISI = \int_0^T u^2(t)\,\mathrm{d}t, \tag{15}$$

where T is the final simulation time.

Since the control signal is usually generated using some kind of energy, then ISI represents an excellent measurement of the energy spent to control the plant. Nowadays, ISI has become extremely important in control schemes, since industrial processes design and operation are focusing on saving energy, as a way of contributing to protect natural resources and planet sustainability.

Although our main goal is showing that the use of the fractional adaptive laws may improve the use of control energy in the adaptive schemes, we have to consider another important variable which is the control error. The integral of the squared control error is usually used as a performance index, measuring the deviation of the controlled variable from its desired value over the time. This index is given in (16) and it will be taken in mind during our studies as well.

$$ISE = \int_0^T e^2(t)\,\mathrm{d}t. \tag{16}$$

A. Numerical Results for the Unstable Plant

Although the order of the adaptive law can be different for each of the four components, let us make a preliminary analysis using the same value for $\alpha_k, \alpha_0, \alpha_1$ and α_2. To get some insight about the behavior of the MRAC scheme depending on the order of the adaptive laws, let us compare the results using the values specified in Table I.

The fractional adaptive laws were implemented using the NID block of the Ninteger toolbox[13], developed for Matlab/Simulink. This implementation requires the definition of the number of poles and zeros of the transfer function (N) to be used in the approximation, as well as the frequency range where approximation is valid and where these poles/zeros lie. In general, large values of N lead to more accurate approximation of the fractional order operator, and the converse is also true. In this paper the Crone approximation[14−18] of order 10 was used, with a frequency interval of $[0.01, 1\,000]$ rad/s. Table I shows the resulting values of ISI and ISE for these simulations.

TABLE I
RESULTING VALUES OF ISI AND ISE FOR REPRESENTATIVE VALUES OF THE ORDERS IN THE ADAPTIVE LAWS, FOR A STABLE PLANT

α_1	α_2	α_0	α_k	ISI	ISE
0.5	0.5	0.5	0.5	5 212.4	6.3651
0.7	0.7	0.7	0.7	58 379	2.1056
0.9	0.9	0.9	0.9	6 033.8	1.2405
1	1	1	1	6 071.7	1.0781

As can be seen from Table I, the lowest ISI value corresponds to the fractional case with lower order ($\alpha_1 = \alpha_2 = \alpha_0 = \alpha_k = 0.5$), increasing from there up to the integer order case. However, the behavior of the ISE is the opposite, being the case with the lowest ISI the one having the highest ISE.

Fig. 1 shows the evolution of control error and the control signal for these simulations. As can be seen, the control signal is smoother for the fractional cases and also converges slowly to its final value, which explains why these cases have lower ISI. However, the convergence of the control error is slower for the fractional cases, which explains why they also have the higher ISE. Thus, there is a trade-off between the magnitudes of the ISI and ISE values, which must be analyzed before making a decision about what values to choose for the orders of the adaptive laws.

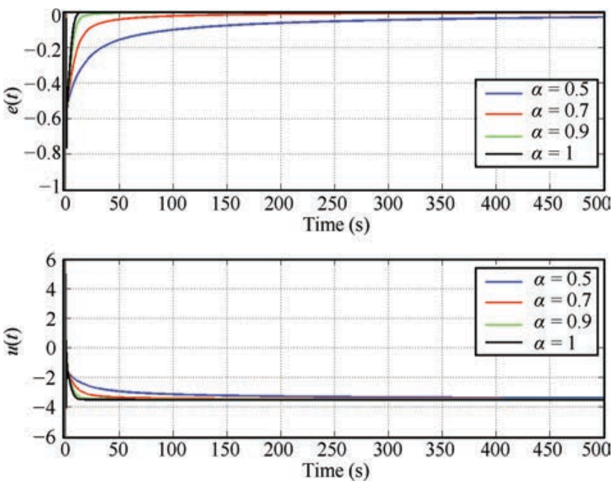

Fig. 1. Control error $e(t)$ (above) and control signal $u(t)$ (below) for representative values of the orders in the adaptive laws, when the reference signal is a unit step.

How to choose the right orders in the adaptive laws is a question that always arises. The answer to this question, however, is not absolute, since it will depend on many factors. It can be seen in the very simple simulation example given here, where the same order was used for the four components of the adaptive laws, that different behaviors will be obtained depending on the selection.

For that reason, the first question we must answer is: how important is the ISI index with respect to the ISE index for our problem? As the reader may note, the answer to this question will strongly depend on the specific application. For example, for processes that are high energy consuming, a reduction of a 2 % of the ISI could lead to million dollars savings in energy, and having probably a bit slower convergence speed of the control error.

Once this question is answered, it is still hard to choose the orders of the adaptive laws. Having in mind that there exists a trade-off between the ISI and the ISE, an optimization procedure appears to be the right option to decide.

In order to see how an optimization procedure can help to choose the orders $\alpha_1, \alpha_2, \alpha_0, \alpha_k$, we performed another simulation study. In this case, an optimization procedure was carried out using particle swarm optimization (PSO)[19], but other techniques could be used at designer will. The objective function used in this optimization process is presented in (17). Certainly, it includes both, the ISE and the ISI indexes, with their corresponding weighting factors to indicate how important is each index in the minimization problem.

$$J_{opt} = w_1\, ISE + w_2\, ISI. \tag{17}$$

For the optimization procedure we consider four cases. The first one takes into account only the ISE. The second, third and fourth take into account both, the ISE and the ISI, using different weighting factors w_1, w_2, as follows:

$$\begin{array}{llll} \text{Case } 1: & w_1 = 1 & \text{and} & w_2 = 0, \\ \text{Case } 2: & w_1 = 0.5 & \text{and} & w_2 = 0.5, \\ \text{Case } 3: & w_1 = 0.8 & \text{and} & w_2 = 0.2, \\ \text{Case } 4: & w_1 = 0.2 & \text{and} & w_2 = 0.8, \end{array} \tag{18}$$

The optimization process delivers the best values of orders $\alpha_1, \alpha_2, \alpha_0$ and α_k minimizing the objective function J_{opt} (17), using the weighting factors (18). The Matlab PSO toolbox[20] was used, with the most representative PSO parameters specified as:

1) Swarm size: 100
2) Number of iterations: 1 000
3) Initial inertia weight: 0.9
4) Final inertia weight: 0.4

The selection of these PSO parameters was made based on the works by [21–23]. The remaining PSO parameters were chosen at their default values.

For every case specified in (18), the optimization process was carried out ten times, obtaining ten sets of values for parameters $\alpha_1, \alpha_2, \alpha_0$ and α_k. In order to select one set of parameters, a criterion function J was calculated for each case, as it is specified in (19)

$$J = w_1\, ISE_{\rm norm} + w_2\, ISI_{\rm norm}, \tag{19}$$

where $ISE_{\rm norm}$ and $ISI_{\rm norm}$ are the normalized values of ISE and ISI respectively. These normalized values were calculated as

$$ISE_{\rm norm} = \frac{ISE - ISE_{\min}}{ISE_{\max} - ISE_{\min}}, \tag{20}$$

and

$$ISI_{\rm norm} = \frac{ISI - ISI_{\min}}{ISI_{\max} - ISI_{\min}}, \tag{21}$$

where $ISE_{\max}$, $ISE_{\min}$, $ISI_{\max}$ and $ISI_{\min}$ are the maximum and minimum values of ISE and ISI, respectively, for the ten simulations.

The values of ISI and ISE were normalized because their absolute values were of very different magnitudes (see Table II), where the resulting orders are specified. Thus, normalization allows the resulting $ISI_{\rm norm}$ and $ISE_{\rm norm}$ to lie in the same interval $[0, 1]$, and then weighting them with weighting factors that are also in the interval $[0, 1]$ is much more fair.

Analyzing the optimal set of parameters for the four cases, some conclusions can be drawn. It can be seen that the resulting optimal orders for Case 1 were all 1, that is, in this case the IOMRAC is the best solution. This means that when the control energy spent in the scheme is not taken into account, then the classic MRAC gives the best results.

However, for Case 2, Case 3 and Case 4, the resulting optimal orders are fractional. This means that, at least for this particular case analyzed, the recommended adaptive laws should not be the classic, if it is taken into account not only the behavior of the control error but also the energy used in the control. This empirical conclusion opens a lot of questions about MRAC, being a topic that deserves more research, from which interesting and useful results could be derived.

B. Numerical Results for the Marginally Stable Plant

As it was done in the case of the unstable plant, optimization process was carried out for the case of the marginally stable plant as well. All the details of the procedure used with the unstable plant were preserved, changing only the plant to be controlled. As a result of the optimization process, the fractional orders detailed in Table III were obtained. The values of the criterion function J for these cases are also specified in Table III.

If we look at Table III, it can be noted that the resulting optimal orders for Case 1 were all 1. This is the same that happened for the unstable plant, that is, in this case the IOMRAC is the best solution. As we mentioned before, this means that when the control energy spent in the scheme is not taken into account, then the classic MRAC gives the best results.

As it was observed for the unstable plant, in this case it can be seen from Table III that for Case 2, Case 3 and Case 4, the resulting optimal orders are fractional or combinations of fractional and integer orders. Thus, when the energy used in the control scheme is taken into account, then the recommended adaptive laws should not be the integer order but fractional.

C. Numerical Results for the Stable Plant

Finally, optimization process was carried out for the case of the stable plant. Again in this case, all the details of the procedure used with the unstable plant were preserved, changing only the plant to be controlled. As a result of the optimization process, the fractional orders and the values of J obtained are detailed in Table IV.

As can be seen from Table IV, the main difference arising in the case of the stable plant is that the resulting optimal orders for Case 1 are not all 1, like in the case of unstable and marginally stable plant, but all fractional. The resulting optimal orders for Case 2, Case 3 and Case 4, are all fractional or combinations of fractional and integer orders, same as in the case of the two previously studied plants. Thus, although for the stable plant the optimal scheme for Case 1 is not the IOMRAC, the fractional orders do remain as the best options when the control energy spent in the scheme is taken into account.

Remark 1. Although the work presented here is preliminary, we must point out an important issue. Beside the orders of the adaptive laws (α_1, α_2, α_0 and α_k), MRAC schemes have some other design parameters such as adaptive gains γ and initial conditions of the controller parameters. In this study, we used specific values for all these design parameters, and only the orders of the adaptive laws were varied. For that reason, a more complete study should include all these parameters in the decision making, being this a topic that is currently under investigation.

V. CONCLUSIONS

In this paper, an empirical analysis of the control energy

TABLE II
RESULTING FRACTIONAL ORDERS FROM THE OPTIMIZATION PROCESS FOR THE UNSTABLE PLANT

	α_1	α_2	α_0	α_k	ISI	ISE	J
Case 1	1	1	1	1	6 071.7	1.0781	0
Case 2	0.01	0.01	0.397	0.6331	5 451	7.7834	0.3881
Case 3	0.8058	0.1657	0.01	0.7619	5 911.7	1.9744	0.1947
Case 4	0.01	0.8818	0.01	0.01	1 471	131.0084	0.1544

TABLE III
RESULTING FRACTIONAL ORDERS FROM THE OPTIMIZATION PROCESS FOR THE MARGINALLY STABLE PLANT

	α_1	α_2	α_0	α_k	ISI	ISE	J
Case 1	1	1	1	1	4.4786	0.7313	0
Case 2	0.7953	1	0.409	1	4.4558	1.0097	0.0174
Case 3	0.6224	0.1333	0.8913	1	4.4693	0.8601	0.0011
Case 4	1	0.4239	1	0.6472	4.4556	1.2604	0.0171

TABLE IV
RESULTING FRACTIONAL ORDERS FROM THE OPTIMIZATION PROCESS FOR THE STABLE PLANT

	α_1	α_2	α_0	α_k	ISI	ISE	J
Case 1	0.6585	0.2147	0.7345	0.01	2.0052×10^5	0.2402	0.2402
Case 2	1	0.6722	0.9677	0.4263	1.9968×10^5	0.2718	0
Case 3	1	1	0.3875	0.1408	1.9969×10^5	0.2588	0.2
Case 4	1	1	0.4185	1	1.9968×10^5	0.2833	0

used in MRAC schemes has been presented, using orders for the adaptive laws in the interval $(0, 1]$. The analysis was made through simulation studies, including optimization procedures using PSO to select the orders of the adaptive laws. The behavior of the control energy spent by the system was analyzed through the integral of the squared control input ISI. The integral of the squared control error ISE was also included in the optimization process.

Simulation studies together with the optimization procedures were carried out for three different types of plants, and they have shown that, when the ISI is included in the objective function of the optimization to determine the orders of the adaptive laws, the resulting orders are fractional or combinations of fractional and integer orders. This is a very interesting result, since it suggests that the use of fractional adaptive laws could play an important role in the control energy management in MRAC schemes, which is an extremely important issue in today industry.

Since the results presented here are preliminary, research should be conducted to include other design parameters of the MRAC schemes into the optimization procedures.

REFERENCES

[1] Narendra K S, Annaswamy A M. *Stable Adaptive Systems*. United States: Dover Publications Inc., 2005.

[2] Kilbas A A, Srivastava H M, Trujillo J J. *Theory and Applications of Fractional Differential Equations*. New York: Elsevier, 2006.

[3] Vinagre B M, Petráš I, Podlubny I, Chen Y Q. Using fractional order adjustment rules and fractional order reference models in model-reference adaptive control. *Nonlinear Dynamics*, 2002, **29**(1−4): 269−279

[4] Ladaci S, Loiseau J, Charef A. Using fractional order filter in adaptive control of noisy plants. In: Proceedings of the 3rd International Conference on Advances in Mechanical Engineering and Mechanics. Hammamet, Tunisia, 2006.

[5] Suárez J I, Vinagre B M, Chen Y Q. A fractional adaptation scheme for lateral control of an AGV. *Journal of Vibration and Control*, 2008, **14**(9−10): 1499−1511

[6] Ma J, Yao Y, Liu D. Fractional order model reference adaptive control for a hydraulic driven flight motion simulator. In: Proceedings of the 41st Southeastern Symposium on System Theory. Tullahoma, TN: IEEE, 2009. 340−343

[7] He Y L, Gong R K. Application of fractional-order model reference adaptive control on industry boiler burning system. In: Proceedings of the 2010 International Conference on Intelligent Computation Technology and Automation (ICICTA). Changsha, China: IEEE, 2010. 750−753

[8] Sawai K, Takamatsu T, Ohmori H. Adaptive control law using fractional calculus systems. In: Proceedings of the 2012 SICE Annual Conference. Akita: IEEE, 2012. 1502−1505

[9] Aguila-Camacho N, Duarte-Mermoud M A. Fractional adaptive control for an automatic voltage regulator. *ISA Transactions*, 2013, **52**(6): 807−815

[10] Ladaci S, Loiseau J J, Charef A. Fractional order adaptive high-gain controllers for a class of linear systems. *Communications in Nonlinear Science and Numerical Simulation*, 2008, **13**(4): 707−714

[11] Charef A, Assabaa M, Ladaci S, Loiseau J J. Fractional order adaptive controller for stabilised systems via high-gain feedback. *IET Control Theory and Applications*, 2013, **7**(6): 822−828

[12] Aguila-Camacho N, Duarte-Mermoud M A. Boundedness of the solutions for certain classes of fractional differential equations with application to adaptive systems. *ISA Transactions*, 2016, **60**: 82−88

[13] Valério D, Da Costa J S. Ninteger: a non-integer control toolbox for Matlab. In: Proceedings of the 2004 Fractional Derivatives and Applications. Bordeaux, France: IFAC, 2004.

[14] Oustaloup A. *Systèmes Asservis Linéaires D'ordre Fractionnaire*. Paris: Masson, 1983.

[15] Oustaloup A. *La Commande CRONE: Commande Robuste D'ordre Non Entier*. Paris: Hermes, 1991.

[16] Lanusse P. De la commande CRONE de première génération à la commande CRONE de troisième generation [Ph. D. dissertation], University of Bordeaux, France, 1994.

[17] Oustaloup A. *Non-Integer Derivation*. Paris: Hermes, 1995.

[18] Oustaloup A, Levron F, Mathieu B, Nanot F M. Frequency-band complex noninteger differentiator: characterization and synthesis. *IEEE Transactions on Circuits and Systems I: Fundamental Theory and Applications*, 2000, **47**(1): 25−39

[19] Olsson A E. *Particle Swarm Optimization: Theory, Techniques and Applications*. New York: Nova Science Publishers, 2011.

[20] Singh J. 03. The PSO toolbox. Tech. Rep.. Source Forge. Available: http://sourceforge.net/projects/psotoolbox, 2011.

[21] Zamani M, Karimi-Ghartemani M, Sadati N, Parniani M. Design of a fractional order PID controller for an AVR using particle swarm optimization. *Control Engineering Practice*, 2009, **17**(12): 1380−1387

[22] Chatterjee A, Mukherjee V, Ghoshal S P. Velocity relaxed and craziness-based swarm optimized intelligent PID and PSS controlled AVR system. *International Journal of Electrical Power & Energy Systems*, 2009, **31**(7−8): 323−333

[23] Ordóñez-Hurtado R H, Duarte-Mermoud M A. Finding common quadratic Lyapunov functions for switched linear systems using particle swarm optimisation. *International Journal of Control*, 2012, **85**(1): 12−25

Norelys Aguila-Camacho received her Automatic Control Engineer title from the Central University in Cuba in 2003, M. Sc. from the Jose Antonio Echeverria Polytechnic Superior Institute of Cuba in 2010 and Ph. D. in electrical engineering from the University of Chile in 2014.

Currently she is a Post Doctoral Fellow at the University of Chile. Her main research interests include fractional adaptive control, nonlinear control and system identification. She is currently focused on applications to grinding circuits in mining industry.

Manuel A. Duarte-Mermoud received his Civil Electrical Engineer title from the University of Chile in 1977 and M. Sc. , M.Phil. and Ph. D. degrees, all in electrical engineering, from Yale University in 1985, 1986 and 1988 respectively.

Currently he is a Professor at the Electrical Engineering Department of the University of Chile. His main research interests include robust adaptive control (linear and nonlinear systems, integer and fractional), system identification, signal processing and pattern recognition. He is focused on applications to mining, energy and wine industry, sensory systems and electrical machines and drives.

Professor Duarte is an IFAC member, and former Treasurer and President of ACCA, the Chilean National Member Organization of IFAC, and former Vice-President of the IEEE-Chile.

An Approach to Design MIMO FO Controllers for Unstable Nonlinear Plants

Arturo Rojas-Moreno, *Senior Member, IEEE*

***Abstract*—This paper develops an approach to control unstable nonlinear multi-inputs multi-output (MIMO) square plants using MIMO fractional order (FO) controllers. The controller design uses the linear time invariant (LTI) state space representation of the nonlinear model of the plant and the diagonal closed-loop transfer matrix (TM) function to ensure decoupling between inputs. Each element of the obtained MIMO controller could be either a transfer function (TF) or a gain. A TF is associated in turn with its corresponding FO TF. For example, a D (Derivative) TF is related to a FO TF of the form D^δ, δ = [0, 1]. Two applications were performed to validate the developed approach via experimentation: control of the angular positions of a manipulator, and control of the car and arm positions of a translational manipulator.**

***Index Terms*—Fractional calculus, modeling of nonlinear system, control of manipulator, multivariable decoupling, multivariable nonlinear system.**

I. Introduction

CURRENTLY research for the design, application, and tuning rules of SISO (Single-input-single-output) FO PID controllers, such as $PI^{-\lambda}D^{\delta}$, is notably growing because controllers designed via fractional calculus improve the control performance and robustness over conventional IO (Integer order) PID controllers, due mainly to the presence of two more tuning parameters[1−3]: fractional numbers λ and δ. However, few results about FO control of MIMO plants have been published.

In [4], the two interacting conical tank process, a two-input two-output stable plant, was controlled by a multiloop FO PID configuration employing two FO PID controllers that were tuned using the cuckoo algorithm. Reference [5] deals with the tuning of FO PID controllers employing a genetic algorithm. Those controllers were applied to a MIMO process. A MIMO FO PID controller was designed in [6] to control stable MIMO time-delay plants. The resulting controller has a diagonal form with each diagonal element being a FO PI controller, whose parameters were tuned using CMAES (Covariance matrix adaptation evolution strategy). In [7], a diagonal-form MIMO FO PI controller was designed to control stable time-delay systems. The design procedure is based on a steady state decoupling of the MIMO system. A MIMO IO (Integer order) PID controller was designed using LMI (Linear matrix inequality) to control a MIMO FO plant in [8]. Design approaches developed in [4, 6] and [7] were tested via simulation.

This paper develops an approach to control stable and unstable nonlinear MIMO square plants using MIMO FO controllers. The design procedure employs the LTI state space representation of the nonlinear model of the the plant. Fig. 1 depicts the linear feedback control system, where the TM function $\boldsymbol{G}_p(s)$ of the plant is computed from its space state description. A selected diagonal closed-loop TM function denoted as $\boldsymbol{G}_T(s)$ ensures decoupling between inputs. For design purposes, each element of this TM function has the form of a first order TF with unity gain. The step response of this TF constitutes the desired output response of the variable under control. Knowing $\boldsymbol{G}_p(s)$ and $\boldsymbol{G}_T(s)$, the MIMO controller $\boldsymbol{G}_c(s)$, actually the structure of the FO MIMO controller $\boldsymbol{G}_{cFO}(s)$ shown in Fig. 2, can be easily computed. The elements of $\boldsymbol{G}_c(s)$ could be either transfer functions or gains. Replacing each TF of $\boldsymbol{G}_c(s)$ with its corresponding FO TF, $\boldsymbol{G}_c(s)$ becomes $\boldsymbol{G}_{cFO}(s)$. For instance, the FO form of the Laplace variable s is s^δ, while the FO form of s^{-1} is $s^{-\lambda}$, where δ and λ are fractional numbers between 0 and 1. The validity of the developed design approach was verified via experimentation using the FO nonlinear control system of Fig. 2. Two applications were performed for such a purpose: control of the angular positions of a manipulator, and control of the car and arm positions of a translational manipulator.

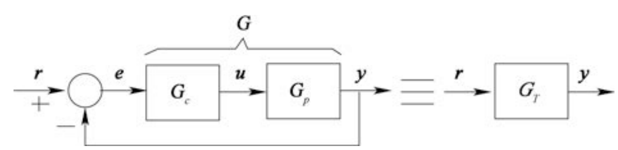

Fig. 1. Block diagram of the linear feedback control system.

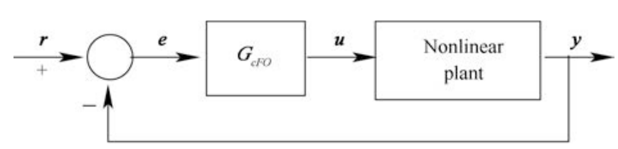

Fig. 2. Block diagram of the nonlinear FO feedback control system.

The MIMO FO controller designed in this work is novel due to its abilities to control not only MIMO stable plants but also nonlinear MIMO unstable ones. On the other hand, the developed approach was verified not only via simulation, but also by means of two real-time applications.

This paper is organized as follows. Section II deals with the design of the MIMO FO controller for MIMO nonlinear pla-

Manuscript received September 6, 2015; accepted February 1, 2016. Recommended by Associate Editor YangQuan Chen.

Citation: Arturo Rojas-Moreno. An approach to design MIMO FO controllers for unstable nonlinear plants. *IEEE/CAA Journal of Automatica Sinica*, 2016, **3**(3): 338−344

Arturo Rojas-Moreno is with the Department of Electrical Engineering, Universidad de Ingenieria y Tecnologia (www.utec.edu.pe), Lima 15063, Peru (email: arojas@utec.edu.pe).

nts. The first and second applications are described in Sections III and IV, respectively, while in Section V, some conclusions derived from this work are presented and discussed.

II. Design of the MIMO FO Controller

A MIMO nonlinear plant can be described by the following steady state representation

$$\dot{X} = \boldsymbol{f}(\boldsymbol{X}, \boldsymbol{U}), \tag{1}$$

where $\boldsymbol{f}$ is the function vector that describes the system dynamics. $\boldsymbol{X}$ and $\boldsymbol{U}$ are the state and control vectors, respectively. All vectors and functions are of known order. The corresponding LTI state-model can be obtained by linearization of (1) about a nominal trajectory. That is

$$\dot{\boldsymbol{x}} = \boldsymbol{A}\boldsymbol{x} + \boldsymbol{B}\boldsymbol{u}, \qquad \boldsymbol{y} = \boldsymbol{C}\boldsymbol{x}, \tag{2}$$

where $\boldsymbol{A}$, $\boldsymbol{B}$, and $\boldsymbol{C}$ are the state, control and output matrices, respectively, and $\boldsymbol{y}$ is the output vector. The TM function of the linear plant (2) is obtained from

$$\boldsymbol{G}_p(s) = \boldsymbol{C}(s\boldsymbol{I} - \boldsymbol{A})^{-1}\boldsymbol{B} + \boldsymbol{D}. \tag{3}$$

In (3), $\boldsymbol{I}$ is the identity matrix and all vectors and matrices are of known orders. Fig. 1 depicts the block diagram of the MIMO LTI control system, where $\boldsymbol{G}_c(s)$ is the MIMO controller, $\boldsymbol{G}(s)$ is the open-loop matrix function

$$\boldsymbol{G}(s) = \boldsymbol{G}_p(s)\boldsymbol{G}_c(s), \tag{4}$$

$\boldsymbol{G}_T(s)$ is the closed-loop matrix function

$$\boldsymbol{G}_T(s) = [\boldsymbol{G}(s) + \boldsymbol{I}]^{-1}\boldsymbol{G}(s), \tag{5}$$

and $\boldsymbol{r}$, $\boldsymbol{e}$, $\boldsymbol{u}$ and $\boldsymbol{y}$ represent reference, error, control and output vectors, respectively.

Consider the following diagonal closed-loop matrix function to ensure complete decoupling between different m inputs

$$\boldsymbol{G}_T(s) = \begin{bmatrix} G_{T11} & & \\ & \ddots & \\ & & G_{Tmm} \end{bmatrix}. \tag{6}$$

From (5)

$$\boldsymbol{G}(s) = \boldsymbol{G}_T(s)[\boldsymbol{I} - \boldsymbol{G}_T(s)]^{-1}. \tag{7}$$

Since $\boldsymbol{G}_T$ is diagonal, $[\boldsymbol{I} - \boldsymbol{G}_T]$ and $[\boldsymbol{I} - \boldsymbol{G}_T]^{-1}$ are also diagonal matrices. Therefore, matrix $\boldsymbol{G}$ takes on the diagonal form

$$\boldsymbol{G}(s) = \begin{bmatrix} \frac{G_{T11}}{1-G_{T11}} & & \\ & \ddots & \\ & & \frac{G_{Tmm}}{1-G_{Tmm}} \end{bmatrix}. \tag{8}$$

From Fig. 1, $\boldsymbol{y}(s) = \boldsymbol{G}_T(s)\boldsymbol{r}(s)$, where $\boldsymbol{r}(s)$ is the reference vector. The system error $\boldsymbol{e}(t)$ is given by

$$\boldsymbol{e}(s) = \boldsymbol{r}(s) - \boldsymbol{y}(s) = [\boldsymbol{I} - \boldsymbol{G}_T(s)]\boldsymbol{r}(s). \tag{9}$$

The necessary condition to make $\boldsymbol{e}(t) = \boldsymbol{0}$ in (9) is

$$\lim_{s\to 0}\boldsymbol{G}_T(s) = \boldsymbol{I}. \tag{10}$$

Introducing condition (10) in (5) results

$$\boldsymbol{I} + \boldsymbol{G}(0) = \boldsymbol{G}(0). \tag{11}$$

This requirement means that each element of the diagonal matrix $\boldsymbol{G}$ must contain at least one integrator. Using (4) in (5), we obtain the MIMO controller $\boldsymbol{G}_c(s)$ depicted in Fig. 1. That is

$$\boldsymbol{G}_c(s) = [\boldsymbol{G}_p(s)]^{-1}\boldsymbol{G}_T(s)[\boldsymbol{I} - \boldsymbol{G}_T(s)]^{-1}. \tag{12}$$

Elements of $\boldsymbol{G}_c(s)$ can be either gains or TF of the form

$$K_c; \qquad \frac{K_i}{s}; \qquad K_d s; \qquad \boldsymbol{G}_x(s) = K\frac{\prod_{i=0}^{M}(s+z_i)}{\prod_{j=0}^{N}(s+p_j)}, \tag{13}$$

where Kc, K_i, K_d and K are real gains, and z_i and p_j are poles and zeros of $\boldsymbol{G}_x(s)$. Note in (13) that $\boldsymbol{G}_x(s)$ is the general form of a TF. To formulate the FO MIMO controller denoted as $\boldsymbol{G}_{cFO}$, terms $\frac{K_i}{s}$ and $K_d s$ of (13) are written as

$$\frac{K_i}{s^\lambda}; \qquad K_d s^\delta, \tag{14}$$

where δ and λ are positive fractional numbers. It is worth mentioning that intensive research is performed in finding the FO counterpart of the TF $\boldsymbol{G}_x(s)$ of (13). For example, a particular case of $\boldsymbol{G}_x(s)$ is the following lead or lag compensator

$$K\frac{(1+s/\omega_b)}{(1+s/\omega_h)}. \tag{15}$$

The corresponding FO counterpart of (15) is written as[9]

$$K\left(\frac{1+s/\omega_k}{1+s/\omega_h}\right)^r \approx K\prod_{k=0}^{N}\left(\frac{1+s/\omega_k'}{1+s/\omega_h}\right),$$

where $0 < \omega_b < \omega_h$, $K > 0$, and, ω_k and ω_k' are corner frequencies that are computed recursively. Fig. 2 depicts the block diagram of the FO feedback control system.

For real-time implementation, it is required to have the discrete form of the controller $\boldsymbol{G}_{cFO}$. The discretization method by Muir's recursion[10] establishes

$$s^\delta \approx \left(\frac{2}{T}\right)^\delta \frac{A_n(z^{-1},\delta)}{A_n(z^{-1},-\delta)}, \tag{16}$$

where T is the sample time. In (16), polynomials $A_n(z^{-1},\delta)$ and $A_n(z^{-1},-\delta)$ can be computed in recursive form from

$$\begin{aligned} &A_n(z^{-1},\delta) = A_{n-1}(z^{-1},\delta) - c_n z^{-n} A_{n-1}(z,\delta), \\ &A_0(z^{-1},\delta) = 1, \\ &\qquad c_n = \begin{cases} \delta/n, & \text{if } n \text{ is odd}, \\ 0, & \text{if } n \text{ is even}. \end{cases} \end{aligned} \tag{17}$$

For $n = 3$, (17) takes on the form

$$\begin{aligned} A_3(z^{-1},\delta) &= -\tfrac{1}{3}\delta z^{-3} + \tfrac{1}{3}\delta^2 z^{-2} - \delta z^{-1} + 1,\\ A_3(z^{-1},-\delta) &= \tfrac{1}{3}\delta z^{-3} + \tfrac{1}{3}\delta^2 z^{-2} + \delta z^{-1} + 1. \end{aligned} \tag{18}$$

The developed design procedure will be validated experimentally with two applications described below.

III. First Application

Base position q_1 and arm position q_2 of a manipulator of 2DOF (2 degrees of freedom) will be controlled using a MIMO FO controller. Fig. 3 shows the experimental setup. The base and the arm of the manipulator are driven by two DC servomotors having reduction mechanism and quadrature encoder to sense angular positions. A NI cRIO-9073 (Compact reconfigurable input/output) device was employed to embed the MIMO FO controller. Modules NI 9263 and NI 9401 were used to acquire angular positions and generate the control signals, respectively. Such signals were amplified using two PWM (Pulse width modulation) Galil motion control amplifiers.

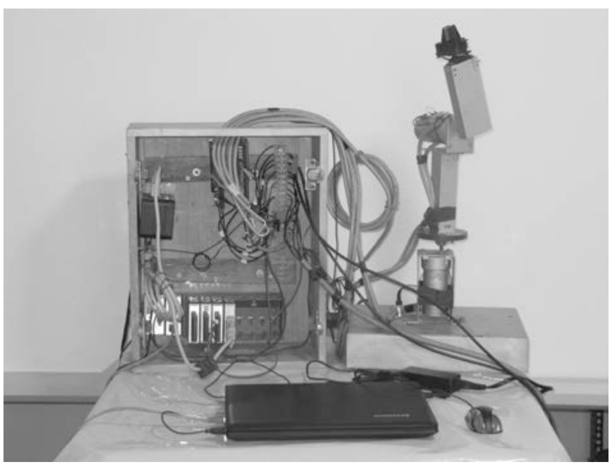

Fig. 3. The experimental setup of the manipulator of 2DOF.

TABLE I
VALUED PARAMETERS OF THE MANIPULATOR

Symbol	Description	Value	Unit
M_a	M. I. (Moment of inertia)	0.057	$\mathrm{kg\cdot m^2}$
J_1	M. I.	0.0394	$\mathrm{kg\cdot m^2}$
J_2	M. I.	0.0767	$\mathrm{kg\cdot m^2}$
J_{eq}	Equivalent M. I.	1.1819	$\mathrm{kg\cdot m^2}$
B_{q1}	F.C. (Friction constant)	0.02	N · m · s/rad
B_{q2}	F. C.	0.02	N · m · s/rad
B_{eq}	Equivalent F. C.	3.2287	N · m · s/rad
D	Torque	1.6481	N · m
n	Gear ratio	12.5	
R_a	Armature resistance	3.5	Ω
K_A	Amplifier gain	2.5	
K_m	Servomotor constant	0.0421	N · m/A
K_b	Back EMF constant	0.0565	V · s/rad
g	Gravitational constant	9.81	$\mathrm{m/s^2}$

The following dynamic model of the manipulator was obtained using Lagrange equations

$$\boldsymbol{M}(\boldsymbol{q})\ddot{\boldsymbol{q}} + \boldsymbol{P}(\boldsymbol{q},\dot{\boldsymbol{q}})\dot{\boldsymbol{q}} + \boldsymbol{d}(\boldsymbol{q}) = \boldsymbol{u}, \tag{19}$$

$$\boldsymbol{M} = \begin{bmatrix} M_{11} & 0\\ 0 & M_{22}\end{bmatrix}, \quad \boldsymbol{P} = \begin{bmatrix} P_{11} & P_{12}\\ P_{21} & P_{22}\end{bmatrix},$$
$$\boldsymbol{d} = \begin{bmatrix} 0\\ d_{21}\end{bmatrix}, \quad \boldsymbol{q} = \begin{bmatrix} q_1\\ q_2\end{bmatrix}, \quad \boldsymbol{u} = \begin{bmatrix} u_1\\ u_2\end{bmatrix},$$

$$\begin{aligned} M_{11} &= \frac{R_a}{nK_mK_A}\left(J_1 + J_{eq} + 2M_a\sin^2 q_2\right),\\ M_{22} &= \frac{R_a}{nK_mK_A}\left(J_2 + J_{eq}\right),\\ P_{11} &= \frac{R_a}{nK_mK_A}\left(B_{eq} + B_{q1} + \frac{n^2K_mK_b}{R_a}\right),\\ P_{12} &= \frac{R_a}{nK_mK_A}\left(4M_a\dot{q}_1\sin q_2\cos q_2\right),\\ P_{21} &= -\frac{R_a}{nK_mK_A}\left(2M_a\dot{q}_1\sin q_2\cos q_2\right),\\ P_{22} &= \frac{R_a}{nK_mK_A}\left(B_{eq} + B_{q2} + \frac{n^2K_mK_b}{R_a}\right),\\ d_{21} &= -\frac{R_a}{nK_mK_A}\left(\sin q_2\right). \end{aligned}$$

In (19), $\boldsymbol{M} = \boldsymbol{M}^{\mathrm{T}}$ is the diagonal inertia matrix, matrices $\boldsymbol{P}$ and $\boldsymbol{d}$ contain Coriolis and centripetal forces, and gravitational torques, respectively. $\boldsymbol{u}$ represents the control vector. Table I describes the valued parameters.

Using in (19) the approximations: $\sin^2 q_2 \approx q_2^2 \approx 0$, $\dot{q}_1\sin q_2\cos q_2 \approx \dot{q}_1 q_2 \approx 0$, $\sin q_2 \approx q_2$, we obtain

$$\overline{\boldsymbol{M}} = \begin{bmatrix} \overline{M}_{11} & 0\\ 0 & \overline{M}_{22}\end{bmatrix}, \overline{\boldsymbol{P}} = \begin{bmatrix} \overline{P}_{11} & \overline{P}_{12}\\ \overline{P}_{21} & \overline{P}_{22}\end{bmatrix}, \bar{\boldsymbol{d}} = \begin{bmatrix} 0\\ \bar{d}_{21}q_2\end{bmatrix}, \tag{20}$$

$$\begin{aligned} &\overline{M}_{11} = \frac{R_a}{nK_mK_A}\left(J_1 + J_{eq}\right), \quad \overline{M}_{22} = M_{22},\\ &\overline{P}_{11} = P_{11}, \quad \overline{P}_{12} = 0, \quad \overline{P}_{21} = 0, \quad \overline{P}_{22} = P_{22},\\ &\bar{d}_{21} = -\frac{R_a}{nK_mK_A}. \end{aligned}$$

Defining as state variables: $x_1 = q_1$, $x_2 = q_2$, $x_3 = \dot{q}_1$, and $x_4 = \dot{q}_2$, the linear model (20) can be transformed into

$$\dot{\boldsymbol{x}} = \boldsymbol{A}\boldsymbol{x} + \boldsymbol{B}\boldsymbol{u}, \qquad \boldsymbol{y} = \boldsymbol{C}\boldsymbol{x}, \tag{21}$$

$$\boldsymbol{A} = \begin{bmatrix} 0 & 0 & 1 & 0\\ 0 & 0 & 0 & 1\\ 0 & 0 & a_{33} & 0\\ 0 & a_{42} & 0 & a_{44}\end{bmatrix}, \quad \boldsymbol{B} = \begin{bmatrix} 0 & 0\\ 0 & 0\\ \frac{1}{\overline{M}_{11}} & 0\\ 0 & \frac{1}{\overline{M}_{22}}\end{bmatrix}$$

$$\boldsymbol{C} = \begin{bmatrix} 1 & 0 & 1 & 0\\ 0 & 1 & 0 & 0\end{bmatrix}$$

$$a_{33} = -\frac{\overline{P}_{11}}{\overline{M}_{11}}, \quad a_{42} = -\frac{\overline{d}_{21}}{\overline{M}_{22}}, \quad a_{44} = -\frac{\overline{P}_{22}}{\overline{M}_{22}},$$
$$b_{31} = -\frac{1}{\overline{M}_{11}}, \quad b_{42} = -\frac{1}{\overline{M}_{22}} \tag{22}$$

It is not difficult to demonstrate that outputs of models given by (19) and (21) have unstable step responses. In order to satisfy condition (10), matrix $\boldsymbol{G}_T(s)$ is selected as

$$\boldsymbol{G}_T(s) = \begin{bmatrix} \frac{1}{1+sT_1} & 0 \\ 0 & \frac{1}{1+sT_2} \end{bmatrix}, \tag{23}$$

where T_1 and T_2 are the chosen time constants of the controlled variables q_1 and q_2. Substituting (23) into (7), we obtain

$$\boldsymbol{G}(s) = \begin{bmatrix} \frac{1}{sT_1} & 0 \\ 0 & \frac{1}{sT_2} \end{bmatrix}. \tag{24}$$

Observe that $\boldsymbol{G}(s)$ in (24) meets requirement (11).

Note that $\boldsymbol{G}_T(s)$ matrices having diagonal elements as

$$\frac{\prod_{i=0}^{M}(T_i s + 1)}{\prod_{j=0}^{N}(T_j s + 1)}$$

fulfill condition (10) but not requirement (11). Therefore, such matrices can not be employed to calculate the controller $\boldsymbol{G}_c(s)$ using (12).

On the other hand, step responses of first order transfer functions as used in (23) constitute a good measure of design specifications to be met by the controlled outputs, because those show no overshoot, null steady state error, and time constants that are about one quarter of the settling times of the outputs under control.

$\boldsymbol{G}_p(s)$ and $\boldsymbol{G}_c(s)$ matrices are obtained using equations (3) and (12), respectively. The controller $\boldsymbol{G}_c(s)$ has the form

$$\boldsymbol{G}_c(s) = \begin{bmatrix} K_{c11} + K_{d11}s & 0 \\ 0 & K_{c22} + K_{d22}s + \frac{K_{i22}}{s} \end{bmatrix}. \tag{25}$$

Parameters in (25) are function of those of (22). The corresponding FO controller is expressed as

$$\boldsymbol{G}_{cFO}(s) = \begin{bmatrix} K_{c11} + K_{d11}s^{\delta} & 0 \\ 0 & K_{c22} + K_{d22}s^{\delta} + \frac{K_{i22}}{s^{\lambda}} \end{bmatrix}. \tag{26}$$

From Fig. 2, the FO control force is described by

$$\boldsymbol{u}(s) = \boldsymbol{G}_{cFO}(s)\boldsymbol{e}(s). \tag{27}$$

Substituting (16) with n = 3 into (26), and using the shift property $z^{-n}u_i(z) = u_i(k-n)$ and $z^{-n}e_i(z) = e_i(k-n)$, i = 1, 2, where k is the discrete time, we obtain the following difference equations for the control forces

$$u_1(k) = \frac{1}{a_0}\left[-\sum_{i=1}^{6} a_i u_1(k-i) + \sum_{j=0}^{6} b_j e_1(k-j)\right],$$
$$u_2(k) = \frac{1}{a_0}\left[-\sum_{i=1}^{6} a_i u_2(k-i) + \sum_{j=0}^{6} h_j e_2(k-j)\right]. \tag{28}$$

In (28), all a_i, b_j and h_j are known constants, for instance

$$a_6 = -\delta\lambda, \qquad a_0 = 1,$$
$$b_6 = \frac{1}{9}K_{d11}\delta\lambda(\frac{2}{T})^{\delta} - \frac{1}{9}K_{c11}\delta\lambda,$$
$$h_6 = \frac{1}{9}K_{d22}\delta\lambda(\frac{2}{T})^{\delta} - \frac{1}{9}K_{c22}\delta\lambda - \frac{1}{9}K_{i22}\delta\lambda(\frac{2}{T})^{-\lambda},$$

where T is the sampling time selected as 1 ms in this work. The FO control system was simulated in Mathscript with time constants T_1 and T_2 and FO parameters δ and λ set to 0.5, 0.5, 0.5 and 0.9, respectively. The other gains were taken from (25): K_{c11} = 10.7, K_{d11} = 0.866, K_{c22} = 26.74, K_{d22} = 4.66, K_{i22} = -13.2786. For the experimentation phase, K_{c11} was set to 15. Figs. 4 and 5 depict the experimental results.

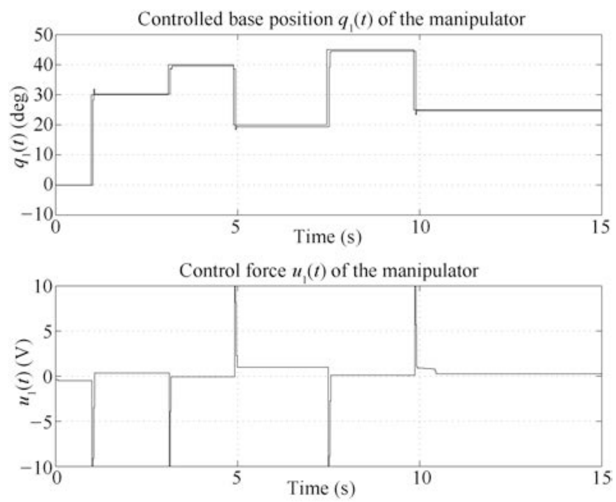

Fig. 4. Controlled base position $q_1(t)$ of the manipulator with respect to step wise references.

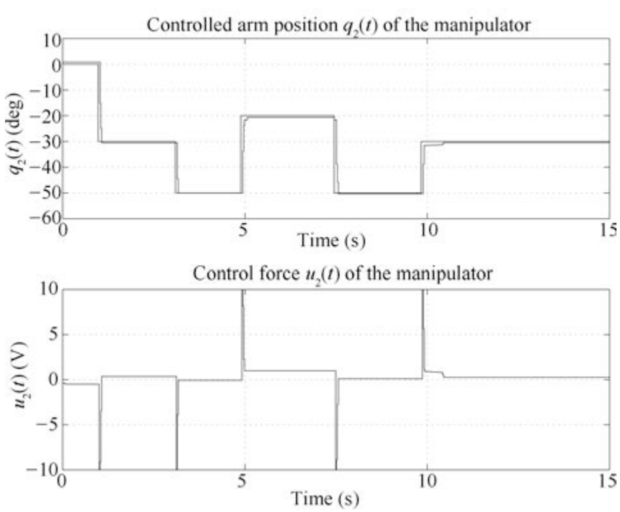

Fig. 5. Controlled arm position $q_2(t)$ of the manipulator with respect to step wise references.

IV. Second Application

The linear position q_1 of the car and the angular position q_2 of the arm of a translational manipulator of 2DOF shown in Fig. 6 will be controlled with a MIMO FO controller. The manipulator possesses two DC servomotors with reduction mechanism and quadrature encoders to sense angular positions. One servomotor is attached to the axis of one of the two pulleys. Those pulleys carry a cable to transmit the force to translate the car, which is mounted on rails. The other servomotor is mounted on the car to drive the arm. This application uses the same experimental setup as the first one.

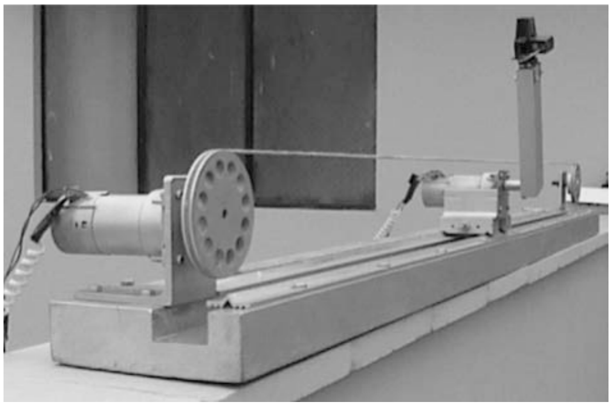

Fig. 6. The translational manipulator of 2DOF.

The dynamic model of the manipulator was also obtained employing Lagrange equations. The resulting nonlinear model takes on the form

$$\boldsymbol{M}(\boldsymbol{q})\ddot{\boldsymbol{q}}+\boldsymbol{P}(\boldsymbol{q},\dot{\boldsymbol{q}})\dot{\boldsymbol{q}}+\boldsymbol{d}(\boldsymbol{q})=\boldsymbol{u} \tag{29}$$

$$\boldsymbol{q}=\begin{bmatrix} q_1\\ q_2\end{bmatrix}=\begin{bmatrix} r\\ \theta\end{bmatrix},\qquad \boldsymbol{u}=\begin{bmatrix} u_1\\ u_2\end{bmatrix},\qquad \boldsymbol{d}=\begin{bmatrix} 0\\ d_{21}\end{bmatrix},$$

$$\boldsymbol{M}=\begin{bmatrix} M_{11} & M_{12}\\ M_{21} & M_{22}\end{bmatrix},\qquad \boldsymbol{P}=\begin{bmatrix} P_{11} & P_{12}\\ 0 & P_{22}\end{bmatrix},$$

$$\begin{aligned}
M_{11}&=\frac{J_x+m_1}{K_xK_{A1}}, & M_{12}&=\frac{m_2}{K_xK_{A1}}\cos\theta,\\
M_{21}&=\frac{m_2}{r_pK_xK_{A2}}\cos\theta, & M_{22}&=\frac{J_{eq2}+J_t}{r_pK_xK_{A2}},\\
P_{11}&=\frac{B_x+B_F}{K_xK_{A1}}, & P_{12}&=-\frac{m_2}{K_xK_{A1}}\dot{\theta}\sin\theta,\\
P_{22}&=\frac{\frac{n^2K_mK_b}{Ra}+B_{eq2}+B_T}{r_pK_xK_{A2}}, & &\\
d_{21}&=-\frac{gm_2}{r_pK_xK_{A2}}\sin\theta. & &
\end{aligned}$$

Observe that matrix $\boldsymbol{M}$ in (29) is neither diagonal nor symmetric which makes the manipulator more challenging to be controlled. Recall that matrix $\boldsymbol{M}$ in (20) was diagonal. Table II describes the valued parameters of the translational manipulator.

TABLE II
VALUED PARAMETERS OF THE MANIPULATOR

Symbol	Description	Value	Units
r_p	Pulley radio	0.05	m
K_A	Amplifier gain	2.5	
K_x	Constant	1.9858	N/A
K_b	Emf constant	0.0565	V · s/rad
R_a	Armature resistance	5.3	Ω
K_m	Motor constant	0.0421	N · m/A
J_x	Mass	450.65	kg
J_t	Moment of inertia	0.0325	kg · m^2
J_{eq2}	Moment of inertia	1.126	kg · m^2
B_T	Friction constant	1.8	N · m/rad/s
B_F	Friction constant	2.81	kg/s
B_x	Constant	2 039.5	kg/s/m^2
B_{eq2}	Friction constant	3.2287	kg/s
m_1	Mass	2.2	kg
m_2	Work	0.0695	kg · m
g	Gravitational constant	9.81	m/s^2
n	Gear ratio	12.5	

On using the approximations $\cos\theta\approx 1$, $\sin\theta\approx\theta$ and $\dot{\theta}\sin\theta\approx 0$ in (29), we obtain

$$\begin{aligned}
&\overline{M}_{11}=M_{11}, \quad \overline{M}_{12}=\frac{m_2}{K_xK_{A1}}, \quad \overline{M}_{21}=\frac{m_2}{r_pK_xK_{A2}},\\
&\overline{M}_{22}=M_{22}, \quad \overline{P}_{11}=P_{11}, \quad \overline{P}_{12}=0, \quad \overline{P}_{22}=P_{22},\\
&\overline{d}_{21}=-\frac{gm_2}{r_pK_xK_{A2}}.
\end{aligned} \tag{30}$$

Defining as state variables: $x_1=r$, $x_2=\theta$, $x_3=\dot{r}$ and $x_4=\dot{\theta}$, the nonlinear model of (29) using (30) can be transformed into the following state equation

$$\dot{\boldsymbol{x}}=\boldsymbol{A}\boldsymbol{x}+\boldsymbol{B}\boldsymbol{u},\qquad \boldsymbol{y}=\boldsymbol{C}\boldsymbol{x}, \tag{31}$$

$$\boldsymbol{A}=\begin{bmatrix} 0&0&1&0\\ 0&0&0&1\\ 0&a_{32}&a_{33}&a_{34}\\ 0&a_{42}&a_{43}&a_{44}\end{bmatrix},\quad \boldsymbol{B}=\begin{bmatrix} 0&0\\ 0&0\\ b_{31}&b_{32}\\ b_{41}&b_{42}\end{bmatrix},$$

$$\boldsymbol{C}=\begin{bmatrix} 1&0&1&0\\ 0&1&0&0\end{bmatrix},$$

$$\begin{aligned}
a_{32}&=\frac{\overline{M}_{12}\overline{d}_{21}}{\overline{den}}, & a_{33}&=-\frac{\overline{M}_{22}\overline{P}_{11}}{\overline{den}},\\
a_{34}&=\frac{\overline{M}_{12}\overline{P}_{22}}{\overline{den}}, & a_{42}&=-\frac{\overline{M}_{11}\overline{d}_{21}}{\overline{den}},\\
a_{43}&=\frac{\overline{M}_{21}\overline{P}_{11}}{\overline{den}}, & a_{44}&=-\frac{\overline{M}_{11}\overline{P}_{22}}{\overline{den}},\\
b_{31}&=\frac{\overline{M}_{22}}{\overline{den}}, & b_{32}&=-\frac{\overline{M}_{12}}{\overline{den}},\\
b_{41}&=-\frac{\overline{M}_{21}}{\overline{den}}, & b_{42}&=\frac{\overline{M}_{11}}{\overline{den}},\\
\overline{den}&=\overline{M}_{11}\overline{M}_{22}-\overline{M}_{12}\overline{M}_{21}. & &
\end{aligned} \tag{32}$$

It is not difficult to prove that outputs of models given by (29) and (31) possess unstable step responses. According to (10), $\boldsymbol{G}_T(s)$ matrix is chosen as in (23). $\boldsymbol{G}_p(s)$, $\boldsymbol{G}_c(s)$ and $\boldsymbol{G}(s)$

matrices are obtained using (3), (12) and (4), respectively. $\boldsymbol{G}(s)$ results in a matrix that has the same form as (24). The $\boldsymbol{G}_c(s)$ matrix is calculated using relation (12)

$$\boldsymbol{G}_c(s) = \begin{bmatrix} K_{c11} + K_{d11}s & K_{c12} + \frac{K_{i12}}{s} + K_{d12}s \\ K_{c21} + K_{d21}s & K_{c22} + \frac{K_{i22}}{s} + K_{d22}s \end{bmatrix}. \quad (33)$$

Parameters of (33) are function of parameters described in (32). The corresponding FO controller is expressed as

$$\begin{aligned} &\boldsymbol{G}_{cFO}(s) \\ &= \begin{bmatrix} K_{c11} + K_{d11}s^{\delta} & K_{c12} + \frac{K_{i12}}{s^{\lambda}} + K_{d12}s^{\delta} \\ K_{c21} + K_{d21}s^{\delta} & K_{c22} + \frac{K_{i22}}{s^{\lambda}} + K_{d22}s^{\delta} \end{bmatrix}. \quad (34) \end{aligned}$$

Compare (33) with (25) and (34) with (26). Replacing (16) with n = 3 in (34), and then employing the shift property, we obtain the following difference equations for the vector control (27)

$$\begin{aligned} u_1(k) &= \frac{1}{a_0}\left[-\sum_{i=1}^{6} a_i u_1(k-i) + \sum_{j=0}^{6} b_j e_1(k-j) \right. \\ &\quad \left. + \sum_{j=0}^{6} c_j e_2(k-j)\right], \\ u_2(k) &= \frac{1}{a_0}\left[-\sum_{i=1}^{6} a_i u_2(k-i) + \sum_{j=0}^{6} g_j e_2(k-j) \right. \\ &\quad \left. + \sum_{j=0}^{6} h_j e_2(k-j)\right]. \quad (35) \end{aligned}$$

In (35), k is the discrete time, and all a_i, b_j and h_j are known constants as in (27). T, the sampling time, was selected to be 1 ms. The FO control system for this manipulator was simulated in Mathscript with time constants T_1 and T_2 and FO parameters δ and λ set to 0.3, 0.5, 0.6 and 0.75, respectively. The other gains were taken from (31): K_{c11} =220, K_{d11} = 1, K_{c12} = 0, K_{i12} = 0; K_{d12} = 0.028, K_{c21} = 0, K_{d21} = 0.0093, K_{c22} = 20, K_{d22} = 10, K_{i22} = -5. For the experimentation phase, K_{c11} was set to 25. Figs. 7 and 8 depict the experimental results.

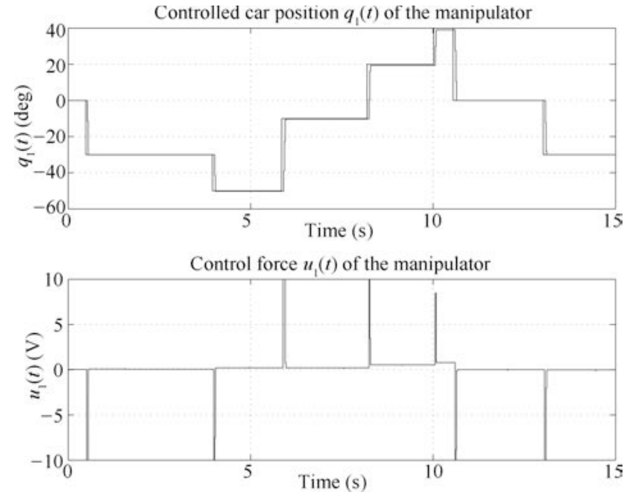

Fig. 7. Controlled car position $q_1(t)$ of the manipulator with respect to step wise references.

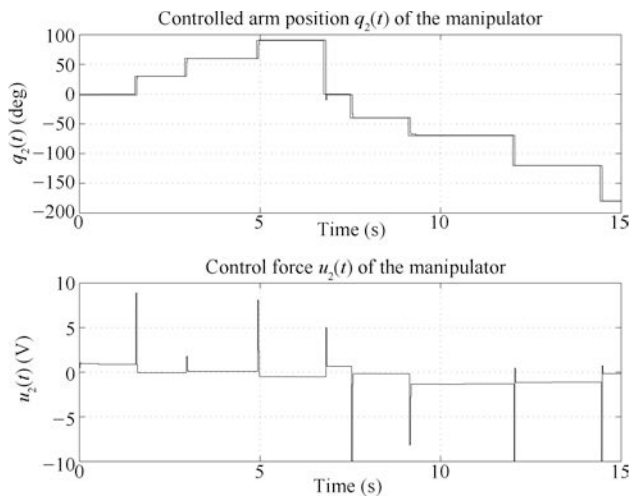

Fig. 8. Controlled arm position $q_2(t)$ of the manipulator with respect to step wise references.

V. Conclusions

In light of the results in Sections III and IV, the main goal of this work has been achieved: experimental verification of the design approach to control nonlinear MIMO processes using MIMO FO controllers.

The nonlinear model of the plant is necessary to obtain the linear model required to design the structure of the FO controller, and to test via simulation the designed FO controller. In the simulation phase, controller parameters were tuned using the trial and error method. Such valued parameters were used with few modifications for the experimentation phase.

Intensive work has been done in tuning rules development for FO SISO (Single-input single-output) controllers. It is still under research to extend the results for FO MIMO controllers. No tuning methods for controllers of the forms given by (26) and (34) have been reported. Moreover, depending on the application, the structure of a FO MIMO controller can change (compare (26) with (34)), making the development of proper tuning rules difficult. For such reasons, this work employed the trial and error method.

MIMO FO controllers designed in [4, 6], and [7] were tuned using different methods, because such controllers have diagonal forms with each diagonal element being a FO SISO controller.

This work is novel because unlike others the designed FO MIMO controller can be applied not only to stable MIMO plants, but also to nonlinear unstable MIMO plants. This approach was tested not only via simulation but also via experimentation.

The proposed design procedure can also be applied to MIMO time-delay plants. In order to obtain a LTI state space description of the plant, TF containing time-delays need to be replaced by equivalent TF. For example[11]

$$\frac{1}{2s+1}\mathrm{e}^{-2s} \approx \frac{1}{(s+1)^4}$$

It is necessary to perform more research related to the design of a FO MIMO controller when the structure of the controller, matrices (25) and (33) for example, has terms of the form

$$G_x(s) = K\frac{\prod\limits_{i=0}^{M}(s+z_i)}{\prod\limits_{j=0}^{N}(s+p_j)}$$

REFERENCES

[1] Karad S, Chatterji S, Suryawanshi P. Performance analysis of fractional order PID controller with the conventional PID controller for bioreactor control. *International Journal of Scientific & Engineering Research*, 2012, **3**(6): 1−6

[2] Singh S, Kosti A. Comparative study of integer order PI-PD controller and fractional order PI-PD controller of a DC motor for speed and position control. *International Journal of Electrical and Electronic Engineering & Telecommunications*, 2015, **4**(2): 22−26

[3] Chen Y, Petrǎš I, Xue D. Fractional order control - a tutorial. In: Proceedings of the 2009 American Control Conference. St. Louis, MO, USA: IEEE, 2009. 1397−1411

[4] Banu U S, Lakshmanaprabu S K. Multiloop fractional order PID controller tuned using cuckoo algorithm for two interacting conical tank process. *World Academy of Science, Engineering and Technology, International Journal of Mechanical and Mechatronics Engineering*, 2015, **2**(1): 742

[5] Moradi M. A genetic-multivariable fractional order PID control to multi-input multi-output processes. *Journal of Process Control*, 2014, **24**(4): 336−343

[6] Sivananaithaperumal S, Baskar S. Design of multivariable fractional order PID controller using covariance matrix adaptation evolution strategy. *Archives of Control Sciences*, 2014, **24**(2): 235−251

[7] Muresan C I, Dulf E H, Ionescu C M. Multivariable fractional order PI controller for time delay processes. In: Proceedings of the 2012 International Conference on Engineering and Applied Science. Colombo, Sri Lanka, 2012.

[8] Song X N, Chen Y Q, Tejado I, Vinagre B M. Multivariable fractional order PID controller design via LMI approach. In: Proceedings of the 18th IFAC World Congress. Milano, Italy: IFAC, 2011. 13960−13965

[9] Malti R, Melchior P, Lanusse P, Oustaloup A. Towards an object oriented CRONE toolbox for fractional differential systems. In: Proceedings of the 18th IFAC World Congress. Milano, Italy: IFAC, 2011. 10830−10835

[10] Vinagre B M, Chen Y Q, Petrǎš I. Two direct Tustin discretization methods for fractional-order differentiator/integrator. *Journal of the Franklin Institute*, 2003, **340**(5): 349−362

[11] Michalowski T. *Applications of MATLAB in Science and Engineering*. Rijeka, Croatia: InTech, 2011.

Arturo Rojas-Moreno graduated from Universidad Nacional de Ingenieria (UNI), Peru, in 1973. He received the M. Sc. degree from UNI in 1979 and the Ph. D. degree from Utah State University, USA, in 1995. He is currently a professor at the Electrical Engineering Department of Universidad de Ingenieria y Tecnologia (UTEC), Peru. His research interest include nonlinear modelling, process control engineering, and motion control, especially the control of robotic manipulators and drones.

Controllability of Fractional Order Stochastic Differential Inclusions with Fractional Brownian Motion in Finite Dimensional Space

T. Sathiyaraj and P. Balasubramaniam

***Abstract*—In this paper, sufficient conditions are formulated for controllability of fractional order stochastic differential inclusions with fractional Brownian motion (fBm) via fixed point theorems, namely the Bohnenblust-Karlin fixed point theorem for the convex case and the Covitz-Nadler fixed point theorem for the nonconvex case. The controllability Grammian matrix is defined by using Mittag-Leffler matrix function. Finally, a numerical example is presented to illustrate the efficiency of the obtained theoretical results.**

***Index Terms*—Controllability, fractional Brownian motion, fractional order derivatives, Mittag-Leffler function, stochastic differential inclusions.**

I. INTRODUCTION

MANY real dynamical systems are better characterized by using a non-integer order dynamic model based on fractional calculus or, differentiation or integration of non-integer order. The concept of fractional calculus has tremendous potential to change the model and control the nature around us. Fractional differential equations serve as an appropriate phenomenon such that it can even describe the real world problems which are impossible to describe using classical integer order differential equations. Over the past decades, the theory of fractional differential equation received more attention, and has obtained a prior position in the field of physics, signal processing, fluid mechanics, viscoelasticity, mathematical biology, electro chemistry and many other science and engineering areas, for details one may refer the books[1−5]. In recent years, fractional control techniques provide an effective way to control dynamic behaviours through the model of fractional differential equations[6]. Tuning and auto-tuning of fractional order controllers for industrial applications have been well developed see [7] and its advanced applications in various branches of physics, economics and engineering sciences, see [8−9] and references therein.

Manuscript received August 18, 2015; accepted January 13, 2016. This work was supported by Council of Scientific and Industrial Research, Extramural Research Division, Pusa, New Delhi, India (25/(0217)/13/EMR-II). Recommended by Associate Editor YangQuan Chen.

Citation: T. Sathiyaraj, P. Balasubramaniam. Controllability of fractional order stochastic differential inclusions with fractional Brownian motion in finite dimensional space. *IEEE/CAA Journal of Automatica Sinica*, 2016, **3**(4): 400−410

T. Sathiyaraj and P. Balasubramaniam are with the Department of Mathematics, The Gandhigram Rural Institute-Deemed University, Gandhigram-624302, Dindigul, Tamil Nadu, India (e-mail: sathiyaraj133@gmail.com; balugru@gmail.com).

Control theory is an interdisciplinary branch of application-oriented mathematics which deals with basic principles underlying the analysis and design of control systems. The objective of control theory is to make systems to perform specific tasks using suitable control actions. Such behaviour is seen in a range of problems from mechanics, optimal control, ecology, industrial robotics, aeronautics, transportation, biotechnology, medical models, etc. Controllability of dynamical systems is one of the fundamental notions of modern control theory. Generally speaking, controllability enables one to steer the control system from an arbitrary initial state to an arbitrary final state using the set of admissible controls. This concept leads to some important conclusions regarding the behaviour of linear and nonlinear dynamical systems. Controllability of fractional order deterministic and stochastic dynamical systems in finite dimensional space has been studied in [10−11]. Controllability for neutral stochastic functional differential inclusions with infinite delay in abstract space has been studied recently in [12]. Controllability of linear stochastic systems has been investigated in [13].

On the other hand, the theory of differential inclusions has become an active area of investigation due to its applications in various fields such as mechanics, electrical engineering, medicine biology, ecology and so on[12,14−15]. Stochastic differential equations driven by fBm have attracted great interest and potential applications in telecommunication networks, finance markets, biology and other fields[16−17].

However, to the best of our knowledge there are limited works considering the existence of solutions, and controllability results of integer order stochastic differential inclusions in finite and infinite dimensional space[12,15]. Fractional order Riemann-Liouville integral inclusions with two independent variables and multiple delays have been illustrated in [14]. Balasubramaniam[15] proposed existence of solutions of functional stochastic differential inclusions, whereas Balachandran and Kokila[10] have obtained the controllability of fractional dynamical systems, although controllability of impulsive neutral stochastic differential equations with fBm was established in [18]. In this paper, we study the controllability of fractional order stochastic differential inclusions with fBm,

$$\begin{aligned} {}^{C}D^{q}x(t) \in Ax(t) + Bu(t) + f(t, x(t)) \\ + \int_0^t G(s, x(s))\mathrm{d}W^H_{(s)},\ t \in J, \end{aligned}$$

$$x(0) = x_0, \tag{1}$$

where $[0,T] := J, {}^C D^q$ denotes Caputo derivative of fractional order q, A and B are matrices of dimensions $n \times n$ and $n \times m$ respectively, $x \in \mathbf{R}^n$, $u \in \mathbf{R}^m$ are the state and control vectors. The nonlinear functions f, G are appropriate functions to be defined later. W_t^H is a fBm with the Hurst parameter $H \in (\frac{1}{2}, 1)$ and defined by its stochastic representation

$$\begin{aligned} W_{(t)}^H := &\frac{1}{\Gamma\left(H+\frac{1}{2}\right)}\Big(\int_{-\infty}^0 [(t-s)^{H-\frac{1}{2}} \\ &- (-s)^{H-\frac{1}{2}}]\mathrm{d}W(s) \\ &+ \int_0^t (t-s)^{H-\frac{1}{2}}\mathrm{d}W(s)\Big), \end{aligned} \tag{2}$$

where Γ represents the Gamma function $\Gamma(\alpha) := \int_0^\infty x^{\alpha-1}\exp(-x)\mathrm{d}x$ and $0 < H < 1$. The integrator W is a stochastic process of ordinary Brownian motion. Note that W is recovered by taking $H = \dfrac{1}{2}$ in (2). The proposed work on the controllability of fractional order stochastic differential inclusions with fBm in finite dimensional space is new to the literature.

The paper is organized as follows: In Section II, we recall some essential results on the basic definitions of fractional integral and derivatives, lemmas, propositions, notations, and some mild conditions to obtain the controllability results successfully. In Section III, we study the controllability results for the fractional system (1) under the fixed point theorems. Numerical example is illustrated in Section IV to show the effectiveness of the derived results. Finally, conclusion and future work is drawn in Section V.

II. Preliminaries

It is well known that the fractional order integral and derivative operators, namely Riemann-Liouville, Caputo and Mittag-Leffler function play a vital role to find the solution of fractional differential equation. The following definitions and properties are well known, for a suitable function $f \in L_1(\mathbf{R}_+), \mathbf{R}_+ = [0, \infty)$. For more details, see [4, 9, 19].

Let $q > 0$, $p > 0$ with $n-1 < q < n$, $n-1 < p < n$, and $n \in \mathbf{N}$. Let $\mathbf{R}^m$ be the m-dimensional Euclidean space.

Definition 1. The fractional integral of order q with the lower limit 0 for a function f is defined as

$$I^q f(t) = \frac{1}{\Gamma(q)}\int_0^t (t-s)^{q-1} f(s)\mathrm{d}s,\ t > 0,$$

provided the right-hand side is pointwise defined on $[0, \infty)$, where $\Gamma(\cdot)$ is the gamma function. The Laplace transform of the Riemann-Liouville fractional integral is given by

$$\mathcal{L}\{I_t^q f(t)\} = \frac{1}{\lambda^q}\hat{f}(\lambda),$$

where

$$\hat{f}(\lambda) = \int_0^\infty \mathrm{e}^{-\lambda t} f(t)\mathrm{d}t, \quad \mathrm{Re}(\lambda) > w.$$

Definition 2. Riemann-Liouville derivative of order q with lower limit zero for a function $f : [0, \infty) \longrightarrow \mathbf{R}$ can be written as

$${}^L D^q f(t) = \frac{1}{\Gamma(n-q)}\frac{\mathrm{d}^n}{\mathrm{d}t^n}\int_0^t \frac{f(s)}{(t-s)^{q+1-n}}\mathrm{d}s.$$

Definition 3. The Caputo fractional derivative of order q for a function $f : [0, \infty) \longrightarrow \mathbf{R}$ can be written as

$$\begin{aligned} {}^C D^q f(t) &= I^{n-q} D^n f(t) \\ &= \frac{1}{\Gamma(n-q)}\int_0^t (t-s)^{n-q+1} f^n(s)\mathrm{d}s. \end{aligned}$$

In particular, $I^{q\,C} D^q f(t) = f(t) - f(0)$. The following is a well-known relation

$$\begin{aligned} {}^C D^q f(t) &= {}^L D^q f(t) \\ &- \sum_{k=0}^{n-1} \frac{t^{k-q}}{\Gamma(k-q+1)} f^{(k)}(0^+), \\ & n = \Re(q) + 1. \end{aligned}$$

Definition 4. Now, consider the well-known Mittag-Leffler function:
A two parameter function of the Mittag-Leffler type function is defined by the series expansion

$$E_{q,p}(z) = \sum_{k=0}^\infty \frac{z^k}{\Gamma(kq+p)}, \quad q, p > 0, \quad z \in \mathbf{C}.$$

The general Mittag-Leffler function satisfies the following identity:

$$\int_0^\infty \mathrm{e}^{-t} t^{p-1} E_{q,p}(t^q z)\mathrm{d}t = \frac{1}{1-z} \text{ for } |z| < 1.$$

The most interesting properties of the Mittag-Leffler function are associated with their Laplace integral

$$\int_0^\infty \mathrm{e}^{-st} t^{p-1} E_{q,p}(\pm a t^q)\mathrm{d}t = \frac{s^{q-p}}{(s^q \mp a)}.$$

That is,

$$\mathcal{L}\{t^{p-1} E_{q,p}(\pm a t^q)\}(s) = \frac{s^{q-p}}{(s^q \mp a)},$$

for $\Re(s) > |a|^{\frac{1}{q}}$ and $\Re(p) > 0$. In particular, for $p = 1$,

$$E_{q,1}(az^q) = E_q(az^q) = \sum_{k=0}^\infty \frac{a^k z^{kq}}{\Gamma(qk+1)},\ a, z \in \mathbf{C},$$

have the interesting property

$${}^C D^q E_q(az^q) = a E_q(az^q),$$

and

$$\mathcal{L}\{E_q(\pm a t^q)\}(s) = \frac{s^{q-1}}{s^q \mp a} \text{ for } p = 1.$$

Let us consider the linear fractional stochastic differential inclusions with fBm is represented in the following form

$$\begin{aligned} {}^C D^q x(t) &\in Ax(t) + Bu(t) + f(t) \\ &+ \int_0^t G(s)\mathrm{d}W_{(s)}^H, \quad t \in J, \\ x(0) &= x_0, \end{aligned} \tag{3}$$

where ${}^C D^q,\ x(t),\ u(t)$ and $W^H_{(s)}$ are same as defined above, $f : J \longrightarrow \mathbf{R}^n$ and $G : J \longrightarrow \mathbf{R}^{n\times n}$. Now applying the Riemann-Liouville integral operator on both sides[20], we get

$$x(t) = x_0 + \frac{1}{\Gamma(q)}\int_0^t (t-s)^{q-1}\Big[Ax(s) + Bu(s) + f(s) + \int_0^s G(\theta)\mathrm{d}W^H_{(\theta)}\Big]\mathrm{d}s.$$

Taking Laplace transformation on both sides, we have

$$\widehat{x}(s) = \frac{1}{s}x_0 + \frac{1}{s^q}A\widehat{x}(s) + \frac{1}{s^q}B\widehat{u}(s) + \frac{1}{s^q}\widehat{f}(s) + \frac{1}{s^q}\widehat{G}(s).$$

Taking inverse Laplace transformation on both sides, we get solution of system (3) by the expression (see [10, 19, 21] given by

$$x(t) = E_q(At^q)x_0 + \int_0^t (t-s)^{q-1}E_{q,q}(A(t-s)^q) \times \left[Bu(s) + f(s) + \int_0^s G(\theta)\mathrm{d}W^H_{(\theta)}\right]\mathrm{d}s.$$

In this paper, we adopt the following notations.

Let $(\Omega, \mathcal{F}, P)$ denote the complete probability space with a right continuous and complete filtration $\{\mathcal{F}_t, t \in J\}$ ($\mathcal{F}_t$ the $\sigma-$algebra generated by the random variables $\{W^H_{(s)}, s \in [0,t]\}$ and $P-$null set) and satisfying $\mathcal{F}_t \subset \mathcal{F}$. Let $L^2(\Omega, \mathcal{F}, \mathbf{R}^n)$ be the space of all square-integrable random variables with values in $\mathbf{R}^n$. Let $\mathcal{B} = \mathcal{C}(J, \mathbf{R}^n)$ be the Banach space. Denote the class of $\mathbf{R}^n-$ valued stochastic processes $\{\xi(t) : t \in J\}$ which is $\mathcal{F}_t-$ adapted and have a finite second moments, that is

$$\|\xi\| = \sup_t \left(\mathrm{E}|\xi(t)|^2\right)^{\frac{1}{2}} < \infty.$$

Definition 5. A normalized fBm $W^H = \{W^H_{(t)} : 0 \le t < \infty\}$ with $0 < H < 1$ on $(\Omega, \mathcal{F}, P)$ is uniquely characterized by the following properties:

1) $W^H_{(t)}$ has stationary increments;
2) $W^H_{(0)} = 0$, and $\mathrm{E}W^H_{(t)} = 0$ for $t \ge 0$;
3) $W^H_{(t)}$ has a Gaussian distribution for $t > 0$.

From the above three properties it follows that the covariance function is given by

$$\begin{aligned} R_H(s,t) &= \mathrm{E}\left(W^H_{(s)}W^H_{(t)}\right) \\ &= \frac{1}{2}\left\{t^{2H} + s^{2H} - |t-s|^{2H}\right\}, \\ &\quad \text{for } 0 < s \le t. \end{aligned} \tag{4}$$

The values of H determines what kind of process the fBm is:

1) if $H = \frac{1}{2}$ then the process is in fact a Brownian motion or Wiener process,

2) if $H > \frac{1}{2}$ then the increments of the process are positively correlated,

3) if $H < \frac{1}{2}$ then the increments of the process are negatively correlated.

Moreover, W^H has the integral representation

$$W^H_{(t)} = \int_0^t K_H(t,s)\mathrm{d}W_{(s)}$$

where W is a standard Wiener process and the kernel $K_H(t,s)$ defined as

$$K_H(t,s) = C_H s^{\frac{1}{2}-H}\int_s^t (u-s)^{H-\frac{3}{2}}u^{H-\frac{1}{2}}\mathrm{d}u$$

and

$$\frac{\partial K}{\partial t}(t,s) = C_H\left(\frac{t}{s}\right)^{H-\frac{1}{2}}(t-s)^{H-\frac{3}{2}}$$

where

$$C_H = \left[\frac{H(2H-1)}{W(2-2H, H-\frac{1}{2})}\right]^{\frac{1}{2}} \quad t > s.$$

Remark 1. For Gaussian process, the mean and covariance structure determine the finite dimensional distribution uniquely. Therefore, we conclude from (4) that $\{W^H_{(at)} : 0 \le t < \infty\}$ and $\{a^H W^H_{(t)} : 0 \le t < \infty\}$ have the same finite-dimensional distribution fBm. In fact, fBm is the only Gaussian process with stationary increments that is self-similar.

Let $(X, \|\cdot\|)$ be a Banach space. Denote $\mathcal{P}_{cl}(X) = \{Y \in \mathcal{P}(X) : Y \text{ is closed}\}, \mathcal{P}_{bd}(X) = \{Y \in \mathcal{P}(X) : Y \text{ is bounded}\}$, $\mathcal{P}_{cp}(X) = \{Y \in \mathcal{P}(X) : Y \text{ is compact}\}$ and $\mathcal{P}_{cp,cv}(X) = \{Y \in \mathcal{P}(X) : Y \text{ is compact and convex}\}$.

For more details on multivalued maps, readers can refer the books[22−25].

Definition 6. A multivalued map $T : X \longrightarrow \mathcal{P}(X)$ is convex (closed) valued if $T(x)$ is convex (closed) for all $x \in X$. T is bounded on bounded sets if $T(B) = \bigcup_{x\in B} T(x)$ is bounded in X for all $B \in \mathcal{P}_{bd}(X)$(i.e. $\sup_{x\in B}\sup_{y\in T(x)}\|y\| < \infty$).

Definition 7. T is called upper semi-continuous on X if for each $x_0 \in X$, the set $T(x_0)$ is a nonempty closed subset of X, and if for each open set N of X containing $T(x_0)$, there exists an open neighborhood N_0 of x_0 such that $T(N_0) \subseteq N$.

Definition 8. T is said to be completely continuous if $T(B)$ is relatively compact for every $B \in \mathcal{P}_{bd}(X)$. T has a fixed point if there is $x \in X$ such that $x \in T(x)$. The fixed point set of the multivalued operator T will be denoted by $FixT$.

Definition 9. A multivalued map $T : X \longrightarrow \mathcal{P}_{cl}(\mathbf{R}^n)$ is said to be measurable if for every $v \in \mathbf{R}^n$, the function $x \mapsto d(v, T(x)) = \inf\{\|v - z\| : z \in T(x)\}$ is measurable.

For each $x \in L_2(J, \mathbf{R}^n), x(t) > 0$ defines the set of selections of G by $\sigma \in N_{G,x} = \{\sigma \in L_2(J, \mathbf{R}^n) : \sigma(t) \in G(t, x(t))$ for almost everywhere (a.e.) $t \in J\}$.

Lemma 1[24]**.** Let T be a completely continuous multivalued map with nonempty compact values, then T is upper semi-continuous if and only if T has a closed graph (i.e. $x_n \longrightarrow x, y_n \longrightarrow y, y_n \in T(x_n)$ imply $y \in T(x)$).

Definition 10. A multivalued map $T : J \times \mathbf{R}^n \longrightarrow \mathcal{P}(\mathbf{R}^n)$ is said to be L_2-Caratheodory if

1) $t \mapsto T(t,x)$ is measurable for each $x \in \mathbf{R}^n$,
2) $x \mapsto T(t,x)$ is upper semi-continuous for almost all $t \in J$,
3) for each $\rho > 0$, there exists $\varphi_\rho \in L^1(J, \mathbf{R}^+)$ such that

$$\|T(t,x)\|^2 := \sup\{\mathrm{E}\|\sigma\|^2 : \sigma \in T(t,x)\} \le \varphi_\rho(t)$$

for all $\|x\|^2_{\mathbf{R}^n} \le \rho$ and for a.e. $t \in J$.

Lemma 2[26]**.** Let X be a Banach space. Let $T : J \times X \longrightarrow \mathcal{P}_{cp,cv}(X)$ be a L_2-Caratheodory multivalued map with $N_{G,x} \neq \emptyset$ and let Λ be a linear continuous mapping from $L^2(J,X)$ to $\mathcal{C}(J,X)$, then the operator

$$\Lambda \circ N_G : \mathcal{C}(J,X) \longrightarrow \mathcal{P}_{cp,cv}(\mathcal{C}(J,X)),$$
$$x \mapsto (\Lambda \circ N_G)(x) := \Lambda(N_{G,x})$$

is a closed graph operator in $\mathcal{C}(J,X) \times \mathcal{C}(J,X)$.

Proposition 1[27]**.** Let X be a separable Banach space. Let $G_1, G_2 : J \longrightarrow \mathcal{P}_{cp}(X)$ be measurable multivalued maps, then the multivalued map $t \mapsto G_1(t) \cap G_2(t)$ is measurable.

Theorem 1[27]**.** Let X be a separable metric space, $(T,\mathcal{L})$ be a measurable space, G is a multivalued map from T to complete nonempty subset of X. If for each open set U in X, $\overline{G}(U) = \{t : G(t) \cap U \neq \emptyset\} \in \mathcal{L}$, then G admits a measurable selection.

Definition 11. A stochastic process $x \in \mathcal{B}$ is said to be a mild solution of system (1) if $x(0) = x_0$, $u(\cdot) \in L^2_{\mathcal{F}_t}(J,\mathbf{R}^m)$ and there exists $\sigma \in N_{G,x}$ such that $\sigma(t) \in G(t,x(t))$, $t \in J$ and

$$\begin{aligned} x(t) &= E_q(At^q)x_0 \\ &\quad + \int_0^t (t-s)^{q-1} E_{q,q}(A(t-s)^q)Bu(s)\mathrm{d}s \\ &\quad + \int_0^t (t-s)^{q-1} E_{q,q}(A(t-s)^q)f(s,x(s))\mathrm{d}s \\ &\quad + \int_0^t (t-s)^{q-1} E_{q,q}(A(t-s)^q) \\ &\quad \times \left(\int_0^s \sigma(\theta)\mathrm{d}W^H_{(\theta)}\right)\mathrm{d}s. \end{aligned}$$

Definition 12. The system (1) is said to be controllable on J if for every $x_0, x_1 \in \mathbf{R}^n$ there exists a control $u(t)$ such that the solution $x(t)$ of (1) satisfies the conditions $x(0) = x_0$ and $x(T) = x_1$.

Let (X,d) be a metric space induced from $(X, \|\cdot\|)$ be a square normed space. Consider $H_d : \mathcal{P}(X) \times \mathcal{P}(X) \longrightarrow \mathbf{R}_+ \cup \{\infty\}$ given by

$$H_d(A,B) = \max\{\sup_{a\in A} d(a,B), \sup_{b\in B} d(A,b)\},$$

where

$$d(A,b) = \inf_{a\in A} d(a,b),\ d(a,B) = \inf_{b\in B} d(a,b).$$

Then $(\mathcal{P}_{bd,cl}(X), H_d)$ is a metric space and $(\mathcal{P}_{cl}(X), H_d)$ is a generalized metric space (see [25]).

Definition 13. A multivalued operator $\Phi : X \longrightarrow \mathcal{P}_{cl}(X)$ is called

1) γ-Lipschitz if and only if there exists $\gamma > 0$ such that

$$H_d(\Phi(x), \Phi(y)) \le \gamma d(x,y)$$

for each $x, y \in X$,

2) a contraction if and only if it is γ-Lipschitz with $\gamma < 1$.

Lemma 3[28] **(Bohnenblust-Karlin).** Let X be a Banach space and $K \in \mathcal{P}_{cl,cv}(X)$ and suppose that the operator $\Phi : K \longrightarrow \mathcal{P}_{cl,cv}(K)$ is upper semi-continuous and the set $\Phi(K)$ is relatively compact in X. Then Φ has a fixed point in K.

Lemma 4[29] **(Covitz-Nadler).** Let (X,d) be a complete metric space. If $\Phi : X \longrightarrow \mathcal{P}_{cl}(X)$ is a contraction, then Φ has fixed points.

In order to prove the controllability results we assume the following mild conditions.

H1) The multivalued map $G : J \times \mathbf{R}^n \longrightarrow \mathcal{P}(\mathbf{R}^n)$ be an L_2-Caratheodory function satisfying the following conditions

  i) for each $t \in J, x \in \mathbf{R}^n$ the function $G(t,\cdot) : \mathbf{R}^n \longrightarrow \mathcal{P}(\mathbf{R}^n)$ is upper semi-continuous. The function $G(\cdot,x) : J \longrightarrow \mathcal{P}(\mathbf{R}^n)$ is measurable and for each $x \in \mathbf{R}^n$ the set $N_{G,x} = \{\sigma \in L_2(J,\mathbf{R}^n) : \sigma(t) \in G(t,x(t))$ for a.e. $t \in J\}$ is nonempty,

  ii) There exists a positive function $\varphi_\rho : J \to \mathbf{R}_+$ such that $\sup\left\{\int_0^t \mathrm{E}\|\sigma(s)\|^2\mathrm{d}s : \sigma(t) \in G(t,x(t))\right\} \le \varphi_\rho(t)$ for a.e. $t \in J$ and the function $s \longrightarrow (t-s)^{q-1}\varphi_\rho(s) \in L^1([0,t],\mathbf{R}_+)$

$$\lim_{\rho\longrightarrow\infty} \inf \frac{\int_0^t (t-s)^{q-1}\varphi_\rho(s)\mathrm{d}s}{\rho} = \eta < \infty.$$

H2) The functions $f : J \times \mathbf{R}^n \longrightarrow \mathbf{R}^n$, $\sigma : J \longrightarrow \mathbf{R}^{n\times n}$ are continuous and there exists a constant $M_f > 0$ such that

  i) $\mathrm{E}\|f(t,x)\|^2 \le M_f(1 + \|x\|^2)$,

  ii) $\mathrm{E}\|\int_0^t \sigma(s)\mathrm{d}W^H_{(s)}\|^2 \le 2Ht^{2H-1}\int_0^t \|\sigma(s)\|^2_{L^2}\mathrm{d}s$.

H3) The linear stochastic differential inclusions (3) are controllable on J if and only if the controllability Grammian matrix

$$\begin{aligned} W = &\int_0^T (T-s)^{q-1}[E_{q,q}(A(T-s)^q)B] \\ &\times [E_{q,q}(A(T-s)^q)B]^*\mathrm{d}s \end{aligned}$$

is positive definite, for some $T > 0$ (see [20]).

H4) The multifunction $G : J \times \mathbf{R}^n \longrightarrow \mathcal{P}_{cp}(\mathbf{R}^n)$ has the property that $G(\cdot,x) : J \longrightarrow \mathcal{P}_{cp}(\mathbf{R}^n)$ is measurable for each $x \in \mathbf{R}^n$.

H5) There exists a non-negative function $m \in L^2(J)$ such that

$$H_d(G(t,x), G(t,y)) \le m(t)\|x-y\|^2$$

for every $x, y \in \mathbf{R}^n$, and

$$d(0, G(t,0)) \le m(t)$$

a.e. $t \in J$.

For convenience, let us introduce the following constants $a_1 = \sup\|E_{q,q}(A(T-s)^q)\|^2$, $a_2 = \sup\|E_q(AT^q)x_0\|^2$, $l = \|W^{-1}\|^2$.

III. Main Results

In this section, we discuss the controllability criteria of fractional order stochastic differential inclusions with fBm. The fixed point technique is effectively used to study the controllability of nonlinear systems. The essential part of this method is to guarantee the existence of an invariant subset for an appropriate nonlinear operator. Due to their importance, several researchers have used different kinds of fixed point theorems. Here the controllability results are obtained by adopting Bohnenblust-Karlin fixed point theorem for the convex case and the Covitz-Nadler for the nonconvex case.

Theorem 2 (Convex Case). Suppose that the hypotheses H1)-H3) are satisfied, then the system (1) is controllable on J, provided that the following holds

$$\begin{aligned}1 > &4a_2\left(1+4\frac{T^{2q}}{q^2}a_1^2\|B\|^2\|B^*\|^2 l\right)+16\frac{T^{2q}}{q^2}\\ &\times a_1^2\|B\|^2 l\|B^*\|^2\|x_1\|^2+4\frac{T^{2q}}{q^2}a_1M_f\\ &\times(1+\mathrm{E}\|x\|^2)\left(1+4\frac{T^{2q}}{q^2}a_1^2\|B\|^2 l\|B^*\|^2\right)\\ &+4\frac{T^q}{q}a_1 2HT^{2H-1}\eta\\ &\times\left(1+4\frac{T^{2q}}{q^2}a_1^2\|B\|^2 l\|B^*\|^2\right).\end{aligned}\tag{5}$$

Proof. For any arbitrary function $x\in\mathbf{R}^n$, we can define the control function $u_x(t)$

$$\begin{aligned}u_x(t)=&B^*E_{q,q}(A^*(T-t)^q)W^{-1}\Big\{x_1-E_q(AT^q)x_0\\ &-\int_0^T(T-s)^{q-1}E_{q,q}(A(T-s)^q)\\ &\times\left[f(s,x(s))+\int_0^s\sigma(\theta)\mathrm{d}W^H_{(\theta)}\right]\mathrm{d}s\Big\}\end{aligned}$$

where $t\in J,\ \sigma\in N_{G,x}$. Using the above control, we show that the operator $\Phi:\mathcal{B}\longrightarrow\mathcal{P}(\mathcal{B})$, defined as

$$\begin{aligned}\Phi(x)=&\Big\{\Psi\in\mathcal{B}:\Psi(t)=E_q(At^q)x_0\\ &+\int_0^t(t-s)^{q-1}E_{q,q}(A(t-s)^q)\\ &\times\left[Bu(s)+f(s,x(s))+\int_0^s\sigma(\theta)\mathrm{d}W^H_{(\theta)}\right]\mathrm{d}s,\\ &\qquad t\in J,\ \sigma\in N_{G,x}\Big\}\end{aligned}$$

has a fixed point x, which is a solution of the system (1). We observe that $x_1\in(\Phi x)(T)$ which means that u_x steers the system (1) from x_0 to x_1 in finite time T. This implies that system (1) is controllable on J.

We now show that Φ satisfies all the conditions of Lemma 3. For the sake of convenience, we subdivide the proof into four steps.

Step 1. Φ is convex, for each $x\in\mathcal{B}$.

In fact, if $\Psi_1,\Psi_2\in\Phi(x)$, then there exists $\sigma_1,\sigma_2\in N_{G,x}$ such that for each $t\in J$, we have

$$\begin{aligned}\Psi_i(t)=&E_q(At^q)x_0+\int_0^t(t-s)^{q-1}E_{q,q}(A(t-s)^q)\\ &\times BB^*E_{q,q}(A^*(T-s)^q)W^{-1}\Big\{x_1\\ &-E_q(AT^q)x_0-\int_0^T(T-s)^{q-1}\\ &\times E_{q,q}(A(T-s)^q)\Big[f(s,x(s))\\ &+\int_0^s\sigma_i(\theta)\mathrm{d}W^H_{(\theta)}\Big]\mathrm{d}s\Big\}(s)\mathrm{d}s\\ &+\int_0^t(t-s)^{q-1}E_{q,q}(A(t-s)^q)\Big[f(s,x(s))\\ &+\int_0^s\sigma_i(\theta)\mathrm{d}W^H_{(\theta)}\Big]\mathrm{d}s,\ i=1,2.\end{aligned}$$

Let $0\leq\lambda\leq1$, then for each $t\in J$, we have

$$\begin{aligned}&[\lambda\Psi_1+(1-\lambda)\Psi_2](t)\\ &\quad=E_q(At^q)x_0+\int_0^t(t-s)^{q-1}E_{q,q}(A(t-s)^q)\\ &\quad\times BB^*E_{q,q}(A^*(T-s)^q)W^{-1}\Big\{x_1\\ &\quad-E_q(AT^q)x_0-\int_0^T(T-s)^{q-1}\\ &\quad\times E_{q,q}(A(T-s)^q)\Big[f(s,x(s))\\ &\quad+\int_0^s[\lambda\sigma_1(\theta)+(1-\lambda)\sigma_2(\theta)]\mathrm{d}W^H_{(\theta)}\Big]\mathrm{d}s\Big\}(s)\mathrm{d}s\\ &\quad+\int_0^t(t-s)^{q-1}E_{q,q}(A(t-s)^q)\Big[f(s,x(s))\\ &\quad+\int_0^s[\lambda\sigma_1(\theta)+(1-\lambda)\sigma_2(\theta)]\mathrm{d}W^H_{(\theta)}\Big]\mathrm{d}s.\end{aligned}$$

It is easy to see that $N_{G,x}$ is convex since G has convex values. So, $\lambda\sigma_1+(1-\lambda)\sigma_2\in N_{G,x}$. Thus, $\lambda\Psi_1+(1-\lambda)\Psi_2\in\Phi(x)$.

Step 2. For each positive number $\rho>0$, let $\mathcal{B}_\rho=\{x\in\mathcal{B}:\|x\|^2_{\mathcal{B}}\leq\rho\}$. Obviously, $\mathcal{B}_\rho$ is a bounded, closed and convex set of $\mathcal{B}$. We claim that there exists a positive number ρ such that $\Phi(\mathcal{B}_\rho)\subset\mathcal{B}_\rho$.

If this is not true, then for each positive number ρ, there exists a function $x^\rho\in\mathcal{B}_\rho$, but $\Phi(x^\rho)\notin\mathcal{B}_\rho$ i.e. $\|\Phi(x^\rho)\|^2_{\mathcal{B}}\equiv\sup\{\|\Psi\|^2_{\mathcal{B}}:\Psi^\rho\in(\Phi x^\rho)\}>\rho$ and

$$\begin{aligned}\Psi^\rho(t)=&E_q(At^q)x_0+\int_0^t(t-s)^{q-1}E_{q,q}(A(T-s)^q)\\ &\times\left[Bu^\rho_x(s)+f(s,x^\rho(s))+\int_0^s\sigma^\rho(\theta)\mathrm{d}W^H_{(\theta)}\right]\mathrm{d}s\end{aligned}$$

for some $\sigma^\rho\in N_{G,x^\rho}$. Using H2) we have

$$\begin{aligned}&\mathrm{E}\|u_x(t)\|^2\\ &\quad\leq4\|B^*\|^2\|E_{q,q}(A^*(T-t)^q)\|^2\left\|W^{-1}\right\|^2\\ &\quad\times\Big\{\|x_1\|^2+\|E_q(AT^q)x_0\|^2\\ &\quad+\mathrm{E}\Big\|\int_0^T(T-s)^{q-1}\end{aligned}$$

$$
\begin{aligned}
&\times E_{q,q}(A(T-s)^q)f(s,x(s))\mathrm{d}s\Big\|^2 \\
&+\mathrm{E}\Big\|\int_0^T (T-s)^{q-1}E_{q,q}(A(T-s)^q) \\
&\times\left(\int_0^s \sigma(\theta)\mathrm{d}W^H_{(\theta)}\right)\mathrm{d}s\Big\|^2\Big\} \\
&\leq 4\|B^*\|^2 a_1 l\|x_1\|^2 \\
&+4\|B^*\|^2 a_1 l a_2 + 4\|B^*\|^2 a_1^2 l\frac{T^{2q}}{q^2}M_f \\
&\times(1+\mathrm{E}\|x\|^2)+4\|B^*\|^2 a_1^2 l 2HT^{2H-1} \\
&\times\frac{T^q}{q}\int_0^T (T-s)^{q-1}\varphi_\rho(s)\mathrm{d}s,
\end{aligned}
$$

and, we find that

$$
\begin{aligned}
\rho &< \mathrm{E}\|(\Phi x^\rho)(t)\|^2 \\
&\leq 4\mathrm{E}\|E_q(At^q)x_0\|^2 \\
&+4\mathrm{E}\Big\|\int_0^t (t-s)^{q-1}E_{q,q}(A(t-s)^q) \\
&\times Bu_x^\rho(s)\mathrm{d}s\Big\|^2 \\
&+4\mathrm{E}\Big\|\int_0^t (t-s)^{q-1}E_{q,q}(A(t-s)^q) \\
&\times f(s,x^\rho(s))\mathrm{d}s\Big\|^2 \\
&+4\mathrm{E}\Big\|\int_0^t (t-s)^{q-1}E_{q,q}(A(t-s)^q) \\
&\times\left(\int_0^s \sigma^\rho(\theta)\mathrm{d}W^H_{(\theta)}\right)\mathrm{d}s\Big\|^2 \\
&\leq 4a_2+16\frac{T^{2q}}{q^2}a_1^2\|B\|^2 l\|B^*\|^2\|x_1\|^2 \\
&+16\frac{T^{2q}}{q^2}a_1^2 a_2\|B\|^2 l\|B^*\|^2+4\frac{T^{2q}}{q^2}a_1\|B\|^2 \\
&\times\left(4\|B^*\|^2 a_1^2 l\frac{T^{2q}}{q^2}M_f(1+\mathrm{E}\|x\|^2)\right) \\
&+4\frac{T^{2q}}{q^2}a_1\|B\|^2 \\
&\times\Big(4\|B^*\|^2 a_1^2 l\frac{T^q}{q}2HT^{2H-1} \\
&\times\int_0^T (T-s)^{q-1}\varphi_\rho(s)\mathrm{d}s\Big) \\
&+4\frac{T^{2q}}{q^2}a_1 M_f(1+\mathrm{E}\|x\|^2) \\
&+4\frac{T^q}{q}a_1 2HT^{2H-1}\int_0^T (T-s)^{q-1}\varphi_\rho(s)\mathrm{d}s \\
&\leq 4a_2\left(1+4\frac{T^{2q}}{q^2}a_1^2\|B\|^2 l\|B^*\|^2\right)+16\frac{T^{2q}}{q^2}a_1^2 \\
&\times\|B\|^2 l\|B^*\|^2\|x_1\|^2+4\frac{T^{2q}}{q^2}a_1 M_f \\
&\times(1+\mathrm{E}\|x\|^2)\left(1+4\frac{T^{2q}}{q^2}a_1^2\|B\|^2 l\|B^*\|^2\right) \\
&+4\frac{T^q}{q}a_1 2HT^{2H-1}\int_0^T (T-s)^{q-1}\varphi_\rho(s)\mathrm{d}s \\
&\times\left(1+4\frac{T^{2q}}{q^2}a_1^2\|B\|^2 l\|B^*\|^2\right).
\end{aligned}
$$

Dividing both sides of the above inequality by ρ and taking limit as $\rho \longrightarrow \infty$, using H1) we get

$$
\begin{aligned}
1 \leq\ & 4a_2\left(1+4\frac{T^{2q}}{q^2}a_1^2\|B\|^2 l\|B^*\|^2\right) \\
&+16\frac{T^{2q}}{q^2}a_1^2\|B\|^2 l\|B^*\|^2\|x_1\|^2+4\frac{T^{2q}}{q^2}a_1 M_f \\
&\times(1+\mathrm{E}\|x\|^2)\left(1+4\frac{T^{2q}}{q^2}a_1^2\|B\|^2 l\|B^*\|^2\right) \\
&+4\frac{T^q}{q}a_1 2HT^{2H-1}\eta \\
&\times\left(1+4\frac{T^{2q}}{q^2}a_1^2\|B\|^2 l\|B^*\|^2\right),
\end{aligned}
$$

which is a contradiction to (5). Hence, for some $\rho > 0,\ \Phi(\mathcal{B}_\rho) \subset \mathcal{B}_\rho$.

Step 3. Compactness of Φ.

To prove this, we first prove that the set $\Phi(\mathcal{B}_\rho)$ is relatively compact in $\mathcal{B}_\rho$. Subsequently, we show that $\Phi(\mathcal{B}_\rho)$ is uniformly bounded. Note that by using the same method as in Step 2, it can be manifested that the operator Φ is uniformly bounded that is

$$
\begin{aligned}
&4a_2\left(1+4\frac{T^{2q}}{q^2}a_1^2\|B\|^2 l\|B^*\|^2\right)+16\frac{T^{2q}}{q^2}a_1^2 \\
&\quad\times\|B\|^2 l\|B^*\|^2\|x_1\|^2+4\frac{T^{2q}}{q^2}a_1 M_f \\
&\quad\times(1+\mathrm{E}\|x\|^2)\left(1+4\frac{T^{2q}}{q^2}a_1^2\|B\|^2 l\|B^*\|^2\right) \\
&\quad+4\frac{T^q}{q}a_1 2HT^{2H-1}\eta \\
&\quad\times\left(1+4\frac{T^{2q}}{q^2}a_1^2\|B\|^2 l\|B^*\|^2\right)<\infty,
\end{aligned}
$$

the set $\Phi(\mathcal{B}_\rho)$ is relatively compact. Finally, we prove that $\Phi(\mathcal{B}_\rho)$ is equicontinuous. For any $x \in \mathcal{B}_\rho$ and $t_1, t_2 \in J$ with $0 < t_1 < t_2 \leq T$, we get

$$
\begin{aligned}
&\mathrm{E}\|\Psi(t_1)-\Psi(t_2)\|^2 \\
&\quad\leq 7\mathrm{E}\|[E_q(At_1^q)-E_q(At_2^q)]x_0\|^2 \\
&\quad+7\mathrm{E}\Big\|\int_{t_1}^{t_2}(t_2-s)^{q-1}E_{q,q}(A(t_2-s)^q)Bu_x(s)\mathrm{d}s\Big\|^2 \\
&\quad+7\mathrm{E}\Big\|\int_0^{t_1}\Big[(t_1-s)^{q-1}E_{q,q}(A(t_1-s)^q) \\
&\quad-(t_2-s)^{q-1}E_{q,q}(A(t_2-s)^q)\Big]Bu_x(s)\mathrm{d}s\Big\|^2 \\
&\quad+7\mathrm{E}\Big\|\int_{t_1}^{t_2}(t_2-s)^{q-1}E_{q,q}(A(t_2-s)^q)
\end{aligned}
$$

$$
\begin{aligned}
&\times f(s,x(s))\mathrm{d}s\Big\|^2 \\
&+7\mathrm{E}\Big\|\int_0^{t_1}\Big[(t_1-s)^{q-1}E_{q,q}(A(t_1-s)^q) \\
&-(t_2-s)^{q-1}E_{q,q}(A(t_2-s)^q)\Big] \\
&\times f(s,x(s))\mathrm{d}s\Big\|^2+7\mathrm{E}\Big\|\int_{t_1}^{t_2}(t_2-s)^{q-1} \\
&\times E_{q,q}(A(t_2-s)^q)\left(\int_0^s\sigma(\theta)\mathrm{d}W^H_{(\theta)}\right)\mathrm{d}s\Big\|^2 \\
&+7\mathrm{E}\Big\|\int_0^{t_1}\Big[(t_1-s)^{q-1}E_{q,q}(A(t_1-s)^q) \\
&-(t_2-s)^{q-1}E_{q,q}(A(t_2-s)^q)\Big] \\
&\times\left(\int_0^s\sigma(\theta)\mathrm{d}W^H_{(\theta)}\right)\mathrm{d}s\Big\|^2 \\
&\le 7\mathrm{E}\,\|[E_q(At_1^q)-E_q(At_2^q)]x_0\|^2 \\
&+\frac{7(t_2-t_1)^q}{q}\int_{t_1}^{t_2}(t_2-s)^{q-1} \\
&\times\|E_{q,q}(A(t_2-s)^q)\|^2\|B\|^2\mathrm{E}\|u_x(s)\|^2\mathrm{d}s \\
&+7t_1\int_0^{t_1}\Big\|[(t_1-s)^{q-1}E_{q,q}(A(t_1-s)^q) \\
&-(t_2-s)^{q-1}E_{q,q}(A(t_2-s)^q)]\Big\|^2\|B\|^2 \\
&\times\mathrm{E}\|u_x(s)\|^2\mathrm{d}s+\frac{7(t_2-t_1)^q}{q}\int_{t_1}^{t_2}(t_2-s)^{q-1} \\
&\times\|E_{q,q}(A(t_2-s)^q)\|^2M_f(1+\mathrm{E}\|x\|^2)\mathrm{d}s \\
&+7t_1\int_0^{t_1}\Big\|[(t_1-s)^{q-1}E_{q,q}(A(t_1-s)^q) \\
&-(t_2-s)^{q-1}E_{q,q}(A(t_2-s)^q)]\Big\|^2 \\
&\times M_f(1+\mathrm{E}\|x\|^2)\mathrm{d}s+\frac{7(t_2-t_1)^q}{q} \\
&\times\int_{t_1}^{t_2}(t_2-s)^{q-1}\|E_{q,q}(A(t_2-s)^q)\|^2\mathrm{d}s \\
&\times 2HT^{2H-1}\int_0^s\mathrm{E}\|\sigma(\theta)\|^2\mathrm{d}\theta \\
&+7t_1\int_0^{t_1}\Big\|[(t_1-s)^{q-1}E_{q,q}(A(t_1-s)^q) \\
&-(t_2-s)^{q-1}E_{q,q}(A(t_2-s)^q)]\Big\|^2\mathrm{d}s \\
&\times 2HT^{2H-1}\int_0^s\mathrm{E}\|\sigma(\theta)\|^2\mathrm{d}\theta.
\end{aligned}
$$

As $t_1 \longrightarrow t_2$, the right-hand side of the above inequality tends to zero. An application of the Arzela-Ascoli theorem yields that Φ maps $\mathcal{B}_\rho$ into $\mathcal{B}$, that is $\Phi:\mathcal{B}_\rho\longrightarrow\mathcal{P}(\mathcal{B})$ is a compact operator. Thus $\Phi(\mathcal{B}_\rho)$ is relatively compact.

Step 4. Φ is upper semi-continuous on $\mathcal{B}_\rho$.

Let $x^n\longrightarrow x^*$, as $n\longrightarrow\infty$ and $\Psi^n\longrightarrow\Psi^*$ as $n\longrightarrow\infty$. We need to show that $\Psi^*\in\Phi(x^*)$. Since $\Psi^n\in\Phi(x^n)$ means that there exists $\sigma^n\in N_{G,x^n}$ such that

$$
\begin{aligned}
\Psi^n(t)=\ &E_q(At^q)x_0+\int_0^t(t-s)^{q-1}E_{q,q}(A(t-s)^q) \\
&\times BB^*E_{q,q}(A^*(T-s)^q)W^{-1}\Big\{x_1 \\
&-E_q(AT^q)x_0-\int_0^T(T-s)^{q-1} \\
&\times E_{q,q}(A(T-s)^q)\Big[f(s,x^n(s)) \\
&+\int_0^s\sigma^n(\theta)\mathrm{d}W^H_{(\theta)}\Big]\mathrm{d}s\Big\}(s)\mathrm{d}s \\
&+\int_0^t(t-s)^{q-1}E_{q,q}(A(t-s)^q) \\
&\times\Big[f(s,x^n(s))+\int_0^s\sigma^n(\theta)\mathrm{d}W^H_{(\theta)}\Big]\mathrm{d}s. \qquad (6)
\end{aligned}
$$

We must show that there exists $\sigma^*\in N_{G,x^*}$ such that

$$
\begin{aligned}
\Psi^*(t)=\ &E_q(At^q)x_0+\int_0^t(t-s)^{q-1}E_{q,q}(A(t-s)^q) \\
&\times BB^*E_{q,q}(A^*(T-s)^q)W^{-1}\Big\{x_1 \\
&-E_q(AT^q)x_0-\int_0^T(T-s)^{q-1} \\
&\times E_{q,q}(A(T-s)^q)\Big[f(s,x^*(s)) \\
&+\int_0^s\sigma^*(\theta)\mathrm{d}W^H_{(\theta)}\Big]\mathrm{d}s\Big\}(s)\mathrm{d}s \\
&+\int_0^t(t-s)^{q-1}E_{q,q}(A(t-s)^q) \\
&\times\Big[f(s,x^*(s))+\int_0^s\sigma^*(\theta)\mathrm{d}W^H_{(\theta)}\Big]\mathrm{d}s.
\end{aligned}
$$

Now, we consider the continuous operator

$$\Lambda:L_2(J,\mathbf{R}^n)\longrightarrow\mathcal{B},\sigma\mapsto\Lambda(\sigma)(t)$$

such that,

$$
\begin{aligned}
\Lambda(\sigma)(t)=&\int_0^t(t-s)^{q-1}E_{q,q}(A(t-s)^q) \\
&\times\Big[\int_0^s\sigma(\theta)\mathrm{d}W^H_{(\theta)}-BB^*E_{q,q}(A^*(T-s)^q) \\
&\times W^{-1}\int_0^T(T-s)^{q-1}E_{q,q}(A(T-s)^q) \\
&\times\left(\int_0^s\sigma(\theta)\mathrm{d}W^H_{(\theta)}\right)\mathrm{d}s\Big](s)\mathrm{d}s.
\end{aligned}
$$

From Lemma 2, it follows that $\Lambda\circ N_G$ is a closed graph operator. Clearly, for each $t\in J$, we have

$$
\begin{aligned}
&\Big(\Psi^n(t)-E_q(At^q)x_0-\int_0^t(t-s)^{q-1} \\
&\quad\times E_{q,q}(A(t-s)^q)\Big[Bu^n(s)+f(s,x^n(s))\Big]\mathrm{d}s\Big) \\
&\quad\in\Lambda(N_{G,x^n}).
\end{aligned}
$$

Since $y^n\longrightarrow y^*$, it follows from Lemma 2 that, for some $y^*\in N_{G,x^*}$, we have

$$
\begin{aligned}
&\Big(\Psi^*(t)-E_q(At^q)x_0-\int_0^t(t-s)^{q-1} \\
&\quad\times E_{q,q}(A(t-s)^q)\Big[Bu^*(s)+f(s,x^*(s))\Big]\mathrm{d}s\Big) \\
&\quad\in\Lambda(N_{G,x^*}).
\end{aligned}
$$

Clearly, for each $t \in J$, we have

$$\Big\|\Big(\Psi^n(t) - E_q(At^q)x_0 - \int_0^t (t-s)^{q-1} \times E_{q,q}(A(t-s)^q)\Big[Bu^n(s) + f(s, x^n(s))\Big]\mathrm{d}s\Big) - \Big(\Psi^*(t) - E_q(At^q)x_0 - \int_0^t (t-s)^{q-1} \times E_{q,q}(A(t-s)^q)\Big[Bu^*(s) + f(s, x^*(s))\Big]\mathrm{d}s\Big)\Big\|_{\mathcal{B}}^2 \longrightarrow 0,$$

as $n \longrightarrow \infty$. From Lemma 1 we can conclude that Φ is upper semi-continuous. As a consequence of Lemma 3, we deduce that Φ has a fixed point which is the solution of the system (1), and it is easy to verify that $x(T) = x_1$. Hence the system (1) is controllable on J. □

Theorem 3 (Non-Convex Case). Assume that conditions H3)-H5) are satisfied, then the system (1) has atleast one solution in J, provided that

$$8\frac{T^{2q}}{q^2}a_1 m(t)\left(1 + T2HT^{2H-1}\right) < 1. \tag{7}$$

Proof. Under the assumption H5) it is easy to see that for each $x \in \mathcal{B}$, the set $N_{G,x}$ is nonempty. Therefore, G has a nonempty measurable selection (by Theorem 1). We shall show that Φ defined in Theorem 2 satisfies the assumption of Lemma 4. The proof will be given in two steps.

Step 1. $\Phi(x) \in \mathcal{P}_{cl}(\mathcal{B})$ for each $x \in \mathcal{B}$.

Indeed, let $(\Psi^n)_{n\geq 0} \in \Phi(x)$ such that $\Psi^n \longrightarrow \Psi$. Then, $\Psi \in \mathcal{B}$ and there exists $\sigma^n \in N_{G,x}$ such that, for each $t \in J$, $\Psi^n(t)$ is defined in (6). Using H5) we have for a.e. $t \in J$

$$|\sigma^n(t)| \leq m(t)\|x\|^2 + m(t),\ n \in \mathbf{N}.$$

The Lebesgue dominated convergence theorem implies that

$$\|\sigma^n - \sigma\|_{L^2} \longrightarrow 0 \text{ as } n \longrightarrow \infty.$$

Hence $\sigma \in N_{G,x}$. Then, for each $t \in J$, $\Psi^n(t) \longrightarrow \Psi(t)$, where

$$\Psi(t) = E_q(At^q)x_0 + \int_0^t (t-s)^{q-1}E_{q,q}(A(t-s)^q)\Big[Bu_x(s) + f(s, x(s)) + \int_0^s \sigma(\theta)\mathrm{d}W^H_{(\theta)}\Big]\mathrm{d}s. \tag{8}$$

So, $\Psi \in \Phi(x)$.

Step 2. There exists $\gamma < 1$ such that $H_d(\Phi(x), \Phi(y)) \leq \gamma\|x - y\|_{\mathcal{B}}$ for each $x, y \in \mathcal{B}$. Let $x, y \in \mathcal{B}$ and $\Psi \in \Phi(x)$. Then, there exists $\sigma \in N_{G,x}$ such that $\Psi(t)$ is defined in (8). From H5), it follows that

$$H_d(G(t, x(t)), G(t, y(t))) \leq m(t)\|x(t) - y(t)\|^2.$$

Hence, there exists $\omega \in N_{G,y}$ such that

$$\|\sigma(t) - \omega(t)\|^2 \leq m(t)\|x(t) - y(t)\|^2,\ t \in J.$$

Consider $U : J \longrightarrow \mathcal{P}(\mathbf{R}^n)$ given by $U(t) = \{\omega(t)|\omega : J \longrightarrow \mathbf{R}^n$ is Lebesgue integrable and $\|\sigma(t) - \omega(t)\|^2 \leq m(t)\|x(t) - y(t)\|^2\}$. Since the multivalued operator $U(t) \cap G(t, y(t))$ is measurable (Proposition 1), there exists a functions $\overline{\sigma}(t)$ which is a measurable selection for U. So, $\overline{\sigma}(t) \in N_{G,y}$, and for each $t \in J$,

$$\|\sigma(t) - \overline{\sigma}(t)\|^2 \leq m(t)\|x(t) - y(t)\|^2.$$

Let us define

$$\overline{\Psi}(t) = E_q(At^q)x_0 + \int_0^t (t-s)^{q-1}E_{q,q}(A(t-s)^q)\Big[Bu_y(s) + f(s, y(s)) + \int_0^s \overline{\sigma}(\theta)\mathrm{d}W^H_{(\theta)}\Big]\mathrm{d}s.$$

Then, for each $t \in J$, we get

$$\begin{aligned}
&\mathrm{E}\|\Psi(t) - \overline{\Psi}(t)\|^2 \\
&\leq 4\mathrm{E}\Big\|\int_0^T (T-s)^{q-1}E_{q,q}(A(T-s)^q) \times [f(s, y(s)) - f(s, x(s))]\mathrm{d}s\Big\|^2 \\
&+ 4\mathrm{E}\Big\|\int_0^T (T-s)^{q-1}E_{q,q}(A(T-s)^q) \times \Big(\int_0^s \Big[\overline{\sigma}(\theta) - \sigma(\theta)\Big]\mathrm{d}W^H_{(\theta)}\Big)\mathrm{d}s\Big\|^2 \\
&+ 4\mathrm{E}\Big\|\int_0^t (t-s)^{q-1}E_{q,q}(A(t-s)^q) \times [f(s, x(s)) - f(s, y(s))]\mathrm{d}s\Big\|^2 \\
&+ 4\mathrm{E}\Big\|\int_0^t (t-s)^{q-1}E_{q,q}(A(t-s)^q) \times \Big(\int_0^s [\sigma(\theta) - \overline{\sigma}(\theta)]\mathrm{d}W^H_{(\theta)}\Big)\mathrm{d}s\Big\|^2 \\
&\leq 4\frac{T^{2q}}{q^2}a_1\mathrm{E}\|f(t, y(t)) - f(t, x(t))\|^2 \\
&+ 4\frac{T^{2q}}{q^2}Ta_1 2HT^{2H-1}\mathrm{E}\|\sigma(t) - \overline{\sigma}(t)\|^2 \\
&+ 4\frac{T^{2q}}{q^2}a_1\mathrm{E}\|f(t, x(t)) - f(t, y(t))\|^2 \\
&+ 4\frac{T^{2q}}{q^2}Ta_1 2HT^{2H-1}\mathrm{E}\|\overline{\sigma}(t) - \sigma(t)\|^2 \\
&\leq 4\frac{T^{2q}}{q^2}a_1 m(t)\|x - y\|^2 \\
&+ 4\frac{T^{2q}}{q^2}Ta_1 2HT^{2H-1}m(t)\|x - y\|^2 \\
&+ 4\frac{T^{2q}}{q^2}a_1 m(t)\|x - y\|^2 \\
&+ 4\frac{T^{2q}}{q^2}Ta_1 2HT^{2H-1}m(t)\|x - y\|^2 \\
&\leq 8\frac{T^{2q}}{q^2}a_1 m(t)\left(1 + T2HT^{2H-1}\right)\|x - y\|^2.
\end{aligned}$$

Thus, for each $t \in J$, we get

$$\mathrm{E}\|\Psi - \overline{\Psi}\|_{\mathcal{B}}^2 \leq 8\frac{T^{2q}}{q^2}a_1 m(t) \times \left(1 + T2HT^{2H-1}\right)\|x-y\|_{\mathcal{B}}^2.$$

By an analogous relation obtained by interchanging the roles of x and y, it follows that

$$H_d(\Phi(x), \Phi(y)) \leq 8\frac{T^{2q}}{q^2}a_1 m(t) \times \left(1 + T2HT^{2H-1}\right)\|x-y\|_{\mathcal{B}}^2.$$

By (7), Φ is a contraction and thus, by Lemma 4, Φ has a fixed point x which is the solution of (1) on J, and it is easy to verify that $x(T) = x_1$. Hence the fractional order system (1) is controllable on J. □

Remark 2. Existence of solutions for integer order stochastic differential inclusions without control vector and fractional Brownian motion have been investigated in [15]. Also the controllability problem for fractional dynamical systems without stochastic differential equations has been studied in [10]. Since fBm has dependent increments, it is an interesting generalization of ordinary Brownian motion to model the noise process in many applications such as finance, network simulations and environmental processes. So, it is significant to study the controllability of fractional order stochastic differential inclusions with fBm due to the potential applications. It should be mentioned that different from literature, this paper makes use of stochastic analysis technique with fBm and the controllability Grammian martrix which is formulated using Mittag-Leffler matrix function. The main advantage of the proposed technique is the utilization of fixed point theorem for both cases of the multivalued map. Moreover, Covitz-Nadler fixed point theorem is utilized for the nonconvex case of the multivalued map to establish controllability of fractional stochastic systems with fBm.

IV. EXAMPLE

In this section an example is illustrated to show the effectiveness of the proposed technique.

As an application of the derived results, we consider the fractional Harmonic Oscillator equation[30]

$$\left(m^C D^{2q} + k\right)x(t) = 0,$$

where k and m are appropriate constants. Introducing a control variable and a nonlinear forcing term, we get the following controlled fractional Harmonic Oscillator equation with Brownian motion:

$$^C D^{2q}x(t) + x(t) = u(t) + \frac{x(t)}{1+3x(t)} + \frac{5x(t)}{1+x(t)}, \quad t \in J,$$

where $x(t)$ specifies the position of the particle or Oscillator at time t, $u(t)$ is a control term, $\frac{x(t)}{1+3x(t)}$ is a nonlinear forcing term and $\frac{5x(t)}{1+x(t)}$ describes a Brownian motion in an external quadratic potential. Introduce the auxiliary variables $x_1(t) = x(t)$ and $x_2(t) = ^C D^q x_1(t)$. Then

$$\begin{aligned} ^C D^q x_1(t) &= {}^C D^q x(t) = x_2(t), \\ ^C D^q x_2(t) &= {}^C D^{2q} x(t) \\ &= -x_1(t) + u(t) + \frac{x_1(t)}{1+3x_1(t)} \\ &\quad + \frac{5x_1(t)}{1+x_1(t)}, \ t \in J. \end{aligned}$$

The above system can be rewritten as follows

$$\begin{aligned} ^C D^q x(t) = \ & Ax(t) + Bu(t) + f(t, x(t)) \\ & + \int_0^t G(s, x(s))\mathrm{d}W_{(s)}^H, \\ & t \in J \end{aligned} \tag{9}$$

with

$$\begin{aligned} & q = \frac{1}{2}, \ A = \begin{pmatrix} 0 & 1 \\ -1 & 0 \end{pmatrix}, \ B = \begin{pmatrix} 0 \\ 1 \end{pmatrix}, \\ & x(t) = \begin{pmatrix} x_1(t) \\ x_2(t) \end{pmatrix}, \ f(t, x(t)) = \begin{pmatrix} 0 \\ \frac{x_1(t)}{1+3x_1(t)} \end{pmatrix} \\ & \text{and} \quad G(t, x(t)) = \begin{pmatrix} \frac{5x_1(t)}{1+x_1(t)} \\ 0 \end{pmatrix}. \end{aligned}$$

The Mittag-Leffler matrix function of the system is given by (see [8])

$$E_q(At^q) = \begin{pmatrix} \sum\limits_{j=0}^{\infty} \frac{(-1)^j t^{2jq}}{\Gamma[1+2jq]} & \sum\limits_{j=0}^{\infty} \frac{(-1)^j t^{(2j+1)q}}{\Gamma[1+(2j+1)q]} \\ -\sum\limits_{j=0}^{\infty} \frac{(-1)^j t^{(2j+1)q}}{\Gamma[1+(2j+1)q]} & \sum\limits_{j=0}^{\infty} \frac{(-1)^j t^{2jq}}{\Gamma[1+2jq]} \end{pmatrix}.$$

By simple matrix calculations, one can see that the controllability matrix

$$\begin{aligned} W &= \int_0^T (T-s)^{q-1}[E_{q,q}(A(T-s)^q)B] \\ &\quad \times [E_{q,q}(A(T-s)^q)B]^* \mathrm{d}s \\ &= \int_0^T (T-s)^{q-1} \\ &\quad \times \begin{pmatrix} S_1^2 + S_2^2 & S_1S_3 + S_2S_4 \\ S_1S_3 + S_2S_4 & S_1^2 + S_2^2 \end{pmatrix} \mathrm{d}s \\ &= \begin{pmatrix} 3.5363 & 0 \\ 0 & 3.5363 \end{pmatrix} > 0 \end{aligned}$$

is positive definite. Here

$$S_1 = S_4 = \sum_{j=0}^{\infty} \frac{(-1)^j (T-s)^{2jq}}{\Gamma[(1+2j)q]},$$

$$S_2 = -S_3 = -\sum_{j=0}^{\infty} \frac{(-1)^j (T-s)^{(2j+1)q}}{\Gamma[2q(j+1)]}.$$

Moreover, it is easy to show that for all $x \in \mathbf{R}^2$, $\|f(t, x(t))\|^2 \leq \frac{\|x_1\|^2}{1+9\|x_1(t)\|^2}$ and $\|G(t, x(t))\|^2 \leq \frac{25\|x_1(t)\|^2}{1+\|x_1(t)\|^2}$. One can see that the inequalities (5) and (7) hold and all other conditions stated in Theorems 2 and 3 are satisfied. Hence, the fractional order stochastic differential inclusions with fBm (9) are completely controllable on J.

V. Conclusion and Future Work

This paper has advanced the controllability result of fractional order stochastic differential inclusions with fBm in finite dimensional space. The results have been obtained upon suitable fixed point theorems, namely the Bohnenblust-Karlin fixed point theorem for the convex case and the Covitz-Nadler for the nonconvex case. Finally, a numerical example has been given to validate the efficiency of the proposed theoretical results.

In recent years, the applications of an integro-differential equations model play an important role in many areas from science and engineering, particularly in the analysis of electrical circuit. Inspired by the applications of fractional order system and integro-differential equation, solving the fractional stochastic integro-differential equations with nonlocal condition deserves our future concern.

References

[1] Miller K S, Ross B. *An Introduction to the Fractional Calculus and Fractional Differential Equations*. New York: Wiley, 1993.

[2] Oldham K B, Spanier J. *The Fractional Calculus: Theory and Applications of Differentiation and Integration to Arbitrary Order*. New York: Academic Press, 1974.

[3] Podlubny I. *Fractional Differential Equations: An Introduction to Fractional Derivatives, Fractional Differential Equations, to Methods of their Solution and some of Their Applications*. California: Academic Press, 1998.

[4] Samko S G, Kilbas A A, Marichev O I. *Fractional Integrals and Derivatives: Theory and Applications*. Amsterdam: Gordon and Breach Science Publisher, 1993.

[5] Sabatier J, Agrawal O P, Tenreiro Machado J A. *Advances in Fractional Calculus*. Netherlands: Springer, 2007.

[6] Monje C A, Chen Y, Vinagre B M, Xue D, Feliu Batlle V. *Fractional-Order Systems and Controls: Fundamentals and Applications*. London: Springer, 2010.

[7] Monje C A, Vinagre B M, Feliu V, Chen Y Q. Tuning and auto-tuning of fractional order controllers for industry applications. *Control Engineering Practice*, 2008, **16**(7): 798−812

[8] Chikriy A A, Matichin I I. Presentation of solutions of linear systems with fractional derivatives in the sense of Riemann-Liouville, Caputo and Miller-Ross. *Journal of Automation and Information Sciences*, 2008, **40**(6): 1−11

[9] Kilbas A A, Srivastava H M, Trujillo J J. *Theory and Applications of Fractional Differential Equations*. Amsterdam: Elsevier Science Limited, 2006.

[10] Balachandran K, Kokila J. On the controllability of fractional dynamical systems. *International Journal of Applied Mathematics and Computer Science*, 2012, **22**(3): 523−531

[11] Sathiyaraj T, Balasubramaniam P. Controllability of nonlinear fractional neutral stochastic dynamical systems with Poisson jumps. *Mathematical Analysis and its Applications*. India: Springer, 2015. 429−438

[12] Balasubramaniam P, Ntouyas S K. Controllability for neutral stochastic functional differential inclusions with infinite delay in abstract space. *Journal of Mathematical Analysis and Applications*, 2006, **324**(1): 161−176

[13] Mahmudov N I, Denker A. On controllability of linear stochastic systems. *International Journal of Control*, 2000, **73**(2): 144−151

[14] Abbas S, Benchohra M. Fractional order Riemann-Liouville integral inclusions with two independent variables and multiple delay. *Opuscula Mathematica*, 2013, **33**(2): 209−222

[15] Balasubramaniam P. Existence of solutions of functional stochastic differential inclusions. *Tamkang Journal of Mathematics*, 2002, **33**(1): 25−34

[16] Boufoussi B, Hajji S. Neutral stochastic functional differential equations driven by a fractional Brownian motion in a Hilbert space. *Statistics & Probability Letters*, 2012, **82**(8): 1549−1558

[17] Caraballo T, Garrido-Atienza M J, Taniguchi T. The existence and exponential behavior of solutions to stochastic delay evolution equations with a fractional Brownian motion. *Nonlinear Analysis: Theory, Methods & Applications*, 2011, **74**(11): 3671−3684

[18] Ahmed H M. Controllability of impulsive neutral stochastic differential equations with fractional Brownian motion. *IMA Journal of Mathematical Control and Information*, 2015, **32**(4): 781−794

[19] Li K X, Peng J G. Laplace Transform and fractional differential equations. *Applied Mathematics Letters*, 2011, **24**(12): 2019−2023

[20] Sakthivel R, Revathi P, Mahmudov N I. Asymptotic stability of fractional stochastic neutral differential equations with infinite delays. *Abstract and Applied Analysis*, 2013, **2013**: Article ID 769257

[21] Zhou Y, Jiao F. Existence of mild solutions for fractional neutral evolution equations. *Computers and Mathematics with Applications*, 2010, **59**(3): 1063−1077

[22] Aubin J B, Cellina A. *Differential Inclusions: Set-Valued Maps and Viability Theory*. Berlin Heidelberg: Springer-Verlag, 1984.

[23] Górniewicz L. *Topological Fixed Point Theory of Multivalued Mappings*. Netherlands: Springer, 1999.

[24] Hu S C, Papageorgiou N S. *Handbook of Multivalued Analysis: Volume II: Applications*. New York: Springer, 2013.

[25] Kisielewicz M. *Differential Inclusions and Optimal Control*. Netherlands: Springer, 1991.

[26] Lasota A, Opial Z. An application of the Kakutani-Ky-Fan theorem in the theory of ordinary differential equation. *Bulletin De Lcadémie Polonaise Des Sciences-Série Des Sciences Mathématiques, Astronomiques Et Physiques*, 1965, **13**(11): 781−786

[27] Castaing C, Valadier M. *Convex Analysis and Measurable Multifunctions.* Berlin Heidelberg: Springer, 1977.

[28] Bohnenblust H F, Karlin S. On a theorem of Ville, contributions to the theory of games. *Annals of Mathematics Studies, 24.* Princeton: Princeton University Press, 1950. 155−160

[29] Covitz H, Nadler S B. Multi-valued contraction mappings in generalized metric spaces. *Israel Journal of Mathematics*, 1970, **8**(1): 5−11

[30] Herrmann R. *Fractional Calculus: An Introduction for Physicists.* London: World Scientific Publishing Company, 2011.

T. Sathiyaraj Under-graduated from Department of Mathematics, AVVM Sri Pushpam College, Poondi, Thanjavur, affiliated with Bharathidasan University, Tiruchirappalli, India, in 2008. He obtained post-graduation and Master of Philosophy from St. Joseph's College, Tiruchirappalli affiliated with Bharathidasan University in 2011 and 2012, respectively. Now, he is pursuing his Ph. D. degree under the guidance of Professor P. Balasubramaniam at Department of Mathematics, The Gandhigram Rural Institute-Deemed University, Gandhigram, Tamil Nadu, India.

His research interests include the analysis and control of fractional order stochastic differential equations.

P. Balasubramaniam Post graduated in the year 1989 and subsequently completed Master of Philosophy in the year 1990 and Doctor of Philosophy (Ph. D.) in 1994 in the field of mathematics with specialized area of control theory from Bharathiar University, Coimbatore, Tamilnadu, India. Soon after his completion of Ph. D. degree, he served as Lecturer in Mathematics in Engineering Colleges for three years. Since February 1997 he served as Lecturer and Reader in Mathematics and now he is rendering his services as a Professor, Department of Mathematics, The Gandhigram Rural Institute-Deemed University, Gandhigram, India, from November 2006 onwards. He has worked as a Visiting Research Professor during the years 2001 and 2005-2006 for promoting research in the field of control theory and neural networks at Pusan National University, Pusan, South Korea. Also he has worked as Visiting Professor in the Institute of Mathematical Sciences, University of Malaya, Malaysia, for the period of six months from September 2011 to March 2012. He is a member of several academic bodies including a life member of Cryptology Research Society of India, Indian Statistical Institute, Kolkata. He has 23 years of experience in teaching and research. He has published more than 211 research papers in various SCI journals holding impact factors with Scopus H-index 29 and web of knowledge H-Index 23. Also he has edited 7 proceedings including a book and 3 international conference proceedings in Springer publications. He is serving as a reviewer of many SCI journals and member of the editorial board of Journal of Computer Science, Advances in Fuzzy Sets and Systems and the Scientific World Journal: Mathematical Analysis, Hindawi Publisling Corporation, USA. He is an Editor-in-Chief of the journal Modern Instrumentation, Scientific Research Publishing Inc. (SCIRP) and Associate Editor of Advances in Difference Equations, Springer, Germany. He has received the Tamilnadu Scientist Award (TANSA) in the discipline of Mathematical Sciences instituted by the Tamilnadu State Council for Science and Technology in the year 2005.

His research interests include the areas of control theory, stochastic differential equations, soft Computing, stability analysis, cryptography, neural networks and image processing. Corresponding author of this paper.

A Note on Robust Stability Analysis of Fractional Order Interval Systems by Minimum Argument Vertex and Edge Polynomials

Baris Baykant Alagoz

***Abstract*—By using power mapping ($s = v^m$), stability analysis of fractional order polynomials was simplified to the stability analysis of expanded degree integer order polynomials in the first Riemann sheet. However, more investigation is needed for revealing properties of power mapping and demonstration of conformity of Hurwitz stability under power mapping of fractional order characteristic polynomials. Contributions of this study have two folds: Firstly, this paper demonstrates conservation of root argument and magnitude relations under power mapping of characteristic polynomials and thus substantiates validity of Hurwitz stability under power mapping of fractional order characteristic polynomials. This also ensures implications of edge theorem for fractional order interval systems. Secondly, in control engineering point of view, numerical robust stability analysis approaches based on the consideration of minimum argument roots of edge and vertex polynomials are presented. For the computer-aided design of fractional order interval control systems, the minimum argument root principle is applied for a finite set of edge and vertex polynomials, which are sampled from parametric uncertainty box. Several illustrative examples are presented to discuss effectiveness of these approaches.**

***Index Terms*—Fractional order systems, robust stability, edge theorem, interval uncertainty.**

I. INTRODUCTION

ROBUST stability analysis is very essential for robust performance of practical control systems working in real applications. Imprecision in system modeling and temporal deviation of system parameters may cause instability of real control systems that are designed according to nominal system models. Implementation of practical and robust control systems requires the system design aspects, which ensure the stability of control systems within the possible ranges of system parameter fluctuations. Several theorems such as Kharitonov's theorem and edge theorem were developed to accomplish parametric robust stability analysis of integer-order system models introducing interval uncertainty of coefficients[1]. These theorems state sufficient conditions for robust stability and thus facilitate robust stability analyses of integer order linear time invariant (LTI) systems with parametric uncertainty. They limit stability checking to the certain number of polynomials sampled from a continuous family of interval characteristic polynomials. Nowadays, fractional order systems are on the focus of control community and confirmation of the validity of well-established robust stability analysis methods for fractional order system models is very beneficial. Robust stability analysis and robust stabilization problems of fractional order systems were addressed in many aspects during the last two decades[2−15]. It can be briefly explained as follows: Stability analysis of fractional order systems according to the pole placement in the complex plane was addressed by Matignon[15]. Minimum argument root principle was a milestone for robust stability analysis of fractional order interval systems. Based on minimum argument of eigenvalues of state space model, an interval boundary box method was presented for stability testing of the fractional order LTI systems with interval uncertainties[5]. Then, stabilization of fractional order LTI systems by using linear matrix inequality (LMI) method was shown in several works[6−9]. Robust stability check based on four Kharitonov's polynomials were also discussed for commensurate order LTI systems[10−11].

In many works, the power mapping of polynomials in complex planes, which is also known as conformal mapping, was employed to simplify stability analysis of fractional order systems by simply transforming them into integer order polynomials[3−4]. By applying $s = v^m$ mapping, stability analyses in the first Riemann sheet were shown for fractional order polynomials[13]. Later, a numerical method based on the exposed edge polynomial sampling was proposed for robust stability analysis of fractional order interval polynomials by using $s = v^m$ mapping[14]. However, it is obvious that there is a need for further works to demonstrate impacts of power mapping on root locus and stability related properties of systems. Thus, implication of edge theorem under power mapping of fractional order characteristic polynomials can be utilized and the robust stability analysis methods based on edge theorem can be developed to reduce computational complexity in robust stability analysis of fractional order interval systems.

In this paper, an investigation on the conformity of Hurwitz stability under power mapping ($s = v^m$) of characteristic polynomials of fractional order systems is presented. After showing that Hurwitz stability is conformal to power mapping, implications of edge theorem for fractional order characteristic polynomial are discussed. Then, robust stability analysis schemes considering combinations of edge and vertex polyno-

Manuscript received August 19, 2015; accepted February 28, 2016. Recommended by Associate Editor Dingyü Xue.

Citation: Baris Baykant Alagoz. A note on robust stability analysis of fractional order interval systems by minimum argument vertex and edge polynomials. *IEEE/CAA Journal of Automatica Sinica*, 2016, **3**(4): 411−421

Baros Baykant Alagoz is with the Department of Computer Engineering, Inonu University, Malatya, Turkey (e-mail: baykant.alagoz@inonu.edu.tr).

mials of the hyper-rectangle are presented and compared with the application of conventional edge theorem given in [14]. Computational complexity and effectiveness of presented methods are discussed by illustrative examples.

II. BASIC DEFINITIONS AND PRELIMINARIES

Definition 1 (Hurwitz stability for integer order polynomials). Let us consider an integer order polynomial with real coefficient, which is expressed as $p(s)=\sum_{i=0}^{n}c_is^i$. Parameters $c_i\in\mathbf{R}$ are real polynomial coefficients, and the parameter $n\in\mathbf{Z}^+$ represents the degree of the polynomials. A characteristic polynomial with real coefficients is said to be Hurwitz stable if and only if all of its roots lie in the left hand side of complex s plane[16−17]. Accordingly, Hurwitz stable polynomials are defined as $\{p(s)|p(s)=0:\forall s\in C\wedge \mathrm{Re}\{s\}<0\}$. If characteristic polynomial of a LTI system model is a Hurwitz stable polynomial, the LTI system model behaves asymptotically stable because time domain solutions consist of exponentially decaying terms. Consequently, root locus of characteristic polynomials has been widely used for the asymptotic stability analyses of LTI systems. The left hand side of complex plane, which is bounded by imaginary axis, is considered as the stability region for root locus analysis of integer order characteristic polynomials $p(s)$.

In general, the characteristic polynomial $p(s)$ is a multivalued function of the complex variable s, whose domain is described by the principle sheet (the first sheet) of Riemann surfaces, defined in an argument range $-\pi<\arg(s)<\pi$[2]. As known, Hurwitz stability region (HSR) for characteristic polynomial roots is the left half plane of the first sheet, which can be defined according to root arguments as $\pi/2<\arg(s)<3\pi/2$. It is convenient to call the argument bounds with angles of $-\pi/2$ and $\pi/2$ as the Hurwitz stability boundary (HSB) for characteristic root locus[18]. The set of complex points with arguments $-\pi/2$ and $\pi/2$ also refers to the imaginary axis.

Definition 2 (Hurwitz stable fractional order polynomials). Let us consider a fractional order polynomial with real coefficients expressed in the form of $p_f(s)=\sum_{i=0}^{n}c_is^{\alpha_i}$, where $\alpha_i\geq 0$ and $\alpha_i\in\mathbf{R}^+$ is the fractional orders of the polynomials. The case of $\alpha_0=0$ yields the constant term of polynomials. In order to facilitate root locus analysis of fractional order LTI systems, $s=v^m$ mapping has been used to transform a fractional order characteristic polynomial to the expanded degree integer order characteristic polynomials. It was shown by many works that one can carry out stability analysis of fractional order systems by examining root locus of the expanded degree integer-order characteristic polynomials, given as $p_f(s)|_{s=v^m}=p_m(v)=\sum_{i=0}^{n}c_iv^{m\alpha_i}$[2−3, 5−6, 13−14]. Here, each $m\alpha_i$ for $i=0,1,2,\ldots,n$ is an integer number. Following the $s=v^m$ mapping, the first Riemann sheet is confined into a plane slice with the argument range $-\pi/m<\arg(v)<\pi/m$[2] and stability analyses were carried out in the first Riemann sheet[10−11, 13−14, 18]. In related works, by applying $s=v^m$ mapping, interval characteristic polynomials were recognized to be stable, in the case that all roots in the first Riemann sheet lie in complex plane slice with argument ranges of $(\pi/2m,\pi/m]$ and $[-\pi/m,-\pi/2m)$. Detailed works on the solution of fractional order characteristic polynomials were elaborated in [18] for analysis and design of control systems. Some useful properties of power mapping can be stated as follows:

Remark 1 (Magnitude and argument properties of power mapping). Let us consider the fraction order real polynomial $p_f(s)$, where complex input variable is defined as $s=M\mathrm{e}^{\mathrm{j}\theta}\in\mathbf{C}$. The $s=v^m$ transformation maps the function $p_f(s)$ to a real polynomial $p_m(v)$, where $v=\tilde{M}\mathrm{e}^{\mathrm{j}\phi}\in C$ such that the magnitude is $\tilde{M}=M^{(1/m)}$ and the argument is $\phi=\theta/m$.

Proof. This remark was previously mentioned in [3−4]. In order to better see mapping properties of $s=v^m$ transformation, one can write reverse transformation as $v=s^{1/m}=M^{(1/m)}\mathrm{e}^{\mathrm{j}\theta/m}$ for a complex point $s=M\mathrm{e}^{\mathrm{j}\theta}$, where parameters M and θ stand for the magnitude and argument of points in s domain. After rearranging $v=M^{(1/m)}\mathrm{e}^{\mathrm{j}\theta/m}$ in the form of $v=\tilde{M}\mathrm{e}^{\mathrm{j}\phi}$, it is obvious that $s=v^m$ transformation maps the complex point in s domain to a point in v domain, where the argument is $\phi=\theta/m$ and the magnitude is $\tilde{M}=M^{(1/m)}$. □

Remark 2 (Hurwitz stability region under $s=v^m$ mapping). An integer order characteristic polynomial is Hurwitz stable, if all characteristic roots lie in the left half side of complex plane. In case of $s=v^m$ mapping, the Hurwitz stability region is mapped into $(\pi/2m,\pi/m]$ for positive root arguments and $[-\pi/m,-\pi/2m)$ for negative root arguments.

Proof. Let us express Hurwitz stability region, given by $-\pi/2<\arg(s)<\pi/2$, as combination of $\pi/2<\theta<\pi$ for positive root arguments and $-\pi<\theta<-\pi/2$ for negative root arguments. Here, θ is the argument of a point in s domain and written as $\theta=\arg(s)$. By considering root argument transformation $\phi=\theta/m$ in Remark 1, Hurwitz stability region is mapped to $(\pi/2m,\pi/m]$ for positive root arguments and $[-\pi/m,\ -\pi/2m)$ for negative root arguments under $s=v^m$ mapping. Fig. 1 depicts the mapping of Hurwitz stability region under $s=v^m$ mapping for stability analysis. □

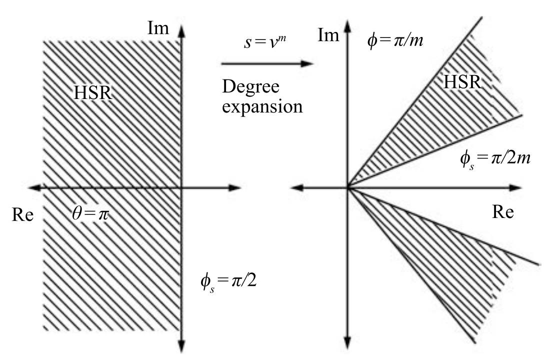

Fig. 1. Hurwitz stability region of fractional order characteristic polynomials under $s=v^m$ mapping[4].

Lemma 1 (Conservation of argument and magnitude relations). $s=v^m$ mapping of real polynomials is conservative in term of argument and magnitude relations. In other words, $s=v^m$ mapping conserves spatial relations between roots of s domain while mapping in v domain. For $m\in\mathbf{Z}^+$, the following root argument relations are valid,

$$\begin{aligned}&\theta_i > \theta_j, \quad \theta_l < \theta_k, \quad \theta_u = \theta_q,\\ &\quad \Rightarrow \phi_i > \phi_j, \quad \phi_l < \phi_k, \quad \phi_u = \phi_q,\end{aligned} \tag{1}$$

and the following root magnitude relations are also valid under $s = v^m$ mapping,

$$\begin{aligned}&M_i > M_j, \quad M_l < M_k, \quad M_u = M_q,\\ &\quad \Rightarrow \tilde{M}_i > \tilde{M}_j, \quad \tilde{M}_l < \tilde{M}_k, \quad \tilde{M}_u = \tilde{M}_q.\end{aligned} \tag{2}$$

Proof. For $m \in \mathbf{Z}^+$, one can write the following relations for arguments according to Remark 1,

$$\theta_i > \theta_j \to \frac{\theta_i}{m} > \frac{\theta_j}{m} \to \phi_i > \phi_j,$$

$$\theta_l > \theta_k \to \frac{\theta_l}{m} > \frac{\theta_k}{m} \to \phi_l > \phi_k,$$

$$\theta_u > \theta_p \to \frac{\theta_u}{m} > \frac{\theta_p}{m} \to \phi_u > \phi_p.$$

And the following relations for magnitudes,

$$M_i < M_j \to M_i^{(\frac{1}{m})} < M_j^{(\frac{1}{m})} \to \tilde{M}_i < \tilde{M}_j,$$

$$M_l > M_k \to M_l^{(\frac{1}{m})} > M_k^{(\frac{1}{m})} \to \tilde{M}_l > \tilde{M}_k,$$

$$M_u > M_q \to M_u^{(\frac{1}{m})} > M_q^{(\frac{1}{m})} \to \tilde{M}_u > \tilde{M}_q.$$

□

This lemma tells us that argument and magnitude relations are conserved under $s = v^m$ mapping.

III. Problem Statement

Fractional order LTI systems are represented by the fractional order differential equations in the form of [19],

$$\begin{aligned}&a_n D^{\alpha_n} y(t) + a_{n-1} D^{\alpha_{n-1}} y(t) + \cdots + a_1 D^{\alpha_1} y(t) + a_0 y(t)\\ &\quad = b_m D^{\varphi_m} u(t) + b_{m-1} D^{\varphi_{m-1}} u(t) + \cdots\\ &\qquad + b_1 D^{\varphi_1} u(t) + b_0 u(t).\end{aligned} \tag{3}$$

By using Laplace transform $L\{D^\alpha f(t)\} = s^\alpha F(s)$ for $f(0^+) = 0$[19], fractional order transfer functions are written to express system model in continuous frequency domain as follows.

$$T(s) = \frac{Y(s)}{U(s)} = \frac{\sum\limits_{i=0}^{m} b_i s^{\varphi_i}}{\sum\limits_{i=0}^{n} a_i s^{\alpha_i}}, \tag{4}$$

where denominator polynomial coefficients a_i and numerator polynomial coefficients b_i are real numbers. The fractional orders of the system are denoted by $\alpha_i \in \mathbf{R}$ $(i = 0, 1, 2, 3, \ldots, n)$ and $\varphi_i \in \mathbf{R}$ $(i = 0, 1, 2, 3, \ldots, m)$. For $\alpha_0 = 0$ and $\varphi_0 = 0$, the system models have constant terms a_0 and b_0. Here, the model orders satisfy $\alpha_n > \alpha_{n-1} > \alpha_{n-2} > \cdots > \alpha_2 > \alpha_1 > 0$ and $\varphi_n > \varphi_{n-1} > \varphi_{n-2} > \cdots > \varphi_2 > \varphi_1 > 0$.

In real systems, unpredictable parameter deviations and change of operating conditions lead to reduce consistency of system modeling. Therefore, a relevant modeling of real systems is not always possible to obtain by means of nominal LTI system models. The system modeling with parametric interval uncertainty is more convenient for the control system design problems compared to nominal system models. Because, systems can operate more effectively in real control application when controller performance is designed robust for possible ranges of system parameter variations. The characteristic polynomials of transfer functions with interval uncertainty are expressed as,

$$\Delta(s) = \sum_{i=0}^{n} [\underline{a}_i \, \bar{a}_i] s^{\alpha_i}, \tag{5}$$

where the parameters $[\underline{a}_i \, \bar{a}_i]$ represent uncertainty of the coefficient a_i, which refers to deviation between a lower $(\underline{a}_i)$ and an upper $(\bar{a}_i)$ bound. In practice, interval uncertainty bounds of the nominal coefficient a_i can be expressed by considering parameter deviation (Δa_i) as $[\underline{a}_i \, \bar{a}_i] = [a_i - \Delta a_i \;\; a_i + \Delta a_i]$. The checking of boundary conditions for robust stability is useful for control system design problems[18]. Example 3 is devoted to searching of the boundaries for allowable parameter deviation of robust stable control system according to edge theorem.

By applying $s = v^m$ to (5), one obtains expanded degree integer order characteristic polynomials in the form of,

$$\Delta^m(v) = \sum_{i=0}^{n} [\underline{a}_i \, \bar{a}_i] v^{\beta_i}, \tag{6}$$

where $\beta_i \in \mathbf{Z}^+ \cup \{0\}$ is expanded degree integer order, which is defined as $\beta_i = m\alpha_i$.

The uncertainty box of interval coefficients defines a hyperrectangle (n-orthotope) denoted by A, which is written as Cartesian product of interval polynomial coefficients $\underline{a}_i \le a_i \le \bar{a}_i$, $i = 1, 2, 3, \ldots, n$,

$$A = \prod_{i=0}^{n} [\underline{a}_i \, \bar{a}_i]. \tag{7}$$

A point of the hyper-rectangle is represented by coefficient vector $a = [a_1\, a_2\, a_3 \cdots a_n]$. Each vector a from hyperrectangle Astands for a fractional order polynomial from the interval polynomial family that is denoted by the set $\Omega \in \mathbf{R}^n$[14]. By considering real positive coefficient vectors, the hyper-rectangle A can be also expressed as $A = \{a : 0 < \underline{a}_i \le a_i \le \bar{a}_i,\ i = 1, 2, 3, \ldots, n\}$[14].

Let us assume that each characteristic polynomial from the set Ω has ξ numbers of complex roots, denoted by v_r in the complex v plane. The number of complex roots depends on the degree of $\Delta^m(v)$ and it can be found by $\xi = m\alpha_n$. The complex roots of the interval polynomial family Ω form a set of roots in the first Riemann sheet, which can be written as[14],

$$\begin{aligned}R(\Omega) = \{&v_r : \Delta^m(a, v_r) = 0 \wedge |\arg(v_r)| < \frac{\pi}{m},\\ &\forall a \in A,\ r = 1, 2, 3, \ldots, \xi\}.\end{aligned} \tag{8}$$

Since expanded degree integer order characteristic polynomials are real coefficient integer order polynomials, complex roots lie symmetrically with respect to the real axis in complex v plane. The root region can be split into three subsets, $R(\Omega) = R(\Omega)^- \cup R(\Omega)^0 \cup R(\Omega)^+$, according to root arguments. Here, $R(\Omega)^+$, $R(\Omega)^-$ and $R(\Omega)^0$ represent subsets of $R(\Omega)$ formed with positive argument roots, negative argument roots and zero argument roots, respectively. The complex conjugate roots present symmetry at positive and negative argument sides[20], that is, one can state $|\arg(R(\Omega)^-)| \equiv |\arg(R(\Omega)^+)|$ for complex conjugate root arguments. Therefore, analysis given for positive arguments roots ($\phi > 0$) is also valid for negative argument roots ($\phi < 0$). This leads us to the conclusion; when $R(\Omega)^0$ is empty set, if only minimum positive argument characteristic roots lie in the stability region $(\pi/2m, \pi/m]$ in the first Riemann sheet under $s = v^m$ mapping, then the interval system can be recognized as Hurwitz stable[5, 15, 18].

$$\min\{\arg(R(\Omega))\} > \frac{\pi}{2m}. \tag{9}$$

Edge theorem is conformal under $s = v^m$ mapping due to Lemma 1. Because, conservation of argument and magnitude relations under power mapping ensures that root constellation in HSR of complex s plane is preserved in HSR of complex v plane and vice versa. Since argument relations of all edge and vertex roots are conserved under power mapping, edge theorem can be extended to complex v plane. On the other hand, due to the conservation of root argument relations according to Lemma 1, it is easy to see that if the minimum argument root in s domain lies in HSR region, it lies in HSR region of v domain. Fig. 2 depicts the mapping relations of the root constellation and vice versa. Lemma 1 also suggests us that vertex and edge of $R(\Omega)$ in v plane are also vertex and edge polynomials in s plane.

Theorem 1. (Conformity of minimum argument roots under power mapping): Under $s = v^m$ mapping ($m > 0$), theminimum argument root of a fractional order polynomial in s plane is mapped to the minimum argument root of its expanded integer order polynomials in v plane. Therefore, Hurwitz stability is conserved under power mapping.

Proof. Let us denote set of root arguments of all edges and vertex roots of $R(\Omega)$ as,

$$\psi = \arg(R(\Omega)) = \{\phi_1, \phi_2, \phi_3, \ldots, \phi_k\}. \tag{10}$$

The minimum argument of root set $R(\Omega)$ is $\phi_{\min} = \min\{\arg(R(\Omega))\}$. If the condition $\phi_{\min} > \pi/2m$ is satisfied, the root set $R(\Omega)$ lies in Hurwitz stability region defined as $(\pi/2m, \pi/m]$ in Remark 2 due to the fact that $\forall\phi_i \in \psi$, $\phi_i \geq \phi_{\min} > \pi/2m$. One can rearrange it as $m\phi_i \geq m\phi_{\min} > \pi/2$, which refers to $\theta_i \geq \theta_{\min} > \pi/2$ where $\theta_{\min} = m\phi_{\min}$ and $\theta_i = m\phi_i$ according to Remark 1. Therefore, if the expanded degree integer order characteristic polynomials are Hurwitz stable, fractional order characteristic polynomial is also Hurwitz stable. It is shown for unstable cases in the same manner. One can state that the stability properties related with root locus are conformal under power mapping. □

It is noteworthy that the root region in v plane is indeed the scaled and rotated image of root region in s plane according to magnitudeand argument properties ($\tilde{M} = M^{(1/m)}$, $\phi = \theta/m$) given in Remark 1. A graph defined by edge and vertices roots on root region $R(\Omega)$ is preserved under power mapping.

IV. Implications of Edge Theorem with Minimum Argument Root Principle for Fractional Order Interval Polynomials

Edge theorem provides consistent solutions for the robust stability analyses of integer-order LTI interval systems[1]. For fractional order interval systems, an application of edge theorem for numerical robust stability analysis was demonstrated by Senol et al.[14]. The boundary of root region in the first Riemann sheet was represented by roots of exposed edge polynomials of interval coefficient hyper-rectangle. In this section, with consideration of minimum argument root principle for vertex and its connected edge polynomials, author aims to reduce computational complexity of the robust stability analysis of fractional order system models. Fig. 3 (a) depicts the exposed edge and vertex polynomials of hyper-rectangle A, which was drawn for the case of three interval coefficients. Fig. 3 (b) illustrates the corresponding roots of exposed edge and vertex polynomials of hyper-rectangle A in the first Riemann sheet. Fig. 3 (c) indicates the minimum argument vertex root and roots of its connected edges. This study suggests that analysis of roots in Fig. 3 (c) can significantly reduce computational complexity of robust stability analysis of fractional order interval polynomials.

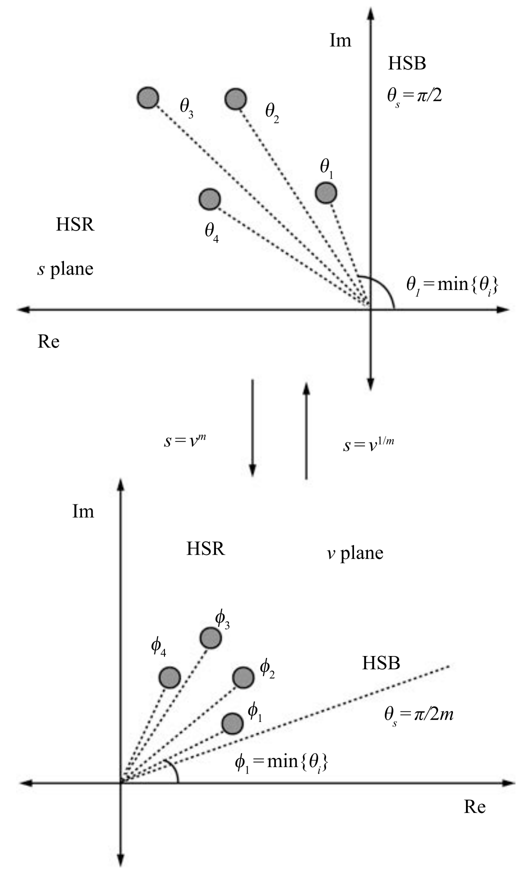

Fig. 2. Argument and magnitude relations are conformal under power mappings (Root placements in s and v planes conserve argument relations).

Edge theorem also implies that boundary of root region is formed by roots of vertex and exposed edge polynomials of uncertainty box, which is represented by hyper-rectangle A of interval coefficients. It is obvious that the change of root location with respect to the change of polynomial coefficients is continuous due to the fact that polynomials and their coefficient intervals are continuous. According to this reason, the most outer roots of root region $R(\Omega)$ can come from edge and vertex polynomials of hyper-rectangle A. A given root region seen in Fig. 4 validates this effect. Boundaries of root region were formed by roots of vertex and exposed edges polynomials of A.

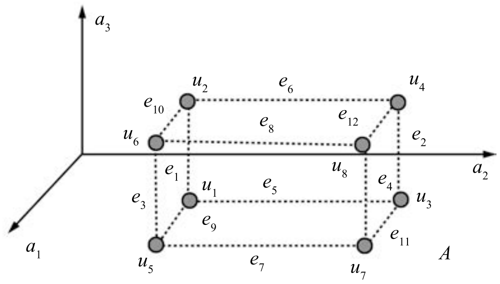

(a)

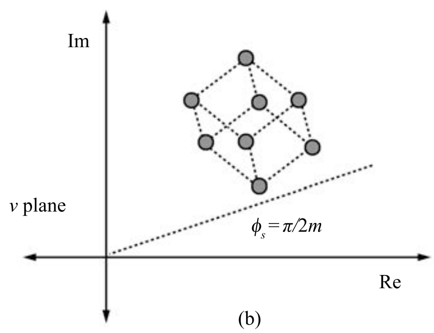

(b)

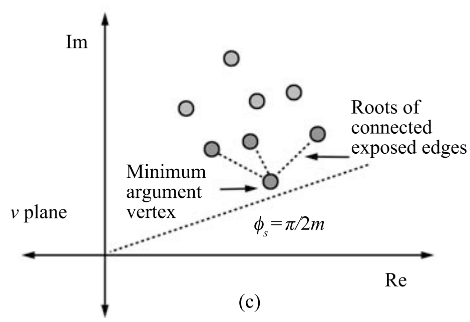

(c)

Fig. 3. Illustrations for three-dimensional hyper-rectangle and root placements ((a) An illustration of vertex $(u_1, u_2, u_3, \ldots, u_8)$ and exposed edges $(e_1, e_2, e_3, \ldots, e_8)$ of hyper-rectangle A build for three interval coefficients; (b) Root locus of exposed edge and vertex polynomials; (c) Root locus of minimum argument vertex polynomial and roots of connected exposed edge polynomials.)

As known, n number of uncertain parameters builds 2^n vertices on the hyper-rectangle. Coefficient vectors of vertex polynomials of A were expressed as Cartesian products of upper and lower bounds of interval coefficients[14],

$$u_k = \{\underline{a}_0, \bar{a}_0\} \times \{\underline{a}_1, \bar{a}_1\} \times \{\underline{a}_2, \bar{a}_2\} \times \cdots \times \left\{\underline{a}_{n-1}, \bar{a}_{n-1}\right\} \times \{\underline{a}_n, \bar{a}_n\}, \quad (11)$$

where "×" represents Cartesian product operator. Let us express vertex polynomials of expanded degree integer order interval polynomials as,

$$\Delta_{u_k} = \Delta^m(u_k, v), \quad k = 1, 2, 3, \ldots, 2^n. \quad (12)$$

Exposed edges are line segments connecting vertices through the surfaces of A as illustrated in Fig. 3 (a). The edge polynomials can be obtained by sampling coefficient vectors from exposed edge of A[14],

$$e_k = \{\underline{a}_0, \bar{a}_0\} \times \{\underline{a}_1, \bar{a}_1\} \times \{\underline{a}_2, \bar{a}_2\} \times \cdots \times s(a_k, \lambda) \times \cdots \times \left\{\underline{a}_{n-1}, \bar{a}_{n-1}\right\} \times \{\underline{a}_n, \bar{a}_n\} \quad (13)$$

where $s(a_k, \lambda)$ is edge sampling function and defined linearly as $s(a_k, \lambda) = \lambda\underline{a}_k + (1-\lambda)\bar{a}_k$, $\lambda \in [0, 1]$. Edge polynomials of expanded degree integer order interval characteristic polynomial are expressed as,

$$\Delta_{e_k} = \Delta^m(e_k, v). \quad (14)$$

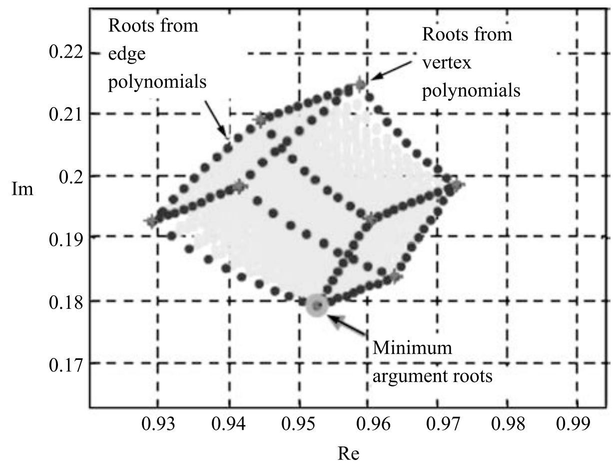

Fig. 4. Root region of expanded degree integer order interval polynomial $\Delta^{10}(v) = [2.1\ 2.6]v^{21} + [1.2\ 1.7]v^8 + [0.7\ 1.3]$ in the first Riemann sheet. Roots from edge polynomials and roots from vertex polynomials of hyper-rectangle A are indicated by blue dots and red asterisks, respectively.

It is unnecessary to check all edge polynomials for robust stability checking. Because, if one can show that minimum argument root lies in stability region, the interval system is robust stable. Computational complexity of robust stability analysis based on root locus strongly depends on the number of tested polynomials and the number of polynomials to be solved increases depending on the number of exposed edges of hyper-rectangle, which is expressed as $n2^{n-1}$, where n is the number of interval coefficients.

Our approach to reduce complexity of numerical analysis is to consider only connected exposed edge polynomials of the minimum argument vertex polynomial. The number of the connected edges of a vertex is n. Complexity reduction depending on edge number can be expressed depending on total edge counts as $G(n) = n/(n2^{n-1}) = 2^{-n+1}$. This indicates an exponential decay of complexity reduction depending on considered edge counts.

Set of vertex roots in the root region $R(\Omega)$ can be expressed as

$$R_u(\Omega) = \{v : \Delta_{u_k}(a, v) = 0 \wedge |\arg(v)| < \frac{\pi}{m}, \forall a \in A,\ k = 1, 2, 3, \ldots, 2^n\}. \quad (15)$$

Set of exposed edge roots in the root region $R(\Omega)$ can be expressed as

$$R_e(\Omega) = \{v : \Delta_{e_k}(a, v) = 0 \wedge |\arg(v)| < \frac{\pi}{m}, \forall a \in A, \ \ k = 1, 2, 3, \ldots, n2^{n-1}\}. \quad (16)$$

Edge theorem suggests that stability checking of all exposed edge polynomials is sufficient to show robust stability of integer order interval characteristic polynomials. Considering this theorem and using power mapping, stability analyses according to test of polynomials taken from all exposed edge and vertex polynomials ($R_u(\Omega) \cup R_e(\Omega)$) were discussed in [14]. In the case of sampling edges with n_p polynomials ($n_p > 2$), the method in [14] requires test of $n_p n 2^{n-1} + 2^n$ polynomials. Here, $n_p n 2^{n-1}$ polynomials are for sampling of edges and 2^n polynomials are for vertex polynomials. In order to simplify robust stability analyses, the following two approaches are proposed in this study:

1) Test of minimum argument vertex with connected edge polynomials (MVCE): For positive interval coefficient polynomials, it can be possible to reduce number of test polynomials by only evaluating stability of the minimum argument vertex polynomial and its connected edge polynomials. It requires the calculation of roots from $R_u(\Omega) \cup R_{ce}(\Omega)$, where $R_{ce}(\Omega) \in R_e(\Omega)$ is a subset of edge roots. It needs only testing of the exposed edge polynomials connected to the minimum argument vertex that is defined as $\min\{\arg(R_u(\Omega))\}$. In the case of an edge polynomial sampling with n_p polynomials, MVCE approach requires the test of $n_p n + 2^n$ polynomials. This approach is valid under the assumption that the branch of edge graph, composed of the minimum argument vertex and its connected edges, includes the minimum argument root of A. Since the boundary of root region is formed by only roots of vertex and exposed edge polynomials of A, minimum argument root is the most likely to be on the minimum argument vertex or its connected edge polynomials.

2) Test of minimum argument vertex (MV): It is possible to reduce further the number of test polynomials by considering only vertex polynomials of hyper-rectangle A. This approach requires calculation of $\min\{\arg(R_u(\Omega))\}$, so it performs the test of 2^n polynomials. This test relies on the assumption that minimum argument roots probably come from vertex polynomials of hyper-rectangle because the interval polynomial coefficients are continuous and lead to continuity of root locus. The most distant polynomials of hyper-rectangle A are vertex polynomials. The roots of vertex polynomials of A form the vertices of root region.

Table I shows the number of the test polynomials required for robust stability analysis for edge theorem based approaches. Fig. 5 shows increase of test polynomials with respect to number of interval coefficients (n) for 20 polynomials edge sampling ($n_p = 20$). It can be seen that the test of minimum argument vertex polynomials (MV) is very advantageous in term of computational complexity.

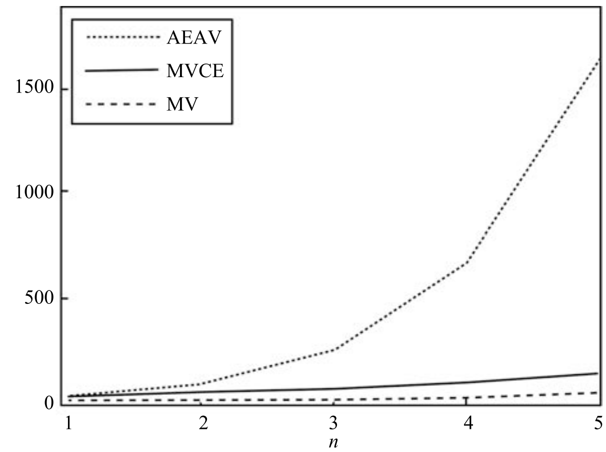

Fig. 5. Number of the tested polynomials required for test of all edge and vertex polynomials (AEAV), for the test of minimum argument vertex with connected edge polynomials (MVCE) and for the test of minimum argument vertex polynomials (MV).

V. ILLUSTRATIVE EXAMPLES

Initial conditions of systems were assumed to be zero for all parameters in numerical analyses.

Example 1. By considering the fractional order LTI nominal system described by fractional order differential equations[3],

$$0.8D^{2.2}y(t) + 0.5D^{0.9}y(t) + y(t) = u(t). \quad (17)$$

Let us check robust stability of this system for interval uncertainty of coefficients given as $0.8 \pm 0.4 = [0.4\ 1.2]$, $0.5 \pm 0.2 = [0.3\ 0.7]$ and $1 \pm 0.3 = [0.7\ 1.3]$.

To simplify analysis of interval system, one can express it in the form of transfer function with zero initial conditions as

$$G(s) = \frac{Y(s)}{U(s)} = \frac{1}{[0.4\ 1.2]s^{2.2} + [0.3\ 0.7]s^{0.9} + [0.7\ 1.3]}, \quad (18)$$

TABLE I

ROBUST STABILITY ANALYSIS APPROACHES BASED ON EDGE THEOREM FOR REAL POSITIVE COEFFICIENT INTERVAL CHARACTERISTIC POLYNOMIALS

Approaches based on edge theorem	Number of test polynomials	Basic assumptions
Test of all edge and vertex polynomials (AEAV)[14]	$n_p n 2^{n-1} + 2^n$	The test of all exposed edge polynomials from A is sufficient to show robust stability
Test of minimum argument vertex with connected edge polynomials (MVCE)	$n_p n + 2^n$	Set of minimum argument vertex with connected edge polynomials generally includes minimum argument root of A
Test of minimum argument vertex polynomials (MV)	2^n	Minimum argument root is probably the root of vertex polynomials of A

and the characteristic polynomial of the system is found as

$$\Delta(s) = [0.4\ 1.2]s^{2.2} + [0.3\ 0.7]s^{0.9} + [0.7\ 1.3]. \quad (19)$$

By applying $s = v^m$ mapping, the expanded degree integer order characteristic polynomial is written as,

$$\Delta^{10}(v) = [0.4\ 1.2]v^{22} + [0.3\ 0.7]v^{9} + [0.7\ 1.3]. \quad (20)$$

Vertex polynomials of expanded degree integer order interval characteristic polynomial were obtained as

$$\begin{aligned}\{\Delta_{u_1} &= \Delta^{10}([0.4\ 0.3\ 0.7], v),\ \Delta_{u_2} = \Delta^{10}([0.4\ 0.3\ 1.3], v),\\ \Delta_{u_3} &= \Delta^{10}([0.4\ 0.7\ 0.7], v),\ \Delta_{u_4} = \Delta^{10}([0.4\ 0.7\ 1.3], v),\\ \Delta_{u_5} &= \Delta^{10}([1.2\ 0.3\ 0.7], v),\ \Delta_{u_6} = \Delta^{10}([1.2\ 0.3\ 1.3], v),\\ \Delta_{u_7} &= \Delta^{10}([1.2\ 0.7\ 0.7], v),\ \Delta_{u_8} = \Delta^{10}([1.2\ 0.7\ 1.3], v)\}\end{aligned}$$

We performed edge sampling with 19 polynomials ($n_p = 19$) in numerical analyses, so edge sampling function can be written as $s(a_k, \lambda) = \lambda\underline{a}_k + (1-\lambda)\bar{a}_k$, where $\lambda \in \{0.05, 0.10, 0.15, 0.20, 0.25, 0.30, 0.35, 0.40, 0.45, 0.50, 0.55, 0.60, 0.65, 0.70, 0.75, 0.80, 0.85, 0.90, 0.95\}$ and $k = \{1, 2, 3\}$. Set of edge polynomials were obtained as,

$$\begin{aligned}\{\Delta_{e_1} &= \Delta^{10}([(\lambda 0.4 + (1-\lambda)1.2)\ 0.3\ 0.7], v),\\ \Delta_{e_2} &= \Delta^{10}([(\lambda 0.4 + (1-\lambda)1.2)\ 0.3\ 1.3], v),\\ \Delta_{e_3} &= \Delta^{10}([(\lambda 0.4 + (1-\lambda)1.2)\ 0.7\ 0.7], v),\\ \Delta_{e_4} &= \Delta^{10}([(\lambda 0.4 + (1-\lambda)1.2)\ 0.7\ 1.3], v),\\ \Delta_{e_5} &= \Delta^{10}([\ 0.4\ (\lambda 0.3 + (1-\lambda)0.7)\ 0.7], v),\\ \Delta_{e_6} &= \Delta^{10}([\ 0.4\ (\lambda 0.3 + (1-\lambda)0.7)\ 1.3], v),\\ \Delta_{e_7} &= \Delta^{10}([\ 1.2\ (\lambda 0.3 + (1-\lambda)0.7)\ 0.7], v),\\ \Delta_{e_8} &= \Delta^{10}([\ 1.2\ (\lambda 0.3 + (1-\lambda)0.7)\ 1.3], v),\\ \Delta_{e_9} &= \Delta^{10}([\ 0.4\ \ 0.3\ (\lambda 0.7 + (1-\lambda)1.3)], v),\\ \Delta_{e_{10}} &= \Delta^{10}([\ 0.4\ \ 0.7\ (\lambda 0.7 + (1-\lambda)1.3)], v),\\ \Delta_{e_{11}} &= \Delta^{10}([\ 1.2\ \ 0.3\ (\lambda 0.7 + (1-\lambda)1.3)], v),\\ \Delta_{e_{12}} &= \Delta^{10}([\ 1.2\ \ 0.7\ (\lambda 0.7 + (1-\lambda)1.3)], v)\}.\end{aligned}$$

Figs. 6 (a) and 6 (b) show roots of vertex and edge polynomials of A in the first Riemann sheet. Roots of vertex polynomials are indicated by blue asterisks. Roots of minimum argument vertex and connected edge polynomial are indicated by red dots in complex v plane. Minimum argument root is the root of vertex polynomial $\Delta_{u_6} = \Delta^{10}([1.2\ 0.3\ 1.3], v)$ and the value of minimum argument is $\phi_{\min} = \min\{\arg(R(\Omega))\} = 0.0487$ radian. Since it is lower than the stability boundary $\phi_s = \frac{\pi}{20}$, the interval system is not robust stable.

Fig. 7 shows step response of 8 vertex polynomials. The step response obtained for $u_6 = [1.2\ 0.3\ 1.3]$ confirms the unstable response of the interval system.

Example 2. By considering the closed loop control of electrical heater, which was modeled by fractional order plant function, $G(s) = \frac{Y(s)}{U(s)} = \frac{1}{39.96s^{1.25}+0.598}$, and the integer

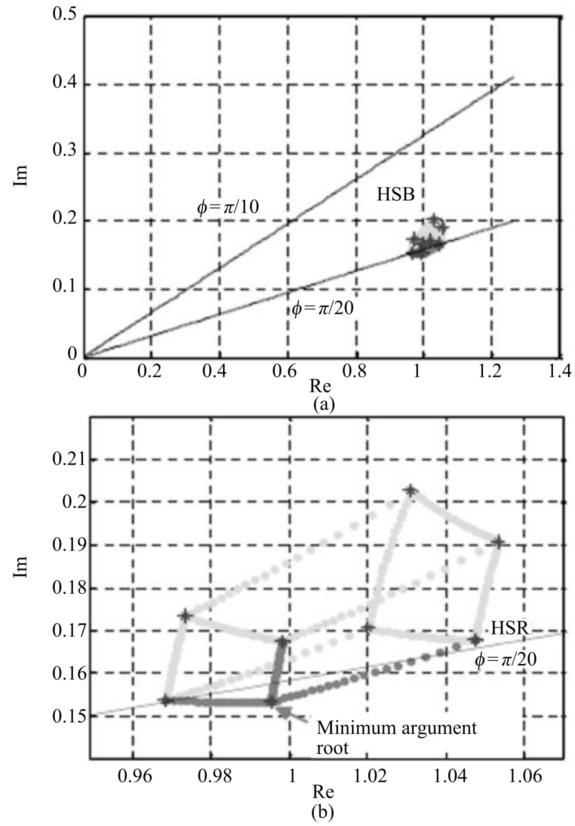

Fig. 6. Root placement for Example 1 ((a) Roots of vertex and edge polynomials; (b) Close view of minimum argument vertex and connected edge polynomials.)

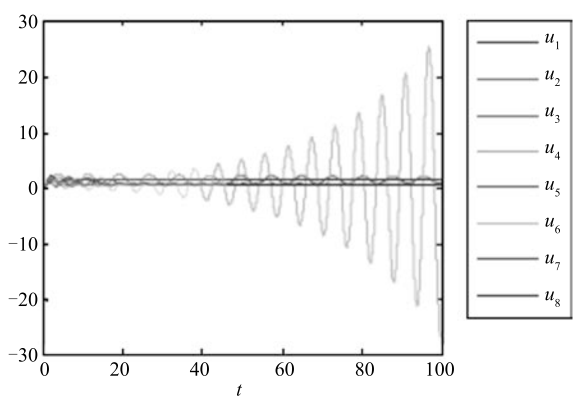

Fig. 7. Step responses of vertex polynomials.

order PD controller, $C(s) = 64.47 + 12.46s$[3], let us check robust stability of closed loop control system for interval uncertainty given as the following:

For electrical heater model, parameter deviations are 39.96 $\pm$ 5.3 = [34.66 45.26] and $0.58 \pm 0.12 = [0.46\ 0.7]$, and for the controller function, parameter deviations are 64.47 ± 11.5 = [52.97 75.97] and $12.46 \pm 3.36 = [9.10\ 15.82]$.

The resulting closed loop transfer function of interval system becomes,

$$\begin{aligned}T(s) &= \frac{Y(s)}{U(s)}\\ &= \frac{[9.10\ \ 15.82]s + [52.97\ \ 75.97]}{[34.66\ \ 45.26]s^{1.25} + [9.10\ \ 15.82]s + [53.43\ \ 76.67]},\end{aligned} \quad (21)$$

and then characteristic polynomial of the system can be expressed as,

$$\Delta(s) = [34.66\ \ 45.26]s^{1.25} + [9.10\ \ 15.82]s + [53.43\ \ 76.67]. \tag{22}$$

By applying $s = v^{100}$ mapping, the expanded degree integer order characteristic polynomial is written as,

$$\begin{aligned}\Delta^{100}(v) = {} & [34.66\ \ 45.26]v^{125} + [9.10\ \ 15.82]v^{100} \\ & + [53.43\ \ 76.67]. \end{aligned}\tag{23}$$

Vertex polynomials of expanded degree integer order interval characteristic polynomial were obtained as

$$\begin{aligned}\{\Delta_{u_1} &= \Delta^{100}([34.66\ 9.10\ 53.43], v),\\ \Delta_{u_2} &= \Delta^{100}([34.66\ 9.10\ 76.67], v),\\ \Delta_{u_3} &= \Delta^{100}([34.66\ 15.83\ 53.43], v),\\ \Delta_{u_4} &= \Delta^{100}([34.66\ 15.83\ 76.67], v),\\ \Delta_{u_5} &= \Delta^{100}([45.26\ 9.10\ 53.43], v),\\ \Delta_{u_6} &= \Delta^{100}([45.26\ 9.10\ 76.67], v),\\ \Delta_{u_7} &= \Delta^{100}([45.26\ 15.82\ 53.43], v),\\ \Delta_{u_8} &= \Delta^{100}([45.26\ 15.82\ 76.67], v)\}.\end{aligned}$$

We used 19 polynomials edge sampling ($n_p = 19$) in numerical analyses. Set of edge polynomials can be written as,

$$\begin{aligned}\{\Delta_{e_1} &= \Delta^{100}([(\lambda 34.66 + (1-\lambda)45.26)\ 9.10\ 53.43], v),\\ \Delta_{e_2} &= \Delta^{100}([(\lambda 34.66 + (1-\lambda)45.26)\ 9.10\ 76.67], v),\\ \Delta_{e_3} &= \Delta^{100}([(\lambda 34.66 + (1-\lambda)45.26)\ 15.82\ 53.43], v),\\ \Delta_{e_4} &= \Delta^{100}([(\lambda 34.66 + (1-\lambda)45.26)\ 15.82\ 76.67], v),\\ \Delta_{e_5} &= \Delta^{100}([\ 34.66\ (\lambda 9.10 + (1-\lambda)\ 15.82)\ 53.43], v),\\ \Delta_{e_6} &= \Delta^{100}([\ 34.66\ (\lambda 9.10 + (1-\lambda)\ 15.82)\ 76.67], v),\\ \Delta_{e_7} &= \Delta^{100}([\ 45.26\ (\lambda 9.10 + (1-\lambda)\ 15.82)\ 53.43], v),\\ \Delta_{e_8} &= \Delta^{100}([\ 45.26\ (\lambda 9.10 + (1-\lambda)\ 15.82)\ 76.67], v),\\ \Delta_{e_9} &= \Delta^{100}([\ 34.66\ 9.10\ (\lambda 53.43 + (1-\lambda)\ 76.67)\ ], v),\\ \Delta_{e_{10}} &= \Delta^{100}([\ 34.66\ 15.82\ (\lambda 53.43 + (1-\lambda)\ 76.67)\ ], v),\\ \Delta_{e_{11}} &= \Delta^{100}([\ 45.26\ 9.10\ (\lambda 53.43 + (1-\lambda)\ 76.67)\ ], v),\\ \Delta_{e_{12}} &= \Delta^{100}([\ 45.26\ 15.82\ (\lambda 53.43 + (1-\lambda)\ 76.67)\ ], v)\}.\end{aligned}$$

Figs. 8 (a) and 8 (b) show roots of vertex and edge polynomials in the first Riemann sheet. Minimum argument root is the root of vertex polynomial $\Delta_{u_6} = \Delta^{100}([45.26\ \ 9.10\ \ 76.67],\ v)$ and the value of minimum argument is $\phi_{\min} = \min\{\arg(R(\Omega))\} = 0.0259$ radian. Since minimum argument root lies in HSR defined with the root argument interval $(\pi/200,\ \pi/100]$, the interval system is robust stable.

Fig. 9 shows step responses of 8 vertex polynomials and confirms robust stability of the closed loop electrical heater control system for the given parameter deviation ranges.

Example 3. By considering the closed loop electrical heater control system given in previous example as the plant function $G(s) = \frac{Y(s)}{U(s)} = \frac{1}{39.96s^{1.25}+0.598}$ and PD controller of system, $C(s) = 64.47 + 12.46s$. By using edge theorem approaches, let us find out interval uncertainly ranges of γ that make the closed loop control system robust stable.

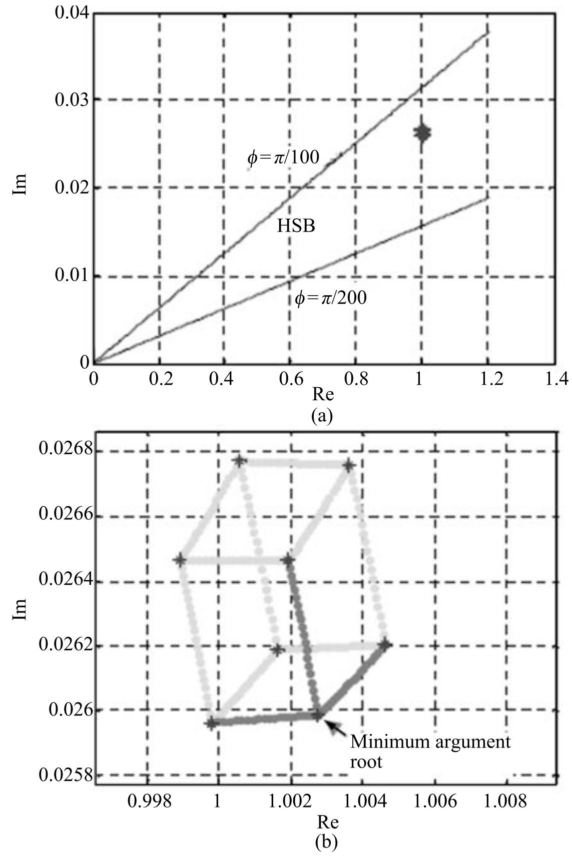

Fig. 8. Root placement for Example 2 ((a) Roots of vertex and edge polynomials; (b) Close view of minimum argument vertex and connected edge polynomials.)

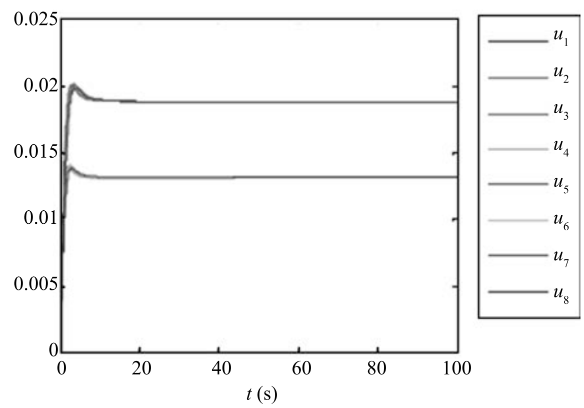

Fig. 9. Step responses of vertex polynomials.

It is convenient to write closed loop transfer function of system:

$$\begin{aligned}T(s) &= \frac{Y(s)}{U(s)}\\ &= \frac{12.46s + 64.47}{(39.96 \pm \gamma)s^{1.25} + (12.46 \pm \gamma)s + (65.068 \pm \gamma)}.\end{aligned}\tag{24}$$

Then, the characteristic polynomial was obtained as,

$$\Delta(s) = (39.96 \pm \gamma)\ s^{1.25} + (12.46 \pm \gamma)s + (65.068 \pm \gamma). \tag{25}$$

By applying $s = v^{100}$ mapping, the expanded degree integer order characteristic polynomial is written as,

$$\Delta^{100}(v) = (39.96 \pm \gamma)\ v^{125} + (12.46 \pm \gamma) v^{100} + (65.068 \pm \gamma). \tag{26}$$

Vertex polynomials of expanded degree integer order interval characteristic polynomial were obtained as

$$\begin{aligned}
\{\Delta_{u_1} &= \Delta^{100}([(39.96-\gamma)\ (12.46-\gamma)\ (65.068-\gamma)], v),\\
\Delta_{u_2} &= \Delta^{100}([(39.96-\gamma)\ (12.46-\gamma)\ (65.068+\gamma)], v),\\
\Delta_{u_3} &= \Delta^{100}([(39.96-\gamma)\ (12.46+\gamma)\ (65.068-\gamma)], v),\\
\Delta_{u_4} &= \Delta^{100}([(39.96-\gamma)\ (12.46+\gamma)\ (65.068+\gamma)], v),\\
\Delta_{u_5} &= \Delta^{100}([(39.96+\gamma)\ (12.46-\gamma)\ (65.068-\gamma)], v),\\
\Delta_{u_6} &= \Delta^{100}([(39.96+\gamma)\ (12.46-\gamma)\ (65.068+\gamma)], v),\\
\Delta_{u_7} &= \Delta^{100}([(39.96+\gamma)\ (12.46+\gamma)\ (65.068-\gamma)], v),\\
\Delta_{u_8} &= \Delta^{100}([(39.96+\gamma)\ (12.46+\gamma)\ (65.068+\gamma)], v)\}.
\end{aligned}$$

We used 19 polynomials edge sampling. Then, edge polynomials were obtained as,

$$\begin{aligned}
\{\Delta_{e_1} &= \Delta^{100}([(\lambda(39.96-\gamma)\\
&\quad + (1-\lambda)(39.96+\gamma))(12.46-\gamma)(65.068-\gamma)], v),\\
\Delta_{e_2} &= \Delta^{100}([(\lambda(39.96-\gamma)\\
&\quad + (1-\lambda)(39.96+\gamma))(12.46-\gamma)(65.068+\gamma)], v),\\
\Delta_{e_3} &= \Delta^{100}([(\lambda(39.96-\gamma)\\
&\quad + (1-\lambda)(39.96+\gamma))(12.46+\gamma)(65.068-\gamma)], v),\\
\Delta_{e_4} &= \Delta^{100}([(\lambda(39.96-\gamma)\\
&\quad + (1-\lambda)(39.96+\gamma))(12.46+\gamma)(65.068+\gamma)], v),\\
\Delta_{e_5} &= \Delta^{100}([(39.96-\gamma)(\lambda(12.46-\gamma)\\
&\quad + (1-\lambda)(12.46+\gamma))(65.068-\gamma)], v),\\
\Delta_{e_6} &= \Delta^{100}([(39.96-\gamma)(\lambda(12.46-\gamma)\\
&\quad + (1-\lambda)(12.46+\gamma))(65.068+\gamma)], v),\\
\Delta_{e_7} &= \Delta^{100}([(39.96+\gamma)(\lambda(12.46-\gamma)\\
&\quad + (1-\lambda)(12.46+\gamma))(65.068-\gamma)], v),\\
\Delta_{e_8} &= \Delta^{100}([(39.96+\gamma)(\lambda(12.46-\gamma)\\
&\quad + (1-\lambda)(12.46+\gamma))(65.068+\gamma)], v),\\
\Delta_{e_9} &= \Delta^{100}([(39.96-\gamma)(12.46-\gamma)(\lambda(65.068-\gamma)\\
&\quad + (1-\lambda)(65.068+\gamma)\ )], v),\\
\Delta_{e_{10}} &= \Delta^{100}([(39.96-\gamma)(12.46+\gamma)(\lambda(65.068-\gamma)\\
&\quad + (1-\lambda)(65.068+\gamma)\ )], v),\\
\Delta_{e_{11}} &= \Delta^{100}([[(39.96+\gamma)(12.46-\gamma)(\lambda(65.068-\gamma)\\
&\quad + (1-\lambda)(65.068+\gamma)\ )], v),\\
\Delta_{e_{12}} &= \Delta^{100}([(39.96+\gamma)(12.46+\gamma)(\lambda(65.068-\gamma)\\
&\quad + (1-\lambda)(65.068+\gamma)\ )], v)\}.
\end{aligned}$$

Figs. 10 (a)-10 (h) show roots of vertex and edge polynomials in the first Riemann sheet for various values of γ. Table II lists minimum argument of vertex roots with respect to value of γ. Graphical results shown in Fig.10 indicate that interval uncertain control system is robust stable for $\gamma \leq 27$.

In this example, all edge and vertex polynomials (AEAV) method[14] requires the test of 236 polynomials ($19.3.2^2+2^3$), minimum argument vertex with connected edge polynomials (MVCE) method requires the test of 65 polynomials ($19.3+2^3$) and minimum argument vertex polynomials (MV) method requires the test of 8 polynomials (2^3). Examples numerically reveal that MVCE and MV can reduce computational complexity of robust stability analysis based on edge theorem; however there is need for theoretical verification of basic assumptions of MVCE and MV approaches.

VI. Conclusions

This study confirms that Hurwitz stability analysis of fractional order characteristic polynomials is valid in v plane under power mapping. As known, it is difficult to calculate root locus of fractional order characteristic polynomials in s domain. The $s = v^m$ power mapping significantly simplifies stability analyses of fractional order polynomials. The problem turns into the Hurwitz stability analysis of expanded degree integer order polynomials in the first Riemann sheet.

It is important to investigate impacts of power mapping on root locus and stability related properties. Preliminarily, this paper revealed properties of $s = v^m$ mapping related with stability analysis and root locus: It was shown that root argument and magnitude relations are conserved under power mapping. This is an important remark of power mapping that leads to conformity of root locus analysis given in v plane for the fractional order systems defined in s plane. The conservation of argument and magnitude relations leads to conservation of the geometrical properties of root constellation under power mapping transformations between complex s and v planes. Thus, the minimum argument root of expanded degree integer order polynomials in complex v plane is also

TABLE II

MINIMUM ARGUMENT OF VERTEX POLYNOMIAL ROOTS AND SYSTEM STABILITY FOR VARIOUS γ

Value of γ	Minimum angle vertex polynomial number (1-8)	Minimum argument of vertex polynomials (Radian)	Robust stability
1	6	0.0263	Stable
5	6	0.0258	Stable
10	6	0.0254	Stable
15	1	0.0246	Stable
20	1	0.0231	Stable
25	1	0.0193	Stable
27	1	0.0158	Stable
28	1	0.0128	Unstable

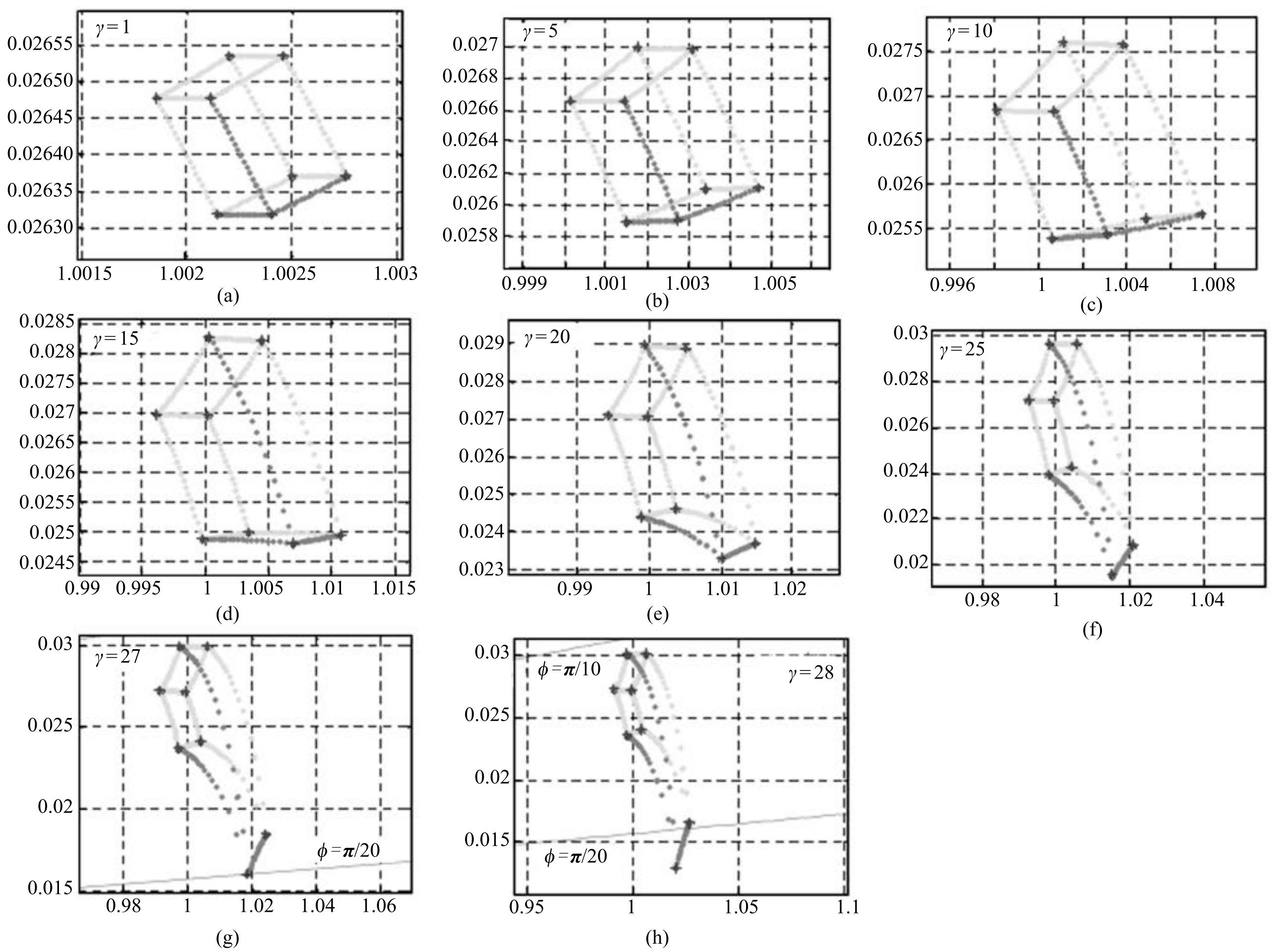

Fig. 10. Root regions of vertex and edge polynomials in the first Riemann sheet for (a) $\gamma = 1$, (b) $\gamma = 5$, (c) $\gamma = 10$, (d) $\gamma = 15$, (e) $\gamma = 20$, (f) $\gamma = 25$, (g) $\gamma = 27$ and (h) $\gamma = 28$.

minimum argument root of fractional order polynomial in the s plane. This property provides the validity of Hurwitz stability and implication of edge theorem under power mapping and it makes possible the robust stability analysis of fractional order interval polynomials according to robust stability of expanded degree integer order polynomials complex v plane.

To utilize edge theorem based approach for robust stability analysis of fractional order control systems. Author numerically demonstrated two robust stability analysis approaches based on minimum root argument analyses of vertex and exposed edge polynomials in v plane. These approaches were shown to reduce the number of test polynomials for the parametric robust stability analyses of fractional order systems. It was observed in numerical calculations that the test of only vertex polynomials can significantly reduce computational complexity of robust stability analyses for interval characteristic polynomials with positive real coefficients. It should be noted that results are valid under the assumption that minimum argument root comes from vertex and/or connected edge polynomials of hyper-rectangle. Results of numerical examples confirm the validity of this assumption. However, there is need for a future study addressing properties of zeros in polynomial arithmetics for the theoretical proof of this assumption.

This study contributes to advance our understanding on implications of power mapping for root locus and stability properties of fractional order systems.

References

[1] Bhattacharyya S P, Keel L H, Chapellat H. *Robust Control: The Parametric Approach*. Englewood Cliffs, NJ: Prentice Hall, 1995. 269−291

[2] Monje C A, Chen Y Q, Vinagre B M, Xue D Y, Feliu-Batlle V. *Fractional-order Systems and Controls: Fundamentals and Applications*. London: Springer, 2010.

[3] Petráš I. Stability of fractional-order systems with rational orders: a survey. *Fractional Calculus and Applied Analysis*, 2009, **12**(3): 269−298

[4] Das S. *Functional Fractional Calculus* (Second edition). Berlin: Springer, 2011.

[5] Chen Y Q, Ahn H S, Podlubny I. Robust stability check of fractional order linear time invariant systems with interval uncertainties. *Signal Processing*, 2006, **86**(10): 2611−2618

[6] Ahn H S, Chen Y Q, Podlubny I. Robust stability test of a class of linear time-invariant interval fractional-order system using Lyapunov inequality. *Applied Mathematics and Computation*, 2007, **187**(1): 27−34

[7] Ahn H S, Chen Y Q. Necessary and sufficient stability condition of fractional-order interval linear systems. *Automatica*, 2008, **44**(11): 2985−2988

[8] Lu J G, Chen G R. Robust stability and stabilization of fractional-order interval systems: an LMI approach. *IEEE Transactions on Automatic Control*, 2009, **54**(6): 1294−1299

[9] N'Doye I, Darouach M, Zasadzinski M, Radhy N E. Robust stabilization of uncertain descriptor fractional-order systems. *Automatica*, 2013, **49**(6): 1907−1913

[10] Petráš I, Chen Y Q, Vinagre B M. A robust stability test procedure for a class of uncertain LTI fractional order systems. In: Proceedings of the 2002 International Carpathian Control Conference ICCC'2002. Malenovice, Czech Republic, 2002. 247−252

[11] Petráš I, Chen Y Q, Vinagre B M. Robust stability test for interval fractional order linear systems. *Unsolved Problems in Mathematical Systems and Control Theory*. Princeton, NJ: Princeton University Press, 2004. 208−210

[12] Lu J G, Chen Y Q. Robust stability and stabilization of fractional-order interval systems with the fractional order α: The $0 \ll \alpha \ll 1$ case. *IEEE Transactions on Automatic Control*, 2010, **55**(1): 152−158

[13] Radwan A G, Soliman A M, Elwakil A S, Sedeek A. On the stability of linear systems with fractional-order elements. *Chaos, Solitons and Fractals*, 2009, **40**(5): 2317−2328

[14] Senol B, Ates A, Alagoz B B, Yeroglu C. A numerical investigation for robust stability of fractional-order uncertain systems. *ISA Transactions*, 2014, **53**(2): 189−198

[15] Matignon D. Stability results for fractional differential equations with applications to control processing. In: Proceedings of the 1996 Computational Engineering in Systems Applications. Lille, France, 1996. 963−968

[16] Minnichelli R J, Anagnost J J, Desoer C A. An elementary proof of Kharitonov's stability theorem with extensions. *IEEE Transactions on Automatic Control*, 1989, **34**(9): 995−998

[17] Podlubny I. *Fractional Differential Equations*. San Diego: Academic Press, 1999.

[18] Xue D Y, Chen Y Q. *Modeling, Analysis and Design of Control Systems in MATLAB and Simulink*. River Edge, NJ, USA: World Scientific Publishing Company, 2014.

[19] Caponetto R, Dongola G, Fortuna L, Petras I. *Fractional Order Systems: Modeling and Control Applications*. Singapore: World Scientific Publishing Company, 2010.

[20] Sheil-Small T. *Complex Polynomials*. Cambridge, UK: Cambridge University Press, 2002.

Baris Baykant Alagoz is working at the Computer Engineering Department in Inonu University. He received the bachelor degree in the Department of Electronics and Communication Engineering, Istanbul Technical University, in 1998, M. S. and Ph. D. degrees in the Department of Electrical-Electronics Engineering, Inonu University, in 2011 and 2015, respectively. His research interests include modeling and simulation of physical systems, control systems, and smart grid.

Criteria for Response Monotonicity Preserving in Approximation of Fractional Order Systems

Mohammad Saleh Tavazoei, *Member, IEEE*

***Abstract*—In approximation of fractional order systems, a significant objective is to preserve the important properties of the original system. The monotonicity of time/frequency responses is one of these properties whose preservation is of great importance in approximation process. Considering this importance, the issues of monotonicity preservation of the step response and monotonicity preservation of the magnitude-frequency response are independently investigated in this paper. In these investigations, some conditions on approximating filters of fractional operators are found to guarantee the preservation of step/magnitude-frequency response monotonicity in approximation process. These conditions are also simplified in some special cases. In addition, numerical simulation results are presented to show the usefulness of the obtained conditions.**

***Index Terms*—Fractional order system, approximation, step response, magnitude-frequency response, monotonicity**

I. INTRODUCTION

THESE days, fractional calculus[1] has found a widespread use in facilitating and dealing with different engineering challenges. On the basis of using fractional order dynamics[2], effective solutions have been proposed for some engineering problems[3] in different fields such as control system design[4−5], system identification[6−7], analysis and synthesis of electrical circuits[8−10], image and signal processing[11−12], robotics[13], electromagnetics[14], biomedical informatics[15], vibration reduction[16−17], wave propagation[18], and viscoelasticity[19].

In practice, sometimes there is a need to approximate fractional order systems. Consequently till now, different useful methods have been proposed for approximating fractional operators (for some sample methods, see [20−26]). But a main concern in using approximation methods is that the significant properties of the original fractional order systems may not be preserved after approximation[27−29]. Considering the importance of preserving the properties of fractional order systems in approximation process, some studies on this subject have been done in literature. For example, the problem of stability preservation has been investigated in [30−31] for methods presenting rational continuous-time filters for approximation of fractional operators. Also, the approximation methods constructed based on the direct discretization of fractional operators have been analyzed in the viewpoint of stability preservation in [32]. In this paper, the aim is to investigate the problem of response monotonicity preserving in approximation of fractional order systems by using rational approximations of fractional operators. Monotonicity of the step response is known as a feature for dynamical systems having desired transient responses[33−37]. Also, a necessary condition to have desired transient response in linear time invariant dynamical systems is monotonicity of the magnitude-frequency response[38]. Considering these points, dynamical systems with monotonic time/frequency responses have been taken into consideration in different applications[33−40]. In these applications, if we deal with a fractional order dynamical system with monotonic time/frequency response (for example in fractional order control system design or in fractional order filter synthesis with the aim of achieving a desired transient response)[41−43], approximating such a system may be unavoidable in practice. In this case, due to the significance of the property of response monotonicity, preserving such a property in approximation process is of great importance. In this paper, general conditions on rational approximations of fractional operators are derived that guarantee the preservation of monotonicity property of the step response or the magnitude-frequency response in approximation process.

The paper is organized as follows. In Section II, some preliminaries on approximation of fractional order systems are presented. Conditions for guaranteeing the preservation of the monotonicity property of the step response and the magnitude-frequency response in approximation of fractional order systems are respectively obtained in Sections III and IV. In these sections, numerical simulation results are also presented to confirm the usefulness of the obtained conditions. Finally, conclusions in Section V close the paper.

II. RATIONAL APPROXIMATION OF FRACTIONAL ORDER SYSTEMS

Consider a SISO LTI fractional order system described by the following pseudo-state space equations

$$\begin{cases} {}_0D_t^{\alpha}x(t) = Ax(t) + Bu(t), \\ y(t) = Cx(t), \end{cases} \tag{1}$$

where $u(t) \in \mathbf{R}$, $y(t) \in \mathbf{R}$, and $x(t) \in \mathbf{R}^n$ are respectively the input, output, and pseudo-state vector of the system[44]. Also, $A \in \mathbf{R}^{n\times n}$, $B \in \mathbf{R}^{n\times 1}$, $C \in \mathbf{R}^{1\times n}$, $\alpha \in (0,1)$, and ${}_0D_t^{\alpha}$ denotes the Caputo derivative operator defined by

Manuscript received August 24, 2015; accepted April 16, 2016. This work was supported by the Research Council of Sharif University of Technology (G930720). Recommended by Associate Editor Dingyü Xue.

Citation: Mohammad Saleh Tavazoei. Criteria for response monotonicity preserving in approximation of fractional order systems. *IEEE/CAA Journal of Automatica Sinica*, 2016, 3(4): 422−429

Mohammad Saleh Tavazoei is with the Electrical Engineering Department, Sharif University of Technology, Tehran 11365-9363, Iran (e-mail: tavazoei@sharif.edu).

Color versions of one or more of the figures in this paper are available online at http://ieeexplore.ieee.org.

$$ {}_0D_t^{\alpha}x(t) = \frac{1}{\Gamma(1-\alpha)}\int_0^t \frac{x'(\tau)}{(t-\tau)^{\alpha}}\mathrm{d}\tau, \quad \alpha \in (0,1). \tag{2}$$

It is worth noting that (1) is the fractional order counterpart of the integer order system

$$\begin{cases} \dot{x}(t) = Ax(t) + Bu(t), \\ y(t) = Cx(t). \end{cases} \tag{3}$$

The transfer function from input $u(t)$ to output $y(t)$ in system (1) is given as follows (See Fig. 1).

$$G(s^{\alpha}) = C\left(s^{\alpha}I - A\right)^{-1}B. \tag{4}$$

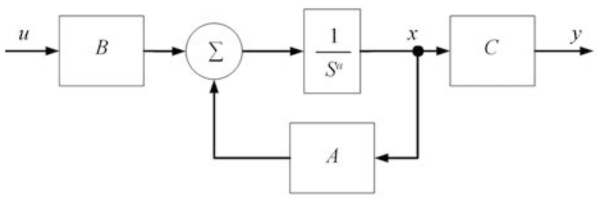

Fig. 1. Block diagram of pseudo-state space system (1).

A common way for approximating fractional order system (1) is to approximate and replace the operator $1/s^{\alpha}$ in block diagram of Fig. 1 by a rational transfer function (Fig. 2)[45]. Assume that the following approximation

$$s^{\alpha} \approx P(s), \tag{5}$$

where

$$P(s) = \frac{b_m s^m + b_{m-1}s^{m-1} + \cdots + b_1 s + b_0}{s^m + a_{m-1}s^{m-1} + \cdots + a_1 s + a_0}, \tag{6}$$

$a_i \geq 0$ for $i = 0, 1, \ldots, m-1$ and $b_i \geq 0$ for $i = 0, 1, ..., m$, is used for approximating fractional order system (1). In this case, the approximated system will be described by rational transfer function $G(P(s))$.

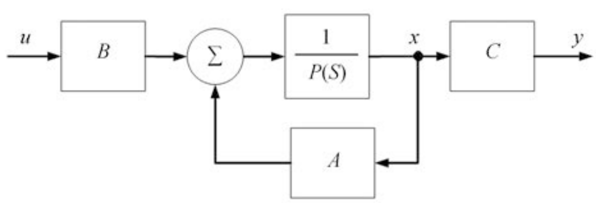

Fig. 2. Block diagram of the approximated integer order system for fractional order system (1) obtained by using approximation (5).

Preservation of the principal properties of the system is an important issue which should be taken into consideration in the approximation process. Considering this importance, on the basis of comparing the stability conditions of the original system (1) and its rational approximation, the stability preservation problem has been previously studied in [31–32]. In this paper, we focus on the monotonicity preservation problem for the time/frequency responses, and obtain conditions on approximation (5) for guaranteeing the preservation of the response monotonicity. Satisfying these conditions guarantees that the monotonicity of the system response is preserved in approximation process, i.e., the approximated integer order system similar as the original fractional order system has a monotonic time/frequency response. The main feature of the conditions obtained in the next sections is the independency of these conditions from the original system dynamics.

III. Step Response Monotonicity

A. Preliminaries

Consider a BIBO stable system described by transfer function $H(s)$. According to the Post-Widder inversion formula[46], the impulse response of this system $(h(t))$, as the inverse Laplace transform of $H(s)$, is given by

$$h(t) = \lim_{k\to\infty}\frac{(-1)^k}{k!}\left(\frac{k+1}{t}\right)^{k+1}H^{(k)}\left(\frac{k+1}{t}\right), \tag{7}$$

where $H^{(k)}(s)$ denotes the $k-th$ derivative of $H(s)$. An interesting consequence of the Post-Widder inversion formula, which has been taken into consideration in the literature[47], is about non-negativeness of the impulse response. According to this formula, if the BIBO stable transfer function $H(s)$ satisfies condition

$$(-1)^r\, H^{(r)}(s)\Big|_{s=\sigma} \geq 0, \tag{8}$$

for r = 1, 2, …and all positive real values of σ, then its impulse response is non-negative for $t > 0$. Conversely, by considering the Laplace transform definition, i.e.

$$H(s) = \int_0^{\infty} \mathrm{e}^{-st}h(t)\,\mathrm{d}t, \tag{9}$$

it is deduced that

$$(-1)^r H^{(r)}(\sigma) = \int_0^{\infty} \mathrm{e}^{-\sigma t}t^r h(t)\,\mathrm{d}t, \tag{10}$$

for $\sigma > 0$, where $H(s)$ is a BIBO stable transfer function with the impulse response $h(t)$. Therefore, if $h(t)$ is non-negative, then condition (8) is satisfied for r = 1, 2, …, and all positive real values of σ[47].

B. Criteria for Step Response Monotonicity

This subsection deals with finding conditions on approximation filter (6) to guarantee monotonicity of the step response. Firstly, the monotonicity condition is derived in a general case (Theorem 1), and then this condition is simplified in some special cases (Corollaries 1-3). In addition, numerical examples are presented to validate the obtained results.

For obtaining the results in this subsection, it is assumed that the original system $(G(s^{\alpha}))$, the approximating filter $(P(s))$, and the approximated system $(G(P(s)))$ are BIBO stable (the conditions on approximating filter $(P(s))$ to preserve the stability of the system in the approximation process can be found in [31]). Now, as a first result consider the following theorem presenting a condition to guarantee the step response monotonicity in the approximation process.

Theorem 1. Assume that system (1) has a monotonic non-decreasing step response. The monotonicity of the step response is preserved by using rational approximation (5) if

$$(-1)^k\, \tilde{P}^{(k)}(s)\Big|_{s=\sigma} \leq 0, \tag{11}$$

for all positive real values of σ and $k \in \mathbf{N}$, where $\tilde{P}(s) = P^{1/\alpha}(s)$.

Proof. Since the BIBO stable system (1) has a monotonic non-decreasing step response, according to discussions of Section III-A

$$(-1)^k \hat{G}^{(k)}(s)\Big|_{s=\sigma} \geq 0, \tag{12}$$

for all $k \in \mathbf{N}$ and $\sigma > 0$ where $\hat{G}(s) = G(s^\alpha) = C(s^\alpha I - A)^{-1}B$. By using the rational approximation (5), the approximated system is described by transfer function $\hat{G}(P^{1/\alpha}(s)) = \hat{G}(\tilde{P}(s))$. According to the Faàdi Bruno's formula (generalization of the chain rule for higher derivatives)[48], the r-th ($r \in \mathbf{N}$) derivative of this transfer function with respect to is given by

$$\frac{\mathrm{d}^r}{\mathrm{d}s^r}\hat{G}\left(\tilde{P}(s)\right) = \sum \frac{r!}{k_1!\, k_2!\, \cdots\, k_r! 1!^{k_1} 2!^{k_2} \cdots r!^{k_r}} \times \hat{G}^{(k_1+k_2+\cdots+k_r)}(x)\Big|_{x=\tilde{P}(s)} \prod_{i=1}^{r}\left(\tilde{P}^{(i)}(s)\right)^{k_i}, \tag{13}$$

where the sum appeared in the right-hand side of (13) is over all r-tuples of non-negative integers satisfying the Diophantine equation

$$k_1 + 2k_2 + \cdots + rk_r = r. \tag{14}$$

The Diophantine equation (14) yields in $\prod_{i=1}^{r}\left((-1)^i\tilde{P}^{(i)}(s)\right)^{k_i} = (-1)^r \prod_{i=1}^{r}\left((-1)^i \tilde{P}^{(i)}(s)\right)^{k_i}$. From this equality and (13),

$$(-1)^r \frac{\mathrm{d}^r}{\mathrm{d}s^r}\hat{G}\left(\tilde{P}(s)\right) = \sum \frac{r!}{k_1!\, k_2! \ldots k_r! 1!^{k_1} 2!^{k_2} \cdots r!^{k_r}} \times \hat{G}^{(k_1+k_2+\cdots+k_r)}(x)\Big|_{x=\tilde{P}(s)} \prod_{i=1}^{r}\left((-1)^i \tilde{P}^{(i)}(s)\right)^{k_i}. \tag{15}$$

If condition (11) is satisfied for all $\sigma > 0$ and $k \in \mathbf{N}$, then $\left((-1)^i\, \tilde{P}^{(i)}(s)\Big|_{s=\sigma}\right)^{k_i}$ and $(-1)^{k_i}$ have the same signs for each $\sigma > 0$ and non-negative integer k_i. Considering this fact and (15), it is deduced that $(-1)^r \frac{\mathrm{d}^r}{\mathrm{d}s^r}\hat{G}\left(\tilde{P}(s)\right)\Big|_{s=\sigma}$ and $(-1)^{k_1+k_2+\cdots+k_r}\hat{G}^{(k_1+k_2+\cdots+k_r)}(x)\Big|_{x=\tilde{P}(\sigma)}$ have the same signs for all $\sigma > 0$. Hence, from (12) it is found that

$$(-1)^r \frac{\mathrm{d}^r}{\mathrm{d}s^r}\hat{G}\left(\tilde{P}(s)\right)\Big|_{s=\sigma} \geq 0, \tag{16}$$

for all $r \in \mathbf{N}$ and $\sigma > 0$. According to (16) and the Post-Widder inversion formula, it is concluded that the BIBO stable system $\hat{G}(\tilde{P}(s))$ (approximated system) has a monotonic non-decreasing step response. □

If α = $1/N$ where $N \in \mathbf{N}$, condition (11) is written as

$$(-1)^k \left(P^N(s)\right)^{(k)}\Big|_{s=\sigma} \leq 0. \tag{17}$$

According to discussions of Section III-A, condition (17) is satisfied for all $k \in \mathbf{N}$, if the BIBO stable transfer function $-P^N(s)$ has a non-negative impulse response for $t > 0$. Consequently, since the impulse response of this transfer function is equal to the negative of the impulse response of transfer function $P^N(s)$, the following corollary is deduced from Theorem 1.

Corollary 1. Assume that $\alpha = 1/N$ ($N \in \mathbf{N}$), and the step response of system (1) is monotonic non-decreasing. In this case, the monotonicity of the step response of system (1) is preserved by using rational approximation (5) if the rational transfer function $P^N(s)$ has a non-positive impulse response for $t > 0$.

Example 1. Consider the approximation $s^{0.5} \approx P(s)$ with (18), Shown at the bottom of the page, which is obtained by the low-frequency continued fraction method[49]. It can be verified that $P^2(s)$ has a non-positive impulse response for $t > 0$ (See Fig. 3). Hence, from Corollary 1 it is concluded that the step response monotonicity is preserved by using the above-mentioned approximation to approximate each fractional order system in the form (1) with α = 1/2 and a monotonic step response. For example, system (1) with α = 1/2, $A = \begin{bmatrix} -1.8 & -1 \\ 1 & 0 \end{bmatrix}$, $B = \begin{bmatrix} 1 & 0 \end{bmatrix}^{\mathrm{T}}$, and $C = [0\ 1]$ is a BIBO stable system having a monotonic step response. As shown in Fig. 4, the monotonicity of the step response of this system is preserved by using the above-mentioned approximation.

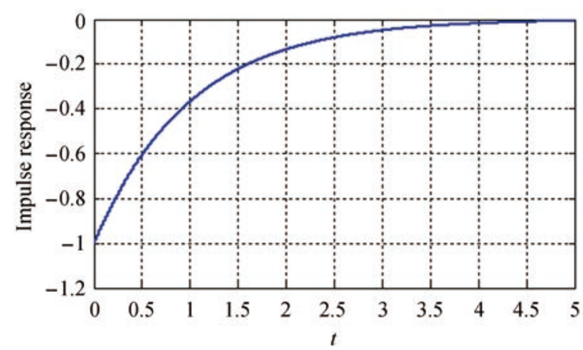

Fig. 3. Impulse response of $P^2(s)$ for $t > 0$ where $P(s)$ is defined by (18).

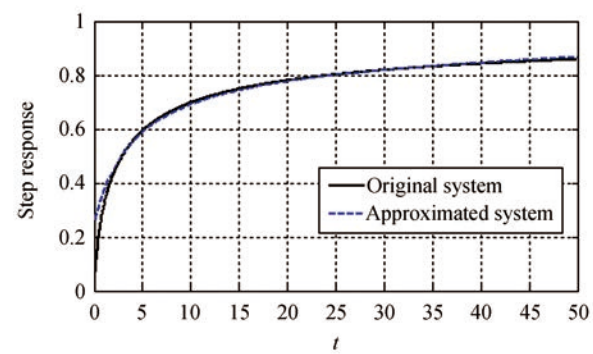

Fig. 4. Monotonic step responses of the original system and its approximation in Example 1.

$$P(s) = \frac{s(s+0.933)(s+0.75)(s+0.5)(s+0.25)(s+0.06699)}{(s+0.983)(s+0.8536)(s+0.6294)(s+0.3706)(s+0.1464)(s+0.01704)}, \tag{18}$$

According to [41, Theorem 3], we know that if (3) is a BIBO stable system with a monotonic step response, then (1) also has a monotonic step response. Hence in such a case, the monotonicity condition is reduced as that stated in the following corollary.

Corollary 2. Assume that the integer order system described by (3) is a BIBO stable system with a monotonic non-decreasing step response. In such a case, the step response of the approximation of system (1) obtained by using (5), similar as the step response of the original system (1), is monotonic if $P(s)$ has a non-positive impulse response for $t > 0$.

It is worth noting that the simple condition presented in Corollary 2 can be satisfied by a large class of rational approximations having interlaced real zeros and poles (For example, the rational approximations proposed in [21, 25, 51]). To show this fact, assume that the transfer function $P(s)$ described by

$$P(s) = k\frac{\prod\limits_{i=1}^{m}(s+z_i)}{\prod\limits_{i=1}^{m}(s+p_i)}, \tag{19}$$

where

$$k > 0 \ \& \ 0 \leq z_1 < p_1 < z_2 < p_2 < \cdots < z_m < p_m \tag{20}$$

is used for approximation of fractional operator s^{α} ($\alpha \in (0,1)$). If condition (20) holds, $P(s)$ can be rewritten as

$$P(s) = k + \sum_{i=1}^{m}\frac{r_i}{s+p_i}, \tag{21}$$

where $r_i < 0$ for $i = 1,...,m$ (See [50]). Since all r_i ($i = 1,...,m$) are negative, transfer function (19) has a non-positive impulse response for $t > 0$. Therefore, the following result is deduced.

Corollary 3. Let assumptions of Corollary 2 hold. Then, the monotonicity of step response is preserved by using approximation (5) if $P(s)$ is in the form (19) and satisfies conditions in (20).

For instance, the approximation methods proposed in [21, 25, 51] satisfy conditions of Corollary 3. Consequently, using these methods results in preservation of the step response monotonicity in approximation of fractional order systems having monotonic step responses.

Example 2. In [41, Example 1], the monotonicity of the step response of a fractional order system is shown. The pseudo-state space representation of the system considered in [41, Example 1] is in the form (1) with the following matrices

$$A = \begin{bmatrix} 0 & 1 & 0 & 0 & 0 & 0 & 0 \\ 0 & 0 & 1 & 0 & 0 & 0 & 0 \\ 0 & 0 & 0 & 1 & 0 & 0 & 0 \\ 0 & 0 & 0 & 0 & 1 & 0 & 0 \\ 0 & 0 & 0 & 0 & 0 & 1 & 0 \\ 0 & 0 & 0 & 0 & 0 & 0 & 1 \\ -0.1 & -1.05 & -4.55 & -10.53 & -14.07 & -11.05 & -4.9 \end{bmatrix},$$

$$B = \begin{bmatrix} 0 & 0 & 0 & 0 & 0 & 0 & 1 \end{bmatrix}^{\mathrm{T}},$$
$$C = \begin{bmatrix} 2 & 1 & 2 & 1 & 0 & 0 & 0 \end{bmatrix}.$$

The step response of this system in the case $\alpha = 0.9$ is shown in Fig. 5. If the approximation

$$s^{0.9} \approx \frac{501.1872(s+0.001259)(s+0.1259)(s+12.59)}{(s+0.07943)(s+7.943)(s+794.3)}, \tag{22}$$

obtained based on the CRONE method[51], is used for approximating the above-described system, according to Corollary 3 the monotonicity of the step response is preserved. The step response of the approximated system shown in Fig. 5 confirms this point.

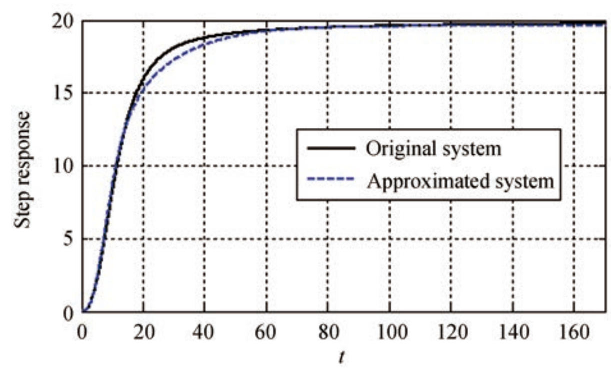

Fig. 5. Monotonic step responses of the original system and its approximation in Example 2.

IV. Magnitude-Frequency Response Monotonicity

The monotonicity of magnitude-frequency response of all-pole fractional order systems has been studied in [42]. In the mentioned study, algebraic conditions have been derived to guarantee the nonexistence of extrema in the magnitude-frequency response of an all-pole fractional order system. In continuation of the work done in [42], in this section it is assumed that (1) describes an all-pole transfer function in the form

$$G(s) = \frac{1}{\sum\limits_{k=0}^{n} d_k s^{k\alpha}}, \quad d_n > 0 \ \& \ d_k \geq 0 \text{ for } k = 0,...,n-1 \tag{23}$$

with the monotonic magnitude-frequency response $|G(\mathrm{j}\omega)|$ for $\omega \in (0,\infty)$. Considering this assumption, the following theorem presents conditions on the approximating filter $P(s)$ in (5) to preserve the monotonicity of the magnitude-frequency response of system (1) in the approximation process.

Theorem 2. The magnitude-frequency response monotonicity of any fractional order system in the form (1) with transfer function (23), which has a monotonic non-increasing magnitude-frequency response, is preserved in the frequency range (ω_i, ω_h) by approximating this system on the basis of approximation (5) if the following sets of conditions

$$\begin{cases} \min\limits_{c\in C^+} \frac{\Psi_c(\omega)}{\cos(\frac{c\alpha\pi}{2})} \geq 0, \\ \min\limits_{c\in C^+} \frac{\Psi_c(\omega)}{\cos(\frac{c\alpha\pi}{2})} \geq \max\limits_{c\in C^-} \frac{\Psi_c(\omega)}{\cos(\frac{c\alpha\pi}{2})}, \end{cases} \quad \forall \omega \in (\omega_l, \omega_h) \tag{24}$$

are satisfied where

$C^+ = \{c \in \{-n,...,n\} |\ \cos(\frac{c\alpha\pi}{2}) \geq 0\}$,

$C^- = \left\{c \in \{-n,...,n\} | \ \cos(\frac{c\alpha\pi}{2}) < 0\right\}$, and

$$\Psi_c(\omega) = \frac{\mathrm{d}\,|P(\mathrm{j}\omega)|}{\mathrm{d}\omega}\cos\left(c\measuredangle P(\mathrm{j}\omega)\right) - \frac{\mathrm{d}\measuredangle P(\mathrm{j}\omega)}{\mathrm{d}\omega}\,|P(\mathrm{j}\omega)|\sin\left(c\measuredangle P(\mathrm{j}\omega)\right). \quad (25)$$

Proof. It can be shown that if the magnitude-frequency response of transfer function (23) is monotonic non-increasing, then

$$f(\omega) \geq 0, \quad \forall\omega \in (0,\infty), \quad (26)$$

where $f(\omega)$ is defined as follows (For more details, see [42: Section 3]).

$$f(\omega) = \sum_{k=0}^{n}\sum_{l=0}^{n} kd_k d_l \cos\left(\frac{(k-l)\alpha\pi}{2}\right)\omega^{k+l-1}. \quad (27)$$

On the other hand, by using approximation (5) the magnitude-frequency response of the approximated system $G(P(s))$ is given by

$$|G\left(P(\mathrm{j}\omega)\right)| = \frac{1}{\sqrt{\rho(\omega)}}, \quad (28)$$

where

$$\rho(\omega) = \left(\sum_{k=0}^{n} d_k\,|P(\mathrm{j}\omega)|^k\cos\left(k\measuredangle P(\mathrm{j}\omega)\right)\right)^2 + \left(\sum_{k=0}^{n} d_k\,|P(\mathrm{j}\omega)|^k\sin\left(k\measuredangle P(\mathrm{j}\omega)\right)\right)^2. \quad (29)$$

The magnitude-frequency response of the approximated system is monotonic non-increasing in the frequency range (ω_i,ω_h) if and only if $\frac{\mathrm{d}\rho(\omega)}{\mathrm{d}\omega} \geq 0$, $\forall\omega \in (\omega_i,\omega_h)$. According to (29),

$$\begin{aligned}\frac{\mathrm{d}\rho(\omega)}{\mathrm{d}\omega} &= 2\left(\sum_{k=0}^{n} d_k\,|P(\mathrm{j}\omega)|^k\cos\left(k\measuredangle P(\mathrm{j}\omega)\right)\right) \\ &\times\left(\begin{array}{c}\sum\limits_{k=0}^{n} kd_k\,|P(\mathrm{j}\omega)|^{k-1}\frac{\mathrm{d}|P(\mathrm{j}\omega)|}{\mathrm{d}\omega}\cos\left(k\measuredangle P(\mathrm{j}\omega)\right) \\ -\,kd_k\,|P(\mathrm{j}\omega)|^k\frac{\mathrm{d}\measuredangle P(\mathrm{j}\omega)}{\mathrm{d}\omega}\sin\left(k\measuredangle P(\mathrm{j}\omega)\right)\end{array}\right) \\ &+ 2\left(\sum_{k=0}^{n} d_k\,|P(\mathrm{j}\omega)|^k\sin\left(kP(\mathrm{j}\omega)\right)\right) \\ &\times\left(\begin{array}{c}\sum\limits_{k=0}^{n} kd_k\,|P(\mathrm{j}\omega)|^{k-1}\frac{\mathrm{d}|P(\mathrm{j}\omega)|}{\mathrm{d}\omega}\sin\left(k\measuredangle P(\mathrm{j}\omega)\right) \\ +\,kd_k\,|P(\mathrm{j}\omega)|^k\frac{\mathrm{d}\measuredangle P(\mathrm{j}\omega)}{\mathrm{d}\omega}\cos\left(k\measuredangle P(\mathrm{j}\omega)\right)\end{array}\right).\end{aligned} \quad (30)$$

By some calculations, (30) is simplified as

$$\frac{\mathrm{d}\rho(\omega)}{\mathrm{d}\omega} = \sum_{k=0}^{n}\sum_{l=0}^{n} kd_k d_l\,|P(\mathrm{j}\omega)|^{k+l-1}\,\Psi_{k-l}(\omega). \quad (31)$$

It is worth noting that condition (26) results in

$$f(|P(\mathrm{j}\omega)|) = \sum_{k=0}^{n}\sum_{l=0}^{n} kd_k d_l\cos\left(\tfrac{(k-l)\alpha\pi}{2}\right)|P(\mathrm{j}\omega)|^{k+l-1} \geq 0, \quad (32)$$

for $\omega \in (0,\infty)$. Define

$$\mu(\omega) = \min_{c\in C^+}\frac{\Psi_c(\omega)}{\cos(\frac{c\alpha\pi}{2})}, \quad \omega \in (\omega_l,\omega_h). \quad (33)$$

Definition (33) yields in

$$\Psi_c(\omega) \geq \mu(\omega)\cos(\frac{c\alpha\pi}{2}), \quad \forall\omega \in (\omega_l,\omega_h) \ \ \& \ \ \forall c \in \mathbf{C}^+. \quad (34)$$

Also if the second part of the conditions in (24) is met, then

$$\Psi_c(\omega) \geq \mu(\omega)\cos(\frac{c\alpha\pi}{2}), \quad \forall\omega \in (\omega_l,\omega_h) \ \ \& \ \ \forall c \in \mathbf{C}^-. \quad (35)$$

According to (31), (34), and (35), we have

$$\frac{\mathrm{d}\rho(\omega)}{\mathrm{d}\omega} \geq \sum_{k=0}^{n}\sum_{l=0}^{n} kd_k d_l\cos\left(\frac{(k-l)\alpha\pi}{2}\right)\mu(\omega)\,|P(\mathrm{j}\omega)|^{k+l-1}, \quad (36)$$

for all $\omega \in (\omega_l,\omega_h)$. If the first part of conditions in (24) (i.e., $\mu(\omega) \geq 0, \forall\omega \in (\omega_l,\omega_h)$ is satisfied, from (32) and (36) it is concluded that $\mathrm{d}\rho(\omega)/\mathrm{d}\omega \geq 0, \forall\omega \in (\omega_l,\omega_h)$. Hence, if the conditions in (24) hold, the approximated system has a monotonic non-increasing magnitude-frequency response in the frequency range (ω_i,ω_h). □

Example 3. The following approximation (37), shown at the bottom of the page, which has been obtained by using the low-frequency continued fraction method[49]. For approximation (37), functions $\min\limits_{c\in\{-1,0,1\}}\frac{\Psi_c(\omega)}{\cos(0.3c\pi)}$ and $\min\limits_{c\in\{-1,0,1\}}\frac{\Psi_c(\omega)}{\cos(0.3c\pi)}/\max\limits_{c\in\{-2,2\}}\frac{\Psi_c(\omega)}{\cos(0.3c\pi)}$ have been respectively plotted versus ω in Figs. 6 and 7. Plotting these functions specify that the conditions in (24) are simultaneously satisfied in the frequency range $(0.074,\infty)$ for $n = 2$. Hence, from Theorem 2 the monotonicity of the magnitude-frequency response is preserved in the frequency range $(0.074,\infty)$ by using approximation (37) in approximating each all-pole fractional order system in the form (1) with $\alpha = 0.6$ and $n = 2$ which has a monotonic magnitude-frequency response. As a sample, consider system (1) with order $\alpha = 0.6$, and matrices $A = \begin{bmatrix} -1/40 & -1/10 \\ 1/16 & 0 \end{bmatrix}$, $B = [1/4 \quad 0]^{\mathrm{T}}$, and $C = [0 \quad 2/5]$. In this case, (1) is an all-pole system with a monotonic magnitude-frequency response (See Fig. 8). Although the magnitude-frequency response of the approximation of this system, obtained on the basis of (37), is not monotonic for all frequencies, the monotonicity of the magnitude-frequency response is preserved in the frequency range $(0.074,\infty)$ (See Fig. 8).

According to (31), a trivial condition which results in the monotonicity of the magnitude-frequency response is non-negative-ness of $\Psi_c(\omega)$. Hence, the following result is deduced.

$$s^{0.6} \approx \frac{s(s+0.8961)(s+0.6405)(s+0.3316)(s+0.08734)}{(s+0.9811)(s+0.8075)(s+0.5167)(s+0.2199)(s+0.03037)}, \quad (37)$$

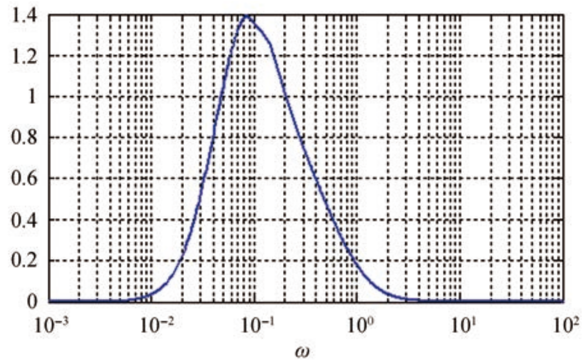

Fig. 6. $\min_{c\in\{-1,0,1\}} \frac{\Psi_c(\omega)}{\cos(0.3c\pi)}$ versus ω (Example 3).

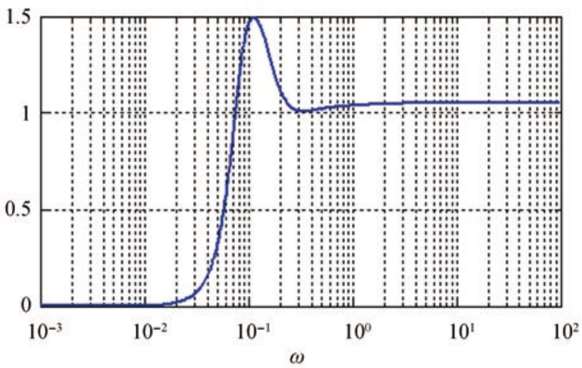

Fig. 7. $\min_{c\in\{-1,0,1\}} \frac{\Psi_c(\omega)}{\cos(0.3c\pi)} / \max_{c\in\{-2,2\}} \frac{\Psi_c(\omega)}{\cos(0.3c\pi)}$ versus ω (Example 3).

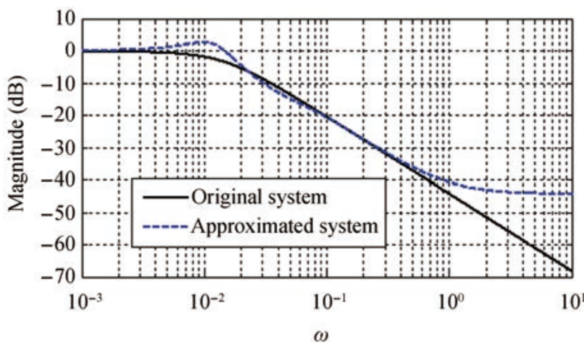

Fig. 8. Magnitude-frequency responses of the original system and its approximation in Example 3.

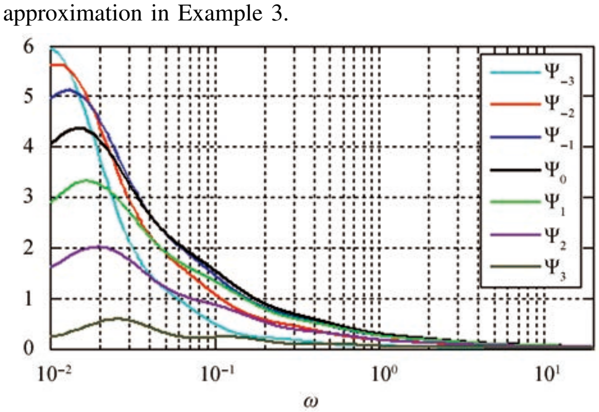

Fig. 9. $\Psi_c(\omega)$ versus ω for $c \in -3, \ldots, 3$ (Example 4).

Corollary 4. If $\Psi_c(\omega) \geq 0$ for all $\omega \in (\omega_i, \omega_h)$ and $c \in -n, ..., n$, then the approximation of system (1) with transfer function (23), which is obtained on the basis of (5), is monotonic non-increasing in the frequency range (ω_i, ω_h).

Example 4. Approximation (38), shown at the bottom of the page, which is obtained by using the CRONE method [51, Sec. 4.1.1]. For this approximation, functions $\Psi_c(\omega)$ for $c \in -3, ..., 3$ are non-negative in the frequency range $(0, \infty)$ (See Fig. 9). Therefore according to Corollary 4, using approximation (38) in approximating system (1) with a transfer function in the form

$$G(s) = \frac{1}{d_3 s^{0.9} + d_2 s^{0.6} + d_1 s^{0.3} + d_0}, \qquad (39)$$

where $d_k \geq 0$ for $k = 0, \ldots, 3$, results in an approximated system with a monotonic magnitude-frequency response (According to [42, Corollary 1], transfer function (39) with condition $d_k \geq 0$ for $k = 0, \ldots, 3$ has a monotonic magnitude-frequency response). For instance if approximation (38) is used for approximating the system

$$\begin{cases} {}_0D_t^{0.3} x(t) = \begin{bmatrix} -2 & -0.5 & -1 \\ 1 & 0 & 0 \\ 0 & 1 & 0 \end{bmatrix} x(t) + \begin{bmatrix} 1 \\ 0 \\ 0 \end{bmatrix} u(t), \\ y(t) = \begin{bmatrix} 0 & 0 & 1 \end{bmatrix} x(t), \end{cases} \qquad (40)$$

as confirmed in Fig. 10 the approximated system similar as the original system has a monotonic magnitude-frequency response.

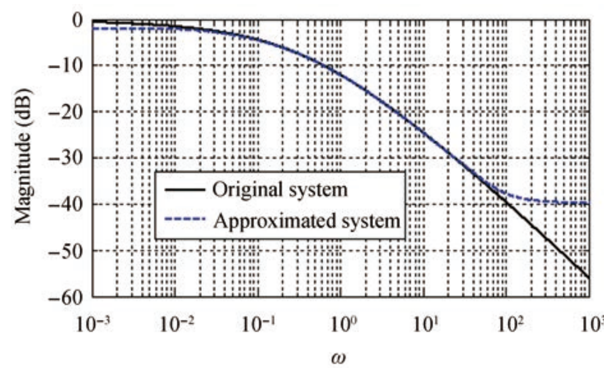

Fig. 10. Magnitude-frequency responses of the original system and its approximation in Example 4.

V. Conclusions

In this paper, the problem of preservation of response monotonicity in approximating fractional order systems by using rational approximations of fractional operators was investigated. In this investigation, conditions on the rational approximation of fractional operators were found to guarantee the monotonicity of step/magnitude-frequency response in approximation process (Theorems 1 and 2). These conditions were also simplified in some special cases (Corollaries 1-4).

$$s^{0.3} \approx 3.9811 \frac{(s+0.01711)(s+0.07943)(s+0.3687)(s+1.711)(s+7.943)(s+36.87)}{(s+0.02712)(s+0.1259)(s+0.5843)(s+2.712)(s+12.59)(s+58.43)}, \qquad (38)$$

Moreover, numerical simulations results were presented to confirm the usefulness of the obtained conditions. The main significance of the conditions, which were obtained on approximating filters to guarantee the monotonicity of step/magnitude-frequency responses in approximation process, is the independency of these conditions from the original system dynamics. This means that if an approximating filter satisfies the obtained conditions, using this filter in approximation of each original system with a monotonic response results in an approximated system having a monotonic response. Generally speaking, this feature can considerably reduce the computational costs for investigating the problem of monotonicity preservation, where the aim is approximation of various fractional order systems having monotonic responses. In this case, the obtained conditions can be only checked for the approximating filter, and if these conditions are satisfied, monotonicity of the response is guaranteed for all the approximated systems resulted from using such an approximating filter. Proposing new monotonicity preserving methods for approximation of fractional order operators or determining the free parameters of the existing approximation methods to guarantee the preservation of the response monotonicity, on the basis of the conditions derived in this paper, can be considered as interesting topics for future research works.

REFERENCES

[1] Oldham K B, Spanier J. *The Fractional Calculus: Theory and Applications of Differentiation and Integration to Arbitrary Order*. UK: Dover Publications Inc., 2006.

[2] Ortigueira M D. An introduction to the fractional continuous- time linear systems: the 21st century systems. *IEEE Circuits and Systems Magazine*, 2008, **8**(3): 19−26

[3] Cafagna D. Fractional calculus: a mathematical tool from the past for present engineers. *IEEE Industrial Electronics Magazine*, 2007, **1**(2): 35−40

[4] Tavazoei M S. From traditional to fractional PI control: a key for generalization. *IEEE Industrial Electronics Magazine*, 2012, **6**(3): 41−51

[5] Ma C B, Hori Y. Fractional-order control: theory and applications in motion control. *IEEE Industrial Electronics Magazine*, 2007, **1**(4): 6−16

[6] Tavakoli-Kakhki M, Tavazoei M S. Proportional stabilization and closed-loop identification of an unstable fractional order process. *Journal of Process Control*, 2014, **24**(5): 542−549

[7] Tavakoli-Kakhki M, Tavazoei M S. Estimation of the order and parameters of a fractional order model from a noisy step response data. *Journal of Dynamic Systems, Measurement and Control*, 2014, **136**(3): 031020

[8] Elwakil A S. Fractional-order circuits and systems: an emerging interdisciplinary research area. *IEEE Circuits and Systems Magazine*, 2010, **10**(4): 40−50

[9] Elwakil A, Maundy B, Fortuna L, Chen G R. Guest editorial fractional-order circuits and systems. *IEEE Journal on Emerging and Selected Topics in Circuits and Systems*, 2013, **3**(3): 297−300

[10] Yang C, Yu H, Shang Y, Fei W. Characterization of CMOS metamaterial transmission line by compact fractional-order equivalent circuit model. *IEEE Transactions on Electron Devices*, 2015, **62**(9): 3012−3018

[11] Ortigueira M D, Ionescu C M, Machado J T, Trujillo J J. Fractional signal processing and applications. *Signal Processing*, 2015, **107**: 197

[12] Cuesta E, Kirane M, Malik S A. Image structure preserving denoising using generalized fractional time integrals. *Signal Processing*, 2012, **92**(2): 553−563

[13] Efe MÖ. ADALINE based robust control in robotics: a Riemann-Liouville fractional differintegration based learning scheme. *Soft Computing*, 2009, **13**(1): 23−29

[14] Rekanos I T, Yioultsis T V. Approximation of Grünwald-Letnikov fractional derivative for FDTD modeling of cole-cole media. *IEEE Transactions on Magnetics*, 2014, **50**(2): 181−184

[15] Du Y C, Chen W L, Lin C H, Kan C D, Wu M J. Residual stenosis estimation of arteriovenous grafts using a dual-channel phonoangiography with fractional-order features. *IEEE Journal of Biomedical and Health Informatics*, 2015, **19**(2): 590−600

[16] Tavazoei M S. Reduction of oscillations via fractional order pre-filtering. *Signal Processing*, 2015, **107**: 407−414

[17] Muresan C I, Dulf E H, Prodan O. A fractional order controller for seismic mitigation of structures equipped with viscoelastic mass dampers. *Journal of Vibration and Control*, 2014. doi: 10.1177/1077546314557553, to be published

[18] Mescia L, Bia P, Caratelli D. Fractional derivative based FDTD modeling of transient wave propagation in Havriliak-Negami media. *IEEE Transactions on Microwave Theory and Techniques*, 2014, **62**(9): 1920−1929

[19] Di Paola M, Pirrotta A, Valenza A. Visco-elastic behavior through fractional calculus: an easier method for best fitting experimental results. *Mechanics of Materials*, 2011, **43**(12): 799−806

[20] Maione G. High-speed digital realizations of fractional operators in the delta domain. *IEEE Transactions on Automatic Control*, 2011, **56**(3): 697−702

[21] Oustaloup A, Levron F, Mathieu B, Nanot F M. Frequency-band complex noninteger differentiator: characterization and synthesis. *IEEE Transactions on Circuits and Systems I: Fundamental Theory and Applications*, 2000, **47**(1): 25−39

[22] Maione G. Closed-form rational approximations of fractional, analog and digital differentiators/integrators. *IEEE Journal on Emerging and Selected Topics in Circuits and Systems*, 2013, **3**(3): 322−329

[23] Chen Y Q, Moore K L. Discretization schemes for fractional-order differentiators and integrators. *IEEE Transactions on Circuits and Systems I: Fundamental Theory and Applications*, 2002, **49**(3): 363−367

[24] Maione G. Continued fractions approximation of the impulse response of fractional-order dynamic systems. *IET Control Theory and Applications*, 2008, **2**(7): 564−572

[25] Charef A. Analogue realisation of fractional-order integrator, differentiator and fractional $PI^{\lambda} D^{\mu}$ controller. *IEE Proceedings-Control Theory and Applications*, 2006, **153**(6): 714−720

[26] Vinagre B M, Podlubny I, Hernández A, Feliu V. Some approximations of fractional order operators used in control theory and applications. *Fractional Calculus and Applied Analysis*, 2000, **3**(3): 231−248

[27] Tavazoei M S, Haeri M. Unreliability of frequency-domain approximation in recognising chaos in fractional-order systems. *IET Signal Processing*, 2007, **1**(4): 171−181

[28] Tavazoei M S. Comments on "Stability analysis of a class of nonlinear fractional-order systems". *IEEE Transactions on Circuits and Systems II: Express Briefs*, 2009, **56**(6): 519−520

[29] Tavazoei M S. Comments on "Chaotic characteristics analysis and circuit implementation for a fractional-order system". *IEEE Transactions on Circuits and Systems I: Fundamental Theory and Applications*, 2015, **62**(1): 329−332

[30] Tavazoei M S, Haeri M. Rational approximations in the simulation and implementation of fractional- order dynamics: a descriptor system approach. *Automatica*, 2010, **46**(1): 94−100

[31] Tavazoei M S, Haeri M, Bolouki S, Siami M. Stability preservation analysis for frequency- based methods in numerical simulation of fractional order systems. *SIAM Journal on Numerical Analysis*, 2008, **47**(1): 321−338

[32] Siami M, Tavazoei M S, Haeri M. Stability preservation analysis in direct discretization of fractional order transfer functions. *Signal Processing*, 2011, **91**(3): 508−512

[33] Darbha S. On the synthesis of controllers for continuous time LTI systems that achieve a non-negative impulse response. *Automatica*, 2003, **39**(1): 159−165

[34] Rachid A. Some conditions on zeros to avoid step-response extrema. *IEEE Transactions on Automatic Control*, 1995, **40**(8): 1501−1503

[35] Tavazoei M S. Overshoot in the step response of fractional-order control systems. *Journal of Process Control*, 2012, **22**(1): 90−94

[36] Bement M, Jayasuriya S. Construction of a set of nonovershooting tracking controllers. *Journal of Dynamic Systems, Measurement, and Control*, 2004, **126**(3): 558−567

[37] Tavazoei M S. On type number concept in fractional-order systems. *Automatica*, 2013, **49**(1): 301−304

[38] Kim Y C, Keel L H, Bhattacharyya S P. Transient response control via characteristic ratio assignment. *IEEE Transactions on Automatic Control*, 2003, **48**(12): 2238−2244

[39] Filanovsky I M. A generalization of filters with monotonic amplitude-frequency response. *IEEE Transactions on Circuits and Systems I: Fundamental Theory and Applications*, 1999, **46**(11): 1382−1385

[40] Kidambi S S. Simple method for design of monotonic analogue filters. *Electronics Letters*, 2000, **36**(4): 287−288

[41] Tavazoei M S. On monotonic and nonmonotonic step responses in fractional order systems. *IEEE Transactions on Circuits and Systems II: Express Briefs*, 2011, **58**(7): 447−451

[42] Tavazoei M S. Algebraic conditions for monotonicity of magnitude-frequency responses in all-pole fractional order systems. *IET Control Theory and Applications*, 2014, **8**(12): 1091−1095

[43] Tavazoei M S. Fractional/distributed-order systems and irrational transfer functions with monotonic step responses. *Journal of Vibration and Control*, 2014, **20**(11): 1697−1706

[44] Tavakoli-Kakhki M, Haeri M, Tavazoei M S. Notes on the state space realizations of rational order transfer functions. *IEEE Transactions on Circuits and Systems I: Fundamental Theory and Applications*, 2011, **58**(5): 1099−1108

[45] Hartley T T, Lorenzo C F, Qammer H K. Chaos in a fractional order Chuas system. *IEEE Transactions on Circuits and Systems I: Fundamental Theory and Applications*, 1995, **42**(8): 485−490

[46] Abate J, Choudhury G L, Whitt W. An introduction to numerical transform inversion and its application to probability models. *Computational Probability*. Boston: Kluwer, 1999. 257−323.

[47] Bryan K. Elementary inversion of the Laplace transform, Preprint [Online]. available: http://www.rose-hulman.edu/ bryan/invlap.pdf. 2006.

[48] Roman S. The formula of Faa di bruno. *American Mathematical Monthly*, 1980, **87**(10): 805−809

[49] Valério D. Toolbox *ninteger* for MatLab [Online]. available: http://web.ist.utl.pt/duarte.valerio/ninteger/ninteger.htm. 2011.

[50] Singh R R. *Electrical Networks*. New Delhi: Tata McGraw-Hill, 2009.

[51] Valério D, da Costa J S. *An Introduction to Fractional Control*. Stevenage: IET, 2013.

Mohammad Saleh Tavazoei received the B.Sc., M.Sc., and Ph.D. degrees in electrical engineering from the Sharif University of Technology, Tehran, Iran, in 2003, 2005, and 2008, respectively. He is currently an associate professor with the Department of Electrical Engineering, Sharif University of Technology. His current research interests include dynamical behavior analysis of fractional order systems and applications of these systems in control system design. Dr. Tavazoei is the recipient of the Young Investigator Award of IEEE Iran Section in 2012.

Fractional-order Generalized Principle of Self-support (FOGPSS) in Control System Design

Hua Chen and YangQuan Chen

***Abstract*—This paper reviews research that studies the principle of self-support (PSS) in some control systems and proposes a fractional-order generalized PSS framework for the first time. The existing PSS approach focuses on practical tracking problem of integer-order systems including robotic dynamics, high precision linear motor system, multi-axis high precision positioning system with unmeasurable variables, imprecise sensor information, uncertain parameters and external disturbances. More generally, by formulating the fractional PSS concept as a new generalized framework, we will focus on the possible fields of the fractional-order control problems such as practical tracking, λ-tracking, etc. of robot systems, multiple mobile agents, discrete dynamical systems, time delay systems and other uncertain nonlinear systems. Finally, the practical tracking of a first-order uncertain model of automobile is considered as a simple example to demonstrate the efficiency of the fractional-order generalized principle of self-support (FOGPSS) control strategy.**

***Index Terms*—Fractional-order, principle of self-support (PSS), practical tracking, first-order automobile model.**

I. INTRODUCTION

THE conception of the principle of self-support (PSS) can be described by the following crucial characteristics for the existence of each phenomenon[1]: 1) Self-existence, each phenomenon (such as thing, fact, single element, unit, set, system, process, etc.) is an entity with its own being and nature. It exists as something (of, by) itself, not as any other thing. 2) Existence as a whole, each phenomenon exists as a whole. It is, or has a wholeness which includes all other phenomena. "Whatever comes into existence, always comes as a whole" (Plato, The Sophist). 3) Existence in a whole, no phenomenon exists entirely alone. Each is a part of other phenomena. Indeed, observing Fig. 1, from a recent report[2], as Alley pointed out that the ice movement may affect the regional climate change and the changes in temperature affects the rising of the sea levels, but instead, changes of the sea surface will also affect the ice movement, so they are reciprocally cause and effect, as they are interrelated and interact and constitute an integral whole (self-support as a whole).

Fig. 1. Interaction between the ice movement and a rise in sea levels.

Fig. 2. One dragon/Uroboros.

Additionally, as seen in Fig. 2, the best representative example for another self-referential (see [1] and references therein) seems to be a medieval paradox, the Uroboros the archetype of a vicious circle formed by a snake, or a dragon, looped in a circle, biting its own tail. How to distinguish where is the beginning and where is the end, why would such a thing happen: how to make it clear which is the cause and which is the effect (Fig. 3)? Based on the PSS idea, it shows just a self-complete whole — a self support system.

Then, as for control systems, how to consider it with these three existences above with PSS?

Manuscript received September 21, 2015; accepted February 28, 2016. This work was supported by the National Natural Science Foundation of China (61304004, 61503205), the Foundation of China Scholarship Council (201406 715056), the Foundation of Changzhou Key Laboratory of Special Robot and Intelligent Technology (CZSR2014005), and the Changzhou Science and Technology Program (CJ20160013). Recommended by Associate Editor Antonio Visioli.

Citation: Hua Chen, YangQuan Chen. Fractional-order generalized principle of self-support (FOGPSS) in control system design. *IEEE/CAA Journal of Automatica Sinica*, 2016, **3**(4): 430−441

Hua Chen is with the Mathematics and Physics Department, Hohai University, Changzhou 213022, China (e-mails: chenhua112@163.com).

YangQuan Chen is with MESA Laboratory, University of California, CA 95343, USA (e-mail: ychen53@ucmerced.edu).

Color versions of one or more of the figures in this paper are available online at http://ieeexplore.ieee.org.

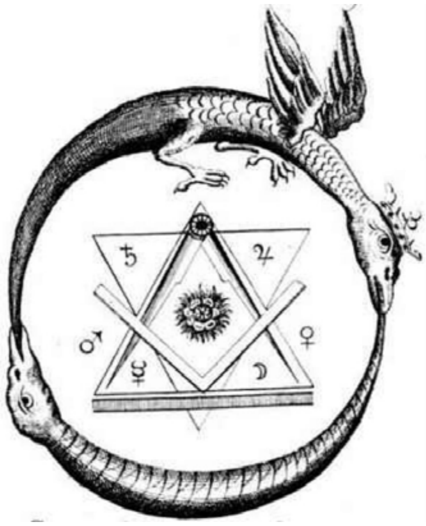

Fig. 3. Two dragons tail to mouth to tail.

A control signal (which is physically an amount of energy provided from the outside to a robotic system, in the form of either an input voltage or current injected to the driving actuators) might be regarded as a self-supported variable, i.e., it is a part of a greater system.

Here, a robotic dynamics is considered as an example by Novaković[3] for introducing the PSS design,

$$M(q)\ddot{q}+d(q,\dot{q})=u, \tag{1}$$

where q, u, $d(q,\dot{q})\in\mathbf{R}^n$ denote the joint coordinates vector, control vector, and the vector grouping the Coriolis centrifugal and gravitational forces or external disturbance, respectively. $M(q)=M(q)^{\mathrm{T}}\in\mathbf{R}^{n\times n}$ is the positive definite non-singular inertia matrix. By the computing torque technique, one can design a state feedback law

$$u=M(q)b+d(q,\dot{q}), \tag{2}$$

where $b\in\mathbf{R}^n$ is to be designed. Using the information about the joint-coordinates error $e=q_d-q$ (q_d is the desired motion of the joints, assuming that the inverse kinematics problem has been solved), let

$$b=\ddot{q}_d+K_d\dot{e}+K_pe,$$

which guarantees that system (1) behaves according to

$$\ddot{e}+K_d\dot{e}+K_pe=0, \tag{3}$$

where K_d, K_p are diagonal matrices whose elements are selected so to guarantee $e\to 0$ in advance. But practically, to consider the issues of robustness to parameter uncertainties, external disturbances, sensor noise and computational complexity, etc., the controller (2) cannot be obtained directly. To overcome this difficulty, the author considered

$$u=\hat{M}(\tilde{q})b+\hat{d}(\tilde{q},\dot{\tilde{q}}), \tag{4}$$

where $\tilde{q}$, $\dot{\tilde{q}}$ are available measured values, $\hat{M}(\tilde{q})$, $\hat{d}(\tilde{q},\dot{\tilde{q}})$ are the estimated values of $M(q)$ and $d(q,\dot{q})$ in model (1). From the basic idea of the PSS, essentially, the controller is seen as a part of (1), which means u can also be substituted into the error system by $M(q)\ddot{q}+d(q,\dot{q})$ to cancel some uncertain terms, thus its maximal limitation $u_{\max}$ can be assumed to be estimated by the bound of $|M(q_d)\ddot{q}_d|+|d(q,\dot{q})|$, then the author proposed some practical tracking control algorithms based on the principle of self-support.

Under the basic idea of PSS, it is not necessary to know the accurate values of q,q_d, and only the estimated error information is enough to design u such that e can be driven into a fixed neighborhood of zero D_ε. For simplicity, let $q=[q_1,\dots,q_n]^{\mathrm{T}}$, $u=[u_1,\dots,u_n]^{\mathrm{T}}$, $b=\mathrm{diag}\{b_i\}$ ($i=1,2,\dots,n$), $q_d=[q_{1d},\dots,q_{nd}]^{\mathrm{T}}$, tracking error $e=[e_1,\dots,e_n]^{\mathrm{T}}$ with $e_i=q_{id}-q_i$, $\max\{|u_i|\}=u_{i\max}$.

When estimating q by $\tilde{q}$, we suppose $\tilde{e}_i=e_i-\int_0^t\omega_i(t)\mathrm{d}t$ for all t, where $\omega_i(t)$ is the measurement function, which is supposed to be bounded ($|\omega_i(t)|\le c_{i1}$) and belong to a class of bounded integrable functions in the sense of Lebesgue integration, i.e., $\omega_i(t)\in L^1_{[0,t]}(f(t))\triangleq\{f(t):\int_{[0,t]}|f(s)|\mathrm{d}s\le c_{i2}\}$, where c_{i1}, c_{i2} are two positive constants given in advance. A PSS feedback law is proposed by $u_i=-b_is_i$, where $b_i>0$ is a design parameter to be given later, $s_i=\dot{\tilde{e}}_i+\rho_i\tilde{e}_i$, $\rho_i>0$. And next, for a given small positive constant ε, we will state that the tracking error $e_i(t)$ can be driven into the neighborhood of zero $D_\varepsilon\triangleq\{e_i:|e_i|\le\frac{\rho_ic_{i2}+c_{i1}}{\rho_i}+\varepsilon\}$ by selecting proper design parameters b_i.

To show how to select the design parameter b_i, take a Lyapunov function $V_1=\frac{1}{2}\sum_{i=1}^n e_i^2$, its time derivative can be calculated

$$\begin{aligned}\dot{V}_1&=\sum_{i=1}^n e_i(\dot{\tilde{e}}_i+\omega_i(t))=\sum_{i=1}^n e_i(s_i-\rho_i\tilde{e}_i+\omega_i(t))\\&=\sum_{i=1}^n e_i\left(-\frac{u_i}{b_i}-\rho_i(e_i-\int_0^t\omega_i(t)\mathrm{d}t)+\omega_i(t)\right)\\&=-\sum_{i=1}^n\rho_ie_i^2-\sum_{i=1}^n e_i\left(\frac{u_i}{b_i}-\rho_i\int_0^t\omega_i(t)\mathrm{d}t+\omega_i(t)\right),\end{aligned}$$

under the boundedness conditions of u_i, $\omega_i(t)$ and $\int_0^t\omega_i(t)\mathrm{d}t$, one has

$$\dot{V}_1\le-\sum_{i=1}^n\rho_ie_i^2+\sum_{i=1}^n|e_i|\left(\frac{u_{i\max}}{b_i}+\rho_ic_{i2}+c_{i1}\right),$$

from which, if $|e_i|>\frac{\rho_ic_{i2}+c_{i1}}{\rho_i}+\varepsilon$, we have

$$\begin{aligned}\dot{V}_1\le&-\sum_{i=1}^n\rho_i\left(\frac{\rho_ic_{i2}+c_{i1}}{\rho_i}+\varepsilon\right)|e_i|\\&+\sum_{i=1}^n|e_i|\left(\frac{u_{i\max}}{b_i}+\rho_ic_{i2}+c_{i1}\right)\\=&-\sum_{i=1}^n|e_i|\left(\rho_i\varepsilon-\frac{u_{i\max}}{b_i}\right).\end{aligned}$$

We can select design parameters b_i such that $\eta=\rho_i\varepsilon-\frac{u_{i\max}}{b_i}>0$, so choosing $b_i>\frac{u_{i\max}}{\rho_i\varepsilon}$ such that

$$\dot{V}_1\le-\eta\sum_{i=1}^n|e_i|\le 0, \tag{5}$$

which means $e_i(t)$ will enter into the region D_ε in a finite time.

On the other hand, once $e_i(t) \in D_\varepsilon$, it has $|e_i(t)| \leq \frac{\rho_i c_{i2}+c_{i1}}{\rho_i} + \varepsilon$ and $|\dot{e}_i(t)|$ is also shown to be upper bounded, since

$$|\dot{e}_i| = |\dot{\widetilde{e}}_i + \omega_i(t)| = |s_i - \rho_i \widetilde{e}_i + \omega_i(t)|,$$

substituting control law and estimated error, we have

$$\begin{aligned}|\dot{e}_i| &= |-\frac{u_i}{b_i} - \rho_i \widetilde{e}_i + \omega_i(t)| \\ &= |-\frac{u_i}{b_i} - \rho_i \left(e_i - \int_0^t \omega_i(t)\mathrm{d}t\right) + \omega_i(t)| \\ &\leq \frac{u_{i\max}}{b_i} + \rho_i \left(\frac{\rho_i c_{i2} + c_{i1}}{\rho_i} + \varepsilon + c_{i2}\right) + c_{i1} \\ &= \frac{u_{i\max}}{b_i} + 2\rho_i c_{i2} + 2c_{i1} + \rho_i \varepsilon,\end{aligned}$$

because $b_i > \frac{u_{i\max}}{\rho_i \varepsilon}$, therefore

$$|\dot{e}_i| < 2\rho_i \left(c_{i2} + \frac{c_{i1}}{\rho_i} + \varepsilon\right). \tag{6}$$

This means that the control algorithm guarantees that e_i will lie in D_ε if $c_{i2} = c_{i1} = 0$, $\varepsilon \to 0^+$.

Remark 1. In an ideal world, $c_{i2} = c_{i1} = 0$ means that the sensors for measuring the tracking error of robotic systems are accurate without any disturbance or noise, i.e., the properties of the final neighborhood of zero D_ε depend on the accuracy of sensors. Therefore, a more generalized case (for any given c_{i1}, c_{i2}) of the tracking problem is discussed here based on the basic PSS idea. Moreover, our further consideration in the next will be the case when the estimated error is assumed to be measured by some cumulative error measurement function with memorability decided by the previous control effect.

Remark 2. Usually, the desired objects to be tracked are moving in a bounded feasible region (the size of which may be very large), for all initial conditions, from (5) and (6), both $\widetilde{e}_i(t)$ and $e_i(t)$ will not escape to infinity before $e_i(t)$ enters into D_ε.

Additionally, there are some research results about PSS in control systems, let us do a brief review on it. In [4], Tan et al. discussed the precision motion control of a permanent magnet linear motor (PMLM) for applications which are inherently repetitive in terms of the motion trajectories, and a feedback-feedforward control structure is proposed with a modest amount of modeling effort. An iterative learning controller (ILC) based on zero-phase filtering is applied as feedforward controller to the existing relay-tuned PID feedback controller to enhance the trajectory tracking performance by utilizing the experience gained from the repeated execution of the same operations. Considering inputs subjected to bounded constraints, Novaković[5] proposed a practical tracking algorithm, the control law is accelerometer-free (or even tacho-free, also), robust to sensor noise, allows the prespecification of the error decay rate, and is realistic from the engineering standpoint that can be implemented using current microprocessor technology. The PSS methodology is introduced for kinematic control of manipulators, in a way that is both mathematically clear and simple to implement[6]. Ulu et al.[7] proposed a new method which is computationally more efficient, more suitable for coupling gain calculations of arbitrary nonlinear contour and easier to implement on multiaxis systems. The tracking and contouring performance of the method on a nonlinear contour is verified through simulations and experiments achieving nanometer level accuracy for the two-axes system.

However, for complicated systems in engineering, designing an integer-order state feedback control law is imperfect especially when dealing with some real-world plants which need the so-called "long term memory property"[8−9]. Compared with integer-order system, fractional calculus has been proven to describe real systems in interdisciplinary fields more effectively, since it can offer a deeper insight into the physical processes underlying a long-range memory behavior[10−14]. To sum up, fractional control related issues can include the fractional order dynamic system or plant to be controlled and the fractional-order controller. However, in control practice it is more common to consider the fractional-order controller[15]. This is due to the fact that the plant model may have already been obtained as an integer order model in the classical sense. In most cases, the task is to apply fractional-order control (FOC) to enhance the system control performance. For example, in [16], the robust control of perturbed integer-order LTI systems is considered by using a fractional order sliding surface design method. A novel control strategy has been proposed, ensuring that the fractional-order (FO) sliding manifold will be hit at an infinite sequence of time instants and becoming denser as time grows. The closed-loop system is proved to be asymptotically robust with respect to a wide class of disturbances with the chattering free FO sliding mode control. To improve control performance or for dealing explicitly with the fractional order behavior of the plants, in [17−18], the authors adopted a fractional order PID controller or the generalized $PI^\lambda D^\mu$ controller. So, naturally, in this paper, we consider to present a fractional-order generalized principle self-support (FOGPSS) control for real application, we also address the questions. What would happen if the PSS controller (4) is replaced by FOGPSS controller? What condition should be satisfied compared with (3), and how to establish a FOGPSS feedback law?

The structure of the article is as follows: Section II presents the FOGPSS statement and a prospect of some possible research interests. Section III provides a simple application example and its simulations. And finally, a conclusion is summarized in Section IV.

II. Problem Formulation of FOGPSS

There are many different definitions of fractional operators[19−30], such as Grunwald-Letnikov fractional derivatives, Hadamard type fractional integrals and fractional derivatives, Liouville fractional integrals and fractional derivatives, Marchaud derivatives, Caputo fractional derivatives, Riemann-Liouville (RL) fractional integrals and fractional derivatives, etc., among which, commonly used are Riemann-Liouville and Caputo fractional order operators. The following subsection will give some basic definitions and properties about these two.

A. Preliminaries of Fractional Calculus

Definition 1[20−30]**.** Given function $f(t) \in L_1[a,b]$ at time instant $t \geq 0$, Riemann-Louville fractional integral with order $\alpha > 0$ is defined as

$$\begin{aligned} {}^{RL}D^{-\alpha}f(t) &= I^{\alpha}f(t) \triangleq D^{-\alpha}f(t) \\ &= \frac{1}{\Gamma(\alpha)}\int_0^t \frac{f(\tau)}{(t-\tau)^{1-\alpha}}\mathrm{d}\tau, \end{aligned}$$

where $\Gamma(\cdot)$ is the Euler gamma function,

$$\Gamma(s) = \int_0^{\infty} \mathrm{e}^{-t}t^{s-1}\mathrm{d}t, \quad s \in \mathbf{C}.$$

The reduction formula for this function holds

$$\Gamma(s+1) = s\Gamma(s) \ \Rightarrow \Gamma(m+1) = m(m-1)! = m!,$$

where $m \in \mathbf{Z}^+ = \{1, 2, 3, \ldots\}$, and $L_p[a,b]$ is (for $1 \leq p \leq \infty$) the usual Lebesgue space.

Definition 2[20−30]**.** The Riemann-Louville fractional derivative of function $f(t)$ with order $\alpha > 0$ is defined as follows:

$${}^{RL}D^{\alpha}f(t) = \frac{1}{\Gamma(m-\alpha)}\frac{\mathrm{d}^m}{\mathrm{d}t^m}\int_0^t \frac{f(\tau)}{(t-\tau)^{\alpha-m+1}}\mathrm{d}\tau,$$

where $m-1 < \alpha \leq m$ and $m \in \mathbf{Z}^+$, $\frac{\mathrm{d}^m}{\mathrm{d}t^m}f(t)$ denotes m-order derivative of $f(t)$.

Definition 3[20−30]**.** The Caputo derivative of fractional order α of a function $f(t)$ is described by

$$\begin{aligned} {}^{C}D^{\alpha}f(t) &= D^{-(m-\alpha)}\frac{\mathrm{d}^m}{\mathrm{d}t^m}f(t) \\ &= \frac{1}{\Gamma(m-\alpha)}\int_0^t \frac{f^{(m)}(\tau)}{(t-\tau)^{1+\alpha-m}}\mathrm{d}\tau, \end{aligned}$$

where $m-1 \leq \alpha < m \in \mathbf{Z}^+$, $f^{(m)}(\tau)$ is the m-order derivative of $f(\tau)$ with respect to τ.

For the fractional-order operators, we select some important properties[20−30] which may be used later:

Property 1. $I^{\alpha}I^{\beta}f(t) = I^{\alpha+\beta}f(t)$, $\alpha, \beta \geq 0$.

Property 2. ${}^{RL}D^{\alpha}\big({}^{RL}D^{-\alpha}(f(t))\big) = f(t)$.

Property 3. ${}^{C}D^{-\alpha}D^{-\beta}f(t) = D^{-(\alpha+\beta)}f(t)$, $\alpha, \beta \geq 0$.

Property 4. ${}^{C}D^{-\alpha}D^{\alpha}f(t) = f(t) - \Sigma_{j=0}^{m-1}\frac{m-1}{i!}f^{(j)(0)}$.

Property 5. ${}^{C}D^{\alpha}I^{\alpha}f(t) = f(t)$.

Next, we will propose the fractional-order generalized principle of self-support (FOGPSS).

B. Conception of FOGPSS

The FOGPSS is proposed by us to define fractional tracking error signals based on "self-support" to replace the general control law. For instance, in order to improve the control performance of robot dynamics (1), we consider to present a fractional-order error state feedback in the PSS control law (4). This is not a simple replica of general PSS, but a challenging task both in control theory and in practical engineering application.

Since under the fractional PSS framework, the corresponding stability issue becomes the most urgent problem to solve, it is not clear that the fractional-order asymptotic stability and Mittag-Leffler stability[31−36] can directly be applied to solve FOGPSS feedback design. In the same example, if we propose a fractional state feedback with PSS in (4) , i.e., the undetermined term b must satisfy some fractional-order ordinary differential equation (ODE) corresponding to (3) such that the closed-loop error system will converge to a bounded neighborhood of zero given in advance. In theory, this process will force the original system into a pre-specified fractional-order error dynamics, it is a big challenge for practical plant with parametric or non-parametric uncertainty and nonlinearity due to the imperfect stability criterion of nonlinear fractional-order systems.

Some useful stability theorems or conclusions of fractional-order systems are listed as follows:

Lemma 1[37]**.** For a differentiable vector $x(t) \in \mathbf{R}^n$, and for any time instant $t \geq 0$,

$$\frac{1}{2}\ {}^{C}D^{\alpha}\big[x^{\mathrm{T}}(t)x(t)\big] \leq x^{\mathrm{T}}(t){}^{C}D^{\alpha}x(t).$$

Lemma 2[31]**.** Let ${}^{C}D^{\alpha}x(t) \geq {}^{C}D^{\alpha}y(t)$, $\forall\alpha \in (0,1)$ and $x(0) = y(0)$, then $x(t) \geq y(t)$.

Lemma 3[38]**.** The linear fractional-order system with commensurate order $0 < \alpha \leq 1$

$${}^{C}D^{\alpha}x(t) = Ax(t)$$

is stable at $x = 0$ if the following conditions are satisfied

$$|\arg(\lambda_i)| > \alpha\frac{\pi}{2},$$

where λ_i are eigenvalues of matrix A.

Lemma 4[31]**.** Consider the non-autonomous nonlinear fractional-order system

$${}^{C}D^{\alpha}x(t) = f(x,t), \quad \alpha \in (0,1), \tag{7}$$

where $f : [0,\infty] \times \Omega \to \mathbf{R}^n$ is piecewise continuous in t and locally Lipschitz in x on $[0,\infty] \times \Omega$, and $\Omega \in \mathbf{R}^n$ is a domain that contains an equilibrium point $x = 0$. If there exists a Lyapunov function $V(x(t),t)$ and class-K functions $\kappa_i(\cdot) : [0,a) \to [0,\infty]$ strictly increasing and $\kappa_i(0) = 0$ ($i =$ 1, 2, 3) satisfying

$$\kappa_1(\|x\|) \leq V(x(t),t) \leq \kappa_2(\|x\|),$$

$${}^{C}D^{\beta}V(x(t),t) \leq -\kappa_3(\|x\|),$$

where $\beta \in (0,1)$. Then the origin of system (7) is asymptotically stable.

On the other hand, to solve the FOGPSS, the available algorithms of fractional-order controller to be implemented in real time should be adopted. Two approximation methods are most frequently used to calculate a linear or nonlinear fractional differential equation (FDE). One is the Adams-Bashford-Moulton (ABM) algorithm, the other is the time-domain method which is a generalization of the ABM approximation algorithm. This method is based on a predictor-corrector scheme using the Caputo definition[39]. We give a brief introduction of this algorithm as follows.

Consider the following fractional-order differential equation:

$$D^{\alpha}x(t) = f(t, x(t)), \quad 0 \leq t \leq T, \tag{8}$$

with $x^{(k)}(0) = x_0^{(k)}$ $(k = 0, 1, 2, \ldots, \lceil\alpha\rceil - 1)$. Equation (8) is equivalent to the following Volterra integral equation

$$x(t) = \sum_{k=0}^{\lceil\alpha\rceil-1} \frac{t^k}{k!} x_0^{(k)} + \frac{1}{\Gamma(\alpha)} \int_0^t (t-\tau)^{\alpha-1} f(\tau, x(\tau)) \mathrm{d}\tau. \quad (9)$$

Set $h = T/N$ $(N \in \mathbf{Z}^+)$, and $t_n = nh$ $(n = 0, 1, 2, \ldots, N)$. Then (9) can be discretized as follows:

$$x_h(t_{n+1}) = \sum_{k=0}^{\lceil\alpha\rceil-1} \frac{t_{n+1}^k}{k!} x_0^{(k)} + \frac{h^\alpha}{\Gamma(\alpha+2)} f(t_{n+1}, x_h^p(t_{n+1})) + \frac{h^\alpha}{\Gamma(\alpha+2)} \sum_{j=0}^{n} a_{j,n+1} f(t_j, x_h(t_j)),$$

where

$$x_h^p(t_{n+1}) = \sum_{k=0}^{\lceil\alpha\rceil-1} \frac{t_{n+1}^k}{k!} x_0^{(k)} + \frac{1}{\Gamma(\alpha)} \sum_{j=0}^{n} b_{j,n+1} f(t_j, x_h(t_j)),$$

$$a_{j,n+1} = \begin{cases} n^{\alpha+1} - (n-\alpha)(n-j)^{\alpha+1}, & j = 0, \\ (n-j+2)^{\alpha+1} + (n-j)^{\alpha+1}, & j = 0, \\ -2(n-j+1)^{\alpha+1}, & 1 \le j \le n, \\ 1, & j = n+1, \end{cases}$$

and

$$b_{j,n+1} = \frac{h^\alpha}{\alpha}((n-j+1)^\alpha - (n-j)^\alpha).$$

The estimation error of this technique is

$$e = \max_{j=0,1,2,\ldots,N} |x(t_j) - x_h(t_j)| = O(h^p),$$

where $p = \min(2, 1+\alpha)$.

C. Possible Research Framework of FOGPSS

We will discuss possible research framework of FOGPSS in this subsection, which mainly includes four aspects: λ-tracking control, tracking of time-delay system, saturated practical tracking and robotic system control.

1) *λ-tracking control*

λ-stabilization or λ-tracking means that the output cannot be controlled to a set-point but into a λ-neighbourhood of the set-point (or the reference trajectory to be tracked), where $\lambda > 0$ is an arbitrarily small constant given in advance[40−41]. For a large class of multivariable nonlinear minimum-phase systems of relative degree one, Allgöwer et al.[42] modified a known adaptive high-gain control strategy $u(t) = -k(t)y(t)$, $\dot{k}(t) = \|y(t)\|^2$ to obtain a λ-tracking in the presence of output corrupted noise. In [43], for a class of high-gain stabilizable multivariable linear infinite-dimensional systems, an adaptive control law is proposed to achieve the approximate asymptotic tracking in the sense that the tracking error converges to a neighborhood of zero with the arbitrary prescribed radius $\lambda > 0$. And a sampled version of the high-gain adaptive λ-tracking controller is considered in [44], because the sampling process from the output of a system may not be available continuously, but only at discrete time instants. Recently, Ilchmann et al.[45−48] considered the temperature control for exothermic chemical reactors by λ-tracking approach with a feedback law subjected to saturation constraints.

By the research motivation above, it is possible to consider the adaptive λ-tracking control under FOGPSS framework, more specifically, we design an error feedback controller

$$u(t) = -k(t)e(t), \quad e(t) = y(t) - y_r(t),$$

where $y(t)$, $y_r(t)$ are output and desired tracking reference signals, respectively. The control gain $k(t)$ satisfies a fractional-order λ-adaptive ODE

$${}^C D^\alpha(k(t)) = \begin{cases} f(e(t), \lambda), & \|e(t)\| \ge \lambda, \\ 0, & \|e(t)\| < \lambda, \end{cases}$$

where the function $f(e(t), \lambda)$ in the equation above is to be designed such that $e(t)$ can be driven into a small λ-neighborhood of zero with pre-given λ. The core task of FOGPSS control is to find an eligible function f so that the FO tracking error closed-loop system is asymptotically stable at zero.

2) *Tracking of systems with time-delay*

Time delay is the property of a physical system by which the response to an applied force (action) is delayed in its effect[49−50]. Time delays are often encountered in many dynamic systems such as rolling mill systems, biological systems, metallurgical processing systems, network systems, and so on[51−52]. It has been shown that the existence of time delays usually becomes the source of instability and degraded performance of systems[51]. Many researches have been devoted to the study of tracking control of systems with time-delay, for example, Fridman[53] considers the sampled-data control of linear systems under uncertain sampling with the known upper bound on the sampling intervals, a time-dependent Lyapunov functional method in the developed framework of input delay approach has been introduced for analysis of this linear system. For a class of perturbed strict-feedback nonlinear time-delay systems, an adaptive fuzzy tracking control scheme has been presented by appropriately choosing Lyapunov-Krasovskii functionals and hyperbolic tangent functions[54]. In [55], the robust tracking and model following for a class of linear systems with known multiple delayed state perturbations, time-varying uncertain parameters, and disturbance have been considered. A class of continuous memoryless state feedback controllers for robust tracking of dynamical signals are proposed, by which, the tracking error can be guaranteed to decrease asymptotically to zero. By using separation technique and the norm of neural weight vector, Wang et al.[56] presented a simple and effective control approach to address the tracking problem for non-affine pure-feedback system with multiple time-varying delay states. For nonlinear discrete-time systems with time delays, the model reference output feedback fuzzy tracking control design and optimal tracking control based on heuristic dynamic programming have been discussed in [57] and [58], respectively. The tracking control for switched linear systems with time-delay is solved by using single Lyapunov function technique and a typical hysteresis switching law so that the H_∞ model reference tracking performance can be satisfied[59]. And Cho et al.[60] considered the robustness in time-delay control in the presence of the nonlinear friction dynamics of robot manipulators that is enhanced with a compensator based on internal model control.

Considering the following nonlinear dynamical system of the form[61−62] with input time delay

$$\begin{aligned}\dot{x} &= Ax + B[f(x) + g(x)u(t-\tau)],\\ y &= Cx,\end{aligned} \tag{10}$$

where

$$A = \begin{bmatrix} 0 & 1 & 0 & \cdots & 0\\ 0 & 0 & 1 & \cdots & 0\\ \vdots & \vdots & \vdots & \ddots & \vdots\\ 0 & 0 & 0 & \cdots & 1\\ 0 & 0 & 0 & 0 & 0 \end{bmatrix},\ B = \begin{bmatrix} 0\\ 0\\ \vdots\\ 0\\ 1 \end{bmatrix},\ C^{\mathrm{T}} = \begin{bmatrix} 1\\ 0\\ \vdots\\ 0\\ 0 \end{bmatrix},$$

$x \in \mathbf{R}^n$ is the state vector, $y, u \in \mathbf{R}$ are the output and control input, respectively. τ denotes the constant of time-delay. Let y_r be the reference signal, $e(t) = y - y_r$ is the tracking error.

Then how to propose a fractional time-delay feedback controller for system (10) or other nonlinear systems with input time delay or state time-delay is an important pioneering research to the best of the authors' knowledge. This study will touch on the field of stability issue about fractional-order time-delay systems combining with the PSS control strategy.

3) *Practical tracking with input saturation*

From a practical point of view, it is important to design saturated controllers for any mechanical systems. That is because any actuator always has a limitation of the physical control inputs (input saturation)[63−76], while the control input signals are a function of the system states, large initial conditions or unmodeled disturbances may cause the controller to exceed physical limitations[77], therefore, lots of saturated controllers design methods have been proposed. Chen et al. considered the saturated stabilization or tracking of dynamic nonholonomic mobile robots[63−65] and robust control for these robotic systems under a fixed camera feedback with input saturation[68−73], respectively. For the systems with time delay, continuous or discrete, linear or nonlinear systems have also been studied under the feedback law subject to input saturation constraints in [75−77]. And Lin et al.[66, 78] have given a semi-global exponential stabilization control strategy including state feedback law or of output feedback type for both discrete-time systems and continuous linear time-invariant systems subject to input saturation. In [67], the robust stabilization of spacecraft in the presence of input saturation constraints, parametric uncertainty, and external disturbances has been addressed by two globally stable control algorithms. In [75], based on linear matrix inequalities (LMIs) technique, the theory of the composite nonlinear feedback control method has been considered for robust tracking and model following of linear systems with time varying delays and input saturation. Recently, the saturated control for multi-agent systems has become a hot research topic, for example, Su et al.[74] studied the observer-based leader-following consensus of a linear multi-agent system on switching networks, in which the input of each agent is subject to saturation. A low-gain output feedback strategy is considered to design the new observer-based consensus algorithms, without requiring any knowledge of the interactive network topology. Also, the global consensus problem of discrete-time multi-agent systems with input saturation constraints under fixed undirected topologies has been discussed in [79], in which, two special cases are considered, where the agent model is either neutrally stable or a double integrator.

Commonly, the saturation function $Sat_\varepsilon(\cdot)$ is a monotonically increasing function whose saturation level is less than ε, i.e., $|Sat_\varepsilon(\cdot)| \le \varepsilon$. Examples of such saturation functions, for instance[64], are

$$\begin{aligned} Sat_\varepsilon(\tilde{z}) &= \varepsilon \tanh(\tilde{z}),\\ Sat_\varepsilon(\tilde{z}) &= \frac{2\varepsilon}{\pi}\arctan(\tilde{z}),\\ Sat_\varepsilon(\tilde{z}) &= \begin{cases} \varepsilon, & \text{if } |\tilde{z}| \ge \varepsilon,\\ \tilde{z}, & \text{otherwise.} \end{cases} \end{aligned}$$

The difficulty of saturating practical tracking feedback based on FOGPSS lies in the fact that we are short of theoretical support because there are only a few results about the control of fractional-order systems with input saturation[80]. It is necessary to find a new control technique for fractional-order system to support this framework in the near future.

4) *Robotic dynamics control*

There are many types of robot systems such as rigid robot manipulators[81−90], humanoid robots[91−95], underwater robots[96−103], space robots[104−106], wheeled mobile robots[107−113], pipe robots[114−116], and so on. Among which, studying of a class of robot systems subject to nonholonomic motion constraints becomes a hot point of research, and control of such mobile robots has attracted considerable attention from the research community because of their practical applications and the theoretical challenges created by the nonholonomic nature of the constraints on it[117−120]. It is because controlling such systems is full of practical engineering interest and theoretically challenging, just as reported by Brockett[121], any nonholonomic system cannot be stabilized to a point with pure smooth (or even continuous) state feedback control law. In order to overcome this design difficulty, many ingenious feedback stabilization methods have been proposed such as discontinuous feedback control law[68−73], time-varying feedback law[63−65], hybrid feedback law[122−123], and optimal feedback law[124−126], etc.

As shown in Fig. 4, the posture kinematic model of a class of nonholonomic wheeled mobile robots can be described by the following differential equations[107]:

$$\begin{cases} \dot{x} = v\cos\theta,\\ \dot{y} = v\sin\theta,\\ \dot{\theta} = \omega, \end{cases} \tag{11}$$

where (x, y) is the position of the mass center of the robot moving in the plane. v is the forward velocity, ω is the steering velocity and θ denotes its heading angle from the horizontal axis.

Different from current approaches, FOGPSS tracking of the wheeled mobile robots (11) is independent of its desired traje-

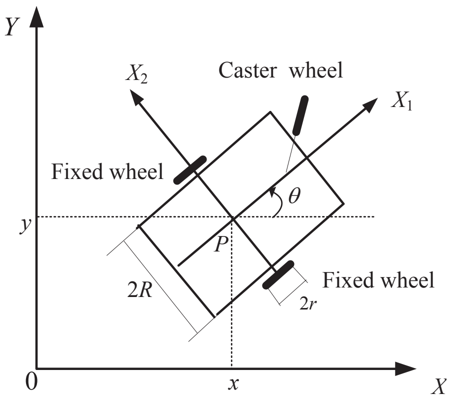

Fig. 4. Nonholonomic wheeled mobile robot.

ctory (x_r, y_r, θ_r) with FO error state feedback $(x_e, y_e, \theta_e) = (x - x_r, y - y_r, \theta - \theta_r)$,

$$\begin{cases} \dot{x}_r = v_r \cos\theta_r, \\ \dot{y}_r = v_r \sin\theta_r, \\ \dot{\theta}_r = \omega_r. \end{cases}$$

For the strong nonlinear robot system model (9), how to design some FO velocity controllers (v, ω) such that the error state (x_e, y_e, θ_e) converges to a small neighborhood of zero given in advance is an important future research objective.

Remark 3. Here, we describe some aspects of control design problems by using FOGPSS, more detailed technical progress will proceed in the next coming months, this paper gives a summarized outline, whereas the most important and the biggest contribution is to bring up the new design idea about fractional order research framework for the first time. And to show the feasibilities of fractional PSS controller, a simple application example is given in the next section.

III. A Simple Application Example of FOGPSS

A. A Simple Tracking Example

A number of simple engineering systems of interest may be represented by a first-order model, for example, the braking of an automobile, the discharge of an electronic flash, or the flow of fluid from a tank may be approximately represented by a first-order differential equation[85]:

$$\dot{x} = -a_p x + b_p u + d(x,t), \tag{12}$$

where $x, u \in \mathbf{R}$ are the state and control input, respectively. a_p, $b_p > 0$ are bounded uncertain parameters (constants), $d(x,t)$ is the external disturbance signal. Let $x_d(t)$ be the desired reference trajectory, $x_e = x_d - x$ is the tracking error.

Here, the control objective is to present a FOGPSS feedback law u such that error state x_e can be driven into a specified ε_0-neighbourhood of zero D_{ε_0} with small positive constant $\varepsilon_0 > 0$ given in advance.

For practice, we make the following assumptions:

Assumption 1. The position of x_d to be tracked is not directly available, but it moves within a known bounded region with a constrained velocity, i.e., $|x_d| \le b_1$, $|\dot{x}_d| \le b_2$, where b_1, $b_2 > 0$ are known constants.

Assumption 2. There exist positive constants $\underline{a}$, $\bar{a}$, $\underline{b}$, $\bar{b}$, $\bar{d}$ for the follower system (12), such that for all x and t,

$$\underline{a} \le |a_p| \le \bar{a}, \quad \underline{b} \le |b_p| \le \bar{b}, \quad |d(x,t)| \le \bar{d}.$$

Assumption 3. The estimate of error measurement x_e can be denoted by

$$\tilde{x}_e = x_e - I^\alpha \omega(t), \quad \alpha \in (0,1),$$

where the estimated error function $\omega(t) \in L_1[a,b]$ satisfies that

$$|\omega(t)| \le c_1, \quad |I^\alpha \omega(t)| \le c_2.$$

By Assumption 2, note that the controller u to be designed in (12) can be seen as an inherent part itself according to PSS[1, 3, 5−6], that means

$$|u| = \left| \frac{\dot{x} + a_p x - d(x,t)}{b_p} \right| \le \frac{|\dot{x}| + \bar{a}|x| + \bar{d}}{\underline{b}}. \tag{13}$$

Tracking the desired trajectory $x_d(t)$, and according to Assumption 1, it is entirely normal to suppose the boundedness of x, $\dot{x}$ in some estimated, feasible motion region by $|x_d|$ and $|\dot{x}_d|$, hence, from (13), we assume that $|u| \le u_{\max}$.

Remark 4. Compared with the existing tracking problem, we suppose x_d cannot be obtained by designer directly in Assumption 1, which is more general. And therefore, in Assumption 3, it is reasonable to assume there is an integrable error function $\omega(t)$ between $\tilde{x}_e$ and x_e under the sense of fractional calculus (Definition 1) due to the possible long term memory property in estimation of tracking error, because it is to consider that the current feedback relies on the previous tracking effects.

For being convenient, we denote the α-order Caputo derivative ${}^C D^\alpha$ by D^α, and the design results will be stated as follows:

Theorem 1. Under Assumptions 1-3, for system (12), taking the FOGPSS feedback law

$$u = \bar{\beta}\tilde{s}, \tag{14}$$

where $\bar{\beta}$ is a design parameter satisfying

$$\bar{\beta} > \frac{u_{\max}}{\delta\varepsilon_0} > 0,$$

where $\delta > 0$ is also a design parameter, $\tilde{s}$ is the fractional-order estimated error feedback signal

$$\tilde{s} = D^\alpha \tilde{x}_e + \delta \tilde{x}_e. \tag{15}$$

Then the real tracking error x_e will be driven into $D_{\varepsilon_0} \triangleq \{x_e : |x_e| \le \frac{\delta c_2 + c_1}{\delta} + \varepsilon_0\}$.

Proof. Take a Lyapunov function $V = \frac{1}{2}x_e^2$, by applying Lemma 1, we have

$$D^\alpha V = D^\alpha \left(\frac{1}{2}x_e^2\right) \le x_e D^\alpha x_e,$$

by Assumption 3 and Property 5 in Definition 3, we have

$$D^\alpha V \le x_e D^\alpha(\tilde{x}_e + I^\alpha \omega(t)) = x_e(D^\alpha(\tilde{x}_e) + \omega(t)).$$

Substituting (15) into the formula above, it has

$$D^\alpha V \le x_e(\tilde{s} - \delta\tilde{x}_e + \omega(t))$$

$$= x_e\left(\frac{u}{\bar{\beta}} - \delta\tilde{x}_e + \omega(t)\right)$$
$$= x_e\left(\frac{u}{\bar{\beta}} - \delta(x_e - I^{\alpha}\omega(t)) + \omega(t)\right).$$

According to Assumption 3 again, we have

$$D^{\alpha}V \le -\delta x_e^2 + |x_e|\left(\frac{u_{\max}}{\bar{\beta}} + \delta c_2 + c_1\right). \quad (16)$$

If $|x_e| > \frac{\delta c_2 + c_1}{\delta} + \varepsilon_0$, from (16), we can obtain

$$\begin{aligned} D^{\alpha}V \le &- \delta\left(\frac{\delta c_2 + c_1}{\delta} + \varepsilon_0\right)|x_e| \\ &+ |x_e|\left(\frac{u_{\max}}{\bar{\beta}} + \delta c_2 + c_1\right) \\ = &- |x_e|\left(\delta(\frac{\delta c_2 + c_1}{\delta} + \varepsilon_0) - \frac{u_{\max}}{\bar{\beta}} - \delta c_2 - c_1\right) \\ = &- \frac{|x_e|}{\bar{\beta}}(\bar{\beta}\delta\varepsilon_0 - u_{\max}). \end{aligned}$$

Let $\hat{\beta} = \left(\bar{\beta}\delta\varepsilon_0 - u_{\max}\right)/\bar{\beta}$, from (14), since $\bar{\beta} > u_{\max}/\delta\varepsilon_0 > 0$, so $\hat{\beta} > 0$, which means

$$D^{\alpha}V \le -\hat{\beta}|x_e| = -\hat{\beta}\sqrt{2}V^{\frac{1}{2}} \le 0,$$

by Lemma 4, $x_e \to 0$ as $t \to \infty$, hence x_e will be driven into $D\varepsilon_0$.

By the similar derivation process as (6) in the introduction section, once $|x_e| \le (\delta c_2 + c_1)/\delta + \varepsilon_0$, from (14)-(16), we have

$$\begin{aligned} |D^{\alpha}x_e| &= |D^{\alpha}\tilde{x}_e + \omega(t)| \\ &= |\frac{u}{\bar{\beta}} - \delta(x_e - I^{\alpha}\omega(t)) + \omega(t)| \\ &\le 2\delta\left(c_2 + \frac{c_1}{\delta} + \varepsilon_0\right). \end{aligned}$$

Then $|D^{\alpha}x_e| < \varepsilon_0 \to 0^+$ as $c_1 = c_2 = 0$, and according to Lemma 4. □

Remark 5. System (12) is a very simple example for describing the FOGPSS idea for the first time in this paper, and the more technical complex systems will be discussed in the further research, such as n-order nonlinear dynamic system with time delay (10), λ-tracking, control of nonholonomic wheeled mobile robots (11), etc.

Remark 6. Since we suppose the feasible tracking moving area can be estimated in advance (Assumption 1), which means the bound of controller $u_{\max}$ is not representative of the mechanical limit of actuator itself but also the constraints of the bounded moving region. Selecting the high gain feedback parameter $\bar{\beta}$ satisfies the condition below (14), one can always tune it at real time according to the data from velocity sensor of controller $u(t)$.

Remark 7. The control process shows that our FOGPSS controller design exhibits good robustness. More generally, the conclusion is also valid even if the uncertain terms a_p, b_p in Assumption 2 are time varying parameters, because the method is directly based on the estimated tracking error but not the model itself.

B. Simulations

In this subsection, when using FOGPSS tracking controller consisting of (14) and (15), we adopt the approximate numerical ABM algorithms (8) and (9) for solving the fractional differential equations for corresponding error system of (12).

In the following simulations, according to Theorem 1, for system (12), given $\varepsilon_0 = 0.3$, $a_p = 1.0 + 0.5\sin t$, $b_p = 1.5 + 0.5\cos t$, $\underline{a} = 0.5$, $\bar{a} = 1.5$, $\underline{b} = 1.0$, $\bar{b} = 2.0$, $d = 0.5\sin(xt)$ and $\bar{d} = 0.5$, by Assumptions 1 and 3, suppose $b_1 = 3.0$, $b_2 = 0.5$, $\omega(t) = -0.045\cos(t)$, $c_1 = 0.1$, $c_2 = 1.5$. From (13), we can estimate that $u_{\max} = 5.5$, then select the design parameters as follows: $\delta = 10$, $\bar{\beta} = 12 > \frac{u_{\max}}{\delta\varepsilon_0} = 1.1$, $\alpha = 0.3$, $\hat{\beta} = \left(\bar{\beta}\delta\varepsilon_0 - u_{\max}\right)/\bar{\beta} = 0.04$. The initial conditions are $x(0) = -1.5$, $x_d(0) = 0.5$, $x_e(0) = \tilde{x}_e(0) = 2.0$.

Some simulation results are shown in Figs. 5-7 performed with MATLAB. From Fig. 5, we can observe that the tracking error state x_e is driven into the small neighborhood of zero

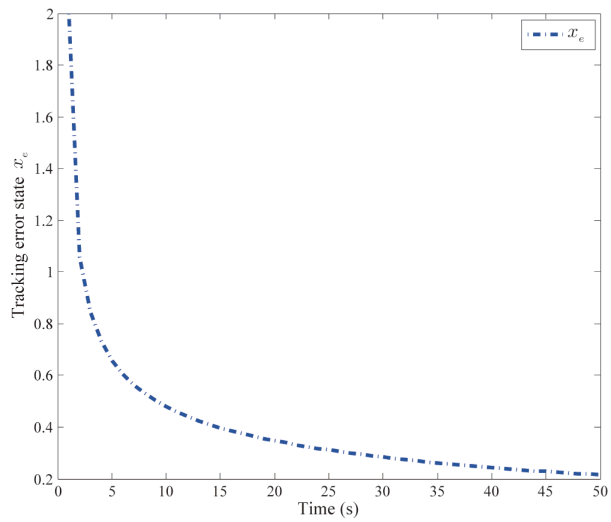

Fig. 5. The response of tracking error state variable x_e with respect to time.

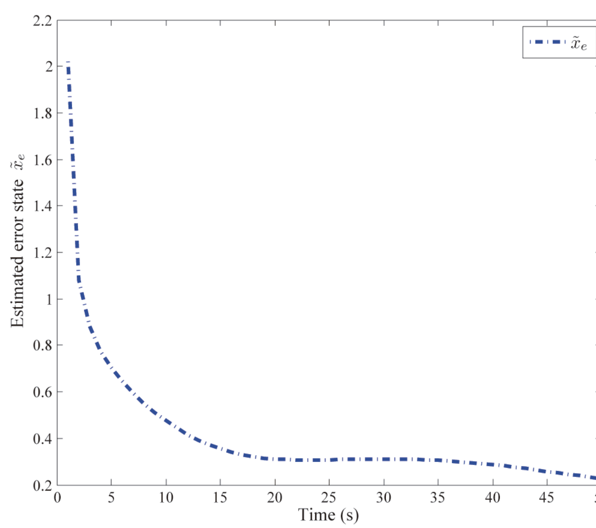

Fig. 6. The response of estimated error state variable $\tilde{x}_e$ with respect to time.

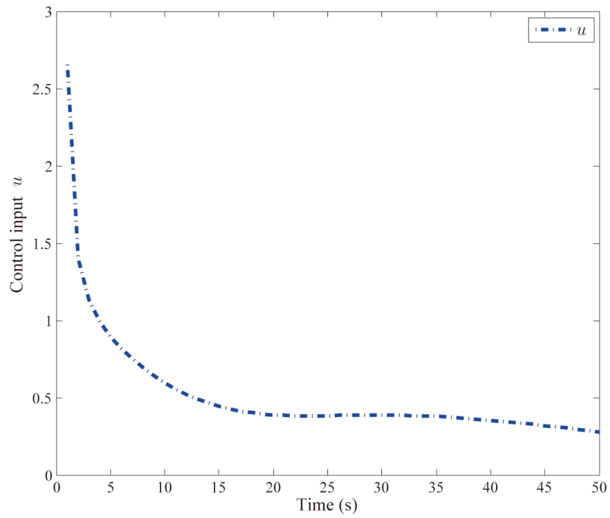

Fig. 7. The response of FOGPSS state feedback input u with respect to time.

for given $\varepsilon_0 = 0.3$, surely, $|x_e| \leq 0.3$ at about $t \geq 30$ s. The response of estimated error state $\tilde{x}_e$ is demonstrated in Fig. 6, from which, it can be seen that the convergence behavior of $\tilde{x}_e$ is not like the x_e, since it is assumed that there exist an error function $\omega(t)$ between x_e and $\tilde{x}_e$, and $\tilde{x}_e$ goes into the ε_0-neighborhood of zero when $t \geq 20$ s. In Fig. 7, the response of control input u looks more like that of $\tilde{x}_e$ in Fig. 3 due to FOGPSS feedback consists of $D^{0.3}\tilde{x}_e$ and $\tilde{x}_e$ by (14) and (15).

If all the information of tracking error $x_{1e} = x - x_d$ is precisely known, we assume the desired tracking trajectory x_d satisfies $\dot{x}_d = -a_p x_d + b_p u_d$ with $u_d = -\sin t \mathrm{e}^{-3t}$ as the desired input. The error dynamics can be obtained easily $\dot{x}_{1e} = -a_p x_{1e} + b_p(u_1 - u_d) + d(x,t)$, here, to distinguish the control input from it in (12), we denote it as u_1. Then according to the conventional sliding mode design[11, 16], a discontinuous integer order controller is designed as $u_1 = u_d - k_s \mathrm{sgn}(x_{1e})$, where the design parameter $k_s \geq \bar{d}/\underline{b}$.

Under the same initial conditions, and selecting $k_s = 0.8$, Figs. 8 and 9 show the traditional integer order sliding mode tracking simulations, compared to the fractional order simula-

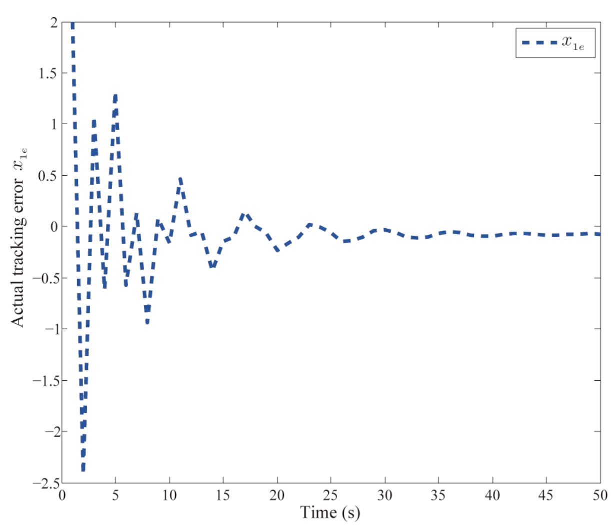

Fig. 8. The response of tracking error x_{1e} by sliding-mode control with respect to time.

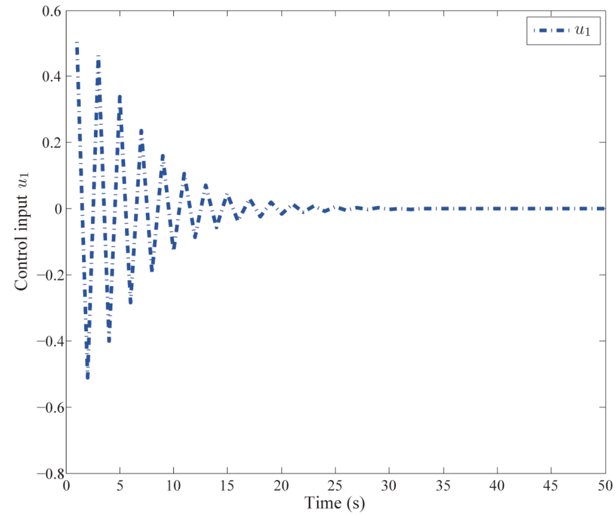

Fig. 9. The response of sliding-mode control input u_1 with respect to time.

tions, we find that the tracking error in Fig. 5 using fractional order controller has a fast convergence speed than the sliding mode case in Fig. 8, moreover, the continuous fractional order feedback in Fig. 7 shows more smoothness than the discontinuous sliding mode controller u_1 in Fig. 9.

Remark 8. Compared to the existing sliding mode control methods, the FOGPSS proposed in this paper is a model-free design technique, which is directly based on the estimated tracking error, while the conventional sliding mode design can not deal with the case when the tracked objects are unavailable.

IV. CONCLUSION

In this article, a new conception of the generalized fractional-order principle of self-support (FOGPSS) is proposed for the first time. After a brief review of PSS, the fractional-order-based framework is considered to deal with the feedback control for practical complex system, which cannot be perfectly controlled by integer-order feedback. And some possible research fields such as practical tracking, λ-tracking, etc. for robot systems, multiple mobile agents, discrete dynamical systems, time delay systems and other uncertain nonlinear systems are discussed using FOGPSS. A simple example is presented to show the efficiency of the fractional-order generalized principle of self-support control strategy.

REFERENCES

[1] Novaković Z R. *The Principle of Self-Support in Control Systems*. Amsterdam, New York: Elsevier Science Ltd., 1992.

[2] Alley R B. *The Two-Mile Time Machine: Ice Cores, Abrupt Climate Change, and Our Future*. Princeton: Princeton University Press, 2014.

[3] Novaković Z R. The principle of self-support in robot control synthesis. *IEEE Transactions on Systems, Man, and Cybernetics*, 1991, **21**(1): 206−220

[4] Tan K K, Dou H F, Chen Y Q, Lee T H. High precision linear motor control via relay-tuning and iterative learning based on zero-phase filtering. *IEEE Transactions on Control Systems Technology*, 2001, **9**(2): 244−253

[5] Novaković Z R. Robust tracking control for robots with bounded input. *Journal of Dynamic Systems, Measurement, and Control*, 1992, **114**(2): 315−319

[6] Novaković Z R. The principle of self-support: a new approach to kinematic control of robots. In: Proceedings of the 5th International Conference on Advanced Robotics, 1991. Robots in Unstructured Environments. Pisa, Italy: IEEE, 1991. 1444−1447

[7] Ulu N G, Ulu E, Cakmakci M. Learning based cross-coupled control for multi-axis high precision positioning systems. In: Proceedings of the 5th ASME Annual Dynamic Systems and Control Conference Joint with the 11th JSME Motion and Vibration Conference. Florida, USA: ASME, 2012. 535−541

[8] Özdemir N, Avci D. Optimal control of a linear time-invariant space-time fractional diffusion process. *Journal of Vibration and Control*, 2014, **20**(3): 370−380

[9] Zhao X, Yang H T, He Y Q. Identification of constitutive parameters for fractional viscoelasticity. *Communications in Nonlinear Science and Numerical Simulation*, 2014, **19**(1): 311−322

[10] Ge Z M, Jhuang W R. Chaos, control and synchronization of a fractional order rotational mechanical system with a centrifugal governor. *Chaos, Solitons and Fractals*, 2007, **33**(1): 270−289

[11] Chen H, Chen W, Zhang B W, Cao H T. Robust synchronization of incommensurate fractional-order chaotic systems via second-order sliding mode technique. *Journal of Applied Mathematics*, 2013, **2013**: Article ID 321253

[12] Jesus I S, Tenreiro Machado J A. Development of fractional order capacitors based on electrolyte processes. *Nonlinear Dynamics*, 2009, **56**(1−2): 45−55

[13] Müller S, Kästner M, Brummund J, Ulbricht V. A nonlinear fractional viscoelastic material model for polymers. *Computational Materials Science*, 2011, **50**(10): 2938−2949

[14] Rivero M, Trujillo J J, Vázquez L, Pilar Velasco M. Fractional dynamics of populations. *Applied Mathematics and Computation*, 2011, **218**(3): 1089−1095

[15] Chen Y Q, Moore K L. Discretization schemes for fractional-order differentiators and integrators. *IEEE Transactions on Circuits and Systems — I: Fundamental Theory and Applications*, 2002, **49**(3): 363−367

[16] Corradini M L, Giambó R, Pettinari S. On the adoption of a fractional-order sliding surface for the robust control of integer-order LTI plants. *Automatica*, 2015, **51**: 364−371

[17] Pisano A, Rapaić M, Jeličić Z, Usai E. Nonlinear fractional PI control of a class of fractional-order systems. In: Proceedings of the 2012 IFAC Conference on Advances in PID Control. Brescia, Italy, 2012. 637−642

[18] Monje C A, Vinagre B M, Feliu V, Chen Y Q. Tuning and auto-tuning of fractional order controllers for industry applications. *Control Engineering Practice*, 2008, **16**(7): 798−812

[19] Monje C A, Chen Y Q, Vinagre B M, Xue D, Feliu-Batlle V. *Fractional-Order Systems and Controls*. London: Springer, 2010.

[20] Kilbas A A, Srivastava H M, Trujillo J J. *Theory and Applications of Fractional Differential Equations*. Amsterdam, The Netherlands: Elsevier, 2006.

[21] Podlubny I. *Fractional Differential Equations*. New York: Academic Press, 1999.

[22] Li C P, Deng W H. Remarks on fractional derivatives. *Applied Mathematics and Computation*, 2007, **187**(2): 777−784

[23] Samko S G, Kilbas A A, Marichev O I. *Fractional Integrals and Derivatives: Theory and Applications*. Switzerland: Gordon and Breach Science Publishers, 1993.

[24] Li C P, Zeng F H. *Numerical Methods for Fractional Calculus*. Boca Raton, FL: Chapman and Hall/CRC, 2015.

[25] Miller K S, Ross B. *An Introduction to the Fractional Calculus and Fractional Differential Equations*. New York: Wiley, 1993.

[26] Oldham K B, Spanier J. *The Fractional Calculus*. New York: Academic Press, 1974.

[27] Li C P, Dao X H, Guo P. Fractional derivatives in complex planes. *Nonlinear Analysis: Theory, Methods, and Applications*, 2009, **71**(5−6): 1857−1869

[28] Li C P, Qian D L, Chen Y Q. On Riemann-Liouville and Caputo derivatives. *Discrete Dynamics in Nature and Society*, 2011, **2011**: Article ID 562494

[29] Li C P, Zhao Z G. Introduction to fractional integrability and differentiability. *The European Physical Journal Special Topics*, 2011, **193**(1): 5−26

[30] Li C P, Zhang F R, Kurths J, Zeng F H. Equivalent system for a multiple-rational-order fractional differential system. *Philosophical Transactions of the Royal Society A: Mathematical, Physical, and Engineering Sciences*, 2013, **371**(1990): 20120156

[31] Li Y, Chen Y Q, Podlubny I. Stability of fractional-order nonlinear dynamic systems: Lyapunov direct method and generalized Mittag-Leffler stability. *Computers and Mathematics with Applications*, 2010, **59**(5): 1810−1821

[32] Li Y, Chen Y Q, Podlubny I. Mittag-Leffler stability of fractional order nonlinear dynamic systems. *Automatica*, 2009, **45**(8): 1965−1969

[33] Ahn H S, Chen Y Q. Necessary and sufficient stability condition of fractional-order interval linear systems. *Automatica*, 2008, **44**(11): 2985−2988

[34] Ahn H S, Chen Y Q, Podlubny I. Robust stability test of a class of linear time-invariant interval fractional-order system using Lyapunov inequality. *Applied Mathematics and Computation*, 2007, **187**(1): 27−34

[35] Lu J G, Chen Y Q. Robust stability and stabilization of fractional-order interval systems with the fractional order α: the $0 \ll \alpha \ll 1$ case. *IEEE Transactions on Automatic Control*, 2010, **55**(1): 152−158

[36] Chen Y Q, Moore K L. Analytical stability bound for a class of delayed fractional-order dynamic systems. *Nonlinear Dynamics*, 2002, **29**(1−4): 191−200

[37] Aguila-Camacho N, Duarte-Mermoud M A, Gallegos J A. Lyapunov functions for fractional order systems. *Communications in Nonlinear Science and Numerical Simulation*, 2014, **19**(9): 2951−2957

[38] Podlubny I. *Fractional Differential Equations: an Introduction to Fractional Derivatives, Fractional Differential Equations, Some Methods of Their Solution and Some of Their Applications*. New York: Academic Press, 1999.

[39] Diethelm K, Ford N J, Freed A D. A predictor-corrector approach for the numerical solution of fractional differential equations. *Nonlinear Dynamics*, 2002, **29**(1−4): 3−22

[40] Ilchmann A, Ryan E P. Universal λ-tracking for nonlinearly-perturbed systems in the presence of noise. *Automatica*, 1994, **30**(2): 337−346

[41] Allgöwer F, Ilchmann A. Multivariable adaptive λ-tracking for nonlinear chemical processes. In: Proceedings of the 3rd European Control Conference. Rome, Italy, 1995. 1645−1651

[42] Allgöwer F, Ashman J, Ilchmann A. High-gain λ-tracking for nonlinear systems. *Automatica*, 1997, **33**(5): 881−888

[43] Ilchmann A, Logemann H. Adaptive λ-tracking for a class of infinite-dimensional systems. *Systems and Control Letters*, 1998, **34**(1−2): 11−21

[44] Ilchmann A, Townley S. Adaptive high-gain λ-tracking with variable sampling rate. *Systems and Control Letters*, 1999, **36**(4): 285−293

[45] Ilchmann A, Thuto M, Townley S. Input constrained adaptive tracking with applications to exothermic chemical reaction models. *SIAM Journal on Control and Optimization*, 2004, **43**(1): 154−173

[46] Ilchmann A, Thuto M, Townley S. λ-tracking for exothermic chemical reactions with saturating inputs. In: Proceedings of the 2001 European Control Conference (ECC). Porto, Portugal: IEEE, 2001. 1928−1933

[47] Ilchmann A, Trenn S. Input constrained funnel control with applications to chemical reactor models. *Systems and Control Letters*, 2004, **53**(5): 361−375

[48] Ilchmann A, Townley S, Thuto M. Adaptive sampled-data tracking for input-constrained exothermic chemical reaction models. *Systems and Control Letters*, 2005, **54**(12): 1149−1161

[49] Shinskey F G. *Process-Control Systems*. New York: McGraw-Hill Book Company, 1967.

[50] Zhong Q C. *Robust Control of Time-Delay Systems*. London: Springer, 2006.

[51] Niculescu S L. *Delay Effects on Stability: A Robust Control Approach*. London: Springer, 2001.

[52] Yi Y, Guo L, Wang H. Adaptive statistic tracking control based on two-step neural networks with time delays. *IEEE Transactions on Neural Networks*, 2009, **20**(3): 420−429

[53] Fridman E. A refined input delay approach to sampled-data control. *Automatica*, 2010, **46**(2): 421−427

[54] Wang M, Chen B, Liu X P, Shi P. Adaptive fuzzy tracking control for a class of perturbed strict-feedback nonlinear time-delay systems. *Fuzzy Sets and Systems*, 2008, **159**(8): 949−967

[55] Wu H S. Adaptive robust tracking and model following of uncertain dynamical systems with multiple time delays. *IEEE Transactions on Automatic Control*, 2004, **49**(4): 611−616

[56] Wang M, Ge S S, Hong K S. Approximation-based adaptive tracking control of pure-feedback nonlinear systems with multiple unknown time-varying delays. *IEEE Transactions on Neural Networks*, 2010, **21**(11): 1804−1816

[57] Tseng C S. Model reference output feedback fuzzy tracking control design for nonlinear discrete-time systems with time-delay. *IEEE Transactions on Fuzzy Systems*, 2006, **14**(1): 58−70

[58] Zhang H G, Song R Z, Wei Q L, Zhang T Y. Optimal tracking control for a class of nonlinear discrete-time systems with time delays based on heuristic dynamic programming. *IEEE Transactions on Neural Networks*, 2011, **22**(12): 1851−1862

[59] Li Q K, Zhao J, Dimirovski G M, Liu X J. Tracking control for switched linear systems with time-delay: a state-dependent switching method. *Asian Journal of Control*, 2009, **11**(5): 517−526

[60] Cho G R, Chang P H, Park S H, Jin M L. Robust tracking under nonlinear friction using time-delay control with internal model. *IEEE Transactions on Control Systems Technology*, 2009, **17**(6): 1406−1414

[61] Wang L X. *Adaptive Fuzzy Systems and Control: Design and Stability Analysis*. Englewood Cliffs, NJ: Prentice-Hall, 1994.

[62] Boulkroune A, Tadjine M, M'Saad M, Farza M. How to design a fuzzy adaptive controller based on observers for uncertain affine nonlinear systems. *Fuzzy Sets and Systems*, 2008, **159**(8): 926−948

[63] Chen H, Wang C L, Yang L, Zhang D K. Semiglobal stabilization for nonholonomic mobile robots based on dynamic feedback with inputs saturation. *Journal of Dynamic Systems, Measurement, and Control*, 2012, **134**(4): 041006

[64] Chen H. Robust stabilization for a class of dynamic feedback uncertain nonholonomic mobile robots with input saturation. *International Journal of Control, Automation, and Systems*, 2014, **12**(6): 1216−1224

[65] Chen H, Wang C L, Zhang B W, Zhang D K. Saturated tracking control for nonholonomic mobile robots with dynamic feedback. *Transactions of the Institute of Measurement and Control*, 2013, **35**(2): 105−116

[66] Lin Z L, Saberi A. Semi-global exponential stabilization of linear discrete-time systems subject to input saturation via linear feedbacks. *Systems and Control Letters*, 1995, **24**(2): 125−132

[67] Boškovic J D, Li S M, Mehra R K. Robust adaptive variable structure control of spacecraft under control input saturation. *Journal of Guidance, Control, and Dynamics*, 2001, **24**(1): 14−22

[68] Chen H, Wang C L, Liang Z Y, Zhang D K, Zhang H J. Robust practical stabilization of nonholonomic mobile robots based on visual servoing feedback with inputs saturation. *Asian Journal of Control*, 2014, **16**(3): 692−702

[69] Chen H, Ding S H, Chen X, Wang L H, Zhu C P, Chen W. Global finite-time stabilization for nonholonomic mobile robots based on visual servoing. *International Journal of Advanced Robotic Systems*, 2014, **11**: 1−13

[70] Li B J, Chen H, Chen J F. Global finite-time stabilization for a class of nonholonomic chained system with input saturation. *Journal of Information and Computational Science*, 2014, **11**(3): 883−890

[71] Chen Hua, Wang Chao-Li, Yang Fang, Xu Wei-Dong. Finite-time saturated stabilization of nonholonomic mobile robots based on visual servoing. *Control Theory and Applications*, 2012, **29**(6): 817−823 (in Chinese)

[72] Chen H, Chen J F, Lei Y, Chen W X, Wang Y W. Further results of semiglobal saturated stabilization for nonholonomic mobile robots. In: Proceedings of the 26th Chinese Control and Decision Conference (2014 CCDC). Changsha, China: IEEE, 2014. 4545−4550

[73] Chen H, Zhang J B. Semiglobal saturated practical stabilization for nonholonomic mobile robots with uncertain parameters and angle measurement disturbance. In: Proceedings of the 25th Chinese Control and Decision Conference (CCDC). Guiyang, China: IEEE, 2013. 3731−3736

[74] Su H S, Chen M Z Q, Wang X F, Lam J. Semiglobal observer-based leader-following consensus with input saturation. *IEEE Transactions on Industrial Electronics*, 2014, **61**(6): 2842−2850

[75] Mobayen S. Robust tracking controller for multivariable delayed systems with input saturation via composite nonlinear feedback. *Nonlinear Dynamics*, 2014, **76**(1): 827−838

[76] Wang X, Saberi A, Stoorvogel A A. Stabilization of discrete-time linear systems subject to input saturation and multiple unknown constant delays. *IEEE Transactions on Automatic Control*, 2014, **59**(6): 1667−1672

[77] Fischer N, Dani A, Sharma N, Dixon W E. Saturated control of an uncertain nonlinear system with input delay. *Automatica*, 2013, **49**(6): 1741−1747

[78] Lin Z L, Saberi A. Semi-global exponential stabilization of linear systems subject to input saturation via linear feedbacks. *Systems and Control Letters*, 1993, **21**(3): 225−239

[79] Yang T, Meng Z Y, Dimarogonas D V, Johansson K H. Global consensus for discrete-time multi-agent systems with input saturation constraints. *Automatica*, 2014, **50**(2): 499−506

[80] Lim Y H, Oh K K, Ahn H S. Stability and stabilization of fractional-order linear systems subject to input saturation. *IEEE Transactions on Automatic Control*, 2013, **58**(4): 1062−1067

[81] Ortega R, Spong M W. Adaptive motion control of rigid robots: a tutorial. *Automatica*, 1989, **25**(6): 877−888

[82] Nicosia S, Tomei P. Robot control by using only joint position measurements. *IEEE Transactions on Automatic Control*, 1990, **35**(9): 1058−1061

[83] Corless M. Control of uncertain nonlinear systems. *Journal of Dynamic Systems, Measurement, and Control*, 1993, **115**(2B): 362−372

[84] Utkin V I. *Sliding Modes and Their Application in Variable Structure Systems*. Moscow: MIR Publishers, 1978.

[85] Slotine J J, Li W P. *Applied Nonlinear Control*. Englewood Cliffs, NJ: Prentice Hall, 1991.

[86] Zhang F, Dawson D M, de Queiroz M S, Dixon W E. Global adaptive output feedback tracking control of robot manipulators. *IEEE Transactions on Automatic Control*, 2000, **45**(6): 1203−1208

[87] Hsu S H, Fu L C. A fully adaptive decentralized control of robot manipulators. *Automatica*, 2006, **42**(10): 1761−1767

[88] Galicki M. An adaptive regulator of robotic manipulators in the task space. *IEEE Transactions on Automatic Control*, 2008, **53**(4): 1058−1062

[89] Galicki M. Control of mobile manipulators in a task space. *IEEE Transactions on Automatic Control*, 2012, **57**(2): 2962−2967

[90] Galicki M. Finite-time control of robotic manipulators. *Automatica*, 2015, **51**: 49−54

[91] Ijspeert A J, Nakanishi J, Schaal S. Movement imitation with nonlinear dynamical systems in humanoid robots. In: Proceedings of the 2002 IEEE International Conference on Robotics and Automation. Washington, DC: IEEE, 2002. 1398−1403

[92] Katić D, Vukobratović M. Survey of intelligent control techniques for humanoid robots. *Journal of Intelligent and Robotic Systems*, 2003, **37**(2): 117−141

[93] Furuta T, Tawara T, Okumura Y, Shimizu M, Tomiyama K. Design and construction of a series of compact humanoid robots and development of biped walk control strategies. *Robotics and Autonomous Systems*, 2001, **37**(2−3): 81−100

[94] Goswami A, Yun S, Nagarajan U, Lee S H, Yin K K, Kalyanakrishnan S. Direction-changing fall control of humanoid robots: theory and experiments. *Autonomous Robots*, 2014, **36**(3): 199−223

[95] Eaton M. Introduction. *Evolutionary Humanoid Robotics*. Berlin Heidelberg: Springer, 2015. 1−7

[96] Yuh J. Design and control of autonomous underwater robots: a survey. *Autonomous Robots*, 2000, **8**(1): 7−24

[97] Antonelli G. *Underwater Robots* (Third edition). Switzerland: Springer, 2014.

[98] Choi S K, Yuh J. Experimental study on a learning control system with bound estimation for underwater robots. *Autonomous Robots*, 1996, **3**(2−3): 187−194

[99] Chu W S, Lee K T, Song S H, Han M W, Lee J Y, Kim H S, Kim M S, Park Y J, Cho K J, Ahn S H. Review of biomimetic underwater robots using smart actuators. *International Journal of Precision Engineering and Manufacturing*, 2012, **13**(7): 1281−1292

[100] Krieg M, Mohseni K. Thrust characterization of a bioinspired vortex ring thruster for locomotion of underwater robots. *IEEE Journal of Oceanic Engineering*, 2008, **33**(2): 123−132

[101] Taylor T. A genetic regulatory network-inspired real-time controller for a group of underwater robots. In: Proceedings of the 8th Conference on Intelligent Autonomous Systems (IAS-8). Amsterdam, 2004. 403−412

[102] Jaulin L. A nonlinear set membership approach for the localization and map building of underwater robots. *IEEE Transactions on Robotics*, 2009, **25**(1): 88−98

[103] Tarn T J, Shoults G A, Yang S P. A dynamic model of an underwater vehicle with a robotic manipulator using Kane's method. *Underwater Robots*. US: Springer, 1996. 195−209

[104] Nakamura Y, Mukherjee R. Nonholonomic path planning of space robots via a bidirectional approach. *IEEE Transactions on Robotics and Automation*, 1991, **7**(4): 500−514

[105] Wee L B, Walker M W. On the dynamics of contact between space robots and configuration control for impact minimization. *IEEE Transactions on Robotics and Automation*, 1993, **9**(5): 581−591

[106] Ulrich S, Sasiadek J Z. Extended Kalman filtering for flexible joint space robot control. In: Proceedings of the 2011 American Control Conference. San Francisco, CA: IEEE, 2011. 1021−1026

[107] Campion G, Bastin G, D'Andrea-Novel B. Structural properties and classification of kinematic and dynamic models of wheeled mobile robots. *IEEE Transactions on Robotics and Automation*, 1996, **12**(1): 47−62

[108] Dixon W E, Dawson D M, Zergeroglu E, Behal A. *Nonlinear Control of Wheeled Mobile Robots*. London: Springer-Verlag, 2001.

[109] Dong W J. Tracking control of multiple-wheeled mobile robots with limited information of a desired trajectory. *IEEE Transactions on Robotics*, 2012, **28**(1): 262−268

[110] Chwa D. Fuzzy adaptive tracking control of wheeled mobile robots with state-dependent kinematic and dynamic disturbances. *IEEE Transactions on Fuzzy Systems*, 2012, **20**(3): 587−593

[111] Siegwart R, Nourbakhsh I R, Scaramuzza D. *Introduction to Autonomous Mobile Robots* (Second edition). Cambridge: MIT Press, 2011.

[112] Blažič S. A novel trajectory-tracking control law for wheeled mobile robots. *Robotics and Autonomous Systems*, 2011, **59**(11): 1001−1007

[113] Wei S M, Uthaichana K, Žefran M, DeCarlo R. Hybrid model predictive control for the stabilization of wheeled mobile robots subject to wheel slippage. *IEEE Transactions on Control Systems Technology*, 2013, **21**(6): 2181−2193

[114] Roman H T, Pellegrino B A, Sigrist W R. Pipe crawling inspection robots: an overview. *IEEE Transactions on Energy Conversion*, 1993, **8**(3): 576−583

[115] Roh S, Choi H R. Differential-drive in-pipe robot for moving inside urban gas pipelines. *IEEE Transactions on Robotics*, 2005, **21**(1): 1−17

[116] Park J, Hyun D, Cho W H, Kim T H, Yang H S. Normal-force control for an in-pipe robot according to the inclination of pipelines. *IEEE Transactions on Industrial Electronics*, 2011, **58**(12): 5304−5310

[117] Murray R M, Walsh G, Sastry S S. Stabilization and tracking for nonholonomic control systems using time-varying state feedback. In: Proceedings of the 2nd IFAC Symposium on Nonlinear Control Systems Design 1992. Bordeaux, France: IFAC, 1993. 109−114

[118] Huang J S, Wen C Y, Wang W, Jiang Z P. Adaptive stabilization and tracking control of a nonholonomic mobile robot with input saturation and disturbance. *Systems and Control Letters*, 2013, **62**(3): 234−241

[119] Chen H, Zhang J B, Chen B Y, Li B J. Global practical stabilization for non-holonomic mobile robots with uncalibrated visual parameters by using a switching controller. *IMA Journal of Mathematical Control and Information*, 2013, **30**(4): 543−557

[120] Chen H, Wang C L, Zhang D K, Yang F. Finite-time robust stabilization of dynamic feedback nonholonomic mobile robots based on visual servoing with input saturation. In: Proceedings of the 10th World Congress on Intelligent Control and Automation (WCICA). Beijing, China: IEEE, 2012. 3686−3691

[121] Brockett R W. Asymptotic stability and feedback stabilization. *Differential Geometric Control Theory*. Boston: Birkhauser, 1983. 181−208

[122] Sordalen O J, Egeland O. Exponential stabilization of nonholonomic chained systems. *IEEE Transactions on Automatic Control*, 1995, **40**(1): 35−49

[123] Prieur C, Astolfi A. Robust stabilization of chained systems via hybrid control. *IEEE Transactions on Automatic Control*, 2003, **48**(10): 1768−1772

[124] Hussein I I, Bloch A M. Optimal control of underactuated nonholonomic mechanical systems. *IEEE Transactions on Automatic Control*, 2008, **53**(3): 668−682

[125] Qu Z, Wang J, Plaisted C E, Hull R A. Global-stabilizing near-optimal control design for nonholonomic chained systems. *IEEE Transactions on Automatic Control*, 2006, **51**(9): 1440−1456

[126] Suruz Miah M, Gueaieb W. Optimal time-varying P-controller for a class of uncertain nonlinear systems. *International Journal of Control, Automation and Systems*, 2014, **12**(4): 722−732

Hua Chen received the B. S. degree from the Department of Mathematics at Yangzhou University, China, 2001, received the M. S. degree from the Department of Management Sciences and Engineering at Nanjing University, China in 2009, and received the Ph. D. degree from the Department of Control Science and Engineering at University of Shanghai for Science and Technology, China in 2012. Currently, he is an associate professor in the Mathematics and Physics Department at Hohai University, Changzhou Campus. His research interests include constrained control design for nonlinear systems, motion control of nonholonomic mobile robots, analysis and control of fractional-order systems. Corresponding author of this paper.

YangQuan Chen received the Ph. D. degree in advanced control and instrumentation from Nanyang Technological University, Singapore, in 1998. Dr. Chen was on the Faculty of Electrical and Computer Engineering at Utah State University before he joined the School of Engineering, University of California, Merced in 2012 where he teached "Mechatronics" for juniors and "Fractional Order Mechanics" for graduates. His current research interests include mechatronics for sustainability, cognitive process control and hybrid lighting control, multi-UAV based cooperative multi-spectral "personal remote sensing" and applications, applied fractional calculus in controls, signal processing and energy informatics, distributed measurement and distributed control of distributed parameter systems using mobile actuator and sensor networks.

Study on Four Disturbance Observers for FO-LTI Systems

Songsong Cheng, Shengguo Wang, *Senior Member, IEEE,* Yiheng Wei, *Member, IEEE,* Qing Liang, *Member, IEEE,* and Yong Wang, *Senior Member, IEEE*

***Abstract*—This paper addresses the problem of designing disturbance observer for fractional order linear time invariant (FO-LTI) systems, where the disturbance includes time series expansion disturbance and sinusoidal disturbance. On one hand, the reduced order extended state observer (ROESO) and reduced order cascade extended state observer (ROCESO) are proposed for the case that the system state can be measured directly. On the other hand, the extended state observer (ESO) and the cascade extended state observer (CESO) are presented for another case when the system state cannot be measured directly. It is shown that combination of ROCESO and CESO can achieve a highly effective observation result. In addition, the way how to tune observer parameters to ensure the stability of the observers and reduce the observation error is presented in this paper. Finally, numerical simulations are given to illustrate the effectiveness of the proposed methods.**

***Index Terms*—Fractional order linear time invariant (FO-LTI) systems, disturbance observer, reduced order, cascade method.**

I. Introduction

In recent years, fractional order systems (FOSs) have attracted considerable attention from control community, since many engineering plants and processes cannot be described concisely and precisely without the introduction of fractional order calculus[1−6]. Due to the tremendous efforts devoted by researchers, a number of valuable results on stability analysis[7−10] and controller synthesis[11−14] of FOSs have been reported in the literature.

Tracking reference signal and disturbance rejection are two of the challenging and significant tasks in engineering plants and processes. It is important to reject disturbance so as to maintain the controlled system running in a fine manner. Aimed at disturbance rejection to enhance control performance, numerous methods have been presented[15]. Sliding mode control (SMC) is an effective method which involves designing of a sliding surface and reaching motion controller. Reference [16] gives the detailed contents to introduce the SMC technique. Guo et al. developed SMC approach to reject disturbance for the Euler-Bernoulli beam in [17]. However, the chattering in sliding surface is the main drawback of SMC. Adaptive control is another method to reject disturbance by adjusting the control parameters automatically[18−19]. While both SMC and adaptive control suppress disturbance passively by improving the robustness of the controller to reduce the sensitivity to external disturbance in the output channel, rather than by actively obtaining the characteristics of the disturbance in time domain or frequency domain. Therefore, the obvious drawback of the two methods is that there is an undesirable trade-off between reference tracking and disturbance rejection[20].

Another idea for disturbance rejection is to utilize the information of the external disturbance to build the feedback compensation, namely, to reject disturbance actively. Active disturbance rejection control (ADRC)[21] technique is proposed by Han in 1998, in which the uncertainties of system model and external disturbance are regarded totally as an extended state which can be observed by an extended state observer. Internal model control is another method to reject disturbance actively. Fedele et al. employed an orthogonal signals generator based on a second-order generalized integrator (OSG-SOGI) to estimate the frequency of the unknown external sinusoidal disturbance, which can be utilized to build internal model control (IMC) algorithm for the disturbed system[22]. However, how to extract the unknown external disturbance for the OSG-SOGI is a difficult issue. Disturbance observer (DOB) is a popular approach to compensate disturbance actively, which was proposed by Nakao et al.[23] in 1987. Chen et al. investigated the disturbance observer based control and related methods in [24]. Park et al. developed DOB algorithm for industrial robots to compensate external disturbance in [25]. While the main drawback of the DOB is that the inverse dynamics of the system, which may cause cancellation of unstable poles and unstable zeros, is required. Ginoya et al. proposed an extended disturbance observer for unmatched uncertain systems based on the assumption that the system state can be measured accurately[26]. However, the assumption cannot be satisfied in many cases. Therefore, it is an important and meaningful issue to develop a method to observe the external disturbance by utilizing the control input and the measured output of the disturbed system.

Motivated by the discussions above, we develop ROESO and ROCESO to observe the external disturbance under the

Manuscript received September 16, 2015; accepted April 18, 2016. This work was supported by the National Natural Science Foundation of China (61573332, 61601431), and Fundamental Research Funds for the Central Universities (WK2100100028). Recommended by Associate Editor YangQuan Chen.

Citation: Songsong Cheng, Shengguo Wang, Yiheng Wei, Qing Liang, Yong Wang. Study on four disturbance observers for FO-LTI systems. *IEEE/CAA Journal of Automatica Sinica*, 2016, **3**(4): 442−450

Songsong Cheng, Yiheng Wei, Qing Liang and Yong Wang are with the Department of Automation, University of Science and Technology of China, Hefei 230027, China (e-mail: sscheng@mail.ustc.edu.cn; neudawei@ustc.edu.cn; liangq@ustc.edu.cn; yongwang@ustc.edu.cn).

Shengguo Wang is with the Department of Engineering Technology and Department of Software and Information Systems, University of North Carolina (UNC) at Charlotte, NC 28223-0001, USA (e-mail: swang@uncc.edu).

Color versions of one or more of the figures in this paper are available online at http://ieeexplore.ieee.org.

assumption that the state can be measured and then propose a way to improve accuracy of the observations. Furthermore, by considering the case that the state cannot be measured directly, ESO is developed to observe the disturbance, in which only the control input and system output signals are utilized. In addition, the CESO is proposed based on ESO to extend the scope of the observations and to get a more effective performance of the observations than the ESO.

The rest of this paper is structured as follows. Section II provides some background materials and the main problem. ROESO and ROCESO for measurable system state and ESO and CESO for unmeasurable system state are presented in Section III. In Section IV, some numerical simulation examples are provided to illustrate the effectiveness of the proposed methods. Conclusions are given in Section V.

Notations. I_n and 0_n are used to denote a $n \times n$ identity matrix and $n \times n$ zero matrix, respectively. $0_{n \cdot m}$ is used to denote a $n \times m$ zero matrix. $\|e(t)\|$ represents the Euclidean norm of $e(t)$. $\mathrm{sym}(M) = M + M^{\mathrm{T}}$. $\Omega^{n \cdot n} = \{X \tan(\pi\alpha/2) + Y : X, Y \in \mathbf{R}^{n \cdot n}, \begin{bmatrix} X & Y \\ -Y & X \end{bmatrix} > 0\}$.

II. Problem Formulation and Preliminaries

Consider the following disturbed FO-LTI system with an assumption that the order α is known in prior:

$$\begin{cases} D^\alpha x(t) = Ax(t) + Bu(t) + Fd(t), \\ y(t) = Cx(t) color1, \end{cases} \tag{1}$$

where the order $0 < \alpha < 1$; $x(t) \in \mathbf{R}^n$, $u(t) \in \mathbf{R}^m$, $d(t) \in \mathbf{R}^q$ and $y(t) \in \mathbf{R}^p$ are the system state, the control input, the disturbance and the measurable output, respectively; the system matrices A, B, F and C are the constant real matrices with appropriate dimensions, and $F = BJ$ where J is a constant matrix, and $\mathrm{rank}(F) = q$. The definition of the fractional order derivative can be referred to [1].

The following Caputo's definition is adopted for fractional derivatives of order α for function $f(t)$

$$D^\alpha f(t) = \frac{1}{\Gamma(m-\alpha)} \int_0^t (t-\tau)^{m-\alpha-1} f^{(m)}(\tau) \mathrm{d}\tau, \tag{2}$$

where $m - 1 < \alpha < m$, $m \in \mathbf{N}$ and $\Gamma(x) = \int_0^\infty \mathrm{e}^{-t} t^{x-1} \mathrm{d}t$. And the Riemann-Liouville's fractional order integral is defined as

$$I^\alpha f(t) = \frac{1}{\Gamma(\alpha)} \int_0^t (t-\tau)^{\alpha-1} f(\tau) \mathrm{d}\tau, \tag{3}$$

where $\alpha > 0$.

In this study, the objective is to develop an approach to ensure the designed observer stable and the external disturbance can be observed by the observer under the following assumptions:

1) Pair $\{A, B\}$ is controllable;
2) Pair $\{A, C\}$ is observable.

In this paper, in order to show the generality of the proposed method, we consider two kinds of disturbances: time series expansion disturbance and sinusoidal disturbance. The time series expansion disturbance has the following form

$$d(t) = \sum_{i=0}^{k} d_i t^{n_i}, \tag{4}$$

where d_i $(i \in \{0, 1, \ldots, k\})$ is constant but unknown, $n_{i-1} \leq n_i$ $(i \in \{1, \ldots, k\})$ and $n_k < 2\alpha$ holds. Based on the relationship between n_k and α, the disturbance can be divided into the following two categories:

1) Slowly varying disturbance $n_k < \alpha$;
2) Slope forms disturbance $\alpha \leq n_k < 2\alpha$.

This paper aims at designing a proper method to observe the external unknown disturbance. For this purpose, the following lemmas are first introduced.

Lemma 1[27]**.** Let $x(t) \in \mathbf{R}$ be a continuous and differentiable function. Then the α-th derivative of $x^2(t)$ has the following properties

$$D^\alpha x^2(t) \leq 2x(t) D^\alpha x(t). \tag{5}$$

Consider a FO-LTI system as follows

$$D^\alpha x(t) = (A + BKC)\, x(t). \tag{6}$$

Based on the system (6), we give our research result in [28] as a lemma as follows.

Lemma 2[28]**.** The system in (6) with $0 < \alpha < 1$ is asymptotically stable, if there exist matrices $Z \in \Omega^{n \cdot n}$, $G \in \mathbf{R}^{m \cdot m}$, and $H \in \mathbf{R}^{m \cdot p}$, such that

$$\begin{bmatrix} \Xi & Z^{\mathrm{T}} B + C^{\mathrm{T}} H^{\mathrm{T}} - {K_0}^{\mathrm{T}} G^{\mathrm{T}} \\ * & -\mathrm{sym}(G) \end{bmatrix} < 0 \tag{7}$$

is feasible, and the matrix K is given by

$$K = G^{-1} H, \tag{8}$$

where $*$ stands for the symmetrical part matrix, $\Xi = \mathrm{sym}(Z^{\mathrm{T}} A + Z^{\mathrm{T}} B K_0)$, and K_0 is an additional initialization matrix, which is derived from $K_0 = QP^{-1}$. The matrices $P \in \Omega^{n \cdot n}$ and $Q \in \mathbf{R}^{m \cdot n}$ satisfy following linear matrix inequality (LMI),

$$\mathrm{sym}(AP + BQ) < 0. \tag{9}$$

III. Main Results

A. Reduced Order Extended State Observer (ROESO)

If the state of the FO-LTI system (1) can be measured directly, we can utilize the state to design a disturbance observer as follows:

$$\begin{cases} \hat{d}(t) = \Lambda \varepsilon(t), \\ \varepsilon(t) = F^+ x(t) - z(t), \\ D^\alpha z(t) = F^+ [Ax(t) + Bu(t)] + \hat{d}(t), \end{cases} \tag{10}$$

where $F^+ = (F^{\mathrm{T}} F)^{-1} F^{\mathrm{T}}$, Λ is a positive definite $q \times q$ diagonal matrix.

Theorem 1. The disturbance can be observed asymptotically by (10), if the disturbance is slowly varying disturbance, namely, $\lim_{t\to\infty} D^\alpha d(t) = 0$.

Proof. Define the observation error $e(t) = d(t) - \hat{d}(t)$ which yields

$$\begin{aligned} D^\alpha e(t) &= D^\alpha d(t) - D^\alpha \hat{d}(t) \\ &= D^\alpha d(t) - \Lambda D^\alpha \varepsilon(t) \\ &= D^\alpha d(t) - \Lambda e(t). \end{aligned} \tag{11}$$

The Laplace transform of (11) is

$$s^{\alpha}E(s)-s^{\alpha-1}e(0)=s^{\alpha}D(s)-s^{\alpha-1}d(0)-\Lambda E(s), \quad (12)$$

where $E(s)$ and $D(s)$ are the Laplace transforms of $e(t)$ and $d(t)$, respectively. Then using the final-value theorem, yields

$$\begin{aligned}e(\infty)&=\lim_{s\to 0} sE(s)\\&=\lim_{s\to 0}(sI_q+\Lambda)^{-1}[s^{1+\alpha}D(s)-s^{\alpha}d(0)+s^{\alpha}e(0)].\end{aligned} \quad (13)$$

Then if $\lim_{s\to 0} s^{1+\alpha}D(s)=0$, that is $\lim_{t\to\infty} D^{\alpha}d(t)=0$, thereby, $\lim_{t\to\infty} e(t)=0$. □

Remark 1. Since the disturbance can be observed asymptotically if $\lim_{t\to\infty} D^{\alpha}d(t)=0$, the constant disturbance, etc. can be observed asymptotically by the ROESO. In addition, square disturbance also satisfies the condition of Theorem 1 when the hopping points are overlooked.

Remark 2. The gain Λ can change the rate of convergence of the observer. The larger value of Λ is, the higher rate of convergence we can get.

B. Reduced Order Cascade Extended State Observer (ROCESO)

In order to expand the scope of the disturbance that can be observed asymptotically based on the system state can be measured directly, we improve the ROESO to ROCESO as follows

$$\begin{cases}\hat{d}(t)=2\Lambda\varepsilon(t)+\Lambda^2 I^{\alpha}\varepsilon(t),\\ \varepsilon(t)=F^{+}x(t)-z(t),\\ D^{\alpha}z(t)=F^{+}\left[Ax(t)+Bu(t)\right]+\hat{d}(t),\end{cases} \quad (14)$$

where Λ is a positive definite $q\times q$ diagonal matrix.

Theorem 2. The disturbance can be observed asymptotically by (14), if the disturbance is of slope form, namely, $\lim_{t\to\infty} D^{2\alpha}d(t)=0$.

Proof. Define the observation error $e(t)=d(t)-\hat{d}(t)$, it yields

$$\begin{aligned}D^{\alpha}e(t)&=D^{\alpha}d(t)-D^{\alpha}\hat{d}(t)\\&=D^{\alpha}d(t)-D^{\alpha}\left[2\Lambda\varepsilon(t)+\Lambda^2I^{\alpha}\varepsilon(t)\right]\\&=D^{\alpha}d(t)-2\Lambda e(t)-\Lambda^2\varepsilon(t).\end{aligned} \quad (15)$$

Based on (15), the 2α-th derivative of $e(t)$ can be expressed as

$$D^{2\alpha}e(t)=D^{2\alpha}d(t)-2\Lambda D^{\alpha}e(t)-\Lambda^2 e(t). \quad (16)$$

If $0<\alpha\leq 0.5$, the Laplace transform of (16) is

$$\begin{aligned}&s^{2\alpha}E(s)-s^{2\alpha-1}e(0)\\&\quad=s^{2\alpha}D(s)-s^{2\alpha-1}d(0)-2\Lambda s^{\alpha}E(s)\\&\qquad+2\Lambda s^{\alpha-1}e(0)-\Lambda^2E(s),\end{aligned} \quad (17)$$

where $E(s)$ and $D(s)$ are the Laplace transforms of $e(t)$ and $d(t)$, respectively. Then using the final-value theorem, yields

$$\begin{aligned}e(\infty)=&\lim_{s\to 0}(s^{2\alpha}I_q+2\Lambda s^{\alpha}+\Lambda^2)^{-1}\\&\times[s^{1+2\alpha}D(s)-s^{2\alpha}d(0)+s^{2\alpha}e(0)+2\Lambda s^{\alpha}e(0)].\end{aligned} \quad (18)$$

Then if $\lim_{s\to 0} s^{1+2\alpha}D(s)=0$, that is $\lim_{t\to\infty} D^{2\alpha}d(t)=0$, thereby, $\lim_{t\to\infty} e(t)=0$. If $0.5<\alpha\leq 1$, the Laplace transform of (16) is

$$\begin{aligned}E(s)&-s^{2\alpha-1}e'(0)-s^{2\alpha-2}e(0)\\&=s^{2\alpha}D(s)-s^{2\alpha-1}d'(0)-s^{2\alpha-2}d(0)\\&\quad-2\Lambda s^{\alpha}E(s)+2\Lambda s^{\alpha-1}e(0)-\Lambda^2E(s),\end{aligned} \quad (19)$$

and it is easy to obtain the same conclusion. All of these discussions establish the Theorem 2. □

Remark 3. Since the disturbance can be observed by ROCESO if $\lim_{t\to\infty} D^{2\alpha}d(t)=0$, the scope of the disturbance observation is expanded from slowly varying disturbance to time series expansion disturbance, which is defined as (2). Therefore, not only the square disturbance, but also the sawtooth disturbance can be observed asymptotically, if $0.5<\alpha\leq 1$.

C. Extended State Observer (ESO)

In the former contents, we have developed ROESO and ROCESO to observe time series expansion disturbance asymptotically based on the ability to directly measure the system state. While, in most cases, the system state cannot be measured directly. And now we are in the position to utilize the control input and output signals only to develop ESO to observe slowly varying disturbance asymptotically and to observe other disturbances with bounded error based on $\lim_{t\to\infty}|D^{\alpha}d(t)|\leq\mu$, with $\mu>0$. In addition, we will propose a way to lower the boundary of the observation error.

Theorem 3. $\{\bar{A},\bar{C}\}$ is observable, if $\{A,C\}$ is observable and $\mathrm{rank}(F^{\mathrm{T}}A^{(n-1)\mathrm{T}}[\begin{matrix}C^{\mathrm{T}} & A^{\mathrm{T}}C^{\mathrm{T}} & \dots & A^{(p-1)\mathrm{T}}C^{\mathrm{T}}\end{matrix}])\geq q$, where $\bar{A}=\begin{bmatrix}A & F\\ 0_{q\cdot n} & 0_q\end{bmatrix}$, $\bar{C}=[\begin{matrix}C & 0_{p\cdot q}\end{matrix}]$.

Proof. According to [1], $\{A,C\}$ is observable, if and only if the observability matrix M_O is full column rank, where $M_O=[\begin{matrix}C^{\mathrm{T}} & A^{\mathrm{T}}C^{\mathrm{T}} & \dots & A^{(n-1)\mathrm{T}}C^{\mathrm{T}}\end{matrix}]^{\mathrm{T}}$.

As a result, the observability matrix $\bar{M}_o$ related to $\{\bar{A},\bar{C}\}$ can be described as

$$\begin{aligned}\bar{M}_o&=[\begin{matrix}\bar{C}^{\mathrm{T}} & \bar{A}^{\mathrm{T}}\bar{C}^{\mathrm{T}} & \dots & \bar{A}^{(n+p-1)\mathrm{T}}\bar{C}^{\mathrm{T}}\end{matrix}]^{\mathrm{T}}\\&=\begin{bmatrix}C^{\mathrm{T}} & A^{\mathrm{T}}C^{\mathrm{T}} & \dots & A^{(n+p-1)\mathrm{T}}C^{\mathrm{T}}\\ 0_{q\cdot p} & F^{\mathrm{T}}C^{\mathrm{T}} & \dots & F^{\mathrm{T}}A^{(n+p-2)\mathrm{T}}C^{\mathrm{T}}\end{bmatrix}^{\mathrm{T}},\end{aligned} \quad (20)$$

which implies that

$$\begin{aligned}&\mathrm{rank}(\bar{M}_o)\\&\quad=\mathrm{rank}\left(\begin{bmatrix}C^{\mathrm{T}} & A^{\mathrm{T}}C^{\mathrm{T}} & \dots & A^{(n+p-1)\mathrm{T}}C^{\mathrm{T}}\\ 0 & F^{\mathrm{T}}C^{\mathrm{T}} & \dots & F^{\mathrm{T}}A^{(n+p-2)\mathrm{T}}C^{\mathrm{T}}\end{bmatrix}\right)\\&\quad\geq\mathrm{rank}([\begin{matrix}C^{\mathrm{T}} & A^{\mathrm{T}}C^{\mathrm{T}} & \cdots & A^{(n-1)\mathrm{T}}C^{\mathrm{T}}\end{matrix}])\\&\qquad+\mathrm{rank}\left([\begin{matrix}F^{\mathrm{T}}A^{(n-1)\mathrm{T}}C^{\mathrm{T}} & \dots & F^{\mathrm{T}}A^{(n+p-2)\mathrm{T}}C^{\mathrm{T}}\end{matrix}]\right)\\&\quad=n+\mathrm{rank}(F^{\mathrm{T}}A^{(n-1)\mathrm{T}}\left[\begin{matrix}C^{\mathrm{T}} & \dots & A^{(p-1)\mathrm{T}}C^{\mathrm{T}}\end{matrix}\right])\\&\quad\geq n+q.\end{aligned} \quad (21)$$

Since $\bar{M}_O\in\mathbf{R}^{p(n+q)\cdot(n+q)}$, we have

$$\begin{aligned}\mathrm{rank}\left(\bar{M}_O\right)&\leq\min\left(p(n+q),(n+q)\right)\\&=n+q.\end{aligned}$$

Proceeding forward, we have

$$\operatorname{rank}\left(\bar{M}_O\right) = n + q. \tag{22}$$

□

Theorem 4. If the α-th order derivative of the disturbance satisfy $\lim_{t\to\infty} D^\alpha d(t) = 0$, the disturbance can be observed asymptotically by following observer

$$\begin{cases} D^\alpha \hat{x}(t) = A\hat{x}(t) + Bu(t) + F\hat{d}(t) + L_1[\hat{y}(t) - y(t)], \\ \hat{y}(t) = C\hat{x}(t), \\ D^\alpha \hat{d}(t) = L_2[\hat{y}(t) - y(t)]. \end{cases} \tag{23}$$

Proof. Defining state observation error $e_x(t) = x(t) - \hat{x}(t)$ and disturbance observation error $e_d(t) = d(t) - \hat{d}(t)$, we can easily get the following equation

$$\begin{aligned} \begin{bmatrix} D^\alpha e_x(t) \\ D^\alpha e_d(t) \end{bmatrix} &= \left(\begin{bmatrix} A & F \\ 0_{q\cdot n} & 0_q \end{bmatrix} + \begin{bmatrix} L_1 \\ L_2 \end{bmatrix} \begin{bmatrix} C & 0_{p\cdot q} \end{bmatrix} \right) \\ &\quad \times \begin{bmatrix} e_x(t) \\ e_d(t) \end{bmatrix} + \begin{bmatrix} 0_{n\cdot q} \\ I_q \end{bmatrix} w_d(t), \end{aligned} \tag{24}$$

where $w_d(t) = D^\alpha d(t)$. If we define the augment state $e(t) = \begin{bmatrix} e_x^{\mathrm{T}}(t) & e_d^{\mathrm{T}}(t) \end{bmatrix}^{\mathrm{T}}$, then (24) can be written as

$$D^\alpha e(t) = (\bar{A} + L\bar{C})e(t) + Gw_d(t), \tag{25}$$

where

$$\bar{A} = \begin{bmatrix} A & F \\ 0_{q\cdot n} & 0_q \end{bmatrix}, \quad L = \begin{bmatrix} L_1 \\ L_2 \end{bmatrix}, \quad G = \begin{bmatrix} 0_{n\cdot q} \\ I_q \end{bmatrix},$$

$$\bar{C}^{\mathrm{T}} = \begin{bmatrix} C^{\mathrm{T}} \\ 0_{q\cdot p} \end{bmatrix}.$$

By using Theorem 3, we can easily search suitable L to make the system (25) asymptotically stable by LMI if $\lim_{t\to\infty} D^\alpha d(t) = 0$, that is, the disturbance can be observed accurately. This establishes Theorem 4. □

By using LMI, we can select L such that the eigenvalues of $\bar{A} + L\bar{C}$ are in the left half plane (LHP), and thereby we can find a positive definite matrix P such that

$$(\bar{A} + L\bar{C})^{\mathrm{T}} P + P(\bar{A} + L\bar{C}) = -Q, \tag{26}$$

for any positive definite matrix Q.

Theorem 5. If the α-th derivative of $d(t)$ is bounded, the ESO can observe the disturbance and state with bounded error and the norm of the estimation error is bounded by

$$\|e(t)\| \le \frac{2\mu \left\|G^{\mathrm{T}} P\right\|}{\lambda_s}, \tag{27}$$

where λ_s is the smallest eigenvalue of Q.

Proof. Consider a Lyapunov function

$$V(t) = e^{\mathrm{T}}(t) P e(t). \tag{28}$$

Seeking for the α-th derivative of $V(t)$, yields

$$\begin{aligned} D^\alpha V(t) &\le e^{\mathrm{T}}(t)[(\bar{A} + L\bar{C})^{\mathrm{T}} P + P(\bar{A} + L\bar{C})]e(t) \\ &\quad + 2w_d(t) G^{\mathrm{T}} P e(t) \\ &\le -e^{\mathrm{T}}(t) Q e(t) + 2w_d(t) G^{\mathrm{T}} P e(t) \\ &\le -\lambda_s \|e(t)\|^2 + 2\mu \left\|G^{\mathrm{T}} P\right\| \|e(t)\| \\ &\le -\|e(t)\| \left(\lambda_s \|e(t)\| - 2\mu \left\|G^{\mathrm{T}} P\right\|\right). \end{aligned} \tag{29}$$

We can easily get that the norm of the observation error is bounded by $\frac{2\mu\left\|G^T P\right\|}{\lambda_s}$. □

Remark 4. Theorem 5 shows that the norm of the observation error is bounded by $\frac{2\mu\left\|G^T P\right\|}{\lambda_s}$, therefore, we can decrease the observation error by increasing the λ_s, which can be realized by placing all of the eigenvalues far from imaginary axis. Then ESO can observe more kinds of disturbance, such as time series expansion disturbance, sinusoidal disturbance.

D. Cascade Extended State Observer (CESO)

From the former contents, the ESO can observe the disturbance $d(t)$ asymptotically if $\lim_{t\to\infty} D^\alpha d(t) = 0$. However, it is invalid for $\lim_{t\to\infty} D^\alpha d(t) \neq 0$. In order to extend the scope of the disturbance observation and get more accurate observation results, the CESO is developed as follows:

$$\begin{cases} D^\alpha \hat{x}(t) = A\hat{x}(t) + Bu(t) + F\hat{d}(t) \\ \qquad + L_1[\hat{y}(t) - y(t)] + L_2 I^\alpha[\hat{y}(t) - y(t)], \\ \hat{y}(t) = C\hat{x}(t), \\ D^\alpha \hat{d}(t) = L_3[\hat{y}(t) - y(t)] + L_4 I^\alpha[\hat{y}(t) - y(t)]. \end{cases} \tag{30}$$

Theorem 6. $\{\bar{A}, \bar{B}\}$ is controllable if $\{A, B\}$ is controllable; $\{\bar{A}, \bar{C}\}$ is observable if $\{A, C\}$ is observable, where

$$\bar{A} = \begin{bmatrix} A & F & 0_n \\ 0_{q\cdot n} & 0_{q\cdot q} & 0_{q\cdot n} \\ I_n & 0_{n\cdot q} & 0_n \end{bmatrix}, \quad \bar{B} = \begin{bmatrix} I_n & 0_{n\cdot q} \\ 0_{q\cdot n} & I_q \\ 0_n & 0_{n\cdot q} \end{bmatrix},$$

$$\bar{C} = \begin{bmatrix} I_n & 0_{n\cdot q} & 0_n \\ 0_n & 0_{n\cdot q} & I_n \end{bmatrix}.$$

Proof. According to [1], $\{A, B\}$ is controllable, if and only if the controllability matrix M_C is full row rank, where $M_C = \begin{bmatrix} B & AB & \dots & A^{n-1}B \end{bmatrix}$. $\{A, C\}$ is observable, if and only if the observability matrix M_O is full column rank, where $M_O = \begin{bmatrix} C^{\mathrm{T}} & A^{\mathrm{T}} C^{\mathrm{T}} & \dots & A^{(n-1)\mathrm{T}} C^{\mathrm{T}} \end{bmatrix}^{\mathrm{T}}$. □

As a result, the controllability matrix $\bar{M}_c$ related to $\{\bar{A}, \bar{B}\}$ can be described as

$$\begin{aligned} \bar{M}_c &= \begin{bmatrix} \bar{B} \,|\bar{A}\bar{B}| \cdots |\bar{A}^{2n+q-1}\bar{B} \end{bmatrix} \\ &= \left[\begin{array}{cc|cc|c|cc} I_n & 0_{n\cdot q} & A & F & & A^{2n+q-1} & A^{2n+q-2}F \\ 0_{q\cdot n} & I_q & 0_{q\cdot n} & 0_q & \cdots & 0_{q\cdot n} & 0_q \\ 0_n & 0_{n\cdot q} & I_n & 0_{n\cdot q} & & A^{2n+q-2} & 0_{n\cdot q} \end{array}\right], \end{aligned} \tag{31}$$

which implies that

$$\begin{aligned} \operatorname{rank}\left(\bar{M}_c\right) &\ge \operatorname{rank}\left(\begin{bmatrix} I_n & 0_{n\cdot q} & A \\ 0_{q\cdot n} & I_q & 0_{q\cdot n} \\ 0_n & 0_{n\cdot q} & I_n \end{bmatrix} \right) \\ &= 2n + q. \end{aligned} \tag{32}$$

By virtue of $\bar{M}_c \in \mathbf{R}^{(2n+q)\cdot((n+q)(2n+q))}$,

$$\begin{aligned} \operatorname{rank}(\bar{M}_c) &\le \min\left((2n+q), (2n+q)(n+q)\right) \\ &= 2n + q. \end{aligned} \tag{33}$$

All of the above stated facts lead to the following

$$\operatorname{rank}(\bar{M}_c) = 2n + q. \tag{34}$$

In the other words, $\{\bar{A}, \bar{B}\}$ is controllable.

The corresponding observability matrix $\bar{M}_O$ satisfies

$$\bar{M}_O = [\ \bar{C}^{\mathrm{T}} \mid \bar{A}^{\mathrm{T}}\bar{C}^{\mathrm{T}} \mid \cdots \mid \bar{A}^{(2n+q)\mathrm{T}}\bar{C}^{\mathrm{T}}\ ]^{\mathrm{T}} = \left[\begin{array}{ccc} I_n & 0_{n\cdot q} & 0_n \\ 0_n & 0_{n\cdot q} & I_n \\ \hline A & F & 0_n \\ I_n & 0_{n\cdot q} & 0_n \\ \hline \vdots & \vdots & \vdots \\ \hline A^{2n+q-1} & A^{2n+q-2}F & 0_n \\ A^{2n+q-2} & A^{2n+q-3}F & 0_n \end{array}\right], \tag{35}$$

which implies that

$$\operatorname{rank}(\bar{M}_O) \geq \operatorname{rank}\left(\begin{bmatrix} I_n & 0_{n\cdot q} & 0_n \\ 0_n & 0_{n\cdot q} & I_n \\ A & F & 0_n \end{bmatrix}\right) = 2n+q. \tag{36}$$

Since $\bar{M}_O \in \mathbf{R}^{2n(2n+q)\cdot(2n+q)}$, we have

$$\operatorname{rank}\left(\bar{M}_O\right) \leq \min\left(2n(2n+q), (2n+q)\right) = 2n+q. \tag{37}$$

Proceeding forward, it follows

$$\operatorname{rank}\left(\bar{M}_O\right) = 2n+q. \tag{38}$$

Consequently, $\{\bar{A}, \bar{C}\}$ is observable. □

Theorem 7. The CESO can observe the state of the disturbed system and α-th order derivative of the disturbance asymptotically, if $\lim_{t\to\infty} D^{2\alpha}d(t) = 0$.

Proof. Defining the observation error

$$e(t) = \begin{bmatrix} e_x(t) \\ e_d(t) \end{bmatrix} = \begin{bmatrix} x(t) - \hat{x}(t) \\ d(t) - \hat{d}(t) \end{bmatrix}. \tag{39}$$

Considering the α-th order derivative of $e(t)$, yields

$$\begin{bmatrix} D^\alpha e_x(t) \\ D^\alpha e_d(t) \end{bmatrix} = \begin{bmatrix} (A+L_1C)e_x(t) + Fe_d(t) + L_2CI^\alpha e_x(t) \\ D^\alpha d(t) + L_3Ce_x(t) + L_4CI^\alpha e_x(t) \end{bmatrix}. \tag{40}$$

Based on (38), considering the 2α-th order derivative of $e(t)$, yields

$$\begin{bmatrix} D^{2\alpha} e_x(t) \\ D^{2\alpha} e_d(t) \end{bmatrix} = \begin{bmatrix} A+L_1C & F \\ L_3C & 0_q \end{bmatrix}\begin{bmatrix} D^\alpha e_x(t) \\ D^\alpha e_d(t) \end{bmatrix} + \begin{bmatrix} L_2C & 0_{n\cdot q} \\ L_4C & 0_q \end{bmatrix}\begin{bmatrix} e_x(t) \\ e_d(t) \end{bmatrix} + \begin{bmatrix} 0_{n\cdot q} \\ I_q \end{bmatrix} w_d(t), \tag{41}$$

where $w_d(t) = D^{2\alpha}d(t)$. Defining the augmented state $\hat{e}(t) = [\ D^\alpha e_x^{\mathrm{T}}(t) \quad D^\alpha e_d^{\mathrm{T}}(t) \quad e_x^{\mathrm{T}}(t) \quad e_d^{\mathrm{T}}(t)\ ]^{\mathrm{T}}$, then (41) can be rewritten as

$$D^\alpha \hat{e}(t) = \hat{A}\hat{e}(t) + Gw_d(t), \tag{42}$$

where

$$\hat{A} = \begin{bmatrix} A+L_1C & F & L_2C & 0_{n\cdot q} \\ L_3C & 0_q & L_4C & 0_q \\ I_n & 0_{n\cdot q} & 0_n & 0_{n\cdot q} \\ 0_{q\cdot n} & I_q & 0_{q\cdot n} & 0_q \end{bmatrix}, \quad G = \begin{bmatrix} 0_{n\cdot q} \\ I_q \\ 0_{n\cdot q} \\ 0_q \end{bmatrix}.$$

Then we extract the state $D^\alpha e_x(t)$, $D^\alpha e_d(t)$ and $e_x(t)$ from $\hat{e}(t)$ to compose a new state $\bar{e}(t)$. Then the state space equation related to $\bar{e}(t)$ can be written as

$$D^\alpha \bar{e}(t) = \begin{bmatrix} A+L_1C & F & L_2C \\ L_3C & 0_q & L_4C \\ I_n & 0_{n\cdot q} & 0_n \end{bmatrix}\bar{e}(t) + \begin{bmatrix} 0_{n\cdot q} \\ I_q \\ 0_{n\cdot q} \end{bmatrix} w_d(t) = \left(\bar{A} + \bar{B}\bar{L}\bar{C}\right)\bar{e}(t) + \bar{G}w_d(t), \tag{43}$$

where

$$\bar{A} = \begin{bmatrix} A & F & 0_n \\ 0_{q\cdot n} & 0_q & 0_{q\cdot n} \\ I_n & 0_{n\cdot q} & 0_n \end{bmatrix}, \quad \bar{B} = \begin{bmatrix} I_n & 0_{n\cdot q} \\ 0_{q\cdot n} & I_q \\ 0_n & 0_{n\cdot q} \end{bmatrix},$$

$$\bar{G} = \begin{bmatrix} 0_{n\cdot q} \\ I_q \\ 0_{n\cdot q} \end{bmatrix}, \quad \bar{L} = \begin{bmatrix} L_1C & L_2C \\ L_3C & L_4C \end{bmatrix},$$

$$\bar{C} = \begin{bmatrix} I_{n\cdot n} & 0 & 0 \\ 0 & 0_{n\cdot q} & I_{n\cdot n} \end{bmatrix}.$$

Based on Theorem 4, we get that $\{\bar{A}, \bar{B}\}$ is controllable and $\{\bar{A}, \bar{C}\}$ is observable. Then based on Lemma 2, we can search $\bar{L}$ by using the MATLAB LMI toolbox to make the system (43) asymptotically stable, if $\lim_{t\to\infty} D^{2\alpha}d(t) = 0$. And the matrix L is given by

$$L = \bar{L}\tilde{C}^-, \tag{44}$$

where $L = \begin{bmatrix} L_1 & L_2 \\ L_3 & L_4 \end{bmatrix}$, $\tilde{C} = \begin{bmatrix} C & 0_{p\cdot n} \\ 0_{p\cdot n} & C \end{bmatrix}$ and $\tilde{C}^-$ is the pseudoinverse of $\tilde{C}$, which can be got by command $\mathrm{pinv}(C)$ in MATLAB. That means, the state of the system in (1) and α-th order derivative of disturbance can be observed accurately by CESO if only $\lim_{t\to\infty} D^{2\alpha}d(t) = 0$. This establishes Theorem 7. □

Remark 5. Although the CESO cannot observe disturbance asymptotically if $\lim_{t\to\infty} D^{2\alpha}d(t) = 0$, the state of disturbed system and α-th derivative of disturbance can be observed asymptotically. Therefore, we can combine the CESO and RO-CESO to observe the disturbance asymptotically. Hereinafter, we denote this observation method as CESO + ROCESO.

Remark 6. The disturbance can be observed by CESO + ROCESO asymptotically if $\lim_{t\to\infty} D^{2\alpha}d(t) = 0$, thereby, the CESO + ROCESO can asymptotically observe more disturbance than the ESO. And if $\lim_{t\to\infty} D^{2\alpha}d(t) \leq \mu$, the CESO + ROCESO can observe it with bounded error, and Theorem 4 and Remark 4 have given the way to reduce the observation error.

Remark 7. Four disturbance observers have been designed in this paper. From the corresponding proofs of Theorem 1, Theorem 2, Theorem 4, and Theorem 7, we can arrive that if and only if these related matrices (Λ in (13) and (18), $\bar{A}+L\bar{C}$)

in (25), and $\bar{A}+\bar{B}\bar{L}\bar{C}$ in (43)) are designed stable and the conditions about the disturbance are satisfied, the convergence of the relevant observation errors are not affected by the initial value of these observation errors.

IV. Illustrative Examples

All the numerical examples illustrated in this paper are implemented via the piecewise numerical approximation algorithm. For more information about the algorithm one can refer to [29].

Example 1. Consider a disturbed fractional order gas-turbine system[30] as follows:

$$\begin{cases} D^{0.84}x(t) = Ax(t) + Bu(t) + Fd(t), \\ y(t) = Cx(t), \end{cases} \tag{45}$$

where

$$A = \begin{bmatrix} 0 & 1 \\ -136.24 & -18.4741 \end{bmatrix}, \quad B = \begin{bmatrix} 0 \\ 1 \end{bmatrix},$$

$$F = \begin{bmatrix} 0 \\ 3 \end{bmatrix}, \quad C^{\mathrm{T}} = \begin{bmatrix} 0 \\ 14164.9 \end{bmatrix},$$

and assume that the state can be measured directly.

We get that the disturbed system is completely controllable and observable. Considering the disturbance is square wave (amplitude $=1$ and frequency $=0.5$). Fig. 1 shows the disturbance observed by ROESO. And in Fig. 1, $d(t)$, $\hat{d}_1(t)$, $\hat{d}_2(t)$, and $\hat{d}_3(t)$ are the primary disturbance and the observed results with $\Lambda = 20, 50, 100$, respectively, and $e_1(t)$, $e_2(t)$, $e_3(t)$ are the corresponding observation errors. The observation results illustrate that the ROESO can asymptotically observe the slowly varying disturbance (square wave). And the bigger value of Λ is, the faster observation convergence rate we can get.

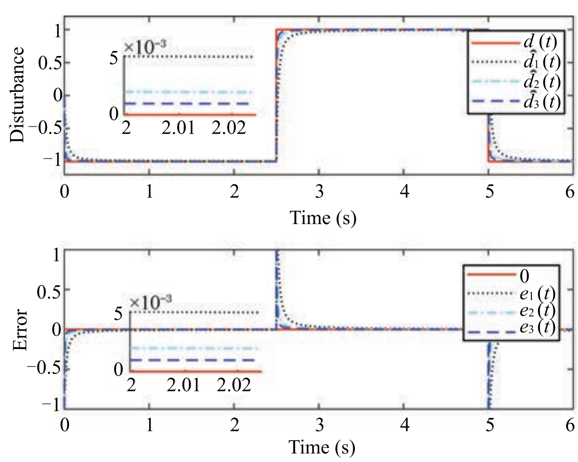

Fig. 1. Observed results for square disturbance of Example 1.

Example 2. Consider system (45) is disturbed by sawtooth wave (amplitude $=1$ and frequency $=0.1$) and assume that the state can be measured directly.

We choose the ROCESO to observe the sawtooth wave and show the observed results as Fig. 2. In Fig. 2, $d(t)$, $\hat{d}_1(t)$, $\hat{d}_2(t)$, and $\hat{d}_3(t)$ are the primary disturbance and the observed results with $\Lambda = 20, 50, 100$, respectively, and $e_1(t)$, $e_2(t)$, $e_3(t)$ are the corresponding observation errors. The observed results illustrate that the ROCESO can asymptotically observe the slope forms disturbance (sawtooth), and then the slowly varying disturbance can be observed by ROCESO certainly. And the bigger value of Λ is, the faster observation convergence rate we can get.

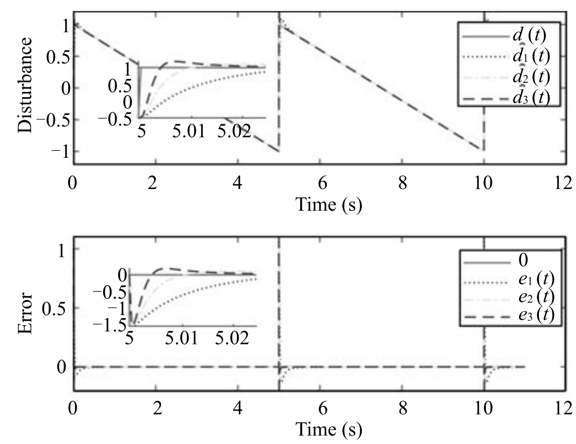

Fig. 2. Observed results for sawtooth disturbance of Example 2.

Example 3. Considering the disturbances in system (45) are square wave (amplitude $=1$ and frequency $=0.1$) and sinusoidal wave as $1+\sin(2t)+2.5\cos(3t)$, and assume that the state cannot be measured directly.

Figs.3-6 show these states and disturbances observed by ESO, respectively. And in these figures, $x_1(t)$, $\hat{x}_{11}(t)$, $\hat{x}_{12}(t)$, $\hat{x}_{13}(t)$ are the system state 1 and the corresponding observed state with $L_1^{\mathrm{T}} = [-0.007 - 0.111]$, $[-0.005 - 0.158]$, $[-0.022 - 2.977]$ and $L_2 = -0.811$, -1.186, -49.370, respectively. And $e_{11}(t)$, $e_{12}(t)$, and $e_{13}(t)$ are the corresponding state observation errors. $\hat{d}_1(t)$, $\hat{d}_2(t)$, and $\hat{d}_3(t)$ are the corresponding observation disturbance and $e_1(t)$, $e_2(t)$, $e_3(t)$ are the corresponding observation errors. The eigenvalues of $\bar{A}+L\bar{C}$ in (23) with respect to the different matrixes $L^{\mathrm{T}} = [L_1^{\mathrm{T}}, L_2^{\mathrm{T}}]$ are shown in Table I. Table I and the simulation results illustrate that the larger distance between the eigenvalues and the imaginary axis is, the more accurate observed result we can get, which demonstrate Theorem 5 and Remark 4 in numerical simulation.

TABLE I
The eigenvalues of $\bar{A}+L\bar{C}$ with respect to the different matrixes L

L_1^{T}	$[-0.007-0.111]$	$[-0.005-0.158]$	$[-0.022-2.977]$
L_2	-0.811	-1.186	-49.370
	$-20.34-7.06\mathrm{i}$	$-33.97-30.82\mathrm{i}$	$-130.24-112.63\mathrm{i}$
eig[1]	$-20.34+7.06\mathrm{i}$	$+33.97+30.82\mathrm{i}$	$-130.24+112.63\mathrm{i}$
	-74.34	-23.96	-70.76

Example 4. Consider another disturbed system as follows:

$$\begin{cases} D^{0.8}x(t) = Ax(t) + Bu(t) + Fd(t), \\ y(t) = Cx(t), \end{cases} \tag{46}$$

[1]The eigenvalues of $\bar{A}+L\bar{C}$

where

$$A=\begin{bmatrix}0 & 1\\ 1 & -2\end{bmatrix},\quad B=\begin{bmatrix}1\\ 1\end{bmatrix},$$
$$F=\begin{bmatrix}3\\ 3\end{bmatrix},\quad C^{\mathrm{T}}=\begin{bmatrix}1\\ 0\end{bmatrix},$$

and assume that the state cannot be measured directly.

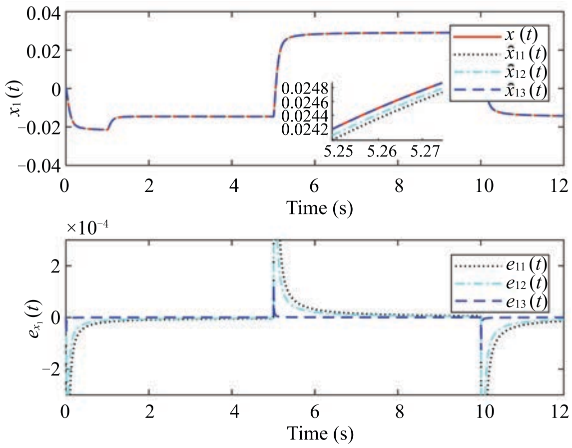

Fig. 3. Observed results for $x_1(t)$ disturbed by square disturbance of Example 3.

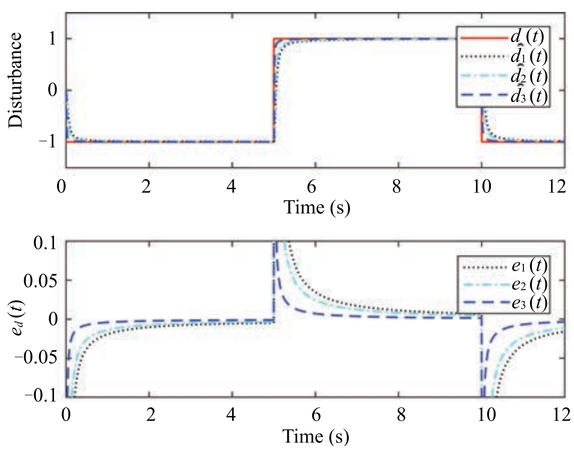

Fig. 4. Observed results for square disturbance of Example 3.

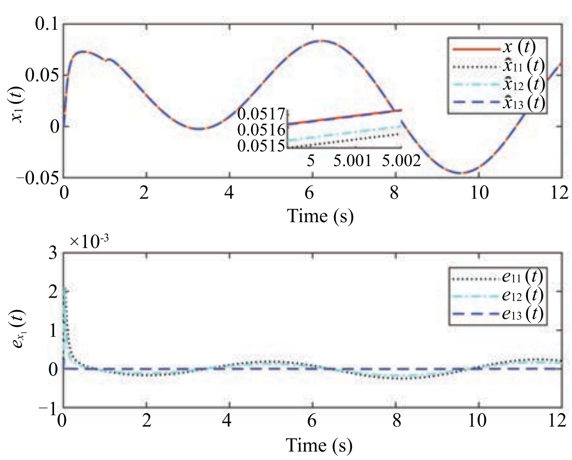

Fig. 5. Observed results for $x_1(t)$ disturbed by sinusoidal disturbance of Example 3.

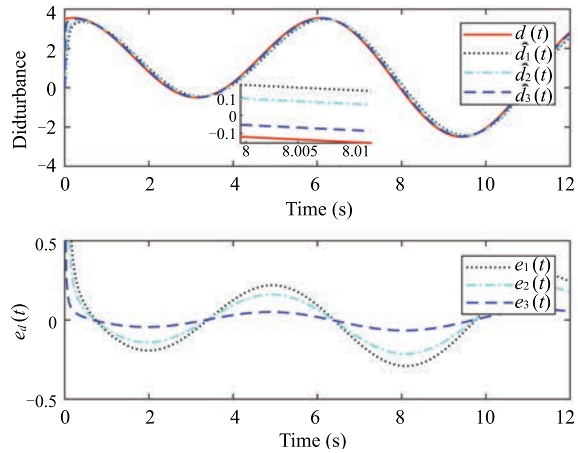

Fig. 6. Observed results for sinusoidal disturbance of Example 3.

It is completely controllable and observable. We can easily get that the system is unstable with poles equal to -2.4142, 0.4142. Consider the disturbances are sawtooth (amplitude $=$ 1 and frequency $= 0.2$) and sinusoidal as $\sin(t)+0.5\sin(1.5t)$. The matrix L of ESO is set as $[-56.59\ 4135.56\ \ -1950.61]$; the Λ of ROCESO is set as 15; the matrixes L_1, L_2, L_3, and L_4 in CESO are set as $[-59.81\ -21.91]^{\mathrm{T}}$, $[-764.93\ -320.81]^{\mathrm{T}}$, -141.98 and -2223.81, respectively. The L in ESO and L_i $(i\in 1,2,3,4)$ in CESO can be sought by MATLAB LMI tool box. Fig. 7 and Fig. 8 show observation results of CESO for the system state, which is disturbed by sawtooth disturbance and sinusoidal disturbance, respectively. In Fig. 9 and Fig. 10, $\hat{d}_1(t)$, $\hat{d}_2(t)$, and $\hat{d}_3(t)$ are the disturbance observation results of ESO, CESO, and ROCESO + CESO, respectively, and $e_1(t)$, $e_2(t)$, and $e_3(t)$ are the corresponding observation errors of $\hat{d}_1(t)$, $\hat{d}_2(t)$, and $\hat{d}_3(t)$. The simulation results show that no matter what the kinds of the disturbance is and no matter the disturbed system whether or not stable, the ROCESO + CESO, which utilize the control input and output signals only, can observe the external unknown disturbance more accurately than ESO and CESO.

V. CONCLUSION

In this article, disturbance observer design for FO-LTI

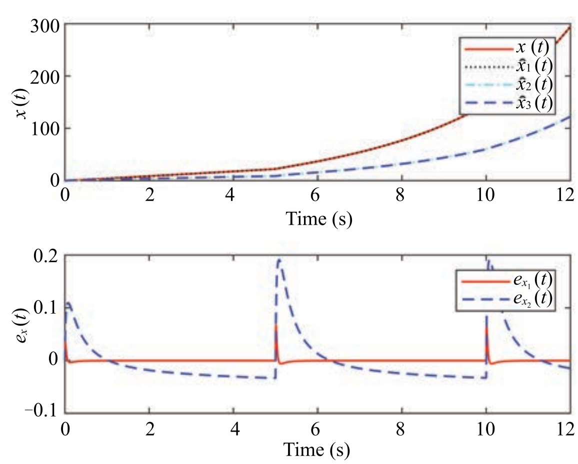

Fig. 7. Observed results of CESO for system state disturbed by sawtooth disturbance of Example 4.

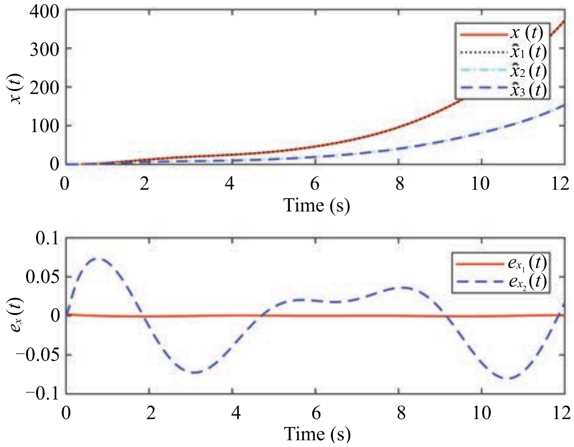

Fig. 8. Observed results of CESO for system state disturbed by sinusoidal disturbance of Example 4.

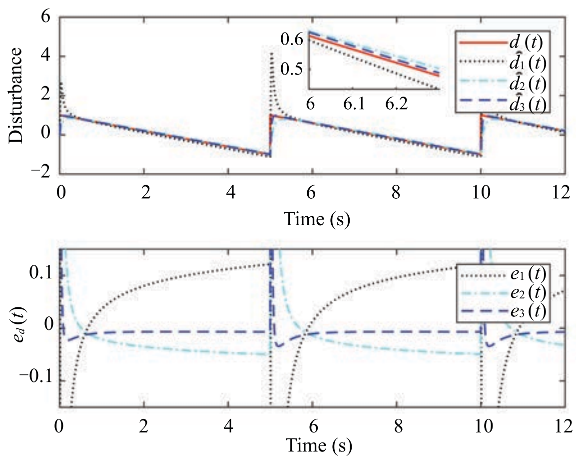

Fig. 9. Observed results for sawtooth disturbance of Example 4.

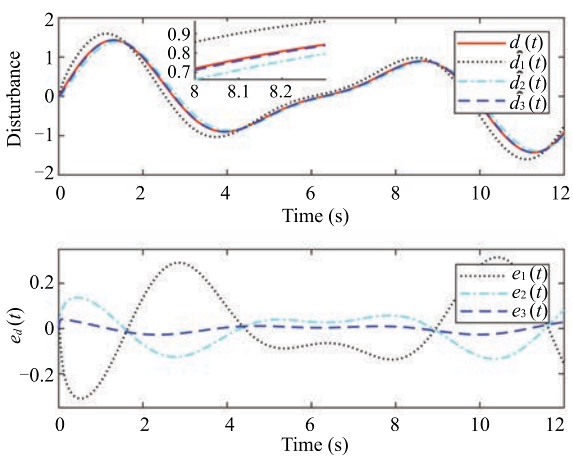

Fig. 10. Observed results for sinusoidal disturbance of Example 4.

systems has been investigated. For the case that state can be measured directly, ROESO and ROCESO are proposed. And then, ESO is developed in the case that the state cannot be measured easily. Furthermore, the CESO has been presented to observe the state and α-th order derivative of disturbance, which can be combined with ROCESO to get a more accurate observation result. In order to show the generality of the proposed observers, we consider two kinds disturbances: time series expansion and sinusoidal. And we have given concrete proofs that the time series expansion can be observed asymptotically and sinusoidal can be observed with bounded error, and in addition, the way how to reduce the observation error has been proposed. The numerical examples have shown the effectiveness of the proposed designing methods. It is believed that the approaches provide a new avenue to observe disturbance. The interesting future topics involve the following cases:

1) To utilize the designed disturbance observer to realize disturbance rejection, as well as the unmatched disturbance;

2) To study the problem of noise effect reduction where the measured output is mixed with measurement noise;

3) To investigate the observer with considering the uncertainties of the system.

REFERENCES

[1] Monje C A, Chen Y Q, Vinagre B M, Xue D Y, Feliu-Batlle V. *Fractional-Order Systems and Controls: Fundamentals and Applications*. London, UK: Springer-Verlag, 2010.

[2] Das S. *Functional Fractional Calculus* (Second edition). Berlin, Heidelberg: Springer, 2011.

[3] Liao Z, Zhu Z T, Liang S, Peng C, Wang Y. Subspace identification for fractional order Hammerstein systems based on instrumental variables. *International Journal of Control, Automation and Systems*, 2012, **10**(5): 947−953

[4] Patil M D, Vyawahare V A, Bhole M K. A new and simple method to construct root locus of general fractional-order systems. *ISA Transactions*, 2014, **53**(2): 380−390

[5] Lan Y H, Li W J, Zhou Y, Luo Y P. Non-fragile observer design for fractional-order one-sided Lipschitz nonlinear systems. *International Journal of Automation and Computing*, 2013, **10**(4): 296−302

[6] Liang S, Peng C, Liao Z, Wang Y. State space approximation for general fractional order dynamic systems. *International Journal of Systems Science*, 2014, **45**(10): 2203−2212

[7] Lu J G, Chen G R. Robust stability and stabilization of fractional-order interval systems: an LMI approach. *IEEE Transactions on Automatic Control*, 2009, **54**(6): 1294−1299

[8] Lu J G, Chen Y Q. Robust stability and stabilization of fractional-order interval systems with the fractional order α: the case $0 \ll \alpha \ll 1$. *IEEE Transactions on Automatic Control*, 2010, **55**(1): 152−158

[9] Ruszewski A. Practical stability and asymptotic stability of interval fractional discrete-time linear state-space system. *Recent Advances in Automation, Robotics and Measuring Techniques*. Switzerland: Springer International Publishing, 2014. 217−227

[10] Liang Shu, Peng Cheng, Wang Yong. Improved linear matrix inequalities stability criteria for fractional order systems and robust stabilization synthesis: the $0 < \alpha < 1$ case. *Control Theory and Applications*, 2013, **30**(4): 531−535 (in Chinese)

[11] NDoye I, Darouach M, Zasadzinski M, Radhy N E. Robust stabilization of uncertain descriptor fractional-order systems. *Automatica*, 2013, **49**(6): 1907−1913

[12] Agrawal S K, Das S. A modified adaptive control method for synchronization of some fractional chaotic systems with unknown parameters. *Nonlinear Dynamics*, 2013, **73**(1−2): 907−919

[13] Li C L, Su K L, Zhang J, Wei D Q. Robust control for fractional-order four-wing hyperchaotic system using LMI. *Optik- International Journal for Light and Electron Optics*, 2013, **124**(22): 5807−5810

[14] Asheghan M M, Delshad S S, Beheshti M T H, Tavazoei M S. Non-fragile control and synchronization of a new fractional order chaotic system. *Applied Mathematics and Computation*, 2013, **222**: 712−721

[15] Guo L, Cao S Y. Anti-disturbance control theory for systems with multiple disturbances: a survey. *ISA Transactions*, 2014, **53**(4): 846−849

[16] Shtessel Y, Edwards C, Fridman L, Levant A. *Sliding Mode Control and Observation*. New York: Springer, 2014.

[17] Guo B Z, Jin F F. The active disturbance rejection and sliding mode control approach to the stabilization of the Euler-Bernoulli beam equation with boundary input disturbance. *Automatica*, 2013, **49**(9): 2911−2918

[18] Yue H Y, Li J M. Adaptive fuzzy dynamic surface control for a class of perturbed nonlinear time-varying delay systems with unknown dead-zone. *International Journal of Automation and Computing*, 2012, **9**(5): 545−554

[19] Li Z, Xia Y, Cao X. Adaptive control of bilateral teleoperation with unsymmetrical time-varying delays. *International Journal of Innovative Computing, Information and Control*, 2013, **9**(2): 753−767

[20] Liu R J, Liu G P, Wu M, Nie Z Y. Disturbance rejection for time-delay systems based on the equivalent-input-disturbance approach. *Journal of the Franklin Institute*, 2014, **351**(6): 3364−3377

[21] Han Jing-Qing. *Active Disturbance Rejection Control Technique — the Technique for Estimating and Compensating the Uncertainties*. Beijing, China: National Defense Industry Press, 2008. (in Chinese)

[22] Fedele G, Ferrise A. Periodic disturbance rejection with unknown frequency and unknown plant structure. *Journal of the Franklin Institute*, 2014, **351**(2): 1074−1092

[23] Nakao M, Ohnishi K, Miyachi K. A robust decentralized joint control based on interference estimation. In: Proceedings of the 1987 IEEE International Conference on Robotics and Automation. Raleigh, North Carolina, USA: 1987. 326−331

[24] Chen W H, Yang J, Guo L, Li S H. Disturbance-observer-based control and related methods: an overview. *IEEE Transactions on Industrial Electronics*, 2016, **63**(2): 1083−1095

[25] Park S K, Lee S H. Disturbance observer based robust control for industrial robots with flexible joints. In: Proceedings of the 2007 International Conference on Control, Automation, and Systems. Seoul, Korea: IEEE, 2007. 584−589

[26] Ginoya D, Shendge P D, Phadke S B. Sliding mode control for mismatched uncertain systems using an extended disturbance observer. *IEEE Transactions on Industrial Electronics*, 2014, **61**(4): 1983−1992

[27] Aguila-Camacho N, Duarte-Mermoud M A, Gallegos J A. Lyapunov functions for fractional order systems. *Communications in Nonlinear Science and Numerical Simulation*, 2014, **19**(9): 2951−2957

[28] Wei Y H, Karimi H R, Liang S, Gao Q, Wang Y. General output feedback stabilization for fractional order systems: an LMI approach. *Abstract and Applied Analysis*, 2014, **2014**: Article ID 737495

[29] Wei Y H, Gao Q, Peng C, Wang Y. A rational approximate method to fractional order systems. *International Journal of Control, Automation, and Systems*, 2014, **12**(6): 1180−1186

[30] Li M D, Li D H, Wang J, Zhao C Z. Active disturbance rejection control for fractional-order system. *ISA Transactions*, 2013, **52**(3): 365−374

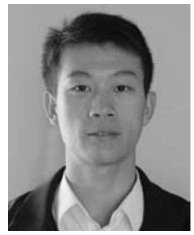

Songsong Cheng received the B. Eng. degree in automation from Anhui University of Science and Technology, China, in 2013. He is currently a Ph. D. candidate of automation at University of Science and Technology of China. His research interests include disturbance rejection control, fractional order systems, LMI, adaptive control, and filtering algorithm.

Shengguo Wang received the B. S. degree and the M. S. degree in electrical engineering from University of Science and Technology of China in 1967 and 1981, respectively, and the Ph. D. degree in electrical and computer engineering from the University of Houston in 1994. Currently, he is a professor in engineering technology and a graduate faculty member at University of North Carolina at Charlotte. His current research interests include systems, control, modeling, robust control, structural control, intelligent control, computer networks, mathematical and numerical analysis, algorithms, and applications.

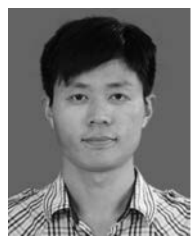

Yiheng Wei received the B. Eng. degree in automation from Northeastern University in 2010 and the Ph. D. degree in navigation, guidance, and control from University of Science and Technology of China, Hefei, China, in 2015. He is currently a postdoctor with the Department of Automation, University of Science and Technology of China, Hefei, China. His research interests include fractional order systems analysis and controller synthesis.

Qing Liang received the B. Sc. degree in automation control and the M. Sc. degree in control theory and applications degrees from University of Science and Technology of China, Hefei, China, in 1983 and 1986, respectively. He has been with the Department of Automation, University of Science and Technology of China since 1986, where he is currently an associate professor. His research interests include aircraft guidance and control, vibration control, and disturbance rejection.

Yong Wang received the B. Eng. degree in automation control from University of Science and Technology of China, Hefei, China, in 1982 and the M. Eng. and Ph. D. degrees in navigation, guidance, and control from Nanjing Aeronautical Institute, Nanjing, China, in 1985 and 1999, respectively. He has been with the Department of Automation, University of Science and Technology of China since 2001, where he is currently a professor. His research interests include active vibration control and fractional order systems. Corresponding author of this paper.

Set-point Filter Design for a Two-degree-of-freedom Fractional Control System

Fabrizio Padula and Antonio Visioli, *Senior Member, IEEE*

***Abstract*—This paper focuses on a new approach to design (possibly fractional) set-point filters for fractional control systems. After designing a smooth and monotonic desired output signal, the necessary command signal is obtained via fractional input-output inversion. Then, a set-point filter is determined based on the synthesized command signal. The filter is computed by minimizing the 2-norm of the difference between the command signal and the filter step response. The proposed methodology allows the designer to synthesize both integer and fractional set-point filters. The pros and cons of both solutions are discussed in details. This approach is suitable for the design of two degree-of-freedom controllers capable to make the set-point tracking performance almost independent from the feedback part of the controller. Simulation results show the effectiveness of the proposed methodology.**

***Index Terms*—Fractional control systems, two-degree-of-freedom control, set-point following, system inversion.**

I. INTRODUCTION

FRACTIONAL systems have been proven to be effective in the design of control systems because of their capability to model complex phenomena and to achieve more challenging control specifications[1−12].

Actually, one of the main issues in a control system is often to achieve a satisfactory performance in the load disturbance rejection and in the set-point following tasks at the same time. An effective solution to this problem is the use of a two degree-of-freedom control system[13], where a suitable set-point filter should be designed in order to recover the set-point following performance independently from the employed feedback controller. Indeed, this approach has been proven to be effective also in the fractional framework. For example, in [14] the use of a set-point weight for fractional-order proportional-integral-derivative controllers is discussed. The use of a Davidson-Cole filter has then been proposed in [15]. In any case, it has to be stressed that such a kind of filter cannot decrease the rise time of the step response but it can just effectively reduce the overshoot[16].

By following another approach, the set-point following performance can be improved by using a suitably designed feedforward control law. In particular, the command signal to be applied to the closed-loop system is determined by exploiting the input-output inversion concept[17−19], that is, is computed in such a way it causes a desired smooth monotonic process variable transition, which is selected as a transition polynomial[20]. In this context, constraints on the control and process variables can be explicitly considered. This technique has been extended successfully also to fractional control systems[16] but it has the drawback that the use of a complex feedforward command signal might lead to implementation problems, especially considering the memory allocation issue.

Thus, in order to simplify significantly the implementation of this strategy by using a standard two-degree-of-freedom control scheme, in this paper, which is an extended version of [21], a methodology to design a set-point filter based on the inversion technique is proposed.

Indeed, the set-point filter is determined as the system that minimizes the 2-norm of the difference between its step response and the synthesized command signal. For this purpose, the differintegrals of both the transition polynomial and the command signal are determined. Then, two techniques to determine either a fractional-order or an integer-order filter are proposed. The advantages of both techniques will be discussed in detail: the integer filter is easier to implement on a commercial off-the-shelf control system, but may become unstable for a small transition time and cannot cope with uncompensated long fractional tails. On the contrary, the fractional filter (which is more complex to implement) is stable for every desired output transition time and works properly independently from the feedback controller tuning.

In this way, the achieved performance is close to the one that would have been obtained by using the synthesized command signal, without the memory allocation problems that would arise from the use of a complex feedforward signal. Moreover, the performance is still independent from the chosen controller and, finally, the filter can be fed with a simple step signal, that is, the overall control system can be implemented in any control setup.

The effectiveness of the proposed methodologies is proven through a series of illustrative examples.

Summarizing, the contribution of the paper is in the design of a (possibly) fractional set-point filter that can be employed in a standard two-degree-of-freedom control scheme and allows the achievement of high performance in terms of low settling time and low overshoot at the same time. This is different from the standard design of set-point filtering that uses a low-pass filtering approach that allows the reduction of the overshoot at the expense of the rise time.

Manuscript received September 1, 2015; accepted June 22, 2016. This work was supported by the Australian Research Council (DP160104994). Recommended by Associate Editor Dingyü Xue.

Citation: Fabrizio Padula, Antonio Visioli. Set-point filter design for a two-degree-of-freedom fractional control system. *IEEE/CAA Journal of Automatica Sinica*, 2016, **3**(4): 451−462

Fabrizio Padula is with the Department of Mathematics and Statistics, Curtin University, Kent St, Bentley WA 6102, Perth, Australia (e-mail: fabrizio.padula@curtin.edu.au).

Antonio Visioli is with the Department of Mechanical and Industrial Engineering, University of Brescia, via Branze 38 25123-Brescia, Italy (e-mail: antonio.visioli@unibs.it).

The paper is organized as follows. In Section II the problem is formalized and, in Section III, the design technique of the command signal is reviewed. The fractional differintegral of both transition polynomial and command signal is obtained in Section IV, while the filter design methodologies are presented in Section V and their use is discussed in Section VI. Illustrative examples are given in Section VII and conclusions are drawn in Section VIII.

Notation. $C^{(i)}$ denotes the space of the scalar real functions which are continuous till the ith time derivative. D^i denotes the ith derivative operator. Finally $[x]$ with $x \in \mathbf{R}$ is the biggest integer lower than x (note that, when $x \in \mathbf{R}\backslash\mathbf{N}$, this is the well-known integer part of x).

II. Problem Formulation

Consider the two degree-of-freedom control system shown in Fig. 1 where the process is a linear time-invariant commensurate strictly proper fractional system, L is the delay term and $\bar{G}(s)$ is minimum-phase.

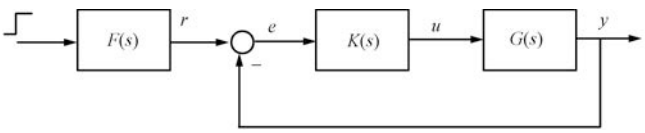

Fig. 1. The two degree-of-freedom unity-feedback control scheme.

$$G(s) = \bar{G}(s)\mathrm{e}^{-Ls} \tag{1}$$

The closed-loop systems transfer function is

$$T(s) = \frac{K(s)G(s)}{1 + K(s)G(s)} \tag{2}$$

and it is assumed to be strictly proper.

It is also assumed that the controller has been designed in order to make the considered feedback loop internally stable.

The goal here is to design a filter $F(s)$ such that process output behaves well. Namely, to obtain, independently from the chosen controller $K(s)$, an output transition as close as possible to a desired output function which exhibits a smooth and monotonic transition from an initial steady-state value to a new one in a finite time interval τ, given a set of bounds on the control and process variables and their derivatives.

In order to do that a suitable command signal $r(t)$ is first synthesized, according to the technique proposed in [16], to obtain a perfect tracking of the desired output function.

Then, a linear (possibly fractional) filter $F(s)$ whose step response is the closest in terms of 2-norm to the determined command signal $r(t)$ is found.

It is worth stressing that in this way, once a suitable filter has been designed and implemented, the control system can be fed directly with a simple step signal instead of a complex command signal $r(t)$, that would require a significant precomputation and memory storage. Moreover, this allows the user to design the feedback controller $K(s)$ independently from the set-point following performance, hence, for example, by better addressing the performance/robustness trade-off (such as focusing the feedback controller design on robustness and/or disturbance rejection).

III. Command Signal Synthesis

For the reader's convenience, the technique proposed in [16] to design $r(t)$ is briefly revisited here. The command signal design problem can be formalized as follows:

Problem 1. Starting from null initial conditions and given a new steady-state output value y_e, design a "sufficiently smooth" τ-parametrized desired output $\bar{y}(\cdot;\tau)$ such that $\bar{y}(0;\tau) = 0$ and $\bar{y}(t;\tau) = 1$ $\forall t \geq \tau$, and $\bar{y}(\cdot;\tau) \in C^{(k)}$ for some $k \in \mathbf{N}$. Then, find $r(\cdot;\tau)$ such that, for the τ-parametrized couple $(r(\cdot;\tau), \bar{y}(\cdot;\tau))$, it holds that

$$\mathcal{L}[\bar{y}(t-L;\tau)] = T(s)\mathcal{L}[r(t;\tau))]. \tag{3}$$

Moreover, determine the minimum time τ^* such that $u(t;\tau^*)$ and the first $l \in \mathbf{N}_0$ ($v \in \mathbf{N}$, respectively) derivatives of $u(t;\tau^*)$ ($\bar{y}(t;\tau^*)$), are bounded:

$$\begin{aligned} &|D^i u(t;\tau^*)| < u_M^i,\ \forall t > 0,\ i = 0, 1, \ldots, l; \\ &|D^i \bar{y}(t;\tau^*)| < y_M^i,\ \forall t > 0,\ i = 1, 2, \ldots, v. \end{aligned} \tag{4}$$

Note that the requirements of null initial conditions and unitary transition are without loss of generality in view of the system linearity.

The simple and computationally efficient τ-parametrized transition polynomial proposed in [20] is chosen as desired output function. It has the nice property of being monotonic, which implies that neither overshoots nor undershoots occur. In the interval $[0,\tau]$ the desired output function is therefore selected as a polynomial

$$\bar{y}(t) := c_0 + c_1 t + \cdots + c_{2n+1}t^{2n+1}, \tag{5}$$

where the coefficients c_i $(i = 0, 1, \ldots, 2n+1)$ are obtained by solving the following system:

$$\begin{cases} \bar{y}(0) = 0, D\bar{y}(0) = 0, \ldots, D^n\bar{y}(0) = 0; \\ \bar{y}(\tau) = 1, D\bar{y}(\tau) = 0, \ldots, D^n\bar{y}(\tau) = 0. \end{cases} \tag{6}$$

Eventually, the solution of the previous systems leads to the desired output function

$$\bar{y}(t;\tau) := \begin{cases} 0, & \text{if} \quad t < 0; \\ \frac{(2n+1)!}{n!\tau^{2n+1}} \sum\limits_{r=0}^{n} \frac{(-1)^{n-r}\tau^r t^{2n-r+1}}{r!(n-r)!(2n-r+1)}, & \text{if} \quad 0 \leq t \leq \tau; \\ 1, & \text{if} \quad t > \tau. \end{cases} \tag{7}$$

Note that, by construction, $\bar{y}(t;\tau)$ allows an arbitrarily smooth transition between 0 and 1; indeed, it is possible to show that $\bar{y}(t;\tau) \in C^{(n)}$[20].

Consider a commensurate minimum-phase fractional system $H(s)$ of commensurate order $\nu \in \mathbf{R}$. By polynomial division the inverse of its transfer function can be always represented as

$$H^{-1}(s) = \gamma_{q-m}s^{\rho} + \gamma_{q-m-1}s^{\rho-\nu} + \cdots + \gamma_1 s^{\nu} + \gamma_0 + H_0(s), \tag{8}$$

where $q\nu$ and $m\nu$, with $q, m \in \mathbf{N}$, are, respectively, the numerator and the denominator orders, $\rho \in \mathbf{R}$ is the relative order and $H_0(s)$ is the zero dynamics of $H(s)$.

By polynomial division it can be shown that $H_0(s)$ is always stable and strictly proper and that it can be represented as

$$H_0(s) = \sum_{i=1}^{m} \frac{g_i}{(s^\nu - \lambda_i)^{k_i+1}}. \tag{9}$$

As a consequence, in the time domain, its impulse response $\eta_0(t)$ can be described as a linear combination of Mittag-Leffler functions[16, 22], that is:

$$\eta_0(t) = \sum_{i=1}^{m} \frac{g_i}{k_i!} \varepsilon_{k_i}(t, \lambda_i; \nu, \nu), \tag{10}$$

where

$$\varepsilon_k(t, \lambda; \alpha, \beta) := t^{k\alpha+\beta-1} \frac{\mathrm{d}^k}{\mathrm{d}(\lambda t^\alpha)^k} E_{\alpha,\beta}(\lambda t^\alpha), \tag{11}$$

with

$$E_{\alpha,\beta}(z) = \sum_{k=0}^{\infty} \frac{z^k}{\Gamma(\alpha k + \beta)} \ \alpha > 0, \beta > 0, \tag{12}$$

The following lemma solves the problem of computing the input signal such that a perfect tracking of the desired output is obtained for the system $H(s)$.

Proposition 1[23]**.** Consider $\bar{y}(t;\tau)$ defined in (7). If $n \geq [\rho] + 1$ then

$$\begin{aligned} u(t;\tau) \ &= \ \gamma_{q-m} D^\rho \bar{y}(t;\tau) + \gamma_{q-m-1} D^{\rho-\nu} \bar{y}(t;\tau) + \cdots \\ &+ \ \gamma_1 D^\nu \bar{y}(t;\tau) + \gamma_0 \bar{y}(t;\tau) + \textstyle\int_0^t \eta_0(t-\xi) \bar{y}(\xi;\tau) \mathrm{d}\xi. \end{aligned} \tag{13}$$

Eventually, for Problem 1, the command signal can be computed by applying Proposition 1 to the delay-free part of the open-loop transfer function, i.e., by defining $H(s) = K(s)\bar{G}(s)$, yielding the signal $r_{ol}(t;\tau)$. Then, a correction term $r_c(t;\tau) = \bar{y}(t-L;\tau)$ must be considered, so that the command signal is

$$r(t;\tau) = r_{ol}(t;\tau) + r_c(t;\tau). \tag{14}$$

Finally, it can be proven that the existence of a suitable command signal is guaranteed under the following condition:

$$n \geq [\rho_{K\bar{G}}] + 1, \tag{15}$$

where $\rho_{k\bar{G}}$ is the relative order of the open-loop transfer function.

$$\begin{cases} n \geq \max\{v; [\rho_{\bar{G}}] + 1 + l\}, \\ \tau \geq \max\{\tau_i^*; \tau_o^*\}, \end{cases} \tag{16}$$

where τ_o^* is the minimum transition time satisfying the output constraints, whereas τ_i^* is minimum transition time such that the input constraints are satisfied for each $\tau \geq \tau_i^*$.

IV. Command Signal Differintegrals

In this section, the differintegral of both the transition polynomial and the command signal are analytically obtained. Indeed, they are necessary to achieve the final result of designing an inversion-based set-point filter.

A. Transition Polynomial Fractional Differintegral

Considering that

$$x^n = (x - \tau + \tau)^n = \sum_{j=0}^{n} \begin{pmatrix} n \\ j \end{pmatrix} (x-\tau)^{n-j} \tau^j \tag{17}$$

the transition polynomial can be represented as

$$\bar{y}(t;\tau) = \begin{cases} 0, & \text{if } t < 0, \\ \dfrac{(2n+1)!}{n!\tau^{2n+1}} \displaystyle\sum_{r=0}^{n} \frac{(-1)^{n-r} \tau^r t^{2n-r+1}}{r!(n-r)!(2n-r+1)}, & \text{if } 0 \leq t \leq \tau, \\ \dfrac{(2n+1)!}{n!\tau^{2n+1}} \displaystyle\sum_{r=0}^{n} \frac{(-1)^{n-r} \tau^r}{r!(n-r)!(2n-r+1)} & \\ \quad \times [t^{2n-r+1} - \displaystyle\sum_{j=0}^{2n-r+1} \begin{pmatrix} 2n-r+1 \\ j \end{pmatrix} & \\ \quad \times (t-\tau)^{2n-r+1-j} \tau^j] + 1(t-\tau), & \text{if } t > \tau, \end{cases} \tag{18}$$

where $1(\cdot)$ is the Heaviside function. The previous expression can be further simplified considering that the transition polynomial is $C^{(n)}$ by construction. Hence, the summation of all the terms that by differentiating till the order n the transition polynomial would lead to impulse-like behaviors at $t = \tau$, is null. Thus, the summation over j can be truncated at $n - r$.

Now consider the fractional differintegral of the transition polynomial. By virtue of the previous reasoning, considering that $D^\alpha x^n = \frac{n!}{\Gamma(n+1-\alpha)} x^{n-\alpha}$, $\alpha \in \mathbf{R}$ and expanding the binomial coefficients in (18), the differintegral of the transition polynomial is finally obtained for $-\infty < \alpha \leq n+1$:

$$D^\alpha \bar{y}(t;\tau) = \begin{cases} 0, & \text{if } t < 0; \\ \frac{(2n+1)!}{n!\tau^{2n+1}} \displaystyle\sum_{r=0}^{n} \frac{(-1)^{n-r} \tau^r (2n-r+1)!}{r!(n-r)!(2n-r+1)\Gamma(2n-r+2-\alpha)} & \\ \quad \times t^{2n-r+1-\alpha}, & \text{if } 0 \leq t \leq \tau; \\ \frac{(2n+1)!}{n!\tau^{2n+1}} \displaystyle\sum_{r=0}^{n} \frac{(-1)^{n-r} \tau^r (2n-r+1)!}{r!(n-r)!(2n-r+1)} & \\ \quad \times \left(\frac{t^{2n-r+1-\alpha}}{\Gamma(2n-r+2-\alpha)} - \displaystyle\sum_{j=0}^{n-r} \frac{\tau^j t^{2n-r+1-j-\alpha}}{j!\Gamma(2n-r+2-j-\alpha)} \right), & \text{if } t > \tau. \end{cases} \tag{19}$$

It is worth stressing the previous equation can also be used for a direct computation of the transition polynomial by selecting $\alpha = 0$.

B. Command Signal Fractional Differintegral

In order to integrate and differentiate the command signal, the following signals must be differintegrated: 1) the transition polynomial (r_c in (14)), 2) the fractional derivatives of the transition polynomial appearing in (13) and 3) the convolution integral appearing in (13).

In order to solve the first point, (19) can be used directly.

However, (19) cannot be applied straightforwardly to the second point since, in general, fractional operators do not commutate[22]. In particular, when using Caputo fractional derivatives, $D^m D^\alpha y(\cdot) \neq D^{m+\alpha} y(\cdot), m \in \mathbf{N}, \alpha \in \mathbf{R}$, unless $D^i y(0) = 0$ $(i = 0, \ldots, m)$. Nevertheless, when differentiating the fractional derivatives of the transition polynomial, in order to guarantee the existence of all the derivatives till a given order m, a sufficient condition is

$$n \geq m + [\rho]. \tag{20}$$

Hence, (19) can be applied. On the contrary, when integrating the fractional derivatives of the transition polynomial, Riemann-Liouville and Grünwald-Letnikov fractional operators do not commutate, that is $D^{-m}D^{\alpha}y(\cdot) \neq D^{-m+\alpha}y(\cdot)$, $m \in \mathbf{N}$, $\alpha \in \mathbf{R}$ unless $D^i y(0) = 0$ $(i = 0, \ldots, [\alpha])$. This condition, considering the transition polynomial, would lead to $n \geq [\rho]$, and it is automatically satisfied by the condition of existence for the inverting signal $n \geq [\rho] + 1$. Evidently, all these conditions must be applied to the specific inverting signal, that is $\rho = \rho_{K\bar{G}}$.

Finally, consider the differintegration of the convolution integral appearing in (13). In this case the operators commutation is guaranteed, independently from the adopted definition because of the strict properness of zero order dynamics, provided (20) is satisfied.

In $[0, \tau]$, considering that the Laplace transform of the convolution integrals equals the product of the Laplace transforms and that $\mathcal{L}[t^{\alpha}] = \Gamma(\alpha + 1)\frac{1}{s^{\alpha+1}}$, starting from (19) its differintegral can be derived as an explicit expression in terms of Mittag-Leffler functions by exploiting the following equality:

$$\mathcal{L}^{-1}\left[\frac{k! s^{\alpha-\beta}}{(s^{\alpha} \pm \lambda)^{k+1}}\right] = \varepsilon_k(t, \mp\lambda; \alpha, \beta). \tag{21}$$

For $t > \tau$ a similar result is achievable by considering that the transition polynomial (19) can be represented as the summation of a polynomial and a delayed one. Hence, the same reasoning previously applied can be used by considering that $\mathcal{L}[(t-\tau)^{\alpha}] = \Gamma(\alpha+1)\frac{1}{s^{\alpha+1}}\mathrm{e}^{-\tau s}$, that is, the integration of a polynomial function, possibly delayed, that can be solved again in terms of Mittag-Leffler functions, leading to

$$\begin{aligned}
&D^{\alpha}\int_0^t \eta_0(t-\xi)y(\xi;\tau)\mathrm{d}\xi \\
&= \sum_{i=1}^{m}\frac{g_i}{k_i!}\frac{(2n+1)!}{n!\tau^{2n+1}}\sum_{r=0}^{n}\frac{(-1)^{n-r}\tau^r}{r!(n-r)!(2n-r+1)}(2n-r+1)! \\
&\times\Bigg[\varepsilon_{k_i}(t,\lambda_i;\nu,2n-r+2+\nu-\alpha) \\
&-\left\{\begin{array}{ll} 0, & \text{if } 0 \leq t \leq \tau \\ \sum\limits_{j=0}^{n-r}\frac{\tau^j}{j!} & \\ \times\varepsilon_{k_i}(t-\tau,\lambda_i;\nu,2n-r+2-j+\nu-\alpha), & \text{if } t > \tau \end{array}\right.\Bigg].
\end{aligned} \tag{22}$$

Again, it is worth mentioning that the previous equation can be used for a direct computation of the convolution integral appearing in (13) in terms of Mittag-Leffler functions by selecting $\alpha = 0$.

It is noteworthy that the computation of (13) by means of (22) only requires the computation of the Mittag-Leffler function, that is widely treated in the literature (see for example [22, 24]). Note that, in the fractional framework, this is a basic requirement since the Mittag-Leffler function plays for fractional systems the same role that the exponential function plays for integer systems.

V. Least-squares Filter Design

In this section, two methodologies will be proposed to obtain the set-point filter. The first one will lead to a fractional-order filter, while the second one to an integer-order one. Also, pros and cons of the two approaches will be discussed in details.

A. Transition Polynomial-based Filter

The first methodology proposed exploits the design of a transfer function whose step response is as close as possible (in terms of 2-norm) to the transition polynomial. In this case, the following transfer function structure is proposed:

$$\tilde{F}(s) = \frac{1}{\sum\limits_{i=1}^{o} a_i s^i + 1}. \tag{23}$$

First $o = n + 1$ is selected, so that the filter step response exhibits the same degree of regularity of the transition polynomial. Then, by sampling at each Δt the transition polynomial and its derivatives obtained via (19), the following matrices are created

$$A = \begin{bmatrix} D^o\bar{y}(0;\tau) & \cdots & D^1\bar{y}(0;\tau) \\ \vdots & \ddots & \vdots \\ D^o\bar{y}(t-\Delta t;\tau) & \cdots & D^1\bar{y}(t-\Delta t;\tau) \\ D^o\bar{y}(t;\tau) & \cdots & D^1\bar{y}(t;\tau) \\ D^o\bar{y}(t+\Delta t;\tau) & \cdots & D^1\bar{y}(t+\Delta t;\tau) \\ \vdots & \ddots & \vdots \\ D^o\bar{y}(3\tau;\tau) & \cdots & D^1\bar{y}(3\tau;\tau) \end{bmatrix}, \tag{24}$$

$$\mathbf{B} = \begin{bmatrix} 1(0) - \bar{y}(0;\tau) \\ \vdots \\ 1(t-\Delta t) - \bar{y}(t-\Delta t;\tau) \\ 1(t) - \bar{y}(t;\tau) \\ 1(t+\Delta t) - \bar{y}(t+\Delta t;\tau) \\ \vdots \\ 1(3\tau) - \bar{y}(3\tau;\tau) \end{bmatrix}. \tag{25}$$

Finally the coefficients vector $\Theta = [a_o \ \cdots \ a_1]^{\mathrm{T}}$ is obtained as $\Theta = A^{\mathrm{T}}(AA^{\mathrm{T}})^{-1}B$. Note that, the transfer function (23) designed in this way has, by construction, unitary dc-gain. Now, using (23) and the process dynamics, the set-point filter can be designed as

$$F(s) = \tilde{F}(s)(\mathrm{e}^{-Ls} + (K(s)\bar{G}(s))^{-1}). \tag{26}$$

It is worth noting that, in this case, the obtained filter is fractional. Hence, it may be difficult to implement with standard industrial control hardware. In order to overcome this problem, in the next subsection a second methodology to design the set point filter is proposed.

B. Command Signal Filter

The second methodology is based on direct design of a filter whose step response is the closest, in terms of 2-norm, to the command signal.

Actually, a double approach to solve this problem is proposed. The first approach consists in identifying a suitable filter using directly the command signal (14). The second approach is based on the separate identification of a transfer function for the transition polynomial and a transfer function for the inverting part of the command signal $r_{ol}(t,\tau)$. The response of the first transfer function can therefore be arbitrarily delayed and, by selecting the system delay, a signal close to $r_c(t;\tau)$ is obtained.

When the first approach is used, the proposed filter structure is

$$F(s) = \frac{\sum_{j=1}^{o-p} b_j s^j + 1}{\sum_{i=1}^{o} a_i s^i + \mu}, \tag{27}$$

where μ is the closed-loop dc-gain and

$$p = n - [\rho_{K\bar{G}}]. \tag{28}$$

Note that the relative order of the filter is chosen in such a way that forces the filter step response to have the greater degree of regularity equal to or smaller than the one of the command signal. Indeed, considering the possibly fractional nature of the considered control systems, the degree of regularity of the command signal is $n - \rho_{K\bar{G}}$. Also, note that the chosen value of p guarantees the accomplishment of condition (20), hence the existence of the derivative of the command signal independently from the adopted definition of fractional operator.

In this case, $o \in \mathbf{R}$ is a design parameter, to be chosen large enough to give to the filter a sufficient number of degrees of freedom. In this case, the identification would require $o-p$ differentiations of the step signal. In order to overcome this problem an integral approach is adopted integrating $o-p$ times both the step signal and the command signal.

Then, by sampling at each Δt the command signal and its integrals obtained via (13), (19) and (22) the following matrices are created

$$A = \left[\begin{array}{ccccccc} D^p r(0;\tau) & \cdots & D^{-o+p+1} r(0;\tau) & -1(0) & \cdots & -\frac{1}{(o-p+1)!}0^{(o-p+1)} \\ \vdots & \ddots & \vdots & \vdots & \ddots & \vdots \\ D^p r(t-\Delta t;\tau) & \cdots & D^{-o+p+1} r(t-\Delta t;\tau) & -1(t-\Delta t) & \cdots & -\frac{1}{(o-p+1)!}(t-\Delta t)^{(o-p+1)} \\ D^p r(t;\tau) & \cdots & D^{-o+p-1} r(t;\tau) & -1(t) & \cdots & -\frac{1}{(o-p+1)!}t^{(o-p+1)} \\ D^p r(t+\Delta t;\tau) & \cdots & D^{-o+p+1} r(t+\Delta t;\tau) & -1(t+\Delta t) & \cdots & -\frac{1}{(o-p+1)!}(t+\Delta t)^{(o-p+1)} \\ \vdots & \ddots & \vdots & \vdots & \ddots & \vdots \\ D^p r(3\tau;\tau) & \cdots & D^{-o+p+1} r(3\tau;\tau) & -1(\psi\tau) & \cdots & -\frac{1}{(o-p+1)!}(\psi\tau)^{(o-p+1)} \end{array}\right], \tag{29}$$

$$B = \left[\begin{array}{c} \frac{1}{(o-p)!}0^{(o-p)} - \mu D^{-o+p} r(0;\tau) \\ \vdots \\ \frac{1}{(o-p)!}(t-\Delta t)^{(o-p)} - \mu D^{-o+p} r(t-\Delta t;\tau) \\ \frac{1}{(o-p)!}t^{(o-p)} - \mu D^{-o+p} r(t;\tau) \\ \frac{1}{(o-p)!}(t+\Delta t)^{(o-p)} - \mu D^{-o+p} r(t+\Delta t;\tau) \\ \vdots \\ \frac{1}{(o-p)!}(\tau)^{(o-p)} - \mu D^{-o+p} r(\psi\tau;\tau) \end{array}\right], \tag{30}$$

where $\psi \in \mathbf{R}$ is a design parameter that must be big enough to capture a sufficient part of the command signal transient (made of action and postaction, see [16] for details) in order to obtain a satisfactory filter. Finally the coefficients vector $\mathbf{\Theta} = [a_o \ \cdots \ a_1 \ b_{o-p} \ \cdots b_1]^{\mathrm{T}}$ is obtained as $\Theta = A^{\mathrm{T}}(AA^{\mathrm{T}})^{-1}B$.

The second approach uses the same filter structure (27) of the first one, but in order to identify the filter parameters it uses $r_{ol}(t;\tau)$ instead of the whole command signal (14) to build the matrices (29) and (30). In order to do that, the following procedure should be used:

1) If the open-loop transfer function $K(s)G(s)$ has a finite dc-gain μ_{ol}, then substitute μ with μ_{ol} both in (27) and (30). Then, use them to compute a filter $\bar{F}(s)$ having the same structure of (27) following the standard procedure;

2) If the open-loop transfer function has an integral behavior of order $\lambda \in \mathbf{R}$, then eliminate from (29) the last $[\lambda] - 1$ columns, eliminate from (30) the integrals of the Heaviside function, set $\mu = 1$ in (30) and use the following filter structure:

$$\bar{F}(s) = \frac{\sum_{j=[\lambda]}^{o-p} b_j s^j}{\sum_{i=1}^{o} a_i s^i + 1}, \tag{31}$$

where $\Theta = [a_o \ \cdots \ a_1 \ b_{o-p} \ \cdots b_{[\lambda]}]^{\mathrm{T}}$.

Then, the technique proposed in the Subsection V-A is employed to design a transfer function $\tilde{F}(s)$ whose step response is close to the transition polynomial $\bar{y}(\cdot)$. Finally, the filter is obtained as

$$F(s) = \bar{F}(s) + \tilde{F}(s)\mathrm{e}^{-Ls}. \tag{32}$$

VI. Discussion

Two methodologies have been proposed in Section V. The first one generates fractional set-point filters, while the second one can be used to obtain different integer-order set-point filters.

Clearly, when able to guarantee the same set-point tracking performance, an integer order filter is preferable for its ease of implementation.

Nevertheless, the second methodology is not always usable. In particular it may present two different problems:

1) When the required transition time τ is too small it may lead to unstable filters. In this case the first methodology i.e., the fractional filter, offers a great advantage. Indeed, the first technique gives the same results independently from the chosen transition time. Actually, when varying the transition time, the transition polynomial is just scaled along the time axis (i.e., it is selfsimilar). So, once a stable filter for a given

τ has been identified, it is possible to obtain many others just scaling its coefficients in such a way that the filter Bode plot is rigidly shifted along the $j\omega$ axes without changing its shape;

2) When the control loop presents uncompensated fractional dynamics (i.e., it is not properly tuned) the integer filter may lead to undershoot or overshoot long time after the application of the step signal. This depends on the fact that the transient response generated by the filter has already expired while the loop dynamics exhibits a slow non exponential decay typical of uncompensated fractional dynamics[25]. It is well known that it is not possible to match this kind of fractional power-law decay using integer systems, hence, in this case, the use of a fractional filter is mandatory in order to obtain a satisfactory result.

Summarizing, the first methodology always guarantees the same level of performance and can be successfully employed on a broader class of control systems, but its use should be carefully evaluated for the intrinsic complexity of implementation that fractional order systems have. Indeed, when usable, the second approach is preferable since, independently from the adopted approach, it leads to integer-order filters, which are easy to implement on off-the-shelf control setups. This issue will be further illustrated in the following section.

VII. Simulation Examples

In this section the proposed techniques will be tested via simulation examples in order to highlight the benefits and the problem that may arise from the use of these set-point filters.

For the purpose of simulation, the fractional-order dynamics has been approximated in the frequency domain by using the well-known Oustaloup approximation[26]. In order to obtain a precise approximation of the real fractional system, a high number of poles and zeros has been used, namely, 20 cells in a frequency band $[0.0001\ \ 10000]$.

A. Example 1

As a first illustrative example consider an unstable fractional system with the following transfer function[16]:

$$G(s)=\frac{3s^{0.5}+1}{s^{1.5}-1}\mathrm{e}^{-0.1s}, \tag{33}$$

whose commensurate order is, evidently, 0.5. A very simple stabilizing controller can be used, indeed a satisfactory set-point tracking performance can be obtained independently from the chosen feedback controller by using a suitable set-point filter. A proportional controller $K(s)=2$ is used here.

The control requirement is to obtain a smooth transition of the output from 0 to 1 constraining both the amplitude and the slew rate of control and process variables (note that these are common requirements in practical applications).

Accordingly, considering that the relative order of the system $\bar{G}(s)$ is $\rho=1$, $n=3$ is chosen, that is sufficient (not necessary) to satisfy conditions (15) and (16), and the transition polynomial $\bar{y}(t;\tau)$ is computed via (7):

$$\bar{y}(t;\tau)=-\frac{20}{\tau^7}t^7+\frac{70}{\tau^6}t^6-\frac{84}{\tau^5}t^5+\frac{35}{\tau^4}t^4. \tag{34}$$

Then, the technique proposed in Section III is applied. The zero dynamics of $K(s)\bar{G}(s)$ is obtained as

$$H_0(s)=\frac{-0.5185}{3s^{0.5}+1} \tag{35}$$

and its time domain version as

$$\eta_0(t)=\frac{-0.5185}{3}\varepsilon_{k_i}\left(t,\frac{1}{3};0.5,0.5\right). \tag{36}$$

Subsequently, the inversion-based part $r_{ol}(t;\tau)$ of the command signal $r(t;\tau)$ can be computed via (13), (19) and (22):

$$\begin{aligned}r_{ol}(t;\tau)\ &= 0.1667D^1y(t;\tau)-0.0556D^{0.5}\bar{y}(t;\tau)+0.0185\\ &+\int_0^t\eta_0(t-\xi)y(\xi;\tau)\mathrm{d}\xi.\end{aligned} \tag{37}$$

Now consider the following set of constraints:

$$\begin{aligned}&u_M^0\le 1.5,\ \ u_M^1\le 5,\\ &y_M^1\le 5.\end{aligned} \tag{38}$$

The minimum transition time can be found by using, for instance, a simple bisection algorithm. It turns out that the most tightening constraint is the one imposed on the derivative of the control variable and the minimum transition time is $\tau^*=\tau_i^*=0.72$.

Once the command signal has been computed, the set-point filter is designed. First, the technique proposed in Subsection V-A is used to identify the parameters of (23) leading to

$$\tilde{F}(s)=\\ 1/(0.0002416s^4+0.004027s^3+0.05374s^2+0.3418s+1). \tag{39}$$

The step response of $\tilde{F}(s)$ is represented in Fig. 2 where it immediately shows the effectiveness of its design. Then, the fractional set-point filter $F(s)$ is obtained via (26) as

$$\begin{aligned}&F(s)=(s^{1.5}+6s\mathrm{e}^{-0.1s}+2\mathrm{e}^{-0.1s}-1)/(0.001450s^{4.5}\\ &+0.0004839s^4+0.02416s^{3.5}+0.008054s^3+0.3224s^{2.5}\\ &+0.1075s^2+2.0509s^{1.5}+0.6836s+6s^{0.5}+2).\end{aligned} \tag{40}$$

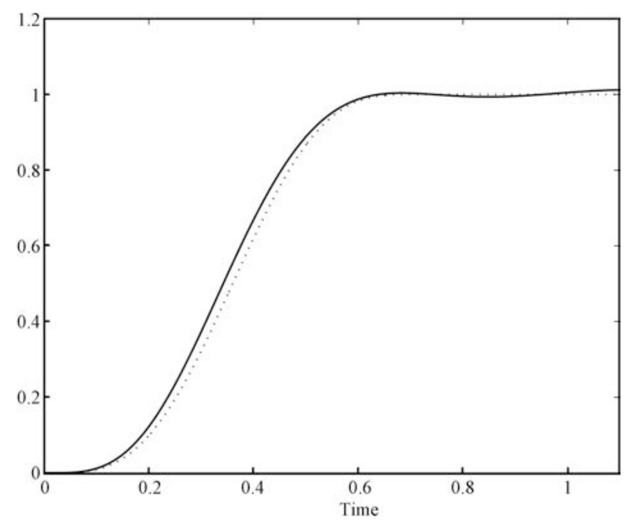

Fig. 2. Transition polynomial (dotted line) and $\tilde{F}(s)$ step response obtained by using the technique of Subsection V-A (solid line) for the set of constraints (38). – Example 1.

Now, also the first methodology proposed in Subsection V-B is implemented selecting $m = 3$, leading to the following integer-order filter

$$F(s) = (0.272s^2 + 15.28s + 1)/(0.001041s^5 + 0.03607s^4 + 0.6633s^3 + 5.473s^2 + 17.91s + 2). \tag{41}$$

Fig. 3 shows the responses obtained with the command signal, the proposed (fractional- and integer-order) set-point filters and, for the sake of comparison, the step command signal (scaled by the closed-loop dc-gain). Indeed, the response using the proposed fractional-order filter is close to the optimal one obtained with the inversion-based command signal and the constraints are almost satisfied. On the contrary, the step response does not respect the constraints and the system is very sluggish. Moreover, because of the long memory of the fractional dynamics, the 2 % settling time has the unacceptable value of 3800. Fig. 3 also reveals that the response of the integer-order filter is not capable to capture the long tail that the fractional dynamics exhibits, causing an unacceptable undershoot. Indeed, because of the very simple controller, the control loop exhibits a sluggish behavior with an uncompensated slow fractional dynamics and a settling time approximately close to the one obtained without the filter.

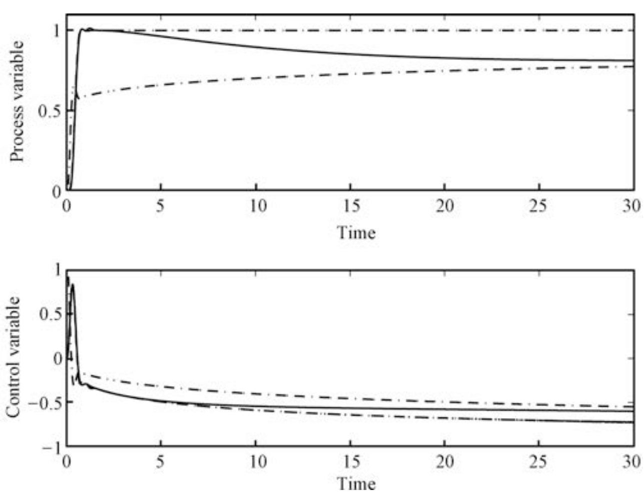

Fig. 3. Process variable (top) and control variable (bottom) obtained by using the command signal (dotted line), the filter designed with the technique of Subsection V-A (dashed line) and Subsection V-B (solid line) and a step command signal (dash-dot line) for the set of constraints (38). – Example 1.

In this context, the fractional-order filter is the only one that is capable to completely compensate this phenomena guaranteeing very good performance despite the simple (detuned) controller. This behavior is even clearer by analyzing the filter responses compared to the ideal command signal, as shown in Fig. 4. By observing Fig. 5, it turns out that the integer-order filter cannot match the whole fractional power-law tail, but it is only capable to match the required command signal only in the first part of the transient response. As a consequence, also the performance of the control system is satisfactory only in the first part of the transient response, as Fig. 6 shows. This depends on the incapability of integer-order systems to match power law decays[25]. It is worth stressing that this is a structural problem that cannot be solved by increasing m in (29) and (30). Moreover, an excessive growth of m would cause a loss of information in the first part of the transient with a consequent decay of the filter performance also in describing that part, which is usually the most exciting for the system dynamics.

Finally, a second simulation has been performed, this time

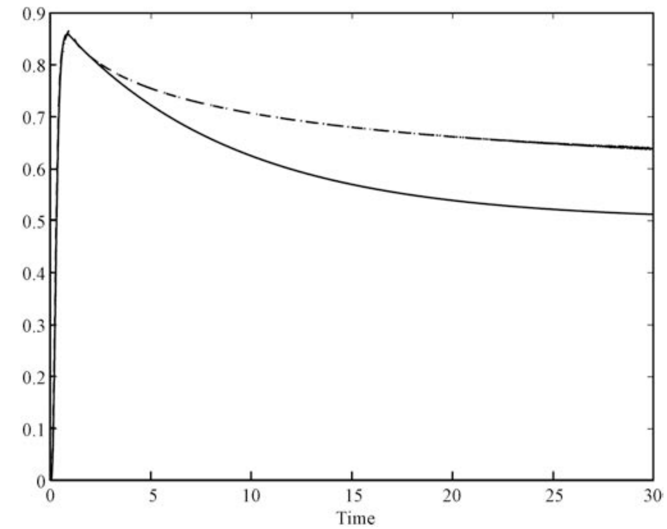

Fig. 4. Command signal (dotted line) and filter step response obtained by using the technique of Subsection V-A (dashed line) and Subsection V-B (solid line) for the set of constraints (38). – Example 1.

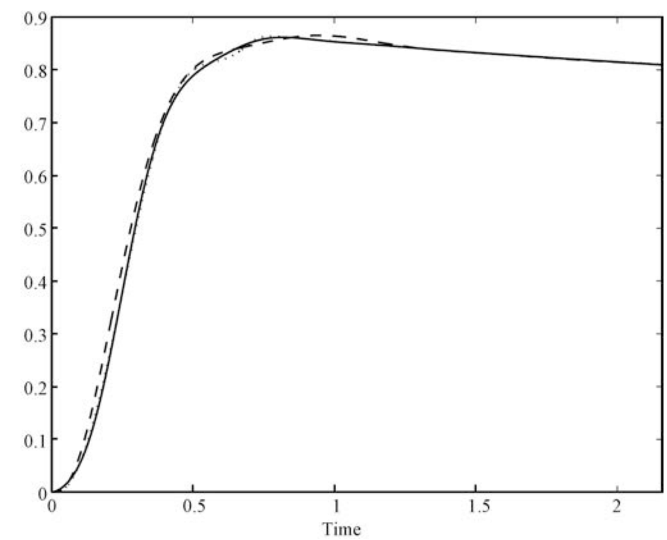

Fig. 5. Zoom of the first part of the command signal (dotted line) and filter step response obtained by using the technique of Subsection V-A (dashed line) and Subsection V-B (solid line) for the set of constraints (38). – Example 1.

neglecting the constraints and reducing the transition time to $\tau = 0.3$. Using this transition time the second methodology cannot be applied since it leads to an unstable filter. On the contrary, the first technique gives the same results independently from the chosen transition time. Indeed, when varying the transition time, the transition polynomial is just scaled along the time axis (i.e., it is selfsimilar). Thus, the Bode plot of the transfer function (23) identified again is identical to the previous one, but just rigidly shifted along the ω axis, as show in Fig. 7. The transfer function is

$$\tilde{F}(s) = 1/(7.28 \cdot 10^{-6}s^4 + 0.0002913s^3 + 0.009328s^2 +0.1424s + 1) \tag{42}$$

and the associated fractional set-point filter is

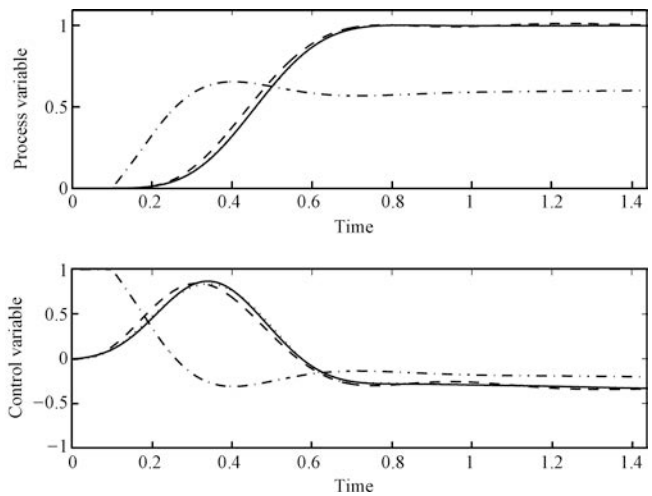

Fig. 6. Zoom of the first part of the process variable (top) and control variable (bottom) obtained by using the command signal (dotted line), the filter designed with the technique of Subsection V-A (dashed line) and Subsection V-B (solid line) and a step command signal (dash-dot line) for the set of constraints (38). – Example 1.

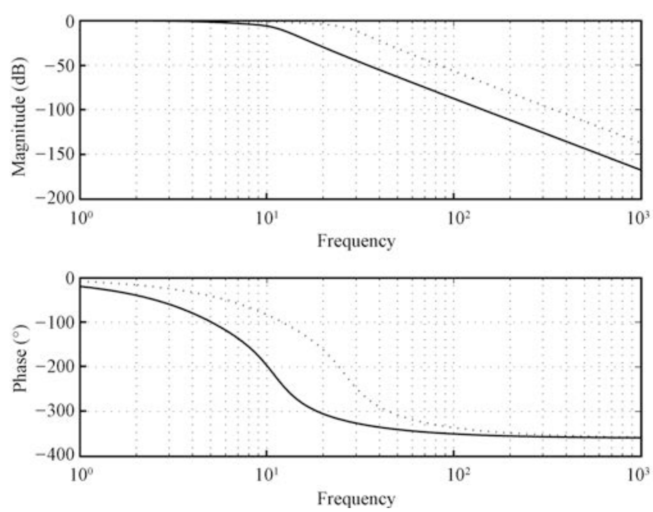

Fig. 7. Bode diagram of $\tilde{F}(s)$ for $\tau = 0.72$ (dotted line) and $\tau = 0.3$ (solid line). – Example 1.

$$F(s) = (s^{1.5} + 6s\mathrm{e}^{-0.1s} + 2\mathrm{e}^{-0.1s} - 1)/(0.00004368s^{4.5} +0.00001456s^4 + 0.001749s^{3.5} + 0.0005826s^3 +0.05597s^{2.5} + 0.01865s^2 + 0.8545s^{1.5} + 0.2848s +6s^{0.5} + 2). \tag{43}$$

Again, the filter is computed via (26), and its step response is quite close to the ideal command signal, as shown in Fig. 8. Finally, Fig. 9 shows that, despite the strong transition time reduction, the process response remains smooth and almost monotonic, close again to the one obtained with the ideal command signal.

B. Example 2

As a second example consider a unity feedback control system where the process and the controller are the ones proposed in [27] and already used as a benchmark in [16]. The controlled process has the transfer function

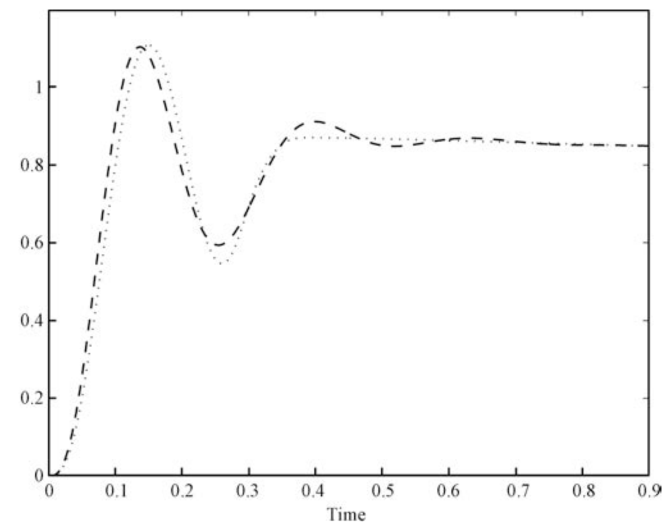

Fig. 8. Command signal (dotted line) and filter step response obtained by using the technique of Subsection V-A (dashed line) for the unconstrained solution. – Example 1.

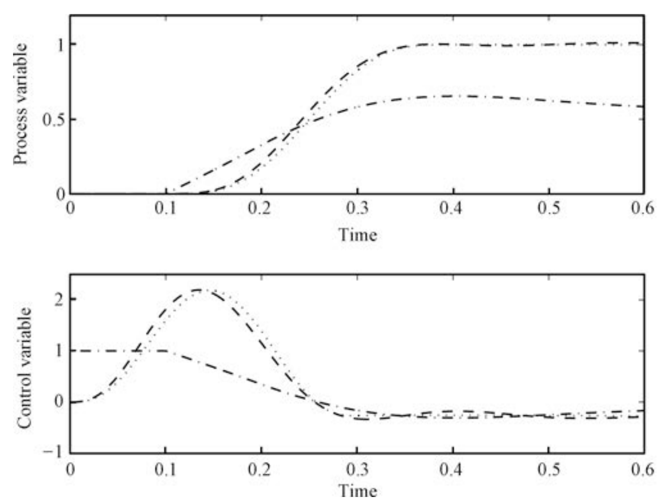

Fig. 9. Process variable (top) and control variable (bottom) obtained by using the command signal (dotted line), the filter designed with the technique of Subsection V-A (dashed line) and a step command signal (dash-dot line) for the unconstrained solution. – Example 1.

$$G(s) = \frac{0.25}{s(s+1)} \tag{44}$$

and the proposed controller is a fractional-order PID tuned in order to achieve the isodamping property:

$$K(s) = 3.8159 + \frac{2.1199}{s^{0.6264}} + 2.2195s^{0.809}. \tag{45}$$

Using the same reasoning proposed in [16], the actual controller is approximated with the following commensurate one

$$\tilde{K}(s) = 3.8159 + \frac{2.1199}{s^{0.6}} + 2.2195s^{0.8}, \tag{46}$$

leading to a control system (only used for design purposes) with commensurate order $\nu = 0.2$. A constraint on the maximum control variable has been considered:

$$u_M^0 \leq 10. \tag{47}$$

Note that, in the case of a servomotor, this is a common choice that means avoiding to saturate the current loop. In order to select the transition polynomial the relative order of the approximate closed-loop transfer function $\rho_{\tilde{T}} = 1.2$ and the relative order of the system $\rho_{\bar{G}} = 2$ have been considered. Applying (15) and (16), the necessary and sufficient condition $n = 2$ is obtained. This choice also satisfies (16) and leads to the following transition polynomial:

$$\bar{y}(t;\tau) = \frac{6}{\tau^5}t^5 - \frac{15}{\tau^4}t^4 + \frac{10}{\tau^3}t^3. \tag{48}$$

Applying the command signal design technique (details are not given for the sake of brevity, they can be found in [16]) it turns out that a transition time $\tau = 1.8$ is sufficient to guarantee the constraint satisfaction.

Finally the filter design methodologies proposed in Section V have been employed, again selecting $m = 3$. It turns out that:

$$\tilde{F}(s) = 1/(0.068s^3 + 0.27s^2 + 0.8819s + 1) \tag{49}$$

that leads to the fractional filter

$$\begin{aligned} F(s) = {} & (s^{2.6} + s^{1.6} + 0.5549s^{1.4} + 0.9540s^{0.6} + 0.5300)/ \\ & (0.0377s^{4.4} + 0.0649s^{3.6} + 0.1498s^{3.4} + 0.0360s^3 \\ & +0.2576s^{2.6} + 0.4893s^{2.4} + 0.1431s^2 + 0.8413s^{1.6} \\ & +0.5549s^{1.4} + 0.4674s + 0.9540s^{0.6} + 0.5300), \end{aligned} \tag{50}$$

while the resulting integer-order filter transfer function (obtained by using the first approach of Section V-B) is

$$\begin{aligned} F(s) = {} & (0.01071s^4 - 0.01051s^3 + 1.133s^2 + 1.222s + 1)/ \\ & (0.003553s^5 + 0.0363s^4 + 0.2631s^3 + 0.8111s^2 \\ & +1.819s + 1). \end{aligned} \tag{51}$$

Again, both filters have been tested, as well as a step command signal and the ideal one. It is worth stressing that the tests have been done using the actual controller and not the approximated one.

Fig. 10 shows that both step responses of the filters are quite close to the ideal command signal. Indeed, in this case, as the fractional slow decay has been well compensated, the integer-order filter step response remains close to ideal command signal also after a long time.

Finally, in Fig. 11 the simulation results are shown. It appears evidently that both methodologies are able to provide responses close to the one obtained using the ideal command signal, notably improving the performance despite the already well-tuned controller.

Among the benefits that both the proposed methodologies provide, a smaller rise and settling times have to be mentioned, as well as a continuous control signal. In particular, this allows the avoidance of a very high peak (or saturation) of the control variable due to the so called "derivative kick" phenomenon[13].

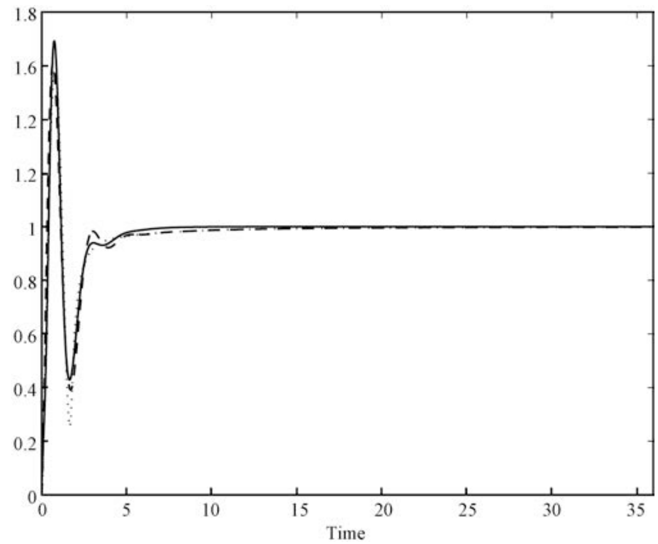

Fig. 10. Command signal (dotted line) and filter step response obtained by using the technique of Subsection V-A (dashed line) and Subsection V-B (solid line) for the set of constraints (47). – Example 2.

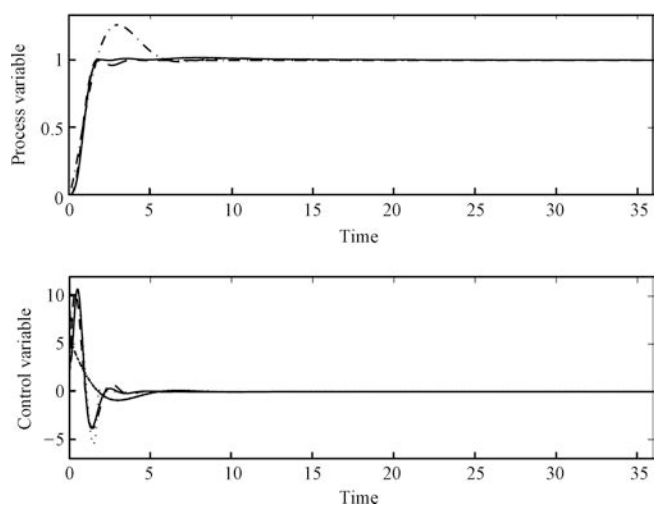

Fig. 11. Process variable (top) and control variable (bottom) obtained by using the command signal (dotted line), the filter designed with the technique of Subsection V-A (dashed line) and Subsection V-B (solid line) and a step command signal (dash-dot line) for the set of constraints (47). – Example 2.

C. Example 3

As a third example consider the following delay-dominant fractional plant

$$G(s)=\frac{1}{s^{1.8}+1}\mathrm{e}^{-3s} \tag{52}$$

and the proportional-integral (PI) controller

$$K(s)=0.12\left(1+\frac{1}{0.65s}\right), \tag{53}$$

tuned in order to achieve a phase margin of approximately $60°$. The system, because of the fractional order of 1.8, exhibits an oscillatory behavior. It is well known that a PI controller is not sufficient to achieve a high performance when dealing with underdamped systems, but in many cases the use of such a controller is in force (in particular in the industry). Bearing in mind this idea, it is shown here how to significantly improve the set-point following performance by using a two-degree-of-freedom controller with suitable set-point filters. Also, note that an integrator is absolutely necessary in the controller in order to reject possible disturbances, since the proportional gain must be very small in order to avoid oscillations because of the strong delay of the plant.

Considering that no constraints are imposed, the condition $n=2$ is sufficient to guarantee the existence of a command signal. Hence, the transition polynomial (48) is obtained. Then, by applying the command signal design procedure, the following results are obtained

$$\begin{aligned}H_0(s)\ &=\tfrac{2.1281}{s^{0.2}+1.0900}+\tfrac{3.3834+1.7277\mathrm{i}}{s^{0.2}+0.3368+1.0366\mathrm{i}}\\ &+\tfrac{3.3834-1.7277\mathrm{i}}{s^{0.2}+0.3368+1.0366\mathrm{i}}+\tfrac{5.4145+1.0678\mathrm{i}}{s^{0.2}-0.8818+0.6407\mathrm{i}}\\ &+\tfrac{5.4145-1.0678\mathrm{i}}{s^{0.2}-0.8818-0.6407\mathrm{i}},\end{aligned} \tag{54}$$

$$\begin{aligned}r_{ol}(t;\tau)\ &=8.3333D^{1.8}\bar{y}(t;\tau)-12.8205D^{0.8}\bar{y}(t;\tau)\\ &+8.3333\bar{y}(t;\tau)+\int_0^t\eta_0(t-\xi)\bar{y}(\xi;\tau)\mathrm{d}\xi,\end{aligned} \tag{55}$$

where the impulse response of the zero-order dynamics is not reported for the sake of readability, but can be easily obtained following the procedure proposed in [16].

After selecting the very small transition time $\tau=1$ (note that it is considerably smaller than the time delay), the technique of Subsection V-A and the second one of Subsection V-B have been applied. It results

$$\tilde{F}(s)=1/(0.01155s^3+0.08333s^2+0.4886s+1). \tag{56}$$

Then, the associated fractional-order filter is determined as

$$\begin{aligned}&F(s)=(s^{2.8}+s+1.2s\mathrm{e}^{-3s}+0.1846\mathrm{e}^{-3s})/(0.001386s^4\\ &+0.01213s^3+0.07402s^2+0.2102s+0.1846),\end{aligned} \tag{57}$$

while, using the integer-order approach we obtain:

$$\begin{aligned}&\bar{F}(s)=(-0.05786s^4+4.801s^3+1.347s^2+5.127s)/\\ &(0.0003913s^5+0.0132s^4+0.09208s^3+0.5454s^2\\ &+1.117s+1).\end{aligned} \tag{58}$$

and the associated integer-order filter is:

$$\begin{aligned}&F(s)=(-0.0006684s^7+0.05064s^6+0.3873s^5+2.459\\ &+s^4+0.01155s^3\mathrm{e}^{-3s}+5.886s^3+0.08333s^2\mathrm{e}^{-3s}\\ &+3.852s^2+0.4886s\mathrm{e}^{-3s}+5.127s+\mathrm{e}^{-3s})/\\ &(4.52\times10^{-6}s^8+0.000185s^7+0.002354s^6+0.02081s^5\\ &+0.1165s^4+0.463s^3+1.175s^2+1.606s+1).\end{aligned} \tag{59}$$

It is worth stressing that here the parameter $m=5$ has been used, because of the large process delay and the small transition time. Indeed, the previous examples choice $m=3$ would not be able to capture the first part of the postaction.

Since here a slow decay tail does not appear, both the techniques work properly. In particular, Fig. 12 shows that both the filters are capable to satisfactorily match the command signal.

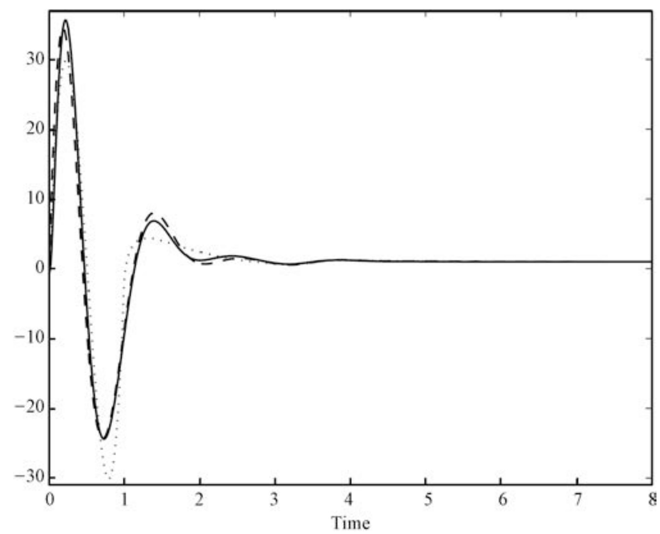

Fig. 12. Command signal (dotted line) and filter step responses obtained by using the technique of Subsection V-A (dashed line) and Subsection V-B (solid line) for the unconstrained problem. – Example 3.

Finally, Fig. 13 shows that both the integer filter and the fractional one are capable to strongly decrease the rise and the settling time contemporarily, guaranteeing a clear improvement of the set-point tracking performance despite the significant delay.

VIII. Conclusions

In this paper, a novel technique to design a set-point filter for a unity-feedback fractional control loop has been proposed.

It is based on a two-step procedure. First, an ideal command signal is synthesized in such away that a smooth and monotonic process output would have been obtained. Then, a linear filter is designed so that its step response is as close as possible, in terms of 2-norm, to the ideal command signal.

Two approaches are proposed, the first one based on a fractional-order filter and the second one on an integer-order one. Summarizing, the use of an integer-order filter should be limited to those cases where the feedback loop is tuned in such a way that no long fractional tails appear (note that this does not prevent the control system to exhibit a fractional dynamics as Examples 2 and 3 show) and the transition time is big enough to guarantee a stable filter. On the contrary, the fractional filter is always usable and guarantees a satisfactory performance, at the price of an increased implementation complexity.

The proposed technique is suitable for the design of two degree-of-freedom control structures and allows the user to design the feedback controller almost independently from the set-point tracking performance, that, on the contrary, mostly depends on the set-point filter.

Simulation results have demonstrated the effectiveness of the proposed methodology.

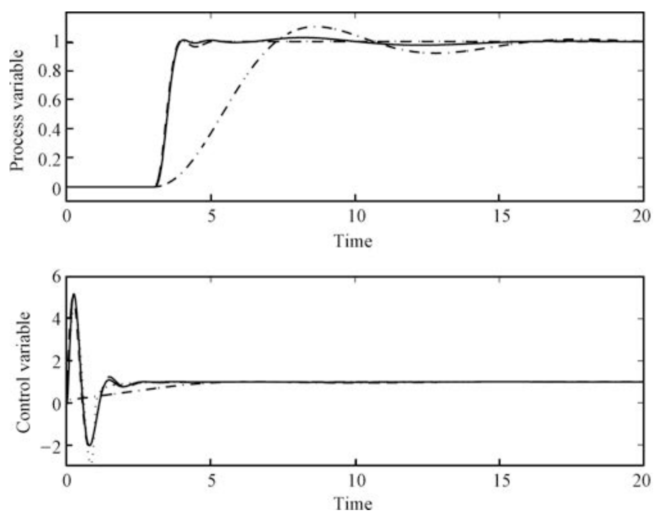

Fig. 13. Process variable (top) and control variable (bottom) obtained by using the command signal (dotted line), the filter designed with the technique of Subsection V-A (dashed line) and Subsection V-B (solid line) and a step command signal (dash-dot line) for the unconstrained problem. – Example 3.

REFERENCES

[1] Valério D, Costa J S. Introduction to single-input, single-output fractional control. *IET Control Theory & Applications*, 2011, **5**(8): 1033−1057

[2] Monje C A, Chen Y Q, Vinagre B M, Xue D Y, Feliu-Batlle V. *Fractional-order Systems and Controls: Fundamentals and Applications.* London, UK: Springer-Verlag, 2010.

[3] Sabatier J, Agrawal O P, Machado J A T. *Advances in Fractional Calculus: Theoretical Developments and Applications in Physics and Engineering.* London, UK: Springer, 2007.

[4] Chen Y Q, Petráš I, Xue D Y. Fractional order control-a tutorial. In: Proceedings of the 2009 Conference on American Control Conference. Piscataway, NJ, USA: IEEE, 2009. 1397−1411

[5] Victor S, Melchior P, Nelson-Gruel D, Oustaloup A. Flatness control for linear fractional MIMO systems: thermal application. In: Proceedings of the 3rd IFAC Workshop on Fractional Differentiation and its Applications. Ankara, Turkey: IFAC, 2008. 1−7

[6] Jallouli-Khlif R, Melchior P, Derbel N, Oustaloup A. Robust path tracking by preshaping approach designed for third generation CRONE control. *International Journal of Modeling, Identification and Control*, 2012, **15**(2): 125−133

[7] Maione G. Continued fractions approximation of the impulse response of fractional-order dynamic systems. *IET Control Theory & Applications*, 2008, **2**(7): 564−572

[8] Caponetto R, Dongola G, Fortuna L, Gallo A. New results on the synthesis of FO-PID controllers. *Communications in Nonlinear Science and Numerical Simulation*, 2010, **15**(4): 997−1007

[9] Padula F, Visioli A. Optimal tuning rules for proportional-integral-derivative and fractional-order proportional-integral-derivative controllers for integral and unstable processes. *IET Control Theory & Applications*, 2012, **6**(6): 776−786

[10] Pisano A, Rapaić M R, Jeličić Z, Usai E. Sliding mode control approaches to the robust regulation of linear multivariable fractional-order dynamics. *International Journal of Robust and Nonlinear Control*, 2010, **20**(18): 2045−2056

[11] Padula F, Vilanova R, Visioli A. H_∞ model matching PID design for fractional FOPDT systems. In: Proceedings of the 2012 American Control Conference. Montreal, CA: ACC, 2012. 5513−5518

[12] Padula F, Visioli A. *Advances in Robust Fractional Control.* Switzerland: Springer, 2015.

[13] Visioli A. *Practical PID Control.* London, UK: Springer, 2006.

[14] Padula F, Visioli A. Set-point weight tuning rules for fractional-order PID controllers. *Asian Journal of Control*, 2013, **15**(3): 678−690

[15] Orsoni B, Melchior P, Oustaloup A, Badie T, Robin G. Fractional motion control: application to an XY cutting table. *Nonlinear Dynamics*, 2002, **29**(1−4): 297−314

[16] Padula F, Visioli A. Inversion-based feedforward and reference signal design for fractional constrained control systems. *Automatica*, 2014, **50**(8): 2169−2178

[17] Piazzi A, Visioli A. Optimal inversion-based control for the set-point regulation of nonminimum-phase uncertain scalar systems. *IEEE Transactions on Automatic Control*, 2001, **46**(10): 1654−1659

[18] Piazzi A, Visioli A. Robust set-point constrained regulation via dynamic inversion. *International Journal of Robust and Nonlinear Control*, 2001, **11**(1): 1−22

[19] Piazzi A, Visioli A. A noncausal approach for PID control. *Journal of Process Control*, 2006, **16**(8): 831−843

[20] Piazzi A, Visioli A. Optimal noncausal set-point regulation of scalar systems. *Automatica*, 2001, **37**(1): 121−127

[21] Padula F, Visioli A. Inversion-based set-point filter design for fractional control systems. In: Proceedings of the 2014 International Conference on Fractional Differentiation and Its Applications. Catania: IEEE, 2014. 1−6

[22] Podlubny I. *Fractional Differential Equations*. San Diego: Academic Press, 1999.

[23] Padula F, Visioli A. Optimal set-point regulation of fractional systems. In: Proceedings of the 6th IFAC Workshop on Fractional Differentiation and Its Applications. Grenoble: Elsevier, 2013. 911−916

[24] Ortigueira M D, Coito F J V, Trujillo J J. A new look into the discrete-time fractional calculus: transform and linear systems. In: Proceedings of the 6th IFAC Workshop on Fractional Differentiation and Its Applications. Grenoble: Elsevier, 2013. 630−635

[25] Sabatier J, Moze M, Farges C. LMI stability conditions for fractional order systems. *Computer & Mathematics with Applications*, 2010, **59**(5): 1594−1609

[26] Oustaloup A, Levron F, Mathieu B, Nanot F M. Frequency-band complex noninteger differentiator: characterization and synthesis. *IEEE Transactions on Circuits and Systems I: Fundamental Theory and Applications*, 2000, **47**(1): 25−39

[27] Monje C A, Vinagre B M, Chen Y Q, Feliu V, Lanusse P, Sabatier J. Proposals for fractional PID tuning. In: Preprints IFAC Workshop on Fractional Differentiation and its Applications. Bordeaux: IFAC, 2004. 156−161

Fabrizio Padula was born in Brescia, Italy, in 1984. He received the M. Sc degree in industrial automation engineering in 2009 and the Ph. D. degree in computer science and automatic control in 2013, both form the University of Brescia. Currently, he is Research Fellow at the Department of Mathematics and Statistics of the Faculty of Science and Engineering at Curtin University, Perth, Australia. His research activity deals with fractional control, inversion-based control and tracking control. He is also interested in robotics and mechatronics.

Antonio Visioli was born in Parma, Italy, in 1970. He received the Laurea degree in electronic engineering from the University of Parma in 1995 and the Ph. D. degree in applied mechanics from the University of Brescia in 1999. Currently he holds a professor position in automatic control at the Department of Mechanical and Industrial Engineering of the University of Brescia. He is a senior member of IEEE and a member of the TC on Education of IFAC, of the IEEE Control Systems Society TC on Control Education and of the IEEE Industrial Electronics Society TC on Factory Automation Subcommittees on Event-Based Control & Signal and on Industrial Automated Systems and Control, and of the national board of Anipla (Italian Association for Automation). His research interests include industrial robot control and trajectory planning, dynamic inversion based control, industrial control, and fractional control. He is the author or co-author or editor of four international book, one textbook and of more than 200 papers in international journals and conference proceedings.

Identification and PID Control for a Class of Delay Fractional-order Systems

Zhuoyun Nie, Qingguo Wang, Ruijuan Liu, and Yonghong Lan

***Abstract*—In this paper, a new model identification method is developed for a class of delay fractional-order system based on the process step response. Four characteristic functions are defined to characterize the features of the normalized fractional-order model. Based on the time scaling technology, two identification schemes are proposed for parameters' estimation. The scheme one utilizes three exact points on the step response of the process to calculate model parameters directly. The other scheme employs optimal searching method to adjust the fractional order for the best model identification. The proposed two identification schemes are both applicable to any stable complex process, such as higher-order, under-damped/over-damped, and minimum-phase/nonminimum-phase processes. Furthermore, an optimal PID tuning method is proposed for the delay fractional-order systems. The requirements on the stability margins and the negative feedback are cast as real part constraints (RPC) and imaginary part constraints (IPC). The constraints are implemented by trigonometric inequalities on the phase variable, and the optimal PID controller is obtained by the minimization of the integral of time absolute error (ITAE) index. Identification and control of a Titanium billet heating process is given for the illustration.**

***Index Terms*—Fractional-order system, time delay, identification, PID control, Titanium billet heating furnace.**

I. INTRODUCTION

FRACTIONAL order appears in many real dynamical processes naturally, such as heating furnace[1], flexible structures[2], materials with memory and hereditary effects[3], and a new electrical circuit element named "fractance"[4]. Compared with the integer model, fractional-order model often provides more reliable description for some real dynamical processes, especially when the Bode diagrams do not show slopes of integer multiplying of 20 dB/decade[5], or when the traditional integer models cannot fit the experiments data well. For these reasons, more and more attention has been paid to the problems of identification and control of fractional-order systems[6−9]. A recent survey of its development is presented in [10] and its applications are introduced in [11].

For unknown processes, fractional-order system identification becomes a difficult problem due to the fractional order present in the physical systems. The aim of identification of fractional-order system is to establish a fractional-order model to describe the system's physical behavior by the observed data. Since the model parameters in identifying consist now not only the coefficients but also the differentiation orders appearing nonlinearly, some standard tools, such as relay feedback method for integer models cannot be used directly to identify fractional-order systems if there is no fundamental improvement in the relay feedback theory. Therefore, the researches on the identification problem for fractional-order system have attracted lots of attention. An overview of the identification issue of fractional-order system is introduced in [12].

There have been some methods developed for the fractional-order system identification using continuous time models. In [13], linear least square (LS) optimization technique is used to estimate the coefficients of fractional differential equation, with the differentiation orders being fixed according to a prior knowledge. When the fractional differentiation orders are not available by the prior knowledge, output error methods are developed in [14], to provide estimation of both coefficients and differentiation orders by nonlinear optimization techniques instead of LS. The above two methods are based on classical identification methods whose parameters are estimated by minimizing a given criterion and data fitting. It is obvious that, the identification procedure becomes complicated when nonlinear optimization is involved[15]. Recently, an optimal identification algorithm is developed with a carefully selected initial value for a class of fractional order modeling[16].

Another identification approach has been presented for fractional-order systems in frequency domain. A new concept of continuous order-distribution is introduced through the development of a fractional/integer-order system identification, which allows the identification of both standard fractional/integer-order systems containing continuous or discrete terms as well as system with continuous order-distributions[17] . Recently, frequency response model identification for fractional-order systems is provided for the purpose of PID auto-tuning[18] . The model assumed to be fractional-order plus time delay form is obtained by model reduction from identified integer model. To estimate the time delay along with continuous-time fractional-order model, a linear filter is introduced for the model identification in an iterative manner by solving simple linear regression[19].

Manuscript received August 20, 2015; accepted February 18, 2016. This work was supported by National Natural Science Foundation of China (61403149, 61573298), Natural Science Foundation of Fujian Province (2015J01261, 2016J05165), and Foundation of Huaqiao University (Z14Y0002). Recommended by Associate Editor Antonio Visioli.

Citation: Zhuoyun Nie, Qingguo Wang, Ruijuan Liu, Yonghong Lan. Identification and PID control for a class of delay fractional-order systems. *IEEE/CAA Journal of Automatica Sinica*, 2016, **3**(4): 463−476

Zhuoyun Nie is with the School of Information Science and Engineering, Huaqiao University, Xiamen 361021, China (e-mail: yezhuyun2004@sina.com).

Qingguo Wang is with the Institute for Intelligent Systems, the University of Johannesburg, Johannesburg 2146, South Africa (e-mail: wangq@uj.ac.za).

Ruijuan Liu is with the School of Applied Mathematics, Xiamen University of Technology, Xiamen 361021, China (e-mail: liuruijuan0313@163.com).

Yonghong Lan is with the School of Information Engineering, Xiangtan University, Xiangtan 411105, China (e-mail: yhlan@xtu.edu.cn).

To obtain PID controller for a fractional-order process, Luo et al.[20] designed integer/fractional-order PID controller for a class of fractional-order system in terms of phase margin and the robustness against the loop gain variations. Based on the magnitude and phase measurements of the plant by relay feedback tests at a frequency of interest, Monje et al.[8−9] developed a method for the auto-tuning of fractional-order PID controllers. Combined with the frequency response estimation for a fractional-order system, an explicit PID tuning rule is proposed, which incorporates both the set-point tracking and the disturbance rejection case[18].

In this paper, a new model identification method is developed for a class of delay fractional-order model. The step responses of the normalized fractional-order model are used for the characteristic functions' definition and fitting. Combined with characteristic functions, the process is identified by time scaling technology. Two identification schemes are developed in the parameter estimation. The scheme one utilizes three exact points' data on the step response of the process to obtain the fractional-order model parameters. The other scheme employs single-variable optimization to adjust the fractional order for the proper parameters. The proposed two identification schemes are both applicable to any stable complex process, such as higher-order, under-damped/over-damped, and minimum-phase/nonminimum-phase processes. Furthermore, an optimal PID tuning method is proposed for the delay fractional-order model. The requirements on the stability margins and the negative feedback structure are cast as real part constraints (RPC) and imaginary part constraints (IPC). The constraints are implemented by trigonometric inequalities on the phase variable, and the optimal controller is obtained by solving a single-variable optimization problem to minimize the integral of time absolute error (ITAE) index. Application results on the Titanium billet heating furnace are provided for the illustration.

The remaining parts of this paper are organized as follows. In Section II, the proposed model identification method based on time scaling technology is developed. In Sections III, optimal PID controller tuning method is presented using ITAE rule. The simulation and comparison results in Section IV are given to illustrate the performance of the proposed methods. In Section V, application results on the titanium billet heating furnace are provided for model identification and control. Finally, conclusion is given in Section VI.

II. Process Model and Identification

In the real-world, many stable physical systems can be well characterized by fractional-order model with non integer-order derivatives. Suppose a stable process is modeled by a delay fractional-order system

$$G(s)=\frac{K}{Ts^{\alpha}+1}\mathrm{e}^{-Ls}, \tag{1}$$

where $L>0$ is time delay, $T>0$ is the time constant, K is the loop gain and $0<\alpha<2$ is the fractional order.

The step responses of (1) for different values of α with $K=1$, $T=0$ and $L=0$ are given in Fig. 1, which shows that the fractional-order model in (1) provides rich complex dynamics, including oscillations and overshoot, to characterize any stable engineering process[9, 19]. It is obvious that, the fractional-order α dominates the behavior of the step response and results in significant performance difference for the case of $0<\alpha\le 1$ and $1<\alpha<2$. When $0<\alpha\le 1$, the outputs have no oscillation and tend to the reference signal very slowly; when $1<\alpha<2$, the oscillations occur in the outputs and are stranger when α is increasing. So, it motivates us to identify the process based on step response depending on the system parameters.

A. Time Scaling Analysis

The process model is normalized to be $K\tilde{G}(\tilde{s})=G(s)$, where

$$\tilde{G}(\tilde{s})=\frac{1}{\tilde{s}^{\alpha}+1}\mathrm{e}^{-\tau\tilde{s}}, \tag{2}$$

$\tilde{s}=\sqrt[\alpha]{T}s$ and $\tau=L/\sqrt[\alpha]{T}$. Denote the step responses by $y(t)$ for the system $G(s)$ and $\tilde{y}(\tilde{t}+\tau)$ for the normalized systems $\tilde{G}(\tilde{s})$. Note that, $\tilde{t}$ stands for the time coordinate in the case of $\tau=0$, and the data $(\tilde{t},\tilde{y}(\tilde{t}+0))$ will be collected and used in our identification.

According to definition of Laplace transform,

$$\mathcal{L}[f(t)]=F(s)=\int_0^{\infty}f(t)\mathrm{e}^{-st}\mathrm{d}t, \tag{3}$$

it is deduced that

$$\mathcal{L}\left[f(\frac{t}{a})\right]=aF(as),\quad a\in\mathbf{R}. \tag{4}$$

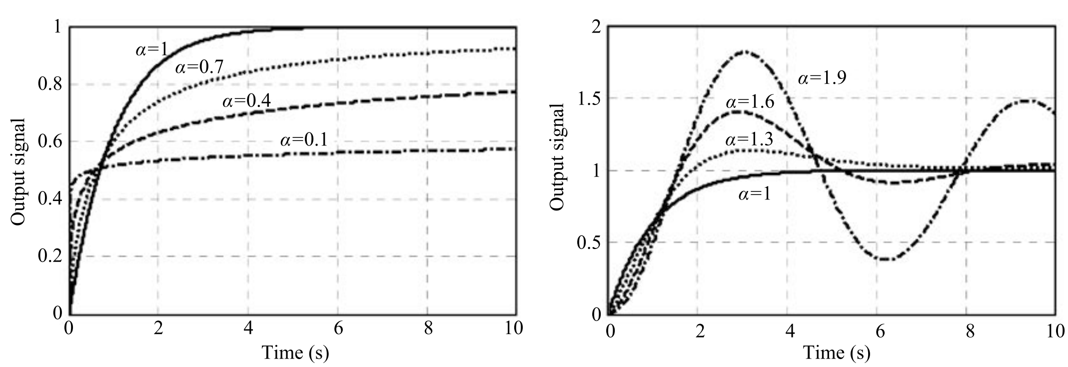

Fig. 1. The step responses for $0<\alpha\le 1$ and $1<\alpha<2$ with $K=1$ and $T=0$.

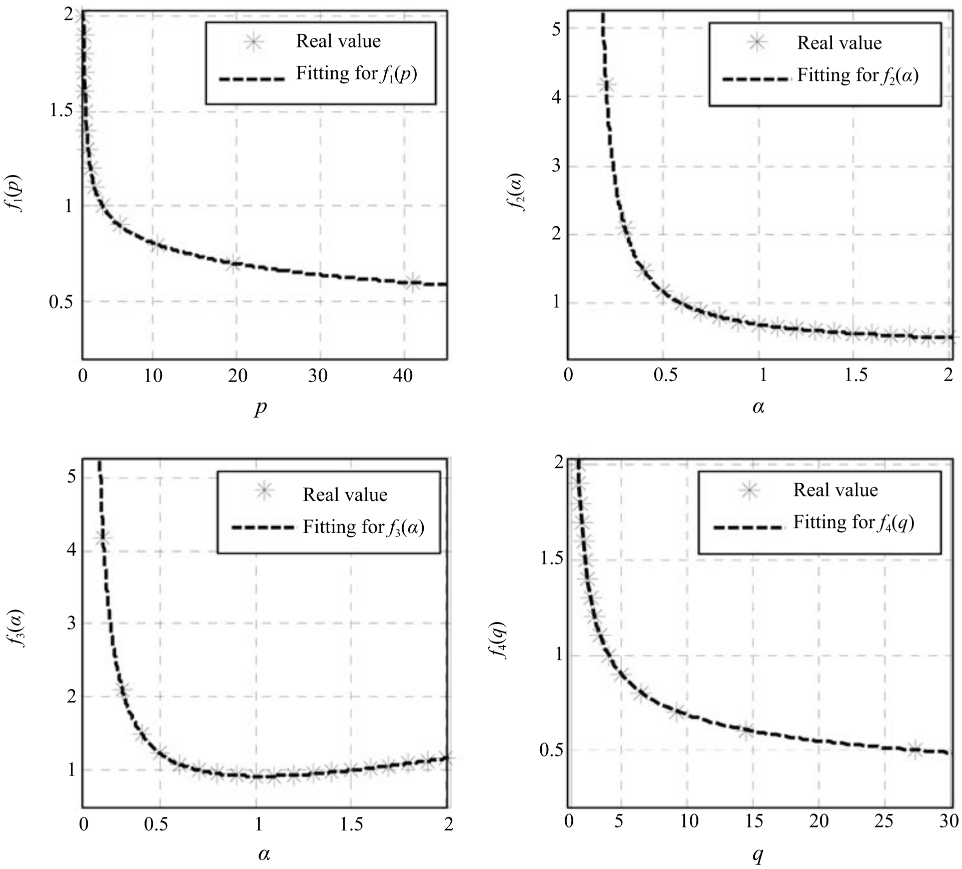

Fig. 2. Curve fitting for $f_1(p)$, $f_2(\alpha)$, $f_3(\alpha)$ and $f_4(q)$.

According to (4), when

$$y(t) = K\tilde{y}(\tilde{t}+\tau), \tag{5}$$

the following equation holds,

$$\tilde{t}+\tau = \frac{t}{\sqrt[\alpha]{T}}. \tag{6}$$

In this way, the relationship between $y(t)$ and $\tilde{y}(\tilde{t}+\tau)$ is well formulated by time scaling.

Denote the step response of the real process by $y_r(t)$. Since the process is modeled by (1), it is reasonable to assume $y_r(t) \approx y(t)$, and specify $y_r(t_i) = K\tilde{y}(\tilde{t}_i+\tau)$ at some points. Then, the parameters can be solved directly using (6). Here, two identifying schemes are proposed for the parameter estimation based on (6).

B. Identification by Three Points

The process gain K is obtained directly by

$$K = \frac{y_r(\infty)}{r(\infty)}, \tag{7}$$

for the stable process. Collect the responses data $(\tilde{t}, \tilde{y}(\tilde{t}+0))$ in Fig. 1, and choose $\tilde{y}(\tilde{t}_1) = \beta_1$, $\tilde{y}(\tilde{t}_2) = \beta_2$ and $\tilde{y}(\tilde{t}_3) = \beta_3$, where $\beta_1 < \beta_2 < \beta_3$ and $\tilde{t}_1 < \tilde{t}_2 < \tilde{t}_3$, in the rising up stage of the step response. Three points are specified as $y_r(t_1)/K = \beta_1$, $y_r(t_2)/K = \beta_2$ and $y_r(t_3)/K = \beta_3$, on the process responses, (6) gives the following equations:

$$\begin{cases} \tilde{t}_1 + \tau = \dfrac{t_1}{\sqrt[\alpha]{T}}, \\ \tilde{t}_2 + \tau = \dfrac{t_2}{\sqrt[\alpha]{T}}, \\ \tilde{t}_3 + \tau = \dfrac{t_3}{\sqrt[\alpha]{T}}. \end{cases} \tag{8}$$

Before solving (8), four characteristic functions are defined

$$\begin{cases} f_1\left(\dfrac{\tilde{t}_3-\tilde{t}_1}{\tilde{t}_2-\tilde{t}_1}\right) := \alpha, \\ f_2(\alpha) := \tilde{t}_2 - \tilde{t}_1, \\ f_3(\alpha) := \tilde{t}_2, \\ f_4\left(\dfrac{\tilde{t}_2}{\tilde{t}_1}\right) := \alpha, \end{cases} \tag{9}$$

where

$$p := \frac{t_3-t_1}{t_2-t_1} = \frac{\tilde{t}_3-\tilde{t}_1}{\tilde{t}_2-\tilde{t}_1}, \tag{10}$$

$$q := \frac{t_2}{t_1} = \frac{\tilde{t}_2}{\tilde{t}_1}. \tag{11}$$

Then, the explicit solution of (8) is given by

$$\begin{cases} \alpha = f_1(p), \\ T = \left(\dfrac{t_2-t_1}{f_2(\alpha)}\right)^{\alpha}, \\ L = t_2 - f_3(\alpha)\sqrt[\alpha]{T}. \end{cases} \tag{12}$$

In (12), $\alpha > 0$ and $T > 0$ hold naturally, since $\tilde{t}_1 < \tilde{t}_2 < \tilde{t}_3$ and $t_1 < t_2 < t_3$. $L < 0$ would occur if

$$t_2 < \tilde{t}_2 \sqrt[\alpha]{T}, \tag{13}$$

because of the complex dynamics caused by high-order poles and zeros, actuator nonlinearities or time varying parameters. In this case, we set $L = 0$ and find the solutions of α and T using two points. Take $\tilde{y}(\tilde{t}_1) = \beta_1$, $\tilde{y}(\tilde{t}_2) = \beta_2$, and we have the solutions

$$\begin{cases} \alpha = f_4(q), \\ T = \left(\dfrac{t_2 - t_1}{f_2(\alpha)}\right)^{\alpha}, \\ L = 0. \end{cases} \tag{14}$$

In this paper, we set $\beta_1 = 0.2$, $\beta_2 = 0.6$ and $\beta_3 = 0.95$ which are listed in Table I as the recommended value for collection of data. Then, four characteristic functions are obtained by curve fitting, as shown in Fig. 2,

$$\begin{cases} f_1(p) = \dfrac{0.4053p^3 + 22.61p^2 + 14.85p - 41.29}{p^3 + 25.22p^2 - 4.519p - 44.52}, \\ f_2(\alpha) = \dfrac{0.3315\alpha + 0.2876}{\alpha - 0.1153}, \\ f_3(\alpha) = \dfrac{2.96\alpha^2 + 1.344\alpha + 4.814}{\alpha^3 - 5.488\alpha^2 + 16.21\alpha - 1.787}, \\ f_4(q) = \dfrac{0.2789q^2 + 14.85q + 11.26}{q^2 + 19.16q - 18.25}. \end{cases} \tag{15}$$

These four functions will play important roles in our process identification because the features of step responses of the normalized model (2) can be well characterized by them. Note that, for any different choice of β_i, the accuracy of the identification results only depend upon the fitting precision.

C. Optimal Identification

Theoretically, the model parameters can be calculated exactly if three points are specified on the step response by (12) or (14), but this would be a strict limitation on the whole curve matching for the responses. Recall that, the fractional-order α dominates the behavior or the shape of the step response. A good choice of α can guarantee a nice shape matching, which motivates us to develop an optimal identification scheme.

Take $\beta_1 = 0.4$ and $\beta_2 = 0.6$ as the recommended value to have $\tilde{y}(\tilde{t}_1) = \beta_1$ and $\tilde{y}(\tilde{t}_2) = \beta_2$, and the values of $\tilde{t}_1$ and $\tilde{t}_2$ are collected in Table II. The function $f_2(\alpha)$, as shown in Fig. 3, is updated in (15) by curve fitting

$$f_2(\alpha) = \frac{0.3704}{\alpha - 0.1097}. \tag{16}$$

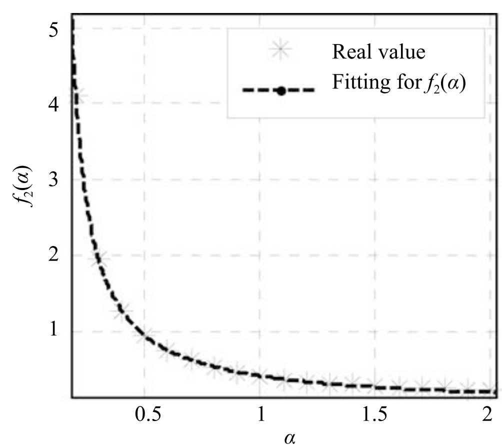

Fig. 3 Curve fitting for $f_2(\alpha)$.

TABLE I
$\tilde{t}_i$ FOR DIFFERENT α IN FIG. 1

α	$\tilde{t}_1$ $\beta_1 = 0.2$	$\tilde{t}_2$ $\beta_1 = 0.6$	$\tilde{t}_3$ $\beta_3 = 0.95$
0.1	$1/\infty$	31.92	∞
0.2	$1/\infty$	4.180	∞
0.3	0.0064	2.102	> 8000
0.4	0.0214	1.497	> 600
0.5	0.0448	1.228	126.3
0.6	0.0744	1.083	41.41
0.7	0.1082	0.9983	17.55
0.8	0.1449	0.952	8.61
0.9	0.1834	0.927	4.71
1.0	0.2233	0.9164	3.02
1.1	0.264	0.9188	2.265
1.2	0.3052	0.9297	1.911
1.3	0.3470	0.9470	1.72
1.4	0.3890	0.9693	1.612
1.5	0.4312	0.9954	1.55
1.6	0.4736	1.0244	1.517
1.7	0.5160	1.0557	1.501
1.8	0.5585	1.0888	1.50
1.9	0.6010	1.1236	1.507
2.0	0.6436	1.1594	1.521

TABLE II
$\tilde{t}_i$ FOR DIFFERENT α IN FIG. 2

α	$\tilde{t}_1$ $\beta_1 = 0.4$	$\tilde{t}_2$ $\beta_1 = 0.6$
0.1	0.0099	31.92
0.2	0.0771	4.180
0.3	0.1551	2.102
0.4	0.2236	1.497
0.5	0.2824	1.228
0.6	0.3342	1.083
0.7	0.3816	0.9983
0.8	0.4262	0.952
0.9	0.4690	0.927
1.0	0.5110	0.9164
1.1	0.5524	0.9188
1.2	0.5937	0.9297
1.3	0.6350	0.9470
1.4	0.6764	0.9693
1.5	0.7180	0.9954
1.6	0.7596	1.0244
1.7	0.8014	1.0557
1.8	0.8433	1.0888
1.9	0.8853	1.1236
2.0	0.9274	1.1594

In our optimal identification, integral square error (ISE) between $y(t)$ and $y_r(t)$ is introduced to find the optimal solution. Then, the minimization problem can be formulated by

$$J_{id} = \min_{\alpha} \left[\int_0^{t*} |y(t) - y_r(t)|^2 \mathrm{d}t \right], \tag{17}$$

$$\text{s.t.} \begin{cases} T = \left(\dfrac{t_2 - t_1}{f_2(\alpha)} \right)^{\alpha}, \\ L = \max \left(t_2 - f_3(\alpha) \sqrt[\alpha]{T}, \quad 0 \right), \end{cases} \tag{18}$$

and solved easily by MATLAB function "fminbnd".

D. Algorithms

The proposed two identification schemes are summarized by the following algorithms.

Algorithm 1. Three points identification (Model 1)

Step 1. Set the recommended value $\beta_1 = 0.2$, $\beta_2 = 0.6$ and $\beta_3 = 0.95$, and calculate the process gain K by (7).

Step 2. Collect t_1, t_2 and t_3 from the step response of the real process to have $y_r(t_1)/K = \beta_1$, $y_r(t_2)/K = \beta_2$ and $y_r(t_3)/K = \beta_3$.

Step 3. Calculate p, q by (10) and (11), respectively.

Step 4. Calculate the value of four functions in (15) to have $\alpha = f_1(p)$, $\tilde{t}_2 - \tilde{t}_1 = f_2(\alpha)$, $\tilde{t}_2 = f_3(\alpha)$ and $\alpha = f_4(q)$.

Step 5. If $t_2 > \tilde{t}_2 \sqrt[\alpha]{T}$, determine the parameters α, T and L by (12), otherwise, by (14).

Algorithm 2. Optimal identification (Model 2)

Step 1. Set the recommended value $\beta_1 = 0.4$ and $\beta_2 = 0.6$, and calculate the process gain K by (7).

Step 2. Collect t_1 and t_2 from the step response of the real process to have $y_r(t_1)/K = \beta_1$ and $y_r(t_2)/K = \beta_2$.

Step 3. Set an initial value of $\alpha = \alpha^* \in (0, 2)$.

Step 4. Update $f_2(\alpha)$ by (16), and calculate T and L by (18).

Step 5. Calculate the cost function (17). If convergent, stop; otherwise, set a new value $\alpha = \alpha_i$ by "fminbnd", and go to Step 4.

In (15) and (16), to reduce the fitting error, rational functions are used with proper order, for curve fitting, which confirms the accuracy of the identification results. Obviously, Algorithm 1 provides a fast identification with only three points used in the calculation, while Algorithm 2 provides more accurate identification results by optimal searching.

Remark 1. The proposed identification procedures in Algorithm 1 and Algorithm 2 allow long dead time, large phase lag and unstable zeros of the system are due to the introduced time delay in the fractional-order model. They can be successfully approximated with equivalent time delay[18].

Remark 2. The proposed identification method is applicable to a wide range of engineering processes. If the process is unstable, one can stabilize the process first by a proportional controller. Then, the method becomes applicable.

Remark 3. The measured noise or disturbance is inevitable in the real process and brings identification errors. To guarantee the accuracy, a filtering algorithm, such as median filtering, can be employed to make pretreatment of the measured data. Then, the measured noise or disturbance is limited.

Remark 4. A similar identification method can be found in [16] for the same model (1). Based on the step response, optimal fitting is carried out with carefully selected initial parameters. For the same points, both methods in this paper and in [16], are trying to extract some typical features of the step response for the model identification. Rather than the direct optimal computation, our basic idea is to make time scaling analysis for the process model (1) and its normalized model (2). Based on such time scaling relationship, the proposed two identification schemes are developed under a unified framework. Then, solving equation set by three exact points or by optimal response shape matching with two points is logical.

E. Simulation Study

To illustrate the utility of the proposed identification method, four typical processes, including minimum phase processes and nonminimum phase processes, are discussed in the simulations.

Process 1. Over-damped process with zero and time delay

$$G_{p1} = \frac{2s+1}{(s+1)^3} \mathrm{e}^{-0.5s}. \tag{19}$$

Process 2. Under-damped process with zero and time delay

$$G_{p2} = \frac{4s+1}{(9s^2+3s+1)(s+1)} \mathrm{e}^{-0.5s}. \tag{20}$$

Process 3. Over-damped process with positive zero and time delay

$$G_{p3} = \frac{-3s+1}{(s+1)^3} \mathrm{e}^{-s}. \tag{21}$$

Process 4. Under-damped process with positive zero and time delay

$$G_{p4} = \frac{-5s+1}{(9s^2+3s+1)(s+1)} \mathrm{e}^{-6s}. \tag{22}$$

The simulations are carried out for the case when the high-order models G_{p1}-G_{p4} have already known to provide the step response data. The identification procedures can also be viewed as model reduction for high-order processes. The above processes are identified to be fractional-order plus time delay models in (1) and a zero initial condition is assumed. The model performance will be compared with a frequency identification method[18].

The basic idea behind the frequency method[18] is to specify a point on the frequency response

$$G_p(\mathrm{j}\omega) = G(\mathrm{j}\omega), \tag{23}$$

which gives the amplitude condition and phase condition to solve T and L for a given value ofα. The parameters are finally determined by solving a single-variable optimization problem to minimize the norm of the frequency response errors between the process and the fractional model:

$$\min_{\alpha}\left[\sum_{i=1}^{n}\left|G_p(\mathrm{j}\omega_i)-G(\mathrm{j}\omega_i,\alpha)\right|^2\right],$$
$$0\leq \omega 1<\omega 2<\cdots<\omega u,$$
$$\begin{cases} k=G_p(0),\\ T=\tau^{\alpha},\\ L=\dfrac{-\angle G_p(\mathrm{j}\omega)+\arctan 2(\tilde{A},\tilde{B})}{\omega}, \end{cases} \tag{24}$$

where

$$\begin{cases} \tau=\left(\dfrac{-\cos(\frac{\alpha\pi}{2})\left|G_P(\mathrm{j}\omega)\right|^2\omega^{\alpha}+\sqrt{A+B}}{\left|G_P(\mathrm{j}\omega)\right|^2\omega^{2\alpha}}\right)^{\frac{1}{\alpha}}\\ A=\cos^2\left(\dfrac{\alpha\pi}{2}\right)\left|G_p(\mathrm{j}\omega)\right|^4\omega^{2\alpha}\\ B=\left|G_p(\mathrm{j}\omega)\right|^2\omega^{2\alpha}(k^2-\left|G_p(\mathrm{j}\omega)\right|^2)\\ \tilde{A}=-\sin\left(\dfrac{\alpha\pi}{2}\right)\tau^{\alpha}\omega^{\alpha}\\ \tilde{B}=\cos\left(\dfrac{\alpha\pi}{2}\right)\tau^{\alpha}\omega^{\alpha}+1\\ \omega\approx\omega_u\ (\text{the ultimate frequency of } G_P) \end{cases}$$

The identification results are given in Table III, and the performance in step responses and frequency responses are given in Figs. 4 and 5. It shows that the proposed method successfully estimates the fractional-order model by step response for all the investigated process with fairly good accuracy. Compared with the frequency method[18], the proposed optimal identification model provides better step response fitting to the real process.

Regarding the frequency response, the proposed models can also fit the processes well. The main fitting error for the nonminimum phase process is caused by the right plane zero, which is equivalent to time delay in the fractional-order model. In the proposed method, such equivalent treatment does not affect the fitting accuracy of the portion of minimum phase. One can see that, when undershoot is ending in Fig. 4, the proposed models follow the step responses of G_{p3} and G_{p4} with little error. So, it is obvious that, there is a trade-off between the step response fitting and frequency response fitting.

III. PID TUNING

In this section, a PID controller tuning method is developed for delay fractional-order processes. The proposed PID tuning rule is derived by ITAE minimization with the constraints on the stability margins.

Since the open loop gain of the Process 1 is less than unity over high frequency range and will not affect stability, the paper measures the robustness by the gain margin A and phase margin ϕ,

$$1+AG(\mathrm{j}\omega_p)C(\mathrm{j}\omega_p)=0, \tag{25}$$

$$1+\mathrm{e}^{-\mathrm{j}\phi}G(\mathrm{j}\omega_g)C(\mathrm{j}\omega_g)=0, \tag{26}$$

where ω_p and ω_g are the phase and gain crossover frequencies of the loop, respectively. According to [21−22], these two

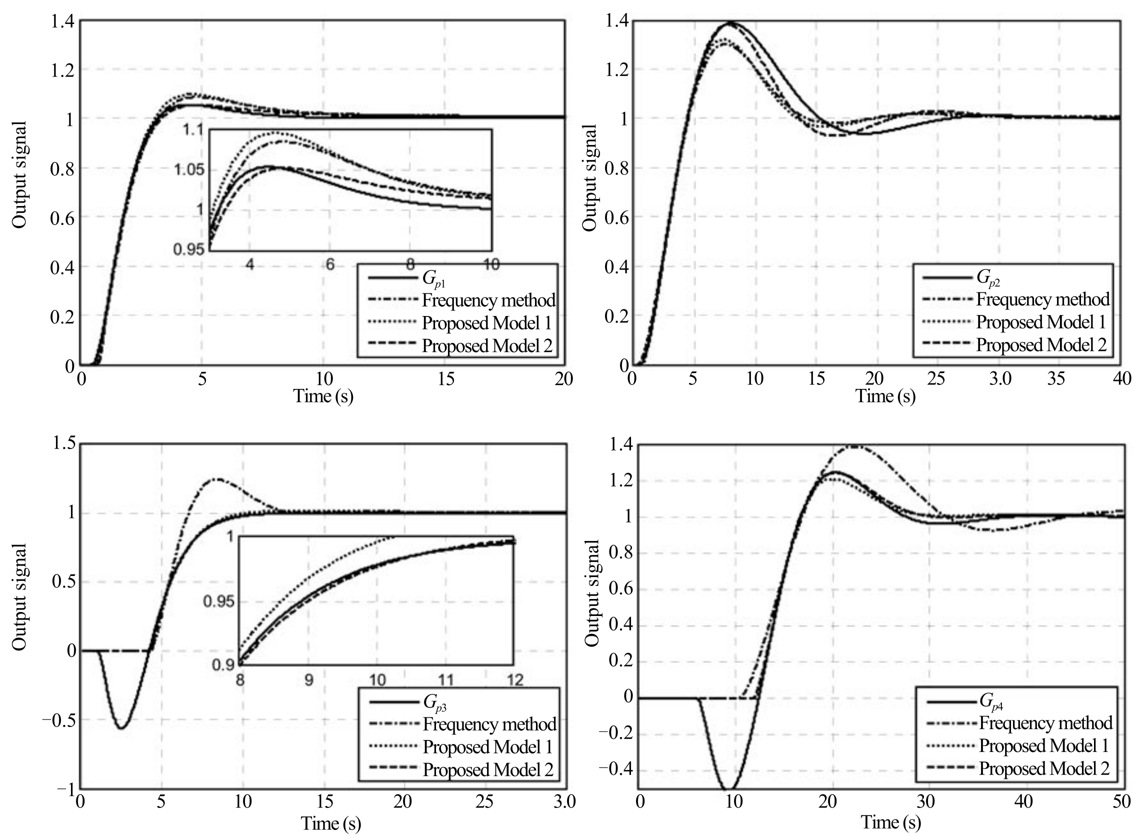

Fig. 4. Results of the process identification method.

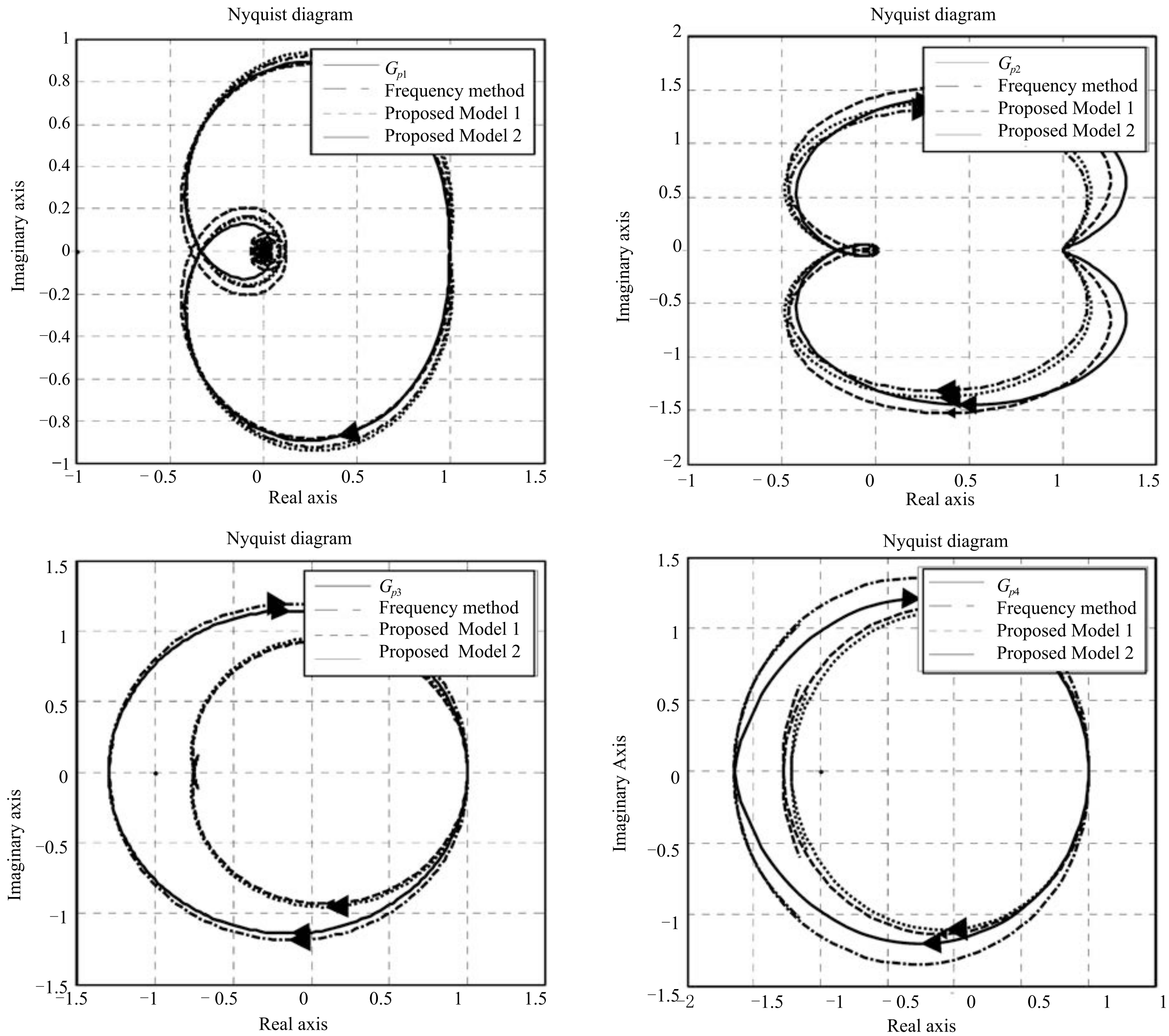

Fig. 5. Frequency responses.

TABLE III
IDENTIFICATION RESULTS FOR FOUR ILLUSTRATIVE EXAMPLES

Process	Proposed (Model 1)	J_{id}	Proposed (Model 2)	J_{id}	Frequency fitting in [18]	J_{id}
1	$\frac{1}{1.2229s^{1.2417}+1}\mathrm{e}^{-0.6786s}$	0.8508	$\frac{1}{1.0905s^{1.16}+1}\mathrm{e}^{-0.783s}$	0.2887	$\frac{1}{1.2427s^{1.2226}+1}\mathrm{e}^{-0.7158s}$	0.7579
2	$\frac{1}{3.5294s^{1.5216}+1}\mathrm{e}^{-0.6265s}$	10.5945	$\frac{1}{4.2556s^{1.58}+1}\mathrm{e}^{-0.37336s}$	5.0937	$\frac{1.0033}{3.5277s^{1.4973}+1}\mathrm{e}^{-0.6699s}$	10.0240
3	$\frac{1}{1.8726s^{1.0694}+1}\mathrm{e}^{-4.2191s}$	46.8204	$\frac{1}{1.6631s^{1.02}+1}\mathrm{e}^{-4.3594s}$	46.5919	$\frac{1.0002}{1.5932s^{1.4409}+1}\mathrm{e}^{-4.2965s}$	80.1147
4	$\frac{1}{3.8241s^{1.3969}+1}\mathrm{e}^{-12.1103s}$	81.148	$\frac{1}{4.4894s^{1.44}+1}\mathrm{e}^{-11.8618s}$	80.6847	$\frac{1}{9.1595s^{1.5844}+1}\mathrm{e}^{-10.385s}$	129.5714

crossover frequencies satisfy $\omega_p \approx A\omega_g$, which motivates us to introduce an additional parameter γ in the formulation

$$\omega_p = \gamma\omega_g, \quad \gamma > 1. \tag{27}$$

This parameter γ plays the same role as ω_p, but it will provide convenience in the analysis of (25) and (26) uniformly under the same frequency variable ω_g.

The constraints on the stability margins are formulated by $A \geq A^*$ and $\pi \geq \phi > \phi^*$, where A^* and ϕ^* are stability lower bounds, and they are determined by the maximum closed-loop amplitude ratio M_T[23],

$$A^* = 1 + \frac{1}{M_T}, \quad \phi^* = 2\sin^{-1}\left(\frac{1}{2M_T}\right). \tag{28}$$

On the other hand, we also require the negative feedback control

$$u(t) = k_p e(t) + k_i \int_0^{\infty} e(t)\mathrm{d}t + k_d \mathrm{d}e(t), \tag{29}$$

with positive controller parameters $k_p > 0$, $k_i \geq 0$ and $k_d \geq 0$.

The transient performance is measured by ITAE index of the step response, that is

$$J_{\mathrm{ITAE}}=\int_0^{\infty} t\,|e(t)|\mathrm{d}t, \tag{30}$$

where $e(t)=r(t)-y(t)$ is the error signal. Combined with all the constraints, the controller design problem is formulated by

$$\min_{k_p,k_i,k_d J_{\mathrm{ITAE}}} = \int_0^{\infty} t\,|e(t)|\mathrm{d}t,$$
$$\text{s.t.}\quad \begin{cases} A\geq A^*,\\ \pi\geq\phi>\phi^*,\\ k_p>0,\\ k_i\geq 0,\\ k_d\geq 0.\end{cases} \tag{31}$$

The problem in (31) can be solved by some classical global searching methods or by intelligent algorithms, such as particle swarm optimization (PSO) or genetic algorithm (GA), without theoretical analysis. In this paper, we try to investigate the constraints (31) and develop an implemented searching algorithm to solve this problem. The constraints in (31) will be analyzed and converted to the implemented form: real parts constraints (RPC) and imaginary parts constraints (IPC), with the help of two characteristic equations (25) and (26).

A. RPC

Let us consider the real parts of (25) and (26), which lead to

$$k_p=\mathrm{Re}\left[-\frac{1}{AG(\mathrm{j}\gamma\omega_g)}\right]=\frac{a}{A(a^2+b^2)}, \tag{32}$$

$$k_p=\mathrm{Re}\left[-\frac{\exp(\mathrm{j}\phi)}{G(\mathrm{j}\omega_g)}\right]=\frac{c\cos\phi+d\sin\phi}{(c^2+d^2)}, \tag{33}$$

where

$$a=\mathrm{Re}(-G(\mathrm{j}\gamma\omega_g)),\quad b=\mathrm{Im}(-G(\mathrm{j}\gamma\omega_g)),$$
$$c=\mathrm{Re}(-G(\mathrm{j}\omega_g)),\quad d=\mathrm{Im}(-G(\mathrm{j}\omega_g)).$$

The relationship of gain margin and phase margin is derived by the following equation

$$A=\frac{a\sqrt{c^2+d^2}}{\sin(\phi+\alpha)(a^2+b^2)}, \tag{34}$$

where

$$\alpha=\begin{cases}\arctan\left(\dfrac{c}{d}\right), & c>0,\ d>0,\\ \pi-\arctan\left(\dfrac{c}{|d|}\right), & c>0,\ d<0,\\ -\pi+\arctan\left(\dfrac{|c|}{|d|}\right), & c<0,\ d<0,\\ -\arctan\left(\dfrac{|c|}{d}\right), & c<0,\ d>0.\end{cases} \tag{35}$$

Therefore, the constraints $k_p>0$, and $A\geq A^*$, are equivalent to the following inequalities

$$RPC:\begin{cases}0<\sin(\phi+\alpha)\leq\dfrac{a\sqrt{c^2+d^2}}{A^*(a^2+b^2)}, & a>0,\\ \phi^*\leq\phi<\pi.\end{cases} \tag{36}$$

B. IPC

The imaginary parts of (25) and (26) are given by

$$k_d\gamma\omega_g-\frac{k_i}{\gamma\omega_g}=\mathrm{Im}\left[-\frac{1}{AG(\mathrm{j}\gamma\omega_g)}\right]=\frac{-b}{A(a^2+b^2)}, \tag{37}$$

$$k_d\omega_g-\frac{k_i}{\omega_g}=\mathrm{Im}\left[-\frac{\exp(\mathrm{j}\phi)}{G(\mathrm{j}\omega_g)}\right]=\frac{c\sin\phi-d\cos\phi}{(c^2+d^2)}, \tag{38}$$

which are solved to get

$$\begin{cases}k_i=-\dfrac{b\gamma\omega_g\sin(\phi+\alpha)-a\omega_g\gamma^2\cos(\phi+\alpha)}{a\sqrt{c^2+d^2}\,(\gamma^2-1)},\\ k_d=-\dfrac{b\gamma\sin(\phi+\alpha)-a\cos(\phi+\alpha)}{a\omega_g\sqrt{c^2+d^2}\,(\gamma^2-1)}.\end{cases} \tag{39}$$

Then, the constraints $k_d\geq 0$ and $k_i\geq 0$ are converted to

$$IPC:\max\left(\frac{b\gamma}{a},\frac{b}{a\gamma}\right)\leq\frac{1}{\tan(\phi+\alpha)}. \tag{40}$$

C. Implementing Optimal Tuning

Based on the analysis above, an explicit PID controller tuning rule and the achieved gain margin are given by

$$\begin{cases}k_p=\dfrac{a}{A(a^2+b^2)}=\dfrac{1}{\sqrt{c^2+d^2}}\sin(\phi+\alpha),\\ k_i=-\dfrac{b\gamma\omega_g\sin(\phi+\alpha)-a\omega_g\gamma^2\cos(\phi+\alpha)}{a\sqrt{c^2+d^2}\,(\gamma^2-1)},\\ k_d=-\dfrac{b\gamma\sin(\phi+\alpha)-a\cos(\phi+\alpha)}{a\omega_g\sqrt{c^2+d^2}\,(\gamma^2-1)},\\ A=\dfrac{a\sqrt{c^2+d^2}}{\sin(\phi+\alpha)(a^2+b^2)}.\end{cases} \tag{41}$$

Theoretically, a suitable value of (ϕ,ω_g,γ) determines a robust stabilizing PID controller and the achieved gain margin in (41). For example, for some typical performance specifications on gain margin A_o, phase margin ϕ_o and the closed-loop bandwidth ω_B, we can set $(\phi,\omega_g,\gamma)\approx(\phi_o,\omega_B,A_o)$ as a recommended value for a robust PID controller in (41) or as an initial value for the optimal searching.

Remark 5. In [21−24], (ϕ,ω_g,A), (ϕ,ω_p,A) or $(\phi,\omega_g,\omega_p, A)$ are used to calculate PID controller parameters, involving some complex computation to solve (25) and (26), the two coupled nonlinear equations. In this paper, with basic variables (ϕ,ω_g,γ), the gain margin and three controller parameters are all decoupled from each other in (41). An explicit PID controller will be more applicable in the practical engineering, which is one of the advantages of the proposed tuning method.

Since (36) and (40) are formulated as trigonometric inequalities on ϕ, RPC and IPC are solved to be

$$\underline{\phi}(\omega_g,\gamma)<\phi<\overline{\phi}(\omega_g,\gamma), \tag{42}$$

where $\overline{\phi}(\omega_g, \gamma)$ and $\underline{\phi}(\omega_g, \gamma)$ stand for the upper bound and lower bound, respectively. Obviously, these two bounds are dependent on an admissible (ω_g, γ). In this way, (42) gives an exact parameter's range, and will help us to find an admissible region of (ϕ, ω_g, γ), which provides great convenience for the optimal searching.

With the equivalent constraint in (42), the optimal controller design problem in (39) can be rewritten in the implemented form

$$\begin{aligned} &\min J_{\text{ITAE}} = \int_0^\infty t\,|e(t)|\mathrm{d}t, \\ &\text{s.t.} \quad \underline{\phi}(\omega_g, \gamma) < \phi < \overline{\phi}(\omega_g, \gamma). \end{aligned} \tag{43}$$

This problem can be solved by MATLAB function "fminbnd" in three dimensions. Set the initial value of (ω_g, γ), and carry on the single-variable searching on ϕ within $[\underline{\phi}(\omega_g, \gamma), \overline{\phi}(\omega_g, \gamma)]$. The value of (ω_g, γ) will be updated by "fminbnd" for the iterations. When finishing the optimal searching in three dimensions, the optimal robust PID controller is decided by (41) accordingly as well as the achieved gain margin, phase margins and two crossover frequencies.

The proposed tuning scheme is summarized by the following algorithm.

Algorithm 3. Optimal PID tuning

Step 1. Give the specification of M_T and calculate the lower bounds of stability margins A^* and ϕ^*.

Step 2. Set the initial value of (ω_g, γ).

Step 3. Solve RPC and IPC by trigonometric calculations to obtain $[\underline{\phi}(\omega_g, \gamma), \overline{\phi}(\omega_g, \gamma)]$.

Step 4. Carry on single-variable searching on ϕ within $[\underline{\phi}(\omega_g, \gamma), \overline{\phi}(\omega_g, \gamma)]$ by "fminbnd".

Step 5. If convergent, go to Step 6; otherwise, update the value of (ω_g, γ) by "fminbnd", and go to Step 3.

Step 6. Substitute the resultant value of (ϕ, ω_g, γ) into (41) for the optimal PID controller.

D. Continuing Simulation Study

Regarding the optimal identified Model 2 in Table III, PID controllers are designed by the proposed method for different values of M_T. Tuning results are exhibited in Table IV, which show that, the maximum closed-loop amplitude ratio M_T is proportional to the overshoot in most cases. With a suitable value of M_T specified, the overshoot will be avoided or limited in the step response.

To illustrate the tuning algorithm, PID controller tuning for the Model 2 of the Process 1 is considered. In Step 1, set $M_T = 1$, and calculate the lower bounds of the stability margins, $A^* = 2$ and $\phi^* = \pi/3$. Given the initial value of $(\omega_g, \gamma) = (0.8, 3)$ in Step 2, RPC and IPC are obtained in Step 3:

$$\begin{cases} 0 < \sin(\phi + 0.1436) \leq 1.2568, \\ \dfrac{\pi}{3} \leq \phi < \pi, \\ -0.0754 \leq \dfrac{1}{\tan(\phi + 0.1436)}, \end{cases} \tag{44}$$

$$1.0472 < \phi \leq 1.4272. \tag{45}$$

TABLE IV
PROPOSED PID PARAMETERS FOR THE IDENTIFIED MODEL 2

Process	M_T	k_p	k_i	k_d	Overshoot (%)
	1	1.2893	0.7587	0.5747	3.3
1	1.2	1.2624	0.7361	0.5885	2.6
	1.4	1.2551	0.7653	0.6021	4.2
	1	4.7749	0.9562	4.6739	11.1
2	1.2	6.2443	1.2211	4.3948	14.9
	1.4	6.8523	1.505	4.0934	21.1
	1	0.266	0.1071	0.3569	0.2
3	1.2	0.5505	0.1579	0.6441	3.2
	1.4	0.5510	0.1582	0.6550	3.2
	1	0.3010	0.0583	0.9809	4.49
4	1.2	0.3074	0.0580	0.9874	6.87
	1.4	0.3157	0.0581	0.9985	7.4

In Step 4, single-variable searching is carried on in the phase range (45) to obtain the minimized index $J_{\text{ITAE}} = 2.6694$. Update the value of (ω_g, γ) for the further searching. Finally, three variables (ϕ, ω_g, γ) are found convergent to $(1.2786, 0.2965, 3.2687)$, and the optimal PID controller is determined by (41),

$$C(s) = 1.2893 + \frac{0.7587}{s} + 0.5747s. \tag{46}$$

Simultaneously, the achieved control performances are obtained

$$A = 2.05\,(\omega_g = 0.3),\ \phi = 1.27\,(\omega_p = 0.96),\ J_{\text{ITAE}} = 1.74. \tag{47}$$

A comparison is made with the design method in [18], which is also using ITAE tuning rule but with no limitation on the stability margin. In [18], the controller parameters are given in Table V, which are obtained based on the frequency fitting model in Table III. In the comparison, we set the controller parameters in Table IV with $M_T = 1$.

TABLE V
CONTROLLER PARAMETERS IN [18]

Process	k_p	k_i	k_d
1	1.3447	1.0022	0.6215
2	2.3722	1.1933	4.7102
3	0.3477	0.1731	0.5272
4	0.2624	0.0645	1.3623

Step response and load disturbance rejection are considered in Fig. 6. Table VI presents ITAE value, overshoot, and the achieved gain and phase margins of the resultant systems. From the tuning results, one can find that the proposed method achieves lower ITAE value and smaller overshoot than results of [18]. Two reasons can support this result: 1) accurate identified models allow better tuning performance for model-based tuning rules. 2) with the limitation on the maximum closed-loop amplitude ratio M_T, ITAE tuning rule would be more applicable in the practical application.

TABLE VI
TUNING RESULTS AND COMPARISON

Process	Proposed PID parameters (Proposed Model 2)				PID parameters[18] (Frequency fitting model)			
	ITAE	Overshoot (%)	Gain margin	Phase margin	ITAE	Overshoot (%)	Gain margin	Phase margin
1	199.11	5	2.907	70.5	199.6429	17	2.7797	61.2
2	236.72	11.9	1.5399	32.3	302.9330	30	1.7298	53.1
3	1.2462E+03	1.8	2.8741	62.4	1.2614E+03	31	2.2029	42
4	1.1269E+04	20.8	2.0114	56.3	1.1303E+04	24.5	1.7681	50.4

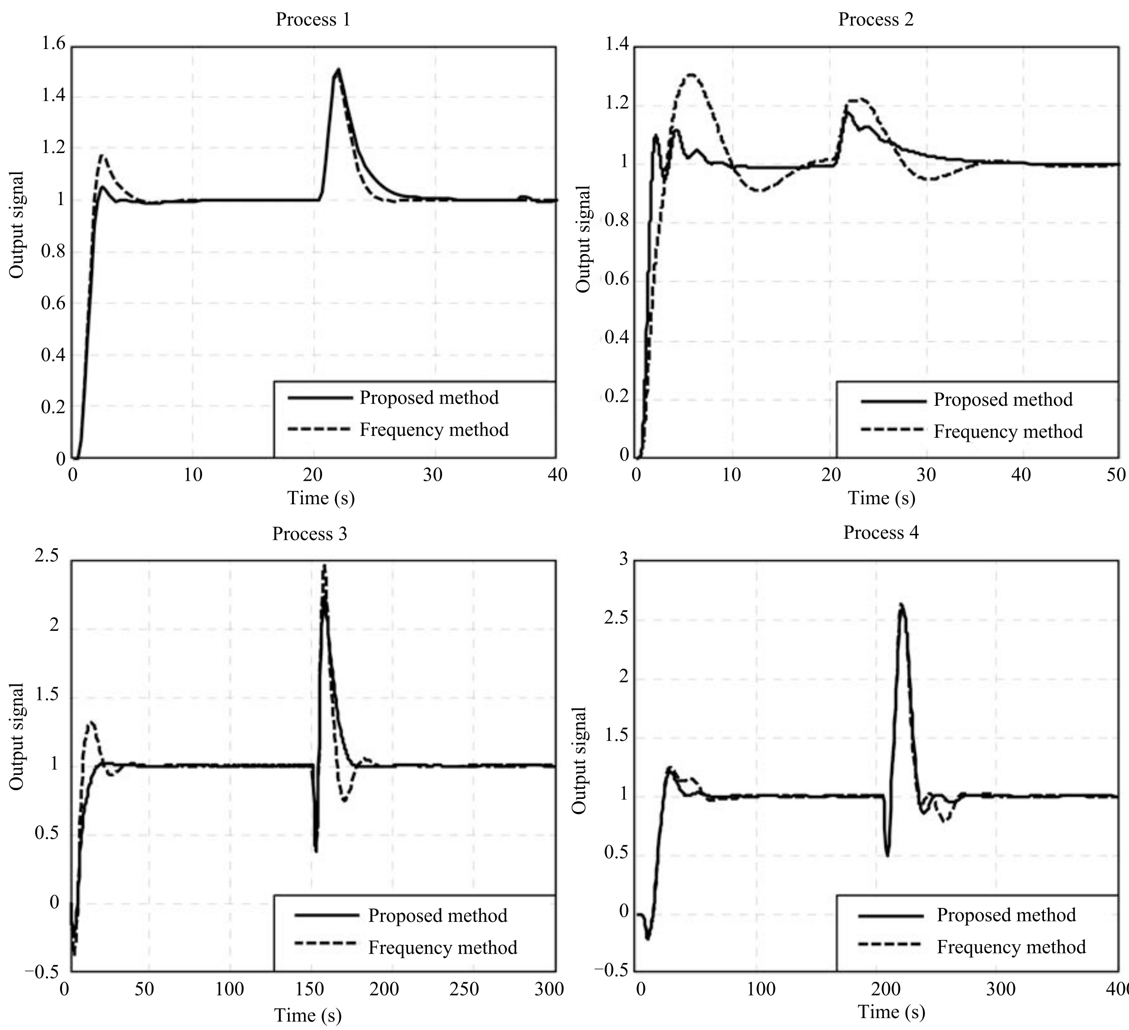

Fig. 6. Closed-loop responses of the PID control systems.

IV. Application to Titanium Billet Heating Furnace

Fractional-order dynamics appears naturally in the heating process when heat conduction occurs between the operating variable (input signal) and the measured physical variable (output signal). An example of heating furnace was considered in [25], which shows that the fractional-order model gives more exact description of the heating process than integer-order model.

Let us consider the temperature control problem of the titanium billet furnace[26]. The titanium billet furnace is divided into three heating areas and the temperature is controlled separately for each area (see Fig. 7). Two kinds of burners, including twelve 200 kW burners and six 350 kW burners, are used in parallel for different heating schedules. The mixed natural gas and air are burned through the 18 burners distributed on both sides of the furnace symmetrically.

The temperature control system is depicted in Fig. 8. Each burner is controlled by a pulse-controller PSF778L independently. The pulse-controller for each burner provides a precise control for the ratio of air and gas, and greatly improves the heating efficiency. All the burners work under the heating task assignment of burners' auto-setting controller PFA700 according to the total control actions generated by the controller SE-504, which is implemented in the form of PID. Note that, PFA700 also controls the process as an inner feedback control loop to guarantee the basic dynamic performance of the heating process. The temperature feedback signals are measured by 6 thermocouples distributed in three areas.

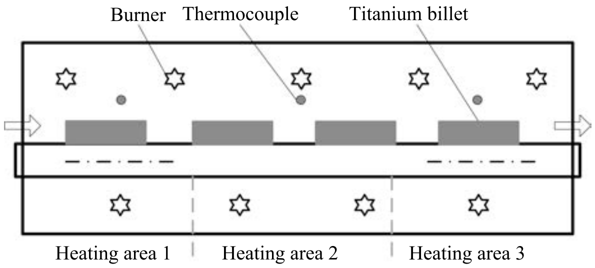

Fig. 7. Titanium billet heating furnace.

Now, consider the model identification for the heating process. We obtain the measured data from a real Titanium billet heating furnace in the first heating stage, with the target temperature 850 °C, which can be viewed as the step response of the heating process. All the measured data are plotted in Fig. 9. It is obvious that, the measured noise is inevitably involved in the sampled data. Especially, the temperature jumping occurs during the whole response, which is caused by the pulse flame of the burners near the thermocouples. To attenuate such temperature jumping and noise, median filtering method is employed to deal with the measured temperature value. Fig. 10 shows the median filtering results. The identification procedure for the Heating area 1 is presented to give the illustration. In the inner control loop, the heating process achieves the setting temperature slowly, that is $y(\infty) \approx 850\,°\mathrm{C}$. The process gain is approximately to be $K \approx 1$.

The process is firstly identified by three points method. Collect $t_1 = 20\,\mathrm{min}$, $t_2 = 81\,\mathrm{min}$ and $t_3 = 374\,\mathrm{min}$ by Step 2 in Algorithm 1. The process is identified by (21),

$$\frac{1}{55.078s^{0.909}+1}\mathrm{e}^{-4.91s}. \tag{48}$$

Then, optimal identification is carried on by Algorithm 2. The cost function (26) is depicted in Fig. 11, and the optimal fractional-order is found by single-variable searching. The process is identified to be

$$\frac{1}{67.1867s^{0.94}+1}\mathrm{e}^{-5.21s}. \tag{49}$$

It is obvious that the step responses of the two resultant models, given in Fig. 12, are very close to the response of the real heating process. In the frequency domain, one can estimate frequency response with fixed frequency resolution using spectral analysis in Fig. 13. It can be seen that the

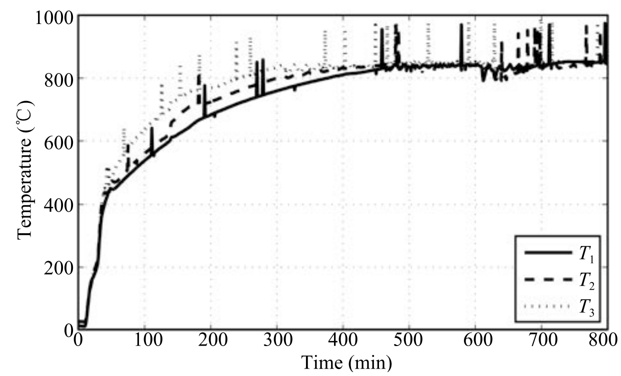

Fig. 9. Step response of three heating areas.

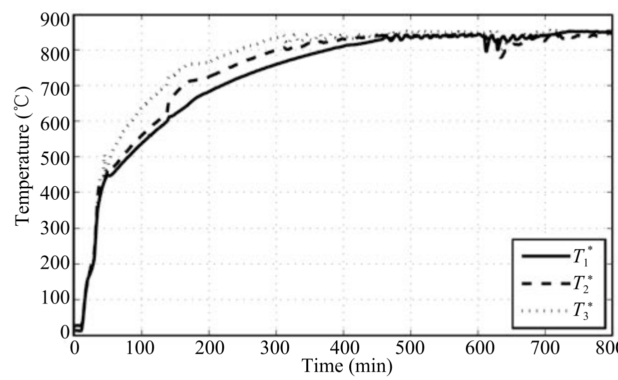

Fig. 10. Step response with median filtering.

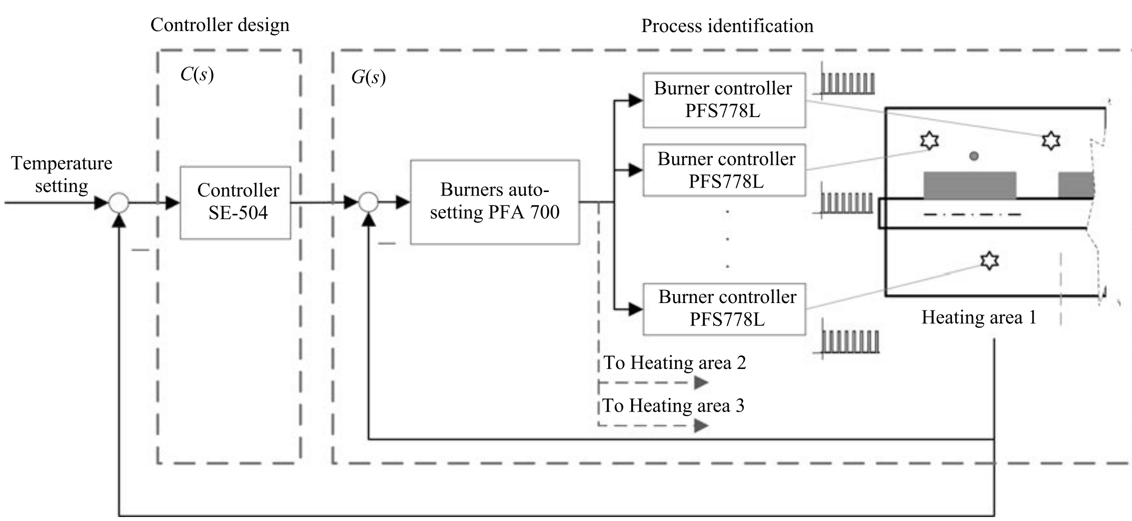

Fig. 8. Temperature control system of Titanium billet heating furnace.

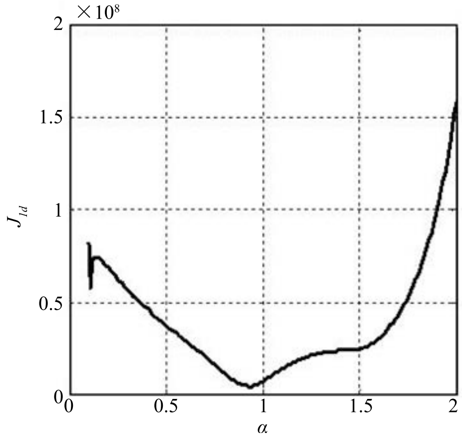

Fig. 11. Cost function for optimal identification.

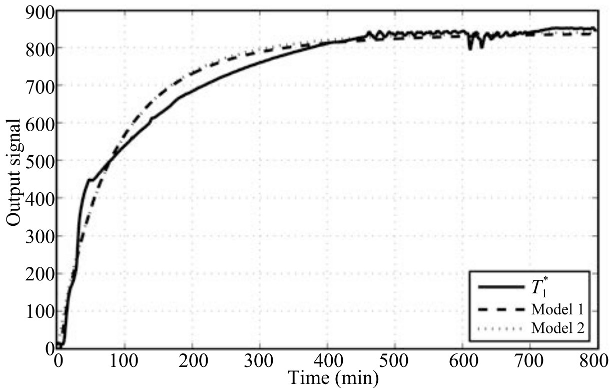

Fig. 12. Identification results for Heating area 1.

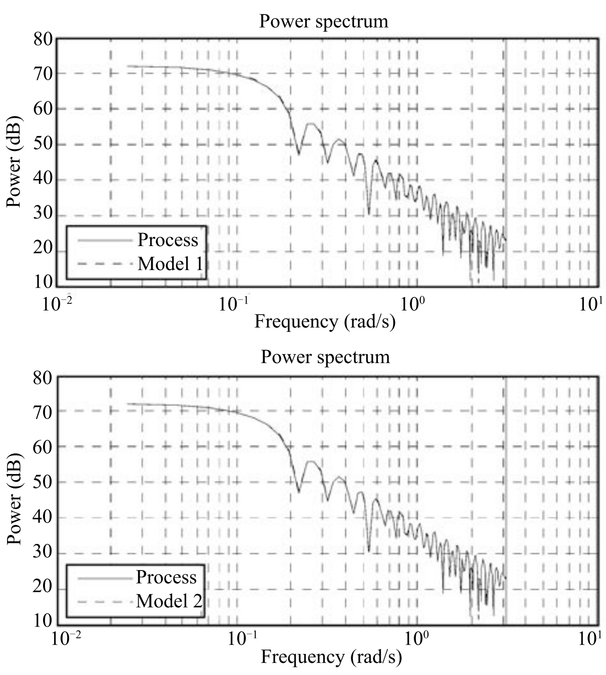

Fig. 13. Frequency spectral analysis.

frequency responses of the resultant models are nearly the same as the frequency response of the real process at low frequencies, which meets the requirement for the process with large inertia time constant. The identification results for the other two heating areas are given in Table VII and the responses are shown in Figs. 14 and 15.

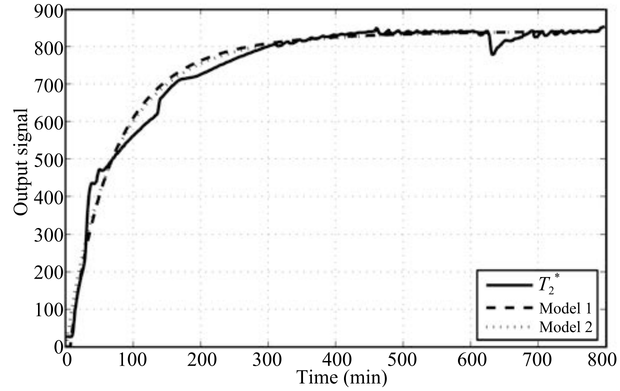

Fig. 14. Identification results for Heating area 2.

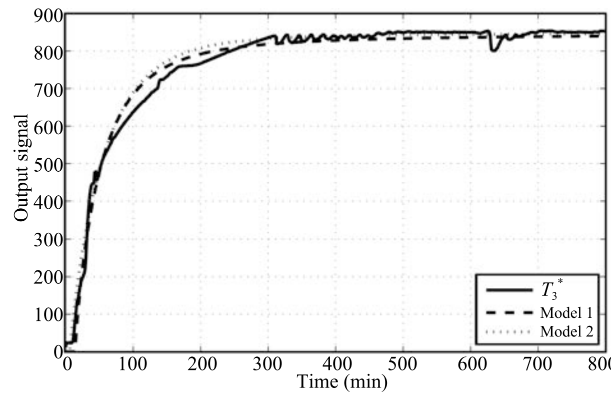

Fig. 15. Identification results for Heating area 3.

Then, we consider the temperature control for each heating area. In this case, we only provide the simulation results to show the control performance. In the simulation, three heating areas are controlled independently, and each controller is designed based on the process Model 2 in Table VII. To avoid overshoot, set $M_T = 1$, and the controller parameters are given in Table VIII. ITAE indexes are obtained in the step input response, and the achieved gain and phase margins of the resultant systems are also exhibited.

A typical heating routine requires the furnace temperature to reach $900\,^\circ$C in three hours. Rather than the typical step input, ramp signal would be more practical in the heating process. According to the heating mechanism, we formulate the reference heating curve by four stages:

$$r_2(t) = \begin{cases} 10t, \\ 600, \\ 3.75(t-90)+600, \\ 900. \end{cases} \tag{50}$$

The responses, tracking errors and control inputs of three heating areas are shown in Figs. 16-18. In the first heating stage, the control inputs are increasing greatly because of the ramp input with a big slope. As we know, the steady output error is inevitable for the ramp input under PID control. The temperature tracking errors are almost kept about $100\,^\circ$C in three areas. After an hour, the input signals maintain $600\,^\circ$C in the second stage for the thermal insulation, and the control inputs decrease when the tracking errors become small. In the

TABLE VII
IDENTIFICATION RESULTS FOR THREE HEATING AREAS AND COMPARISONS

Process	Fractional-order model			
	Proposed (Model 1)	$J_{id} \times 10^6$	Proposed (Model 2)	$J_{id} \times 10^6$
Heating area 1	$\frac{1}{55.078s^{0.909}+1}\mathrm{e}^{-4.91s}$	4.8788	$\frac{1}{67.1867s^{0.94}+1}\mathrm{e}^{-5.21s}$	4.4843
Heating area 2	$\frac{1}{50.006s^{0.922}+1}\mathrm{e}^{-6.91s}$	3.3877	$\frac{1}{56.7735s^{0.93}+1}\mathrm{e}^{-5.92s}$	3.1368
Heating area 3	$\frac{1}{27.593s^{0.879}+1}\mathrm{e}^{-13.49s}$	4.2200	$\frac{1}{42.817s^{0.95}+1}\mathrm{e}^{-5.9596s}$	3.1494

TABLE VIII
PID CONTROLLERS FOR EACH HEATING AREA

Process model	k_p	k_i	k_d	ITAE	Gain margin	Phase margin
$\frac{1}{67.1867s^{0.94}+1}\mathrm{e}^{-5.21s}$	8.2019	0.1153	0.8750	77.2937	2.871	63.8848
$\frac{1}{56.7735s^{0.93}+1}\mathrm{e}^{-5.92s}$	7.1244	0.1090	3.9377	87.3280	2.7074	63.6843
$\frac{1}{42.817s^{0.95}+1}\mathrm{e}^{-5.9596s}$	5.2301	0.1006	5.8289	81.9108	2.8153	65.6896

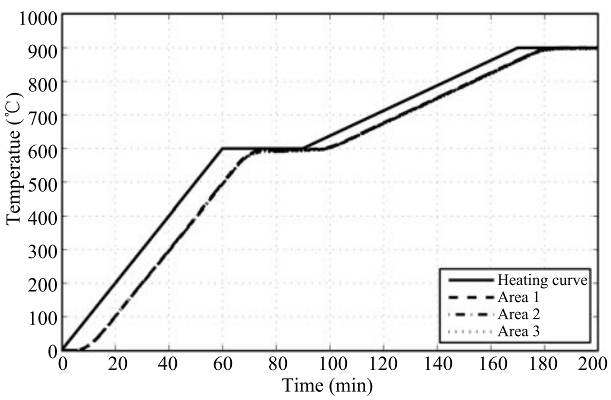

Fig. 16. Responses of three heating areas under PID control.

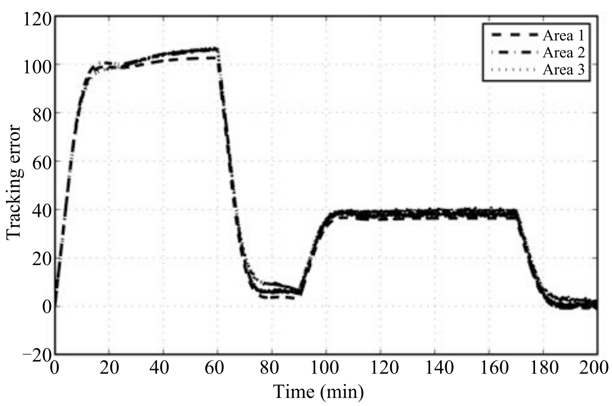

Fig. 17. Tracking Errors.

third heating stage, the control inputs increase continues with the ramp reference inputs, and the tracking errors are about 40 °C. Finally, reference inputs are kept 900 °C for half an hour in the last stage and the control inputs decrease and tend to a constant. After the temperature field distributed uniformly, all the temperature in three areas achieve 900 °C. One can see that, the proposed three PID controllers provide good control performance for the heating furnace without any overshoot and oscillation, in the whole heating process.

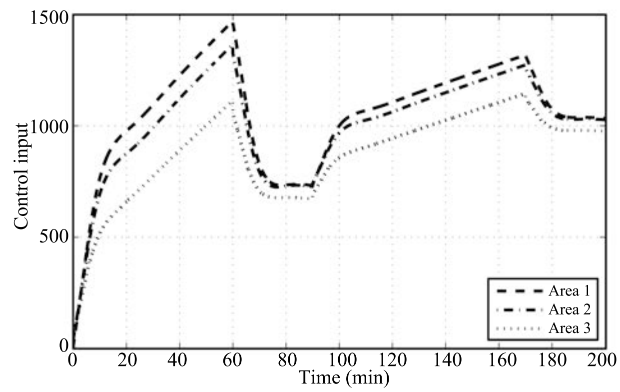

Fig. 18. Control inputs.

V. CONCLUSION

This paper has presented a new model identification method for a class of delay fractional-order system based on the process step response. In this method, the features of the normalized fractional-order model were analyzed and formulated by four defined characteristic functions based on the step responses. Two identification schemes were proposed based on time scaling analysis. Scheme one utilized three exact points on the step response of the process to calculate model parameters directly, and the other scheme employed optimal searching method to adjust the fractional order for the best model parameters. Simulation results show that the proposed two identification schemes were both applicable to any stable complex process, such as higher-order, under-damped/over-damped, and minimum-phase/nonminimum-phase processes.

To design a PID controller, an optimal tuning method was proposed for the delay fractional-order model. The requirements on the stability margins and negative feedback were formulated by RPC and IPC, which were implemented by trigonometric inequalities on the phase variable. With the basic variables (ϕ, ω_g, γ), an explicit PID was derived without any tedious computation, as well as the achieving of gain margins. Under the constraints of PRC and IPC, an optimal controller was obtained by the minimization of ITAE index.

Finally, the proposed method is applied to the Titanium billet heating process. Step responses of the real process were obtained and used to identify fractional-order models for three heating areas. Regarding the identified model, optimal PID controller was designed for each heating area. The application results illustrated the effectiveness of the proposed method.

REFERENCES

[1] Zhao C N, Xue D Y, Chen Y Q. A fractional order PID tuning algorithm for a class of fractional order plants. In: Proceedings of the 2005 IEEE International Conference Mechatronics and Automation. Canada: IEEE, 2005. 216−221

[2] Manabe S. A suggestion of fractional-order controller for flexible spacecraft attitude control. *Nonlinear Dynamics*, 2002, **29**(1−4): 251−268

[3] Torvik P J, Bagley R L. On the appearance of the fractional derivative in the behavior of real materials. *Journal of Applied Mechanics*, 1984, **51**(2): 294−298

[4] Nakagawa M, Sorimachi K. Basic characteristics of a fractance device. *IEICE Transactions on Fundamentals of Electronics, Communications and Computer Sciences*, 1992, **E75-A**(12): 1814−1819

[5] Özbay H, Bonnet C, Fioravanti A R. PID controller design for fractional-order systems with time delays. *Systems and Control Letters*, 2012, **61**(1): 18−23

[6] Caponetto R, Dongola G, Pappalardo F L, Tomasello V. Autotuning method for PIλDμ controllers design. *International Journal of Innovative Computing, Information and Control*, 2013, **9**(10): 4043−4055

[7] Caponetto R, Dongola G, Pappalardo F, Tomasello V. Auto-tuning and fractional order controller implementation on hardware in the loop system. *Journal of Optimization Theory and Applications*, 2013, **156**(1): 141−152

[8] Monje C A, Vinagre B M, Feliu V, Chen Y Q. Tuning and auto-tuning of fractional order controllers for industry applications. *Control Engineering Practice*, 2008, **16**(7): 798−812

[9] Monje C A, Chen Y Q, Vinagre B M, Xue D Y, Feliu-Batlle V. *Fractional-Order Systems and Controls: Fundamentals and Applications*. London: Springer-Verlag, 2010.

[10] Tavazoei M S. Time response analysis of fractional-order control systems: a survey on recent results. *Fractional Calculus and Applied Analysis*, 2014, **17**(2): 440−461

[11] Luo Y, Zhang T, Lee B, Kang C, Chen Y Q. Fractional-order proportional derivative controller synthesis and implementation for hard-disk-drive servo system. *IEEE Transactions on Control Systems Technology*, 2014, **22**(1): 281−289

[12] Oustaloup A, Sabatier J, Lanusse P, Malti R, Melchior P, Moreau X, Moze M. An overview of the crone approach in system analysis, modeling and identification, observation and control. In: Proceedings of the 17th IFAC World Congress. COEX, Korea, South: IFAC, 2008. 14254−14265

[13] Mathieu B, Le Lay L, Oustaloup A. Identification of non integer order systems in the time-domain. In: CESA'96 IMACS Multiconference: Computational Engineering in Systems Applications. 1996. 843−847

[14] Trigeassou J C, Poinot T, Lin J, Oustaloup A, Levron F. Modeling and identification of a non integer order system. In: Proceedings of the 1999 European Control Conference (ECC). Karlsruhe: IEEE, 1999. 2453−2458

[15] Poinot T, Trigeassou J C. Identification of fractional systems using an output-error technique. *Nonlinear Dynamics*, 2004, **38**(1−4): 133−154

[16] Guevara E, Meneses H, Arrieta O, Vilanova R, Visioli A, Padula F. Fractional order model identification: computational optimization. In: Proceedings of the 20th IEEE Conference on Emerging Technologies and Factory Automation (ETFA). Luxembourg: IEEE, 2015. 1−4

[17] Hartley T T, Lorenzo C F. Fractional-order system identification based on continuous order-distributions. *Signal Processing*, 2003, **83**(11): 2287−2300

[18] Jin C Y, Ryu K H, Sung S W, Lee J, Lee I B. PID auto-tuning using new model reduction method and explicit PID tuning rule for a fractional order plus time delay model. *Journal of Process Control*, 2014, **24**(1): 113−128

[19] Narang A, Shah S L, Chen T. Continuous-time model identification of fractional-order models with time delays. *IET Control Theory and Applications*, 2011, **5**(7): 900−912

[20] Luo Y, Chen Y Q, Wang C Y, Pi Y G. Tuning fractional order proportional integral controllers for fractional order systems. *Journal of Process Control*, 2010, **20**(7): 823−831

[21] Wang Y G, Shao H H. PID autotuner based on gain- and phase-margin specifications. *Industrial and Engineering Chemistry Research*, 1999, **38**(8): 3007−3012

[22] Ho W K, Lee T H, Gan O P. Tuning of multiloop proportional-integral-derivative controllers based on gain and phase margin specifications. *Industrial and Engineering Chemistry Research*, 1997, **36**(6): 2231−2238

[23] Li K Y. PID tuning for optimal closed-loop performance with specified gain and phase margins. *IEEE Transactions on Control Systems Technology*, 2013, **21**(3): 1024−1030

[24] Fung H W, Wang Q G, Lee T H. PI tuning in terms of gain and phase margins. *Automatica*, 1998, **34**(9): 1145−1149

[25] Li M D, Li D H, Wang J, Zhao C Z. Active disturbance rejection control for fractional-order system. *ISA Transactions*, 2013, **52**(3): 365−374

[26] Lv Y, Wu M, Lei Q, Nie Z Y. Soft sensor based on a Pso-Bp neural network for a titanium billet furnace-temperature. *Intelligent Automation and Soft Computing*, 2011, **17**(8): 1207−1216

Zhuoyun Nie received the Ph. D. degree in control theory and control engineering from Central South University, China in 2012. He was a visiting scholar at the National University of Singapore. He is currently a lecturer at the School of Information Engineering, Huaqiao University, China. His research interests include robust control, process identification, internet of things, and financial forecasting. Corresponding author of this paper.

Qingguo Wang received the B. Eng. degree in chemical engineering in 1982, M. Eng. degree in 1984 and Ph. D. degree in 1987 both in industrial automation, all from Zhejiang University, China, respectively. He held Alexander-von-Humboldt Research Fellowship of Germany from 1990 to 1992. From 1992 to 2015, he was with the Department of Electrical and Computer Engineering of the National University of Singapore, where he became a full professor in 2004. He has published over 250 international journal papers and 6 books. He received nearly 1 1000 citations with h-index of 58. He is currently a distinguished professor with the Institute for Intelligent Systems, University of Johannesburg, South Africa. His present research interests include modeling, estimation, prediction, control, optimization and automation for complex systems, including but not limited to, industrial and environmental processes, new energy devices, defense systems, medical engineering, and financial markets.

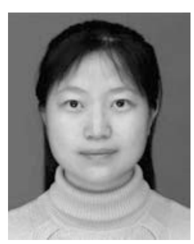

Ruijuan Liu received the Ph. D. degree in control theory and control engineering from Central South University, China in 2014. She was a visiting scholar at the University of South Wales. She is currently a lecturer at the School of Applied Mathematics, Xiamen University of Technology, China. Her research interests include robust control, nonlinear control, and disturbance rejection.

Yonghong Lan received the B. S. and M. S. degrees in applied mathematics from Xiangtan University, Xiangtan, China in 1999 and 2004, respectively; and the Ph. D. degree in control theory and control engineering from Central South University, Changsha, China in 2010. He is currently an assistant professor at the School of Information Engineering, Xiangtan University, Xiangtan, China. His current research interests include fractional order control systems.

Robust Output Feedback Control for Fractional Order Nonlinear Systems with Time-varying Delays

Changchun Hua, Tong Zhang, Yafeng Li, and Xinping Guan

***Abstract*—Robust controller design problem is investigated for a class of fractional order nonlinear systems with time varying delays. Firstly, a reduced-order observer is designed. Then, an output feedback controller is designed. Both the designed observer and controller are independent of time delays. By choosing appropriate Lyapunov functions, we prove the designed controller can render the fractional order system asymptotically stable. A simulation example is given to verify the effectiveness of the proposed approach.**

***Index Terms*—Fractional order systems, time-varying delays, Laypunov function, backstepping.**

I. Introduction

Fractional calculus is an ancient concept, which can be dated back to the end of 17th century, the time when the classical integer order calculus was established. It is a generalization of the ordinary differentiation and integration to arbitrary order[1]. Although it has a long history, it has not attracted much attention until recently in the control field. It is found that many systems with memory feature or complex material can be more concisely and actually described by fractional order derivatives, such as the diffusion process, the heat transfer process and the effect of the frequency in induction machines. It also has been proved that fractional order controllers, like fractional order PID controllers and fractional order model reference adaptive controllers, can capture much better effect and robustness[2]. For some basic theory of fractional order calculus and fractional order systems, one can refer to [1−6] and the references therein.

Stability analysis is one of the most fundamental and essential issues for the control system. In [7], Matignon firstly studied the stability of fractional-order linear differential systems with the Caputo definition. Since then, many further achievements have been obtained[8−11]. In [8−9], the authors presented the sufficient and necessary conditions for the asymptotical stability of fractional order interval systems with fractional order α satisfying $0 < \alpha < 1$ and $1 < \alpha < 2$, respectively. Reference [10] designed both state and output feedback controllers for fractional order linear systems in triangular form by introducing appropriate transformations of coordinates. Based on Gronwall-Bellman lemma and sector bounded condition, the stability and stabilization of fractional order linear systems subject to input saturation were studied in [11]. For the nonlinear fractional order systems, the stability analysis is much more difficult than that of the linear systems. We can find some sufficient conditions in [12−14]. In [15], the authors introduced Mittag-Leffler stability by using Lyapunov direct method.

Time delay is an inherent phenomenon in the interconnected systems or processes, which makes the stability analysis and controller design challenging. Robust output control problem for a class of nonlinear time-delay systems was studied in [16]. The necessary and sufficient stability conditions for linear fractional-order differential equations and linear time-delayed fractional differential equations have already been obtained in [17−19]. Reference [20] investigated the stability of α-dimensional linear fractional-order differential systems with order $1 < \alpha < 2$. References [21−22] contain the stability analysis of fractional order nonlinear time delay system based on Lyapunov direct method and by using properties of Mittag-Leffler function and Laplace transform.

In recent years, the backstepping technique has attracted much attention as a powerful method for controlling the strict feedback nonlinear systems. There are a few works using backstepping technique to handle fractional order systems. Using Lyapunov indirect method, the authors of [23] presented a new method to design an adaptive backstepping controller for triangular fractional order nonlinear systems. In [24], a new adaptive fractional-order backstepping method is proposed for a class of commensurate fractional order nonlinear systems with uncertain constant parameters. However, for fractional order nonlinear systems with time-varying delays, there is none related work. Motivated by the mentioned situation, we devote to solve the stabilization problem of fractional order nonlinear systems with time-varying delays.

The contributions of this paper are as follows: 1) A reduced-order observer is designed to estimate the state of the system; 2) Based on the backstepping method, we design a robust output feedback controller for a class of fractional order nonlinear time-varying delay systems; 3) With a novel class of fractional Lyapunov functions, we prove the stability of fractional order nonlinear systems.

The remainder of this paper is organized as follows: Section II presents some basic concepts about fractional order calculus and the stability of fractional order nonlinear systems. In Sec-

Manuscript received September 8, 2015, accepted March 3, 2016. This work was partially supported by National Natural Science Foundation of China (61290322, 61273222, 61322303, 61473248, 61403335), Hebei Province Applied Basis Research Project (15967629D), and Top Talents Project of Hebei Province and Yanshan University Project (13LGA020).

Citation: Changchun Hua, Tong Zhang, Yafeng Li, Xinping Guan. Robust output feedback control for fractional order nonlinear systems with time-varying delays. *IEEE/CAA Journal of Automatica Sinica*, 2016, **3**(4): 477−482

Changchun Hua, Tong Zhang, and Yafeng Li are with the Institute of Electrical Engineering, Yanshan University, Qinhuangdao 066004, China (e-mail: cch@ysu.edu.cn; 13230929204@163.com; y.f.li@foxmail.com).

Xinping Guan is with the Department of Automation, Shanghai Jiao Tong University, Shanghai 200030, China (e-mail: xpguan@ysu.edu.cn).

tion III, as the main part of this note, an adaptive controller is designed by using the backstepping method for fractional order nonlinear time-varying delayed systems. An example is presented to show the effectiveness of the proposed controller in Section IV. Finally, Section V gives the conclusion of this paper.

Notations . Throughout this paper, $\mathbf{R}$ denotes the set of real numbers, $\mathbf{R}^n$ for n-dimensional Euclidean vector space and $\mathbf{R}^{n\times n}$ for the space of $n\times n$ real matrices. X^{T} and X^{-1} represent the transpose and the inverse of matrix X, respectively. I denotes the unit matrix with proper dimensions. For any matrix $A\in\mathbf{R}^{n\times n}$, $\lambda_i(A)$ stands for the i-th eigenvalue of A. For simplicity, ${}_0^C D_t^\alpha$ is mentioned as D^α.

II. Preliminaries

In this section, we provide some basic knowledge of fractional calculus and fractional order systems (details can be found in [1−2]). There are several definitions of fractional order derivatives, among which the Riemann-Liouville and Caputo definitions are well known and most commonly used. In this paper, we choose the Caputo definition for the fractional order derivatives. The Caputo derivative and fractional integral are defined as follows.

Definition 1 (Caputo fractional derivative). The Caputo fractional derivative of order $\alpha\geq 0$ for a function $f:[0,\infty]\to\mathbf{R}$ is defined as

$$ {}_0D_t^\alpha f(t)=\frac{1}{\Gamma(n-\alpha)}\int_0^t\frac{f^{(n)}(s)}{(t-s)^{\alpha+1-n}}\mathrm{d}s,\quad t>0, \tag{1}$$

where n is the first integer that is larger than α and $\Gamma(\cdot)$ is the well known Gamma function which is defined as follows:

$$\Gamma(t)=\int_0^\infty x^{t-1}\mathrm{e}^{-x}\mathrm{d}x.$$

Definition 2 (Fractional integral). The fractional integral of order $\alpha\geq 0$ for a function $f:[0,\infty]\to\mathbf{R}$ is defined as

$$ {}_0I_t^\alpha f(t)=\frac{1}{\Gamma(\alpha)}\int_0^t\frac{f(s)}{(t-s)^{1-\alpha}}\mathrm{d}s,\quad t>0. \tag{2}$$

Definition 3 (Class-K function). A continuous function $\gamma:[0,t)\to[0,\infty)$ is said to belong to class-K function if it is strictly increasing and $\gamma(0)=0$.

Here are some lemmas we could use in this paper.

Lemma 1 (General Leibnitz's rule). If f and g are differentiable and continuous functions, the product $f\cdot g$ is also differentiable and its α-th ($\alpha\geq 0$) derivative is given by

$$D^\alpha(f\cdot g)=(D^\alpha f)\cdot g+\sum_{k=1}^\infty\frac{\Gamma(\alpha+1)D^{\alpha-k}f\cdot D^k g}{\Gamma(k+1)\Gamma(\alpha-k+1)}. \tag{3}$$

According to Lemma 1, the α-th order time derivative of $V(x)=2x^{\mathrm{T}}x$ can be extended as $D^\alpha V(x)=(D^\alpha x)^{\mathrm{T}}x+x^{\mathrm{T}}D^\alpha x+2\gamma$, where x is a column vector and $\gamma=\sum_{k=1}^\infty\frac{\Gamma(\alpha+1)(D^{\alpha-k}x)^{\mathrm{T}}D^kx}{\Gamma(k+1)\Gamma(\alpha-k+1)}$.

Lemma 2 (Fractional comparison principle). Let $D^\alpha x(t)\geq D^\alpha y(t)$ and $x(0)=y(0)$, where $\alpha\in(0,1)$. Then $x(t)\geq y(t)$. In particular, if $x(t)=c$, where c is a constant, $D^\alpha c=0$ and $y(0)=c$, we will have $y(t)\leq c$.

Theorem 1[15]**.** Let $x=0$ be an equilibrium point for $D^\alpha x(t)=f(t,x)$ and $D\subset\mathbf{R}^n$ be a domain containing $x=0$. Let $V(t,x):[0,\infty)\times D\to\mathbf{R}$ be a continuously differentiable function such that for $\forall t\geq 0$, $\forall x\in D$, $0<\alpha<1$,

$$\begin{aligned}&W_1(x)\leq V(t,x)\leq W_2(x),\\&D^\alpha V(t,x)\leq -W_3(x),\end{aligned} \tag{4}$$

where $W_1(x)$, $W_2(x)$, and $W_3(x)$ are class-K functions on D. Then $x=0$ is asymptotically stable.

Lemma 4[12]**.** Let $x(t)\in\mathbf{R}^n$ be a differentiable and continuous function. Then, for $\forall t\geq t_0$ and $\forall\alpha\in(0,1)$

$$\frac{1}{2}D^\alpha(x^{\mathrm{T}}(t)x(t))\leq x^{\mathrm{T}}(t)D^\alpha x(t). \tag{5}$$

Lemma 5 (Schur complement lemma). The linear matrix inequality (LMI)

$$M=\begin{bmatrix}A & B\\ B^{\mathrm{T}} & C\end{bmatrix}<0,$$

where $A=A^{\mathrm{T}}$, $C=C^{\mathrm{T}}$ and C is invertible, is equivalent to

$$C<0,\quad A-BC^{-1}B^{\mathrm{T}}<0.$$

III. Main Results

Consider the following fractional order nonlinear system with $0<\alpha<1$ and time-varying delays:

$$\begin{cases}D^\alpha x_1=x_2+F_1(x_1)+H_1(y(t),y(t-d_1(t))),\\ D^\alpha x_i=x_{i+1}+F_i(\bar{x}_i)+H_i(y(t),y(t-d_i(t))),\\ D^\alpha x_n=u+F_n(\bar{x}_n)+H_n(y(t),y(t-d_n(t))),\\ y=x_1,\end{cases} \tag{6}$$

where $x(t)=[x_1(t),x_2(t),\ldots,x_n(t)]^{\mathrm{T}}\in\mathbf{R}^n$ is the state and $x_i(\theta)=\phi_i(\theta)$, $\theta\in[-d_i(0),0)$, $i=1,\ldots,n$, $x(0)=0$, $u(t)\in\mathbf{R}$ and $y(t)\in\mathbf{R}$ are the control input and the output of the system, respectively; $\bar{x}_i(t)=[x_1(t),x_2(t),\ldots,x_i(t)]^{\mathrm{T}}$; $F_i(\cdot)$ and $H_i(\cdot)$ are smooth nonlinear functions and $F_i(0,\ldots,0)=H_i(0,0)=0$; $d_i(t)$ is the time-varying delay and there exists positive scalar η_i such that $\dot{d}_i(t)\leq\eta_i<1$.

We impose the following assumptions on system (6).

Assumption 1. Nonlinear functions $H_i(\xi_1,\xi_2)$ $(i=1,2,\ldots,n)$ satisfy the following inequality:

$$|H_i(\xi_1,\xi_2)|\leq\bar{H}_{i1}(\xi_1)\xi_1+\bar{H}_{i2}(\xi_2)\xi_2, \tag{7}$$

where $\bar{H}_{i1}(\cdot)$ and $\bar{H}_{i2}(\cdot)$ are known functions.

Let $H_{i1}(\xi_1)=2\bar{H}_{i1}^2(\xi_1)\xi_1$, $H_{i2}(\xi_2)=2\bar{H}_{i2}^2(\xi_2)\xi_2$, then we can have the following inequality:

$$|H_i(\xi_1,\xi_2)|^2\leq H_{i1}(\xi_1)\xi_1+H_{i2}(\xi_2)\xi_2. \tag{8}$$

Assumption 1 is very common in nonlinear time delay systems, by which the term $y(t-d_i(t))$ can be separated from the delay-function, so that we can handle the delay problems.

Assumption 2. For nonlinear functions $F_i(\cdot)$, there exist some positive scalars l_i such that the following inequalities hold for $i=1,2,3,\ldots,n$:

$$|F_i(\bar{\zeta}_i)-F_i(\hat{\bar{\zeta}}_i)|\leq l_i\left\|\bar{\zeta}_i-\hat{\bar{\zeta}}_i\right\|, \tag{9}$$

where $\bar{\zeta}_i=[\zeta_1,\zeta_2,\ldots,\zeta_i]^{\mathrm{T}}$, $\hat{\bar{\zeta}}_i=[\zeta_1,\hat{\zeta}_2,\ldots,\hat{\zeta}_i]^{\mathrm{T}}$ and l_i is a known positive parameter.

We can use the following expression for $F_i(\bar{x}_i)$

$$F_i(\bar{x}_i) = n_{i1}x_1 + \bar{F}_i(\bar{x}_i), \quad i = 1, \ldots, n, \tag{10}$$

where n_{i1} is a constant which could be zero.

In this paper, we focus on solving the following problem. For system (6) satisfying Assumptions 1 and 2, design a reduced-order observer based memoryless output feedback controller to render the closed-loop system stable.

Considering system (6) with unmeasured state variables, we propose the following reduced-order observer:

$$\begin{cases} D^\alpha \lambda_i(t) = \lambda_{i+1}(t) + k_{i+1}x_1(t) + F_i(\widehat{\bar{x}}_i(t)) \\ \qquad\qquad -k_i(\lambda_2(t) + k_2 y(t) + F_1(y(t))), \\ D^\alpha \lambda_n(t) = u(t) + F_n(\widehat{\bar{x}}_n(t)) \\ \qquad\qquad -k_n(\lambda_2(t) + k_2 y(t) + F_1(y(t))), \\ \hat{x}_i(t) = \lambda_i + k_i y(t), \quad i = 2, \ldots, n, \end{cases} \tag{11}$$

where $\widehat{\bar{x}}_i(t) = [x_1(t), \hat{x}_2(t), \ldots, \hat{x}_i(t)]^{\mathrm{T}}$ and parameters k_i ($i = 2, \ldots, n$) are to be specified later.

Similar to (10), we can change $F_i(\widehat{\bar{x}}_i(t))$ into

$$F_i(\widehat{\bar{x}}_i(t)) = n_{i1}x_1 + \bar{F}_i(\widehat{\bar{x}}_i(t)).$$

Remark 1. In this paper, we introduce the reduced-order observer instead of the full-order one. In this way, some of the states can be derived from the real output, making the results more precise and simplifying the structure and computation complexity. To our best knowledge, it is the first time that the reduced-order observer is introduced to fractional order nonlinear systems.

The estimation errors are defined as

$$e_i(t) = x_i(t) - \hat{x}_i(t). \tag{12}$$

From (11) and (12), we can get

$$D^\alpha e(t) = Ae(t) + \widetilde{F}(t) + \widetilde{H}(t), \tag{13}$$

where

$$e(t) = [e_2(t), \ldots, e_n(t)]^{\mathrm{T}},$$

$$A = \begin{bmatrix} -k_2 & 1 & 0 & \cdots & 0 \\ -k_3 & 0 & 1 & \cdots & 0 \\ \vdots & \vdots & \vdots & \ddots & \vdots \\ -k_n & 0 & 0 & \cdots & 0 \end{bmatrix},$$

$$\begin{aligned} \tilde{F}(t) = [&F_2(\bar{x}_2(t)) - F_2(\widehat{\bar{x}}_2(t)), \ldots, \\ &F_n(\bar{x}_n(t)) - F_n(\widehat{\bar{x}}_n(t))]^{\mathrm{T}}, \end{aligned} \tag{14}$$

$$\begin{aligned} \tilde{H}(t) = [&H_2(y(t), y(t-d_2))) - k_2 H_1(y(t), y(t-d_1))), \\ &\ldots, H_n(y(t), y(t-d_n))) - k_n H_1(y(t), y(t-d_1)))]^{\mathrm{T}}. \end{aligned} \tag{15}$$

Next, we extend the backstepping technique to the fractional order nonlinear system with time-varying delays described by (6). The virtual controllers α_i ($i = 1, \ldots, n-1$) are developed at each step. Finally, at step n, the actual controller u is designed. First, we introduce the following transformation of states.

$$\begin{aligned} &z_1(t) = y(t), \\ &z_i(t) = \lambda_i(t) - \alpha_{i-1}, \quad i = 2, \ldots, n. \end{aligned} \tag{16}$$

Then we choose the Lyapunov function as

$$V = V_e + V_z + V_d, \tag{17}$$

where

$$V_e = I^{1-\alpha} e^{\mathrm{T}} P e, \tag{18}$$

and P is a real symmetric positive matrix.

$$V_z = I^{1-\alpha} \sum_{i=1}^{n} M_i, \tag{19}$$

$$M_i = \frac{1}{2} z_i^2,$$

$$\begin{aligned} V_d = &\left(2\sum_{i=2}^{n} k_i^2 + 1\right) \int_{t-d_1(t)}^{t} \frac{1}{1-\eta_1} H_{12}(y(t))y(t)\mathrm{d}t \\ &+ 2\sum_{i=2}^{n} \int_{t-d_i(t)}^{t} \frac{1}{1-\eta_i} H_{i2}(y(t))y(t)\mathrm{d}t. \end{aligned} \tag{20}$$

Next, we will give the derivative of V_e, V_z, V_d, and V in turn. From Lemma 4, the derivative of V_e is:

$$\begin{aligned} \dot{V}_e &= D^\alpha e(t)^{\mathrm{T}} P e(t) \\ &\le (D^\alpha e(t))^{\mathrm{T}} P e(t) + e^{\mathrm{T}}(t) P D^\alpha e(t) \end{aligned} \tag{21}$$

$$\begin{aligned} &= (Ae(t) + \tilde{F}(t) + \tilde{H}(t))^{\mathrm{T}} P e(t) \\ &\quad + e^{\mathrm{T}}(t) P (Ae(t) + \tilde{F}(t) + \tilde{H}(t)) \\ &= e^{\mathrm{T}}(t)(A^{\mathrm{T}}P + PA)e(t) + \tilde{F}^{\mathrm{T}}(t) P e(t) \\ &\quad + e^{\mathrm{T}}(t) P \tilde{F}(t) + \tilde{H}^{\mathrm{T}}(t) P e(t) + e^{\mathrm{T}}(t) P \tilde{H}(t) \end{aligned} \tag{22}$$

According to Assumption 2, we can get

$$\begin{aligned} \tilde{F}^{\mathrm{T}}(t)\tilde{F}(t) &= \sum_{i=2}^{n} (F_i(\bar{x}_i(t)) - F_i(\widehat{\bar{x}}_i(t)))^2 \\ &\le \sum_{i=2}^{n} l_i^2 \left\|\bar{x}_i - \widehat{\bar{x}}_i\right\|^2 \\ &\le \rho \left\|\bar{x}_n - \widehat{\bar{x}}_n\right\|^2, \end{aligned}$$

where $\rho = \sum_{i=2}^{n} l_i^2$.

$$\begin{aligned} \dot{V}_e &\le e^{\mathrm{T}}(t)(A^{\mathrm{T}}P + PA)e(t) + \rho e^{\mathrm{T}}(t)e(t) \\ &\quad + \tilde{H}^{\mathrm{T}}(t)\tilde{H}(t) + 2e^{\mathrm{T}}(t)PPe(t) \\ &\le e^{\mathrm{T}}(t)(A^{\mathrm{T}}P + PA + \rho I + 2PP)e(t) + \tilde{H}^{\mathrm{T}}(t)\tilde{H}(t) \\ &\le e^{\mathrm{T}}(t)(A^{\mathrm{T}}P + PA + \rho I + 2PP)e(t) \\ &\quad + 2\sum_{i=2}^{n} H_i^2 + 2\sum_{i=2}^{n} k_i^2 H_1^2 \end{aligned} \tag{23}$$

and P and k_i ($i = 2, \ldots, n$) satisfy

$$A^{\mathrm{T}}P + PA + \rho I + 2PP < -\frac{n}{2\epsilon_1} I. \tag{24}$$

To solve inequality (24), we decompose $A = \bar{A} + kB$ with

$$\bar{A} = \begin{bmatrix} 0 & I_{(n-2)\times(n-2)} \\ 0 & 0 \end{bmatrix}, \quad k = \begin{bmatrix} k_2 \\ \vdots \\ k_n \end{bmatrix}_{(n-1)\times 1},$$

$$B = [-1, 0, \ldots, 0]_{1\times(n-1)}.$$

According to Lemma 5, inequality (24) is equivalent to the following LMI

$$\begin{bmatrix} P\bar{A}+WB+B^{\mathrm{T}}W^{\mathrm{T}}+\bar{A}^{\mathrm{T}}P+(\rho+\frac{n}{2\epsilon_1})I & P \\ P & -0.5I \end{bmatrix} < 0, \tag{25}$$

where $W=Pk$. Further, we can use LMI toolbox in Matlab to obtain P and k.

The derivative of V_z is:

$$\dot{V}_z=\sum_{i=1}^{n} D^{\alpha} M_i. \tag{26}$$

Next, by the backstepping method, the virtual controllers α_i ($i=1,2,\ldots,n-1$) and controller u are designed respectively.

Step 1.

$$\begin{aligned} D^{\alpha}M_1 =& \frac{1}{2}D^{\alpha}z_1^2 \le z_1 D^{\alpha} z_1 \\ =& z_1(z_2+\alpha_1+k_2x_1+e_2+F_1(y(t)) \\ &+H_1(y(t),y(t-d_1(t)))) \\ \le& \left(\frac{1}{4}+\frac{\epsilon_1}{2}\right)z_1^2+\frac{1}{2\epsilon_1}e_2^2+H_1^2(y(t),y(t-d_1(t))) \\ &+z_1(\alpha_1+k_2x_1+F_1(x_1(t)))+z_1z_2, \end{aligned} \tag{27}$$

where ϵ_1 is a positive constant.

Choose

$$\begin{aligned} \alpha_1 =& -\left(c_1+\frac{1}{4}+\frac{\epsilon_1}{2}+k_2+n_{11}\right)z_1-\bar{F}_1(y(t)) \\ &-\left(2\sum_{i=2}^{n}k_i^2+1\right)\left(H_{11}(y(t))+\frac{1}{1-\eta_1}H_{12}(y(t))\right) \\ &-2\sum_{i=2}^{n}\left(H_{i1}(y(t))+\frac{1}{1-\eta_i}H_{i2}(y(t))\right) \\ =& -K_1z_1-\bar{\alpha}_1, \end{aligned} \tag{28}$$

where c_i ($i=1,2,\ldots,n$) are positive constants,

$$\begin{aligned} K_1 =& c_1+\frac{1}{4}+\frac{\epsilon_1}{2}+k_2+n_{11} \\ \bar{\alpha}_1 =& \bar{F}_1(y(t))+\left(2\sum_{i=2}^{n}k_i^2+1\right)(H_{11}(y(t)) \\ &+\frac{1}{1-\eta_1}H_{12}(y(t)))+2\sum_{i=2}^{n}(H_{i1}(y(t)) \\ &+\frac{1}{1-\eta_i}H_{i2}(y(t))). \end{aligned}$$

Step 2.

$$\begin{aligned} D^{\alpha}M_2 =& \frac{1}{2}D^{\alpha}z_2^2 \le z_2D^{\alpha}z_2 \\ =& z_2(z_3+\alpha_2+k_3x_1+F_2(\hat{\bar{x}}_2(t)) \\ &-k_2(\lambda_2+k_2x_1+F_1(x_1))-D^{\alpha}\alpha_1) \\ \le& z_2z_3+\frac{1}{2\epsilon_1}e_2^2+z_2(\alpha_2+k_3x_1+F_2(\hat{\bar{x}}_2(t)) \\ &-k_2(\lambda_2+k_2x_1+F_1(x_1))+D^{\alpha}\bar{\alpha}_1 \\ &+K_1(z_2+\alpha_1+k_2x_1+F_1(y(t)))+\frac{K_1\epsilon_1}{2}z_2^2. \end{aligned} \tag{29}$$

Choose

$$\begin{aligned} \alpha_2 =& -z_1-\left(c_2+\frac{K_1\epsilon_1}{2}\right)z_2-k_3x_1-n_{21}z_1 \\ &-\bar{F}_2(\hat{\bar{x}}_2(t))-K_1(z_2+\alpha_1+k_2x_1+F_1(y(t))) \\ &+k_2(\lambda_2+k_2x_1(t)+F_1(x_1(t)))-D^{\alpha}\bar{\alpha}_1 \\ =& -K_2z_1-\bar{\alpha}_2, \end{aligned} \tag{30}$$

where

$$\begin{aligned} K_2 =& 1+(K_1-k_2)(n_{11}+k_2)+n_{21}+k_3 \\ \bar{\alpha}_2 =& \left(c_2+\frac{K_1\epsilon_1}{2}\right)z_2+\bar{F}_2(\hat{\bar{x}}_2(t)) \\ &+(K_1-k_2)(z_2+\alpha_1+\bar{F}_1(y(t)))+D^{\alpha}\bar{\alpha}_1. \end{aligned}$$

Step i.

$$\begin{aligned} D^{\alpha}M_i =& \frac{1}{2}D^{\alpha}z_i^2 \le z_iD^{\alpha}z_i \\ =& z_i(z_{i+1}+\alpha_i+k_{i+1}x_1+F_i(\hat{\bar{x}}_i(t)) \\ &-k_i(\lambda_2+k_2x_1(t)+F_1(x_1(t)))-D^{\alpha}\alpha_{i-1}) \\ =& z_iz_{i+1}+\frac{1}{2\epsilon_1}e_2^2+z_i(\alpha_i+k_{i+1}x_1+F_i(\hat{\bar{x}}_i(t))) \\ &-k_i(\lambda_2+k_2x_1(t)+F_1(x_1(t)))+D^{\alpha}\bar{\alpha}_{i-1} \\ &+K_{i-1}(z_2+\alpha_1+k_2x_1+F_1(y(t))))+\frac{K_{i-1}\epsilon_1}{2}z_i^2. \end{aligned} \tag{31}$$

Choose

$$\begin{aligned} \alpha_i =& -z_{i-1}-\left(c_i+\frac{K_{i-1}\epsilon_1}{2}\right)z_i-k_{i+1}x_1-n_{i1}z_1 \\ &-\bar{F}_i(\hat{\bar{x}}_i(t))+k_i(\lambda_2+k_2x_1(t)+F_1(x_1(t))) \\ &-D^{\alpha}\bar{\alpha}_{i-1}-K_{i-1}(z_2+\alpha_1+k_2x_1+F_1(y(t))) \\ =& -K_iz_1-\bar{\alpha}_i, \end{aligned} \tag{32}$$

where

$$\begin{aligned} K_i =& (K_{i-1}-k_i)(n_{11}+k_2)+n_{i1}+k_{i+1} \\ \bar{\alpha}_i =& z_{i-1}+\left(c_i+\frac{K_{i-1}\epsilon_1}{2}\right)z_i+\bar{F}_i(\hat{\bar{x}}_i(t)) \\ &+(K_{i-1}-k_i)(z_2+\alpha_1+\bar{F}_1(y(t)))+D^{\alpha}\bar{\alpha}_{i-1}. \end{aligned}$$

Step n.

$$\begin{aligned} D^{\alpha}M_n =& \frac{1}{2}D^{\alpha}z_n^2 \le z_nD^{\alpha}z_n \\ =& z_n(u+F_n(\hat{\bar{x}}_n(t))-k_n(\lambda_2+k_2x_1(t) \\ &+F_1(x_1(t)))-D^{\alpha}\alpha_{n-1}) \\ =& \frac{1}{2\epsilon_1}e_2^2+\frac{K_{n-1}\epsilon_1}{2}z_n^2+z_n(u+F_n(\hat{\bar{x}}_n(t)) \\ &+D^{\alpha}\bar{\alpha}_{n-1}-k_n(\lambda_2+k_2x_1(t)+F_1(x_1(t))) \\ &+K_{n-1}(z_2+\alpha_1+k_2x_1+F_1(y(t)))). \end{aligned} \tag{33}$$

Then

$$\begin{aligned} u =& -z_{n-1}-\left(c_n+\frac{K_{n-1}\epsilon_1}{2}\right)z_n-F_n(\hat{\bar{x}}_n(t)) \\ &+k_n(\lambda_2+k_2x_1(t)+F_1(x_1(t))) \\ &-K_{n-1}(z_2+\alpha_1+k_2x_1+F_1(x_1(t)))-D^{\alpha}\bar{\alpha}_{n-1}. \end{aligned} \tag{34}$$

The derivative of V_d is:

$$\begin{aligned}\dot{V}_d =& \left(2\sum_{i=2}^{n} k_i^2 + 1\right)\\ &\times\left(\frac{\mathrm{d}}{\mathrm{d}t}\left(\int_{t-d_1(t)}^{t}\frac{1}{1-\eta_1}H_{12}(y(t))y(t)\mathrm{d}t\right)\right)\\ &+2\sum_{i=2}^{n}\left(\frac{\mathrm{d}}{\mathrm{d}t}\left(\int_{t-d_i(t)}^{t}\frac{1}{1-\eta_i}H_{i2}(y(t))y(t)\mathrm{d}t\right)\right)\\ \le& \left(2\sum_{i=2}^{n} k_i^2 + 1\right)\left(\frac{1}{1-\eta_1}H_{12}(y(t)\right)y(t)\\ &- H_{12}(y(t-d_1(t)))y(t-d_1(t)))\\ &+2\sum_{i=2}^{n}(\frac{1}{1-\eta_i}H_{i2}(y(t))y(t)\\ &- H_{i2}(y(t-d_i(t)))y(t-d_i(t))). \end{aligned} \tag{35}$$

Then, we have

$$\begin{aligned}\dot{V} =& \dot{V}_e + \dot{V}_z + \dot{V}_d\\ \le& e^{\mathrm{T}}(t)\left(A^{\mathrm{T}}P + PA + \left(\rho + \frac{n}{2\epsilon_1}\right)I + 2PP\right)e(t)\\ &-\sum_{i=1}^{n} c_i z_i^2. \end{aligned}\tag{36}$$

So

$$\dot{V} \le -W(e(t), \bar{z}_n), \tag{37}$$

where $\bar{z}_i = [z_1, z_2, \ldots, z_n]$ and $W(\cdot)$ and $W_1(\cdot)$ are class-K functions.

According to the definition of the Caputo fractional derivative, Lemma 2 and (37)

$$D^{\alpha}V = I^{1-\alpha}\dot{V} \le -I^{1-\alpha}W(e(t), \bar{z}_n) \le -W_1(e(t), \bar{z}_n)$$

Finally, we present the main result of this paper as follows:

Theorem 2. For a system described by (6) satisfying Assumptions 1 and 2, controller (34) can render the closed-loop system asymptotically stable.

IV. Simulation

In this section, an example is given to show the effectiveness of the proposed controller.

Consider the following system:

$$\begin{cases} D^{\alpha}x_1(t) = x_2(t) - 0.8x_1(t) + 0.5x_1^2(t-d_1(t))\sin t,\\ D^{\alpha}x_2(t) = u - 0.8x_2(t) + 0.5x_1^3(t-d_2(t))\sin t, \end{cases}$$

where $d_1(t) = 0.5(1+\sin t)$, $d_2(t) = 0.5(1+\cos t)$. We can see that the aforementioned system satisfies the above assumptions with $P = I$, $\eta_1 = \eta_2 = 0.5$, $l = 0.8$, $\rho = 0.64$, $n_{11} = -0.8$, $\bar{F}_1(x_1) = 0$, $n_{21} = 0$, $\bar{F}_2(\bar{x}_2) = -0.8x_2$, $H_{11}(t) = H_{21}(t) = 0$, $H_{12}(t-d_1(t)) = 0.25x_1^3(t-d_1(t))$ and $H_{22}(t-d_1(t)) = 0.25\ x_1^5(t-d_1(t))$. Choosing $\epsilon_1 = 1$, $k_2 = 2$, $c_1 = 0.05$ and $c_2 = 0.8$, we can obtain the reduced-order observer and the function $\beta_1(x_1(t))$:

$$\begin{aligned} &D^{\alpha}\lambda_2(t) = u - 2.8\lambda_2(t) - 4x_1(t),\\ &\alpha_1(x_1(t)) = -2x_1(t) - 4.5x_1^3(t) - x_1^5(t). \end{aligned}$$

Then, $K_1 = 2$, $\bar{\alpha}_1 = 4.5x_1^3 + x_1^5$, the controller can be designed as

$$u(t) = 0.6x_1(t) - \lambda_2(t) + 1.8\alpha_1(x_1(t)) - D^{\alpha}\bar{\alpha}_1.$$

The simulation results are shown in Figs. 1 and 2, from which we can see that the constructed controller renders the closed-loop system stable.

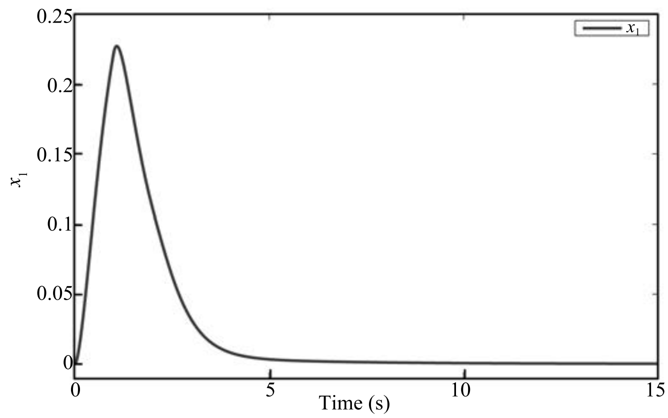

Fig. 1. The output response of the closed-loop system.

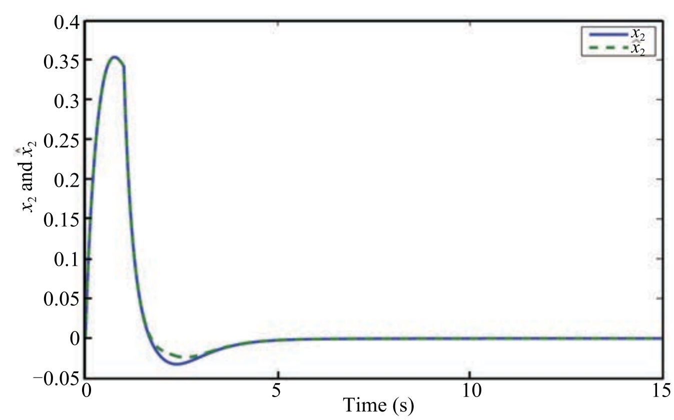

Fig. 2. The trajectories of x_2 and $\hat{x}_2$.

V. Conclusion

In this paper, we study the controller design problem for fractional order nonlinear time-varying delay systems, using the well known backstepping method. Also, we extend the Lyapunov method to fractional order systems. Both the designed observer and controller are independent of time delays. Through the simulation presented in Section IV, the effectiveness of the proposed controller has been verified. As put in [25], fractional order systems have a memory feature, which could make difficulties in the process of controller design. In the future, we will further consider the memory feature and its influence. Based on the result of this paper, we will study the stability and stabilization problems for fractional nonlinear delayed systems with fractional order $1 < \alpha < 2$ and the stability of fractional order nonlinear systems with fractional order $\alpha > 2$.

REFERENCES

[1] Podlubny I. *Fractional Differential Equations: An Introduction to Fractional Derivatives, Fractional Differential Equations, Some Methods of Their Solution and Some of Their Applications.* San Diego: Academic Press, 1999.

[2] Pan I, Das S. *Intelligent Fractional Order Systems and Control.* Berlin Heidelberg: Springer, 2013.

[3] Kilbas A A, Srivastava H M, Trujillo J J. *Theory and Applications of Fractional Differential Equations, Volume 204 (North-Holland Mathematics Studies).* New York: Elsevier Science Inc., 2006.

[4] Lakshmikantham V, Leela S, Vasundhara Devi J. *Theory of Fractional Dynamic Systems.* Cambridge, UK: Cambridge Scientific Publishers, 2009.

[5] Diethelm K. *The Analysis of Fractional Differential Equations.* Berlin: Springer, 2010.

[6] Lakshmikantham V, Vatsala A S. Basic theory of fractional differential equations. *Nonlinear Analysis: Theory, Methods and Applications*, 2008, **69**(8): 2677−2682

[7] Matignon D. Stability results for fractional differential equations with applications to control processing. *Computational Engineering in Systems Applications*, 1996, **2**: 963−968

[8] Lu J G, Chen Y Q. Robust stability and stabilization of fractional-order interval systems with the fractional order α: the $0 \ll \alpha \ll 1$ case. *IEEE Transactions on Automatic Control*, 2010, **55**(1): 152−158

[9] Lu J G, Chen G R. Robust stability and stabilization of fractional-order interval systems: an LMI approach. *IEEE Transactions on Automatic Control*, 2009, **54**(6): 1294−1299

[10] Zhang X F, Liu L, Feng G, Wang Y Z. Asymptotical stabilization of fractional-order linear systems in triangular form. *Automatica*, 2013, **49**(11): 3315−3321

[11] Lim Y H, Oh K K, Ahn H S. Stability and stabilization of fractional-order linear systems subject to input saturation. *IEEE Transactions on Automatic Control*, 2013, **58**(4): 1062−1067

[12] Aguila-Camacho N, Duarte-Mermoud M A, Gallegos J A. Lyapunov functions for fractional order systems. *Communications in Nonlinear Science and Numerical Simulation*, 2014, **19**(9): 2951−2957

[13] Wen X J, Wu Z M, Lu J G. Stability analysis of a class of nonlinear fractional-order systems. *IEEE Transactions on Circuits and Systems II: Express Briefs*, 2008, **55**(11): 1178−1182

[14] Delavari H, Baleanu D, Sadati J. Stability analysis of Caputo fractional-order nonlinear systems revisited. *Nonlinear Dynamics*, 2012, **67**(4): 2433−2439

[15] Li Y, Chen Y Q, Podlubny I. Stability of fractional-order nonlinear dynamic systems: Lyapunov direct method and generalized Mittag-Leffler stability. *Computers and Mathematics with Applications*, 2010, **59**(5): 1810−1821

[16] Hua C C, Guan X P, Shi P. Robust backstepping control for a class of time delayed systems. *IEEE Transactions on Automatic Control*, 2005, **50**(6): 894−899

[17] Bonnet C, Partington J R. Coprime factorizations and stability of fractional differential systems. *Systems and Control Letters*, 2000, **41**(3): 167−174

[18] Deng W H, Li C P, Lv J H. Stability analysis of linear fractional differential system with multiple time delays. *Nonlinear Dynamics*, 2007, **48**(4): 409−416

[19] Kheirizad I, Tavazoei M S, Jalali A A. Stability criteria for a class of fractional order systems. *Nonlinear Dynamics*, 2010, **61**(1−2): 153−161

[20] Zhang F R, Li C P. Stability analysis of fractional differential systems with order lying in $(1, 2)$. *Advances in Difference Equations*, 2011, **2011**: Article ID 213485

[21] Wen Y H, Zhou X F, Zhang Z X, Liu S. Lyapunov method for nonlinear fractional differential systems with delay. *Nonlinear Dynamics*, 2015, **82**(1−2): 1015−1025

[22] Yu W, Li T Z. Stability analysis of fractional-order nonlinear systems with delay. *Mathematical Problems in Engineering*, 2014, **2014**(4): Article ID 301235

[23] Wei Y H, Chen Y Q, Liang S, Wang Y. A novel algorithm on adaptive backstepping control of fractional order systems. *Neurocomputing*, 2015, **165**: 395−402

[24] Ding D S, Qi D L, Meng Y, Xu L. Adaptive Mittag-Leffler stabilization of commensurate fractional-order nonlinear systems. In: Proceedings of the 53rd IEEE Conference on Decision and Control (CDC). Los Angeles, CA: IEEE, 2014. 6920−6926

[25] Syta A, Litak G, Lenci S, Scheffler M. Chaotic vibrations of the duffing system with fractional damping. *Chaos: An Interdisciplinary Journal of Nonlinear Science*, 2014, **24**(1): 013107

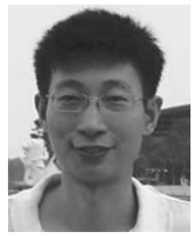

Changchun Hua received the Ph. D. degree in electrical engineering from Yanshan University, Qinhuangdao, China, in 2005. He was a research fellow in National University of Singapore from 2006 to 2007. From 2007 to 2009, he worked in Carleton University, Canada, funded by Province of Ontario Ministry of Research and Innovation Program. From 2009 to 2011, he worked in University of Duisburg-Essen, Germany, funded by Alexander von Humboldt Foundation. Now he is a full professor at Yanshan University, China. He is the author or coauthor of more than 110 papers in mathematical, technical journals, and conferences. He has been involved in more than 10 projects supported by the National Natural Science Foundation of China, the National Education Committee Foundation of China, and other important foundations. His research interests include nonlinear control systems, control systems design over network, teleoperation systems, and intelligent control. Corresponding author of this paper.

Tong Zhang received the B. S. degree in electrical engineering from Yanshan University, Qinhuangdao, China, in 2014. She is currently working toward the M. S. degree in electrical engineering. Her research interests include fractional order system control.

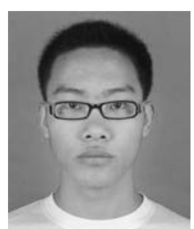

Yafeng Li received the B. S. degree in electrical engineering from Hebei University of Science and Technology, Shijiazhuang, China, in 2013. He is currently working toward the Ph. D. degree in Yanshan University. His research interests include nonlinear system control and multi-agent system control.

Xinping Guan received the B. S. degree in mathematics from Harbin Normal University, Harbin, China, and the M. S. degree in applied mathematics and the Ph. D. degree in electrical engineering, both from Harbin Institute of Technology, in 1986, 1991, and 1999, respectively. He is with the Department of Automation, Shanghai Jiao Tong University. He is the (co)author of more than 200 papers in mathematical, technical journals, and conferences. As (a)an (co)-investigator, he has finished more than 20 projects supported by National Natural Science Foundation of China (NSFC), the National Education Committee Foundation of China, and other important foundations. He is Cheung Kong Scholars Programme Special appointment professor. His current research interests include networked control systems, robust control and intelligent control for complex systems and their applications. Dr. Guan is serving as a reviewer of Mathematic Review of America, a member of the Council of Chinese Artificial Intelligence Committee, and chairman of Automation Society of Hebei Province, China.

State Feedback Control for a Class of Fractional Order Nonlinear Systems

Yige Zhao, Yuzhen Wang, and Haitao Li

***Abstract*—Using the Lyapunov function method, this paper investigates the design of state feedback stabilization controllers for fractional order nonlinear systems in triangular form, and presents a number of new results. First, some new properties of Caputo fractional derivative are presented, and a sufficient condition of asymptotical stability for fractional order nonlinear systems is obtained based on the new properties. Then, by introducing appropriate transformations of coordinates, the problem of controller design is converted into the problem of finding some parameters, which can be certainly obtained by solving the Lyapunov equation and relevant matrix inequalities. Finally, based on the Lyapunov function method, state feedback stabilization controllers making the closed-loop system asymptotically stable are explicitly constructed. A simulation example is given to demonstrate the effectiveness of the proposed design procedure.**

***Index Terms*—Fractional order system, triangular system, asymptotical stabilization, state feedback, Lyapunov function method.**

I. INTRODUCTION

FRACTIONAL order systems have been of great interest in the last two decades. It is caused both by the intensive development of the theory of fractional calculus itself and by the applications. Apart from diverse areas of mathematics, fractional order systems play an important role in physics, chemistry, engineering and so on[1−2].

As we all know, stability is an essential issue to control systems, certainly including fractional order systems. The earliest study on the stability of fractional differential equations can be traced back to 1960s[3], where it was shown that the stability problem of fractional differential equations comes down to the eigenvalue problem of system matrices. For fractional order systems, there are many papers related to the stability theory[4−10] such as root-locus, asymptotical stability, bounded input bounded output stability, internal stability, external stability, robust stability, finite-time stability, etc.

Recently, the Lyapunov function method has also been used to study the stability of fractional order systems[11−17]. On one hand, some Lyapunov functions were constructed in works related to fractional sliding mode control[13−14], and the classic Lyapunov function method was presented to stabilize fractional order systems. On the other hand, Li et al. investigated the Mittag-Leffler stability and the asymptotical stability of fractional order nonlinear systems by using the fractional Lyapunov's direct method[15−16]. It is usually difficult to construct a positive definite function and calculate its fractional derivative for a given fractional order system. Recently, a new property for Caputo fractional derivative of a quadratic function has been presented in [17]. The result allows the use of classic quadratic Lyapunov functions in the stability analysis of fractional order systems. In some cases, those simple quadratic functions[17] cannot work, and more general quadratic Lyapunov functions should be used instead. These results are very important in the sense that they have provided a basic tool for the stability analysis and controller design of fractional order systems.

However, it should be pointed out that it is usually difficult to construct a positive definite function and calculate its fractional derivative for a given fractional order system. The Leibniz rule for Caputo fractional derivative does not work very well like that for classical derivative. To this end, this work will present some new and useful properties for Caputo fractional derivative which allow finding a simple Lyapunov candidate function for many fractional order systems. Furthermore, to the authors' best knowledge, fewer works have been done to study the stabilization problems for fractional order nonlinear systems in the triangular form. For fractional order nonlinear systems in the triangular form, such as the ones considered in this work, it is difficult or even impossible to solve the feedback stabilizer design problem by the existing approaches.

In this paper, using the Lyapunov function method, we investigate the design of state feedback stabilization controllers for fractional order nonlinear systems in the upper triangular form. The main contributions of this paper are as follows: 1) Some new properties for Caputo fractional derivative are presented, which allow finding a simple Lyapunov candidate function for many fractional order systems. As an application, a sufficient condition of asymptotical stability for fractional order nonlinear systems is obtained based on the new properties. 2) By introducing appropriate transformations of coordinates, the problems of controller design are converted into the problems of finding some parameters, which can be certainly obtained by solving the Lyapunov equation and relevant matrix inequalities. By designing state feedback stabilization controllers for fractional order nonlinear systems in the upper

Manuscript received August 9, 2015; accepted December 3, 2015. This work was supported by National Natural Science Foundation of China (61374065, 61374002, 61503225, 61573215), the Research Fund for the Taishan Scholar Project of Shandong Province of China, and the Natural Science Foundation of Shandong Province (ZR2015FQ003). Recommended by Associate Editor Antonio Visioli.

Citation: Yige Zhao, Yuzhen Wang, Haitao Li. State feedback control for a class of fractional order nonlinear systems. *IEEE/CAA Journal of Automatica Sinica*, 2016, **3**(4): 483−488

Yige Zhao is with School of Mathematical Sciences, University of Jinan, Jinan 250022, China (e-mail: zhaoeager@126.com).

Yuzhen Wang is with School of Control Science and Engineering, Shandong University, Jinan 250061, China (e-mail: yzwang@sdu.edu.cn).

Haitao Li is with the School of Mathematical Science, Shandong Normal University, Jinan 250014, China (e-mail: haitaoli09@gmail.com).

triangular form, asymptotical stability for closed-loop systems is considered based on the Lyapunov function method.

The rest of this paper is organized as follows: Section II presents some necessary preliminaries. Section III gives new properties on Caputo fractional derivative and presents a sufficient condition of asymptotical stability for fractional order nonlinear systems. Section IV investigates the design of state feedback controller for the upper triangular fractional order nonlinear systems. Section V gives an illustrative example to illustrate our new results, which is followed by the conclusion in Section VI.

Notation. $\mathbf{R}$ denotes the set of real numbers, $\mathbf{R}^n$ denotes the n-dimensional Euclidean space, and $\mathbf{R}^{n\times n}$ denotes the set of $n\times n$ real matrices. For real symmetric matrices X and Y, the notation $X>Y$ ($X\geq Y$) means that matrix $X-Y$ is positive definite (positive semi-definite), and similarly, $X<Y$ ($X\leq Y$) means that matrix $X-Y$ is negative definite (negative semi-definite). I is the identity matrix with appropriate dimension. X^{T} and X^{-1} represent the transpose and the inverse of matrix X, respectively. $\|\cdot\|$ denotes the Euclidean norm for a vector, or the induced Euclidean norm for a matrix.

II. Preliminaries

In this section, we first give some definitions and properties for Caputo fractional derivative, and then present a Lyapunov-based stability theorem for fractional order systems. Throughout this paper, we use Caputo fractional derivative as our main tools, which is given in [2].

Definition1[2] **.** Caputo fractional derivative of order $\alpha>0$ of a continuous function $f(t)$ is given by

$$ {}_0^CD_t^\alpha f(t)=\frac{1}{\Gamma(n-\alpha)}\int_0^t\frac{f^{(n)}(s)}{(t-s)^{\alpha-n+1}}\mathrm{d}s, $$

where n is the smallest integer greater than or equal to α and $\Gamma(\cdot)$ denotes the Gamma function, provided that the right side is pointwise defined on $(0,+\infty)$.

The Leibniz rule for Caputo fractional derivative is the following.

Lemma 1[2]**.** If φ and f along with all its derivatives are continuous in $(0,+\infty)$, then the Leibniz rule for Caputo fractional derivative takes the form

$$ \begin{aligned} &{}_0^CD_t^\alpha\left(\varphi(t)f(t)\right)\\ &=\sum_{k=0}^{\infty}\frac{\Gamma(1+\alpha)}{\Gamma(1+k)\Gamma(1-k+\alpha)}\varphi^{(k)}(t)\ {}_0^CD_t^{\alpha-k}f(t), \end{aligned} $$

where $\alpha\in(0,1)$, $\Gamma(\cdot)$ denotes the Gamma function.

Remark 1. By Lemma 1, we can easily see that

$$ {}_0^CD_t^\alpha\left(\varphi(t)f(t)\right)\neq{}_0^C D_t^\alpha\varphi(t)f(t)+\varphi(t){}_0^CD_t^\alpha f(t), $$

where $\alpha\in(0,1)$. Obviously, the Leibniz rule for Caputo fractional derivative does not have the form like that for classical derivative.

The following lemma is the property for Caputo fractional derivative of a matrix.

Lemma 2. Let $A(t)=(a_{i,j}(t))_{n\times n}$ be a time-varying matrix and $a_{i,j}(t)$ be continuous and derivable functions, and $Q\in\mathbf{R}^{n\times n}$. Then the following equalities:

$$ \begin{aligned} &{}_0^CD_t^\alpha A(t)=\left({}_0^CD_t^\alpha a_{i,j}(t)\right)_{n\times n},\\ &{}_0^CD_t^\alpha(QA(t))=Q{}_0^CD_t^\alpha A(t) \end{aligned} $$

hold, where ${}_0^CD_t^\alpha$ is Caputo fractional derivative, $\alpha\in(0,1]$.

Proof. The proof is straightforward. □

The property for Caputo fractional derivative of a quadratic function is the following.

Lemma 3[17]**.** Let $x(t)\in\mathbf{R}$ be a continuous and derivable function. Then, for any time instant $t\geq0$,

$$ \frac{1}{2}{}_0^CD_t^\alpha x^2(t)\leq x(t){}_0^CD_t^\alpha x(t),\qquad\forall\ \alpha\in(0,1). $$

Remark 2[17]**.** In the case when $x(t)\in\mathbf{R}^n$, Lemma 3 is still valid. That is, for $\forall\ \alpha\in(0,1)$ and $\forall\ t\geq0$,

$$ \frac{1}{2}{}_0^CD_t^\alpha\left(x^{\mathrm{T}}(t)x(t)\right)\leq x^{\mathrm{T}}(t){}_0^CD_t^\alpha x(t). $$

Finally, we recall a useful result on the Lyapunov-based stability theorem for fractional order systems[15−16].

Lemma 4. Let $\tilde{x}=0$ be an equilibrium point of fractional order systems

$$ {}_0^CD_t^\alpha x(t)=f(t,x),\quad x_0\in\mathbf{R}^n, \tag{1} $$

where ${}_0^CD_t^\alpha$ denotes Caputo fractional derivative, $0<\alpha<1$. Assume that there exists a Lyapunov function $V(t,x(t))$ and class-$\mathcal{K}$ functions β_i ($i=1,\ 2,\ 3$) satisfying

$$ \begin{aligned} &\beta_1(\|x\|)\leq V(t,x(t))\leq\beta_2(\|x\|),\\ &{}_0^CD_t^\alpha V(t,x(t))\leq-\beta_3(\|x\|). \end{aligned} $$

Then the equilibrium point of the system (1) is asymptotically stable.

III. New properties for Caputo fractional derivative

In this section, we give some new properties for Caputo fractional derivative. To this end, we need the following lemma, which is about the decomposition of a positive definite matrix.

Lemma 5. Let $A\in\mathbf{R}^{n\times n}$ be a positive definite matrix. Then there exists a positive definite matrix $B\in\mathbf{R}^{n\times n}$, such that $A=B^2$.

Proof. The proof is straightforward. □

According to this lemma, some new properties for Caputo fractional derivative of a general quadratic function are given in the following.

Theorem 1. Let $x(t)=(x_1(t),\ x_2(t),\ \ldots,\ x_n(t))^{\mathrm{T}}\in\mathbf{R}^n$, $x_i(t)$ ($i=1,\ 2,\ \ldots,\ n$) be continuous and derivable functions, and $\alpha\in(0,1]$. Then, for any time instant $t\geq0$, there exists a positive definite matrix $P\in\mathbf{R}^{n\times n}$ such that

$$ \frac{1}{2}{}_0^CD_t^\alpha\left(x^{\mathrm{T}}(t)Px(t)\right)\leq x^{\mathrm{T}}(t)P{}_0^CD_t^\alpha x(t). \tag{2} $$

Proof. For convenience, we divide the proof into two cases.

Case 1. $\alpha=1$.

This case corresponds to the chain rule for the integer order derivatives, which states that

$$\frac{1}{2}\frac{\mathrm{d}}{\mathrm{d}t}\left(x^{\mathrm{T}}(t)Px(t)\right) = x^{\mathrm{T}}(t)P\frac{\mathrm{d}}{\mathrm{d}t}x(t).$$

Case 2. $0 < \alpha < 1$.

By Lemma 5, there exists a positive definite matrix $Q \in \mathbf{R}^{n\times n}$ such that $P = Q^2$. Then we have

$$\frac{1}{2}{}_0^C D_t^\alpha \left(x^{\mathrm{T}}(t)Px(t)\right) = \frac{1}{2}{}_0^C D_t^\alpha \left(x^{\mathrm{T}}(t)Q^{\mathrm{T}}Qx(t)\right).$$

Let $y(t) = Qx(t)$. From Lemma 2 and Remark 2, we obtain

$$\begin{aligned}\frac{1}{2}{}_0^C D_t^\alpha \left(x^{\mathrm{T}}(t)Px(t)\right) &= \frac{1}{2}{}_0^C D_t^\alpha \left(x^{\mathrm{T}}(t)Q^{\mathrm{T}}Qx(t)\right)\\ &= \frac{1}{2}{}_0^C D_t^\alpha \left(y^{\mathrm{T}}(t)y(t)\right)\\ &\le y^{\mathrm{T}}(t){}_0^C D_t^\alpha y(t)\\ &= x^{\mathrm{T}}(t)Q^{\mathrm{T}}{}_0^C D_t^\alpha (Qx(t))\\ &= x^{\mathrm{T}}(t)Q^{\mathrm{T}}Q{}_0^C D_t^\alpha x(t)\\ &= x^{\mathrm{T}}(t)P{}_0^C D_t^\alpha x(t).\end{aligned}$$

□

Remark 3. In the case when $P = I$, the conclusion of Theorem 1 turns to be the conclusion of Remark 2.

Remark 4. Inequality (2) is equivalent to any one of the following inequalities:

$$\frac{1}{2}{}_0^C D_t^\alpha \left(x^{\mathrm{T}}(t)Px(t)\right) \le \left({}_0^C D_t^\alpha x(t)\right)^{\mathrm{T}} Px(t),$$

$${}_0^C D_t^\alpha \left(x^{\mathrm{T}}(t)Px(t)\right) \le \left({}_0^C D_t^\alpha x(t)\right)^{\mathrm{T}} Px(t) + x^{\mathrm{T}}(t)P{}_0^C D_t^\alpha x(t). \tag{3}$$

As an application of Theorem 1 and inequality (3), we present a sufficient condition of stability for fractional order nonlinear system by Lyapunov function method.

Consider the fractional order nonlinear system with Caputo fractional derivative

$${}_0^C D_t^\alpha x(t) = f(t, x(t)), \tag{4}$$

where $\alpha \in (0, 1]$, $x(t) \in \mathbf{R}^n$ is the state, $f:\ \mathbf{R}\times\mathbf{R}^n \to \mathbf{R}^n$, $f_i\ (i = 1,\ 2,\ \ldots,\ n)$ are continuous functions.

Theorem 2. The system (4) is asymptotically stable if there exists a positive definite matrix $P \in \mathbf{R}^{n\times n}$ and a class-$\mathcal{K}$ function γ such that for $\forall\ x(t) \in \mathbb{R}^n$, $x^T(t)Pf(t, x(t)) < -\gamma(\|x\|)$.

Proof. Let $V(t) = x^{\mathrm{T}}(t)Px(t)$. Because $P \in \mathbf{R}^{n\times n}$ is a positive definite matrix, then V is positive definite. By using (3), we have

$$\begin{aligned}{}_0^C D_t^\alpha V(t)|_4 &= {}_0^C D_t^\alpha x^{\mathrm{T}}(t)Px(t)\\ &\le \left({}_0^C D_t^\alpha x(t)\right)^{\mathrm{T}} Px(t) + x^{\mathrm{T}}(t)P{}_0^C D_t^\alpha x(t)\\ &= f^{\mathrm{T}}(t, x(t))Px(t) + x^{\mathrm{T}}(t)Pf(t, x(t))\\ &= 2x^{\mathrm{T}}(t)Pf(t, x(t)) < -2\gamma(\|x\|).\end{aligned}$$

Thus, according to Lemma 4, the system (4) is asymptotically stable. □

IV. State feedback stabilizers design

In this section, state feedback stabilizers are designed for the upper triangular fractional order nonlinear system.

Consider the following fractional order nonlinear system in the upper triangular form:

$$\begin{cases} {}_0^C D_t^\alpha x_1(t) = x_2(t) + \phi_1(t, x(t)),\\ {}_0^C D_t^\alpha x_2(t) = x_3(t) + \phi_2(t, x(t)),\\ \qquad\vdots\\ {}_0^C D_t^\alpha x_{n-2}(t) = x_{n-1}(t) + \phi_{n-2}(t, x(t)),\\ {}_0^C D_t^\alpha x_{n-1}(t) = x_n(t),\\ {}_0^C D_t^\alpha x_n(t) = u(t),\end{cases} \tag{5}$$

where $\alpha \in (0, 1]$, $x(t) = (x_1(t), x_2(t), \ldots, x_n(t))^T \in \mathbf{R}^n$ is the state, $u \in \mathbf{R}$ is the control input. The arguments of the functions will be omitted or simplified whenever no confusion can arise from the context. In this paper, $x_i(t)$ and $z_i(t)$ are always denoted by x_i and z_i. The functions $\phi_i : \mathbf{R}\times\mathbf{R}^n \to \mathbf{R}$, $i = 1, 2, \ldots, n-2$ are continuous, and satisfy the following growth condition:

Assumption 1.

$$\begin{aligned}&|\phi_i(t, x)| \le c(|x_{i+2}| + |x_{i+3}| + \cdots + |x_n|),\\ &i = 1, 2, \ldots, n-2,\end{aligned} \tag{6}$$

where $c \ge 0$ is a constant.

Remark 5. It is noted that the condition (6) was widely used in the synthesis of nonlinear triangular systems in the literatures[18−20].

In the following, we consider the state feedback controller design for system (5).

Theorem 3. Under the Assumption 1, constants $a_i\,(i = 1, 2, \ldots, n)$ and r can be chosen, such that the system (5) is globally asymptotically stable by a linear state feedback controller of the form

$$u = -\sum_{i=1}^{n}\left(\frac{a_i}{r^{n-i+1}}x_i\right).$$

Proof. For the convenience of readers, we divide the proof into two parts.

Part 1. State transformation of nonlinear system.

Introduce a state transformation for (5):

$$z_i = \frac{x_i}{r^{n-i+1}}, \quad i = 1, 2, \ldots, n, \tag{7}$$

where $r > 1$ is a parameter to be determined later. System (5) can be converted into the following system:

$${}_0^C D_t^\alpha z = \frac{1}{r}\Omega z + \frac{1}{r}Gu + \Phi, \tag{8}$$

where

$$z=\begin{pmatrix} z_1\\ z_2\\ \vdots\\ z_{n-1}\\ z_n\end{pmatrix},\quad \Omega=\begin{pmatrix} 0 & 1 & 0 & \cdots & 0\\ 0 & 0 & 1 & \cdots & 0\\ \vdots & \vdots & \vdots & \ddots & \vdots\\ 0 & 0 & 0 & \cdots & 1\\ 0 & 0 & 0 & \cdots & 0\end{pmatrix},$$

$$G=\begin{pmatrix} 0\\ 0\\ \vdots\\ 0\\ 1\end{pmatrix},\quad \Phi=\begin{pmatrix} \frac{\phi_1}{r^n}\\ \frac{\phi_2}{r^{n-1}}\\ \vdots\\ \frac{\phi_{n-2}}{r^3}\\ 0\\ 0\end{pmatrix}.$$

Let $a_j>0$ $(j=1,2,\ldots,n)$ be coefficients of the Hurwitz polynomial

$$q(s)=s^n+a_ns^{n-1}+\cdots+a_2s+a_1.$$

Next, choose $r>1$ such that the closed-loop system (8) with

$$u=-(a_1z_1+a_2z_2+\cdots+a_nz_n) \tag{9}$$

is globally asymptotically stable at the equilibrium $z=0$.

The closed-loop system consisting of (8) and (9) is

$${}_0^CD_t^\alpha z=\frac{1}{r}Az+\Phi, \tag{10}$$

where

$$A=\begin{pmatrix} 0 & 1 & 0 & \cdots & 0\\ 0 & 0 & 1 & \cdots & 0\\ \vdots & \vdots & \vdots & \ddots & \vdots\\ 0 & 0 & 0 & \cdots & 1\\ -a_1 & -a_2 & -a_3 & \cdots & -a_n\end{pmatrix}.$$

Up to now, the problem of designing controller for (5) is converted into that of finding an appropriate r, such that the system (10) is asymptotically stable at $z=0$.

Part 2. Stability analysis.

Since $q(s)$ is a Hurwitz polynomial, it can be concluded that A is a stable matrix. Therefore, there exists a positive definite matrix $P>0$ such that

$$PA+A^{\rm T}P=-I.$$

Choose Lyapunov function $V=z^{\rm T}Pz$. Observing Assumption 1, the change of coordinate (7) and $r>1$, gives, for any $i(i=1,2,\ldots,n-2)$,

$$\begin{aligned}\left|\frac{\phi_i}{r^{n-i+1}}\right| &\le \frac{c}{r^{n-i+1}}(|x_{i+2}|+|x_{i+3}|+\cdots+|x_n|)\\ &\le \frac{c}{r^2}\sum_{j=1}^{n}\frac{|x_j|}{r^{n-j+1}}\\ &=\frac{c}{r^2}\sum_{i=1}^{n}|z_j|\le\frac{c\sqrt{n}}{r^2}\|z\|.\end{aligned}$$

Hence,

$$\begin{aligned}{}_0^CD_t^\alpha V\big|_{(10)} &= {}_0^CD_t^\alpha\left(z^{\rm T}Pz\right)\\ &\le \left({}_0^CD_t^\alpha z\right)^{\rm T}Pz+z^{\rm T}P{}_0^CD_t^\alpha z\\ &=(\frac{1}{r}Az+\Phi)^{\rm T}Pz+z^{\rm T}P(\frac{1}{r}Az+\Phi)\\ &\le -\frac{1}{r}\|z\|^2+2\|z\|\cdot\|P\|\cdot\|\Phi\|\\ &\le -\frac{1}{r}\|z\|^2+2\|z\|\cdot\|P\|(\frac{c\sqrt{n}}{r^2}\|z\|)\\ &\quad\cdot\left\|(1,1,\cdots,1,0,0)^{\rm T}\right\|\\ &\le -\frac{1}{r}\|z\|^2+\frac{2nc}{r^2}\|P\|\cdot\|z\|^2\\ &=-\frac{1}{r^2}\left(r-2nc\|P\|\right)\cdot\|z\|^2.\end{aligned}$$

Choose

$$r>\max\{1,2nc\|P\|+\eta\},$$

where $\eta>0$. By Lemma 4, we can get ${}_0^CD_t^\alpha V\big|_{(10)}<-\frac{\eta}{r^2}\|z\|^2$ which indicates that (10) is asymptotically stable at $z=0$. Therefore, the closed-loop system consisting of (8) and (9) is asymptotically stable at $z=0$.

Noticing (9) and the change of coordinate (7), we can get the state feedback controller of system (5):

$$u=-\frac{1}{r^n}\left(a_1x_1+a_2rx_2+a_3r^2x_3+\cdots+a_nr^{n-1}x_n\right).$$

□

Remark 5. The conclusion of Theorem 3 also holds for the following fractional order nonlinear system:

$$\begin{cases} {}_0^CD_t^\alpha x_1(t)=d_1x_2(t)+\phi_1(t,x(t)),\\ {}_0^CD_t^\alpha x_2(t)=d_2x_3(t)+\phi_2(t,x(t)),\\ \qquad\vdots\\ {}_0^CD_t^\alpha x_{n-2}(t)=d_{n-2}x_{n-1}(t)+\phi_{n-2}(t,x(t)),\\ {}_0^CD_t^\alpha x_{n-1}(t)=d_{n-1}x_n(t),\\ {}_0^CD_t^\alpha x_n(t)=d_nu(t),\end{cases} \tag{11}$$

where $d_i,\ i=1,2,\ldots,n$ are known nonzero real constants. In fact, by introducing an appropriate state transformation, system (11) can be converted into another system having the same form as system (5).

Remark 6. It should be pointed out that the recent novel work presented in [21] investigated the state feedback H_∞ control problem for commensurate fractional order linear time-invariant systems. When $w=0$, the system (3) in [21] is reduced to the general fractional order linear system. The advantage of [21] was dealing with exogenous disturbance input w for commensurate linear fractional order systems by introducing a new flexible matrix variable. Compared with [21], the main feature of this paper is to deal with the nonlinear terms in fractional order nonlinear systems by the Lyapunov function method (also see Remark 8).

V. EXAMPLE

In this section, we present an example to illustrate the main results.

Example 1. Consider the following fractional order nonlinear system:

$$\begin{cases} {}_0^C D_t^\alpha x_1 = x_2 + \frac{\sin x_1}{7+7e^{-t}} x_3, \\ {}_0^C D_t^\alpha x_2 = x_3, \\ {}_0^C D_t^\alpha x_3 = u, \end{cases} \tag{12}$$

where $\alpha \in (0, 1]$.

It is easy to see that Assumption 1 is satisfied with $c = 1/7$.

Let $a_j > 0,\ j = 1, 2, 3$ be the coefficients of the Hurwitz polynomial

$$q(s) = s^3 + a_3 s^2 + a_2 s + a_1.$$

Choose $a_1 = 6$, $a_2 = 11$, $a_3 = 6$. Then

$$A = \begin{pmatrix} 0 & 1 & 0 \\ 0 & 0 & 1 \\ -6 & -11 & -6 \end{pmatrix}.$$

Solving the Lyapunov equation

$$A^{\mathrm{T}} P + PA = -I$$

leads to

$$P = \begin{pmatrix} 23/15 & -1/2 & -7/10 \\ -1/2 & 7/10 & -1/2 \\ -7/10 & -1/2 & 17/10 \end{pmatrix} > 0.$$

Choose $r = 2 > 6c\|P\| = 1.9911$, we can get the linear state feedback controller for the system (12),

$$u = -\frac{6}{r^3} x_1 - \frac{11}{r^2} x_2 - \frac{6}{r} x_3. \tag{13}$$

Figure 1 shows the state response of the closed-loop system consisting of (12) and (13) with $\alpha = 0.8$ for the initial condition $(x_1(0), x_2(0), x_3(0)) = (1, 4, 3)$, which clearly demonstrates the asymptotic stability of the closed-loop system.

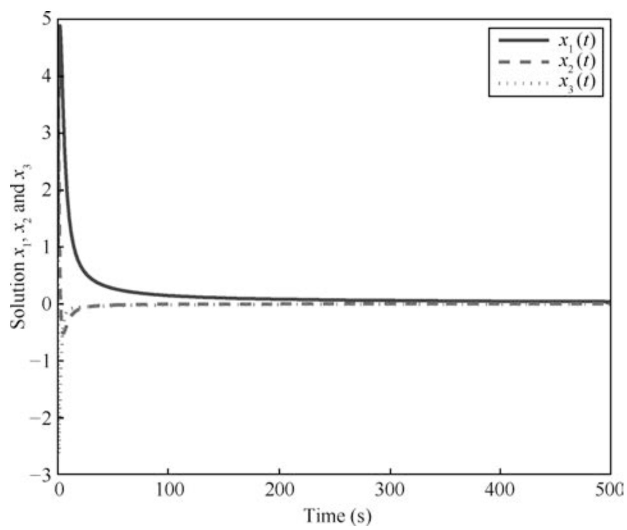

Fig. 1 The state of the closed-loop system consisting of (12) and (13) with $\alpha = 0.8$.

Remark 7. In Example 1, the nonlinear terms $\left|\frac{\sin x_1}{7+7e^{-t}} x_3\right| < \frac{1}{7}|x_3|$, which implies that the condition (6) is satisfied with $c = 1/7$.

Remark 8. In Example 1, we can easily deal with the nonlinear terms "$\frac{\sin x_1}{7+7e^{-t}} x_3$" by the method presented in this paper. However, it is clear that one cannot deal with these nonlinear terms by the method presented in [21].

VI. CONCLUSION

In this paper, we have investigated the design of state feedback stabilization controllers for fractional order nonlinear systems in upper triangular form by the Lyapunov function method. We have presented some new properties for Caputo fractional derivative to allow finding a simple Lyapunov candidate function for many fractional order systems. As an application, we have given a sufficient condition of asymptotical stability for fractional order nonlinear systems based on the new properties. By introducing appropriate transformations of coordinates, we have converted the problem of controller design into the problem of finding some parameters, which could be certainly obtained by solving the Lyapunov equation and relevant matrix inequalities. In addition, based on the Lyapunov function method, asymptotical stability for closed-loop systems has been considered by designing state feedback stabilization controllers for fractional order nonlinear systems in upper triangular form. The study of an illustrative example has shown that the new results presented in this paper are very effective.

REFERENCES

[1] Podlubny I. *Fractional Differential Equations*. New York: Academic Press, 1998.

[2] Kilbas A A, Srivastava H H, Trujillo J J. *Theory and Applications of Fractional Differential Equations*. Amsterdam: Elsevier Science, 2006.

[3] Manabe S. The non-integer integral and its application to control systems. *Electrotechnical Journal of Japan*, 1961, **6**(3−4): 83−87

[4] Ahn H S, Chen Y Q, Podlubny I. Robust stability test of a class of linear time-invariant interval fractional-order system using Lyapunov inequality. *Applied Mathematics and Computation*, 2007, **187**(1): 27−34

[5] Tavazoei M S, Haeri M. A note on the stability of fractional order systems. *Mathematics and Computers in Simulation*, 2009, **79**(5): 1566−1576

[6] Chen Y Q, Ahn H S, Xue D Y. Robust controllability of interval fractional order linear time invariant systems. *Signal Processing*, 2006, **86**(10): 2794−2802

[7] Daftardar-Gejji V, Babakhani A. Analysis of a system of fractional differential equations. *Journal of Mathematical Analysis and Applications*, 2004, **293**(2): 511−522

[8] Yu Y, Jiao Z, Sun C Y. Sufficient and necessary condition of admissibility for fractional-order singular system. *Acta Automatica Sinica*, 2013, **39**(12): 2160−2164

[9] Lazarevic M P, Spasic A M. Finite-time stability analysis of fractional order time-delay systems: Gronwall's approach. *Mathematical and Computer Modelling*, 2009, **49**(3−4): 475−481

[10] Shen J, Lam J. Non-existence of finite-time stable equilibria in fractional-order nonlinear systems. *Automatica*, 2014, **50**(2): 547−551

[11] Lakshmikantham V, Leela S, Sambandham M. Lyapunov theory for fractional differential equations. *Communications in Applied Analysis*, 2008, **12**(4): 365−376

[12] Burton T A. Fractional differential equations and Lyapunov functionals. *Nonlinear Analysis: Theory, Methods & Applications*, 2011, **74**(16): 5648−5662

[13] Si-Ammour A, Djennoune S, Bettayeb M. A sliding mode control for linear fractional systems with input and state delays. *Communications in Nonlinear Science and Numerical Simulation*, 2009, **14**(5): 2310−2318

[14] Kamal S, Raman A, Bandyopadhyay B. Finite-time stabilization of fractional order uncertain chain of integrator: an integral sliding mode approach. *IEEE Transactions on Automatic Control*, 2013, **58**(6): 1597−1602

[15] Li Y, Chen Y Q, Podlubny I. Mittag-Leffler stability of fractional order nonlinear dynamic systems. *Automatica*, 2009, **45**(8): 1965−1969

[16] Li Y, Chen Y Q, Podlubny I. Stability of fractional-order nonlinear dynamic systems: Lyapunov direct method and generalized Mittag-Leffler stability. *Computers and Mathematics with Applications*, 2010, **59**(5): 1810−1821

[17] Aguila-Camacho N, Duarte-Mermoud M A, Gallegos J A. Lyapunov functions for fractional order systems. *Communications in Nonlinear Science and Numerical Simulation*, 2014, **19**(9): 2951−2957

[18] Qian C J, Lin W. Output feedback control of a class of nonlinear systems: a nonseparation principle paradigm. *IEEE Transactions on Automatic Control*, 2002, **47**(10): 1710−1715

[19] Choi H L, Lim J T. Global exponential stabilization of a class of nonlinear systems by output feedback. *IEEE Transactions on Automatic Control*, 2005, **50**(2): 255−257

[20] Zhang X F, Cheng Z L. Output feedback stabilization of nonlinear systems with delays in the input. *Applied Mathematics and Computation*, 2005, **167**(2): 1026−1040

[21] Shen J, Lam J. State feedback H_∞ control of commensurate fractional-order systems. *International Journal of Systems Science*, 2014, **45**(3): 363−372

Yige Zhao received the B. S. and M. S. degrees from the School of Mathematical Sciences, University of Jinan, China, in 2008 and 2011, respectively, and the Ph. D. degree from the School of Control Science and Engineering, Shandong University in 2016. Since 2016, he has been with the School of Mathematical Sciences, University of Jinan, China, where he is currently an assistant professor. His research interests include fractional order system, triangular system, and time delay systems. Corresponding author of this paper.

Yuzhen Wang graduated from Tai'an Teachers College in 1986, received his M. S. degree from Shandong University of Science and Technology in 1995 and his Ph.D. degree from the Institute of Systems Science, Chinese Academy of Sciences in 2001. Since 2003, he is a professor with the School of Control Science and Engineering, Shandong University, China, and now the Dean of the School of Control Science and Engineering, Shandong University. From 2001 to 2003, he worked as a Postdoctoral Fellow in Tsinghua University, Beijing, China. From Mar. 2004 to Jun. 2004, from Feb. 2006 to May 2006 and from Nov. 2008 to Jan. 2009, he visited City University of Hong Kong as a Research Fellow. From Sept. 2004 to May 2005, he worked as a visiting Research Fellow at the National University of Singapore. His research interests include nonlinear control systems, Hamiltonian systems and Boolean networks. Prof. Wang received the Prize of Guan Zhaozhi in 2002, the Prize of Huawei from the Chinese Academy of Sciences in 2001, the Prize of Natural Science from Chinese Education Ministry in 2005, and the National Prize of Natural Science of China in 2008. Currently, he is an associate editor of IMA Journal of Math Control and Inform., and a Technical Committee member of IFAC (TC2.3).

Haitao Li received the B. S. and M. S. degrees from the School of Mathematical Science, Shandong Normal University in 2007 and 2010, respectively, and the Ph.D. degree from the School of Control Science and Engineering, Shandong University in 2014. Since 2015, he has been with the School of Mathematical Science, Shandong Normal University, China, where he is currently an associate professor. From Jan. 2014 to Jan. 2015, he worked as a Research Fellow in Nanyang Technological University, Singapore. His research interests include logical dynamic systems, switched systems, etc. He received the Prize of Best Student Paper Award at the 10th World Congress on Intelligent Control and Automation, and the Prize of Guan Zhaozhi at the 31st Chinese Control Conference.

Synthesis of Fractional-order PI Controllers and Fractional-order Filters for Industrial Electrical Drives

Paolo Lino, *Member, IEEE,* Guido Maione, *Senior Member, IEEE,* Silvio Stasi, Fabrizio Padula, and Antonio Visioli, *Senior Member, IEEE*

***Abstract*—This paper introduces an electrical drives control architecture combining a fractional-order controller and a set-point pre-filter. The former is based on a fractional-order proportional-integral (PI) unit, with a non-integer order integral action, while the latter can be of integer or non-integer type. To satisfy robustness and dynamic performance specifications, the feedback controller is designed by a loop-shaping technique in the frequency domain. In particular, optimality of the feedback system is pursued to achieve input-output tracking. The set-point pre-filter is designed by a dynamic inversion technique minimizing the difference between the ideal synthesized command signal (i.e., a smooth monotonic response) and the pre-filter step response. Experimental tests validate the methodology and compare the performance of the proposed architecture with well-established control schemes that employ the classical PI-based symmetrical optimum method with a smoothing pre-filter.**

***Index Terms*—Dynamic inversion, electrical drives, fractional-order PI controller, loop-shaping, set-point pre-filter.**

I. Introduction

IN the last two decades, the applications of fractional calculus spread across several engineering fields [1], [2], ranging from control systems [3], [4] to electrical circuits [5], to signal processing and communications [6]−[8], to antennas and propagation [9], [10], etc. In particular, several efforts aimed to take advantage of fractional differentiation/integration for developing effective and easy-to-use control design methods and tuning techniques [11]. Frequently, the innovations are based on the idea of extending the proportional-integral-derivative (PID) controllers by differential or integral operators of non-integer order [12].

Manuscript received November 3, 2015; accepted April 1, 2016. Fabrizio Padula's research contributing to these results has been partially supported by the Australian Research Council (DP160104994). Recommended by Associate Editor Dingyü Xue.

Citation: P. Lino, G. Maione, S. Stasi, F. Padula, and A. Visioli, "Synthesis of fractional-order PI controllers and fractional-order filters for industrial electrical drives," *IEEE/CAA Journal of Automatica Sinica*, vol. 4, no. 1, pp. 58−69, Jan. 2017.

P. Lino, G. Maione, and S. Stasi are with the Dipartimento di Ingegneria Elettrica e dell'Informazione, Politecnico di Bari, Bari I-70125, Italy (e-mail: paolo.lino@poliba.it; guido.maione@poliba.it; silvio.stasi@poliba.it).

F. Padula is with the Department of Mathematics and Statistics, Curtin University, Perth WA6102, Australia (e-mail: fabrizio.padula@curtin.edu.au).

A. Visioli is with the Department of Mechanical and Industrial Engineering, University of Brescia, Brescia 25123, Italy (e-mail: antonio.visioli@unibs.it).

Color versions of one or more of the figures in this paper are available online at http://ieeexplore.ieee.org.

Digital Object Identifier 10.1109/JAS.2017.7510325

These controllers are often named fractional-order controllers (FOC), where the order of differentiation and integration can be any non-integer number, even complex [13]. However, to be successful in industrial applications, the FOC must compete with the wide diffusion of PID controllers [14]. Namely, it is well-known that FOC may guarantee superior robustness and dynamic performance indexes with respect to PID, especially if the controlled plants are themselves modeled as fractional-order systems [15]. However, affordable realizations are required for low-cost implementation. To this aim, the irrational transfer functions of FOC must be approximated by rational transfer functions. Then, efficient, easy-to-use, and convenient realization techniques are necessary. Indeed a good trade-off between accuracy and efficiency would be a great benefit for many industrial control loops using PID [14].

Regarding robust control systems, the seminal Bode's idea is to approximate an ideal loop gain ω_c/s^ν as much as possible. This transfer function includes an integrator of non-integer (fractional) order ν and the gain crossover angular frequency ω_c [11], [12], [16], [17]. The solutions based on integration of non-integer order reduce the sensitivity of the control loop to gain variations and to parametric uncertainties and achieve a better disturbance rejection. However, to be more accepted in industry, the FOC must easily achieve good time- or frequency-domain performance specifications and improve the robustness guaranteed by PID-based solutions. On the other hand, to obtain the same robustness of FOC, often more complex high integer-order controllers are necessary.

Hence this paper analyzes the benefits and limits of a new scheme with fractional-order PI (FOPI) controllers and fractional-order filters. The control scheme is tested on real electrical drives, that are important constituent parts of many industrial control systems. There are many approaches to design and then realize FOC (e.g., see [11], [12], [17]−[20]). In this paper, a new methodology is proposed to combine: 1) a loop-shaping strategy to design a feedback FOPI controller and 2) an input-output inversion technique to design an integer or non-integer order set-point pre-filter. The main contributions are the following ones:

1) extending the symmetrical optimum tuning method for classical PI to the FOPI counterparts, i.e., extending a well-known and widely used method to FOPI to make easier the acceptance from the industrial drives area;

2) extending, in this context, the standard combination of

the PI with a smoothing pre-filter to the combination of the FOPI with an integer- or fractional-order pre-filter.

The proposed solution improves the control dynamic performance and disturbance rejection. Then, it may help reducing the issues depending on control efforts, energy consumption to compensate disturbances. Moreover, the control architecture implies a simple updating of the usually employed elements (i.e., a FOPI replaces a PI controller and a fractional-order filter replaces a smoothing filter). The limitations could be determined by the practical implementation of the irrational transfer functions. The orders of realization, however, are kept low both in the controller and in the pre-filter.

The rest of the paper is organized as follows. Section II provides background on the considered electrical drives. Section III describes the approach to design the FOPI controller and Section IV illustrates the design of set-point pre-filters. Section V shows results of experimental tests. Finally, Section VI draws the conclusions.

II. The Modeled Electrical Systems

Many industrial loops employ permanent magnet DC-motors or permanent magnet synchronous motor (PMSM) drives. Hence, in this paper, these two systems are test beds for measuring the performance obtained by the proposed control architecture. This section briefly recalls the respective characteristics, properties, and operation and presents sufficiently accurate mathematical system models.

A. The DC-motor

The DC-motor armature voltage equations are given by:

$$v_a \,=\, R_a\,(1+T_a\,p)\,i_a + K_v\,\Phi\,\omega_r \tag{1}$$

where R_a, L_a, and $T_a = L_a/R_a$ are the armature winding resistance, inductance, and time constant, respectively; Φ is the constant excitation flux due to permanent magnets or independent field excitation winding; v_a, i_a and e_a are the armature voltage, current, and back-electromotive force, respectively; finally ω_r is the rotor speed, K_v is the voltage constant and $p = d/dt$. The mechanical equations are:

$$J\,p\,\omega_r \,=\, C_e - B\,\omega_r - C_L \quad\text{and}\quad p\,\theta_r \,=\, \omega_r \tag{2}$$

where $C_e = K_v\,\Phi\,i_a$ is the electromagnetic torque developed by the motor, J is the inertia moment of the rotor and connected load, B is the viscous friction coefficient, C_L is the external load torque, and θ_r is the rotor position. In the Laplace-transform s-domain, the previous equations become:

$$\begin{aligned} I_a &= \frac{\frac{1}{R_a}}{1+T_a\,s}\,(V_a - K_v\,\Phi\,\Omega_r) \\ \Omega_r &= \frac{1}{J\,s+B}\,(C_e - C_L) \Rightarrow \Theta_r = \frac{1}{s(Js+B)}(C_e - C_L). \end{aligned} \tag{3}$$

Taking into account the static friction, the mechanical model can be extended by including a pure time delay ϑ.

B. The PMSM Drive

The PMSM drives voltage equations in the d-q rotor reference frame are [21]:

$$\begin{aligned} v_{s,d} &= R_s\,i_{s,d} + L_{s,d}\,\frac{di_{s,d}}{dt} - \omega_r\,L_{s,q}\,i_{s,q} \\ v_{s,q} &= R_s\,i_{s,q} + L_{s,q}\,\frac{di_{s,q}}{dt} + \omega_r\,(L_{s,d}\,i_{s,d} + \Psi_{PM}) \end{aligned} \tag{4}$$

where $v_{s,d}$, $v_{s,q}$, $i_{s,d}$ and $i_{s,q}$ are the stator voltage and current vector d-q components, R_s is the resistance of each stator phase, $L_{s,d}$ and $L_{s,q}$ are the d- and q-axis stator inductances, Ψ_{PM} is the permanent magnet flux linked to the stator windings, and ω_r is the electrical motor speed.

The electromagnetic torque developed by the motor is:

$$C_e \,=\, 1.5\,n_p\,[\Psi_{PM}\,i_{s,q} + (L_{s,d} - L_{s,q})\,i_{s,q}\,i_{s,d}] \tag{5}$$

where n_p is the number of pole pairs. In case of superficial PMSM, magnetic isotropy leads to $L_{s,d} = L_{s,q}$. Then C_e does not contain the term due to saliency (reluctance torque):

$$C_e \,=\, 1.5\,n_p\,\Psi_{PM}\,i_{s,q} \,=\, K_c\,i_{s,q}. \tag{6}$$

Equations (4) show the dynamic coupling between the two axes. Independent control requires the coupling terms to be compensated by injecting feed-forward decoupling signals:

$$\begin{aligned} v_{s,dcomp} &= -\omega_r\,L_{s,q}\,i_{s,q} \\ v_{s,qcomp} &= \omega_r\,(L_{s,d}\,i_{s,d} + \Psi_{PM}). \end{aligned} \tag{7}$$

Thus the control system will give the reference signals of d-q voltages as follows:

$$\begin{aligned} v^*_{s,d} &= v_{s,d} + \omega_r L_{s,q} i_{s,q} = R_s i_{s,d} + L_{s,d}\frac{di_{s,d}}{dt} \\ v^*_{s,q} &= v_{s,q} - \omega_r (L_{s,d} i_{s,d} + \Psi_{PM}) = R_s i_{s,q} + L_{s,q}\frac{di_{s,q}}{dt}. \end{aligned} \tag{8}$$

In the Laplace-transform s-domain, (8) becomes:

$$\begin{aligned} V^*_{s,d} &= (R_s + L_{s,d}\,s)\,I_{s,d} \,=\, R_s\,(1+T_d\,s)\,I_{s,d} \\ V^*_{s,q} &= (R_s + L_{s,q}\,s)\,I_{s,q} \,=\, R_s\,(1+T_q\,s)\,I_{s,q} \end{aligned} \tag{9}$$

where $T_d = T_q$ for superficial PMSM.

The PMSM is controlled by two inner loops for the d- and q-axis current components, and an outer loop for rotor speed (Fig. 1). The d-axis current reference signal is set equal to zero, by the maximum torque per ampere criterion for a superficial PMSM. Moreover, time delays associated with several necessary operations are represented as first-order systems with small time constants. If T_c is the sampling period, delays are due to: signal sampling ($T_c/2$) and holding ($T_c/2$), inverter operation ($T_c/2$), computation of the control algorithm (T_c), and speed (τ_{sp}) and current (τ_L) measurement. Note that k_{inv} is the converter static gain. Fig. 2 shows the block diagram for both the d- and q- axis current control loops.

The open-loop transfer function of both the current control loops is simplified by considering an equivalent unitary feedback loop and by summing up all the small time constants in $\tau_{\Sigma i} = 5T_c/2 + \tau_L$. The current PI controller $G_{PI_{isq}}(s) = K_{isq}(1+\tau_{isq}s)/\tau_{isq}s$ is designed by applying the zero-pole cancelation to the plant pole and the absolute value optimum criterion [22]. The controller parameters are given by

$$\tau_{isq} \,=\, T_d \,=\, T_q \quad\text{and}\quad K_{isq} \,=\, \frac{R_s\,\tau_{isq}}{2\,k_{inv}\,\tau_{\Sigma i}} \tag{10}$$

and the closed-loop transfer function of the inner loop is

$$G_{0,isq}(s) \,=\, \frac{1}{1-\tau_L s}\,\frac{1}{1-\frac{T_c}{2}s}\,\frac{1}{1+2\,\tau_{\Sigma i}\,s+2\,\tau_{\Sigma i}^2\,s^2} \tag{11}$$

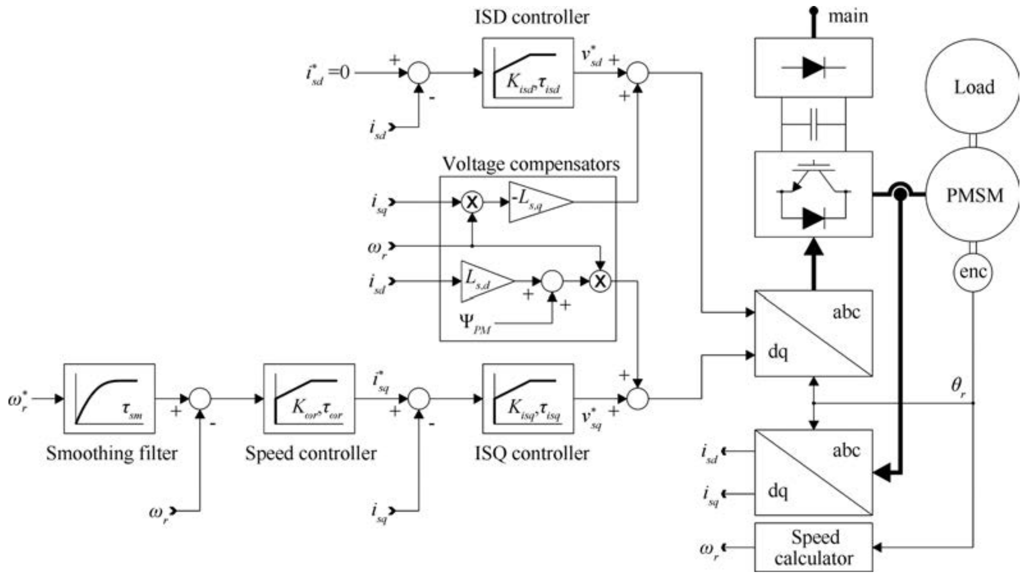

Fig. 1. Scheme of the vector controlled PMSM drive.

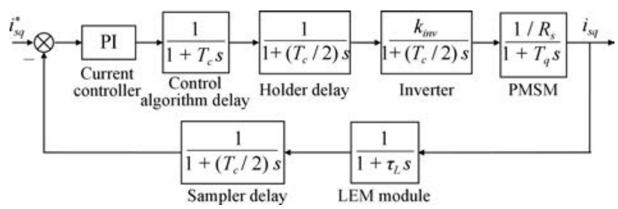

Fig. 2. Scheme of the q-axis current control loop.

where the first two factors respectively approximate $(1+\tau_L s)$ and $(1+T_c s/2)$. Namely, these last terms are originated by the equivalent representation with unitary feedback to include the time delays τ_L and $T_c/2$, respectively, in the forward path.

The block diagram implementing the speed control loop is shown in Fig. 3. The open-loop transfer function for speed control is simplified by neglecting the very small term $2\,\tau_{\Sigma i}^2\,s^2$ and by summing up all the small time constants $\tau_{\Sigma\omega} = 44\,T_c/2 + 44\,T_c - T_c/2 - \tau_L + 2\,\tau_{\Sigma i} + \tau_{sp}$. Note that the coefficients in the previous formula are determined by a sampling in the outer speed loop different from the inner current loop. Then the process transfer function is

$$G_{p,\omega r}(s) \;=\; \frac{K_c\,n_p}{J\,s\,(1+\tau_{\Sigma\omega}\,s)}. \tag{12}$$

The usual choice for speed control is to tune an integer-order PI controller $G_{PI_{\omega r}}(s) = K_{\omega r}(1+\tau_{\omega r}\,s)/\tau_{\omega r}\,s$ by the symmetrical optimum criterion [23], [24]. The method is based on tuning the controller parameters as:

$$\tau_{\omega r} \;=\; 4\,\tau_{\Sigma\omega} \;\text{ and }\; K_{\omega r} \;=\; \frac{J}{2\,\tau_{\Sigma\omega}\,K_c\,n_p}. \tag{13}$$

The word "symmetrical" refers to the obtained symmetry of the compensated Bode diagram with respect to the gain crossover. The word "optimum" refers to the higher ability of disturbance rejection. Moreover, a smoothing first order filter with a time constant in $(4\,\tau_{\Sigma\omega}, 4.8\,\tau_{\Sigma\omega})$ lowers the overshoot.

III. Fractional-order PI Controller Design

A. The Design Approach

The initial assumption is that both DC-motors and PMSM drives are modeled as first-order systems with an integrator

$$G_p(s) \;=\; \frac{K}{s\,(1+T\,s)} \tag{14}$$

which is common when controlling position of DC-motors (see (3)) and speed of PMSM drives (see (12)), respectively, and is suitable for many industrial applications. In case of DC-motor speed control, the plant transfer function is

$$G_p(s) \;=\; \frac{K}{1+T\,s}. \tag{15}$$

All the elements in the control loop introduce delays that are associated with an equivalent time constant, which is indicated by T and is obtained in Section II.

A fractional-order PI controller, FOPI for short, also named PI^{ν} controller, is used. The integrator is of non-integer order ν. A FOPI controller is chosen because it is the closest one to the standard integer-order PI controller that is applied in most industrial control loops. The FOPI transfer function is

$$G_c(s) \;=\; K_P + \frac{K_I}{s^{\nu}} \;=\; \frac{K_I\,(1+T_I\,s^{\nu})}{s^{\nu}} \tag{16}$$

where K_P and K_I are the proportional and integral gain, respectively, and $T_I = K_P/K_I$. Moreover, the non-integer order is $1<\nu<2$, such that $1/s^{\nu} = (1/s)\cdot(1/s^{\mu})$, with $\mu = \nu - 1$ and $0<\mu<1$. Then, the integer order integrator $1/s$ rejects common torque disturbances on the motor input, and the residual non-integer order integrator is given by the operator $1/s^{\mu}$. For practical implementation, the irrational transfer function is approximated as shown in Section III-B.

The open-loop transfer function $G(s) = G_c(s)\,G_p(s)$ is

$$G(s) \;=\; \begin{cases} a: \dfrac{K\,K_I\,(1+T_I s^{\nu})}{s^{\nu+1}\,(1+Ts)} & \text{with plant (14)} \\ b: \dfrac{K\,K_I\,(1+T_I s^{\nu})}{s^{\nu}\,(1+Ts)} & \text{with plant (15).} \end{cases} \tag{17}$$

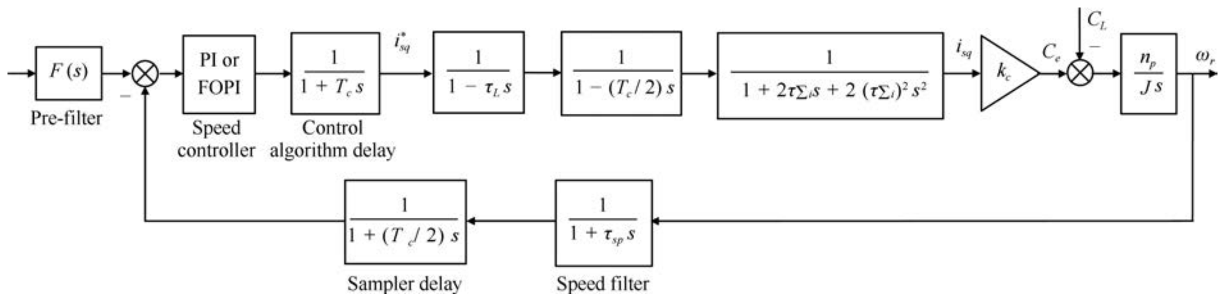

Fig. 3. Scheme of the speed control loop: the reference is given by the employed pre-filter, which is a smoothing one with an integer-order PI, an integer- or fractional-order pre-filter with a FOPI.

The controller is designed to obtain superior robustness to parametric variations and to achieve a nearly optimal feedback system [25]. Let us first consider the robustness requirement. To this aim, the non-integer integrator must lead to the fractal robustness. In other words, the open-loop frequency response (OLFR) must be characterized by a nearly flat phase diagram and a constant slope of the magnitude diagram in a sufficiently wide interval around the gain crossover frequency. To this aim, the fractional integrator provides a constant phase plot of $-\nu\pi/2$ and a magnitude plot with slope of -20ν dB/decade. Then replacing $s = j\omega$ yields the OLFR $G(j\omega)$ and the phase function $\angle G(j\omega)$ which must guarantee the robustness specification by imposing the desired phase margin at the crossover frequency, say ω_c. This ensures a stable performance despite parameter variations.

Regarding the optimality, consider the closed-loop frequency response $G_{cl}(j\omega) = 1/(1+G^{-1}(j\omega))$. It is well-known that a feedback system is optimal if and only if the magnitude of the return difference $|1 + G^{-1}(j\omega)|$ is unitary for all frequencies [26]. In this condition, indeed, a perfect input/output tracking is achieved, whichever is the input signal. Unfortunately, this condition cannot be satisfied by real systems. Moreover, since $|G(j\omega)| \gg 1$ may lead to instability, the OLFR is shaped around ω_c so that the gain is high at low frequency and rolls off at high frequency. Then, the optimal requirement is only approximated in a specified bandwidth, say ω_B, in which it is desired to achieve a good tracking performance.

To start with, consider the OLFR given by

$$G(j\omega) = \begin{cases} a: \dfrac{K\,K_I\,\left[1 + T_I\,\omega^{\nu}\,(C + j\,S)\right]}{\omega^{\nu+1}(-S + j\,C)\,(1 + j\omega T)} \\[2ex] b: \dfrac{K\,K_I\,\left[1 + T_I\,\omega^{\nu}\,(C + j\,S)\right]}{\omega^{\nu}\,(C + j\,S)\,(1 + j\,\omega\,T)} \end{cases} \tag{18}$$

with $C = \cos(\pi\nu/2)$ and $S = \sin(\pi\nu/2)$, which can be expressed in terms of a normalized angular frequency $\overline{\omega} = \omega\,T$:

$$G(j\overline{\omega}) = \begin{cases} a: \dfrac{K\,K_I\,\left[1 + T_I\,\left(\frac{\overline{\omega}}{T}\right)^{\nu}\,(C + j\,S)\right]}{\left(\frac{\overline{\omega}}{T}\right)^{\nu+1}\,(-S + j\,C)\,(1 + j\,\overline{\omega})} \\[2ex] b: \dfrac{K\,K_I\,\left[1 + T_I\,\left(\frac{\overline{\omega}}{T}\right)^{\nu}\,(C + j\,S)\right]}{\left(\frac{\overline{\omega}}{T}\right)^{\nu}\,(C + j\,S)\,(1 + j\,\overline{\omega})}. \end{cases} \tag{19}$$

Then the magnitude of the OLFR is given by

$$|G(j\overline{\omega})| = \begin{cases} a: \dfrac{K\,K_I}{\left(\frac{\overline{\omega}}{T}\right)^{\nu+1}} \sqrt{\dfrac{1 + 2\,T_I\,\left(\frac{\overline{\omega}}{T}\right)^{\nu}\,C + T_I^2\,\left(\frac{\overline{\omega}}{T}\right)^{2\nu}}{1 + \overline{\omega}^2}} \\[2ex] b: \dfrac{K\,K_I}{\left(\frac{\overline{\omega}}{T}\right)^{\nu}} \sqrt{\dfrac{1 + 2\,T_I\,\left(\frac{\overline{\omega}}{T}\right)^{\nu}\,C + T_I^2\,\left(\frac{\overline{\omega}}{T}\right)^{2\nu}}{1 + \overline{\omega}^2}} \end{cases} \tag{20}$$

and the phase of the OLFR is given by

$$\angle G(j\overline{\omega}) = \begin{cases} a: \varphi_1(\overline{\omega}) - \varphi_2(\overline{\omega}) - \dfrac{\pi(\nu+1)}{2} \\[2ex] b: \varphi_1(\overline{\omega}) - \varphi_2(\overline{\omega}) - \dfrac{\pi\nu}{2} \end{cases} \tag{21}$$

where $\varphi_1(\overline{\omega}) = \tan^{-1}\left(T_I S\left(\frac{\overline{\omega}}{T}\right)^{\nu}/(1 + T_I C\left(\frac{\overline{\omega}}{T}\right)^{\nu})\right)$ and $\varphi_2(\overline{\omega}) = \tan^{-1}(\overline{\omega})$.

Now, the design procedure begins with choosing the bandwidth $\overline{\omega}_B = \omega_B T$ where input/output tracking is desired. The value $\overline{\omega}_B$ is chosen higher than the plant bandwidth. Moreover, as it will be shown below, the integral time constant T_I depends on $\overline{\omega}_B$. So, $T_I > 0$ must hold true for a stable controller. More in details, $\overline{\omega}_B$ was maximized after a trial-and-error procedure. It is also remarked that maximizing $\overline{\omega}_B$ reduces the rise time of the closed-loop response, but it also increases the crossover $\overline{\omega}_c$, which could be shifted too much with respect to a centered position in the range where the phase diagram is flat or slowly changing. Then, a tradeoff must be reached between performance and robustness, as it is usual.

Next, the crossover $\overline{\omega}_c$ is determined by a relation that is commonly used for estimation: $\overline{\omega}_c \in [\overline{\omega}_B/1.7, \overline{\omega}_B/1.3]$ [27], e.g., $\overline{\omega}_c = \overline{\omega}_B/1.5$, but this interval allows changing the value of $\overline{\omega}_c$. Obviously, other methods can be used to set $\overline{\omega}_c$.

Hence, the phase margin specification is enforced as a robustness measure. Since $PM = \pi + \angle G(j\overline{\omega}_c)$, it holds

$$PM = \begin{cases} a: \varphi_1(\overline{\omega}_c) - \varphi_2(\overline{\omega}_c) + \dfrac{\pi(1-\nu)}{2} \\[2ex] b: \varphi_1(\overline{\omega}_c) - \varphi_2(\overline{\omega}_c) + \dfrac{\pi(2-\nu)}{2}. \end{cases} \tag{22}$$

Now, $\varphi_1(\overline{\omega}_c) - \varphi_2(\overline{\omega}_c) = \pi/2$ is set in case a or $\varphi_1(\overline{\omega}_c) - \varphi_2(\overline{\omega}_c) = 0$ is set in case b. These settings introduce a constraint on T_I but give the advantage of a strict, closed-form, and simple relation between the specified phase margin and the required fractional order. Namely, in both cases a and b, the previous settings yield $PM = \pi(2-\nu)/2$. If the specification PM_s is given, then the following relation is established

$$PM_s = (2-\nu)\pi/2 \Leftrightarrow \nu = 2 - 2PM_s/\pi. \tag{23}$$

The introduced constraint yields a closed-form expression that is used as tuning rule for the integral time constant:

$$T_I = \begin{cases} a: \dfrac{-1}{\left(\dfrac{\overline{\omega}_c}{T}\right)^{\nu}(S\,\overline{\omega}_c + C)} \\ b: \dfrac{\overline{\omega}_c}{\left(\dfrac{\overline{\omega}_c}{T}\right)^{\nu}(S - \overline{\omega}_c\,C)}. \end{cases} \tag{24}$$

To set the remaining parameter K_I, the condition $|G^{-1}(j\overline{\omega}_c)|^2 = 1$ uses the gain crossover normalized angular frequency $\overline{\omega}_c$ and leads to another closed-form expression that is exploited as a rule for the integral gain:

$$K_I = \begin{cases} a: \dfrac{1}{K}\left(\dfrac{\overline{\omega}_c}{T}\right)^{\nu+1}\sqrt{\dfrac{1+\overline{\omega}_c^2}{1+2\,T_I\,\left(\frac{\overline{\omega}_c}{T}\right)^{\nu}C + T_I^2\,\left(\frac{\overline{\omega}_c}{T}\right)^{2\nu}}} \\ b: \dfrac{1}{K}\left(\dfrac{\overline{\omega}_c}{T}\right)^{\nu}\sqrt{\dfrac{1+\overline{\omega}_c^2}{1+2\,T_I\,\left(\frac{\overline{\omega}_c}{T}\right)^{\nu}C + T_I^2\,\left(\frac{\overline{\omega}_c}{T}\right)^{2\nu}}} \end{cases} \tag{25}$$

in which T_I is the value given by (24). The proportional gain is $K_P = K_I\,T_I$.

If the plant includes a pure time delay ϑ, i.e., $G_p(s)$ of (14) and (15) is replaced by $G_p(s)\,e^{-\vartheta s}$, or if the control loop is affected by a significant dead-time ϑ, the OLFR becomes $G(j\overline{\omega})\,e^{-j\overline{\omega}\vartheta/T}$. For example, as already mentioned in Section II-A, it is necessary to model the static friction effect of the DC-motor. In this case, the design procedure is easily extended. Namely, the magnitude does not change, whereas the argument is modified as

$$\angle G(j\overline{\omega}) = \begin{cases} a: \varphi_1(\overline{\omega}) - \varphi_2(\overline{\omega}) - \dfrac{\pi\,(\nu+1)}{2} - \dfrac{\overline{\omega}\,\vartheta}{T} \\ b: \varphi_1(\overline{\omega}) - \varphi_2(\overline{\omega}) - \dfrac{\pi\,\nu}{2} - \dfrac{\overline{\omega}\,\vartheta}{T} \end{cases} \tag{26}$$

then the phase margin becomes

$$PM = \begin{cases} a: \ \varphi_1(\overline{\omega}_c) - \varphi_2(\overline{\omega}_c) + \dfrac{\pi\,(1-\nu)}{2} - \dfrac{\overline{\omega}_c\,\vartheta}{T} \\ b: \ \varphi_1(\overline{\omega}_c) - \varphi_2(\overline{\omega}_c) + \dfrac{\pi\,(2-\nu)}{2} - \dfrac{\overline{\omega}_c\,\vartheta}{T}. \end{cases} \tag{27}$$

In this case, the settings are $\varphi_1(\overline{\omega}_c) - \varphi_2(\overline{\omega}_c) - \overline{\omega}_c\vartheta/T = \pi/2$ in case a and $\varphi_1(\overline{\omega}_c) - \varphi_2(\overline{\omega}_c) - \overline{\omega}_c\vartheta/T = 0$ in case b. The formulas for T_I are updated as follows:

$$T_I = \begin{cases} a: \dfrac{\overline{\omega}_c\gamma - 1}{\left(\dfrac{\overline{\omega}_c}{T}\right)^{\nu}[(\gamma+\overline{\omega}_c)S + (1-\gamma\overline{\omega}_c)C]} \\ b: \dfrac{\overline{\omega}_c + \gamma}{\left(\dfrac{\overline{\omega}_c}{T}\right)^{\nu}[(1-\gamma\overline{\omega}_c)S - (\overline{\omega}_c+\gamma)C]} \end{cases} \tag{28}$$

where $\gamma = \tan(\overline{\omega}_c\vartheta/T)$. Note that (28) coincides with (24) when $\vartheta \to 0$. Since the magnitude keeps unchanged, the crossover specification sets the integral gain by the same rule (25).

B. Realization of the FOPI Controller

The final step in the synthesis procedure is to realize the FOPI transfer function. Namely, in (16) the irrational operator s^{ν} requires an approximation as rational transfer function. Literature discloses several methods [11], [13], [28]−[30]. Here, a methodology is employed to a priori guarantee that zeros and poles of the rational transfer function are interlaced with each other in the negative real half-axis of the s-plane [31], [32]. This method warrants stability and minimum-phase properties, that are important for control purpose. Finally, it is based on closed-form formulas that can be easily applied to obtain the coefficients of the rational transfer function, depending on ν and the number N of zero-pole pairs in the approximation. The greater is N, the better is the approximation of s^{ν}, but also the more complex and memory-demanding is the implementation. More precisely, a continued fractions expansion is truncated and converted to a rational transfer function

$$s^{\lambda} \approx \frac{\alpha_{N,0}(\lambda)\,s^N + \alpha_{N,1}(\lambda)\,s^{N-1} + \cdots + \alpha_{N,N}(\lambda)}{\beta_{N,0}(\lambda)\,s^N + \beta_{N,1}(\lambda)\,s^{N-1} + \cdots + \beta_{N,N}(\lambda)} \tag{29}$$

where $0 < \lambda < 1$, $N \geq 1$ is the number of zero-pole interlaced pairs and the coefficients $\alpha_{N,j}(\lambda) = \beta_{N,N-j}(\lambda)$, for $j = 0, \ldots, N$, depend on λ. The coefficients can be computed very easily and rapidly by a closed-form formula:

$$\alpha_{N,j}(\lambda) = (-1)^j \binom{N}{j} (\lambda+j+1)_{(N-j)}(\lambda-N)_{(j)} \tag{30}$$

in which $(\lambda+j+1)_{(N-j)} = (\lambda+j+1)(\lambda+j+2)\cdots(\lambda+N)$ and $(\lambda-N)_{(j)} = (\lambda-N)(\lambda-N+1)\cdots(\lambda-N+j-1)$, with $(\lambda+N+1)_{(0)} = (\lambda-N)_{(0)} = 1$. Simple algebraic manipulations lead to [33], [34]:

$$\alpha_{N,j} = C(N,j)\,(j+1+\lambda)_{(N-j)}\,(N-\lambda)_{(j)^*} \tag{31}$$

$$\beta_{N,j} = C(N,j)\,(N-j+1+\lambda)_{(j)}\,(N-\lambda)_{(N-j)^*} \tag{32}$$

where $(N-\lambda)_{(j)^*} := (N-\lambda)(N-\lambda-1)\cdots(N-\lambda-j+1)$ and $(N-\lambda)_{(N-j)^*} := (N-\lambda)(N-\lambda-1)\cdots(j-\lambda+1)$ are falling factorials, with $(N-\lambda)_{(0)^*} = 1$. Similar methods and considerations can be applied for digital realizations [35]−[38].

IV. Set-point Pre-filter Design

To improve the set-point following performance, the design is completed by adding a suitable set-point pre-filter. The filter $F(s)$ is designed by the method recently proposed in [39], which is briefly revisited here for the reader's convenience and suitably adapted for the considered problem, where a feedback filter has to be taken into account.

The control loop includes the designed fractional-order PI controller, $G_c(s)$, a linear time-invariant commensurate strictly proper minimum-phase system, that can be of integer or non-integer order (a fractional system), and a possible feedback filter $R(s)$. The set-point pre-filter $F(s)$ aims at obtaining, independently from $G_c(s)$, an output transition as close as possible to a desired output function, that is a smooth and monotonic transition from an initial steady-state value to a new one in a finite time interval τ. The first step is to employ the technique in [40] to synthesize a suitable command signal $r(t)$ that provides a perfect tracking of the desired output function. The second step is to find an integer or non-integer (fractional) pre-filter $F(s)$ that is able to provide a step response as close as possible, in terms of 2-norm, to the synthesized $r(t)$.

The synthesis of $r(t)$ is as follows [40]. The desired output signal $\bar{y}(t;\tau)$ was proposed in [41]. It can be represented, together with its fractional differintegral, as in (33)

$$D^{\alpha}\bar{y}(t;\tau) = \begin{cases} 0, & t<0 \\ \dfrac{(2n+1)!}{n!\tau^{2n+1}}\displaystyle\sum_{r=0}^{n}\dfrac{(-1)^{n-r}\tau^{r}(2n-r)!\,t^{2n-r+1-\alpha}}{r!(n-r)!\Gamma(2n-r+2-\alpha)} & t\le\tau \\ \dfrac{(2n+1)!}{n!\tau^{2n+1}}\displaystyle\sum_{r=0}^{n}\dfrac{(-1)^{n-r}\tau^{r}(2n-r)!}{r!(n-r)!} \times\left(\dfrac{t^{2n-r+1-\alpha}}{\Gamma(2n-r+2-\alpha)}-\displaystyle\sum_{j=0}^{n-r}\dfrac{\tau^{j}t^{2n-r+1-j-\alpha}}{j!\Gamma(2n-r+2-j-\alpha)}\right) & t>\tau \end{cases} \quad (33)$$

where $-\infty<\alpha\le n+1$. The previous τ-parameterized signal exhibits a smooth monotonic transition from 0 to 1 in a finite time interval τ and its degree of regularity is C^n.

To compute a command signal $r(t)$ such that a perfect tracking of the τ-parameterized output function $\bar{y}(t;\tau)$ is obtained, the open-loop transfer function $G(s)=G_c(s)G_p(s)$ is first considered. The input-output technique in [40] is straightforwardly applied to $G(s)$ (or to the delay-free part $\bar{G}$ of $G(s)=\bar{G}(s)e^{-\vartheta s}$ if there is a pure time delay ϑ in the loop), yielding the signal

$$\begin{aligned} r_{ol}(t;\tau) &= \gamma_{n-m}D^{\rho}\bar{y}(t;\tau)+\gamma_{n-m-1}D^{\rho-\nu}\bar{y}(t;\tau) \\ &\quad+\cdots+\gamma_1 D^{\nu}\bar{y}(t;\tau)+\gamma_0\bar{y}(t;\tau) \\ &\quad+\int_0^t \eta_0(t-\xi)\bar{y}(\xi;\tau)d\xi \end{aligned} \quad (34)$$

where ρ is the relative order of the open-loop transfer function and $\eta_0(t)$ is its zero order dynamics. Then, a correction term $r_c(t;\tau)=\mathcal{L}^{-1}[R(s)\bar{Y}(s;\tau)e^{-\vartheta s}]$ must be considered, so that the ideal command signal is

$$r(t;\tau) = r_{ol}(t;\tau)+r_c(t;\tau). \quad (35)$$

Details on the computation of (35), together with the proof of existence of the command signal, can be found in [40].

A. Transition Polynomial-Based Filter

The first method proposed for designing the set-point pre-filter $F(s)$ relies on the design of a transfer function whose step response is as close as possible (in terms of 2-norm) to the transition polynomial. The following transfer function structure is employed

$$\tilde{F}(s)=\frac{1}{\sum_{i=1}^{o}a_i s^i+1} \quad (36)$$

where $o=n+1$, so that the pre-filter step response exhibits the same degree of regularity of the transition polynomial. By sampling at each Δt the transition polynomial and its derivatives obtained via (33), the following matrices are created

$$A=\begin{bmatrix} D^{o}\bar{y}(0;\tau) & \cdots & D^{1}\bar{y}(0;\tau) \\ \vdots & & \vdots \\ D^{o}\bar{y}(t-\Delta t;\tau) & \cdots & D^{1}\bar{y}(t-\Delta t;\tau) \\ D^{o}\bar{y}(t;\tau) & \cdots & D^{1}\bar{y}(t;\tau) \\ D^{o}\bar{y}(t+\Delta t;\tau) & \cdots & D^{1}\bar{y}(t+\Delta t;\tau) \\ \vdots & \ddots & \vdots \\ D^{o}\bar{y}(3\tau;\tau) & \cdots & D^{1}\bar{y}(3\tau;\tau) \end{bmatrix} \quad (37)$$

$$B=\begin{bmatrix} 1(0)-\bar{y}(0;\tau) \\ \vdots \\ 1(t-\Delta t)-\bar{y}(t-\Delta t;\tau) \\ 1(t)-\bar{y}(t;\tau) \\ 1(t+\Delta t)-\bar{y}(t+\Delta t;\tau) \\ \vdots \\ 1(3\tau)-\bar{y}(3\tau;\tau) \end{bmatrix}. \quad (38)$$

Finally, the coefficients vector $\Theta=[a_o\cdots a_1]^T$ is obtained as $\Theta = A^T(AA^T)^{-1}B$. Now, using (36) and the process dynamics, the set-point pre-filter is designed as

$$F(s) = \tilde{F}(s)(R(s)e^{-\vartheta s}+\bar{G}^{-1}(s)) \quad (39)$$

where $\bar{G}^{-1}(s)$ is obtained straightforwardly by considering that $\bar{G}(s)$ is the delay free-part of the process. Moreover, it is worth stressing that, given the properness of $\tilde{F}(s)$, the overall filter $F(s)$ is always proper. Note that, in this case, the obtained filter is fractional. If a unitary-feedback loop is considered with no time delay, then $F(s) = \tilde{F}(s)(1+\bar{G}^{-1}(s))$.

B. Command Signal Filter

The second methodology for designing the set-point pre-filter $F(s)$ is based on the direct design of an integer order pre-filter whose step response is the closest, in terms of 2-norm, to the command signal (35). The proposed filter structure is

$$F(s) = \frac{\sum_{j=1}^{o-p}b_j s^j+1}{\sum_{i=1}^{o}a_i s^i+\mu} \quad (40)$$

where μ is the closed-loop dc-gain, $p=n-[\rho_G]$, with ρ_G the relative order of the open-loop transfer function, and $o\in\mathbb{R}$ is a design parameter. In this case, the identification would require $o-p$ differentiation of the step signal. To overcome this problem, both the step and the command signals are integrated $o-p$ times yielding (41)–(42), shown at the bottom of the next page.

Finally, the coefficients vector is defined as $\Theta = [a_o\ \cdots\ a_1\ b_{o-p}\ \cdots b_1]^T$ and is obtained by the same formula $\Theta=A^T(AA^T)^{-1}B$.

V. Experimental Validation

In this section, the proposed control scheme combining a feedback FOPI controller and a set-point pre-filter is tested. It is also compared with an industrial solution, combining a PI controller, which is tuned by the classical symmetrical optimum method, and a smoothing pre-filter. The tests are done by simulation of identified input/output models and by experiments performed on real equipment. Two different test beds are considered.

The first one is a 370 W brushed DC-servomotor (AMIRA DR300), that is driven by a device equipped with a power supply, a servo amplifier, a signal adaption unit, and a module for measuring outputs. PC-commands to the device are processed and sent by an interface board (a floating point 250 Mhz Motorola PPC dSPACE board DS1104). Then, all control functions can be generated directly by the PC which integrates the board. A 1024 pulses digital incremental encoder is mounted at the motor free drive-shaft to measure rotor position or speed. Feedback from the encoder arrives the board processor, that computes and sends the control action to the power unit. The board uses 16 bit A/D-D/A converters to process signals and commands, generates the position and speed references, applies the Euler's discretization rule and runs the controllers in discrete time. The PI or FOPI controllers and the set-point pre-filters are part of a Simulink block diagram the board uses to directly control the real plant or its I/O model. The board compiles the Simulink scheme, generates a real-time executable code, and downloads it to the board memory. Fig. 4 shows all the experimental set-up. The plant parameters are identified by a frequency-domain technique as: $K = 0.9843$, $T = 0.0651$ s, $\vartheta = 0.02$ s. Then, formulas (28) and (25) are used to design the FOPI controller.

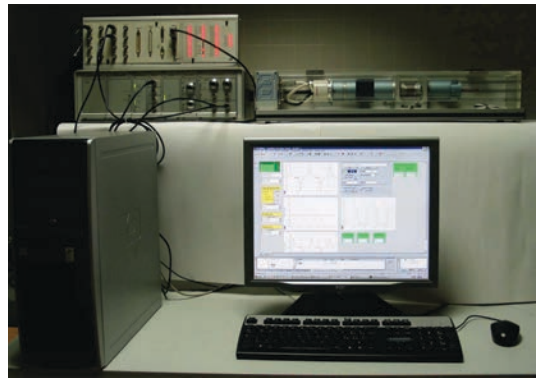

Fig. 4. Experimental set-up for controlling the DC-servomotor.

The second test bed system is a PMSM drive (SIEMENS series 1FK7 CT) with the characteristics and parameters shown in Table I. This system is tested by the experimental set-up in Fig. 5. The diagram in Fig. 1 accurately represents the controlled system. If $T_c = 0.1$ ms, $\tau_{sp} = 6 \cdot 10^{-6}$ ms, and $\tau_L = 0.7$ ms, then $\tau_{\Sigma i} = 0.95$ ms and the Absolute Value Optimum Criterion settings provide $\tau_{isq} = 0.0114$ s and $K_{isq} = 6.5253$ for the current PI controller. Moreover, for the

$$A = \begin{bmatrix} D^p r(0;\tau) & \cdots & D^{-o+p+1} r(0;\tau) & \cdots & -1(0) & \cdots & -\dfrac{1}{(o-p+1)!} 0^{(o-p+1)} \\ \vdots & \ddots & \vdots & \ddots & \vdots & \ddots & \vdots \\ D^p r(t-\Delta t;\tau) & \cdots & D^{-o+p+1} r(t-\Delta t;\tau) & \cdots & -1(t-\Delta t) & \cdots & -\dfrac{1}{(o-p+1)!}(t-\Delta t)^{(o-p+1)} \\ D^p r(t;\tau) & \cdots & D^{-o+p+1} r(t;\tau) & \cdots & -1(t) & \cdots & -\dfrac{1}{(o-p+1)!} t^{(o-p+1)} \\ D^p r(t+\Delta t;\tau) & \cdots & D^{-o+p+1} r(t+\Delta t;\tau) & \cdots & -1(t+\Delta t) & \cdots & -\dfrac{1}{(o-p+1)!}(t+\Delta t)^{(o-p+1)} \\ \vdots & \ddots & \vdots & \ddots & \vdots & \ddots & \vdots \\ D^p r(3\tau;\tau) & \cdots & D^{-o+p+1} r(3\tau;\tau) & \cdots & -1(3\tau) & \cdots & -\dfrac{1}{(o-p+1)!}(3\tau)^{(o-p+1)} \end{bmatrix} \tag{41}$$

$$B = \begin{bmatrix} \dfrac{1}{(o-p)!} 0^{(o-p)} - \mu D^{-o+p} r(0;\tau) \\ \vdots \\ \dfrac{1}{(o-p)!}(t-\Delta t)^{(o-p)} - \mu D^{-o+p} r(t-\Delta t;\tau) \\ \dfrac{1}{(o-p)!} t^{(o-p)} - \mu D^{-o+p} r(t;\tau) \\ \dfrac{1}{(o-p)!}(t+\Delta t)^{(o-p)} - \mu D^{-o+p} r(t+\Delta t;\tau) \\ \vdots \\ \dfrac{1}{(o-p)!}(3\tau)^{(o-p)} - \mu D^{-o+p} r(3\tau;\tau) \end{bmatrix} \tag{42}$$

speed loop, the I/O plant model parameters in (12) are $K = K_c n_p / J = 728.5343$ and $T = \tau_{\Sigma\omega} = 0.0078\,\mathrm{s}$. Then, for the PI designed with the Symmetrical Optimum Criterion, $\tau_{\omega r} = 0.0310\,\mathrm{s}$ and $K_{\omega r} = 0.0886$. Whereas, formulas (24) and (25) (case a) are used to design the FOPI controller.

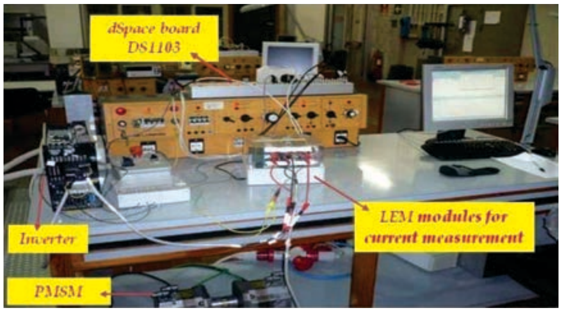

Fig. 5. Experimental set-up for controlling the PMSM drive.

A. First Case: Control of DC-motor

The control approach is applied both to the position and speed of the DC-motor. The tests are performed both in simulation and by experiments. Simulation employs the models $G_p(s) = K\,e^{-\vartheta\,s}/(s\,(1 + T\,s))$ for position control and $G_p(s) = K\,e^{-\vartheta\,s}/(1 + T\,s)$ for speed control. Experiments are made by directly applying the controllers to the real system through the dSpace board.

As basis for comparison, a PI controller, that is tuned by the symmetrical optimum method (for position control) or by the absolute value optimum criterion (for speed control) with a smoothing pre-filter, is applied. On the other side, the FOPI controller is designed by (28) and (25). For robustness specifications, the fractional orders $\nu = 1.4, 1.5, 1.6$ are used as good trade-off values respectively providing the phase margins $54°, 45°, 36°$ by (23). Moreover, the performance specifications are $\overline{\omega}_c = 0.5$, for position control, and $\overline{\omega}_c = 1.8$, for speed control. The designed values of the controller gains are shown in Table II. All the FOPI controllers are realized by rational transfer functions with $N = 5$ zero-pole pairs. Finally, the integer-order and fractional-order pre-filters are designed by the method in Section IV.

TABLE I
PMSM NAME PLATE DATA AND PARAMETERS

Description	Value (Measure unit)
Nominal power	2.14 (KW)
Nominal current	4.40 (A)
Nominal torque	6.80 (Nm)
Power factor ($\cos(\varphi)$)	0.80
Frequency	200 (Hz)
Nominal speed	3000 (rpm)
No. of pole pairs	4
Stator resistance: R_s	1.09 (Ω)
d- & q- axis inductances: L_{sd}, L_{sq}	12.4, 12.4 (mH)
Inertia moment: J	0.006 (Kg m^2)
Viscous friction coefficient: B	0 (0.05) (Nms)
Permanent magnets flux: Ψ_{PM}	0.1821 (Wb)
Torque constant: K_c	1.0928 (Nm/A)

Fig. 6 shows the reference step responses both for position control (above) and for speed control (below), corresponding to the selected values of ν. Moreover, the response to speed reversal and to load application is shown in the same figure. The responses obtained with PI control are green, the ones obtained with FOPI control and an integer-order pre-filter are blue, and the ones with FOPI control and a fractional-order

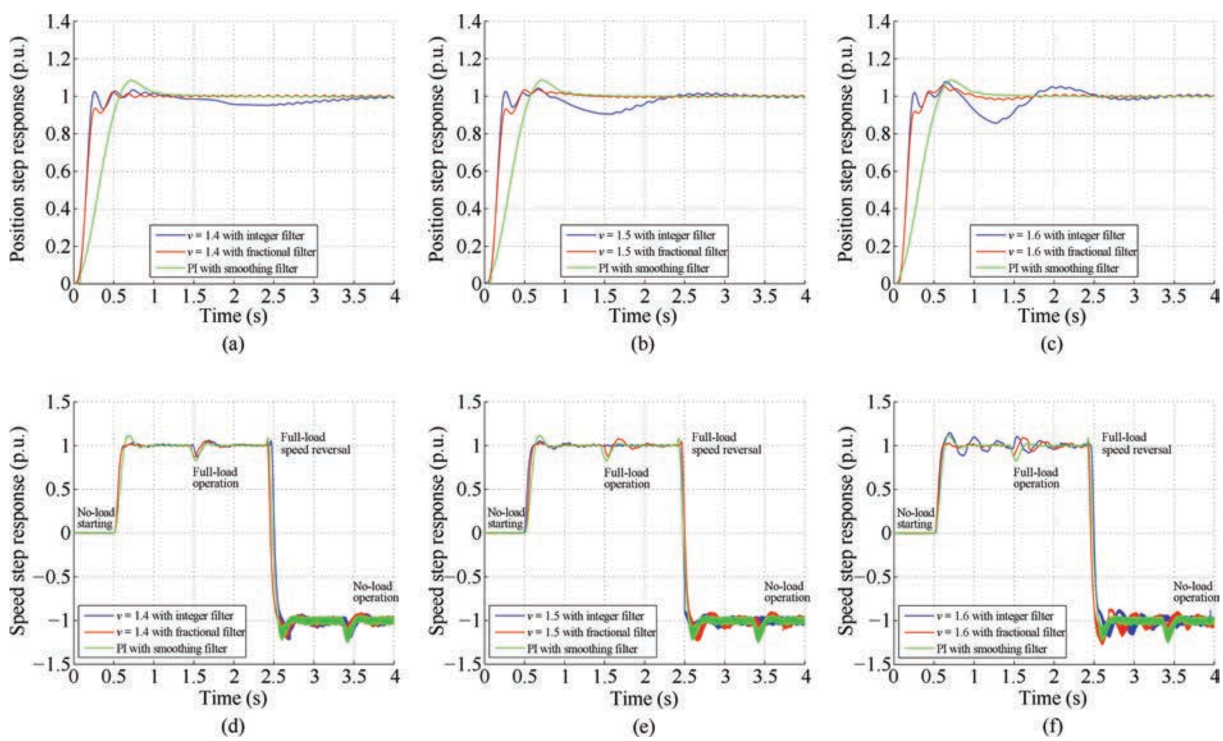

Fig. 6. PI and FOPI control of DC-motor position and speed: PI with smoothing filter (green), FOPI with integer-order (blue) or fractional-order filters (red).

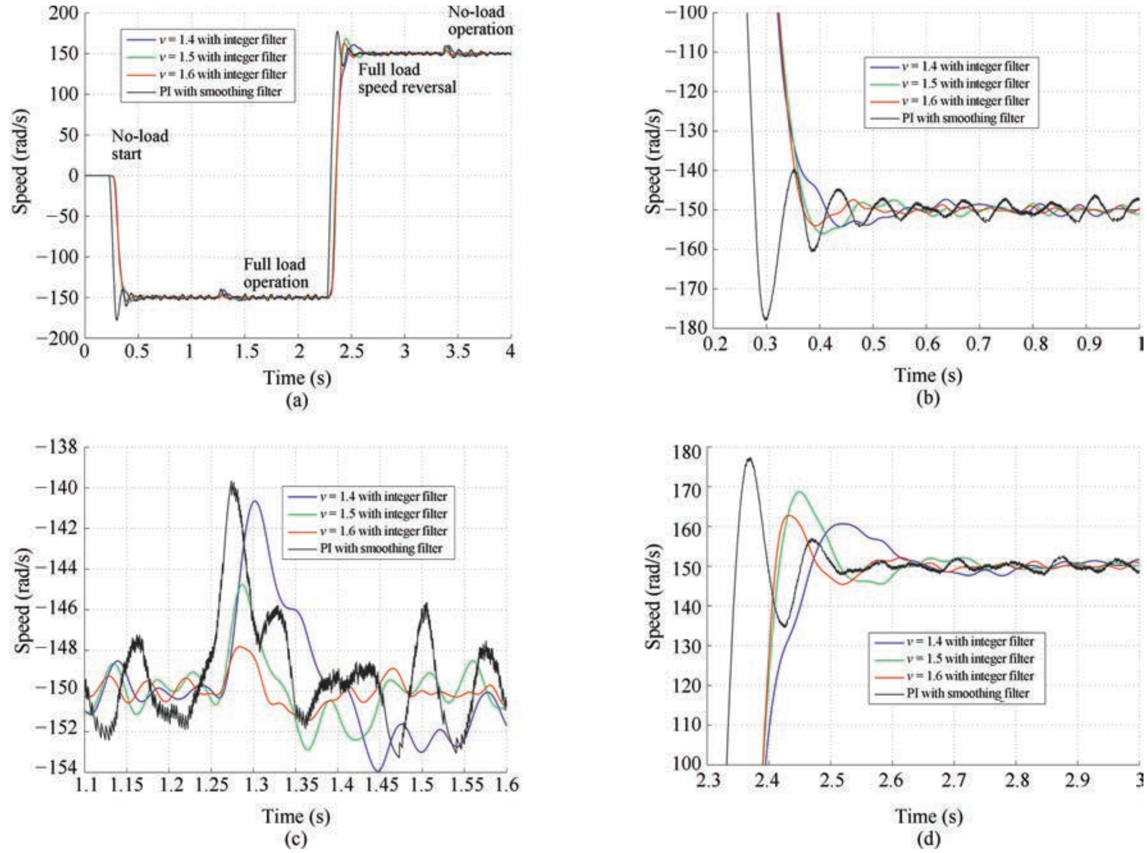

Fig. 7. Control of the speed of a PMSM by FOPI controllers and integer filters. (a) General view. (b) Zoom in the no-load start period. (c) Zoom in the full load operational period. (d) Zoom in the period after full load speed reversal.

pre-filter are red. Only experimental results are shown, namely simulation matches the experiments to a large extent.

TABLE II
FOPI CONTROLLER GAINS FOR DC-MOTOR AND PMSM DRIVES

	DC position control		DC speed control		PMSM Speed control	
ν	K_P	K_I	K_P	K_I	K_P	K_I
1.4	8.7936	2.0706	2.5831	148.3770	0.1314	5.9296
1.5	10.0609	43.9481	2.9554	289.8783	0.2004	29.7201
1.6	12.1033	123.7699	3.5553	563.3830	0.3616	119.5887

It is remarkable that the fractional pre-filters almost cancel the oscillations. The improvement is even more relevant in the case of speed control. The overshoot is greatly reduced and the settling and rise times are also reduced with respect to the PI-controlled system. Disturbance is better rejected by the FOPI with fractional filters that show a fast settling. The performance obtained by PI or FOPI when speed is reverted is comparable. This last result is due to the opposite action of the brushes when the sense of rotation is not the preferred one. Regarding the effect of changes in ν, the oscillations increase with ν (the phase margin decreases according to (23)).

B. Second Case: Control of PMSM Drive

Now the PMSM speed is controlled. The model is given by (14). Then, (24) and (25) are used for design purpose. Again, the orders $\nu = 1.4, 1.5, 1.6$ are chosen. Moreover, the desired performance is specified by the maximum bandwidth $\overline{\omega}_B$ that allows $T_I > 0$: by $\overline{\omega}_c = \overline{\omega}_B/1.7$, the necessary values are $\overline{\omega}_c = 0.6$ ($\overline{\omega}_B = 1.02$) for $\nu = 1.4$, $\overline{\omega}_c = 0.8$ ($\overline{\omega}_B = 1.36$) for $\nu = 1.5$, and $\overline{\omega}_c = 1.2$ ($\overline{\omega}_B = 2.04$) for $\nu = 1.6$. The values of the controllers' gains are shown in Table II and realization is by $N = 5$ zero-pole pairs.

To execute a suitable and intense test to verify performance and robustness, a reference step input of -150 rad/s (half of the rated speed) is first applied at $t = 0.225$ s. Then, an operation period follows in which a load disturbance of 2.2 Nm is superposed at $t = 1.253$ s. The motion is reverted at $t = 2.268$ s. Finally, the load is removed at $t = 3.361$s. The control scheme combining a FOPI controller and an integer/fractional pre-filter is compared with the traditional scheme that combines a smoothing pre-filter and a PI controller tuned by the symmetrical optimum method [23], [24]. Note that, in both schemes, the internal current loop includes the PI controller tuned by the absolute value optimum criterion. Figs. 7(a) and 8(a) show a general view of the entire test duration with integer filters and fractional filters, respectively.

First of all, the performance analysis of the reference step response without load applied, at the start of the operational test (see zoom in Figs. 7(b) and 8(b), is considered. The FOPI controllers provide a reasonable fast response and small overshoot with respect to the PI controller, especially with $\nu = 1.6$ and with fractional filters on the set-point (Fig. 8(b)).

In all the cases employing integer or fractional filters, improvements are obtained. Namely, the responses provided by the PI controller with a smoothing filter show lower rise

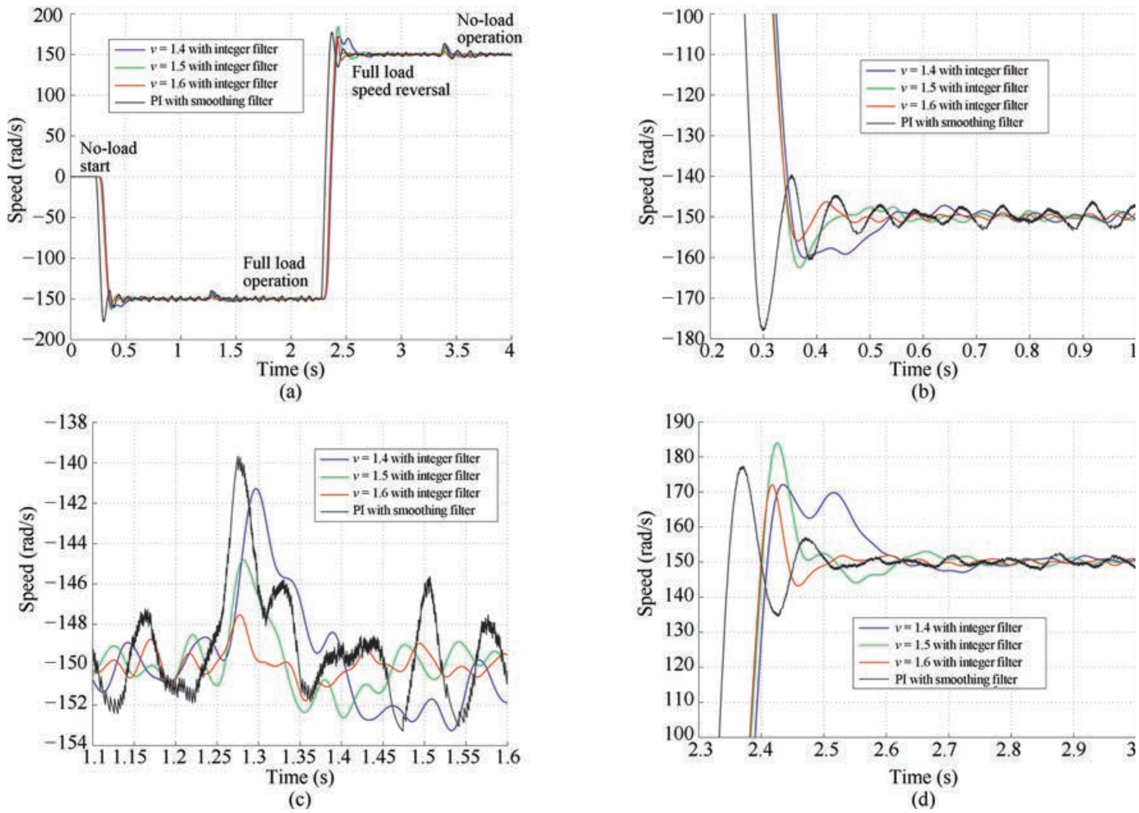

Fig. 8. Control of the speed of a PMSM by FOPI controllers and fractional filters. (a) General view. (b) Zoom in the no-load start period. (c) Zoom in the full load operational period. (d) Zoom in the period after full load speed reversal.

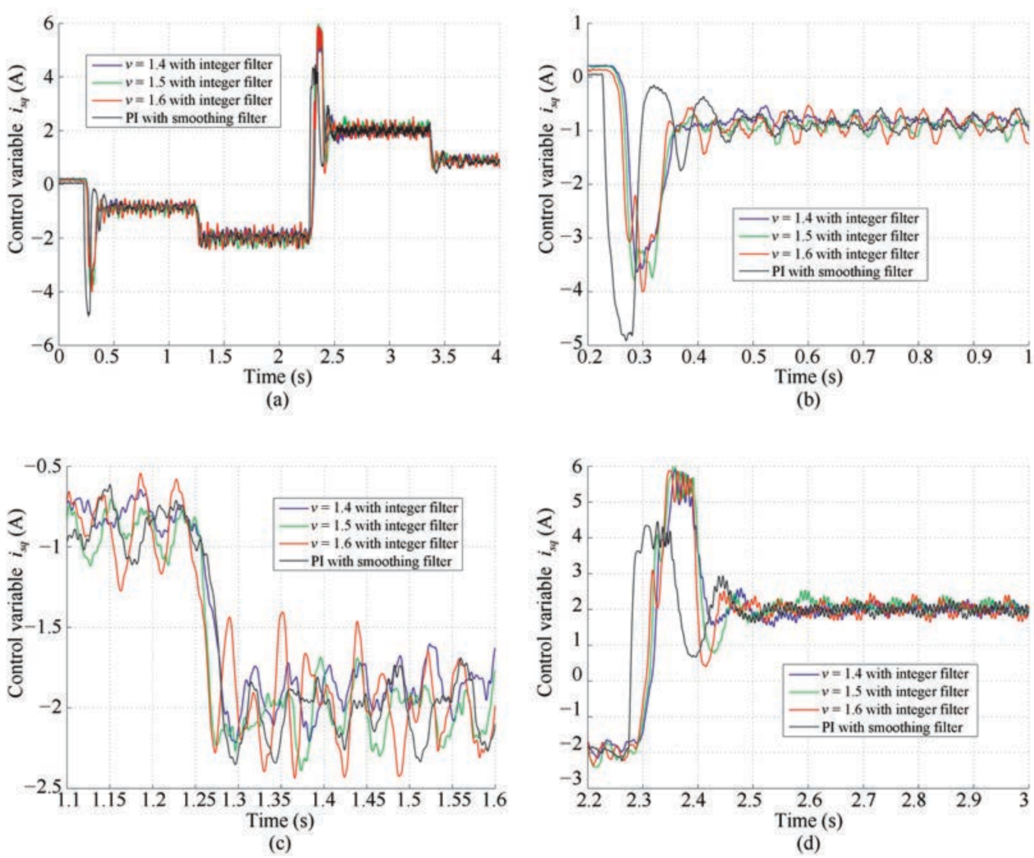

Fig. 9. Control variable when applying FOPI controllers and fractional filters. (a) General view. (b) Zoom in the no-load start period. (c) Zoom in the full load operational period. (d) Zoom in the period after full load speed reversal.

times, but they have much more oscillations (see Figs. 7(b)−7(c) and 8(b)−8(c)) and settle after slower transients.

In particular, using FOPI and integer filters reduces overshoots and undershoots with respect to using a standard PI with a smoothing pre-filter (see zoom in Fig. 7(b)), especially if ν is increased (the best response is with $\nu = 1.6$). The settling time is also reduced. Similar considerations hold true if fractional filters are employed (see zoom in Fig. 8(b)). The oscillations are much reduced with respect to the PI controller and a slightly faster response is obtained also with respect to integer filters.

Now, consider the ability to reject disturbances, then see the intermediate test period, which is better shown by Figs. 7(c) and 8(c). The zoom highlights that FOPI controllers achieve a better rejection of the applied load, especially if $\nu = 1.6$. Namely, the amplitude of the undershoot is much lower and the response settles in almost the same time as with a PI controller. To synthesize, the FOPI controller is beneficial for disturbance rejection which is very important in industrial applications.

Finally, Figs. 7(d) and 8(d) exhibit the last period in which the motion is reverted. Also in this condition, a FOPI controller with $\nu = 1.6$ reduces oscillations and obtains a fast settlement.

To complete the performance analysis, the control variable can be examined as well, for $\nu = 1.4, 1.5, 1.6$. Figs. 9(a)–9(d) show the results with fractional filters. An improvement is obtained with respect to the PI with a smoothing filter. Namely, see the reduction in oscillations and a faster response, which occurs especially after the reference input is applied (see Fig. 9(b)) and after the motion is reverted (see Fig. 9(d)). In any case, the speed response obtained by the PI with a smoothing filter is more rough, not completely clean and sensitive to disturbances (see Figs. 7 – 8).

VI. Conclusions

This paper proposes a new control scheme of DC-motor or PMSM drives, which are modeled as first-order systems plus a time delay. The scheme employs a fractional-order PI feedback controller and a set-point pre-filter, that can be of integer or fractional order. The feedback controller design is based on systematic closed-form expressions. The formulas allow easy and fast computation both of the controller parameters satisfying dynamic performance and robustness specifications (see (24) and (25) or (28)) and of the rational transfer function realization (see (29), (31), (32)). The pre-filter is designed by a dynamic inversion method that allows reducing overshoot to a large extent. The proposed scheme is compared with a classical one based on a standard PI controller combined with a smoothing pre-filter. The PI controller is tuned by the symmetrical optimum method, which is frequently employed in industrial cases. An extensive experimental (and simulation) analysis has shown the superior performance of the novel scheme and its potential impact.

References

[1] M. D. Ortigueira, *Fractional Calculus for Scientists and Engineers*. Dordrecht, The Netherlands: Springer, 2011.

[2] J. Sabatier, O. P. Agrawal, and J. A. Tenreiro Machado, *Advances in Fractional Calculus: Theoretical Developments and Applications in Physics and Engineering*. Netherlands: Springer, 2007.

[3] R. Caponetto, G. Dongola, L. Fortuna, and I. Petráš, *Fractional Order Systems: Modeling and Control Applications*. Singapore: World Scientific, 2010.

[4] C. A. Monje, Y. Q. Chen, B. M. Vinagre, D. Y. Xue, and V. Feliu, *Fractional-Order Systems and Controls: Fundamentals and Applications*. London, UK: Springer-Verlag, 2010.

[5] P. Arena, R. Caponetto, L. Fortuna, and D. Porto, *Nonlinear Noninteger Order Circuits and Systems: An Introduction*. Singapore: World Scientific, 2000.

[6] M. D. Ortigueira and J. A. Tenreiro Machado, "Special issue editorial: Fractional signal processing and applications," *Signal Process.*, vol. 83, no. 11, pp. 2285−2286, Nov. 2003.

[7] Y. Q. Chen and B. M. Vinagre, "A new IIR-type digital fractional order differentiator," *Signal Process.*, vol. 83, no. 11, pp. 2359−2365, Nov. 2003.

[8] R. R. Nigmatullin, C. Ceglie, G. Maione, and D. Striccoli, "Reduced fractional modeling of 3D video streams: The FERMA approach," *Nonlinear Dyn.*, vol. 80, no. 4, pp. 1869−1882, Jun. 2015.

[9] N. Engheta, "On the role of fractional calculus in electromagnetic theory," *IEEE Antennas Propag. Mag.*, vol. 39, no. 4, pp. 35−46, Aug. 1997.

[10] P. Bia, D. Caratelli, L. Mescia, R. Cicchetti, G. Maione, and F. Prudenzano, "A novel FDTD formulation based on fractional derivatives for dispersive Havriliak-Negami media," *Signal Process.*, vol. 107, pp. 312−318, Feb. 2015.

[11] A. Oustaloup, *La Commande CRONE. Commande Robuste d'Ordre Non Entiér*. Paris: Editions Hermés, 1991.

[12] I. Podlubny, "Fractional-order systems and $PI^{\lambda}D^{\mu}$-controllers," *IEEE Trans. Autom. Control*, vol. 44, no. 1, pp. 208−214, Jan. 1999.

[13] A. Oustaloup, F. Levron, B. Mathieu, and F. M. Nanot, "Frequency-band complex noninteger differentiator: characterization and synthesis," *IEEE Trans. Circuits Syst. I, Fundam. Theory Appl.*, vol. 47, no. 1, pp. 25−39, Jan. 2000.

[14] K. J. Åström and T. Hägglund, *PID Controllers: Theory, Design, and Tuning*, 2nd ed. Research Triangle Park, NC: Instrument Society of America, 1995.

[15] Y. Q. Chen, "Ubiquitous fractional order controls?," in *Proc. 2nd IFAC Symp. Fractional Derivatives and Applications FDA'06*, Porto, Portugal, 2006, pp. 168−173.

[16] H. W. Bode, *Network Analysis and Feedback Amplifier Design*. New York: Van Nostrand, 1945.

[17] C. A. Monje, B. M. Vinagre, V. Feliu, and Y. Q. Chen, "Tuning and auto-tuning of fractional order controllers for industry applications," *Control Eng. Pract.*, vol. 16, no. 7, pp. 798−812, Jul. 2008.

[18] R. S. Barbosa, J. A. Tenreiro Machado, and I. M. Ferreira, "Tuning of PID controllers based on Bode's ideal transfer function," *Nonlinear Dyn.*, vol. 38, no. 1−4, pp. 305−321, Dec. 2004.

[19] H. S. Li, Y. Luo, and Y. Q. Chen, "A fractional order proportional and derivative (FOPD) motion controller: Tuning rule and experiments," *IEEE Trans. Control Syst. Technol.*, vol. 18, no. 2, pp. 516−520, Mar. 2010.

[20] F. Padula, R. Vilanova, and A. Visioli, "H_{∞} optimization-based fractional-order PID controllers design," *Int. J. Robust Nonlinear Control*, vol. 24, no. 17, pp. 3009−3026, Nov. 2014.

[21] S. Stasi, L. Salvatore, and F. Cupertino, "Speed sensorless control of PMSM via linear Kalman filtering," *J. Electr. Eng.*, vol. 6, no. 4, pp. 1−8, 2006.

[22] R. C. Oldenbourg and H. Sartorius, "A uniform approach to the optimum adjustments of control loops," in *Frequency Response*, R. Oldenburger, Ed. New York: The Macmillan Co., 1956.

[23] C. Kessler, "Das symmetrische optimum," *Regelungstechnik*, vol. 6, pp. 395−400, 432−436, 1958.

[24] A. A. Voda and I. D. Landau, "A method for the auto-calibration of PID controllers," *Automatica*, vol. 31, no. 1, pp. 41−53, Jan. 1995.

[25] P. Lino and G. Maione, "Loop-shaping and easy tuning of fractional-order proportional integral controllers for position servo systems," *Asian J. Control*, vol. 15, no. 3, pp. 796−805, May 2013.

[26] R. E. Kalman, "When is a linear control system optimal?," *Trans. ASME Ser. D: J. Basic Eng.*, vol. 86, no. 1, pp. 51−60, Mar. 1964.

[27] J. M. Maciejowski, *Multivariable Feedback Design*. Wokingham, UK: Addison-Wesley, 1989.

[28] B. M. Vinagre, I. Podlubny, A. Hernández, and V. Feliu, "Some approximations of fractional order operators used in control theory and applications," *Fract. Calc. Appl. Anal.*, vol. 3, no. 3, pp. 231−248, 2000.

[29] Y. Q. Chen, B. M. Vinagre, and I. Podlubny, "Continued fraction expansion approaches to discretizing fractional order derivatives-an expository review," *Nonlinear Dyn.*, vol. 38, no. 1−4, pp. 155−170, Dec. 2004.

[30] R. S. Barbosa, J. A. Tenreiro Machado, and M. F. Silva, "Time domain design of fractional differintegrators using least-squares," *Signal Process.*, vol. 86 no. 10, pp. 2567−2581, Oct. 2006.

[31] G. Maione, "Continued fractions approximation of the impulse response of fractional-order dynamic systems," *IET Control Theory Appl.*, vol. 2, no. 7, pp. 564−572, Jul. 2008.

[32] G. Maione, "Conditions for a class of rational approximants of fractional differentiators/integrators to enjoy the interlacing property," in *Proc. of the 18th IFAC World Congr.*, S. Bittanti, A. Cenedese, S. Zampieri, Eds. Milan, Italy: IFAC, 2011, pp. 13984−13989.

[33] G. Maione, "Closed-form rational approximations of fractional, analog and digital differentiators/integrators," *IEEE J. Emerg. Sel. Topics Circuits Syst.*, vol. 3, no. 3, pp. 322−329, Sep. 2013.

[34] G. Maione, "Correction to "Closed-form rational approximations of fractional, analog and digital differentiators/integrators," *IEEE J. Emerg. Sel. Topics Circuits Syst.*, vol. 3, no. 4, pp. 654, Dec. 2013.

[35] G. Maione, "A rational discrete approximation to the operator $s^{0.5}$," *IEEE Signal Process. Lett.*, vol. 13, no. 3, pp. 141−144, Mar. 2006.

[36] G. Maione, "Concerning continued fractions representation of noninteger order digital differentiators," *IEEE Signal Process. Lett.*, vol. 13, no. 12, pp. 725−728, Dec. 2006.

[37] G. Maione, "High-speed digital realizations of fractional operators in the delta domain," *IEEE Trans. Autom. Control*, vol. 56, no. 3, pp. 697−702, Mar. 2011.

[38] G. Maione, "On the Laguerre rational approximation to fractional discrete derivative and integral operators," *IEEE Trans. Autom. Control*, vol. 58, no. 6, pp. 1579−1585, Jun. 2013.

[39] F. Padula and A. Visioli, "Inversion-based set-point filter design for fractional control systems," in *Proc. 2014 Int. Conf. on Fractional Differentiation and Its Applications*, Catania, Italy: IEEE, 2014, pp. 1−6.

[40] F. Padula and A. Visioli, "Inversion-based feedforward and reference signal design for fractional constrained control systems," *Automatica*, vol. 50, no. 8, pp. 2169−2178, Aug. 2014.

[41] A. Piazzi and A. Visioli, "Optimal noncausal set-point regulation of scalar systems," *Automatica*, vol. 37, no. 1, pp. 121−127, Jan. 2001.

Paolo Lino received the Laurea degree in electrical engineering from Politecnico di Bari, Italy, in 2000 and the Ph.D. degree in electronics and automation from the University of Catania, Italy, in 2004. In 2003 he has been a visiting researcher at the University of New Mexico, Albuquerque, NM, USA. Currently he is an assistant professor in automatic control at Politecnico di Bari. His main research interests are in intelligent control, predictive control and modeling and control of electro-mechanical and automotive systems. He is co-author of more than 60 peer reviewed papers in journals, book chapters, and conference proceedings. Dr. Lino is member of IEEE and IEEE Control Systems Society.

Guido Maione received the Laurea degree with honors in electronic engineering in 1992 and the Ph.D. degree in electrical engineering in 1997, both from Politecnico di Bari. In 1996 he joined the University of Lecce, Italy, where he was assistant professor in automatic control. In 2002 he moved to Politecnico di Bari. He visited the Rensselaer Polytechnic Institute of Troy, NY, USA, in 1997 and 1998, and the Queen's University of Belfast (UK) in 2007, 2009, and 2013. His research interests include fractional-order systems and controllers, automotive systems, discrete event systems, multi-agent systems, Petri nets and digraph models. He is the author or co-author of more than 120 peer reviewed papers in journals, book chapters and conference proceedings. Dr. Maione is senior member of IEEE, IEEE Control Systems Society, and he is an IFAC affiliate. In 1996 he founded the IEEE Student Branch at Politecnico di Bari and served as first ad interim president. Corresponding author of this paper.

Silvio Stasi received the M.Sc. degree in electrical engineering from the University of Bari, Italy, in 1989, and the Ph.D. degree in electrical engineering from Politecnico di Bari, in 1993. From 1990 to 1993, he was with the Electric Drives and Machines Group, Politecnico di Bari, where he carried out research on control and state and parameter estimation of electrical drives and, since November 2002, he has been an associate professor of electrical machines and drives in the Department of Electrical and Information Engineering. His research interests include control of electric drives, fuzzy logic, neural networks, power electronics, and motor parameter estimation.

Fabrizio Padula received the M.Sc. degree in industrial automation engineering in 2009 and the Ph.D. degree in computer science and automatic control in 2013, both form the University of Brescia. Currently, he is research fellow at the Department of Mathematics and Statistics of the Faculty of Science and Engineering at Curtin University, Perth, Australia. His research activity deals with fractional control, inversion-based control and tracking control. He is also interested in robotics and mechatronics.

Antonio Visioli received the Laurea degree in electronic engineering from the University of Parma in 1995 and the Ph.D. degree in applied mechanics from the University of Brescia in 1999. Currently he holds a professor position in automatic control at the Department of Mechanical and Industrial Engineering of the University of Brescia. He is a senior member of IEEE and a member of the TC on Education of IFAC, of the IEEE Control Systems Society TC on Control Education and of the IEEE Industrial Electronics Society TC on Factory Automation Subcommittees on Event-Based Control & Signal and on Industrial Automated Systems and Control, and of the National Board of Anipla (Italian Association for Automation). His research interests include industrial robot control and trajectory planning, dynamic inversion based control, industrial control, and fractional control. He is the author or co-author or editor of four international books, one textbook and more than 200 papers in international journals and conference proceedings.

Maximum Power Point Tracking With Fractional Order High Pass Filter for Proton Exchange Membrane Fuel Cell

Jianxin Liu, Tiebiao Zhao, and YangQuan Chen

***Abstract*—Proton exchange membrane fuel cell (PEMFC) is widely recognized as a potentially renewable and green energy source based on hydrogen. Maximum power point tracking (MPPT) is one of the most important working conditions to be considered. In order to improve the performance such as convergence and robustness under disturbance and uncertainty, a fractional order high pass filter (FOHPF) is applied for the MPPT controller design based on the traditional extremum seeking control (ESC). The controller is designed with integer-order integrator (IO-I) and low pass filter (IO-LPF) together with fractional order high pass filter (FOHPF), by substituting the normal HPF in the original ESC system. With this FOHPF ESC, better convergence and smoother performance are achieved while maintaining the robust specifications. First, tracking stability is discussed under the commensurate-order condition. Then, simulation results are included to validate the proposed new FOHPF ESC scheme under disturbance. Finally, comparison results between FOHPF ESC and the traditional ESC method are also provided.**

***Index Terms*—Extremum seeking control (ESC), fractional order high pass filter (FOHPF), fuel cell, fractional controller stability, maximum power point tracking (MPPT).**

I. Introduction

PROBLEMS Problems about energy crisis and environment pollution related to fossil fuel are intensively studied all over the world [1]−[3]. Energy saving and looking for new-generation reproductive energy source are considered helpful for attenuating these problems. Nuclear energy, solar cell, wind, fuel cell, and hydro power are alternative green power sources [4],[5]. Recently, the fuel cell (FC) has gained attention as a new power source because of higher energy density than fossil fuels. Moreover, the FC is eco-friendly because only water and heat are produced as by-products [6]. Hydrogen fuel cell is a kind of power source to gain electric power from chemical one under control, which is considered as an emerging renewable green power source. However, due to its low reaction rate and difficulty of hydrogen availability, many different fuel cell types have been tried, such as alkaline (AFC), proton exchange membrane (PEMFC), direct methanol (DMFC), phosphoric acid (PAFC), molten carbonate (MCFC), solid oxide (SOFC) [7]. Among various types of FC, the PEMFC is suitable for some special applications such as unmanned aerial vehicles (UAVs) because of high loading capability due to relatively lighter weight, and ease of miniaturization, low operating temperature at which ion conductivity is adequate to generate high power and use of solid-state electrolyte.

Since the cost of PEMFC is a little expensive now, so, in many cases, efficiency must be the most important factor taken into consideration when designing a PEMFC and the related controller. However, sometimes, how to extract the maximum power fast and stably should be placed on the first position. For a typical application scenario, a working UAV should have four stages: taking-off, climbing, cruising and landing, as shown in Fig. 1. It is well known that taking off and landing will draw more power from the energy system, requiring the FC system to work at maximum power point [8]. However, it is also known that the power output of PEMFC is dependent not only on internal chemical reaction but also on external load impedance [9]. And the operating point is the intersection of PEMFC's characteristic P-I curve and the load line, as shown in Fig. 2. If the current drawn from the cell is tuned to the maximum power point with value of I^*, then the cell works under the maximum power point P^* which is an equilibrium

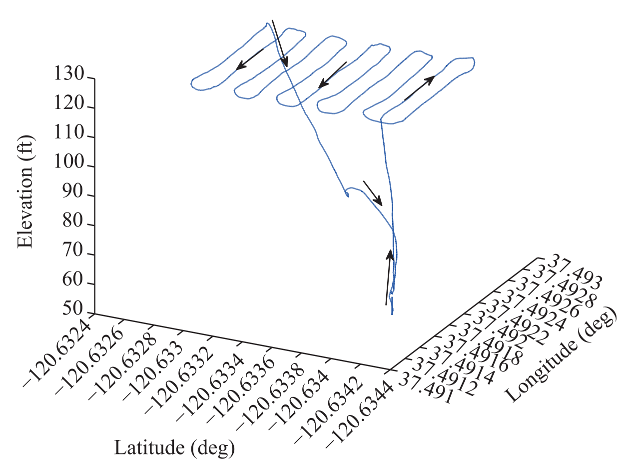

Fig. 1. Drone trajectory as an example during implementing a task.

Manuscript received Septempber 1, 2015; accepted February 28, 2016. This work was supported by the Research Project Granted by Xihua University. Recommended by Associate Editor Dingyü Xue.

Citation: J. X. Liu, T. B. Zhao, and Y. Q. Chen, "Maximum power point tracking with fractional order high pass filter for proton exchange membrane fuel cell," *IEEE/CAA Journal of Automatica Sinica*, vol. 4, no. 1, pp. 70−79, Jan. 2017.

J. X. Liu is with the School of Mechanical Engineering, Xihua University, Chengdu 610039, China (e-mail: jamson_liu@163.com).

T. B. Zhao and Y. Q. Chen are with University of California, Merced, CA95343, USA (e-mail: tzhao@ucmerced.edu; ychen53@ucmerced.edu).

Color versions of one or more of the figures in this paper are available online at http://ieeexplore.ieee.org.

Digital Object Identifier 10.1109/JAS.2017.7510328

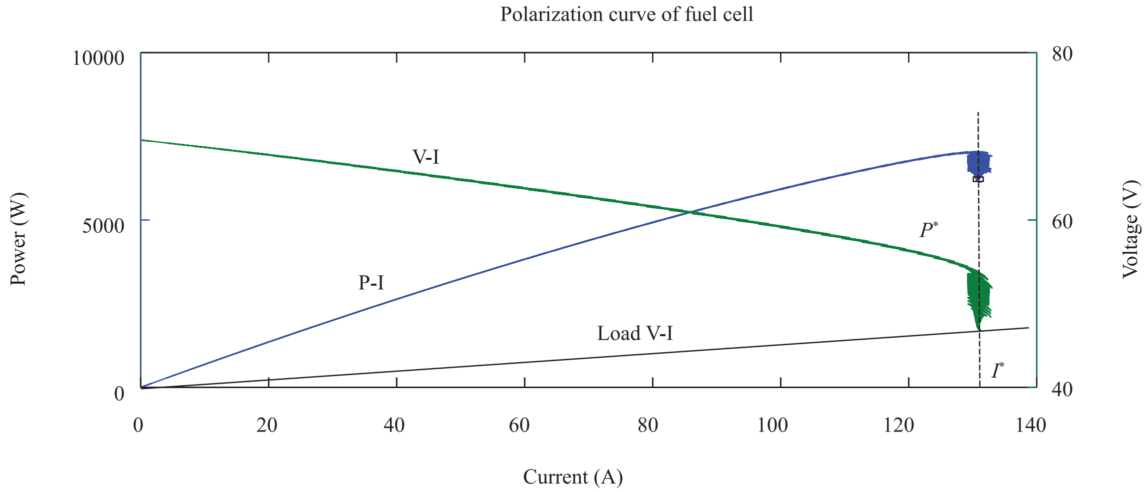

Fig. 2. Typical polarization curve and the maximum power point.

point. It is worthy to point out that the polarization curve is nonlinear and time-variant. So the setpoint is inclined to shift when the working parameters are changed, and the MPPT for PEMFC is in fact a dynamic optimization problem thus control schemes with capability of more robustness via adaptation are needed.

The problem of extracting the maximum power from renewable energy sources was first done for processes like photovoltaic panels (PV) and wind turbines [10]. Up to now, extensive research work has been done on photovoltaic power applications, such as the perturbation and observe (P&O) method, the conductance incremental method, the parasitic capacitance method, the short current method, model-based methods, and artificial intelligence methods. But relatively few researches on fuel cell MPPT control have been reported. Among them the P&O algorithm is by far the most commonly used in practice because of its ease of implementation [11]. However, due to the limitation that P&O exhibits erratic and unstable behavior under rapidly changing environments, thus the algorithm is unsuitable for the job of tracking the frequently moving MPP.

Extremum seeking is an adaptive nonlinear control method which has been used since 1950s, but its theoretical foundations for its stability and performance were established very late by [12]. Yin *et al*. discussed a class of nonlinear systems controlled by fractional order slide-mode extremum seeking control strategy and succeeded in lighting control applications [13], [14]. Bizon applied an ESC scheme to PEMFC, by setting the dither amplitude to be proportional with the magnitude of first harmonics of the processed FC power [15]. Fig. 3 is the simplest peak searching scheme. The higher order extremum seeking (hoES) control scheme is based on the classical control extremum seeking scheme, which is augmented with a low pass filter (LPF) and/or a high pass filter (HPF), as shown in Fig. 4. Usually, the HPF is used to eliminate the slowly changing DC component from the signal P which is demodulated by multiplication with sinusoidal signals. The integrator could attenuate the high-frequency periodical signal around zero. Finally, the gradient of the output power is calculated.

In Fig. 4, if P is the output power of the controlled fuel cell with current I, the DC component of P is attenuated by high pass filter (HPF) and the left component will be in phase or out of phase with the perturbation signal if the current is less than or greater than the optimum value. So, after being modulated using the multiplication operation, the DC component extracted by the low pass filter (LPF) is greater or less than zero. Finally, the gradient of I is used to force the power to converge to the maximum point.

So far, different algorithms have been proposed for fuel cell MPP tracking. Zhong *et al*., reported a first attempt to track MPP by an extremum seeking algorithm [9]. Bizon proposed an architecture of hybrid power source for vehicle application operating at MPP of the fuel cell using extremum seeking [15]. Dargahi et al. proposed MPP tracking for fuel cell in fuel cell/battery hybrid power systems using perturbation and observe (P&O) algorithm [16].

The main contribution of this work lies in two aspects. One is discussing the influence of fractional order integrator and high pass filter (HPF) on the stability of maximum power point tracking (MPPT) based on extremum seeking control (ESC). Another one is demonstrating the response smoothness of ESC with fractional order HPF (FOHPF) when applied to PEMFC. The objective is to improve PEMFC performance and robustness under disturbance, through a fractional order control scheme instead of an integer order one.

The paper is organized as follows. The preliminaries of stability of fractional order transfer functions are discussed

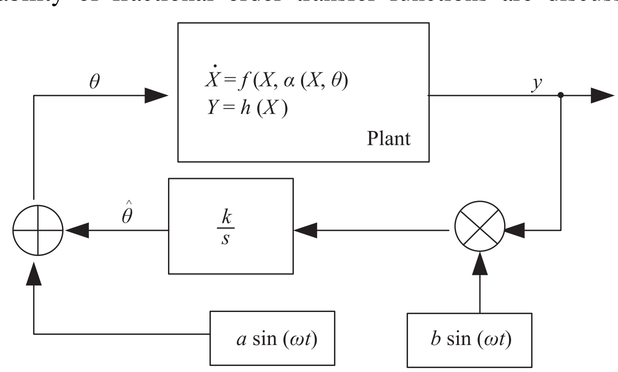

Fig. 3. The simplest peak searching scheme.

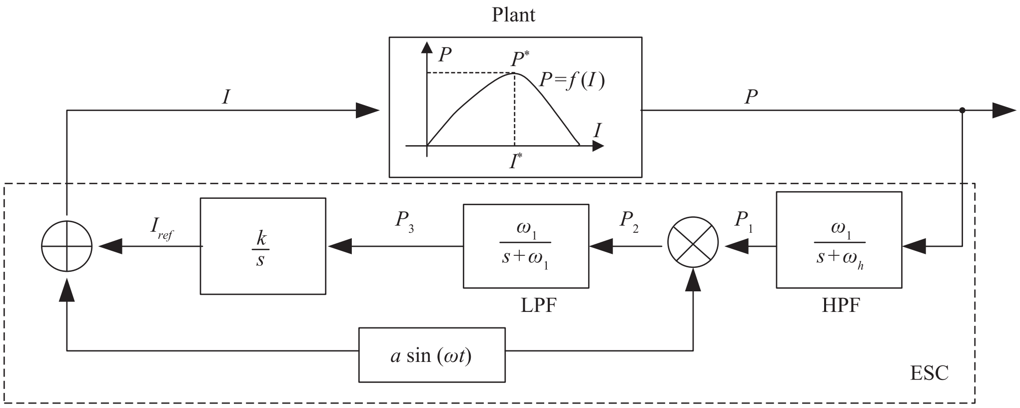

Fig. 4. General ESC control scheme.

in Section II; and in Section III, an adaptive MPPT controller is designed. In Section IV extremum seeking is applied to the fuel cell power system and simulation results are discussed in detail.

II. Stability of Fractional Order Transfer Function (TF)

Usually, linear time invariant (LTI) fractional order (FO) system can be described by fractional order differential equation (FODE) of the form

$$\begin{aligned}&(a_nD^{\alpha_n}+a_{n-1}D^{\alpha_{n-1}}+\cdots+a_1D^{\alpha_1}+a_0)y(t)\\&\quad=(b_mD^{\beta_m}+b_{m-1}D^{\beta_{m-1}}+\cdots+b_1D^{\beta_1}+b_0)x(t)\quad(1)\end{aligned}$$

where $D^\gamma={}_0D_t^\gamma$; $y(t)$ and $x(t)$ represent the system output and input signals, respectively; $a_i\,(i=0,\dots,n)$ and $b_j\,(j=0,\dots,m)$ are constants; $\alpha_i\,(i=0,\dots,n)$ and $\beta_j\,(j=0,\dots,m)$ are arbitrary real numbers.

Under zero initial conditions, the transfer function of fractional order systems can be obtained as

$$\begin{aligned}G(s)&=\frac{Y(s)}{X(s)}=\frac{b_ms^{\beta_m}+b_{m-1}s^{\beta_{m-1}}+\cdots+b_1s^{\beta_1}+b_0}{a_ns^{\alpha_n}+a_{n-1}s^{\alpha_{n-1}}+\cdots+a_1s^{\alpha_1}+a_0}\\&=\frac{Num(s)}{Den(s)}.\end{aligned}\quad(2)$$

Provided that $s^{1/\nu}$ is the greatest common factor of $Num(s)$ and $Den(s)$, $G(s)$ can be transformed to integer order transfer function in w-domain with $w=s^{1/\nu}$, which is the so called commensurate-order system.

With this transformation, the Riemann surface consists of Riemann sheets and the principal Riemann sheet (PRS) located in the area

$$-\frac{\pi}{\nu}<\arg(w)<\frac{\pi}{\nu}.\quad(3)$$

The stability condition is expressed as:

$$|\arg(w_i)|>\frac{1}{\nu}\cdot\frac{\pi}{2}\quad(4)$$

where w_i is the root of the characteristic polynomial in w-domain.

III. Design and Stability Analysis of MPPT Controller Based on ESC

A. Fractional Order Average Linear Model

The averaged linearized model relating the optimized point and the error signal for integer order ESC (IO-ESC) in Fig. 4 is [17]:

$$\frac{\tilde{\theta}}{\theta^*}=\frac{1}{1+L(s)}\quad(5)$$

where

$$L(s)=\frac{ka^2}{2s}\Big(\frac{s+j\omega}{s+j\omega+\omega_h}+\frac{s-j\omega}{s-j\omega+\omega_h}\Big).\quad(6)$$

So,

$$\begin{aligned}\frac{\tilde{\theta}}{\theta^*}&=\frac{1}{1+L(s)}\\&=\frac{s(s^2+2\omega_hs+\omega_h^2+\omega^2)}{s^3+(2\omega_h+ka^2)s^2+(\omega_h^2+\omega^2+ka^2\omega_h)s+ka^2\omega^2}.\end{aligned}\quad(7)$$

By replacing s with s^q, Malek deduced the averaged linearized model for the FO-ESC as shown in Fig. 5 [18]:

$$\begin{aligned}\frac{\tilde{\theta}}{\theta^*}&=\frac{1}{1+L(\lambda)}\\&=\frac{\lambda(\lambda^2+2\omega_h\lambda+\omega_h^2+\omega^2)}{\lambda^3+(2\omega_h+ka^2)\lambda^2+(\omega_h^2+\omega^2+ka^2\omega_h)\lambda+ka^2\omega^2}\end{aligned}\quad(8)$$

where $\lambda=s^q$.

When ka^2 is small relative to ω, the IO-ESC transfer function is asymptotically stable for all $k>0$, with a pair of closed-loop poles making the system lightly damped. On the other hand, in the FO-ESC model, there is no pole close to the stability boundaries. However, the problem of stability in the cases of the integrator, LPF and HPF with different order value q for s^q is necessary to be discussed further. Combinations of integrator, LPF, HPF with or without fractional order operation are also valuable to discuss. Without loss of generality, the case considering only an integrator or a HPF utilizing fractional order operation without a low-pass filter (LPF) will be discussed first, as shown in Fig. 6.

B. FO-ESC Model With Different Fractional Order of Integrator and HPF

In Fig. 6, the ESC system can be modeled as:

$$P(t)=f^*(t)+(\theta(t)-\theta^*(t))\quad(9)$$

$$\theta_0(t)=a\sin(\omega t),\quad(10)$$

$$\theta(t)=\theta_0(t)+\frac{k}{s^\alpha}[P_3(t)]\quad(11)$$

$$\tilde{\theta}(t)=\theta^*-\theta(t)+\theta_0(t)\quad(12)$$

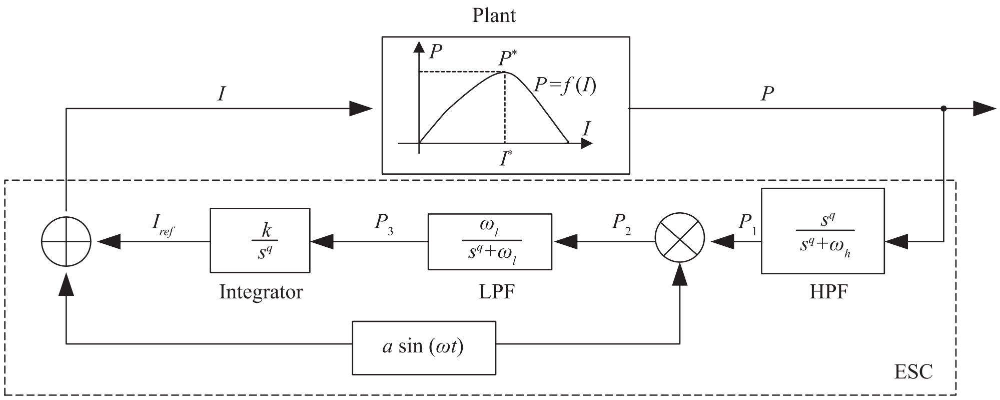

Fig. 5. Fractional order ESC (FO-ESC) control scheme.

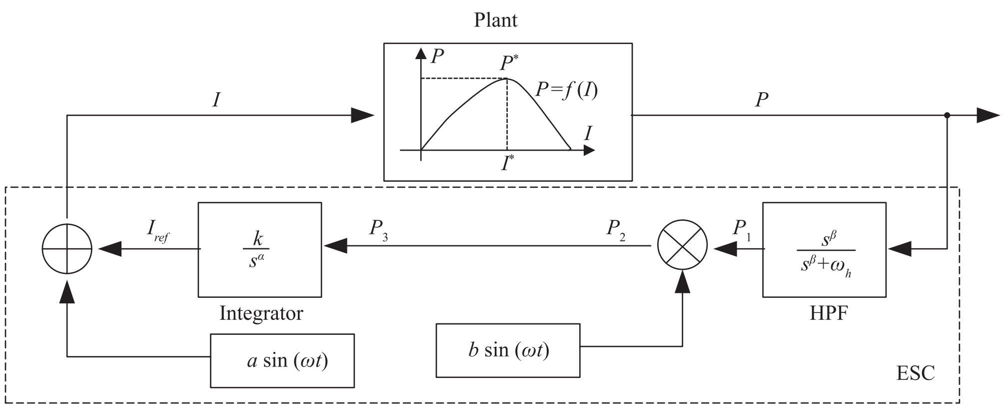

Fig. 6. Fractional order ESC (FO-ESC) without LPF.

$$P_3(t) = b\sin(\omega t)\frac{s^\beta}{s^\beta + \omega_h}[P(t)] \tag{13}$$

where $G(s)[u(t)]$ means a time-domain signal obtained as an output of system $G(s)$ using $u(t)$ as the input signal [17], and $\theta(t)$ represents input current I of fuel cell and $y(t)$ represents the output power P. Therefore,

$$\begin{aligned}\tilde{\theta} &= \theta^* - \frac{k}{s^\alpha}[b\sin(\omega t)\frac{s^\beta}{s^\beta + \omega_h}[P]] \\ &= \theta^* - \frac{k}{s^\alpha}[b\sin(\omega t)\frac{s^\beta}{s^\beta + \omega_h}[f^* + (\theta - \theta^*)^2]]\end{aligned} \tag{14}$$

$$\tilde{\theta} + \frac{2kab}{s^\alpha}[\sin(\omega t)\frac{s^\beta}{s^\beta + \omega_h}[\tilde{\theta}\sin(\omega t)]] = \theta^* + \varepsilon \tag{15}$$

where ε is the dynamic response part attenuating to zero.

C. ESC With Fractional Order Integrator

Considering the case of a fractional order integrator working with an integer order HPF in ESC, which means $1/s^\alpha$ $(0 < \alpha < 1)$ is adopted as an integrator, the transfer function is:

$$\begin{aligned}\frac{\tilde{\theta}}{\theta^*} &= \frac{1}{1+L(s)} \\ &= \frac{s^\alpha(s^2+2\omega_h s+\omega_h^2+\omega^2)}{s^{\alpha+2}+kabs^2+2\omega_h s^{\alpha+1} + (\omega_h^2+\omega^2)s^\alpha+kab\omega_h s+kab\omega^2}.\end{aligned} \tag{16}$$

And the roots of the characteristic equation determine this ESC system's stability.

$$\begin{aligned}D(s) = \; & s^{\alpha+2} + kabs^2 + 2\omega_h s^{\alpha+1} + (\omega_h^2 + \omega^2)s^\alpha \\ & + kab\omega_h s + kab\omega^2 = 0.\end{aligned} \tag{17}$$

D. ESC With Fractional Order HPF (FO-HPF)

Considering the case of a FO-HPF working with an integer order integrator in ESC, here, the FO-HPF is defined as

$$G_{\text{FO-HPF}}(s) = \frac{s^\beta}{s^\beta + \omega_h}, \quad 0 < \beta < 1 \tag{18}$$

Finally, the transfer function can be obtained as

$$\begin{aligned}\frac{\tilde{\theta}}{\theta^*} &= \frac{1}{1 + L(s)} \\ &= \frac{s(s^{2\beta}+2\omega_h s^{2\beta}+\omega_h^2+\omega^2)}{s(s^{2\beta}+2\omega_h s^\beta+\omega_h^2+\omega^2)+kab(s^{2\beta}+2\omega_h s^\beta+\omega_h^2+\omega^2)}.\end{aligned} \tag{19}$$

E. Approximation of Fractional Order Integrator $1/s^\alpha$

Since FO-HPF can be represented as a closed-loop with fractional order integrator as shown in Fig. 7, therefore, the main calculation in the situation of fractional order integrator and FO-HPF is related to the approximation of fractional order integrator $1/s^\alpha$ with integer order rational polynomial. The MATLAB Toolbox Ninteger [19] is chosen to approximate the fractional order integrator $1/s^\alpha$.

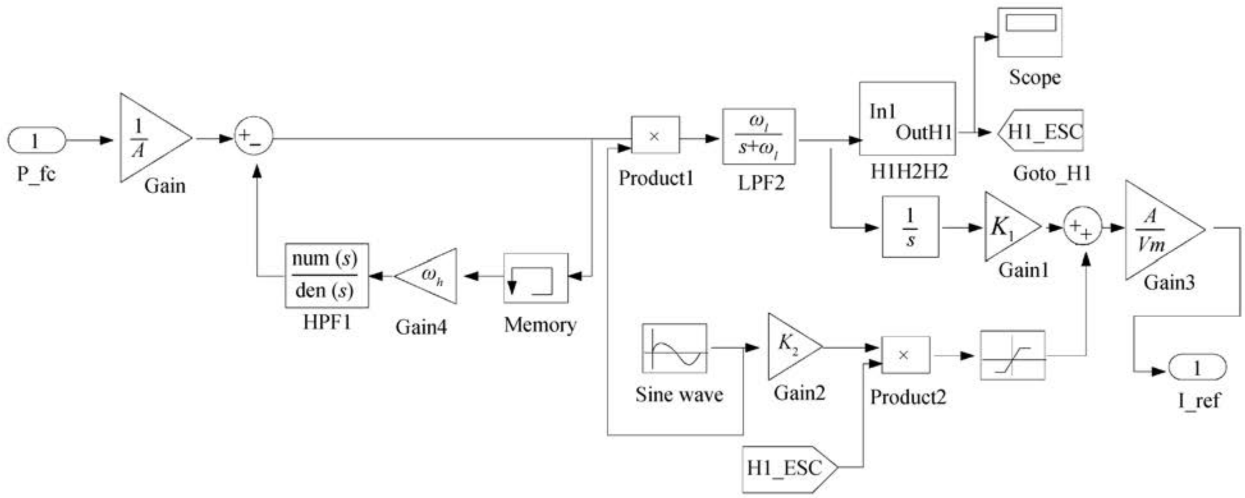

Fig. 7. MPPT controller with FO-HPF in Simulink.

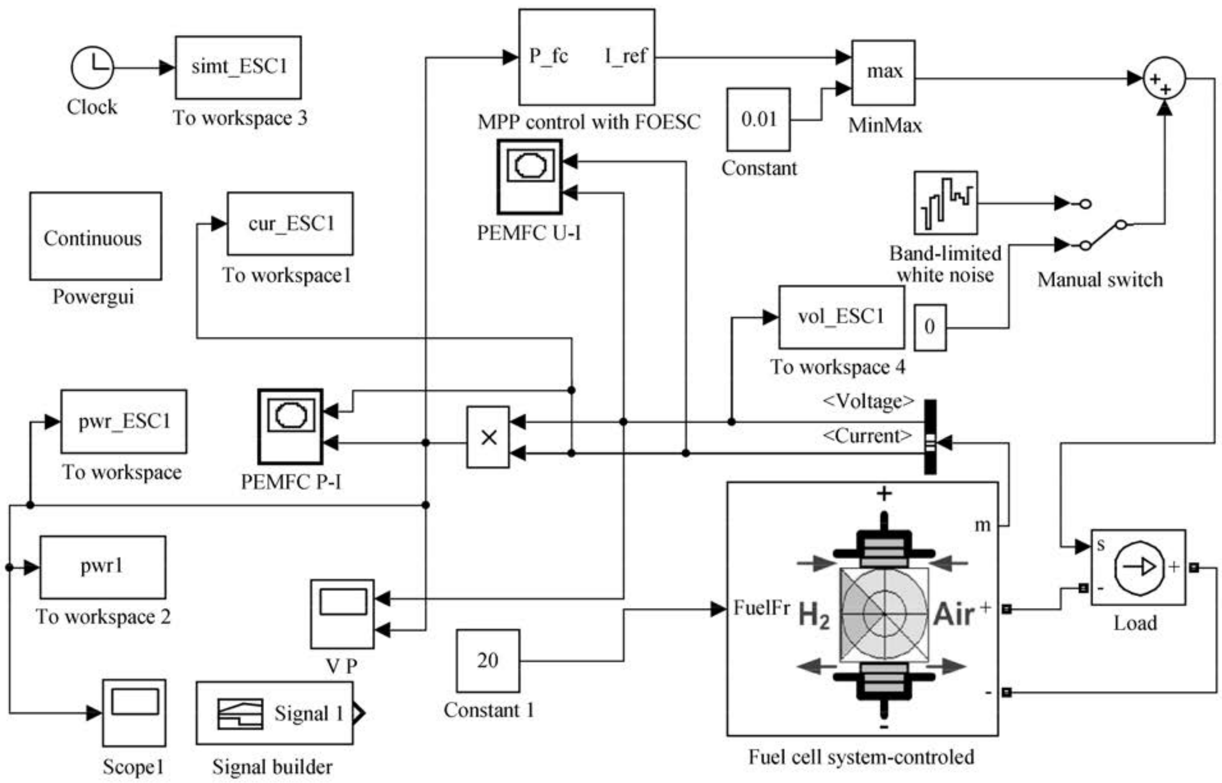

Fig. 8. Fuel cell with MPPT controller in Simulink.

IV. Simulation Results and Discussions

The focus of this paper is to discuss the role of fractional order controller in ESC. Here, the fuel cell model in MATLAB/Simulink as shown in Fig. 8 is adopted. The fuel cell model is a 6 kW & 45 V PEMFC stack from the SimPowerSystem Toolbox in MATLAB, which is fueled with hydrogen (FuelFr value) and air at nominal flow rate of 50 lpm (liters per minute) and 300 lpm, respectively. As a comparison, the model in [20] is used as the reference. The simulation models of the ESC controller with FO-HPF used in Simulink are shown in Fig. 4. The MPP here for comparison relates to the case when the FuelFr value is given as 20 lpm, without loss of generality. Some key parameters are given in Table I.

TABLE I
Simulation Parameters

Parameters	Formula	Value
Frequency f_1(Hz)		100
Cutoff radian frequency of HPF ω_h		62.8
Perturbation radian frequency		628
Activation area $A\,(\mathrm{cm}^2)$		56
Loop gain K_1	$4 * f_1$	400
Sine gain K_2		10
V_m		45
Gain k	K_1/V_m	8.9
Magnitude a		1
Magnitude b	$K_2 * H_1 * A/V_m$	$12.4 * H_1$

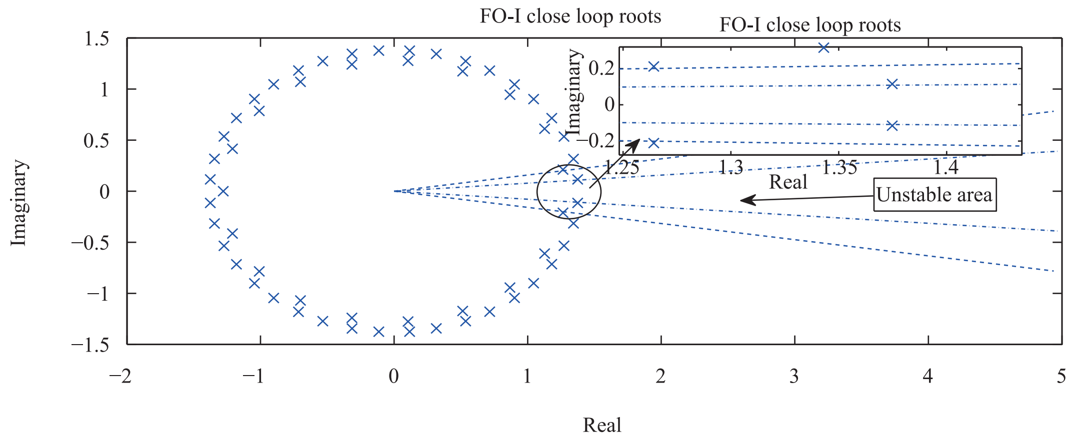

Fig. 9. Root map of ESC with fractional order integrator.

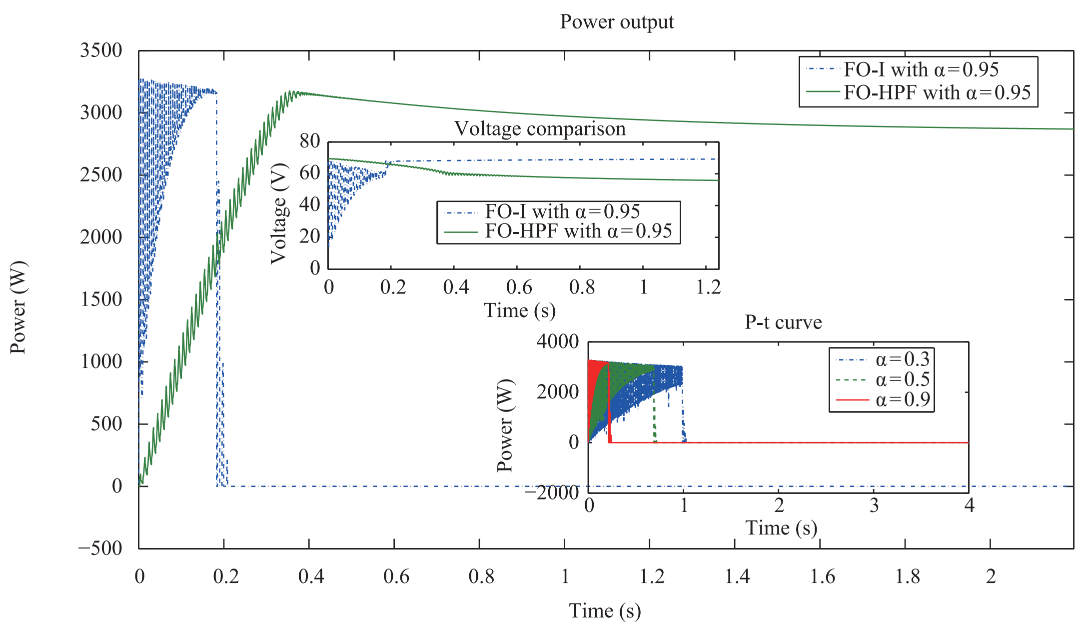

Fig. 10. Power/voltage output using ESC with fractional order integrator.

A. Performance of ESC Using Fractional Order Integrator With Order α

During simulation, when α varies between 0.3 and 1, the tracking of the MPP fails and when α is less than 0.3, no simulation result can be gained, showing that the tracking process is nonconvergent and the system is unstable. So, it is necessary to explain why this phenomenon occurs. Taking $\alpha = 0.95$ as an example, the characteristic polynomial is:

$$D(s) = s^{\frac{59}{20}} + c_1 s^{\frac{40}{20}} + c_2 s^{\frac{39}{20}} + c_3 s^{\frac{20}{20}} + c_4 s^{\frac{19}{20}} + c_5. \quad (20)$$

This is a commensurate-order system, and the closed-loop root map in the $\lambda = s^{1/20}$ plane is shown in Fig. 9. It can be found that there are two roots $1.375 \pm j0.115$ with angle of 0.0785 radians very close to the stability boundary angle of $1/20(\pi/2)$. So, the stability condition is very poor which leads to the abnormal voltage output, and it fails to track the MPP, as shown in Fig. 10. This phenomenon also exists in other cases using different order $0.3 < \alpha < 1$.

B. Performance of ESC Using FO-HPF With Order β

The characteristic polynomial is:

$$D(s) = s(s^{2\beta}+2\omega_h s^{\beta}+\omega_h^2+\omega^2)+kab(s^{2\beta}+2\omega_h s^{\beta}+\omega_h^2+\omega^2). \quad (21)$$

Given $\beta = 0.95$,

$$D(s) = s^{\frac{58}{20}} + d_1 s^{\frac{39}{20}} + d_2 s^{\frac{38}{20}} + d_3 s^{\frac{20}{20}} + d_4 s^{\frac{19}{20}} + d_5. \quad (22)$$

This is also a commensurate-order system, and the closed-loop root map in the $\lambda = s^{1/20}$ plane is shown in Fig. 11. It can be found that there are roots $1.398 \pm j0.128$ with angle of 0.091 radian which is less close to the critical stable boundary angle of $1/20(\pi/2)$ than the case using fractional order integrator, which means FO-HPF improves the tracking stability. And the power vs. time curves under different fractional orders are shown in Fig. 12. It can also be found that the larger the fractional order α the faster the power responses, but the integer-order HPF has the fastest response speed.

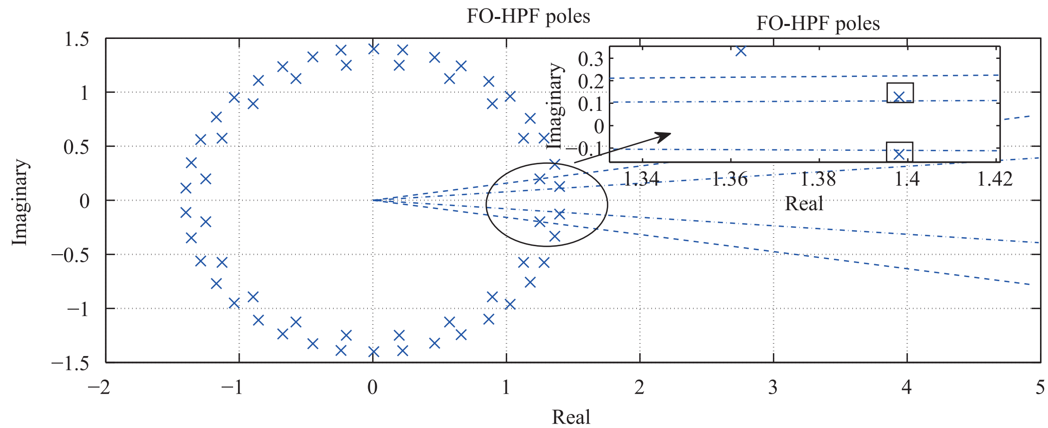

Fig. 11. Root map of FO-HPF-ESC.

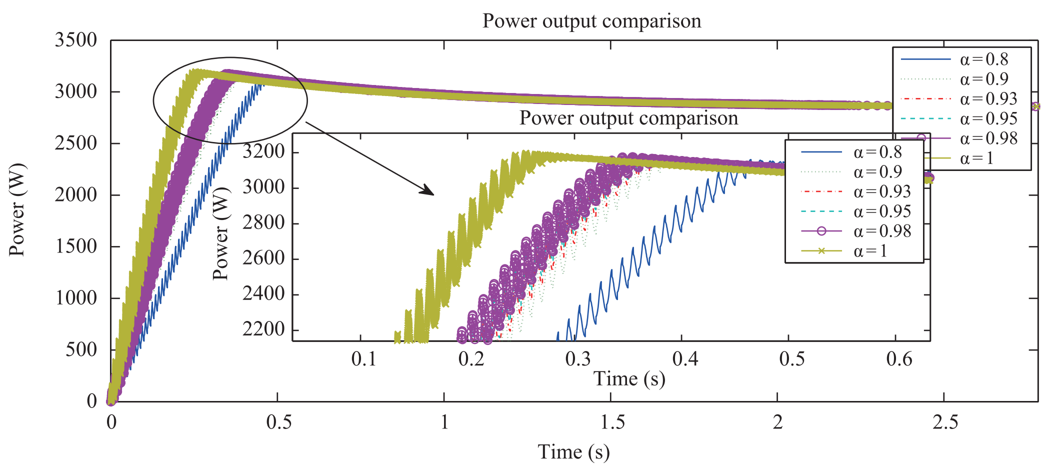

Fig. 12. Power output with FO-HPF-ESC.

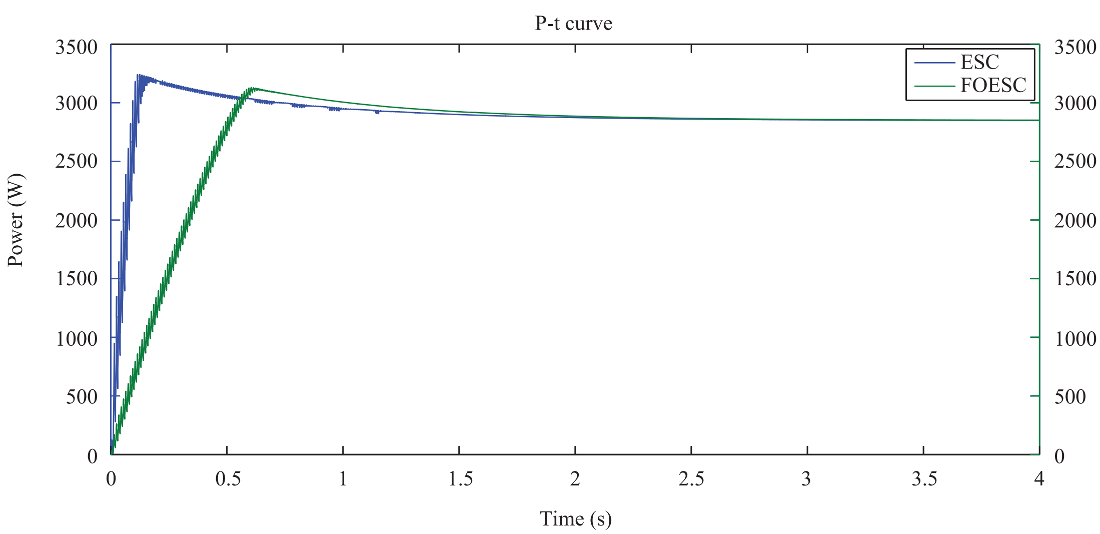

Fig. 13. Power-time curve comparison.

C. Performance of ESC Using FO-HPF With LPF

The ESC controller using fractional high-pass filter, together with integer-order integrator and integer-order low-pass filter, has the structure shown in Fig. 7.

1) Power Output Comparison

As shown in Fig. 13, the fuel cell controlled by an integer-order ESC, which uses dither amplitude proportional to the magnitude of the first harmonics of the processed FC power, has faster response speed than the one using FO-HPF ESC and marked with green color.

2) Attraction Range of MPPT

When the fuel input is 20 lpm, as an example, the relationship between the fuel cell power output and the current is shown in Fig. 14. It is obvious that the current fluctuation when using the FO-HPF ESC (green one) during tracking is smaller near the maximum power point, with range 52−53, comparing to 51−57 of the regular ESC method.

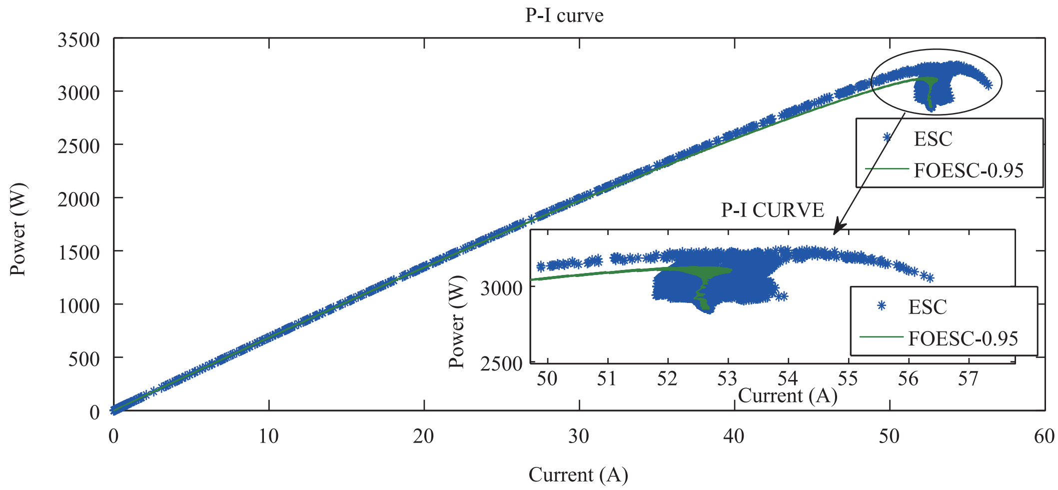

Fig. 14. Power output vs current during tracking.

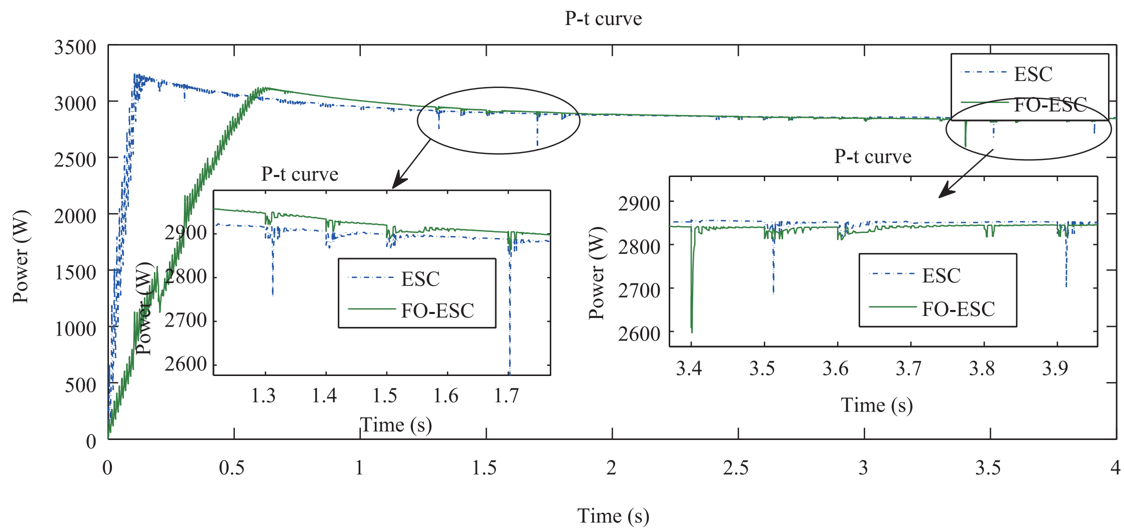

(a) Power-time curve comparison ESC

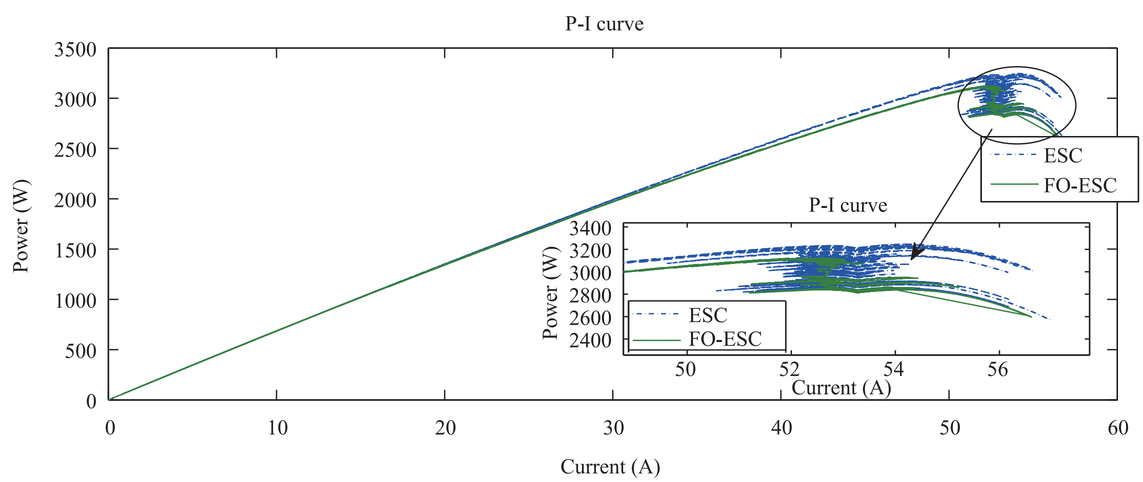

(b) Power-current curve comparison

Fig. 15. MPPT performance under white noise.

3) Robustness Under White Noise

If band-limited white noise with power of 0.04 is applied, fuel cell power outputs are shown in Fig. 15. It is obvious that the tracking process with FO-HPF (the blue curve) outperforms the one using normal HPF. Fig. 16 shows the MPPT when the load varies in the case of Fig. 17. So, FO-HPF-ESC offers more stable tracking ability than the usual ESC.

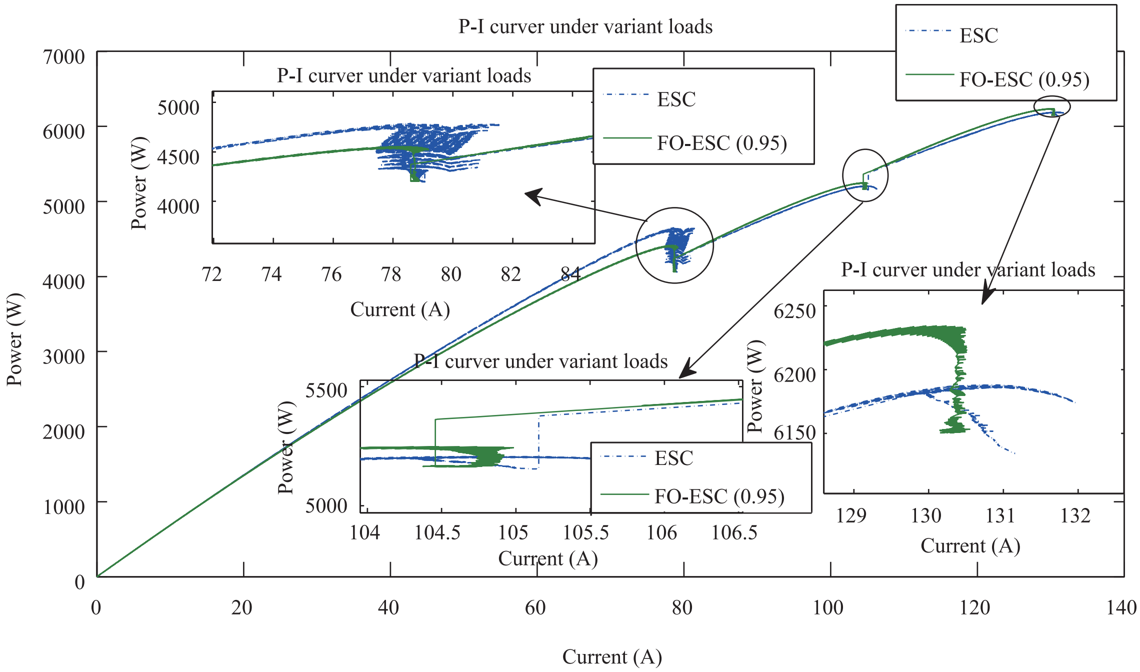

Fig. 16. MPPT performance under variant loads.

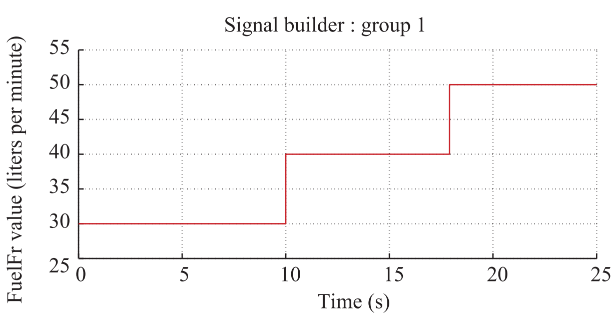

Fig. 17. Variant loads.

V. Conclusions

In this paper, a novel ESC algorithm is presented which is an ESC with FO-HPF. As discussed in this paper, separate fractional order integrator may cause the tracking failure because of the poor tracking stability, and using FO-HPF in the ESC structure reduces the dynamic response fluctuation. In addition, FO-HPF-ESC increases the robustness compared to the regular ESC. As can be seen in our simulation results, FO-HPF-ESC not only can follow the maximum power point smoother than the regular ESC, but also shows more robustness in the presence of disturbance in the system. However, for the given application case, only adjusting the order of FO-HPF is difficult to improve the response speed. Furthermore, how to optimize the order of FO-HPF instead of trial-and-error is still open and worthy of intensive research.

Acknowledgements

The authors would like to thank Prof. Nicu Bizon at the University of Pitesti, Romania and Prof. WoonKi Na at the California State University, Fresno, USA, and Dr. Hadi Malek, for their help and valuable advices in this work.

References

[1] X. P. Zhou, S. Yuan, C. Wu, B. Song, and S. L. Peng, "Potential production and distribution of microalgae in China," *J. Renew. Sustain. Energ.*, vol. 5, no. 5, pp. 053101, 2013.

[2] H. B. Khalil and S. J. H. Zaidi, "Energy crisis and potential of solar energy in Pakistan," *Renew. Sustain. Energ. Rev.*, vol. 31, pp. 194−201, Mar. 2014.

[3] J.-M. Chevalier, *The New Energy Crisis: Climate, Economics and Geopolitics*. London: Palgrave Macmillan, 2009.

[4] A. Rashid, K. Yousaf, S. Shah, and N. Shaukat, "Electricity crisis and the significance of indigenous coal for electric power generation," *Electronic Devic.*, vol. 4, no. 1, pp. 1−11, Mar. 2015.

[5] A. Omri and A. Chaibi, "Nuclear energy, renewable energy, and economic growth in developed and developing countries: a modelling analysis from simultaneous-equation models," Technical Report, Department of Research, IPAG Business School, Paris, 2014.

[6] O. Z. Sharaf and M. F. Orhan, "An overview of fuel cell technology: fundamentals and applications," *Renew. Sustain. Energ. Rev.*, vol. 32, pp. 810−853, Apr. 2014.

[7] J. Larminie and A. Dicks, *Fuel cell systems explained* (Second edition). New York: Wiley, 2003.

[8] K. N. Mobariz, A. M. Youssef, and M. Abdel-Rahman, "Long endurance hybrid fuel cell-battery powered UAV," *World J. Modell. Simul.*, vol. 11, no. 1, pp. 69−80, 2015.

[9] Z. D. Zhong, H. B. Huo, X. J. Zhu, G. Y. Cao, and Y. Ren, "Adaptive maximum power point tracking control of fuel cell power plants," *J. Power Sourc.*, vol. 176, no. 1, pp. 259−269, Jan. 2008.

[10] N. Karami, R. Outbib, and N. Moubayed, "Maximum power point tracking with reactant flow optimization of proton exchange membrane fuel cell," *J. Fuel Cell Sci. Technol.*, vol. 10, no. 5, pp. 051008, Aug. 2013.

[11] D. P. Hohm and M. E. Ropp, "Comparative study of maximum power point tracking algorithms," *Progr. Photovolt.: Res. Applic.*, vol. 11, no. 1, pp. 47−62, Jan. 2003.

[12] M. Krstić and H.-H. Wang, "Stability of extremum seeking feedback for general nonlinear dynamic systems," *Automatica*, vol. 36, no. 4, pp. 595−601, Apr. 2000.

[13] C. Yin, B. Stark, Y. Q. Chen, and S. M. Zhong, "Adaptive minimum energy cognitive lighting control: integer order vs fractional order strategies in sliding mode based extremum seeking," *Mechatronics*, vol. 23, no. 7, pp. 863−872, Oct. 2013.

[14] C. Yin, Y. Q. Chen, and S. M. Zhong, "Fractional-order sliding mode based extremum seeking control of a class of nonlinear systems," *Automatica*, vol. 50, no. 12, pp. 3173−3181, Dec. 2014.

[15] N. Bizon, "FC energy harvesting using the MPP tracking based on advanced extremum seeking control," *Int. J. Hydrogen Energ.*, vol. 38, no. 4, pp. 1952−1966, Feb. 2013.

[16] M. Dargahi, J. Rouhi, M. Rezanejad, and M. Shakeri, "Maximum power point tracking for fuel cell in fuel cell/battery hybrid power systems," *Eur. J. Sci. Res.*, vol. 25, no. 4, pp. 538−548, Jan. 2009.

[17] M. Krstić, "Performance improvement and limitations in extremum seeking control," *Syst. Contr. Lett.*, vol. 39, no. 5, pp. 313−326, Apr. 2000.

[18] H. Malek, "Control of grid-connected photovoltaic systems using fractional order operators," Ph. D. dissertation, Utah State University, Logan, Utah, 2014.

[19] D. Valério, "Toolbox Ninteger for MATLAB, v. 2.3 (September 2005)," 2015. [Online]. Available: http://web.ist.utl.pt/duarte.valerio/ninteger/ninteger.htm

[20] N. Bizon, "On tracking robustness in adaptive extremum seeking control of the fuel cell power plants," *Appl. Energ.*, vol. 87, no. 10, pp. 3115−3130, Oct. 2010.

Jianxin Liu graduated from Wuhan Iron and Steel University (WISU), China, in 1991. He received the M.E. degree from WISU in 1994 and the Ph.D. degree from the Chongqing University, China, in 1997. He is currently a professor at the School of Mechanical Engineering, Xihua University, China. His research interests include robotics and automation, especially the control of robots such as visual servoing control and intelligent control. Corresponding author of this paper.

Tiebiao Zhao graduated from Yantai University, China, 2009. He received his M.Sc. degree in control theory and control engineering from University of Science and Technology of China, China, 2012. Currently he is the third year Ph.D. candidate in University of California, Merced. His research interests include applications of small unmanned aerial systems (sUAS) in precision agriculture, especially water stress detection and yield prediction.

YangQuan Chen received his Ph.D. degree in advanced control and instrumentation from Nanyang Technological University, Singapore, in 1998. Dr. Chen was on the Faculty of Electrical and Computer Engineering at Utah State University before he joined the School of Engineering, University of California, Merced in 2012 where he teaches mechatronics for juniors and fractional order mechanics for graduates. His current research interests include mechatronics for sustainability, cognitive process control and hybrid lighting control, multi-UAV based cooperative multi-spectral personal remote sensing and applications, applied fractional calculus in controls, signal processing and energy informatics; distributed measurement and distributed control of distributed parameter systems using mobile actuator and sensor networks.

Constrained Fractional Variational Problems of Variable Order

Dina Tavares, Ricardo Almeida, and Delfim F. M. Torres

***Abstract*—Isoperimetric problems consist in minimizing or maximizing a cost functional subject to an integral constraint. In this work, we present two fractional isoperimetric problems where the Lagrangian depends on a combined Caputo derivative of variable fractional order and we present a new variational problem subject to a holonomic constraint. We establish necessary optimality conditions in order to determine the minimizers of the fractional problems. The terminal point in the cost integral, as well as the terminal state, are considered to be free, and we obtain corresponding natural boundary conditions.**

***Index Terms*—Fractional calculus, fractional calculus of variations, holonomic constraints, isoperimetric constraints, optimization, variable fractional order.**

I. INTRODUCTION

MANY real world phenomena are better described by noninteger order derivatives. In fact, fractional derivatives have unique characteristics that may model certain dynamics more efficiently. To start, we can consider any real order for the derivatives, and thus we are not restricted to integer-order derivatives only. Secondly, they are nonlocal operators, in opposite to the usual derivatives, containing memory. With the memory property one can take into account the past of the processes. This subject, called Fractional Calculus, although as old as ordinary calculus itself, only recently has found numerous applications in mathematics, physics, mechanics, biology and engineering. The order of the derivative is assumed to be fixed along the process, that is, when determining what is the order $\alpha > 0$ such that the solution of the fractional differential equation $D^{\alpha}y(t) = f(t, y(t))$ better approaches the experimental data, we consider the order to be a fixed constant. Of course, this may not be the best option, since trajectories are a dynamic process, and the order may vary. So, the natural solution to this problem is to consider the order to be a function, $\alpha(\cdot)$, depending on time. Then we may seek what is the best function $\alpha(\cdot)$ such that the variable order fractional differential equation $D^{\alpha(\cdot)}y(t) = f(t, y(t))$ better describes the real data. This approach is very recent, and many work has to be done for a complete study of the subject (see, e.g., [1]−[5]).

Manuscript received September 16, 2015; accepted June 22, 2016. This work was supported by Portuguese Funds through the Center for Research and Development in Mathematics and Applications (CIDMA) and the Portuguese Foundation for Science and Technology (FCT) (UID/MAT/04106/2013). Tavares was also supported by FCT through the Ph.D. fellowship SFRH/BD/42557/2007. Recommended by Associate Editor YangQuan Chen.

Citation: D. Tavares, R. Almeida, and D. F. M. Torres, "Constrained fractional variational problems of variable order," *IEEE/CAA Journal of Automatica Sinica*, vol. 4, no. 1, pp. 80−88, Jan. 2017.

D. Tavares is with the Department of Mathematics, Polytechnic Institute of Leiria, 2410-272 Leiria, Portugal (email: dtavares@ipleiria.pt).

R. Almeida and D. F. M. Torres are with the Department of Mathematics, University of Aveiro, 3810-193 Aveiro, Portugal (email: ricardo.almeida@ua.pt; delfim@ua.pt).

Digital Object Identifier 10.1109/JAS.2017.7510331

The most common fractional operators considered in the literature take into account the past of the process: they are usually called left fractional operators. But in some cases we may be also interested in the future of the process, and the computation of $\alpha(\cdot)$ to be influenced by it. In that case, right fractional derivatives are then considered. Our goal is to develop a theory where both fractional operators are taken into account, and for that we define a combined fractional variable order derivative operator that is a linear combination of the left and right fractional derivatives. For studies with fixed fractional order see [6]−[8].

Variational problems are often subject to one or more constraints. For example, isoperimetric problems are optimization problems where the admissible functions are subject to integral constraints. This direction of research has been recently investigated in [9], where variational problems with dependence on a combined Caputo derivative of variable fractional order are considered and necessary optimality conditions deduced. Here variational problems are considered subject to integral or holonomic constraints.

The text is organized in four sections. In Section II we review some important definitions and results about combined Caputo derivative of variable fractional order, and present some properties that will be need in the sequel. For more on the subject we refer the interested reader to [3], [10], [11]. In Section III we present two different isoperimetric problems and we study necessary optimality conditions in order to determine the minimizers for each of the problems. We end Section III with an example. In Section IV we consider a new variational problem subject to a holonomic constraint.

II. FRACTIONAL CALCULUS OF VARIABLE ORDER

In this section we collect definitions and preliminary results on fractional calculus, with variable fractional order, needed in the sequel. The variational fractional order is a continuous function of two variables, $\alpha : [a, b]^2 \to (0, 1)$. Let $x : [a, b] \to \mathbb{R}$. Two different types of fractional derivatives are considered.

Definition 1 (Riemann–Liouville fractional derivatives): The left and right Riemann–Liouville fractional derivatives of order $\alpha(\cdot, \cdot)$ are defined respectively by

$$
\begin{aligned}
&{}_aD_t^{\alpha(\cdot,\cdot)}x(t)\\
&\quad = \frac{d}{dt}\int_a^t \frac{1}{\Gamma(1-\alpha(t,\tau))}(t-\tau)^{-\alpha(t,\tau)}x(\tau)d\tau
\end{aligned}
$$

and

$$
\begin{aligned}
&{}_tD_b^{\alpha(\cdot,\cdot)}x(t)\\
&\quad = \frac{d}{dt}\int_t^b \frac{-1}{\Gamma(1-\alpha(\tau,t))}(\tau-t)^{-\alpha(\tau,t)}x(\tau)d\tau.
\end{aligned}
$$

Definition 2 (Caputo fractional derivatives): The left and right Caputo fractional derivatives of order $\alpha(\cdot,\cdot)$ are defined respectively by

$$
\begin{aligned}
&{}^C_a D_t^{\alpha(\cdot,\cdot)} x(t)\\
&= \int_a^t \frac{1}{\Gamma(1-\alpha(t,\tau))}(t-\tau)^{-\alpha(t,\tau)} x^{(1)}(\tau)d\tau
\end{aligned}
$$

and

$$
\begin{aligned}
&{}^C_t D_b^{\alpha(\cdot,\cdot)} x(t)\\
&= \int_t^b \frac{-1}{\Gamma(1-\alpha(\tau,t))}(\tau-t)^{-\alpha(\tau,t)} x^{(1)}(\tau)d\tau.
\end{aligned}
$$

Of course the fractional derivatives just defined are linear operators. The next step is to define a new fractional derivative, combining the previous ones into a single one.

Definition 3: Let $\alpha,\, \beta : [a,b]^2 \to (0,1)$ be the fractional orders, and define the constant vector $\gamma = (\gamma_1, \gamma_2) \in [0,1]^2$. The combined Riemann–Liouville fractional derivative of a function x is defined by

$$
D_\gamma^{\alpha(\cdot,\cdot),\beta(\cdot,\cdot)} x(t) = \gamma_1\, {}_aD_t^{\alpha(\cdot,\cdot)} x(t) + \gamma_2\, {}_tD_b^{\beta(\cdot,\cdot)} x(t).
$$

The combined Caputo fractional derivative of a function x is defined by

$$
{}^C D_\gamma^{\alpha(\cdot,\cdot),\beta(\cdot,\cdot)} x(t) = \gamma_1\, {}^C_a D_t^{\alpha(\cdot,\cdot)} x(t) + \gamma_2\, {}^C_t D_b^{\beta(\cdot,\cdot)} x(t).
$$

For the sequel, we also need the generalization of fractional integrals for a variable order.

Definition 4 (Riemann–Liouville fractional integrals): The left and right Riemann–Liouville fractional integrals of order $\alpha(\cdot,\cdot)$ are defined respectively by

$$
{}_aI_t^{\alpha(\cdot,\cdot)} x(t) = \int_a^t \frac{1}{\Gamma(\alpha(t,\tau))}(t-\tau)^{\alpha(t,\tau)-1} x(\tau)d\tau
$$

and

$$
{}_tI_b^{\alpha(\cdot,\cdot)} x(t) = \int_t^b \frac{1}{\Gamma(\alpha(\tau,t))}(\tau-t)^{\alpha(\tau,t)-1} x(\tau)d\tau.
$$

We remark that in contrast to the fixed fractional order case, variable-order fractional integrals are not the inverse operation of the variable-order fractional derivatives.

For the next section, we need the following fractional integration by parts formulas.

Theorem 1 (Theorem 3.2 of [11]): If $x, y \in C^1[a,b]$, then

$$
\begin{aligned}
&\int_a^b y(t)\, {}^C_a D_t^{\alpha(\cdot,\cdot)} x(t)dt\\
&= \int_a^b x(t)\, {}_tD_b^{\alpha(\cdot,\cdot)} y(t)dt + \left[x(t)\, {}_tI_b^{1-\alpha(\cdot,\cdot)} y(t)\right]_{t=a}^{t=b}
\end{aligned}
$$

and

$$
\begin{aligned}
&\int_a^b y(t)\, {}^C_t D_b^{\alpha(\cdot,\cdot)} x(t)dt\\
&= \int_a^b x(t)\, {}_aD_t^{\alpha(\cdot,\cdot)} y(t)dt - \left[x(t)\, {}_aI_t^{1-\alpha(\cdot,\cdot)} y(t)\right]_{t=a}^{t=b}.
\end{aligned}
$$

III. Fractional Isoperimetric Problems

Consider the set

$$
D = \Big\{(x,t) \in C^1([a,b]) \times [a,b] : {}^C D_\gamma^{\alpha(\cdot,\cdot),\beta(\cdot,\cdot)} x(t) \\ \text{exists and is continuous on } [a,b]\Big\}
$$

endowed with the norm

$$
\|(x,t)\| := \max_{a\le t\le b} |x(t)| + \max_{a\le t\le b} \left| {}^C D_\gamma^{\alpha(\cdot,\cdot),\beta(\cdot,\cdot)} x(t)\right| + |t|.
$$

Throughout the text, we denote by $\partial_i z$ the partial derivative of a function $z : \mathbb{R}^3 \to \mathbb{R}$ with respect to its i-th argument. Also, for simplification, we consider the operator

$$
[x]_\gamma^{\alpha,\beta}(t) := \left(t, x(t), {}^C D_\gamma^{\alpha(\cdot,\cdot),\beta(\cdot,\cdot)} x(t)\right).
$$

The main problem of the fractional calculus of variations with variable order is described as follows. Let $L : C^1\left([a,b]\times\mathbb{R}^2\right) \to \mathbb{R}$ and consider the functional $\mathcal{J} : D \to \mathbb{R}$ of the form

$$
\mathcal{J}(x,T) = \int_a^T L[x]_\gamma^{\alpha,\beta}(t)dt + \phi(T, x(T)) \tag{1}
$$

where $\phi : [a,b]\times\mathbb{R} \to \mathbb{R}$ is of class C^1. In the sequel, we need the auxiliary notation of the dual fractional derivative:

$$
D_{\overline{\gamma},c}^{\beta(\cdot,\cdot),\alpha(\cdot,\cdot)} = \gamma_2\, {}_aD_t^{\beta(\cdot,\cdot)} + \gamma_1\, {}_tD_c^{\alpha(\cdot,\cdot)} \tag{2}
$$

where $\overline{\gamma} = (\gamma_2, \gamma_1)$ and $c \in (a,b]$.

Remark 1: Fractional derivatives (2) can be regarded as a generalization of usual fractional derivatives. For advantages of applying them to fractional variational problems see [8], [12], [13].

In [9] we obtained necessary conditions that every local minimizer of functional $\mathcal{J}$ must fulfill.

Theorem 2 [9]: If $(x,T) \in D$ is a local minimizer of functional (1), then (x,T) satisfies the fractional differential equation

$$
\partial_2 L[x]_\gamma^{\alpha,\beta}(t) + D_{\overline{\gamma},T}^{\beta(\cdot,\cdot),\alpha(\cdot,\cdot)} \partial_3 L[x]_\gamma^{\alpha,\beta}(t) = 0
$$

on $[a,T]$ and

$$
\gamma_2\left({}_aD_t^{\beta(\cdot,\cdot)} \partial_3 L[x]_\gamma^{\alpha,\beta}(t) - {}_TD_t^{\beta(\cdot,\cdot)} \partial_3 L[x]_\gamma^{\alpha,\beta}(t)\right) = 0
$$

on $[T,b]$.

Remark 2: In general, analytical solutions to fractional variational problems are hard to find. For this reason, numerical methods are often used. The reader interested in this subject is referred to [14], [15] and references therein.

Fractional differential equations as the ones given by Theorem 2, are known in the literature as fractional Euler–Lagrange equations, and they provide us with a method to determine the candidates for solutions of the problem addressed. Solutions of such fractional differential equations are called extremals for the functional. In this paper, we proceed the study initiated in [9] by considering additional constraints to the problems. We will deal with two types of isoperimetric problems, which we now describe.

A. Problem I

The fractional isoperimetric problem of the calculus of variations consists to determine the local minimizers of $\mathcal{J}$ over all $(x,T)\in D$ satisfying a boundary condition

$$x(a)=x_a \tag{3}$$

for a fixed $x_a\in\mathbb{R}$ and an integral constraint of the form

$$\int_a^T g[x]_\gamma^{\alpha,\beta}(t)dt=\psi(T) \tag{4}$$

where $g:C^1\left([a,b]\times\mathbb{R}^2\right)\to\mathbb{R}$ and $\psi:[a,b]\to\mathbb{R}$ are two differentiable functions. The terminal time T and terminal state $x(T)$ are free. In this problem, the condition of the form (4) is called an isoperimetric constraint. The next theorem gives fractional necessary optimality conditions to this isoperimetric problem.

Theorem 3: Suppose that (x,T) gives a local minimum for functional (1) on D subject to the boundary condition (3) and the isoperimetric constraint (4). If (x,T) does not satisfies the Euler–Lagrange equations with respect to the isoperimetric constraint, that is, if one of the two following conditions is not verified,

$$\partial_2 g[x]_\gamma^{\alpha,\beta}(t)+D_{\gamma,T}^{\beta(\cdot,\cdot),\alpha(\cdot,\cdot)}\partial_3 g[x]_\gamma^{\alpha,\beta}(t)=0 \tag{5}$$

for $t\in[a,T]$, or

$$\gamma_2\left[{}_aD_t^{\beta(\cdot,\cdot)}\partial_3 g[x]_\gamma^{\alpha,\beta}(t)-{}_TD_t^{\beta(\cdot,\cdot)}\partial_3 g[x]_\gamma^{\alpha,\beta}(t)\right]=0 \tag{6}$$

for $t\in[T,b]$, then there exists a constant λ such that, if we define the function $F:[a,b]\times\mathbb{R}^2\to\mathbb{R}$ by $F=L-\lambda g$, (x,T) satisfies the fractional Euler – Lagrange equations

$$\partial_2 F[x]_\gamma^{\alpha,\beta}(t)+D_{\gamma,T}^{\beta(\cdot,\cdot),\alpha(\cdot,\cdot)}\partial_3 F[x]_\gamma^{\alpha,\beta}(t)=0 \tag{7}$$

on the interval $[a,T]$ and

$$\gamma_2\left({}_aD_t^{\beta(\cdot,\cdot)}\partial_3 F[x]_\gamma^{\alpha,\beta}(t)\ -{}_TD_t^{\beta(\cdot,\cdot)}\partial_3 F[x]_\gamma^{\alpha,\beta}(t)\right)=0 \tag{8}$$

on the interval $[T,b]$. Moreover, (x,T) satisfies the transversality conditions

$$\begin{cases} F[x]_\gamma^{\alpha,\beta}(T)+\partial_1\phi(T,x(T)) \\ \quad +\partial_2\phi(T,x(T))x'(T)+\lambda\psi'(T)=0 \\ \Big[\gamma_1\,{}_tI_T^{1-\alpha(\cdot,\cdot)}\partial_3 F[x]_\gamma^{\alpha,\beta}(t) \\ \quad -\gamma_2\,{}_TI_t^{1-\beta(\cdot,\cdot)}\partial_3 F[x]_\gamma^{\alpha,\beta}(t)\Big]_{t=T} \\ \quad +\partial_2\phi(T,x(T))=0 \\ \gamma_2\Big[{}_TI_t^{1-\beta(\cdot,\cdot)}\partial_3 F[x]_\gamma^{\alpha,\beta}(t) \\ \quad -{}_aI_t^{1-\beta(\cdot,\cdot)}\partial_3 F[x]_\gamma^{\alpha,\beta}(t)\Big]_{t=b}=0. \end{cases} \tag{9}$$

Proof: Consider variations of the optimal solution (x,T) of the type

$$(x^*,T^*)=(x+\epsilon_1h_1+\epsilon_2h_2,T+\epsilon_1\Delta T) \tag{10}$$

where, for each $i\in\{1,2\}$, $\epsilon_i\in\mathbb{R}$ is a small parameter, $h_i\in C^1([a,b])$ satisfies $h_i(a)=0$, and $\triangle T\in\mathbb{R}$. The additional term ϵ_2h_2 must be selected so that the admissible variations (x^*,T^*) satisfy the isoperimetric constraint (4). For a fixed choice of h_i, let

$$i(\epsilon_1,\epsilon_2)=\int_a^{T+\epsilon_1\triangle T}g[x^*]_\gamma^{\alpha,\beta}(t)dt-\psi(T+\epsilon_1\triangle T).$$

For $\epsilon_1=\epsilon_2=0$, we obtain that

$$\begin{aligned} i(0,0)&=\int_a^T g[x]_\gamma^{\alpha,\beta}(t)dt-\psi(T)\\ &=\psi(T)-\psi(T)=0. \end{aligned}$$

The derivative $\dfrac{\partial i}{\partial\epsilon_2}$ is given by

$$\begin{aligned} \frac{\partial i}{\partial\epsilon_2}=\int_a^{T+\epsilon_1\triangle T}&\big(\partial_2 g[x^*]_\gamma^{\alpha,\beta}(t)h_2(t)\\ &+\partial_3 g[x^*]_\gamma^{\alpha,\beta}(t)^C D_\gamma^{\alpha(\cdot,\cdot),\beta(\cdot,\cdot)}h_2(t)\big)dt. \end{aligned}$$

For $\epsilon_1=\epsilon_2=0$ one has

$$\begin{aligned} \left.\frac{\partial i}{\partial\epsilon_2}\right|_{(0,0)}=\int_a^T&\big(\partial_2 g[x]_\gamma^{\alpha,\beta}(t)h_2(t)\\ &+\partial_3 g[x]_\gamma^{\alpha,\beta}(t)^C D_\gamma^{\alpha(\cdot,\cdot),\beta(\cdot,\cdot)}h_2(t)\big)dt. \end{aligned} \tag{11}$$

The second term in (11) can be written as

$$\begin{aligned} &\int_a^T\partial_3 g[x]_\gamma^{\alpha,\beta}(t)^C D_\gamma^{\alpha(\cdot,\cdot),\beta(\cdot,\cdot)}h_2(t)dt\\ &=\int_a^T\partial_3 g[x]_\gamma^{\alpha,\beta}(t)\left[\gamma_1\,{}_a^CD_t^{\alpha(\cdot,\cdot)}h_2(t)\right.\\ &\quad\left.+\gamma_2\,{}_t^CD_b^{\beta(\cdot,\cdot)}h_2(t)\right]dt\\ &=\gamma_1\int_a^T\partial_3 g[x]_\gamma^{\alpha,\beta}(t){}_a^CD_t^{\alpha(\cdot,\cdot)}h_2(t)dt\\ &\quad+\gamma_2\left[\int_a^b\partial_3 g[x]_\gamma^{\alpha,\beta}(t){}_t^CD_b^{\beta(\cdot,\cdot)}h_2(t)dt\right.\\ &\quad\left.-\int_T^b\partial_3 g[x]_\gamma^{\alpha,\beta}(t){}_t^CD_b^{\beta(\cdot,\cdot)}h_2(t)dt\right]. \end{aligned} \tag{12}$$

Using the fractional integrating by parts formula, (12) is equal to

$$\begin{aligned} &\int_a^T h_2(t)\left[\gamma_1{}_tD_T{}^{\alpha(\cdot,\cdot)}\partial_3 g[x]_\gamma^{\alpha,\beta}(t)\right.\\ &\qquad\left.+\gamma_2{}_aD_t{}^{\beta(\cdot,\cdot)}\partial_3 g[x]_\gamma^{\alpha,\beta}(t)\right]dt\\ &+\int_T^b\gamma_2h_2(t)\left[{}_aD_t^{\beta(\cdot,\cdot)}\partial_3 g[x]_\gamma^{\alpha,\beta}(t)\right.\\ &\qquad\left.-{}_TD_t{}^{\beta(\cdot,\cdot)}\partial_3 g[x]_\gamma^{\alpha,\beta}(t)\right]dt\\ &+\left[h_2(t)\Big(\gamma_1{}_tI_T{}^{1-\alpha(\cdot,\cdot)}\partial_3 g[x]_\gamma^{\alpha,\beta}(t)\right.\\ &\qquad\left.-\gamma_2{}_TI_t{}^{1-\beta(\cdot,\cdot)}\partial_3 g[x]_\gamma^{\alpha,\beta}(t)\Big)\right]_{t=T}\\ &+\left[\gamma_2h_2(t)\Big({}_TI_t{}^{1-\beta(\cdot,\cdot)}\partial_3 g[x]_\gamma^{\alpha,\beta}(t)\right.\\ &\qquad\left.-\ {}_aI_t{}^{1-\beta(\cdot,\cdot)}\partial_3 g[x]_\gamma^{\alpha,\beta}(t)\Big)\right]_{t=b}. \end{aligned}$$

Substituting these relations into (11), and considering the fractional operator $D^{\beta(\cdot,\cdot),\alpha(\cdot,\cdot)}_{\overline{\gamma},c}$ as defined in (2), we obtain that

$$\begin{aligned}
&\left.\frac{\partial i}{\partial \epsilon_2}\right|_{(0,0)}\\
&= \int_a^T h_2(t)\left[\partial_2 g[x]^{\alpha,\beta}_{\gamma}(t) + D^{\beta(\cdot,\cdot),\alpha(\cdot,\cdot)}_{\overline{\gamma},T}\partial_3 g[x]^{\alpha,\beta}_{\gamma}(t)\right]dt\\
&\quad + \int_T^b \gamma_2 h_2(t)\left[{}_aD_t^{\beta(\cdot,\cdot)}\partial_3 g[x]^{\alpha,\beta}_{\gamma}(t)\right.\\
&\qquad\qquad \left. - {}_TD_t{}^{\beta(\cdot,\cdot)}\partial_3 g[x]^{\alpha,\beta}_{\gamma}(t)\right]dt\\
&\quad + \left[h_2(t)\left(\gamma_{1\,t}I_T{}^{1-\alpha(\cdot,\cdot)}\partial_3 g[x]^{\alpha,\beta}_{\gamma}(t)\right.\right.\\
&\qquad\qquad \left.\left. - \gamma_{2\,T}I_t{}^{1-\beta(\cdot,\cdot)}\partial_3 g[x]^{\alpha,\beta}_{\gamma}(t)\right)\right]_{t=T}\\
&\quad + \left[\gamma_2 h_2(t)\left({}_TI_t{}^{1-\beta(\cdot,\cdot)}\partial_3 g[x]^{\alpha,\beta}_{\gamma}(t)\right.\right.\\
&\qquad\qquad \left.\left. - {}_aI_t{}^{1-\beta(\cdot,\cdot)}\partial_3 g[x]^{\alpha,\beta}_{\gamma}(t)\right)\right]_{t=b}.
\end{aligned}$$

Since (5) or (6) fails, there exists a function h_2 such that

$$\left.\frac{\partial i}{\partial \epsilon_2}\right|_{(0,0)} \neq 0.$$

In fact, if not, from the arbitrariness of the function h_2 and the fundamental lemma of the calculus of the variations, (5) and (6) would be verified. Thus, we may apply the implicit function theorem, that ensures the existence of a function $\epsilon_2(\cdot)$, defined in a neighborhood of zero, such that $i(\epsilon_1, \epsilon_2(\epsilon_1)) = 0$. In conclusion, there exists a subfamily of variations of the form (10) that verifies the integral constraint (4). We now seek to prove the main result. For that purpose, consider the auxiliary function $j(\epsilon_1, \epsilon_2) = \mathcal{J}(x^*, T^*)$. By hypothesis, function j attains a local minimum at $(0,0)$ when subject to the constraint $i(\cdot,\cdot) = 0$, and we proved before that $\nabla i(0,0) \neq 0$. Applying the Lagrange multiplier rule, we ensure the existence of a number λ such that

$$\nabla\left(j(0,0) - \lambda i(0,0)\right) = 0.$$

In particular,

$$\frac{\partial\left(j - \lambda i\right)}{\partial \epsilon_1}(0,0) = 0. \tag{13}$$

Let $F = L - \lambda g$. The relation (13) can be written as

$$\begin{aligned}
0 &= \int_a^T h_1(t)\Big[\partial_2 F[x]^{\alpha,\beta}_{\gamma}(t)\\
&\qquad + D^{\beta(\cdot,\cdot),\alpha(\cdot,\cdot)}_{\overline{\gamma},T}\partial_3 F[x]^{\alpha,\beta}_{\gamma}(t)\Big]dt\\
&\quad + \int_T^b \gamma_2 h_1(t)\left[{}_aD_t^{\beta(\cdot,\cdot)}\partial_3 F[x]^{\alpha,\beta}_{\gamma}(t)\right.\\
&\qquad \left. - {}_TD_t^{\beta(\cdot,\cdot)}\partial_3 F[x]^{\alpha,\beta}_{\gamma}(t)\right]dt\\
&\quad + h_1(T)\left[\gamma_{1\,t}I_T^{1-\alpha(\cdot,\cdot)}\partial_3 F[x]^{\alpha,\beta}_{\gamma}(t)\right.\\
&\qquad \left. - \gamma_{2\,T}I_t^{1-\beta(\cdot,\cdot)}\partial_3 F[x]^{\alpha,\beta}_{\gamma}(t) + \partial_2\phi(t,x(t))\right]_{t=T}\\
&\quad + \Delta T\Big[F[x]^{\alpha,\beta}_{\gamma}(t) + \partial_1\phi(t,x(t))\\
&\qquad + \partial_2\phi(t,x(t))x'(t) + \lambda\psi'(t)\Big]_{t=T}\\
&\quad + h_1(b)\gamma_2\left[{}_TI_t^{1-\beta(\cdot,\cdot)}\partial_3 F[x]^{\alpha,\beta}_{\gamma}(t)\right.\\
&\qquad \left. - {}_aI_t^{1-\beta(\cdot,\cdot)}\partial_3 F[x]^{\alpha,\beta}_{\gamma}(t)\right]_{t=b}.
\end{aligned}\tag{14}$$

As h_1 and $\triangle T$ are arbitrary, we can choose $\triangle T = 0$ and $h_1(t) = 0$ for all $t \in [T, b]$. But h_1 is arbitrary in $t \in [a, T)$. Then, we obtain the first necessary condition (7):

$$\partial_2 F[x]^{\alpha,\beta}_{\gamma}(t) + D^{\beta(\cdot,\cdot),\alpha(\cdot,\cdot)}_{\overline{\gamma},T}\partial_3 F[x]^{\alpha,\beta}_{\gamma}(t) = 0$$

for all $t \in [a, T]$. Analogously, considering $\triangle T = 0$ and $h_1(t) = 0$ for all $t \in [a, T] \cup \{b\}$, and h_1 arbitrary on (T, b), we obtain the second necessary condition (8):

$$\begin{aligned}
&\gamma_2\left({}_aD_t^{\beta(\cdot,\cdot)}\partial_3 F[x]^{\alpha,\beta}_{\gamma}(t)\right.\\
&\qquad \left. - {}_TD_t^{\beta(\cdot,\cdot)}\partial_3 F[x]^{\alpha,\beta}_{\gamma}(t)\right) = 0 \quad \forall t \in [T, b].
\end{aligned}$$

As (x, T) is a solution to the necessary conditions (7) and (8), then (14) takes the form

$$\begin{aligned}
0 &= h_1(T)\left[\gamma_{1\,t}I_T^{1-\alpha(\cdot,\cdot)}\partial_3 F[x]^{\alpha,\beta}_{\gamma}(t)\right.\\
&\qquad \left. - \gamma_{2\,T}I_t^{1-\beta(\cdot,\cdot)}\partial_3 F[x]^{\alpha,\beta}_{\gamma}(t) + \partial_2\phi(t,x(t))\right]_{t=T}\\
&\quad + \Delta T\Big[F[x]^{\alpha,\beta}_{\gamma}(t) + \partial_1\phi(t,x(t))\\
&\qquad + \partial_2\phi(t,x(t))x'(t) + \lambda\psi'(t)\Big]_{t=T}\\
&\quad + h_1(b)\left[\gamma_2\left({}_TI_t^{1-\beta(\cdot,\cdot)}\partial_3 F[x]^{\alpha,\beta}_{\gamma}(t)\right.\right.\\
&\qquad \left.\left. - {}_aI_t^{1-\beta(\cdot,\cdot)}\partial_3 F[x]^{\alpha,\beta}_{\gamma}(t)\right)\right]_{t=b}.
\end{aligned}\tag{15}$$

Transversality conditions (9) are obtained for appropriate choices of variations. ■

In the next theorem, considering the same Problem I, we rewrite the transversality conditions (9) in terms of the increment on time ΔT and on the increment of space Δx_T given by

$$\Delta x_T = (x + h_1)(T + \Delta T) - x(T). \tag{16}$$

Theorem 4: Let (x, T) be a local minimizer to the functional (1) on D subject to the boundary condition (3) and the isoperimetric constraint (4). Then (x, T) satisfies the transversality conditions

$$\begin{cases}
F[x]^{\alpha,\beta}_{\gamma}(T) + \partial_1\phi(T,x(T)) + \lambda\psi'(T)\\
\quad + x'(T)\left[\gamma_{2\,T}I_t^{1-\beta(\cdot,\cdot)}\partial_3 F[x]^{\alpha,\beta}_{\gamma}(t)\right.\\
\qquad \left. - \gamma_{1\,t}I_T^{1-\alpha(\cdot,\cdot)}\partial_3 F[x]^{\alpha,\beta}_{\gamma}(t)\right]_{t=T} = 0\\
\left[\gamma_{1\,t}I_T^{1-\alpha(\cdot,\cdot)}\partial_3 F[x]^{\alpha,\beta}_{\gamma}(t)\right.\\
\quad \left. - \gamma_{2\,T}I_t^{1-\beta(\cdot,\cdot)}\partial_3 F[x]^{\alpha,\beta}_{\gamma}(t)\right]_{t=T}\\
\quad + \partial_2\phi(T,x(T)) = 0\\
\gamma_2\left[{}_TI_t^{1-\beta(\cdot,\cdot)}\partial_3 F[x]^{\alpha,\beta}_{\gamma}(t)\right.\\
\quad \left. - {}_aI_t^{1-\beta(\cdot,\cdot)}\partial_3 F[x]^{\alpha,\beta}_{\gamma}(t)\right]_{t=b} = 0.
\end{cases}\tag{17}$$

Proof: Suppose (x^*, T^*) is an admissible variation of the form (10) with $\epsilon_1 = 1$ and $\epsilon_2 = 0$. Using Taylor's expansion up to first order for a small ΔT, and restricting the set of variations to those for which $h_1'(T) = 0$, we obtain the increment Δx_T on x:

$$(x + h_1)(T + \Delta T) = (x + h_1)(T) + x'(T)\Delta T + O(\Delta T)^2.$$

Relation (16) allows us to express $h_1(T)$ in terms of ΔT and Δx_T:

$$h_1(T) = \Delta x_T - x'(T)\Delta T + O(\Delta T)^2.$$

Substituting this expression into (15), and using appropriate choices of variations, we obtain the new transversality conditions (17). ■

Theorem 5: Suppose that (x, T) gives a local minimum for functional (1) on D subject to the boundary condition (3) and the isoperimetric constraint (4). Then, there exists $(\lambda_0, \lambda) \neq (0, 0)$ such that, if we define the function $F : [a, b] \times \mathbb{R}^2 \to \mathbb{R}$ by $F = \lambda_0 L - \lambda g$, (x, T) satisfies the following fractional Euler–Lagrange equations:

$$\partial_2 F[x]_\gamma^{\alpha,\beta}(t) + D_{\overline{\gamma},T}^{\beta(\cdot,\cdot),\alpha(\cdot,\cdot)} \partial_3 F[x]_\gamma^{\alpha,\beta}(t) = 0$$

on the interval $[a, T]$, and

$$\gamma_2 \left({}_aD_t^{\beta(\cdot,\cdot)} \partial_3 F[x]_\gamma^{\alpha,\beta}(t) - {}_TD_t^{\beta(\cdot,\cdot)} \partial_3 F[x]_\gamma^{\alpha,\beta}(t) \right) = 0$$

on the interval $[T, b]$.

Proof: If (x, T) does not verifies (5) or (6), then the hypothesis of Theorem 3 is satisfied and we prove Theorem 5 considering $\lambda_0 = 1$. If (x, T) verifies (5) and (6), then we prove the result by considering $\lambda = 1$ and $\lambda_0 = 0$. ■

B. Problem II

We now consider a new isoperimetric type problem with the isoperimetric constraint of form

$$\int_a^b g[x]_\gamma^{\alpha,\beta}(t)dt = C \tag{18}$$

where C is a given real number.

Theorem 6: Suppose that (x, T) gives a local minimum for functional (1) on D subject to the boundary condition (3) and the isoperimetric constraint (18). If (x, T) does not satisfies the Euler–Lagrange equation with respect to the isoperimetric constraint, that is, the condition

$$\partial_2 g[x]_\gamma^{\alpha,\beta}(t) + D_{\overline{\gamma},b}^{\beta(\cdot,\cdot),\alpha(\cdot,\cdot)} \partial_3 g[x]_\gamma^{\alpha,\beta}(t) = 0$$

for $t \in [a, b]$ is not satisfied, then there exists $\lambda \neq 0$ such that, if we define the function $F : [a, b] \times \mathbb{R}^2 \to \mathbb{R}$ by $F = L - \lambda g$, (x, T) satisfies the fractional Euler–Lagrange equations

$$\begin{aligned} \partial_2 F[x]_\gamma^{\alpha,\beta}(t) &+ D_{\overline{\gamma},T}^{\beta(\cdot,\cdot),\alpha(\cdot,\cdot)} \partial_3 L[x]_\gamma^{\alpha,\beta}(t) \\ &- \lambda D_{\overline{\gamma},b}^{\beta(\cdot,\cdot),\alpha(\cdot,\cdot)} \partial_3 g[x]_\gamma^{\alpha,\beta}(t) = 0 \end{aligned} \tag{19}$$

on the interval $[a, T]$, and

$$\begin{aligned} &\gamma_2 \left({}_aD_t^{\beta(\cdot,\cdot)} \partial_3 F[x]_\gamma^{\alpha,\beta}(t) - {}_TD_t^{\beta(\cdot,\cdot)} \partial_3 L[x]_\gamma^{\alpha,\beta}(t) \right) \\ &-\lambda \left(\partial_2 g[x]_\gamma^{\alpha,\beta}(t) + \gamma_1 {}_tD_b^{\alpha(\cdot,\cdot)} \partial_3 g[x]_\gamma^{\alpha,\beta}(t) \right) = 0 \end{aligned} \tag{20}$$

on the interval $[T, b]$. Moreover, (x, T) satisfies the transversality conditions

$$\begin{cases} L[x]_\gamma^{\alpha,\beta}(T) + \partial_1 \phi(T, x(T)) \\ \quad + \partial_2 \phi(T, x(T)) x'(T) = 0 \\ \Big[\gamma_1 {}_tI_T^{1-\alpha(\cdot,\cdot)} \partial_3 L[x]_\gamma^{\alpha,\beta}(t) \\ \quad - \gamma_2 {}_TI_t^{1-\beta(\cdot,\cdot)} \partial_3 L[x]_\gamma^{\alpha,\beta}(t) \\ \quad + \partial_2 \phi(t, x(t)) \Big]_{t=T} = 0 \\ \Big[- \lambda \gamma_1 {}_tI_b^{1-\alpha(\cdot,\cdot)} \partial_3 g[x]_\gamma^{\alpha,\beta}(t) \\ \quad + \gamma_2 \Big({}_TI_t^{1-\beta(\cdot,\cdot)} \partial_3 L[x]_\gamma^{\alpha,\beta}(t) \\ \quad - {}_aI_t^{1-\beta(\cdot,\cdot)} \partial_3 F[x]_\gamma^{\alpha,\beta}(t) \Big) \Big]_{t=b} = 0. \end{cases} \tag{21}$$

Proof: Similarly as done to prove Theorem 3, let

$$(x^*, T^*) = (x + \epsilon_1 h_1 + \epsilon_2 h_2, T + \epsilon_1 \Delta T)$$

be a variation of the solution, and define

$$i(\epsilon_1, \epsilon_2) = \int_a^b g[x^*]_\gamma^{\alpha,\beta}(t)dt - C.$$

The derivative $\dfrac{\partial i}{\partial \epsilon_2}$, when $\epsilon_1 = \epsilon_2 = 0$, is

$$\begin{aligned} \frac{\partial i}{\partial \epsilon_2}\bigg|_{(0,0)} = \int_a^b \Big(&\partial_2 g[x]_\gamma^{\alpha,\beta}(t) h_2(t) \\ &+ \partial_3 g[x]_\gamma^{\alpha,\beta}(t) {}^C D_\gamma^{\alpha(\cdot,\cdot),\beta(\cdot,\cdot)} h_2(t) \Big) dt. \end{aligned}$$

Integrating by parts and choosing variations such that $h_2(b) = 0$, we have

$$\begin{aligned} \frac{\partial i}{\partial \epsilon_2}\bigg|_{(0,0)} = \int_a^b h_2(t) \Big[&\partial_2 g[x]_\gamma^{\alpha,\beta}(t) \\ &+ D_{\overline{\gamma},b}^{\beta(\cdot,\cdot),\alpha(\cdot,\cdot)} \partial_3 g[x]_\gamma^{\alpha,\beta}(t) \Big] dt. \end{aligned}$$

Thus, there exists a function h_2 such that

$$\frac{\partial i}{\partial \epsilon_2}\bigg|_{(0,0)} \neq 0.$$

We may apply the implicit function theorem to conclude that there exists a subfamily of variations satisfying the integral constraint. Consider the new function $j(\epsilon_1, \epsilon_2) = \mathcal{J}(x^*, T^*)$. Since j has a local minimum at $(0, 0)$ when subject to the constraint $i(\cdot, \cdot) = 0$ and $\nabla i(0, 0) \neq 0$, there exists a number λ such that

$$\frac{\partial}{\partial \epsilon_1} (j - \lambda i)(0, 0) = 0. \tag{22}$$

Let $F = L - \lambda g$. Relation (22) can be written as

$$\begin{aligned} 0 = \int_a^T h_1(t) \Big[&\partial_2 F[x]_\gamma^{\alpha,\beta}(t) \\ &+ D_{\overline{\gamma},T}^{\beta(\cdot,\cdot),\alpha(\cdot,\cdot)} \partial_3 L[x]_\gamma^{\alpha,\beta}(t) \\ &- \lambda D_{\overline{\gamma},b}^{\beta(\cdot,\cdot),\alpha(\cdot,\cdot)} \partial_3 g[x]_\gamma^{\alpha,\beta}(t) \Big] dt \\ + \int_T^b h_1(t) \Big[&\gamma_2 \Big({}_aD_t^{\beta(\cdot,\cdot)} \partial_3 F[x]_\gamma^{\alpha,\beta}(t) \end{aligned}$$

$$
\begin{aligned}
&- {}_T D_t^{\beta(\cdot,\cdot)} \partial_3 L[x]_\gamma^{\alpha,\beta}(t)\Big) \\
&- \lambda\Big(\partial_2 g[x]_\gamma^{\alpha,\beta}(t) \\
&+ \gamma_1 {}_t D_b^{\alpha(\cdot,\cdot)} \partial_3 g[x]_\gamma^{\alpha,\beta}(t)\Big)\Big]\, dt \\
+ h_1(T) &\Big[\gamma_1\, {}_t I_T^{1-\alpha(\cdot,\cdot)} \partial_3 L[x]_\gamma^{\alpha,\beta}(t) \\
&- \gamma_2\, {}_T I_t^{1-\beta(\cdot,\cdot)} \partial_3 L[x]_\gamma^{\alpha,\beta}(t) \\
&+ \partial_2 \phi(t, x(t))\Big]_{t=T} \\
+ \Delta T &\Big[L[x]_\gamma^{\alpha,\beta}(t) + \partial_1 \phi(t, x(t)) \\
&+ \partial_2 \phi(t, x(t)) x'(t)\Big]_{t=T} \\
+ h_1(b) &\Big[-\lambda \gamma_1 {}_t I_b^{1-\alpha(\cdot,\cdot)} \partial_3 g[x]_\gamma^{\alpha,\beta}(t) \\
&+ \gamma_2 \Big({}_T I_t^{1-\beta(\cdot,\cdot)} \partial_3 L[x]_\gamma^{\alpha,\beta}(t) \\
&- {}_a I_t^{1-\beta(\cdot,\cdot)} \partial_3 F[x]_\gamma^{\alpha,\beta}(t)\Big)\Big]_{t=b}.
\end{aligned}
$$

Considering appropriate choices of variations, we obtain the first (19) and the second (20) necessary optimality conditions, and also the transversality conditions (21). ■

Similarly to Theorem 5, the following result holds.

Theorem 7: Suppose that (x, T) gives a local minimum for functional (1) on D subject to the boundary condition (3) and the isoperimetric constraint (18). Then there exists $(\lambda_0, \lambda) \neq (0, 0)$ such that, if we define the function $F : [a, b] \times \mathbb{R}^2 \to \mathbb{R}$ by $F = \lambda_0 L - \lambda g$, (x, T) satisfies the fractional Euler–Lagrange equations

$$
\begin{aligned}
&\partial_2 F[x]_\gamma^{\alpha,\beta}(t) + D_{\overline{\gamma},T}^{\beta(\cdot,\cdot),\alpha(\cdot,\cdot)} \partial_3 L[x]_\gamma^{\alpha,\beta}(t) \\
&- \lambda D_{\overline{\gamma},b}^{\beta(\cdot,\cdot),\alpha(\cdot,\cdot)} \partial_3 g[x]_\gamma^{\alpha,\beta}(t) = 0
\end{aligned}
$$

on the interval $[a, T]$, and

$$
\gamma_2 \left({}_a D_t^{\beta(\cdot,\cdot)} \partial_3 F[x]_\gamma^{\alpha,\beta}(t) - {}_T D_t^{\beta(\cdot,\cdot)} \partial_3 L[x]_\gamma^{\alpha,\beta}(t)\right)
$$

$$
-\lambda \left(\partial_2 g[x]_\gamma^{\alpha,\beta}(t) + \gamma_1 {}_t D_b^{\alpha(\cdot,\cdot)} \partial_3 g[x]_\gamma^{\alpha,\beta}(t)\right) = 0
$$

on the interval $[T, b]$.

C. An example

Let $\alpha(t, \tau) = \alpha(t)$ and $\beta(t, \tau) = \beta(\tau)$. Define the function

$$
\psi(T) = \int_0^T \left(\frac{t^{1-\alpha(t)}}{2\Gamma(2-\alpha(t))} + \frac{(b-t)^{1-\beta(t)}}{2\Gamma(2-\beta(t))}\right)^2 dt
$$

on the interval $[0, b]$ with $b > 0$. Consider the functional J defined by

$$
\begin{aligned}
J(x, t) = \int_0^T &\Bigg[\alpha(t) + \left({}^C D_\gamma^{\alpha(\cdot,\cdot),\beta(\cdot,\cdot)} x(t)\right)^2 \\
&+ \left(\frac{t^{1-\alpha(t)}}{2\Gamma(2-\alpha(t))} + \frac{(b-t)^{1-\beta(t)}}{2\Gamma(2-\beta(t))}\right)^2\Bigg] dt
\end{aligned}
$$

for $t \in [0, b]$ and $\gamma = (1/2, 1/2)$, subject to the initial condition

$$
x(0) = 0
$$

and the isoperimetric constraint

$$
\begin{aligned}
\int_0^T {}^C D_\gamma^{\alpha(\cdot,\cdot),\beta(\cdot,\cdot)} x(t) &\left(\frac{t^{1-\alpha(t)}}{2\Gamma(2-\alpha(t))} + \frac{(b-t)^{1-\beta(t)}}{2\Gamma(2-\beta(t))}\right)^2 dt \\
&= \psi(T).
\end{aligned}
$$

Define $F = L - \lambda g$ with $\lambda = 2$, that is,

$$
\begin{aligned}
F = \alpha(t) + \Big(&{}^C D_\gamma^{\alpha(\cdot),\beta(\cdot)} x(t) \\
&- \frac{t^{1-\alpha(t)}}{2\Gamma(2-\alpha(t))} - \frac{(b-t)^{1-\beta(t)}}{2\Gamma(2-\beta(t))}\Big)^2.
\end{aligned}
$$

Consider the function $\overline{x}(t) = t$ with $t \in [0, b]$. Because

$$
{}^C D_\gamma^{\alpha(\cdot,\cdot),\beta(\cdot,\cdot)} \overline{x}(t) = \frac{t^{1-\alpha(t)}}{2\Gamma(2-\alpha(t))} + \frac{(b-t)^{1-\beta(t)}}{2\Gamma(2-\beta(t))}
$$

we have that $\overline{x}$ satisfies conditions (7), (8) and the two last of (9). Using the first condition of (9), that is,

$$
\alpha(t) + 2\left(\frac{T^{1-\alpha(T)}}{2\Gamma(2-\alpha(T))} + \frac{(b-T)^{1-\beta(T)}}{2\Gamma(2-\beta(T))}\right)^2 = 0
$$

we obtain the optimal time T.

IV. Holonomic Constraints

Consider the space

$$
\begin{aligned}
U = \{&(x_1, x_2, T) \in C^1([a, b]) \times C^1([a, b]) \times [a, b] : \\
&x_1(a) = x_{1a} \wedge x_2(a) = x_{2a}\}
\end{aligned} \tag{23}
$$

for fixed reals $x_{1a}, x_{2a} \in \mathbb{R}$. In this section we consider the functional $\mathcal{J}$ defined in U by

$$
\begin{aligned}
\mathcal{J}(x_1, x_2, T) = \int_a^T L\Big(&t, x_1(t), x_2(t), {}^C D_\gamma^{\alpha(\cdot,\cdot),\beta(\cdot,\cdot)} x_1(t), \\
&{}^C D_\gamma^{\alpha(\cdot,\cdot),\beta(\cdot,\cdot)} x_2(t)\Big) dt + \phi(T, x_1(T), x_2(T))
\end{aligned} \tag{24}
$$

with terminal time T and terminal states $x_1(T)$ and $x_2(T)$ free. The Lagrangian $L : [a, b] \times \mathbb{R}^4 \to \mathbb{R}$ is a continuous function and continuously differentiable with respect to its i-th argument, $i \in \{2, 3, 4, 5\}$. To define the variational problem, we consider a new constraint of the form

$$
g(t, x_1(t), x_2(t)) = 0, \quad t \in [a, b] \tag{25}
$$

where $g : [a, b] \times \mathbb{R}^2 \to \mathbb{R}$ is a continuous function and continuously differentiable with respect to second and third arguments. This constraint is called a holonomic constraint. The next theorem gives fractional necessary optimality conditions to the variational problem with a holonomic constraint. To simplify the notation, we denote by x the vector (x_1, x_2); by ${}^C D_\gamma^{\alpha(\cdot,\cdot),\beta(\cdot,\cdot)} x$ the vector $({}^C D_\gamma^{\alpha(\cdot,\cdot),\beta(\cdot,\cdot)} x_1, {}^C D_\gamma^{\alpha(\cdot,\cdot),\beta(\cdot,\cdot)} x_2)$; and we use the operator

$$
[x]_\gamma^{\alpha,\beta}(t) := \left(t, x(t), {}^C D_\gamma^{\alpha(\cdot,\cdot),\beta(\cdot,\cdot)} x(t)\right).
$$

Theorem 8: Suppose that (x, T) gives a local minimum to functional $\mathcal{J}$ as in (24), under the constraint (25) and the boundary conditions defined in (23). If

$$
\partial_3 g(t, x(t)) \neq 0 \quad \forall t \in [a, b]
$$

then there exists a piecewise continuous function $\lambda : [a, b] \to \mathbb{R}$ such that (x, T) satisfies the following fractional Euler–Lagrange equations:

$$\begin{aligned}&\partial_2 L[x]^{\alpha,\beta}_{\gamma}(t) + D^{\beta(\cdot,\cdot),\alpha(\cdot,\cdot)}_{\overline{\gamma},T}\partial_4 L[x]^{\alpha,\beta}_{\gamma}(t)\\ &\quad + \lambda(t)\partial_2 g(t, x(t)) = 0\end{aligned} \tag{26}$$

and

$$\begin{aligned}&\partial_3 L[x]^{\alpha,\beta}_{\gamma}(t) + D^{\beta(\cdot,\cdot),\alpha(\cdot,\cdot)}_{\overline{\gamma},T}\partial_5 L[x]^{\alpha,\beta}_{\gamma}(t)\\ &\quad + \lambda(t)\partial_3 g(t, x(t)) = 0\end{aligned} \tag{27}$$

on the interval $[a, T]$, and

$$\begin{aligned}&\gamma_2 \Big({}_aD_t^{\beta(\cdot,\cdot)}\partial_4 L[x]^{\alpha,\beta}_{\gamma}(t) - {}_TD_t{}^{\beta(\cdot,\cdot)}\partial_4 L[x]^{\alpha,\beta}_{\gamma}(t)\\ &\quad + \lambda(t)\partial_2 g(t, x(t))\Big) = 0\end{aligned} \tag{28}$$

and

$$\begin{aligned}&{}_aD_t^{\beta(\cdot,\cdot)}\partial_5 L[x]^{\alpha,\beta}_{\gamma}(t) - {}_TD_t{}^{\beta(\cdot,\cdot)}\partial_5 L[x]^{\alpha,\beta}_{\gamma}(t)\\ &\quad + \lambda(t)\partial_3 g(t, x(t)) = 0\end{aligned} \tag{29}$$

on the interval $[T, b]$. Moreover, (x, T) satisfies the transversality conditions

$$\begin{cases} L[x]^{\alpha,\beta}_{\gamma}(T) + \partial_1\phi(T, x(T)) \\ \quad + \partial_2\phi(T, x(T))x_1'(T) \\ \quad + \partial_3\phi(T, x(T))x_2'(T) = 0 \\ \Big[\gamma_1\, {}_tI_T^{1-\alpha(\cdot,\cdot)}\partial_4 L[x]^{\alpha,\beta}_{\gamma}(t) \\ \quad - \gamma_2\, {}_TI_t^{1-\beta(\cdot,\cdot)}\partial_4 L[x]^{\alpha,\beta}_{\gamma}(t)\Big]_{t=T} \\ \quad + \partial_2\phi(T, x(T)) = 0 \\ \Big[\gamma_1{}_tI_T{}^{1-\alpha(\cdot,\cdot)}\partial_5 L[x]^{\alpha,\beta}_{\gamma}(t) \\ \quad - \gamma_2{}_TI_t{}^{1-\beta(\cdot,\cdot)}\partial_5 L[x]^{\alpha,\beta}_{\gamma}(t)\Big]_{t=T} \\ \quad + \partial_3\phi(T, x(T)) = 0 \\ \gamma_2\Big[{}_TI_t^{1-\beta(\cdot,\cdot)}\partial_4 L[x]^{\alpha,\beta}_{\gamma}(t) \\ \quad - {}_aI_t^{1-\beta(\cdot,\cdot)}\partial_4 L[x]^{\alpha,\beta}_{\gamma}(t)\Big]_{t=b} = 0 \\ \gamma_2\Big[{}_TI_t^{1-\beta(\cdot,\cdot)}\partial_5 L[x]^{\alpha,\beta}_{\gamma}(t) \\ \quad - {}_aI_t^{1-\beta(\cdot,\cdot)}\partial_5 L[x]^{\alpha,\beta}_{\gamma}(t)\Big]_{t=b} = 0. \end{cases} \tag{30}$$

Proof: Consider admissible variations of the optimal solution (x, T) of the type

$$(x^*, T^*) = (x + \epsilon h, T + \epsilon\Delta T)$$

where $\epsilon \in \mathbb{R}$ is a small parameter,

$$h = (h_1, h_2) \in C^1([a, b]) \times C^1([a, b])$$

satisfies $h_i(a) = 0$, $i = 1, 2$, and $\triangle T \in \mathbb{R}$. Because

$$\partial_3 g(t, x(t)) \neq 0 \quad \forall t \in [a, b]$$

by the implicit function theorem there exists a subfamily of variations of (x, T) that satisfy (25), that is, there exists a unique function $h_2(\epsilon, h_1)$ such that the admissible variation (x^*, T^*) satisfies the holonomic constraint (25):

$$g(t, x_1(t) + \epsilon h_1(t), x_2(t) + \epsilon h_2) = 0 \quad \forall t \in [a, b].$$

Differentiating this condition with respect to ϵ and considering $\epsilon = 0$, we obtain that

$$\partial_2 g(t, x(t))h_1(t) + \partial_3 g(t, x(t))h_2(t) = 0$$

which is equivalent to

$$\frac{\partial_2 g(t, x(t))h_1(t)}{\partial_3 g(t, x(t))} = -h_2(t). \tag{31}$$

Define j on a neighborhood of zero by

$$\begin{aligned}j(\epsilon) = &\int_a^{T+\epsilon\triangle T} L[x^*]^{\alpha,\beta}_{\gamma}(t)dt\\ &+ \phi(T + \epsilon\triangle T, x^*(T + \epsilon\triangle T)).\end{aligned}$$

The derivative $\dfrac{\partial j}{\partial \epsilon}$ for $\epsilon = 0$ is

$$\begin{aligned}\frac{\partial j}{\partial\epsilon}\bigg|_{\epsilon=0} = &\int_a^T \Big(\partial_2 L[x]^{\alpha,\beta}_{\gamma}(t)h_1(t)\\ &\quad + \partial_3 L[x]^{\alpha,\beta}_{\gamma}(t)h_2(t)\\ &\quad + \partial_4 L[x]^{\alpha,\beta}_{\gamma}(t)^C D_{\gamma}^{\alpha(\cdot,\cdot),\beta(\cdot,\cdot)}h_1(t)\\ &\quad + \partial_5 L[x]^{\alpha,\beta}_{\gamma}(t)^C D_{\gamma}^{\alpha(\cdot,\cdot),\beta(\cdot,\cdot)}h_2(t)\Big)dt\\ &+ L[x]^{\alpha,\beta}_{\gamma}(T)\triangle T + \partial_1\phi(T, x(T))\triangle T\\ &+ \partial_2\phi(T, x(T))\left[h_1(T) + x_1'(T)\triangle T\right]\\ &+ \partial_3\phi(T, x(T))\left[h_2(T) + x_2'(T)\triangle T\right].\end{aligned} \tag{32}$$

The third term in (32) can be written as

$$\begin{aligned}&\int_a^T \partial_4 L[x]^{\alpha,\beta}_{\gamma}(t)^C D_{\gamma}^{\alpha(\cdot,\cdot),\beta(\cdot,\cdot)}h_1(t)dt\\ &= \int_a^T \partial_4 L[x]^{\alpha,\beta}_{\gamma}(t)\\ &\qquad \times \left[\gamma_1\, {}^C_aD_t^{\alpha(\cdot,\cdot)}h_1(t) + \gamma_2\, {}^C_tD_b^{\beta(\cdot,\cdot)}h_1(t)\right]dt\\ &= \gamma_1\int_a^T \partial_4 L[x]^{\alpha,\beta}_{\gamma}(t){}^C_aD_t^{\alpha(\cdot,\cdot)}h_1(t)dt\\ &\quad + \gamma_2\left[\int_a^b \partial_4 L[x]^{\alpha,\beta}_{\gamma}(t){}^C_tD_b^{\beta(\cdot,\cdot)}h_1(t)dt\right.\\ &\quad \left. - \int_T^b \partial_4 L[x]^{\alpha,\beta}_{\gamma}(t){}^C_tD_b^{\beta(\cdot,\cdot)}h_1(t)dt\right].\end{aligned} \tag{33}$$

Integrating by parts, (33) can be written as

$$\begin{aligned}&\int_a^T h_1(t)\left[\gamma_1{}_tD_T{}^{\alpha(\cdot,\cdot)}\partial_4 L[x]^{\alpha,\beta}_{\gamma}(t)\right.\\ &\qquad \left. + \gamma_2{}_aD_t{}^{\beta(\cdot,\cdot)}\partial_4 L[x]^{\alpha,\beta}_{\gamma}(t)\right]dt\\ &+ \int_T^b \gamma_2 h_1(t)\left[{}_aD_t^{\beta(\cdot,\cdot)}\partial_4 L[x]^{\alpha,\beta}_{\gamma}(t)\right.\\ &\qquad \left. - {}_TD_t{}^{\beta(\cdot,\cdot)}\partial_4 L[x]^{\alpha,\beta}_{\gamma}(t)\right]dt\\ &+ \left[h_1(t)\Big(\gamma_1{}_tI_T{}^{1-\alpha(\cdot,\cdot)}\partial_4 L[x]^{\alpha,\beta}_{\gamma}(t)\right.\\ &\qquad \left. - \gamma_2{}_TI_t{}^{1-\beta(\cdot,\cdot)}\partial_4 L[x]^{\alpha,\beta}_{\gamma}(t)\Big)\right]_{t=T}\end{aligned}$$

$$+\left[\gamma_2 h_1(t)\left({}_TI_t{}^{1-\beta(\cdot,\cdot)}\partial_4 L[x]^{\alpha,\beta}_\gamma(t) - {}_aI_t{}^{1-\beta(\cdot,\cdot)}\partial_4 L[x]^{\alpha,\beta}_\gamma(t)\right)\right]_{t=b}.$$

By proceeding similarly to the 4th term in (32), we obtain an equivalent expression. Substituting these relations into (32) and considering the fractional operator $D^{\beta(\cdot,\cdot),\alpha(\cdot,\cdot)}_{\overline{\gamma},c}$ as defined in (2), we get

$$\begin{aligned}0 = &\int_a^T \left[h_1(t)\left[\partial_2 L[x]^{\alpha,\beta}_\gamma(t) + D^{\beta(\cdot,\cdot),\alpha(\cdot,\cdot)}_{\overline{\gamma},T}\partial_4 L[x]^{\alpha,\beta}_\gamma(t)\right] + h_2(t)\left[\partial_3 L[x]^{\alpha,\beta}_\gamma(t) + D^{\beta(\cdot,\cdot),\alpha(\cdot,\cdot)}_{\overline{\gamma},T}\partial_5 L[x]^{\alpha,\beta}_\gamma(t)\right]\right]dt\\
&+\gamma_2\int_T^b\left[h_1(t)\left[{}_aD_t^{\beta(\cdot,\cdot)}\partial_4 L[x]^{\alpha,\beta}_\gamma(t) - {}_TD_t{}^{\beta(\cdot,\cdot)}\partial_4 L[x]^{\alpha,\beta}_\gamma(t)\right] + h_2(t)\left[{}_aD_t^{\beta(\cdot,\cdot)}\partial_5 L[x]^{\alpha,\beta}_\gamma(t) - {}_TD_t{}^{\beta(\cdot,\cdot)}\partial_5 L[x]^{\alpha,\beta}_\gamma(t)\right]\right]dt\\
&+h_1(T)\left[\gamma_1{}_tI_T{}^{1-\alpha(\cdot,\cdot)}\partial_4 L[x]^{\alpha,\beta}_\gamma(t) - \gamma_2{}_TI_t{}^{1-\beta(\cdot,\cdot)}\partial_4 L[x]^{\alpha,\beta}_\gamma(t) + \partial_2\phi(t,x(t))\right]_{t=T}\\
&+h_2(T)\left[\gamma_1{}_tI_T{}^{1-\alpha(\cdot,\cdot)}\partial_5 L[x]^{\alpha,\beta}_\gamma(t) - \gamma_2{}_TI_t{}^{1-\beta(\cdot,\cdot)}\partial_5 L[x]^{\alpha,\beta}_\gamma(t) + \partial_3\phi(t,x(t))\right]_{t=T}\\
&+\triangle T\left[L[x]^{\alpha,\beta}_\gamma(t) + \partial_1\phi(t,x(t)) + \partial_2\phi(t,x(t))x_1'(t) + \partial_3\phi(t,x(t))x_2'(t)\right]_{t=T}\\
&+h_1(b)\left[\gamma_2\left({}_TI_t{}^{1-\beta(\cdot,\cdot)}\partial_4 L[x]^{\alpha,\beta}_\gamma(t) - {}_aI_t{}^{1-\beta(\cdot,\cdot)}\partial_4 L[x]^{\alpha,\beta}_\gamma(t)\right)\right]_{t=b}\\
&+h_2(b)\left[\gamma_2\left({}_TI_t{}^{1-\beta(\cdot,\cdot)}\partial_5 L[x]^{\alpha,\beta}_\gamma(t) - {}_aI_t{}^{1-\beta(\cdot,\cdot)}\partial_5 L[x]^{\alpha,\beta}_\gamma(t)\right)\right]_{t=b}.\end{aligned}\tag{34}$$

Define the piecewise continuous function λ by

$$\lambda(t) = \begin{cases} -\dfrac{\partial_3 L[x]^{\alpha,\beta}_\gamma(t)}{\partial_3 g(t,x(t))} - \dfrac{D^{\beta(\cdot,\cdot),\alpha(\cdot,\cdot)}_{\overline{\gamma},T}\partial_5 L[x]^{\alpha,\beta}_\gamma(t)}{\partial_3 g(t,x(t))} & t\in[a,T]\\ -\dfrac{({}_aD_t^{\beta(\cdot,\cdot)}\partial_5 L[x]^{\alpha,\beta}_\gamma(t)}{\partial_3 g(t,x(t))} + \dfrac{{}_TD_t^{\beta(\cdot,\cdot)}\partial_5 L[x]^{\alpha,\beta}_\gamma(t)}{\partial_3 g(t,x(t))} & t\in[T,b].\end{cases}\tag{35}$$

Using (31) and (35), we obtain that

$$\lambda(t)\partial_2 g(t,x(t))h_1(t) = \begin{cases}(\partial_3 L[x]^{\alpha,\beta}_\gamma(t) + D^{\beta(\cdot,\cdot),\alpha(\cdot,\cdot)}_{\overline{\gamma},T}\partial_5 L[x]^{\alpha,\beta}_\gamma(t))h_2(t) & t\in[a,T]\\ ({}_aD_t^{\beta(\cdot,\cdot)}\partial_5 L[x]^{\alpha,\beta}_\gamma(t) -{}_T D_t^{\beta(\cdot,\cdot)}\partial_5 L[x]^{\alpha,\beta}_\gamma(t))h_2(t) & t\in[T,b].\end{cases}$$

Substituting in (34), we have

$$\begin{aligned}0 = &\int_a^T h_1(t)\left[\partial_2 L[x]^{\alpha,\beta}_\gamma(t) + D^{\beta(\cdot,\cdot),\alpha(\cdot,\cdot)}_{\overline{\gamma},T}\partial_4 L[x]^{\alpha,\beta}_\gamma(t) + \lambda(t)\partial_2 g(t,x(t))\right]dt\\
&+\gamma_2\int_T^b h_1(t)\left[{}_aD_t^{\beta(\cdot,\cdot)}\partial_4 L[x]^{\alpha,\beta}_\gamma(t) - {}_TD_t{}^{\beta(\cdot,\cdot)}\partial_4 L[x]^{\alpha,\beta}_\gamma(t) + \lambda(t)\partial_2 g(t,x(t))\right]dt\\
&+h_1(T)\left[\gamma_1{}_tI_T{}^{1-\alpha(\cdot,\cdot)}\partial_4 L[x]^{\alpha,\beta}_\gamma(t) - \gamma_2{}_TI_t{}^{1-\beta(\cdot,\cdot)}\partial_4 L[x]^{\alpha,\beta}_\gamma(t) + \partial_2\phi(t,x(t))\right]_{t=T}\\
&+h_2(T)\left[\gamma_1{}_tI_T{}^{1-\alpha(\cdot,\cdot)}\partial_5 L[x]^{\alpha,\beta}_\gamma(t) - \gamma_2{}_TI_t{}^{1-\beta(\cdot,\cdot)}\partial_5 L[x]^{\alpha,\beta}_\gamma(t) + \partial_3\phi(t,x(t))\right]_{t=T}\\
&+\triangle T\left[L[x]^{\alpha,\beta}_\gamma(t) + \partial_1\phi(t,x(t)) + \partial_2\phi(t,x(t))x_1'(t) + \partial_3\phi(t,x(t))x_2'(t)\right]_{t=T}\\
&+h_1(b)\left[\gamma_2\left({}_TI_t{}^{1-\beta(\cdot,\cdot)}\partial_4 L[x]^{\alpha,\beta}_\gamma(t) - {}_aI_t{}^{1-\beta(\cdot,\cdot)}\partial_4 L[x]^{\alpha,\beta}_\gamma(t)\right)\right]_{t=b}\\
&+h_2(b)\left[\gamma_2\left({}_TI_t{}^{1-\beta(\cdot,\cdot)}\partial_5 L[x]^{\alpha,\beta}_\gamma(t) - {}_aI_t{}^{1-\beta(\cdot,\cdot)}\partial_5 L[x]^{\alpha,\beta}_\gamma(t)\right)\right]_{t=b}.\end{aligned}$$

Considering appropriate choices of variations, we obtained the first (26) and the third (28) necessary conditions, and also the transversality conditions (30). The remaining conditions (27) and (29) follow directly from (35). ■

We end this section with a simple illustrative example. Consider the following problem:

$$J(x,t)=\int_0^T\Bigg[\alpha(t)+\Bigg({}^{C}D_{\gamma}^{\alpha(\cdot,\cdot),\beta(\cdot,\cdot)}x_1(t)-\frac{t^{1-\alpha(t)}}{2\Gamma(2-\alpha(t))}-\frac{(b-t)^{1-\beta(t)}}{2\Gamma(2-\beta(t))}\Bigg)^2+\Big({}^{C}D_{\gamma}^{\alpha(\cdot,\cdot),\beta(\cdot,\cdot)}x_2(t)\Big)^2\Bigg]dt\longrightarrow\min$$

$$x_1(t)+x_2(t)=t+1,\quad x_1(0)=0,\quad x_2(0)=1.$$

It is a simple exercise to check that $x_1(t)=t$, $x_2(t)\equiv 1$ and $\lambda(t)\equiv 0$ satisfy our Theorem 8.

V. CONCLUSION

Nowadays, optimization problems involving fractional derivatives constitute a very active research field due to several applications [14], [16], [17]. Here we obtained optimality conditions for two isoperimetric problems and for a new variational problem subject to a holonomic constraint, where the Lagrangian depends on a combined Caputo derivative of variable fractional order. Main results include Euler-Lagrange and transversality type conditions. For simplicity, we considered here only linear combinations between the left and right operators. Using similar techniques as the ones developed here, one can obtain analogous results for fractional variational problems with Lagrangians containing left-sided and right-sided fractional derivatives of variable order. More difficult and interesting, would be to develop a "multi-term fractional calculus of variations". The question seems however nontrivial, even for the nonvariable order case, because of difficulties in application of integration by parts. For the variable order case, as we consider in our work, there is yet no formula of fractional integration by parts for higher-order derivatives. This is under investigation and will be addressed elsewhere.

REFERENCES

[1] A. Atangana and A. Kilicman, "On the generalized mass transport equation to the concept of variable fractional derivative," *Math. Probl. Eng.*, vol. 2014, Art. ID 542809, 9 pages, Mar. 2014.

[2] C. M. Soon, C. F. M. Coimbra, and M. H. Kobayashi, "The variable viscoelasticity oscillator," *Ann. Phys.*, vol. 14, no. 6, pp. 378−389, Apr. 2005.

[3] S. G. Samko and B. Ross, "Integration and differentiation to a variable fractional order," *Integral Transform. Spec. Funct.*, vol. 1, no. 4, pp. 277−300, Dec. 1993.

[4] H. Sheng, H. Sun, C. Coopmans, Y. Chen, and G. W. Bohannan, "Physical experimental study of variable-order fractional integrator and differentiator," in *Proc. 4th IFAC Workshop Fractional Differentiation and Its Applications*, Badajoz, Spain, 2010.

[5] D. Valério, G. Vinagre, J. Domingues, and J. S. da Costa, "Variable-order fractional derivatives and their numerical approximations I–real orders," in *Symp. Fractional Signals and Systems Lisbon 09*, Lisbon, Portugal, 2009.

[6] A. B. Malinowska and D. F. M. Torres, "Fractional calculus of variations for a combined Caputo derivative," *Fract. Calc. Appl. Anal.*, vol. 14, no. 4, pp. 523−537, Dec. 2011.

[7] A. B. Malinowska and D. F. M. Torres, "Multiobjective fractional variational calculus in terms of a combined Caputo derivative," *Appl. Math. Comput.*, vol. 218, no. 9, pp. 5099−5111, Jan. 2012.

[8] T. Odzijewicz, A. B. Malinowska, and D. F. M. Torres, "Fractional variational calculus with classical and combined Caputo derivatives," *Nonlinear Anal.*, vol. 75, no. 3, pp. 1507−1515, Feb. 2012.

[9] D. Tavares, R. Almeida, and D. F. M. Torres, "Optimality conditions for fractional variational problems with dependence on a combined Caputo derivative of variable order," *Optimization*, vol. 64, no. 6, pp. 1381−1391, Feb. 2015.

[10] T. Odzijewicz, A. B. Malinowska, and D. F. M. Torres, "Fractional variational calculus of variable order," in *Advances in Harmonic Analysis and Operator Theory, The Stefan Samko Anniversary Volume, Operator Theory: Advances and Applications*, A. Almeida, L. Castro, and F. O. Speck, Eds. Basel: Birkhäuser Verlag, 2013, pp. 291−301.

[11] T. Odzijewicz, A. B. Malinowska, and D. F. M. Torres, "Noether's theorem for fractional variational problems of variable order," *Cent. Eur. J. Phys.*, vol. 11, no. 6, pp. 691−701, Jun. 2013.

[12] J. Cresson, "Fractional embedding of differential operators and Lagrangian systems," *J. Math. Phys.*, vol. 48, no. 3, Art. ID 033504, 34 pages, Mar. 2007.

[13] A. B. Malinowska and D. F. M. Torres, "Towards a combined fractional mechanics and quantization," *Fract. Calc. Appl. Anal.*, vol. 15, no. 3, pp. 407–417, Sep. 2012.

[14] R. Almeida, S. Pooseh, and D. F. M. Torres, *Computational Methods in the Fractional Calculus of Variations*, London: Imperial College Press, 2015.

[15] D. Tavares, R. Almeida, and D. F. M. Torres, "Caputo derivatives of fractional variable order: numerical approximations," *Commun. Nonlinear Sci. Numer. Simul.* vol. 35, pp. 69−87, Jun. 2016.

[16] A. B. Malinowska, T. Odzijewicz, and D. F. M. Torres, *Advanced methods in the fractional calculus of variations*. Cham: Springer, 2015.

[17] A. B. Malinowska and D. F. M. Torres, *Introduction to the Fractional Calculus of Variations*. London: Imperial College Press, 2012.

Dina Tavares is a Ph. D. student in the doctoral programme in mathematics and applications of Universities of Aveiro and Minho. She obtained her bachelor and master degrees in mathematics from University of Aveiro. She is a teaching assistant in the Polytechnic Institute of Leiria since 2006. Her research interests include fractional calculus, calculus of variations and mathematics education.

Ricardo Almeida received his bachelor and master degrees in mathematics from University of Porto, Portugal, and his Ph. D. degree in mathematics from University of Aveiro, Portugal. He is currently an assistant professor in the University of Aveiro. His research interests include fractional calculus, calculus of variations and optimal control theory. Corresponding author of this paper.

Delfim F. M. Torres is a full professor of mathematics at the University of Aveiro since 2015 and coordinator of the Systems and Control Group of CIDMA since 2010. He obtained his Ph. D. in mathematics in 2002 and his D. Sc. (Habilitation) in mathematics in 2011. Professor Torres has been awarded in 2015 with the title of ISI Highly Cited Researcher. He has written more than 350 publications, including two books with Imperial College Press, in 2012 and 2015, and two books with Springer, in 2014 and 2015. Torres was, from 2011 to 2014, a key scientist of the European Marie Curie Project SADCO, a Network for Initial Training. He is the director of the FCT Doctoral Programme of Excellence in mathematics and applications of Universities of Minho, Aveiro, Porto and UBI since 2013. Eleven Ph. D. students in mathematics have successfully finished under his supervision.

Robust Attitude Control for Reusable Launch Vehicles Based on Fractional Calculus and Pigeon-inspired Optimization

Qiang Xue and Haibin Duan, *Senior Member, IEEE*

***Abstract*—In this paper, a robust attitude control system based on fractional order sliding mode control and dynamic inversion approach is presented for the reusable launch vehicle (RLV) during the reentry phase. By introducing the fractional order sliding surface to replace the integer order one, we design robust outer loop controller to compensate the error introduced by inner loop controller designed by dynamic inversion approach. To take the uncertainties of aerodynamic parameters into account, stochastic robustness design approach based on the Monte Carlo simulation and Pigeon-inspired optimization is established to increase the robustness of the controller. Some simulation results are given out which indicate the reliability and effectiveness of the attitude control system.**

***Index Terms*—Attitude control, fractional calculus, pigeon-inspired optimization, reusable launch vehicle (RLV), sliding mode control.**

I. INTRODUCTION

WITH the necessity of the development of reusable space transportation system as well as the hypersonic weapons with high penetration ability and kill efficiency, reusable launch vehicle (RLV) technology becomes a hot research field all over the world [1]. Unpowered gliding reentry vehicle is one of the implementations which have the aerodynamic configuration with high lift-to-drag ratio (L/D). During the reentry phase, the flight envelope ranges from over Mach 20 to Mach 1 and altitude ranges from 100 km to 20 km [2]. When reusable launch vehicle maneuvers in the so called near space, the flow field around the vehicle would present the hypersonic flow dynamic characteristics, such as viscous interference, thin shock layer, low density effect and so on [3]. Thus, complex coupling between state variables and control variables, high nonlinear terms and strongly time varying characteristics take into the dynamics of reentry vehicles.

Facing with these challenges, the guidance and control technology becomes one of the key issues in the development process of reusable launch vehicles [4]. Guidance subsystem leads the vehicle to steer the reference trajectory or predict trajectory onboard, while control subsystem stabilizes the attitude and takes attitude maneuver to track guidance commands. By introducing advanced control theories such as adaptive control theory, dynamic inversion approach and sliding mode control, the robustness and effectiveness of the flight control systems were obviously improved [4], compared with some classical design techniques such as gain-scheduling methods. Recently, the dynamic inversion technique was applied into the flight control law design process, especially in reentry flight control and high angle of attack maneuver, demonstrated several advantages [5]. However, it required a precise model to avoid the error introduced by inversion, which might strongly influence the control qualities. The saturation of actuators is also an additional serious problem which should be avoided. However, another nonlinear control method named sliding mode control approach as a robust control technique has been widely applied in the flight control law design which could tolerate the uncertainties of models and disturbance. Unfortunately, there are some problems when applying the sliding mode method directly. For example, the order of the sliding mode method would be high when the controlled model is complex, which might make the algorithm difficult to be employed.

Fractional calculus theory, which is about integration and differential with non-integer orders, has a rapid development with an increasing attention since hundred years ago. More and more attention focuses on the application of fractional calculus in the modeling and control in engineering viewpoint [6]. Some designs based on fractional calculus for flight control system also present the possibility of the application and the advantages compared with traditional integer control approach [7]. In general, the fractional order of integral or derivation is more flexible and widely used than the integer order. To introduce the fractional calculus in these control method, the performance of closed-loop systems could probably be improved and control inputs could be reduced. Therefore, applying fractional calculus in reusable launch vehicle attitude control would be a beneficial trial.

In fact, the uncertainties of aerodynamic coefficients are also necessary to be taken into consideration in the process of control law design. It demands that the control system could tolerate these uncertainties of the coefficients and endure any dispersion. In order to improve the robustness of control system, the stochastic robustness method based on Pigeon-inspired optimization is introduced. By this procedure, the optimal parameters of the controller have been obtained and the controller is optimal in terms of stochastic robustness. Therefore, a combined and robust control structure based on stochastic robustness design method is established to overcome these challenges mentioned previously. In this

Manuscript received August 30, 2015; accepted November 17, 2015. This work was supported by National Natural Science Foundation of China (61425008, 61333004, 61273054), Top-Notch Young Talents Program of China, and Aeronautical Foundation of China (2015ZA51013). Recommended by Associate Editor YangQuan Chen.

Citation: Q. Xue and H. B. Duan, "Robust attitude control for reusable launch vehicles based on fractional calculus and pigeon-inspired optimization," *IEEE/CAA Journal of Automatic Sinica*, vol. 4, no. 1, pp. 89−97, Jan. 2017.

Q. Xue and H. B. Duan are with Bio-inspired Autonomous Flight Systems (BAFS) Research Group, the Science and Technology on Aircraft Control Laboratory, School of Automation Science and Electrical Engineering, Beihang University (BUAA), Beijing 100083, China (e-mail: xueqiang@buaa.edu.cn; hbduan@buaa.edu.cn).

Color versions of one or more of the figures in this paper are available online at http://ieeexplore.ieee.org.

Digital Object Identifier 10.1109/JAS.2017.7510334

structure, the dynamic inversion is applied to design the inner loop controller, while the fractional sliding mode approach is applied to design the outer loop controller. The fractional sliding mode approach could weak the integral action and decrease the control input. It could also smooth the time history of controlled variables. The stochastic robustness method based on PIO algorithm allows us to obtain the optimal controller in terms of stochastic robustness. The organization of this paper is as follows. In Section II, the description of the reusable launch vehicle model is presented. In Section III, the control system including control law and control allocation algorithm is established. The control law is based on fractional sliding mode control (FSMC) and dynamic inversion (DI) approach, and the control allocation algorithm is a commonly used algorithm. In Section IV, the stochastic robustness design method based on a new swarm intelligent algorithm, i.e., pigeon-inspired optimization is introduced, based on which we design stochastic robustness optimal controller. In Section V, we give the design examples and simulation results to demonstrate the robustness and effectiveness of the control system, and the influence of different fractional orders of FSMC to the closed-loop system is discussed.

II. Attitude Control Problem

A. Mathematical Model of Attitude Dynamics

The mathematical equations of reentry dynamics consist of the translational motion associated with flight path variables and the rotational motion associated with attitude angles which used to be aerodynamic angles during the reentry phase. The three-degree-of-freedom model of unpowered reentry attitude dynamics is given out as follows [8]:

$$\begin{aligned}\dot{\alpha} &= q - (p\cos\alpha + r\sin\alpha)\tan\beta \ - \dot{\gamma}\cos\mu/\cos\beta \\ &\quad - \dot{\chi}\cos\gamma\sin\mu/\cos\beta \qquad (1)\\ \dot{\beta} &= p\sin\alpha - r\cos\alpha - \dot{\gamma}\sin\mu + \dot{\chi}\cos\gamma\cos\mu \qquad (2)\\ \dot{\mu} &= p\cos\alpha/\cos\beta + r\sin\alpha/\cos\beta \\ &\quad + \dot{\chi}(\sin\gamma + \tan\beta\sin\mu\cos\gamma) + \dot{\gamma}\tan\beta\cos\mu \qquad (3)\end{aligned}$$

where α is the angle of attack, β is the angle of sideslip, μ is the bank angle, γ is the flight-path angle, and χ is the airspeed heading angle.

The rotational dynamic equation is as follows:

$$\begin{aligned}\dot{p} &= I_{lp}M_x + I_{np}M_z + \frac{(I_y - I_z)I_z - I_{xz}^2}{I_xI_z - I_{xz}^2}qr \\ &\quad + \frac{(I_x - I_y + I_z)I_{xz}}{I_xI_z - I_{xz}^2}pq \qquad (4)\\ \dot{q} &= I_{mq}M_y + \frac{I_z - I_x}{I_y}pr - \frac{I_{xz}}{I_y}(p^2 - r^2) \qquad (5)\end{aligned}$$

$$\begin{aligned}\dot{r} &= I_{lr}M_x + I_{nr}M_z + \frac{I_x(I_x - I_y) + I_{xz}^2}{I_xI_z - I_{xz}^2}pq \\ &\quad - \frac{(I_x - I_y + I_z)I_{xz}}{I_xI_z - I_{xz}^2}qr \qquad (6)\end{aligned}$$

$$\begin{aligned}I_{lp} &= \frac{I_z}{I_xI_z - I_{xz}^2}, \quad I_{np} = \frac{I_{xz}}{I_xI_z - I_{xz}^2}, \quad I_{mq} = \frac{1}{I_y} \\ I_{lr} &= \frac{I_{xz}}{I_xI_z - I_{xz}^2}, \quad I_{nr} = \frac{I_x}{I_xI_z - I_{xz}^2} \qquad (7)\end{aligned}$$

where $\vec{w} = (p, q, r)^T$ are the roll rate, the pitch rate and the yaw rate, $\vec{M} = (M_x, M_y, M_z)$are the moments acting on the vehicle, consisting of aerodynamic trim moments and control torques generated by aerodynamic surfaces and reaction control systems.

$$I = \begin{bmatrix} I_x & -I_{xy} & -I_{xz} \\ -I_{xy} & I_y & -I_{yz} \\ -I_{xz} & -I_{yz} & I_z \end{bmatrix}$$

which is the inertia matrix.

B. Improved Aerodynamic Model of RLV

The aerodynamic moments generated by the aerodynamic control surfaces could be calculated by the following standard formulation:

$$\bar{L} = C_{l,total}q_{bar}SL_{ref} \qquad (8)$$

$$M = C_{m,total}q_{bar}SL_{ref} \qquad (9)$$

$$N = C_{n,total}q_{bar}SL_{ref} \qquad (10)$$

where $\bar{L}$ is the roll aerodynamic moment, M is the pitch aerodynamic moment, N is the yaw aerodynamic moment, q_{bar} is the dynamic pressure, S is the reference area, L_{ref} is the reference length, $C_{l,total}$ is the non-dimensional roll moment coefficient, $C_{m,total}$ it he non-dimensional pitch moment coefficient, and $C_{n,total}$ is the non-dimensional yaw moment coefficient.

The reusable launch vehicle used in this study is configured with several aerodynamic surfaces: four body flaps placed at the tail, two elevons and one rudder. In order to simplify the relationship between the motion channel and the control surface deflection, nominal control surfaces are introduced to replace the actual aerodynamic surfaces with the transformational matrix as follows [9]:

$$\begin{bmatrix} 0 & 0 & 0 & 0 & 0.5 & -0.5 & 0 \\ 0 & 0 & 0 & 0 & 0.5 & 0.5 & 0 \\ 0 & 0 & 0 & 0 & 0 & 0 & 1 \\ 0.5 & 0.5 & 0 & 0 & 0 & 0 & 0 \\ 0 & 0 & 0.5 & 0.5 & 0 & 0 & 0 \\ 0.5 & -0.5 & 0.5 & -0.5 & 0 & 0 & 0 \end{bmatrix} \begin{bmatrix} \delta_{LLBP} \\ \delta_{LRBP} \\ \delta_{ULBP} \\ \delta_{URBP} \\ \delta_{WL} \\ \delta_{WR} \\ \delta_r \end{bmatrix} = \begin{bmatrix} \delta_a \\ \delta_e \\ \delta_r \\ \delta_{f+} \\ \delta_{f-} \\ \delta_{\Delta f} \end{bmatrix}. \qquad (11)$$

As for our specific developed reentry vehicle, the original formulations of the moment coefficients are shown in (12)−(14) [10].

$$\begin{aligned}C_{l,total} &= C_{l\beta,basic}\beta + \Delta C_{l,BF} + \Delta C_{l,rudder} \\ &\quad + \Delta C_{l.Elevon} + \Delta C_{l\beta,GE}\beta + \Delta C_{l\beta,LG}\beta \\ &\quad + \Delta C_{lp}\frac{pb}{2V} + \Delta C_{lr}\frac{rb}{2V} \qquad (12)\end{aligned}$$

$$\begin{aligned}C_{m,total} &= C_{m,basic} + \Delta C_{m,BF} + \Delta C_{m,Elevon} \\ &\quad + \Delta C_{m,rudder} + \Delta C_{m,GE} + \Delta C_{m,LG} + \Delta C_{mq}\frac{qc}{2V} \qquad (13)\end{aligned}$$

$$\begin{aligned}C_{n,total} &= C_{n\beta,basic}\beta + \Delta C_{n,BF} + \Delta C_{n,elevon} \\ &\quad + \Delta C_{n,rudder} + \Delta C_{n\beta,GE}\beta + \Delta C_{n\beta,LG}\beta \\ &\quad + \Delta C_{np}\frac{pb}{2V} + \Delta C_{nr}\frac{pr}{2V}. \qquad (14)\end{aligned}$$

According to the relations between the actual surfaces and nominal surfaces, and converting the aerodynamic coefficients to the aerodynamic derivatives by $C_{i,j} = \Delta C_{i,j}/\Delta\delta_j$, the developed formulation of the moment coefficients could be obtained as follows:

$$C_{l,total} = C_{l\beta,basic}\beta + C_{l\delta_a}\delta_a + C_{l\delta_r}\delta_r + C_{l\delta_{\Delta f}}\delta_{\Delta f} + C_{lp}\frac{pb}{2V} + C_{lr}\frac{rb}{2V} \tag{15}$$

$$C_{m,total} = C_{m,basic} + C_{m\delta_e}\delta_e + C_{m\delta_{f+}}\delta_{f+} + C_{m\delta_{f-}}\delta_{f-} + \Delta C_{mq}\frac{qc}{2V} \tag{16}$$

$$C_{n,total} = C_{n\beta,basic}\beta + C_{n\delta_a}\delta_a + C_{n\delta_r}\delta_r + C_{np}\frac{pb}{2V} + C_{nr}\frac{pr}{2V} \tag{17}$$

where $\delta = [\delta_a\ \delta_e\ \delta_r\ \delta_{f+}\ \delta_{f-}\ \delta_{\Delta f}]$ is deflection vector of the aerodynamic control surfaces ranking as the aileron, elevator, rudder, body flap positive deflection, body flap negative deflection and body flap differential deflection.

These aerodynamic coefficients and derivatives mentioned above could be obtained from the complete set of the coefficient and derivative lookup table vs Mach and AOA using interpolation algorithm.

C. Attitude Control Strategy

In the design process of reentry flight attitude control law, adequate engineering practices present the feasibility and effectiveness of the application of time-scale separation principle to deal with the flight state variables [5], [11]. The aerodynamic angles including angle of attack and slip slide angle and bank angle are regarded as the slow variables of the outer loop, while the angle rates around body axis are regarded as the fast variables of the inner loop. Dual loop control framework could be designed for the inner loop and outer loop: the function of inner loop controller is to track the angular rate commands generated by the outer loop, while the outer loop controller operates to control aerodynamic commands.

In this study, dynamic inversion approach is chosen to design the dual loop controller and obtain three channel decoupling model of aerodynamic angles, and sliding mode technique improved by fractional calculus is used to design to provide the desired time-scale separation [2]. Thus, when guidance commands are given out from guidance subsystem, the required total control torque would be generated by the control law. The control torque allocation algorithm presents the mapping relation between the control torque and control surface deflections. By combining control law and control torque allocation, the complete attitude control system is established. The framework of the whole system is shown in Fig. 1.

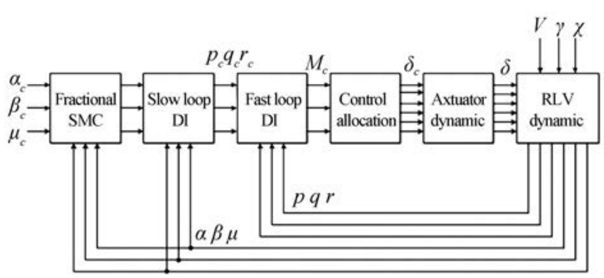

Fig. 1. The diagram of control system.

III. Implementation of the Attitude Control System

A. Fractional Calculus and Approximate Form of Fractional Calculus Operator

The Caputo's definition of the fractional derivative of order α with respect to variable t and initial point at $t = 0$ is as follows [12]:

$$_0D_t^\alpha f(t) = \frac{1}{\Gamma(1-\delta)}\int_0^t \frac{f^{(m+1)}(\tau)}{(t-\tau)^\delta}d\tau \quad (\alpha = m+\delta;\ m \in \mathbb{Z};\ 0 < \delta \le 1) \tag{18}$$

where $\Gamma(\cdot)$ is the gamma function [12]:

$$\Gamma(\xi) = \int_0^\infty e^{-m}m^{\xi-1}dm. \tag{19}$$

The Grunwald-Letnikov's fractional derivative of order m is defined as follows:

$$_aD_t^m f(t) = \lim_{h\to\infty} h^{-m}\sum_{j=0}^{\frac{t-m}{h}}(-1)^j\binom{m}{j}f(t-jh) \tag{20}$$

where h is the step size, a is the lower limit of integral and t is the upper limit of integral. The Laplace transform of fractional derivative is given as follows:

$$L\{_0D_t^\alpha f(t)\} = s^\alpha F(s) - [_0D_t^{\alpha-1}f(t)]_{t=0} \tag{21}$$

$$L\{_0D_t^{-\alpha} f(t)\} = s^{-\alpha}F(s). \tag{22}$$

One of the digital implement of fractional derivative is using the discrete filter to approximate it which can be easily applied in engineering practice [13]. In this study, the directly discretization method is conducted to obtain the equivalent discrete filter. Firstly, apply Tustin mapping function to transform the fractional derivative from S domain to Z domain:

$$s^{\pm\alpha} = (w(z^{-1}))^{\pm\alpha} \tag{23}$$

where $w(\cdot)$ is the Tustin mapping function as follows:

$$w(z^{-1}) = \frac{2}{T}\frac{1-z^{-1}}{1+z^{-1}}. \tag{24}$$

Then the CFE (continued fraction expansion) method is used to obtain the rationalization result of the fractional derivative model in Z domain. The whole procedure of Tustin with CFE method is as follows [14]:

$$D_E^{\pm\alpha}(z) = \left(\frac{1}{T}\right)^{\pm\alpha} CFE\{(1-z^{-1})^{\pm\alpha}\}_{p,q} = \left(\frac{1}{T}\right)^{\pm\alpha}\frac{P_p(z^{-1})}{Q_q(z^{-1})} \tag{25}$$

B. Dual Loop Control Law Designed by Nonlinear Dynamic Inversion Approach

According to time-scale separation principle, control law could be designed separately for the fast loop variables and the slow loop variables. It is assumed that the dynamic of fast loop is so fast that does not affect the responses of slow loop.

For the fast loop, a first-order desired dynamic could be chosen as follows [2], [5]:

$$\begin{bmatrix}\dot{p}\\ \dot{q}\\ \dot{r}\end{bmatrix}_{des} = K_w\left(\begin{bmatrix}p_c\\ q_c\\ r_c\end{bmatrix} - \begin{bmatrix}p\\ q\\ r\end{bmatrix}\right). \tag{26}$$

Combined with the rotational dynamic (4)−(6), the required total torque could be calculated as follows:

$$\begin{bmatrix} M_x \\ M_y \\ M_z \end{bmatrix} = \begin{bmatrix} I_{lp} & 0 & I_{np} \\ 0 & I_{mq} & 0 \\ I_{lr} & 0 & I_{nr} \end{bmatrix}^{-1} \times \left(\begin{bmatrix} \dot{p} \\ \dot{q} \\ \dot{r} \end{bmatrix}_{des} - \begin{bmatrix} \frac{(I_y - I_z)I_z - I_{xz}^2}{I_x I_z - I_{xz}^2} qr + \frac{(I_x - I_y + I_z)I_{xz}}{I_x I_z - I_{xz}^2} pq \\ \frac{I_z - I_x}{I_y} pr - \frac{I_{xz}}{I_y}(p^2 - r^2) \\ \frac{I_x(I_x - I_y) + I_{xz}^2}{I_x I_z - I_{xz}^2} pq - \frac{(I_x - I_y + I_z)I_{xz}}{I_x I_z - I_{xz}^2} qr \end{bmatrix} \right). \tag{27}$$

Subtracting the basic aerodynamic moments and damping aerodynamic moments from the total required torque, the required control torque is obtained as in (28).

$$M_c = M - M_a. \tag{28}$$

The fast loop control law allows the angular rates to be able to track the angular rate commands, while the angular rate commands are generated by the slow loop. The characteristics of fast loop dynamic such as the bandwidth depend on parameter K_w.

For the slow loop, the rotational motion equations about aerodynamic angles could be rearranged in vector form as follows [2]:

$$\begin{aligned} \begin{bmatrix} \dot{\alpha} \\ \dot{\beta} \\ \dot{\mu} \end{bmatrix} &= \begin{bmatrix} -\cos\alpha\tan\beta & 1 & -\sin\alpha\tan\beta \\ \sin\alpha & 0 & -\cos\alpha \\ \cos\alpha/\cos\beta & 0 & \sin\alpha/\cos\beta \end{bmatrix} \begin{bmatrix} p \\ q \\ r \end{bmatrix} + \begin{bmatrix} v_\alpha \\ v_\beta \\ v_\mu \end{bmatrix} \\ &= L \begin{bmatrix} p \\ q \\ r \end{bmatrix} + \begin{bmatrix} v_\alpha \\ v_\beta \\ v_\mu \end{bmatrix} \end{aligned} \tag{29}$$

$$\begin{bmatrix} v_\alpha \\ v_\beta \\ v_\mu \end{bmatrix} = \begin{bmatrix} -1/\cos\beta(\dot{\gamma}\cos\mu + \dot{\chi}\cos\gamma\sin\mu) \\ \dot{\chi}\cos\mu\cos\gamma - \dot{\gamma}\sin\mu \\ \dot{\gamma}\cos\mu\tan\beta + \dot{\chi}(\cos\gamma\sin\mu\tan\beta + \sin\gamma) \end{bmatrix}. \tag{30}$$

When β satisfies the inequality $\beta \neq \pm 90°$, matrix L is invertible, while in the reentry flight phase this condition is always satisfied. Thus, assuming v is the virtual control input, the fast loop input, i.e., angular rate commands could be obtained as follows:

$$\begin{bmatrix} p \\ q \\ r \end{bmatrix}_c = \begin{bmatrix} 0 & \sin\alpha & \cos\alpha\cos\beta \\ 1 & 0 & \sin\beta \\ 0 & -\cos\alpha & \sin\alpha\cos\beta \end{bmatrix} \left(v - \begin{bmatrix} v_\alpha \\ v_\beta \\ v_\mu \end{bmatrix} \right). \tag{31}$$

According to time-scale separation principle, the fast loop dynamic is so fast compared with the dynamic of the slow loop which allows us to suppose that the angular rate is equal to the angular rate command.

By introducing the dual loop control law, the three channels have been decoupled and a linear system is obtained as follows:

$$\begin{bmatrix} \dot{\alpha} \\ \dot{\beta} \\ \dot{\mu} \end{bmatrix} = v. \tag{32}$$

C. Sliding Mode Control Design Based on Fractional Calculus

For the decoupling linear system about three aerodynamic angle channels, a sliding mode control law based on fractional calculus is designed to obtain the virtual control input v of dual loop dynamic inversion law and compensating the error generated by dynamic inversion approach.

First, define the attitude error as in (33), and choose the fractional sliding surface function as in (34).

$$e = [\alpha_c - \alpha \quad \beta_c - \beta \quad \mu_c - \mu]^T \tag{33}$$

$$S = e + K \cdot {}_0D_t{}^\lambda e. \tag{34}$$

The fractional exponential reaching law is chosen as follows:

$${}_0D_t{}^\eta S = -\kappa S - \sigma\,\mathrm{sign}(S) \tag{35}$$

where the parameters above are defined as:

$$\kappa = \mathrm{diag}\{\kappa_\alpha, \kappa_\beta, \kappa_\mu\}, \quad \sigma = \mathrm{diag}\{\sigma_\alpha, \sigma_\beta, \sigma_\mu\}$$
$$\kappa_\alpha, \kappa_\beta, \kappa_\mu > 0; \quad \sigma_\alpha, \sigma_\beta, \sigma_\mu > 0.$$

Combine (34) and (35), the virtual control input v could be obtained.

$$\begin{aligned} \dot{S} &= \frac{d}{dt}(e + K \cdot {}_0D_t{}^\lambda e) \\ &= \dot{e} + K \cdot {}_0D_t{}^{\lambda+1} e = {}_0D_t{}^{1-\eta}(-\kappa S - \sigma\,\mathrm{sign}(S)) \end{aligned} \tag{36}$$

$$\begin{aligned} v &= \begin{bmatrix} \dot{\alpha} \\ \dot{\beta} \\ \dot{\mu} \end{bmatrix} \\ &= \begin{bmatrix} \dot{\alpha}_c + k_{\alpha 0} D_t{}^{\lambda+1}(\alpha_c - \alpha) + {}_0D_t{}^{1-\eta}[\kappa_\alpha S_\alpha + \sigma_\alpha\,\mathrm{sign}(S_\alpha)] \\ \dot{\beta}_c + k_{\beta 0} D_t{}^{\lambda+1}(\beta_c - \beta) + {}_0D_t{}^{1-\eta}[\kappa_\beta S_\beta + \sigma_\beta\,\mathrm{sign}(S_\beta)] \\ \dot{\mu}_c + k_{\mu 0} D_t{}^{\lambda+1}(\mu_c - \mu) + {}_0D_t{}^{1-\eta}[\kappa_\mu S_\mu + \sigma_\mu\,\mathrm{sign}(S_\mu)] \end{bmatrix} \end{aligned} \tag{37}$$

where $S = [S_\alpha\, S_\beta\, S_\mu]^T$. In the next, D^λ is used to replace the description ${}_0D_t{}^\lambda$.

D. Control Allocation Algorithm

The control law designed above generates the required control torque command to steer the guidance commands, while the control torque is generated by vehicle's control surfaces. For reentry vehicles, they always configure with hybrid control surfaces including aerodynamic control surfaces and reaction control systems (RCS). During early reentry phase, both aerodynamic control surfaces and RCS are operated, while pure aerodynamic control surfaces are operated during final reentry phase. In this study, the terminal of reentry phase is focused on and pure aerodynamic control surfaces are used to generate all the control torques:

$$\begin{bmatrix} M_{cx} \\ M_{cy} \\ M_{cz} \end{bmatrix} = qSL_{ref}C \begin{bmatrix} \delta_a \\ \delta_e \\ \delta_r \\ \delta_{f+} \\ \delta_{f-} \\ \delta_{\Delta f} \end{bmatrix} = qSL_{ref}C\delta \tag{38}$$

where C is the control matrix with aerodynamic derivatives:

$$C = \begin{bmatrix} C_{l\delta_a} & 0 & C_{l\delta_r} & 0 & 0 & C_{l\delta_{\Delta f}} \\ 0 & C_{m\delta_e} & 0 & C_{m\delta_{f+}} & C_{m\delta_{f-}} & 0 \\ C_{n\delta_a} & 0 & C_{n\delta_r} & 0 & 0 & 0 \end{bmatrix} \tag{39}$$

$$\mathrm{rank}(C) = 3. \tag{40}$$

The reference control allocation strategy is chosen in [8], [15]:

$$\delta_{c,rtd} = Q^{-1}C^T[CQ^{-1}C^T]^{-1}\frac{M_c}{qSL_{ref}}. \tag{41}$$

If the rated deflection of aerodynamic surfaces is saturated, the saturated value is chosen to be the deflection command, although it is important to try to avoid these conditions.

IV. Principles of PIO Algorithm and Stochastic Robustness Design

A. PIO Algorithm Description and Principles

PIO algorithm, firstly proposed by Duan and Qiao, is a swarm intelligence algorithm inspired by the behavior of homing pigeons [16]. As presented in [16], homing pigeons are considered to go home by three homing tools: magnetic field, sun and landmarks. The homing behaviors depending on different homing tools are mapping to the update formulations in this new evolution algorithm. The detailed description of PIO is as follows [16]:

Individual in the pigeon swarm is initialized with initial velocity V_i and the initial position X_i in D-dimension research space randomly, while the position is the vector formed by parameters to be optimized and the velocity is the vector to update the position vector. Each individual is related to a value named the fitness value which is the cost function and always depends on the position of the individual. The evolution algorithm is to find the best position which has the maximum or minimum cost function. Two operators, map and compass operator and landmark operator, are introduced to model the two homing behaviors as mentioned early. At the early moment, pigeons are supposed to adjust their direction to the destination by the map shaped in their brains and compass. Thus, in this map and compass operator, the pigeon is trend to the global best position by the update formulations as follows:

$$V_i(t) = V_i(t-1)\cdot e^{-Rt} + \mathrm{rand}\cdot(X_{g,best} - X_i(t-1)) \tag{42}$$

$$X_i(t) = X_i(t-1) + V_i(t) \tag{43}$$

where R is defined as the map and compass factor, $X_{g,best}$ denotes the global best position among all individual in current iteration, rand signifies a random number.

With pigeons approaching to the destination, they switch their homing tool from map and compass to landmark, which means the landmark operator starts. In the landmark operator, pigeons are halved in every iteration generation. The pigeons which are familiar to the landmark fly straight to the destination, while others are supposed to follow the ones which are familiar to the landmark. In this model, the destination is regarded as the center of all pigeons in current iteration generation and can be calculated by weighted average of the position, the formulation is as follows:

$$X_c(t) = \frac{\sum\limits_{N_p} X_k(t)\cdot \mathrm{fitness}(X_k(t))}{\sum\limits_{N_p}\mathrm{fitness}(X_k(t))}. \tag{44}$$

In addition, the number of pigeons would be updated as follows:

$$N_p(t) = \frac{N_p(t-1)}{2}. \tag{45}$$

In this operator, the update formulation of the position of pigeons can be written as follows:

$$X_i(t) = X_i(t-1) + \mathrm{rand}\cdot(X_c(t) - X_i(t-1)). \tag{46}$$

Several papers indicate the effectiveness and robustness to solve some optimization problems or converted optimization problem, such as target detection, air robot path planning problem, UAVs formation cooperative control problem and so on [16]−[19]. In this study, PIO algorithm is selected to design parameters of the controller using stochastic robustness design method.

B. Stochastic Robustness Design Method

Due to the difficulties of the application of classical robust control theoretics in engineering practice, R.F. Stengel *et al.* introduced the concept of stochastic robustness and established a new robust control design method named stochastic robustness analysis and design (SRAD) in 1990s, which has been widely applied in engineering practice especially in flight control area in the past years [20]−[22].

In Stengel's theoretic, for linear time invariant (LTI) system, suppose that there are uncertain parameters $v \in \mathcal{Q}$, the instability probability can be defined as follows [23]:

$$P_{\text{instability}} = 1 - \int_{v\in\mathcal{Q}, g(v)\le 0} f(x)dx \tag{47}$$

where $g(v) = [\sigma_1(v)\sigma_2(v)\cdots\sigma_n(v)]^T$ is the vector formed by the real parts of the eigenvalues of closed-loop system, $f[g(v)]$ is the combined probability density distribution function. In practical application, the instability probability can be calculated by sample frequency calculation instead of the integral calculation, i.e.,

$$\int_{v\in\mathcal{Q}, g(v)\le 0} f(x)dx = \lim_{N\to\infty}\frac{M[g_{\max}(v)\le 0]}{N}\bigg|_{v\in\mathcal{Q}} \tag{48}$$

where $g_{\max}(v) = \max\{\sigma_1(v), \sigma_2(v), \ldots, \sigma_n(v)\}$, $M(\cdot)$ is the number of the maximum real part of eigenvalue less than zero in N times estimates. Moreover, the stochastic robust stability and stochastic robust performance can be introduced.

Similar to the definition of the instability probability, the probability that the dynamic out of performance envelope or the control variable saturated could be weighted summed to describe the performance of the closed-loop system. The sum is which named stochastic robustness cost function. When the structure of the controller has been chosen, the parameters of the controller can be designed by optimizing the cost function. The optimal control law from the point of stochastic robustness concepts is obtained.

For each performance demand, a two-valued indicator function is introduced to tell whether the closed-loop system satisfies this requirement in once simulation:

$$I[G(v), C(d)] = \begin{cases} 0, & \text{satified}, \\ 1, & \text{unsatified}, \end{cases} \quad v\in\mathcal{Q} \tag{49}$$

where d is the parameters to be designed, $\mathcal{Q}$ is the value set of uncertain parameters. Supposing that $f(v)$ is the combined probability density distribution function about v, the probability that closed-loop system violate this performance demand can be defined as follows [20]:

$$p = \int_{v\in\mathbb{Q}} I[G(v), C(d)]f(v)dv. \tag{50}$$

In practical application, this integral can be approximately calculated through Monte-Carlo simulation:

$$\hat{p} = \frac{1}{N}\sum_{k=1}^{N} I[H(v_k), G(d)] \tag{51}$$

where N is the simulation times, and $\hat{p}$ is the estimate of the violate probability.

Synthesize all the performance violate probability and instability probability, the stochastic robustness cost function can be defined as follows:

$$J(d) = \sum_{i=1}^{M} [w_i \hat{p}_i(d)] \tag{52}$$

where w_i is the weight, and M is the number of the indicators.

After the stochastic robustness cost function is defined, the last step is to use an optimization method to optimize this cost function. PIO algorithm introduced previously is applied in this optimization procedure. So far, the main principle of the stochastic robustness method has been presented.

V. Simulation Results and Analysis

In this section, the simulation results of the closed-loop system composed of the RLV and the controller designed by stochastic robustness design method are presented. Firstly, some simulation parameters setting are given out at the beginning of this section.

The test flight condition of the reusable launch vehicle is selected to give a design instance and evaluate the performance of the controller. This flight condition is selected refer to the flight envelope of the X-38. The flight condition selected is in Table I.

TABLE I
The Selected Flight Condition

h (m)	Ma	γ	$d\gamma/dt$	χ	$d\chi/dt$
30 000	2.8	−5	0	0	0

The evaluation commands are: angle of attack 5 degree step command, angle of side slip remains at the zero point, bank angle −5 degree step command.

The uncertainties of aerodynamic coefficients are supposed to subject to normal distribution, i.e.,:

$$v \sim \mathrm{N}(1, 0.15^2), \quad C_{ij} = vC_{ij} \tag{53}$$

where C_{ij} is the aerodynamic coefficients.

The design process goes for the different fractional order of the fractional SMC to give a preliminary study of the influence of the fractional orders. The parameters and performance indicators of stochastic robustness design method are set as in Table II, while the simulation times of Monte Carlo simulation $N = 50$.

The parameters to be optimized are the control parameters: $d = [k_w\ k_\alpha\ k_\beta\ k_\mu\ \sigma_\alpha\ \sigma_\beta\ \sigma_\mu\ \kappa_\alpha\ \kappa_\beta\ \kappa_\mu]^T$.

The parameters of PIO algorithm are set as follows: the number of pigeon $n = 20$, the map and compass operator $R = 0.02$, the iteration times of the map and compass operator $T_1 = 30$, the iteration times of landmark operator $T_2 = 5$.

Case 1: In this case, the stochastic robustness design for selected fractional order is focused on and the Monte-Carlo simulation is carried out to evaluate the designed parameters of the controller.

TABLE II
The Stability and Performance Metrics

Index	Weight	Indicator	Performance demand
1	8	I1	outputs convergence
2	0.1	I2	Regulation time at point 10% less than 1s
3	1	I3	Regulation time at point 10% less than 2s
4	1	I4	Overshoot less than 20%
5	0.1	I5	Overshoot less than 10%
6	1	I6	Deflection of aileron less than 40 deg
7	0.5	I7	Deflection of aileron less than 30 deg
8	1	I8	Deflection of elevator less than 40 deg
9	0.5	I9	Deflection of elevator less than 30 deg
10	1	I10	Deflection of rudder less than 40 deg
11	0.5	I11	Deflection of rudder less than 30 deg
12	1	I12	Deflection of body flap less than50 deg
13	0.5	I13	Deflection of body flap less than 40 deg

The fractional order of FSMC selected: $\lambda = -0.8, \eta = 0.9$.

The result of design parameter is:

$$\begin{aligned} d = [&1.8359\ \ 1.0651\ \ 2.1960\ \ 1.0364\ \ 3.4948\times10^{-5} \\ &8.1261\times10^{-5}\ \ 6.2807\times10^{-5}\ \ 0.7458\ \ 1.2157\ \ 1.4024] \end{aligned}$$

Fig. 2 shows the history of the stochastic robustness cost function in the design process based on PIO algorithm. Then the Monte-Carlo simulation goes for the closed loop system with the designed control parameters. Fig. 3 is the simulation results from which we can evaluate the robustness of the control system. The time history of attitude angles shows that they can steer the evaluation step command quickly and robustly though angle of attack has a tolerant steady-state error.

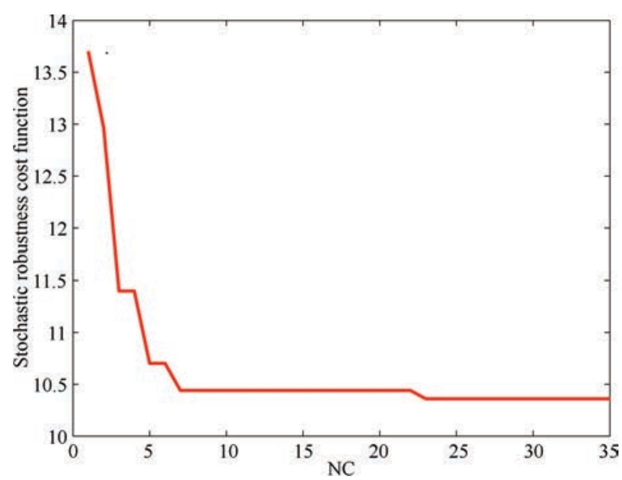

Fig. 2. The fitness value curve of PIO algorithm.

From the simulation results, the controller based on FSMC and DI can tolerate the uncertainties of aerodynamic parameters through the stochastic robustness design process.

Case 2: In this case, the design results based on stochastic robustness design method for the different fractional orders are compared, from which we can find out the influence of the fractional order in FSMC to the closed loop system.

Six groups of the fractional order are selected:

$$\begin{aligned} &\lambda_1 = -1, \quad \eta_1 = 0.9; \quad \lambda_2 = -0.9, \quad \eta_2 = 0.9 \\ &\lambda_3 = -0.8, \quad \eta_3 = 0.9; \quad \lambda_4 = -0.7, \quad \eta_4 = 0.9 \\ &\lambda_5 = -0.7, \quad \eta_5 = 1; \quad \lambda_6 = -1, \quad \eta_6 = 1. \end{aligned}$$

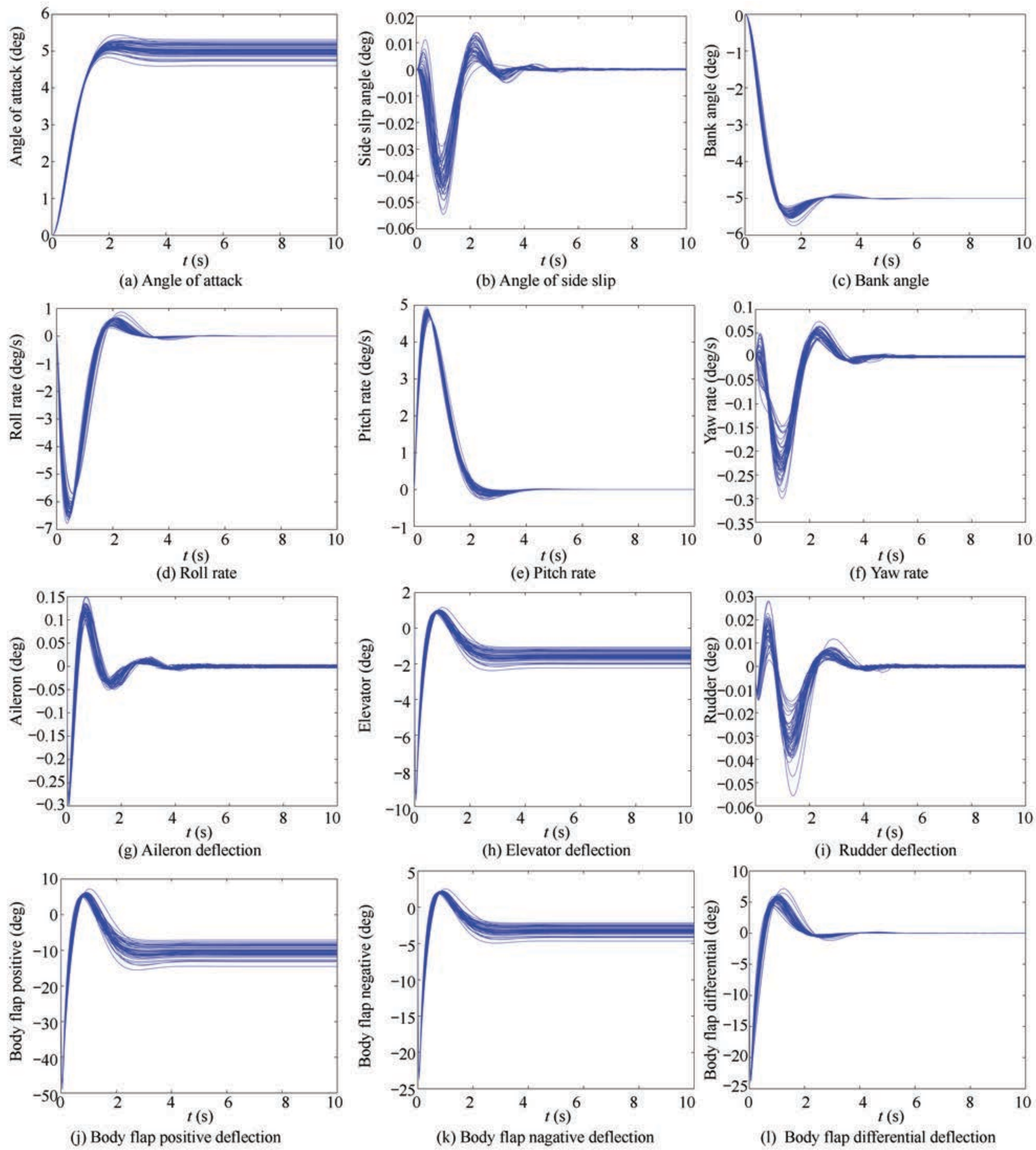

Fig. 3. Results of Monte Carlo simulation experiments.

These groups include different fractional order in the sliding surface function and fractional reaching law, as well as integral order sliding surface and reaching law. Through the stochastic robustness design procedure above, we obtain the optimal design parameters of the each controller with different fractional orders and integral order. The simulations of these closed-loop systems with different FSMC and SMC have been carried out. Fig. 4 gives the compared results of these closed-loop systems.

It should be noted that in these figures, symbol a represents the fractional integral order, while symbol b represents the fractional integral order. These compared results show how the different fractional orders in FSMC influence the performance of the closed loop system. For the group 1 to group 4, these groups all have the same fractional order of the reaching law and different fractional order of the sliding surface. The group 2 and group 3 have the similar performance, the response of the attitude angle is smoother and faster which means a shorter settling time and a smaller overshoot. Compared the control surface deflection, the group 2 and group 3 have a smaller control effectors but the group 1 and group 4 have one aerodynamic surface saturated. With the above factors combined, the group 2 and group 3 have more desirable performance. By Comparing the group 3 with the group 6

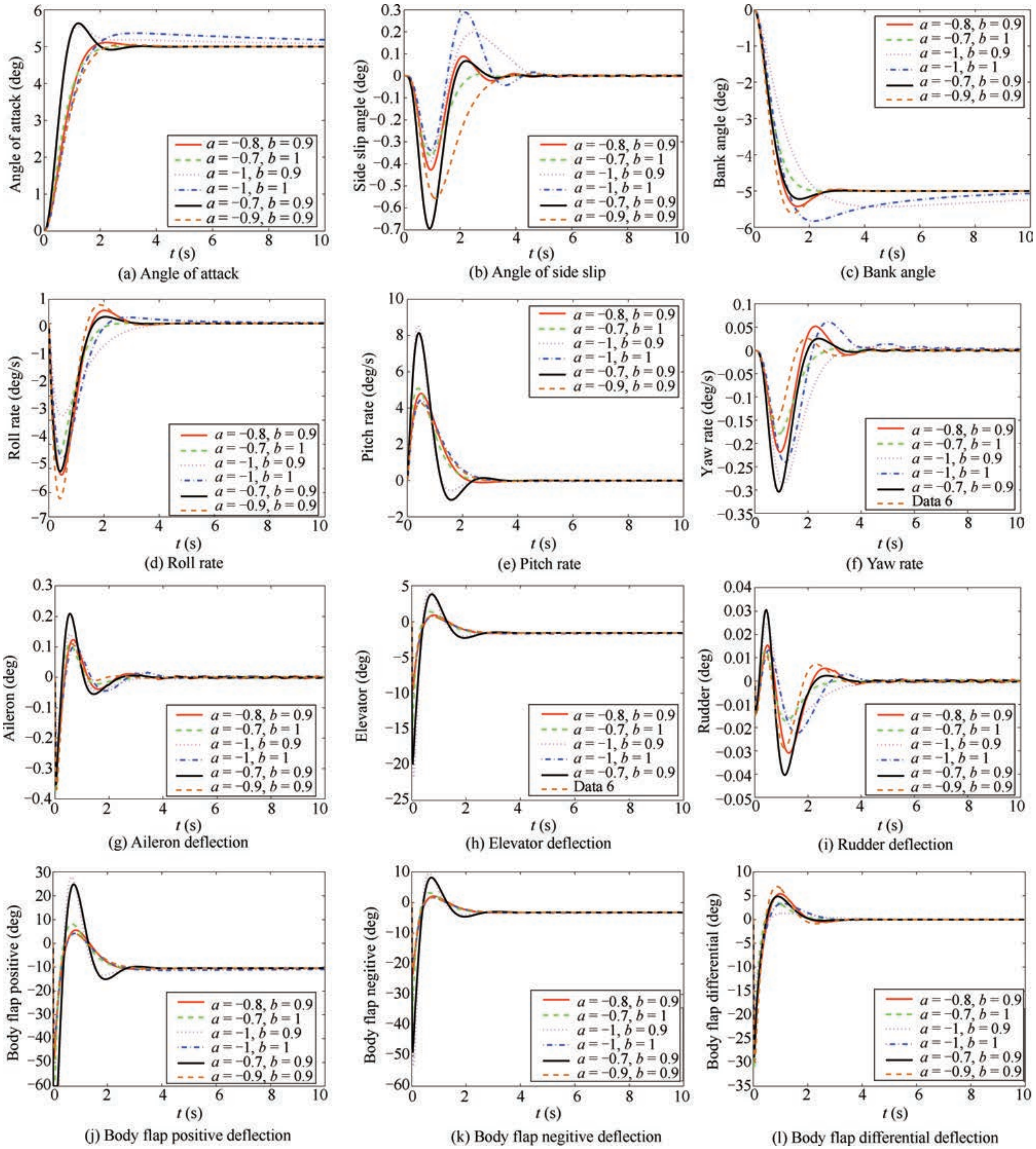

Fig. 4. Results of simulation experiments of different FSMC.

which has integral order sliding surface and reaching law, we can see that the attitude angle response of group 3 is smoother and faster than that of group 6. The control surface deflection in the group 6 is smaller than that in the group 3. Comparing the group 1, group 4, group 5 and group 6, we can see that the fractional order obviously influence the control variables. So the optimal fractional order or integral order in FSMC should been chosen by taking both the dynamic characters and control effects into count. In this study, the stochastic robustness design method for the different fractional orders also influence the performance of these controllers. The more credible mean to find the optimal fractional order in the controller remains a question.

VI. Conclusions

In this paper, we have established a robust controller for reusable launch vehicle based on fractional sliding mode technology and dynamic inversion approach. For the parameters of the controller, stochastic robustness design method based on PIO algorithm and Monte-Carlo simulations is applied to obtain the optimal values. The influence of different fractional order of the FSMC to the performance of closed loop system is discussed. The experimental results validate the effectiveness and robustness of the combined robust controller when considering sufficient dispersion of aerodynamic coefficients. In addition, the fractional orders in sliding mode method improve the performance of the closed-loop system.

It should be pointed out that FSMCs with several different fractional orders in our control law are designed to compare the performance of the closed-loop systems. The direct analysis to obtain the optimal fractional order in FSMC for the closed-loop system has not been given out. In addition, how to simply the algorithm and make it more convenient in engineering is still a challenge. The more relative further work and details would be conducted in these issues in the future.

REFERENCES

[1] E. Mooij, "Aerospace-plane flight dynamics: analysis of guidance and control concepts," Ph.D. dissertation, Delft University of Technology, The Netherlands, 1998.

[2] A. J. Roenneke and K. H. Well, "Nonlinear flight control for a high-lift reentry vehicle," in *Guidance, Navigation, and Control Conf., Guidance, Navigation, and Control and Co-located Conf.*, Baltimore, MD, 1995, pp. 1798−1805.

[3] H. X. Wu and B. Meng, "Review on the control of hypersonic flight vehicles," *Adv. Mechan.*, vol. 39, no. 6, pp. 756−765, Nov. 2009.

[4] J. M. Hanson, "A plan for advanced guidance and control technology for 2nd generation reusable launch vehicles," in *AIAA Guidance, Navigation, and Control Conf. and Exhibit, Guidance, Navigation, and Control and Co-located Conf.* Monterey, California, USA, 2002, pp. 1−9.

[5] D. Ito, J. Georgie, J. Valasek, and D. T. Ward, "Reentry vehicle flight controls design guidelines: dynamic inversion," Technical Report NASA/TP-2002-210771, Mar. 1, 2002.

[6] C. Y. Wang, Y. Luo, and Y. Q. Chen, "An analytical design of fractional order proportional integral and [proportional integral] controllers for robust velocity servo," in *Proc. 4th IEEE Conf. Industrial Electronics and Applications (ICIEA 2009)*, Xi'an, China, 2009, pp. 3448−3453.

[7] B. C. Zhang, S. F. Wang, Z. P. Han, and C. M. Li, "Using fractional-order PID controller for control of aerodynamic missile," *J. Astronaut.*, vol. 26, no. 5, pp. 653−656, Sep. 2005.

[8] R. J. Adams, J. M. Buffington, and S. S. Banda, "Design of nonlinear control laws for high-angle-of-attack flight," *J. Guid. Contr. Dynam.*, vol. 17, no. 4, pp. 737−746, Jul. 1994.

[9] E. B. Jackson and C. I. Cruz, "Preliminary subsonic aerodynamic model for simulation studies of the HL-20 lifting body," Technical Report NASA TM-4302, Sep. 1992.

[10] E. B. Jackson, C. I. Cruz, and W. A. Ragsdale, "Real-time simulation model of the HL-20 lifting body," Technical Report NASA TM-107580, Aug. 1992.

[11] J. Reiner, G. J. Balas, and W. L. Garrard, "Flight control design using robust dynamic inversion and time-scale separation," *Automatica*, vol. 32, no. 11, pp. 1493−1504, Nov. 1996.

[12] I. Podlubny, "Fractional-order systems and $PI^{\lambda}D^{\mu}$-controllers," *IEEE Trans. Automat. Contr.*, vol. 44, no. 1, pp. 208−214, Jan. 1999.

[13] X. Yuan, H. Y. Zhang, and J. B. Yu, "Fractional-order derivative and design of fractional digital differentiators," *Acta Electron. Sin.*, vol. 32, no. 10, pp. 1658−1665, Oct. 2004.

[14] J. Y. Cao and B. G. Cao, "Digital realization and characteristics of fractional order controllers," *Contr. Theor. Appl.*, vol. 23, no. 5, pp. 791−799, Oct. 2006.

[15] W. T. Ma, Q. Z. Zhang, B. B. Shi, and C. Gao, "Robust control approach for re-entry vehicle based on inversion model," in *Proc. 29th Chinese Control Conf.*, Beijing, China, 2010, pp. 2005−2009.

[16] H. B. Duan and P. X. Qiao, "Pigeon-inspired optimization: a new swarm intelligence optimizer for air robot path planning," *Int. J. Intell. Comput. Cybernet.*, vol. 7, no. 1, pp. 24−37, Feb. 2014.

[17] H. B. Duan and X. H. Wang, "Echo state networks with orthogonal pigeon-inspired optimization for image restoration," *IEEE Trans. Neural Network. Learn. Syst.*, vol. 27, no. 11, pp. 2413−2425, Nov. 2016.

[18] H. B. Duan, H. X. Qiu, and Y. M. Fan, "Unmanned aerial vehicle close formation cooperative control based on predatory escaping pigeon-inspired optimization," *Sci. China Technol. Sci.*, vol. 45, no. 6, pp. 559−572, Apr. 2015.

[19] B. Zhang and H. B. Duan, "Three-dimensional path planning for uninhabited combat aerial vehicle based on predator-prey pigeon-inspired optimization in dynamic environment," *IEEE/ACM Trans. Computat. Biol. Bioinf.*, 2017, to be published, DOI:10.1109/TCBB.2015.2443789.

[20] L. R. Ray and R. F. Stengel, "Application of stochastic robustness to aircraft control systems," *J. Guid. Contr. Dynam.*, vol. 14, no. 6, pp. 1251−1259, Nov. 1991.

[21] C. I. Marrison and R. F. Stengel, "Design of robust control systems for a hypersonic aircraft," *J. Guid. Contr. Dynam.*, vol. 21, no. 1, pp. 58−63, Jan. 1998.

[22] Q. Wang and R. F. Stengel, "Robust nonlinear control of a hypersonic aircraft," *J. Guid. Contr. Dynam.*, vol. 23, no. 4, pp. 577−585, Jul. 2000.

[23] S. T. Wu, *Stochastic Robustness Analysis and Design for Guidance and Control System of Winged Missile*. Beijing: National Defense Industry Press, 2010.

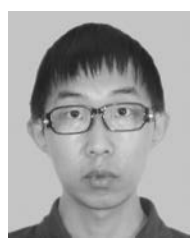

Qiang Xue is a master student at the School of Automation Science and Electrical Engineering, Beihang University, China. He received his bachelor degree from Beihang University in 2015. He is a member of BUAA Bio-inspired Autonomous Flight Systems (BAFS) Research Group. His reserach interests include multiple UAVs cooperative control and flight control.

Haibin Duan is a professor in the School of Automation Science and Electrical Engineering, Beihang University, China. He received his Ph.D. degree from Nanjing University of Aeronautics and Astronautics in 2005. He is the head of BUAA Bio-inspired Autonomous Flight Systems (BAFS) Research Group. His research interests include multiple UAVs cooperative control, biological computer vision and bio-inspired computation. Corresponding author of this paper.

Numerical Solutions of Fractional Differential Equations by Using Fractional Taylor Basis

Vidhya Saraswathy Krishnasamy, Somayeh Mashayekhi, and Mohsen Razzaghi

***Abstract*—In this paper, a new numerical method for solving fractional differential equations (FDEs) is presented. The method is based upon the fractional Taylor basis approximations. The operational matrix of the fractional integration for the fractional Taylor basis is introduced. This matrix is then utilized to reduce the solution of the fractional differential equations to a system of algebraic equations. Illustrative examples are included to demonstrate the validity and applicability of this technique.**

***Index Terms*—Caputo derivative, fractional differential equations (FEDs), fractional Taylor basis, operational matrix, Riemann-Liouville fractional integral operator.**

I. Introduction

THE fractional differential equations (FDEs) have drawn increasing attention and interest due to their important applications in science and engineering. A history of the development of fractional differential operators can be found in [1]−[3].

Many mathematical modelings contain FDEs. To mention a few, fractional derivatives are used in visco-elastic systems [4], economics [5], continuum and statistical mechanics [6], solid mechanics [7], electrochemistry [8], biology [9] and acoustics [10]. Generally speaking, most of the FDEs do not have exact analytic solutions. Therefore, seeking numerical solutions of these equations becomes more and more important. Recently, several numerical methods to solve FDEs have been given, such as Fourier transforms [11], Laplace transforms [12], Adomian decomposition method [13], variational iteration method [14], the power series method [15], truncated fractional power series method [16], fractional differential transform method (FDTM) [17], homotopy analysis method [18], fractional-order Legendre functions method [19], modified homotopy perturbation method (MHPM) [20] and enhanced homotopy perturbation method (EHPM) [21].

Moreover, for solving FDEs in [22], the Bernstein polynomials are used to solve the fractional Riccati type differential equations. In [22], the Bernstein polynomials were first expanded into fractional Taylor polynomials. The operational matrix of fractional differentiation (OMFD) of fractional Taylor polynomials were then used for calculating OMFD for Bernstein polynomials. In addition, the Chebyshev, Legendre and Bernoulli wavelets operational matrices of fractional integration (OMFI) were calculated in [23]−[25], respectively. For obtaining OMFI in [23], [24], these wavelets were first expanded into block-pulse functions. Then, OMFI of block-pulse were used for calculating OMFI for Chebyshev and Legendre wavelets in [23], [24], respectively. In [25], for obtaining the OMFI for Bernoulli wavelets, these wavelets were expanded into Bernoulli polynomials.

In this paper, a new numerical method for solving the initial and boundary value problems for fractional differential equations is presented. The method is based upon the fractional Taylor basis approximations. The OMFI for the fractional Taylor basis is calculated. This matrix is then utilized to reduce the solution of the FDEs to the solution of algebraic equations. This method is applicable for linear equations or nonlinear equations with square nonlinearities.

The outline of this paper is as follows: In Section II, we introduce some necessary definitions and properties of fractional calculus. Section III is devoted to the basic formulation of the fractional Taylor basis. In Section IV, we derive the Fractional Taylor OMFI. In Section V, the problem statement is given. Section VI is devoted to the numerical method for solving the initial and boundary value problems for FDEs and, in Section VII we report our numerical findings and demonstrate the accuracy of the proposed numerical scheme by considering five numerical examples.

II. Preliminaries

A. The Fractional Integral and Derivative

In this section, we present some notations, definitions, and preliminary facts of the fractional calculus theory which will be used further in this work.

Definition 1: The Riemann-Liouville fractional integral operator of order α is defined as [12]

$$I^{\alpha}y(t)=\begin{cases}\frac{1}{\Gamma(\alpha)}\int_0^t(t-s)^{\alpha-1}y(s)ds, & \alpha>0\\ y(t), & \alpha=0.\end{cases}$$

The Riemann-Liouville fractional integral operator has the following properties:

$$I^{\alpha}\ t^{\gamma}=\frac{\Gamma(\gamma+1)}{\Gamma(\gamma+\alpha+1)}\ t^{\gamma+\alpha},\quad \alpha\geq 0;\gamma>-1 \tag{1}$$

$$I^{\alpha}I^{\beta}y(t)=I^{\beta}I^{\alpha}y(t)=I^{\alpha+\beta}y(t),\quad \alpha,\ \ \beta>0. \tag{2}$$

Manuscript received August 8, 2015; accepted April 18, 2016. Recommended by Associate Editor YangQuan Chen.

Citation: V. S. Krishnasamy, S. Mashayekhi, and M. Razzaghi, "Numerical solutions of fractional differential equations by using fractional Taylor basis," *IEEE/CAA Journal of Automatica Sinica*, vol. 4, no. 1, pp. 98−106, Jan. 2017.

V. S. Krishnasamy and M. Razzaghi are with the Department of Mathematics and Statistics, Mississippi State University, MS 39762, USA (e-mail: vk81@msstate.edu; razzaghi@math.msstate.edu).

S. Mashayekhi is with the Department of Mathematics, Florida State University, Tallahassee, FL 32306, USA (e-mail: sm2395@msstate.edu).

Color versions of one or more of the figures in this paper are available online at http://ieeexplore.ieee.org.

Digital Object Identifier 10.1109/JAS.2017.7510337

Also the fractional integral is a linear operator, that is for constants λ_1 and λ_2, we have

$$I^\alpha(\lambda_1 y_1(t)+\lambda_2 y_2(t))=\lambda_1 I^\alpha y_1(t)+\lambda_2 I^\alpha y_2(t).$$

Definition 2: The Caputo fractional derivative of order α is defined as [12]

$$D^\alpha y(t)=I^{n-\alpha}\left(\frac{d^n}{dt^n}y(t)\right),\ \ n-1<\alpha\le n;\ n\in\mathbb{N}. \tag{3}$$

The fractional integral operator and fractional derivative operator do not commute in general, but we have the following property

$$I^\alpha(D^\alpha y(t))=y(t)-\sum_{k=0}^{n-1}y^{(k)}(0)\ \frac{t^k}{k!}. \tag{4}$$

III. The Properties of Fractional Taylor Basis

A. Fractional Taylor Basis Vector

In this paper, we define the fractional Taylor basis vector as

$$T_{m\gamma}(t)=[1,t^\gamma,t^{2\gamma},\ldots,t^{m\gamma}]^T \tag{5}$$

where m is a positive integer and $\gamma>0$, is a real number.

B. Function Approximation

Let $H=L^2[0,1]$, and assume that $T_{m\gamma}(t)\subset H$, S = span $\{1,t^\gamma,t^{2\gamma},\ldots,t^{m\gamma}\}$ and y be an arbitrary element in H. Since S is a finite dimensional vector subspace of H, y has a unique best approximation out of S such as $y_0\in S$, that is

$$\forall\hat{y}\in S,\quad ||y-y_0||\le||y-\hat{y}||.$$

Since $y_0\in S$, there exist unique coefficients $c_0,c_1,c_2,\ldots,c_m$, such that

$$y\simeq y_0=\sum_{i=0}^{m}c_i t^{i\gamma}=C^T T_{m\gamma}(t) \tag{6}$$

where

$$C^T=[c_0,c_1,c_2,\ldots,c_m]. \tag{7}$$

C. Error Bound for the Best Approximation

To obtain the error bound for the best approximation, we use the following formula.

Generalized Taylor formula [15]: Suppose that $D^{k\gamma}y(t)\in\mathbb{C}[0,1]$ for $k=0,1,\ldots,m$, where $0<\gamma\le 1$, then

$$y(t)=\sum_{i=0}^{m}\frac{(t)^{i\gamma}}{\Gamma(i\gamma+1)}[D^{i\gamma}y(t)]_{t=0}+R_m^\gamma(t,0) \tag{8}$$

where $D^{i\gamma}=\underbrace{D^\gamma D^\gamma\cdots D^\gamma}_{i\ \text{times}}$, with D^γ defined similar to D^α in (3), and

$$R_m^\gamma(t,0)=\frac{(t)^{(m+1)\gamma}}{\Gamma((m+1)\gamma+1)}[D^{(m+1)\gamma}y(t)]_{t=\xi}$$
$$0\le\xi\le t;\quad\forall t\in[0,1].$$

Theorem 1: Let y_0 be the best approximation of y out of S and suppose $D^{k\gamma}y(t)\in C[0,1]$, $k=0,1,\ldots,$ then

$$||y(t)-y_0(t)||_{L^2[0,1]}\le\frac{M_\gamma}{\Gamma((m+1)\gamma+1)}\sqrt{\frac{1}{2(m+1)\gamma+1}}$$

where

$$M_\gamma=\sup_{t\in[0,1]}|D^{(m+1)\gamma}y(t)|.$$

Proof: Similar to [19], since y_0 is the best approximation of y out of S, by using (8) we have

$$\begin{aligned}||y-y_0||^2_{L^2[0,1]}&\le\frac{M_\gamma^2}{(\Gamma((m+1)\gamma+1))^2}\int_0^1(t)^{2(m+1)\gamma}dt\\&=\frac{M_\gamma^2}{(\Gamma((m+1)\gamma+1))^2}\frac{1}{2(m+1)\gamma+1}.\end{aligned} \tag{9}$$

By using (9), the result can be obtained. ∎

D. Error Bound for Fractional Integration

In this section we obtain the error bound for $I^\alpha y(t)$.

Theorem 2: Suppose all the conditions in Theorem 1 are true and $\alpha>1$, then

$$||I^\alpha y(t)-I^\alpha y_0(t)||_{L^2[0,1]}\le\frac{M_\gamma}{\Gamma((m+1)\gamma+1)\Gamma(\alpha)}\sqrt{\frac{1}{2(m+1)\gamma+1}}.$$

Proof: By using Definition 1, we have

$$\begin{aligned}&||I^\alpha y(t)-I^\alpha y_0(t)||_{L^2[0,1]}\\&=||I^\alpha\left(y(t)-y_0(t)\right)||_{L^2[0,1]}\\&\le\frac{1}{\Gamma(\alpha)}\int_0^t||(t-s)^{\alpha-1}(y(s)-y_0(s))||_{L^2[0,1]}\ ds\\&\le\frac{1}{\Gamma(\alpha)}\int_0^1||(1-s)^{\alpha-1}(y(s)-y_0(s))||_{L^2[0,1]}\ ds\\&\le\frac{1}{\Gamma(\alpha)}\int_0^1||(y(s)-y_0(s))||_{L^2[0,1]}\ ds.\end{aligned} \tag{10}$$

By using (9) and (10), the result can be obtained. ∎

IV. The Operational Matrices

A. Operational Matrix of the Fractional Integration

In this section we derive the fractional Taylor operational matrix of the fractional integration.

By using (1) and (5), we have

$$\begin{aligned}I^\alpha(T_{m\gamma}(t))&=\left[\frac{1}{\Gamma(\alpha+1)}t^\alpha,\frac{\Gamma(\gamma+1)}{\Gamma(\gamma+\alpha+1)}t^{\gamma+\alpha},\right.\\&\left.\frac{\Gamma(2\gamma+1)}{\Gamma(2\gamma+\alpha+1)}t^{2\gamma+\alpha},\ldots,\frac{\Gamma(m\gamma+1)}{\Gamma(m\gamma+\alpha+1)}t^{m\gamma+\alpha}\right]^T\\&=t^\alpha F_\alpha T_{m\gamma}(t)\end{aligned} \tag{11}$$

where

$$F_\alpha=\operatorname{diag}\left[\frac{1}{\Gamma(\alpha+1)},\ \frac{\Gamma(\gamma+1)}{\Gamma(\gamma+\alpha+1)},\ \frac{\Gamma(2\gamma+1)}{\Gamma(2\gamma+\alpha+1)},\ \ldots,\ \frac{\Gamma(m\gamma+1)}{\Gamma(m\gamma+\alpha+1)}\right].$$

Equation (11) can be rewritten as

$$I^\alpha(T_{m\gamma}(t))=t^\alpha G_\alpha * T_{m\gamma}(t) \tag{12}$$

where

$$G_\alpha = \left[\frac{1}{\Gamma(\alpha+1)},\ \frac{\Gamma(\gamma+1)}{\Gamma(\gamma+\alpha+1)},\ \frac{\Gamma(2\gamma+1)}{\Gamma(2\gamma+\alpha+1)},\right.$$
$$\left.\ldots,\ \frac{\Gamma(m\gamma+1)}{\Gamma(m\gamma+\alpha+1)}\right]^T$$

and * denotes term by term multiplication of two matrices of the same dimensions.

B. Operational Matrix of Product

The following property of the product of two fractional Taylor vectors will also be used.

$$I^\alpha(T_{m\gamma}(t)T_{m\gamma}^T(t)) \ = \ t^\alpha S_\alpha * (T_{m\gamma}(t)T_{m\gamma}^T(t)) \tag{13}$$

where S_α is given by

$$S_\alpha = \begin{bmatrix} \frac{1}{\Gamma(\alpha+1)} & \frac{\Gamma(\gamma+1)}{\Gamma(\gamma+\alpha+1)} & \cdots & \frac{\Gamma(m\gamma+1)}{\Gamma(m\gamma+\alpha+1)} \\ \frac{\Gamma(\gamma+1)}{\Gamma(\gamma+\alpha+1)} & \frac{\Gamma(2\gamma+1)}{\Gamma(2\gamma+\alpha+1)} & \cdots & \frac{\Gamma((m+1)\gamma+1)}{\Gamma((m+1)\gamma+\alpha+1)} \\ \frac{\Gamma(2\gamma+1)}{\Gamma(2\gamma+\alpha+1)} & \frac{\Gamma(3\gamma+1)}{\Gamma(3\gamma+\alpha+1)} & \cdots & \frac{\Gamma((m+2)\gamma+1)}{\Gamma((m+2)\gamma+\alpha+1)} \\ \vdots & \vdots & \ddots & \vdots \\ \frac{\Gamma(m\gamma+1)}{\Gamma(m\gamma+\alpha+1)} & \frac{\Gamma((m+1)\gamma+1)}{\Gamma((m+1)\gamma+\alpha+1)} & \cdots & \frac{\Gamma(2m\gamma+1)}{\Gamma(2m\gamma+\alpha+1)} \end{bmatrix}. \tag{14}$$

To illustrate the calculation procedure, by using (5), we have

$$T_{m\gamma}(t)T_{m\gamma}^T(t)$$
$$= \begin{bmatrix} 1 & t^\gamma & t^{2\gamma} & \cdots & t^{m\gamma} \\ t^\gamma & t^{2\gamma} & t^{3\gamma} & \cdots & t^{(m+1)\gamma} \\ t^{2\gamma} & t^{3\gamma} & t^{4\gamma} & \cdots & t^{(m+2)\gamma} \\ \vdots & \vdots & \vdots & \ddots & \vdots \\ t^{m\gamma} & t^{(m+1)\gamma} & t^{(m+2)\gamma} & \cdots & t^{2m\gamma} \end{bmatrix}. \tag{15}$$

From (1) and (15), we get (16), shown at the bottom of the page.

Therefore from (13) and (15), we get S_α in (14).

V. Problem Statement

In this paper we focus on the following FDE problems [24].

A. Problem a

Caputo fractional differential equation

$$\begin{aligned} &D^\alpha y(t) = f(t, y(t), D^\beta y(t)) \\ &\quad 0 \le t \le 1;\quad 0 < \alpha \le 2;\quad 0 \le \beta \le \alpha \end{aligned} \tag{17}$$

with the initial conditions

$$y(0) = Y_0, \quad y'(0) = Y_1. \tag{18}$$

The existence and uniqueness results for solution of this problem are given in [26].

B. Problem b

Caputo fractional differential equation in (17) with the boundary conditions

$$y(0) = Y_0, \quad y(1) = \bar{Y}_1. \tag{19}$$

For this problem, we have the following Lemma 1.

Lemma 1: Assume that $f : [0,1]\times\mathbb{R}\times\mathbb{R} \to \mathbb{R}$ is continuous. Then $y(t)\in\mathbb{C}[0,1]$ is a solution of the boundary value problem in (17) and (19) if and only if $y(t)$ is the solution of [24].

$$\begin{aligned} y(t) = \ & I^\alpha f(t, y(t), D^\beta y(t)) - tI^\alpha f(1, y(1), D^\beta y(1)) \\ & + (\bar{Y}_1 - Y_0)t + Y_0. \end{aligned} \tag{20}$$

The existence and uniqueness results for solution of this problem are given in [24].

VI. The Numerical Method

In this section, we use the fractional Taylor vector in (5) for solving Problem a given in (17) and (18) and Problem b given in (17) and (19).

A. Problem a

In this case, by using (4) and (17), we have

$$y(t) - \sum_{k=0}^{n-1} y^k(0)\ \frac{t^k}{k!} = I^\alpha f(t, y(t), D^\beta y(t)). \tag{21}$$

$$I^\alpha(T_{m\gamma}(t)T_{m\gamma}^T(t)) = \begin{bmatrix} \frac{1}{\Gamma(\alpha+1)}t^\alpha & \frac{\Gamma(\gamma+1)}{\Gamma(\gamma+\alpha+1)}t^{\gamma+\alpha} & \cdots & \frac{\Gamma(m\gamma+1)}{\Gamma(m\gamma+\alpha+1)}t^{m\gamma+\alpha} \\ \frac{\Gamma(\gamma+1)}{\Gamma(\gamma+\alpha+1)}t^{\gamma+\alpha} & \frac{\Gamma(2\gamma+1)}{\Gamma(2\gamma+\alpha+1)}t^{2\gamma+\alpha} & \cdots & \frac{\Gamma((m+1)\gamma+1)}{\Gamma((m+1)\gamma+\alpha+1)}t^{(m+1)\gamma+\alpha} \\ \frac{\Gamma(2\gamma+1)}{\Gamma(2\gamma+\alpha+1)}t^{2\gamma+\alpha} & \frac{\Gamma(3\gamma+1)}{\Gamma(3\gamma+\alpha+1)}t^{3\gamma+\alpha} & \cdots & \frac{\Gamma((m+2)\gamma+1)}{\Gamma((m+2)\gamma+\alpha+1)}t^{(m+2)\gamma+\alpha} \\ \vdots & \vdots & \ddots & \vdots \\ \frac{\Gamma(m\gamma+1)}{\Gamma(m\gamma+\alpha+1)}t^{m\gamma+\alpha} & \frac{\Gamma((m+1)\gamma+1)}{\Gamma((m+1)\gamma+\alpha+1)}t^{(m+1)\gamma+\alpha} & \cdots & \frac{\Gamma(2m\gamma+1)}{\Gamma(2m\gamma+\alpha+1)}t^{2m\gamma+\alpha} \end{bmatrix} \tag{16}$$

Substituting (6) and (18) in (21), we obtain

$$C^T T_{m\gamma}(t) - Y_0 - Y_1 t = I^\alpha f\left(t, C^T T_{m\gamma}(t), D^\beta(C^T T_{m\gamma}(t)\right). \quad (22)$$

Next, we use the operational matrices obtained in Section 4 as needed and collocate (22) at the following equidistant nodes t_i given by

$$t_i = \frac{i}{m}, \quad i = 0, 1, 2, \ldots m. \quad (23)$$

These equations give $m+1$ algebraic equations, which can be solved for the unknown vector C^T using Newton's iterative method. It is known that the initial guess for Newton's iterative method is very important. According to the conditions in (18) the solution $y(t)$ will pass through the point $(0, Y_0)$ and have a slope Y_1 at this point. We choose our initial guess $y_0(t)$ such that $y_0(t) = Y_1 t + Y_0$.

B. Problem b

For Problem b, by substituting (6) in (20) we get (24), shown at the bottom of the page.

By using the operational matrices obtained in Section IV wherever needed and collocating (24) at the equidistant nodes t_i, given in (23), we get a system of algebraic equations, which can be solved for the unknown vector C^T using Newton's iterative method. In this case, the initial values required to start Newton's iterative method have been chosen by taking $y(t)$ as a linear function between the initial value $y(0) = Y_0$ and the final value $y(1) = \bar{Y}_1$.

VII. Illustrative Examples

In this section, five examples are given to demonstrate the applicability and accuracy of our method. Examples 1−4 are initial value problems and Example 5 is a boundary value problem. Example 1 is an initial value FDE, which was first considered in [19]. The exact solution of Example 1 is a polynomial, and the exact solution can be obtained using the proposed method. Examples 2 and 3 are FDEs describing the fractional Riccati equation, which were first considered in [20] by using modified homotopy perturbation method, it was also studied in [21] by applying the enhanced homotopy perturbation method, in [22] by using Bernstein polynomials and in [25] by applying Bernoulli wavelets. For Examples 2 and 3, we compare our findings with the numerical results in [20]−[22], [25]. Example 4 was first considered in [27] by using a predictor corrector approach; it was also solved in [28] by converting the FDE to a Volterra type integral equation and in [24] by using Legendre wavelet method. For Example 4 we compare our method with [24] which has been shown to be comparable or superior to [27], [28]. Example 5 was solved in [24] by using Legendre wavelet. For Example 5, we compare our results with [24]. In Examples 2−5 the package of Mathematica ver. 9.0 has been used to solve the test problems. Here, we first give a method for selecting γ in (5) for our examples. We select $\gamma = 1$ if $\alpha = 1$ or $\alpha = 2$. Otherwise, we select $\gamma = \alpha$. For Example 5, similar to [29] we have also used $\gamma = \alpha - \lfloor \alpha \rfloor$, and we get better results than α. Here $\lfloor \alpha \rfloor$ is the floor function which is the greatest integer less than or equal to the α.

A. Example 1

Consider the following linear fractional differential equation given in [19].

$$\begin{gathered} D^2 y(t) + D^{\frac{3}{2}} y(t) + y(t) = 1 + t \\ 0 < t \leq 1; \quad y(0) = 1; \quad y'(0) = 1. \end{gathered} \quad (25)$$

The exact solution of this problem is

$$y(t) = 1 + t.$$

Here, we solve this problem by using the proposed method with $\gamma = 1$ and $m = 1$.

Let

$$y(t) \cong C^T T_{m\gamma}(t) = [c_0,\ c_1] \begin{bmatrix} 1 \\ t \end{bmatrix}. \quad (26)$$

By using (1)−(4) and (25), we have

$$y(t) - 1 - t + I^{\frac{1}{2}}\left(I^{\frac{3}{2}} D^{\frac{3}{2}} y(t)\right) + I^2 y(t) = \frac{t^2}{2} + \frac{t^3}{6}. \quad (27)$$

By substituting (26) in (27), we get

$$C^T T_{m\gamma}(t) - 1 - t + I^{\frac{1}{2}}\left(C^T T_{m\gamma}(t) - y(0) - y'(0)t\right) + I^2 C^T T_{m\gamma}(t) = \frac{t^2}{2} + \frac{t^3}{6}.$$

From (12), we have (28), shown at the bottom of the page. where

$$G_{\frac{1}{2}} = [\frac{1}{\Gamma(\frac{3}{2})}, \frac{1}{\Gamma(\frac{5}{2})}]^T, \qquad G_2 = [\frac{1}{2}, \frac{1}{6}]^T. \quad (29)$$

Substituting (29) in (28) and collocating the resulting equation at $t_0 = 0$ and $t_1 = 1$, we get

$$c_0 = 1, \quad c_1 = 1.$$

Then, by using (26), we get $y(t) = 1 + t$, which is the exact solution.

B. Example 2

Consider the fractional Riccati differential equation [22].

$$D^\alpha y(t) + y^2(t) = 1, \quad y(0) = 0; \quad 0 < \ \alpha \ \leq 1. \quad (30)$$

$$C^T T_{m\gamma}(t) - I^\alpha f(t, C^T T_{m\gamma}(t), D^\beta C^T T_{m\gamma}(t)) + tI^\alpha\left(\ f(1, C^T T_{m\gamma}(t), D^\beta C^T T_{m\gamma}(t))|_{t=1}\right) - (\bar{Y}_1 - Y_0)t - Y_0 = 0 \quad (24)$$

$$C^T T_{m\gamma}(t) - 1 - t + t^{\frac{1}{2}} C^T \left(G_{\frac{1}{2}} * T_{m\gamma}(t) - \frac{t^{\frac{1}{2}}}{\Gamma(\frac{3}{2})} \ - \frac{t^{\frac{3}{2}}}{\Gamma(\frac{5}{2})}\right) + t^2 C^T (G_2 * T_{m\gamma}(t)) = \frac{t^2}{2} + \frac{t^3}{6} \quad (28)$$

TABLE I
COMPARISON OF NUMBERICAL RESULTS FOR $\alpha = 0.75$

t_i	BPM [22], $N=8$	Proposed method, $m=8$	BPM [22], $N=11$	Proposed method, $m=11$	IABMM [21]	EHPM [21]	MHPM [20]
0	0	0	0	0	0	0	0
0.2	0.30996891	0.30997496	0.30997552	0.30997528	0.3117	0.3214	0.3138
0.4	0.48162749	0.48163161	0.48163184	0.48163169	0.4855	0.5077	0.4929
0.6	0.59777979	0.59778262	0.59778277	0.59778267	0.6045	0.6259	0.5974
0.8	0.67884745	0.67884945	0.67884957	0.67884949	0.6880	0.7028	0.6604
1	0.73684181	0.73683663	0.73683686	0.73683667	0.7478	0.7542	0.7183

TABLE II
COMPARISON OF NUMBERICAL RESULTS FOR $\alpha = 0.9$

t_i	BPM [22], $N=8$	Proposed method, $m=8$	BPM [22], $N=11$	Proposed method, $m=11$	IABMM [21]	EHPM [21]	MHPM [20]
0	0	0	0	0	0	0	0
0.2	0.23878798	0.23878894	0.23878915	0.23878913	0.2393	0.2647	0.2391
0.4	0.42258214	0.42258305	0.42258309	0.42258308	0.4234	0.4591	0.4229
0.6	0.56617082	0.56617156	0.56617157	0.56617156	0.5679	0.6031	0.5653
0.8	0.67462642	0.67462706	0.67462700	0.67462699	0.6774	0.7068	0.6740
1	0.75460256	0.75458885	0.75458901	0.75458880	0.7584	0.7806	0.7569

TABLE III
COMPARISON OF ABSOLUTE ERROR FOR $\alpha = 1$

t_i	BPM [22], $N=5$	Proposed method, $m=5$	BPM [22], $N=11$	Proposed method, $m=11$	Proposed method, $m=20$	MHPM [20]
0	0	0	0	0	0	0
0.2	5.1734E−05	1.1440E−06	2.6847E−10	4.3055E−11	5.5511E−17	3.2022E−7
0.4	2.5969E−05	8.4839E−08	2.5057E−10	1.2536E−11	1.1102E−16	4.9622E−6
0.6	4.0657E−05	1.0711E−06	2.1577E−10	1.4442E−11	0	0.0001925
0.8	1.2390E−05	1.0920E−06	2.9392E−10	5.7991E−11	1.1102E−16	0.0023307
1	7.5141E−04	5.8350E−06	6.8444E−08	1.8625E−10	1.1102E−16	0.0155622

The exact solution of this problem for $\alpha = 1$ is

$$y(t) = \frac{e^{2t}-1}{e^{2t}+1}.$$

To compare the proposed method with [20]−[22], we solve (30) for $\alpha = 0.75$, $\alpha = 0.9$, and $\alpha = 1$. Now, we solve (30), with $m = 3$ and $\gamma = \alpha = 0.75$.

Let

$$y(t) \cong C^T T_{m\gamma}(t) \tag{31}$$

where

$$C^T = [c_0,\ c_1,\ c_2,\ c_3]$$

and

$$T_{m\gamma}(t) = [1,\ t^{0.75},\ t^{1.5},\ t^{2.25}]^T.$$

By using (22), (30), and (31), we get

$$C^T T_{m\gamma}(t) + t^\alpha\ C^T (S_\alpha * (T_{m\gamma}(t) T_{m\gamma}^T(t))C - \frac{t^\alpha}{\Gamma(\alpha+1)} = 0 \tag{32}$$

where

$$T_{m\gamma}(t).T_{m\gamma}^T(t) = \begin{bmatrix} 1 & t^{0.75} & t^{1.5} & t^{2.25} \\ t^{0.75} & t^{1.5} & t^{2.25} & t^3 \\ t^{1.5} & t^{2.25} & t^3 & t^{3.75} \\ t^{2.25} & t^3 & t^{3.75} & t^{4.5} \end{bmatrix}$$

and

$$S_\alpha(t) = \begin{bmatrix} 1.08807 & 0.691367 & 0.521462 & 0.424876 \\ 0.691367 & 0.521462 & 0.424876 & 0.361746 \\ 0.521462 & 0.424876 & 0.361746 & 0.316877 \\ 0.424876 & 0.361746 & 0.316877 & 0.283147 \end{bmatrix}.$$

By collocating (32) at the nodes given in (23), and solving the resulting equations we get,

$$c_0 = 0,\ c_1 = 1.03094,\ c_2 = -0.165321,\ \text{and}\ c_3 = -0.1044.$$

Then, by using (31), we have

$$y(t) = 1.03094\ t^{0.75} - 0.165321\ t^{1.5} - 0.1044\ t^{2.25}.$$

In Tables I and II, we compare our results with the solutions of the modified homotopy perturbation method (MHPM) in [20], the improved Adams-Bashforth-Moulton method (IABMM) in [21], the enhanced homotopy perturbation method (EHPM) in [21] and with the Bernstein polynomials method (BPM) in [22] for $\gamma = \alpha = 0.75$ and $\gamma = \alpha = 0.9$ for different values of m. In Table III, we compare the absolute error of our method for $\gamma = \alpha = 1$ with MHPM [20] and BPM [22], for different values of m. In Tables I−III, N represents the degree of the Bernstein polynomial used in [22]. Also, Fig. 1 shows the approximate solutions obtained for different values of α using the proposed method with $m = 5$. From these results, it is seen that the approximate solutions converge to the exact solution for α=1. In addition, the absolute difference between the exact and approximate solutions for $\alpha = 1$ with $m = 5$ is plotted in Fig. 2. The absolute difference between the exact and approximate solutions for $k = 1$ and $M = 5$ or $\hat{m} = 2^{k-1}M = 5$ and $\alpha = 1$ by Bernoulli wavelets method is plotted in [25]. Here, k and M are the order of wavelets and Bernoulli polynomials respectively. From our figures and those in [25], we can conclude that the result obtained by the proposed method has less error compared to Bernoulli wavelets method.

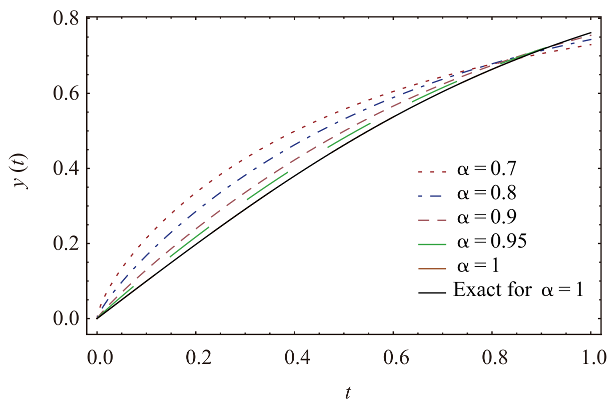

Fig. 1. Comparison of the computed solutions for different values of α with exact solution for $\gamma = \alpha = 1$ for Example 2 with $m = 5$.

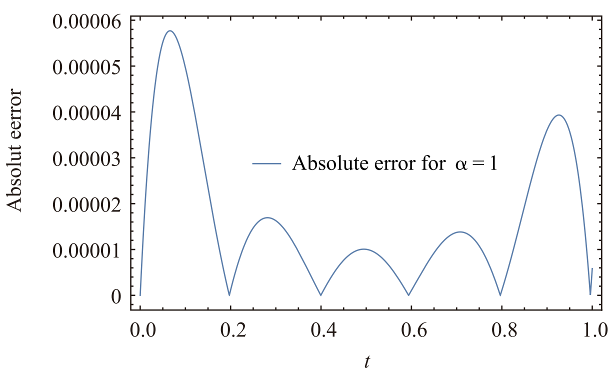

Fig. 2. The absolute error for $\gamma = \alpha = 1$ for Example 2 with $m = 5$.

C. Example 3

Consider the following Riccati fractional differential equation given in [22].

$$D^{\alpha}y(t) = 2\,y(t) - y^2(t) + 1, \quad y(0) = 0; \quad 0 < \alpha \leq 1. \tag{33}$$

To solve this problem by using the proposed method, we let

$$y(t) \cong C^T T_{m\gamma}(t) \tag{34}$$

where C^T and $T_{m\gamma}(t)$ are given in (5) and (7) respectively. Using (22), (33), and (34), we have

$$\begin{aligned} &C^T T_{m\gamma}(t) - 2t^{\alpha}C^T(G_\alpha * T_{m\gamma}(t)) \\ &\quad + t^{\alpha}C^T(S_\alpha * (T_{m\gamma}(t)T_{m\gamma}^T(t)))C - \tfrac{t^\alpha}{\Gamma(\alpha+1)} = 0. \end{aligned} \tag{35}$$

Now, by collocating (35) at the nodes given in (23), we get $m + 1$ nonlinear algebraic equations which can be solved for the unknown vector C^T using Newton's iterative method. It is well known that the initial guesses for Newton's iterative method are very important. For this problem, by using $y(0) = 0$, and (34), we choose the initial guesses such that $C^T T_{m\gamma}(0) = 0$. The exact solution of this problem for α = 1 is

$$y(t) = 1 + \sqrt{2}\tanh\left(\sqrt{2}t + \frac{1}{2}\ln(\frac{\sqrt{2}-1}{\sqrt{2}+1})\right).$$

Table IV shows the comparison of our numerical results with [20]−[22] for $\gamma = \alpha = 0.9$. In Table V, we compare the absolute error of our numerical method with [20] and [22] for α=1. Also, Fig. 3 shows the approximate solutions obtained for different values of α using the proposed method with $m = 5$. From these results, it is seen that the approximate solutions converge to the exact solution for $\alpha = 1$. From Table V it is seen that our results with $m = 18$ has less error than the results in the table given in [25], with $k = 2$ and $M = 10$ or $\hat{m} = 2^{k-1}M = 20$ using Bernoulli wavelets method.

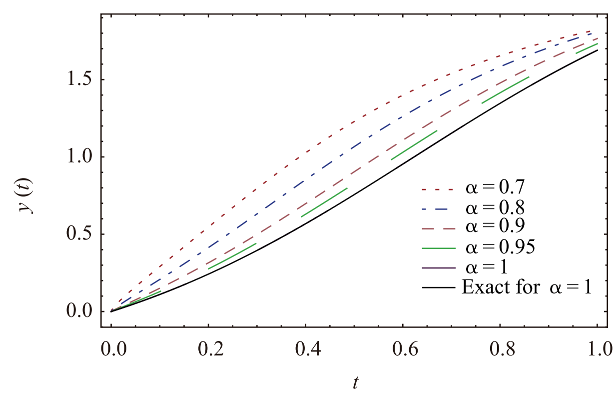

Fig. 3. Comparison of the computed solutions for different values of α with exact solution for $\alpha = 1$ for Example 3 with $m = 5$.

D. Example 4

Consider the FDE [24]

$$D^{\alpha}y(t) + y(t) = 0, \quad 0 < \alpha \leq 2 \tag{36}$$

with $y(0) = 1$ and $y'(0) = 0$. The condition $y'(0) = 0$ is for $1 < \alpha \leq 2$ only.

The exact solution of this problem is $y(t) = E_a(-t^{\alpha})$ [24], where

$$E_a(z) = \sum_{k=0}^{\infty}\frac{z^k}{\Gamma(\alpha k + 1)}$$

is the Mittag-Leffler function with order α. To solve this problem by using the proposed method, similar to (34) in Example 3 we let

$$y(t) \cong C^T T_{m\gamma}(t). \tag{37}$$

Using (22), (36), and (37), we have

$$C^T T_{m\gamma}(t) - 1 + t^{\alpha}C^T(G_\alpha * T_{m\gamma}(t)) = 0.$$

TABLE IV
COMPARISON OF NUMBERICAL RESULTS FOR $\alpha = 0.9$

t_i	BPM [22], $N = 8$	Proposed method, $m = 8$	BPM [22], $N = 11$	Proposed method, $m = 11$	IABMM [21]	EHPM [21]	MHPM [20]
0	0	0	0	0	0	0	0
0.2	0.31488815	0.31485423	0.31486902	0.31486367	-	-	-
0.4	0.69756771	0.69751826	0.69754441	0.69753816	-	-	-
0.5	0.90369502	0.90364539	0.90367312	0.90366680	0.8621	1.4614	0.9010
0.6	1.10789047	1.10783899	1.10786695	1.10786083	-	-	-
0.8	1.47772823	1.47768008	1.47770748	1.47770236	-	-	-
1	1.76452008	1.76525852	1.76529044	1.76527469	1.7356	2.0697	1.8720

TABLE V
COMPARISON OF ABSOLUTE ERROR FOR $\alpha = 1$

t_i	BPM [22], $N = 5$	Proposed method, $m = 5$	BPM [22], $N = 11$	Proposed method, $m = 11$	Proposed method, $m = 18$	MHPM [20]
0	0	0	0	0	0	0
0.2	6.9332E−04	1.7402E−04	2.3521E−07	5.7111E−08	5.2301E−12	0.00001
0.4	6.2509E−04	1.9080E−04	3.0542E−07	6.3894E−08	6.7869E−12	0.00030
0.6	9.1370E−04	2.1689E−04	3.3836E−07	7.0059E−08	7.4832E−12	0.00469
0.8	3.9346E−04	2.0848E−04	3.4201E−07	7.1896E−08	7.0779E−12	0.01887
1	7.1367E−03	1.3840E−04	1.1799E−05	3.1903E−08	5.9701E−12	0.03431

TABLE VI
COMPARISON OF ABSOLUTE ERROR WITH [24] FOR $\alpha = 1.5$

t_i	LWM [24], $\hat{M} = 384$	Proposed method, $m = 3$	Proposed method, $m = 4$	Proposed method, $m = 5$	Proposed method, $m = 10$
0.1	4.207E−7	3.06933E−6	3.60303E−8	2.8731E−10	2.5259E−17
0.2	1.944E−7	4.52543E−6	2.57570E−8	1.17022E−11	2.3353E−16
0.3	5.705E−8	1.45914E−6	3.43268E−8	3.89751E−10	7.0728E−17
0.4	4.605E−8	4.53425E−6	6.35744E−8	3.84075E−12	3.6902E−18
0.5	1.282E−7	8.96162E−6	1.91067E−10	6.05008E−10	7.2132E−17
0.6	1.944E−7	6.66709E−6	1.10701E−7	2.24834E−11	2.6174E−16
0.7	2.471E−7	5.03679E−6	1.02038E−7	1.58912E−9	6.2367E−17
0.8	2.878E−7	2.24058E−5	1.90389E−7	2.93859E−11	3.0854E−16
0.9	3.176E−7	3.05511E−5	5.93256E−7	7.70141E−9	2.8515E−16

TABLE VII
ABSOLUTE ERROR OF OUR METHOD FOR DIFFERENT VALUES OF α WITH $m = 10$

t_i	$\alpha = 1.1$	$\alpha = 1.3$	$\alpha = 1.5$	$\alpha = 1.6$	$\alpha = 1.8$	$\alpha = 2$
0.1	1.95877E−16	4.86487E−17	2.52589E−17	6.61786E−17	8.17143E−18	5.5437E−17
0.2	1.48822E−16	2.00823E−16	2.33527E−16	2.28488E−16	1.70503E−16	1.02528E−18
0.3	2.9433E−16	1.60699E−17	7.07283E−17	1.87274E−17	1.90848E−17	2.66293E−17
0.4	4.38831E−17	3.31082E−17	3.69019E−18	1.86397E−17	9.881E−17	7.59506E−17
0.5	2.29268E−16	1.72008E−16	7.21322E−17	6.88831E−17	1.32945E−16	4.27994E−17
0.6	4.46312E−16	1.77538E−18	2.61743E−16	3.10642E−17	1.78043E−17	3.43499E−17
0.7	4.04245E−16	1.85026E−16	6.23670E−17	9.06418E−17	1.30585E−16	1.05295E−16
0.8	4.16117E−16	1.31649E−16	3.08539E−16	2.75084E−16	7.1246E−17	1.84848E−17
0.9	5.21935E−16	1.84856E−17	2.85145E−16	1.22344E−16	2.10206E−17	6.86984E−17
1	9.45424E−17	1.87242E−16	1.70220E−17	8.38901E−18	1.07569E−16	5.90071E−17

By collocating at the points given in (23) we get $m+1$ algebraic equations, which can be solved for the unknown vector C^T. Table VI shows the absolute error obtained for different values of t and for $\alpha = 1.5$ by using the proposed method with different values of m and the Legendre wavelets method (LWM) in [24], with $k = 8$ and $M_1 = 3$ or $\hat{M} = 2^{k-1}M_1 = 384$. Here, M_1 shows the order of Legendre polynomials. In Table VII, the absolute error obtained using the proposed method for different values of α with $m = 10$ is given.

TABLE IX
ABSOLUTE ERROR FOR DIFFERENT α WITH $M = 3$

t_i	$\alpha = 1.1$	$\alpha = 1.3$	$\alpha = 1.5$	$\alpha = 1.6$	$\alpha = 1.8$	$\alpha = 2$
0.1	1.33357E−17	5.01444E−18	2.71728E−18	7.76899E−18	5.36765E−18	8.84514E−19
0.2	1.04083E−17	6.07153E−18	1.22515E−17	1.85399E−17	1.55041E−17	2.19551E−18
0.3	6.93889E−18	0	3.1225E−17	2.38524E−17	2.32019E−17	2.1684E−19
0.4	2.77556E−17	1.04083E−17	5.89806E−17	1.9082E−17	2.34188E−17	1.04083E−17
0.5	5.55112E−17	1.38778E−17	9.71445E−17	0	1.04083E−17	3.1225E−17
0.6	5.55112E−17	0	1.38778E−16	2.77556E−17	1.38778E−17	6.93889E−17
0.7	5.55112E−17	0	1.38778E−16	5.55112E−17	2.77556E−17	9.71445E−17
0.8	0	5.55112E−17	1.66533E−16	5.55112E−17	5.55112E−17	1.66533E−16
0.9	1.11022E−16	1.11022E−16	1.11022E−16	0	1.11022E−16	1.11022E−16
1	3.33067E−16	3.33067E−16	0	0	3.33067E−16	0

E. Example 5

Consider the following FDE with boundary value conditions [24]

$$D^{\alpha}y(t) + ay^{n}(t) = g(t), \quad y(0) = 0; \quad y(1) = 1 \tag{38}$$

where $1 < \alpha \leq 2$, $a = \exp(-2\pi)$ and $n = 2$. For $\alpha = 1.5$ and $g(t) = 105\sqrt{\pi}t^2/32 + \exp(-2\pi)t^7$, the exact solution is given by

$$y(t) = t^{\frac{7}{2}}.$$

Using (20) and (38), we have

$$\begin{aligned} y(t) = I^{\alpha}g(t) - aI^{\alpha}y^2(t) - t(I^{\alpha}g(t))|_{t=1} \\ - a\ t(I^{\alpha}y^2(t))|_{t=1} + t. \end{aligned} \tag{39}$$

Similar to (34) in Example 3, we let

$$y(t) \cong C^T T_{m\gamma}(t). \tag{40}$$

Using (39) and (40), we get

$$\begin{aligned} &C^T T_{m\gamma}(t) - \frac{105\sqrt{\pi}\Gamma(3)}{32\Gamma(3+\alpha)}t^{2+\alpha} - \frac{\exp(-2\pi)\Gamma(8)}{\Gamma(8+\alpha)}t^{7+\alpha} \\ &\quad + \exp(-2\pi)t^{\alpha}C^T(S_{\alpha} * T_{m\gamma}(t)\ T^T_{m\gamma}(t))C \\ &\quad +\ t\frac{105\sqrt{\pi}\Gamma(3)}{32\Gamma(3+\alpha)} +\ t\ \frac{\exp(-2\pi)\Gamma(8)}{\Gamma(8+\alpha)} \\ &\quad +\ \exp(-2\pi)tC^T(S_{\alpha} * T_{m\gamma}(1)\ T^T_{m\gamma}(1))C -\ t = 0. \end{aligned}$$

By collocating at the points given in (23) we get $m+1$ algebraic equations, which can be solved for the unknown vector C^T. Table VIII shows the absolute error obtained for different values of t and for $m = 10$ by using the proposed method for $\alpha = 1.5$ with $\gamma = \alpha$ and $\gamma = \alpha - \lfloor\alpha\rfloor$, together with the absolute error obtained by the Legendre wavelets method in [24], with $k = 3$ and $M_1 = 3$ or $\hat{M} = 2^{k-1}M_1 = 12$. Here, M_1 shows the order of Legendre polynomials.

More generally, the exact solution for (38) with

$$g(t) = \frac{\Gamma(3\alpha+1)}{\Gamma(2\alpha+1)}t^{2\alpha} + \exp(-2\pi)t^{6\alpha}$$

and keeping the other coefficients the same is

$$y(t) = t^{3\alpha}.$$

In Table IX, we show the absolute error of our numerical results for different values of α with $m = 3$.

TABLE VIII
COMPARISON OF ABSOLUT ERROR FOR $\alpha = 1.5$

t_i	LWM[24] $\hat{M} = 12$	Proposed method $m = 10$ $\gamma = \alpha$	Proposed method $m = 10$ $\gamma = \alpha - \lfloor\alpha\rfloor$
0.1	9.6996E−5	1.34431E−9	1.06794E−17
0.2	9.3927E−4	2.68845E−9	1.38778E−17
0.3	1.5087E−3	4.03315E−9	8.67362E−18
0.4	3.3989E−4	5.37645E−9	4.16334E−17
0.5	2.4163E−3	6.72324E−9	2.77556E−17
0.6	3.1023E−4	8.05974E−9	2.77556E−17
0.7	1.4799E−3	9.43278E−9	0
0.8	6.3407E−4	1.06306E−8	1.66533E−16
0.9	4.6701E−3	1.30547E−8	2.22045E−16

VIII. CONCLUSION

In the present work the fractional Taylor basis is used to solve FDEs. The integral operational matrix F_{α} and S_{α} have been derived. The error bounds are also included. The problem has been reduced to a problem of solving a system of algebraic equations. Illustrative examples are solved by using the proposed method to show that this approach can solve the problem effectively.

REFERENCES

[1] K. B. Oldham and J. Spanier, *The Fractional Calculus*. New York: Academic Press, 1974.

[2] K. S. Miller and B. Ross, *An Introduction to the Fractional calculus and Fractional Differential Equations*. New York: Wiley, 1993.

[3] J. T. Machado, V. Kiryakova, and F. Mainardi, “Recent history of fractional calculus,” *Commun. Nonlinear Sci. Numer. Simul.*, vol. 16, no. 3, pp. 1140−1153, Mar. 2011.

[4] R. L. Bagley and P. J. Torvik, “Fractional calculus in the transient analysis of viscoelastically damped structures,” *AIAA J.*, vol. 23, no. 6, pp. 918−925, Jun. 1985.

[5] R. T. Baillie, “Long memory processes and fractional integration in econometrics,” *J. Econometr.*, vol. 73, no. 1, pp. 5−59, Jul. 1996.

[6] F. Mainardi, “Fractional calculus: some basic problems in continuum and statistical mechanics,” *Fractals and Fractional Calculus in Continuum Mechanics*, A. Carpinteri and F. Mainardi, Eds. Vienna: Springer-Verlag, 1997, pp. 291−348.

[7] Y. A. Rossikhin and M. V. Shitikova, "Applications of fractional calculus to dynamic problems of linear and nonlinear hereditary mechanics of solids," *Appl. Mech. Rev.*, vol. 50, no. 1, pp. 15−67, Jan. 1997.

[8] K. B. Oldham, "Fractional differential equations in electrochemistry," *Adv. Eng. Softw.*, vol. 41, no. 1, pp. 9−12, Jan. 2010.

[9] V. S. Ertürk, Z. M. Odibat, and S. Momani, "An approximate solution of a fractional order differential equation model of human T-cell lymphotropic virus I (HTLV-I) infection of $CD4^+$ T-cells," *Comput. Math. Appl.*, vol. 62, no. 3, pp. 996−1002, Aug. 2011.

[10] S. A. El-Wakil, E. M. Abulwafa, E. K. El-Shewy, and A. A. Mahmoud, "Ion-acoustic waves in unmagnetized collisionless weakly relativistic plasma of warm-ion and isothermal-electron using time-fractional KdV equation," *Adv. Space Res.*, vol. 49, no. 12, pp. 1721−1727, Jun. 2012.

[11] L. Gaul, P. Klein, and S. Kemple, "Damping description involving fractional operators," *Mech. Syst. Signal Proc.*, vol. 5, no. 2, pp. 81−88, Mar. 1991.

[12] I. Podlubny, *Fractional Differential Equations: an Introduction to Fractional Derivatives, Fractional Differential Equations, to Methods of their Solution and Some of their Applications*. New York: Academic Press, 1998.

[13] S. Momani and K. Al-Khaled, "Numerical solutions for systems of fractional differential equations by the decomposition method," *Appl. Math. Comput.*, vol. 162, pp. 1351−1365, Mar. 2005.

[14] Z. M. Odibat and S. Momani, "Application of variational iteration method to nonlinear differential equations of fractional order," *Int. J. Nonlinear Sci. Numer. Simul.*, vol. 7, no. 1, pp. 27−34, Mar. 2006.

[15] Z. M. Odibat and N. T. Shawagfeh, "Generalized Taylor's formula," *Appl. Math. Comput.*, vol. 186, no. 1, pp. 286−293, Mar. 2007.

[16] J. S. Duan, T. Chaolu, and R. Rach, "Solutions of the initial value problem for nonlinear fractional ordinary differential equations by the Rachdomianeyers modified decomposition method," *Appl. Math. Comput.*, vol. 218, no. 17, pp. 8370−8392, May 2012.

[17] A. Arikoglu and I. Ozkol, "Solution of fractional integro-differential equations by using fractional differential transform method," *Chaos Solit. Fract.*, vol. 40, no. 2, pp. 521−529, Apr. 2009.

[18] I. Hashim, O. Abdulaziz, and S. Momani, "Homotopy analysis method for fractional IVPs," *Commun. Nonlinear Sci. Numer. Simul.*, vol. 14, no. 3, pp. 674−684, Mar. 2009.

[19] S. Kazem, S. Abbasbandy, and S. Kumar, "Fractional-order Legendre functions for solving fractional-order differential equations," *Appl. Math. Model.*, vol. 37, no. 7, pp. 5498−5510, Apr. 2013.

[20] Z. Odibat and S. Momani, "Modified homotopy perturbation method: application to quadratic Riccati differential equation of fractional order," *Chaos Solit. Fract.*, vol. 36, no. 1, pp. 167−174, Apr. 2008.

[21] S. H. Hosseinnia, A. Ranjbar, and S. Momani, "Using an enhanced homotopy perturbation method in fractional differential equations via deforming the linear part," *Comput. Math. Appl.*, vol. 56, no. 12, pp. 3138−3149, Dec. 2008.

[22] S. Yüzbaşi, "Numerical solutions of fractional Riccati type differential equations by means of the Bernstein polynomials," *Appl. Math. Comput.*, vol. 219, no. 11, pp. 6328−6343, Feb. 2013.

[23] Y. L. Li, "Solving a nonlinear fractional differential equation using Chebyshev wavelets," *Commun. Nonlinear Sci. Numer. Simul.*, vol. 15, no. 9, pp. 2284−2292, Sep. 2010.

[24] M. ur Rehman and R. Ali Khan, "The Legendre wavelet method for solving fractional differential equations," *Commun. Nonlinear Sci. Numer. Simul.*, vol. 16, no. 11, pp. 4163−4173, Nov. 2011.

[25] E. Keshavarz, Y. Ordokhani, and M. Razzaghi, "Bernoulli wavelet operational matrix of fractional order integration and its applications in solving the fractional order differential equations," *Appl. Math. Model.*, vol. 38, no. 24, pp. 6038−6051, Dec. 2014.

[26] A. A. Kilbas, H. M. Srivastava, and J. J. Trujillo, *Theory and Applications of Fractional Differential Equations*. Amsterdam: Elsevier, 2006.

[27] K. Diethelm, N. J. Ford, and A. D. Freed, "A predictor-corrector approach for the numerical solution of fractional differential equations," *Nonlinear Dyn.*, vol. 29, no. 1−4, pp. 3−22, Jul. 2002.

[28] P. Kumar and O. P. Agrawal, "An approximate method for numerical solution of fractional differential equations," *Signal Proc. -Fract. Calcul. Appl. Signal. Syst.*, vol. 86, no. 10, pp. 2602−2610, Oct. 2006.

[29] X. H. Ma and C. M. Huang, "Numerical solution of fractional integro-differential equations by a hybrid collocation method," *Appl. Math. Comput.*, vol. 219, no. 12, pp. 6750−6760, Feb. 2013.

Vidhya Saraswathy Krishnasamy received her undergraduate and master's degree in mathematics from Sri G.V.G. Vishalakshi College for Women, Udumalpet, India. She graduated from Mississippi State University (MSU), USA with her Ph.D. degree in August, 2016.

She has diverse research interests, which include fractional calculus, orthogonal functions and its applications to dynamical systems, graph theory, number theory, cryptography and its applications.

Somayeh Mashayekhi graduated from Mississippi State University (MSU), USA, in 2015. She received her first Ph.D. degree from Alzahra University in 2013, and her second Ph.D. degree from MSU in 2015. She is, currently, a post doctoral research associate in computational science and engineering, Department of Mathematics, Florida State University.

Her research interests include optimal control, delay system, fractional calculus, orthogonal functions and its applications to dynamical systems.

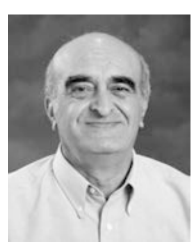

Mohsen Razzaghi received his undergraduate degree in mathematics from the University of Sussex in England. He went to Canada and received his master's degree in applied mathematics from the University of Waterloo. He returned to the University of Sussex and obtained his Ph.D.. After that, he has taught and served in several administrative positions in Iran and in the USA. Since 1986, he has been at the Department of Mathematics and Statistics at Mississippi State University, where he is currently a professor and the department head. During the academic years 2011-2012 and 2015-2016, he was a Fulbright Scholar at the Department of Mathematics and Computer Science at the Technical University of Civil Engineering in Bucharest, Romania.

His area of research centers on optimal control, orthogonal functions and wavelets in dynamical system, and fractional calculus. He has over 150 refereed journal publications in mathematics, mathematical physics, and engineering. Corresponding author of this paper.

Artificial Bee Colony Algorithm-based Parameter Estimation of Fractional-order Chaotic System with Time Delay

Wenjuan Gu, Yongguang Yu, and Wei Hu

Abstract—**It is an important issue to estimate parameters of fractional-order chaotic systems in nonlinear science, which has received increasing interest in recent years. In this paper, time delay and fractional order as well as system's parameters are concerned by treating the time delay and fractional order as additional parameters. The parameter estimation is converted into a multi-dimensional optimization problem. A new scheme based on artificial bee colony (ABC) algorithm is proposed to solve the optimization problem. Numerical experiments are performed on two typical time-delay fractional-order chaotic systems to verify the effectiveness of the proposed method.**

Index Terms—**Artificial bee colony (ABC) algorithm, fractional-order chaotic system, parameters estimation, time delay.**

I. INTRODUCTION

FRACTIONAL calculus is a branch of mathematics which deals with differentiation and integration of arbitrary orders and is as old as calculus [1]. Although the classical calculus has been playing a dominant role in explaining and modeling dynamical processes observed in real world, the fractional calculus has gradually attracted the attention of scientists during the last decades because of its capability in describing important phenomena of non-local dynamics and memory effects. It has been introduced into various engineering and science domains, such as image processing [2], robotics [3], diffusion [4], mechanics [5], and others [1].

Time delay is commonly encountered in real systems, such as chemistry, climatology, biology, economy and crypto systems [6]. Time-delay differential equation is a differential equation in which the derivative of the function at any time depends on the solution at previous time. Introduction of time delay in the model can enrich its dynamics and provide a precise description of real life phenomenon [7]. Particularly, since Mackey and Glass [8] firstly detected chaos in time-delay systems, control and synchronization of time-delay chaotic systems have obtained increasing attention [9], [10], which can produce more complex and adequate dynamic behavior than those free of time delays.

Recently, chaotic behavior has been found in time-delay fractional-order systems, such as fractional-order financial system [11], fractional-order Chen system [12], fractional-order Liu system [13] and so on. Many control methods are valid for the fractional-order chaotic systems with known parameters and time-delays [14]−[16]. However, in some applications such as secure communications and chaos synchronization, the chaotic system is partially known. It means that the form of differential equation is known, but some or all of the time delays, fractional orders and system's parameters are unknown. Therefore, estimating the unknown parameters of time-delay fractional-order chaotic system is of vital significance in controlling and utilizing chaos.

Up to now, for the parameter estimation of chaotic systems, considerable methods have been put forward, such as the least-squares method [17], the symbolic time series analysis-based method [18], the adaptive control method [19]. Besides, by transforming the parameter estimation in dynamical systems as a multi-dimensional optimization problem, many evolutionary algorithms have been proposed to deal with the problem, such as differential evolution (DE) [20], particle swarm optimization (PSO) [21], cuckoo search (CS) [22], biogeography-based optimization (BBO) [23]. However, most of the works mentioned so far are involved mainly with integer-order chaotic systems or fractional-order chaotic systems without time delays. That is, very few have addressed the estimation problem on fractional-order chaotic systems with time delay.

Artificial bee colony (ABC) algorithm is a relatively new optimization technique which is developed by Karaboga in 2005 based on simulating the foraging behavior of honey-bee swarm. It has been shown to be competitive to other population-based algorithms for global numerical optimization problem with the advantage of employing fewer control parameters [24]−[26]. For example, apart from the maximum iteration number and population size, a standard GA has three more control parameters (crossover rate, mutation rate, generation gap) [27], a standard DE has at least two control parameters (crossover rate, scaling factor) [28] and a basic PSO has three control parameters (cognitive and social factors, inertia weight) [29]. Besides, limit values for the velocities $v_{\max}$ have a significant effect on the performance of PSO. The ABC algorithm has only one control parameter (limit)

Manuscript received September 6, 2015; accepted January 13, 2016. This work was supported by National Natural Science Foundation of China (11371049). Recommended by Associate Editor Dingyü Xue.

Citation: W. J. Gu, Y. G. Yu, and W. Hu, "Artificial bee colony algorithm-based parameter estimation of fractional-order chaotic system with time delay," *IEEE/CAA Journal of Automatica Sinica*, vol. 4, no. 1, pp. 107−113, Jan. 2017.

W. J. Gu is with the School of Economics and Management, Beijing Jiaotong University, Beijing 100044, China (e-mail: guwj0423@163.com).

Y. G. Yu and W. Hu are with the School of Science, Beijing Jiaotong University, Beijing 100044, China (e-mail: ygyu@bjtu.edu.cn; 13121527@bjtu.edu.cn).

Digital Object Identifier 10.1109/JAS.2017.7510340

apart from colony size and maximum cycle number. Although it uses less control parameters, the performance of ABC algorithm is better than or similar to that of these algorithms and it can be efficiently used for solving multimodal and multidimensional optimization problems.

Based on the above discussion, in this paper, a scheme based on artificial bee colony algorithm is firstly proposed to estimate the parameters of unknown time-delay fractional-order chaotic system. Numerical simulations are performed to estimate two well-known fractional-order chaotic systems with time delay. The simulation results demonstrate the good performance of the ABC algorithm, and thus the ABC algorithm proves to be a promising candidate for parameter estimation of time-delay fractional-order chaotic systems.

The rest of the paper is organized as follows. In Section II, the Caputo fractional-order derivative is introduced. In Section III, the problem of parameter estimation for time-delay fractional-order chaotic system is formulated from the view of optimization. In Section IV, a parameter estimation scheme is proposed after briefly introducing the ABC algorithm. Numerical simulations and conclusions are given in Sections V and VI.

II. Caputo Fractional-order Derivative

In general, three best-known definitions of fractional-order derivatives are widely used: Grunwald-Letnikov, Riemann-Liouville and Caputo definitions [1]. In particular, the main advantage of Caputo fractional-order derivative is that it owns same initial conditions with integer-order derivatives, which have well-understood features of physical situations and more applicable to real world problems. Thus, the Caputo fractional-order derivative is employed in this paper.

Definition 1 (Caputo fractional-order derivative): The Caputo fractional-order derivative of order $\alpha > 0$ for a function $f(t) \in C^{n+1}([t_0, +\infty), R)$ is defined as

$$ {}_{t_0}D_t^{\alpha} f(t) = \frac{1}{\Gamma(n-\alpha)} \int_{t_0}^{t} \frac{f^{(n)}(\tau)}{(t-\tau)^{\alpha+1-n}} d\tau \tag{1}$$

where $\Gamma(\cdot)$ denotes the gamma function and n is a positive integer such that $n-1 < \alpha \leq n$.

Property 1: When C is any constant, ${}_{t_0}D_t^{\alpha} C = 0$ holds.

Property 2: For constants μ and ν, the linearity of Caputo fractional-order derivative is described by

$$ {}_{t_0}D_t^{\alpha}(\mu f(t) + \nu g(t)) = \mu \ {}_{t_0}D_t^{\alpha} f(t) + \nu \ {}_{t_0}D_t^{\alpha} g(t).$$

III. Problem Formulation

The problem formulation of parameter estimation for time-delay fractional-order chaotic systems is presented in this section.

Let us consider the following time-delay fractional-order chaotic system described by delay differential equation

$$ {}_0D_t^{\alpha} Y(t) = f(Y(t), Y(t-\tau), Y_0, \theta) \tag{2}$$

where $Y(t) = (y_1(t), y_2(t), \ldots, y_n(t))^T \in \mathbb{R}^n$ denotes the state vector of system (2), $Y_0 = Y(0)$ denotes the initial value for $t \leq \tau$, $\theta = (\theta_1, \theta_2, \ldots, \theta_m)^T$ denotes the set of system's parameters, $\alpha = (\alpha_1, \alpha_2, \ldots, \alpha_n)$ $(0 < \alpha_i < 1$, $i = 1, 2, \ldots, n)$ is the fractional derivative orders. $f(Y(t), Y(t-\tau), Y_0, \theta) = (f_1(Y(t), Y(t-\tau), Y_0, \theta)$, $f_2(Y(t), Y(t-\tau), Y_0, \theta)$, $\ldots$, $f_n(Y(t), Y(t-\tau), Y_0, \theta))^T$. In this paper, the delay time τ and fractional order α are treated as additional parameters to be estimated.

Suppose the structure of system (2) is known, then the corresponding estimated system can be written as

$$ {}_0D_t^{\tilde{\alpha}} \tilde{Y}(t) = f(\tilde{Y}(t), \tilde{Y}(t-\tilde{\tau}), Y_0, \tilde{\theta}) \tag{3}$$

where $\tilde{Y}(t) = (\tilde{y}_1(t), \tilde{y}_2(t), \ldots, \tilde{y}_n(t))^T \in \mathbb{R}^n$ is the state vector of the estimated system (3), $\tilde{\theta} = (\tilde{\theta}_1, \tilde{\theta}_2, \ldots, \tilde{\theta}_m)^T$ is a set of estimated systematic parameters, $\tilde{\alpha} = (\tilde{\alpha}_1, \tilde{\alpha}_2, \ldots, \tilde{\alpha}_n)^T$ is the estimated fractional orders, and $\tilde{\tau}$ is the estimated time delay. Besides, systems (2) and (3) have the same initial conditions Y_0.

Based on the measurable state vector $Y(t) = (y_1(t), y_2(t), \ldots, y_n(t))^T \in \mathbb{R}^n$, we define the following objective function or fitness function

$$\begin{aligned} J(\tilde{\alpha}, \tilde{\theta}, \tilde{\tau}) &= \arg \min_{(\tilde{\alpha}, \tilde{\theta}, \tilde{\tau}) \in \Omega} F \\ &= \arg \min_{(\tilde{\alpha}, \tilde{\theta}, \tilde{\tau}) \in \Omega} \sum_{k=1}^{N} \|Y_k - \tilde{Y}_k\|_2 \end{aligned} \tag{4}$$

where $k = 1, 2, \ldots, N$ is the sampling time point and N denotes the length of data used for parameter estimation. Y_k and $\tilde{Y}_k$ respectively denote the state vector of the original system (2) and the estimated system (3) at time kh. h is the step size employed in the predictor-corrector approach for the numerical solutions of time-delay fractional-order differential equations [7]. $\|\cdot\|$ is Euclid norm. Ω is the searching area suited for parameters $\tilde{\alpha}$, $\tilde{\theta}$ and $\tilde{\tau}$.

Obviously, the parameter estimation for system (2) is multi-dimensional continuous optimization problem, where the decision vectors are $\tilde{\alpha}$, $\tilde{\theta}$ and $\tilde{\tau}$. The optimal solution can be achieved by searching suitable $\tilde{\alpha}$, $\tilde{\theta}$ and $\tilde{\tau}$ in the searching space Ω such that the objective function (4) is minimized. In this paper, a novel scheme based on artificial bee colony algorithm is proposed to solve this problem.

The time-delay fractional-order chaotic systems are not easy to estimate because of the unstable dynamics of the chaotic system and the complexity of the fractional-order nonlinear systems. Besides, due to multiple variables in the problem and multiple local search optima in the objective functions, it is easily trapped into local optimal solution and the computation amount is great. So it is not easy to search the global optimal solution effectively and accurately using the traditional general methods. Therefore, we aim to solve this problem by the effective artificial bee colony algorithm in this paper. The general principle of parameter estimation by ABC algorithm is shown in Fig. 1.

IV. A Novel Parameter Estimation Scheme

A. An Overview of the Original Artificial Bee Colony Algorithm

In the natural bee swarm, there are three kinds of honey bees to search foods generally, which include the employed bees, the onlookers and the scouts (both onlookers and the scouts are also called unemployed bees). The employed bees search the food around the food source in their memory. At the same time, they pass their food information to the onlookers. The onlookers tend to select good food sources from those found by the employed bees, then further search the foods around the selected food source. The scouts are transformed from a few employed bees, which abandon their food sources and search new ones. In short, the food search of bees is collectively performed by the employed bees, the onlookers and the scouts.

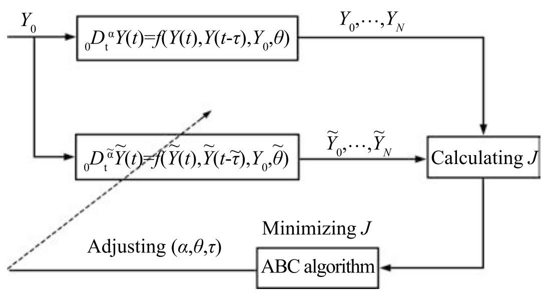

Fig. 1. The general principle of parameter estimation by ABC algorithm.

By simulating the foraging behaviors of honey bee swarm, Karaboga proposed a competitive optimization technique called artificial bee colony (ABC) algorithm [24]−[26]. In the original ABC algorithm, each cycle of the search consists of three steps: moving the employed and onlooker bees onto the food sources and calculating their nectar amounts; and determining the scout bees and directing them onto possible food sources. A food source position represents a possible solution to the problem to be optimized. The amount of nectar of a food source corresponds to the quality of the solution represented by that food source. Onlookers are placed on the food sources by using a probability based selection process. As the nectar amount of a food source increases, the probability value with which the food source is preferred by onlookers increases, too. Every bee colony has scouts that are the colony's explorers. The explorers do not have any guidance while looking for food. They are primarily concerned with finding any kind of food source. As a result of such behavior, the scouts are characterized by low search costs and a low average in food source quality. Occasionally, the scouts can accidentally discover rich, entirely unknown food sources. In the case of artificial bees, the artificial scouts could have the fast discovery of the group of feasible solutions as a task. In this work, one of the employed bees is selected and classified as the scout bee. The selection is controlled by a control parameter called limit. If a solution representing a food source is not improved by a predetermined number of trials, then the food source is abandoned by its employed bee and the employed bee is converted to a scout. The number of trials for releasing a food source is equal to the value of limit which is an important control parameter of ABC. In a robust search process, exploration and exploitation process must be carried out together. In the ABC algorithm, while onlookers and employed bees carry out the exploitation process in the search space, the scouts control the exploration process. Besides, the number of employed bees is equal to the number of onlooker bees which is also equal to the number of food sources. The detailed searching process is described as following:

At the first step, the ABC algorithm produces a randomly distributed initial population with the following equation:

$$x_{i,j} = x_{\min,j} + \mathrm{rand}(0,1)(x_{\max,j} - x_{\min,j}) \tag{5}$$

where $i = 1, 2, \ldots, SN$, $j = 1, 2, \ldots, D$. SN is the size of the solutions (food sources), D is the dimension of the optimization parameters. $x_{\min,j}$ and $x_{\max,j}$ are the lower and upper bounds for the dimension j, respectively.

After initialization, the population of the food sources (solutions) is subjected to repeated cycles. An employed bee makes a modification on the position in her memory depending on the local information as

$$v_{i,j} = x_{i,j} + \phi_{i,j}(x_{i,j} - x_{k,j}) \tag{6}$$

where $k = 1, 2, \ldots, SN$ and $j = 1, 2, \ldots, D$. k and j are randomly generated, and k must be different from i. $\phi_{i,j}$ is a random number in $[-1, 1]$. Then, the employed bee tests the nectar amount of the new source. If the nectar amount of the new one is higher than that of the previous one in her memory, the bee memorizes the new position and forgets the old one. Otherwise, she keeps the position of the previous one in her memory.

Then, an onlooker bee evaluates the nectar information taken from all employed bees and chooses a food source with a probability related to its nectar amount and calculated as

$$p_i = \frac{fit_i}{\sum\limits_{j=1}^{SN} fit_j} \tag{7}$$

where fit_i denotes the fitness value of solution X_i. As in the case of the employed bee, she produces a modification on the position in her memory and checks the nectar amount of the candidate source. Besides, the fitness value fit_i is defined as follows:

$$fit_i = \begin{cases} \dfrac{1}{1+f(X_i)}, & \text{if } f(X_i) \geq 0 \\ 1 + |f(X_i)|, & \text{if } f(X_i) < 0 \end{cases} \tag{8}$$

where $f(X_i)$ represents the objective function value of the decision vector X_i.

In ABC, if a position cannot be improved further through a predetermined number of cycles (called limit), then that food source is assumed to be abandoned. The corresponding employed bee becomes a scout bee and a new food source is generated with (5).

Some more details can be found from [24]−[26] and the main steps of the original ABC algorithm are described in Algorithm 1 (see the top of next page).

B. A Novel Parameter Estimation Scheme

As far as we are concerned, little research has been done for the parameter estimation of time-delay fractional-order chaotic systems. Thus, in this paper, the parameter estimation

Algorithm 1 The main procedure of the original artificial bee colony algorithm

Step 0: Predefine some parameters: SN (population size number), D (searching dimension), $LOWER$ (lower bound), $UPPER$ (upper bound), $limit$ (control parameter), MCN (maximum cycle number)
Step 1: The population initialization phase:
  Step 1.1: Randomly generate $0.5 \times SN$ points in the search space to form an initial population via (5).
  Step 1.2: Evaluate the objective function values of population.
  Step 1.3: cycle=1.
Step 2: The employed bees phase:
  For $i = 1$ **to** $0.5 \times SN$ **do**
    Step 2.1:
      Step 2.1.1: Generate a candidate solution V_i by **(6)**.
      Step 2.1.2: Evaluate $f(V_i)$.
    Step 2.2: If $f(V_i) < f(X_i)$, set $X_i = V_i$, otherwise, set $trial_i = trial_i + 1$.
  End For
Step 3: Calculating the probability values p_i by (7), set $t = 0$, $i = 1$.
Step 4: The onlooker bees phase:
  While $t \leq 0.5 \times$ SN, **do**
    Step 4.1:
      If $\mathrm{rand}(0, 1) < p_i$
        Step 4.1.1: Generate a candidate solution V_i by **(6)**.
        Step 4.1.2: Evaluate $f(V_i)$.
        Step 4.1.3: If $f(V_i) < f(X_i)$, set $X_i = V_i$, otherwise, set $trial_i = trial_i + 1$.
        Step 4.1.4: Set $t = t + 1$.
      End If
    Step 4.2: Set $i = i + 1$, if $i = 0.5 \times SN$, set $i = 1$.
  End While
Step 5: The scout bees phase:
  If $\max(trial_i) > limit$, replace X_i with a new candidate solution generated via (5).
Step 6: Set $cycle = cycle + 1$, and **if** $cycle > MCN$, then stop and output the best solution achieved so far, otherwise, go to Step 2.

for time-delay fractional-order chaotic systems is studied. It is converted into a nonlinear optimization problem via a functional extreme model in Section III. In Section IV-A, the artificial bee colony algorithm is described in details. In this subsection, a method based on ABC algorithm is firstly proposed and applied to estimate the unknown parameters of the time-delay fractional-order chaotic systems. The procedure of the new method for parameter estimation of time-delay fractional-order chaotic systems is outlined in Algorithm 2 (see the top of next page).

V. Simulations

To test the effectiveness of ABC algorithm, two typical time-delay fractional-order chaotic systems are selected to show the performance. The simulations were done using MATLAB 7.1 on Intel (R) Core (TM) i5-3470 CPU, 3.2 GHz with 4 GB RAM. The predictor-corrector approach for the numerical solutions of time-delay fractional-order differential equations is used, which can be found in [7]. It is obvious that if the population and the maximum cycle number are larger, the corresponding probability of finding the global optimum is larger as well. However, a larger population and maximum cycle number need a larger number of function evaluations. In the following simulations, for the ABC algorithm, the population size (SN) and maximum cycle number (MCN) are set as: $SN = 100$, $MCN = 300$. Besides, the control parameter limit is chosen as 15. The ABC algorithm is run for 15 independent times for each example, and all runs are terminated after the predefined maximum number of iterations is reached.

Example 1: Fractional-order financial system with time-delay [11] is described as:

$$\begin{cases} {}_0D_t^{\alpha_1} x(t) = z(t) + (y(t-\tau) - a)x(t) \\ {}_0D_t^{\alpha_2} y(t) = 1 - by(t) - x^2(t-\tau) \\ {}_0D_t^{\alpha_3} z(t) = -x(t-\tau) - cz(t) \end{cases} \tag{9}$$

when $(\alpha_1, \alpha_2, \alpha_3) = (0.76, 1, 1)$, $(a, b, c) = (3, 0.1, 1)$, $\tau = 0.08$ and initial point is $(0.1, 4, 0.5)$, system (9) is chaotic. In order to demonstrate the performance of ABC algorithm clearly, the true values of fractional order α_1, system's parameter c and time delay τ are assumed as unknown parameters which need to be estimated. The searching spaces of the unknown parameters are set as $(\alpha_1, c, \tau) \in [0.4, 1.4] \times [0.5, 1.5] \times [0.01, 0.1]$. The No. of samples is set as $N = 250$ and the step size $h = 0.01$.

The corresponding objective function can be written as

$$F(\tilde{\alpha}_1, \tilde{c}, \tilde{\tau}) = \sum_{k=1}^{N} \|Y_k - \tilde{Y}_k\|_2 \tag{10}$$

therefore, the parameter estimation of system (9) is converted into a nonlinear function optimization problem as (10). In particular, the smaller F is, the better combination of parameters (α_1, c, τ) is. The distribution of the objective function value for the time-delay fractional-order financial system (9) is shown in Fig. 2. As viewed in different colors in Fig. 2, it can be found that the objective function values are smaller in the neighborhood of the point $(\alpha_1, c, \tau) = (0.76, 1, 0.08)$ than those in other places.

To show the performance of ABC algorithm, the statistical results in terms of the best, the mean, and the worst estimated parameters over 15 independent runs are listed in Table I, it can be easily seen that the estimated value obtained via the ABC algorithm is close to the true parameter value, implying that it can estimate the unknown parameters of the time-delay fractional-order chaotic system accurately. The evolutionary

Algorithm 2 A novel parameter estimation method based on ABC algorithm

Step 1: The initialization phase:
  Step 1.1: Initialize the parameters for ABC algorithm and time-delay fractional-order chaotic system (2).
  Step 1.2: Generate the initial population in the feasible domain Ω referred to in Section III.
Step 2: The optimization phase:
  Repeat
    Optimize the function (4) by ABC algorithm (Algorithm 1).
  Until Termination condition is satisfied.

curves of the parameters and fitness values estimated by ABC algorithm are shown in Figs. 3 and 4 in a single run, which can also illustrate the effectiveness of the proposed method.

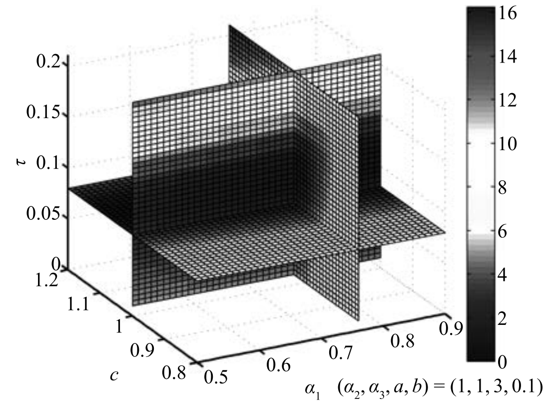

Fig. 2. The distribution of the objective function values for system (9).

TABLE I
SIMULATION RESULTS FOR SYSTEM (9) OVER 15 INDEPENDENT RUNS

	Best	Mean	Worst
α_1	0.7599999995	0.7600001772	0.7600028911
$\frac{\lvert\alpha_1-0.76\rvert}{0.76}$	5.06E−10	1.77E−07	2.89E−06
c	0.9999999791	0.9999994842	0.9999723488
$\frac{\lvert c-1\rvert}{1}$	2.09E−08	5.16E−07	2.77E−05
τ	0.0794338076	0.0796012039	0.0844809056
$\frac{\lvert\tau-0.08\rvert}{0.08}$	5.66E−04	3.99E−04	4.48E−03
F	1.57E−07	2.39E−05	1.41E−04

Example 2: Fractional-order Chen system with time-delay [12] is described as:

$$\begin{cases} {}_0D_t^{\alpha_1}x(t) = a(y(t) - x(t-\tau)) \\ {}_0D_t^{\alpha_2}y(t) = (c-a)x(t-\tau) - x(t)z(t) + cy(t) \\ {}_0D_t^{\alpha_3}z(t) = x(t)y(t) - bz(t-\tau) \end{cases} \tag{11}$$

when $\alpha_1 = \alpha_2 = \alpha_3 = 0.94 = \alpha$, $(a, b, c) = (35, 3, 27)$, $\tau = 0.009$ and initial point is $(0.2, 0, 0.5)$, system (11) is chaotic. In this example, the fractional order α, system parameter b and time delay τ are treated as unknown parameters to be estimated. The searching spaces of the unknown parameters are set as $(\alpha, b, \tau) \in [0.4, 1.4] \times [2.5, 3.5] \times [0.001, 0.015]$.

The No. of samples is set as $N = 250$ and the step size $h = 0.001$. Similarly, the corresponding objective function can be written as

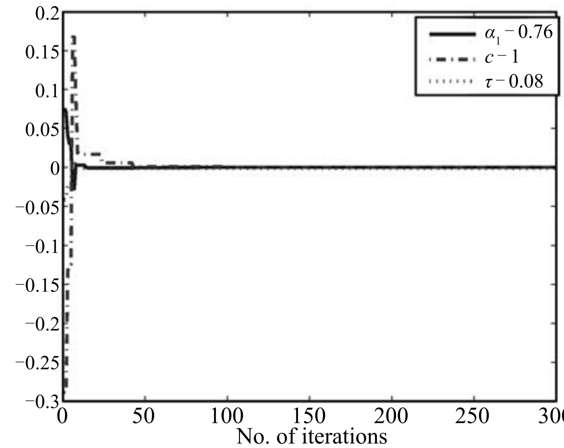

Fig. 3. Evolutionary curve in terms of estimated error values with the ABC algorithms on system (9) in a single run.

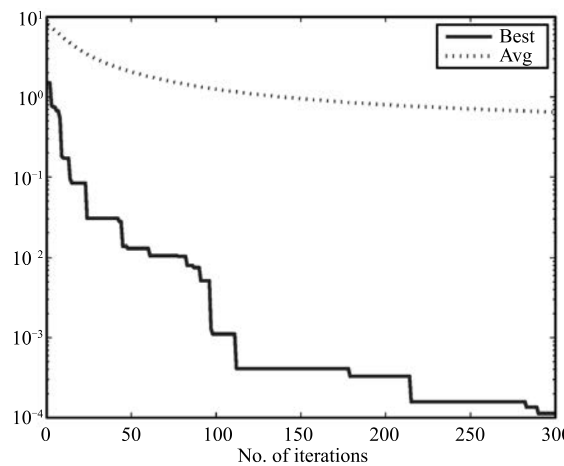

Fig. 4. Evolutionary curve in terms of fitness values with the ABC algorithms on system (9) in a single run.

$$F(\tilde{\alpha}, \tilde{b}, \tilde{\tau}) = \sum_{k=1}^{N} \|Y_k - \tilde{Y}_k\|_2 \tag{12}$$

therefore, the parameter estimation of system (11) is converted into a nonlinear function optimization problem as (12). Fig. 5 shows the distribution of the objective function value for the time-delay fractional-order Chen system (11).

The statistical results of the best, the mean and the worst estimated parameters with their corresponding relative error values over 15 independent runs are displayed in Table II. From Table II, it can be seen that the ABC algorithm can efficiently estimate the parameters of system (11). Figs. 6 and 7 depict the convergence profile of the evolutionary processes of the estimated parameters and the fitness values. From the figures, it can be seen that ABC algorithm can converge to the optimal solution rapidly.

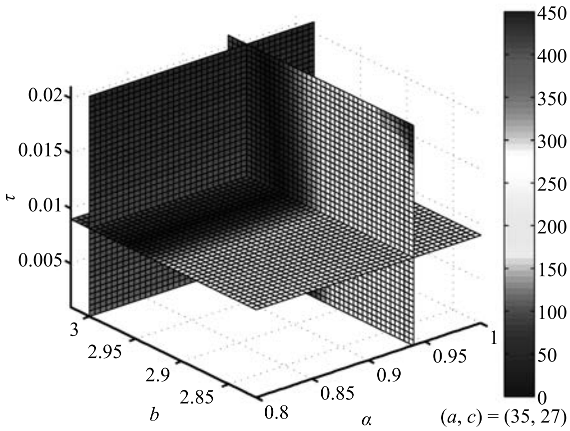

Fig. 5. The distribution of the objective function values for system (11).

TABLE II
SIMULATION RESULTS FOR SYSTEM (11) OVER 15 INDEPENDENT RUNS

	Best	Mean	Worst
α	0.9400000256	0.9400899098	0.9415600675
$\frac{\lvert\alpha-0.94\rvert}{0.94}$	2.56E−08	8.99E−05	1.56E−03
b	2.9999503453	2.9925101632	3.2099938577
$\frac{\lvert b-3\rvert}{3}$	4.97E−05	7.49E−03	2.10E−01
τ	0.0089214355	0.0089894034	0.0099489787
$\frac{\lvert\tau-0.009\rvert}{0.009}$	7.86E−05	1.06E−05	9.49E−04
F	1.48E−04	1.21E−01	1.11E+00

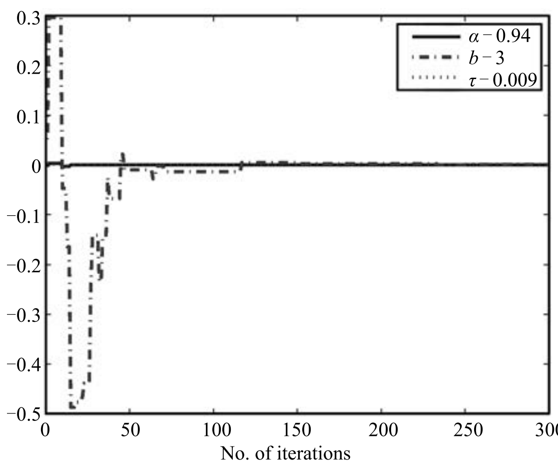

Fig. 6. Evolutionary curve in terms of estimated error values with the ABC algorithms on system (11) in a single run.

VI. CONCLUSIONS

In this paper, the parameter estimation of time-delay fractional-order chaotic systems is concerned by converting it into an optimization problem. A method based on artificial bee colony algorithm is proposed to deal with the optimization problem via functional extreme model. In simulations, the proposed method is applied to identify two typical time-delay fractional-order chaotic systems. And the simulation results show that the fractional order, the time delay and the system's parameter of chaotic system can be successfully estimated with the proposed scheme.

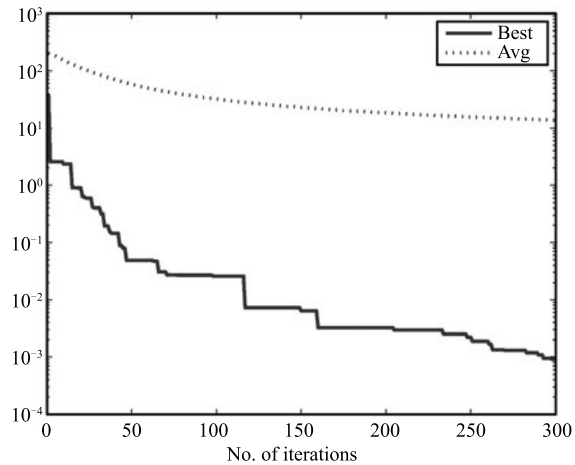

Fig. 7. Evolutionary curve in terms of fitness values with the ABC algorithms on system (11) in a single run.

The aim of this paper is to design a scheme based on ABC algorithm to estimate the unknown fractional orders, system's parameters and time delays. The proposed method can avoid the design of parameter update law in synchronization analysis of the time-delay fractional-order chaotic systems with unknown parameters. Though it is not good enough, we hope this method will contribute to the application of chaos control and synchronization for the time-delay fractional-order chaotic systems.

REFERENCES

[1] I. Podlubny, *Fractional Differential Equations*. San Diego: Academic Press, 1998.

[2] B. Mathieu, P. Melchior, A. Oustaloup, and C. Ceyral, "Fractional differentiation for edge detection," *Signal Proc.*, vol. 83, no. 11, pp. 2421−2432, Nov. 2003.

[3] M. F. Silva, J. A. T. Machado, and A. M. Lopes, "Fractional order control of a hexapod robot," *Nonlinear Dyn.*, vol. 38, no. 1−4, pp. 417−433, Dec. 2004.

[4] W. Chen, L. J. Ye, and H. G. Sun, "Fractional diffusion equations by the Kansa method," *Comput. Math. Appl.*, vol. 59, no. 5, pp. 1614−1620, Mar. 2010.

[5] M. A. E. Herzallah and D. Baleanu, "Fractional-order Euler-Lagrange equations and formulation of Hamiltonian equations," *Nonlinear Dyn.*, vol. 58, no. 1−2, pp. 385−391, Oct. 2009.

[6] M. Lakshmanan and D. V. Senthilkumar, *Dynamics of Nonlinear Time-Delay Systems*. Berlin Heidelberg: Springer, 2011.

[7] S. Bhalekar and V. Daftardar-Gejji, "A predictor-corrector scheme for solving nonlinear delay differential equations of fractional order," *J. Fract. Calculus Appl.*, vol. 1, no. 5, pp. 1−9, Jan. 2011.

[8] M. C. Mackey and L. Glass, "Oscillation and chaos in physiological control systems," *Science*, vol. 197, no. 4300, pp. 287−289, Jul. 1977.

[9] E. M. Shahverdiev and K. A. Shore, “Synchronization in multiple time delay chaotic laser diodes subject to incoherent optical feedbacks and incoherent optical injection,” *Nonlinear Anal. Real World Appl.*, vol. 12, no. 6, pp. 3114−3124, Dec. 2011.

[10] H. Wang, X. Wang, X. J. Zhu, and X. H. Wang, “Linear feedback controller design method for time-delay chaotic systems,” *Nonlinear Dyn.*, vol. 70, no. 1, pp. 355−362, Oct. 2012.

[11] Z. Wang, X. Huang, and G. D. Shi, “Analysis of nonlinear dynamics and chaos in a fractional order financial system with time delay,” *Comput. Math. Appl.*, vol. 62, no. 3, pp. 1531−1539, Aug. 2011.

[12] V. Daftardar-Gejji, S. Bhalekar, and P. Gade, “Dynamics of fractional-ordered Chen system with delay,” *Pramana*, vol. 79, no. 1, pp. 61−69, Jul. 2012.

[13] S. Bhalekar and V. Daftardar-Gejji, “Fractional ordered Liu system with time-delay,” *Commun. Nonlinear Sci. Numer. Simul.*, vol. 15, no. 8, pp. 2178−2191, Aug. 2010.

[14] Z. M. Odibat, N. Corson, M. A. Aziz-Alaoui, and C. Bertelle, “Synchronization of chaotic fractional-order systems via linear control,” *Int. J. Bifurc. Chaos*, vol. 20, no. 1, pp. 81−97, Jan. 2010.

[15] X. Y. Wang, X. P. Zhang, and C. Ma, “Modified projective synchronization of fractional-order chaotic systems via active sliding mode control,” *Nonlinear Dyn.*, vol. 69, no. 1−2, pp. 511−517, Jul. 2012.

[16] S. Bhalekar and V. Daftardar-Gejji, “Synchronization of different fractional order chaotic systems using active control,” *Commun. Nonlinear Sci. Numer. Simul.*, vol. 15, no. 11, pp. 3536−3546, Nov. 2010.

[17] R. Konnur, “Synchronization-based approach for estimating all model parameters of chaotic systems,” *Phys. Rev. E*, vol. 67, no. 2, pp. 027204, Feb. 2003.

[18] N. Q. Li, W. Pan, L. S. Yan, B. Luo, M. F. Xu, N. Jiang, and Y. L. Tang, “On joint identification of the feedback parameters for hyperchaotic systems: an optimization-based approach,” *Chaos Solit. Fract.*, vol. 44, no. 4−5, pp. 198−207, May 2011.

[19] M. F. Hu, Z. Y. Xu, R. Zhang, and A. H. Hu, “Parameters identification and adaptive full state hybrid projective synchronization of chaotic (hyper-chaotic) systems,” *Phys. Lett. A*, vol. 361, no. 3, pp. 231−237, Jan. 2007.

[20] Y. G. Tang, X. Y. Zhang, C. C. Hua, L. X. Li, and Y. X. Yang, “Parameter identification of commensurate fractional-order chaotic system via differential evolution,” *Phys. Lett. A*, vol. 376, no. 4, pp. 457−464, Jan. 2012.

[21] Y. Huang, F. Guo, Y. L. Li, and Y. F. Liu, “Parameter estimation of fractional-order chaotic systems by using quantum parallel particle swarm optimization algorithm,” *PLoS One*, vol. 10, no. 1, pp. e0114910, Jan. 2015.

[22] Z. Sheng, J. Wang, S. D. Zhou, and B. H. Zhou “Parameter estimation for chaotic systems using a hybrid adaptive cuckoo search with simulated annealing algorithm,” *Chaos* , vol. 24, no. 1, pp. 013133, Mar. 2014.

[23] J. Lin, “Parameter estimation for time-delay chaotic systems by hybrid biogeography-based optimization,” *Nonlinear Dyn.*, vol. 77, no. 3, pp. 983−992, Aug. 2014.

[24] D. Karaboga, “An idea based on honey bee swarm for numerical optimization,” Tech. Rep. TR06, Erciyes University, Engineering Faculty, Computer Engineering Department, Jan. 2005.

[25] D. Karaboga and B. Akay, “A comparative study of artificial bee colony algorithm,” *Appl. Math. Comput.*, vol. 214, no. 1, pp. 108−132, Aug. 2009.

[26] D. Karaboga and B. Basturk, “On the performance of artificial bee colony (ABC) algorithm,” *Appl. Soft Comput.*, vol. 8, no. 1, pp. 687−697, Jan. 2008.

[27] K. S. Tang, K. F. Man, S. Kwong, and Q. He, “Genetic algorithms and their applications,” *IEEE Signal Proc. Mag.*, vol. 13, no. 6, pp. 22−37, Nov. 1996.

[28] K. Price, R. M. Storn, and J. A. Lampinen, *Differential Evolution: A Practical Approach to Global Optimization*. Berlin Heidelberg: Springer, 2005.

[29] J. Kennedy, “Particle swarm optimization,” in *Encyclopedia of Machine Learning*, C. Sammut and G. I. Webb, Eds. US: Springer, 2010, pp. 760−766.

Wenjuan Gu received her B.S. degree at the School of Mathematics and Statistics, Ludong University, China in 2013. She is currently working toward the MEcons degree at the School of Economics and Management, Beijing Jiaotong University, China. Her research interests include intelligent optimization algorithms and its applications, logistic optimization, parameter estimation, data mining and analysis, applied statistics.

Yongguang Yu received his M.S. degree in the Department of Mathematical Science, Inner Mongolia University, China in 2001, and his Ph.D. degree at the Institute of Applied Mathematics, Academy of Mathematics and System Sciences, Chinese Academy of Sciences, China in 2004. From 2007 to 2009, he was a research fellow at City University of Hong Kong, China. Since 2010, he has been a professor with the Department of Mathematics, School of Science, Beijing Jiaotong University, China. His research interests include chaotic dynamics, chaos control and synchronization, complex networks, nonlinear control, and multi-agent systems. Corresponding author of this paper.

Wei Hu received his B.S. degree at the School of Mathematics and Statistics, Ludong University, China in 2013. He is currently working toward the M.S. degree in the Department of Mathematics, Beijing Jiaotong University, China. His research interests include parameter estimation of chaotic systems, chaos control and synchronization, and coordination control of multi-agent systems.

Stability Analysis, Chaos Control of Fractional Order Vallis and El-Nino Systems and Their Synchronization

Subir Das and Vijay K Yadav

***Abstract*—In this article the authors have studied the stability analysis and chaos control of the fractional order Vallis and El-Nino systems. The chaos control of these systems is studied using nonlinear control method with the help of a new lemma for Caputo derivative and Lyapunov stability theory. The synchronization between the systems for different fractional order cases and numerical simulation through graphical plots for different particular cases clearly exhibit that the method is easy to implement and reliable for synchronization of fractional order chaotic systems. The comparison of time of synchronization when the systems pair approaches from standard order to fractional order is the key feature of the article.**

***Index Terms*—El-Nino system, fractional derivative, nonlinear control method, stability analysis, synchronization, Vallis systems.**

I. INTRODUCTION

THE chaotic system is a nonlinear deterministic system which possess complex dynamical behaviors which are extremely sensitive to initial conditions and having bounded trajectories in the phase space. The study of dynamic behavior in nonlinear fractional order systems has become an interesting topic to the scientists and engineers. Fractional calculus is playing an important role for the analysis of nonlinear dynamical systems. Through fractional calculus approach many systems in interdisciplinary fields can be described by the fractional differential equation such as dielectric polarization, viscoelastic system, electrode-electrolyte polarization and electronic wave [1]−[4]. Another importance of fractional calculus is that it provides an excellent tool for the description of memory and hereditary properties, for which it is used in various physical areas of science and engineering such as material science [5], fluid mechanics [6], colored noise, biological modeling [7], [8], etc.

Effect of chaos in nonlinear dynamics is studied during last few decades by the researchers from different parts of the world. This effect is most common and has been detected in a number of dynamical systems of various types of physical nature. In practice it is usually undesirable and restricts the operating range of many mechanical and electrical devices. This type of control of dynamical system has attracted a great deal of attention by the researchers in society of engineering. The chaos control of systems can be divided into two categories, first one is to suppress the chaotic dynamical behaviors and second one is to generate or enhance chaos in nonlinear systems known as chaotincation or anti-control of chaos. So far various types of methods and techniques have been proposed for control of chaos such as feedback and non-feedback control [9]−[11], adaptive control [12], [13] and backstepping method [14] etc. Synchronization of two dynamical systems is the phenomenon where one dynamical system behaves according to the behavior of the other dynamical system. In chaos synchronization, two or more chaotic systems are coupled or one chaotic system drives another system. L. M. Pecora and T. L. Carroll [15] were first to introduce a method to synchronize drive and response systems of two identical or non-identical systems with different initial conditions.

In this manuscript, the authors have studied the chaos control and stability analysis of Vallis and El-Nino systems with fractional order, and also the synchronization between the considered systems. A nonlinear control method is used for chaos control of fractional order Vallis and El-Nino systems, and also during their synchronization. Both the systems were proposed by Vallis in 1986 for the description of temperature fluctuations in the western and eastern parts of equatorial ocean, which have a strong influence on the Earth's global climate. The first model Vallis system does not allow trade winds, whereas the second model El-Nino system describes the nonlinear interactions of the atmosphere, and trade winds in the equatorial part of pacific ocean. The main feature of this article is the study of time of synchronization between the systems through numerical simulation for different particular cases as systems' pair approaches fractional order from integer order.

II. SOME PRELIMINARIES AND STABILITY CONDITION

A. Definitions and Lemma

Definition 1 [16]: The Caputo derivative for fractional order q is defined as

$$ {}_a^cD_t^q\phi(t) = \frac{1}{\Gamma(n-q)}\int_a^t \frac{\phi^{(n)}(\tau)}{(t-\tau)^{q+1-n}}\,d\tau, \quad t > a $$

Manuscript received September 16, 2015; accepted February 1, 2016. Recommended by Associate Editor Antonio Visioli.

Citation: S. Das and V. K. Yadav, "Stability analysis, chaos control of fractional order Vallis and El-Nino systems and their synchronization," *IEEE/CAA Journal of Automatica Sinica*, vol. 4, no. 1, pp. 114−124, Jan. 2017.

S. Das and V. K. Yadav are with the Department of Mathematical Sciences, Indian Institute of Technology, Banaras Hindu University, Varanasi 221005, India (e-mail: sdas.apm@iitbhu.ac.in; vijayky999@gmail.com).

Color versions of one or more of the figures in this paper are available online at http://ieeexplore.ieee.org.

Digital Object Identifier 10.1109/JAS.2017.7510343

where $q \in \mathbb{R}^+$ on the half axis $\mathbb{R}^+$ and $n = \min\{k \in \mathbb{N}/k > q\}$, $q > 0$.

Lemma 1 [17]: Let $x(t) \in \mathbb{R}$ be a continuous and derivable function. Then for any time instant $t \geq t_0$,

$$\frac{1}{2}{}_{t_0}^{c}D_t^q x^2(t) \leq x(t){}_{t_0}^{c}D_t^q x(t) \quad \forall\, q \in (0,1).$$

Definition 2 [18]: An equilibrium point E of a system is called a saddle point of index 1 if the Jacobian matrix at point E has one eigenvalue with a non-negative real part (i.e., unstable).

Definition 3: An equilibrium point E of a system is called a saddle point of index 2 if the Jacobian matrix at point E has two unstable eigen values.

The scrolls are generated only around the saddle points of index 2. Saddle point of index 1 is responsible only for connecting scrolls.

B. Stability of the System

Consider a fractional order dynamical system as

$$\begin{aligned} D_t^q x(t) &= f_1(x,\, y,\, z)\\ D_t^q y(t) &= f_2(x,\, y,\, z)\\ D_t^q z(t) &= f_3(x,\, y,\, z) \end{aligned} \tag{1}$$

where $q \in (0,\, 1)$ and D_t^q is the Caputo derivative. The Jacobian matrix at equilibrium points of the above system is

$$J = \begin{bmatrix} \frac{\partial f_1}{\partial x} & \frac{\partial f_1}{\partial y} & \frac{\partial f_1}{\partial z}\\ \frac{\partial f_2}{\partial x} & \frac{\partial f_2}{\partial y} & \frac{\partial f_2}{\partial z}\\ \frac{\partial f_3}{\partial x} & \frac{\partial f_3}{\partial y} & \frac{\partial f_3}{\partial z} \end{bmatrix}. \tag{2}$$

Theorem 1 [19], [20]: The system (1) is locally asymptotically stable if all the eigenvalues of the Jacobian matrix at its equilibrium point satisfy the condition

$$|\arg(\lambda)| > \frac{q\pi}{2}. \tag{3}$$

III. Design of Controller for Fractional Order Chaotic System Using Nonlinear Control Method

Consider the fractional order chaotic system as the master system as

$$D_t^q x = Px + Qf(x) \tag{4}$$

where $0 < q \leq 1$ is the order of the fractional time derivative, $x = [x_1, x_2, \ldots, x_n]^T \in \mathbb{R}^n$ is the state vector, P and Q are the $n \times n$ matrices consisting of the system parameters and $f: \mathbb{R}^n \to \mathbb{R}^n$ is a nonlinear function of the system.

Consider another fractional order chaotic system as a slave system described as

$$D_t^q y = P_1 y + Q_1 g(y) + u(t) \tag{5}$$

where $y = [y_1, y_2, \ldots, y_n]^T \in \mathbb{R}^n$ is the state vector of the system, P_1 and Q_1 are the $n \times n$ matrices of the system parameters, $g: \mathbb{R}^n \to \mathbb{R}^n$ is a nonlinear part of the function of the system and $u(t)$ is the controller of the system (5).

During synchronization, defining the error as $e = y - x$, the error dynamical system is obtained as

$$D_t^q e = P_1 e + Q_1 g(y) + (P_1 - P)x - Qf(x) + u(t). \tag{6}$$

During the synchronization, our aim is to find the appropriate feedback controller $u(t)$, so that we may stabilize the error dynamics (6) in order to get $\lim_{t\to\infty} \|e(t)\| = 0, \forall\, e(0) \in \mathbb{R}^n$.

Now, we define the following Lyapunov function as $V(e) = \frac{1}{2}e^T e$, whose q-th order fractional derivative w. r. to t is (using Lemma 1)

$$\begin{aligned} \frac{d^q V(e)}{dt^q} &= \frac{1}{2}\frac{d^q(e^{\mathrm{T}}e)}{dt^q} = \frac{1}{2}\frac{d^q}{dt^q}\left(e_1^2 + e_2^2 + \cdots + e_n^2\right)\\ &\leq \left(e_1\frac{d^q e_1}{dt^q} + e_2\frac{d^q e_2}{dt^q} + \cdots + e_n\frac{d^q e_n}{dt^q}\right). \end{aligned} \tag{7}$$

Substituting the values of $\frac{d^q e_1}{dt^q}, \frac{d^q e_2}{dt^q}, \ldots, \frac{d^q e_n}{dt^q}$ and choosing appropriate control function $u(t)$, the q-th order derivative of the Lyapunov function $V(e)$ becomes negative i.e., $\frac{d^q V(e)}{dt^q} < 0$, which helps to get synchronization between the systems (4) and (5).

IV. System Description and Its Stability

A. Fractional Order Vallis System

The Vallis model [21], [22] is described by

$$\begin{aligned} \frac{dx}{dt} &= \mu y - ax\\ \frac{dy}{dt} &= xz - y\\ \frac{dz}{dt} &= 1 - xy - z \end{aligned} \tag{8}$$

where x is the speed of water molecules on the surface of ocean, $y = (T_w - T_e)/2$, $z = (T_w + T_e)/2$, T_w and T_e are temperatures accordingly in western and eastern parts of ocean, μ and a are positive parameters.

The fractional order Vallis system can be described as

$$\begin{aligned} \frac{d^q x}{dt^q} &= \mu y - ax\\ \frac{d^q y}{dt^q} &= xz - y\\ \frac{d^q z}{dt^q} &= 1 - xy - z, \quad 0 < q < 1. \end{aligned} \tag{9}$$

1) Equilibrium Points and Stability: To find the equilibrium points of the system (9), we have

$$D_t^q x = D_t^q y = D_t^q z = 0$$

where $D_t^q = \frac{d^q}{dt^q}$.

The equilibrium points are obtained as

$$\begin{aligned} E_1 &= (0,\ 0,\ 1)\\ E_{2,3} &= \left(\pm\sqrt{\frac{(\mu - a)}{a}},\ \pm\frac{\sqrt{a(\mu - a)}}{\mu},\ \frac{a}{\mu}\right). \end{aligned}$$

For convenience the point E_1 is shifted to the point of origin through the transformation $z \to z + 1$ and the system (9) reduces to

$$\frac{d^q x}{dt^q} = \mu y - ax$$
$$\frac{d^q y}{dt^q} = xz + x - y$$
$$\frac{d^q z}{dt^q} = -xy - z \tag{10}$$

where $0 < q < 1$. For the parameters $\mu = 121$ and $a = 5$ and the initial condition $(0.1, 1.2, 0.5)$, the trajectories of the Vallis system are depicted through Figs. 1 (a)−1 (d) for fractional order $q = 0.97$. Again for the same parameters' values and initial conditions the Vallis system shows chaotic behavior at the lowest fractional order $q = 0.981$, the trajectories of which are described through Figs. 2 (a)−2 (d).

The equilibrium points of the system (10) are $E_1 = (0,\ 0,\ 0)$, $E_2 = (4.8166,\ 0.1990,\ -0.9586)$ and $E_3 = (-4.8166,\ -0.1990,\ -0.9586)$.

The Jacobian matrix of the Vallis system (10) at the equilibrium point $\bar{E}(\bar{x},\ \bar{y},\ \bar{z})$ is

$$J(\bar{E}) = \begin{bmatrix} -a & \mu & 0 \\ \bar{z}+1 & -1 & \bar{x} \\ -\bar{y} & -\bar{x} & -1 \end{bmatrix}. \tag{11}$$

Putting the values of $a = 5$ and $\mu = 121$, the characteristic polynomial of the above Jacobian matrix will be

$$P(\lambda) = \lambda^3 + 7\lambda^2 - (-\bar{x}^2 + 121\bar{z} + 110)\lambda - 121\bar{z} + 5\bar{x}^2 + 121\bar{x}\bar{y} - 116. \tag{12}$$

At the equilibrium point $E_1 = (0,\ 0,\ 0)$, (12) becomes

$$P(\lambda) = \lambda^3 + 7\lambda^2 - 110\lambda - 116. \tag{13}$$

The eigenvalues of the equation (13) are $\lambda_1 = -14.1803$, $\lambda_2 = 8.1803$, $\lambda_3 = -1.0000$.

It is seen that the equilibrium point E_1 is a saddle point of index 1 and from Definition 2 it is unstable for $0 < q < 1$.

At the equilibrium point $E_2 = (4.8166,\ 0.1990,\ -0.9586)$, the equation (12) becomes

$$P(\lambda) = \lambda^3 + 7\lambda^2 + 29.1902\lambda + 231.9676. \tag{14}$$

The eigenvalues of (14) are $\lambda_1 = -7.3331$, $\lambda_{2,3} = 0.1666 \pm 5.6219i$. The equilibrium point E_2 is the saddle point of index 2 (Definition 2). E_2 is stable for $0 < q < 0.981$. Similarly the equilibrium point $E_3 = (-4.8166, -0.1990,\ -0.9586)$ is also stable for $0 < q < 0.981$.

2) Control of Chaos Using Nonlinear Control Method: Let the fractional order Vallis system is taken as a controlled system with control functions $u_i(t),\ i = 1,\ 2,\ 3$ to stabilize unstable periodic orbit or fixed point as given in (10).

Let $(\bar{x},\ \bar{y},\ \bar{z})$ is the solution of the system (10), then we have

$$\frac{d^q \bar{x}}{dt^q} = \mu\bar{y} - a\bar{x}$$
$$\frac{d^q \bar{y}}{dt^q} = \bar{x}\bar{z} + \bar{x} - \bar{y}$$
$$\frac{d^q \bar{z}}{dt^q} = -\bar{x}\bar{y} - \bar{z}. \tag{15}$$

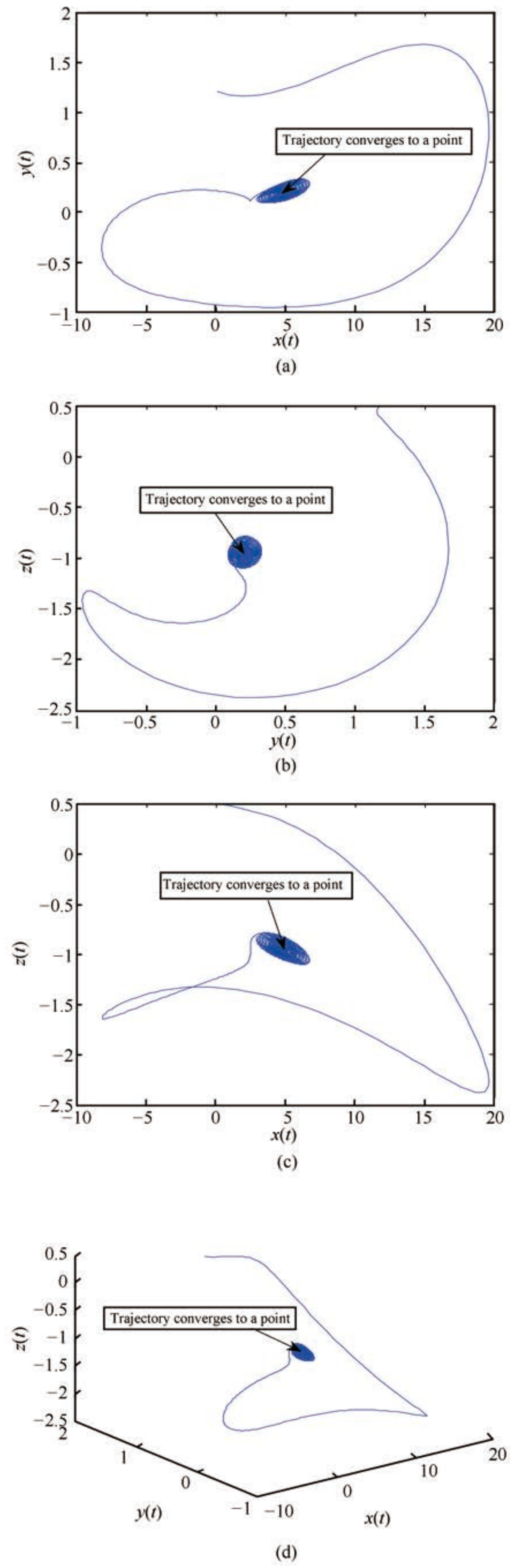

Fig. 1. Phase portraits of fractional order Vallis system for fractional order $q = 0.97$.

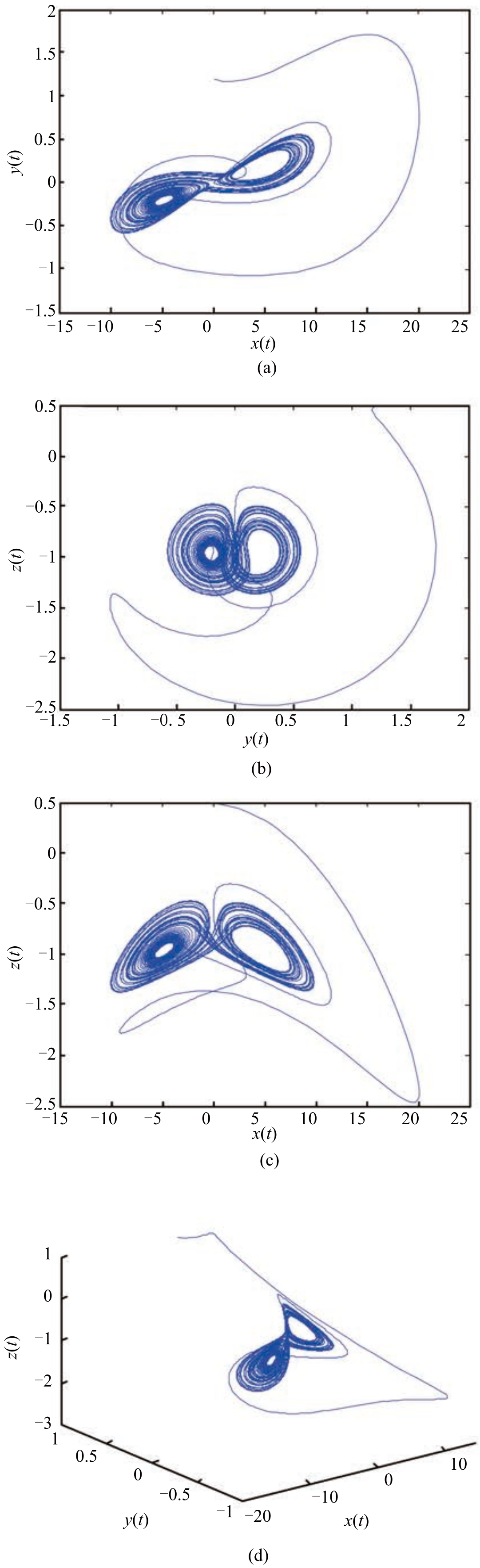

Fig. 2. Phase portraits of fractional order Vallis system for fractional order $q = 0.981$.

Defining error functions as $e_1 = x - \bar{x}$, $e_2 = y - \bar{y}$ and $e_3 = z - \bar{z}$, we obtain the following error system as

$$\begin{aligned}\frac{d^q e_1}{dt^q} &= \mu e_2 - a e_1 + u_1(t)\\ \frac{d^q e_2}{dt^q} &= e_1 - e_2 + xz - \bar{x}\bar{z} + u_2(t)\\ \frac{d^q e_3}{dt^q} &= -e_3 - xy + \bar{x}\bar{y} + u_3(t).\end{aligned} \tag{16}$$

To stabilize the error system, define the Lyapunov function as

$$V = \frac{1}{2}e_1^2 + \frac{1}{2}e_2^2 + \frac{1}{2}e_3^2$$

whose q-th order fractional derivative is (from Lemma 1)

$$\begin{aligned}\frac{d^q V}{dt^q} &= \frac{1}{2}\frac{d^q e_1^2}{dt^q} + \frac{1}{2}\frac{d^q e_2^2}{dt^q} + \frac{1}{2}\frac{d^q e_3^2}{dt^q}\\ &\le e_1\frac{d^q e_1}{dt^q} + e_2\frac{d^q e_2}{dt^q} + e_3\frac{d^q e_3}{dt^q}\end{aligned}$$

i.e.,

$$\begin{aligned}\frac{d^q V}{dt^q} \le\ & e_1[\mu e_2 - a e_1 + u_1(t)]\\ &+ e_2[e_1 - e_2 + xz - \bar{x}\bar{z} + u_2(t)]\\ &+ e_3[-e_3 - xy + \bar{x}\bar{y} + u_3(t)].\end{aligned}$$

If we take $u_1(t) = -\mu e_2$, $u_2(t) = -e_1 - xz + \bar{x}\bar{z}$ and $u_3(t) = xy - \bar{x}\bar{y}$, it becomes $\frac{d^q V}{dt^q} \le -a e_1^2 - e_2^2 - e_3^2 < 0$. This shows that the trajectories $(x(t), y(t), z(t))$ converge to the point $(\bar{x}, \bar{y}, \bar{z})$.

3) Stabilizing the Points E_1, E_2 and E_3: It is clear from Figs. 3 (a)–3 (c) that at $(\bar{x}, \bar{y}, \bar{z}) = (0, 0, 0) = E_1$, the system (10) is stable at the point E_1 for the order $0 < q < 1$. Similarly for $(\bar{x}, \bar{y}, \bar{z}) = (4.8166, 0.1990, -0.9586) = E_2$ and $(\bar{x}, \bar{y}, \bar{z}) = (-4.8166, -0.1990, -0.9586) = E_3$, the system (10) is also stable for the order $0 < q < 1$. The plots of the control functions $u_1(t)$, $u_2(t)$, $u_3(t)$ used to stabilize the fractional order chaotic system are depicted through Fig. 3 (d), which clearly show that the chosen functions tend to zero as time approaches infinity at the equilibrium point E_1. It can be shown that the nature of the above functions at other two equilibrium points E_2 and E_3 are similar.

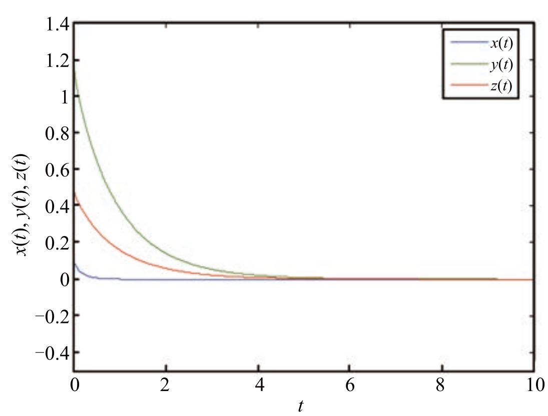

(a)

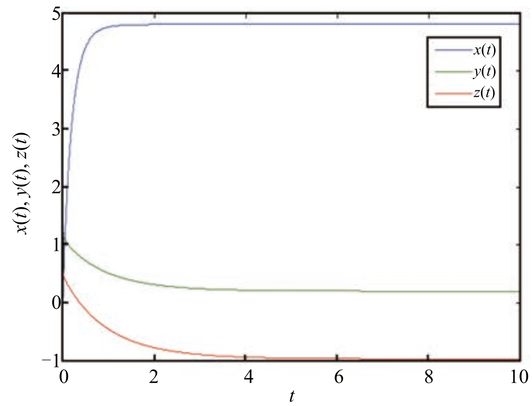

(b)

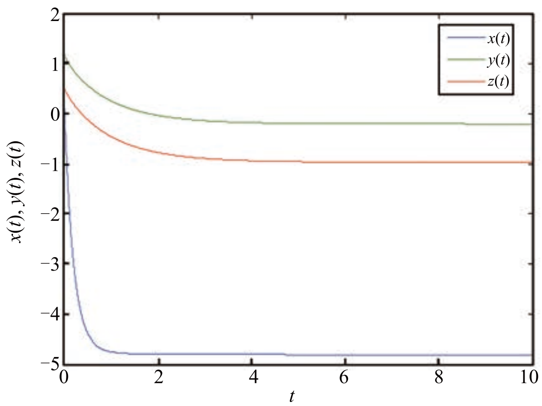

(c)

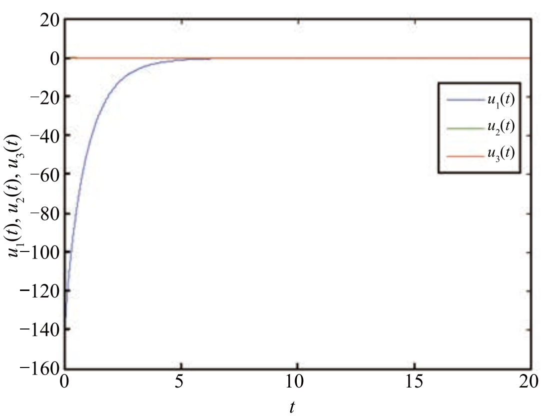

(d)

Fig. 3. Plots of $x(t)$, $y(t)$, $z(t)$ of the controlled system (10). (a) At equilibrium point E_1. (b) At the equilibrium point E_2. (c) At the equilibrium point E_3. (d) Plots of control functions $u_1(t)$, $u_2(t)$, $u_3(t)$ at E_1.

B. Fractional Order El-Nino System

El-Nino system is nonlinear and non-autonomous system represented by three differential equations as [21], [22]

$$\begin{aligned}\frac{dx}{dt} &= \mu'(y-z) - b(x - f(t))\\ \frac{dy}{dt} &= xz - y + c\\ \frac{dz}{dt} &= -xy - z + c \end{aligned} \tag{17}$$

where x, y and z are the speed of surface ocean current, temperature of water accordingly on western and eastern bounds of water pool respectively, $f(t)$ is the periodic function considering influence of trades winds.

Taking $f(t) = 0$ to make an autonomous system as

$$\begin{aligned}\frac{dx}{dt} &= \mu'(y-z) - bx\\ \frac{dy}{dt} &= xz - y + c\\ \frac{dz}{dt} &= -xy - z + c. \end{aligned} \tag{18}$$

The fractional order El-Nino system is described as

$$\begin{aligned}\frac{d^q x}{dt^q} &= \mu'(y-z) - bx\\ \frac{d^q y}{dt^q} &= xz - y + c\\ \frac{d^q z}{dt^q} &= -xy - z + c, \quad 0 < q < 1. \end{aligned} \tag{19}$$

1) Equilibrium Points and Stability: To find the equilibrium points of the system (19), we have

$$\begin{aligned} &\mu'(y-z) - bx = 0\\ &xz - y + c = 0\\ &-xy - z + c = 0. \end{aligned}$$

The equilibrium points are obtained as

$$\begin{aligned} P_1 &= (0,\ c,\ c)\\ P_2 &= \left(\sqrt{\frac{2\mu c}{b} - 1},\ \frac{b + \sqrt{2\mu bc - b^2}}{2\mu},\ \frac{b - \sqrt{2\mu bc - b^2}}{2\mu}\right)\\ P_3 &= \left(-\sqrt{\frac{2\mu c}{b} - 1},\ \frac{b - \sqrt{2\mu bc - b^2}}{2\mu},\ \frac{b + \sqrt{2\mu bc - b^2}}{2\mu}\right). \end{aligned}$$

Making a shifting through $y \to y + c$ and $z \to z + c$, the system (19) will be reduced to the following form

$$\begin{aligned}\frac{d^q x}{dt^q} &= \mu'(y-z) - bx\\ \frac{d^q y}{dt^q} &= xz + xc - y\\ \frac{d^q z}{dt^q} &= -xy - xc - z. \end{aligned} \tag{20}$$

For the parameters $\mu' = 83.6$, $b = 10$ and $c = 12$ and the initial condition $(-2,\ 3,\ 5)$, the El-Nino system shows chaotic behavior at $q = 0.934$, the lowest fractional order (see Figs. 4 (a)−4 (d)). For the same values of parameters and initial conditions the trajectories of the system at $q = 0.93$ are described through Figs. 5 (a)−5 (d).

The equilibrium points of the system (20) are calculated as

$$\begin{aligned} P_1 &= (0,\ 0,\ 0)\\ P_2 &= (14.1294,\ -11.0951,\ -12.7852)\\ P_3 &= (-14.1294,\ -12.7852,\ -11.0951). \end{aligned}$$

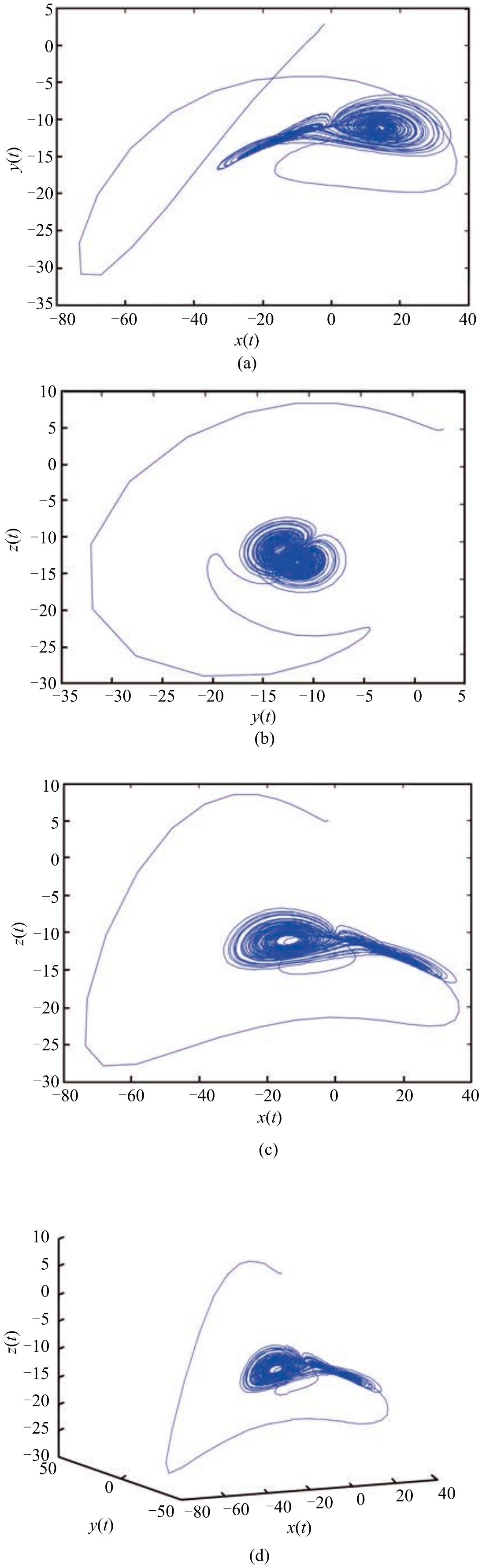

Fig. 4. Phase portraits of fractional order El-Nino system for fractional order $q = 0.934$.

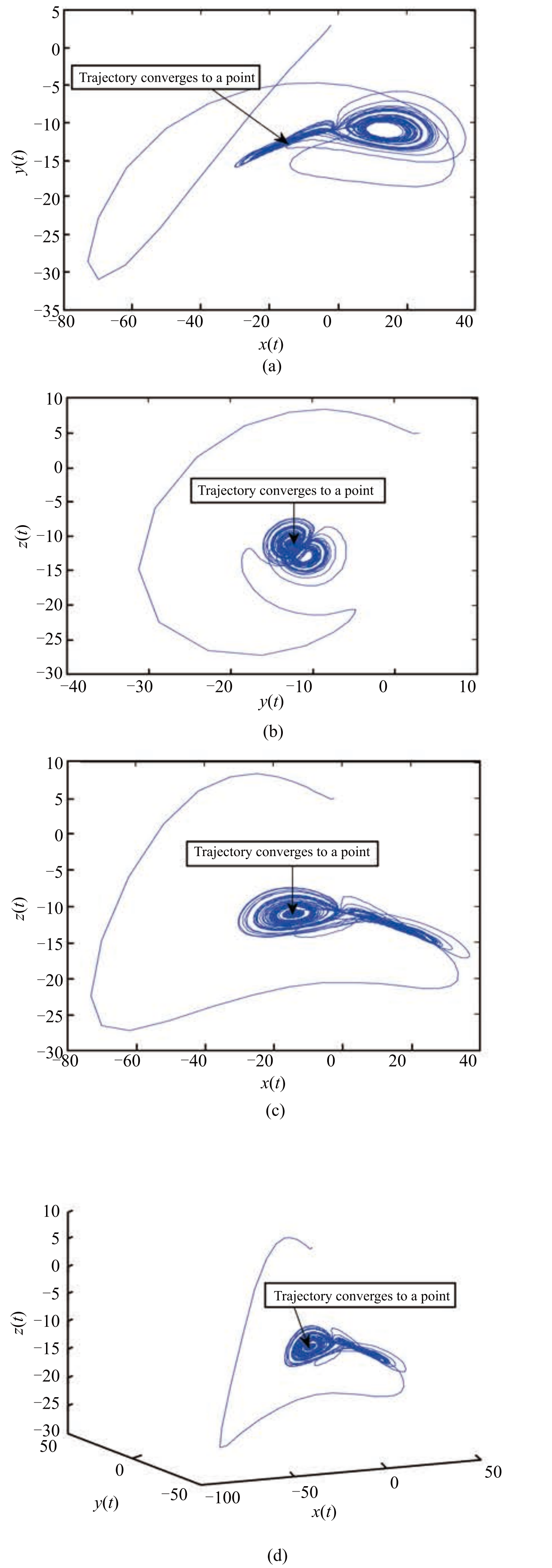

Fig. 5. Phase portraits of fractional order El-Nino system for fractional order $q = 0.93$.

The Jacobian matrix of the El-Nino system (20) at the equilibrium point $\bar{P}(\bar{x},\ \bar{y},\ \bar{z})$ is

$$J(\bar{P}) = \begin{bmatrix} -b & \mu' & -\mu' \\ \bar{z}+c & -1 & \bar{x} \\ -\bar{y}-c & -\bar{x} & -1 \end{bmatrix}.$$

Putting the values of $\mu' = 83.6$, $b = 10$ and $c = 12$, we obtain characteristic polynomial of the above Jacobian matrix as

$$\begin{aligned} P(\lambda) = {} & \lambda^3 + 12\lambda^2 - (-\bar{x}^2 + 83.6\bar{y} + 83.6\bar{z} + 1985.40)\lambda \\ & + 10\bar{x}^2 - 83.6\bar{y} - 83.6\bar{z} + 83.6\bar{x}\,\bar{y} \\ & - 83.6\bar{x}\,\bar{z} - 1996.40. \end{aligned}$$

At the equilibrium point $P_1 = (0,\ 0,\ 0)$,

$$P(\lambda) = \lambda^3 + 12\lambda^2 - 1985.40\lambda - 1996.40$$

which gives $\lambda_1 = -50.5183$, $\lambda_2 = 39.5183$, $\lambda_3 = -1.0000$.

Now P_1 is a saddle point of index 1 and from Definition 2 it is unstable for $0 < q < 1$. At the equilibrium point $P_2 = (14.1294,\ -11.0951,\ -12.7852)$,

$$P(\lambda) = \lambda^3 + 12\lambda^2 + 210.6330\lambda + 3992.7687$$

and thus the eigenvalues are $\lambda_1 = -15.2956$, $\lambda_{2,\,3} = 1.6478 \pm 16.0725i$. P_2 is the saddle point of index 2 (Definition 2). So P_2 is stable for $0 < q < 0.934$. Similarly at $P_3 = (-14.1294,\ -12.7852,\ -11.0951)$, the eigenvalues are obtained as $\lambda_1 = -15.2956$, $\lambda_{2,\,3} = 1.6478 \pm 16.0725i$, and this shows that P_3 is stable for $0 < q < 0.934$.

2) Control of Chaos Using Nonlinear Control Method: Consider the fractional order El-Nino system as a controlled system with control functions $u_1(t)$, $u_2(t)$ and $u_3(t)$, for stabilizing unstable periodic orbit and $(\bar{x},\ \bar{y},\ \bar{z})$ be the solution of the system (20) so that

$$\begin{aligned} \frac{d^q\bar{x}}{dt^q} &= \mu'(\bar{y} - \bar{z}) - b\bar{x} \\ \frac{d^q\bar{y}}{dt^q} &= \bar{x}\bar{z} + \bar{x}c - \bar{y} \\ \frac{d^q\bar{z}}{dt^q} &= -\bar{x}\bar{y} - \bar{x}c - \bar{z}. \end{aligned} \tag{21}$$

Defining the error function $e(t)$ and Lyapunov function V as in Section IV-A for stabilizing the error system, we get the q-th order derivative of V as

$$\begin{aligned} \frac{d^qV}{dt^q} \le {} & e_1[\mu'(e_2 - e_3) - be_1 + u_1(t)] \\ & + e_2[ce_1 - e_2 + xz - \bar{x}\bar{z} + u_2(t)] \\ & + e_3[-ce_1 - e_3 - xy + \bar{x}\bar{y} + u_3(t)]. \end{aligned}$$

Taking $u_1(t) = -\mu'(e_2 - e_3)$, $u_2(t) = -ce_1 - xz + \bar{x}\bar{z}$ and $u_3(t) = ce_1 + xy - \bar{x}\bar{y}$, we get $\frac{d^qV}{dt^q} \le -be_1^2 - e_2^2 - e_3^2 < 0$, which implies the trajectories $(x(t),\ y(t),\ z(t))$ converge to $(\bar{x},\ \bar{y},\ \bar{z})$.

3) Stabilizing the Points P_1, P_2, and P_3: It is seen from Figs. 6 (a)−6 (c) that at $P_1 = (0,\ 0,\ 0)$, $P_2 = (14.1294,\ -11.0951,\ -12.7852)$ and $P_3 = (-14.1294,\ -12.7852,\ -11.0951)$, the system (20) is stable for the order $0 < q < 1$. Like previous system, the chosen control functions for this fractional order chaotic system converge to zero at all the equilibrium points P_1, P_2, P_3 as time approaches infinity. The plots at P_1 are shown through Fig. 6 (d).

V. Synchronization Between Fractional Order Vaallis and EL-Nino Systems Using Nonlinear Control Method

In this section to study the synchronization between fractional order Vallis and El-Nino systems, we consider the fractional order Vallis system as the master system as

$$\begin{aligned} \frac{d^qx_1}{dt^q} &= \mu y_1 - ax_1 \\ \frac{d^qy_1}{dt^q} &= x_1z_1 + x_1 - y_1 \\ \frac{d^qz_1}{dt^q} &= -x_1y_1 - z_1 \end{aligned} \tag{22}$$

and the fractional order El-Nino system as slave system as

$$\begin{aligned} \frac{d^qx_2}{dt^q} &= \mu'(y_2 - z_2) - bx_2 + v_1(t) \\ \frac{d^qy_2}{dt^q} &= x_2z_2 + x_2c - y_2 + v_2(t) \\ \frac{d^qz_2}{dt^q} &= -x_2y_2 - x_2c - z_2 + v_3(t) \end{aligned} \tag{23}$$

where $v_1(t)$, $v_2(t)$ and $v_3(t)$ are the control functions. Defining error functions as

$$e_1 = x_2 - x_1, \quad e_2 = y_2 - y_1, \quad e_3 = z_2 - z_1.$$

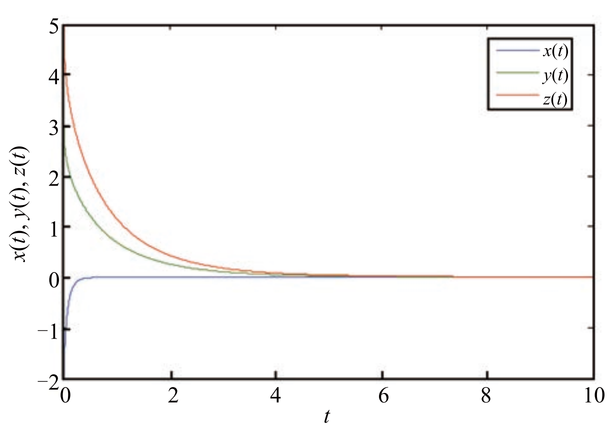

(a)

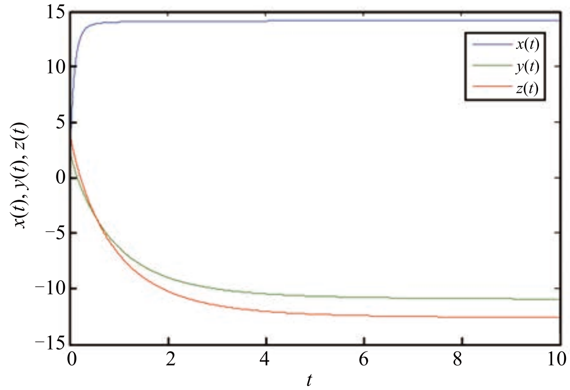

(b)

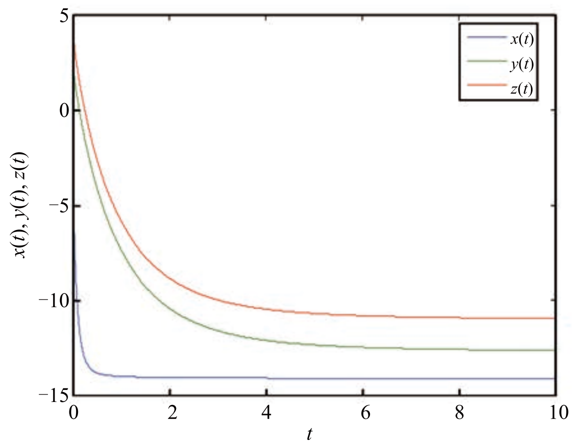

(c)

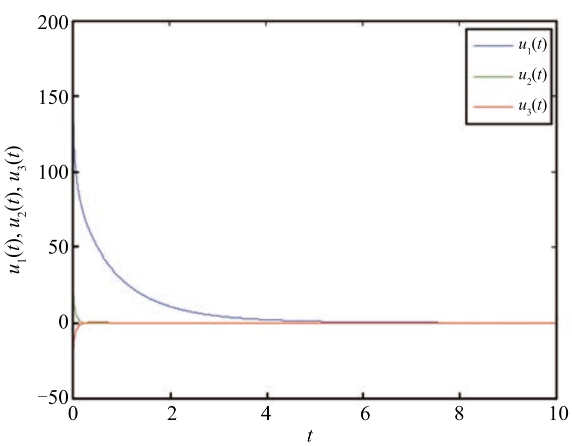

(d)

Fig. 6. Plots of $x(t)$, $y(t)$, $z(t)$of the controlled system (20). (a) At the equilibrium point P_1. (b) At the equilibrium point P_2. (c) At the equilibrium point P_3. (d) Plots of control functions $u_1(t)$, $u_2(t)$, $u_3(t)$ at P_1.

We obtain the following error system as

$$\begin{aligned}\frac{d^q e_1}{dt^q} &= \mu'(e_2 - e_3) - be_1 + (a-b)x_1 + (\mu' - \mu)y_1 \\ &\quad - \mu' z_1 + v_1(t) \\ \frac{d^q e_2}{dt^q} &= ce_1 - e_2 + (c-1)x_1 + x_2 z_2 - x_1 z_1 + v_2(t) \\ \frac{d^q e_3}{dt^q} &= -ce_1 - e_3 - x_1 c - x_2 y_2 + x_1 y_1 + v_3(t). \end{aligned} \tag{24}$$

In order to stabilize the error system, let us consider the Lyapunov function as

$$V(e) = \frac{1}{2}\left(e_1^2 + e_2^2 + e_3^2\right). \tag{25}$$

Choosing the control functions as

$$\begin{aligned} v_1(t) &= -\mu'(e_2 - e_3) - (a-b)x_1 - (\mu' - \mu)y_1 + \mu' z_1 \\ v_2(t) &= -ce_1 - (c-1)x_1 - x_2 z_2 + x_1 z_1 \\ v_3(t) &= ce_1 + x_1 c + x_2 y_2 - x_1 y_1 \end{aligned}$$

the q-th order derivative of the Lyapunov function $V(e)$ becomes $\frac{d^q V(e)}{dt^q} \leq -be_1^2 - e_2^2 - e_3^2 < 0$, which concludes that $\lim_{t\to\infty} \|e(t)\| = 0$, and hence the synchronization between master and response systems is achieved.

VI. Numerical Simulation and Results

In this section, we take the earlier considered values of the parameters of systems. The initial conditions of master and slave systems are $(x_1(0),\ y_1(0),\ z_1(0)) = (0.1,\ 1.2,\ 0.5)$ and $(x_2(0),\ y_2(0),\ z_2(0)) = (-2,\ 3,\ 5)$, respectively. Hence the initial conditions of error system will be $(e_1(0),\ e_2(0),\ e_3(0)) = (-2.1,\ 1.8,\ 4.5)$. During synchronization of the systems the time step size is taken as 0.005. The synchronization between $x_1 - x_2$, $y_1 - y_2$ and $z_1 - z_2$ are depicted through Figs. 7–10 at $q = 0.7,\ 0.9,\ 0.981,\ 1.0$. The time for synchronization of the considered fractional order chaotic systems clearly exhibits that it takes less time for synchronization when the order of the derivative approaches from standard order to the fractional order.

VII. Conclusion

The authors have achieved four important goals through the analysis of the present study. First one is the stability analysis to locate the range of fractional order beyond which the systems show chaotic behavior. Second one is the synchronization between the considered fractional order systems and also chaos control of both the systems using nonlinear control method. The third one is the proper design of the control functions so that the error states decay to zero as time approaches infinity which helps to get the required time for synchronization. The most important part of the study is the comparison of time of synchronization through effective numerical simulation and graphical presentations for different particular cases as systems pair approaches from standard order to fractional order. The authors believe that the outcome of the results will be appreciated and utilized by the scientists and engineers working in the field of atmospheric science and oceanography.

Acknowledgement

The second author acknowledges the financial support from the UGC, New Delhi, India under the SRF scheme.

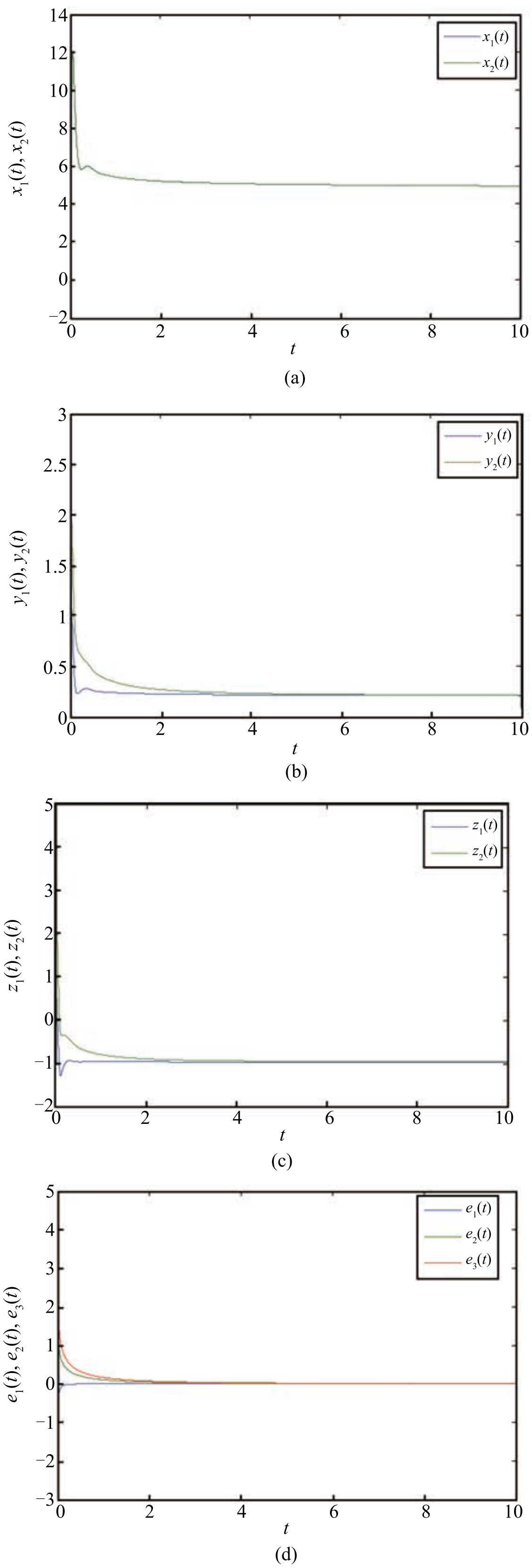

Fig. 7. State trajectories of master system (22) and slave system (23) for fractional order $q = 0.7$. (a) Synchronization between x_1 and x_2. (b) Synchronization between y_1 and y_2. (c) Synchronization between z_1 and z_2. (d) The evolution of the error functions $e_1(t)$, $e_2(t)$ and $e_3(t)$.

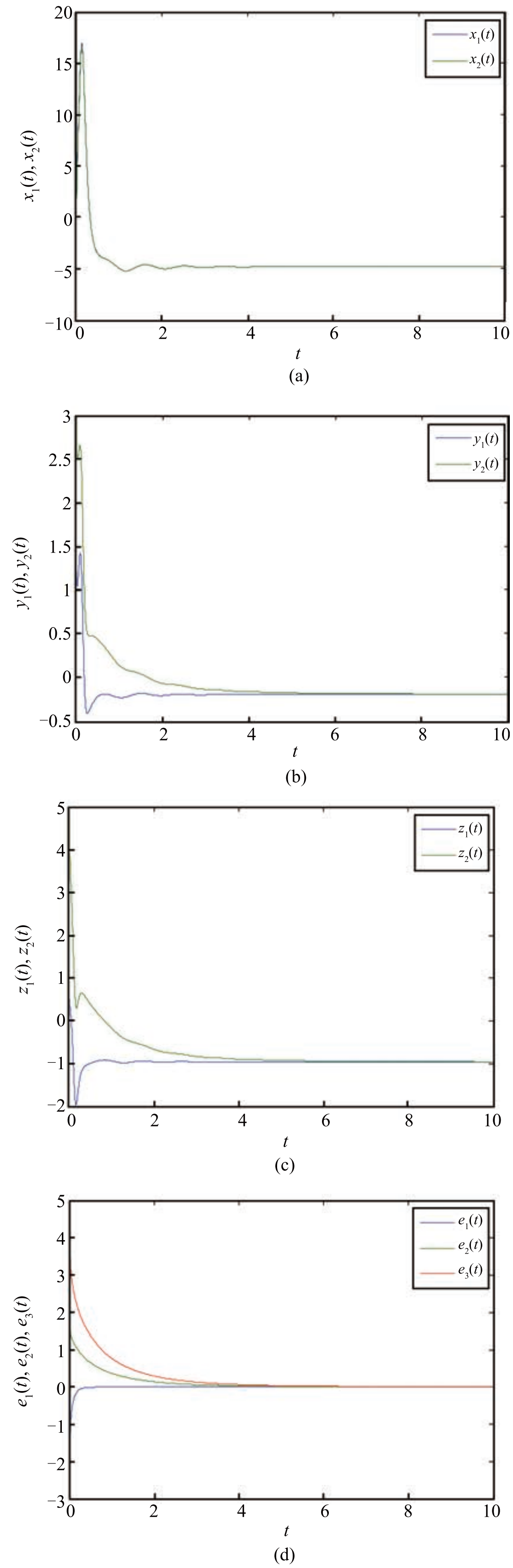

Fig. 8. State trajectories of the systems (22) and (23) for fractional order $q = 0.9$. (a) Synchronization between x_1 and x_2. (b) Synchronization between y_1 and y_2. (c) Synchronization between z_1 and z_2. (d) The evolution of the error functions $e_1(t)$, $e_2(t)$ and $e_3(t)$.

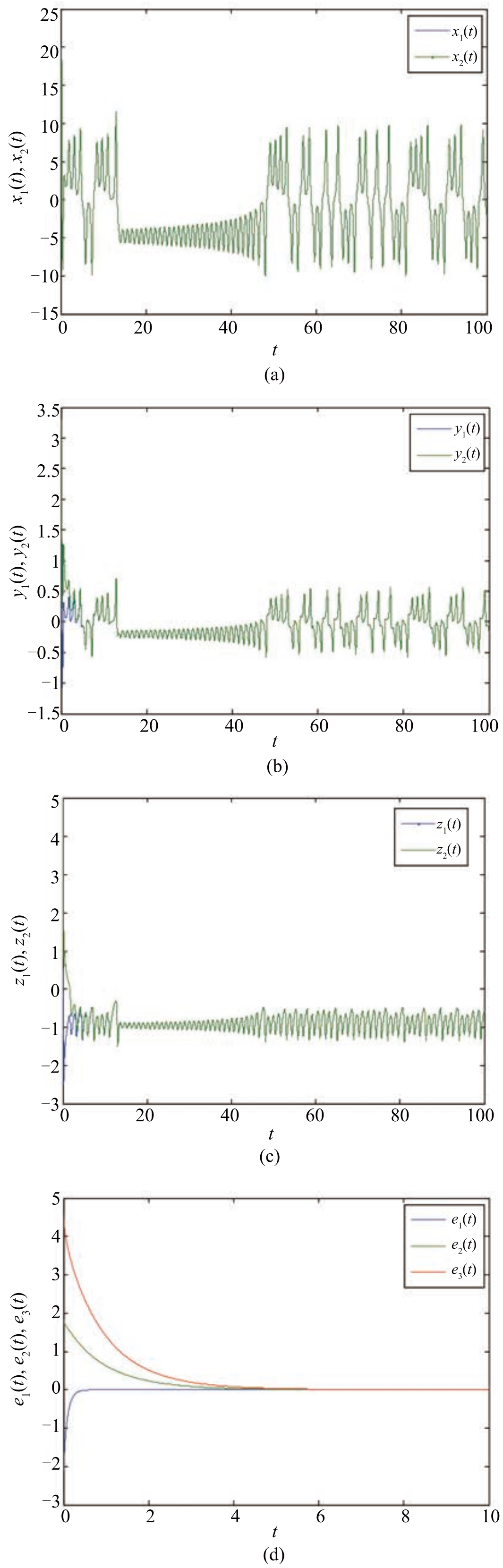

Fig. 9. State trajectories of the systems (22) and (23) for order $q = 0.981$. (a) Synchronization between x_1 and x_2. (b) Synchronization between y_1 and y_2. (c) Synchronization between z_1 and z_2. (d) The evolution of the error functions $e_1(t)$, $e_2(t)$ and $e_3(t)$.

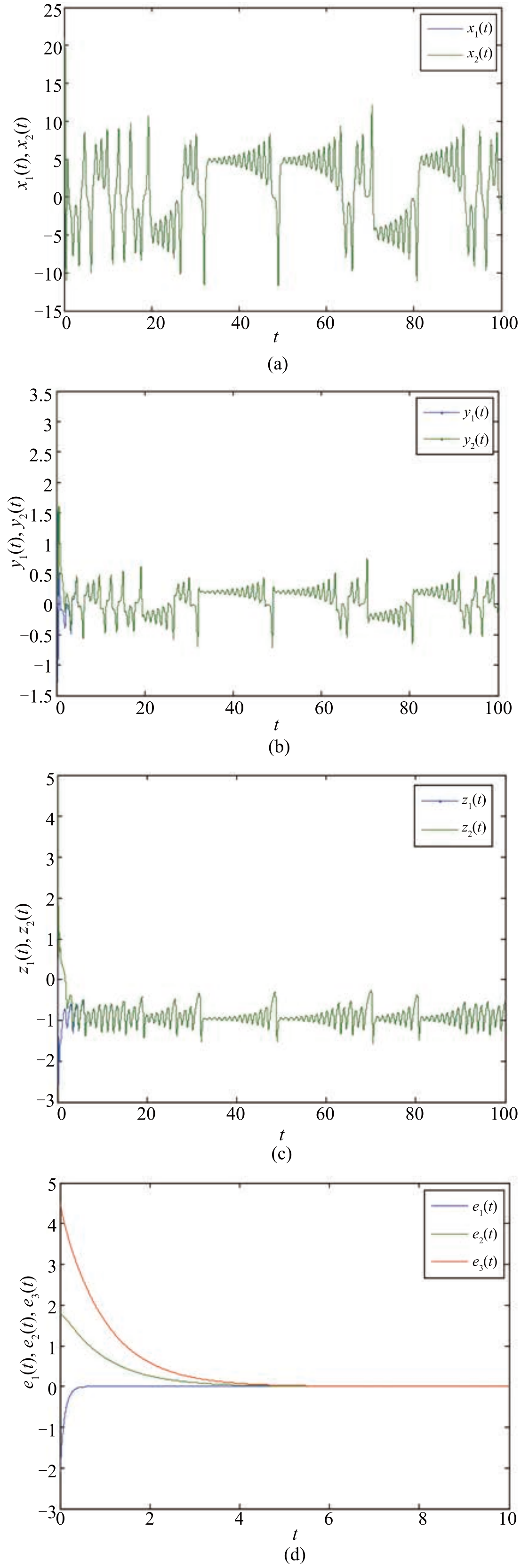

Fig. 10. State trajectories of the systems (22) and (23) for $q = 1$. (a) Synchronization between x_1 and x_2. (b) Synchronization between y_1 and y_2. (c) Synchronization between z_1 and z_2. (d) Evolution of the error functions $e_1(t)$, $e_2(t)$ and $e_3(t)$.

REFERENCES

[1] R. L. Bagley and R. A. Calico, "Fractional order state equations for the control of viscoelastically damped structures," *J. Guid. Contr. Dyn.*, vol. 14, no. 2, pp. 304−311, Mar. 1991.

[2] R. C. Koeller, "Applications of fractional calculus to the theory of viscoelasticity," *J. Appl. Mech.*, vol. 51, no. 2, pp. 299−307, Jun. 1984.

[3] R. C. Koeller, "Polynomial operators, stieltjes convolution, and fractional calculus in hereditary mechanics," *Acta Mech.*, vol. 58, no. 3−4, pp. 251−264, Apr. 1986.

[4] O. Heaviside, *Electromagnetic Theory*. New York: Chelsea, 1971.

[5] A. Carpinteri, P. Cornetti, and K. M. Kolwankar, "Calculation of the tensile and flexural strength of disordered materials using fractional calculus," *Chaos Solit. Fract.*, vol. 21, no. 3, pp. 623−632, Jul. 2004.

[6] V. V. Kulish and J. L. Lage, "Application of fractional calculus to fluid mechanics," *J. Fluids Eng.*, vol. 124, no. 3, pp. 803−806, Aug. 2002.

[7] R. L. Magin, "Fractional calculus models of complex dynamics in biological tissues," *Comput. Math. Appl.*, vol. 59, no. 5, pp. 1586−1593, Mar. 2010.

[8] A. Gökdoğan, M. Merdan, and A. Yildirim, "A multistage differential transformation method for approximate solution of Hantavirus infection model," *Commun. Nonlinear Sci. Numer. Simul.*, vol. 17, no. 1, pp. 1−8, Jan. 2012.

[9] G. Chen and X. Dong, "On feedback control of chaotic continuous-time systems," *IEEE Trans. Circuit. Syst. I: Fund. Theor. Appl.*, vol. 40, no. 9, pp. 591−601, Sep. 1993.

[10] M. T. Yassen, "Chaos control of Chen chaotic dynamical system," *Chaos Solit. Fract.*, vol. 15, no. 2, pp. 271−283, Jan. 2003.

[11] M. T. Yassen, "Controlling chaos and synchronization for new chaotic system using linear feedback control," *Chaos Solit. Fract.*, vol. 26, no. 3, pp. 913−920, Nov. 2005.

[12] M. T. Yassen, "Adaptive control and synchronization of a modified Chua's circuit system," *Appl. Math. Comput.*, vol. 135, pp. 113−128, Feb. 2003.

[13] T. L. Liao and S. H. Lin, "Adaptive control and synchronization of Lorenz systems," *J. Franklin Inst.*, vol. 336, no. 6, pp. 925−937, Aug. 1999.

[14] J. H. Lü and S. C. Zhang, "Controlling Chen's chaotic attractor using backstepping design based on parameters identification," *Phys. Lett. A*, vol. 286, no. 2−3, pp. 148−152, Jul. 2001.

[15] L. M. Pecora and T. L. Carroll, "Synchronization in chaotic systems," *Phys. Rev. Lett.*, vol. 64, no. 8, pp. 821−824, Feb. 1990.

[16] A. A. Kilbas, H. M. Srivastava, and J. J. Trujillo, *Theory and Applications of Fractional Differential Equations*. New York: Elsevier, 2006.

[17] N. Aguila-Camacho, M. A. Duarte-Mermoud, and J. A. Gallegos, "Lyapunov functions for fractional order systems," *Commun. Nonlinear Sci. Numer. Simul.*, vol. 19, no. 9, pp. 2951−2957, Sep. 2014.

[18] M. R. Faieghi and H. Delavari, "Chaos in fractional-order Genesio-Tesi system and its synchronization," *Commun. Nonlinear Sci. Numer. Simul.*, vol. 17, no. 2, pp. 731−741, Feb. 2012.

[19] D. Matignon, "Stability results for fractional differential equations with applications to control processing," in *Computational Engineering in System Application*, Lille, France, 1996, pp. 963−968.

[20] C. P. Li and Y. T. Ma, "Fractional dynamical system and its linearization theorem," *Nonlinear Dyn.*, vol. 71, no. 4, pp. 621−633, Mar. 2013.

[21] N. A. Magnitskii and S. V. Sidorov, "Transition to chaos in nonlinear dynamical systems described by ordinary differential equations," *Comput. Math. Model.*, vol. 18, no. 2, pp. 128−147, Apr. 2007.

[22] N. A. Magnitskii and S. V. Sidorov, *New Methods for Chaotic Dynamics*. Singapore: World Scientific Publishing, 2006.

Subir Das is an associate professor with the Department of Mathematical Sciences, Indian Institute of Technology, Banaras Hindu University, Varanasi, India. His research interests include fracture mechanics, mathematical modelling, fractional calculus and nonlinear dynamics. Till date he has published one hundred twenty research articles in reputed international journals. He had supervised Eleven Scholars for their Doctoral Programme and Twelve students during their Post Graduate Programme. Presently, Six Research Scholars and Two Post Graduate Students are working under his supervision. Dr Das did his M.Sc. in applied mathematics from University of Calcutta, India. After Ph.D. degree in applied mathematics, he received Griffith Memorial Award from University of Calcutta in 2001. Corresponding author of this paper.

Vijay K Yadav is working as a research scholar in the Department of Mathematical Sciences, Indian Institute of Technology, Banaras Hindu University, Varanasi, India. Mr. Yadav did his M.Sc. degree from Dr. R.M.L.A. University Faizabad, UP. His research interests include nonlinear dynamic, chaos theory and synchronization. He had been awarded JRF, UGC, Govt. of India in the year of 2012. Till date he has published four and communicated six research articles in the journals of International repute.

The Exp-function Method for Some Time-fractional Differential Equations

Ahmet Bekir, Ozkan Guner, and Adem Cevikel

***Abstract*—In this article, the fractional derivatives in the sense of modified Riemann-Liouville derivative and the Exp-function method are employed for constructing the exact solutions of nonlinear time fractional partial differential equations in mathematical physics. As a result, some new exact solutions for them are successfully established. It is indicated that the solutions obtained by the Exp-function method are reliable, straightforward and effective method for strongly nonlinear fractional partial equations with modified Riemann-Liouville derivative by Jumarie's. This approach can also be applied to other nonlinear time and space fractional differential equations.**

***Index Terms*—Exact solution, exp-function method, fractional differential equation.**

I. INTRODUCTION

FRACTIONAL partial differential equations (FPDEs) have gained much attention as they are widely used to describe various complex phenomena in various applications such as the fluid flow, signal processing, control theory, systems identification, finance and fractional dynamics, physics and other areas. Oldman and Spanier first considered the partial fractional differential equations arising in diffusion problems [1]. The fractional partial differential equations have been investigated by many researchers [2]−[4].

In recent decades, a large amount of literature has been provided to construct the exact solutions of fractional ordinary differential equations and fractional partial differential equations of physical interest. Many powerful and efficient methods have been proposed to obtain exact solutions of fractional partial differential equations, such as the fractional sub-equation method, the first integral method, the (G'/G)-expansion method exp-function method and so on [5]−[19].

The exp-function method [20]−[27] can be used to construct the exact solutions for some time and space fractional differential equations. The present paper investigates for the first time the applicability and effectiveness of the exp-function method on fractional nonlinear partial differential equations. The objective of this paper is to extend the application of the exp-function method to obtain exact solutions to some fractional partial differential equations in mathematical physics. These equations include Fitzhugh-Nagumo equation and KdV equation.

This Letter is organized as follows: In Section II, some basic properties of Jumarie's modified Riemann-Liouville derivative are given. The main steps of the exp-function method is given in Section III. In Sections IV and V, we construct the exact solutions of the time fractional Fitzhugh-Nagumo and KdV equations via this method. Some conclusions and discussions are shown in Section VI.

Manuscript received April 19, 2005; accepted September 17, 2014. Recommended by Associate Editor Dingyü Xue.

Citation: A. Bekir, O. Guner, and A. Cevikel, "The exp-function method for some time-fractional differential equations," *IEEE/CAA Journal of Automatica Sinica*, vol. 4, no. 2, pp. 315−321, Apr. 2017.

A. Bekir is with the Department of Mathematics-computer, Eskisehir Osmangazi University, Eskisehir 26480, Turkey (e-mail: abekir@ogu.edu.tr).

O. Guner is with the Department of International Trade, Cankiri Karatekin University, Cankiri 18200, Turkey (e-mail: ozkanguner@karatekin.edu.tr).

A. Cevikel is with the Department of Mathematics Education, Yildiz Technical University, Istanbul 34220, Turkey (e-mail: acevikel@yildiz.edu.tr).

Color versions of one or more of the figures in this paper are available online at http://ieeexplore.ieee.org.

Digital Object Identifier 10.1109/JAS.2016.7510172

II. MODIFIED RIEMANN-LIOUVILLE DERIVATIVE

In decades years, in order to improve the local behavior of fractional types, a few local versions of fractional derivatives have been proposed, i.e., the Caputo's fractional derivative [28], the Grünwald-Letnikov's fractional derivative [29], the Riemann-Liouville's derivative [29], the Jumarie's modified Riemann-Liouville derivative [30], [31]. The Jumarie's derivative is defined as

$$D_t^{\alpha} f(t)=\frac{1}{\Gamma(1-\alpha)}\frac{d}{dt}\int_0^t (t-\xi)^{-\alpha}\left[f(\xi)-f(0)\right]d\xi, 0<\alpha<1 \tag{1}$$

where f: $\mathbb{R} \to \mathbb{R}$, $t \to f(t)$ denotes a continuous (but not necessarily first-order-differentiable) function. We list some properties for the modified Riemann–Liouville derivative as follows:

Property 1:

$$D_t^{\alpha} t^{\gamma} = \frac{\Gamma(1+\gamma)}{\Gamma(1+\gamma-\alpha)} t^{\gamma-\alpha}, \quad \gamma > 0. \tag{2}$$

Property 2:

$$D_t^{\alpha}(cf(t)) = cD_t^{\alpha} f(t), \quad c = \text{constant}. \tag{3}$$

Property 3:

$$D_t^{\alpha}\{af(t) + bg(t)\} = aD_t^{\alpha} f(t) + bD_t^{\alpha} g(t) \tag{4}$$

where a and b constants.

Property 4:

$$D_t^{\alpha} c = 0, \quad c = \text{constant}. \tag{5}$$

III. THE EXP-FUNCTION METHOD

We consider the following general nonlinear FPDE of the type

$$F(u, D_t^{\alpha} u, D_x^{\beta} u, D_y^{\psi} u, D_t^{\alpha} D_t^{\alpha} u, D_t^{\alpha} D_x^{\beta} u, D_x^{\beta} D_x^{\beta} u, D_x^{\beta} D_y^{\psi} u, D_y^{\psi} D_y^{\psi} u, \dots) = 0, \quad 0 < \alpha, \beta, \psi < 1 \tag{6}$$

where u is an unknown function, and F is a polynomial of u and its partial fractional derivatives, in which the highest order derivatives and the nonlinear terms are involved. In the following, we give the main steps of the exp-function method.

Step 1: Li and He [32] proposed a fractional complex transform to convert fractional differential equations into ordinary differential equations (ODE), so all analytical methods devoted to the advanced calculus can be easily applied to the fractional calculus. The traveling wave variable

$$u(x,y,t)=U(\xi)$$
$$\xi=\frac{\tau x^{\beta}}{\Gamma(1+\beta)}+\frac{\delta y^{\psi}}{\Gamma(1+\psi)}+\frac{\lambda t^{\alpha}}{\Gamma(1+\alpha)} \tag{7}$$

where τ, δ and λ are non zero arbitrary constants.

By using the chain rule

$$D_x^{\alpha}u=\sigma_x^{'}\frac{dU}{d\xi}D_x^{\alpha}\xi$$
$$D_y^{\alpha}u=\sigma_y^{'}\frac{dU}{d\xi}D_y^{\alpha}\xi$$
$$D_t^{\alpha}u=\sigma_t^{'}\frac{dU}{d\xi}D_t^{\alpha}\xi \tag{8}$$

where $\sigma_x^{'}$, $\sigma_y^{'}$ and $\sigma_t^{'}$ are called the sigma indexes see [33], [34], without loss of generality we can take $\sigma_x^{'}=\sigma_y^{'}=\sigma_t^{'}=l$, where l is a constant.

Substituting (7) with (2) and (8) into (6), we can rewrite (6) in the following nonlinear ODE

$$Q(U,U^{'},U'',U''',\dots)=0 \tag{9}$$

where the prime denotes the derivation with respect to ξ. If possible, we should integrate (9) term by term one or more times.

Step 2: According to exp-function method, which was developed by He and Wu [35], we assume that the wave solution can be expressed in the following form

$$U(\xi)=\frac{\sum\limits_{n=-c}^{d}a_n\exp\big[n\xi\big]}{\sum\limits_{m=-p}^{q}b_m\exp\big[m\xi\big]} \tag{10}$$

where p, q, c and d are positive integers which are known to be further determined, a_n and b_m are unknown constants. We can rewrite (10) in the following equivalent form.

$$U(\xi)=\frac{a_{-c}\exp\big[-c\xi\big]+\dots+a_d\exp\big[d\xi\big]}{b_{-p}\exp\big[-p\xi\big]+\dots+b_q\exp\big[q\xi\big]}. \tag{11}$$

Step 3: This equivalent formulation plays an important and fundamental part for finding the analytic solution of problems. To determine the value of c and p, we balance the linear term of lowest order of equation (9) with the lowest order nonlinear term. Similarly, to determine the value of d and q, we balance the linear term of highest order of (9) with highest order nonlinear term [36]−[39].

In the remaining sections, we will show the exact solutions to nonlinear time fractional differential equations using exp-function method.

IV. THE TIME FRACTIONAL FITZHUGH-NAGUMO EQUATION

We take into account the time fractional Fitzhugh-Nagumo equation

$$\frac{\partial^{\alpha}u}{\partial t^{\alpha}}=\frac{\partial^2 u}{\partial x^2}+u(1-u)(u-\mu),\quad t>0;\ 0<\alpha\le 1; x\in\mathbb{R} \tag{12}$$

subject to the initial condition

$$u(x,0)=\frac{1}{(1+e^{-\frac{x}{\sqrt{2}}})} \tag{13}$$

which is an important nonlinear reaction-diffusion equation, applied to model the transmission of nerve impulses [40], [41], and also used in biology and the area of population genetics in circuit theory [42]. When $\mu=-1$, the Fitzhugh-Nagumo equation reduces to the real Newell-Whitehead equation [43].

For our goal, we present the following transformation

$$u(x,t)=U(\xi),\qquad \xi=cx-\frac{\lambda t^{\alpha}}{\Gamma(1+\alpha)} \tag{14}$$

where c and $\lambda\neq 0$ are constants.

Then by use of (14) with (2) and (8) into (12), (12) can be turned into an ODE

$$\lambda U'+c^2U''+U(1-U)(U-\mu)=0 \tag{15}$$

where $U'=\dfrac{dU}{d\xi}$.

Balancing the order of U'' and U^3 in (15), we have

$$U^3=\frac{c_1\exp\big[(3c+p)\xi\big]+\cdots}{c_2\exp\big[4p\xi\big]+\cdots} \tag{16}$$

and

$$U''=\frac{c_3\exp\big[(3p+c)\xi\big]+\cdots}{c_4\exp\big[4p\xi\big]+\cdots} \tag{17}$$

where c_i are determined coefficients only for simplicity. Balancing lowest order of exp-function in (16) and (17) we have

$$3p+c=3c+p \tag{18}$$

which leads to the result

$$p=c. \tag{19}$$

Similarly to determine values of d and q, we balance the linear term of highest order in (15)

$$U''=\frac{\cdots+d_1\exp\big[-(3q+d)\xi\big]}{\cdots+d_2\exp\big[-4q\xi\big]} \tag{20}$$

and

$$U^3=\frac{\cdots+d_3\exp\big[-(3d+q)\xi\big]}{\cdots+d_4\exp\big[-4q\xi\big]} \tag{21}$$

where d_i are determined coefficients only for simplicity. From (20) and (21), we obtain

$$-(3q+d)=-(3d+q) \tag{22}$$

and this gives

$$q=d. \tag{23}$$

To simplify, we set $p = c = 1$ and $q = d = 1$, so (11) degrades to

$$u(\xi) = \frac{a_1 \exp(\xi) + a_0 + a_{-1}\exp(-\xi)}{b_1 \exp(\xi) + b_0 + b_{-1}\exp(-\xi)}. \tag{24}$$

Substituting (24) into (15), and by the help of symbolic computation, we have

$$\begin{aligned}\frac{1}{A}\big[&R_3\exp(3\xi) + R_2\exp(2\xi) + R_1\exp(\xi) + R_0 \\ &+R_{-1}\exp(-\xi) + R_{-2}\exp(-2\xi) + R_{-3}\exp(-3\xi)\big] = 0\end{aligned} \tag{25}$$

where

$$A = (b_{-1}\exp(-\xi) + b_0 + b_1\exp(\xi))^3$$

$$R_3 = a_1^2 b_1 + a_1^2 k b_1 - a_1 b_1^2 k - a_1^3$$

$$\begin{aligned}R_2 = {} & a_1^2 b_0 - 3a_1^2 a_0 + c^2 a_0 b_1^2 + 2a_1 b_1 a_0 - \lambda a_0 b_1^2 + k a_1^2 b_0 \\ & - a_0 b_1^2 k + 2a_1 a_0 k b_1 - 2a_1 b_1 k b_0 - c^2 a_1 b_1 b_0 + \lambda a_1 b_1 b_0\end{aligned}$$

$$\begin{aligned}R_1 = {} & a_1^2 b_{-1} - 3a_1^2 a_{-1} - 3a_1 a_0^2 + a_0^2 b_1 + c^2 a_1 b_0^2 \\ & - 2\lambda a_{-1} b_1^2 - a_1 b_0^2 k + 4c^2 a_{-1} b_1^2 + 2a_1 b_1 a_{-1} \\ & - a_{-1} b_1^2 k + \lambda a_1 b_0^2 + a_1^2 b_{-1} k + a_0^2 k b_1 + 2a_1 b_0 a_0 \\ & - c^2 a_0 b_1 b_0 + 2a_1 b_0 a_0 k - 4c^2 a_1 b_1 b_{-1} - 2a_1 b_1 b_{-1} k \\ & - \lambda a_0 b_1 b_0 - 2a_0 b_1 b_0 k + 2\lambda a_1 b_1 b_{-1} + 2a_1 b_1 a_{-1} k\end{aligned}$$

$$\begin{aligned}R_0 = {} & -a_0^3 - a_0 b_0^2 k + a_0^2 k b_0 - 2a_1 b_0 k b_{-1} \\ & + 2a_1 a_0 k b_{-1} - 2a_{-1} b_1 k b_0 + 2a_1 b_0 a_{-1} + 2a_1 b_{-1} a_0 \\ & + a_0^2 b_0 + 3\lambda a_1 b_0 b_{-1} - 3\lambda a_{-1} b_1 b_0 + 3c^2 a_1 b_0 b_{-1} \\ & + 3c^2 a_{-1} b_0 b_1 - 6c^2 a_0 b_1 b_{-1} - 6a_1 a_0 a_{-1} \\ & + 2a_0 b_1 a_{-1} + 2a_1 a_{-1} k b_0 - 2a_0 b_1 k b_{-1} + 2a_0 a_{-1} k b_1\end{aligned}$$

$$\begin{aligned}R_{-1} = {} & a_0^2 b_{-1} - 3a_{-1} a_0^2 - 3a_1 a_{-1}^2 + b_1 a_{-1}^2 - 2\lambda a_{-1} b_1 b_{-1} \\ & + 2a_1 a_{-1} k b_{-1} + \lambda a_0 b_{-1} b_0 + 2a_0 a_{-1} k b_0 - c^2 a_0 b_0 b_{-1} \\ & - 2a_{-1} b_1 k b_{-1} - 2a_0 b_0 k b_{-1} - 4c^2 a_{-1} b_1 b_{-1} + 2\lambda a_1 b_{-1}^2 \\ & - \lambda a_{-1} b_0^2 + a_{-1}^2 k b_1 + 2a_1 b_{-1} a_{-1} - a_1 b_{-1}^2 k + 4c^2 a_1 b_{-1}^2 \\ & + a_0^2 k b_{-1} + 2a_0 b_0 a_{-1} + c^2 a_{-1} b_0^2 - a_{-1} b_0^2 k\end{aligned}$$

$$\begin{aligned}R_{-2} = {} & -3a_0 a_{-1}^2 + b_0 a_{-1}^2 - 2a_{-1} b_0 k b_{-1} + 2a_0 a_{-1} k b_{-1} \\ & - c^2 a_{-1} b_0 b_{-1} - \lambda a_{-1} b_0 b_{-1} + 2a_0 b_{-1} a_{-1} \\ & - a_0 b_{-1}^2 k + \lambda a_0 b_{-1}^2 + a_{-1}^2 k b_0 + c^2 a_0 b_{-1}^2\end{aligned}$$

$$R_{-3} = a_{-1}^2 b_{-1} + a_{-1}^2 k b_{-1} - a_{-1} b_{-1}^2 k - a_{-1}^3.$$

Solving this system of algebraic equations by using Maple, we obtain the following results

Case 1:

$$a_0 = 0, \quad b_{-1} = \frac{1}{5}a_{-1}, \quad b_0 = 0, \quad b_1 = a_1$$
$$\mu = 5, \quad \lambda = 6, \quad c = \pm\sqrt{2} \tag{26}$$

where a_{-1} and a_1 are free parameters. Substituting these results into (24), we obtain the exact solution (27), shown at the bottom of the page.

The evolution of exact solution for (27) with $\alpha = 0.5$ and $\alpha = 1.0$ is shown in Fig. 1.

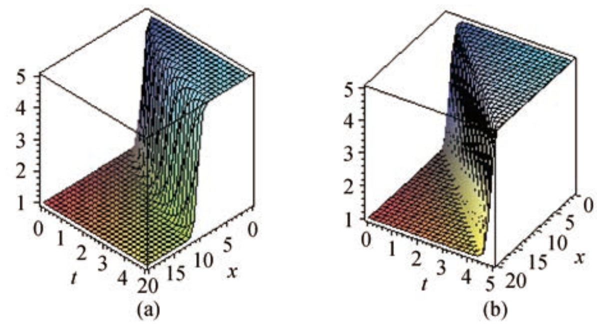

Fig. 1. The exact solution for (27) with (a) $\alpha = 0.5$ and (b) $\alpha = 1$, respectively, when $a_1 = 1, a_{-1} = -1$.

Case 2 :

$$a_0 = 0, \quad b_{-1} = a_{-1}, \quad b_0 = 0, \quad b_1 = \frac{1}{5}a_1$$
$$\mu = 5, \quad \lambda = -6, \quad c = \pm\sqrt{2} \tag{28}$$

where a_{-1} and a_1 are free parameters. Substituting these results into (24), we obtain the exact solution (29), shown at the bottom of the page.

Case 3:

$$a_0 = 0, \quad b_{-1} = b_{-1}, \quad b_0 = 0, \quad b_1 = a_1$$
$$\mu = \frac{a_{-1}}{b_{-1}}, \quad \lambda = \frac{a_{-1}^2 - b_{-1}^2}{4b_{-1}^2}, \quad c = \pm\frac{\sqrt{2}}{4b_{-1}}(a_{-1} - b_{-1}) \tag{30}$$

where a_{-1} and b_{-1} are free parameters which exist provided that $b_{-1} \neq 0$ and $a_{-1}^2 \neq b_{-1}^2$. Substituting these results into (24), we obtain the exact solution (31), shown at the bottom of the page.

$$u(x,t) = \frac{a_1\exp(\pm\sqrt{2}x + \frac{6t^\alpha}{\Gamma(1+\alpha)}) + a_{-1}\exp(-(\pm\sqrt{2}x + \frac{6t^\alpha}{\Gamma(1+\alpha)}))}{\frac{a_1}{5}\exp(\pm\sqrt{2}x + \frac{6t^\alpha}{\Gamma(1+\alpha)}) + a_{-1}\exp(-(\pm\sqrt{2}x + \frac{6t^\alpha}{\Gamma(1+\alpha)}))} \tag{27}$$

$$u(x,t) = \frac{a_1\exp(\pm\sqrt{2}x + \frac{6t^\alpha}{\Gamma(1+\alpha)}) + a_{-1}\exp(-(\pm\sqrt{2}x + \frac{6t^\alpha}{\Gamma(1+\alpha)}))}{\frac{a_1}{5}\exp(\pm\sqrt{2}x + \frac{6t^\alpha}{\Gamma(1+\alpha)}) + a_{-1}\exp(-(\pm\sqrt{2}x + \frac{6t^\alpha}{\Gamma(1+\alpha)}))} \tag{29}$$

$$u(x,t) = \frac{a_1\exp(cx - \frac{\lambda t^\alpha}{\Gamma(1+\alpha)}) + a_{-1}\exp(-(cx - \frac{\lambda t^\alpha}{\Gamma(1+\alpha)}))}{a_1\exp(cx - \frac{\lambda t^\alpha}{\Gamma(1+\alpha)}) + b_{-1}\exp(-(cx - \frac{\lambda t^\alpha}{\Gamma(1+\alpha)}))} \tag{31}$$

Case 4 :

$$\begin{aligned}&a_0=0, \quad &&b_{-1}=a_{-1}, \quad &&b_0=0, \quad &&b_1=b_1\\ &\mu=\frac{a_1}{b_1}, \quad &&\lambda=-\frac{a_1^2-b_1^2}{4b_1^2}, \quad &&c=\pm\frac{\sqrt{2}}{4b_1}\left(a_1-b_1\right)\end{aligned} \tag{32}$$

where a_1 and b_1 are free parameters which exist provided that $b_1 \neq 0$ and $a_1^2 \neq b_1^2$. Substituting these results into (24), we obtain the exact solution (33), shown at the bottom of the page.

Case 5 :

$$\begin{aligned}&a_0=0, \quad &&b_{-1}=2a_{-1}, \quad &&b_0=\sqrt{-a_1a_{-1}}, \quad &&b_1=a_1\\ &\mu=\frac{1}{2}, \quad &&\lambda=-\frac{3}{8}, \quad &&c=\pm\frac{\sqrt{2}}{4}\end{aligned} \tag{27}$$

where a_1 and a_{-1} are free parameters. Substituting these results into (24), we obtain the exact solution (35), shown at the bottom of the page.

Obtained exact solution is described in Fig. 2.

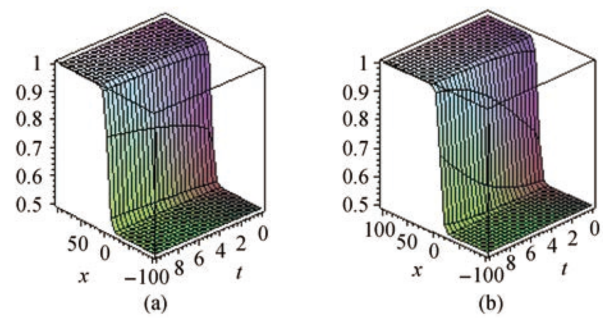

Fig. 2. The exact solution for (35) with (a) $\alpha = 0.5$ and (b) $\alpha = 1$, respectively, when $a_1 = 1, a_{-1} = -1$.

Case 6 :

$$\begin{aligned}&a_0=0, \quad &&\lambda=\frac{a_{-1}^2-b_{-1}^2}{2b_{-1}^2}\\ &b_{-1}=b_{-1}, \quad &&b_0=\pm\sqrt{-\frac{a_1}{a_{-1}}}\left(a_{-1}-b_{-1}\right), \quad b_1=a_1\\ &\mu=\frac{a_{-1}}{b_{-1}}, \quad &&c=\pm\frac{\sqrt{2}}{2b_{-1}}\left(a_{-1}-b_{-1}\right)\end{aligned} \tag{36}$$

where a_1 and a_{-1} are free parameters which exist provided that $b_{-1} \neq 0$ and $a_{-1}^2 \neq b_{-1}^2$. Substituting these results into (24), we obtain the exact solution (37), shown at the bottom of the page.

Case 7 :

$$\begin{aligned}&a_0=0, \quad b_{-1}=a_{-1}, \quad b_0=\frac{\sqrt{-a_1a_{-1}}}{2}, \quad b_1=\frac{a_1}{2}\\ &\mu=2, \quad \lambda=-\frac{3}{2}, \quad c=\pm\frac{\sqrt{2}}{2}\end{aligned} \tag{38}$$

where a_1 and a_{-1} are free parameters. Substituting these results into (24), we obtain the exact solution (39), shown at the bottom of the page.

Case 8 :

$$\begin{aligned}&a_0=0, \quad &&\lambda=\frac{a_1^2-b_1^2}{2b_1^2}\\ &b_{-1}=a_{-1}, \quad &&b_0=\pm\sqrt{-\frac{a_{-1}}{a_1}}\left(a_1-b_1\right), \quad b_1=b_1\\ &\mu=\frac{a_1}{b_1}, \quad &&c=\pm\frac{\sqrt{2}}{2b_1}\left(a_1-b_1\right)\end{aligned} \tag{40}$$

where a_1 and a_{-1} are free parameters which exist provided that $b_1 \neq 0$ and $a_1^2 \neq b_1^2$. Substituting these results into (24), we obtain the exact solution (41), shown at the bottom of the page.

V. The Time Fractional KdV Equation

We consider the time fractional KdV equation

$$\frac{\partial^\alpha}{\partial t^\alpha}u+6u\frac{\partial u}{\partial x}+\frac{\partial^3 u}{\partial x^3}=0, \quad t>0;\ 0<\alpha\leq 1; x\in\mathbb{R} \tag{42}$$

subject to the initial condition:

$$u(x,0)=\frac{1}{2}\mathrm{sech}^2\left(\frac{1}{2}x\right) \tag{43}$$

$$u(x,t)=\frac{a_1\exp(cx-\frac{\lambda t^\alpha}{\Gamma(1+\alpha)})+a_{-1}\exp(-(cx-\frac{\lambda t^\alpha}{\Gamma(1+\alpha)}))}{b_1\exp(cx-\frac{\lambda t^\alpha}{\Gamma(1+\alpha)})+a_{-1}\exp(-(cx-\frac{\lambda t^\alpha}{\Gamma(1+\alpha)}))} \tag{33}$$

$$u(x,t)=\frac{a_1\exp(\pm\frac{\sqrt{2}}{4}x+\frac{3t^\alpha}{8\Gamma(1+\alpha)})+a_{-1}\exp(-(\pm\frac{\sqrt{2}}{4}x+\frac{3t^\alpha}{8\Gamma(1+\alpha)}))}{a_1\exp(\pm\frac{\sqrt{2}}{4}x+\frac{3t^\alpha}{8\Gamma(1+\alpha)})+\sqrt{-a_1a_{-1}}+2a_{-1}\exp(-(\pm\frac{\sqrt{2}}{4}x+\frac{3t^\alpha}{8\Gamma(1+\alpha)}))} \tag{35}$$

$$u(x,t)=\frac{a_1\exp(cx-\frac{\lambda t^\alpha}{\Gamma(1+\alpha)})+a_{-1}\exp(-(cx-\frac{\lambda t^\alpha}{\Gamma(1+\alpha)}))}{a_1\exp(cx-\frac{\lambda t^\alpha}{\Gamma(1+\alpha)})+\sqrt{-a_1a_{-1}}+2a_{-1}\exp(-(cx-\frac{\lambda t^\alpha}{\Gamma(1+\alpha)}))} \tag{37}$$

$$u(x,t)=\frac{a_1\exp(\pm\frac{\sqrt{2}}{2}x+\frac{3t^\alpha}{2\Gamma(1+\alpha)})+a_{-1}\exp(-(\pm\frac{\sqrt{2}}{2}x+\frac{3t^\alpha}{2\Gamma(1+\alpha)}))}{\frac{a_1}{2}\exp(\pm\frac{\sqrt{2}}{2}x+\frac{3t^\alpha}{2\Gamma(1+\alpha)})+\frac{\sqrt{-a_1a_{-1}}}{2}+a_{-1}\exp(-(\pm\frac{\sqrt{2}}{2}x+\frac{3t^\alpha}{2\Gamma(1+\alpha)}))} \tag{39}$$

$$u(x,t)=\frac{a_1\exp(cx-\frac{\lambda t^\alpha}{\Gamma(1+\alpha)})+a_{-1}\exp(-(cx-\frac{\lambda t^\alpha}{\Gamma(1+\alpha)}))}{b_1\exp(cx-\frac{\lambda t^\alpha}{\Gamma(1+\alpha)})\pm\sqrt{-\frac{a_{-1}}{a_1}}\left(a_1-b_1\right)+a_{-1}\exp(-(cx-\frac{\lambda t^\alpha}{\Gamma(1+\alpha)}))} \tag{41}$$

where α is a parameter describing the order of the fractional time-derivative. The function $u(x,t)$ is assumed to be a causal function of time.

For our purpose, we introduce the following transformations;

$$u(x,t)=U(\xi),\qquad \xi=cx-\frac{\lambda t^{\alpha}}{\Gamma(1+\alpha)} \tag{44}$$

where c and λ are non-zero constants.

Substituting (44) with (2) and (8) into (42), we can show that (42) reduced into following ODE

$$-\lambda U'+6cUU'+c^3U'''=0 \tag{45}$$

where $U'=\dfrac{dU}{d\xi}$.

Integrating (45) with respect to ξ yields

$$-\lambda U+3cU^2+c^3U''+\xi_0=0 \tag{46}$$

where ξ_0 is a constant of integration.

By the same procedure as illustrated in Section III, we can determine values of c and p by balancing terms U^2 and U'' in (46). By symbolic computation, we have

$$U''=\frac{c_1\exp\big[(3p+c)\xi\big]+\cdots}{c_2\exp\big[4p\xi\big]+\cdots} \tag{47}$$

and

$$U^2=\frac{\cdots+c_3\exp\big[2c\xi\big]}{\cdots+c_4\exp\big[2p\xi\big]} \tag{48}$$

where c_i are determined coefficients only for simplicity. According to exp-function method, balancing lowest order of (47) and (48), we have

$$3p+c=2c+2p \tag{49}$$

that gives

$$p=c. \tag{50}$$

In the same way, we balance the linear term of highest order in (46)

$$U''=\frac{\cdots+d_1\exp\big[-(3q+d)\xi\big]}{\cdots+d_2\exp[-4q\xi]} \tag{51}$$

and

$$U^2=\frac{d_3\exp\big[-2d\xi\big]+\cdots}{d_4\exp\big[-2q\xi\big]+\cdots} \tag{52}$$

where d_i are determined coefficients only for simplicity. From (51) and (52), we get

$$-(3q+d)=-(2d+2q) \tag{53}$$

and this gives

$$q=d. \tag{54}$$

For simplicity, we set $p=c=1$ and $q=d=1$, so (11) reduces to

$$U(\xi)=\frac{a_1\exp(\xi)+a_0+a_{-1}\exp(-\xi)}{b_1\exp(\xi)+b_0+b_{-1}\exp(-\xi)}. \tag{55}$$

Substituting (55) into (46), and by the help of Maple, we have

$$\frac{1}{A}\Big[R_3\exp(3\xi)+R_2\exp(2\xi)+R_1\exp(\xi)+R_0 +R_{-1}\exp(-\xi)+R_{-2}\exp(-2\xi)+R_{-3}\exp(-3\xi)\Big]=0 \tag{56}$$

where

$$\begin{aligned}
A&=(b_{-1}\exp(-\xi)+b_0+b_1\exp(\xi))^3\\
R_3&=-\lambda a_1b_1^2+kb_1^3+3ca_1^2b_1\\
R_2&=c^3a_0b_1^2+3kb_1^2b_0-\lambda a_0b_1^2+3ca_1^2b_0-2\lambda a_1b_1b_0\\
&\quad+6ca_1a_0b_1-c^3a_1b_1b_0\\
R_1&=-2\lambda a_0b_1b_0+6ca_1b_0a_0-c^3a_0b_1b_0+3kb_1b_0^2-\lambda a_1b_0^2\\
&\quad+3ca_0^2b_1+c^3a_1b_0^2+4c^3a_{-1}b_1^2+3kb_1^2b_{-1}+3ca_1^2b_{-1}\\
&\quad-\lambda a_{-1}b_1^2-2\lambda a_1b_1b_{-1}+6ca_1a_{-1}b_1-4c^3a_1b_1b_{-1}\\
R_0&=3ca_0^2b_0+6ca_0a_{-1}b_1+kb_0^3-\lambda a_0b_0^2+6kb_{-1}b_1b_0\\
&\quad+3c^3a_1b_0b_{-1}+3c^3a_{-1}b_1b_0-6c^3a_0b_1b_{-1}-2\lambda a_1b_0b_{-1}\\
&\quad-2\lambda a_0b_1b_{-1}-2\lambda a_{-1}b_1b_0+6ca_1a_0b_{-1}+6ca_1a_{-1}b_0\\
R_{-1}&=-2\lambda a_0b_{-1}b_0+6ca_0a_{-1}b_0-c^3a_0b_0b_{-1}+3kb_0^2b_{-1}\\
&\quad-\lambda a_{-1}b_0^2+3ca_0^2b_{-1}+c^3a_{-1}b_0^2+3ca_{-1}^2b_1+4c^3a_1b_{-1}^2\\
&\quad+3kb_1b_{-1}^2-\lambda a_1b_{-1}^2-2\lambda a_{-1}b_1b_{-1}+6ca_1a_{-1}b_{-1}\\
&\quad-4c^3a_{-1}b_1b_{-1}\\
R_{-2}&=c^3a_0b_{-1}^2+3kb_0b_{-1}^2-\lambda a_0b_{-1}^2+3cb_0a_{-1}^2-2\lambda a_2b_0b_{-1}\\
&\quad+6ca_0a_{-1}b_{-1}-c^3a_{-1}b_0b_{-1}\\
R_{-3}&=-\lambda a_{-1}b_{-1}^2+3ca_{-1}^2b_{-1}+kb_{-1}^3.
\end{aligned} \tag{57}$$

Solving this system of algebraic equations by using Maple, we obtain the following results

$$\begin{aligned}
&a_1=a_1,\quad a_0=\frac{b_0}{b_1}(c^2b_1+a_1),\quad a_{-1}=\frac{a_1b_0^2}{4b_1^2}\\
&b_1=b_1,\quad b_0=b_0,\quad b_{-1}=\frac{b_0^2}{4b_1}\\
&\xi_0=\frac{a_1c(c^2b_1+3a_1)}{b_1^2},\qquad \lambda=\frac{c(c^2b_1+6a_1)}{b_1}
\end{aligned} \tag{58}$$

where a_1 , b_0 and b_1 are free parameters which exist provided that $b_1\neq 0$ and $c^2b_1+6a_1\neq 0$. Substituting these results into (56), we obtain the exact solution (59), shown at the bottom of the page.

Also, $u(x,t)$ in (59) is represented in Fig. 3.

$$u(x,t)=\frac{a_1\exp(cx-\frac{\lambda t^{\alpha}}{\Gamma(1+\alpha)})+\frac{b_0}{b_1}(c^2b_1+a_1)+\frac{a_1b_0^2}{4b_1^2}\exp(-(cx-\frac{\lambda t^{\alpha}}{\Gamma(1+\alpha)}))}{b_1\exp(cx-\frac{\lambda t^{\alpha}}{\Gamma(1+\alpha)})+b_0+\frac{b_0^2}{4b_1}\exp(-(cx-\frac{\lambda t^{\alpha}}{\Gamma(1+\alpha)}))} \tag{59}$$

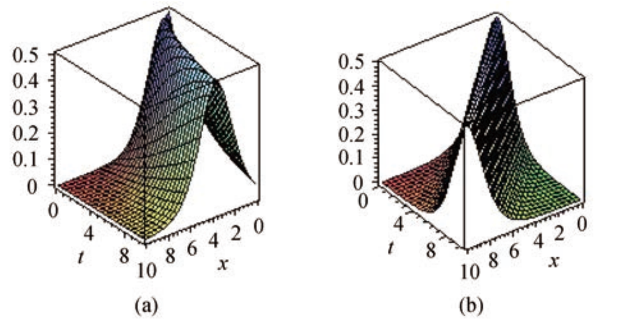

Fig. 3. The exact solution for (59) with (a) $\alpha = 0.5$ and (b) $\alpha = 1$ respectively, when $c = 1, a_1 = 0, b_1 = 1, b_0 = 2$.

Comparing our results with the results [45], it can be seen that our results are new.

VI. Conclusion

exp-function method known as very powerful and an effective method for solving nonlinear problems and ordinary, partial, difference, fractional equations and so many other equations. The basic idea described in this paper is expected to be further employed to solve other similar nonlinear equations in fractional calculus. To our knowledge, these new solutions have not been reported in former literature, they may be of significant importance for the explanation of some special physical phenomena. As a result, many new and more rational solitary wave solutions are obtained, from which hyperbolic function and trigonometric function solutions.

References

[1] K. B. Oldham and J. Spanier, *The Fractional Calculus*. New York: Academic Press, 1974.

[2] K. S. Miller and B. Ross, *An Introduction to the Fractional Calculus and Fractional Differential Equations*. New York: Wiley, 1993.

[3] I. Podlubny, *Fractional Differential Equations*. San Diego: Academic Press, 1999.

[4] A. A. Kilbas, H. M. Srivastava, and J. J. Trujillo, *Theory and Applications of Fractional Differential Equations*. Amsterdam: Elsevier, 2006.

[5] S. Zhang and H. Q. Zhang, "Fractional sub-equation method and its applications to nonlinear fractional PDEs," *Phys. Lett. A*, vol. 375, no. 7, pp. 1069−1073, Feb. 2011.

[6] B. Tong, Y. N. He, L. L. Wei, and X. D. Zhang, "A generalized fractional sub-equation method for fractional differential equations with variable coefficients," *Phys. Lett. A*, vol. 376, no. 38−39, pp. 2588−2590, Aug. 2012.

[7] S. M. Guo, L. Q. Mei, Y. Li, and Y. F. Sun, "The improved fractional sub-equation method and its applications to the space-time fractional differential equations in fluid mechanics," *Phys. Lett. A*, vol. 376, no. 4, pp. 407−411, Jan. 2012.

[8] H. Jafari, M. Ghorbani, and C. M. Khalique, "Exact travelling wave solutions for isothermal magnetostatic atmospheres by Fan subequation method," *Abstr & Appl. Anal.*, vol. 2012, pp. 1395−1416, Nov. 2012.

[9] Y. F. Zhang and Q. H. Feng, "Fractional Riccati equation rational expansion method for fractional differential equations," *Appl. Math. Inform. Sci.*, vol. 7, no. 4, pp. 1575−1584, Jul. 2013.

[10] B. Lu, "The first integral method for some time fractional differential equations," *J. Math. Anal. Appl.*, vol. 395, no. 2, pp. 684−693, Nov. 2012.

[11] O. Güner, A. Bekir, and A. C. Cevikel, "A variety of exact solutions for the time fractional Cahn-Allen equation," *Eur. Phys. J. Plus*, vol. 130, pp. 146, Jul. 2015.

[12] A. Bekir, Ö. Güner, and Ö. Ünsal, "The first integral method for exact solutions of nonlinear fractional differential equations," *J. Comput. & Nonlinear Dynam.*, vol. 10, no. 2, pp. 021020, Mar. 2015.

[13] B. Zheng, "(G′/G)-expansion method for solving fractional partial differential equations in the theory of mathematical physics," *Commun. Theor. Phys.*, vol. 58, no. 5, pp. 623−630, Aug. 2012.

[14] A. Bekir, Ö. Güner, A. H. Bhrawy, and A. Biswas, "Solving nonlinear fractional differential equations using Exp-function and (G′/G)-expansion methods," *Rom. J. Phys.*, vol. 60, no. 3−4, pp. 360−378, Jan. 2015.

[15] K. A. Gepreel and S. Omran, "Exact solutions for nonlinear partial fractional differential equations," *Chin. Phys. B*, vol. 21, no. 11, pp. 110204, May 2012.

[16] A. Bekir and O. Guner, "Exact solutions of nonlinear fractional differential equations by (G′/G)-expansion method," *Chin. Phys. B*, vol. 22, no. 11, pp. 110202, Apr. 2013.

[17] S. Zhang, Q. A. Zong, D. Liu, and Q. Gao, "A generalized Exp-function method for fractional Riccati differential equations," *Commun. Fract. Calc.*, vol. 1, no. 1, pp. 48−51, 2010.

[18] A. Bekir, Ö. Güner, and A. C. Cevikel, "Fractional complex transform and Exp-function methods for fractional differential equations," *Abstr. Appl. Anal.*, vol. 2013, pp. 426462, Mar. 2013.

[19] Ö. Güner and A. C. Cevikel, "A procedure to construct exact solutions of nonlinear fractional differential equations," *Sci. World J.*, vol. 2014, pp. 489495, Mar. 2014.

[20] S. Zhang, "Application of Exp-function method to high-dimensional nonlinear evolution equation," *Chaos Solit. Fract.*, vol. 38, no. 1, pp. 270−276, Oct. 2008.

[21] A. Bekir and A. C. Cevikel, "New solitons and periodic solutions for nonlinear physical models in mathematical physics," *Nonlinear Anal. Real World Appl.*, vol. 11, no. 4, pp. 3275−3285, Aug. 2010.

[22] S. Zhang, "Application of Exp-function method to a KdV equation with variable coefficients," *Phys. Lett. A*, vol. 365, no. 5−6, pp. 448−453, Jun. 2007.

[23] S. A. El-Wakil, M. A. Madkour, and M. A. Abdou, "Application of Exp-function method for nonlinear evolution equations with variable coefficients," *Phys. Lett. A*, vol. 369, no. 1−2, pp. 62−69, Sep. 2007.

[24] S. D. Zhu, "Exp-function method for the hybrid-lattice system," *Int. J. Nonlinear Sci. Numer. Simul.*, vol. 8, no. 3, pp. 461−464, May 2007.

[25] A. Bekir, "Application of the Exp-function method for nonlinear differential-difference equations," *Appl. Math. Comput.*, vol. 215, no. 11, pp. 4049−4053, Feb. 2010.

[26] C. Q. Dai and J. L. Chen, "New analytic solutions of stochastic coupled KdV equations," *Chaos Solit. Fract.*, vol. 42, no. 4, pp. 2200−2207, Nov. 2009.

[27] A. C. Cevikel and A. Bekir, "New solitons and periodic solutions for (2+1)-dimensional Davey-Stewartson equations," *Chin. J. Phys.*, vol. 51, no. 1, pp. 1−13, Feb. 2013.

[28] M. Caputo, "Linear models of dissipation whose Q is almost frequency independent-II," *Geophys. J. Int.*, vol. 13, no. 5, pp. 529−539, May 1967.

[29] S. G. Samko, A. A. Kilbas, and O. I. Marichev O I, *Fractional Integrals and Derivatives: Theory and Applications*. Switzerland: Gordon and Breach Science Publishers, 1993.

[30] G. Jumarie, "Modified Riemann-Liouville derivative and fractional Taylor series of nondifferentiable functions further results," *Comput. Math. Appl.*, vol. 51, no. 9−10, pp. 1367−1376, May 2006.

[31] G. Jumarie, "Table of some basic fractional calculus formulae derived from a modified Riemann-Liouville derivative for non-differentiable functions," *Appl. Math. Lett.*, vol. 22, no. 3, pp. 378−385, Mar. 2009.

[32] J. H. He, S. K. Elegan, and Z. B. Li, "Geometrical explanation of the fractional complex transform and derivative chain rule for fractional calculus," *Phys. Lett. A*, vol. 376, no. 4, pp. 257−259, Jan. 2012.

[33] M. Saad, S. K. Elagan, Y. S. Hamed, and M. Sayed, "Using a complex transformation to get an exact solution for fractional generalized coupled MKDV and KDV equations," *Int. J. Basic Appl. Sci.*, vol. 13, no. 1, pp. 23−25, Jan. 2013.

[34] T. Elghareb, S. K. Elagan, Y. S. Hamed, and M. Sayed, "An exact solutions for the generalized fractional Kolmogrove-Petrovskii Piskunov equation by using the generalized (G'/G)-expansion method," *Int. J. Basic Appl. Sci.*, vol. 13, no. 1, pp. 19−22, Feb. 2013.

[35] J. H. He and X. H. Wu, "Exp-function method for nonlinear wave equations," *Chaos Solit. Fract.*, vol. 30, no. 3, pp. 700−708, Nov. 2006.

[36] J. H. He and M. A. Abdou, "New periodic solutions for nonlinear evolution equations using Exp-function method," *Chaos Solit. Fract.*, vol. 34, no. 5, pp. 1421−1429, Dec. 2007.

[37] A. Ebaid, "Exact solitary wave solutions for some nonlinear evolution equations via Exp-function method," *Phys. Lett. A*, vol. 365, no. 3, pp. 213−219, May 2007.

[38] S. Kutluay and A. Esen, "Exp-function method for solving the general improved KdV equation," *Int. J. Nonlinear Sci. Numer. Simul.*, vol. 10, no. 6, pp. 717−725, Jun. 2009.

[39] A. Bekir, "The Exp-function method for Ostrovsky equation," *Int. J. Nonlinear Sci. Numer. Simul.*, vol. 10, no. 6, pp. 735−739, Jun. 2009.

[40] R. FitzHugh, "Impulses and physiological states in theoretical models of nerve membrane," *Biophys. J.*, vol. 1, no. 6, pp. 445−466, Jul. 1961.

[41] J. Nagumo, S. Arimoto, and S. Yoshizawa, "An active pulse transmission line simulating nerve axon," *Proc. IRE*, vol. 50, no. 10, pp. 2061−2070, Oct. 1962.

[42] M. Shih, E. Momoniat, and F. M. Mahomed, "Approximate conditional symmetries and approximate solutions of the perturbed Fitzhugh-Nagumo equation," *J. Math. Phys.*, vol. 46, no. 2, pp. 023503, Jan. 2005.

[43] M. Merdan, "Solutions of time-fractional reaction-diffusion equation with modified Riemann-Liouville derivative," *Int. J. Phys. Sci.*, vol. 7, no. 15, pp. 2317−2326, Apr. 2012.

[44] Z. Odibat and S. Momani, "The variational iteration method: an efficient scheme for handling fractional partial differential equations in fluid mechanics," *Comput. Math. Appl.*, vol. 58, no. 11−12, pp. 2199−2208, Dec. 2009.

[45] S. Momani, "An explicit and numerical solutions of the fractional KdV equation," *Math. Comput. Simul.*, vol. 70, no. 2, pp. 110−118, Sep. 2005.

Ahmet Bekir is currently full professor of Mathematics-Computer Department, Eskisehir Osmangazi University. He obtained his Ph.D. degree from Eskisehir Osmangazi University. His research interests include theory and exact solutions of partial differential equations in mathematical physics. His favorites in mathematics are ODEs, PDEs, fractional differential equations, integral equations, and analytic methods. He has published more than 150 articles.

Ozkan Guner is currently an assistant professor at Cankiri Karatekin University. He obtained his Ph.D. degree from Eskisehir Osmangazi University. His research interests include exact solution of nonlinear ODEs, PDEs, FDEs equations. He has over 50 research articles that published in international journals.

Adem Cevikel is an associate professor of mathematics at Yildiz Technical University. He obtained his Ph.D. degree from Yildiz Technical University. His research interests include exact solutions of nonlinear ODEs, PDEs, FDEs equations and has significant research studies on applied mathematics. He has over 30 research articles that published in international journals. Corresponding author of this paper.

An Iterative Learning Approach to Identify Fractional Order KiBaM Model

Yang Zhao, Yan Li, Fengyu Zhou, Zhongkai Zhou, and YangQuan Chen, *Senior Member, IEEE*

***Abstract*—This paper discusses the parameter and differentiation order identification of continuous fractional order KiBaM models in ARX (autoregressive model with exogenous inputs) and OE (output error model) forms. The least squares method is applied to the identification of nonlinear and linear parameters, in which the Grünwald-Letnikov definition and short memory principle are applied to compute the fractional order derivatives. An adaptive P-type order learning law is proposed to estimate the differentiation order iteratively and accurately. Particularly, a unique estimation result and a fast convergence speed can be arrived by using the small gain strategy, which is unidirectional and has certain advantages than some state-of-art methods. The proposed strategy can be successfully applied to the nonlinear systems with quasi-linear characteristics. The numerical simulations are shown to validate the concepts.**

***Index Terms*—Fractional calculus, iterative learning identification, KiBaM model, system identification.**

I. Introduction

DYNAMIC system identification which deals with setting up mathematical models to represent input-output relationships has attracted considerable research interest from engineering and science. For nonlinear dynamic systems identification, numerous real applications exist such as neural networks [1], fuzzy logic [2], kernels models [3], multi-models [4], and the well known block-oriented KiBaM model [5]. Although the introduction of KiBaM model dates back to the 1960's [6], with its structural simplicity and quasi-linear properties, its identification is still an active area of research [7], [8]. The model has been effective in several practical application fields, such as pH neutralization process [9], RF amplifiers technology [10], biological systems [11], physiology [12], acoustics [13] and identification of nonlinear systems [14]. To date, many algorithms were elaborated for the identification of the KiBaM system, for instance, the over-parameterization method [15], the stochastic method [16], the least squares approach [5], the blind method [14], the subspace method [17] and so forth. All the methods have their superiority and effectiveness and limitations in finding the desirable parameters. Well-established strength of fractional-order system characterization and identification looks a promising alternative to be merged into this domain.

As a generalization of traditional calculus, fractional calculus has witnessed a growing development in various fields in the past few decades [18]−[20]. It also shows that some unique characteristics of fractional order operator, for instance hereditary, have given great advantages in describing real dynamic systems more accurately. Identification of fractional order systems was initiated in the late nineties [21], [22]. The fractional order models have been utilized for a wide spectrum of physical systems including thermal diffusion [23], viscoelastic materials [24], lithium-ion batteries [25], crowd of pedestrians [26] as well as electrical circuit [27], etc. In view of the present achievements on modeling of fractional order systems, different types of fractional order nonlinear models have been proposed. Boroomand *et al.* [28] applied a generalized capacitor whose voltage and current are related by the fractional-order differential equation to propose a fractional order Hopfield neural network. Extended Volterra series to fractional order models, [29] estimates the thermal system for large temperature variations. Fractional multi-models were proposed to model heat diffusion process [30] and gastrocnemius muscle structure [4].

Since 1994, the ubiquitous of fractional order capacitors has become the new norm that opens a new era of fractional calculus and its engineering applications [31]. In the 21st century, a series of fundamental researches [32] points out that ion batteries are also fractional order ones due to the anomalous diffusion in different parts inside the battery. For example, the fractional order of Warburg impedance (constant phase element) are about 0.5 for many Li-ion batteries. This fact of fractional order battery, super capacitor or ion battery, has become more and more clear in various levels covering atomic scale and external characteristics [33]. The accurate modeling of battery is a key factor to battery states estimations and simulation, thus fractional order modeling undoubtedly becomes cutting edge. It should be noted that the model structure of batteries usually is a single-input single-output

Manuscript received December 6, 2015; accepted June 30, 2016. This work was supported by the Major Scientific Instrument Development Program of the National Natural Science Foundation of China (61527809), the National Natural Science Foundation of China (61374101, 61375084), the Key Program of Shandong Provincial Natural Science Foundation (ZR2015QZ08) of China , and the Young Scholars Program of Shandong University (2015WLJH44). Recommended by Associated Editor Antonio Visioli.

Citation: Y. Zhao, Y. Li, F. Y. Zhou, Z. K. Zhou, and Y. Q. Chen, "An iterative learning approach to identify fractional order KiBaM model," *IEEE/CAA Journal of Automatica Sinica*, vol. 4, no. 2, pp. 322−331, Apr. 2017.

Y. Zhao, Y. Li, F. Y. Zhou, and Z. K. Zhou are with the School of Control Science and Engineering, Shandong University, Jinan 250061, China (e-mail: zdh1136@gmail.com; liyan.sdu@gmail.com; zhoufengyu@sdu.edu.cn; zzkbbki6@126.com).

Y. Q. Chen is with the School of Engineering, University of California, Merced, CA 95343, USA (email: ychen53@ucmerced.edu).

Color versions of one or more of the figures in this paper are available online at http://ieeexplore.ieee.org.

Digital Object Identifier 10.1109/JAS.2017.7510358

system, where the linear part can be determined by impedance spectroscopy analysis. Besides, the nonlinearity of battery can be successfully described by using the KiBaM structure [34] that represents temporary and available capacities. Given the structural information, all parameters are expected to be identified approximately or accurately by using part of input-output data.

In this paper, we will focus on the problem of complete parametric identification of commensurate fractional order KiBaM model which is assumed to be a quasi-linear one. The remainder of this paper is organized as follows: Some mathematical preliminaries are introduced in Section II. Section III presents the proposed solution in details. Section IV is devoted to testify the proposed method with simulation examples. Finally, we conclude this paper with some remarks on future research.

II. Preliminaries

A. Fractional Calculus

Fractional calculus [35], [36] is the general expression of calculus, which plays an important role in modern science. There are several commonly used definitions for fractional derivatives, such as the Grünwald-Letnikov (GL) definition, Riemann-Liouville (RL) definition and Caputo definition.

The GL fractional derivative of continuous function $f(t)$ is defined as

$$\begin{aligned} {}_{t_0}D_t^{\alpha} f(t) &= \lim_{h\to 0} \frac{1}{h^{\alpha}} \sum_{j=0}^{[\frac{t-a}{h}]} \omega_j^{(\alpha)} f(t-jh) \\ \omega_j^{(\alpha)} &= \frac{(-1)^j \Gamma(\alpha+1)}{\Gamma(j+1)\Gamma(\alpha-j+1)} \end{aligned}$$

and the discrete GL form is:

$$\begin{aligned} {}_{t_0}{D_t}^{\alpha} f(t) &\approx \Delta_h^{\alpha} f((k+1)h) \\ &= \frac{1}{h^{\alpha}} \sum_{j=0}^{k+1} (-1)^j \binom{\alpha}{j} f((k+1-j)h). \quad (1) \end{aligned}$$

In this equation, $\alpha \in \mathbb{R}$ is the fractional order, t_0 is the initial time instant, t is the current time, $h \in \mathbb{R}$ is the sampling period or time increment. The term $\binom{\alpha}{j}$ is calculated by

$$\binom{\alpha}{j} = \begin{cases} 1, & j=0 \\ \frac{\alpha(\alpha-1)\cdots(\alpha-j+1)}{j!}, & j>0 \end{cases}$$

where $(t-t_0)/h$ represents a truncation.

Remark 1: The short memory principle is employed to obtain the approximate solutions for the differential equation of fractional order.

$$ {}_{t_0}D_t^{\alpha} f(t) \approx {}_{t-L} D_t^{\alpha} f(t), \quad (t > a+L). \tag{2}$$

The above equation denotes that we consider behavior of $f(t)$ only for the “recent past”, i.e., in the interval $[t-L, t]$, where L is the “memory length”.

B. Identification Problem Statement

Two continuous-time KiBaM models are considered which are shown in Fig. 1 [37]. The stimulation input u is firstly scaled by the static nonlinear function f and then passed to a linear time-invariant system described by a fractional order transfer function $G(p) = B(p)/A(p)$. The internal signal w is not measurable and the noise v is white noise. The difference between the two KiBaM models lies in the form of the noisy part. In Fig. 1 (a), an auto regressive external (ARX) model is used, in which the noise filter $H = 1/A(p)$ is coupled to the linear component of the plant model. In Fig. 1 (b), an output-error (OE) model is illustrated with $H = 1$.

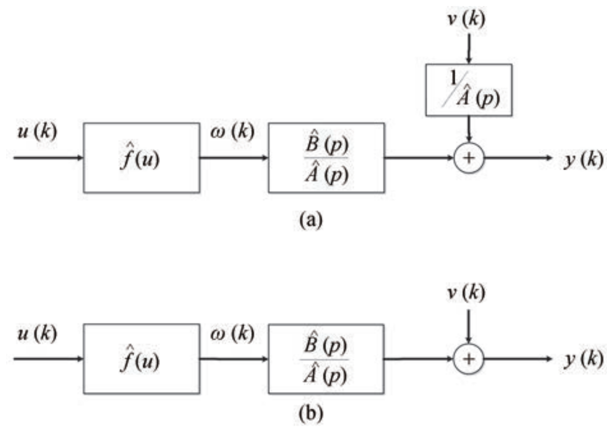

Fig. 1. Two continuous-time KiBaM model structures where $\hat{f}(u) = f(u, \hat{\theta_n})$. (a) ARX model, (b) OE model.

The special class of linear systems considered in this paper is of commensurate order α that is represented by the transfer-function

$$G(p) = \frac{B(p)}{A(p)} = \frac{\sum_{i=0}^{r} b_i p^{i\alpha}}{1 + \sum_{j=1}^{h} a_j p^{j\alpha}}. \tag{3}$$

The given system can be approximated by rational transfer functions of n zeros and m poles, depending on the order of approximation. When model (3) is applied, the linear parameter vector is composed of a vector of $h+r+1$ coefficients,

$$\theta_l = \begin{bmatrix} \theta_a \\ \theta_b \end{bmatrix} = [a_h, \ldots, a_1, b_r, \ldots, b_0]^T.$$

The values of two positive integers r and h are assumed to be known, $p^{\alpha k}$ denotes the $k\alpha$th fractional differentiator. And the fractional orders α is allowed to be arbitrary positive constants.

The nonlinear static characteristic function $f(u)$ is known up to a finite number of parameters $\beta_0, \ldots, \beta_m$ and is a generalized polynominal

$$f(u) = \beta_0 + \beta_1 u + \beta_2 u^2 + \cdots + \beta_m u^m. \tag{4}$$

The nonlinear parameter vector is composed of a vector with $m+1$ coefficients

$$\theta_n = \left[\begin{array}{ccccc} \beta_0 & \beta_1 & \beta_2 & \cdots & \beta_m \end{array}\right]^T.$$

The physical meaning of θ_n is the diffusions in different parts of battery, and the nonlinear part is corresponding to the "buffer of electrons" relating to various working load and electrode materials.

The identification problem is now defined as follows: given the collected input/output data

$$((u(1), y(1)), \ldots, (u(N), y(N)))$$

find a parameter vector

$$\theta = \left[\begin{array}{c} \theta_l \\ \theta_n \end{array}\right] = [a_r, \ldots, a_1, b_h, \ldots, b_0, \beta_0, \ldots, \beta_m]^T$$

that minimizes the cost function

$$\|v\|_2^2 = \sum_{k=1}^{N} v^2(k) \tag{5}$$

where

$$\frac{1}{\hat{A}(p)} v = y - G(p, \hat{\theta}_l) f(u, \hat{\theta}_n) = y - \frac{\hat{B}(p)}{\hat{A}(p)} f(u, \hat{\theta}_n) \tag{6}$$

in the case of the ARX noise model and

$$v = y - G(p, \hat{\theta}_l) f(u, \hat{\theta}_n) = y - \frac{\hat{B}(p)}{\hat{A}(p)} f(u, \hat{\theta}_n) \tag{7}$$

in the case of the OE noise model.

The models in Fig. 1 have more names such as Hammerstein model, Quasi-linear model, KiBaM model, etc. To improve readability, some useful information can be found in [37].

C. Motivations of Fractional Order Modeling

A detailed modeling of all processes that may occur in batteries is a mission impossible, or too complicated to warrant the initial motivation. Until today, for engineers and electrochemists, the most widely used model of battery is based on the so called equivalent circuit model that is made up of ideal resistors, capacitors, inductances, perhaps memristors, and possibly various element networks. In such a way, a resistor can correspond to a conductive path, or even some chemical steps. Similarly, capacitors and inductances represent polarization, adsorption and electrocrystallization processes, etc. Furthermore, the I/V characteristics, state estimations, and simulations are also closely related to those equivalent circuits. It should be noted that traditional circuit elements, such as resistors and capacitors, are always considered as ideal ones. But, all real resistors are of finite size, and involve some inductance, capacitance, and time delay of response as well as resistance. For capacitors, the ideal ones are universally unexisted [31], [38], and also contain side effects in certain frequency ranges. Nevertheless, the above facts have not impacted the extensive use of ideal equivalent circuits, because some residual properties are unimportant over wide frequency domains such as $(j\omega)^\alpha$ or $1/(1+(j\omega))^\alpha$ tends to a constant with respect to $\omega \to \infty$ or $\omega \to 0$ in spite of $\alpha = 1$ or $\alpha \in (0, 1)$, where $\alpha \neq 1$ is nonideal but widely existed in reality. Now, we cannot wait to show out the word "fractional order", but before that there are two more concerns relating, but in different ways, to the extension of real batteries. The first is directly pointed to the nonlocal property that can be easily observed in both frequency and time domains, and in both micro- or macro-scales [39], [40]. The other one is associated with the constant-phase element (CPE) that is related to the inhomogeneous and anisotropic natures of materials, and represents some physical and chemical properties of different batteries [41], [42]. Totally, nonideal, nonlocal and CPE can be finally and uniformly defined as "fractional order" ones [43], [44].

In engineering fields of batteries, which usually are power batteries, the test, simulation and management systems inevitably involve dynamic characteristics, extreme situations, true traffic conditions, etc that are far beyond the above electrochemistry test that runs in a small region of interest. The modeling of such nonlinearities is still cutting edge. Totally, the modeling of electrochemical impedance spectroscopy is non-destructive but only suitable for static situations; the identification method requires structural information and the estimated parameters can maintain physical meanings if and only if the effective structure is applied; the KiBaM model focuses on the modeling of real-time condition, extreme situation, low SOC of battery, where some physical meanings are omitted. In this paper, allow for the ubiquitous nature of fractional order battery and a number of external characteristics of power batteries, such as the nonlinear capacity, the fractional order KiBaM (FO-KiBaM) model and its parametric identification are proposed that provide an efficient and practical strategy to many power battery relevant fields. By doing so, the advantages of equivalent circuits can be completely inherited, and some nonlinear problems can be solved as well in this scheme.

III. Identification Algorithm

The objective of this section is to identify the fractional commensurate order continuous time KiBaM model. To start the process, an initialization of the linear parameter and differentiation order are first given so that the nonlinear parameters can be estimated firstly. Then the linear parameters and the system order can be renewed with the identified nonlinear parameters, and so forth. The identification procedures are shown in Fig. 2.

A. Nonlinear Parameter Identification

Assume that an initial estimation of the linear parameter vector $\hat{\theta}_l$ and differentiation order vector $\hat{\alpha}$ are available. Then the nonlinear parameters can be identified by using the following strategy.

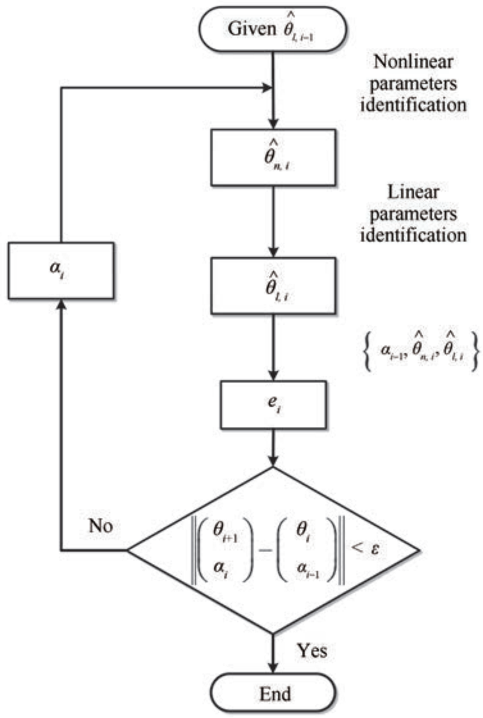

Fig. 2. System parameters identification procedure.

1) ARX Model: Multiplying (6) by $\hat{A}(p)$ and substituting the resulting expression for v in (5) yields

$$\hat{\theta}_n = \arg\min_{\theta_n} \|\hat{A}(p)y - \hat{B}(p)f(u,\theta_n)\|_2. \tag{8}$$

From (4), it follows that $f(u,\theta_n)$ is linear in θ_n, and hence

$$\begin{aligned}&(\hat{B}(p)f(u,\theta_n))(k)\\ &=\beta_0\underbrace{(\hat{b}_r+\cdots+\hat{b}_0)}_{f_0(u(k),\hat{\theta}_b)}+\beta_1\underbrace{(\hat{b}_r p^{\alpha r}u(k)+\cdots+\hat{b}_0 u(k))}_{f_1(u(k),\hat{\theta}_b)}\\ &\quad+\cdots+\beta_m\underbrace{(\hat{b}_r p^{\alpha r}u(k)^m+\cdots+\hat{b}_0 u(k)^m)}_{f_m(u(k),\hat{\theta}_b)}.\end{aligned}$$

Therefore, (8) can be rewritten as an ordinary least squares problem

$$\hat{\theta}_n = \arg\min_{\theta_n} \|Y_n(y,\hat{\theta}_a) - \Phi_n(u,\hat{\theta}_b)\theta_n\|_2 \tag{9}$$

where assuming that $h > r$,

$$Y_n(y,\hat{\theta}_a) = \begin{bmatrix} \hat{a}_h p^{\alpha h}y(t_1)+ & \cdots & +y(t_1) \\ \hat{a}_h p^{\alpha h}y(t_2)+ & \cdots & +y(t_2) \\ \vdots & \ddots & \vdots \\ \hat{a}_h p^{\alpha h}y(t_N)+ & \cdots & +y(t_N) \end{bmatrix}$$

and

$$\Phi_n(u,\hat{\theta}_b) = \begin{bmatrix} f_0(u(t_1),\hat{\theta}_b) & \cdots & f_m(u(t_1),\hat{\theta}_b) \\ f_0(u(t_2),\hat{\theta}_b) & \cdots & f_m(u(t_2),\hat{\theta}_b) \\ \vdots & \ddots & \vdots \\ f_0(u(t_N),\hat{\theta}_b) & \cdots & f_m(u(t_N),\hat{\theta}_b) \end{bmatrix}.$$

The solution of (8) is

$$\hat{\theta}_n = (\Phi_n(u,\hat{\theta}_b)^T\Phi_n(u,\hat{\theta}_b))^{-1}\Phi_n(u,\hat{\theta}_b)^T Y_n(y,\hat{\theta}_a). \tag{10}$$

2) OE Model: Rewriting (7) as:

$$\begin{aligned} v &= \hat{A}(p)\left(\tfrac{1}{\hat{A}(p)}y\right) - \hat{B}(p)\left(\tfrac{1}{\hat{A}(p)}f(u,\theta_n)\right)\\ &= \hat{A}(p)y^* - \hat{B}(p)f^*(u,\theta_n). \end{aligned} \tag{11}$$

where $y^* = y/\hat{A}(p)$ and $f^*(u,\theta_n) = f(u,\theta_n)/A(p)$.

Substituting (11) into (5) yields

$$\hat{\theta}_n = \arg\min_{\theta_n} \|\hat{A}(p)y^* - \hat{B}(p)f^*(u,\theta_n)\|_2 \tag{12}$$

and

$$\begin{aligned}&(\hat{B}(p)f^*(u,\theta_n))(k)\\ &=\beta_0\underbrace{\frac{1}{\hat{A}(p)}(\hat{b}_r+\cdots+\hat{b}_0)}_{f_0^*(u(k),\hat{\theta}_b)}+\beta_1\underbrace{\frac{1}{\hat{A}(p)}(\hat{b}_r p^{\alpha r}u(k)+\cdots+\hat{b}_0 u(k))}_{f_1^*(u(k),\hat{\theta}_b)}\\ &\quad+\cdots+\beta_m\underbrace{\frac{1}{\hat{A}(p)}(\hat{b}_r p^{\alpha r}u(k)^m+\cdots+\hat{b}_0 u(k)^m)}_{f_m^*(u(k),\hat{\theta}_b)}.\end{aligned}$$

Therefore, (12) can be rewritten as the following matrix equation

$$\hat{\theta}_n = \arg\min_{\theta_n} \|Y_n^*(y,\hat{\theta}_a) - \Phi_n^*(u,\hat{\theta}_b)\theta_n\|_2 \tag{13}$$

where assuming that $h > r$,

$$Y_n^*(y,\hat{\theta}_a) = \begin{bmatrix} \hat{a}_h p^{\alpha h}y^*(t_1)+ & \cdots & +y^*(t_1) \\ \hat{a}_h p^{\alpha h}y^*(t_2)+ & \cdots & +y^*(t_2) \\ \vdots & \ddots & \vdots \\ \hat{a}_h p^{\alpha h}y^*(t_N)+ & \dots & +y^*(t_N) \end{bmatrix}$$

and

$$\Phi_n^*(u,\hat{\theta}_b) = \begin{bmatrix} f_0^*(u(t_1),\hat{\theta}_b) & \cdots & f_m^*(u(t_1),\hat{\theta}_b) \\ f_0^*(u(t_2),\hat{\theta}_b) & \cdots & f_m^*(u(t_2),\hat{\theta}_b) \\ \vdots & \ddots & \vdots \\ f_0^*(u(t_N),\hat{\theta}_b) & \cdots & f_m^*(u(t_N),\hat{\theta}_b) \end{bmatrix}.$$

The solution of (8) is

$$\hat{\theta}_n = (\Phi_n^*(u,\hat{\theta}_b)^T\Phi_n^*(u,\hat{\theta}_b))^{-1}\Phi_n^*(u,\hat{\theta}_b)^T Y_n^*(y,\hat{\theta}_a). \tag{14}$$

B. Linear Parameters Identification

Given an estimation of $\hat{\theta}_n$, the internal signal w can be estimated as: $w(k) = f(u,\hat{\theta}_n)u(k)$, which is the input of the linear system. Then the fractional order linear part can be written as follows:

$$a_h p^{\alpha h}y_k + \cdots + a_1 p^{\alpha}y_k + y_k = b_r p^{\alpha r}\hat{w}_k + \cdots + b_0\hat{w}_k.$$

The above equation can be rewritten as

$$\underbrace{\begin{bmatrix} Y_k \\ Y_{k-1} \\ \vdots \end{bmatrix}}_{Y_l} = \underbrace{\begin{bmatrix} \hat{\varphi}_k \\ \hat{\varphi}_{k-1} \\ \vdots \end{bmatrix}}_{\Psi_l} \theta_l \tag{15}$$

where

$$\hat{\varphi}_k = \begin{bmatrix} -p^{\alpha h}y_{t_k}\cdots - p^{\alpha}y_{t_k} & p^{\alpha r}\hat{w}_{t_k}\cdots\hat{w}_{t_k} \end{bmatrix}$$

$$\hat{\theta}_l = \left[\begin{array}{cc} a_h \cdots a_1 & b_r \cdots b_0 \end{array} \right]^T, \quad Y_k = [y_{t_k}].$$

The estimated value of $\hat{\theta}_l$ can be calculated as

$$\hat{\theta}_l = ({\Psi_l}^T \Psi_l)^{-1}) {\Psi_l}^T Y_l.$$

C. Differentiation Order Estimation

After the above coefficient identification method, a general and applicable iterative learning identification technique is applied to differentiation orders by using the P-type order learning law [45].

For systems (3) and (4), the linear and nonlinear coefficients are derived from the above proposed identification methods with the knowledge of α_{k-1}. The order identification is to estimate the value of α from the following P-type order learning law

$$\alpha_{k+1} \triangleq \alpha_k + \Gamma_k e_k(T), \ \alpha_{k+1} \in [0,1] \tag{16}$$

where $\triangleq$ denotes

$$\alpha_{k+1} = \begin{cases} 0, & \alpha_k + \Gamma_k e_k(T) < 0 \\ \alpha_k + \Gamma_k e_k(T), & 0 \le \alpha_k + \Gamma_k e_k(T) \le 1 \\ 1, & \alpha_k + \Gamma_k e_k(T) > 1. \end{cases}$$

Theorem 1: For system (3) and (4) and order learning law (16), it can be proved that $\alpha_d - \alpha_k \to 0$ monotonically if there exists a $\rho \in [0, 1)$ satisfying either of the following conditions:

1) any Γ_k satisfying $|1 - \Gamma_k \Lambda_k| \le \rho$,

2)

$$\begin{cases} \|\hat{\Gamma}_k\| \cdot [\max\limits_{\alpha_\xi, \alpha_\eta} \|\tilde{\Lambda}_k\|] \le 1 + \rho, \\ 1 \le \tilde{\Gamma}_k e_{k-1}(T), \end{cases} \Rightarrow \Gamma_k = \frac{\tilde{\Gamma}_k}{(-1)^k \mathrm{sgn}\{\delta\alpha_0\}},$$

3)

$$\begin{cases} \|\hat{\Gamma}_k\| \cdot [\max\limits_{\alpha_\xi, \alpha_\eta} \|\tilde{\Lambda}_k\|] \le 1, \\ 1 - \rho \le \tilde{\Gamma}_k e_{k-1}(T), \end{cases} \Rightarrow \Gamma_k = \frac{\tilde{\Gamma}_k}{\mathrm{sgn}\{\delta\alpha_0\}}$$

where Λ_k, $\tilde{\Lambda}_k$, $\hat{\Gamma}_k$, $\tilde{\Gamma}_k$ and the order learning gains Γ_k are defined in the following proof, f is locally Lipschitz on y_k with Lipschitz constant K, and

$$\|\tilde{\Lambda}_k\| = \int_0^T (T-\tau)^{\alpha_\xi - 1} E_{\alpha_\xi, \alpha_\xi}[K(T-\tau)^{\alpha_\xi}] \left\| \left. \frac{\partial \varepsilon_k(\tau)}{\partial \alpha} \right|_{\tilde{\alpha}_\xi} \right\| d\tau.$$

Proof: This proof is divided into two parts.

Part I:

It can be proved that

$$y_d^{(\alpha_d)}(t) - y_k^{(\alpha_k)}(t) = f(t, y_d, u_d) - f_k(t, y_k, u_d)$$

$$\Leftrightarrow \left. \frac{\partial y_d^{(\alpha)}(t)}{\partial \alpha} \right|_{\alpha_\xi} \delta\alpha_k + e_k^{(\alpha_k)}(t) = f(t, y_d, u_d) - f_k(t, y_k, u_d)$$

where $e_k(t) = y_d(t) - y_k(t)$ and $\delta\alpha_k = \alpha_d - \alpha_k$, It follows from $y_{d0} = y_{k0}$ that there exists a kernel function $H(\cdot)$ and the order sensitivity function $\frac{\partial \varepsilon_k}{\alpha}$ satisfying

$$e_k(t) = \int_0^t H(t, \tau, \alpha_k, h_k(t,\tau)) \left. \frac{\partial \varepsilon_k(\tau)}{\partial \alpha} \right|_{\tilde{\alpha}_\xi} d\tau \delta\alpha_k \tag{17}$$

where $h_k(t, \tau)$ is iteration dependent and related to the estimation of other coefficients. Thus the convergence condition can be written as

$$|1 - \Gamma_k \Lambda_k| \le \rho < 1 \tag{18}$$

where $\Lambda_k = \int_0^T H(T, \tau, \alpha_k, h_k(t, \tau)) \left. \frac{\partial \varepsilon_k(\tau)}{\partial \alpha} \right|_{\tilde{\alpha}_\xi} d\tau$.

Part II:

It is obvious that (18) holds if either of the following conditions is satisfied:

$$1 \le \Gamma_k \Lambda_k \le 1 + \rho \tag{19}$$

$$1 - \rho \le \Gamma_k \Lambda_k \le 1 \tag{20}$$

which are sufficient conditions.

Moreover, applying Lemma 1 of [45] to $\Gamma_k \Lambda_k$ yields

$$\Gamma_k \Lambda_k \le \|\Gamma_k\| \|\tilde{\Lambda}_k\|.$$

On the other hand, because $\delta\alpha_k = [1 - \Gamma_k \Lambda_k]\delta\alpha_{k-1}$,

1) for (19), $\mathrm{sgn}\{\delta\alpha_k\} = -\mathrm{sgn}\{\delta\alpha_{k-1}\} = (-1)^k \mathrm{sgn}\{\delta\alpha_0\}$,

2) for (20), $\mathrm{sgn}\{\delta\alpha_k\} = \mathrm{sgn}\{\delta\alpha_{k-1}\} = \mathrm{sgn}\{\delta\alpha_0\}$.

Firstly, for (19), the order leaning gain Γ_k is derived from the following steps:

Step 1: Find $\hat{\Gamma}_k$ satisfying $\|\hat{\Gamma}_k\| \cdot \left[\max\limits_{\alpha_\xi, \alpha_\eta} \|\tilde{\Lambda}_k\|\right] \le 1 + \rho$.

Step 2: Choose $\tilde{\Gamma}_k \in \{\hat{\Gamma}_k, -\hat{\Gamma}_k\}$ satisfying $1 \le \tilde{\Gamma}_k e_{k-1}(T)$.

Step 3: It follows that

$$1 \le \tilde{\Gamma}_k e_{k-1}(T) \le \frac{\tilde{\Gamma}_k e_{k-1}(T)}{\mathrm{sgn}\{\delta\alpha_k\}} \delta\alpha_k = \frac{\tilde{\Gamma}_k e_{k-1}(T)}{(-1)^k \mathrm{sgn}\{\delta\alpha_0\} \delta\alpha_k}.$$

Step 4: Let $\Gamma_k = \frac{\tilde{\Gamma}_k}{(-1)^k \mathrm{sgn}\delta\alpha_0}$, we have

$$\begin{cases} \Gamma_k \Lambda_k \le \|\Gamma_k\| \|\tilde{\Lambda}_k\| \le 1 + \rho \\ 1 \le \dfrac{\Gamma_k e_{k-1}(T)}{\delta\alpha_k} = \Gamma_k \Lambda_k. \end{cases}$$

It follows from $\delta\alpha_k = [1 - \Gamma_k \Lambda_k]\delta\alpha_{k-1}$ that $\lim_{k\to\infty} \alpha_k = \alpha_d$.

Secondly, for (20), the order learning gain Γ_k is derived from the following steps:

Step 1: Find $\hat{\Gamma}_k$ satisfying $\|\hat{\Gamma}_k\| \cdot \left[\max\limits_{\alpha_\xi, \alpha_\eta} \|\tilde{\Lambda}_k\|\right] \le 1$.

Step 2: Choose $\tilde{\Gamma}_k \in \{\hat{\Gamma}_k, -\hat{\Gamma}_k\}$ satisfying $1 - \rho \le \tilde{\Gamma}_k e_{k-1}(T)$.

Step 3: It follows that

$$1 - \rho \le \tilde{\Gamma}_k e_{k-1}(T) \le \frac{\tilde{\Gamma}_k e_{k-1}(T)}{\mathrm{sgn}\{\delta\alpha_k\}} \delta\alpha_k = \frac{\tilde{\Gamma}_k e_{k-1}(T)}{(-1)^k \mathrm{sgn}\{\delta\alpha_0\} \delta\alpha_k}.$$

Step 4: Let $\Gamma_k = \frac{\tilde{\Gamma}_k}{\mathrm{sgn}\delta\alpha_0}$, we have

$$\begin{cases} \Gamma_k \Lambda_k \le \|\Gamma_k\| \, \|\tilde{\Lambda}_k\| \le 1 \\ 1 - \rho \le \dfrac{\Gamma_k e_{k-1}(T)}{\delta\alpha_k} = \Gamma_k \Lambda_k. \end{cases}$$

It follows from $\delta\alpha_k = [1-\Gamma_k\Lambda_k]\delta\alpha_{k-1}$ that $\lim_{k\to\infty}\alpha_k = \alpha_d$.

Lastly, the universal way to determine $\mathrm{sgn}\{\delta\alpha_0\}$ is

$$\mathrm{sgn}\{\delta\alpha_0\} = \mathrm{sgn}\{\alpha_d - \alpha_0\} = \begin{cases} +1, & \text{if } \alpha_0 = 0 \\ -1, & \text{if } \alpha_0 = 1. \end{cases} \quad \blacksquare$$

Remark 2: Comparing to the identification of integer order KiBaM model, an extra parameter "fractional order α" is introduced to the linear part of the model, and the computations of other parameters are accordingly related to the fractional order derivatives of certain variables. Thus, there exist two essential difficulties: how to find α accurately, and how to compute fractional order derivatives accurately. On one hand, the identification of α is just dependent on the structure of system, i.e., the linear part of the model is a SISO one due to the physical meanings of the system such as the distributed property or the averaging method, and the input and output can represent the current and voltage. A small gain can always guarantee the convergence of the iterative learning identification method. Besides, this method arrives at a unique value of $\hat{\alpha}$, and the initial α_0 can be chosen as 0 or 1. Besides, it will be shown in the next section that a number of state-of-art methods such as internal partition method, GA, NN, etc, may fail to find the real α. On the other hand, the short memory principle guarantees the accuracy of fractional order derivatives, and reveals the importance of preconditioning before real experiments [46]. To sum up, because of the adaptiveness of α estimation, a faster convergence speed and a more accurate result can surely be expected.

IV. Illustrated Examples

Example 1: In this simulation example a FO-KiBaM model is considered where the nonlinear and linear parts (structural information) are assumed as:

$$\begin{aligned} f(u,\theta_n) &= \beta u^3 \\ G(s) &= \frac{b_1 s^\alpha + b_0}{a_2 s^{3\alpha} + a_1 s^{2\alpha} + a_0 s^\alpha + 1} \end{aligned} \tag{21}$$

where the true values are

$$\begin{aligned} &\alpha = 0.5, \quad \beta = 2 \\ &b_1 = 3, \quad b_0 = 2 \\ &a_2 = 2, \quad a_1 = 3, \quad a_0 = 5 \end{aligned}$$

and the input signal is $u = 0.5\sin(t)$.

Given the initial value of $\alpha_0 = 0.1$, and $N = 6693$ samples of the input/output data for the identification of structure (21). The linear coefficient vector was initialized as $a_2 = 1, a_1 = 1, a_0 = 1, b_1 = 1, b_0 = 1$. The matrices of Φ_n and Y_n in the nonlinear identification process are:

$$Y_n(y,\hat{\theta}_a) = \begin{bmatrix} \hat{a}_2 p^{3\alpha} y(t_1) + & \cdots & +y(t_1) \\ \hat{a}_2 p^{3\alpha} y(t_{k+1}) + & \cdots & +y(t_{k+1}) \\ \vdots & \ddots & \vdots \\ \hat{a}_2 p^{3\alpha} y(t_N) + & \cdots & +y(t_N) \end{bmatrix}$$

and

$$\Phi_n(u,\hat{\theta}_b) = \begin{bmatrix} \hat{b}_1 p^\alpha u^3(t_1) + \hat{b}_0 u^3(t_1) \\ \hat{b}_1 p^\alpha u^3(t_{k+1}) + \hat{b}_0 u^3(t_{k+1}) \\ \vdots \\ \hat{b}_1 p^\alpha u^3(t_N) + \hat{b}_0 u^3(t_N) \end{bmatrix}.$$

The matrices of $\hat{\varphi}_k$ and Y_k in the linear identification process are:

$$\hat{\varphi}_k = \begin{bmatrix} -p^{3\alpha} y_{t_k} & -p^{2\alpha} y_{t_k} & -p^\alpha y_{t_k} & p^\alpha \hat{w}_{t_k} & \hat{w}_{t_k} \end{bmatrix}$$

$$\hat{\theta}_l = \begin{bmatrix} a_2 & a_1 & b_1 & b_0 \end{bmatrix}^T, \; Y_k = [y_{t_k}].$$

Refer to the above fractional order KiBaM system (21), two identification strategies are discussed by using different order identification methods, i.e., the interval partition method and the iterative learning order identification method. With the interval partition method, the identification procedure is basically as follows:

1) Given the increment of α, such as $\Delta\alpha = 0.1$, that divides $[0, 1]$ into $\alpha/\Delta\alpha$ parts, identify the linear and nonlinear parameters with the $\alpha/\Delta\alpha$ values of α, respectively.

2) Compare the $\alpha/\Delta\alpha$ identification results according to the 2-norm of their output error. Find the two smaller results which construct the renewed domain of α.

3) Repeat the above procedure until the domain cannot be divided or the precision of α has arrived to the requirement.

Fig. 3 illustrates the 2-norm of output errors according to different $\alpha \in [0, 1]$. As shown in Fig. 3, the 2-norm of the identified system's output error is not monotonically convergent to the real value $\alpha = 0.5$, which restricts the validation of the interval partition method in fractional order identification, and this phenomenon always happens in fractional order nonlinear system identifications.

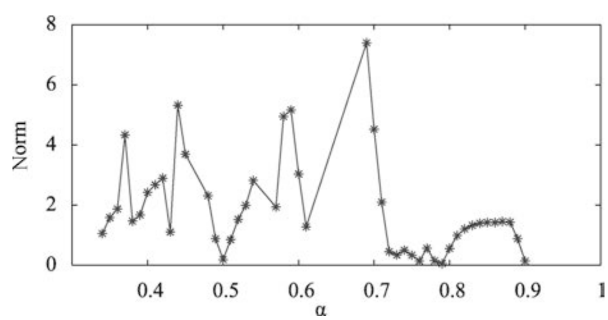

Fig. 3. The 2-norm of output errors by using the interval partition method, where the minimum point corresponds to $\alpha = 0.79$ instead of the true value 0.5.

On the other hand, by using the iterative learning order identification method, the learning laws of α_k are assumed as:

$$\alpha_{k+1} \triangleq \alpha_k + 0.01 e_k(T).$$

Combined with the nonlinear and linear parameters learning laws (10) and (14), the identification process is proceeded as Fig. 2 shown and the result is shown as follows:

$$f(u,\theta_n) = 1.6174u^3$$
$$G(s) = \frac{1.7397s^{0.4988} + 2.1601}{0.9852s^{1.4964} + 1.7439s^{0.9976} + 3.2185s^{0.4988} + 1}$$

which is very precise for there is no noise introduced into the example system. Simulate the above identified system with the input data u. After 12 iterations, the iteration converges when the 2-norm of the output error arrived at 0.0388. Comparison between the identified system output and the original system output is illustrated in Fig. 4.

Example 2: Consider a FO-KiBaM model described as

$$f(u,\theta_n) = \beta u^2$$
$$G(s) = \frac{b_1 s^{\alpha} + b_0}{a_1 s^{2\alpha} + a_0 s^{\alpha} + 1} \tag{22}$$

with

$$\alpha = 0.5, \quad \beta = 1, \quad b_1 = 3, \quad b_0 = 2, \quad a_1 = 3, \quad a_0 = 1$$

and the input signal is $u = 0.5\sin(t)$.

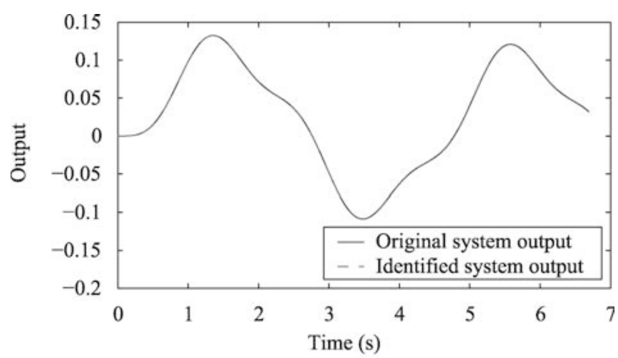

Fig. 4. Comparisons of the outputs between the ideal system and the identified one in Example 1.

With $N = 6693$ samples of the input/output data of the structure (22), parameter estimation is performed using the approaches proposed in Section III. Besides the order learning law is assumed as: $\alpha_{k+1} \triangleq \alpha_k + 0.01e_k(T)$. Fig. 5 presents the results of modeling of the actual and modeled outputs of the KiBaM system (22). The estimation results are:

$$f(u,\theta_n) = 1.496u^2$$
$$G(s) = \frac{1.9965s^{0.4988} + 1.2598}{2.9216s^{0.9976} + 0.9464s^{0.4988} + 1}.$$

Example 3: A real-world application of this paper is illustrated in this example. Given the structure of fractional order KiBaM model in Fig. 6, where R_s represents the nonlinear term, and a linear circuit is cascaded after it. Based on the standard of dynamic stress test (DST), the I/V data is applied to estimate those parameters, where the order of Warburg impedance $\beta = 0.5$ is assumed due to the property of Lithium-ion battery ($\beta = 0.25$ for fuel cells), then it, follows that

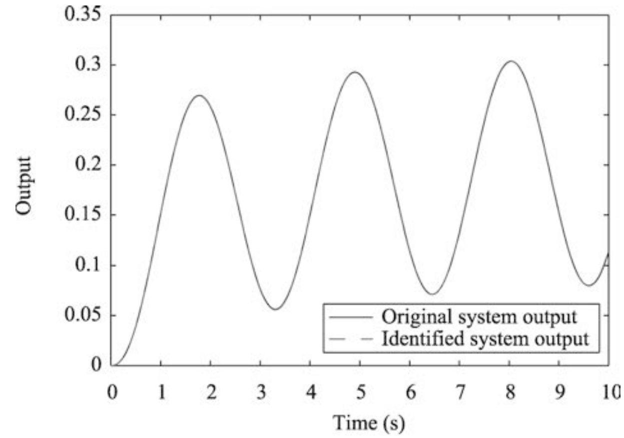

Fig. 5. Comparisons of the outputs between the ideal system and the identified one in Example 2.

$R_s = 19.1$ MΩ, $R_p = 15.6$ MΩ, $Y_0 = 1.24$ mho, $Y_1 = 370$ mho, α=0.665. Thus the electrochemical impedance spectroscopy is

$$G(s) = R_s + \frac{R_p Y_0 s^{\alpha} + R_p Y_1 s^{\beta} + 1}{R_p Y_0 Y_1 s^{\alpha+\beta} + Y_1 s^{\beta}}$$

where the nonlinear term Rs is varying according to the error e. The measured fractional order and fractional order KiBaM outputs are compared in Fig. 7, where $R_s \in [34, 37.7]$. It can be seen that the nonlinear term plays crucial role in the above real-time traffic test.

Remark 3: It should be noted that, given an accurate α, many methods can derive accurate models for sure, such as the prony technique. This α is a key parameter in FO KiBaM model which reveals a number of physical, chemical and distributed characteristics as introduced in Section II-C.

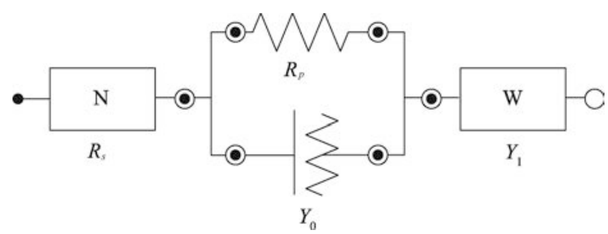

Fig. 6. Structural information of a fractional order KiBaM model.

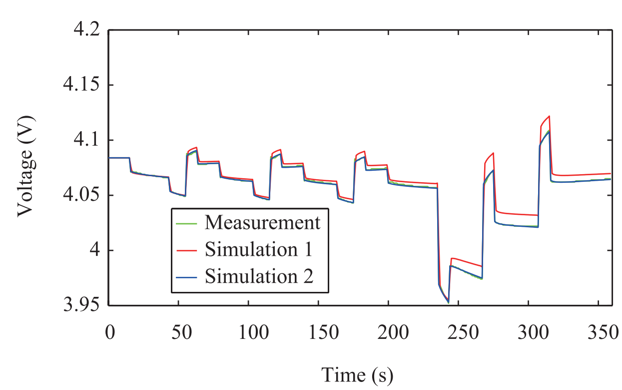

Fig. 7. Comparisons of the outputs between the fractional order model (FOM) and the discussed fractional order KiBaM model in Example 3.

Besides, the computations of other parameters are accordingly related to the fractional order derivatives of certain variables. Thus how to find α accurately, and how to compute fractional order derivatives accurately become primary tasks. In Example 1, the interval partition method failed to work because a too different α was obtained. But, the proposed method in Section III-C is adaptive to those linear parameters, and can converge to the real α in terms of other parameters in less than 20 iterations, where the errors are set to be in range $0.01-0.05$. The similar convergence accuracy and speed can be observed in various other simulations that we have done previously which are excluded in this paper such as more complicated nonlinear terms [25], [47]–[53].

Lastly, in the above examples, the small gain learning law guarantees the convergence, but sacrifices the convergence speed. But fortunately, this learning gain can be tuned from a small enough one to a large and optimized one so that the convergence speed is improved accordingly, where the whole tuning process is unidirectional. By doing so, the accuracy and convergence speed can be improved simultaneously.

V. Conclusions and Future Works

This paper deals with the parameter and order identifications of commensurate fractional order KiBaM systems in continuous-time domain. The least square method is applied to the linear and nonlinear parameters identification. A P-type order learning law associated with the terminal value of system error is applied to identify the system order accurately. The performance of the proposed algorithms has been testified by illustrative examples. Based on results presented in this paper, it is anticipated that the proposed identification algorithms will lead to more precise construction of fractional order quasi-linear systems. The other part of this work is the identification of variable order system which is another representation of nonlinearity.

References

[1] G. P. Liu, "*Nonlinear Identification and Control: A Neural Network Approach,*" Berlin: Springer Science and Business Media, 2012.

[2] M. Mahfouf, D. A. Linkens, and D. Xue, "A new generic approach to model reduction for complex physiologically based drug models," *Control Eng. Pract.*, vol. 10, no. 1, pp. 67–81, Jan. 2002.

[3] C. Campbell, "Kernel methods: a survey of current techniques," *Neurocomputing*, vol. 48, no. 1–4, pp. 63–84, Oct. 2002.

[4] L. Sommacal, P. Melchior, A. Oustaloup, J. M. Cabelguen, and A. J. Ijspeert, "Fractional multi-models of the frog gastrocnemius muscle," *J. Vibr. Control*, vol. 14, no. 9–10, pp. 1415–1430, Sep. 2008.

[5] W. X. Zhao, "Parametric identification of Hammerstein systems with consistency results using stochastic inputs," *IEEE Trans. Autom. Control*, vol. 55, no. 2, pp. 474–480, Feb. 2010.

[6] K. S. Narendra and P. G. Gallman, "An iterative method for the identification of nonlinear systems using a Hammerstein model," *IEEE Trans. Autom. Control*, vol. 11, no. 3, pp. 546–550, Jul. 1966.

[7] Y. Liu and E. W. Bai, "Iterative identification of Hammerstein systems," *Automatica*, vol. 43, no. 2, pp. 346–354, Feb. 2007.

[8] Y. W. Mao and F. Ding, "Multi-innovation stochastic gradient identification for Hammerstein controlled autoregressive autoregressive systems based on the filtering technique," *Nonlinear Dyn.*, vol. 79, no. 3, pp. 1745–1755, Feb. 2015.

[9] X. F. Zhu and D. E. Seborg, "Nonlinear predictive control based on Hammerstein models," *Control Theory Appl.*, vol. 11, no. 5, pp. 564–575, Oct. 1994.

[10] D. R. Morgan, Z. X. Ma, J. Kim, M. G. Zierdt, and J. Pastalan, "A generalized memory polynomial model for digital predistortion of RF power amplifiers," *IEEE Trans. Signal Process.*, vol. 54, no. 10, pp. 3852–3860, Oct. 2006.

[11] I. W. Hunter and M. J. Korenberg, "The identification of nonlinear biological systems: Wiener and Hammerstein cascade models," *Biol. Cybern.*, vol. 55, no. 2–3, pp. 135–144, Nov. 1986.

[12] E. W. Bai, Z. J. Cai, S. Dudley-Javorosk, and R. K. Shields, "Identification of a modified Wiener-Hammerstein system and its application in electrically stimulated paralyzed skeletal muscle modeling," *Automatica*, vol. 45, no. 3, pp. 736–743, Mar. 2009.

[13] J. P. Costa, A. Lagrange, and A. Arliaud, "Acoustic echo cancellation using nonlinear cascade filters," in *Proc. Int. Conf. Acoustics, Speech, and Signal Processing*. Hong Kong, China, 2003.

[14] L. Vanbeylen, R. Pintelon, and J. Schoukens, "Blind maximum likelihood identification of Hammerstein systems," *Automatica*, vol. 44, no. 12, pp. 3139–3146, Dec. 2008.

[15] M. Boutayeb, D. Aubry, and M. Darouach, "A robust and recursive identification method for MISO Hammerstein model," in *Proc. Int. Conf. Control '96*. Washington DC, USA, 1996, pp. 447–452.

[16] W. Greblicki, "Continuous-time Hammerstein system identification," *IEEE Trans. Autom. Control*, vol. 45, no. 6), 1232–1236, Jun. 2000.

[17] I. Goethals, K. Pelckmans, J. A. K. Suykens, and B. De Moor, "Subspace identification of Hammerstein systems using least squares support vector machines," *IEEE Trans. Autom. Control*, vol. 50, no. 10, pp. 1509–1519, Oct. 2005.

[18] T. Pritz, "Five-parameter fractional derivative model for polymeric damping materials," *J. Sound Vibr.*, vol. 265, no. 5, pp. 935–952, Aug. 2003.

[19] A. Dumlu and K. Erenturk, "Trajectory tracking control for a 3-DOF parallel manipulator using fractional-order $PI^{\lambda}D^{\mu}$ control," *IEEE Trans. Ind. Electron.*, vol. 61, no. 7, pp. 3417–3426, Jul. 2014.

[20] S. Gulistan, M. Abbas, and A. A. Syed, "Fractional dual fields for a slab placed in unbounded dielectric magnetic medium," *Int. J. Appl. Electrom. Mech.*, vol. 46, no. 1, pp. 11–21, Jan. 2014.

[21] K. B. Oldham and J. Spanier, "The replacement of Ficks laws by a formulation involving semidifferentiation," *J. Electroanal. Chem. Interf. Electrochem.*, vol. 26, no. 2–3, pp. 331–341, Jul. 1970.

[22] K. B. Oldham and J. Spanier, *The Fractional Calculus-Theory and Applications of Differentiation and Integration to Arbitrary Order*. New York and London: Academic Press, 1974.

[23] S. Victor, R. Malti, H. Garnier, and A. Oustaloup, "Parameter and

differentiation order estimation in fractional models," *Automatica*, vol. 49, no. 4, pp. 926−935, Apr. 2013.

[24] N. Heymans and J. C. Bauwens, "Fractal rheological models and fractional differential equations for viscoelastic behavior," *Rheol. Acta*, vol. 33, no. 3, pp. 210−219, May 1994.

[25] J. Sabatier, M. Merveillaut, J. M. Francisco, F. Guillemard, and D. Porcelatto, "Fractional models for lithium-ion batteries," in *Proc. 2013 European Control Conf.*, Zurich, Switzerland, 2013, pp. 3458−3463.

[26] K. C. Cao, Y. Q. Chen, D. Stuart, and D. Yue, "Cyber-physical modeling and control of crowd of pedestrians: a review and new framework," *IEEE/CAA J. Autom. Sinica*, vol. 2, no. 3, pp. 334−344, Jul. 2015.

[27] M. Ichise, Y. Nagayanagi, and T. Kojima, "An analog simulation of non-integer order transfer functions for analysis of electrode processes," *J. Electroanal. Chem. Interf. Electrochem.*, vol. 33, no. 2, pp. 253−265, Dec. 1971.

[28] A. Boroomand and M. B. Menhaj, "Fractional-order Hopfield neural networks," in *Advances in Neuro-Information Processing*, Springer Berlin Heidelberg, 2009, pp. 883−890.

[29] A. Maachou, R. Malti, P. Melchior, J. L. Battaglia, A. Oustaloup, and B. Hay, "Thermal system identification for large temperature variations using fractional Volterra series," in *Proc. 4th IFAC Workshop on Fractional Differentiation and its Applications*, Badajoz, Spain, 2010.

[30] S. Oukacine, T. Djamah, S. Djennoune, R. Mansouri, and M. Bettayeb, "Multi-model identification of a fractional non linear system," in *Proc. 6th IFAC Workshop on Fractional Differentiation and its Applications*, 2013, pp. 48−53.

[31] S. Westerlund and L. Ekstam, "Capacitor theory," *IEEE Trans. Dielectr. Electr. Insul.*, vol. 1, no. 5, pp. 826−839, Oct. 1994.

[32] E. Barsoukov and J. R. Macdonald, *Impedance Spectroscopy Theory, Experiment, and Applications*. 2nd ed. Manhattan: John Wiley & Sons, 2005.

[33] A. Seaman, T. S. Dao, and J. McPhee, "A survey of mathematics-based equivalent-circuit and electrochemical battery models for hybrid and electric vehicle simulation," *J. Power Sources*, vol. 256, pp. 410−423, Jun. 2014.

[34] T. Kim and W. Qiao, "A hybrid battery model capable of capturing dynamic circuit characteristics and nonlinear capacity effects," *IEEE Trans. Energy Convers.*, vol. 26, no. 4, pp. 1172−1180, Dec. 2011.

[35] J. Sabatier, O. P. Agrawal, and J. A. T. Machado, *Advances in Fractional Calculus: Theoretical Developments and Applications in Physics and Engineering*. Dordrecht: Springer, 2007.

[36] I. Podlubny, *Fractional Differential Equations*. Pittsburgh: Academic Press, 1998.

[37] F. M. Le, I. Markovsky, C. T. Freeman, and E. Rogers, "Identification of electrically stimulated muscle models of stroke patients," *Control Eng. Pract.*, vol. 18, no. 4, pp. 396−407, Apr. 2010.

[38] J. D. Gabano, T. Poinot, and H. Kanoun, "LPV continuous fractional modeling applied to ultracapacitor impedance identification," *Control Eng. Pract.*, vol. 45, pp. 86−97, Dec. 2015.

[39] L. J. Gao, S. Y. Liu, and R. A. Dougal, "Dynamic lithium-ion battery model for system simulation," *IEEE Trans. Compon. Packaging Technol.*, vol. 25, no. 3, pp. 495−505, Sep. 2002.

[40] P. Rong and M. Pedram, "An analytical model for predicting the remaining battery capacity of lithium-ion batteries," *IEEE Trans. Very Large Scale Integr. Syst.*, vol. 14, no. 5, pp. 441−451, May 2006.

[41] C. C. Weng, S. Y. Chen, and J. C. Chang, "Predicting remaining discharge time of a Lithium-ion battery by using residual capacity and workload," in *Proc. 17th Int. Symp. Consumer Electronics (ISCE)*, Hsinchu City, Taiwan, China, 2013, pp. 179−180.

[42] K. A. Smith, C. D. Rahn, and C. Y. Wang, "Model-based electrochemical estimation and constraint management for pulse operation of lithium ion batteries," *IEEE Trans. Control Syst. Technol.*, vol. 18, no. 3, pp. 654−663, May 2010.

[43] N. M. Yusof, N. Ishak, M. H. F. Rahiman, R. Adnan, and M. Tajjudin, "Fractional-order model identification for electro-hydraulic actuator," in *Proc. 10th Asian Control Conference (ASCC)*, Kota Kinabalu, Malaysia, 2015, pp. 1−5.

[44] M. R. Kumar, S. Ghosh, and S. Das, "Identification of fractional order circuits from frequency response data using seeker optimization algorithm," in *Proc. Int. Conf. Industrial Instrumentation and Control (ICIC)*, Pune, India, 2015, pp. 197−202.

[45] Y. Li, Y. Q. Chen, and H. S. Ahn, "On P-type fractional order iterative learning identification," in *Proc. 13th Int. Conf. Control, Automation and Systems*, Gwangju, Korea, 2013, pp. 219−225.

[46] Y. Li, Y. Q. Chen, and H. S. Ahn, "Fractional order iterative learning control for fractional order system with unknown initialization," in *Proc. American Control Conf.*, Portland, OR, USA, 2014, pp. 5712−5717.

[47] J. Sabatier, M. Aoun, A. Oustaloup, G. Grégoire, F. Ragot, and P. Roy, "Fractional system identification for lead acid battery state of charge estimation," *Signal Process.*, vol. 86, no. 10, pp. 2645−2657, Oct. 2006.

[48] J. Sabatier, M. Cugnet, S. Laruelle, S. Grugeon, B. Sahut, A. Oustaloup, and J. M. Tarascon, "A fractional order model for lead-acid battery crankability estimation," *Commun. Nonlinear Sci. Numer. Simul.*, vol. 15, no. 5, pp. 1308−1317, May 2010.

[49] Efe M Ö, "Battery power loss compensated fractional order sliding mode control of a quadrotor UAV," *Asian J. Control*, vol. 14, no. 2, pp. 413−425, Mar. 2012.

[50] J. Sabatier, M. Merveillaut, J. M. Francisco, F. Guillemard, and D. Porcelatto, "Lithium-ion batteries modeling involving fractional differentiation," *J. Power Sources*, vol. 262, pp. 36−43, Sep. 2014.

[51] J. M. Francisco, J. Sabatier, L. Lavigne, F. Guillemard, M. Moze, M. Tari, M. Merveillaut, and A. Noury, "Lithium-ion battery state of charge estimation using a fractional battery model," in *Proc. Int. Conf. Fractional Differentiation and Its Applications (ICFDA)*, Catania, Italy, 2014, pp. 1−6.

[52] T. J. Freeborn, B. Maundy, and A. S. Elwakil, "Fractional-order models of supercapacitors, batteries and fuel cells: a survey," *Mater. Renew. Sustain. Energy*, vol. 4, no. 3, pp. 9, Sep. 2015.

[53] T. Takamatsu and H. Ohmori, "State and parameter estimation of lithium-ion battery by Kreisselmeier-type adaptive observer for fractional calculus system," in *Proc. 54th Annu. Conf. Society of Instrument and Control Engineers of Japan (SICE)*,

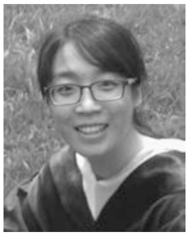

Yang Zhao is currently a Ph.D. candidate at the School of Control Science and Engineering at Shandong University, Jinan, China. She received her M.S. degree in control engineering from the School of Control Science and Engineering at Shandong University, Jinan, China, in 2011. Her research interests include applied fractional calculus in control, iterative learning control, system identification and robotics.

Yan Li received the Ph.D. degree in applied mathematics from Shandong University, Jinan, China, in 2008. During 2007−2010, he was invited by Dr. YangQuan Chen and Huifang Dou as a research fellow at Center for Self-Organizing Intelligent Systems (CSOIS). He is currently an associate professor and Ph.D. supervisor of the School of Control Science and Engineering at Shandong University. His recent research interests include fractional calculus, modeling of complex system, stability analysis of fractional order systems, and intelligent control. Corresponding author of this paper.

Fengyu Zhou received the Ph.D. degree in electrical engineering from Tianjin University, Tianjin, China, in 2008. He is currently a professor of the School of Control Science and Engineering at Shandong University, Jinan, China. His research interests include robotics and automation.

Zhongkai Zhou is currently a Ph.D. candidate at the School of Control Science and Engineering at Shandong University, Jinan, China. He received the B.E. degree in automation from Qufu Normal University, Rizhao, China, in 2013. His research interests include battery management systems and more particularly on active balancing, modeling for batteries.

YangQuan Chen received his Ph.D. degree in advanced control and instrumentation from Nanyang Technological University, Singapore, in 1998. Dr. Chen was on the Faculty of Electrical and Computer Engineering at Utah State University before he joined the School of Engineering, University of California, Merced in 2012 where he teaches mechatronics for juniors and fractional order mechanics for graduates. His research interests include mechatronics for sustainability, cognitive process control and hybrid lighting control, multi-UAV based cooperative multi-spectral personal remote sensing and applications, applied fractional calculus in controls, signal processing and energy informatics; distributed measurement and distributed control of distributed parameter systems using mobile actuator and sensor networks.

Pinning Synchronization Between Two General Fractional Complex Dynamical Networks With External Disturbances

Weiyuan Ma, Yujiang Wu, and Changpin Li

***Abstract*—In this paper, the pinning synchronization between two fractional complex dynamical networks with nonlinear coupling, time delays and external disturbances is investigated. A Lyapunov-like theorem for the fractional system with time delays is obtained. A class of novel controllers is designed for the pinning synchronization of fractional complex networks with disturbances. By using this technique, fractional calculus theory and linear matrix inequalities, all nodes of the fractional complex networks reach complete synchronization. In the above framework, the coupling-configuration matrix and the inner-coupling matrix are not necessarily symmetric. All involved numerical simulations verify the effectiveness of the proposed scheme.**

***Index Terms*—External disturbance, fractional complex network, nonlinear coupling, pinning control, time delay.**

I. Introduction

FRACTIONAL calculus is as old as the conventional calculus. However, fractional calculus has become a hot topic in recent two decades due to its advantages in applications of physics and engineering. As a generalization of ordinary differential equation, fractional differential equation can capture non-local relations in space and time. Thus, the fractional-order models are believed to be more accurate than the integer-order models. Fractional models have been proven to be excellent instrument to describe the memory and hereditary properties of various materials and processes, such as dielectric polarization, electrode-electrolyte polarization, electromagnetic waves, viscoelastic systems, quantitative finance and waves [1]−[4].

It is demonstrated that fractional differential systems also behave chaotically or hyperchaotically, such as the fractional Lorenz system [5], the fractional Chua system [6], and the fractional Chen system [7]. Many complex networks usually consist of a large number of highly interconnected fractional dynamical units. Generally speaking, there are two main advantages of the fractional complex dynamical networks: one is infinite memory; the other is that the derivative order of a parameter enriches the system performance by increasing one degree of freedom. A fractional neural network is made up of thousands of neurons and their interactions. On the other hand, fractional differentiation provides neurons with a fundamental and general computation ability which can contribute to efficient information processing. Time delays are ubiquitous in neural networks due to finite switching speed of amplifiers. They usually occur in the signal transmission among neurons [8]−[10]. Therefore, it is more valuable and practical to investigate fractional complex networks with time delays.

Following these findings, synchronization of fractional chaotic systems becomes a challenging and interesting realm due to its potential applications in secure communication and control processing [11]−[16]. Many of complex networks normally have a large number of nodes, therefore it is usually expensive to control a complex network by designing the controllers for all nodes. To reduce the number of controllers, a pinning control method is proposed. Wang and Chen investigated a scale-free dynamical network by controlling a fraction of network nodes [17]. Sorrentino *et al.* explored the pinning controllability of the complex networks [18]. Liang and Wang revealed the relationship between the coupling matrix and the synchronizability of complex networks via pinning control [19]. Yu *et al.* studied synchronization via pinning control of general complex dynamical networks [20]. Nian and Wang investigated the optimal scheme of pinning synchronization of directed networks [21]. In addition, Liang and Wang proposed a method to quickly calculating pinning nodes on pinning synchronization in complex networks [22]. In [23]−[25], the authors investigated the pinning control of integer-order complex networks with time delays. However, pinning synchronization of integer-order complex networks was well-studied. Due to global dependent property of fractional complex networks, as far as we know, the literature on pinning synchronization of fractional complex networks is still sparse. In [26], based on the eigenvalue analysis and fractional

Manuscript received September 11, 2015; accepted January 13, 2016. This work was supported by National Natural Science Foundation of China (11372170, 11471150, 41465002) and Fundamental Research Funds for the Central Universities (31920130003). Recommended by Associate Editor Dingyü Xue.

Citation: W. Y. Ma, Y. J. Wu, and C. P. Li, "Pinning synchronization between two general fractional complex dynamical networks with external disturbances," *IEEE/CAA Journal of Automatica Sinica*, vol. 4, no. 2, pp. 332−339, Apr. 2017.

W. Y. Ma is with the School of Mathematics and Statistics, Lanzhou University, Lanzhou 730000, China, and also with the School of Mathematics and Computer Science, Northwest University for Nationalities, Lanzhou 730000, China (e-mail: mwy2004@126.com).

Y. J. Wu is with the School of Mathematics and Statistics, Lanzhou University, Lanzhou 730000, China (e-mail: myjaw@lzu.edu.cn).

C. P. Li is with the Department of Mathematics, Shanghai University, Shanghai 200444, China (e-mail: lcp@shu.edu.cn).

Color versions of one or more of the figures in this paper are available online at http://ieeexplore.ieee.org.

Digital Object Identifier 10.1109/JAS.2016.7510202

stability theory, local stability properties of pinned fractional networks were derived. The pinning synchronization of new uncertain fractional unified chaotic systems were discussed in [27]. In [28], Chai *et al.* proposed a global pinning synchronization for fractional complex dynamical networks. Xiang *et al.* investigated the robust synchronization problem for a class of systems with external disturbances [29]. Wang *et al.* provided a method to achieve projective synchronization of two fractional chaotic systems with external disturbances [30]. However, the effects of both time delay and external disturbance of the fractional complex network have seldom been considered.

Lyapunov direct method is important for synchronization analysis of complex networks with integer-order, but this method is difficult to be directly extended to fractional case [28], [31], [32]. Thus, to find out new ways to cope with these problems is still challenging. Motivated by the above discussions, pinning synchronization between the drive-response fractional complex networks with nonlinear coupling and time delays is studied. A novel modified Lyapunov method is used to analyze the global asymptotical synchronization criteria of fractional systems with time delays. These criteria rely on the coupling strength and the number of nodes pinned to the networks, there is no extra constraint on the two coupling matrices, such as symmetric or irreducible case.

The rest of this paper is arranged as follows. In Section II, the general drive and response fractional complex dynamical network models are introduced and some necessary preliminaries are given. A Lyapunov-like criteria for delayed fractional system is obtained. In Section III, based on the Lyapunov stability theorem, pinning controllers are designed to ensure the drive and response systems with external disturbances achieve synchronization. The illustrative numerical simulations are displayed in Section IV. Section V concludes this paper.

Throughout this paper, let $\|\cdot\|$ the Euclidean norm, I_n the identity matrix. If A is a vector or matrix, its transpose is denoted by A^T. Let $\lambda_{\min}(A)$ and $\lambda_{\max}(A)$ be the smallest and largest eigenvalue of symmetric matrix A, respectively.

II. Preliminaries and Mathematical Models

A. Fractional Complex Dynamical Networks With Nonlinear Coupling and Time Delays

In this section, we introduce some notations, definitions and preliminaries which will be used later on.

At present, there are several definitions of fractional differential operators [4], such as Grünwald-Letnikov definition, Riemann-Liouville definition, Caputo definition. Among them, the initial conditions for Caputo derivatives have the same form as those for integer-order ones. And Caputo derivative not only has a clearly interpretable physical meaning, but can also be properly measured to initializing in the simulation. So it may be the most appropriate choice for practical applications. Now we give the definition of Caputo fractional derivative ${}_CD^{\alpha}_{0,t}f(t)$, of order α with respect to time t as follows

$$ {}_CD^{\alpha}_{0,t}f(t) = \frac{1}{\Gamma(m-\alpha)}\int_0^t (t-\tau)^{m-\alpha-1}f^{(m)}(\tau)d\tau \tag{1}$$

where $m-1<\alpha<m\in\mathbb{Z}^+$.

Consider a general fractional delayed dynamical system consisting of N nodes, which can be described as follows:

$$\begin{aligned} {}_CD^{\alpha}_{0,t}x_i(t) &= Ax_i(t) + f(x_i(t)) + c\sum_{j=1}^N b_{ij}Hx_j(t) \\ &\quad + \bar{c}\sum_{j=1}^N \bar{b}_{ij}\bar{H}g(x_j(t-\tau)) + \xi_i(t) \end{aligned} \tag{2}$$

where $i=1,2,\ldots,N$, $0<\alpha<1$ is the fractional order, $x_i(t)=(x_{i1}(t),\ldots,x_{in}(t))^T\in\mathbb{R}^n$ is the state variable of the ith node. $A\in\mathbb{R}^{n\times n}$ is a given linear matrix, and $f(x_i)=[f_1(x_i),f_2(x_i),\ldots,f_n(x_i)]^T:\mathbb{R}^n\to\mathbb{R}^n$ is a smooth function describing the nonlinear dynamics of the node. c and $\bar{c}$ are two parameters of the non-delay and delay coupling strengths, respectively. $H\in\mathbb{R}^{n\times n}$ and $\bar{H}\in\mathbb{R}^{n\times n}$ are inner coupling matrices. $B=(b_{ij})_{N\times N}$ and $\bar{B}=(b_{ij})_{N\times N}$ denote the coupling configuration matrices of the network. If there is a connection from node i to node j $(i\neq j)$, then $b_{ij}>0$ (or $\bar{b}_{ij}>0$); otherwise, $b_{ij}=0$ (or $\bar{b}_{ij}=0$). The diagonal elements of matrix B and $\bar{B}$ are given by $b_{ii}=-\sum_{j=1,j\neq i}^N b_{ij}$ and $\bar{b}_{ii}=-\sum_{j=1,j\neq i}^N \bar{b}_{ij}$, respectively. $g(x_i(t-\tau))=[g_1(x_i(t-\tau)),\, g_2(x_i(t-\tau)),\ldots,g_n(x_i(t-\tau))]^T:\mathbb{R}^n\to\mathbb{R}^n$ is the nonlinear coupling function. $\xi_i(t)\in\mathbb{R}^n$ are external disturbance vectors.

If model (2) is referred as the drive system, the response complex network can be chosen as

$$\begin{aligned} {}_CD^{\alpha}_{0,t}y_i(t) &= Ay_i(t) + f(y_i(t)) + c\sum_{j=1}^N b_{ij}Hy_j(t) \\ &\quad + \bar{c}\sum_{j=1}^N \bar{b}_{ij}\bar{H}g(y_j(t-\tau)) + \eta_i(t) + u_i(t) \end{aligned} \tag{3}$$

where $y_i(t)=(y_{i1}(t),y_{i2}(t),\ldots,y_{in}(t))^T\in\mathbb{R}^n$ is the response state vector of the ith node; $\eta_i(t)\in\mathbb{R}^n$ are external disturbance vectors. $u_i(t)\in\mathbb{R}^n$ $(i=1,2,\ldots,N)$ are the controllers to be designed; the other parameters have the same meanings as those in (2).

It is not necessary to assume that the inner coupling matrix H (or $\bar{H}$) and coupling configuration matrix B (or $\bar{B}$) are symmetric and irreducible. Meanwhile, the corresponding topological graph can be directed or undirected. Throughout the paper, we always assume that nonlinear functions $f(x)$ and $g(x)$ satisfy the uniform Lipschitz conditions,

$$\|f(x)-f(y)\|\le L\|x-y\| \tag{4}$$

$$\|g(x)-g(y)\|\le \bar{L}\|x-y\|. \tag{5}$$

We also assume the time-varying disturbances $\xi_i(t)$ and $\eta_i(t)$ are bounded and satisfy the following condition

$$\|\xi_i(t)-\eta_i(t)\|\le \tilde{L}_i \tag{6}$$

where $\tilde{L}_i>0$.

According to systems (2) and (3), the error system is described by

$$ {}_CD^{\alpha}_{0,t}e_i(t) = Ae_i(t) + f(y_i(t)) - f(x_i(t))$$

$$+ c\sum_{j=1}^{N} b_{ij}He_j(t) + [\eta_i(t) - \xi_i(t)] + u_i(t)$$
$$+ \bar{c}\sum_{j=1}^{N} \bar{b}_{ij}\bar{H}[g(y_j(t-\tau)) - g(x_j(t-\tau))] \quad (7)$$

where $e_i(t) = y_i(t) - x_i(t)$, $i = 1, 2, \ldots, N$. Thus, our objective is to design a suitable controller $u_i(t)$ such that error dynamical system (7) is asymptotically stable, i.e.,

$$\lim_{t\to\infty} \|y_i(t; t_0, x_0) - x_i(t; t_0', x_0')\| = 0, \quad i = 1, 2, \ldots, N$$

which implies the drive system (2) and the response system (3) are synchronized.

B. Some Lemmas

Now we present some lemmas for later use.

Lemma 1 [33]: Let $x(0) = y(0)$ and ${}_CD_{0,t}^{\alpha}x(t) \geq {}_CD_{0,t}^{\alpha}y(t)$, where $\alpha \in (0, 1)$. Then $x(t) \geq y(t)$.

Lemma 2 [9], [10]: Consider the following linear fractional system with time delays:

$${}_CD_{0,t}^{\alpha}X(t) = AX(t) + X(t_\tau), \quad \alpha \in (0, 1) \quad (8)$$

where $A = (a_{ij})_{n\times n}$, $X(t) = (x_1(t), x_2(t), \ldots, x_n(t))^T$, $X(t_\tau) = (\sum_{j=1}^{n} k_{1j}x_j(t - \tau_{1j}), \sum_{j=1}^{n} k_{2j}x_k(t- \tau_{2j}), \ldots, \sum_{j=1}^{n} k_{nj}x_j(t - \tau_{nj}))^T$. Let $M = (k_{ij} + a_{ij})_{n\times n}$ and $B = (k_{ij}\exp(-s\tau_{ij}) + a_{ij})_{n\times n}$. If all the eigenvalues of M satisfy $|\arg(\lambda)| > \pi/2$ and the characteristic equation $\det(\Delta(s)) = |s^{\alpha}I_n - B| = 0$ has no purely imaginary roots for any $\tau_{ij} > 0$, $i, j = 1, 2, \ldots, n$, then the zero solution of system (8) is Lyapunov asymptotically stable.

Lemma 3 [34]: Let $x(t) = (x_1(t), \ldots, x_n(t))^T \in \mathbb{R}^n$ be a real continuous and differentiable vector function. Then

$${}_CD_{0,t}^{\alpha}[x^T(t)Px(t)] \leq 2x^T(t)P\,{}_CD_{0,t}^{\alpha}x(t)$$

where $0 < \alpha < 1$, P is a symmetric and positive definite matrix.

Lemma 4 [35]: Let X and Y be arbitrary n-dimensional real vectors, K a positive definite matrix, and $H \in \mathbb{R}^{n\times n}$. Then, the following matrix inequality holds:

$$2X^THY \leq X^THK^{-1}X + Y^TKY.$$

Lemma 5 [36]: Assume that $Q = (q_{ij})_{N\times N}$ is symmetric. Let $M^* = \mathrm{diag}\{m_1^*, m_2^*, \ldots, m_l^*, \underbrace{0, \ldots, 0}_{N-l}\}$, $1 \leq l \leq N$, $m_i^* > 0$ $(i = 1, 2, \ldots, l)$, $Q - M^* = \begin{pmatrix} E - \widetilde{M}^* & S \\ S^T & Q_l \end{pmatrix}$, $\widetilde{M}^* = \mathrm{diag}\{m_1^*, \ldots, m_l^*\}$, $m^* = \min_{1\leq i\leq l}\{m_i^*\}$, Q_l is the minor matrix of Q by removing its first l $(1 \leq l \leq N)$ row-column pairs, E and S are matrices with appropriate dimensions. When $m^* > \lambda_{\max}(E - SQ_l^{-1}S^T)$, then $Q - M^* < 0$ is equivalent to $Q_l < 0$.

C. Lyapunov-like Method for Fractional Nonlinear System With Time Delays

Consider the Caputo fractional non-autonomous system with time delays

$${}_CD_{0,t}^{\alpha}x(t) = f(t, x(t), x(t-\tau)) \quad (9)$$

with initial condition $x(t) = x_0(t)$, $t \in [-\tau, 0]$, where $\alpha \in (0, 1)$, $f : [0, \infty) \times \Omega \to \mathbb{R}^n$ is piecewise continuous on t and locally Lipschitz with respect to x. $\Omega \in \mathbb{R}^n$ is a domain that contains the origin $x = 0$. We always assume that (9) has an equilibrium $x = 0$.

It is well known, by using the Lyapunov direct method, we can get the asymptotic stability of the non-delays systems. Next, we extend the Lyapunov direct method to the time delays case, which leads to the Lyapunov asymptotic stability. Based on [9], [10], [33], we could obtain the following theorem.

Theorem 1: Let $x = 0$ be an equilibrium point of system (9). If there exists a Lyapunov-like function $V(t, x(t)) : [-\tau, \infty] \times \Omega \to \mathbb{R}$ which is continuously differentiable and locally Lipschitz with respect to x such that

$$\alpha_1\|x(t)\|^a \leq V(t, x(t)) \leq \alpha_2\|x(t)\|^{ab} \quad (10)$$

$${}_CD_{0,t}^{\alpha}V(t, x(t)) \leq -\alpha_3\|x(t)\|^{ab} + \alpha_4\|x(t-\tau)\|^a \quad (11)$$

$$\nu < \mu\sin\left(\frac{\alpha\pi}{2}\right) \quad (12)$$

where a, b, α_1, α_2, α_3 are positive constants, $\mu = \alpha_3/\alpha_2$ and $\nu = \alpha_4/\alpha_1$. Then $x = 0$ of system (9) is Lyapunov asymptotically stable.

Proof: It follows from (10) and (11) that

$${}_CD_{0,t}^{\alpha}V(t, x(t)) \leq -\frac{\alpha_3}{\alpha_2}V(t, x(t)) + \frac{\alpha_4}{\alpha_1}V(t-\tau, x(t-\tau)) \quad (13)$$

where $t \geq 0$.

Consider the following system:

$${}_CD_{0,t}^{\alpha}W(t, x(t)) = -\mu W(t, x(t)) + \nu W(t-\tau, x(t-\tau)) \quad (14)$$

where $W(t, x(t))$ has the same initial conditions with $V(t, x(t))$, $\mu = \alpha_3/\alpha_2$ and $\nu = \alpha_4/\alpha_1$. Using Lemma 1, we have

$$0 \leq V(t, x(t)) \leq W(t, x(t)). \quad (15)$$

By Lemma 2, the characteristic equation of (14) is $\det(\Delta(s)) = s^{\alpha} + \mu - \nu\exp(-s\tau) = 0$. Suppose that $s = \omega i = |\omega|(\cos(\pi/2) + i\sin(\pm\pi/2))$. Substituting s into $\det(\Delta(s))$ gives

$$|\omega|^{\alpha}\left(\cos\left(\frac{\alpha\pi}{2}\right) + i\sin\left(\pm\frac{\alpha\pi}{2}\right)\right) + \mu - \nu\left(\cos(\tau\omega) - i\sin(\tau\omega)\right) = 0.$$

Separating real and imaginary parts gives

$$|\omega|^{\alpha}\cos\left(\frac{\alpha\pi}{2}\right) + \mu = \nu\cos(\tau\omega) \quad (16)$$

$$|\omega|^{\alpha}\sin\left(\pm\frac{\alpha\pi}{2}\right) = -\nu\sin(\tau\omega). \quad (17)$$

According to (16) and (17), one has

$$|\omega|^{2\alpha} + 2\mu \cos\left(\frac{\alpha\pi}{2}\right)|\omega|^{\alpha} + \mu^2 - \nu^2 = 0. \tag{18}$$

Obviously, when $\nu < \mu\sin(\alpha\pi/2)$, no real number ω satisfies (18). Furthermore, the eigenvalue of M in equation is $\nu - \mu$. When $\nu < \mu\sin(\alpha\pi/2)$, that is $\nu < \mu$, implying $|\arg(\lambda(M))| > \pi/2$. So, $W(t, x(t)) \to 0$, as $t \to +\infty$.

From (15), $V(t, x(t)) \to 0$, as $t \to +\infty$, which means all the solutions of system (9) converge to $x = 0$. ■

III. Pinning Synchronization of Fractional Complex Networks With Nonlinear Coupling and External Disturbances

In this section, some global asymptotically stable criteria are presented below.

To realize synchronization between (2) and (3), assume that first l $(1 \le l \le N)$ nodes are pinned, the pinning controllers are chosen as

$$\begin{cases} u_i(t) = -p_i e_i(t) - q\dfrac{\text{sgn}(e_i(t))}{\sum\limits_{j=1}^{n}|e_{ij}(t)|}, & 1 \le i \le l \\ u_i(t) = 0, & l+1 \le i \le N \end{cases} \tag{19}$$

where $p_i > 0$ are feedback gains, $\text{sgn}(e_i(t)) = (\text{sgn}(e_{i1}(t)), \text{sgn}(e_{i2}(t)), \ldots, \text{sgn}(e_{in}(t)))^T$ are signum vectors, and $q = \frac{1}{2l}\sum_{i=1}^{N}\tilde{L}_i^2$.

Theorem 2: Suppose that the dynamical function f and nonlinear coupling function g satisfy Lipschitz conditions (4) and (5), respectively. If there exists a matrix P satisfying the following conditions

$$1)\ \ \bar{\mu} = -\lambda_{\max}\left[\left(a + L + \frac{1}{2} + \frac{\bar{c}\beta_2\bar{h}(1+\bar{L})}{2}\right)I_N + ch\hat{B} - P\right] > 0 \tag{20}$$

$$2)\ \ \bar{\nu} < \bar{\mu}\sin\left(\frac{\alpha\pi}{2}\right) \tag{21}$$

where $a = \|A\|$, $h = \|H\|$, $\bar{h} = \|\bar{H}\|$, $\beta_1 = \max\{\bar{b}_{ij}, j \ne i\}$, $\beta_2 = \max\{|\bar{b}_{ii}|\}$ and $\bar{\nu} = \frac{\bar{c}\bar{L}}{2}(N\beta_1\bar{L} + \bar{h}\beta_2)$, then the fractional response network (3) asymptotically synchronizes to the drive network (2).

Proof: Construct the following Lyapunov-like function:

$$V(t, e(t)) = \frac{1}{2}\sum_{i=1}^{N} e_i^T(t)e_i(t). \tag{22}$$

Using (7) and Lemma 3, the fractional derivative of $V(t, e(t))$ yields

$$\begin{aligned} {}_C D_{0,t}^{\alpha} V(t, e(t)) &\le \sum_{i=1}^{N} e_i^T(t)\, {}_C D_{0,t}^{\alpha} e_i(t) \\ &= \sum_{i=1}^{N} e_i^T(t)Ae_i(t) + \sum_{i=1}^{N} e_i^T(t)[f(y_i(t)) - f(x_i(t))] \\ &\quad + c\sum_{i=1}^{N}\sum_{j=1}^{N} b_{ij}e_i^T(t)He_j(t) + \sum_{i=1}^{N} e_i^T(t)[\eta_i(t) - \xi_i(t)] \\ &\quad + \bar{c}\sum_{i=1}^{N}\sum_{j=1}^{N}\bar{b}_{ij}e_i^T(t)\bar{H}[g(y_j(t-\tau)) - g(x_j(t-\tau))] \\ &\quad - \sum_{i=1}^{l} p_i e_i^T(t)e_i(t) - \sum_{i=1}^{l} q\frac{e_i^T(t)\text{sgn}(e_i(t))}{\sum\limits_{j=1}^{n}|e_{ij}(t)|} \\ &\le (a+L)\sum_{i=1}^{N} e_i^T(t)e_i(t) + c\sum_{i=1}^{N}\sum_{j=1}^{N} b_{ij}e_i^T(t)He_j(t) \\ &\quad - \sum_{i=1}^{l} p_i e_i^T(t)e_i(t) - lq \\ &\quad + \bar{c}\sum_{i=1}^{N}\sum_{j=1}^{N}\bar{b}_{ij}e_i^T(t)\bar{H}[g(y_j(t-\tau)) - g(x_j(t-\tau))] \\ &\quad + \sum_{i=1}^{N} e_i^T(t)[\eta_i(t) - \xi_i(t)]. \end{aligned} \tag{23}$$

From Lemma 4, we have (24), shown at the bottom of this page, and

$$\begin{aligned} &\sum_{i=1}^{N}\sum_{j=1}^{N}\bar{b}_{ij}e_i^T(t)\bar{H}\Big[g(y_j(t-\tau)) - g(x_j(t-\tau))\Big] \\ &\le \sum_{i=1}^{N}\sum_{j=1, j\ne i}^{N}\bar{b}_{ij}\Big[(g(y_j(t-\tau)) - g(x_j(t-\tau)))^T(g(y_j(t-\tau)) - g(x_j(t-\tau))) \\ &\qquad + e_i^T(t)\bar{H}e_i(t)\Big] + 2\bar{h}\bar{L}\sum_{i=1}^{N}|\bar{b}_{ii}|\cdot\|e_i(t)\|\cdot\|e_i(t-\tau)\| \\ &\le \sum_{i=1}^{N}\sum_{j=1, j\ne i}^{N}\bar{b}_{ij}\Big[\bar{L}^2 e_j^T(t-\tau)e_j(t-\tau) + \bar{h}e_i^T(t)e_i(t)\Big] \\ &\qquad + \bar{h}\bar{L}\sum_{i=1}^{N}|\bar{b}_{ii}|\Big[e_i^T(t)e_i(t) + e_i^T(t-\tau)e_i(t-\tau)\Big] \\ &\le \beta_2\bar{h}(1+\bar{L})\sum_{i=1}^{N} e_i^T(t)e_i(t) + \bar{L}(N\beta_1\bar{L} + \beta_2\bar{h})\sum_{i=1}^{N} e_i^T(t-\tau)e_i(t-\tau) \end{aligned} \tag{24}$$

$$\begin{aligned}&\sum_{i=1}^{N}\sum_{j=1}^{N} b_{ij}e_i^T(t)He_j(t)\\&\quad=\sum_{i=1}^{N}\sum_{j=1,j\neq i}^{N} b_{ij}e_i^T(t)He_j(t)\\&\qquad+\sum_{i=1}^{N} b_{ii}e_i^T(t)\left(\frac{H+H^T}{2}\right)e_i(t)\\&\quad\leq h\sum_{i=1}^{N}\sum_{j=1,j\neq i}^{N} b_{ij}\|e_i(t)\|\cdot\|e_j(t)\|\\&\qquad+\rho_{\min}\sum_{i=1}^{N} b_{ii}e_i^T(t)e_i(t)\end{aligned}\tag{25}$$

where $\rho_{\min}$ is the minimum eigenvalue of the matrix $(H+H^T)/2$. Using Lemma 4 and (6), we get

$$\begin{aligned}&\sum_{i=1}^{N} e_i^T(t)[\eta_i(t)-\xi_i(t)]-lq\\&\quad\leq\frac{1}{2}\sum_{i=1}^{N} e_i^T(t)e_i(t)\\&\qquad+\frac{1}{2}\sum_{i=1}^{N}[\eta_i(t)-\xi_i(t)]^T[\eta_i(t)-\xi_i(t)]-lq\\&\quad\leq\frac{1}{2}\sum_{i=1}^{N} e_i^T(t)e_i(t)+\frac{1}{2}\sum_{i=1}^{N}\tilde{L}_i^2-lq\\&\quad=\frac{1}{2}\sum_{i=1}^{N} e_i^T(t)e_i(t).\end{aligned}\tag{26}$$

Substituting (24)−(26) into (23), and from Lemma 3, we obtain that

$$\begin{aligned}&{}_CD_{0,t}^{\alpha}V(t,e(t))\\&\quad\leq\|e(t)\|^T\Bigg[\left(a+L+\frac{1}{2}+\frac{\bar{c}\beta_2\bar{h}(1+\bar{L})}{2}\right)I_N\\&\qquad+ch\hat{B}-P\Bigg]\|e(t)\|\\&\qquad+\frac{\bar{c}\bar{L}}{2}(N\beta_1\bar{L}+\bar{h}\beta_2)\|e(t-\tau)\|^T\cdot\|e(t-\tau)\|\\&\quad\leq-\bar{\mu}\sum_{i=1}^{N} e_i^Te_i(t)+\bar{\nu}\sum_{i=1}^{N} e_i(t-\tau)^Te_i(t-\tau)\end{aligned}\tag{27}$$

where $\|e(t)\| = (\|e_1(t)\|, \|e_2(t)\|, \ldots, \|e_N(t)\|)^T$, $P = \mathrm{diag}(\underbrace{p_1, p_2, \ldots, p_l}_{l}, \underbrace{0, 0, \ldots, 0}_{N-l})$, $\hat{B} = (\tilde{B}^T + \tilde{B})/2$ and $\tilde{B}$ is a modifying matrix of B via replacing the diagonal elements b_{ii} by $(\rho_{\min}/h)b_{ii}$.

According to Theorem 1, we have $\|e_i(t)\| \to 0$, that is $\|y_i(t) - x_i(t)\| \to 0$ as $t \to \infty$, which means that the asymptotical synchronization between drive system (2) and response system (3) is realized. ■

Furthermore, from (27), let $Q = (a + L + 1/2 + \bar{c}\beta_2\bar{h}(1 + \bar{L})/2)I_N + ch\hat{B}$, and $Q - P = \begin{pmatrix} E-P^* & S\\ S^T & Q_l\end{pmatrix}$, where $1 \leq l \leq N$, $P^* = \mathrm{diag}\{p_1, p_2, \ldots, p_l\}$, Q_l is the part matrix of Q by removing its first l row-column pairs, E and S are matrices with appropriate dimensions. Based on Lemma 5, and supposing that p_i $(i = 1, \ldots, l)$ are suitably large, $Q-P < 0$ is equivalent to $Q_l = [(a+L+1/2+\bar{c}\beta_2\bar{h}(1+\bar{L})/2)I_N+ch\hat{B}]_l < 0$. One has $\lambda_{\max}[(a+L+1/2+\bar{c}\beta_2\bar{h}(1+\bar{L})/2)I_N+ch\hat{B}]_l = (a+L+1/2+\bar{c}\beta_2\bar{h}(1+\bar{L})/2)+ch\lambda_{\max}(\hat{B}_l) < 0$. So, the following corollary can be immediately obtained.

Corollary 1: Under assumptions (4) and (5), the fractional response network (3) asymptotically synchronizes to the drive one (2) under the controller (28), where p_i $(i = 1, \ldots, l)$ are sufficiently large, and the following conditions satisfied :

$$\begin{aligned}\bar{\mu}=&-\Bigg[\left(a+L+\frac{1}{2}+\frac{\bar{c}\beta_2\bar{h}(1+\bar{L})}{2}\right)\\&+ch\lambda_{\max}(\hat{B}_l)\Bigg]>0\\\bar{\nu}<&\ \bar{\mu}\sin\left(\frac{\alpha\pi}{2}\right)\end{aligned}$$

in which $\bar{\nu} = \frac{\bar{c}\bar{L}}{2}(N\beta_1\bar{L} + \bar{h}\beta_2)$.

Corollary 2: If $g(x_j(t-\tau)) = x_j(t-\tau)$ and $g(y_j(t-\tau)) = y_j(t-\tau)$, the synchronous conditions between (2) and (3) are reduced to:

$$\begin{aligned}\bar{\mu}=&-\lambda_{\max}\Bigg[\left(a+L+\frac{1}{2}+\bar{c}\beta_2\bar{h}\right)I_N\\&+ch\hat{B}-P\Bigg]>0\\\bar{\nu}<&\ \bar{\mu}\sin\left(\frac{\alpha\pi}{2}\right)\end{aligned}$$

where $\nu = \frac{\bar{c}}{2}(N\beta_1 + \bar{h}\beta_2)$.

Corollary 3: Assume $\xi_i(t) = \eta_i(t) = 0$, the fractional complex networks (2) and (3) do not contain the disturbances. Under the assumptions (4) and (5), fractional systems (2) and (3) can be asymptotically synchronized under the controllers

$$\begin{cases}u_i(t)=-p_ie_i(t), & 1\leq i\leq l\\ u_i(t)=0, & l+1\leq i\leq N\end{cases}\tag{28}$$

and the following control conditions:

$$\begin{aligned}\bar{\mu}=&-\lambda_{\max}\Bigg[\left(a+L+\frac{\bar{c}\beta_2\bar{h}(1+\bar{L})}{2}\right)I_N\\&+ch\hat{B}-P\Bigg]>0\\\bar{\nu}<&\ \bar{\mu}\sin\left(\frac{\alpha\pi}{2}\right)\end{aligned}$$

where $\bar{\nu} = \frac{\bar{c}\bar{L}}{2}(N\beta_1\bar{L} + \bar{h}\beta_2)$.

IV. NUMERICAL EXAMPLE

In this section, a numerical example is presented. Consider a complex network with 10 nodes, the fractional dynamical equation of each node is described by the following fractional chaotic Lorenz system

$$\begin{cases}{}_CD_{0,t}^{\alpha}x_{i1}=a_L(x_{i2}-x_{i1})\\{}_CD_{0,t}^{\alpha}x_{i2}=b_Lx_{i1}-x_{i1}x_{i3}-x_{i2}\\{}_CD_{0,t}^{\alpha}x_{i3}=x_{i1}x_{i2}-c_Lx_{i3}\end{cases}\tag{29}$$

where $i = 1, 2, \ldots, 10$. The parameters are chosen as $a_L = 10$, $b_L = 28$, $c_L = 8/3$ and $\alpha = 0.995$. From (2) and (3), we know that $A = \begin{pmatrix} -a & a & 0 \\ b & -1 & 0 \\ 0 & 0 & -c \end{pmatrix}$, $f(x_i(t)) = \begin{pmatrix} 0 \\ -x_{i1}x_{i3} \\ x_{i1}x_{i2} \end{pmatrix}$, and that system (29) is chaotic, see Fig. 1.

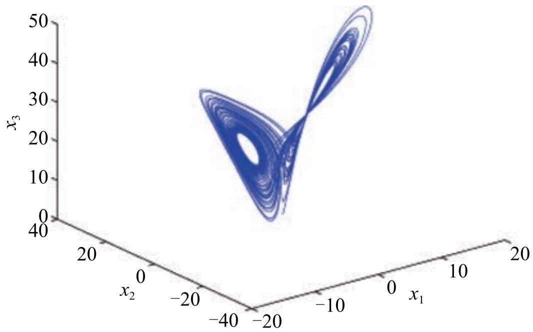

Fig. 1. Chaotic attractor of fractional Lorenz system with order $\alpha = 0.995$.

For convenience, let $H = \bar{H} = I$, the coupling configuration matrices B and $\bar{B}$ are given as follows,

$$\begin{pmatrix} -2 & 1 & 0 & 1 & 0 & 0 & 0 & 0 & 0 & 0 \\ 0 & -2 & 1 & 0 & 1 & 0 & 0 & 0 & 0 & 0 \\ 1 & 0 & -3 & 0 & 0 & 1 & 1 & 0 & 0 & 0 \\ 0 & 0 & 1 & -1 & 0 & 0 & 0 & 0 & 0 & 0 \\ 0 & 1 & 0 & 1 & -3 & 0 & 0 & 0 & 1 & 0 \\ 0 & 0 & 1 & 0 & 1 & -2 & 0 & 0 & 0 & 0 \\ 0 & 0 & 0 & 0 & 0 & 1 & -3 & 1 & 0 & 1 \\ 0 & 1 & 0 & 1 & 0 & 0 & 0 & -3 & 1 & 0 \\ 1 & 0 & 1 & 0 & 0 & 0 & 1 & 0 & -4 & 1 \\ 0 & 0 & 1 & 1 & 0 & 0 & 0 & 0 & 0 & -2 \end{pmatrix}.$$

The nonlinear coupling function is chosen as

$$\begin{aligned} g(x_j(t-\tau)) = (&x_{j1}(t-\tau) + \sin(x_{j1}(t-\tau)), \\ &x_{j2}(t-\tau) + \sin(x_{j2}(t-\tau)), \\ &x_{j3}(t-\tau) + \sin(x_{j3}(t-\tau)))^T. \end{aligned}$$

It is known that the Lorenz system is bounded. Actually, $\|x_{i1}\| \le 25$, $\|x_{i2}\| \le 30$, $\|x_{i3}\| \le 60$, $\|y_{i1}\| \le 25$, $\|y_{i2}\| \le 30$, $\|y_{i3}\| \le 60$, $i = 1, 2, \ldots, 10$, and

$$\begin{aligned} &\|f(x_i) - f(y_i)\| \\ &\le \sqrt{(-x_{i1}x_{i3} + y_{i1}y_{i3})^2 + (x_{i1}x_{i2} - y_{i1}y_{i2})^2} \\ &\le 75.83\|e_i\| \end{aligned}$$

that is $L = 75.83$. Obviously, $\bar{L} = 2$. According to the method proposed in [15], whose out-degrees are bigger than their in-degrees, it should be selected as pinned candidates. The out-degrees of nodes 2, 3 and 4 are bigger than their in-degrees, so we choose them as the pinned nodes. Rearrange the network nodes and the new order will be 4, 3, 2, 1, 6, 10, 5, 7, 8, 9.

Under the no disturbance case, that is $\xi_i(t) = \eta_i(t) = (0, 0, 0)^T$, let $p_i = 910$, $i = 1, 2, 3$, when $\alpha = 0.9$, $c = 100$, $\bar{c} = 0.01$, one has $\bar{\mu}\sin(\alpha\pi/2) = 0.2808$ and $\bar{\nu} = 0.2400$. From Corollary 3, it is clear that pinning conditions hold. The simulation results are shown in Fig. 2, which shows the time waveforms of errors e_{i1}, e_{i2}, e_{i3}, $i = 1, 2, \ldots, 10$. From the figures, fractional complex networks (2) and (3) are synchronized, which demonstrate the effectiveness of the proposed method.

Now, we come to the disturbance case. Let $p_i = 930$, $i = 1, 2, 3$, $\xi_i(t) = (0, 0, 0)^T$, $\eta_i(t) = (0.3\sin t\cos t, 0.1\sin t, 0.5\cos t)^T$, $\alpha = 0.9$, $c = 100$, $\bar{c} = 0.01$, one has $q = 0.5833$, $\bar{\mu}\sin(\alpha\pi/2) = 0.2489$ and $\bar{\nu} = 0.2400$. From Theorem 2, it is clear that pinning conditions hold. Fig. 3 illustrates the synchronization phenomenon in noisy environment. It shows the error trajectories of drive and response networks, from which we can see that the synchronization between the driving and response networks is achieved successfully.

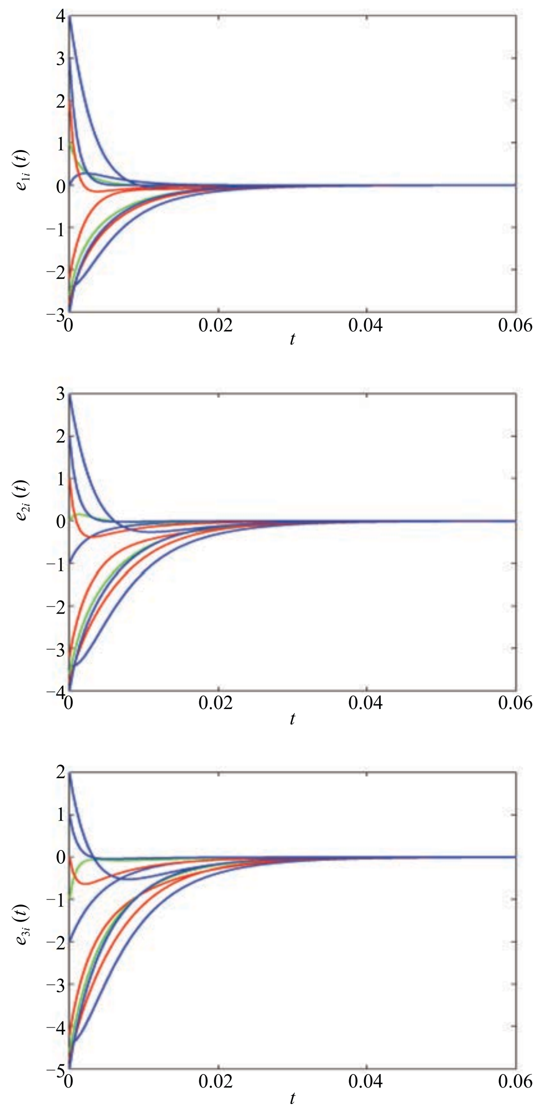

Fig. 2. Time evolution of the error states e_{1i}, e_{2i} and e_{3i} with no disturbance.

V. Conclusion

In this paper, we proposed a fractional pinning controller and presented a synchronization law for the delayed fractional complex networks with nonlinear couplings and disturbances. Some new synchronization criteria are proposed based on the Lyapunov-like stability theory. This method can be applied to many types of fractional complex networks. Furthermore, the coupling configuration matrices and the inner-coupling matrices are not assumed to be symmetric or irreducible. It means that this method is more general. The numerical results showed the effectiveness of the proposed controllers.

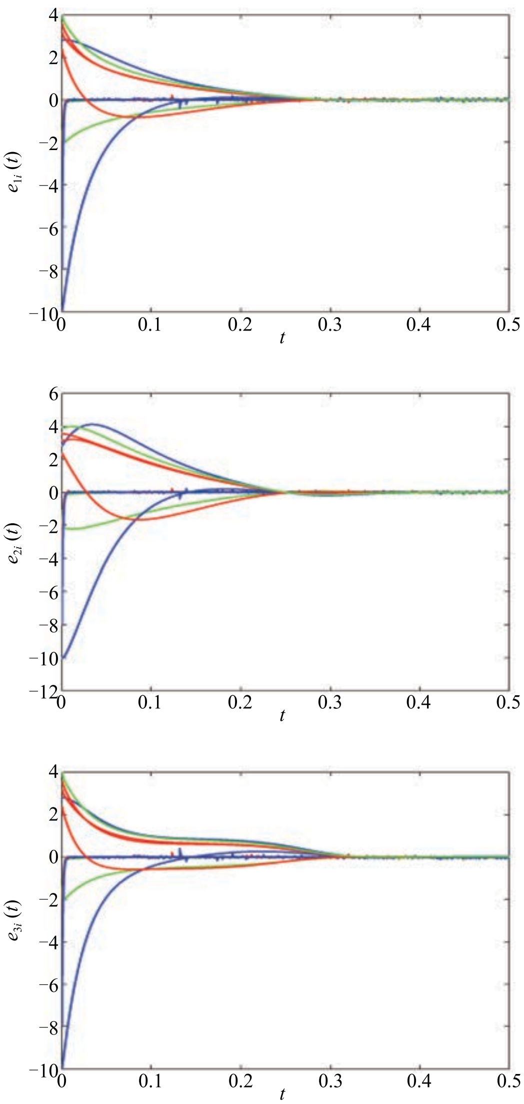

Fig. 3. Time evolution of the error states e_{1i}, e_{2i} and e_{3i} with disturbances.

REFERENCES

[1] R. C. Koeller, "Polynomial operators, stieltjes convolution, and fractional calculus in hereditary mechanics," *Acta Mech.*, vol. 58, no. 3−4, pp. 251−264, Apr. 1986.

[2] P. J. Torvik and R. L. Bagley, "On the appearance of the fractional derivative in the behavior of real materials," *J. Appl. Mech.*, vol. 51, no. 2, pp. 294−298, Jun. 1984.

[3] O. Heaviside, *Electromagnetic Theory*. New York, USA: Chelsea, 1971, pp. 1−130.

[4] I. Podlubny, *Fractional Differential Equations*. New York, USA: Academic Press, 1998, pp. 201−307.

[5] I. Grigorenko and E. Grigorenko, "Chaotic dynamics of the fractional Lorenz system," *Phys. Rev. Lett.*, vol. 91, no. 3, pp. 034101, Jul. 2003.

[6] T. T. Hartley, C. F. Lorenzo, and H. K. Qammer, "Chaos in a fractional order Chuaś system," *IEEE Trans. Circ. Syst. I Fund. Theory Appl.*, vol. 42, no. 8, pp. 485−490, Aug. 1995.

[7] C. G. Li and G. R. Chen, "Chaos in the fractional order Chen system and its control," *Chaos Solitons Fractals*, vol. 22, no. 3, pp. 549−554, Nov. 2004.

[8] B. N. Lundstrom, M. H. Higgs, W. J. Spain, and A. L. Fairhall, "Fractional differentiation by neocortical pyramidal neurons," *Nat. Neurosci.*, vol. 11, no. 11, pp. 1335−1342, Oct. 2008.

[9] H. Wang, Y. G. Yu, G. G. Wen, S. Zhang, and J. Z. Yu, "Global stability analysis of fractional-order Hopfield neural networks with time delay," *Neurocomputing*, vol. 154, pp. 15−23, Apr. 2015.

[10] W. H. Deng, C. P. Li, and J. H. Lv, "Stability analysis of linear fractional differential system with multiple time delays," *Nonlinear Dyn.*, vol. 48, no. 4, pp. 409−416, Jun. 2007.

[11] C. P. Li, W. H. Deng, and D. Xu, "Chaos synchronization of the Chua system with a fractional order," *Phys. A: Stat. Mech. Appl.*, vol. 360, no. 2, pp. 171−185, Feb. 2006.

[12] W. Y. Ma, C. P. Li, and Y. J. Wu, "Impulsive synchronization of fractional Takagi-Sugeno fuzzy complex networks," *Chaos: An Interdisciplinary J. of Nonlinear Sci.*, vol. 26, no. 8, pp. 084311, 2016.

[13] X. J. Wu and Y. Lu, "Generalized projective synchronization of the fractional-order Chen hyperchaotic system," *Nonlinear Dyn.*, vol. 57, no. 1−2, pp. 25−35, Jul. 2009.

[14] L. P. Chen, Y. Chai, and R. C. Wu, "Linear matrix inequality criteria for robust synchronization of uncertain fractional-order chaotic systems," *Chaos Interdiscip. J. Nonlinear Sci.*, vol. 21, no. 4, Article ID 043107, Oct. 2011.

[15] Z. Odibat, "A note on phase synchronization in coupled chaotic fractional order systems," *Nonlinear Anal. Real World Appl.*, vol. 13, no. 2, pp. 779−789, Apr. 2012.

[16] Y. C. Wang, H. G. Zhang, X. Y. Wang, and D. S. Yang, "Networked synchronization control of coupled dynamic networks with time-varying delay," *IEEE Trans. Syst. Man Cybern. B Cybern.*, vol. 40, no. 6, pp. 1468−1479, Dec. 2010.

[17] X. F. Wang and G. R. Chen, "Pinning control of scale-free dynamical networks," *Phys. A: Stat. Mech. Appl.*, vol. 310, no. 3−4, pp. 521−531, Jul. 2002.

[18] F. Sorrentino, M. di Bernardo, F. Garofalo, and G. R. Chen, "Controllability of complex networks via pinning," *Phys. Rev. E*, vol. 75, no. 4, pp. 046103, Apr. 2007.

[19] Y. Liang and X. Y. Wang, "Synchronizability on complex networks via pinning control," *Pramana*, vol. 80, no. 4, pp. 593−606, Apr. 2013.

[20] W. W. Yu, G. R. Chen, J. H. Lv, and J. Kurths, "Synchronization via pinning control on general complex networks," *SIAM J. Control Optim.*, vol. 51, no. 2, pp. 1395−1416, Apr. 2013.

[21] F. Z. Nian and X. Y. Wang, "Optimal pinning synchronization on directed complex network," *Chaos Interdiscip. J. Nonlinear Sci.*, vol. 21, no. 4, pp. 043131, Dec. 2011.

[22] Y. Liang and X. Y. Wang, "A method of quickly calculating the number of pinning nodes on pinning synchronization in complex networks," *Appl. Math. Comput.*, vol. 246, pp. 743−751, Nov. 2014.

[23] Y. Liang, X. Y. Wang, and J. Eustace, "Adaptive synchronization in complex networks with non-delay and variable delay couplings via pinning control," *Neurocomputing*, vol. 123, pp. 292−298, Jan. 2014.

[24] Y. H. Xu, C. R. Xie, and D. B. Tong, "Adaptive synchronization for dynamical networks of neutral type with time-delay," *Optik Int. J. Light Electr. Opt.*, vol. 125, no. 1, pp. 380−385, Jan. 2014.

[25] R. R. Cheng, M. S. Peng, and W. B. Yu, "Pinning synchronization of delayed complex dynamical networks with nonlinear coupling," *Phys. A: Stat. Mech. Appl.*, vol. 413, pp. 426−431, Nov. 2014.

[26] Y. Tang, Z. D. Wang, and J. A. Fang, "Pinning control of fractional-order weighted complex networks," *Chaos Interdiscip. J. Nonlinear Sci.*, vol. 19, no. 1, pp. 013112, Feb. 2009.

[27] L. Pan, W. N. Zhou, J. A. Fang, and D. Q. Li, "Synchronization and anti-synchronization of new uncertain fractional-order modified unified chaotic systems via novel active pinning control," *Commun. Nonlinear Sci. Numer. Simul.*, vol. 15, no. 12, pp. 3754−3762, Dec. 2010.

[28] Y. Chai, L. P. Chen, R. C. Wu, and J. Sun, "Adaptive pinning synchronization in fractional-order complex dynamical networks," *Phys. A: Stat. Mech. Appl.*, vol. 391, no. 22, pp. 5746−5758, Nov. 2012.

[29] W. Xiang and F. Q. Chen, "Robust synchronization of a class of chaotic systems with disturbance estimation," *Commun. Nonlinear Sci. Numer. Simul.*, vol. 16, no. 8, pp. 2970−2977, Aug. 2011.

[30] D. F. Wang, J. Y. Zhang, and X. Y. Wang, "Robust modified projective synchronization of fractional-order chaotic systems with parameters perturbation and external disturbance," *Chin. Phys. B*, vol. 22, no. 10, pp. 100504, Apr. 2013.

[31] T. D. Ma and J. Zhang, "Hybrid synchronization of coupled fractional-order complex networks," *Neurocomputing*, vol. 157, pp. 166−172, Jun. 2015.

[32] L. X. Yang and J. Jiang, "Adaptive synchronization of drive-response fractional-order complex dynamical networks with uncertain parameters," *Commun. Nonlinear Sci. Numer. Simul.*, vol. 19, no. 5, pp. 1496−1506, May 2014.

[33] Y. Li, Y. Q. Chen, and I. Podlubny, "Mittag-Leffler stability of fractional order nonlinear dynamic systems," *Automatica*, vol. 45, no. 8, pp. 1965−1969, Aug. 2009.

[34] M. A. Duarte-Mermoud, N. Aguila-Camacho, J. A. Gallegos, and R. Castro-Linares, "Using general quadratic Lyapunov functions to prove Lyapunov uniform stability for fractional order systems," *Commun. Nonlinear Sci. Numer. Simul.*, vol. 22, no. 1−3, pp. 650−659, May 2015.

[35] J. S. Wu and L. C. Jiao, "Synchronization in complex delayed dynamical networks with nonsymmetric coupling," *Phys. A: Stat. Mech. Appl.*, vol. 386, no. 1, pp. 513−530, Dec. 2007.

[36] Q. Song and J. D. Cao, "On pinning synchronization of directed and undirected complex dynamical networks," *IEEE Trans. Circ. Syst. I Regul. Pap.*, vol. 57, no. 3, pp. 672−680, Mar. 2010.

Weiyuan Ma received the B. Sc. degree in mathematics at Northwest Normal University, Lanzhou, China, in 2004, and received the M. Sc. degree in mathematics at Lanzhou University, Lanzhou, China, in 2007. He is working toward the Ph. D. degree in computational mathematics at Lanzhou University, Lanzhou, China. He is currently an associate professor at the School of Mathematics and Computer Science, Northwest University for Nationalities, China. His research interests include complex networks, nonlinear systems, and chaos control.

Yujiang Wu received the B. Sc. and M. Sc. degrees in mathematics at Lanzhou University, Lanzhou, China, in 1982 and 1985, respectively, and he received the Ph. D. degree in mathematics at Shanghai University, Shanghai, China, in 1997. He is currently a professor at the School of Mathematics and Statistics, Lanzhou University, China. His main research interest is scientific computing. Corresponding author of this paper.

Changpin Li received his Ph. D. degree in computational mathematics from Shanghai University, China in 1998. After graduation, he worked in the same university and became a full professor in 2007 and director of the Institute of Computational Mathematics in 2012. Dr. Li is in the broad area of applied theory and computation of bifurcation and chaos, dynamics of fractional ordinary differential equations, dynamics of complex networks, numerical methods and computations of fractional partial differential equations, fractional modeling. Dr Li's current work is focused on fractional modeling of anomalous diffusion with mathematical analysis and numerical calculations. Dr Li has published nearly 100 papers in referred journals with more than 2500 citations. He has co-edited one book published by World Scientific, and has published one book by CRC press. He is on the editorial boards of several journals such as *Fractional Calculus and Applied Analysis*, *International Journal of Bifurcation and Chaos*, *International Journal of Computer Mathematics*, etc. He was also the lead guest editor of *European Physical Journal-Special Topics* (2011), *International Journal of Bifurcation and Chaos* (2012), and *Philosophical Transactions of the Royal Society A: Mathematical, Physical and Engineering Sciences* (2013). He was awarded the Shanghai Natural Science Prize in 2010, Bao Steel Prize in 2011, and Riemann-Liouville Award: Best FDA Paper (theory) in FDA'12 in 2012.

Variational Calculus With Conformable Fractional Derivatives

Matheus J. Lazo and Delfim F. M. Torres

***Abstract*—Invariant conditions for conformable fractional problems of the calculus of variations under the presence of external forces in the dynamics are studied. Depending on the type of transformations considered, different necessary conditions of invariance are obtained. As particular cases, we prove fractional versions of Noether's symmetry theorem. Invariant conditions for fractional optimal control problems, using the Hamiltonian formalism, are also investigated. As an example of potential application in Physics, we show that with conformable derivatives it is possible to formulate an Action Principle for particles under frictional forces that is far simpler than the one obtained with classical fractional derivatives.**

***Index Terms*—Conformable fractional derivative, fractional calculus of variations, fractional optimal control, invariant variational conditions, Noether's theorem.**

I. Introduction

FRACTIONAL calculus is a generalization of (integer) differential calculus, allowing to define integrals and derivatives of real or complex order [1]–[3]. It had its origin in the 1600 s and for three centuries the theory of fractional derivatives developed as a pure theoretical field of mathematics, useful only for mathematicians. The theory took more or less finished form by the end of the 19th century. In the last few decades, fractional differentiation has been "rediscovered" by applied scientists, proving to be very useful in various fields: physics (classic and quantum mechanics, thermodynamics, etc.), chemistry, biology, economics, engineering, signal and image processing, and control theory [4]. One can find in the existent literature several definitions of fractional derivatives, including the Riemann-Liouville, Caputo, Riesz, Riesz-Caputo, Weyl, Grunwald-Letnikov, Hadamard, and Chen derivatives. Recently, a simple solution to the discrepancies between known definitions was presented with the introduction of a new fractional notion, called the conformable derivative [5]. The new definition is a natural extension of the usual derivative, and satisfies the main properties one expects in a derivative: the conformable derivative of a constant is zero; satisfies the standard formulas of the derivative of the product and of the derivative of the quotient of two functions; and satisfies the chain rule. Besides simple and similar to the standard derivative, one can say that the conformable derivative combines the best characteristics of known fractional derivatives [6]. For this reason, the subject is now under strong development: see [7]–[10] and references therein.

The fractional calculus of variations was introduced in the context of classical mechanics when Riewe [11] showed that a Lagrangian involving fractional time derivatives leads to an equation of motion with non-conservative forces such as friction. It is a remarkable result since frictional and non-conservative forces are beyond the usual macroscopic variational treatment [12]. Riewe generalized the usual calculus of variations for a Lagrangian depending on Riemann-Liouville fractional derivatives [11] in order to deal with linear non-conservative forces. Actually, several approaches have been developed to generalize the calculus of variations to include problems depending on Caputo fractional derivatives, Riemann-Liouville fractional derivatives, Riesz fractional derivatives and others [13]–[19] (see [20]–[22] for the state of the art). Among theses approaches, recently it was shown that the action principle for dissipative systems can be generalized, fixing the mathematical inconsistencies present in the original Riewe's formulation, by using Lagrangians depending on classical and Caputo derivatives [23].

In this paper we work with conformable fractional derivatives in the context of the calculus of variations and optimal control [20]. In order to illustrate the potential application of conformable fractional derivatives in physical problems we show that it is possible to formulate an action principle with conformable fractional calculus for the frictional force free from the mathematical inconsistencies found in the Riewe original approach and far simpler than the formulations proposed in [23]. Furthermore, we obtain a generalization of Noether's symmetry theorem for fractional variational problems and we also consider conformable fractional optimal control problems. Emmy Noether was the first who proved, in 1918, that the notions of invariance and constant of motion are connected: when a system is invariant under a family of transformations, then a conserved quantity along the Euler-Lagrange extremals can be obtained [24], [25]. All conservation laws of Mechanics, e.g., conservation of energy or conservation of momentum, are easily explained from Noether's theorem. In this paper we study necessary conditions for invariance under a family of continuous transformations,

Manuscript received October 1, 2015; accepted June 22, 2016. This work was partially supported by CNPq and CAPES (Brazilian research funding agencies), and Portuguese funds through the Center for Research and Development in Mathematics and Applications (CIDMA), and also the Portuguese Foundation for Science and Technology (FCT), within project UID/MAT/04106/2013. Recommended by Associate Editor YangQuan Chen.

Citation: M. J. Lazo, D. F. M. Torres, "Variational calculus with conformable fractional derivatives," *IEEE/CAA Journal of Automatica Sinica*, vol. 4, no. 2, pp. 340−352, Apr. 2017.

M. J. Lazo is with the Instituto de Matemática, Estatística e Física — FURG, Rio Grande, RS 96.201-900, Brazil (e-mail: matheuslazo@furg.br).

D. F. M. Torres is with the Center for Research and Development in Mathematics and Applications (CIDMA), Department of Mathematics, University of Aveiro, Aveiro 3810-193, Portugal (e-mail: delfim@ua.pt).

Digital Object Identifier 10.1109/JAS.2016.7510160

where the Lagrangian contains a conformable fractional derivative of order $\alpha \in (0,1)$. When $\alpha \to 1$, we obtain some well-known results, in particular the Noether theorem [25]. The advantages of our fractional results are clear. Indeed, the classical constants of motion appear naturally in closed systems while in practical terms closed systems do not exist: forces that do not store energy, so-called nonconservative or dissipative forces, are always present in real systems. Fractional dynamics provide a good way to model nonconservative systems [11]. Nonconservative forces remove energy from the systems and, as a consequence, the standard Noether constants of motion are broken [26]. Our results assert that it is still possible to obtain Noether-type theorems, which cover both conservative and nonconservative cases, and that this is done in a particularly simple and elegant way via the conformable fractional approach. This is in contrast with the approaches followed in [27]–[30].

The paper is organized as follows. In Section II we collect some necessary definitions and results on the conformable fractional calculus needed in the sequel. In Section III we obtain the conformable fractional Euler-Lagrange equation and in Section IV we formulate an action principle for dissipative systems, as an example of application and motivation to study the conformable calculus of variations. In Section V, we present an immediate consequence of the Euler-Lagrange equation that we use later in Sections VI and VII, where we prove, respectively, some necessary conditions for invariant fractional problems and a conformable fractional Noether theorem. We then review the obtained results using the Hamiltonian language in Section VIII. In Section IX, we consider the conformable fractional optimal control problem, where the dynamic constraint is given by a conformable fractional derivative. Using the Hamiltonian language, we provide an invariant condition. In Section X we consider the multi-dimensional case, for several independent and dependent variables.

II. Preliminaries

In this section we review the conformable fractional calculus [5]–[7]. The conformable fractional derivative is a new well-behaved definition of fractional derivative, based on a simple limit definition. We review in this section the generalization of [5] proposed in [6].

Definition 1: The left conformable fractional derivative of order $0 < \alpha \leq 1$ starting from $a \in \mathbb{R}$ of a function $f : [a,b] \to \mathbb{R}$ is defined by

$$\frac{d_a^\alpha}{dx_a^\alpha} f(x) = f_a^{(\alpha)}(x) = \lim_{\epsilon \to 0} \frac{f(x + \epsilon(x-a)^{1-\alpha}) - f(x)}{\epsilon}. \qquad (1)$$

If the limit (1) exist, then we say that f is left α-differentiable. Furthermore, if $f_a^{(\alpha)}(x)$ exist for $x \in (a,b)$, then

$$f_a^{(\alpha)}(a) = \lim_{x \to a^+} f_a^{(\alpha)}(x)$$

and

$$f_a^{(\alpha)}(b) = \lim_{x \to b^-} f_a^{(\alpha)}(x).$$

The right conformable fractional derivative of order $\alpha \in (0,1]$ terminating at $b \in \mathbb{R}$ of a function $f : [a,b] \to \mathbb{R}$ is defined by

$$\frac{{}_b d^\alpha}{{}_b dx^\alpha} f(x) = {}_b f^{(\alpha)}(x) = -\lim_{\epsilon \to 0} \frac{f(x + \epsilon(b-x)^{1-\alpha}) - f(x)}{\epsilon}. \qquad (2)$$

If the limit (2) exist, then we say that f is right α-differentiable. Furthermore, if ${}_b f^{(\alpha)}(x)$ exist for $x \in (a,b)$, then

$${}_b f^{(\alpha)}(a) = \lim_{x \to a^+} {}_b f^{(\alpha)}(x)$$

and

$${}_b f^{(\alpha)}(b) = \lim_{x \to b^-} {}_b f^{(\alpha)}(x).$$

It is important to note that for $\alpha = 1$ the conformable fractional derivatives (1) and (2) reduce to first order ordinary derivatives. Furthermore, despite the definition of the conformable fractional derivatives (1) and (2) can be generalized for $\alpha > 1$ [6], we consider only $0 < \alpha \leq 1$ in the present work. Is is also important to note that, differently from the majority of definitions of fractional derivative, including the popular Riemann-Liouville and Caputo fractional derivatives, the fractional derivatives (1) and (2) are local operators and are related to ordinary derivatives if the function is differentiable (see Remark 1). For more on local fractional derivatives, we refer the reader to [31], [32] and references therein.

Remark 1: If $f \in C^1[a,b]$, then we have from (1) that

$$f_a^{(\alpha)}(x) = (x-a)^{1-\alpha} f'(x) \qquad (3)$$

and from (2) that

$${}_b f^{(\alpha)}(x) = -(b-x)^{1-\alpha} f'(x) \qquad (4)$$

where $f'(x)$ stands for the ordinary first order derivative of $f(x)$.

From (3) and (4) it is easy to see that the conformable fractional derivative of a constant is zero, differently from the Riemann-Liouville derivative of a constant, and for the power functions $(x-a)^p$ and $(b-x)^p$ one has

$$\frac{d_a^\alpha}{dx_a^\alpha}(x-a)^p = p(x-a)^{p-\alpha}$$

and

$$\frac{{}_b d^\alpha}{{}_b dx^\alpha}(b-x)^p = p(b-x)^{p-\alpha}$$

for all $p \in \mathbb{R}$.

The most remarkable consequence of definitions (1) and (2) is that the conformable fractional derivatives satisfy very simple fractional versions of chain and product rules.

Proposition 1 [5], [6]: Let $0 < \alpha < 1$ and f and g be α-differentiable functions. Then,

1)
$$(c_1 f + c_2 g)_a^{(\alpha)}(x) = c_1 f_a^{(\alpha)}(x) + c_2 g_a^{(\alpha)}(x)$$
and
$${}_b(c_1 f + c_2 g)^{(\alpha)}(x) = c_1 {}_b f^{(\alpha)}(x) + c_2 {}_b g^{(\alpha)}(x)$$

for all $c_1, c_2 \in \mathbb{R}$.

2)
$$(fg)_a^{(\alpha)}(x) = f_a^{(\alpha)}(x)g(x) + f(x)g_a^{(\alpha)}(x)$$
and
$${}_b(fg)^{(\alpha)}(x) = {}_bf^{(\alpha)}(x)g(x) + f(x){}_bg^{(\alpha)}(x).$$

3)
$$\left(\frac{f}{g}\right)_a^{(\alpha)}(x) = \frac{f_a^{(\alpha)}(x)g(x) - f(x)g_a^{(\alpha)}(x)}{g^2(x)}$$
and
$${}_b\left(\frac{f}{g}\right)^{(\alpha)}(x) = \frac{{}_bf^{(\alpha)}(x)g(x) - f(x){}_bg^{(\alpha)}(x)}{g^2(x)}.$$

4) If $g(x) \geq a$, then
$$(f \circ g)_a^{(\alpha)}(x) = f_a^{(\alpha)}(g(x))g_a^{(\alpha)}(x)(g(x) - a)^{\alpha - 1}.$$

5) If $g(x) \leq b$, then
$${}_b(f \circ g)^{(\alpha)}(x) = {}_bf^{(\alpha)}(g(x)){}_bg^{(\alpha)}(x)(b - g(x))^{\alpha - 1}.$$

6) If $g(x) < a$, then
$$(f \circ g)_a^{(\alpha)}(x) = -{}_af^{(\alpha)}(g(x))g_a^{(\alpha)}(x)(a - g(x))^{\alpha - 1}.$$

7) If $g(x) > b$, then
$${}_b(f \circ g)^{(\alpha)}(x) = -f_b^{(\alpha)}(g(x)){}_bg^{(\alpha)}(x)(g(x) - b)^{\alpha - 1}.$$

The simple chain and product rules given in Proposition 1 justify the increasing interest in the study of the conformable fractional calculus, since it enable us to investigate its potential applications as a tool to practical modeling of complex problems in science and engineering.

The conformable fractional integrals are defined as follows [5], [6].

Definition 2: The left conformable fractional integral of order $0 < \alpha \leq 1$ starting from $a \in \mathbb{R}$ of a function $f \in L^1[a, b]$ is defined by
$$I_a^\alpha f(x) = \int_a^x f(u) d_a^\alpha u = \int_a^x \frac{f(u)}{(u - a)^{1-\alpha}} du \tag{5}$$
and the right conformable fractional integral of order $0 < \alpha \leq 1$ terminating at $b \in \mathbb{R}$ of a function $f \in L^1[a, b]$ is defined by
$${}_bI^\alpha f(x) = \int_x^b f(u) {}_bd^\alpha u = \int_x^b \frac{f(u)}{(b - u)^{1-\alpha}} du. \tag{6}$$

It is important to mention that the conformable fractional integrals (5) and (6) differ from the traditional fractional Riemann-Liouville integrals [1]–[3] only by a multiplicative constant. Moreover, for $\alpha = 1$, the conformable fractional integrals reduce to ordinary first order integrals.

In addition to these definitions, in the present work we make use of the following properties of conformable fractional derivatives and integrals.

Theorem 1: Let $f \in C[a, b]$ and $0 < \alpha \leq 1$. Then,
$$\frac{d_a^\alpha}{dx_a^\alpha} I_a^\alpha f(x) = f(x)$$
and
$$\frac{{}_bd^\alpha}{{}_bdx^\alpha} {}_bI^\alpha f(x) = f(x)$$
for all $x \in [a, b]$.

Theorem 2 (Fundamental theorem of conformable fractional calculus): Let $f \in C^1[a, b]$ and $0 < \alpha \leq 1$. Then,
$$I_a^\alpha f_a^{(\alpha)}(x) = f(x) - f(a)$$
and
$${}_bI^\alpha {}_bf^{(\alpha)}(x) = f(x) - f(b)$$
for all $x \in [a, b]$.

Theorem 3 (Integration by parts): Let $f, g : [a, b] \to \mathbb{R}$ be two functions such that fg is differentiable. Then,
$$\int_a^b f(x)g_a^{(\alpha)}(x)d_a^\alpha x = f(x)g(x)|_a^b - \int_a^b g(x)f_a^{(\alpha)}(x)d_a^\alpha x \tag{7}$$
and
$$\int_a^b f(x){}_bg^{(\alpha)}(x){}_bd^\alpha x = -f(x)g(x)|_a^b - \int_a^b g(x){}_bf^{(\alpha)}(x){}_bd^\alpha x. \tag{8}$$

If $f, g : [a, b] \to \mathbb{R}$ are differentiable functions, then
$$\int_a^b f(x)g_a^{(\alpha)}(x)d_a^\alpha x = f(x)g(x)|_a^b + \int_a^b g(x){}_bf^{(\alpha)}(x){}_bd^\alpha x.$$

The proof of Theorem 1 follows directly from (3), (4), (5) and (6) since $I_a^\alpha f(x)$ and ${}_bI^\alpha f(x)$ are differentiable. On the other hand, the fundamental theorem of the conformable fractional calculus (Theorem 2) is a direct consequence of (3), (4) and definitions (5) and (6) since $f, g : [a, b] \to \mathbb{R}$ are differentiable functions. Finally, the integration by parts (7) and (8) follow from Proposition 1 and Theorem 1. We also need the following result.

Theorem 4 (Chain rule for functions of several variables): Let $f : \mathbb{R}^N \to \mathbb{R}$ ($N \in \mathbb{N}$) be a differentiable function in all its arguments and $y_1, \ldots, y_N : \mathbb{R} \to \mathbb{R}$ be α-differentiable functions. Then,
$$\frac{d_a^\alpha}{dx_a^\alpha} f(y_1(x), \ldots, y_N(x)) = \frac{\partial f}{\partial y_1} {y_1}_a^{(\alpha)} + \frac{\partial f}{\partial y_2} {y_2}_a^{(\alpha)} + \cdots + \frac{\partial f}{\partial y_N} {y_N}_a^{(\alpha)} \tag{9}$$
and
$$\frac{{}_bd^\alpha}{{}_bdx^\alpha} f(y_1(x), \ldots, y_N(x)) = \frac{\partial f}{\partial y_1} {}_b{y_1}^{(\alpha)} + \frac{\partial f}{\partial y_2} {}_b{y_2}^{(\alpha)} + \cdots + \frac{\partial f}{\partial y_N} {}_b{y_N}^{(\alpha)}. \tag{10}$$

Proof : For simplicity, we prove (9) only for $N = 2$. The proofs for a general N and of (10) are similar. From (1) we have for $N = 2$ that (by writing $\overline{x} = x + \epsilon(x - a)^{1-\alpha}$ for simplicity)

$$\begin{aligned}
&\frac{d_a^\alpha}{dx_a^\alpha} f(y_1(x), y_2(x)) \\
&= \lim_{\epsilon\to 0} \frac{f(y_1(\overline{x}), y_2(\overline{x})) - f(y_1(x), y_2(x))}{\epsilon} \\
&= \lim_{\epsilon\to 0} \frac{f(y_1(\overline{x}), y_2(\overline{x})) - f(y_1(x), y_2(\overline{x}))}{y_1(\overline{x}) - y_1(x)} \frac{y_1(\overline{x}) - y_1(x)}{\epsilon} \\
&\quad + \lim_{\epsilon\to 0} \frac{f(y_1(x), y_2(\overline{x})) - f(y_1(x), y_2(x))}{y_2(\overline{x}) - y_2(x)} \frac{y_2(\overline{x}) - y_2(x)}{\epsilon} \\
&= \frac{\partial f}{\partial y_1} {y_1}_a^{(\alpha)} + \frac{\partial f}{\partial y_2} {y_2}_a^{(\alpha)}
\end{aligned}$$

since f is differentiable. ∎

III. The Conformable Euler–Lagrange Equation

Let us first consider the fractional variational integral

$$\mathcal{J}(y) = \int_a^b L\left(x, y(x), y_a^{(\alpha)}(x)\right) d_a^\alpha x \tag{11}$$

defined on the set of continuous functions $y : [a, b] \to \mathbb{R}$ such that $y_a^{(\alpha)}$ exists on $[a, b]$, where the Lagrangian L, $L(x, y, y_a^{(\alpha)}) : [a, b] \times \mathbb{R}^2 \to \mathbb{R}$, is of class C^1 in each of its arguments. The fundamental problem of the calculus of variations consists in finding which functions extremize functional (11). In order to obtain a necessary condition for the extremum of (11) we need the following Lemma.

Lemma 1 (Fundamental lemma for the conformable calculus of variations): Let M and η be continuous functions on $[a, b]$. If

$$\int_a^b \eta(x) M(x) d_a^\alpha x = 0 \tag{12}$$

for any $\eta \in C\,[a, b]$ with $\eta(a) = \eta(b) = 0$, then

$$M(x) = 0 \tag{13}$$

for all $x \in [a, b]$.

Proof : We do the proof by contradiction. From (12) we have that

$$\int_a^b \eta(x) M(x) d_a^\alpha x = \int_a^b \eta(x) \frac{M(x)}{(x-a)^{1-\alpha}} dx = 0. \tag{14}$$

Suppose that there exist an $x_0 \in (a, b)$ such that $M(x_0) \neq 0$. Without loss of generality, let us assume that $M(x_0) > 0$. Since M is continuous on $[a, b]$, there exists a neighborhood $N^\delta(x_0) \subset (a, b)$ such that

$$M(x) > 0 \quad \text{for all} \quad x \in N^\delta(x_0).$$

Let us choose

$$\eta(x) = \begin{cases} (x - x_0 - \delta)^2 (x - x_0 + \delta)^2, & \text{if } x \in N^\delta(x_0) \\ 0, & \text{if } x \notin N^\delta(x_0). \end{cases} \tag{15}$$

Clearly, $\eta(x)$ given by (15) is continuous and satisfy $\eta(a) = 0$ and $\eta(b) = 0$. Inserting (15) into (14), we obtain that

$$\begin{aligned}
&\int_a^b \eta(x) M(x) d_a^\alpha x \\
&= \int_{x_0-\delta}^{x_0+\delta} (x - x_0 - \delta)^2 (x - x_0 + \delta)^2 \frac{M(x)}{(x-a)^{1-\alpha}} dx > 0
\end{aligned}$$

which contradicts our hypothesis. Thus,

$$\frac{M(x)}{(x-a)^{1-\alpha}} > 0 \quad \text{for all} \quad x \in (a, b).$$

Since $(x-a)^{1-\alpha} > 0$ for $x \in (a, b)$, and since $M \in C\,[a, b]$, we get

$$M(x) = 0 \quad \text{for all} \quad x \in [a, b].$$

∎

Theorem 5 (The conformable fractional Euler–Lagrange equation): Let $\mathcal{J}$ be a functional of form (11) with $L \in C^1\left([a, b] \times \mathbb{R}^2\right)$, and $0 < \alpha \leq 1$. Let $y : [a, b] \to \mathbb{R}$ be a α-differentiable function with $y(a) = y_a$ and $y(b) = y_b$, y_a, $y_b \in \mathbb{R}$. Furthermore, let $y \frac{\partial L}{\partial y_a^{(\alpha)}}$ be a differentiable function and $\frac{\partial L}{\partial y_a^{(\alpha)}}$ be α-differentiable. If y is an extremizer of $\mathcal{J}$, then y satisfies the following fractional Euler–Lagrange equation:

$$\frac{\partial L}{\partial y} - \frac{d_a^\alpha}{dx_a^\alpha} \left(\frac{\partial L}{\partial y_a^{(\alpha)}} \right) = 0. \tag{16}$$

Proof : Let y^* give an extremum to (11). We define a family of functions

$$y(x) = y^*(x) + \epsilon \eta(x) \tag{17}$$

where ϵ is a constant and η is an arbitrary α-differentiable function satisfying $\eta \frac{\partial L}{\partial {y^*}_a^{(\alpha)}} \in C^1$ and the boundary conditions $\eta(a) = \eta(b) = 0$ (weak variations). From (17), the boundary conditions $\eta(a) = \eta(b) = 0$, and the fact that $y^*(a) = y_a$ and $y^*(b) = y_b$, it follows that function y is admissible: y is α-differentiable with $y(a) = y_a$, $y(b) = y_b$, and $y \frac{\partial L}{\partial {y^*}_a^{(\alpha)}}$ is differentiable. Let the Lagrangian L be $C^1([a, b] \times \mathbb{R}^2)$. Because y^* is an extremizer of functional $\mathcal{J}$, the Gateaux derivative $\delta\mathcal{J}(y^*)$ needs to be identically null. For the functional (11),

$$\begin{aligned}
\delta\mathcal{J}(y^*) &= \lim_{\epsilon\to 0} \frac{1}{\epsilon} \left(\int_a^b L\left(x, y, y_a^{(\alpha)}\right) d_a^\alpha x - \int_a^b L\left(x, y^*, {y^*}_a^{(\alpha)}\right) d_a^\alpha x \right) \\
&= \int_a^b \left(\eta(x) \frac{\partial L\left(x, y^*, {y^*}_a^{(\alpha)}\right)}{\partial y^*} + \eta_a^{(\alpha)}(x) \frac{\partial L\left(x, y^*, {y^*}_a^{(\alpha)}\right)}{\partial {y^*}_a^{(\alpha)}} \right) d_a^\alpha x = 0.
\end{aligned}$$

Using the integration by parts formula (7) ($\eta \frac{\partial L}{\partial {y^*}_a^{(\alpha)}}$ is differentiable), we get

$$\delta\mathcal{J}(y^*) = \int_a^b \eta(x) \left(\frac{\partial L\left(x, y^*, {y^*}_a^{(\alpha)}\right)}{\partial y^*} - \frac{d_a^\alpha}{dx_a^\alpha} \frac{\partial L\left(x, y^*, {y^*}_a^{(\alpha)}\right)}{\partial {y^*}_a^{(\alpha)}} \right) d_a^\alpha x = 0 \tag{18}$$

since $\eta(a)=\eta(b)=0$. The fractional Euler–Lagrange equation (16) follows from (18) by using the fundamental Lemma 1. ■

Definition 3: A continuous function y solution of (16) is said to be an extremal of (11).

Remark 2: For $\alpha=1$, the functional $\mathcal{J}$ given by (11) reduces to the classical variational functional

$$\mathcal{J}(y)=\int_0^1 L\left(x,y(x),y'(x)\right)dx$$

and the associated Euler–Lagrange equation (16) is

$$\frac{\partial L}{\partial y}-\frac{d}{dx}\left(\frac{\partial L}{\partial y'}\right)=0. \tag{19}$$

Let us now consider the more general case where the Lagrangian depends on both integer order and fractional order derivatives. In this case the following theorem holds.

Theorem 6 (The generalized conformable fractional Euler–Lagrange equation): Let $\mathcal{J}$ be a functional of form

$$\mathcal{J}(y)=\int_a^b L\left(x,y(x),y'(x),y_a^{(\alpha)}(x)\right)dx \tag{20}$$

with $L\in C^1\left([a,b]\times\mathbb{R}^3\right)$, and $0<\alpha\le 1$. Let $y:[a,b]\to\mathbb{R}$ be a differentiable function with $y(a)=y_a$ and $y(b)=y_b$, $y_a,y_b\in\mathbb{R}$. If y is an extremizer of $\mathcal{J}$, then y satisfies the following fractional Euler–Lagrange equation:

$$\frac{\partial L}{\partial y}-\frac{d}{dx}\left(\frac{\partial L}{\partial y'}\right)-\frac{1}{(x-a)^{1-\alpha}}\frac{d_a^\alpha}{dx_a^\alpha}\left(\frac{\partial \tilde{L}}{\partial y_a^{(\alpha)}}\right)=0 \tag{21}$$

where $\tilde{L}\left(x,y,y',y_a^{(\alpha)}\right)=(x-a)^{1-\alpha}L\left(x,y,y',y_a^{(\alpha)}\right)$.

Proof : Let y^* give an extremum to (20). We define a family of functions as in (17) but with $y\in C^1[a,b]$. From (17) and the boundary conditions $\eta(a)=\eta(b)=0$, and the fact that $y^*(a)=y_a$ and $y^*(b)=y_b$, it follows that function y is admissible. Because y^* is an extremizer of $\mathcal{J}$, the Gateaux derivative $\delta\mathcal{J}(y^*)$ needs to be identically null. For the functional (20) we have

$$\begin{aligned}\delta\mathcal{J}(y^*)&=\lim_{\epsilon\to 0}\frac{1}{\epsilon}\left(\int_a^b L\left(x,y,y',y_a^{(\alpha)}\right)dx\right.\\&\qquad\left.-\int_a^b L\left(x,y^*,y'^*,{y^*}_a^{(\alpha)}\right)dx\right)\\&=\int_a^b\left(\eta(x)\frac{\partial L\left(x,y^*,y'^*,{y^*}_a^{(\alpha)}\right)}{\partial y^*}\right.\\&\qquad\left.+\eta'(x)\frac{\partial L\left(x,y^*,y'^*,{y^*}_a^{(\alpha)}\right)}{\partial y'^*}\right)dx\\&\quad+\int_a^b\eta_a^{(\alpha)}(x)\frac{\partial L\left(x,y^*,y'^*,{y^*}_a^{(\alpha)}\right)}{\partial {y^*}_a^{(\alpha)}}dx\\&=\int_a^b\eta(x)\left(\frac{\partial L\left(x,y^*,y'^*,{y^*}_a^{(\alpha)}\right)}{\partial y^*}\right.\\&\qquad\left.-\frac{d}{dx}\frac{\partial L\left(x,y^*,y'^*,{y^*}_a^{(\alpha)}\right)}{\partial y'^*}\right)dx\\&\quad+\int_a^b\eta_a^{(\alpha)}(x)\frac{\partial \tilde{L}\left(x,y^*,y'^*,{y^*}_a^{(\alpha)}\right)}{\partial {y^*}_a^{(\alpha)}}d_a^\alpha x=0\end{aligned}$$

where we performed an integration by parts in the second term in the first integral (since $\eta(a)=\eta(b)=0$), and we rewrote the second integral as a conformable integral by using definition (5). Using the integration by parts formula (7) ($\eta\frac{\partial L}{\partial {y^*}_a^{(\alpha)}}$ is differentiable), we get

$$\begin{aligned}\delta\mathcal{J}(y^*)&=\int_a^b\eta(x)\left(\frac{\partial L\left(x,y^*,y'^*,{y^*}_a^{(\alpha)}\right)}{\partial y^*}\right.\\&\qquad\left.-\frac{d}{dx}\frac{\partial L\left(x,y^*,y'^*,{y^*}_a^{(\alpha)}\right)}{\partial y'^*}\right)dx\\&\quad-\int_a^b\eta(x)\frac{d_a^\alpha}{dx_a^\alpha}\frac{\partial \tilde{L}\left(x,y^*,y'^*,{y^*}_a^{(\alpha)}\right)}{\partial {y^*}_a^{(\alpha)}}d_a^\alpha x\\&=\int_a^b\eta(x)\left((x-a)^{1-\alpha}\frac{\partial L\left(x,y^*,y'^*,{y^*}_a^{(\alpha)}\right)}{\partial y^*}\right.\\&\qquad-(x-a)^{1-\alpha}\frac{d}{dx}\frac{\partial L\left(x,y^*,y'^*,{y^*}_a^{(\alpha)}\right)}{\partial y'^*}\\&\qquad\left.-\frac{d_a^\alpha}{dx_a^\alpha}\frac{\partial \tilde{L}\left(x,y^*,y'^*,{y^*}_a^{(\alpha)}\right)}{\partial {y^*}_a^{(\alpha)}}\right)d_a^\alpha x=0\end{aligned} \tag{22}$$

since $\eta(a)=\eta(b)=0$. The fractional Euler–Lagrange equation (21) follows from (22) by using the fundamental Lemma 1. ■

IV. LAGRANGIAN FORMULATION FOR FRICTIONAL FORCES

As an example of potential application of the variational calculus with conformable fractional derivatives, we formulate an action principle for dissipative systems free from the mathematical inconsistencies found in the Riewe approach [23] and far simpler than the formulation proposed in [23]. The action principle we propose states that the equation of motion for dissipative systems is obtained by taking the limit $a\to b$ in the extremal of the action

$$S=\int_a^b L\left(x,x',x_a^{(\alpha)}\right)dt \tag{23}$$

that satisfy the fractional Euler–Lagrange equation (see (21))

$$\frac{\partial L}{\partial x}-\frac{d}{dt}\frac{\partial L}{\partial x'}-\frac{1}{(t-a)^{1-\alpha}}\frac{d_a^\alpha}{dt_a^\alpha}\frac{\partial \tilde{L}}{\partial x_a^{(\alpha)}}=0 \tag{24}$$

where $\tilde{L}\left(x, x', x_a^{(\alpha)}\right) = (t-a)^{1-\alpha} L\left(x, x', x_a^{(\alpha)}\right)$, $x(t)$ is the path of the particle and t is the time. It is important to emphasize that the condition $a \to b$ (also considered in the original Riewe's approach) applied to the action principle does not imply any restrictions for conservative systems, since in this case $x(t)$ is the action's extremal for any time interval $[a,b]$, even when $a \to b$. Furthermore, our action principle is simpler than the formulation in [23] and free from the mathematical inconsistencies present in Riewe's approach (see [23] for a detailed discussion). In order to show that our method provides us with physical Lagrangians, let us consider the simple problem of a particle under a frictional force proportional to velocity. A quadratic Lagrangian for a particle under a frictional force proportional to the velocity is given by

$$L\left(x, x', x_a^{(\frac{1}{2})}\right) = \frac{1}{2} m \left(x'\right)^2 - U(x) + \frac{\gamma}{2}\left(x_a^{(\frac{1}{2})}\right)^2 \tag{25}$$

where the three terms in (25) represent the kinetic energy, potential energy, and the fractional linear friction energy, respectively. Note that, differently from Riewe's Lagrangian [11], our Lagrangian (25) is a real function with a linear friction energy, which is physically meaningful. Since the equation of motion is obtained in the limit $a \to b$, if we consider the last term in (25) up to first order in $\Delta t = t - a$, we get

$$\frac{\gamma}{2}\left(x_a^{(\frac{1}{2})}\right)^2 = \frac{\gamma}{2}\left(x' \Delta t^{\frac{1}{2}}\right)^2 \approx \frac{\gamma}{2} x' \Delta x$$

that coincides, apart from the multiplicative constant $1/2$, with the work from the frictional force $\gamma x'$ in the displacement $\Delta x \approx x' \Delta t$. The appearance of an additional multiplicative constant is a consequence of the use of fractional derivatives in the Lagrangian and does not appear in the equation of motion after we apply the action principle [23].

Remark 3: It is important to stress that the order of the fractional derivative should be fixed to $\alpha = 1/2$ in order to obtain, by a fractional Lagrangian, a correct equation of motion of a dissipative system. For α different from $1/2$, the Lagrangian does not describe a frictional system under a frictional force proportional to the velocity. Consequently, the fractional linear friction energy makes sense only for $\alpha = 1/2$.

The Lagrangian (25) is physical in the sense it provides physically meaningful relations for the momentum and the Hamiltonian. If we define the canonical variables

$$q_1 = x', \quad q_{\frac{1}{2}} = x_a^{(\frac{1}{2})}$$

and

$$p_1 = \frac{\partial L}{\partial q_1} = m x', \quad p_{\frac{1}{2}} = \frac{\partial L}{\partial q_{\frac{1}{2}}} = \gamma x_a^{(\frac{1}{2})}$$

we obtain the Hamiltonian

$$H = q_1 p_1 + q_{\frac{1}{2}} p_{\frac{1}{2}} - L = \frac{1}{2} m \left(x'\right)^2 + U(x) + \frac{\gamma}{2}\left(x_a^{(\frac{1}{2})}\right)^2. \tag{26}$$

From (26) we can see that the Lagrangian (25) is physical in the sense it provides us a correct relation for the momentum $p_1 = m\dot{x}$ and a physically meaningful Hamiltonian (it is the sum of all energies). Furthermore, the additional fractional momentum $p_{\frac{1}{2}} = \gamma x_a^{(\frac{1}{2})}$ goes to zero when we take the limit $a \to b$, since $x \in C^2[a,b]$.

Finally, the equation of motion for the particle is obtained by inserting our Lagrangian (25) into the Euler–Lagrange equation (24),

$$\begin{aligned} m x'' + \gamma (t-a)^{-\frac{1}{2}} \frac{d_a^{\frac{1}{2}}}{dt_a^{\frac{1}{2}}} &\left[(t-a)^{\frac{1}{2}} x_a^{(\frac{1}{2})}\right] \\ &= m x'' + \gamma x' + \gamma (t-a) x'' = F(x) \end{aligned} \tag{27}$$

where we have used (3) since $x \in C^2[a,b]$ and

$$F(x) = -\frac{d}{dx} U(x)$$

is the external force. By taking the limit $a \to b$ with $t \in [a,b]$, we finally obtain the correct equation of motion for a particle under a frictional force:

$$m x'' + \gamma x' = F(x).$$

V. The Conformable DuBois–Reymond Condition

In the remainder of the present work, we are going to consider only the simplest case where we have no mixed integer and fractional derivatives. We now present the DuBois–Reymond condition in the conformable fractional context. It is an immediate consequence of the chain rule (9) and the Euler–Lagrange equation (16).

Theorem 7 (The conformable fractional DuBois-Reymond condition): If y is an extremal of $\mathcal{J}$ as in (11), then

$$\frac{d_a^\alpha}{dx_a^\alpha}\left(L - \frac{\partial L}{\partial y_a^{(\alpha)}} y_a^{(\alpha)}\right) = \frac{\partial L}{\partial x} \cdot (x-a)^{1-\alpha}. \tag{28}$$

Proof : By the chain rule (9) and the Leibniz rule in Proposition 1:

$$\begin{aligned} &\frac{d_a^\alpha}{dx_a^\alpha}\left(L - \frac{\partial L}{\partial y_a^{(\alpha)}} y_a^{(\alpha)}\right) \\ &\quad = \frac{\partial L}{\partial x} x_a^{(\alpha)} + \frac{\partial L}{\partial y} y_a^{(\alpha)} + \frac{\partial L}{\partial y_a^{(\alpha)}} \frac{d_a^\alpha}{dx_a^\alpha} y_a^{(\alpha)} \\ &\quad\quad - \frac{d_a^\alpha}{dx_a^\alpha}\left(\frac{\partial L}{\partial y_a^{(\alpha)}}\right) y_a^{(\alpha)} - \frac{\partial L}{\partial y_a^{(\alpha)}} \frac{d_a^\alpha}{dx_a^\alpha} y_a^{(\alpha)} \\ &\quad = \frac{\partial L}{\partial x} x_a^{(\alpha)} + y_a^{(\alpha)}\left[\frac{\partial L}{\partial y} - \frac{d_a^\alpha}{dx_a^\alpha}\left(\frac{\partial L}{\partial y_a^{(\alpha)}}\right)\right] \\ &\quad = \frac{\partial L}{\partial x} \cdot (x-a)^{1-\alpha}. \end{aligned}$$

■

Corollary 1: If (11) is autonomous, that is, if $L = L(y, y_a^{(\alpha)})$ does not depend on x, then

$$\frac{d_a^\alpha}{dx_a^\alpha}\left(L - \frac{\partial L}{\partial y_a^{(\alpha)}} y_a^{(\alpha)}\right) = 0$$

along any extremal y.

Remark 4: When $\alpha = 1$ and $y \in C^1$, Theorem 7 is the classical DuBois–Reymond condition: if $y \in C^1$ is an extremal of $\mathcal{J}(y) = \int_0^1 L(x, y, y') dx$ (i.e., y satisfies (19)), then

$$\frac{d}{dx}\left(L - \frac{\partial L}{\partial y'} y'\right) = \frac{\partial L}{\partial x}.$$

VI. FRACTIONAL INVARIANT CONDITIONS

We consider invariance transformations in the (x, y)-space, depending on a real parameter ϵ. To be more precise, we consider transformations of type

$$\begin{cases} \overline{x} = x + \epsilon\tau(x, y(x)) \\ \overline{y} = y + \epsilon\xi(x, y(x)) \end{cases} \tag{29}$$

where the generators τ and ξ are such that $\overline{x} \geq a$ and there exist $\tau_a^{(\alpha)}$ and $\xi_a^{(\alpha)}$.

Definition 4: We say that the fractional variational integral (11) is invariant under the family of transformations (29) up to the Gauge term Λ, if a function $\Lambda = \Lambda(x, y)$ exists such that for any function y and for any real $x \in [a, b]$, we have

$$L\left(\overline{x}, \overline{y}, \frac{d_a^\alpha \overline{y}}{d\overline{x}_a^\alpha}\right)\frac{d_a^\alpha \overline{x}}{d_a^\alpha x} = L(x, y, y_a^{(\alpha)}) + \epsilon\frac{d_a^\alpha \Lambda}{dx_a^\alpha}(x, y) + o(\epsilon) \tag{30}$$

for all ϵ in some neighborhood of zero, where $\frac{d_a^\alpha \overline{x}}{d_a^\alpha x}$ stands for

$$\frac{\dfrac{d_a^\alpha \overline{x}}{dx_a^\alpha}}{\dfrac{d_a^\alpha x}{dx_a^\alpha}} = 1 + \epsilon\frac{\tau_a^{(\alpha)}}{(x-a)^{1-\alpha}}. \tag{31}$$

We note that for $\alpha = 1$ our Definition 4 coincides with the standard approach (see, e.g., [33]). When $\Lambda \equiv 0$, one obtains the concept of absolute invariance. The presence of a new function Λ is due to the presence of external forces in the dynamical system, like friction. The function Λ is called a Gauge term. In fact, many phenomena are nonconservative and this has to be taken into account in the conservation laws [26], [34]. We give an example.

Example 1: Consider the transformation

$$\begin{cases} \overline{x} = x \\ \overline{y} = y + \epsilon\frac{1}{2\alpha}(x-a)^\alpha \end{cases} \tag{32}$$

and the functional

$$\mathcal{J}(y) = \int_a^b \left(y_a^{(\alpha)}(x)\right)^2 d_a^\alpha x. \tag{33}$$

Since

$$\frac{d_a^\alpha}{dx_a^\alpha}\frac{1}{2\alpha}(x-a)^\alpha = \frac{1}{2}$$

it is easy to verify that (33) is invariant under (32) up to the Gauge function $\Lambda = y$.

Definition 5: Given a function $C = C(x, y, y_a^{(\alpha)})$, we say that C is a conserved quantity for (11) if

$$\frac{d_a^\alpha C}{dx_a^\alpha}(x, y(x), y_a^{(\alpha)}(x)) = 0 \tag{34}$$

along any solution y of (16) (i.e., along any extremal of (11)).

Remark 5: Applying the conformable integral (5) to both sides of equation (34), Definition 5 is equivalent to $C(x, y(x), y_a^{(\alpha)}(x)) \equiv$ const.

We now provide a necessary condition of invariance.

Theorem 8: If $\mathcal{J}$ given by (11) is invariant under a family of transformations (29), then

$$\begin{aligned} &\frac{\partial L}{\partial x}\tau + \frac{\partial L}{\partial y}\xi \\ &+ \frac{\partial L}{\partial y_a^{(\alpha)}}\left[\xi_a^{(\alpha)} - y_a^{(\alpha)}\left((\alpha-1)\frac{\tau}{(x-a)} + \frac{\tau_a^{(\alpha)}}{(x-a)^{1-\alpha}}\right)\right] \\ &+ L\frac{\tau_a^{(\alpha)}}{(x-a)^{1-\alpha}} = \frac{d_a^\alpha \Lambda}{dx_a^\alpha}. \end{aligned} \tag{35}$$

Proof : By the fractional chain rule (see Proposition 1),

$$\begin{aligned} \frac{d_a^\alpha \overline{y}}{d\overline{x}_a^\alpha} &= \frac{\dfrac{d_a^\alpha \overline{y}}{dx_a^\alpha}}{(\overline{x}-a)^{\alpha-1}\dfrac{d_a^\alpha \overline{x}}{dx_a^\alpha}} \\ &= \frac{y_a^{(\alpha)} + \epsilon\xi_a^{(\alpha)}}{(x+\epsilon\tau-a)^{\alpha-1}[(x-a)^{1-\alpha} + \epsilon\tau_a^{(\alpha)}]}. \end{aligned}$$

Substituting this formula into (30), differentiating with respect to ϵ and then putting $\epsilon = 0$, we obtain relation (35).■

Remark 6: Allowing α to be equal to 1, for $\Lambda \equiv 0$ our equation (35) becomes the standard necessary condition of invariance (cf., e.g., [24]):

$$\frac{\partial L}{\partial x}\tau + \frac{\partial L}{\partial y}\xi + \frac{\partial L}{\partial y'}(\xi' - y'\tau') + L\tau' = 0.$$

For $\alpha = 1$ and an arbitrary Λ, see [33].

In particular, if we consider "time invariance" (i.e., $\tau \equiv 0$), we obtain the following result.

Corollary 2: Let $\overline{y} = y + \epsilon\xi(x, y(x))$ be a transformation that leaves invariant $\mathcal{J}$ in the sense that

$$L(x, \overline{y}, \overline{y}_a^{(\alpha)}) = L(x, y, y_a^{(\alpha)}) + \epsilon\frac{d_a^\alpha \Lambda}{dx_a^\alpha}(x, y) + o(\epsilon).$$

Then,

$$\frac{\partial L}{\partial y}\xi + \frac{\partial L}{\partial y_a^{(\alpha)}}\xi_a^{(\alpha)} = \frac{d_a^\alpha \Lambda}{dx_a^\alpha}.$$

VII. THE CONFORMABLE NOETHER THEOREM

Noether's theorem is a beautiful result with important implications and applications in optimal control [35]−[37]. We provide here a conformable fractional Noether theorem in the context of the calculus of variations. Later, in Section IX, we provide a conformable fractional optimal control version (see Theorem 11).

Theorem 9 (The conformable fractional Noether theorem): If $\mathcal{J}$ given by (11) is invariant under (29) and if y is an extremal of $\mathcal{J}$, then

$$\begin{aligned} &\frac{d_a^\alpha}{dx_a^\alpha}\left[\left(L - \frac{\partial L}{\partial y_a^{(\alpha)}}y_a^{(\alpha)}\right)\tau + \frac{\partial L}{\partial y_a^{(\alpha)}}\xi(x-a)^{1-\alpha}\right] \\ &= (1-\alpha)\frac{\partial L}{\partial y_a^{(\alpha)}}\left[\xi(x-a)^{1-2\alpha} - \frac{y_a^{(\alpha)}\tau}{(x-a)^\alpha}\right] \\ &+ \frac{d_a^\alpha \Lambda}{dx_a^\alpha}(x-a)^{1-\alpha}. \end{aligned} \tag{36}$$

Proof : From Theorem 8, and using the conformable fractional Euler-Lagrange equation (16) and the DuBois-Reymond condition (28), we deduce successively that

$$\begin{aligned}
&\frac{d_a^\alpha \Lambda}{dx_a^\alpha}(x-a)^{1-\alpha}\\
&=\left[\frac{d_a^\alpha}{dx_a^\alpha}\left(L-\frac{\partial L}{\partial y_a^{(\alpha)}}y_a^{(\alpha)}\right)\frac{\tau}{(x-a)^{1-\alpha}}\right.\\
&\quad\left.+\frac{d_a^\alpha}{dx_a^\alpha}\left(\frac{\partial L}{\partial y_a^{(\alpha)}}\right)\xi+\frac{\partial L}{\partial y_a^{(\alpha)}}\xi_a^{(\alpha)}\right](x-a)^{1-\alpha}\\
&\quad-\frac{\partial L}{\partial y_a^{(\alpha)}}y_a^{(\alpha)}\left[\frac{(\alpha-1)\tau}{(x-a)^\alpha}+\tau_a^{(\alpha)})\right]+L\tau_a^{(\alpha)}\\
&=\left[\frac{d_a^\alpha}{dx_a^\alpha}\left(L-\frac{\partial L}{\partial y_a^{(\alpha)}}y_a^{(\alpha)}\right)\tau+\frac{d_a^\alpha}{dx_a^\alpha}\left(\frac{\partial L}{\partial y_a^{(\alpha)}}\xi\right)(x-a)^{1-\alpha}\right]\\
&\quad-\frac{\partial L}{\partial y_a^{(\alpha)}}y_a^{(\alpha)}\left[\frac{(\alpha-1)\tau}{(x-a)^\alpha}+\tau_a^{(\alpha)})\right]+L\tau_a^{(\alpha)}\\
&=\frac{d_a^\alpha}{dx_a^\alpha}\left[\left(L-\frac{\partial L}{\partial y_a^{(\alpha)}}y_a^{(\alpha)}\right)\tau+\frac{\partial L}{\partial y_a^{(\alpha)}}\xi(x-a)^{1-\alpha}\right]\\
&\quad-\frac{\partial L}{\partial y_a^{(\alpha)}}y_a^{(\alpha)}\left[\frac{(\alpha-1)\tau}{(x-a)^\alpha}+\tau_a^{(\alpha)}\right]\\
&\quad+L\tau_a^{(\alpha)}-\left(L-\frac{\partial L}{\partial y_a^{(\alpha)}}y_a^{(\alpha)}\right)\tau_a^{(\alpha)}\\
&\quad-\frac{\partial L}{\partial y_a^{(\alpha)}}\xi(1-\alpha)(x-a)^{1-2\alpha}\\
&=\frac{d_a^\alpha}{dx_a^\alpha}\left[\left(L-\frac{\partial L}{\partial y_a^{(\alpha)}}y_a^{(\alpha)}\right)\tau+\frac{\partial L}{\partial y_a^{(\alpha)}}\xi(x-a)^{1-\alpha}\right]\\
&\quad+\frac{\partial L}{\partial y_a^{(\alpha)}}y_a^{(\alpha)}\frac{(1-\alpha)\tau}{(x-a)^\alpha}-\frac{\partial L}{\partial y_a^{(\alpha)}}\xi(1-\alpha)(x-a)^{1-2\alpha}.
\end{aligned}$$

Thus, we obtain equation (36). ■

Remark 7: When $\alpha=1$, equation (36) is simply Noether's conservation law in the presence of external forces: for any extremal of $\mathcal{J}$ and for any family of transformations $(\overline{x},\overline{y})$ for which $\mathcal{J}$ is invariant, the conservation law

$$\left(L-\frac{\partial L}{\partial y'}y'\right)\tau+\frac{\partial L}{\partial y'}\xi=\Lambda+\text{constant}$$

holds [33, Theorem 2.1]. In addition, if system is conservative ($\Lambda\equiv 0$), then one has the classical Noether theorem

$$\left(L-\frac{\partial L}{\partial y'}y'\right)\tau+\frac{\partial L}{\partial y'}\xi=\text{constant}.$$

Corollary 3 (The conformable fractional Noether theorem under the presence of an external force f): If $\mathcal{J}$ given by (11) is invariant under (29), y is an extremal of $\mathcal{J}$, and the function $f=f(x,y,y_a^{(\alpha)})$ satisfies the equation

$$\begin{aligned}\frac{d_a^\alpha f}{dx_a^\alpha}=&(1-\alpha)\frac{\partial L}{\partial y_a^{(\alpha)}}\left[\xi(x-a)^{1-2\alpha}-\frac{y_a^{(\alpha)}\tau}{(x-a)^\alpha}\right]\\&+\frac{d_a^\alpha\Lambda}{dx_a^\alpha}(x-a)^{1-\alpha}\end{aligned}$$

then

$$\left(L-\frac{\partial L}{\partial y_a^{(\alpha)}}y_a^{(\alpha)}\right)\tau+\frac{\partial L}{\partial y_a^{(\alpha)}}\xi(x-a)^{1-\alpha}-f$$

is a conserved quantity.

Corollary 4: If $\mathcal{J}$ given by (11) is invariant under the transformation $\overline{x}=x$, $\overline{y}=y+\epsilon\xi(x,y(x))$, and if y is an extremal of $\mathcal{J}$, then

$$\frac{\partial L}{\partial y_a^{(\alpha)}}\xi-\Lambda$$

is a conserved quantity.

Proof : Given that

$$\frac{d_a^\alpha(x-a)^{1-\alpha}}{dx_a^\alpha}=(1-\alpha)(x-a)^{1-2\alpha}$$

the result follows immediately from Theorem 9. ■

VIII. The Hamiltonian Formalism

The Hamiltonian formalism is related to the Lagrangian one by the so called Legendre transformation, from coordinates and velocities to coordinates and momenta. Let the momenta be given by

$$p(x)=\frac{\partial L}{\partial y_a^{(\alpha)}}(x,y(x),y_a^{(\alpha)}(x)) \tag{37}$$

and the Hamiltonian function by

$$H(x,y,v,\psi)=-L(x,y,v)+\psi\, v. \tag{38}$$

To simplify notation, $[y](x)$ and $\{y\}(x)$ will denote $(x,y(x),y_a^{(\alpha)}(x))$ and $(x,y(x),y_a^{(\alpha)}(x),p(x))$, respectively. Differentiating (38), and using definition (37), it follows that

$$\begin{aligned}
&\frac{d_a^\alpha H}{dx_a^\alpha}\{y\}(x)\\
&=-\frac{\partial L}{\partial x}[y](x)x_a^{(\alpha)}-\frac{\partial L}{\partial y}[y](x)\cdot y_a^{(\alpha)}(x)\\
&\quad-\frac{\partial L}{\partial v}[y](x)\cdot\frac{d_a^\alpha}{dx_a^\alpha}y_a^{(\alpha)}(x)+p_a^{(\alpha)}(x)\cdot y_a^{(\alpha)}(x)\\
&\quad+\frac{\partial L}{\partial v}[y](x)\cdot\frac{d_a^\alpha}{dx_a^\alpha}y_a^{(\alpha)}(x)\\
&=-\frac{\partial L}{\partial x}[y](x)\cdot(x-a)^{1-\alpha}-\frac{\partial L}{\partial y}[y](x)\cdot y_a^{(\alpha)}(x)\\
&\quad+p_a^{(\alpha)}(x)\cdot y_a^{(\alpha)}(x).
\end{aligned} \tag{39}$$

On the other hand, by the definition of Hamiltonian (38), one has immediately that

$$\begin{cases}\dfrac{\partial H}{\partial x}(x,y,v,\psi)=-\dfrac{\partial L}{\partial x}(x,y,v)\\ \dfrac{\partial H}{\partial y}(x,y,v,\psi)=-\dfrac{\partial L}{\partial y}(x,y,v)\\ \dfrac{\partial H}{\partial \psi}(x,y,v,\psi)=v\end{cases}$$

and so we can write (39) in the form

$$\begin{aligned}\frac{d_a^\alpha H}{dx_a^\alpha}&\{y\}(x)\\ =&\frac{\partial H}{\partial x}\{y\}(x)(x-a)^{1-\alpha}\\ &+\frac{\partial H}{\partial y}\{y\}(x)\cdot y_a^{(\alpha)}(x)+\frac{\partial H}{\partial \psi}\{y\}(x)\cdot p_a^{(\alpha)}(x).\end{aligned}\tag{40}$$

If y is an extremal of $\mathcal{J}$, then by the conformable fractional Euler-Lagrange equation (16) one has

$$\frac{\partial L}{\partial y}[y](x)-\frac{d_a^\alpha}{dx_a^\alpha}\left(\frac{\partial L}{\partial v}[y]\right)(x)=-\frac{\partial H}{\partial y}\{y\}(x)-p_a^{(\alpha)}(x)=0$$

and we can write

$$\begin{cases}y_a^{(\alpha)}(x)=\dfrac{\partial H}{\partial \psi}\{y\}(x)\\ p_a^{(\alpha)}(x)=-\dfrac{\partial H}{\partial y}\{y\}(x).\end{cases}\tag{41}$$

The system (41) is nothing else than the conformable fractional Euler-Lagrange equation in Hamiltonian form. Substituting the expressions of (41) into (40), we get the analog to the DuBois–Reymond condition (28) in Hamiltonian form:

$$\frac{d_a^\alpha H}{dx_a^\alpha}\{y\}(x)=\frac{\partial H}{\partial x}\{y\}(x)(x-a)^{1-\alpha}.\tag{42}$$

If the Lagrangian L is autonomous, i.e., L does not depend on x, then

$$\frac{\partial L}{\partial x}=0$$

and, consequently, by (42) H is a conserved quantity. If the Lagrangian L does not depend on y, then

$$\frac{\partial L}{\partial y}=-\frac{\partial H}{\partial y}=0$$

and so $p_a^{(\alpha)}=0$, i.e., p is a conserved quantity.

We now exhibit Corollary 3 within the Hamiltonian framework.

Theorem 10 (Conformable fractional Noether's theorem in Hamiltonian form under the presence of an external force f): If $\mathcal{J}$ given by (11) is invariant under (29), y is an extremal of $\mathcal{J}$, and function $f=f(x,y(x),y_a^{(\alpha)}(x))$ satisfies the equation

$$\begin{aligned}\frac{d_a^\alpha f}{dx_a^\alpha}&(x,y(x),y_a^{(\alpha)}(x))\\ &=(1-\alpha)p(x)\left[\xi(x-a)^{1-2\alpha}-\frac{y_a^{(\alpha)}(x)\tau}{(x-a)^\alpha}\right]\\ &\quad+\frac{d_a^\alpha\Lambda}{dx_a^\alpha}(x,y(x))(x-a)^{1-\alpha}\end{aligned}$$

then

$$p(x)\xi(x-a)^{1-\alpha}-H\{y\}(x)\tau-f(x,y(x),y_a^{(\alpha)}(x))$$

is a conserved quantity.

IX. Conformable Fractional Optimal Control

The conformable fractional optimal control problem is stated as follows: find a pair of functions $(y(\cdot),v(\cdot))$ that minimizes

$$\mathcal{J}(y,v)=\int_a^b L(x,y(x),v(x))\,d_a^\alpha x\tag{43}$$

when subject to the (nonautonomous) fractional control system

$$y_a^{(\alpha)}(x)=\varphi(x,y(x),v(x)).\tag{44}$$

A pair $(y(\cdot),v(\cdot))$ that minimizes functional (43) subject to (44) is called an optimal process. The reader interested on the fractional optimal control theory is referred to [28], [29], [38]. Here we note that if $\alpha=1$, then (43) and (44) is the standard optimal control problem: to minimize

$$\mathcal{J}(y,v)=\int_a^b L(x,y(x),v(x))\,dx$$

subject to the control system

$$y'(x)=\varphi(x,y(x),v(x)).$$

We assume that the Lagrangian L and the velocity vector φ are functions at least of class C^1 in their domain $[a,b]\times\mathbb{R}^2$. Also, the admissible state trajectories y are such that $y_a^{(\alpha)}$ exist.

Remark 8: In case $\varphi\equiv v$, the previous problem (43) and (44) reduces to the fundamental problem of the conformable fractional variational calculus (11), as stated in Section III.

Following the standard approach [37], [39], we consider the augmented conformable fractional functional

$$\begin{aligned}\mathcal{I}(y,v,p)=\int_a^b[\,&L(x,y(x),v(x))+p(x)(y_a^{(\alpha)}(x)\\ &-\varphi(x,y(x),v(x)))]\,d_a^\alpha x\end{aligned}\tag{45}$$

where p is such that $p_a^{(\alpha)}$ exists. Consider a variation vector of type $(y+\epsilon y_1,v+\epsilon v_1,p+\epsilon p_1)$ with $|\epsilon|\ll 1$. For convenience, we restrict ourselves to the case $y_1(a)=y_1(b)=0$. If $(y(\cdot),v(\cdot))$ is an optimal process, then the first variation is zero when $\epsilon=0$. Thus, using the conformable fractional integration by parts formula (Theorem 3), we obtain that

$$\begin{aligned}0&=\int_a^b\Bigg[\frac{\partial L}{\partial y}y_1+\frac{\partial L}{\partial v}v_1+p_1(y_a^{(\alpha)}-\varphi)\\ &\qquad+p\left({y_1}_a^{(\alpha)}-\tfrac{\partial\varphi}{\partial y}y_1-\tfrac{\partial\varphi}{\partial v}v_1\right)\Bigg]d_a^\alpha x\\ &=\int_a^b\Bigg[y_1\left(\frac{\partial L}{\partial y}-p\frac{\partial\varphi}{\partial y}-p_a^{(\alpha)}\right)+v_1\left(\frac{\partial L}{\partial v}-p\frac{\partial\varphi}{\partial v}\right)\\ &\qquad+p_1(y_a^{(\alpha)}-\varphi)\Bigg]d_a^\alpha x.\end{aligned}$$

By the arbitrariness of the the variation functions, we obtain the following system, called the Euler–Lagrange equations for the conformable fractional optimal control problem:

$$\begin{cases}y_a^{(\alpha)}(x)=\varphi(x,y(x),v(x))\\ p_a^{(\alpha)}(x)=\dfrac{\partial L}{\partial y}(x,y(x),v(x))-p(x)\dfrac{\partial\varphi}{\partial y}(x,y(x),v(x))\\ \dfrac{\partial L}{\partial v}(x,y(x),v(x))-p(x)\dfrac{\partial\varphi}{\partial v}(x,y(x),v(x))=0.\end{cases}\tag{46}$$

These equations give necessary conditions for finding the optimal solutions of problem (43) and (44). We remark that they are similar to the standard ones, in case of integer order derivatives, but in this case they contain conformable fractional derivatives, as expected. The solution can be stated using the Hamiltonian formalism. Consider the Hamiltonian function

$$H(x,y,v,p) = -L(x,y,v) + p(x)\varphi(x,y,v). \tag{47}$$

Then (46) gives:

1) The fractional Hamiltonian system

$$\begin{cases} y_a^{(\alpha)}(x) = \dfrac{\partial H}{\partial p}(x,y,v,p) \\ p_a^{(\alpha)}(x) = -\dfrac{\partial H}{\partial y}(x,y,v,p). \end{cases} \tag{48}$$

2) The stationary condition

$$\frac{\partial H}{\partial v}(x,y,v,p) = 0. \tag{49}$$

Definition 6: Any triplet (y,v,p) satisfying system (48) and (49) is called a conformable fractional Pontryagin extremal.

Remark 9: In the particular case $\varphi \equiv v$, i.e., when the conformable fractional optimal control problem is reduced to the fundamental conformable fractional problem of the calculus of variations, we obtain

$$H = -L(x,y,v) + pv\,, \quad y_a^{(\alpha)} = v$$

and the equations

$$p_a^{(\alpha)} = -\frac{\partial H}{\partial y} = \frac{\partial L}{\partial y}\,, \quad p = \frac{\partial L}{\partial v}.$$

Therefore, we obtain the conformable fractional Euler–Lagrange equation (16):

$$\frac{\partial L}{\partial y} = \frac{d_a^\alpha}{dx_a^\alpha}\left(\frac{\partial L}{\partial y_a^{(\alpha)}}\right).$$

Let us now considerer the augmented fractional variational functional (45) written in the Hamiltonian form:

$$\mathcal{I}(y,v,p) = \int_0^1 \left(-H(x,y(x),v(x),p(x)) + p(x)y_a^{(\alpha)}(x)\right) d_a^\alpha x \tag{50}$$

where H is given by expression (47). For a parameter ϵ, with $|\epsilon| \ll 1$, consider the family of transformations

$$\begin{cases} \overline{x} = x + \epsilon\tau(x,y(x),v(x),p(x)) \\ \overline{y} = y + \epsilon\xi(x,y(x),v(x),p(x)) \\ \overline{v} = v + \epsilon\sigma(x,y(x),v(x),p(x)) \\ \overline{p} = p + \epsilon\pi(x,y(x),v(x),p(x)). \end{cases} \tag{51}$$

We now define the notion of invariance of (43)–(44) in terms of the Hamiltonian H and the augmented conformable fractional variational functional (50).

Definition 7: The conformable fractional optimal control problem (43) and (44) is invariant under the transformations (51) up to the Gauge term Λ, if a function $\Lambda = \Lambda(x,y)$ exists such that for any functions y, v and p, and for any real $x \in [0,1]$, the following equality holds:

$$\begin{aligned}\left[-H\left(\overline{x},\overline{y},\overline{v},\overline{p}\right) + \overline{p}\frac{d_a^\alpha \overline{y}}{d\overline{x}_a^\alpha}\right]\frac{d_a^\alpha \overline{x}}{d_a^\alpha x} \\ = -H(x,y,v,p) + py_a^{(\alpha)} + \epsilon\frac{d_a^\alpha\Lambda}{dx_a^\alpha}(x,y) + o(\epsilon)\end{aligned} \tag{52}$$

for all ϵ in some neighborhood of zero, where as in Definition 4 $\frac{d_a^\alpha \overline{x}}{d_a^\alpha x}$ stands for (31).

Theorem 11 (Fractional Noether's theorem for the fractional optimal control problem (43)–(44)): If (43) and (44) is invariant under (51) in the sense of Definition 7, and if (y,v,p) is a conformable fractional Pontryagin extremal, then

$$\begin{aligned}\frac{d_a^\alpha}{dx_a^\alpha}(p\xi) - \tau\left(\frac{\partial H}{\partial x} + (\alpha-1)\frac{py_a^{(\alpha)}}{x-a}\right) \\ - H\frac{\tau_a^{(\alpha)}}{(x-a)^{1-\alpha}} = \frac{d_a^\alpha\Lambda}{dx_a^\alpha}.\end{aligned} \tag{53}$$

Proof: Differentiating (52) with respect to ϵ, then choosing $\epsilon = 0$, we get

$$\begin{aligned}&-\frac{\partial H}{\partial x}\tau - \frac{\partial H}{\partial y}\xi - \frac{\partial H}{\partial v}\sigma - \frac{\partial H}{\partial p}\pi + \pi y_a^{(\alpha)} \\ &+ p\left[\xi_a^{(\alpha)} - y_a^{(\alpha)}\left((\alpha-1)\frac{\tau}{x-a} + \frac{\tau_a^{(\alpha)}}{(x-a)^{1-\alpha}}\right)\right] \\ &+ \left[-H + py_a^{(\alpha)}\right]\frac{\tau_a^{(\alpha)}}{(x-a)^{1-\alpha}} = \frac{d_a^\alpha\Lambda}{dx_a^\alpha}.\end{aligned}$$

Equation (53) follows because (y,v,p) is a conformable fractional Pontryagin extremal. ■

Remark 10: When $\alpha = 1$ and $\Lambda = 0$, equation (53) becomes

$$\frac{d}{dx}(p\xi) - \tau\frac{\partial H}{\partial x} - H\tau' = 0.$$

Using relations (48) and (49) with $\alpha = 1$, we deduce that

$$-H\tau + p\xi \equiv \text{ constant}$$

which is the optimal control version of Noether's theorem [35]–[37]. For $\alpha \in (0,1)$, Theorem 11 extends the main result of [28].

X. The Multi-dimensional Case

In this section, we show a necessary condition of invariance, when the Lagrangian depends on two independent variables x_1 and x_2 and on m functions $y_1, \ldots, y_m$. First, we define conformable fractional partial derivatives and conformable multiple fractional integrals in a natural way, similarly as done in the integer case. In addition, we are going to use the following properties.

Theorem 12 (Conformable Green's theorem for a rectangle): Let f and g be two continuous and α-differentiable functions whose domains contain $R = [a,b] \times [c,d] \subset \mathbb{R}^2$. Then,

$$\begin{aligned}\int_a^b (f(x_1,c) - f(x_1,d))\, d_a^\alpha x_1 + \int_c^d (g(b,x_2) - g(a,x_2))\, d_c^\alpha x_2 \\ = \int_R \left(\frac{\partial_a^\alpha}{\partial {x_1}_a^\alpha}g(x_1,x_2) - \frac{\partial_c^\alpha}{\partial {x_2}_c^\alpha}f(x_1,x_2)\right) d_a^\alpha x_1 d_c^\alpha x_2.\end{aligned} \tag{54}$$

Proof : By Theorem 2, we have

$$f(x_1,d)-f(x_1,c)=\int_c^d \frac{\partial_c^\alpha}{\partial {x_2}_c^\alpha} f(x_1,x_2) d_c^\alpha x_2$$

and

$$g(b,x_2)-g(a,x_2)=\int_a^b \frac{\partial_a^\alpha}{\partial {x_1}_a^\alpha} g(x_1,x_2) d_a^\alpha x_1.$$

Therefore,

$$\begin{aligned}
&\int_a^b (f(x_1,c)-f(x_1,d))\, d_a^\alpha x_1+\int_c^d (g(b,x_2)-g(a,x_2))\, d_c^\alpha x_2\\
&= -\int_a^b\int_c^d \frac{\partial_c^\alpha}{\partial {x_2}_c^\alpha} f(x_1,x_2) d_c^\alpha x_2 d_a^\alpha x_1\\
&\quad +\int_c^d\int_a^b \frac{\partial_a^\alpha}{\partial {x_1}_a^\alpha} g(x_1,x_2) d_a^\alpha x_1 d_c^\alpha x_2\\
&= \int_R \left(\frac{\partial_a^\alpha}{\partial {x_1}_a^\alpha} g(x_1,x_2)-\frac{\partial_c^\alpha}{\partial {x_2}_c^\alpha} f(x_1,x_2)\right) d_a^\alpha x_1 d_c^\alpha x_2.
\end{aligned}$$

■

Remark 11: From Definition 2 and Remark 1, it is easy to verify that for C^1 functions our fractional Green's theorem over a rectangular domain (Theorem 12) reduces to the conventional Green's identity for

$$\tilde{f}(x_1,x_2)=f(x_1,x_2)(x_1-a)^{\alpha-1}$$

and

$$\tilde{g}(x_1,x_2)=g(x_1,x_2)(x_2-a)^{\alpha-1}.$$

Lemma 2: Let F, G and h be α-differentiable continuous functions whose domains contain $R=[a,b]\times[c,d]$. If $h=0$ on the boundary ∂R of R, then

$$\begin{aligned}
&\int_R \bigg(G(x_1,x_2)\frac{\partial_a^\alpha}{\partial {x_1}_a^\alpha} h(x_1,x_2)\\
&\qquad -F(x_1,x_2)\frac{\partial_c^\alpha}{\partial {x_2}_c^\alpha} h(x_1,x_2)\bigg) d_a^\alpha x_1 d_c^\alpha x_2\\
&\quad = -\int_R \left(\frac{\partial_a^\alpha}{\partial {x_1}_a^\alpha} G(x_1,x_2)-\frac{\partial_c^\alpha}{\partial {x_2}_c^\alpha} F(x_1,x_2)\right)\\
&\qquad \times h(x_1,x_2) d_a^\alpha x_1 d_c^\alpha x_2.
\end{aligned} \tag{55}$$

Proof : By choosing $f=Fh$ and $g=Gh$ in Green's formula (54), we obtain that

$$\begin{aligned}
&\int_a^b (F(x_1,c)h(x_1,c)-F(x_1,d)h(x_1,d))\, d_a^\alpha x_1\\
&+\int_c^d (G(b,x_2)g(b,x_2)-G(a,x_2)h(a,x_2))\, d_c^\alpha x_2\\
&= \int_R \bigg(\frac{\partial_a^\alpha}{\partial {x_1}_a^\alpha} G(x_1,x_2)\\
&\qquad -\frac{\partial_c^\alpha}{\partial {x_2}_c^\alpha} F(x_1,x_2)\bigg) h(x_1,x_2) d_a^\alpha x_1 d_c^\alpha x_2\\
&\quad +\int_R \bigg(G(x_1,x_2)\frac{\partial_a^\alpha}{\partial {x_1}_a^\alpha} h(x_1,x_2)\\
&\qquad -F(x_1,x_2)\frac{\partial_c^\alpha}{\partial {x_2}_c^\alpha} h(x_1,x_2)\bigg) d_a^\alpha x_1 d_c^\alpha x_2.
\end{aligned}$$

Since $h=0$ on the boundary ∂R of R, we have

$$\begin{aligned}
&\int_R \bigg(G(x_1,x_2)\frac{\partial_a^\alpha}{\partial {x_1}_a^\alpha} h(x_1,x_2)\\
&\qquad -F(x_1,x_2)\frac{\partial_c^\alpha}{\partial {x_2}_c^\alpha} h(x_1,x_2)\bigg) d_a^\alpha x_1 d_c^\alpha x_2\\
&= -\int_R \left(\frac{\partial_a^\alpha}{\partial {x_1}_a^\alpha} G(x_1,x_2)-\frac{\partial_c^\alpha}{\partial {x_2}_c^\alpha} F(x_1,x_2)\right)\\
&\qquad \times h(x_1,x_2) d_a^\alpha x_1 d_c^\alpha x_2.
\end{aligned}$$

■

Remark 12: In the very recent and general paper [40], a vector calculus with deformed derivatives (as the conformable derivative) is formally introduced. We refer the reader to [40] for a detailed discussion of a vector calculus with deformed derivatives and more properties on the multi-dimensional conformable calculus.

Let us now consider the fractional variational integral

$$\mathcal{J}(y)=\int_R L\left(x,y,\frac{\partial_a^\alpha y}{\partial x_a^\alpha}\right) d_a^\alpha x \tag{56}$$

where for simplicity we choose $R=[a,b]\times[a,b]$, and where $x=(x_1,x_2)$, $y=(y_1,\ldots,y_m)$, $d_a^\alpha x=d_a^\alpha x_1 d_a^\alpha x_2$, and

$$\frac{\partial_a^\alpha y}{\partial x_a^\alpha}=\left(\frac{\partial_a^\alpha y_1}{\partial {x_1}_a^\alpha},\frac{\partial_a^\alpha y_1}{\partial {x_2}_a^\alpha},\ldots,\frac{\partial_a^\alpha y_m}{\partial {x_1}_a^\alpha},\frac{\partial_a^\alpha y_m}{\partial {x_2}_a^\alpha}\right).$$

We are assuming that the Lagrangian

$$L=L(x_1,x_2,y_1,\ldots,y_m,v_{1,1},v_{1,2},\ldots,v_{m,1},v_{m,2})$$

is at least of class C^1, that the domains of y_k, $k\in\{1,\ldots,m\}$, contain R, and that all these partial conformable fractional derivatives exist.

Theorem 13 (The multi-dimensional fractional Euler-Lagrange equation): Let y be an extremizer of (56) with

$$y|_{\partial R}=\psi(x_1,x_2)$$

for some given function $\psi=(\psi_1,\ldots,\psi_m)$. Then, the following equation holds:

$$\frac{\partial L}{\partial y_k}-\frac{\partial_a^\alpha}{\partial {x_1}_a^\alpha}\left(\frac{\partial L}{\partial v_{k,1}}\right)-\frac{\partial_a^\alpha}{\partial {x_2}_a^\alpha}\left(\frac{\partial L}{\partial v_{k,2}}\right)=0 \tag{57}$$

for all $k\in\{1,\ldots,m\}$.

Proof : Let $y^*=(y_1^*,\ldots,y_m^*)$ give an extremum to (56). We define m families of functions

$$y_k(x_1,x_2)=y_k^*(x_1,x_2)+\epsilon\eta_k(x_1,x_2) \tag{58}$$

where $k\in\{1,\ldots,m\}$, ϵ is a constant, and η_k is an arbitrary α-differentiable function satisfying the boundary conditions $\eta_k|_{\partial R}=0$ (weak variations). From (58), the boundary conditions $\eta_k|_{\partial R}=0$ and $y_k|_{\partial R}=\psi_k(x_1,x_2)$, it follows that function y_k is admissible. Let the Lagrangian L be C^1. Because y^* is an extremizer of functional $\mathcal{J}$, the Gateaux derivative

$\delta\mathcal{J}(y^*)$ needs to be identically null. For the functional (56),

$$\begin{aligned}\delta\mathcal{J}(y^*) &= \lim_{\epsilon\to 0}\frac{1}{\epsilon}\left(\int_R L\left(x, y, \frac{\partial_a^\alpha y}{\partial x_a^\alpha}\right) d_a^\alpha x\right.\\ &\qquad \left. - \int_R L\left(x, y^*, \frac{\partial_a^\alpha y^*}{\partial x_a^\alpha}\right) d_a^\alpha x\right)\\ &= \sum_{k=1}^m \int_R \left(\eta_k(x_1,x_2)\frac{\partial L\left(x, y^*, \frac{\partial_a^\alpha y^*}{\partial x_a^\alpha}\right)}{\partial y_k^*}\right.\\ &\qquad + \frac{\partial_a^\alpha}{\partial {x_1}_a^\alpha}\eta_k(x_1,x_2)\frac{\partial L\left(x, y^*, \frac{\partial_a^\alpha y^*}{\partial x_a^\alpha}\right)}{\partial v_{k,1}}\\ &\qquad \left. + \frac{\partial_a^\alpha}{\partial {x_2}_a^\alpha}\eta_k(x_1,x_2)\frac{\partial L\left(x, y^*, \frac{\partial_a^\alpha y^*}{\partial x_a^\alpha}\right)}{\partial v_{k,2}}\right) d_a^\alpha x\\ &= 0.\end{aligned}$$

Using (55), we get that

$$\begin{aligned}&\sum_{k=1}^m \int_R \eta_k(x_1,x_2)\left(\frac{\partial L\left(x, y^*, \frac{\partial_a^\alpha y^*}{\partial x_a^\alpha}\right)}{\partial y_k^*}\right.\\ &\qquad - \frac{\partial_a^\alpha}{\partial {x_1}_a^\alpha}\frac{\partial L\left(x, y^*, \frac{\partial_a^\alpha y^*}{\partial x_a^\alpha}\right)}{\partial v_{k,1}}\\ &\qquad \left. - \frac{\partial_a^\alpha}{\partial {x_2}_a^\alpha}\frac{\partial L\left(x, y^*, \frac{\partial_a^\alpha y^*}{\partial x_a^\alpha}\right)}{\partial v_{k,2}}\right) d_a^\alpha x = 0 \qquad (59)\end{aligned}$$

since $\eta_k|_{\partial R} = 0$. The fractional Euler–Lagrange equation (57) follows from (59) by using the fundamental lemma of the conformable fractional calculus of variations (Lemma 1). ∎

Let ϵ be a real, and consider the following family of transformations:

$$\begin{cases}\overline{x}_i = x_i + \epsilon\tau_i(x, y(x)), & i \in \{1,2\},\\ \overline{y}_k = y_k + \epsilon\xi_k(x, y(x)), & k \in \{1,\ldots,m\}\end{cases} \qquad (60)$$

where τ_i and ξ_k are such that there exist $\frac{\partial_a^\alpha \tau_i}{\partial {x_j}_a^\alpha}$ and $\frac{\partial_a^\alpha \xi_k}{\partial {x_j}_a^\alpha}$ for all $i, j \in \{1,2\}$ and all $k \in \{1,\ldots,m\}$. Denote by $\left[\frac{\partial_a^\alpha \overline{x}}{\partial_a^\alpha x}\right]$ the matrix

$$\begin{bmatrix}\dfrac{\dfrac{\partial_a^\alpha \overline{x}_1}{\partial {x_1}_a^\alpha}}{\dfrac{\partial_a^\alpha x_1}{\partial {x_1}_a^\alpha}} & \dfrac{\dfrac{\partial_a^\alpha \overline{x}_1}{\partial {x_2}_a^\alpha}}{\dfrac{\partial_a^\alpha x_2}{\partial {x_2}_a^\alpha}}\\[2ex] \dfrac{\dfrac{\partial_a^\alpha \overline{x}_2}{\partial {x_1}_a^\alpha}}{\dfrac{\partial_a^\alpha x_1}{\partial {x_1}_a^\alpha}} & \dfrac{\dfrac{\partial_a^\alpha \overline{x}_2}{\partial {x_2}_a^\alpha}}{\dfrac{\partial_a^\alpha x_2}{\partial {x_2}_a^\alpha}}\end{bmatrix}$$

$$= \begin{bmatrix} 1 + \dfrac{\epsilon}{(x_1-a)^{1-\alpha}}\dfrac{\partial_a^\alpha \tau_1}{\partial {x_1}_a^\alpha} & \dfrac{\epsilon}{(x_2-a)^{1-\alpha}}\dfrac{\partial_a^\alpha \tau_1}{\partial {x_2}_a^\alpha}\\ \dfrac{\epsilon}{(x_1-a)^{1-\alpha}}\dfrac{\partial_a^\alpha \tau_2}{\partial {x_1}_a^\alpha} & 1 + \dfrac{\epsilon}{(x_2-a)^{1-\alpha}}\dfrac{\partial_a^\alpha \tau_2}{\partial {x_2}_a^\alpha}\end{bmatrix}.$$

Definition 8: Functional $\mathcal{J}$ as in (56) is invariant under the family of transformation (60) if for all y_k and for all $x_i \in [0,1]$ we have

$$\begin{aligned}&L\left(\overline{x}, \overline{y}, \frac{\partial_a^\alpha \overline{y}}{\partial \overline{x}_a^\alpha}\right)\det\left[\frac{\partial_a^\alpha \overline{x}}{\partial_a^\alpha x}\right]\\ &\qquad = L\left(x, y, \frac{\partial_a^\alpha y}{\partial x_a^\alpha}\right) + \epsilon\frac{d_a^\alpha \Lambda}{dx_a^\alpha}(x,y) + o(\epsilon)\end{aligned}$$

for all ϵ in some neighborhood of zero.

Using the same techniques as in the proof of Theorem 8, we obtain a necessary condition of invariance for the fractional variational problem (56).

Theorem 14: If $\mathcal{J}$ given by (56) is invariant under transformations (60), then

$$\begin{aligned}&\sum_{i=1}^2\frac{\partial L}{\partial x_i}\tau_i + \sum_{k=1}^m\frac{\partial L}{\partial y_k}\xi_k + \sum_{k=1}^m\sum_{i=1}^2\frac{\partial L}{\partial v_{k,i}}\left[\frac{\partial_a^\alpha \xi_k}{\partial {x_i}_a^\alpha}\right.\\ &\left. - \frac{\partial_a^\alpha y_k}{\partial {x_i}_a^\alpha}\left((\alpha-1)\frac{\tau_i}{x_i-a} + \frac{1}{(x_i-a)^{1-\alpha}}\frac{\partial_a^\alpha \tau_i}{\partial {x_i}_a^\alpha}\right)\right]\\ &+ L\left(\frac{1}{(x_1-a)^{1-\alpha}}\frac{\partial_a^\alpha \tau_1}{\partial {x_1}_a^\alpha} + \frac{1}{(x_2-a)^{1-\alpha}}\frac{\partial_a^\alpha \tau_2}{\partial {x_2}_a^\alpha}\right) = \frac{d^\alpha \Lambda}{dx^\alpha}.\end{aligned} \qquad (61)$$

Proof : Using relations

$$\frac{\partial_a^\alpha \overline{y}_k}{\partial {\overline{x}_i}_a^\alpha} = \frac{\dfrac{\partial_a^\alpha y_k}{\partial {x_i}_a^\alpha} + \epsilon\dfrac{\partial_a^\alpha \xi_k}{\partial {x_i}_a^\alpha}}{(x_i + \epsilon\tau_i - a)^{\alpha-1}\left[(x_i-a)^{1-\alpha} + \epsilon\dfrac{\partial_a^\alpha \tau_i}{\partial {x_i}_a^\alpha}\right]}$$

and

$$\begin{aligned}&\frac{d}{d\epsilon}\det\left[\frac{\partial^\alpha \overline{x}}{\partial^\alpha x}\right]\Bigg|_{\epsilon=0}\\ &\qquad = \frac{1}{(x_1-a)^{1-\alpha}}\frac{\partial_a^\alpha \tau_1}{\partial {x_1}_a^\alpha} + \frac{1}{(x_2-a)^{1-\alpha}}\frac{\partial_a^\alpha \tau_2}{\partial {x_2}_a^\alpha}\end{aligned}$$

we conclude that (61) holds. ∎

Remark 13: When $\alpha = 1$ and $\Lambda \equiv 0$, Theorem 14 reduces to the standard one [24]: equality (61) simplifies to

$$\begin{aligned}&\sum_{i=1}^2\frac{\partial L}{\partial x_i}\tau_i + \sum_{k=1}^m\frac{\partial L}{\partial y_k}\xi_k + \sum_{k=1}^m\sum_{i=1}^2\frac{\partial L}{\partial v_{k,i}}\left[\frac{\partial \xi_k}{\partial x_i} - \frac{\partial y_k}{\partial x_i}\frac{\partial \tau_i}{\partial x_i}\right]\\ &\qquad + L\left(\frac{\partial \tau_1}{\partial x_1} + \frac{\partial \tau_2}{\partial x_2}\right) = 0.\end{aligned}$$

Corollary 5: If $\mathcal{J}$ given by (56) is invariant under (60), $\tau_1 \equiv 0 \equiv \tau_2$, and no Gauge term is involved (i.e., $\Lambda \equiv 0$), then

$$\sum_{k=1}^m\frac{\partial L}{\partial y_k}\xi_k + \sum_{k=1}^m\sum_{i=1}^2\frac{\partial L}{\partial v_{k,i}}\frac{\partial_a^\alpha \xi_k}{\partial {x_i}_a^\alpha} = 0.$$

It remains an open question how to obtain a Noether constant of motion for the conformable fractional multi-dimensional case.

REFERENCES

[1] A. A. Kilbas, H. M. Srivastava, and J. J. Trujillo, *Theory and Applications of Fractional Differential Equations, Volume 204 (North-Holland Mathematics Studies)*. Amsterdam: Elsevier Science, 2006.

[2] K. S. Miller and B. Ross, *An Introduction to the Fractional Calculus and Fractional Differential Equations*. New York: Wiley-Interscience, 1993.

[3] I. Podlubny, *Fractional Differential Equations, Mathematics in Science and Engineering*. San Diego, CA: Academic Press, Inc., 1999.

[4] J. T. Machado, V. Kiryakova, and F. Mainardi, "Recent history of fractional calculus," *Commun. Nonlinear Sci. Numer. Simul.*, vol. 16, no. 3, pp. 1140−1153, Mar. 2011.

[5] R. Khalil, M. Al Horani, A. Yousef, and M. Sababheh, "A new definition of fractional derivative," *J. Comput. Appl. Math.*, vol. 264, pp. 65−70, Jul. 2014.

[6] T. Abdeljawad, "On conformable fractional calculus," *J. Comput. Appl. Math.*, vol. 279, pp. 57−66, May 2015.

[7] D. R. Anderson and R. I. Avery, "Fractional-order boundary value problem with Sturm-Liouville boundary conditions," *Electron. J. Diff. Equ.*, vol. 2015, no. 29, pp. 10, Jan. 2015.

[8] H. Batarfi, J. Losada, J. J. Nieto, and W. Shammakh, "Three-point boundary value problems for conformable fractional differential equations," *J. Funct. Spaces*, vol. 2015, Article ID 706383, 2015.

[9] B. Bayour and D. F. M. Torres, "Existence of solution to a local fractional nonlinear differential equation," *J. Comput. Appl. Math.*, vol. 312, pp. 127–133, Mar. 2017.

[10] N. Benkhettou, S. Hassani, and D. F. M. Torres, "A conformable fractional calculus on arbitrary time scales," *J. King Saud Univ. Sci.*, vol. 28, no. 1, pp. 93−98, Jan. 2016.

[11] F. Riewe, "Mechanics with fractional derivatives," *Phys. Rev. E*, vol. 55, no. 3, pp. 3581−3592, Mar. 1997.

[12] P. S. Bauer, "Dissipative dynamical systems. I," *Proc. Natl. Acad. Sci. USA*, vol. 17, pp. 311−314, Jun. 1931.

[13] O. P. Agrawal, "Formulation of Euler-Lagrange equations for fractional variational problems," *J. Math. Anal. Appl.*, vol. 272, no. 1, pp. 368−379, Aug. 2002.

[14] R. Almeida and D. F. M. Torres, "Necessary and sufficient conditions for the fractional calculus of variations with Caputo derivatives," *Commun. Nonlinear Sci. Numer. Simul.*, vol. 16, no. 3, pp. 1490−1500, 2011.

[15] D. Baleanu and O. P. Agrawal, "Fractional Hamilton formalism within Caputo's derivative," *Czechoslovak J. Phys.*, vol. 56, no. 10−11, pp. 1087−1092, Oct. 2006.

[16] J. Cresson, "Fractional embedding of differential operators and Lagrangian systems," *J. Math. Phys.*, vol. 48, no. 3, pp. 033504, Mar. 2007.

[17] M. J. Lazo and D. F. M. Torres, "The DuBois-Reymond fundamental lemma of the fractional calculus of variations and an Euler-Lagrange equation involving only derivatives of Caputo," *J. Optim. Theory Appl.*, vol. 156, no. 1, pp. 56−67, Jan. 2013.

[18] T. Odzijewicz, A. B. Malinowska, and D. F. M. Torres, "Fractional variational calculus with classical and combined Caputo derivatives," *Nonlinear Anal.*, vol. 75, no. 3, pp. 1507−1515, Feb. 2012.

[19] T. Odzijewicz, A. B. Malinowska, and D. F. M. Torres, "Fractional calculus of variations in terms of a generalized fractional integral with applications to physics," *Abstr. Appl. Anal.*, vol. 2012, Article ID 871912, 2012.

[20] R. Almeida, S. Pooseh, and D. F. M. Torres, *Computational Methods in the Fractional Calculus of Variations*. London: Imperial College Press, 2015.

[21] A. B. Malinowska, T. Odzijewicz, and D. F. M. Torres, *Advanced Methods in the Fractional Calculus of Variations*. New York: Springer International Publishing, 2015.

[22] A. B. Malinowska and D. F. M. Torres, *Introduction to the Fractional Calculus of Variations*. London: Imperial College Press, 2012.

[23] M. J. Lazo and C. E. Krumreich, "The action principle for dissipative systems," *J. Math. Phys.*, vol. 55, no. 12, pp. 122902, 2014.

[24] J. D. Logan, *Invariant Variational Principles. Vol. 138. Mathematics in Science and Engineering*. New York, San Francisco, Lindon: Academic Press, 1977.

[25] D. F. M. Torres, "Proper extensions of Noether's symmetry theorem for nonsmooth extremals of the calculus of variations," *Commun. Pure Appl. Anal.*, vol. 3, no. 3, pp. 491−500, Sep. 2004.

[26] G. S. F. Frederico and D. F. M. Torres, "Non-conservative Noether's theorem for fractional action-like variational problems with intrinsic and observer times," *Int. J. Ecol. Econ. Stat.*, vol. 9, no. F07, pp. 74−82, Nov. 2007.

[27] G. S. F. Frederico and D. F. M. Torres, "A formulation of Noether's theorem for fractional problems of the calculus of variations," *J. Math. Anal. Appl.*, vol. 334, no. 2, pp. 834−846, Oct. 2007.

[28] G. S. F. Frederico and D. F. M. Torres, "Fractional conservation laws in optimal control theory," *Nonlinear Dyn.*, vol. 53, no. 3, pp. 215−222, Aug. 2008.

[29] G. S. F. Frederico and D. F. M. Torres, "Fractional optimal control in the sense of Caputo and the fractional Noether's theorem," *Int. Math. Forum*, vol. 3, no. 10, pp. 479−493, Sep. 2008.

[30] G. S. F. Frederico and D. F. M. Torres, "Fractional Noether's theorem in the Riesz-Caputo sense," *Appl. Math. Comput.*, vol. 217, no. 3, pp. 1023−1033, Oct. 2010.

[31] N. Benkhettou, A. M. C. Brito Da Cruz, and D. F. M. Torres, "A fractional calculus on arbitrary time scales: Fractional differentiation and fractional integration," *Signal Proc.*, vol. 107, pp. 230−237, Feb. 2015.

[32] N. Benkhettou, A. M. C. Brito da Cruz, and D. F. M. Torres, "Nonsymmetric and symmetric fractional calculi on arbitrary nonempty closed sets," *Math. Methods Appl. Sci.*, vol. 39, no. 2, pp. 261−279, Jan. 2016.

[33] W. Sarlet and F. Cantrijn, "Generalizations of Noether's theorem in classical mechanics," *SIAM Rev.*, vol. 23, no. 4, pp. 467−494, 1981.

[34] G. S. F. Frederico and D. F. M. Torres, "Nonconservative Noether's theorem in optimal control," *Int. J. Tomogr. Stat.*, vol. 5, no. W07, pp. 109−114, 2007.

[35] D. F. M. Torres, "On the Noether theorem for optimal control," *Eur. J. Control*, vol. 8, no. 1, pp. 56−63, 2002.

[36] D. F. M. Torres, "Conservation laws in optimal control," in *Dynamics, Bifurcations, and Control*, vol. 273, F. Colonius and L Grüne, Eds. Berlin: Springer, 2002, pp. 287−296.

[37] D. F. M. Torres, "Quasi-invariant optimal control problems," *Port. Math.*, vol. 61, no. 1, pp. 97−114, 2004.

[38] S. Pooseh, R. Almeida, and D. F. M. Torres, "Fractional order optimal control problems with free terminal time," *J. Ind. Manag. Optim.*, vol. 10, no. 2, pp. 363−381, Apr. 2014.

[39] D. S. Dukić, "Noether's theorem for optimum control systems," *Int. J. Control*, vol. 18, no. 3, pp. 667−672, Jul. 1973.

[40] A. S. Balankin, J. Bory-Reyes, and M. Shapiro, "Towards a physics on fractals: differential vector calculus in three-dimensional continuum with fractal metric," *Phys. A*, vol. 444, pp. 345−359, Feb. 2016.

Matheus J. Lazo received the B.P., M.S.P. and Ph.D. degrees in physics all from the University of São Paulo, São Carlos-Brazil, in 1999, 2001 and 2006, respectively. He is currently a professor at the Federal University of Rio Grande in Brazil. His research interests include mathematical physics, fractional calculus and applications, and the calculus of variations.

Delfim F. M. Torres is a full professor of mathematics at the University of Aveiro since 2015 and coordinator of the Systems and Control Group of CIDMA since 2010. He obtained his Ph.D. in mathematics in 2002 and his D.Sc. (Habilitation) in mathematics in 2011. Professor Torres has been awarded in 2015 with the title of ISI Highly Cited Researcher. He has written more than 350 publications, including two books with Imperial College Press, in 2012 and 2015, and two books with Springer, in 2014 and 2015. Torres was, from 2011 to 2014, a key scientist of the European Marie Curie Project SADCO, a network for initial training. He is the director of the FCT Doctoral Programme of Excellence in mathematics and applications of Universities of Minho, Aveiro, Porto and UBI since 2013. Eleven Ph.D. students in mathematics have successfully finished under his supervision. Corresponding author of this paper.

Fractional Envelope Analysis for Rolling Element Bearing Weak Fault Feature Extraction

Jianhong Wang, Liyan Qiao, Yongqiang Ye, *Senior Member, IEEE*, and YangQuan Chen, *Senior Member, IEEE*

***Abstract*—The bearing weak fault feature extraction is crucial to mechanical fault diagnosis and machine condition monitoring. Envelope analysis based on Hilbert transform has been widely used in bearing fault feature extraction. A generalization of the Hilbert transform, the fractional Hilbert transform is defined in the frequency domain, it is based upon the modification of spatial filter with a fractional parameter, and it can be used to construct a new kind of fractional analytic signal. By performing spectrum analysis on the fractional envelope signal, the fractional envelope spectrum can be obtained. When weak faults occur in a bearing, some of the characteristic frequencies will clearly appear in the fractional envelope spectrum. These characteristic frequencies can be used for bearing weak fault feature extraction. The effectiveness of the proposed method is verified through simulation signal and experiment data.**

***Index Terms*—Fractional analytic signal, fractional envelope analysis, fractional Hilbert transform, rolling element bearing, weak fault feature extraction.**

I. INTRODUCTION

ROLLING element bearings are at the heart of almost every rotating machine. Therefore, they have received a lot of attention in the field of vibration analysis as they represent a common source of faults, which can be detected at an early stage [1]. Recently, to ensure the reliability and safety of modern large-scale industrial processes, data-driven methods have been receiving considerably increasing attention, particularly for the purpose of process monitoring [2], [3]. The collected vibration data from defective rolling element bearings are generally non-stationary. If processed properly by a fault feature extraction technique, this data can indicate the existence and location of certain faults. However, the vibration signal is still an indirect source of information, as it is often severely corrupted by various noise effects. As a result, the weak signature is even more difficult to be detected at the early stage of defect development. Its effectiveness in fault feature extraction largely relies on the availability of proper signal processing techniques [4]. A signal feature enhancing method is required to provide more evident information for incipient defect detection of rolling element bearings.

While operating a roller bearing with local faults impulse is created, the high-frequency shock vibration is then generated and the amplitude of vibration is modulated by the pulse force. Therefore resonance demodulation technique provides an important and effective approach to analyze the fault signals of high-frequency impact vibration. Envelope analysis, sometimes known as the high frequency resonance demodulation technique is by far the most successful method for rolling element bearings diagnostics [5]−[9]. At present, the Hilbert transform based envelope analysis has been widely used in rolling element bearings fault diagnosis as one of the most common envelope analysis methods because the characteristic information can be obtained by Hilbert transform, which has quick algorithm and could extract envelope of the rolling element bearings fault vibration signal effectively [10], [11].

However, in the traditional Hilbert transform based envelope analysis method, the fault is identified through the peak value of envelope spectrum. Thus, this traditional method has inherent disadvantages. Fast Fourier transform method is widely used in the spectrum analysis of envelope signals; however, it could only give the global energy-frequency distributions and fail to reflect the details of a signal. So it is hard to analyze a signal effectively when the fault signal is weaker than the interfering signal. At the same time, it is easy to diffuse and truncate the signal's energy as fast Fourier transform regards harmonic signals as basic components, which will lead to energy leakage and cause lower accuracy.

One of the early works in connection with fractional is that of Lohmann *et al.* [12], who proposed two fractional generalizations of the classical Hilbert transform. One definition is a modification of the spatial filter with a fractional parameter, and the other is based on the fractional Fourier transform. In [13], Pei and Yeh developed the discrete version of the fractional Hilbert transform and applied it to the edge detection of images. Tseng and Pei [14] considered optimized design strategies for finite impulse response designs and infinite impulse response models of the discrete-time fractional Hilbert transform, and proposed a novel secure SSB communication application. So far, the research application of fractional Hilbert transform is very young and needs to be explored.

A generalization of Hilbert transform based envelope anal-

Manuscript received September 11, 2015; accepted March 15, 2016. This work was supported by National Natural Science Foundation of China (61074161, 61273103, 61374061) and Nantong Science and Technology Plan Project (MS22016051). Recommended by Associate Editor Antonio Visioli.

Citation: J. H. Wang, L. Y. Qiao, Y. Q. Ye, and Y. Q. Chen, "Fractional envelope analysis for rolling element bearing weak fault feature extraction," *IEEE/CAA Journal of Automatica Sinica*, vol. 4, no. 2, pp. 353−360, Apr. 2017.

J. H. Wang is with the School of Science, Nantong University, Nantong 226019, China (e-mail: ntuwjh@163.com).

L. Y. Qiao and Y. Q. Chen are with the School of Engineering, University of California, Merced CA 95343, USA (e-mail: qiaoliyan@163.com; yqchen@ieee.org).

Y. Q. Ye is with the College of Automation Engineering, Nanjing University of Aeronautics and Astronautics, Nanjing 210016, China (e-mail: melvinye@nuaa.edu.cn).

Color versions of one or more of the figures in this paper are available online at http://ieeexplore.ieee.org.

Digital Object Identifier 10.1109/JAS.2016.7510166

ysis, called fractional envelope analysis, is introduced here, which provides a tool to process signal in the fractional Fourier plane instead of a conventional Fourier plane. This method hugs the signal optimally, and could reduce the interference of noise to some extent. Thus, this relatively new signal processing technique has the capability of providing more diagnostic information than conventional Hilbert transform based envelope analysis. Reference [5] describes that the Kurtosis value is very sensitive to bearing fault signal. Therefore, the Kurtosis is feasible to be the index for selecting the optimal fractional order envelope analysis.

The remainder of the paper is organized as follows: Section II presents necessary theoretical background of Hilbert transform. The fractional envelope analysis based upon the modification of spatial filter with a fractional parameter is introduced in Section III. Simulations and experimental validations are performed consequently in Sections IV and V. Conclusions are drawn in Section VI.

II. Hilbert Transform

The Hilbert transform of the function $x(t)$ is defined by an integral transform [11], [15]:

$$H[x(t)] = \hat{x}(t) = \frac{1}{\pi}\int_{-\infty}^{\infty}\frac{x(\tau)}{t-\tau}d\tau. \tag{1}$$

Because of a possible singularity at $t=\tau$, the integral has to be considered as a Cauchy principal value. Mathematically, the Hilbert transform $\hat{x}(t)$ of the original function represents a convolution of $x(t)$ and $1/(\pi t)$, which can be written as:

$$\hat{x}(t) = x(t) * \left(\frac{1}{\pi t}\right). \tag{2}$$

Note that the Hilbert transform of a time-domain signal $x(t)$ is another time-domain signal $\hat{x}(t)$. If $x(t)$ is real-valued, then so is $\hat{x}(t)$. The transfer function of Hilbert transform becomes

$$H_1(\omega) = -j\mathrm{sgn}(\omega) = \begin{cases} -j, & \omega > 0 \\ 0, & \omega = 0 \\ j, & \omega < 0. \end{cases} \tag{3}$$

Physically, the Hilbert transform can be viewed as a filter of unity amplitude and phase $\pm 90^\circ$ depending on the sign of the frequency of the input signal spectrum. The Hilbert filter takes an input signal and returns the Hilbert transform of the signal as an output signal. This is also referred to as a Hilbert transformer, a quadrature filter, or a 90° phase shifter.

III. Fractional Envelope Analysis

Note that the Heaviside step function, or unit step function, is defined by [12], [15]:

$$H(\omega) = \frac{1}{2}(1+\mathrm{sgn}(\omega)) = \begin{cases} 1, & \omega > 0 \\ \frac{1}{2}, & \omega = 0 \\ 0, & \omega < 0. \end{cases} \tag{4}$$

Equation (3) can be rewritten in terms of the Heaviside step function as follows:

$$H_1(\omega) = -jH(\omega) + jH(-\omega). \tag{5}$$

Equation (5) can be put in the following form:

$$H_1(\omega) = \exp\left(-j\frac{\pi}{2}\right)H(\omega) + \exp\left(j\frac{\pi}{2}\right)H(-\omega). \tag{6}$$

A fractional generalization of this result can be written as follows:

$$H_p(\omega) = \exp\left(-jp\frac{\pi}{2}\right)H(\omega) + \exp\left(jp\frac{\pi}{2}\right)H(-\omega). \tag{7}$$

This can be conveniently rewritten as

$$H_p(\omega) = \cos\left(p\frac{\pi}{2}\right) - j\mathrm{sgn}(\omega)\sin\left(p\frac{\pi}{2}\right) \tag{8}$$

or

$$H_p(\omega) = \cos\left(p\frac{\pi}{2}\right)H_0(\omega) + \sin\left(p\frac{\pi}{2}\right)H_1(\omega). \tag{9}$$

In fact, the transfer function of Hilbert transform (3) can be written as

$$\begin{aligned} H_1(\omega) &= -j\mathrm{sgn}(\omega) \\ &= \begin{cases} \exp\left(-j\frac{\pi}{2}\right), & \omega > 0 \\ \dfrac{\exp\left(-j\frac{\pi}{2}\right)+\exp\left(j\frac{\pi}{2}\right)}{2}, & \omega = 0 \\ \exp\left(j\frac{\pi}{2}\right), & \omega < 0. \end{cases} \end{aligned} \tag{10}$$

We introduce the kth-order Hilbert operator $H_k = H^k$ to represent the kth-repetition of the Hilbert transform. Thus, the Fourier transform of the kth-order Hilbert transform can be expressed as

$$F[H_k x(t)] = F(\omega)\cdot[-j\mathrm{sgn}(\omega)]^k. \tag{11}$$

The formula (11) can be generalized to a non-integer p and the transfer function of the pth-order Hilbert operator H_p is

$$\begin{aligned} H_p(\omega) &= [-j\mathrm{sgn}(\omega)]^p \\ &= \begin{cases} \exp\left(-jp\frac{\pi}{2}\right), & \omega > 0 \\ \dfrac{\exp\left(-jp\frac{\pi}{2}\right)+\exp\left(jp\frac{\pi}{2}\right)}{2}, & \omega = 0 \\ \exp\left(jp\frac{\pi}{2}\right), & \omega < 0. \end{cases} \end{aligned} \tag{12}$$

This can be conveniently rewritten as (8). Thus, the pth-order Hilbert operator H_p can be expressed as

$$H_p = \cos\left(p\frac{\pi}{2}\right)\cdot I + \sin\left(p\frac{\pi}{2}\right)\cdot H_1 \tag{13}$$

where $H_0 = I$ is the identity operator. The pth-order Hilbert transform is

$$\hat{x}(t) = H_p[x(t)] = \cos\left(p\frac{\pi}{2}\right)\cdot x(t) + \sin\left(p\frac{\pi}{2}\right)\cdot H_1(t). \tag{14}$$

The parameter p is called the order. The above definition of fractional Hilbert transform is a weighted sum of the original signal and its conventional Hilbert transform, and it is based upon modifying the spatial filter with fractional parameter. The magnitude response and the phase response are

$$|H_p(\omega)| = 1 \tag{15}$$

and

$$\varphi(\omega) = \begin{cases} -p\frac{\pi}{2}, & \omega > 0 \\ p\frac{\pi}{2}, & \omega < 0 \end{cases} \tag{16}$$

respectively.

Fig. 1 shows the block diagram for implementing the generalized fractional Hilbert transform.

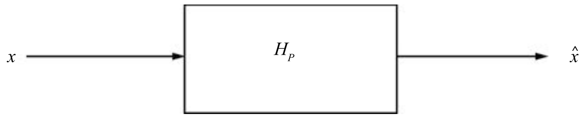

Fig. 1. Block diagram for implementation of the generalized fractional Hilbert transform.

As we know, Fourier transform is fundamental tool in fractional-order systems and controls [16]. In fact, among Hilbert, fractional Hilbert, and fractional calculus there are the following transfer function, magnitude response, and phase response relations (Table I).

TABLE I
COMPARISON OF HILBERT, FRACTIONAL HILBERT, AND FRACTIONAL CALCULUS

	Hilbert	Fractional Hilbert	Fractional calculus
Transfer	$-i\mathrm{sgn}(\omega)$	$[-i\mathrm{sgn}(\omega)]^p$	$(i\omega)^\nu$
Magnitude	1	1	$\lvert\omega\rvert^\nu$
Phase	$-\frac{\pi}{2}\mathrm{sgn}(\omega)$	$-\frac{p\pi}{2}\mathrm{sgn}(\omega)$	$\frac{\nu\pi}{2}\mathrm{sgn}(\omega)$

From Table I, the phase characteristic of the fractional calculus operator ($\nu = -p$) is the same as the phase characteristic of the fractional Hilbert. However, the fractional calculus operator is actually a singular low-pass ($\nu < 0$) filter, or a singular high-pass ($\nu > 0$) filter (Fig. 2), although the fractional Hilbert is an all-pass filter.

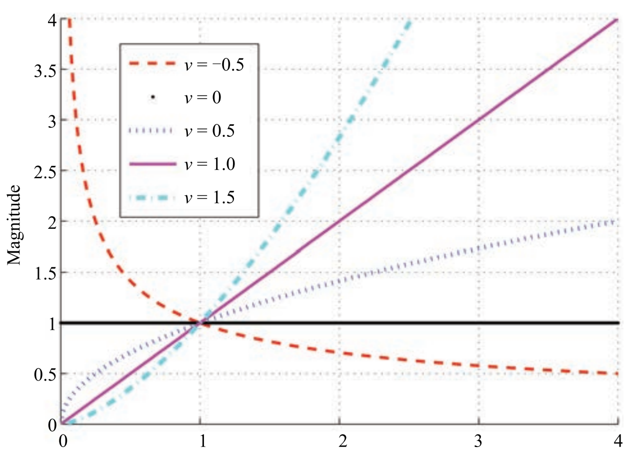

Fig. 2. Magnitude response of the fractional calculus operator.

The real signal $x(t)$ and its fractional Hilbert transform $\hat{x}(t)$ can form a new complex signal, which is called the fractional analytical signal, such that

$$y(t) = x(t) + j\hat{x}(t). \tag{17}$$

The envelope $A(t)$ of the complex signal $y(t)$ is defined as

$$A(t) = |x(t) + j\hat{x}(t)| = \sqrt{x^2(t) + \hat{x}^2(t)}. \tag{18}$$

The application to fractional envelope analysis is shown in Fig. 3 [5]. Fig. 3 depicts the envelope as the modulus of the analytic signal obtained by inverse transformation of the selected one-sided frequency band.

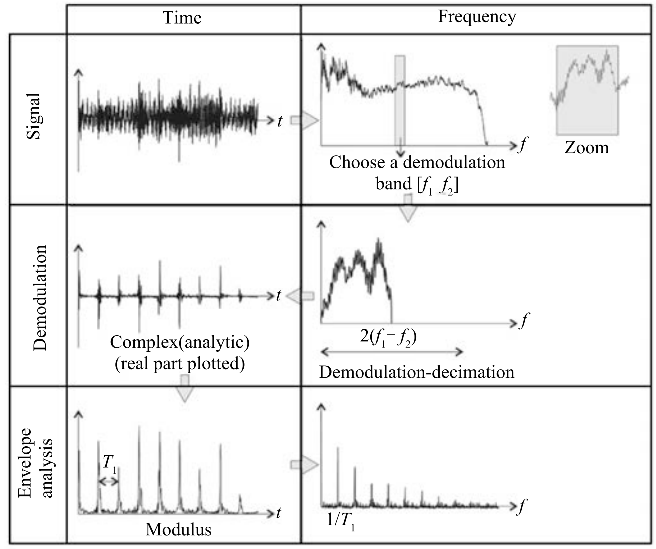

Fig. 3. Procedure for envelope analysis using the fractional Hilbert transform method.

By performing spectrum analysis on the envelope signal $A(t)$, the fractional envelope spectrum can be obtained. When faults occur on a bearing, some of the characteristic frequencies will clearly appear in the fractional envelope spectrum. These characteristic frequencies can be used for bearing weak fault feature extraction.

The algorithm for rolling element bearing fractional envelope analysis consists of the following steps:

Step 1: Rolling element bearing vibration signal acquisition.

Step 2: Taking fractional Hilbert transform of vibration signal.

Step 3: Taking magnitude of fractional analytical signal to obtain fractional envelope signal.

Step 4: Taking fast Fourier transform (FFT) of fractional envelope signal.

Step 5: Analyzing envelope spectrum at bearing fault frequencies.

IV. SIMULATION ANALYSIS

In this section, a simple simulation is used to illustrate the fractional envelope characteristic of the bearing fault signal with strong background noise. The bearing system including the transducer is simplified as a single degree of freedom (SDOF) system and the vibration induced by a single defect in the rolling element bearing can be given by [8]

$$x(t) = \sum_{k=0}^{+\infty} A_k e^{-\xi\omega_n(t-T_k)} \times \sin(\omega_n(t - T_k)) \tag{19}$$

where ω_n denotes the resonance angular frequency of the system and $\omega_n = 2\pi f_n$, where f_n denotes the resonance frequency. The amplitude of the kth transient response A_k

is set to be 5, the sampling frequency f_s is 20 kHz, the resonance frequency f_n of system is 3 kHz, the maximal slip ratio of its period T is 0.01 s, the relative damping ratio ξ is 0.1. The profile of a typical signal, contaminated with -2 dB additive Gaussian noise, (i.e., $\mathrm{SNR} = -2$), is shown in Fig. 4. Figs. 4 (a) and 4 (b) display the time waveform of the original signal and noisy signal. The frequency spectrum of the noisy signal is shown in Fig. 4 (c). It is hard to reveal some useful information from Fig. 4 (c). Therefore, the proposed method is used to achieve the enhancement of fault detection.

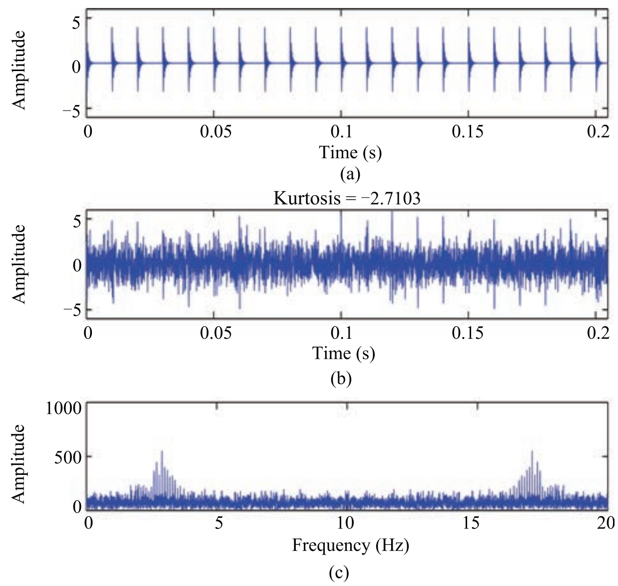

Fig. 4. Simulated signal: (a) time waveform of original signal, (b) time waveform of signal contaminated with -2 dB additive Gaussian noise and (c) frequency spectrum waveform.

As a matter of fact, the Kurtosis has often been employed in the signal processing community to solve "blind" problems: blind identification and equalisation of systems by output Kurtosis maximisation, blind separation of mixed signals by individual maximisation of the source Kurtosis, etc [17]. Here, the sample version of the Kurtosis (20) is used to blindly identify the optimal order of fractional Hilbert transformer. This Kurtosis is taken as the normalised fourth order moment given by [5]

$$K = \frac{m_4}{m_2^2} = \frac{\frac{1}{N}\sum_{i=1}^{N}(x_i-\bar{x})^4}{\left(\frac{1}{N}\sum_{i=1}^{N}(x_i-\bar{x})^2\right)^2} \tag{20}$$

where m_4 is the fourth sample moment about the mean, m_2 is the second sample moment about the mean (sample variance), N is the number of samples, x_i is the ith sample and $\bar{x}$ is the sample mean. For symmetric unimodal distributions, positive Kurtosis indicates heavy tails and peakedness relative to the normal distribution, whereas negative Kurtosis indicates light tails and flatness [18].

Table II presents the comparison of Kurtosis using different order Hilbert transformer filtering simulation signal (19) contaminated with -2 dB additive white Gaussian noise. Note that, 0.2-order is suitable for this envelope spectrum analysis. For this reason, our method has larger design flexibility than the integer (1-order) Hilbert transform-based method. The 0.2-order envelope signal and 0.2-order envelope spectrum of the 0.2-order Hilbert transformer filtered signal are shown in Fig. 5. It can be seen that in Fig. 5 (b) the characteristic frequencies clearly appear in the 0.2-order envelope spectrum. These characteristic frequencies can be used for bearing fault diagnosis.

TABLE II
COMPARISON OF KURTOSIS BETWEEN DIFFERENT ORDER HILBERT TRANSFORM

Order	0	0.1	0.2	0.3	0.4
Kurtosis	3.0461	3.3907	3.7015	3.5582	2.9891
0.5	0.6	0.7	0.8	0.9	1.0
2.5702	2.7531	3.1859	3.3133	3.0536	2.7558

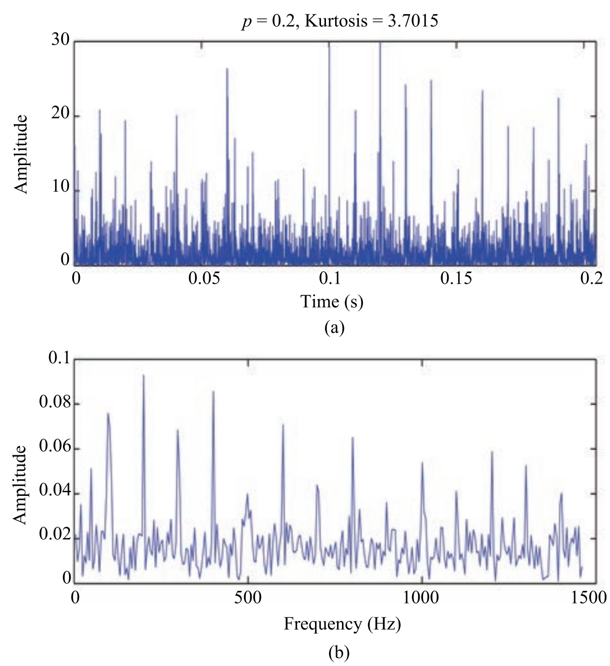

Fig. 5. Envelope spectrum obtained by the 0.2-order Hilbert transform.

V. EXPERIMENTAL VALIDATION

The success of the proposed method in detecting early defect under strong additive stationary noise is clearly demonstrated in the above simulation. In this section, the application to actual vibration signals collected in a rolling element bearing accelerated life test is presented.

Generally, the vibration spectrum of a healthy bearing contains only the information related to the shaft rotation speed and its harmonics, which is shown as Zone I in Fig. 6. Any other frequencies might indicate noise, or frequencies related to other rotating parts operating at the same time with the bearing under test [19]. A rolling element bearing fault could appear at the outer, the inner race and (or) on the rolling elements. During its early stages, the damage on the surface is mostly only localized. The vibration signal in this case includes repetitive impacts of the moving components on the defect. These impacts might create repetition frequencies that depend on whether the defect is on the outer or the inner race, or on the rolling element (Fig. 7).

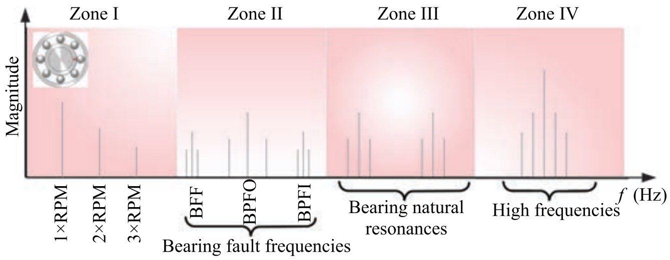

Fig. 6. Frequency content of a vibration signal of a damaged rolling element bearing.

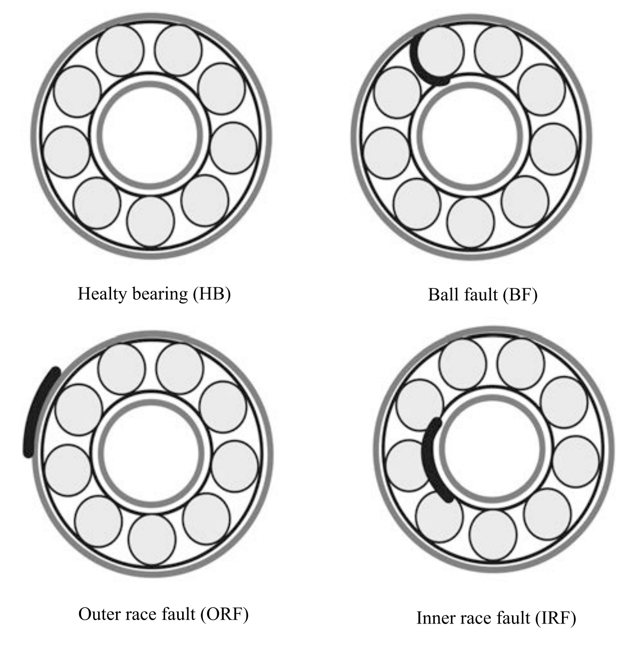

Fig. 7. A series of bearing components with faults induced in them indicated in bold line [20].

The repetition rates are denoted bearing frequencies. The formulae for the ball passing frequency outer (BPFO) race, ball passing frequency inner (BPFI) race, and ball fault frequency (BFF) are as follows [5]:

$$f_{\text{BPFO}} = \frac{n}{2} f_r \left(1 - \frac{d}{D}\cos\theta\right)$$
$$f_{\text{BPFI}} = \frac{n}{2} f_r \left(1 + \frac{d}{D}\cos\theta\right)$$
$$f_{\text{BFF}} = \frac{D}{2d} f_r \left[1 - \left(\frac{d}{D}\cos\theta\right)^2\right] \tag{21}$$

where n is the number of rolling elements, f_r is the shaft rotational frequency (RPM), d is the diameter of rolling element, (i.e., ball) diameter, D is the pitch diameter, and θ is the angle of the load from the radial plane.

For early faults, the repetition impulses could create initially an increase of frequencies in the high frequency range (Zone IV), and may excite the resonant frequencies of the bearing parts later in Zone III, as well as the repetition frequencies of Zone II (BPFO, BPFI, BFF).

The vibration signals collected in the bearing center of case western reserve university (CWRU) [21] are used to illustrate the fractional envelope analysis. The test stand consists of a 2 hp drive induction motor, a torque transducer/encoder, a dynamometer, and control electronics (Figs. 8 and 9). The test bearings which support the motor shaft have single point faults with the diameters of 0.007 inch, 0.014 inch, 0.021 inch, and 0.028 inch on the outer race, inner race, and ball of the drive end bearings produced by an electro-discharge machine. Faulted bearings were reinstalled into the test motor and vibration data was recorded for motor loads of 0 to 3 horsepower (motor speeds of 1797 to 1720 rpm). The number n of rolling elements is 9 and the angle θ of the load from the radial plane is 0°. Vibration data was collected using a 16 channel DAT recorder at 12 000 samples per second. The bearing is a deep groove ball bearing and the model is 6205-2RS JEM SKF. The diameter and depth of the pit are 0.18 mm and 0.28 mm respectively. The geometry (outside diameter, inside diameter, thickness, ball diameter, and pitch diameter) and defect frequencies of the bearing are listed in Tables III and IV.

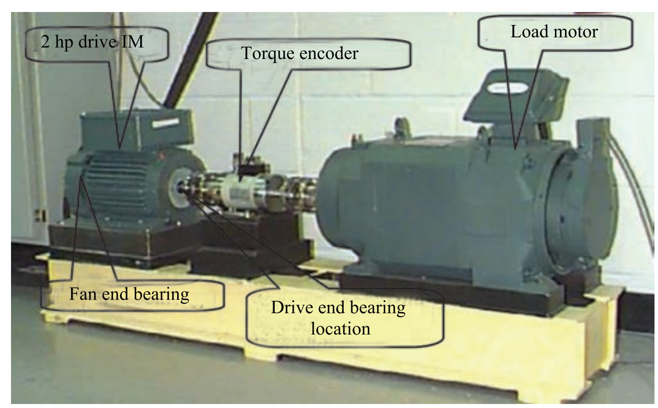

Fig. 8. Experimental test rig, composed of a 2 hp drive induction motor, a torque transducer/encoder, load [21].

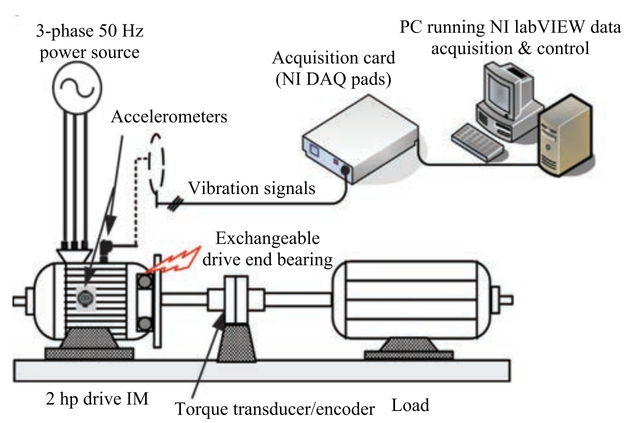

Fig. 9. Schematic of the experimental test rig [22].

TABLE III
SIZE OF ROLLING ELEMENT BEARING (MM)

Type	Outside	Inside	Thickness	Ball	Pitch
SKF6025	51.9989	25.0012	15.0012	7.9400	39.0398

TABLE IV
DEFECT FREQUENCIES OF ROLLING ELEMENT BEARING, (MULTIPLE OF RUNNING SPEED)

Type	Outer ring	Inner ring	Rolling element
SKF6025	3.5848	5.4152	4.7135

A. Case 1: Outer Race Fault

The outer race fault is located at the 6 o'clock position and the accelerometer is attached to the housing with a magnetic base. In this case, the shaft frequency f_r is 29.17 Hz (1750/60, shaft rotates at the speed of 1750 rpm). The characteristic bearing defect frequency $f_{\rm BPFO}$ is equal to 3.5848 times the shaft rotation speed based on (21). Thus, the fault characteristic frequency $f_{\rm BPFO}$ is 104.56 Hz.

Fig. 10 (a) gives the temporal waveform of outer race fault diameter of 0.007 inch. Fig. 10 (b) shows the corresponding optimal fractional (0.1-order, Table V) envelope spectrum. The fault characteristic frequency $f_{\rm BPFO}$ is located at 105 Hz, and its associated harmonics, at 209.8 Hz, 314.8 Hz, 419.7 Hz, and so on, can be easily detected.

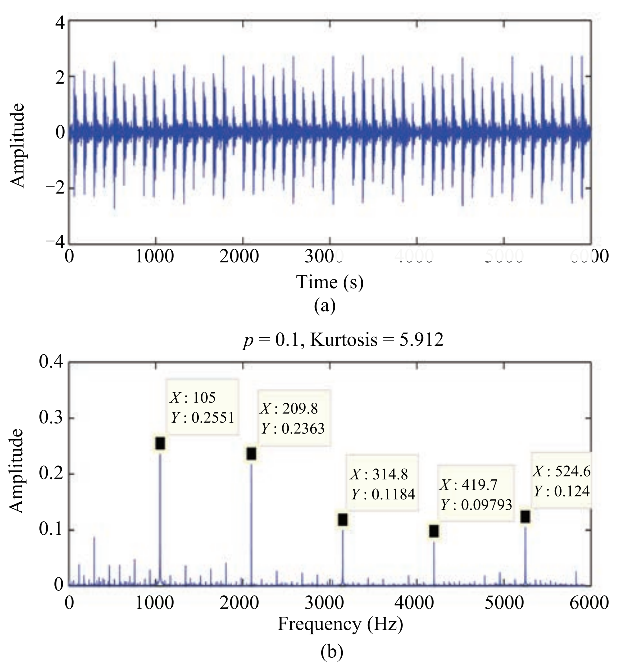

Fig. 10. The temporal waveform of the signal of OR007@6-2 and the corresponding envelope spectrum obtained by the 0.1-order Hilbert transform.

B. Case 2: Inner Race Fault

In this case, the shaft frequency f_r is 29.13 Hz (shaft rotates at the speed of 1748 rpm). The characteristic bearing defect frequency $f_{\rm BPFI}$ is equal to 5.4152 times the shaft rotation speed based on (22). Thus, the fault characteristic frequency $f_{\rm BPFI}$ is 157.76 Hz.

TABLE V
COMPARISON OF KURTOSIS BETWEEN DIFFERENT ORDER HILBERT TRANSFORM

Order	0	0.1	0.2	0.3	0.4
Kurtosis	5.8875	5.9120	5.8019	5.3508	4.2234
0.5	0.6	0.7	0.8	0.9	1.0
3.0349	1.3953	0.4235	0.3769	0.9572	1.8214

Fig. 11 (a) gives the temporal waveform of inner race fault diameter of 0.007 inch and the corresponding optimal fractional (0.5-order, Table VI) envelope spectrum is shown in Fig. 11 (b). It can be seen that the 1×, 2×, 3× BPFI are very clear in Fig. 11 (b).

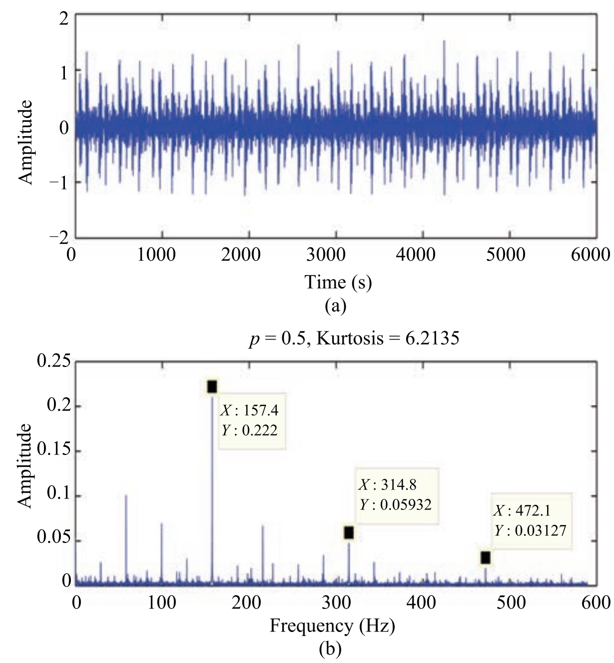

Fig. 11. The temporal waveform of the signal of IR007-2 and the corresponding envelope spectrum obtained by the 0.5-order Hilbert transform.

TABLE VI
COMPARISON OF KURTOSIS BETWEEN DIFFERENT ORDER HILBERT TRANSFORM

Order	0	0.1	0.2	0.3	0.4
Kurtosis	4.7495	4.7805	4.7163	4.2787	3.1397
0.5	0.6	0.7	0.8	0.9	1.0
6.2135	0.4184	0.4780	1.1967	1.6665	1.6513

C. Case 3: Ball Fault

In this case, the shaft frequency f_r is 29.13 Hz (shaft rotates at the speed of 1748 rpm). The characteristic bearing defect frequency $f_{\rm BFF}$ is equal to 4.7135 times the shaft rotation speed based on (23). Thus, the fault characteristic frequency $f_{\rm BFF}$ is 137.30 Hz.

Fig. 12 (a) gives the temporal waveform of ball fault diameter of 0.028 inch. It can be seen that there are many obvious periodic impulses in Fig. 12 (a), which may be caused by the interaction between the faulty parts and connected rolling element surfaces. In order to obtain clear fault information, the corresponding optimal fractional (0.9-order, Table VII) envelope spectrum is shown in Fig. 12 (b). It can be seen that the characteristic frequencies are $1\times$, $2\times$, $3\times$ BFF and its harmonics modulated by f_r (Fig. 6), which implies the occurrence of ball fault. Moreover, there are some frequency components in Fig. 12 (b). The fault information can hardly be obtained from single fractional envelope analysis without prior filtration. The possible reason for other frequency components may be that the signals collected are usually disturbed by the nearby bearings or other background noise [19].

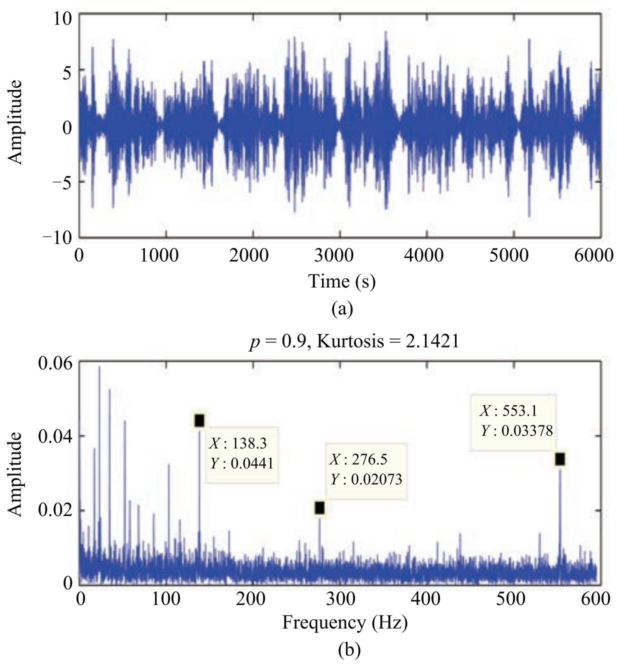

Fig. 12. The temporal waveform of the signal of B028-2 and the corresponding envelope spectrum obtained by the 0.9-order Hilbert transform.

TABLE VII
COMPARISON OF KURTOSIS BETWEEN DIFFERENT ORDER HILBERT TRANSFORM

Order	0	0.1	0.2	0.3	0.4
Kurtosis	1.9349	1.9552	1.9037	1.5660	0.6402
0.5	0.6	0.7	0.8	0.9	1.0
0.9391	1.0778	1.4084	1.7998	2.1421	1.0845

Figs. 10−12 altogether show that the proposed fractional Hilbert transform based envelop analysis provides better envelop detection results and achieves better Kurtosis performance than the envelop analysis based on traditional Hilbert transform on the studied bearing fault signals. These results demonstrate the excellent compromise capability of the fractional Hilbert transformer in detect accuracy and filtering noisy bearing fault signal. This method may therefore serve as an effective framework for the model-based detection of noisy rolling element bearings.

VI. CONCLUSION

The fractional Hilbert transform signal detect model based upon the modification of spatial filter with a fractional parameter technique is constructed in this work, which breaks the thought that the traditional fault detect model can only be based on integer-order Hilbert transform. By setting a flexible fractional order, our model can better enhance the compromise capability in detect accuracy and filtering noisy bearing fault signal. The effectiveness of the method is demonstrated on both simulated signal and actual data are collected in rolling bearing accelerated life test. The proposed technique exhibits excellent performances on visual sense and quantitative comparison. While the cyclic frequency error has some influence on the performance of the proposed method, how to reduce the cyclic frequency error and extract the coupled faults are worthy of further study.

REFERENCES

[1] N. Sawalhi, R. B. Randall, and H. Endo, "The enhancement of fault detection and diagnosis in rolling element bearings using minimum entropy deconvolution combined with spectral kurtosis," *Mech. Syst. Signal Process.*, vol. 21, no. 6, pp. 2616−2633, Aug. 2007.

[2] S. Yin, S. X. Ding, X. C. Xie, and H. Luo, "A review on basic data-driven approaches for industrial process monitoring," *IEEE Trans. Ind. Electron.*, vol. 61, no. 11, pp. 6418−6428, Nov. 2014.

[3] B. P. Cai, Y. H. Liu, Q. Fan, Y. W. Zhang, Z. K. Liu, S. L. Yu, and R. J. Ji, "Multi-source information fusion based fault diagnosis of ground-source heat pump using Bayesian network," *Appl. Energy*, vol. 114, pp. 1−9, Feb. 2014.

[4] W. Sun, G. A. Yang, Q. Chen, A. Palazoglu, and K. Feng, "Fault diagnosis of rolling bearing based on wavelet transform and envelope spectrum correlation," *J. Vib. Control*, vol. 19, no. 6, pp. 924−941, Apr. 2013.

[5] R. B. Randall and J. Antoni, "Rolling element bearing diagnostics-a tutorial," *Mech. Syst. Signal Process.*, vol. 25, no. 2, pp. 485−520, Feb. 2011.

[6] Y. Ming, J. Chen, and G. M. Dong, "Weak fault feature extraction of rolling bearing based on cyclic Wiener filter and envelope spectrum," *Mech. Syst. Signal Process.*, vol. 25, no. 5, pp. 1773−1785, Jul. 2011.

[7] P. Borghesani, P. Pennacchi, and S. Chatterton, "The relationship between kurtosis- and envelope-based indexes for the diagnostic of rolling element bearings," *Mech. Syst. Signal Process.*, vol. 43, no. 1−2, pp. 25−43, Feb. 2014.

[8] A. B. Ming, W. Zhang, Z. Y. Qin, and F. L. Chu, "Envelope calculation of the multi-component signal and its application to the deterministic component cancellation in bearing fault diagnosis," *Mech. Syst. Signal Process.*, vol. 50−51, pp. 70−100, Jan. 2015.

[9] R. H. Jiang, S. L. Liu, Y. F. Tang, and Y. H. Liu, "A novel method of fault diagnosis for rolling element bearings based on the accumulated envelope spectrum of the wavelet packet," *J. Vib. Control*, vol. 21, no. 8, pp. 1580−1593, Jun. 2015.

[10] M. Feldman, "Hilbert transform in vibration analysis," *Mech. Syst. Signal Process.*, vol. 25, no. 3, pp. 735−802, Apr. 2011.

[11] M. Feldman, *Hilbert Transform Applications in Mechanical Vibration*. Chichester, UK: John Wiley and Sons, 2011.

[12] A. W. Lohmann, D. Mendlovic, and Z. Zalevsky, "Fractional Hilbert transform," *Opt. Lett.*, vol. 21, no. 4, pp. 281−283, Feb. 1996.

[13] S. C. Pei and M. H. Yeh, "Discrete fractional Hilbert transform," *IEEE Trans. Circ. Syst. II: Analog Digit. Signal Process.*, vol. 47, no. 11, pp. 1307−1311, Nov. 2000.

[14] C. C. Tseng and S. C. Pei, "Design and application of discrete-time fractional Hilbert transformer," *IEEE Trans. Circ. Syst. II: Analog Digit. Signal Process.*, vol. 47, no. 12, pp. 1529−1533, Dec. 2000.

[15] F. W. King, *Hilbert Transforms*. Cambridge, UK: Cambridge University Press, 2009.

[16] C. A. Monje, Y. Q. Chen, B. M. Vinagre, D. Y. Xue, and V. Feliu, *Fractional-order Systems and Controls: Fundamentals and Applications*. London, UK: Springer, 2010.

[17] J. Antoni and R. B. Randall, "The spectral Kurtosis: Application to the vibratory surveillance and diagnostics of rotating machines," *Mech. Syst. Signal Process.*, vol. 20, no. 2, pp. 308−331, Feb. 2006.

[18] L. T. DeCarlo, "On the meaning and use of kurtosis," *Psychol. Methods*, vol. 2, no. 3, pp. 292−307, Sep. 1997.

[19] L. Saidi, J. B. Ali, and F. Fnaiech, "The use of spectral kurtosis as a trend parameter for bearing faults diagnosis," in *Proc. 15th Int. Conf. Sciences and Techniques of Automatic Control and Computer Engineering*, Hammamet, Tunisia, 2014, pp. 394−399.

[20] L. Saidi, J. B. Ali, and F. Fnaiech, "Bi-spectrum based-EMD applied to the non-stationary vibration signals for bearing faults diagnosis," *ISA Trans.*, vol. 53, no. 5, pp. 1650−1660, Sep. 2014.

[21] K. A. Loparo, Bearings vibration data set. Case Western Reserve University. [Online]. Available: http://csegroups.case.edu/bearingdatacenter/pages/12k-drive-end-bearing-fault-data.

[22] L. Saidi, J. B. Ali, and F. Fnaiech, "Application of higher order spectral features and support vector machines for bearing faults classification," *ISA Trans.*, vol. 54, pp. 193−206, Jan. 2015.

Jianhong Wang received the B. S. degree in mathematics and applied mathematics from Jiangsu Normal University, China, in 2000, the M. S. degree in operations research and control theory from Shanghai Jiao Tong University, China, in 2007, and the Ph. D. degree in control theory and control engineering from Nanjing University of Aeronautics and Astronautics, China, in 2016. He was a visiting scholar with the School of Engineering at the University of California, Merced, USA, in 2015. He is currently an associate professor at the School of Science, Nantong University, China. His current research interests include applied fractional calculus in intelligent control, signal processing, image processing, and big data processing. Corresponding author of this paper.

Liyan Qiao received the B. S. degree in radio engineering from Harbin Institute of Technology, China, in 1992, the M. S. degree in communication and electronics system from Harbin Institute of Technology, China, in 1996, and the Ph. D. degree in instrumentation science and technology from Harbin Institute of Technology, China, in 2005. He is at the Automatic Test and Control Faculty of School of Electrical Engineering and Automation, Harbin Institute of Technology, Harbin, China. His research interests include automatic test system, data acquiring technic through internet, flash storage system, and signal analysis.

Yongqiang Ye received the B. S. and M. S. degrees from Zhejiang University, China, in 1994 and 1997, respectively, and the Ph. D. degree from Nanyang Technological University, Singapore, in 2004, all in electrical engineering. He had been a faculty member with the School of Information, Zhejiang University of Finance and Economics, China, for more than four years. He had also been a postdoctoral fellow with the Department of Electrical Engineering at Lakehead University, the Department of Systems and Computer Engineering at Carleton University, and the Department of Mechanical Engineering, Dalhousie University, Canada, respectively. He joined the Department of Automation Engineering at Nanjing University of Aeronautics and Astronautics in 2009 as a professor. He is a Senior Member of IEEE. His research interests include computer vision, pattern recognition, learning and repetitive control, and power electronics control.

YangQuan Chen received his Ph. D. degree in advanced control and instrumentation from Nanyang Technological University, Singapore, in 1998. Dr. Chen was on the Faculty of Electrical and Computer Engineering at Utah State University before he joined the School of Engineering, University of California, Merced in 2012 where he teaches "Mechatronics" for juniors and "Fractional Order Mechanics" for graduates. His current research interests include mechatronics for sustainability, cognitive process control and hybrid lighting control, multi-UAV based cooperative multi-spectral "personal remote sensing" and applications, applied fractional calculus in controls, signal processing and energy informatics; distributed measurement and distributed control of distributed parameter systems using mobile actuator and sensor networks.

Local Bifurcation Analysis of a Delayed Fractional-order Dynamic Model of Dual Congestion Control Algorithms

Min Xiao, *Member, IEEE*, Guoping Jiang, *Member, IEEE*, Jinde Cao, *Fellow, IEEE*, and Weixing Zheng, *Fellow, IEEE*

***Abstract*—In this paper, we propose a delayed fractional-order congestion control model which is more accurate than the original integer-order model when depicting the dual congestion control algorithms. The presence of fractional orders requires the use of suitable criteria which usually make the analytical work so harder. Based on the stability theorems on delayed fractional-order differential equations, we study the issue of the stability and bifurcations for such a model by choosing the communication delay as the bifurcation parameter. By analyzing the associated characteristic equation, some explicit conditions for the local stability of the equilibrium are given for the delayed fractional-order model of congestion control algorithms. Moreover, the Hopf bifurcation conditions for general delayed fractional-order systems are proposed. The existence of Hopf bifurcations at the equilibrium is established. The critical values of the delay are identified, where the Hopf bifurcations occur and a family of oscillations bifurcate from the equilibrium. Same as the delay, the fractional order normally plays an important role in the dynamics of delayed fractional-order systems. It is found that the critical value of Hopf bifurcations is crucially dependent on the fractional order. Finally, numerical simulations are carried out to illustrate the main results.**

***Index Terms*—Congestion control algorithm, fractional-order congestion control algorithm model, Hopf bifurcation, stability.**

I. INTRODUCTION

FRACTIONAL calculus and its applications to physics, biology and engineering have become a subject of intense research activities. It has been found that dynamical equations using fractional derivatives are useful and more accurate in the mathematical modeling of real world phenomena arising from several interdisciplinary fields, such as diffusion and wave propagation [1], electromagnetic waves [2], viscoelastic liquids [3], dielectric polarization [4], control [5], and biology [6]. As a result of growing applications, the study of dynamics of fractional-order systems has attracted considerable interest of many researchers and numerous important results have been reported, including the stability [7], bifurcations [8], chaos [9], and synchronization [10].

With the rapid development of the Internet, the congestion control mechanism is a focus of interest to many researchers in the past few years [11]−[13] since the seminal work [14]. One of the important properties of congestion control algorithms is the stability. Sufficient conditions for stability are given for congestion control systems [15]−[18]. However, it is found in [19], [20] that some common AQM (active queue management) schemes coupled with the current congestion avoidance TCP (transmission control protocol) algorithm may lose the local stability due to an increase in delays or capacity, or a decrease in the number of connections. The loss of stability causes some nonlinear dynamical behaviors such as chaos and bifurcation. Therefore, in addition to investigation of stability, the Hopf bifurcation and control have also begun to draw much attention from researchers [21]−[26].

Unlike integer-order derivatives that are local operators, fractional-order derivatives are non-local integro-differential operators [27]. As such, they can be used to represent memory effects and long-range dispersion processes. In the last decade, fractional-order models have been an active field of research both from a theoretical and applied perspective. For instance, the resistance-capacitance-inductance (RLC) interconnect model of a transmission line is a fractional-order model [28]. Heat conduction can be more adequately modeled by fractional-order models than by their integer order counterparts [29]. In biology, it has been shown that the membranes of cells of biological organism have a fractional-order electrical conductance [30]. In economics, it is known that some financial systems can display fractional-order dynamics [31].

There have been many results on Hopf bifurcations for a variety of delayed integer-order congestion control systems recently [21]−[26]. However, to the best of our knowledge, few studies of Hopf bifurcations for delayed fractional-order congestion control systems have been, reported. It should be

Manuscript received September 7, 2015; accepted June 2, 2016. This work was supported by National Natural Science Foundation of China (61573194, 61374180, 61573096), China Postdoctoral Science Foundation Funded Project (2013M530229), China Postdoctoral Science Special Foundation Funded Project (2014T70463), Six Talent Peaks High Level Project of Jiangsu Province (ZNDW-004), Science Foundation of Nanjing University of Posts and Telecommunications (NY213095), and Australian Research Council (DP120104986). Recommended by Associate Editor Antonio Visioli.

Citation: M. Xiao, G. P. Jiang, J. D. Cao, and W. X. Zheng, "Local bifurcation analysis of a delayed fractional-order dynamic model of dual congestion control algorithms", *IEEE/CAA Journal of Automatica Sinica*, vol. 4, no. 2, pp. 361−369, Apr. 2017.

M. Xiao and G. P Jiang are with the College of Automation, Nanjing University of Posts and Telecommunications, Nanjing 210023, China (e-mail: candymanxm2003@aliyun.com; jianggp@njupt.edu.cn).

J. D. Cao is with the Research Center for Complex Systems and Network Sciences, Southeast University, Nanjing 210096, China (e-mail: jdcao@seu.edu.cn).

W. X. Zheng is with the School of Computing, Engineering and Mathematics, Western Sydney University, Sydney, NSW 2751, Australia (e-mail: w.zheng@westernsydney.edu.au).

Digital Object Identifier 10.1109/JAS.2016.7510151

mentioned that the qualitative theory of Hopf bifurcations for the case of fractional-order dynamical systems has not completely settled yet. Thus, the Hopf bifurcation theory in fractional-order dynamical systems is still an open problem. In this paper, we will establish some bifurcation conditions for delayed fractional-order dynamical systems.

Motivated by the above discussions, this paper is devoted to investigating the stability and bifurcations for a delayed fractional-order congestion control model. The sufficient conditions for the stability of the equilibrium are given for the delayed fractional-order congestion control model. The Hopf bifurcation conditions are proposed for delayed fractional-order systems when the delay is chosen as the bifurcation parameter. Then, the critical values of the delay are identified in the delayed fractional-order congestion control model, where Hopf bifurcations occur and a family of oscillations bifurcate from the equilibrium. It is worth mentioning that the observations in this paper can help to design the Hopf bifurcation of congestion control systems with the desired bifurcation point via adjusting the delay and fractional-order.

The paper is organized as follows. In Section II, some preliminaries on delayed fractional-order systems are summarized. In Section III, a delayed fractional-order model of fair dual congestion control algorithms is proposed. In Section IV, by analyzing the associated characteristic equation, the stability condition is derived for the delayed fractional-order congestion control model. The existence of the Hopf bifurcation is established when the communication delay is chosen as the bifurcation parameter. In Section V, numerical simulations are given to illustrate the results. Finally, the conclusions are drawn in Section VI.

II. Preliminaries

Generally speaking, there are three definitions of fractional derivative, i.e., the Grünwald-Letnikov fractional derivative, Riemann-Liouville fractional derivative, and Caputo fractional derivative [27]. Due to taking on the same form as integer order differential on the initial conditions, which has well-understood physical meanings and has more applications in engineering, here we only discuss the Caputo derivative which is defined as follows:

$$ {}_a^C D_t^\alpha f(t) = \frac{1}{\Gamma(n-\alpha)} \int_a^t (t-\tau)^{n-\alpha-1} f^{(n)}(\tau) d\tau \tag{1}$$

where $n-1 < \alpha < n$, $n \in \mathbb{N}$, and $\Gamma(\cdot)$ is the Gamma function. The symbol α denotes the value of the fractional order that is usually chosen in the range $0 < \alpha \le 1$ in engineering.

The Laplace transform of the Caputo fractional derivative (1) at $a = 0$ is given by

$$\mathscr{L}\{{}_0^C D_t^\alpha f(t)\} = s^\alpha F(s) - \sum_{k=0}^{n-1} s^{\alpha-k-1} f^{(k)}(0). \tag{2}$$

If $f^{(k)}(0) = 0, k = 0, 1, \ldots, n-1$, then $\mathscr{L}\{{}_0^C D_t^\alpha f(t)\} = s^\alpha F(s)$.

A class of n-dimensional linear fractional-order systems with multiple time delays can be represented in the following form [32]:

$$\begin{aligned}
\frac{d^{\alpha_1} x_1}{dt^{\alpha_1}} &= a_{11} x_1(t-\tau_{11}) + a_{12} x_2(t-\tau_{12}) \\
&\quad + \cdots + a_{1n} x_n(t-\tau_{1n}) \\
\frac{d^{\alpha_2} x_2}{dt^{\alpha_2}} &= a_{21} x_1(t-\tau_{21}) + a_{22} x_2(t-\tau_{22}) \\
&\quad + \cdots + a_{2n} x_n(t-\tau_{2n}) \\
&\vdots \\
\frac{d^{\alpha_n} x_n}{dt^{\alpha_n}} &= a_{n1} x_1(t-\tau_{n1}) + a_{n2} x_2(t-\tau_{n2}) \\
&\quad + \cdots + a_{nn} x_n(t-\tau_{nn})
\end{aligned} \tag{3}$$

where $0 < \alpha_i \le 1$ for $i = 1, 2, \ldots, n$, and the notation $\dfrac{d^{\alpha_i}}{dt^{\alpha_i}}$ is chosen as the Caputo fractional derivative (1). The initial values $x_i(t) = \phi_i(t)$ are given for $-\tau_{\max} \le t \le 0$, $i = 1, 2, \ldots, n$, where $\tau_{\max} = \max_{1\le i,j\le n}\{\tau_{ij}\}$.

Next, we introduce some stability results on the delayed fractional-order system (3). The stability of the zero solution of system (3) depends on the distribution of roots of the associated characteristic equation (4), as shown at the bottom of this page.

Theorem 1 [32]: The zero solution of system (3) is Lyapunov globally asymptotically stable if all the roots of the characteristic equation (4) have negative real parts.

Remark 1: If $\alpha_i = 1$, $i = 1, 2, \ldots, n$, then the characteristic equation of (3) is reduced to the characteristic equation of delay differential equations. If $\tau_{ij} = 0$, $i, j = 1, 2, \ldots, n$ and $\alpha_i = 1$, $i = 1, 2, \ldots, n$, then the characteristic equation of (3) is reduced to $\det(sI - A) = 0$, where the coefficient $A = (a_{ij})_{n\times n}$. This coincides with the definition of the characteristic equation for ordinary differential equations.

Corollary 1 [32]: Suppose that $\tau_{ij} = 0, i, j = 1, 2, \ldots, n$ and $\alpha_i = \alpha \in (0, 1]$, $i = 1, 2, \ldots, n$. If all the roots of the characteristic equation $\det(sI - A) = 0$ satisfy $|\arg(s)| > \alpha\pi/2$, then the zero solution of system (3) is Lyapunov globally asymptotically stable.

Corollary 1 is the Matignon criterion (Theorem 2 of [33]).

Corollary 2 [32]: If $\alpha_i = \alpha \in (0, 1]$, $i = 1, 2, \ldots, n$, all the eigenvalues λs of A satisfy $|\arg(s)| > \alpha\pi/2$ and the

$$\det \begin{pmatrix} s^{\alpha_1} - a_{11}e^{-s\tau_{11}} & -a_{12}e^{-s\tau_{12}} & \cdots & -a_{1n}e^{-s\tau_{1n}} \\ -a_{21}e^{-s\tau_{21}} & s^{\alpha_2} - a_{22}e^{-s\tau_{22}} & \cdots & -a_{2n}e^{-s\tau_{2n}} \\ \vdots & \vdots & \ddots & \vdots \\ -a_{n1}e^{-s\tau_{n1}} & -a_{n2}e^{-s\tau_{n2}} & \cdots & s^{\alpha_n} - a_{nn}e^{-s\tau_{nn}} \end{pmatrix} = 0 \tag{4}$$

characteristic equation (4) has no purely imaginary roots for any $\tau_{ij} > 0,\ i,\ j = 1, 2, \ldots, n$, then the zero solution of system (3) is Lyapunov globally asymptotically stable.

There are a number of substantial differences between integer-order dynamical systems and fraction-order dynamical systems. Therefore, most results on the delayed integer-order model of congestion control algorithms cannot be simply extended to the case of fractional order one. As is well known, limit cycles of integer-order dynamical systems are isolated periodic oscillations, whose appearance can be explained using the Hopf bifurcation theory [34]. However, to the best of our knowledge, there is no Hopf bifurcation qualitative theory developed thoroughly for the case of fractional-order dynamical systems yet, and thus, the Hopf bifurcation theory in fractional-order dynamical systems is still an open problem.

The Hopf bifurcation conditions for fractional-order dynamical systems without delays were proposed based on numerical simulations, but were not proved in [35], [36]. There are seldom reports about the Hopf bifurcation of delayed fractional-order dynamical systems.

In this paper, we are interested in the stability and bifurcation in delayed fractional-order congestion control systems.

III. MODEL DESCRIPTIONS

The dual algorithms are a subset of a larger class of congestion control mechanisms. In these algorithms the resource determines its congestion measure or price, by an averaging process at the link, which is then communicated back to the end-systems. To facilitate a control theoretic study, caricatures of rate control or window-based algorithms are often converted into delayed integer-order differential equations [19], [37]−[39]. It has been found from the study of such integer-order equations that some congestion control mechanisms may lose the local stability with an increase in delays or capacity, or a decrease in the number of connections, which is triggered by the Hopf bifurcation.

Raina [19] introduced the following dynamical representation of a fair dual congestion control algorithm:

$$\frac{d}{dt}p(t) = \kappa p(t)(x(t-\tau) - C) \tag{5}$$

where the variable p is the price at the link, τ is the communication delay, $\kappa > 0$ is the gain parameter, and the scalar $C > 0$ is the capacity. In addition, $x(t) = \mathcal{D}(p(t))$ with $\mathcal{D}(p)$, $p \geq 0$, a non-negative, continuous and strictly decreasing demand function, and $\mathcal{D}(p)$ can be expressed by $(w/p)^{1/\gamma}$, where $w > 0$ may be viewed as a willingness to pay parameter of the user, and $\gamma > 0$ is the fair allocation parameter [40].

The integer-order dual algorithm model (5) has been extensively studied regarding its bifurcation and control by many researchers in the past years [19], [23], [41]. The local Hopf bifurcation was studied for model (5) by choosing the non-dimensional parameter κ as the bifurcation parameter [19]. Explicit conditions were derived to ensure the onset of stable limit cycles as model (5) just loses its local stability, and the direction of Hopf bifurcations was also determined by applying the normal form theory and center manifold theorem. On the other hand, unlike the work in [19] where the gain parameter κ was considered as the bifurcation parameter, the authors used the communication delay τ as the bifurcation parameter [23]. It was demonstrated that model (5) loses its stability and a Hopf bifurcation occurs when the delay τ passes through a critical value. Moreover, the bifurcating periodic solution was calculated by means of the perturbation method. A hybrid control strategy using both the state feedback and parameter perturbation was applied to control the undesirable Hopf bifurcation of model (5) [41]. It was shown that this proposed method can delay the onset of bifurcations effectively, and thus extend the stable range in the parameter space and improve the performance of congestion control systems.

Compared with the classical integer-order models, fractional-order models are characterized by infinite memory. Congestion control systems include round trip propagation delays. Therefore, the incorporation of a memory term into a congestion control model is an extremely important improvement. Moreover, the fractional-order congestion control models are more accurate than the original integer-order models when modeling some congestion control algorithms. Thus, studying fractional-order congestion control models is of great significance.

In this paper, we replace the usual integer-order derivative by the fractional-order Caputo derivative (1) in the fair dual congestion control algorithm model (5). The new model is then described by the following delayed fractional-order differential equation:

$$\frac{d^\alpha p}{dt^\alpha} = \kappa p(t)(x(t-\tau) - C) \tag{6}$$

where $\alpha \in (0, 1]$.

Suppose that p^* is a non-zero equilibrium of (6). Then it satisfies the following equation:

$$\mathcal{D}(p^*) = C. \tag{7}$$

It should be underlined that p^* is an equilibrium of model (6) with the fractional order α if and only if it is an equilibrium of the integer-order model (5).

IV. STABILITY AND BIFURCATION ANALYSIS

In this section, we investigate the stability and bifurcation of the delayed fractional-order model (6) of fair dual congestion control algorithms.

A. Stability Analysis

Let $u(t) = p(t) - p^*$ and the equilibrium p^* is shifted to the origin. The linearized model of (6) is

$$\frac{d^\alpha u}{dt^\alpha} = \kappa p^* \mathcal{D}'(p^*) u(t-\tau) \tag{8}$$

with the characteristic equation

$$s^\alpha - \kappa p^* \mathcal{D}'(p^*) e^{-s\tau} = 0. \tag{9}$$

Theorem 2: If $[-\kappa p^* \mathcal{D}'(p^*)]^{1/\alpha} \neq [(2k+1)\pi - \alpha\pi/2]/\tau$, where $k \in \mathbb{Z}$, then the equilibrium p^* of model (6) is Lyapunov globally asymptotically stable.

Proof: Let $s = i\omega = \omega(\cos\pi/2 + i\sin\pi/2)(\omega > 0)$ be a root of (9). Then

$$\omega^\alpha(\cos\frac{\alpha\pi}{2} + i\sin\frac{\alpha\pi}{2}) - \kappa p^* \mathcal{D}'(p^*)(\cos\omega\tau - i\sin\omega\tau) = 0.$$

Separating the real and imaginary parts gives

$$\begin{aligned}&\omega^\alpha \cos\frac{\alpha\pi}{2} - \kappa p^* \mathcal{D}'(p^*)\cos\omega\tau = 0\\&\omega^\alpha \sin\frac{\alpha\pi}{2} + \kappa p^* \mathcal{D}'(p^*)\sin\omega\tau = 0.\end{aligned} \tag{10}$$

Taking square on the both sides of (10) and summing them up give

$$\begin{aligned}&(\omega^\alpha)^2 + [\kappa p^*\mathcal{D}'(p^*)]^2\\&\quad -2\omega^\alpha \kappa p^*\mathcal{D}'(p^*)\cos(\tfrac{\alpha\pi}{2}+\omega\tau) = 0.\end{aligned} \tag{11}$$

Notice that $\kappa > 0, p^* > 0$, and $\mathcal{D}'(p^*) < 0$. It is straightforward to obtain that

$$\begin{aligned}&(\omega^\alpha)^2 + [\kappa p^*\mathcal{D}'(p^*)]^2 - 2\omega^\alpha\kappa p^*\mathcal{D}'(p^*)\cos(\frac{\alpha\pi}{2}+\omega\tau)\\&\geq (\omega^\alpha)^2 + [\kappa p^*\mathcal{D}'(p^*)]^2 + 2\omega^\alpha\kappa p^*\mathcal{D}'(p^*)\\&= [\omega^\alpha + \kappa p^*\mathcal{D}'(p^*)]^2.\end{aligned}$$

Obviously, if $[-\kappa p^*\mathcal{D}'(p^*)]^{1/\alpha} \neq [(2k+1)\pi - \alpha\pi/2]/\tau$, then (11) has no positive real roots, meaning that (9) has no purely imaginary roots with positive imaginary parts.

Let $s = i\omega = -\omega[\cos\pi/2 + i\sin(-\pi/2)]$ $(\omega < 0)$ be a root of (9). It is similar to prove that (9) has no purely imaginary roots with negative imaginary parts under the assumption $[-\kappa p^*\mathcal{D}'(p^*)]^{1/\alpha} \neq [(2k+1)\pi - \alpha\pi/2]/\tau$.

Thus, if $[-\kappa p^*\mathcal{D}'(p^*)]^{1/\alpha} \neq [(2k+1)\pi - \alpha\pi/2]/\tau$, then the characteristic equation (9) has no purely imaginary roots.

On the other hand, it is easy to see that the coefficient A of the linearized model (8) has one eigenvalue $s = \kappa p^*\mathcal{D}'(p^*) < 0$ satisfying $|\arg(s)| > \alpha\pi/2$.

Applying Corollary 2, the equilibrium p^* of model (6) is Lyapunov globally asymptotically stable. ■

Remark 2: Although nonlinear dynamics of integer-order congestion control systems were investigated in [19], [23], [37]−[41], to date, the theoretical results on the stability with respect to the system parameters and order have not been reported yet for fractional-order congestion control systems.

For illustration of Theorem 2, we consider the fractional-order model (6) with $\kappa = 0.02, C = 40, \tau = 1, \alpha = 0.9$, and the proportional fairness [19] with $\gamma = 1, w = 1$. The equilibrium can be found by solving (7), yielding $p^* = 0.025$. It is easy to verify that the condition $[-\kappa p^*\mathcal{D}'(p^*)]^{1/\alpha} \neq [(2k+1)\pi - \alpha\pi/2]/\tau$ holds. Fig. 1 shows that the state $p(t)$ of model (6) is globally asymptotically decreasing toward the equilibrium p^*.

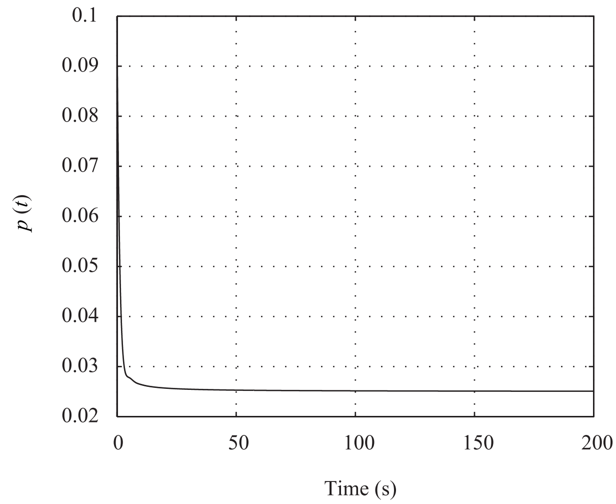

Fig. 1. Equilibrium $p^* = 0.025$ of model (6) is Lyapunov globally asymptotically stable when $\kappa = 0.02, C = 40, \tau = 1, \gamma = 1, w = 1, \alpha = 0.9$, and the initial condition $p^0 = 0.1$.

B. Hopf Bifurcation

It is well known that the Hopf bifurcation is the birth of a limit cycle from an equilibrium in integer-order dynamical systems, when the equilibrium changes the stability via a pair of purely imaginary eigenvalues. However, the qualitative theory of Hopf bifurcations for fractional-order dynamical systems has not been constructed yet. In this Subsection, we study the local bifurcation of the delayed fractional-order model (6) by regarding the delay τ as the bifurcation parameter.

First, we put forward the Hopf bifurcation conditions for general delayed fractional-order systems. Consider the following n-dimensional fractional-order system with delay:

$$\frac{d^\alpha x_i}{dt^\alpha} = f_i(x_1, x_2, \ldots, x_n; \tau),\ i = 1, 2, \ldots, n \tag{12}$$

where $0 < \alpha \leq 1$ and the time delay $\tau \geq 0$. According to Corollary 2, we propose the conditions of (12) to undergo a Hopf bifurcation at the equilibrium $x^* = (x_1^*, x_2^*, \ldots, x_n^*)$ when $\tau = \tau_0$ as follows:

1) All the eigenvalues of the coefficient matrix of the linearized system of (12) satisfy $|\arg(s)| > \alpha\pi/2$.

2) The characteristic equation of (12) has a purely imaginary roots $\pm i\omega_0$ when $\tau = \tau_0$.

3) $\frac{d\mathrm{Re}[s(\tau)]}{d\tau}\Big|_{\tau=\tau_0} > 0$, where $\mathrm{Re}\{\cdot\}$ denotes the real part of the complex eigenvalue.

Remark 3: The condition 1) guarantees the stability of the equilibrium x^* of the delayed fractional-order system (12) when $\tau = 0$. It is well known that the Routh-Hurwitz criterion is the necessary and sufficient condition for the stability of the equilibrium of integer-order dynamical systems. It should be noted that this criterion can also ensure the stability of the equilibrium of fractional-order dynamical systems.

Remark 4: The condition 3) is the transversality condition of Hopf bifurcations of the delayed fractional-order system (12).

Remark 5: The Hopf bifurcation conditions for fractional-order dynamical systems without time delays by the observations from numerical simulations were proposed in [35], [36]. We formulate the conditions of Hopf bifurcation of fractional-order dynamical systems with time delays in this paper.

Lemma 1: If $\tau = \tau_k, k = 0, 1, \ldots$, then (9) has a purely imaginary roots $\pm i\omega_0 (\omega_0 > 0)$, where

$$\begin{aligned}\tau_k &= \frac{(2k+1)\pi - \frac{\alpha\pi}{2}}{[-\kappa p^*\mathcal{D}'(p^*)]^{1/\alpha}}\\ \omega_0 &= [-\kappa p^*\mathcal{D}'(p^*)]^{1/\alpha}.\end{aligned} \tag{13}$$

Proof: From the proof of Theorem 2, we can see that (9) has a pair of purely imaginary roots when $[-\kappa p^*\mathcal{D}'(p^*)]^{1/\alpha} = [(2k+1)\pi - \alpha\pi/2]/\tau$. Therefore, the conclusion follows immediately. ■

Remark 6: Lemma 1 illustrates that the proposed condition 2) of Hopf bifurcation is reached for the delayed fractional-order model (6).

Lemma 2: Let $s(\tau) = \rho(\tau) + i\omega(\tau)$ be the root of (9) satisfying $\rho(\tau_k) = 0$ and $\omega(\tau_k) = \omega_0 > 0, k = 0, 1, \ldots$. Then,

$$\frac{d\mathrm{Re}[s(\tau)]}{d\tau}\Big|_{\tau=\tau_k} > 0.$$

Proof: Substituting $s(\tau)$ into (9) and differentiating both sides of the resulting equation with respect to τ, we obtain

$$\alpha s^{\alpha-1}\frac{ds}{d\tau} + \kappa p^*\mathcal{D}'(p^*)e^{-s\tau}[\tau\frac{ds}{d\tau} + s] = 0.$$

Thus

$$\frac{ds}{d\tau} = \frac{-\kappa p^*\mathcal{D}'(p^*)se^{-s\tau}}{\alpha s^{\alpha-1} + \kappa p^*\mathcal{D}'(p^*)\tau e^{-s\tau}}.$$

Note that $s(\tau) = \rho(\tau) + i\omega(\tau) = r(\cos\theta + i\sin\theta)$ is the root of (9). Then we have

$$\frac{ds}{d\tau} = \frac{-\kappa p^*\mathcal{D}'(p^*)[\rho + \mathrm{i}\omega]e^{-\rho\tau}[\cos(\omega\tau) - \mathrm{i}\sin(\omega\tau)]}{\alpha[\rho + \mathrm{i}\omega]^{\alpha-1} + \kappa p^*\mathcal{D}'(p^*)\tau e^{-\rho\tau}[\cos(\omega\tau) - \mathrm{i}\sin(\omega\tau)]}.$$

From this we obtain

$$\frac{d\mathrm{Re}[s(\tau)]}{d\tau} = -\kappa p^*\mathcal{D}'(p^*)e^{-\rho\tau}\frac{P(\tau)M(\tau) + Q(\tau)N(\tau)}{M^2(\tau) + N^2(\tau)}$$

in which

$$P(\tau) = \rho\cos\omega\tau + \omega\sin\omega\tau$$
$$Q(\tau) = \omega\cos\omega\tau - \rho\sin\omega\tau$$
$$M(\tau) = \alpha r^{\alpha-1}\cos(\alpha-1)\theta + \kappa p^*\mathcal{D}'(p^*)\tau e^{-\rho\tau}\cos\omega\tau$$
$$N(\tau) = \alpha r^{\alpha-1}\sin(\alpha-1)\theta - \kappa p^*\mathcal{D}'(p^*)\tau e^{-\rho\tau}\sin\omega\tau.$$

Replacing τ by τ_k, it follows that:

$$\begin{aligned}\frac{d\mathrm{Re}[s(\tau)]}{d\tau}\bigg|_{\tau=\tau_k} &= -\kappa p^*\mathcal{D}'(p^*)\frac{P(\tau_k)M(\tau_k) + Q(\tau_k)N(\tau_k)}{M^2(\tau_k) + N^2(\tau_k)} \\ &= -\kappa p^*\mathcal{D}'(p^*)\frac{\alpha(\omega_0)^\alpha\sin[\omega_0\tau_k + (\alpha-1)\frac{\pi}{2}]}{M^2(\tau_k) + N^2(\tau_k)}\end{aligned}$$

where

$$P(\tau_k) = \omega_0\sin(\omega_0\tau_k)$$
$$Q(\tau_k) = \omega_0\cos(\omega_0\tau_k)$$
$$M(\tau_k) = \alpha(\omega_0)^{\alpha-1}\cos(\alpha-1)\frac{\pi}{2} + \kappa p^*\mathcal{D}'(p^*)\tau_k\cos(\omega_0\tau_k)$$
$$N(\tau_k) = \alpha(\omega_0)^{\alpha-1}\sin(\alpha-1)\frac{\pi}{2} - \kappa p^*\mathcal{D}'(p^*)\tau_k\sin(\omega_0\tau_k).$$

It can be seen from (13) that $\omega_0\tau_k = (2k+1)\pi - \alpha\pi/2$, implying that $\sin\ [\omega_0\tau_k + (\alpha-1)\pi/2] = 1$. Moreover, note that $-\kappa p^*\mathcal{D}'(p^*) > 0$. Therefore

$$\frac{d\mathrm{Re}[s(\tau)]}{d\tau}\bigg|_{\tau=\tau_k^+} > 0.$$

The conclusion follows. ■

Remark 7: Lemma 2 implies that the transversality condition 3) of Hopf bifurcations is satisfied for the delayed fractional-order model (6).

Theorem 3: For model (6), the following results hold.

1) The equilibrium p^* of model (6) is asymptotically stable for $\tau \in [0, \tau_0)$, and unstable when $\tau > \tau_0$.

2) Model (6) undergoes a Hopf bifurcation at the equilibrium p^* when $\tau = \tau_0$.

Proof: Note that the coefficient matrix of the linearized (8) has the eigenvalue $\lambda = \kappa p^*\mathcal{D}'(p^*) < 0$ satisfying the inequality $|\arg(s)| > \alpha\pi/2$. Thus, the condition 1) of Hopf bifurcations is satisfied for model (6).

1) It is easy to see that all the roots of (9) with $\tau = 0$ have negative real parts. From Lemma 1, the definition of τ_0 implies that all the roots of (9) have negative real parts for $\tau \in [0, \tau_0)$. The conclusion in Lemma 2 indicates that (9) has at least one root with positive real part when $\tau > \tau_0$. Thus, the conclusion follows.

2) From Remarks 6 and 7, we know that the conditions 2) and 3) of Hopf bifurcations are satisfied for model (6). Hence, a Hopf bifurcation occurs at the equilibrium p^* when $\tau = \tau_0$. ■

Remark 8: The Hopf bifurcation theory in fractional-order dynamical systems is still an open problem. The Hopf bifurcation conditions for fractional-order systems without delays are proposed based on the observations from numerical simulations [35], [36]. However, there are few results on the Hopf bifurcation of delayed fractional-order systems.

Remark 9: The integer-order congestion control model (5) may display a Hopf bifurcation when the delay τ passes through the critical values [23]. However, the corresponding fractional-order model (6) will not produce the bifurcation at the same values, which will be confirmed by numerical simulations later.

Remark 10: The order and system parameter were chosen as the bifurcation parameters in fractional-order neural network models in [8]. In this paper, we use the delay τ as the bifurcation parameter in fractional-order congestion control models.

V. Numerical Simulations

In this section, we present some numerical results to illustrate the analytical results obtained in the previous section, displaying the Hopf bifurcation phenomenon of the delayed fractional-order model (6) of fair dual congestion control algorithms. Simulations are performed using the method introduced in [42] to find the solution of delayed fractional-order differential equations. This method is the improved version of the Adams-Bashforth-Moulton algorithm and is proposed based on the predictor correctors scheme.

For a consistent comparison, we discuss model (6) with the same system parameters used in [23]: $\kappa = 0.01, C = 50$, and the proportional fairness [19] with $\mathcal{D}(p) = 1/p$. From (7), model (6) has a unique non-zero equilibrium $p^* = 0.02$. For model (6) with $\alpha = 1$ (integer-order model (5)), it follows from Theorem 1 in [23] that

$$\tau_0 = 3.1416, \quad \omega_0 = 0.5.$$

The dynamical behavior of the integer-order model (5) is illustrated in Figs. 2–4. From Theorem 1 in [23], it is shown

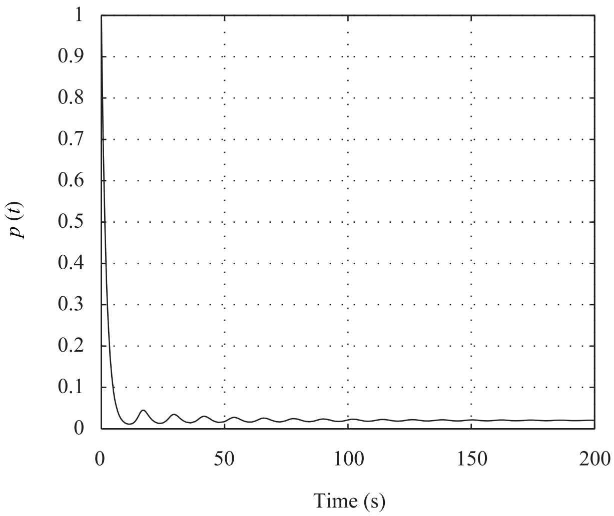

Fig. 2. The equilibrium $p^* = 0.02$ of the integer-order model (5) is asymptotically stable, where $\kappa = 0.01, C = 50, \mathcal{D}(p) = 1/p$, the initial condition $p^0 = 1$, and $\tau = 2.95 < \tau_0 = 3.1416$.

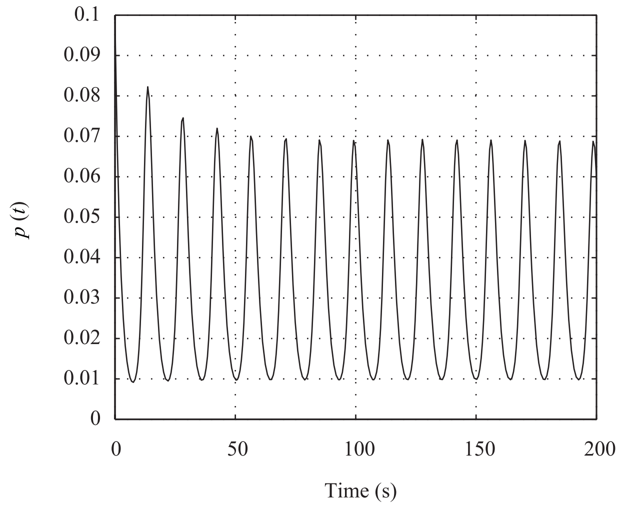

Fig. 4. A periodic oscillation bifurcates from the equilibrium $p^* = 0.02$ of the integer-order model (5), where $\kappa = 0.01, C = 50, \mathcal{D}(p) = 1/p$, the initial condition $p^0 = 0.1$, and $\tau = 3.45 > \tau_0 = 3.1416$.

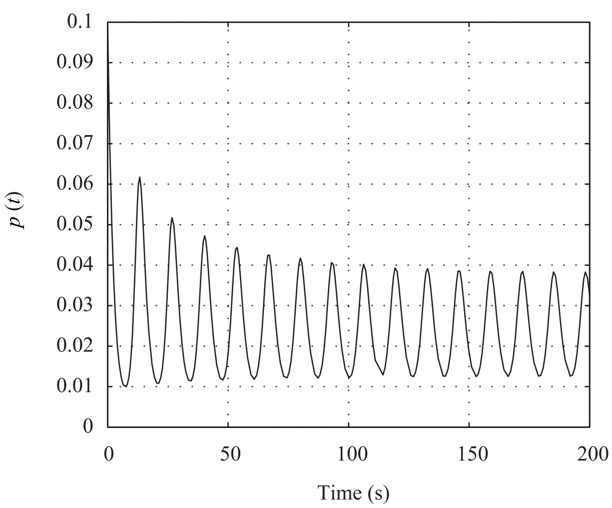

Fig. 3. A periodic oscillation bifurcates from the equilibrium $p^* = 0.02$ of the integer-order model (5), where $\kappa = 0.01, C = 50, \mathcal{D}(p) = 1/p$, the initial condition $p^0 = 0.1$, and $\tau = 3.25 > \tau_0 = 3.1416$.

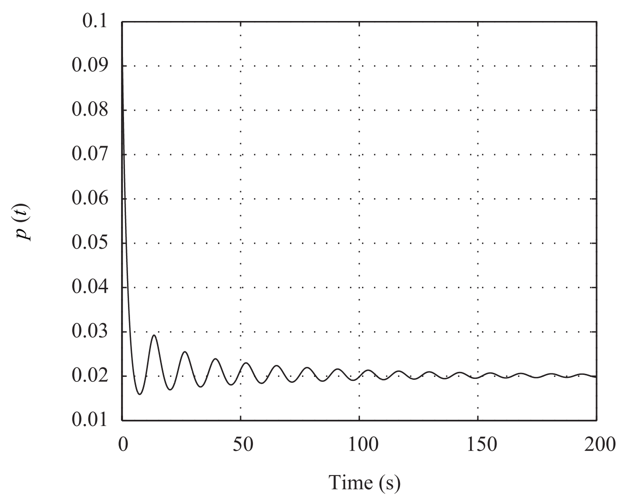

Fig. 5. The equilibrium $p^* = 0.02$ of model (6) with $\alpha = 0.92$ is asymptotically stable, where $\kappa = 0.01, C = 50, \mathcal{D}(p) = 1/p$, the initial condition $p^0 = 0.1$, and $\tau = 3.45 < \tau_0 = 3.6037$.

that when $\tau < \tau_0$, the trajectory converges to the equilibrium p^* (see Fig. 2), while as τ is increased to pass through τ_0, p^* loses its stability and a Hopf bifurcation occurs (see Figs. 3 and 4).

Next, using our Theorem 3, we display the Hopf bifurcation for the fractional-order model (6) with $\alpha \in (0, 1)$. For example, by choosing $\alpha = 0.92$, we can apply (13) in Lemma 1 to obtain

$$\tau_0 = 3.6037, \quad \omega_0 = 0.4708.$$

Note that the fractional-order model (6) with $\alpha = 0.92$ has the same equilibrium as that of the integer-order model (5), but the critical value τ_0 increases from 3.1416 to 3.6037, implying that the onset of Hopf bifurcations is delayed.

When $\alpha = 0.92$, we choose $\tau = 3.45 < \tau_0 = 3.6037$, which is the same value as that used in Fig. 4. According to Theorem 3, we conclude that instead of having a Hopf bifurcation, the fractional-order model (6) with $\alpha = 0.92$ converges to the equilibrium $p^* = 0.02$, as shown in Fig. 5.

When $\alpha = 0.92$, we choose $\tau = 3.8 > \tau_0 = 3.6037$. From Theorem 3, the equilibrium $p^* = 0.02$ is unstable, as shown in Fig. 6. It can be seen that when τ passes through the critical value $\tau_0 = 3.6037$, a Hopf bifurcation occurs (see Figs. 5 and 6).

When $\alpha = 0.92$, we choose $\tau = 3.45 < \tau_0 = 3.6037$, which is the same value as that used in Fig. 4. According to Theorem 3, we conclude that instead of having a Hopf bifurcation, the fractional-order model (6) with $\alpha = 0.92$ converges to the equilibrium $p^* = 0.02$, as shown in Fig. 5.

When $\alpha = 0.92$, we choose $\tau = 3.8 > \tau_0 = 3.6037$. From Theorem 3, the equilibrium $p^* = 0.02$ is unstable, as shown in Fig. 6. It can be seen that when τ passes through the critical value $\tau_0 = 3.6037$, a Hopf bifurcation occurs (see Figs. 5 and 6).

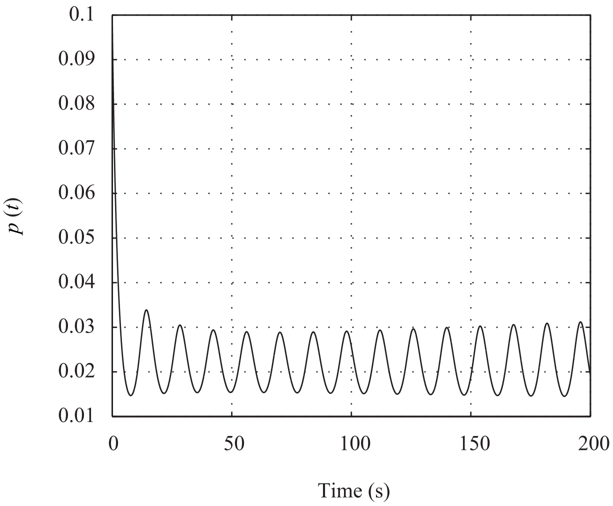

Fig. 6. A periodic oscillation bifurcates from the equilibrium $p^* = 0.02$ of model (6) with $\alpha = 0.92$, where $\kappa = 0.01, C = 50, \mathcal{D}(p) = 1/p$, the initial condition $p^0 = 0.1$, and $\tau = 3.8 > \tau_0 = 3.6037$.

It can be shown that if we choose a smaller value of α, then the fractional-order model (6) may not have a Hopf bifurcation even for the larger values of τ. This indicates that the order α can delay the onset of Hopf bifurcations, thus guaranteeing a stationary sending rate for the larger values of τ. For example, when choosing $\alpha = 0.86$, the fractional-order model (6) converges to the equilibrium $p^* = 0.02$ if $\tau < \tau_0 = 4.0092$, as shown in Fig. 7.

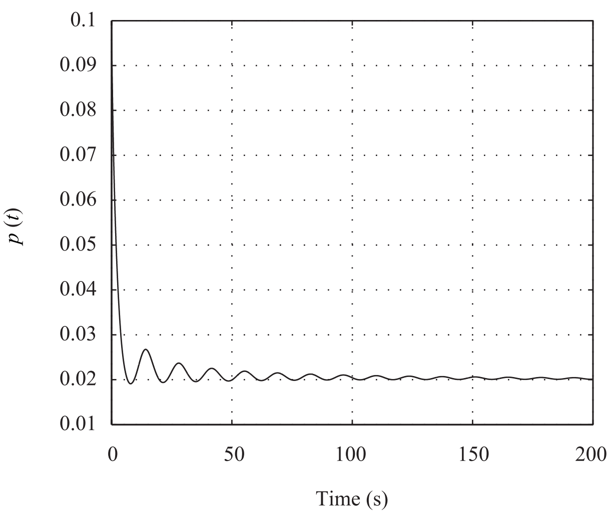

Fig. 7. Equilibrium $p^* = 0.02$ of model (6) with $\alpha = 0.86$ is asymptotically stable, where $\kappa = 0.01, C = 50, \mathcal{D}(p) = 1/p$, the initial condition $p^0 = 0.1$, and $\tau = 3.9 < \tau_0 = 4.0092$.

The effect of the order α on the values of τ_0 and ω_0 is shown in Table I. The critical value τ_0 decreases clearly with the order α, which means that the value of τ_0 is sensitive to the change of the order α.

VI. Conclusion

In this paper, we have extended a delayed integer-order model of dual congestion control algorithms to a fractional-order counterpart. We have considered the stability and bifurcations of network congestion control in the presence of communication delays and fractional order. A stability criterion for the delayed fractional-order congestion control model has been established. We have also proposed some conditions of Hopf-type bifurcations for delayed fractional-order systems. The delayed fractional-order congestion control model can exhibit a Hopf bifurcation (i.e., periodic oscillations appear) as the delay achieves a critical value which can be determined exactly. It is observed that an increase in the order may lead to a decrease of the critical value. The observations allow us to design Hopf bifurcations of congestion control systems with the desired bifurcation points by adjusting the delays and order.

TABLE I

Values of ω_0 and τ_0 for (6) With $\kappa = 0.01$, $C = 50$, $D(P) = 1/P$, and Different Values of α : $\alpha = 1, 0.9, 0.8, 0.7, 0.6, 0.5, 0.4, 0.3, 0.2$, and 0.1

Fractional order of model (6)	ω_0	τ_0
$\alpha = 1$	0.5	3.1416
$\alpha = 0.9$	0.4629	3.7324
$\alpha = 0.8$	0.4204	4.4832
$\alpha = 0.7$	0.3715	5.4968
$\alpha = 0.6$	0.3150	6.9818
$\alpha = 0.5$	0.2500	9.4248
$\alpha = 0.4$	0.1768	14.2172
$\alpha = 0.3$	0.0992	26.9155
$\alpha = 0.2$	0.0313	90.4779
$\alpha = 0.1$	9.7656E−004	3.0561E+003

References

[1] B. I. Henry and S. L. Wearne, "Existence of Turing instabilities in a two-species fractional reaction-diffusion system," *SIAM J. Appl. Math.*, vol. 62, no. 3, pp. 870−887, Feb. 2002.

[2] N. Engheia, "On the role of fractional calculus in electromagnetic theory," *IEEE Antennas Propag. Mag.*, vol. 39, no. 4, pp. 35−46, Aug. 1997.

[3] N. Heymans and J. C. Bauwens, "Fractal rheological models and fractional differential equations for viscoelastic behavior," *Rheol. Acta*, vol. 33, no. 3, pp. 210−219, May 1994.

[4] H. Sun, A. Abdelwahab, and B. Onaral, "Linear approximation of transfer function with a pole of fractional power," *IEEE Trans. Automat. Control*, vol. 29, no. 5, pp. 441−444, May 1984.

[5] D. Baleanu, J. A. T. Machado, and A. C. J. Luo, " *Fractional Dynamics and Control*. Berlin: Springer, 2012.

[6] V. D. Djordjević, J. Jarić, B. Fabry, J. J. Fredberg, and D. Stamenović, "Fractional derivatives embody essential features of cell rheological behavior," *Ann. Biomed. Eng.*, vol. 31, no. 6, pp. 692−699, Jun. 2003.

[7] Y. H. Lim, K. K. Oh, and H. S. Ahn, "Stability and stabilization of fractional-order linear systems subject to input saturation," *IEEE Trans. Automat. Control*, vol. 58, no. 4, pp. 1062−1067, Apr. 2013.

[8] M. Xiao, W. X. Zheng, G. P. Jiang, and J. D. Cao, "Undamped oscillations generated by Hopf bifurcations in fractional- order recurrent neural networks with Caputo derivative," *IEEE Trans. Neural Networks Learn. Syst.*, vol. 26, no. 12, pp. 3201−3214, Dec. 2015.

[9] T. T. Hartley, C. F. Lorenzo, and H. K. Qammer, "Chaos in a fractional order Chua's system," *IEEE Trans. Circuits Syst. I Fund. Theory Appl.*, vol. 42, no. 8, pp. 485−490, Aug. 1995.

[10] I. N'Doye, H. Voos, and M. Darouach, "Observer-based approach for fractional-order chaotic synchronization and secure communication," *IEEE J. Emerg. Sel. Topics Circuits Syst.*, vol. 3, no. 3, pp. 442−450, Sep. 2013.

[11] A. Papachristodoulou and A. Jadbabaie, "Delay robustness of nonlinear Internet congestion control schemes," *IEEE Trans. Automat. Control*, vol. 55, no. 6, pp. 1421−1427, Jun. 2010.

[12] J. Barrera and A. Garcia, "Dynamic incentives for congestion control," *IEEE Trans. Automat. Control*, vol. 60, no. 2, pp. 299−310, Feb. 2015.

[13] X. Zhang and A. Papachristodoulou, "Improving the performance of network congestion control algorithms," *IEEE Trans. Automat. Control*, vol. 60, no. 2, pp. 522−527, Feb. 2015.

[14] F. P. Kelly, A. K. Maulloo, and D. K. H. Tan, "Rate control for communication networks: shadow prices, proportional fairness and stability," *J. Oper. Res. Soc.*, vol. 49, no. 3, pp. 237−252, Mar. 1998.

[15] Y. P. Zhang and D. Loguinov, "Local and global stability of delayed congestion control systems," *IEEE Trans. Automat. Control*, vol. 53, no. 10, pp. 2356−2360, Nov. 2008.

[16] P. Ranjan, R. J. La, and E. H. Abed, "Global stability conditions for rate control with arbitrary communication delays," *IEEE/ACM Trans. Network.*, vol. 14, no. 1, pp. 94−107, Feb. 2006.

[17] M. L. Sichitiu and P. H. Bauer, "Asymptotic stability of congestion control systems with multiple sources," *IEEE Trans. Automat. Control*, vol. 51, no. 2, pp. 292−298, Feb. 2006.

[18] Y. P. Tian, "Stability analysis and design of the second-order congestion control for networks with heterogeneous delays," *IEEE/ACM Trans. Network.*, vol. 13, no. 5, pp. 1082−1093, Oct. 2005.

[19] G. Raina, "Local bifurcation analysis of some dual congestion control algorithms," *IEEE Trans. Automat. Control*, vol. 50, no. 8, pp. 1135−1146, Aug. 2005.

[20] C. G. Li, G. R. Chen, X. F. Liao, and J. B. Yu, "Hopf bifurcation in an Internet congestion control model," *Chaos Solitons Fractals*, vol. 19, no. 4, pp. 853−862, Mar. 2004.

[21] M. Xiao, W. X. Zheng, and J. D. Cao, "Bifurcation control of a congestion control model via state feedback," *Int. J. Bifurc. Chaos*, vol. 23, no. 6, pp. 1330018, Jun. 2013.

[22] W. Y. Xu, J. D. Cao, and M. Xiao, "Bifurcation analysis of a class of (n+1)-dimension Internet congestion control systems," *Int. J. Bifurc. Chaos*, vol. 25, no. 2, pp. 1550019, Feb. 2015.

[23] D. W. Ding, J. Zhu, X. S. Luo, and Y. L. Liu, "Delay induced Hopf bifurcation in a dual model of Internet congestion control algorithm," *Nonlinear Anal. Real World Appl.*, vol. 10, no. 5, pp. 2873−2883, Oct. 2009.

[24] M. Xiao, G. P. Jiang, and L. D. Zhao, "State feedback control at Hopf bifurcation in an exponential RED algorithm model," *Nonlinear Dyn.*, vol. 76, no. 2, pp. 1469−1484, Apr. 2014.

[25] F. Liu F, H. O. Wang, and Z. H. Guan, "Hopf bifurcation control in the XCP for the Internet congestion control system," *Nonlinear Anal. Real World Appl.*, vol. 13, no. 3, pp. 1466−1479, Jun. 2012.

[26] M. Xiao and J. D. Cao, "Delayed feedback-based bifurcation control in an Internet congestion model," *J. Math. Anal. Appl.*, vol. 332, no. 2, pp. 1010−1027, Aug. 2007.

[27] I. Podlubny, *Fractional Differential Equations*. New York: Academic Press, 1999.

[28] G. Q. Chen and E. G. Friedman, "An RLC interconnect model based on fourier analysis," *IEEE Trans. Comp. Aided Des. Integr. Circuits Syst.*, vol. 24, no. 2, pp. 170−183, Feb. 2005.

[29] V. G. Jenson and G. V. Jeffreys, *Mathematical Methods in Chemical Engineering*. 2nd ed. New York: Academic Press, 1977.

[30] R. L. Magin, "Fractional calculus models of complex dynamics in biological tissues," *Comput. Math. Appl.*, vol. 59, no. 5, pp. 1586−1593, Mar. 2010.

[31] N. Laskin, "Fractional market dynamics," *Phys. A*, vol. 287, no. 3−4, pp. 482−492, Dec. 2000.

[32] W. H. Deng, C. P. Li, and J. H. Lü, "Stability analysis of linear fractional differential system with multiple time delays," *Nonlinear Dyn.*, vol. 48, no. 4, pp. 409−416, Jun. 2007.

[33] D. Matignon, "Stability results for fractional differential equations with applications to control processing," in *Multiconference: Computational Engineering in Systems and Application*, Lille, France, 1996, pp. 963−968.

[34] Y. A. Kuznetsov, *Elements of Applied Bifurcation Theory*. New York: Springer-Verlag, 2004.

[35] H. A. El-Saka, E. Ahmed, M. I. Shehata, and A. M. A. El-Sayed, "On stability, persistence, and Hopf bifurcation in fractional order dynamical systems," *Nonlinear Dyn.*, vol. 56, no. 1−2, pp. 121−126, Jul. 2008.

[36] M. S. Abdelouahab, N. E. Hamri, and J. W. Wang, "Hopf bifurcation and chaos in fractional-order modified hybrid optical system," *Nonlinear Dyn.*, vol. 69, no. 1−2, pp. 275−284, Jul. 2012.

[37] S. S. Kunniyur and R. Srikant, "Stable, scalable, fair congestion control and AQM schemes that achieve high utilization in the Internet," *IEEE Trans. Automat. Control*, vol. 48, no. 11, pp. 2024−2028, Nov. 2003.

[38] S. Liu, T. Basar, and R. Srikant, "Exponential-RED: a stabilizing AQM scheme for low- and high-speed TCP protocols," *IEEE/ACM Trans. Network.*, vol. 13, no. 5, pp. 1068−1081, Oct. 2005.

[39] P. Ranjan, E. H. Abed, and R. J. La, "Nonlinear instabilities in TCP-RED," *IEEE/ACM Trans. Network.*, vol. 12, no. 6, pp. 1079−1092, Dec. 2004.

[40] F. Kelly, "Fairness and stability of end-to-end congestion control," *Eur. J. Control*, vol. 9, no. 2−3, pp. 159−176, 2003.

[41] D. W. Ding, X. M. Qin, N. Wang, T. T. Wu, and D. Liang, "Hybrid control of Hopf bifurcation in a dual model of Internet congestion control system," *Nonlinear Dyn.*, vol. 76, no. 2, pp. 1041−1050, Apr. 2014.

[42] S. Bhalekar and V. Daftardar-Gejji, "A predictor-corrector scheme for solving nonlinear delay differential equations of fractional order," *J. Fract. Calculus Appl.*, vol. 1, no. 5, pp. 1−9, Jul. 2011.

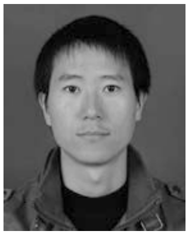

Min Xiao (M'11) received the B.S. and M.S. degrees in mathematics and fundamental mathematics from Nanjing Normal University, Nanjing, China, in 1998 and 2001, respectively, and the Ph.D. degree in applied mathematics from Southeast University, Nanjing, China, in 2007. He is currently a professor at the College of Automation, Nanjing University of Posts and Telecommunications, Nanjing, China. His current research interests include memristor-based neural networks, fractional order systems, networked control systems, bifurcation control, and smart networks of power. Corresponding author of this paper.

Guoping Jiang (M'03–SM'13) received the B.E. degree in Electrical Engineering from Hohai University, Nanjing, China, in 1988, and the Ph.D. degree in control theory and engineering from Southeast University, Nanjing, China, in 1997. He is currently a professor and the vice president of Nanjing University of Posts and Telecommunications, Nanjing, China. He has authored or coauthored more than 200 published academic articles. Professor Jiang received the Academic Leader for the Youthful and Middle-Aged Scholars of Jiangsu Province, China, in 2002, and the New Century Excellent Talents of Ministry of Education, China, in 2006. His research interests include chaos synchronization and control, and complex dynamical networks.

Jinde Cao received the B.S. degree from Anhui Normal University, Wuhu, China, the M.S. degree from Yunnan University, Kunming, China, and the Ph.D. degree from Sichuan University, Chengdu, China, all in mathematics/applied mathematics, in 1986, 1989, and 1998, respectively. He is currently a distinguished professor, the dean of Department of Mathematics and the Director of the Research Center for Complex Systems and Network Sciences at Southeast University, Nanjing, China. Professor Cao was an associate editor of the *IEEE Transactions on Neural Networks*, *Journal of the Franklin Institute* and *Neurocomputing*. He is an associate editor of the *IEEE Transactions on Cybernetics*, *Differential Equations and Dynamical Systems*, *Mathematics and Computers in Simulation*, and *Neural Networks*. He is a fellow of IEEE(2016), and a member of the Academy of Europe(2016). He has been named as Highly-Cited Researcher in Mathematics, Computer Science and Engineering listed by Thomson Reuters. His research interests include nonlinear systems, neural networks, complex systems and complex networks, stability theory, and applied mathematics.

Weixing Zheng received the B.S. degree in 1982, the M.S. degree in 1984, and the Ph.D. degree in 1989, all from the Southeast University, Nanjing, China. He is currently a professor at the Western Sydney University, Sydney, Australia. Dr. Zheng serves as an associate editor of *Automatica*, *IEEE Transactions on Automatic Control*, and other IEEE journals. He is a fellow of IEEE and a Thomson Reuters Highly Cited Researcher. His research interests include system identification, networked control systems, multi-agent systems, complex networks and signal processing.

Modified Grey Model Predictor Design Using Optimal Fractional-order Accumulation Calculus

Yang Yang, and Dingyü Xue

***Abstract*—The major advantage of grey system theory is that both incomplete information and unclear problems can be processed precisely. Considering that the modeling of grey model (GM) depends on the preprocessing of the original data, the fractional-order accumulation calculus could be used to do preprocessing. In this paper, the residual sequence represented by Fourier series is used to ameliorate performance of the fractional-order accumulation $\mathrm{GM}\,(1,1)$ and improve the accuracy of predictor. The state space model of optimally modified $\mathrm{GM}\,(1,1)$ predictor is given and genetic algorithm (GA) is used to find the smallest relative error during the modeling step. Furthermore, the fractional form of continuous $\mathrm{GM}\,(1,1)$ is given to enlarge the content of prediction model. The simulation results illustrated that the fractional-order calculus could be used to depict the GM precisely with more degrees of freedom. Meanwhile, the ranges of the parameters and model application could be enlarged with better performance. The method of modified GM predictor using optimal fractional-order accumulation calculus is expected to be widely used in data processing, model theory, prediction control and related fields.**

***Index Terms*—Fractional-order accumulation, grey model (GM), genetic algorithm (GA), fourier series.**

I. INTRODUCTION

GREY system theory was firstly proposed in 1982 and GM was built for prediction or decision-making with unclear and incomplete information [1]. Compared with the conventional statistical models, only small samples of data is required to estimate the behavior of unknown systems in the GM using a special differential equation according to the output data predicted [1]−[4]. $\mathrm{GM}\,(1,1)$ is the basic form and most commonly used due to its computational efficiency and prediction accuracy [3]−[5]. Furthermore, extraordinary differential equations (for example Non-linear, Delayed and Fractional-order) are also popularly used in mathematical modeling of many engineering and scientific problems.

Although, fractional-order differential equations (FODEs) have been efficient tools for model simulation and theoretical analysis, it is difficult to get the solution due to the existence of fractional derivatives, especially with the initial value problem [6]−[9]. Several Matlab programs and interfaces have been given for fractional-order systems. For example, Simulink model method for fractional-order nonlinear system is proposed in ref [10] for initial value problem. A Ninteger toolbox is developed for fractional-order controllers [11] and FOMCON is a modeling and control toolbox for fractional-order system [12]. The state space representation [13], [14], robust stability research and system analysis are also hot topics. In ref [13], two methods for the state space representation are presented based on the differentiation and integration operator approximation respectively. The robust stability of Fractional-order Linear Time Invariant (FO-LTI) system with interval uncertainties has been investigated in ref [14], [15]. Furthermore, parameter and differentiation order estimation in fractional models are discussed in ref [16].

Based on the fractional-order accumulation, many researches have been carried out to study the model performance in the GMs, for example, the model properties, perturbation problems and stability analysis of the fractional-order accumulation calculus by $\alpha = p/q$ [17]−[22]. Furthermore, several new GMs are proposed based on the fractional-order accumulation, for example, non-homogenous discrete grey model (NDGM) with fractional-order accumulation is put forward in ref [19], the fractional-order accumulating generation operator is applied in the $\mathrm{GM}\,(2,1)$ in ref [20], the grey discrete power $\mathrm{GM}\,(1,1)$ model is constructed by the fractional-order accumulation in ref [21], the fractional-order accumulation time-lag model $\mathrm{GM}\,(1,\mathrm{N},\tau)$ is proposed in [22]. Apart from this, the residual information are also used in some modified GMs. For example, Fourier residual, Markov Chain model and Artificial Neural Network have been used to correct the periodicity and randomness of residuals and improve the model performance [23]−[25].

Compared with the work being published, the GM using fractional-order accumulation, the modified optimal model and the model state space descriptions are all practical questions. In order to settle the problems above, the works described in this paper include the discrete GM $(1,1)$ using fractional-order accumulation and the fractional form of continuous GM $(1,1)$ by fractional calculus are studied; the modified optimal model is obtained based on GA and Fourier series; the state space models for the predictor are also given.

The rest of this paper is organized as follows. In Section II, the basic knowledge of fractional accumulation calculus is introduced. In Section III, the form and model by fractional-order accumulation calculus in GM $(1,1)$ is analyzed. In Sec-

This article has been accepted for publication in a future issue of this journal, but has not been fully edited. Content may change prior to final publication.

This work was supported by the National Natural Science Foundation of China (61174145). Recommended by Associate Editor YangQuan Chen.

Citation: Y. Yang, and D. Y. Xue, "Modified grey model predictor design using optimal fractional-order accumulation calculus," *IEEE/CAA Journal of Automatica Sinica*, pp. 1−10, 2017. DOI: 10.1109/JAS.2017.7510355.

Y. Yang is with the College of Information Science and Engineering, Northeastern University, Shenyang 110004, China, and also with the College of Engineering, Bohai University, Jinzhou, 121013, China(email: yangy195@163.com).

D. Y. Xue is with the College of Information Science and Engineering, Northeastern University, Shenyang 110004, China(email: xuedingyu@ise.neu.edu.cn).

tion IV, the state space models of modified optimal fractional accumulation GM $(1,1)$ predictor are studied. In Section V, the fractional form of continuous GM $(1,1)$ is given. In Section VI, the properties of fractional-order accumulation calculus are showed by a simple sequence and one case of modified optimal fractional-order accumulation GM $(1,1)$ predictor is discussed and tested. The conclusion part is given finally.

II. Fractional Accumulation Calculus

A. Fractional Calculus

Fractional calculus is a generalization of differentiation and integration to non-integer-order fundamental operator. The continuous differential-integral operator is

$$ {}_aD_t^\gamma = \frac{\mathrm{d}^\gamma}{\mathrm{d}t^\gamma}, \qquad \gamma > 0 \tag{1a}$$
$$ {}_aD_t^\gamma = 1, \qquad \gamma = 0 \tag{1b}$$
$$ {}_aD_t^\gamma = \int_a^t (\mathrm{d}\tau)^{-\gamma}, \qquad \gamma < 0 \tag{1c}$$

where γ is a complex number, a is a real number related to initial value. $\Gamma(n)$ is Euler's Gamma function and

$$\Gamma(n) = \int_o^\infty t^{n-1}e^{-t}\mathrm{d}t \text{ for } \mathrm{Re}(n) > 0 \tag{2}$$

It is also called Euler's integral of the second kind. It is clear that the restriction $\mathrm{Re}(n) > 0$ assures the convergence of the integral. The Grünwald–Letnikov (GL), the Riemann–Liouville (RL) or Caputo derivative are the three most frequently used definitions for the general fractional differintegral, and the GL definition [26]−[28] is given as

$$ {}_aD_t^\gamma f(\mathrm{t}) = \frac{\mathrm{d}^\gamma f(t)}{\mathrm{d}t^\gamma} = \lim_{h\to 0}\frac{1}{h^\gamma}\sum_{j=0}^{(t-a)/h}(-1)^j\binom{\gamma}{j}f(t-jh) \tag{3}$$

where the binomial coefficients are defined as

$$\binom{\gamma}{j} = \frac{\gamma!}{j!\,(\gamma-j)!} \tag{4}$$

For arbitrary non-integer and even complex $\gamma \neq -1, -2, \cdots$ and j:

$$\begin{aligned}\binom{\gamma}{j} &= \frac{\Gamma(1+\gamma)}{\Gamma(1+j)\Gamma(1+\gamma-j)} \\ &= \frac{\sin[(j-\gamma)\pi]}{\pi}\frac{\Gamma(1+\gamma)\Gamma(j-\gamma)}{\Gamma(1+j)}\end{aligned} \tag{5}$$

For an integer $j = n$ and non-integer γ

$$\begin{aligned}\binom{\gamma}{n} &= \frac{\gamma(\gamma-1)\cdots(\gamma-n+1)}{n!} \\ &= \frac{(-1)^{n-1}\mu\Gamma(n-\gamma)}{n!\Gamma(1-\mu)} = O(n^{-\mu-1}), \quad n\to\infty\end{aligned} \tag{6}$$

B. Fractional Accumulation Calculus

In the accumulation theory, for α is arbitrary positive integer number, the definition of integral-order accumulation for sequence $x(j)$ $j = 1, 2, \cdots, m$ is given as in (7) [29].

$$\begin{aligned}
\sum_{j=1}^m {}^{(1)}x(j) &= \sum_{j=1}^m C_{m-j}^{m-j}x(j) = \sum_{j=1}^m x(j) \quad \alpha = 1 \\
\sum_{j=1}^m {}^{(2)}x(j) &= \sum_{j=1}^m\sum_{i=1}^j {}^{(1)}x(j) = \sum_{j=1}^m C_{m-j+1}^{m-j}x(j) \\
&= \sum_{j=1}^m C_{m-j+1}^{1}x(j) \quad \alpha = 2 \\
&\vdots \\
\sum_{j=1}^m {}^{(k)}x(j) &= \sum_{j=1}^m\sum_{i=1}^j {}^{(k-1)}x(j) \\
&= \frac{1}{(k-1)!}\sum_{j=1}^m (m-j+1)(m-j+2) \\
&\quad \cdots[m-j+(k-1)]x(j) \\
&= \sum_{j=1}^m C_{m-j+k-1}^{m-j}x(j) \\
&= \frac{(m-j+k-1)(m-j+k-2)\cdots(k+1)k}{(m-j)!} \\
&\quad \cdot x(j) \quad \alpha = k
\end{aligned} \tag{7}$$

where $\alpha = 1, 2, \cdots, k$ are the integer-orders. For $\alpha = \frac{p}{q}$, the accumulation for sequence $x(j)$ $j = 1, 2, \cdots, m$ has been given in ref [17] and the definition is

$$\sum_{j=1}^m {}^{(\frac{p}{q})}x(j) = \sum_{j=1}^m C_{m-j+\frac{p}{q}-1}^{m-j}x(j) \tag{8}$$

where

$$C_{\frac{p}{q}-1}^0 = 1,$$
$$C_{m-j+\frac{p}{q}-1}^{m-j} = \frac{(m-j+\frac{p}{q}-1)(m-j+\frac{p}{q}-2)\cdots(\frac{p}{q}+1)\frac{p}{q}}{(m-j)!}.$$

Based on the fractional-order and accumulation theory [9], [17], [29], the definition of fractional-order accumulation is given by Gamma function in this paper. For sequence $x(j)$ $j = 1, 2, \cdots, m$, the fractional-order accumulation is defined as in (9) with the order $k > 0$.

$$\sum_{j=1}^m {}^{(k)}x(j) = \sum_{j=1}^m \frac{\Gamma(m-j+k)}{\Gamma(m-j+1)\Gamma(k)}x(j) \tag{9}$$

and

$$\sum_{j=1}^m {}^{(k)} = \frac{\Gamma(m-j+k)}{\Gamma(m-j+1)\Gamma(k)} = \begin{cases} C_{k-1}^0 = 1 & m = j \\ C_{m-j+k-1}^{m-j} = \frac{(m-j+k-1)(m-j+k-2)\cdots(k+1)k}{(m-j)!} & m \neq j\end{cases} \tag{10}$$

The proof can be easily obtained using the properties of Gamma function. The expression by (9) is generalization of integer or $\alpha = \frac{p}{q}$. The parameter w_j is defined as the weighting factor of accumulation as in (11).

$$w_j = \frac{\Gamma(m-j+k)}{\Gamma(m-j+1)\Gamma(k)} \quad j = 1, 2, \cdots, m \tag{11}$$

Using the fractional-order calculus, the weighted form of the overall data information is considered. Therefore, the fractional-order accumulation can be used to do data preprocessing and mine the information from the data. The estimated data by the model can be obtained from the following equation.

$$\hat{x}^{(0)}(m) = x^{(1)}(m) - \sum_{j=1}^{m-1} \frac{\Gamma(m-j+k)}{\Gamma(m-j+1)\Gamma(k)} \hat{x}^{(0)}(j) \tag{12}$$

III. Fractional-order Accumulation in GM $(1,1)$

Suppose $x^{(0)} = \left(x^{(0)}(1), x^{(0)}(2), \cdots, x^{(0)}(m)\right)$ is the sequence of raw data with non-nonnegative values usually. Denote its fractional-order accumulation generated sequence by $x^{(1)} = \left(x^{(1)}(1), x^{(1)}(2), \cdots, x^{(1)}(m)\right)$.

The image form for continuous data of GM $(1,1)$ is [30]–[32].

$$\frac{\mathrm{d}x^{(1)}}{\mathrm{d}t} + ax^{(1)} = b \tag{13}$$

where a and b are referred as the development coefficient and grey action quantity, respectively. Using the difference instead of differential form, $\Delta t = (t+1) - t = 1$, as in (13), it can be rewritten as $x^{(1)}(i+1) - x^{(1)}(i) + ax^{(1)}(i+1) = b$, which is the basic form of the fractional-order accumulation GM $(1,1)$. The matrix form can be given as

$$\begin{bmatrix} x^{(1)}(2) - x^{(1)}(1) \\ x^{(1)}(3) - x^{(1)}(2) \\ \vdots \\ x^{(1)}(m) - x^{(1)}(m-1) \end{bmatrix} = \begin{bmatrix} -x^{(1)}(2) & 1 \\ -x^{(1)}(3) & 1 \\ \vdots & 1 \\ -x^{(1)}(m) & 1 \end{bmatrix} \begin{bmatrix} a \\ b \end{bmatrix} \tag{14}$$

Suppose

$$xx(j) = \frac{\Gamma(m-j+k)}{\Gamma(m-j+1)\Gamma(k)} x(j) = w_j x(j) \quad j = 1, 2, \cdots, m.$$

By using the least squares to estimate the model as in (14), it satisfies that

$$[a \quad b]^T = B^{-1} Y \tag{15}$$

where

$$B = \begin{bmatrix} -x^{(1)}(2) & 1 \\ -x^{(1)}(3) & 1 \\ \vdots & \vdots \\ -x^{(1)}(m) & 1 \end{bmatrix}$$

$$= \begin{bmatrix} -\sum_{j=1}^{2} \frac{\Gamma(m-j+k)}{\Gamma(m-j+1)\Gamma(k)} x(j) & 1 \\ -\sum_{j=1}^{3} \frac{\Gamma(m-j+k)}{\Gamma(m-j+1)\Gamma(k)} x(j) & 1 \\ \vdots & \vdots \\ -\sum_{j=1}^{m} \frac{\Gamma(m-j+k)}{\Gamma(m-j+1)\Gamma(k)} x(j) & 1 \end{bmatrix}$$

$$= \begin{bmatrix} 1 & 1 & 0 & \cdots & 0 \\ 1 & 1 & 1 & \cdots & 0 \\ \vdots & \vdots & \vdots & \ddots & \vdots \\ 1 & 1 & 1 & \cdots & 1 \end{bmatrix}_{(m-1)\times m} \begin{bmatrix} -xx(1) & 1 \\ -xx(2) & 0 \\ \vdots & \vdots \\ -xx(m) & 0 \end{bmatrix}_{m\times 2}$$

$$Y = [x^{(1)}(2) - x^{(1)}(1), x^{(1)}(3) - x^{(1)}(2), \cdots, \\ x^{(1)}(m) - x^{(1)}(m-1)]^T.$$

If $k = 1$, the model by (15) becomes the traditional one-order GM $(1,1)$.

Denote the fractional-order accumulation generated sequence by $x^{(1)}$ and $z^{(1)}$, $z^{(1)}$ is the average value of the adjacent neighbors of $x^{(1)}(k)$ and it can be expressed as

$$z^{(1)}(i) = \frac{x^{(1)}(i) + x^{(1)}(i+1)}{2}, \quad i = 1, 2, \cdots, m-1.$$

The matrix form is

$$\begin{bmatrix} x^{(1)}(2) - x^{(1)}(1) \\ x^{(1)}(3) - x^{(1)}(2) \\ \vdots \\ x^{(1)}(m) - x^{(1)}(m-1) \end{bmatrix} = \begin{bmatrix} -z^{(1)}(2) & 1 \\ -z^{(1)}(3) & 1 \\ \vdots & \vdots \\ -z^{(1)}(m) & 1 \end{bmatrix} \begin{bmatrix} a \\ b \end{bmatrix} \tag{16}$$

By using the least squares to estimate the model in equation (16), the parameters which also satisfies as in (15) are

$$B = \begin{bmatrix} -\frac{1}{2} & -\frac{1}{2} & 0 & \cdots & 0 & 0 \\ 0 & -\frac{1}{2} & -\frac{1}{2} & \cdots & 0 & 0 \\ \vdots & \vdots & \vdots & \ddots & \vdots & \vdots \\ 0 & 0 & 0 & \cdots & -\frac{1}{2} & -\frac{1}{2} \end{bmatrix}_{(m-1)\times m}$$

$$\begin{bmatrix} 1 & 0 & \cdots & 0 \\ 1 & 1 & \cdots & 0 \\ \vdots & \vdots & \ddots & \vdots \\ 1 & 1 & \cdots & 1 \end{bmatrix}_{m\times m} \begin{bmatrix} xx(1) & -1 \\ xx(2) & 0 \\ \vdots & \vdots \\ xx(m) & 0 \end{bmatrix}_{m\times 2}$$

$$= \begin{bmatrix} -\frac{1}{2} & -\frac{1}{2} & 0 & \cdots & 0 & 0 \\ 0 & -\frac{1}{2} & -\frac{1}{2} & \cdots & 0 & 0 \\ \vdots & \vdots & \vdots & \ddots & \vdots & \vdots \\ 0 & 0 & 0 & \cdots & -\frac{1}{2} & -\frac{1}{2} \end{bmatrix}_{(m-1)\times m}$$

$$\begin{bmatrix} w_1 & 0 & \cdots & 0 \\ w_1 & w_2 & \cdots & 0 \\ \vdots & \vdots & \ddots & \vdots \\ w_1 & w_2 & \cdots & w_m \end{bmatrix}_{m\times m} \begin{bmatrix} x^{(0)}(1) & -\frac{1}{w_1} \\ x^{(0)}(2) & 0 \\ \vdots & \vdots \\ x^{(0)}(m) & 0 \end{bmatrix}_{m\times 2}$$

$$Y = [x^{(1)}(2) - x^{(1)}(1), x^{(1)}(3) - x^{(1)}(2), \ldots, x^{(1)}(m) - x^{(1)}(m-1)]^T.$$

IV. Fractional Accumulation GM (1, 1) Predictor Theory

A. Prediction Theory

Suppose the original data and the fractional-order accumulation generated sequence are $(x^{(0)}(1), x^{(0)}(2), \cdots, x^{(0)}(m))$, $(x^{(1)}(1), x^{(1)}(2), \cdots, x^{(1)}(m))$ and $(z^{(1)}(1), z^{(1)}(2), \cdots, z^{(1)}(m))$. $z^{(1)}(i) = [x^{(1)}(i) + x^{(1)}(i+1)]/2$, $i = 1, 2, \cdots, m-1$. For $0 < k \leq 1$, the estimated data from the model can be obtained by (12) and $\hat{x}^{(0)} = (\hat{x}^{(0)}(1), \hat{x}^{(0)}(2), \cdots, \hat{x}^{(0)}(m))$. The estimated prediction data $x^{(0)}(m+1)$ can be obtained from the following equation.

$$\hat{x}^{(0)}(m+1) = x^{(1)}(m+1) - \sum_{j=1}^{m} \frac{\Gamma(m+1-j+k)}{\Gamma(m-j+2)\Gamma(k)} \hat{x}^{(0)}(j) \tag{17}$$

The relative error is defined as

$$\begin{aligned} \Delta &= \left| \frac{\hat{x}^{(0)} - x^{(0)}}{x^{(0)}} \right| \times 100\% \\ &= \Bigg(\left| \frac{\hat{x}^{(0)}(1) - x^{(0)}(1)}{x^{(0)}(1)} \right| \times 100\%, \left| \frac{\hat{x}^{(0)}(2) - x^{(0)}(2)}{x^{(0)}(2)} \right| \\ &\quad \times 100\%, \cdots, \left| \frac{\hat{x}^{(0)}(m) - x^{(0)}(m)}{x^{(0)}(m)} \right| \times 100\% \Bigg) \end{aligned} \tag{18}$$

and $\overline{\Delta} = \frac{1}{m} \sum_{i=1}^{m} \Delta_i$ is the average relative error for the series modeling.

GA is a stochastic technique and popularly used in the optimization problems. It is inspired by the natural genetics and biological evolutionary process. Reproduction, crossover and mutation are three basic operators used to manipulate the genetic composition of a population. GA evaluates a population and generates a new one iteratively with each successive population (generation) [33]. In this paper, the fitness function is the minimization of the average model error and $\min_k \overline{\Delta} = \frac{1}{m} \sum_{i=1}^{m} \Delta_i$.

B. Modified Predictor Model

The model residual sequence can be written as

$$\begin{aligned} \varepsilon^{(0)} &= (\varepsilon^{(0)}(2), \varepsilon^{(0)}(3), \cdots, \varepsilon^{(0)}(m))^{\mathrm{T}} \\ &= (x^{(0)}(2) - \hat{x}^{(0)}(2), x^{(0)}(3) - \hat{x}^{(0)}(3), \cdots, \\ &\quad x^{(0)}(m) - \hat{x}^{(0)}(m))^T \end{aligned}$$

The periodical feature hidden in the residual series can be extracted by the Fourier series and it is

$$\begin{aligned} &\varepsilon^{(0)}(j) = 0.5a_0 + \sum_{i=1}^{z} \left[a_i \cos \frac{2\pi i}{T} j + b_i \sin \frac{2\pi i}{T} j \right] \\ &j = 2, 3, \cdots, m, T = m-1, z = [(m-1)/2] - 1 \end{aligned} \tag{19}$$

where z is the integral part of $(m-1)/2 - 1$. It can be also written in the matrix form as below [25], [34].

$$\begin{bmatrix} \varepsilon^{(0)}(2) \\ \varepsilon^{(0)}(3) \\ \vdots \\ \varepsilon^{(0)}(m) \end{bmatrix} = \begin{bmatrix} 0.5 & \cos \frac{4\pi}{T} & \sin \frac{4\pi}{T} & \cdots & \cos \frac{4\pi z}{T} & \sin \frac{4\pi z}{T} \\ 0.5 & \cos \frac{6\pi}{T} & \sin \frac{6\pi}{T} & \cdots & \cos \frac{6\pi z}{T} & \sin \frac{6\pi z}{T} \\ \vdots & \vdots & \vdots & \ddots & \vdots & \vdots \\ 0.5 & \cos \frac{2m\pi}{T} & \sin \frac{2m\pi}{T} & \cdots & \cos \frac{2m\pi z}{T} & \sin \frac{2m\pi z}{T} \end{bmatrix} \begin{bmatrix} a_0 \\ a_1 \\ b_1 \\ \vdots \\ a_z \\ b_z \end{bmatrix} \tag{20}$$

If

$$P = \begin{bmatrix} 0.5 & \cos \frac{4\pi}{T} & \sin \frac{4\pi}{T} & \cdots & \cos \frac{4\pi z}{T} & \sin \frac{4\pi z}{T} \\ 0.5 & \cos \frac{6\pi}{T} & \sin \frac{6\pi}{T} & \cdots & \cos \frac{6\pi z}{T} & \sin \frac{6\pi z}{T} \\ \vdots & \vdots & \vdots & \ddots & \vdots & \vdots \\ 0.5 & \cos \frac{2m\pi}{T} & \sin \frac{2m\pi}{T} & \cdots & \cos \frac{2m\pi z}{T} & \sin \frac{2m\pi z}{T} \end{bmatrix},$$

$C = \begin{bmatrix} a_0 \\ a_1 \\ b_1 \\ \vdots \\ a_z \\ b_z \end{bmatrix}$, then the matrix can be written as $\varepsilon^{(0)} = PC$.

Based on the least square method, $\hat{C} = (P^T P)^{-1} P^T \varepsilon^{(0)}$. Therefore, the estimated residual error can be given as

$$\begin{aligned} &\hat{\varepsilon}^{(0)}(j) = 0.5\hat{a}_0 + \sum_{i=1}^{z} \left[\hat{a}_i \cos \frac{2\pi i}{T} j + \hat{b}_i \sin \frac{2\pi i}{T} j \right] \\ &j = 2, 3, \cdots, m, T = m-1, z = \frac{[m-1]}{2} - 1 \end{aligned} \tag{21}$$

The modified model output $\hat{x}_F^{(0)}(j)$ by Fourier series is

$$\hat{x}_F^{(0)}(j) = \hat{x}^{(0)}(j) + \hat{\varepsilon}^{(0)}(j) \tag{22}$$

The process of calculating modified optimal fractional accumulation GM (1, 1) is:

(1)

1) Use GA to find the optimal fractional-order model with the minimization of the average relative error for modeling;
2) Analyze the estimated residual error using Fourier series;
3) Obtain the modified prediction model;
4) Analyze the model and the prediction results.

C. State Space Model for Prediction

For the data sequence $x(j)$ $j = 1, 2, \cdots, m$, suppose we obtain the optimal fractional accumulation data sequence $x^{(1)}$ by GA, the fractional-order accumulation GM (1, 1) can be also represented by the state variable and the form is

$$\begin{aligned} x^{(1)}(n+1) &= A^{(1)}x^{(1)}(n) + B^{(1)}u(n) \\ y^{(1)}(n+1) &= x^{(1)}(n+1) \end{aligned} \tag{23}$$

where $x^{(1)}$ is the state variable vector and

$$x^{(1)}(n) = \sum_{j=1}^{n} {}^{(k)}x^{(0)}(j) = \sum_{j=1}^{n} \frac{\Gamma(n-j+k)}{\Gamma(n-j+1)\Gamma(k)} x(j),$$

y is the output variable, u is the input variable and equal to 1. Compared with the basic fractional accumulation GM (1, 1), when the model form is $x^{(1)}(i+1) - x^{(1)}(i) + ax^{(1)}(i+1) = b$, $A^{(1)} = 1/(1+a), B^{(1)} = b/(1+a)$. When the model form is $x^{(1)}(i+1) - x^{(1)}(i) + az^{(1)}(i+1) = b$, $A^{(1)} = (2-a)/(2+a), B^{(1)} = b/(2+a)$. For $n < m$ and $n \geq m$, the state space model becomes a constructing and predicting model equation respectively.

As in (23), it can be also written as

$$\sum_{j=1}^{n+1} {}^{(k)}x^{(0)}(j) = A^{(1)} \sum_{j=1}^{n} {}^{(k)}x^{(0)}(j) + B^{(1)}u(n)$$

and

$$x^{(0)}(n+1) = A^{(0)}x^{(0)}(n) + B^{(0)}u(n) + \omega(n) \tag{24}$$

where, $A^{(0)} = A^{(1)} - \frac{k}{\Gamma(2)}, B^{(0)} = B^{(1)}, \omega(n) = \sum_{j=1}^{n-1} \frac{A^{(1)}\Gamma(n-j+k)\Gamma(n-j+2) - \Gamma(n-j+1)\Gamma(n-j+k+1)}{\Gamma(n-j+1)\Gamma(n-j+2)\Gamma(k)} x^{(0)}(j)$.

The solution of (23) can be obtained using irritation method, and

$$x^{(1)}(n) = \Phi(n,1)x(1) + \sum_{j=1}^{n-1} \Phi(n, j+1)B^{(1)}(j)u(j),$$

where, $\Phi(n,p) = A^{(1)}(n-1)A^{(1)}(n-2)...A^{(1)}(p)$, $\Phi(p,p) = I$. For $n < m$, take a difference operation on the left and right side in (23), then the difference of the state space equation can be written as:

$$\begin{aligned} \Delta x^{(1)}(n+1) &= A^{(1)}\Delta x^{(1)}(n) \\ y^{(1)}(n+1) - y^{(1)}(n) &= \Delta x^{(1)}(n+1) \\ &= A^{(1)}(x^{(1)}(n) - x^{(1)}(n-1)). \end{aligned}$$

The modeling process in (23) can be rewritten as

$$\begin{aligned} \begin{bmatrix} \Delta x^{(1)}(n+1) \\ y^{(1)}(n+1) \end{bmatrix} &= \begin{bmatrix} A^{(1)} & O_m^T \\ A^{(1)} & 1 \end{bmatrix} \begin{bmatrix} \Delta x^{(1)}(n) \\ y^{(1)}(n) \end{bmatrix} \\ y^{(1)}(n) &= \begin{bmatrix} O_m & 1 \end{bmatrix} \begin{bmatrix} \Delta x^{(1)}(n) \\ y^{(1)}(n) \end{bmatrix} \end{aligned},$$

where $O_m = \begin{bmatrix} 0 & 0 & \cdots & 0 \end{bmatrix}$. Define new variables $y(k)$ and $z(k) = \begin{bmatrix} \Delta x^{(1)}(k) \\ y^{(1)}(k) \end{bmatrix}$. It can be also given as

$$\begin{aligned} z(k+1) &= Az(k) \\ y(k) &= Cz(k) \end{aligned},$$

where $A = \begin{bmatrix} A^{(1)} & O_m^T \\ A^{(1)} & 1 \end{bmatrix}$, $C = \begin{bmatrix} O_m & 1 \end{bmatrix}$.

The characteristic equation of A can be calculated as

$$\begin{aligned} \det(\lambda I - A) &= \det \begin{bmatrix} \lambda I - A^{(1)} & -O_m^T \\ -A^{(1)} & \lambda I - 1 \end{bmatrix} \\ &= (\lambda - 1)\det(\lambda I - A^{(1)}). \end{aligned}$$

The future state variables for the prediction can be calculated from the following equation. That is $Y = Fz(k)$, where $F = \begin{bmatrix} A \\ A^2 \\ ... \\ A^h \end{bmatrix}$ and h is number of samples predicted for the future state variables.

Base on the Fourier series, the modified state space model for prediction is given as

$$\begin{aligned} \hat{x}(n+1) &= \hat{A}\hat{x}(n) + \hat{B}u(n) + e(n+1) \\ \hat{y}(n+1) &= \hat{x}(n+1) \end{aligned} \tag{25}$$

where,

$$e(n+1) = 0.5\hat{a}_0 + \sum_{i=1}^{z} \left[\hat{a}_i \cos\frac{2\pi i}{T}(n+1) + \hat{b}_i \sin\frac{2\pi i}{T}(n+1) \right].$$

V. Fractional-order Grey Model

The fractional form for continuous data of GM (1, 1) model is defined as GM $(\alpha, 1)$, and it is

$$\frac{\mathrm{d}^\alpha x}{\mathrm{d}t^\alpha} + ax = b \tag{26}$$

where a and b are referred as the development coefficient and grey action quantity, respectively, the fractional-order α should be more than zero and the number of variables is one. It can also be written as

$$D_t^\alpha x + ax = b, \quad \text{or} \quad \frac{1}{b}D_t^\alpha x + \frac{a}{b}x = 1.$$

The state space representation for GM $(\alpha, 1)$ is

$$\begin{aligned} D_t^\alpha x(t) &= Ax(t) + Bu(t) \\ y(t) &= x(t) \end{aligned}$$

where $A, B, u(t)$ are the state, input and output vectors of the system and $A = -a, B = b, u(t) = 1$.

In order to simplify the problem, here, we only consider the zero initial condition. The model solution can be obtained by using Laplace transform $X(s) = \frac{b}{s(s^{\alpha}+a)}$ and

$$x(t) = b\varepsilon_0(t, -a; \alpha, \alpha+1) = bt^{\alpha}E_{\alpha,\alpha+1}(-at^{\alpha}),$$

where

$$\varepsilon_k(t, \lambda; \mu, v) = t^{\mu k+v-1}E^{(k)}_{\mu,v}(\lambda t^{\mu})(k = 0, 1, 2, \cdots)$$

is the Mittag-Leffler type introduced by Podlubny.

If $x^{(0)} = (x^{(0)}(1), x^{(0)}(2), \cdots, x^{(0)}(m))$ is a sequence of raw data which are usually non-negative values, its fractional-order accumulation generated sequence is given by $x^{(1)} = (x^{(1)}(1), x^{(1)}(2), \cdots, x^{(1)}(m))$, then $D^{\alpha}_t x^{(1)} + ax^{(1)} = b$ is referred to fractional-order whitenization or image equation of the GM$(\alpha, 1)$.

By using forward difference with G-L definition, the following equation is obtained [35] which can be used for the discretization of continuous models.

$$\begin{aligned} D^{\alpha}x(kT) &\approx \frac{1}{T^{\alpha}}\sum_{i=0}^{k+1}(-1)^i\begin{pmatrix}\alpha\\ i\end{pmatrix}x((k+1-i)T)\\ &= \frac{1}{T^{\alpha}}(x((k+1)T) - \begin{pmatrix}\alpha\\ 1\end{pmatrix}x(kT)\\ &+\sum_{i=2}^{k+1}(-1)^i\begin{pmatrix}\alpha\\ i\end{pmatrix}x((k+1-i)T) \end{aligned} \tag{27}$$

VI. Simulation Experiments

Consider a discrete sequence $x^{(0)}(j) = (1, 2, 3, 4, 5), j = 1, 2, \cdots, 5$. The results of fractional-order weighted factor and accumulation generated sequence can be seen from Fig. 1 and Fig. 2. The fractional-order in the range of zero and one could model the system well compared with one-order generation and obey the new information priority rule.

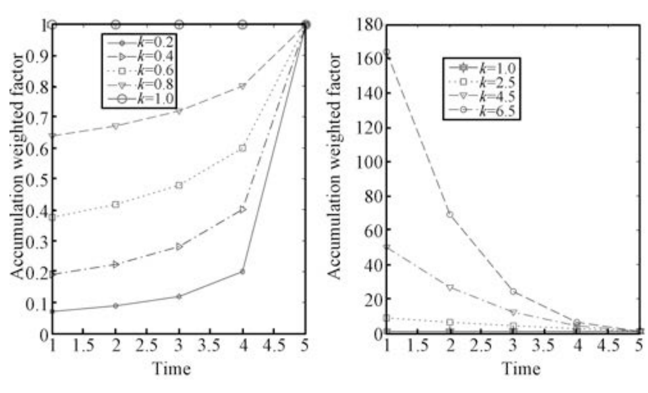

Fig. 1. Weighted factor with fractional-order less than and larger than one.

The original data of main indicators on internet development (based on number of users) taken at the end of years (2006-2012), from China statistical yearbook-2013, People's Republic of China National Bureau of Statistics, which can be seen in Table I. The model and error analysis results based on two models with fractional-order from 0.1 to 1.0 can be seen from Fig. 3 and Fig. 4, the prediction result and error analysis also show the predictor has better performance than the traditional GM$(1, 1)$. The modified model result using Fourier series can be seen in Fig. 5 and Fig. 6. The optimal model and prediction result are obtained and can be seen in Fig. 7 and Fig. 8. The state space model for optimal order result is given in Table II. Error analysis of different fractional-order accumulations using Fourier series are given in Table III. The data of modified optimal fractional-order accumulation model can be seen in Table IV. In Table III, we can see that the average model and prediction error in the classical GM$(1, 1)$ is larger than fractional-order accumulation ones. The modified model has better results than the traditional ones without using Fourier series in modeling and prediction. From Table IV, the modified GM using optimal fractional-order accumulation can obtain good performance compared with some classical GMs.

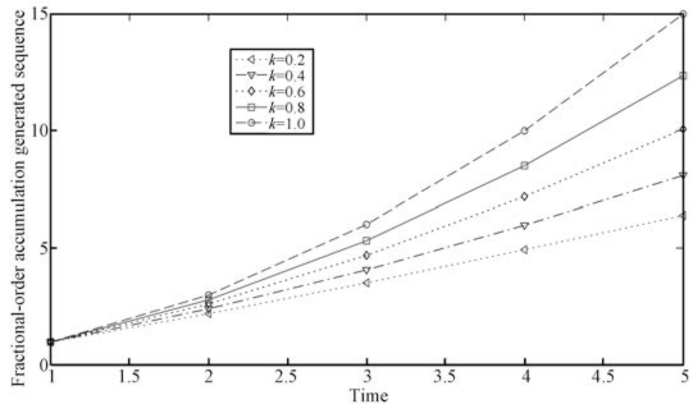

Fig. 2. Accumulation generated sequence with fractional-order.

Table I
Original Data of Number of Users Taken at the and of Years

Year	2006	2007	2008	2009	2010	2011	2012
Number of Internet Users (10^6 persons)	137.0	210.0	298.0	384.0	457.3	513.1	564.0

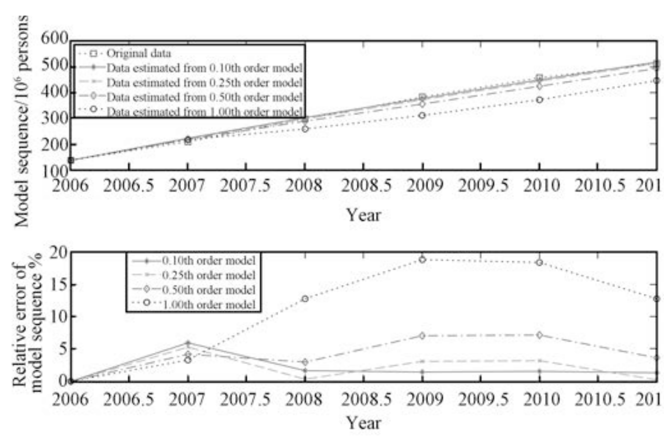

Fig. 3. Internet data modeling and error analysis using $x^{(1)}(k+1) - x^{(1)}(k) + ax^{(1)}(k+1) = b$.

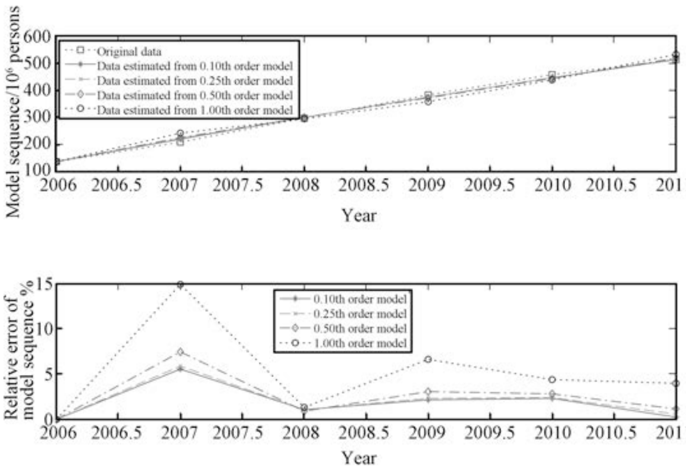

Fig. 4. Internet data modeling and error analysis using $x^{(1)}(k+1) - x^{(1)}(k) + az^{(1)}(k+1) = b$.

Table II
STATE SPACE MODEL FOR OPTIMAL ORDER

GM model	Optimal order	$A^{(1)}$	$B^{(1)}$	A	C
$x^{(1)}(k+1) - x^{(1)}(k) + ax^{(1)}(k+1) = b$	0.2311	1.0112	114.9412	$\begin{bmatrix} 1.0112 & 0 \\ 1.0112 & 1 \end{bmatrix}$	$\begin{bmatrix} 0 & 1 \end{bmatrix}$
$x^{(1)}(k+1) - x^{(1)}(k) + az^{(1)}(k+1) = b$	1.6736×10^{-5}	0.9427	46.1318	$\begin{bmatrix} 0.9427 & 0 \\ 0.9427 & 1 \end{bmatrix}$	$\begin{bmatrix} 0 & 1 \end{bmatrix}$

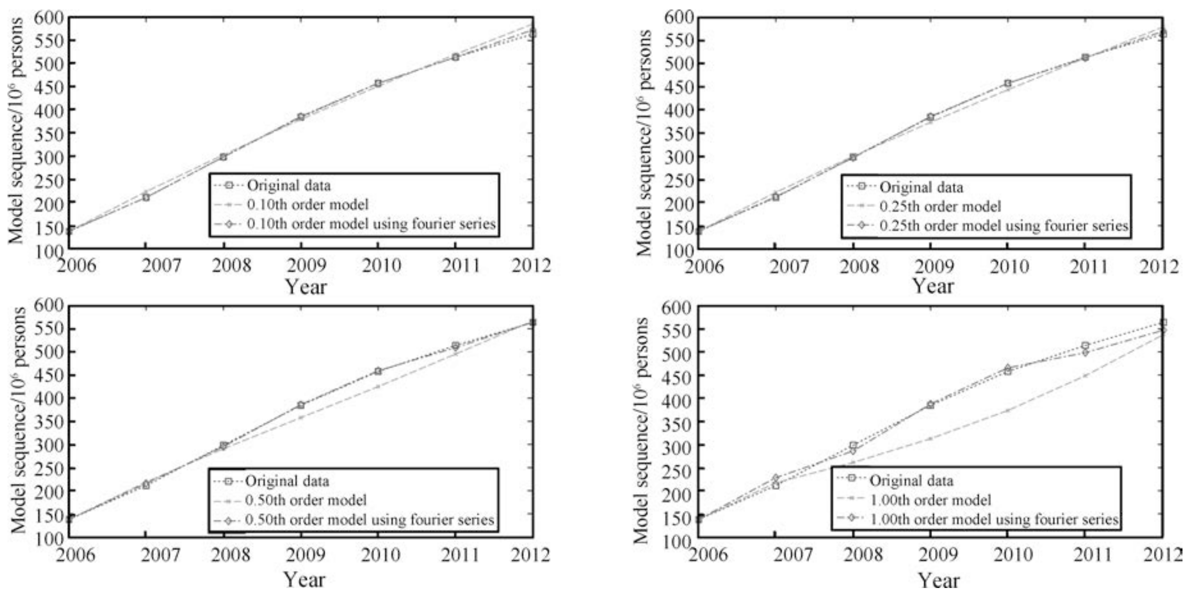

Fig. 5. Modified model output of internet data modeling using Fourier series analysis based on $x^{(1)}(k+1) - x^{(1)}(k) + ax^{(1)}(k+1) = b$.

Table III
ERROR ANALYSIS USING SERIES OF INTERNET DEVELOPMENT

order	method	$x^{(1)}(k+1) - x^{(1)}(k) + ax^{(1)}(k+1) = b$ Δ (%)	Δ_7 (%)	$x^{(1)}(k+1) - x^{(1)}(k) + az^{(1)}(k+1) = b$ Δ (%)	Δ_7 (%)
0.10	common	1.9236	3.7190	1.8549	2.5575
	Fourier series	0.1118	1.5075	0.1927	0.6877
0.25	common	1.9736	2.7617	2.0085	3.4366
	Fourier series	0.2456	1.0420	0.1693	1.3721
0.50	common	4.1491	0.5578	2.5374	5.7856
	Fourier series	0.8681	0.1029	0.2047	3.1108
0.75	common	7.2293	2.1057	3.4459	9.6037
	Fourier series	1.7676	1.5565	0.3419	5.8862
0.80	common	7.9322	2.6635	3.6752	10.5827
	Fourier series	1.9792	1.8657	0.3842	6.5982
0.90	common	9.4185	3.7836	4.3567	12.7859
	Fourier series	2.4345	2.4880	0.0168	8.2046
1.00	common	11.0073	4.8934	5.1734	15.3407
	Fourier series	2.9336	3.1033	0.6211	10.0767

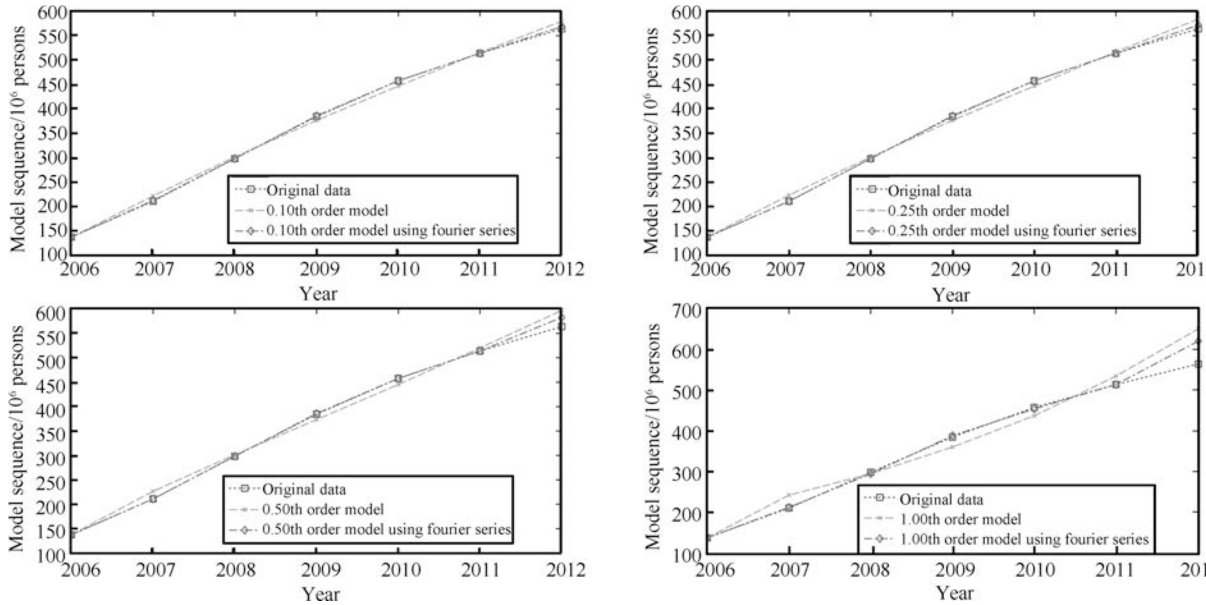

Fig. 6. Modified model output of internet data modeling using Fourier series analysis based on $x^{(1)}(k+1)-x^{(1)}(k)+az^{(1)}(k+1)=b$.

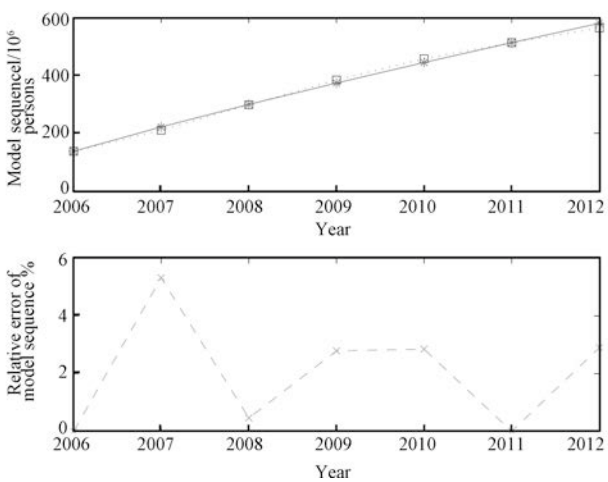

Fig. 7. Internet data optimal modeling and error analysis using $x^{(1)}(k+1)-x^{(1)}(k)+ax^{(1)}(k+1)=b$.

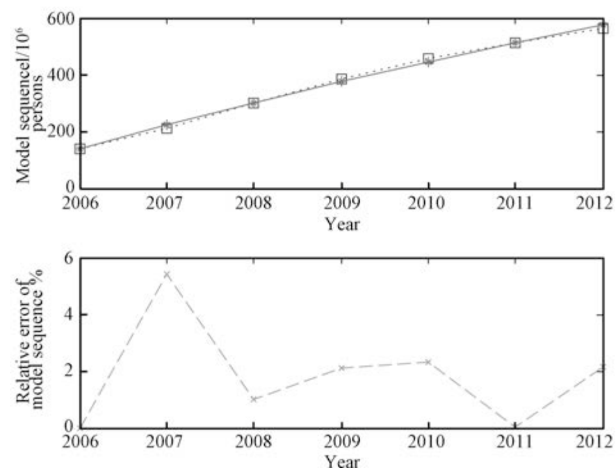

Fig. 8. Internet data optimal modeling and error analysis using $x^{(1)}(k+1)-x^{(1)}(k)+az^{(1)}(k+1)=b$.

Table IV
OPTIMAL MODEL ANALYSIS AND PREDICTION RESULT DATA USING GA BY FOURIER SERIES

$x^{(1)}(k+1)-x^{(1)}(k)+ax^{(1)}(k+1)=b$	$\overline{\Delta}$(%)	Prediction value	Δ_7(%)
GA method	1.9044	580.3567	2.9001
GA method by Fourier series	0.2176	570.2651	1.1108
One-order accumulation GM(1,1)	11.0073	536.4013	4.8934
$x^{(1)}(k+1)-x^{(1)}(k)+az^{(1)}(k+1)=b$	$\overline{\Delta}$(%)	Prediction value	Δ_7(%)
GA method	1.8126	576.0692	2.1399
GA method by Fourier series	0.2240	565.9218	0.3407
One-order accumulation GM(1,1)	5.1734	650.5216	15.3407
Model	$\overline{\Delta}$(%)	Prediction value	Δ_7(%)
DGM(1,1)	5.7740	653.7459	15.9124
Model	$\overline{\Delta}$(%)	Prediction value	Δ_7(%)
DGM(2,1)	11.0738	618.3561	9.6376

From the above results, the model prediction performance can be greatly improved by Fouries series method, and the modified optimal predictor could describe the system more precisely than the traditional GM(1,1) in model construction and prediction. The difference of $x^{(1)}(k+1)-x^{(1)}(k)+ax^{(1)}(k+1)=b$ and $x^{(1)}(k+1)-x^{(1)}(k)+az^{(1)}(k+1)=b$ is that the latter model considers the neighbour information in the data modeling. From the optimal order analysis and other data results, when the model is different, the optimal fractional-order is also different for the same problem. Several other results also show the proposed method of fractional accumulation order using GA by Fourier series can improve the model performance greatly and can be perfectly put into the application of predictor design and model construction.

VII. Conclusion

Fractional calculus studies the possibility of differentiation and integration with arbitrary real or complex orders of the differential operator. The fractional-order accumulation model can mine the data information more precisely than the classical order, which can reduce the randomness of the original data and exhibit better performance. The GM$(1,1)$ predictor based on the fractional-order accumulation has more degrees of freedom and better performance compared with the traditional one-order GM. The modified optimal fractional-order accumulation method can be used to ameliorate the model performance and improve the accuracy of predictor. The GM$(\alpha,1)$ application scope will also be enlarged with more freedom. The proposed method can be widely used in data processing, modeling theory, multi-step prediction, predictor design and related fields. The discrete and continuous forms for GM by fractional calculus, other forms of GMs by fractional accumulation, for example, delay model, power exponent model and feedback model, which also need our further researches.

References

[1] Deng J L. The introduction of grey system. *The Journal of Grey System*, 1982, **1**(1): 1−24

[2] Lee Y C, Wu C H, Tsai S B. Grey system theory and fuzzy time series forecasting for the growth of green electronic materials. *International Journal of Production Research*, 2014, **52**(10): 2931−2945

[3] Wang X, Qi L, Chen C, et al. Grey System Theory based prediction for topic trend on Internet. *Engineering Applications of Artificial Intelligence*, 2014, 29: 191−200

[4] Liu X, Peng H, Bai Y, et al. Tourism Flows Prediction based on an Improved Grey GM (1, 1) Model. *Procedia-Social and Behavioral Sciences*, 2014, 138: 767−775

[5] Xiao X P, Guo H, Mao S H. The modeling mechanism, extension and optimization of grey GM (1, 1) model. *Applied Mathematical Modelling*, 2014, **38**(5): 1896−1910

[6] Abbasbandy S, Hashemi M S, Hashim I. On convergence of homotopy analysis method and its application to fractional integro-differential equations. *Quaestiones Mathematicae*, 2013, **36**(1): 93−105.

[7] Garrappa R, Popolizio M. Exponential quadrature rules for linear fractional differential equations. *Mediterranean Journal of Mathematics,* 2013, **12**(1): 219−244

[8] Shen S, Liu F, Anh V, et al. Detailed analysis of a conservative difference approximation for the time fractional diffusion equation. *Journal of Applied Mathematics and Computing*, 2006, **22**(3): 1−19

[9] Abdelkawy M A, Taha T M. An operational matrix of fractional derivatives of Laguerre polynomials. *Walailak Journal of Science and Technology (WJST)*, 2014, **11**(12): 1041−1055

[10] Xue D Y, Zhao C N, Pan F. Simulation model method and application of fractional order nonlinear system. *Journal of System Simulation*, 2006, **9**(18): 2405−2408

[11] Valerio D, Costa.J. Ninteger: A non-integer control toolbox for Matlab. *1st IFAC Workshop on Fractional Differentiation and its Applications*. France: Bordeaux, 2004. 208−213

[12] Tepljakov A, Petlenkov E, Belikov J. FOMCON: a MATLAB toolbox for fractional-order system identification and control. *International Journal of Microelectronics and Computer Science*, 2011, **2**(2): 51−62

[13] Rachid M, Maamar B, Said D. Comparison between two approximation methods of state space fractional systems. *Signal Processing*, 2011, **91**(3): 461−469

[14] Sabatier J, Farges C, Trigeassou J C. Fractional systems state space description: some wrong ideas and proposed solutions. *Journal of Vibration and Control*, 2014, **20**(7): 1076−1084

[15] Ahn H S, Chen Y Q, Podlubny I. Robust stability test of a class of linear time-invariant interval fractional-order system using Lyapunov inequality. *Applied Mathematics and Computation*, 2007, **187**(1): 27−34

[16] Victor S, Malti R, Garnier H, et al. Parameter and differentiation order estimation in fractional models. *Automatica*. 2013, **49**(4): 926−935

[17] Wu L F, Liu S F, Liu J. GM(1,1) model based on fractional order accumulating method and its stability. *Control and Decision*, 2014, **29**(5): 919−924

[18] Wu L, Liu S, Yao L, et al. Grey system model with the fractional order accumulation. *Communications in Nonlinear Science and Numerical Simulation*, 2013, **18**(7): 1775−1785

[19] Wu L F, Liu S F, Cui W, et al. Non-homogenous discrete grey model with fractional-order accumulation. *Neural Computing and Applications*, 2014, **25**(5): 1215−1221

[20] Wu L, Liu S, Yao L, et al. Using fractional order accumulation to reduce errors from inverse accumulated generating operator of grey model. *Soft Computing*, 2015, **19**(2): 483−488.

[21] Liu J F, Liu S F, Wu L F, et al. Fractioanl order reverse accumulative discrete grey model and its application. *Systems Engineering and Electronics*, 2016, **38**(3): 719−724

[22] Mao S H, Cao M Y, Xiao X P. Frational order accumulation time-lag GM(1,N,τ) model and its application. *Systems Engineering-Theroy & Practice*, 2015, **35**(2): 430−436

[23] Hsu L C. Applying the grey prediction model to the global integrated circuit industry. *Technological Forecasting and Social Change*, 2003, **70**(6): 563−574

[24] Liang M T, Zhao G F, Chang C W, et al. Evaluating the carbonation damage to concrete bridges using a grey forecasting model combined with a statistical method. *Journal of the Chinese Institute of Engineers*, 2001, **24**(1): 85−94

[25] Wang Z X. Grey forecasting method for small sample oscillating sequences based on Fourier series. *Control and Decision*, 2014, **29**(5): 270−274

[26] Benson D A, Meerschaert M M, Revielle J. Fractional calculus in hydrologic modeling: A numerical perspective. *Advances in water resources*, 2013, 51: 479−497

[27] Sabatier J, Lanusse P, Melchior P, et al. Fractional Order Differentiation and Robust Control Design: CRONE. *H-infinity and Motion Control*. New York: Springer, 2015. 1−10

[28] Yucra E A, Yuz J I, Goodwin G C. Sampling zeros of discrete models for fractional order systems. *Automatic Control, IEEE Transactions on*. 2013, **58**(9): 2383−2388

[29] Cao D A. *Theory of Accumulation*. Beijing: Science Press, 2011. 163−177

[30] Chen C I, Huang S J. The necessary and sufficient condition for GM (1,1) grey prediction model. *Applied Mathematics and Computation*. 2013, **219**(11): 6152−6162

[31] Liu S F, Lin Y. *Grey information: theory and practical applications*. London: Springer-Verlag, 2006. 194−216

[32] Xiao X P, Mao S H. *Grey prediction and decision methods*. Beijing: Science Press, 2013. 165−201

[33] Moradi M H, Abedini M. A combination of genetic algorithm and particle swarm optimization for optimal DG location and sizing in distribution systems. *International Journal of Electrical Power & Energy Systems*, 2012, **34**(1): 66−74

[34] Lin Y H, Lee P C. *Novel high-precision grey forecasting model*. Automation in construction, 2007, **16**(6): 771−777

[35] Monje C A, Chen Y Q, Vinagre B M. *Fractional-order systems and controls-fundamentals and applications*. London: Springer-Verlag, 2010. 60−65

Yang Yang graduated from Northeast Normal university(NENU),China, in 2006. She received the Master degree from NENU in 2009. She is currently a Ph. D. candidate at Northeastern University. Her main research interests are signal processing and fractional-order control.

Dingyü Xue received the Ph. D. degree from University of Sussex (UK). Now he is a professor at Northeastern University. His main research interests include fractional-order control system modeling, simulation and computer aided design, robot control and computer vision.

Applications of Fractional Lower Order Time-Frequency Representation to Machine Bearing Fault Diagnosis

Junbo Long, Haibin Wang, Peng Li and Hongshe Fan

***Abstract*—The machinery fault signal is a typical non-Gaussian and non-stationary process. The fault signal can be described by $S\alpha S$ distribution model because of the presence of impulses. Time-frequency distribution is a useful tool to extract helpful information of the machinery fault signal. Various fractional lower order (FLO) time-frequency distribution methods have been proposed based on fractional lower order statistics, which include fractional lower order short time Fourier transform (FLO-STFT), fractional lower order Wigner-Ville distributions (FLO-WVDs), fractional lower order Cohen class time-frequency distributions (FLO-CDs), fractional lower order adaptive kernel time-frequency distributions (FLO-AKDs) and adaptive fractional lower order time-frequency auto-regressive moving average (FLO-TFARMA) model time-frequency representation method. The methods and the exiting methods based on second order statistics in $S\alpha S$ distribution environments are compared, simulation results show that the new methods have better performances than the existing methods. The advantages and disadvantages of the improved time-frequency methods have been summarized. Last, the new methods are applied to analyze the outer race fault signals, the results illustrate their good performances.**

***Index Terms*—Alpha stable distribution; non-stationary signal; adaptive function; auto-regressive (AR) model; parameter estimation; time frequency representation.**

I. Introduction

THe machinery vibration signal is a non-stationary signal, its spectrum characteristic changes with the time. The time-frequency analysis is a powerful tool to provide the frequency spectrum information for the non-stationary signals. The traditional short time Fourier transform (STFT) time-frequency distributions[1], Wigner-Ville distributions (WVDs)[2], wavelet transform (WT) time-frequency[3], Hilbert-Huang transform (HHT) time-frequency[4−6], the time-frequency analysis methods have been widely used in mechanical fault diagnosis. Recently, some improved methods based on traditional time-frequency distribution are also used in fault diagnosis, such as the evolutionary spectrum based on STFT[6] and the improved cyclic WVD spectrum analysis based on WVD[7]. The time-frequency distribution cannot change according to the signal's characteristic, hence, the adaptive time-frequency analysis method has been focused and applied to the mechanical fault diagnosis because of its high performance. The time-frequency analysis method based on adaptive kernel function is proposed in literature[8], and the adaptive optimization criterion can adaptively adjust the kernel function according to the characteristics of the signals.

Recently, the adaptive time-frequency analysis method is developed rapidly, such as adaptive time-frequency distribution based on radial Gaussian kernel function, cone-shaped kernel function[9−10] and butterworth kernel function[11]. The new adaptive parabola kernel function time-frequency distribution method has been proposed in [12]. The improved basis function chirplet adaptive time-frequency method is introduced in literature[13], and it is applied to the bearings and gear box fault analysis. An improved radial parabolic kernel time-frequency method has been used to the bearing fault diagnosis, which can effectively improve the bearing fault diagnosis time-frequency resolution and suppress the cross-term interference[14]. Shi Dong-feng proposed a kind of adaptive time-frequency decomposition algorithm based on Gaussian linear frequency-modulation[15], the method has good performance in the machinery critical vibration analysis. Recently, the adaptive time-frequency method is proposed based on AR parameter model by Michael Jachan[16−17], whereafter, the improved vector time-frequency AR (VTFAR) and TFARMA adaptive time-frequency algorithm are put forward[18−19]. The model time-frequency methods have been applied in mechanical engineering[20−21], the TFAR model method has illustrated fine time-frequency resolution when it is used to analyze the vibration signals of a faulty gearbox[20], more application examples with parametric models method could be found in literature[21]. However, the TFARMA model method has not been applied for the machinery fault signals analysis.

Gaussian model and second order statistics are used to analyze the fault signals in the above methods, but some actual mechanical fault signals have obvious pulsing characteristics, and they are non-Gaussian, hence there will be a certain deviation. Therefore, Nikias first proposed a new statistical model for the typical signal Alpha (α) stable distribution process[22−25]. When $0 < \alpha < 2$, the performance of the time-frequency analysis method based on Gaussian model degenerates, therefore, the new methods based on α stable distribution model are put forward, and they are applied to

This article has been accepted for publication in a future issue of this journal, but has not been fully edited. Content may change prior to final publication.

This work was financially supported by Natural Science Foundation of China (61261046), Jiangxi province natural science foundation of China (20142BAB207006), Science and technology project of provincial education department of jiangxi (GJJ14738, GJJ14739). Recommended by Associate Editor Yangquan Chen.

Junbo Long, Ping Li and Hongshe Fan are with the Department of Electrical and Engineering, jiujiang university, jiujiang 332005, China (e-mail: ljb829@qq.com).

Haibin Wang is with the Information Science and Engineering Technology, jiujiang university, jiujiang 332005, China (e-mail: wanghaibin00@163.com).

Digital Object Identifier 10.1109/JAS.2016.7510190

the mechanical fault diagnosis. Chang-Ning Li proved that the bearing fault signals belong to α stable distribution[26]. A new support vector machine fault diagnosis algorithm based on the stable distribution model is proposed in [27], it can effectively improve small sample learning and convergence speed. A rolling bearing fault diagnosis method is put forward with fractional lower order statistics instead of second order statistics based on α stable model and kurtogram[28], which effectively improve the performance. However, few research works are studied on applications of time-frequency distribution in machine fault diagnosis with α stable distribution model. The adaptive time-frequency analysis method based on α stable distribution is worth investigating. More realistic statistical model will bring new machine fault detection and diagnosis methods for rotating machines. In addition, the fractional-order differential calculus methods have been applied in many fields[29−31].

In this paper, several new time-frequency representation methods based on α stable distribution statistical modeling are proposed for machine fault diagnosis. The paper is structured in the following manner. α stable distribution and its statistical moment are introduced in Section 2. The bearing fault signals are introduced in Section 3. The improved fractional lower order time-frequency representation methods are demonstrated, and the simulations comparisons with the conventional methods are performed to demonstrate justifiability of the proposed methods in Section 4. The simulations of the outer race fault signals diagnosis are presented in Section 5. Finally, the conclusions and future research are given in Section 6.

II. α STABLE DISTRIBUTION AND ITS STATISTICS

A. α stable distribution

α stable distribution is a kind of generalized Gaussian distribution, the process is not limited in variance and its probability density function has a serious tail, its characteristic function can be described as[22−25]

$$\phi(t) = \exp\{j\mu t - \gamma|t|^{\alpha}[1 + j\beta sign(t)\omega(\tau,\alpha)]\} \qquad (1)$$

where α is the characteristic index, when $0 < \alpha < 2$ it (type 1) is lower order α stable distribution, when $\alpha = 2$ it is Gaussian distribution. β is the symmetry coefficient, γ is the dispersion coefficient, μ is the location parameter. When $\beta = 0$, $\mu = 0$, $\gamma = 1$, When α= 0.5, 1.0, 1.5 and 2.0, the time-domain waveforms of $S\alpha S$ distribution are shown in Fig. 1, and their probability density function (PDF) are shown in Fig. 2.

Waveforms of $S\alpha S$ stable dαvariance are shown in Fig. 3 when sample numbers successively increase with $\alpha = 0.5, 1.0, 1.5$ and 2.0. When $0 < \alpha < 2$, the results show that variances are not limited, the variance is convergent when $\alpha = 2$ (Gaussian distribution), $\gamma = 2\sigma^2 = 2(\sigma = 1)$.

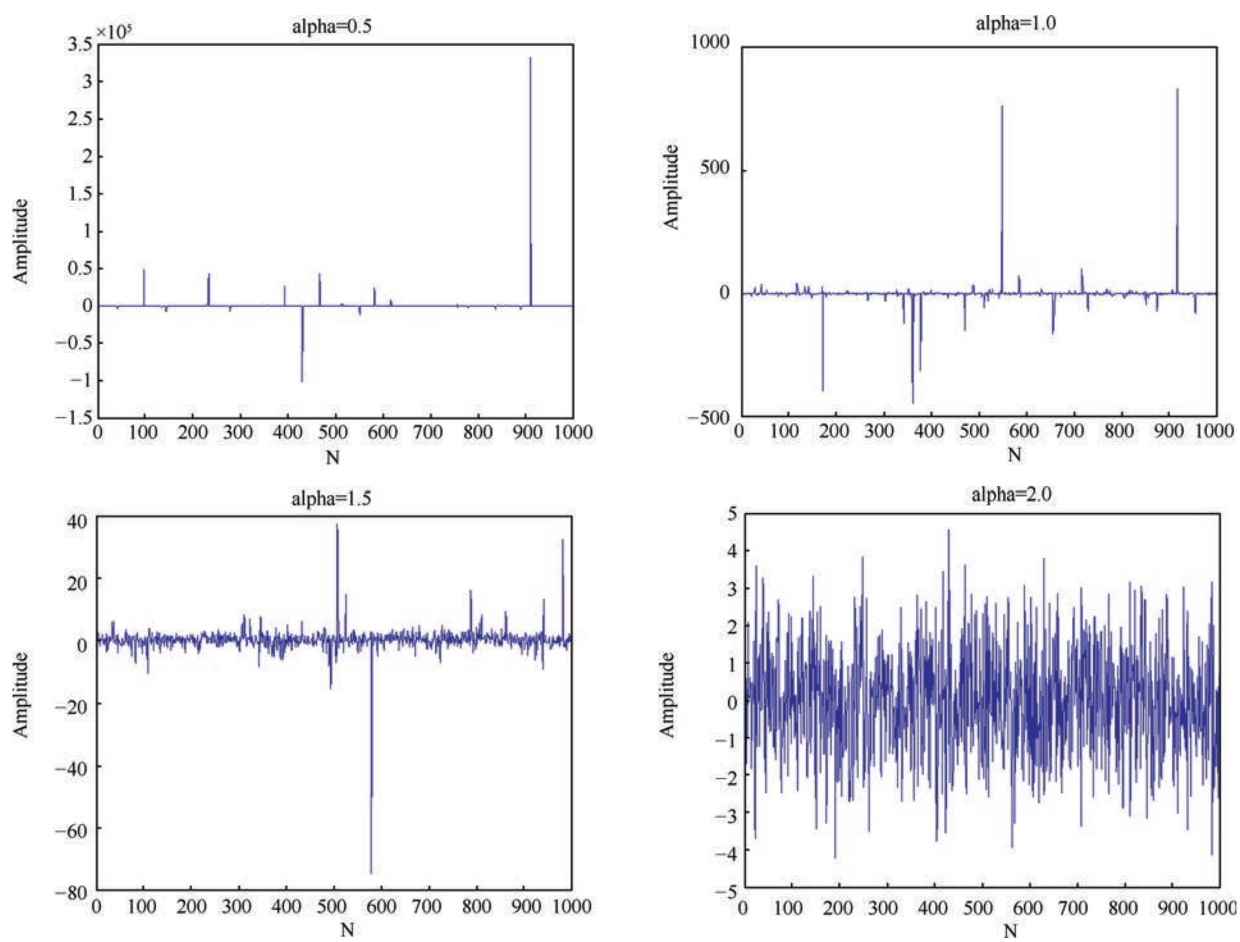

Fig. 1 Waveform of $S\alpha S$ distribution under $\alpha = 0.5, 1.0, 1.5$ and 2.0 in time domain

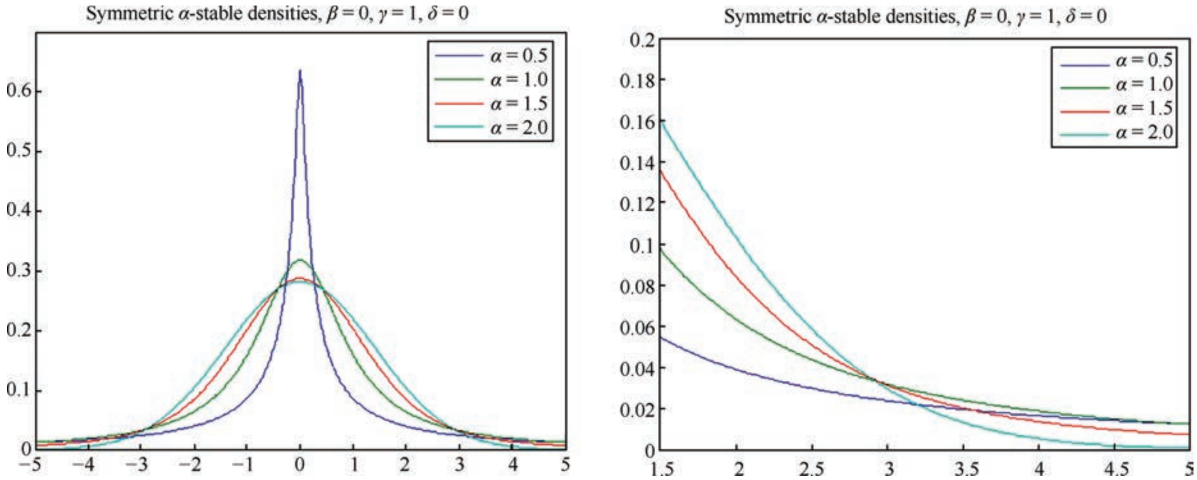

Fig. 2 PDF of $S\alpha S$ distribution with different alpha α

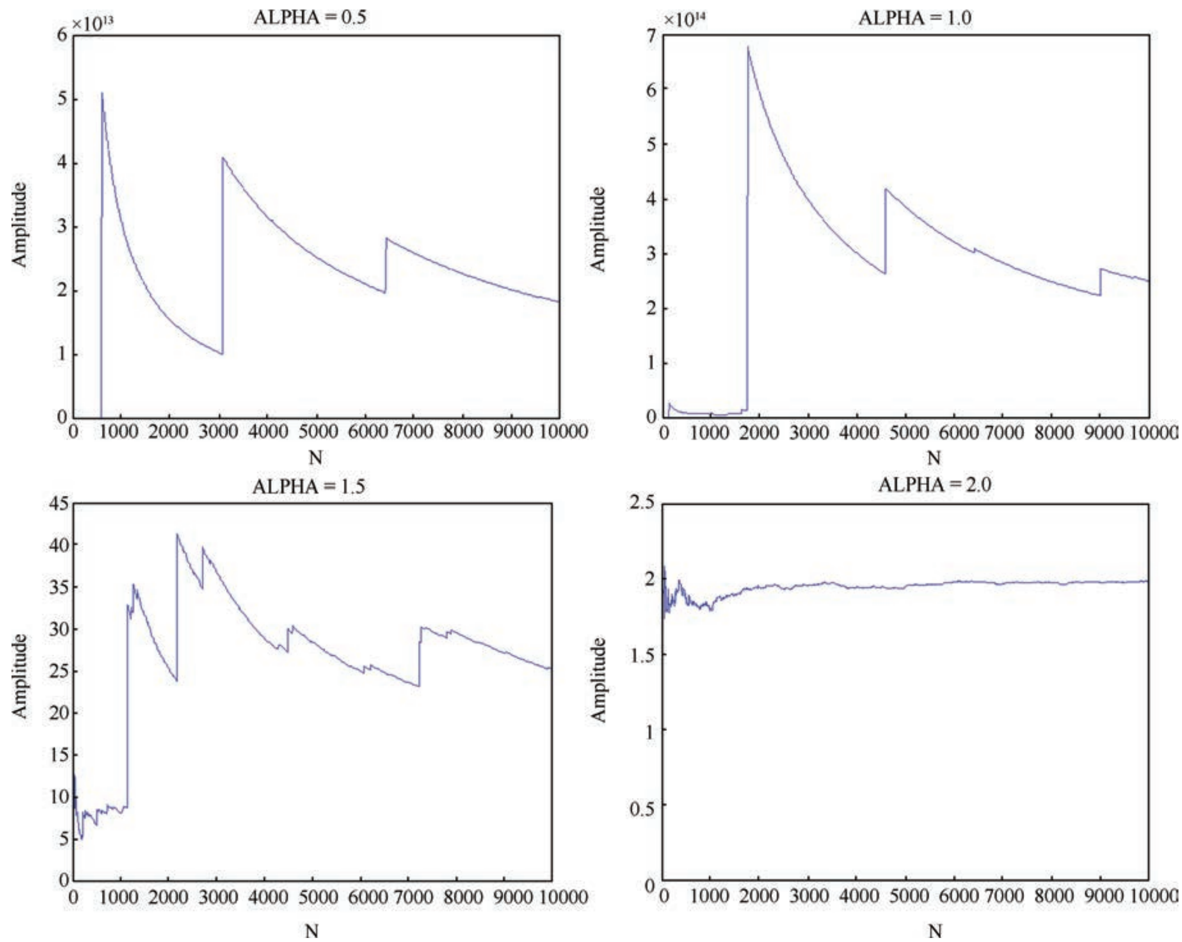

Fig. 3 Variance of $S\alpha S$ distribution with successively increase of sample numbers with different alpha (α)

B. fractional lower order statistics

1) Fractional lower order covariation coefficient: The covariance of $S\alpha S$ distribution is not existing because of its limited variance. Hence, the covariation concept is put forward by Miller in 1978, it is similar to the covariance of Gaussian random process. Covariation of two $S\alpha S$ distribution random variables X and Y is defined as

$$[X,Y]_\alpha = \int_s xy^{<\alpha-1>}\mu(ds), 1<\alpha\leq 2 \tag{2}$$

where S denotes the unit circle, $< >$ denotes the operation $z^{<\alpha>} = |z|^\alpha sign(z)$, the covariation coefficient of $X$and $Y$is defined as

$$\lambda_{XY} = \frac{[X,Y]_\alpha}{[Y,Y]_\alpha} \tag{3}$$

If the dispersion coefficient of Y is γ_y, the covariation and covariation coefficient can be written as

$$[X,Y]_\alpha = \frac{E(XY^{<p-1>})}{E(|Y|^p)}\gamma_y, 1 \le p < \alpha \le 2 \quad (4)$$

$$\lambda_{XY} = \frac{E(XY^{<p-1>})}{E(|Y|^p)}, 1 \le p < \alpha \le 2 \quad (5)$$

According to the definition of covariation coefficient, the covariation coefficient of a real observation sequence $X(n)(n = 0, 1, \ldots N)$can be defined as[21]:

$$\lambda(m) = \frac{E(X(n)X(n+m)^{<p-1>})}{E(|X(n+m)|^p)}, 1 \le p < \alpha \le 2 \quad (6)$$

$$\hat{\lambda}(m) = \frac{\sum_{m=1}^{N} X(n)|X(n+m)|^{p-1} sign[X(n+m)]}{\sum_{m=1}^{N} |X(n+m)|^p}, \quad 1 \le p < \alpha \le 2 \quad (7)$$

where $\hat{\lambda}(m)$ is the approximate estimation of $\lambda(m)$. The simplified fractional lower order moment is used in array signal processing, and it is expressed as[23, 24]:

$$\lambda_{FLOM}(m) = E(X(n)X(n+m)^{<p-1>}), 1 \le p < \alpha \le 2 \quad (8)$$

when X(n) is real

$$\hat{\lambda}_{FLOM}(m) = \frac{1}{L_2 - L_1} \sum_{n=L_1+1}^{L_2} X(n)|X(n+m)|^{p-1} sign[X(n+m)] \quad (9)$$

when X(n) is complex

$$\hat{\lambda}_{FLOM}(m) = \frac{1}{L_2 - L_1} \sum_{n=L_1+1}^{L_2} X(n)|X(n+m)|^{p-2} X^*(n+m) \quad (10)$$

where $1 \le p < \alpha \le 2, L_1 = \max(0, -m), L_2 = \min(N - m, N)$.

2) Fractional lower order covariance: Because the fractional lower order covariation and fractional lower order moment define α as $1 < \alpha \le 2$ and the range from 0 to 1 is not defined, hence, fractional lower order covariance (FLOC) is given in [25], in which $0 < \alpha \le 2$ is defined. Fractional lower order auto-covariance (FLOAC) of N pairs of the observations $X(n)(n = 0, 1, \cdots N)$ based on the definition of FLOC[25] can be defined as:

$$R_d(m) = E\left\{X(n)^{<a>}X(n+m)^{<b>}\right\}, \quad 0 \le a < \alpha/2, 0 \le b < \alpha/2 \quad (11)$$

where $0 < \alpha \le 2$, if $X(n)$ is real, the FLOAC can be estimated with the sample FLOAC $\hat{R}_d(m)$.

$$\hat{R}_d(m) = \frac{1}{L_2 - L_1} \sum_{n=L_1+1}^{L_2} |X(n)|^a |X(n+m)|^b sign[X(n)X(n+m)] \quad (12)$$

And if $X(n)$ is complex, the FLOAC is estimated with the sample FLOAC $\hat{R}_d(m)$

$$\hat{R}_d(m) = \frac{1}{L_2 - L_1} \sum_{n=L_1+1}^{L_2} |X(n)|^{a-1}|X(n+m)|^{b-1} X^*(n)X^*(n+m) \quad (13)$$

where $L_1 = \max(0, -m)$, $L_2 = \min(N - m, N)$, $*$ denotes the conjugate operation.

III. Bearing Fault Signals

The data of real bearing fault signals are got from the Case Western Reserve University (CWRU) bearing data center[29]. As shown in Figure 4, the diameter of the bearing fault in the test motor is 0.007 inches, and the fault points include inner race fault, ball fault and outer race fault. The experiments are conducted with a 2hp reliance electric motor, and the acceleration data are measured at proximal and distal points of motor bearings, the points include the drive end accelerometer (DE), fan end accelerometer (FE) and base accelerometer (BA). The motor speed is 1797 RPM (revolutions per minute), and the digital data are collected with a speed of 12, 000 samples per second.

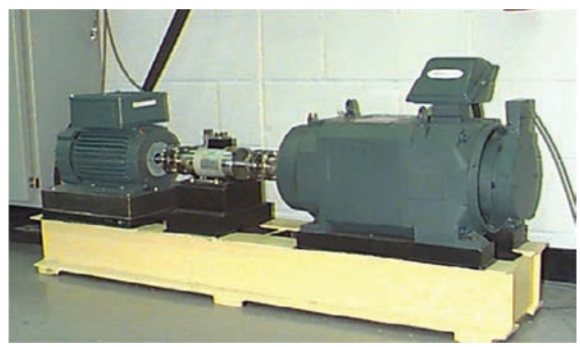

Fig. 4 The apparatus of bearing fault test data

When the single fault point appears in inner race, outer race or ball, we collect the fault signals. Waveforms are shown in Figure 4 a, b, c and d, where it is shown that fault points cause different impulse intensities. The ball fault has very small impulse intensity, while the impulse intensity of outer race is higher.

Statistical characteristics of these bearing fault signals should be analyzed to obtain the condition information. Hence, the stable distribution statistical model is used to estimate parameters of the inner race fault signals, ball fault signals and outer race fault signals, the estimated four parameters are shown in Table 1. As it can be seen, bearing signals in normal condition are Gaussian distribution for $\alpha = 2$, and they are non-Gaussian α stable distribution for $\alpha < 2$. Probability density function (PDF) of the inner race fault signals, the ball fault signals and the outer race fault signals are shown in Figure 6. By comparing PDF of normal signals and fault signals, we know that PDF of fault signals have serious trailing. Table 1 shows that the β value around zero, and Fig. 6 shows that bearing fault signals generally have symmetric PDF, hence, $S\alpha S$ distribution statistical model is concise and accurate for bearing fault signals.

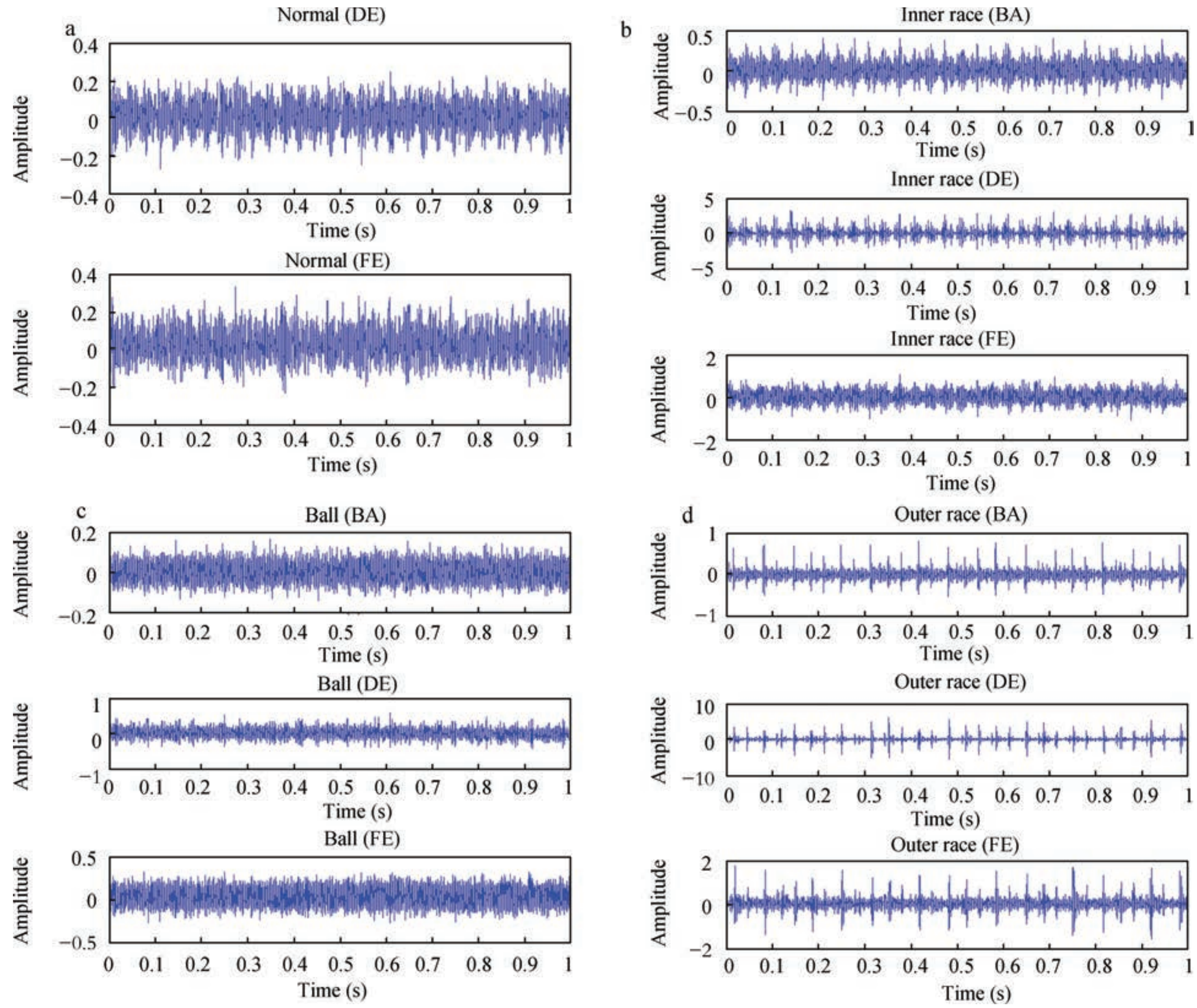

Fig. 5 Bearing fault waveforms (a. The waveform of normal signals in DE and FE b. the waveform of the inner race fault signals in DE, FE and BA c. the waveform of the ball fault signals in DE, FE and BA d. the waveform of the outer race fault signals in DE, FE and BA)

Table I α stable distribution model parameter estimates of bearing fault signals

parameters		α	β	γ	μ
Normal	DE	2.000	–0.283	0.1304	0.1317
	FE	2.000	1.000	0.0583	0.0236
Inner race	BA	1.7682	0.0872	0.0590	0.0062
	DE	1.4195	0.0155	0.2407	0.0175
	FE	1.8350	0.0322	0.1495	0.0291
Ball	BA	1.9790	0.0592	0.0293	0.0055
	DE	1.8697	0.1215	0.0772	0.0193
	FE	1.998	–0.0371	0.0674	0.0321
Outer race	BA	1.6077	–0.1731	0.0530	0.0012
	DE	1.1096	0.0433	0.1341	0.0367
	FE	1.5435	–0.0169	0.0968	0.0296

IV. Fractional lower order time-frequency distributions

A. Fractional lower order short-time Fourier transform

1) Principle: Short time Fourier transform (STFT) time-frequency distribution is free from cross-term interference, but the time-frequency resolution is low and it is governed by the Heisenberg uncertainty principle. The conventional STFT of an analytic signal $x(t)$ is defined as

$$STFT_x(t,\omega)=\int_{-\infty}^{+\infty}x(\tau)h(\tau-t)e^{-j\omega\tau}\mathrm{d}\tau \tag{14}$$

The discrete equation is defined as

$$STFT_x(n,\varpi)=\sum_m x(m)h(m-n)e^{-jn\varpi} \tag{15}$$

STFT is one of Fourier transform, which is added with time window h(t) at each specific time of $x(t)$, in α stable distribution environment, fractional low order short time Fourier transform (FLO-STFT) based on P order moment can be defined as

$$FLOSTFT_x(t,\omega)=\int_{-\infty}^{+\infty}x^{<P>}(\tau)h(\tau-t)e^{-j\omega\tau}\mathrm{d}\tau \tag{16}$$

FLO-STFT discrete equation is defined as

$$FLOSTFT_x(n,\varpi)=\sum_m x^{<P>}(m)h(m-n)e^{-jn\varpi} \tag{17}$$

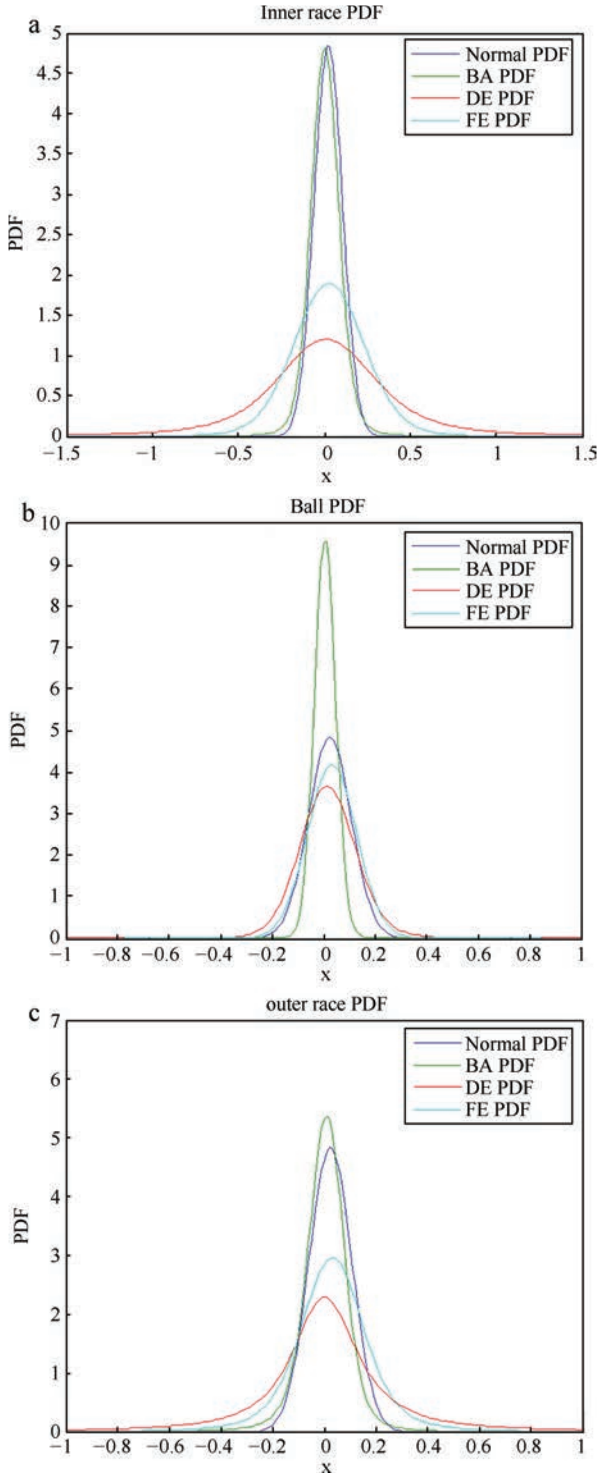

Fig. 6 PDF of the bearing fault signals (a. PDF of inner race fault signals in DE, FE and BA; b. PDF of the ball fault signals in DE, FE and BA; c. PDF of the outer race fault signals in DE, FE and BA)

In the equations 16-17, the moving window function can satisfy that P moment of non-stationary signal is stationary and integrable within the time window, however, the traditional STFT method is no longer stationary and integrable because $E[|s|] = \infty$ when $\alpha < 1$.

2) Application review: We apply FLO-STFT time-frequency distribution to estimate the time-varying spectral, the signal x added with $S\alpha S$ distribution noise is defined as

$$\begin{aligned} x &= e^{-a(n-80)^2+j\omega_1(n-80)} + e^{-a(n-190)^2+j\omega_2(n-190)} + S\alpha S \\ &= y + S\alpha S \end{aligned} \tag{18}$$

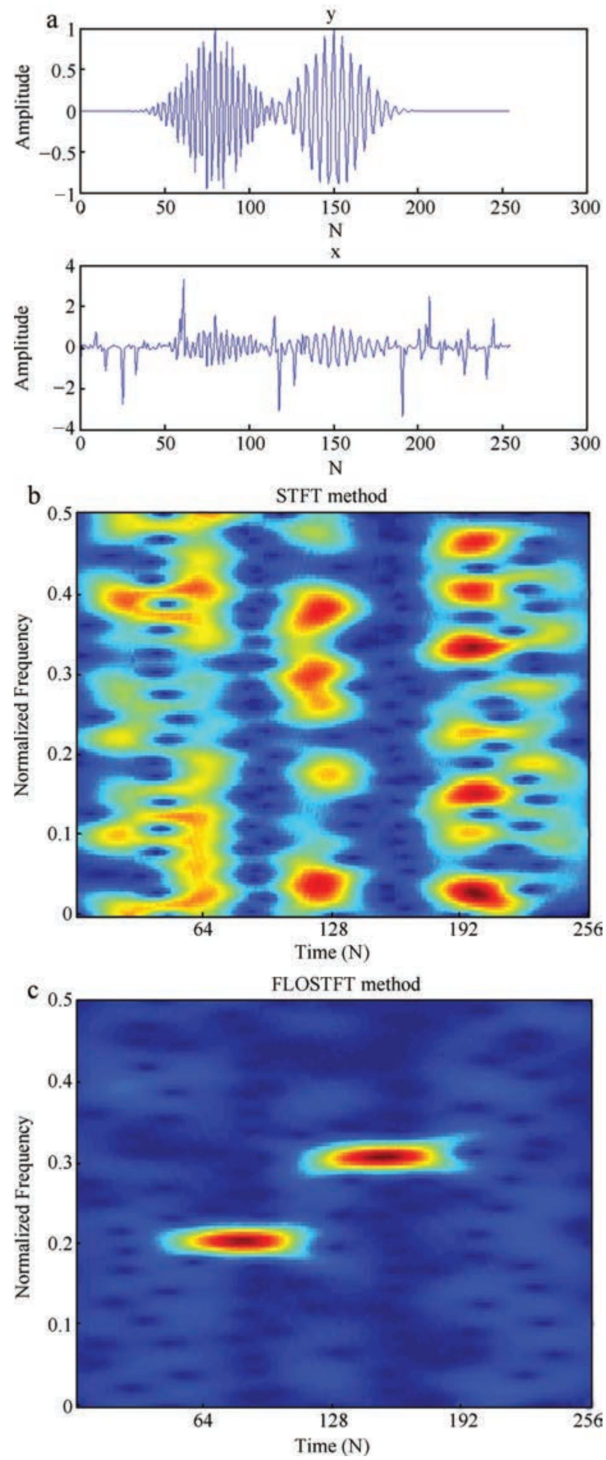

Fig. 7 Time-frequency representations of the signal x in $S\alpha S$ noise environment. (a. Waveform of x and y ; b. STFT time-frequency representation of the signal x; c. FLO-STFT time-frequency representation of the signal x)

where $a = 0.002, \omega_1 = 1.85, \omega_2 = 1.2, n = 1, 2, \cdots 256, \alpha = 1.5, MSNR = 15$ db (Mixed Signal to Noise Ratio), $MNSR = 10\log(E\left\{|s(t)|^2\right\}/\gamma^{\alpha})$. The traditional STFT method and FLO-STFT method are used to estimate time-frequency representations of the signal x, simulation results are shown in Figure 7.

3) Remarks: Figure 7. b shows that the traditional STFT time-frequency method fails in noise environment, the improved FLOC-STFT method shows good robustness in Fig. 7.c. However, the time-frequency resolution of the FLO-STFT method is controlled by the length of the window function like STFT method. In real application, the shorter time window should be used when we want to get the information of higher frequency components, and if we wish to closely localize the frequency location of lower frequency components, a longer time window is preferred. As a result, STFT time-frequency method is only suitable to analyze signals in Gaussian environment, but FLO-STFT can work in Gaussian and noise environment, which is robust.

B. Fractional lower order Wigner-Ville Distributions

1) Principle: Wigner-Ville Distribution (WVD) of the signal $x(t)$ is defined as

$$WVD_x(t,\omega) = \int_{-\infty}^{+\infty} x(t+\tau/2)x(t-\tau/2)e^{-j\omega\tau}\mathrm{d}\tau \quad (19)$$

WVD time-frequency is a quadratic transformation, it has serious cross-terms, hence, the smoothing window function $h(\tau)$ is used to reduce the cross-term interference, Pseudo WVD (PWVD) is expressed as

$$PWVD_x(t,\omega) = \int_{-\infty}^{+\infty} h(\tau)x(t+\tau/2)x(t-\tau/2)e^{-j\omega\tau}\mathrm{d}\tau \quad (20)$$

In α stable distribution environment, Fractional Low Order Wigner-Ville Distribution (FLO-WVD) based on P order moment can be expressed as

$$\begin{aligned} &FLOWVD_x(t,\omega) \\ &= \int_{-\infty}^{+\infty} x^{<P>}(t+\tau/2)x^{-<P>}(t-\tau/2)e^{-j\omega\tau}\mathrm{d}\tau \end{aligned} \quad (21)$$

The FLO-WVD discrete equation of the signal $x(t)$ is expressed as

$$\begin{aligned} &FLOWVD_x(n,\varpi) \\ &= 2\sum_m x^{<P>}(n+m)x^{-<P>}(n-m)e^{-jm\varpi} \end{aligned} \quad (22)$$

FLO-PWVD of the signal $x(t)$ can be defined as

$$\begin{aligned} &FLOPWVD_x(t,\omega) = \\ &\int_{-\infty}^{+\infty} h(\tau)x^{<P>}(t+\tau/2)x^{-<P>}(t-\tau/2)e^{-j\omega\tau}\mathrm{d}\tau \end{aligned} \quad (23)$$

The instantaneous auto-covariance of the signal $x(t)$ is defined as

$$R_x^C(t,\tau) = x^{<P>}(t+\tau/2)x^{-<P>}(t-\tau/2) \quad (24)$$

According to the equation (24), FLO-WVD changes as

$$FLOWVD_x(t,\omega) = \int_{-\infty}^{+\infty} R_x^C(t,\tau)e^{-j\omega\tau}\mathrm{d}\tau \quad (25)$$

According to the equation (24), we can know that FLO-WVD of the signal $x(t)$ is the Fourier transform of instantaneous auto-covariance in time delay τ.

2) Application review: The traditional WVD method, PWVD method, the improved FLO-WVD method and FLO-PWVD method are used to estimate time-frequency distributions of the signal $x(t)$, and their simulation results are shown in Figure 8.

3) Remarks: Fig. 8.a and Fig. 8.c respectively are WVD and PWVD time-frequency representations of the synthetic signal x, Fig8. b and Fig8. d respectively are FLO-WVD and FLO-PWVD of the synthetic signal x. Simulation results show WVD and PWVD time-frequency methods cannot work, but FLO-WVD and FLO-PWVD time-frequency methods have good performance in $S\alpha S$ environment. FLO-WVD method is an improved WVD time-frequency method, FLO-WVD has high time-frequency resolution, but it has serious cross-term interference. Hence, its application is inevitably hindered by the cross-term interference. FLO-PWVD is FLO-WVD added the window function, it can better suppress the cross term interference.

Fractional lower order Cohen class time-frequency distributions

1) $Principle$: The Cohen-class time-frequency distribution is intended to obtain the expected properties like higher resolution, non-negativeness and removal of cross-terms with a kernel function, Cohen class Time-frequency distribution (CTFD) of the analytic signal $x(t)$ is defined as

$$\begin{aligned} &C_x(t,\omega) = \frac{1}{2\pi}\int_{-\infty}^{+\infty}\int_{-\infty}^{+\infty}\int_{-\infty}^{+\infty} \\ &x(t+\tau/2)x(t-\tau/2)\Phi(\theta,\tau)e^{j\theta t-j\omega\tau-j\theta u}d\theta\mathrm{d}\tau du \end{aligned} \quad (26)$$

Ambiguity function (AF) of the signal $x(t)$ is expressed as

$$\begin{aligned} AF_x(\theta,\tau) &= \int_{-\infty}^{+\infty} x(t+\tau/2)x(t-\tau/2)e^{-j\theta t}dt \\ &= \int_{-\infty}^{+\infty} R_x^C(t,\tau)e^{-j\theta t}\mathrm{d}t \end{aligned} \quad (27)$$

Fractional Low Order Ambiguity function (FLOAF) of the analytic signal $x(t)$ based on P order moment is defined as

$$\begin{aligned} &FLOAF_x(\theta,\tau) = \int_{-\infty}^{+\infty} R_x^C(t,\tau)e^{-j\theta t}\mathrm{d}t \\ &= \int_{-\infty}^{+\infty} x^{<P>}(t+\tau/2)x^{-<P>}(t-\tau/2)e^{-j\theta t}\mathrm{d}t \end{aligned} \quad (28)$$

When the inverse Fourier transform of equation (28) is computed, we can get:

$$R_x^C(t,\tau) = \frac{1}{2\pi}\int_{-\infty}^{+\infty} FLOAF_x(\theta,\tau)e^{j\theta t}d\theta \quad (29)$$

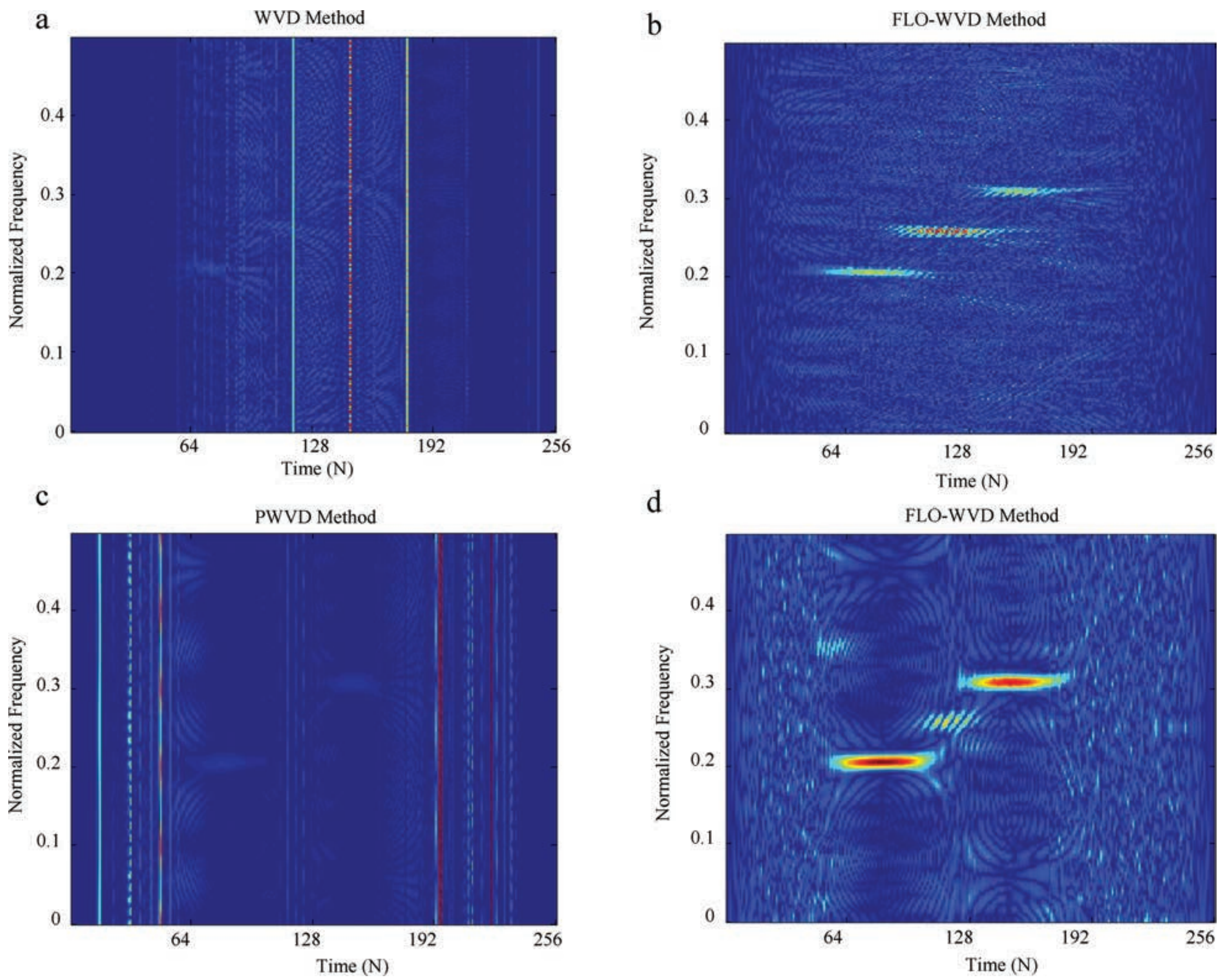

Fig. 8 Time-frequency representations of the signal x in $S\alpha S$ noise environment (a. WVD time-frequency representation of the signal x; b. FLO-WVD time-frequency representation of the signal x; c. PWVD time-frequency representation of the signal x; d. FLO-PWVD time-frequency representation of the signal x)

If the equation (29) is substituted to equation (25), we get the following form.

$$FLOWVD_x(t,\omega) = \frac{1}{2\pi}\int_{-\infty}^{+\infty}\int_{-\infty}^{+\infty} FLOAF_x(\theta,\tau)e^{j\theta t-j\omega\tau}d\theta\mathrm{d}\tau \tag{30}$$

From the equation (30), we know that FLOWVD of the signal $x(t)$ is two-dimensional Fourier transform of FLOC-AF, FLOWVD is three-dimensional (3-D) indication of the signal $x(t)$ in time, frequency and energy, and FLOC-AF is 3-D indication in time-delay, frequency deviation and the correlation. The images of FLOWVD and FLOC-AF have the components and cross-terms, the components of FLOWVD method are on both sides, and the cross terms are in the middle. However, the components of FLOC-AF are in the middle, and the cross terms are in both sides. When FLOC-AF of the signal $x(t)$ is computed, and a low-pass filter is used to filter cross-terms in AF plane, finally, the time-frequency distribution is calculated. FLO-Cohen distribution of the signal $x(t)$ is defined as

$$FLO-C_x(t,\omega) = \frac{1}{2\pi}\int_{-\infty}^{+\infty}\int_{-\infty}^{+\infty}\Phi(\theta,\tau) FLOAF_x(\theta,\tau)e^{j\theta t-j\omega\tau}d\theta\mathrm{d}\tau \tag{31}$$

$\Phi(\theta,\tau)$ is the kernel function, a different distribution is got when a different kernel function is used. If $\Phi(\theta,\tau)=1$, FLO-Cohen time-frequency representation degenerates into FLOWVD method, when $\Phi(\theta,\tau)$ is a moving window function, FLO-Cohen method is called pseudo FLOWVD time-frequency representation, if $\Phi(\theta,\tau)=\cos(\theta\tau/2)$, FLO-Cohen method is called FLO- Rihaczek time-frequency representation, when $\Phi(\theta,\tau)=e^{j\theta\tau/2}$, FLO-Cohen method is called FLO-Page time-frequency representation, if $\Phi(\theta,\tau)=e^{-\theta^2\tau^2/\sigma}$, FLO-Cohen method is called FLO-Choi-Williams time-frequency representation, $\sigma$is a constant between 0.2-8, if $\Phi(\theta,\tau)=g(\tau)\,|\tau|\sin(\beta\theta\tau)/\beta\theta\tau$, it is called as FLO-conical kernel distribution.

4) Application review: Choi-Williams and FLO-Choi-Williams time-frequency methods are used to estimate time-frequency distributions of the synthetic signal x (equation 18), simulation results are shown in Figure 9.

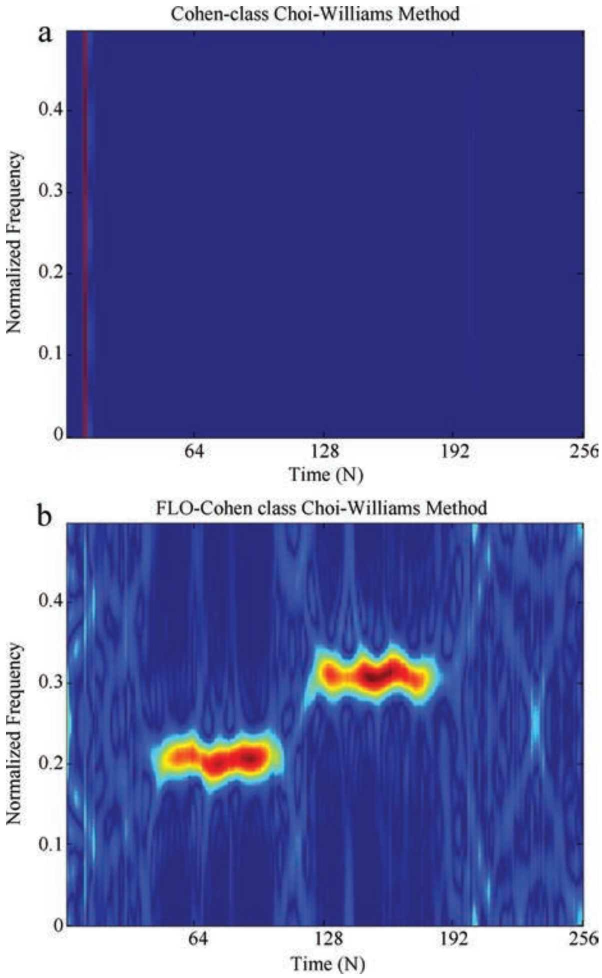

Fig. 9 Time-frequency representations of the signal x in $S\alpha S$ noise environment. (a. Choi-Williams time-frequency representation of the signal x;b. FLO-Choi-Williams time-frequency representation of the signal x)

5) $Remarks$ Fig. 9.a shows the Choi-Williams time-frequency representation of the synthetic signal x, and Fig. 9.b is the FLO-Choi-Williams time-frequency representation of the synthetic signal x. In view of the $S\alpha S$ stable distribution noise environment, the Choi-Williams method fails, and FLO-Choi-Williams method can better represent time-frequency distribution. FLO-Choi-Williams time-frequency method smoothing by the kernel function get rid of most of the cross-terms, but the time-frequency resolution is reduced.

C. FLO adaptive kernel time-frequency representation method

1) Principle: The kernel functions of traditional Cohen-class time-frequency method and fractional lower order Cohen-class time-frequency method are fixed, a class kernel function is only suitable for one type of signal, which can not meet all the signals. However, the adaptive kernel time-frequency distribution can change optimal kernel function$\Phi(\theta, \tau)$according to the feature of the different signals. Hence, adaptive optimal kernel time-frequency method is focused, and adaptive optimal kernel time-frequency representation in stable distribution environment will be a new direction.

According to the definition of FLOC-Cohen method, we use the optimal kernel function $\Phi_{opt}(\theta, \tau)$ instead of the fixed kernel function $\Phi(\theta, \tau)$, then we can get a new fractional low-order adaptive kernel time-frequency distribution. the polar coordinates expression of optimal kernel can be defined as:

$$\max_{\Phi} \int_0^{2\pi} \int_0^{+\infty} |AF_x(r, \phi)\Phi(r, \phi)|^2 r\mathrm{d}r\mathrm{d}\phi \tag{32}$$

when the kernel function is a radial Gaussian kernel function, the optimal kernel function is defined as:

$$\Phi(r, \phi) = e^{-\frac{r^2}{2\sigma^2(\phi)}} \tag{33}$$

Where ϕ is radial angle$\phi = \arctan \frac{\tau}{\theta} \sigma(\phi)$ is radial extension functionit controls the radial shape of $\Phi(\theta, \tau)$, constraint condition in polar coordinates is defined as:

$$\begin{aligned} &\frac{1}{4\pi^2} \int_0^{2\pi} \int_0^{+\infty} |\Phi(r, \phi)|^2 r\mathrm{d}r\mathrm{d}\phi \\ &= \frac{1}{4\pi^2} \int_0^{2\pi} \int_0^{+\infty} \left| e^{-\frac{r^2}{2\sigma^2(\phi)}} \right|^2 r\mathrm{d}r\mathrm{d}\phi \\ &= \frac{1}{4\pi^2} \int_0^{2\pi} \sigma^2(\phi) d\phi \leq \beta \end{aligned} \tag{34}$$

When $\Phi_{opt}(\theta, \tau)$ is a radial optimal parabolic kernel function, its function is defined as:

$$\Phi(\theta, \tau) = 1 - \frac{w(\theta^2 + \tau^2)}{2\sigma^2(\phi)}, (0 \leq \frac{w(\theta^2 + \tau^2)}{2\sigma^2(\phi)} \leq 1) \tag{35}$$

The constraint condition in polar coordinates is expressed as:

$$\frac{1}{6w\pi} \int_0^{\pi} \sigma^2(\phi) d\phi \leq \beta \tag{36}$$

If we use the equation (32), (33) and (34) to choose kernel function, the method can be called fractional lower order adaptive Gaussian-kernel time-frequency distribution (FLO-AGK-TFD). When we use the equation (32), (35) and (36) to choose kernel function, it is called fractional lower order adaptive parabolic kernel time-frequency distribution (FLO-APK-TFD).

2) Application review: The adaptive kernel function time-frequency distribution and FLO-adaptive kernel function time-frequency distribution are used to estimate time-frequency distributions of the synthetic signal x(the equation 18), the optimal radial Gaussian kernel function is used in the methods. Simulation results are shown in Figure 10.

3) Remarks: The adaptive kernel time-frequency distributions of synthetic signal x are illustrated in Fig. 10.a, and Fig. 10.b illustrate the FLO-adaptive optimal kernel time-frequency distributions of synthetic signal x. As shown in the figures, two components of the FLO-adaptive optimal kernel time-frequency method can be clearly resolved in fine resolution, but adaptive optimal kernel time-frequency method cannot represent time-frequency distributions. From Figure 10.b, we know that the FLO-adaptive kernel function method can effectively suppress the cross-terms, and it has a better timeCfrequency resolution. The FLO-adaptive kernel method requires that the auto-terms of the signals concentrate around the origin on the ambiguity plane, the cross-terms distribute in an area is far from the origin, and it will not be effective to separate the auto-terms and cross-terms when they overlap regardless of what volume of parameter is used.

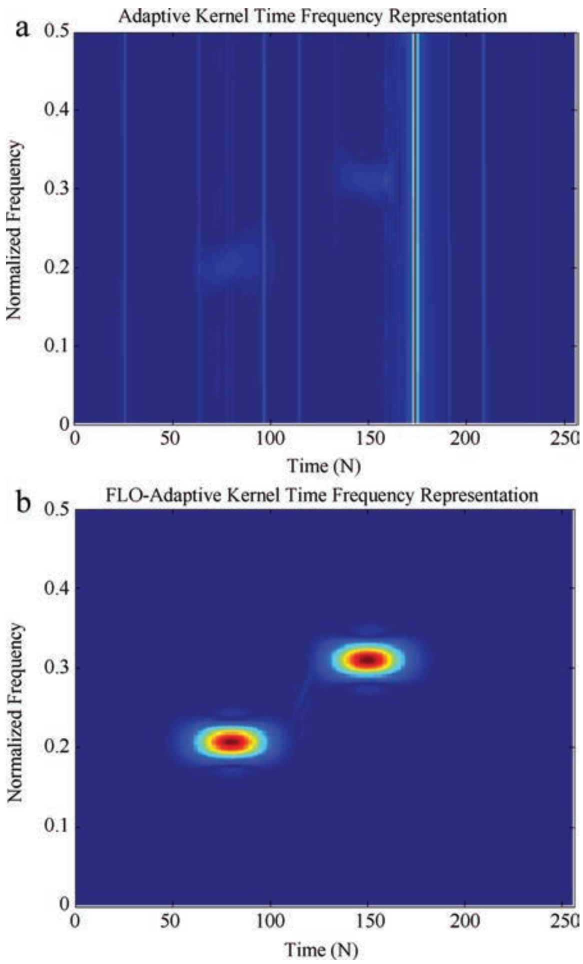

Fig. 10 Time-frequency representations of the signal x in $S\alpha S$ noise environment. (a. Adaptive kernel time-frequency representation of the signal x; b. FLO- adaptive kernel time-frequency representation of the signal)

D. Adaptive FLO-TFARMA Time-Frequency Representation method

TFARMA model of a non-stationary random process is defined as[19]

$$x[n] = -\sum_{i=1}^{M} a_i[n]x[n-i] + \sum_{i=0}^{L} b_i[n]e[n-i], n = 0, 1, 2, \cdots N-1 \tag{37}$$

Where $a_i[n]$ and $b_i[n]$ are the time-varying parameters of the TFAR and TFMA part, M and L are orders, $e(n)$ is stationary white noise. When the noise $e(n)$ is a stationary $S\alpha S$ distribution process $u(n)$, according to the definition method of the equation (37) TFARMA, we can also define a non-stationary time-frequency auto-regressive moving average $S\alpha S$ process TFARMA (M, L, A, B) as

$$x[n] = -\sum_{i=1}^{M} a_i[n]x[n-i] + \sum_{i=0}^{L} b_i[n]u[n-i], n = 0, 1, 2, \cdots N-1 \tag{38}$$

where

$$\begin{aligned} a_i[n] &= \sum_{l=-A}^{A} a_{i,l} f_l[n] = \sum_{l=-A}^{A} a_{i,l} e^{j\frac{2\pi}{N}nl}, n = 0, 1, 2, \cdots N-1 \\ b_i[n] &= \sum_{l=-B}^{B} b_{i,l} f_l[n] = \sum_{l=-B}^{B} b_{i,l} e^{j\frac{2\pi}{N}nl}, n = 0, 1, 2, \cdots N-1 \\ f_l[n] &= e^{j\frac{2\pi}{N}nl}, l = 0, 1, 2, \cdots, \max\{A, B\} \end{aligned} \tag{39}$$

We call it as fractional lower order time-frequency auto-regressive moving average (FLO -TFARMA) process, where M, L, A and B are the orders of the model, and M and L are the order in time domain, A and B are the order in frequency domain (the bandwidth of the model are $[-A, A]$ and $[-B, B]$), $a_i[n]$ and $b_i[n]$ are the parameters of the FLO -TFAR model, the numbers are as high as $N(M+L+1)$, $a_{i,l}$ and $b_{i,l}$ are basis expansion of the parameter functions, the number of $a_{i,l}$ is $M(2A+1)$, the number of $b_{i,l}$ is $(L+1)(2B+1)$. When $L=0$, $B=0$, FLO - TFARMA model will degrade into FLO-TFAR (M, A) model, and if $A=0$, $B=0$, it will degrade into FLO-TFMA (M, L) model. $f_l[n]$ is the basis functions, $u(n)$ is a stationary white noise $S\alpha S$ process, γ is its dispersion coefficient($\gamma = 1$).

1) FLO-TFMA Time-Frequency Representations: The α spectrum of the α stable distribution process is defined as

$$\begin{aligned} S_\alpha(z) &= \left[X[n], \sum_{i=-q}^{q} X(n-i)z^i \right] \\ &= \gamma \left[(\frac{1}{z})^{<\alpha-1>} \right] [H(z)]^{<\alpha-1>} \end{aligned} \tag{40}$$

When inserting $z = e^{j\omega}$ into the equation (40), α spectrum on the unit circle is calculated as

$$S_\alpha(e^{j\omega}) = \gamma H(e^{j\omega}) \cdot [H(e^{j\omega})]^{<\alpha-1>} = \gamma \left| H(e^{j\omega}) \right|^\alpha \tag{41}$$

When Z transformation with respect to both sides of the equation (38) is computed, we obtain

$$H[Z] = \frac{1 + \sum\limits_{i=1}^{L} b_i[n]Z^{-i}}{1 + \sum\limits_{i=1}^{M} a_i[n]Z^{-i}} = \frac{B(Z)}{A(Z)} \tag{42}$$

By inserting the equation (42) into the equation (40), FLO-TFARMA model spectrum estimation of a $S\alpha S$ process $X[n]$ can be defined as

$$S_\alpha(n,k) = \gamma\left|\frac{1+\sum\limits_{i=1}^{L} b_i[n]e^{-j\frac{2\pi}{N}ik}}{1+\sum\limits_{i=1}^{M} a_i[n]e^{-j\frac{2\pi}{N}ik}}\right|^\alpha = \gamma\left|\frac{1+\sum\limits_{i=1}^{L}\sum\limits_{l=-B}^{B} b_{i,l}e^{-j\frac{2\pi}{N}(ik-nl)}}{1+\sum\limits_{i=1}^{M}\sum\limits_{l=-A}^{A} a_{i,l}e^{-j\frac{2\pi}{N}(ik-nl)}}\right|^\alpha \tag{43}$$

For getting $a_{i,l}$ and $b_{i,l}$ of FLO-TFARMA model parameters, we solve the parameters $a_{i,l}$ of FLO-TFAR model, and then solve the parameters $b_{i,l}$ of FLO - TFMA model.

2) FLO-TFAR parameters estimation: If both sides of the equation (38) are multiplied by $x^{<P-1>}[n-i']$ and taken expectation, it can be written as

$$\sum_{i'=0}^{M} a_i[n]E\left\{x[n-i']x^{<P-1>}[n-i']\right\} = \sum_{i'=0}^{L} b_i[n]E\left\{U[n-i']x^{<P-1>}[n-i']\right\} \tag{44}$$

A simplified fractional lower order covariance is defined in [21], it simplifies to equation (44), and then we can get

$$\sum_{i'=0}^{M}\sum_{l'=-A}^{A} a_{i',l'}C_x[n-i',i-i']e^{j\frac{2\pi}{N}nl'} = \sum_{i'=0}^{L}\sum_{l'=-B}^{B} b_{i',l'}C_{U,x}[n-i',i-i']e^{j\frac{2\pi}{N}nl'} \tag{45}$$

where $C_x[n-i',i-i']\triangleq E\left\{x[n-i']x^{<P-1>}[n-i']\right\}\triangleq E\left\{x[n-i']|x[n-i']|^{P-2}X^*[n-i']\right\}$ is auto-covariance function of $x[n]$,

$C_{U,x}[n-i',i-i']\triangleq E\left\{U[n-i']x^{<P-1>}[n-i']\right\}\triangleq E\left\{U[n-i']|x[n-i']|^{P-2}\cdot x^*[n-i']\right\}$ is cross-covariance of $x[n]$ and $U[n]$, N points of discrete Fourier transform (DFT) with respect to both sides of the equation (45) can be expressed as

$$\sum_{i'=0}^{M}\sum_{l'=-A}^{A} a_{i',l'}\lambda_x[i-i',l-l']e^{-j\frac{2\pi}{N}i'(l-l')} = \sum_{i'=0}^{L}\sum_{l'=-B}^{B} b_{i',l'}\lambda_{U,x}[i-i',l-l']e^{-j\frac{2\pi}{N}i'(l-l')} \tag{46}$$

$$\lambda_x[i-i',l-l']\triangleq\sum_{n=0}^{N-1} C_x[n-i',i-i']e^{-j\frac{2\pi}{N}nl'}$$
$$\lambda_{U,x}[i-i',l-l']\triangleq\sum_{n=0}^{N-1} C_{U,x}[n-i',i-i']e^{-j\frac{2\pi}{N}nl'} \tag{47}$$

where $\lambda_x[i-i',l-l']$ and $\lambda_{U,x}[i-i',l-l']$are similar to Cohen-class time-frequency distribution expected ambiguity function (EAF) based on the second-order correlation function $A_x[i,l]\triangleq\sum\limits_{n=0}^{N-1} R_X[n,i]e^{-j\frac{2\pi}{N}nl}$, its auto-correlation is replaced by auto-covariance, it can be named as fractional order discrete expect ambiguity function (FLO-EAF), it represents statistical covariance of the time shift and frequency shift in time-frequency domain. When $i\ge A$, $x[n]$, $U[n]$ are statistically independent from each other and $C_{U,x}[n-i',i-i']=0$, the equation (46) can be written as

$$\sum_{i'=0}^{M}\sum_{l'=-A}^{A} a_{i',l'}\lambda_x[i-i',l-l']e^{-j\frac{2\pi}{N}i'(l-l')} = 0$$
$$\sum_{i'=1}^{M}\sum_{l'=-A}^{A} a_{i',l'}\lambda_x[i-i',l-l']e^{-j\frac{2\pi}{N}i'(l-l')} = -\lambda_x[i,l]$$
$$A+1\le i\le A+M \quad -L\le l\le L \tag{48}$$

The equation (48) can be written as

$$\Gamma a=-\theta \quad or\ a=-\Gamma^{-1}\theta \tag{49}$$

where Γ is $(2L+1)M\times(2L+1)M$ Toeplitz-block matrix, $a=\left[{a_1}^T,{a_2}^T,\cdots,{a_M}^T\right]^T$, $a_m=\left[a_{i,-L},a_{i,-L+1},\cdots,a_{i,L}\right]^T$, $\theta=\left[{\theta_{A+1}}^T,{\theta_{A+2}}^T,\cdots{\theta_{A+M}}^T\right]^T$.

The equation (49) has $(2L+1)M$ independent equations, and the required parameters $a_{i',l'}$ are $(2L+1)M$. The lengths of θ and a are $(2L+1)M$, and through the solution of Toeplitz matrices using equation (49), we can obtain the vector a and FLO - TFAR model parameters $a_{i,l}$.

3) FLO-TFMA parameters estimation: A $S\alpha S$ distribution signal $y[n]$ can be produced by $S\alpha S$ noise distribution $U[n]$ through causal linear time-varying (LTV) system (TFMA), we can also obtain it when $U[n]$ is passed through a TFARMA system and then through a TFAR model system. Then, we can take advantage of the observation sequence $x[n]$ that is discussed in Section 5.2 with the help of TFAR model filter to obtain TFMA process $y[n]$, this whole process can be expressed as

$$y[n]=\sum_{i=0}^{L} b_i[n]U[n-i]=\sum_{i=0}^{L}\sum_{l=-B}^{B} b_{i,l}[n]e^{j\frac{2\pi}{N}nl}U[n-i] \tag{50}$$

The both sides of the equation (50) are multiplied by $x^{<P-1>}[n-i']$ and taken expectation, then, N points of discrete Fourier transform (DFT) with respect to both sides of the equation (50) can be written as

$$\sum_{i'=0}^{L}\sum_{l'=-B}^{B} b_{i',l'}[n]\lambda_{U,y}[i-i',l-l']e^{-j\frac{2\pi}{N}i'(l-l')} = \lambda_y[i,l]$$
$$0\le i\le L \quad -B\le i\le B \tag{51}$$

When $LB<<N$, phase factor $e^{-j\frac{2\pi}{N}i'(l-l')}\approx 1$, it can be expressed as

$$\sum_{i'=0}^{L}\sum_{l'=-B}^{B} b_{i',l'}[n]\lambda_{U,y}[i-i',l-l'] = \lambda_y[i,l]$$
$$0\le i\le L \quad -B\le i\le B \tag{52}$$

According to the method in section 5.2, the equation (49) is written as Toeplitz matrix form $\Gamma b = \theta$, and then the model parameters $b_{i,l}$ are solved.

However, $U[n]$ and $\lambda_{U,y}[i - i', l - l']$ are unknown from the observations of a random signal $x[n]$, in that way, we cannot evaluate $b_{i,l}$ through the above method. We can use improved fractional lower order complex time-frequency spectrum (FLO-CTFC) algorithm to calculate FLO-TFMA coefficient $b_{i,l}$[17], where, the second order correlation is replaced by fractional low-order covariance.

4) Application review: We will study the performances of the TFAR, TFMA and TFARMA, the proposed FLO-TFAR, FLO-TFMA and FLO-TFARMA, they are applied to estimate the time frequency representations of the synthetic signal x (the equation 18) in $S\alpha S$ stable distribution noise environment. The length of the signal N=256, its time frequency representations are shown in Fig. 11-Fig. 13.

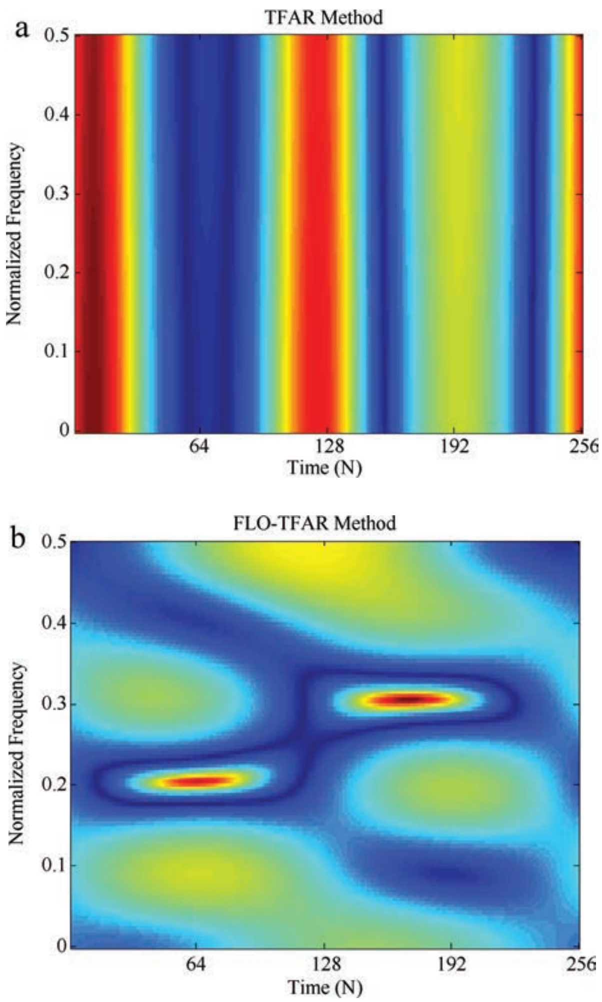

Fig. 11 The model time-frequency representations of the signal x in $S\alpha S$ noise environment (a. TFAR (5, 1) model time-frequency representation of the signal x; b. FLO- TFAR (5, 1) model time-frequency representation of the signal)

5) Remarks: The results show that TFAR (5, 1) model time-frequency spectrum is a failure in Fig. 11.a, the overall resolution of FLO-TFAR (5, 1) is poorer than that of the nonparametric FLO-PWVD in Fig. 11.b. but it can better suppress the cross term interference. TFMA (2, 2) method failed in Fig. 12.a, and FLO-TFMA (2, 2) spectrum is very poor in Fig. 12.b. Finally, TFARMA (2, 2, 1, 2) model method cannot work in $S\alpha S$ noise environment in Fig. 13.a, but FLO-TFARMA (2, 2, 1, 2) model time-frequency spectrum exhibits better resolution than FLO-TFAR and FLO-TFMA in Fig. 13.b, and it does not contain any cross terms as does FLO-PWVD.

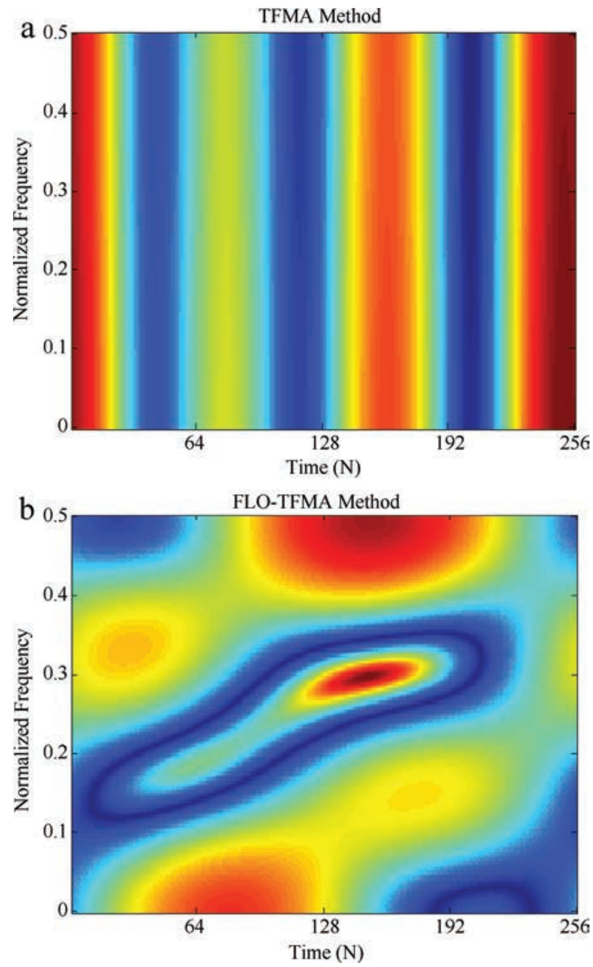

Fig. 12 The model time-frequency representations of the signal x in $S\alpha S$ noise environment (a. TFMA (2, 2) model time-frequency representation of the signal x; b. FLO- TFMA (2, 2) model time-frequency representation of the signal)

The improved FLO-TFAR, FLO-TFMA and FLO-TFARMA methods are effective for slowly time-varying signals, and they are free from cross-term interference. The timeCfrequency resolution of the FLO-TFAR and FLO-TFMA methods are relatively low, and FLO-TFARMA method illustrates better resolution. In addition, the complicated algorithm for estimating model parameters makes FLO-TFARMA method computationally demanding. Therefore, some works will be made to improve the time-frequency resolution and model parameter estimation process for practical fault signal analysis.

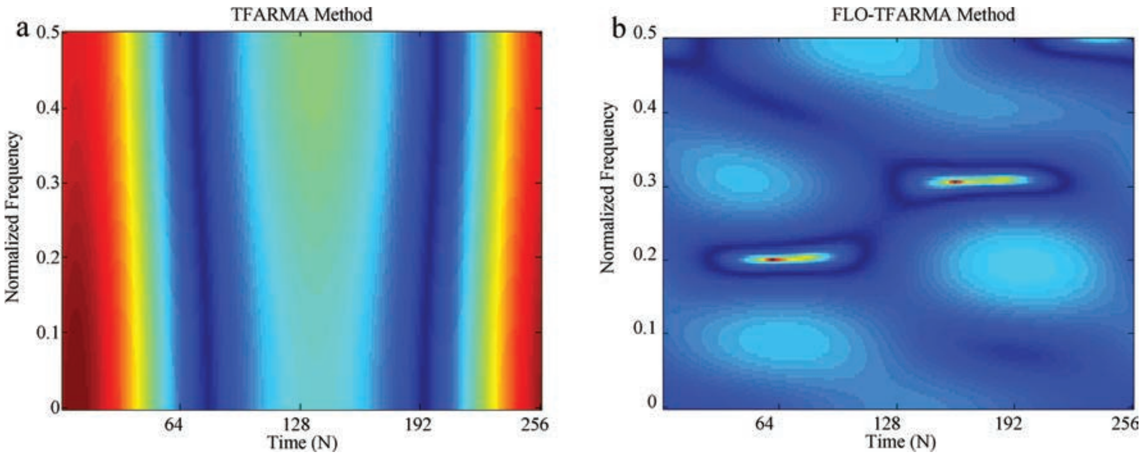

Fig. 13 The model time-frequency representations of the signal x in $S\alpha S$ noise environment (a. TFARMA (2, 2, 1, 2) model time-frequency representation of the signal x; b. FLO- TFARMA (2, 2, 1, 2) model time-frequency representation of the signal)

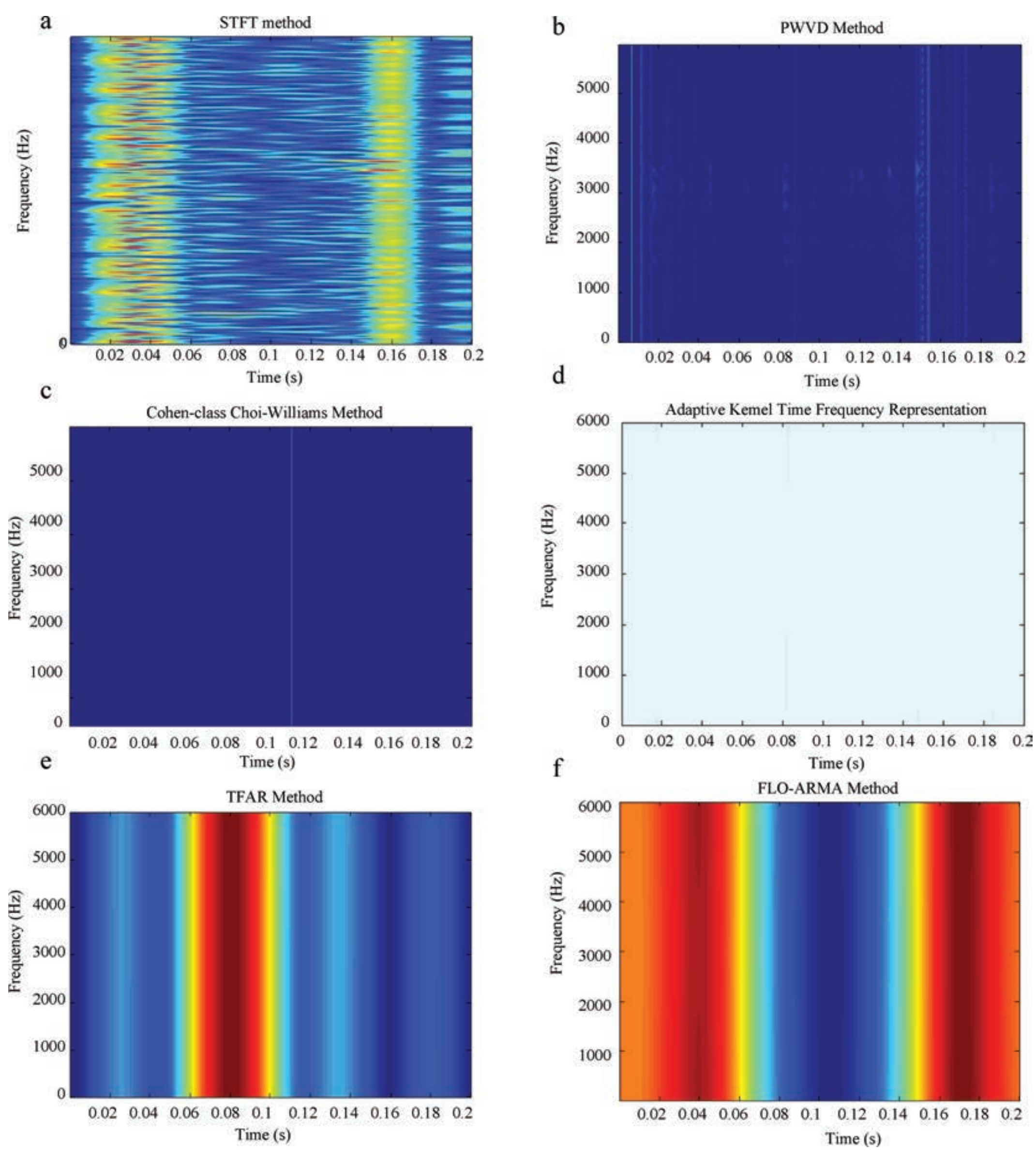

Fig. 14 The conventional time-frequency representations of the outer race fault signal in α stable distribution environment (a. The conventional STFT time-frequency representation; b. The conventional PWVD time-frequency representation; c. The conventional CWD time-frequency representation; d. The conventional adaptive kernel time-frequency representation; e. The TFAR model time-frequency representation; f. The TFARMA model time-frequency representation)

V. Application simulations

The impulse of the outer race fault signals in the vibration position of the drive end accelerometer, the fan end accelerometer and the base accelerometer is generated because of the local defects of rolling element bearings, as shown Fig. 5.d and Table. 1. The fault signals are non-Gaussian and non-stationary α stable distribution because of the presence of impulses. α stable distribution noises are added to the fault signals in the experiment, setting α=0.8, MSNR=20 dB, and letting N=2400. The conventional time-frequency distribution methods including STFT, PWVD, CWD, the adaptive kernel time-frequency method, TFMA, TFARMA model time-frequency method, and the improved lower order time-frequency distribution methods including FLO-STFT, FLO-PWVD, FLO-CWD, the FLO-adaptive kernel time-frequency method, FLO-TFMA and FLO-TFARMA model time-frequency method are applied to analyze the vibration signal of a bearing with an artificially seeded defect on outer race in the position of DE in α stable distribution environment. FLO-TFMA (2, 2) and FLO-TFARMA (2, 2, 1, 2) model time-frequency spectrum methods are used to analyze the signals in the experiment. The results are shown in Fig. 14 and Fig. 15.

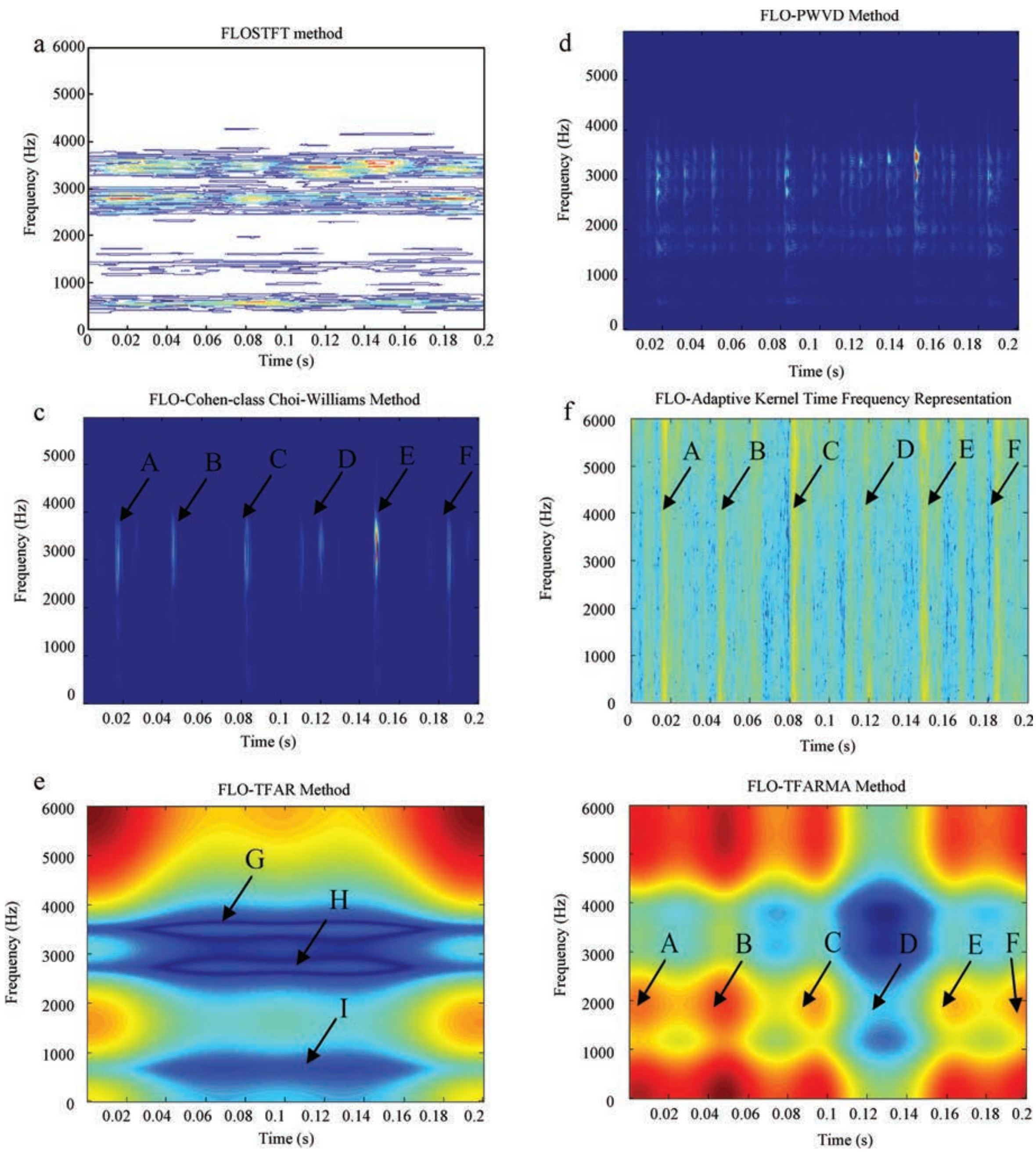

Fig. 15 The new time-frequency representations of the outer race fault signal in α stable distribution environment (a. The FLO-STFT time-frequency representation; b. The FLO-PWVD time-frequency representation; c. The FLO-CWD time-frequency representation; d. The FLO-adaptive kernel time-frequency representation; e. The FLO-TFAR model time-frequency representation; f. The FLO-TFARMA model time-frequency representation;)

Table II The comparison of various FLO-time-frequency distribution methods

Methods	Advantages	Disadvantages	Application to fault Diagnosis
FLO-STFT time-frequency distribution	Free from cross-terms, Low computational complexity, Definite physical meaning	Low time-frequency resolution	Revealing the time-frequency structure of the fault signals as a preprocessing tool
FLO-WVD time-frequency distribution	High time-frequency resolution	Serious cross-terms interference	Analyzing the fault signals after getting the signals structure
FLO-Cohen class time-frequency distribution	Suppressed cross-terms compared with FLO-WVD method	Reduced time-frequency resolution, certain cross-term interference	Analyzing the fault signals after getting the signals structure
FLO-adaptive kernel time-frequency distribution	Suppressed cross-terms, improved timeCfrequency resolution	High computationally complex	Suitable to the computational complexity fault signals
FLO-ARMA time-frequency distribution	Free from cross-terms	High computational complexity, low time-frequency resolution	Suitable to analyzing the slowly time-varying fault signals

STFT time-frequency representation of the outer race fault signal is shown in Figure. 14.a, Fig. 14.b is the PWVD time-frequency distribution, CWD method time-frequency representation is shown in Fig. 14.c, the adaptive kernel time-frequency representation is in Figure. 15.d, Figure. 15.e and Figure. 15.f respectively are TFAR model time-frequency representation and TFARMA model time-frequency distribution. The results show that the conventional time-frequency methods fail in α stable distribution environment. FLO-STFT time-frequency representations of the outer race fault signal in Figure. 15.a show the shock pulse is mainly distributed in low-frequency band from 0 Hz to 4000 Hz, and the transient harmonic vibration components of about 600 Hz, 2800 Hz and 3500 Hz dominate frequency-domain. Its vertical resolution is bad, the fault characteristic frequency cannot be seen. FLO-PWVD time-frequency representations in Fig. 15.b have a good vertical resolution, but there are serious cross terms, which render it not conducive to observe. FLO-CWD method preferably restrains the cross-term interference in Fig. 15.c, it can be seen clearly that the gap regularly changes between the impact, the interval between the impulses A, B, C, D, E and F is approximately 30ms, the interval corresponds to the characteristic frequency of outer race as 33.333Hz. We can also know the interval between A, B, C, D, E and F is about 30ms from FLO-adaptive kernel time-frequency representation in Figure. 15.d, the impact frequency band expanded into 0-6000 Hz because of its poor lateral resolution. The results show that the transient harmonic vibration components are 600Hz, 2800Hz and 3500Hz from the FLO-TFAR model time-frequency representation in Fig. 15.e, but its vertical resolution is bad, so we cannot see the effect of the time interval. However, FLO-TFARMA model time-frequency distributions in Fig. 15.f show the interval between the impulses A, B, C, D, E and F is approximately 30ms, as well as that the dominant frequency of 600Hz, 2800Hz and 3500Hz, FLO-TFARMA has certain ability in the horizontal and vertical, but the overall resolution is low.

The simulations show that the improved methods have their respective advantages and disadvantages as shown in this paper. The fractional lower order short time Fourier transform time-frequency representation has low computational complexity and definite physical meaning, but the time-frequency resolution is low, hence it is suitable to analyze the non-stationary machinery fault signals whose local stationary is larger. The fractional lower Wigner-ville time-frequency representation has high time-frequency resolution, however, there are serious cross-terms interference. The fractional lower order pseudo Wigner-Ville time-frequency representation added window function and the different kernel function fractional low-order Cohen class time-frequency distribution can suppress certain cross-term interference, but it leads to reduced the time-frequency resolution. The fractional lower order adaptive kernel time-frequency representation can suppress cross-term interference, and effectively improve the time-frequency resolution, but the computational complexity is higher. The fractional lower order ARMA model time-frequency representation has no interference of cross-terms, but the time-frequency resolution is low, hence it is suitable for analyzing the changing slowly non-stationary machinery fault signals. The methods are summarized in Table 2. In real applications, several methods can be selected to analyze the fault signals according to their specific characteristics.

VI. CONCLUSIONS

The paper has presented an accurate statistical parameter model $S\alpha S$ distribution for bearing fault signals diagnosis. The time-frequency analysis methods are key tools for machinery fault diagnosis, they can be used to identify the constituent components and time variation of the signals. We have presented FLO-STFT, FLO-WVD, FLO-PWVD, FLO-CWD, FLO-AKTFD and FLO-ARMA time-frequency analysis methods based on $S\alpha S$ stable distribution statistical model. The methods have better performances than the conventional methods including STFT, WVD, PWVD, CWD, AKTFD and ARMATFD. The traditional methods fail in $S\alpha S$ stable distribution environment, but the proposed methods can regularly work in the noise environment, which shows robustness. The proposed time-frequency analysis methods are used to analyze the bearing fault signals, they have respective advantages and disadvantages, the FLO-STFT method has low computational complexity and low resolution. FLO-WVD has better resolution, but there are serious cross terms. The FLO-PWVD and FLO-CWD methods suppress the cross-term interference through adding the window function, but they still suffer from cross-term interference. The FLO-AKTFD methods could be effective to improve time-frequency resolution and suppress cross-terms. The FLO-TFARMA model method is free from cross-term interference, however, the timeCfrequency resolution is not as high as expected. The improved time-frequency analysis method is applied to the bearing fault diagnosis, which can better get fault features of the signals. In the actual bearing fault diagnosis analysis, we can use the above several kinds of comprehensive methods to analyze together, and take their respective advantages to comprehensive judgment, and hence better results can be obtained.

REFERENCES

[1] S.V Narasimhan, S Pavanalatha, *Estimation of evolutionary spectrum based on short time Fourier transform and modified group delay*, Signal Processing. 2004, 84(11):2139-2152.

[2] Baoping Tang, Wenyi Liu, Tao Song, *Wind turbine fault diagnosis based on Morlet wavelet transformation and Wigner-Ville distribution*, Renewable Energy. 2010, 7(35): 2862-2866.

[3] Z.K. Penga, P.W. Tsea, F.L. Chub, *A comparison study of improved Hilbert-Huang transform and wavelet transform: Application to fault diagnosis for rolling bearing*, Mechanical Systems and Signal Processing. 2005, 19(5): 974-988.

[4] Zhipeng Feng, Ming Liang, Fulei Chu, *Recent advances in timeCfrequency analysis methods for machinery fault diagnosis: A review with application examples*, Mechanical Systems and Signal Processing. 2013, 3(38): 165-205.

[5] Jianhong Wang, Liyan Qiao, Yongqiang Ye, YangQuan Chen, *Fractional Hilbert transform in rolling element bearings diagnostics*, Proceedings of the 2015 International Symposium on Fractional Signals and Systems. Romania, 2015, (10):1-3.

[6] A.L MANIE, W.J WANG, *Time-frequency analysis evolutionary periodogram with application in gear fault diagnosis*, International Journal of Wavelets, Multi-resolution and Information Processing. 2010, 8(5): 679C693.

[7] Guangming DongJinChen, *Noise resistant time frequency analysis and application in fault diagnosis of rolling element bearings*, Mechanical Systems and Signal Processing. 2012, 7(33):212C236.

[8] Richard G.B, Douglas L.J, *Signal dependent time-frequency analysis using radially Gaussian kernel*, Signal Processing. 1993, 32(3):263-284.

[9] Richard G.B, Douglas L.J, *A signal-dependent time-frequency representation: optimal kernel design*, IEEE Transactions on Signal Processing. 1993, 41(4):1589-1602.

[10] Richard G.B, Douglas L.J, *Adaptive cone-kernel time-frequency analysis*, IEEE Transactions on Signal Processing. 1995, 43(7):1715-1719.

[11] Dong-sheng Wu, Morris J.M, *Time-frequency representations using a radial Butterworth kernel, Time-Frequency and Time-Scale Analysis*, Proceedings of the IEEE-SP International Symposium on. Philadelphia, 1994:60-63.

[12] S.C. Wang, J. Han, *Adaptive Signal Analysis Based on Radial Parabola Kernel*, Applied Mechanics and Materials. 2008, 10(12):737-741.

[13] Li Hui, Liu Xiao-feng, Bo Lin, *Chirplet Time-Frequency Spectrum Analysis of Gear and Rolling Bearing Fault*, Journal of Vibration, Measurement and Diagnosis. 2011, 31(5):591-595.

[14] WANG Sheng-Chun HAN Jie LI Zhi-Nong LI Jian-Feng, *Adaptive Radial Parabola Kernel Representation and its Application in the Fault Diagnosis*, Journal of Mechanical Strength. 2007, 29(2) : 180-184.

[15] Shi Dongfeng, Shen Fan, Bao Ming, Qu Liang-sheng, *Adaptive Time-Frequency Analysis and its Application in Large Rotating Machinery Diagnosis* , Journal of Vibration Engineering. 2000, 13(2):271-276.

[16] M Jachan, G Matz and F Hlawatsch, *Time-Frequency Autoregressive Random Processes: Modeling and Fast Parameter Estimation*, IEEE ICASSP-2003. 2003:125-128.

[17] M Jachan, G Matz and F Hlawatsch, *Least-squares and Maximum-likelihood TFAR Parameter estimation for nonstationary processes*, IEEE ICASSP-2006. 2006, vol(III):492C495.

[18] M Jachan, G Matz and F Hlawatsch, *Vector Time-Frequency AR Models for Nonstationary Multivariate Random Processes*, IEEE transactions on signal processing. 2009, 57(12): 4646-4658.

[19] M Jachan, G Matz and F Hlawatsch, *Time-Frequency ARMA Models and Parameter Estimators for Underspread Nonstationary Random Processes*, IEEE transactions on signal processing. 2007, 55(9):4366-4380.

[20] L.R.Padovese, *Hybrid time-frequency methods for non-stationary mechanical signal analysis*, Mechanical Systems and Signal Processing. 2004, 18:1047-1064.

[21] G.Poulimenos, S.D.Fassois, *Parametric time-domain methods for non-stationary random vibration modeling and analysis-A critical survey and comparison*, Mechanical Systems and Signal Processing. 2006, 20(4):763-816.

[22] Min Shao, C L Nikias, *Signal processing with fractional lower order moments :stable processes and their applications*, Proceedings of the IEEE. 1993, 81(7):986-1010.

[23] Xinyu Ma, C L Nikias, *Parameter estimation and blind channel identification in impulsive signal environments*, IEEE Transactions on Signal Processing. 1995, 43(12):2884-2897.

[24] Tsung-Hsien Liu, Jerry M. Mendel, *A Subspace-Based Direction Finding Algorithm Using Fractional Lower Order Statistics*, IEEE transactions on signal processing. 2001, 49(8):1605-1613.

[25] Xinyu Ma, C L Nikias, *Joint estimation of time delay and frequency delay in impulsive noise using fractional lower order statistics*, IEEE Transactions on Signal Processing. 1996, 44(11):2669-2687.

[26] Changning Li, Gang Yu, *A New Statistical Model For Rolling Element Bearing Fault Signals Based On Alpha-Stable Distribution*, Second International Conference on Computer Modeling and Simulation. 2010:386-390.

[27] YU Xiang-Mei, SHU Tong, *Fault Diagnosis Method for Gearbox Based on -Stable Distribution Parameters and Support Vector Machines*, Measurement and Control Technology. 2012, 31(8):21-30.

[28] Gang Yu, Chang-Ning Li, Jian-feng Zhang, *A new statistical modeling and detection method for rolling element bearing faults based on alphaCstable distribution*, Mechanical Systems and Signal Processing. 2013, 10(41):155C175.

[29] Jianhong Wang, Yongqiang Ye.et, *Fractional zero-phase filtering based on the Riemann-Liouville integral*, Signal Processing. 2014, 98(5):150-157.

[30] Jianhong Wang, Yongqiang Ye.et, *Fractional compound integral with application to ECG signal denoising*, Circuits, Systems, Signal Processing. 2015, 34:1915-1930.

[31] Jianhong Wang, Yongqiang Ye.et, *Parallel-type fractional zero-phase filtering for ECG signal denoising*, Biomedical Signal Processing and Control. 2015, 18:36-41.

[32] *CWRU bearing data center:(http://csegroups.case.edu/bearingdatacenter/*.

[33] M Jachan, G Matz, and F Hlawatsch, *Time-frequency-moving-average processes: pinciples and cepstralmethods for parameter estimation*, IEEE ICASSP-2004. 2004, vol(II):757C760.

[34] WANG Shouyong, ZHU Xiaobo, *α spectrum estimation method for ARMA $S\alpha S$ process based on FLOC*, Journal on Communications. 2007, 28(7):98-103.

Junbo Long graduated from Hunan normal University, China, in 2003. He received the M. Sc.degree from Dalian university of technology, China, in 2013. He is currently a lecturer at jiujiang University. Her research interests include fractional lower order signal processing and time-frequency signal processing.email: 18488870 @qq.com

Wang Haibin graduated from Hunan normal University, China, in 2003. He received the M. Sc.degree from Huazhong university of science and technology, China, in 2010. He is currently a lecturer at jiujiang University. Her research interests include fractional lower order signal processing and image signal processing. email: 18488870 @qq.com

Li Peng graduated from Central China Normal University, China, in 2003. He received the M. Sc.degree from Huazhong university of science and technology, China, in 2008. He is currently a lecturer at jiujiang University. Her research interests include non-Gaussian signal processing and time-frequency signal processing. email: 47071565 @qq.com

Fan Hongshe graduated from Shaanxi University of technology, China, in 1998. He received the M. Sc.degree from radar university, China, in 2004. He is currently a professor at jiujiang University. Her research interests include radar signal processing and communication signal processing. 819285223@qq.com

An Exploration on Adaptive Iterative Learning Control for a Class of Commensurate High-order Uncertain Nonlinear Fractional Order Systems

Jianming Wei, Yun-an Hu, and Meimei Sun

***Abstract*—This paper explores the adaptive iterative learning control method in the control of fraction order systems for the first time. An adaptive iterative learning control (AILC) scheme is presented for a class of commensurate high-order uncertain nonlinear fractional order systems in the presence of disturbance. To facilitate the controller design, a sliding mode surface of tracking errors is designed by using sufficient conditions of linear fraction order. To relax the assumption of the identical initial condition in iterative learning control (ILC), a new boundary layer function is proposed by employing Mittag-Leffler function. The uncertainty in the system is compensated for by utilizing radial basis function neural network. Fractional order differential type updating laws and difference type learning law are designed to estimate unknown constant parameters and time-varying parameter, respecitvely. The hyperbolic tangent function and a convergent series sequence are used to design robust control term for neural network approximation error and bounded disturbance, simultaneously guaranteeing the learning convergence along iteration. The system output is proved to converge to a small neighborhood of the desired trajectory by constructing Lyapnov-like composite energy function (CEF) containing new integral type Lyapunov function, while keeping all the closed-loop signals bounded. Finally, a simulation example is presented to verify the effectiveness of the proposed approach.**

***Index Terms*—Adaptive iterative learning control, fractional order nonlinear systems, Mittag-Leffler function, boundary layer function, composite energy function, fractional order differential learning law .**

I. Introduction

PAST decades have witnessed tremendous research efforts aiming at the development of systematic design methods for the iterative learning control (ILC) of nonlinear systems performing control task over a finite interval repeatedly. ILC has been proven to be the most suitable and effective control scheme for such repeatable control tasks owing to its capacity of achieving perfect tracking by learning along iteration. Generally, according to the stability analysis tool, ILC can be categorized into two classes: traditional ILC [1]−[5] and adaptive ILC (AILC) [6]−[16]. The basic idea of traditional ILC is to use information of the previous execution to design the control signal for current operation by a learning mechanism, which allows to achieve improving performance from iteration to iteration. Furthermore, the stability conclusion of traditional ILC is usually obtained by using contraction mapping theorem and fixed point theorem, which enables traditional ILC to deal with nonlinear plants without needing any information of the system. Traditional ILC has been developed greatly in theory and application because of its simplicity and availability. However, the main drawback of traditional ILC lies in the requirement of the global Lipschitz continuous condition, which restricts its application to certain nonlinear systems. Besides, the usage of contraction mapping theorem rather than Lyapunov method as the key tool of stability analysis in traditional ILC makes it difficult to relax the global Lipschitz condition to local Lipschitz or even non-Lipschitz condition and cooperate with the mainstream methods of nonlinear control theory, such as adaptive control and neural control. To overcome the constraints of traditional ILC, some researchers tried to introduce the idea of adaptive control into ILC and proposed adaptive iterative learning control (AILC) [6], [7]. AILC takes advantage of both adaptive control and ILC, which successfully overcomes the restriction of global Lipschitz condition, thus it enables us to use fuzzy logic systems or neural networks as approximators to deal with nonlinear uncertainties. In general, the control parameters of AILC methods are tuned along the iteration axis, and the so-called composite energy function (CEF) [8] is usually constructed to analyze the stability and convergence property of the closed-loop systems. The past decade has witnessed great progress in AILC of uncertain nonlinear systems [9]−[16].

Fractional calculus is a promising topic for more than 300 years. But the researches are mainly in the field of mathematical sciences [17], [18]. Until recent decade, the applications of fractional calculus develop rapidly [19], [20]. Fractional order systems allow us to describe and model a real object more accurately than the classical integer order dynamical systems. Among the investigations of fractional order systems in the past decades, control design for some fractional order systems has been a hot topic. Many different control methods have been proposed for various kinds of fractional systems [20]−[28]. Especially, the research on control and synchronization control design for fractional order chaotic systems is very active [29]−[39].

Comparing with such a large number of results, the papers

This article has been accepted for publication in a future issue of this journal, but has not been fully edited. Content may change prior to final publication.

This work was supported by National Natural Science Foundation of China (60674090). Recommended by Associate Editor Yangguan Chen.

Citation: J. M. Wei, Y. A. Hu, and M. M. Sun, “An exploration on adaptive iterative learning control for a class of commensurate high-order uncertain nonlinear fractional order systems,” *IEEE/CAA Journal of Automatica Sinica*, pp. 1–10, 2017. DOI: 10.1109/JAS.2017.7510361.

J. M. Wei, Y. A. Hu, and M. M. Sun are with the Department of Control Engineering, Naval Aeronautical Engineering Institute, Yantai 264001, China (e-mail: wjm604@163.com; hya507@sina.com; smm6224582@sina.cn).

on the ILC control of fractional order systems are relatively less. Only a few works are reported in the filed of ILC [40]-[53]. Moreover, all these literatures are from the viewpoint of traditional ILC and the stability conclusions are obtained by using contraction mapping theorem method. Therefore, as results of integer-order systems, global Lipschitz condition is required for traditional ILC schemes. As for AILC problem of fractional order systems, to the best of our knowledge, there are no results having been reported.

In this paper, we present an AILC scheme for a class of nonlinear fractional order system with both parametric and nonparametric uncertainties in the presence of disturbance. As far as we know, up till now no works have been presented for such a problem. In the proposed AILC scheme, adaptive iterative learning controller with fractional order differential type and difference type learning laws are presented and the CEF containing new integral type Lyapunov function is constructed to analyze the stability and convergence property. The main contributions of the proposed AILC scheme and stability analysis are highlighted as follows: 1) To the best of our knowledge, it is the first time, in the literature, that AILC problem of fractional order system is investigated. 2) A sliding mode surface of tracking errors is designed by using the sufficient condition for linear fractional order systems. 3) A new boundary layer function using Mittag-Leffler function is designed to deal with the initial condition problem in the ILC design of fractional order system. 4) Fractional order differential type learning laws with alignment method for unknown constant parameters is used in the AILC method for the first time and integral type Lyapunov function is used to analyze the convergence of estimation errors. 5) The hyperbolic tangent function is used to design robust control term for neural network approximation error and bounded disturbance, and a convergent series is introduced to guarantee the learning convergence along iteration index.

The rest of this paper is organized as follow. The problem formulation and preliminaries are given in Section II. The AILC design with parameter updating laws is developed in section III. In Section IV, the CEF-based stability analysis is presented. A simulation example is presented to verify the validity of the proposed scheme in Section V, followed by conclusion in Section VI.

II. Problem Formulation and Preliminaries

A. Preliminaries

In this subsection, some basic definitions and useful lemmas are given.

Definition 1 [18]: Fractional calculus is a generalization of integration and differentiation to noninteger-order fundamental operator ${}_aD_t^\alpha$, where a and t are the bounds of the operation and $\alpha \in \mathbf{R}$. The continuous integro-differential operator is defined as

$$ {}_aD_t^\alpha = \begin{cases} \frac{d^\alpha}{\mathrm{d}t^\alpha}, & \alpha > 0, \\ 1, & \alpha = 0, \\ \int_a^t (\mathrm{d}\sigma)^\alpha, & \alpha < 0. \end{cases} \tag{1} $$

Definition 2 [17]: The most important function used in fractional calculus-Euler's gamma function is defined as

$$ \Gamma(\alpha) = \int_0^\infty \mathrm{e}^{-\sigma}\sigma^{\alpha-1}\mathrm{d}\sigma. \tag{2} $$

Definition 3 [17]: Another important function in the fractional calculus named Mittag-Leffler type with two parameters is defined as

$$ E_{\alpha,\ \beta}(z) = \sum_{j=0}^{\infty} \frac{z^j}{\Gamma(\alpha j+\beta)}, \alpha > 0, \beta > 0. \tag{3} $$

Especially, when $\beta = 1$, we obtain the Mittag-Leffler function with one parameter

$$ E_{\alpha,\ 1}(z) = \sum_{j=0}^{\infty} \frac{z^j}{\Gamma(\alpha j+1)} \triangleq E_\alpha(z). \tag{4} $$

For integer values of α, (4) reduces to the well-known Cauchy repeated integration formula.

The three most frequently used definitions for the general fractional differintegral are: The Grünwald-Letnikov (GL) definition, the Riemann-Liouville (RL) and Caputo definitions.

Definition 4 [17]: The Grünwald-Letnikov derivative definition of order α is described as

$$ {}_aD_t^\alpha f(t) = \lim_{h\to 0}\frac{1}{h^\alpha}\sum_{j=0}^{\infty}(-1)^j \begin{pmatrix} \alpha \\ j \end{pmatrix} f(t-jh) \tag{5} $$

with

$$ \begin{pmatrix} \alpha \\ j \end{pmatrix} = \frac{\alpha!}{j!(\alpha-j)!} = \frac{\Gamma(\alpha+1)}{\Gamma(j-1)\Gamma(\alpha-j+1)}. \tag{6} $$

Definition 5 [54]: The Riemann-Liouville fractional integral of order α of function $f(t)$ at a time instant $t \geq 0$ is defined as:

$$ {}_aI_t^\alpha f(t) = {}_aD_t^{-\alpha} f(t) = \frac{1}{\Gamma(\alpha)}\int_a^t f(\sigma)(t-\sigma)^{\alpha-1}\mathrm{d}\sigma. \tag{7} $$

From (7) we can write formula for the Riemann-Liouville definition of fractional derivative of order α in the following form

$$ {}_aD_t^\alpha f(t) = \frac{1}{\Gamma(n-\alpha)}\frac{\mathrm{d}^n}{\mathrm{d}t^n}\int_a^t \frac{f(\sigma)}{(t-\sigma)^{\alpha-n+1}}\mathrm{d}\sigma, \tag{8} $$

for $n-1 < \alpha < n$.

Definition 6 [17]: The Caputo fractional integral of order α of function $f(t)$ at time $t \geq 0$ is defined as

$$ {}_aD_t^\alpha f(t) = \frac{1}{\Gamma(n-\alpha)}\int_a^t \frac{f^{(n)}(\sigma)}{(t-\sigma)^{\alpha-n+1}}\mathrm{d}\sigma, \tag{9} $$

for $n-1 < \alpha < n$.

Remark 1: Actually, the above three definitions are equivalent under some conditions. We will use the Caputo definition in this paper. In the rest of this paper, the notation $D^\alpha(\cdot)$ indicates the Caputo derivative of order α with $a = 0$, i.e., $D^\alpha(\cdot) \triangleq {}_0D_t^\alpha(\cdot)$.

Lemma 1 [55], [56]: Consider the following fractional order autonomous system

$$ D^\alpha x(t) = Ax(t), x(0) = x_0, \tag{10} $$

where $0<\alpha<1$, $x\in\mathbf{R}^n$ and $A\in\mathbf{R}^{n\times n}$. This system is asymptotically stable if and only if $|\arg(\lambda(A))|>\alpha\frac{\pi}{2}$. In this situation, the components of the state vector decay toward zero like $t^{-\alpha}$.

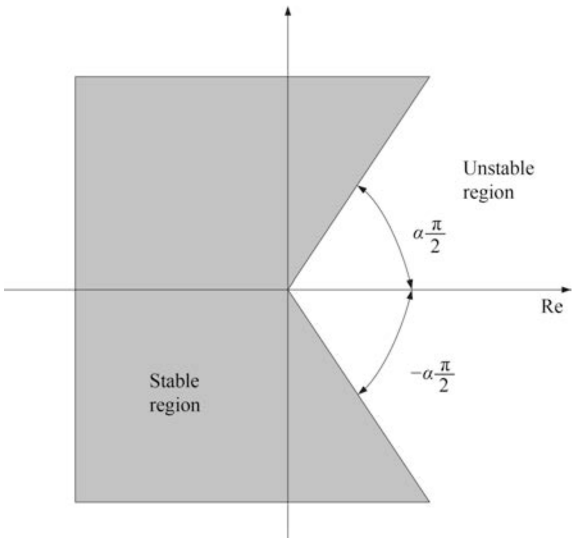

Fig. 1. Stability domain for fractional order linear systems with $0<\alpha<1$.

Lemma 1 [57]: The fractional system $D^\alpha y(t)=u(t)$, $0<\alpha<1$, is equivalent to the following continuous frequency distributed model

$$\begin{cases}\frac{\partial z(\omega,t)}{\partial t}=-\omega z(\omega,t)+u(t),\\ y(t)=\int_0^\infty \mu(\omega)z(\omega,t)\mathrm{d}\omega,\end{cases}\tag{11}$$

with weighting function $\mu(\omega)=\frac{\sin(\alpha\pi)}{\pi\omega^\alpha}$, $z(\omega,t)\in\mathbf{R}$.

B. Problem Formulation

In this paper, we consider a class of commensurate high-order uncertain nonlinear systems in the presence of disturbance which runs on a finite interval $[0,T]$ repeatedly given by

$$\begin{cases}D^\alpha x_{i,k}(t)=x_{i+1,k}(t), i=1,\cdots,n-1,\\ D^\alpha x_{n,k}(t)=f(x_k(t))+\theta(t)\xi(x_k(t))+u_k(t)+d(t),\\ y_k(t)=x_{1,k}(t),\end{cases}\tag{12}$$

where $t\in[0,T]$ is the time, $k\in\mathbf{N}$ denotes the times of iteration; $x_{i,k}(t)\in\mathbf{R}$ $i=1,\cdots,n$ and $y_k(t)$ are the pseudo state and output variables, respectively; $x_k(t)=\left[x_{1,k}(t),x_{2,k}(t),\cdots,x_{n,k}(t)\right]^{\mathrm{T}}\in\mathbf{R}^n$ is the pseudo state vector; $f(\cdot)$ is an unknown smooth function. $d(t)$ is unknown bounded external disturbance. $u_k(t)\in\mathbf{R}$ is the control input. The control objective of this paper is to design the adaptive iterative learning controller to steer the output $y_k(t)$ to follow the desired reference signal $r(t)$.

Define $r_1(t)=r(t)$ and $r_{i+1}(t)=D^\alpha r_i(t)$, $i=1,2,\cdots,n-1$. Then we can write the desired reference vector as $x_d(t)=[r_1(t),r_2(t),\cdots,r_n(t)]^{\mathrm{T}}$. Define the tracking errors as $e_{i,k}(t)=x_{i,k}(t)-r_i(t)$, $i=1,2,\cdots,n$. Then the tracking error vector can be given by $e_k(t)=x_k(t)-x_d(t)=\left[e_{1,k}(t),e_{2,k}(t),\cdots,e_{n,k}(t)\right]^{\mathrm{T}}$. In the rest of this paper, the denotation t will be omitted when no confusion arises.

Choose the sliding surface as $e_{s,k}=\left[\Lambda^{\mathrm{T}}\ 1\right]e_k$, where $\Lambda=\left[\lambda_1,\lambda_2,\cdots,\lambda_{n-1}\right]^{\mathrm{T}}$ and $\lambda_1,\cdots,\lambda_{n-1}$ are chosen suitably such that the eigenvalues of the matrix B satisfy condition of Lemma 1, where the matrix B is given by

$$B=\begin{bmatrix}0 & & \\ \vdots & I_{n-2} & \\ 0 & & \\ -\lambda_1 & \cdots & -\lambda_{n-1}\end{bmatrix},\tag{13}$$

with I_{n-2} as unit matrix of $n-2$ dimensions. Then keeping the system's errors on this surface leads to the asymptotic stability of error systems and therefore output tracking of the desired reference signal.

To facilitate control system design, the following reasonable assumptions are made.

Assumption 1: The unknown external disturbance is bounded.

Assumption 2: The desired state trajectory $x_d(t)$ is continuous, bounded and available.

Assumption 3: The initial state errors $e_{i,k}(0)$ at each iteration are not necessarily zero, small and fixed, but assumed to be bounded.

C. RBF Neural Networks

In control engineering, two types of artificial neural networks are usually used to approximate unknown smooth functions, which specifically are linearly parameterized neural networks (LPNNs) and multilayer neural networks (MNNs). As a kind of LPNNs, the radial basis function (RBF) neural network (NN) [58] is usually used as a tool to model unknown nonlinear functions owing to its nice approximation capabilities. The RBF NN can be seen as a two-layer network in which hidden layer performs a fixed nonlinear transformation with no adjustable parameters, i.e., the input space is mapped into a new space. The output layer then combines the outputs in the latter space linearly. Generally, the RBF NN approximates the continuous function $Q(Z):\mathbf{R}^q\to\mathbf{R}$ as follows

$$Q_{nn}(Z)=W^{\mathrm{T}}\phi(Z),$$

where $Z\in\Omega_Z\subset\mathbf{R}^q$ is the input vector, $W=[w_1,w_2,\cdots,w_l]^{\mathrm{T}}\in R^l$ is the weight vector, the NN node number $l>1$; and $\phi(Z)=[\varphi_1(Z),\cdots,\varphi_l(Z)]^{\mathrm{T}}$, with $\varphi_i(Z)$ as the commonly used Gaussian functions, i.e., $\varphi_i(Z)=e^{-(Z-\mu_i)^{\mathrm{T}}(Z-\mu_i)/\sigma_i^2}$, $i=1,\cdots,l$, where $\mu_i=[\mu_{i1},\mu_{i2},\cdots,\mu_{iq}]$ is the center of the receptive field and σ_i is the width of the Gaussian function. It has been proven that if l is chosen sufficiently large, $W^{\mathrm{T}}\phi(Z)$ can approximate any continuous function, $Q(Z)$, to any desired accuracy over a compact set $\Omega_Z\subset\mathbf{R}^q$ in the form of $Q(Z)=W^{*\mathrm{T}}\phi(Z)+\varepsilon(Z)$, $\forall Z\in\Omega_Z\subset\mathbf{R}^q$ where W^* is the ideal constant weight vector, and $\varepsilon(Z)$ is the approximation error which is bounded over the compact set, i.e., $|\varepsilon(Z)|\le\varepsilon^*$, $\forall Z\in\Omega_Z$, where $\varepsilon^*>0$ is an unknown constant. The ideal weight vector W^* is an artificial quantity required for analytical purposes. W^* is defined as the value of W that minimizes $|\varepsilon(Z)|$ for all $Z\in\Omega_Z\subset\mathbf{R}^q$, i.e., $W^*:=\arg\min_{W\in\mathbf{R}^l}\left\{\sup_{Z\in\Omega_Z}\left|h(Z)-W^{\mathrm{T}}\phi(Z)\right|\right\}$.

III. AILC Scheme Design

According to the systems dynamic equation (10) and definition of tracking errors, we can have the dynamics of tracking errors

$$\begin{cases} D^{\alpha}e_{i,k}(t) = & e_{i+1,k}(t), i=1,\cdots,n-1, \\ D^{\alpha}e_{n,k}(t) = & f(x_k(t))+\theta(t)\xi(x_k(t))+u_k(t) \\ & +d(t)-D^{\alpha}r_n. \end{cases} \tag{14}$$

By taking the derivative of order α of sliding surface, one has

$$\begin{aligned} D^{\alpha}e_{s,k} &= D^{\alpha}e_{n,k}+D^{\alpha}\left(\sum_{i=1}^{n-1}\lambda_i e_{i,k}\right) \\ &= D^{\alpha}e_{n,k}+\sum_{i=1}^{n-1}\lambda_i D^{\alpha}e_{i,k} \\ &= f(x_k(t))+\theta(t)\xi(x_k(t))+u_k(t)+d(t) \\ &\quad -D^{\alpha}r_n+\sum_{i=1}^{n-1}\lambda_i e_{i+1,k}. \end{aligned} \tag{15}$$

According to Assumption 3, there exist known constants ε_i, such that, $|e_{i,k}(0)|\le\varepsilon_i$, $i=1,2,\cdots,n$ for any $k\in\mathbf{N}$. In order to overcome the uncertainty from initial resetting errors, we define a novel boundary layer function by employing Mittag-Leffler function

$$\eta(t)=\varepsilon E_{\alpha}(-Kt), K>0, \tag{16}$$

where $\varepsilon=\left[\Lambda^{\mathrm{T}}\ 1\right][\varepsilon_1,\varepsilon_2,\cdots,\varepsilon_n]^{\mathrm{T}}$.

Remark 2: As the boundary layer function[13−15] in integer order case, $\eta(t)$ has good property of decreasing along time axis with initial condition $\eta(0)=\varepsilon$. Moreover, it is clear that $D^{\alpha}\eta(t)=\varepsilon D^{\alpha}E_{\alpha}(-Kt)=-K\varepsilon E_{\alpha}(-Kt)=-K\eta(t)$.

Then we can define an auxiliary error signal as

$$s_k(t)=e_{s,k}(t)-\eta(t)\mathrm{sat}\left(\frac{e_{s,k}(t)}{\eta(t)}\right), \tag{17}$$

where $\mathrm{sat}(\cdot)$ is the saturation function which is defined as

$$\mathrm{sat}(\cdot)=\mathrm{sgn}(\cdot)\cdot\min\{|\cdot|,1\}, \tag{18}$$

with $\mathrm{sgn}(\cdot)=\begin{cases} 1, \text{if } \cdot >0 \\ 0, \text{if } \cdot =0 \\ -1, \text{if } \cdot <0 \end{cases}$ as the sign function.

Subsequently, it can be easily obtained that

$$\begin{aligned} |e_{sk}(0)| &= |\lambda_1 e_{1,k}(0)+\lambda_2 e_{2,k}(0)+\cdots+e_{n,k}(0)| \\ &\le \lambda_1|e_{1,k}(0)|+\lambda_2|e_{2,k}(0)|+\cdots+|e_{n,k}(0)| \\ &\le \lambda_1\varepsilon_1+\lambda_2\varepsilon_2+\cdots+\varepsilon_n=\eta(0), \end{aligned} \tag{19}$$

which implies that $s_k(0)=e_{sk}(0)-\eta(0)\frac{e_{sk}(0)}{\eta(0)}=0$ is satisfied for all $k\in\mathbf{N}$. Moreover, there exists the fact that

$$\begin{aligned} s_k(t)\,\mathrm{sat}\left(\frac{e_{sk}(t)}{\eta(t)}\right) &= \begin{cases} 0, & \text{if } \left|\frac{e_{sk}(t)}{\eta(t)}\right|\le 1 \\ s_k(t)\,\mathrm{sgn}(e_{sk}(t)), & \text{if } \left|\frac{e_{sk}(t)}{\eta(t)}\right|>1 \end{cases} \\ &= s_k(t)\,\mathrm{sgn}(s_k(t))=|s_k(t)|. \end{aligned} \tag{20}$$

To overcome the design difficulty from uncertainty $f(x_k(t))$, we employ radial basis function neural network to approximate $f(x_k(t))$ in the form of

$$f(x_k(t))=W^{*\mathrm{T}}\phi(x_k)+\varepsilon(x_k). \tag{21}$$

From Lemma 2, we can obtain the equivalent continuous frequency distributed model of dynamical system of s_k

$$\begin{cases} \frac{\partial z_k(\omega,t)}{\partial t}=-\omega z_k(\omega,t)+D^{\alpha}s_k, \\ s_k(t)=\int_0^{\infty}\mu(\omega)z_k(\omega,t)\mathrm{d}\omega, \end{cases} \tag{22}$$

with weighting function $\mu(\omega)=\frac{\sin(\alpha\pi)}{\pi\omega^{\alpha}}$, $z_k(\omega,t)\in\mathbf{R}$ is the true error variable.

Define a smooth scalar positive function as

$$V_{s,k}(t)=\frac{1}{2}\int_o^{\infty}\mu(\omega)z_k^2(\omega,t)\mathrm{d}\omega. \tag{23}$$

The time derivative of $V_{s,k}(t)$ can be expressed as

$$\begin{aligned} \dot V_{s,k}(t) &= \int_0^{\infty}\mu(\omega)z_k(\omega,t)\frac{\partial z_k(\omega,t)}{\partial t}\mathrm{d}\omega \\ &= \int_0^{\infty}\mu(\omega)z_k(\omega,t)(-\omega z_k(\omega,t)+D^{\alpha}s_k)\mathrm{d}\omega \\ &= -\int_0^{\infty}\mu(\omega)\omega z_k^2(\omega,t)\mathrm{d}\omega+s_kD^{\alpha}s_k \\ &= \begin{cases} -\int_0^{\infty}\mu(\omega)\omega z_k^2(\omega,t)\mathrm{d}\omega \\ +s_k\left(D^{\alpha}e_{s,k}-D^{\alpha}\eta(t)\,\mathrm{sgn}(s_k)\right), |e_{s,k}|>\eta(t) \\ -\int_0^{\infty}\mu(\omega)\omega z_k^2(\omega,t)\mathrm{d}\omega, |e_{s,k}|\le\eta(t) \end{cases} \\ &= -\int_0^{\infty}\mu(\omega)\omega z_k^2(\omega,t)\mathrm{d}\omega+s_k\left(D^{\alpha}e_{s,k}-D^{\alpha}\eta(t)\,\mathrm{sgn}(s_k)\right) \\ &= -\int_0^{\infty}\mu(\omega)\omega z_k^2(\omega,t)\mathrm{d}\omega+s_k\big(W^{*\mathrm{T}}\phi(x_k)+\varepsilon(x_k) \\ &\quad +\theta(t)\xi(x_k)+u_k+d(t)-D^{\alpha}r_n+\sum_{i=1}^{n-1}\lambda_i e_{i+1,k} \\ &\quad +K\eta(t)\,\mathrm{sgn}(s_k)\big) \\ &= -\int_0^{\infty}\mu(\omega)\omega z_k^2(\omega,t)\mathrm{d}\omega+s_k\big(W^{*\mathrm{T}}\phi(x_k)+\varepsilon(x_k) \\ &\quad +\theta(t)\xi(x_k)+u_k+d(t)-D^{\alpha}r_n+\sum_{i=1}^{n-1}\lambda_i e_{i+1,k} \\ &\quad -Ke_{s,k}+Ke_{s,k}+K\eta(t)\,\mathrm{sgn}(s_k)\big) \\ &= -\int_0^{\infty}\mu(\omega)\omega z_k^2(\omega,t)\mathrm{d}\omega+s_k\Big(W^{*\mathrm{T}}\phi(x_k)+\theta(t)\xi(x_k) \\ &\quad +u_k+\bar d(t)-D^{\alpha}r_n+\sum_{i=1}^{n-1}\lambda_i e_{i+1,k}+Ke_{s,k}\Big)-Ks_k^2, \end{aligned} \tag{24}$$

where $\bar d(t)=d(t)+\varepsilon(x_k)$ and using the equality

$$\begin{aligned} & s_k(t)(-Ke_{sk}(t)+K\eta(t)\,\mathrm{sgn}(s_k(t))) \\ &= s_k(t)\left(-Ks_k(t)-K\eta(t)\,\mathrm{sat}\left(\frac{e_{sk}(t)}{\eta(t)}\right)\right. \\ &\quad \left.+K\eta(t)\,\mathrm{sgn}(s_k(t))\right) \\ &= -Ks_k^2(t)-K\eta(t)|s_k(t)|+K\eta(t)|s_k(t)| \\ &= -Ks_k^2(t). \end{aligned} \tag{25}$$

Obviously, $\bar d(t)$ is bounded, i.e., there exists an unknown positive constant ρ such that $|\bar d(t)|\le\rho$.

Then we can determine the control law as

$$u_k(t) = D^\alpha r_n - \sum_{i=1}^{n-1} \lambda_i e_{i+1,k} - K e_{s,k} - \hat{W}_k^{\mathrm{T}} \phi(x_k) - \hat{\theta}_k(t)\,\xi(x_k) - \hat{\rho}_k \tanh\left(\frac{s_k \hat{\rho}_k}{\Delta_k}\right), \quad (26)$$

where $\hat{W}_k$, $\hat{\theta}_k(t)$ and $\hat{\rho}_k$ are the estimates of W^*, $\theta(t)$ and ρ, respectively, Δ_k is a convergent series sequence which is defined as $\Delta_k = \frac{q}{k^m}$, l and q are constant design parameters and $q(\in \mathbf{R}) > 0$, $m(\in \mathbf{Z}_+) \geq 2$. For preceding analysis, we need the following lemmas.

Lemma 3 [59]: For any $\Delta_k > 0$ and $x \in \mathbf{R}$, the inequality $|x| - x\tanh(x/\Delta_k) \leq \gamma\Delta_k$ is established, where γ is a positive constant and $\gamma = \mathrm{e}^{-(\gamma+1)}$ or $\gamma = 0.2785$.

Lemma 4 [60]: $\lim_{k\to\infty} \sum_{j=1}^{k} \Delta_j \leq 2q$.

The adaptive learning laws for unknown parameters are designed as

$$\begin{cases} D^\alpha \hat{W}_k(t) = \Gamma_W s_k(t)\,\phi(x_k), \\ \hat{W}_k(0) = \hat{W}_{k-1}(T),\, \hat{W}_1(0) = 0, \end{cases} \quad (27)$$

$$\begin{cases} \hat{\theta}_k(t) = \hat{\theta}_{k-1}(t) + q_\theta s_k(t)\,\xi(x_k), \\ \hat{\theta}_0(t) = 0,\, t \in [0,T], \end{cases} \quad (28)$$

$$\begin{cases} D^\alpha \hat{\rho}_k(t) = q_\rho |s_k(t)|, \\ \hat{\rho}_k(0) = \hat{\rho}_{k-1}(T),\, \hat{\rho}_1(0) = 0, \end{cases} \quad (29)$$

where $\Gamma_W \in \mathbf{R}^{l\times l}$ is a positive square matrix and $q_\theta, q_\rho > 0$ are design parameters. In the following parts, we define the estimation error of $\Theta(t)$ as $\tilde{\Theta}_k(t) = \hat{\Theta}_k(t) - \Theta(t)$ where $\Theta(t)$ denotes W^*, $\theta(t)$ and ρ.

Substituting the controller (26) back into (24) yields

$$\begin{aligned} \dot{V}_{s,k}(t) \leq & -\int_0^\infty \mu(\omega)\,\omega z_k^2(\omega,t)\mathrm{d}\omega - s_k \tilde{W}_k^{\mathrm{T}} \phi(x_k) \\ & - s_k \tilde{\theta}_k(t)\,\xi(x_k) + |s_k|\rho - |s_k|\hat{\rho}_k \\ & + |s_k|\hat{\rho}_k - s_k\hat{\rho}_k \tanh\left(\frac{s_k\hat{\rho}_k}{\Delta_k}\right) - Ks_k^2 \\ \leq & -\int_0^\infty \mu(\omega)\,\omega z_k^2(\omega,t)\mathrm{d}\omega - s_k \tilde{W}_k^{\mathrm{T}} \phi(x_k) \\ & - s_k \tilde{\theta}_k(t)\,\xi(x_k) - |s_k|\tilde{\rho}_k + \gamma\Delta_k - Ks_k^2 \\ \leq & -s_k \tilde{W}_k^{\mathrm{T}} \phi(x_k) - s_k \tilde{\theta}_k(t)\,\xi(x_k) \\ & - |s_k|\tilde{\rho}_k + \gamma\Delta_k - Ks_k^2. \end{aligned} \quad (30)$$

From adaptive updating laws (27) and (29) it follows

$$D^\alpha \tilde{W}_k = D^\alpha \hat{W}_k - D^\alpha W^* = D^\alpha \hat{W}_k, \quad (31)$$

$$D^\alpha \tilde{\rho}_k = D^\alpha \hat{\rho}_k - D^\alpha \rho = D^\alpha \hat{\rho}_k. \quad (32)$$

According to Lemma 2, we can obtain the distributed frequency model of (31) and (32) as follows

$$\begin{cases} \frac{\partial z_{W,k}(\omega,t)}{\partial t} = -\omega z_{W,k}(\omega,t) + \Gamma_W s_k(t)\,\phi(x_k), \\ \tilde{W}_k(t) = \int_0^\infty \mu(\omega)\, z_{W,k}(\omega,t)\mathrm{d}\omega, \end{cases} \quad (33)$$

$$\begin{cases} \frac{\partial z_{\rho,k}(\omega,t)}{\partial t} = -\omega z_{\rho,k}(\omega,t) + q_\rho |s_k(t)|, \\ \tilde{\rho}_k(t) = \int_0^\infty \mu(\omega)\, z_{\rho,k}(\omega,t)\mathrm{d}\omega, \end{cases} \quad (34)$$

where $z_{W,k}(\omega,t) \in \mathbf{R}^l$ and $z_{\rho,k}(\omega,t) \in \mathbf{R}$ are the true estimation error variables.

Define a positive scalar positive function of parameter estimation errors as

$$V_{p,k}(t) = \frac{1}{2}\int_o^\infty \mu(\omega)\, z_{W,k}^{\mathrm{T}}(\omega,t)\,\Gamma_W^{-1} z_{W,k}(\omega,t)\mathrm{d}\omega + \frac{1}{2q_\rho}\int_o^\infty \mu(\omega)\, z_{\rho,k}^2(\omega,t)\mathrm{d}\omega. \quad (35)$$

Taking the time derivative of $V_{p,k}(t)$ results in

$$\begin{aligned} \dot{V}_{p,k}(t) = & \int_o^\infty \mu(\omega)\, z_{W,k}^{\mathrm{T}}(\omega,t)\,\Gamma_W^{-1} \frac{\partial z_{W,k}(\omega,t)}{\partial t}\mathrm{d}\omega \\ & + \frac{1}{q_\rho}\int_o^\infty \mu(\omega) z_{\rho,k}(\omega,t) \frac{\partial z_{\rho,k}(\omega,t)}{\partial t}\mathrm{d}\omega \\ = & -\int_o^\infty \mu(\omega)\,\omega z_{W,k}^{\mathrm{T}}(\omega,t)\,\Gamma_W^{-1} z_{W,k}(\omega,t)\mathrm{d}\omega \\ & + \Gamma_W^{-1} D^\alpha \tilde{W}_k^{\mathrm{T}} \int_o^\infty \mu(\omega)\, z_{W,k}(\omega,t)\mathrm{d}\omega \\ & - \frac{1}{q_\rho}\int_o^\infty \mu(\omega)\,\omega z_{\rho,k}^2(\omega,t)\mathrm{d}\omega \\ & + \frac{1}{q_\rho} D^\alpha \tilde{\rho}_k \int_o^\infty \mu(\omega)\, z_{\rho,k}(\omega,t)\mathrm{d}\omega \\ \leq & s_k \tilde{W}_k^{\mathrm{T}} \phi(x_k) + |s_k|\tilde{\rho}_k. \end{aligned} \quad (36)$$

Define a Lyapunov candidate as $V_k(t) = V_{s,k}(t) + V_{p,k}(t)$. Hence, we can obtain the derivative of $V_k(t)$ with respect to time by combining (30) and (36)

$$\dot{V}_k \leq -Ks_k^2 - s_k\tilde{\theta}_k(t)\,\xi(x_k) + \gamma\Delta_k. \quad (37)$$

IV. Analysis of Stability and Convergence

In this section, we will prove that the controller can guarantee the stability of the closed-loop system and the convergence of tracking errors.

The stability of the proposed AILC scheme is summarized as follows.

Theorem 1: Considering the fractional order system (12), and designing adaptive iterative learning controller (26) and with parameter adaptive learning algorithms (27)−(29), the following properties can be guaranteed: 1) all the signals of the closed-loop system are bounded; 2) the pseudo error variable $s_k(t)$ converges to zero as $k \to \infty$, i.e., $\lim_{k\to\infty} \int_0^T (s_k(\sigma))^2 \mathrm{d}\sigma \leq 0$.

Proof: Define the Lyapunov-like CEF as

$$E_k(t) = V_k(t) + \frac{1}{2q_\theta}\int_0^t \tilde{\theta}_k^2(\sigma)\,\mathrm{d}\sigma. \quad (38)$$

The proof includes four parts.

1) Difference of $E_k(t)$

Compute the difference of $E_k(t)$, which is

$$\begin{aligned} \Delta E_k(t) = & E_k(t) - E_{k-1}(t) \\ = & V_k(t) - V_{k-1}(t) \\ & + \frac{1}{2q_\theta}\int_0^t \left[\tilde{\theta}_k^2(\sigma) - \tilde{\theta}_{k-1}^2(\sigma)\right]\mathrm{d}\sigma. \end{aligned} \quad (39)$$

Considering (37), one has

$$V_k(t) \le V_k(0) + \int_0^t \left(-Ks_k^2 - s_k\tilde{\theta}_k(t)\xi(x_k) + \gamma\Delta_k\right)\mathrm{d}\sigma$$
$$= V_{p,k}(0) - K\int_0^t s_k^2 \mathrm{d}\sigma - \int_0^t s_k\tilde{\theta}_k(\sigma)\xi(x_k)\mathrm{d}\sigma + \gamma\Delta_k t. \tag{40}$$

Utilizing the algebraic relation $(\boldsymbol{a}-\boldsymbol{b})^{\mathrm{T}}(\boldsymbol{a}-\boldsymbol{b}) - (\boldsymbol{a}-\boldsymbol{c})^{\mathrm{T}}(\boldsymbol{a}-\boldsymbol{c}) = (\boldsymbol{c}-\boldsymbol{b})^{\mathrm{T}}[2(\boldsymbol{a}-\boldsymbol{b})+(\boldsymbol{b}-\boldsymbol{c})]$ and taking the adaptive learning laws (28) into consideration, we have

$$\frac{1}{2q_\theta}\int_0^t \left[\tilde{\theta}_k^2(\sigma) - \tilde{\theta}_{k-1}^2(\sigma)\right]\mathrm{d}\sigma$$
$$= \int_0^t s_k\tilde{\theta}_k(\sigma)\xi(x_k)\mathrm{d}\sigma - \frac{q_\theta}{2}\int_0^t s_k^2(\sigma)\xi^2(x_k)\mathrm{d}\sigma. \tag{41}$$

Substituting (40) and (41) back into (39), it follows that

$$\Delta E_k(t) \le V_{p,k}(0) - V_{k-1}(t) - K\int_0^t s_k^2\mathrm{d}\sigma + \gamma\Delta_k t. \tag{42}$$

Let $t=T$ in (42). From the adaptive parameter updating laws we know $V_{p,k}(0) = V_{p,k-1}(T)$. Therefore, it follows from (42) that

$$\Delta E_k(T) \le V_{p,k}(0) - V_{p,k-1}(T) - V_{s,k-1}(T)$$
$$- K\int_0^t s_k^2\mathrm{d}\sigma + \gamma\Delta_k T$$
$$\le -K\int_0^t s_k^2\mathrm{d}\sigma + \gamma\Delta_k T. \tag{43}$$

2) The finiteness of $E_k(T)$

According to (38), we know

$$E_1(t) = V_1(t) + \frac{1}{2q_\theta}\int_0^t \tilde{\theta}_1^2(\sigma)\mathrm{d}\sigma. \tag{44}$$

Recalling adaptive updating law (28), we can have $\hat{\theta}_1(t) = q_\theta s_1(t)\xi(x_1)$, which leads to time derivative of $E_1(t)$ as follows

$$\dot{E}_1(t) = \dot{V}_1(t) + \frac{1}{2q_\theta}\tilde{\theta}_1^2(t)$$
$$\le -Ks_1^2 - s_1\tilde{\theta}_1(t)\xi(x_1) + \gamma\Delta_1$$
$$+ \frac{1}{2q_\theta}\left(\tilde{\theta}_1^2(t) - 2\tilde{\theta}_1(t)\hat{\theta}_1(t)\right) + \frac{1}{q_\theta}\tilde{\theta}_1(t)\hat{\theta}_1(t)$$
$$= -Ks_1^2 - s_1\tilde{\theta}_1(t)\xi(x_1) + \gamma\Delta_1 + s_1\tilde{\theta}_1(t)\xi(x_1)$$
$$+ \frac{1}{2q_\theta}\left[\left(\hat{\theta}_1(t) - \theta(t)\right)^2 - 2\left(\hat{\theta}_1(t) - \theta(t)\right)\hat{\theta}_1(t)\right]$$
$$\le -Ks_1^2 + \gamma\Delta_1 + \frac{1}{2q_\theta}\theta^2(t). \tag{45}$$

Denote $c = \max_{t\in[0,T]}\left\{\theta^2(t)/(2q_\theta)\right\}$. Integrating the above inequality over $[0,t]$ yields

$$E_1(t) - E_1(0) \le -K\int_0^t s_1^2(\sigma)\mathrm{d}\sigma + t\cdot c + \theta\Delta_1 t. \tag{46}$$

According to the adaptive updating laws it is clear that $E_1(0) = V_{p,1}(0)$, which is determined by W^* and ρ. Thus the boundedness of $E_1(t)$ can be ensured since

$$E_1(t) \le -K\int_0^t s_1^2(\sigma)\mathrm{d}\sigma + t\cdot c + \theta\Delta_1 t + V_{p,1}(0),\ t\in[0,T]. \tag{47}$$

Letting $t=T$ in (47), we can obtain the boundedness of $E_1(T)$

$$E_1(T) \le -K\int_0^T s_1^2(\sigma)\mathrm{d}\sigma + T(c+\gamma\Delta_1) + V_{p,1}(0)$$
$$< \infty. \tag{48}$$

Applying (43) repeatedly, we may have

$$E_k(T) = E_1(T) + \sum_{j=2}^k \Delta E_j(T)$$
$$\le -K\sum_{j=1}^k\int_0^T s_j^2(\sigma)\mathrm{d}\sigma + T\cdot c_{\max} + \gamma T\sum_{j=1}^k\Delta_k + V_{p,1}(0)$$
$$\le T\cdot c_{\max} + \gamma T\sum_{j=1}^k\Delta_k + V_{p,1}(0). \tag{49}$$

Recalling Lemma 4 we have $\gamma T\sum_{j=1}^k\Delta_k \le \lim_{k\to\infty}\gamma T\sum_{j=1}^k\Delta_k \le 2\gamma Tq$, which further implies the boundedness of $E_k(T)$.

3) The finiteness of $E_k(t)$

Next we will prove the boundedness of $E_k(t)$ by induction. The boundedness of $E_k(T)$ is guaranteed for all iterations. Consequently, $\forall k\in\mathbf{N}$, there exists a constant M_1 satisfying $\int_0^{\mathrm{T}}\tilde{\theta}_k^2(\sigma)\mathrm{d}\sigma \le M_1$, thus it follows

$$E_k(t) = V_k(t) + \int_0^t \tilde{\theta}_k^2(\sigma)\mathrm{d}\sigma$$
$$\le V_k(t) + \int_0^T \tilde{\theta}_k^2(\sigma)\mathrm{d}\sigma$$
$$\le V_k(t) + M_1. \tag{50}$$

On the other hand, from (42), we obtain

$$\Delta E_{k+1}(t) \le V_{p,k+1}(0) - V_k(t) - K\int_0^t s_{k+1}^2 d\sigma + \gamma\Delta_{k+1}t. \tag{51}$$

Adding (51) to (50) leads to

$$E_{k+1}(t) = E_k(t) + \Delta E_{k+1}(t)$$
$$\le V_k(t) + M_1 + V_{p,k+1}(0) - V_k(t)$$
$$- K\int_0^t s_{k+1}^2\mathrm{d}\sigma + \gamma\Delta_{k+1}t$$
$$\le M_1 + V_{p,k}(T) + \gamma\Delta_{k+1}t. \tag{52}$$

As we have proven that $E_1(t)$ is bounded, therefore $E_k(t)$ is finite by induction. In the sequel, we can obtain the boundedness of $\hat{W}_k(t)$, $\hat{\theta}_k(t)$ and $\hat{\rho}_k$.

4) Learning convergence property

Rewrite inequality (49) as

$$\sum_{j=1}^k\int_0^T s_j^2(\sigma)\mathrm{d}\sigma$$
$$\le \frac{\left(T\cdot c_{\max} + \gamma T\sum\limits_{j=1}^k\Delta_k + V_{p,1}(0) - E_k(T)\right)}{K}. \tag{53}$$

Taking the limitation of (53), it follows that

$$\begin{aligned}
&\lim_{k\to\infty}\sum_{j=1}^{k}\int_0^T s_j^2(\sigma)\mathrm{d}\sigma \\
&\le \lim_{k\to\infty}\left(T\cdot c_{\max}+\gamma T\sum_{j=1}^{k}\Delta_k+V_{p,1}(0)-E_k(T)\right)/K \\
&\le T\cdot c_{\max}+2\gamma qT+V_{p,1}(0). \qquad (54)
\end{aligned}$$

According to the convergence theorem of the sum of series, $\lim_{k\to\infty}\int_0^T s_k^2(\sigma)\mathrm{d}\sigma=0$. Since x_d is bounded, the boundedness of x_k is established. Based on the above reasoning, we can arrive at that $u_k(t)$ is bounded. □

V. SIMULATION STUDY

In this section, a simulation study is presented to verify the effectiveness of the AILC scheme. Consider the following second-order nonlinear fractional order system:

$$\begin{cases}
D^{\alpha}x_{1,k}(t)=x_{2,k}(t), \\
D^{\alpha}x_{2,k}(t)=f(x_k)+\theta(t)\xi(x_k)+u_k(t)+d(t), \\
y_k(t)=x_{1,k}(t),
\end{cases}$$

where $\alpha=0.9$, $f(x_k)=-x_{1,k}x_{2,k}\sin(x_{1,k}x_{2,k})$, $\theta(t)=1+0.5\sin t$, $\xi(x_k)=\sin(x_{1,k})\cos(x_{2,k})$, $d(t)=0.1*rand*\sin(t)$ with *rand* presenting a Gaussian white noise. The desired reference trajectory is given by $r(t)=\sin t$. The design parameters are chosen as $\varepsilon_1=\varepsilon_2=1$, $\lambda=2$, $K=6$, $\Gamma_W=\mathrm{diag}\{0.6\}$, $q_\theta=2$, $q_\rho=0.8$, $\varepsilon=\lambda\varepsilon_1+\varepsilon_2=3$. It is clear that $|\lambda|>\frac{\alpha}{2}\pi$. Additionally, the boundary layer function is specified by $\eta(t)=3E_{0.9}(-Kt)$, a graphic representation of $\eta(t)$ is shown in Fig. 2.

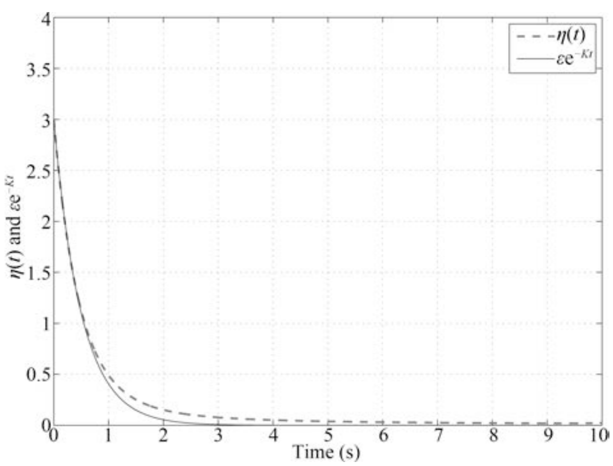

Fig. 2. Mittag-Leffler type boundary layer function $\eta(t)$.

The parameters for neural network are chosen as $l=30$, $\mu_j=\frac{1}{l}(2j-l)[2,3]$, $\sigma_j=2$, $j=1,2,\cdots,l$. The initial condition $x_{1,k}(0)$ and $x_{2,k}(0)$ are randomly taken as $r(0)+0.5(1-2rand)$ and $r_1(0)+0.5(1-2rand)$, respectively. For ease of programming, we use the Grünwald-Letnikov definition in the simulation. The system runs on $[0,2\pi]$ repeatedly. Parts of the simulation results are shown in Fig. 3 ∼ Fig. 7.

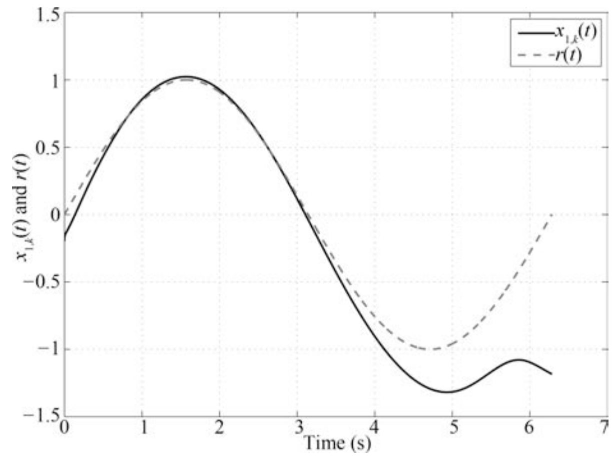

Fig. 3. System output $y_k(t)$ on $r(t)$ $(k=1)$.

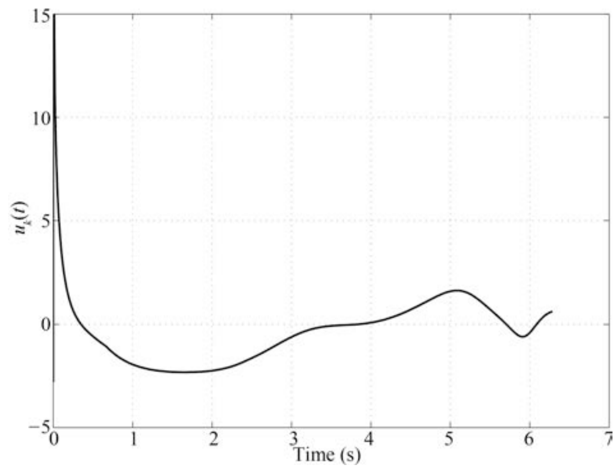

Fig. 4. Control input $(k=1)$.

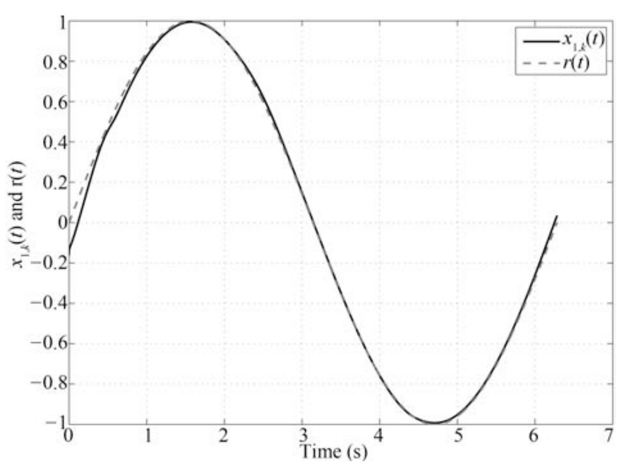

Fig. 5. System output $y_k(t)$ on $r(t)$ $(k=30)$.

Figs. 3 ∼ 4 and Figs. 5 ∼ 6 show the output tracking trajectory and control input of the 1st and the 30th iteration. Obviously, the signals are bounded and the tracking performance of 1st iteration is much worse than that of 30th iteration. Fig. 7 gives the convergence of $\int_0^{\mathrm{T}} s_k^2(t)\,\mathrm{d}t$ along the iteration axis, which indicates that the proposed AILC scheme achieves perfect tracking by learning.

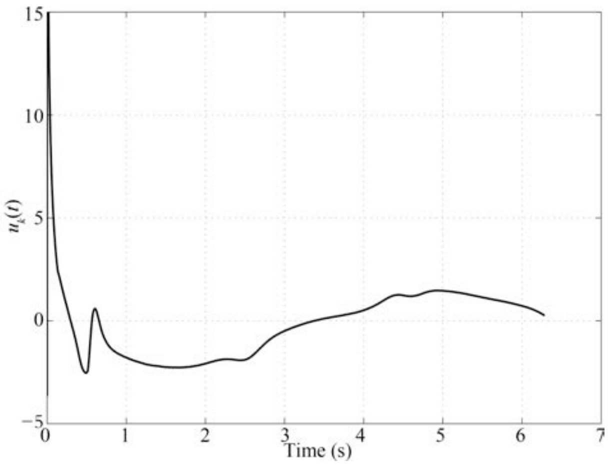

Fig. 6. Control input ($k = 30$).

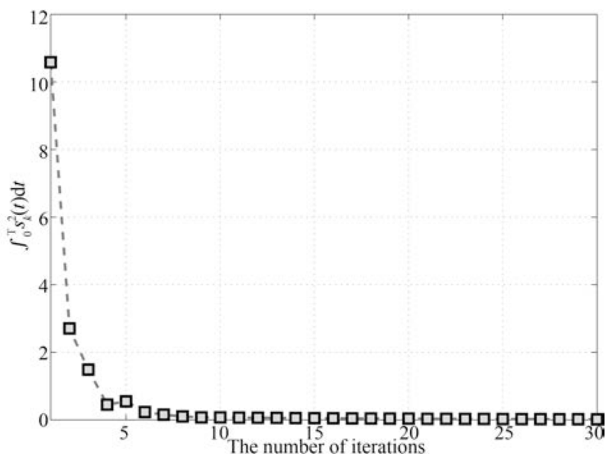

Fig. 7. $\int_0^T s_k^2(t)\,\mathrm{d}t$ versus the number of iterations.

VI. Conclusions

In this paper, an adaptive iterative learning control scheme has been presented for a class of nonlinear fractional order systems in the presence of disturbance. A new boundary layer function by introducing Mittag-Leffler function is designed to deal with the initial condition problem of ILC. RBF NN is utilized to approximate the system uncertainty while fractional order differential type updating laws are designed to estimate ideal neural weight and the upper bound of neural approximation error and disturbance. The hyperbolic tangent function with a convergent series sequence is employed to form the robust control term. Theoretical analysis by constructing Lyapunov-like CEF has been presented to show the boundedness of all signals and convergence along iteration of tracking error. Simulation results have been provided to show the validity the proposed scheme. This is the first time consideration of the AILC problem of fractional order system. Compared with traditional ILC of fractional systems, our AILC scheme relaxes the global Lipschitz condition and a new framework of stability analysis by using Lyapunov-like CEF is presented. Although we only consider the class of fraction as (12), the idea of the proposed AILC method can be applied to more kinds of fractional order systems and provide a reference for AILC design of fractional order systems.

References

[1] Arimoto S, Kawamrua S, Miyazaki. Bettering operation of robots by learning. *Journal of Robotic System*, 1984, **11**(2): 123−140

[2] Kuc T Y, Nam K, Lee J S. An iterative learning control of robot manipulators. *IEEE Transactions on Robotics and Automation*, 1991, **7**(6): 835−841

[3] Chen Y Q, Wen C Y. *Iterative learning control- Convergence, robustness and applications*. UK, London: Spring-Verlag, 1999

[4] Bien Z, Xu J X. *Iterative learning control - analysis, design, integration and applications*. USA, Boston: Kluwer Academic Publisher, 1998

[5] Xu J X, Tan Y. *Linear and nonlinear iterative learning control*. Berlin: Springer-Verlag, 2003

[6] Xu J X, Qu Z H. Robust iterative learning control for a class of nonlinear systems. *Automatica*, 1998, **34**(8): 983−988

[7] French M, Rogers E. Nonlinear iterative learning control by an adaptive Lyapunov technique. *International Journal of Control*, 2000, **73**(10): 840−850

[8] Xu J X, Tan Y. A composite energy function-based learning control approach for nonlinear systems with time-varying parametric uncertainties. *IEEE Transactions on Automatic Control*, 2002, **47**(11): 1940−1945

[9] Chi R H, Hou Z S, Xu J X. Adaptive ILC for a class of discrete-time systems with iteration-varying trajectory and random initial condition. *Automatica*, 2008, **44**(8): 2207−2213

[10] Chi R H, Sui S L, Hou Z S. A New Discrete-time Adaptive ILC for Nonlinear Systems with Time-varying Parametric Uncertainties. *Acta Automatica Sinica*, 2008, **34**(7): 805−808

[11] Yin C, Xu J X, Hou Z. An ILC scheme for a class of nonlinear continuous-time systems with time-iteration-varying parameters subject to second-order internal model. *Asian Journal of Control*, 2011, **13**(1): 126−135

[12] Zhang R, Hou Z, Chi R, et al. Adaptive iterative learning control for nonlinearly parameterised systems with unknown time-varying delays and input saturations. *International Journal of Control*, 2015, **88**(6): 1133−1141

[13] Wang Y C, Chien C J, Teng C C. Direct adaptive iterative learning control of nonlinear systems using an output-recurrent fuzzy neural network. *IEEE Transactions on Systems, Man, and Cybernetics-Part B: Cybernetics*, 2004, **34**(3): 1348−1359

[14] Chien C J. A Combined Adaptive Law for Fuzzy Iterative Learning Control of Nonlinear Systems With Varying Control Tasks. *IEEE Transactions on Fuzzy Systems*, 2008, **16**(1): 40−51

[15] Wang Y C, Chien C J. Decentralized Adaptive Fuzzy Neural Iterative Learning Control for Nonffine Nonlinear Interconnected Systems. *Asian Journal of Control*, 2011, **13**(1): 94−106

[16] Zhang C, Li J. Adaptive iterative learning control for nonlinear pure feedback systems with initial state error based on fuzzy approximation. *Journal of the Franklin Institute*, 2014, **351**(3): 1483−1500

[17] Podlubny I. *Fractional differential equations: an introduction to fractional derivatives, fractional differential equations, to methods of their solution and some of their applications*. New York: Academic Press, 1999

[18] Petráš I. *Fractional-order nonlinear systems-modeling, analysis and simulation*. Berlin: Spring-Verlag, 2010

[19] Gabano J D, Poinot T. Fractional modelling and identification of thermal systems. *Signal Processing*, 2011, **91**(3): 531−541

[20] Luo Y, Chen Y Q. Stabilizing and robust fractional order PI controller synthesis for first order plus time delay systems. *Automatica*, 2012, **48**(9): 2159−2167

[21] Efe, Mehmet Önder. Fractional fuzzy adaptive sliding-mode control of a 2-DOF direct-drive robot arm. *IEEE Transactions on Systems, Man, and Cybernetics-Part B: Cybernetics*, 2008, **38**(6): 1561−1570

[22] Delavari H, Ghaderi R, Ranjbar A, et al. Fuzzy fractional order sliding mode controller for nonlinear systems. *Communications in Nonlinear Science and Numerical Simulation*, 2010, **15**(4): 963−978

[23] Li J, Lu J G, Chen Y. Robust decentralized control of perturbed fractional-order linear interconnected systems. *Computers and Mathematics with Applications*, 2013, **66**(5): 844−859

[24] Tang X D, Tao G, Suresh M J. Adaptive actuator failure compensation for parametric strict feedback systems and an aircraft application. *Automatica*, 2003, **39**(12): 1975−1982

[25] Wang X S, Su C Y, Hong H. Robust adaptive control of a class of nonlinear systems with unknown dead-zone. *Automatica*, 2004, **40**(3): 407−413

[26] Zhang T P, Ge S S. Adaptive neural control of MIMO nonlinear state time-varying delay systems with unknown dead-zones and gain signs. *Automatica*, 2007, **43**(6): 1021−1033

[27] Zhang T P, Ge S S. Adaptive dynamic surface control of nonlinear systems with unknown dead zone in pure feedback form. *Automatica*, 2008, **44**(7): 1895−1903

[28] Xu J X, Xu J, Lee T H. Iterative Learning Control for Systems With Input Deadzone. *IEEE Transactions on Automatic Control*, 2005, **50**(9): 1455−1459

[29] Razminia A, Torres D F M. Control of a novel chaotic fractional order system using a state feedback technique. *Mechatronics*, 2013, **23**(7): 755−763

[30] Li C, Su K, Zhang J, et al. Robust control for fractional-order four-wing hyperchaotic system using LMI. *Optik*, 2013, **124**(22): 5807−5810

[31] Yin C, Dadras S, Zhong S, et al. Control of a novel class of fractional-order chaotic systems via adaptive sliding mode control approach. *Applied Mathematical Modelling*, 2013, **37**(4): 2469−2483

[32] Yang C C, Ou C J. Adaptive terminal sliding mode control subject to input nonlinearity for synchronization of chaotic gyros. *Communications in Nonlinear Science and Numerical Simulation*, 2013, **18**(3): 682−691

[33] Huang X, Wang Z, Li Y, et al. Design of fuzzy state feedback controller for robust stabilization of uncertain fractional-order chaotic systems. *Journal of the Franklin Institute*, 2014, **351**(12): 5480−5493

[34] Pan I, Das S, Das S. Multi-objective active control policy design for commensurate and incommensurate fractional order chaotic financial systems. *Applied Mathematical Modelling*, 2015, **39**(2): 500−514

[35] Bhalekar S, Daftardar-Gejji V. Synchronization of different fractional order chaotic systems using active control. *Communications in Nonlinear Science and Numerical Simulation*, 2010, **15**(11): 3536−3546

[36] Li T, Wang Y, Yang Y. Designing synchronization schemes for fractional-order chaotic system via a single state fractional-order controller. *Optik*, 2014, **125**(22): 6700−6705

[37] Agrawal S K, Das S. Function projective synchronization between four dimensional chaotic systems with uncertain parameters using modified adaptive control method. *Journal of Process Control*, 2014, **24**(5): 517−530

[38] Gao L, Wang Z, Zhou K, et al. Modified sliding mode synchronization of typical three-dimensional fractional-order chaotic systems. *Neurocomputing*, 2015, **166**: 53−58

[39] Gao Y, Liang C, Wu Q, et al. A new fractional-order hyperchaotic system and its modified projective synchronization. *Chaos, Solitons & Fractals*, 2015, **76**: 190−204

[40] YangQuan Chen, Kevin L. Moore. On D α Iterative learning control. Proceedings of the 40th IEEE Conference on Decision and Control, Orlando, Florida, USA, 2001. 4451−4456

[41] Ahn H S, Moore K L, Chen Y Q. Stability analysis of discrete-time iterative learning control systems with interval uncertainty. *Automatica*, 2007, **43**(5): 892−902

[42] Li Y, Chen Y Q, Ahn H S. Fractional Order Iterative Learning Control. ICROS-SICE International Joint Conference 2009, Fukuoka, Japan, 2009. 3106−3110

[43] Li H S , Huang J C, Liu D, et al. Design of Fractional Order Iterative Learning Control on Frequency Domain. Proceedings of the 2011 IEEE International Conference on Mechatronics and Automation, Beijing, China, 2011. 2056−2060

[44] Li Y, Chen Y Q, Ahn H S. A Generalized Fractional-Order Iterative Learning Control. 2011 50th IEEE Conference on Decision and Control and European Control Conference (CDC-ECC), Orlando, USA, 2011. 5356−5361

[45] Li Y, Chen Y Q, Ahn H S. On the PDα-Type Iterative Learning Control for the Fractional-Order Nonlinear Systems. 2011 American Control Conference, San Francisco, CA, USA, 2011. 4320−4325

[46] Lan Y H. Iterative learning control with initial state learning for fractional order nonlinear systems. *Computers and Mathematics with Applications*, 2012, **64**(10): 3210−3216

[47] Li Y, Chen Y Q, Ahn H S. On P-type Fractional Order Iterative Learning Identification. 13th International Conference on Control. Automation and Systems, Gwangju, Korea, 2013. 219−225

[48] Lan Y H, Zhou Y. D $\alpha-$ Type Iterative Learning Control for Fractional-Order Linear Time-Delay Systems. *Asian Journal of Control*, 2013, **15**(3): 669−677

[49] Li Y, Zhai L, Chen Y Q, et al. Fractional-order Iterative Learning Control and Identification for Fractional-order Hammerstein System. Proceeding of the 11th World Congress on Intelligent Control and Automation, Shenyang, China, 2014. 840−845

[50] Li Y, Chen Y Q, Ahn H S. Fractional Order Iterative Learning Control for Fractional Order System with Unknown Initialization. 2014 American Control Conference (ACC), Portland, Oregon, USA, 2014. 5712−5717

[51] Li Y, Chen Y Q, Ahn H S. A High-gain Adaptive Fractional-order Iterative Learning Control. 11th IEEE International Conference on Control & Automation (ICCA), Taichung, Taiwan, 2014. 1150−1155

[52] Lazarević M, Mandić P. Feedback-feedforward iterative learning control

for fractional order uncertain time delay system-PD alpha type. International Conference on Fractional Differentiation and its Applications (ICFDA), 2014. 1−6

[53] Yan L, Wei J. Fractional order nonlinear systems with delay in iterative learning control. *Applied Mathematics and Computation*, 2015, **257**: 546−552

[54] Kilbas A A, Srivastava H M, Trujillo J J. *Theory and applications of fractional differential equations*. The Netherlands: Elsevier, 2006. 69−83

[55] Matignon D. Stability results of fractional differential equations with applications to control processing. Computational Engineering in Systems and Application multiconference, IMACS, IEEE-SMC, Lille, France, 1996. 963−968

[56] Sabatier J, Moze M, Farges C. LMI stability conditions for fractional order systems. *Computers and Mathematics with Applications*, 2010, **59**: 1594−1609

[57] Trigeassou J C, Maamri N, Oustaloup A. Lyapunov stability of linear fractional systems: part 1-definition of fractional energy. ASME 2013 International Design Engineering Technical Conferences and Computers and Information in Engineering Conference, 2013

[58] Gupta M M, Rao D H. *Neuro-Control Systems:Theory and Applications*. New York, USA: IEEE Press, 1994

[59] Polycarpou M M. Stable adaptive neural control scheme for nonlinear systems. *IEEE Transactions on Automatic Control*, 1996, **41**(3): 447−451

[60] Zhu S, Sun M X, He X X. Iterative learning control of strict-feedback nonlinear time-varying systems. *Acta Automatica Sinica*, 2010, **36**(3): 454−458

Jianming Wei graduated from Naval Aeronautical and Astronautical University, China, in 2009. He received the M. S. degree and the Ph. D. degree from Naval Aeronautical and Astronautical University in 2011 and 2015, respectively. He is currently with Naval Aeronautical and Astronautical University, as a lecturer. His research interests include iterative learning control and nonlinear control. Corresponding author of this paper.

Yun-an Hu graduated from Huazhong Institute of Technology, China, in 1985. He received the M. S. degree from Naval Engineering Institute in 1988 and Ph. D. degree from Harbin Institute of Technology in 2004. He is currently a professor at Naval Aeronautical and Astronautical University. His research interests include aircraft guidance and control system design, nonlinear control.

Meimei Sun graduated from Naval Aeronautical and Astronautical University, China, in 2009. She received the M. S. degree and the Ph. D. degree from Naval Aeronautical and Astronautical University in 2011 and 2015, respectively. She is currently with Naval Aeronautical Engineering Institute, as a lecturer. Her research interests include chaotic systems and nonlinear control.

Design and Implementation of Digital Fractional Order PID Controller using Optimal Pole-Zero Approximation Method for Magnetic Levitation System

Amit S. Chopade, Swapnil W. Khubalkar, A. S. Junghare, M. V. Aware, and Shantanu Das

***Abstract*—The aim of this paper is to employ fractional order proportional integral derivative (FO-PID) controller and integer order PID controller to control the position of the levitated object in a magnetic levitation system (MLS), which is inherently nonlinear and unstable system. The proposal is to deploy discrete optimal pole-zero approximation method for realization of digital fractional order controller. An approach of phase shaping by slope cancellation of asymptotic phase plots for zeros and poles within given bandwidth is explored. The controller parameters are tuned using dynamic particle swarm optimization (dPSO) technique. Effectiveness of the proposed control scheme is verified by simulation and experimental results. The performance of realized digital FO-PID controller has been compared with that of the integer order PID controllers. It is observed that effort required in fractional order control is smaller as compared with its integer counterpart for obtaining the same system performance.**

***Index Terms*—Digital control, Position control, Fractional calculus, Particle swarm optimization (PSO), Approximation methods, Magnetic levitation, Discretization, Fractional order PID controller (FOPID).**

I. INTRODUCTION

IN 1914, American inventor Emile Bachelet presented his idea of a magnetically levitated (maglev) vehicle with a display model. In magnetic levitation system (MLS), ferromagnetic object levitate by the electromagnetic force induced due to electric current flowing through coil around a solenoid[1−5]. The MLS is inherently nonlinear and unstable[6−10]. However, the advantage is that, as the suspended object has no mechanical support, there is no friction and noise. This allows us to position it accurately - a major advantage, explored in many applications such as magnetically levitated train, magnetic bearing, conveyor system, etc.[1].

In recent years, various methods have been proposed to improve control in MLS-based applications. In 2006, Chiang et al. proposed the concept of integral variable-structure grey control[2]. Yang et al. introduced the concept of adaptive robust output-feedback control with K-filter approach in 2008[3]. In 2011, Chih-Min Lin et al. developed an adaptive PID controller and a fuzzy compensation controller for MLS[1]. In the same year, Rafael Morales et al. proposed generalized proportional integral output feedback controller[4]. Recently in 2014, Chih-Min Lin et al. proposed a function-link cerebellar model articulation control system design based on the neural network concept[5]. However, in spite of all these developments, there is scope for improving efficiency of the controller. The energy required to achieve and maintain the object's position (in the face of disturbances) form an important part of improving the control action. The aim of this paper is to control and maintain the desired object's position, with lesser controller effort. The controller effort minimization is reported in literature[11−14].

The conventional integer order controllers such as, PD and PID controller have been applied in industry for over half-a-century to control linear and nonlinear systems[15]. Recently, such control schemes have been extended to their generalized form using fractional calculus[16−17] (differentiation and integration of an arbitrary order). The FO-PID controller has fractional differ-integrator operations. This makes the controller have memory (i.e. its action will memorize its past states) and avoids instantaneous actions. Using the definition of convolution integral, the expression for the fractional integration (which also is embedded in the fractional differentiation) can be written as the convolution of the function and the power function, which is elaborately explained in [17].

In last few decades, the fractional order approach to represent the plant and its controllers are increasingly used to describe the dynamic process accurately[17]. The fractional order transfer function is approximated by integer order transfer function using various methods[16−20]. The proposed method can achieve the desired accuracy over a much larger bandwidth than has been achieved using earlier methods. In applications, where non-integer order controllers are used for integer order

This article has been accepted for publication in a future issue of this journal, but has not been fully edited. Content may change prior to final publication.

This work was supported by the Board of Research in Nuclear sciences of the Department of Atomic Energy, India. Sanction no. 2012/36/69-BRNS/2012. Recommended by Associate Editor Antonio Visioli.

Amit S. Chopade, Swapnil W. Khubalkar, Anjali S. Junghare, and Mohan V. Aware are with the Department of Electrical Engineering, Visvesvaraya National Institute of Technology, Nagpur, India 440010 e-mail: (a.s.chopade@ieee.org, swapnil.w.khubalkar@ieee.org, asjunghare@eee.vnit.ac.in, mvaware@eee.vnit.ac.in).

Shantanu Das is with Reactor Control Division, Bhabha Atomic Research Centre, India. e-mail: (shantanu@barc.gov.in).

Digital Object Identifier 10.1109/JAS.2016.7510181

plant, there is more flexibility in adjusting the gain and phase characteristics as compared to integer order controllers. This flexibility makes fractional order control a more versatile tool in designing robust and precise control systems.

This paper presents the control of magnetic levitation system using FO-PID controller based on optimal pole-zero approximation method. An algorithm is developed to realize digital FO-differentiators and FO-integrators. The proposed design procedure aims to ensure that the performance is within required tolerance bandwidth. Five parameters $(k_p, k_i, k_d, \alpha, \beta)$ of FO-PID need to be tuned for designing the controller. This paper utilizes dynamic PSO optimization (dPSO) method to achieve the required values. Finally, a comparative study of the performance parameters of the controller is presented to evaluate the advantages of deployment of FO-PID against the conventionally used integer-order controllers. The control effort minimization by FO-PID controller is quantified and demonstrated.

This work is organized as follows: section II presents the system description. Design procedure of proposed digital FO-PID controller using discrete optimal pole-zero approximation method and dPSO technique is discussed in section III. In section IV simulation and experimental results on MLS are provided to validate effectiveness of the proposed controller. Paper concludes with a summary of the results obtained in section V.

II. System Identification of MLS Model

A laboratory scale magnetic levitation system is used to evaluate the performance of proposed controller in a controlled environment. MLS levitates an object (metallic ball with mass m) in a desired position by controlling the electromagnetic field counteracting the gravitational force. The applied control input is voltage, which is converted into current via embedded driver[21]. Fig.1 shows the schematic diagram of MLS. The system model is nonlinear, that means at least one of the two states (i–current, x–ball position) is an argument of a nonlinear function. The nonlinear model of MLS relating the ball position x and coil current i is given as (1):

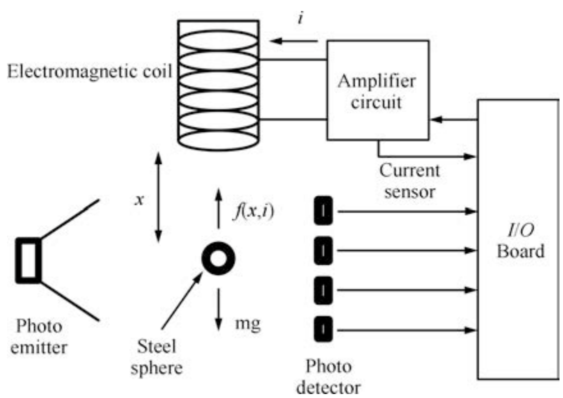

Fig. 1. Schematic diagram of MLS.

$$m\ddot{x} = mg - k\frac{i^2}{x^2} \tag{1}$$

$$i = k_1 u \tag{2}$$

where, k is a constant depending on coil (electromagnet) parameters, m is the mass of sphere, g is gravitational force, k_1 is an input conductance, u is control voltage, and x is a ball position. The values of these parameters are given in Appendix-A. A relation between control voltage x and coil current i is given in (2). The control signal ranges between $[-5V, +5V]$.

A. Linearization of MLS Model

The nonlinear form of maglev model is linearized for analysis of the system[21]. The linear form of the model is obtained from (1) as follows:

$$\ddot{x} = g - f(x, i) \tag{3}$$

where, $f(x,i) = k\frac{i^2}{mx^2}$

Equilibrium point is calculated by setting $\ddot{x} = 0$,

$$g = f(x, i)|_{i_o, x_o} \tag{4}$$

Linearization is carried out about the equilibrium point of $x_o = -1.5V$ (the position is expressed in volts), $i_o = 0.8A$[8]. Using series expansion method, (5) is obtained.

$$\ddot{x} = -\Big(\frac{\partial f(i,x)}{\partial i}\Big|_{i_o,x_o} \triangle i + \frac{\partial f(i,x)}{\partial x}\Big|_{i_o,x_o} \triangle x\Big) \tag{5}$$

Application of Laplace Transform on (5) simplifies it to (6).

$$\frac{\triangle X(s)}{\triangle I(s)} = \frac{-K_i}{s^2 + K_x} \tag{6}$$

where, $K_i = \frac{2mg}{i_o}$ and $K_x = -\frac{2mg}{x_o}$

Linearized model transfer function (6) has two poles, one of which is in the right half plane at $\sqrt{(2mg/x_0)}$, which makes the MLS open-loop unstable. Transfer function, obtained by the linearization, is verified using system identification procedure.

B. Integer Order System Identification of MLS Model

System identification is a process for obtaining mathematical model using input and output system response. The identified model response should fit with measured response for input applied to the system model[21]. Usually there are two methods for system identification, least mean square (LMS) method and instrumental variable method. The identification of MLS is generally accomplished via traditional least squares method, and is implemented in MATLAB[21−22].

As MLS is unstable, it has to be identified with a running, stabilizing controller i.e. closed loop identification. Fig.2 shows the scheme of unstable system identification. LMS method minimizes error between the model and plant output. The optimal model parameters, for which the square of the error is minimal is the result of identification. In order to carry out identification experiment, a discrete controller has to be applied, in the absence of which, the ball falls down, rendering dentification impossible. The reference signal $r(t)$ i.e. random binary sequence signal is given to excite the MLS and output $y(t)$ is monitored. 2500 samples of the input, output signals are collected from the system with sampling period of $0.01s$.

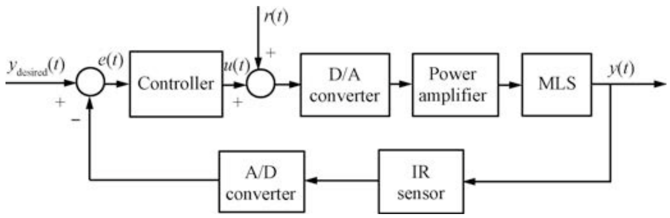

Fig. 2. Block diagram of MLS control and close loop system identification.

Fig.3 presents the comparison between measured and identified model output. Input and output data is taken from MLS system for real-time identification. The best fit obtained is 90.78% for integer order identification, which gives close loop discrete transfer function as in (7):

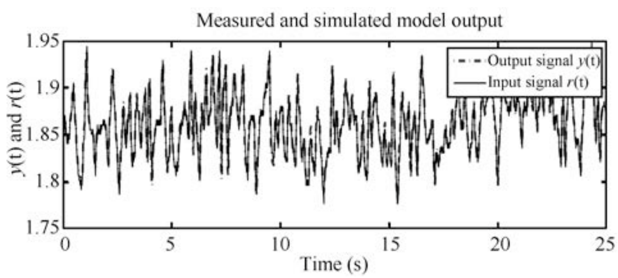

Fig. 3. Measured and simulated model output.

$$Y(z^{-1}) = \frac{G(z^{-1})}{1 + C(z^{-1})G(z^{-1})} \tag{7}$$

where, $Y(z^{-1})$ is complete system transfer function, $C(z^{-1})$ is controller transfer function, and $G(z^{-1})$ is MLS model transfer function in discrete domain.

III. DESIGN OF DIGITAL FRACTIONAL ORDER PID CONTROLLER

A. Fractional Calculus

Fractional calculus is a branch of mathematics that studies the possibility of taking real or complex number powers of differential and integral operator. Basic definitions of fractional calculus and approximation of fractional integrator and fractional differentiator are described in the literature[16−17]. The real order operator is generalized as follows in (8):

$$D^{\alpha} = \left\{ \begin{array}{cc} \frac{d^{\alpha}}{\mathrm{d}t} & \alpha > 0 \\ 1 & \alpha = 0 \\ \int_a^t (\mathrm{d}\tau)^{-\alpha} & \alpha < 0 \end{array} \right\} \tag{8}$$

where, $\alpha \in \mathbf{R}$

Some popular definitions used for general fractional derivatives/integrals in fractional calculus are :

1) : Riemann-Liouville (RL) definition is given in (9).

$$_aD_t^{\alpha} f(t) = \frac{1}{\Gamma(n-\alpha)} \left(\frac{\mathrm{d}}{\mathrm{d}t}\right)^n \int_a^t \frac{f(\tau)}{(t-\tau)^{\alpha-n+1}} \mathrm{d}\tau \tag{9}$$

for $(n-1) \le \alpha < n$
where, n is an integer, α is a real number, and Γ is Euler gamma function. Laplace transform of the RL fractional derivative/integral (9), under zero initial conditions, is given in (10).

$$L\{_aD_t^{\pm\alpha} f(t)\} = s^{\pm\alpha} F(s) \tag{10}$$

2) : Another definition is based on the concept of fractional differentiation i.e. Grunewald-Letnikov (GL) definition. It is given in (11).

$$_aD_t^{\alpha} f(t) = \lim_{h \to 0} h^{-\alpha} \Sigma_{j=0}^{\left[\frac{t-a}{h}\right]} (-1)^j \binom{\alpha}{j} f(t-jh) \tag{11}$$

where, $\left[\frac{t-a}{h}\right] \longrightarrow Integer$
3) : One more option for computing fractional derivatives is Caputo fractional derivative, its definition is as follows (12):

$$^C_aD_t^{\alpha} f(t) = \frac{1}{\Gamma(n-\alpha)} \int_a^t \frac{f^n(\tau)}{(t-\tau)^{\alpha+1-n}} \mathrm{d}\tau \tag{12}$$

where, $(n-1) \le \alpha < n$, n is an integer, and α is a real number.

Initial conditions for Caputo's derivatives are expressed in terms of initial values of integer order derivatives. It is noted that for zero initial conditions RL, GL, and Caputo fractional derivatives coincide. Hence, any of the mentioned methods may be used, using the case of zero initial conditions. That would then eliminate the differences arising due to different initial conditions (amongst the three methods).

B. Digital Realization of Fractional Order Differintegrals with Optimal Pole-Zero for Phase Shaping

The aim behind the choice of frequency domain rational approximation of FO-PID controller is to realize the controller in real time using existing analog/digital filters[16−20, 23−25]. Precise hardware implementation of multi-dimensional natured of fractional order operator is difficult. However, recent research work revealed that band-limited implementation of FO-PID controllers using higher order integer transfer function approximation of the differintegrals give satisfactory performance[26]. This paper, hence utilizes optimal pole-zero algorithm to realize fractional differintegrals in the frequency domain.

1) Optimal pole-zero approximation for phase shaping: Any rational transfer function is characterized by its poles and zeros. The Bode magnitude plot of non-integer order transfer function has a slope of $\pm\alpha 20$ dB/dec and the Bode phase plot lies in the range of $\pm\alpha 90^o$ (α is a real number). This is achieved by the interlacing of real poles and zeros alternately on the negative real axis[19−20, 27−28]. Thus, depending on the error band ϵ around required phase angle $\alpha_{req} = \alpha 90^o$

and the frequency band of interest (ω_L, ω_H), the n^{th} order approximation is obtained[28]. The proposed algorithm is developed to obtain the number of optimal pole-zero pairs to maintain the phase value within the tolerance, of around 1^o. In this algorithm, poles and zeros given by (13) are obtained as follows:

$$\begin{aligned} First\ pole,\ p_1 &= 10^{[\frac{\phi_{req}+45log\omega_l}{45}+1]} \\ First\ zero,\ z_1 &= 10\omega_l \\ Second\ pole,\ p_2 &= 10^{[log(p_1)+2-\mu]} \\ Second\ zero,\ z_2 &= 10^{[log(z_1)+2-\mu]} \\ &\vdots \\ till\ p_n &\geq \omega_h \end{aligned} \tag{13}$$

As a particular case, asymptotic phase plot for fractional order integrator circuit having $\alpha = -0.4$, $\phi_{req} = -36^o$, $\omega_L = 0.1$rad/s and $\omega_H = 100$rad/s is given in Fig.4 - Fig.6. The selection of three pairs of poles and zeros with $\alpha = -0.4$ fraction is shown in Fig.4. The asymptotic phase plot is a straight line at ϕ_{req}, but the actual phase plot is oscillating about asymptotic phase plot, apart from that the average value of phase angle -37.31^o is also different from ϕ_{req}. In Fig.4 the required correction of phase is achieved over three decades by three pole-zero pairs only, which is however less in pursuit of more accuracy. This problem is rectified by increasing the pole-zero density, i.e. having more pole-zero pairs in the desired frequency band. Number of pole-zero pairs depend on the permissible error and the desired band of frequency.

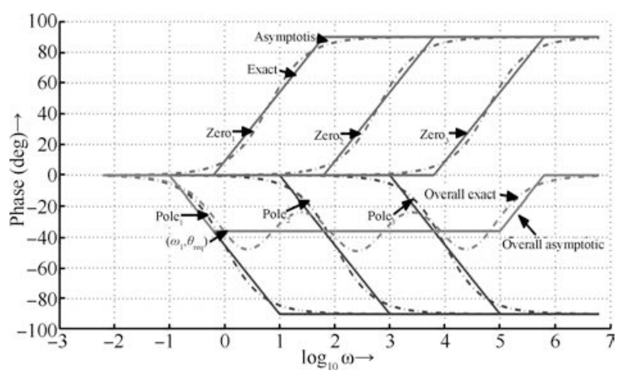

Fig. 4. Asymptotic phase plot with three pole-zero pairs for $\alpha = -0.4(-36^o)$.

Generally, three pole-zero pairs per decade give the phase plot within $\varepsilon = \pm 1^o$ error, but it depends on the value of α as well. For the same parameters, i.e. $\alpha = -0.4, \phi_{req} = 36^o$, $\omega_L = 0.1$rad/s and $\omega_H = 100$ rad/s with seven pole-zero pairs, phase plot is shown in Fig.5. The actual phase plot is oscillating with rms error of $0.6471^o (< 1^o)$. Apart from that, average value of phase angle $(-35.9999^o \approx -36^o)$ is same as ϕ_{req}. Moreover, this is achieved over 3 decades of cycle by seven pole-zero pairs. In order to maintain the phase margin tolerance within the lower limits, more pole-zero pairs in the desired frequency band are required. This can be done by adjusting $z_1, p_2, z_3....$ closer towards left. To achieve this shift, design parameter μ is introduced. Frequency band of constant phase shrinks on both the ends with increasing μ for constant number of pole-zero pairs. Fig.6 shows the basic idea of frequency band tightening. The problem regarding frequency band shrinking is tackled by designing the rational approximation on wider frequency band $(\frac{\omega_l}{10^\gamma}, 10^\delta\omega_h)$ followed by curtailing the frequency overhang on either side, such that the phase remains within $\phi_{req} \pm \varepsilon$ in range of (ω_l, ω_h). Nominal values to expand frequency band are $\gamma = 3, \delta = 2$.

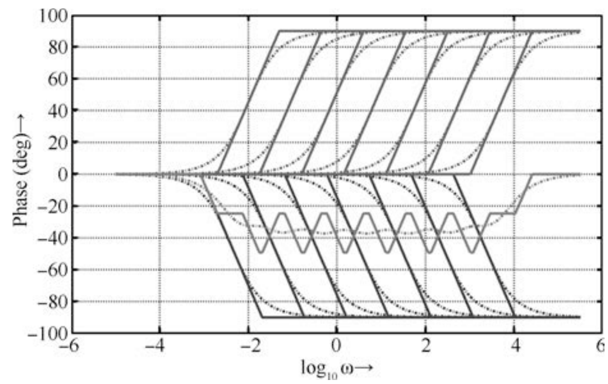

Fig. 5. Asymptotic phase plot with seven pole-zero pairs.

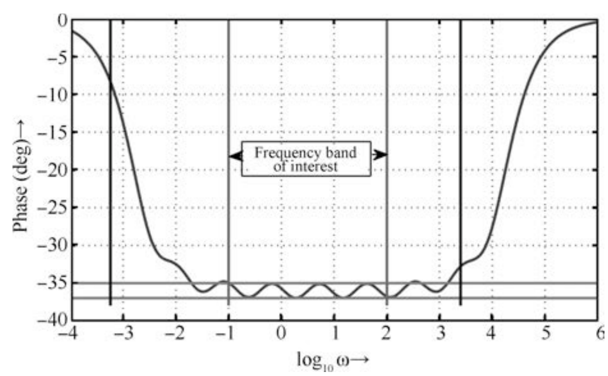

Fig. 6. The basic idea of frequency band tightening.

2) Design of Digital Fractional Order Integrator: The key point in digital implementation of fractional order controller is discretization of fractional order differintegral[24, 27−29]. Contributions related to the discretization have been reported in literature[30−33]. The pole-zero pairs obtained by algorithm in the above case are discretized using first order hold (foh), zero order hold (zoh), Tustin operator, impulse invariant, matched pole-zero, and Tustin with pre-warp frequency methods. In Fig.7, Bode plot for $s^{-0.4}$ digital integrator is shown and it depicts that digital integrator with Tustin approximation method matches closely with continuous time integrator. Tustin approximation method with a sample time of $0.01s$ is used for discretization. To relate s-domain and z-domain transfer functions, Tustin and bilinear methods use the following approximation as (14).

$$z = e^{sT_s} \approx \frac{1 + sT_s/2}{1 - sT_s/2} \tag{14}$$

The optimal pole-zero algorithm for digital fractional integrator of $s^{-0.4}$ within desired band of frequency $\omega_L = 0.1$rad/s and $\omega_H = 100$rad/s gives pole-zero pairs which are listed in Table 1 with gain value 0.010127.

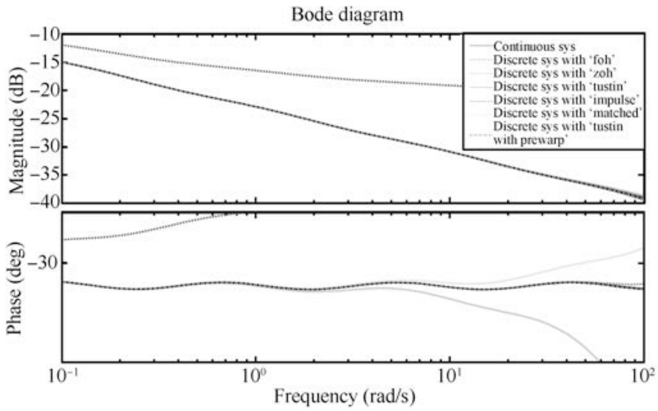

Fig. 7. Bode plot of $s^{-0.4}$ digital integrator.

Table I
THE POLE-ZERO PAIRS OF THE RATIONAL APPROXIMATION OF $s^{-0.4}$ ON $(10^{-1}, 10^{2})rad/s$

i	1	2	3	4	5	6	7
z_i	−0.9253	−0.4842	0.9307	0.992	0.9991	1	0.5136
p_i	−0.8286	0.7651	0.9707	0.9967	1	1	−0.0875

Digital fractional differentiator is designed along the lines of approach similar to that of digital fractional integrator. The architecture of digital FO-PID with digital fractional integrator and digital fractional differentiator is shown in Fig.8.

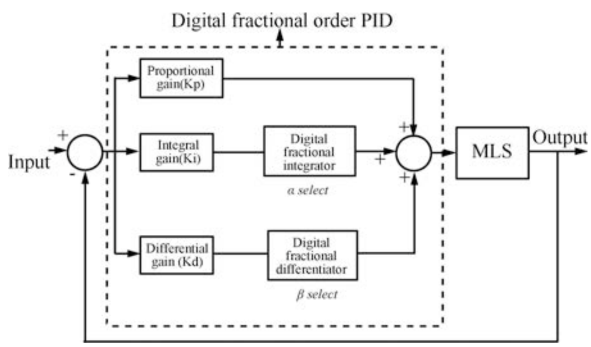

Fig. 8. Digital FO-PID controller.

3) dynamic Particle Swarm Optimization: Recently, many researchers have focused on fractional order controllers tuning, and have obtained meaningful results[34−47]. In this work, dPSO method is used to tune the gains and orders of the controller. PSO is a method for optimizing hard numerical functions, analogous to social behavior of flocks of birds, schools of fish, etc. Here, each particle in swarm represents a solution to the problem defined by its instantaneous position and velocity[48]. The position vector of each particle is represented by unknown parameters to be ascertained. In present case, five control parameters $(k_p, k_i, k_d, \alpha, \beta)$ of FO-PID controller need to be ascertained. The desired number of particles is known as population. The population is varied to carry out a search in multidimensional space. Each particle in population will travel with the updated velocity and direction to converge as early as possible to the optimal solution point. Dynamic PSO is an improvement in PSO by adding the product of differences in objective function value between a particle and its individual best or the global best. Here, the change in position of a particle is directly proportional to iteration, which further depends on individual best, global best, and a random velocity[49]. dPSO searches the workspace similar to a simple PSO and velocity of a particle is obtained by (15):

$$\begin{aligned} v_{id} = {} & (f(p_{id}) - f(x_{id})) \times (p_{id} - x_{id}) \times sf_1 \\ & + (f(p_{gd}) - f(x_{id})) \times (p_{gd} - x_{id}) \times sf_2 \\ & + rand() \times signis() \times sf_3 \end{aligned} \tag{15}$$

where, v_{id}: velocity of a particle, p_{id}: individual best, x_{id}: current position of a particle, p_{gd}: global best, rand: random function, sf_1, sf_2, sf_3: to scale the calculated value in the range of the control variable, $signis$: function which generates random positive or negative value.

Population size is taken as 100, maximum iteration is set as 50, lower and higher translation frequencies are taken as $\omega_L = 0.1$rad/s and $\omega_H = 100$rad/s. ITAE (Integral Time Absolute Error) is chosen as performance criterion. The values of controller parameters, obtained from dPSO, are implemented in PD, PID, and FO-PID controller in simulation as well as in real time mode on MLS. The optimized values of the controllers are presented in Table II.

Table II
dPSO OPTIMIZED GAIN AND FRACTIONAL ORDER VALUES USED FOR DIFFERENT CONTROLLERS (α :ORDER OF INTEGRATOR, β :ORDER OF DIFFERENTIATOR)

Sr. No.	Controllers	Gain and Fractional Order Value				
		K_p	K_i	K_d	α	β
1.	**PD**	4	–	2	–	1
2.	**PID**	5.5	2	0.2	1	1
3.	**FOPID**	7	12	1	0.4	0.8

IV. MLS CONTROL: SIMULATION AND HARDWARE

A. Closed-Loop Control System Simulation

Control of MLS using optimized PD, PID, and FO-PID controller is studied by MATLAB simulation. A sinusoidal excitation signal is used to study the effects. The controller generates a compensating control signal (based on the positional error) to achieve desired ball position. Controller parameters are tuned using dPSO method as discussed in section III-B-3. Fig.9 - Fig.11 present simulation results of the controlled output of MLS using PD, PID, and FO-PID controller respectively. Here, encircled part pointed by an arrow shows deviation between desired and actual ball position.

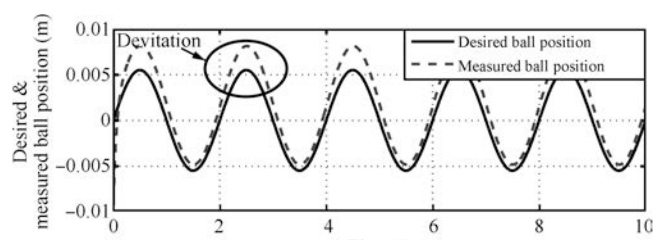

Fig. 9. Controlled output result of MLS using PD.

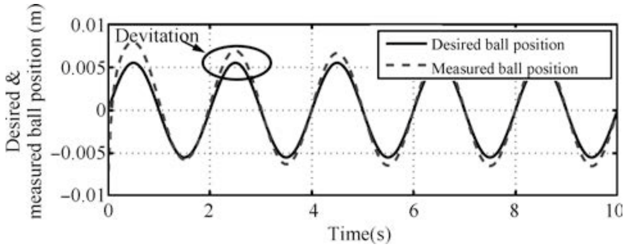

Fig. 10. Controlled output result of MLS using PID.

The measured and desired ball positions with PD, PID, and FO-PID controllers are quantitatively presented in Table III. The simulation results indicate that deviation between measured and desired ball positions by using dPSO tuned FO-PID controller, is less as compared to PD or PID controllers.

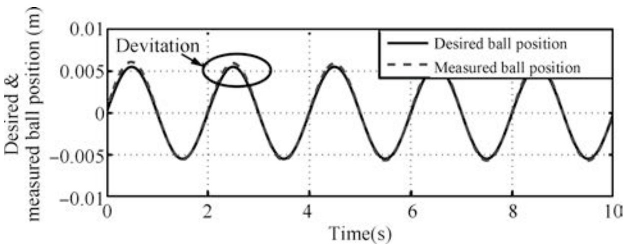

Fig. 11. Controlled output result of MLS using FO-PID.

Error values presented in Table III are calculated using (16):

$$Percent\ error = \frac{desired\ position - actual\ position}{actual\ position} \times 100\% \tag{16}$$

From the data presented in Table III, it is observed that FO-PID controller tracks the desired position more efficiently than PD or PID controllers.

B. Real Time Implementation of Closed-Loop System

The MLS used for experimentation is shown in Fig.12. Due to high nonlinearity and open-loop instability, MLS system is a very challenging plant. Assembly of MLS consists of a mechanical unit labeled A in Fig.12. Analogue control interface unit labeled A is used to transfer control signals between computing system and MLS. Advanced PCI1711 I/O card has been inserted into a PCI computer slot and connected with SCSI adapter box using SCSI cable. Mathworks software tools are used to implement control algorithm. It includes MATLAB control toolbox, real time windows workshop (RTW), real time windows target (RTWT), and visual C as programming environment. The flowchart required to obtain executable file is shown in Fig.13. RTW builds a C++ source code from the Simulink Model. C code compiler compiles and links the code to produce executable program. RTWT communicates with executable program acting as the control program and interfaces with hardware through input/output board. The block diagram of MLS close loop control is shown in Fig.14.

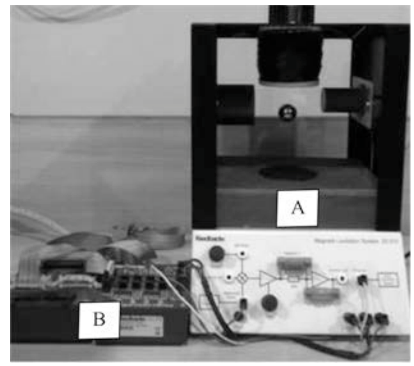

Fig. 12. Experimental setup.

1) Experimental Results using a PD Controller: The measured and desired ball positions using real time PD controller is shown in Fig.15(a) and control signal c(t) before digital to analog (D/A) conversion is given in Fig.15(b). This control signal is used to levitate the object at desired position. The plant input signal m(t) after D/A conversion and output signal y(t), captured on the digital storage oscilloscope (DSO), is presented in Fig.16.

The control effort required by controller to maintain object's position can be observed from the control signal c(t). The ball position is tracked by infrared sensor and is fed back to Simulink environment via analog to digital (A/D) converter. It is observed from Fig.15 - Fig.16 that there is more deviation in ball position and control effort required by the controller, and is higher in case of PD controller. Hence, integral action is added to the PD controller to achieve an improved control over desired ball position. The quantitative analysis of desired and actual ball position achieved by the controller is presented in Table IV and the control effort analysis of controller is shown in Table V.

Table III
MEASURED AND DESIRED BALL POSITIONS FOR DIFFERENT CONTROLLERS IN SIMULATION

Ball Positions (m)		**Controllers**		
		PD	**PID**	**FO-PID**
Measured ball position	Max.	8.12×10^{-3}	6.92×10^{-3}	5.94×10^{-3}
	Min.	-4.83×10^{-3}	-6.68×10^{-3}	-5.65×10^{-3}
Desired ball position	Max.	5.5×10^{-3}	5.5×10^{-3}	5.5×10^{-3}
	Min.	-5.5×10^{-3}	-5.5×10^{-3}	-5.5×10^{-3}
Error		23.06%	19.09%	5.03%

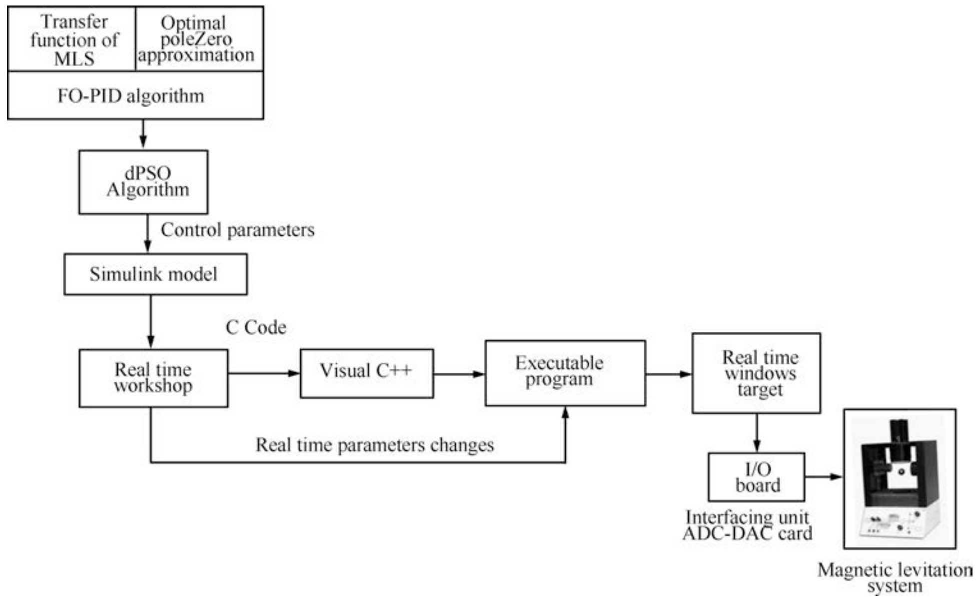

Fig. 13. Control system development flow diagram.

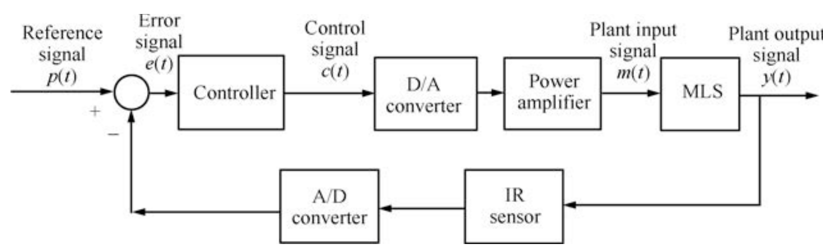

Fig. 14. Block diagram of MLS close loop control.

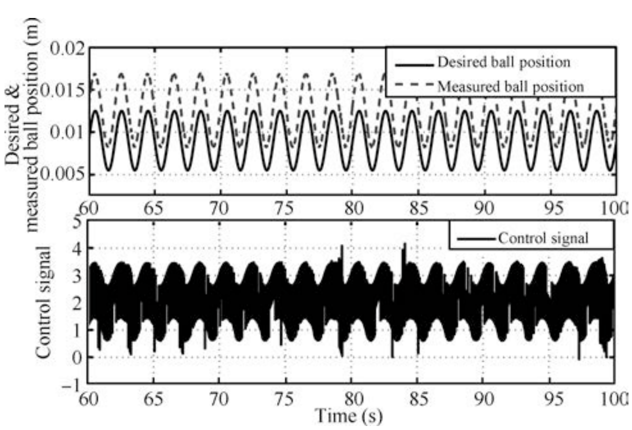

Fig. 15. (a) Controlled output result of MLS using a PD controller (b) Control signal of PD controller.

2) Experimental Results using a PID Controller: Fig.17(a) shows measured and desired ball positions using PID controller and output of controller c(t) is shown in Fig.17(b). The captured controller output signal c(t) and output signal are presented in Fig.18. The deviation in the ball position is minimized to an extent by employing the PID controller. However, the control effort required by controller is still similar to that of PD controller while achieving the improvement.

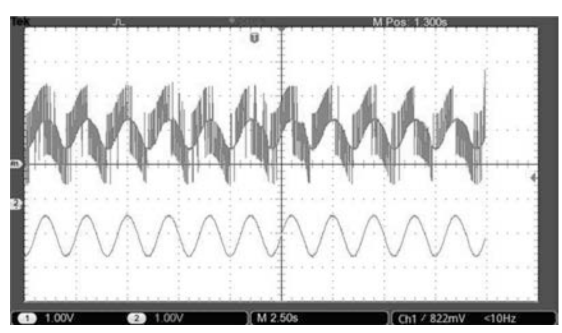

Fig. 16. Experimental PD controller output and object's trajectory captured on DSO.

3) Experimental Results using a FO-PID Controller: The deviation in ball positions using real time FO-PID controller is shown in Fig.19(a). It depicts that error in desired and actual ball positions has reduced in comparison to both PD or PID control actions. The control signal c(t) of FO-PID controller is presented in Fig.19(b). It shows that effort required by the controller is least as compared to PD or PID controllers. Plant input signal m(t) and output signal y(t) are presented in Fig.20.

Table IV
MEASURED AND DESIRED BALL POSITIONS FOR DIFFERENT CONTROLLERS IN REAL TIME IMPLEMENTATION

Ball Positions (m)		**Controllers** PD	PID	FO-PID
Measured ball position	Max.	16.8×10^{-3}	13.1×10^{-3}	12.6×10^{-3}
	Min.	8.3×10^{-3}	4.85×10^{-3}	5.24×10^{-3}
Desired ball position	Max.	12.5×10^{-3}	12.5×10^{-3}	12.5×10^{-3}
	Min.	5.5×10^{-3}	5.5×10^{-3}	5.5×10^{-3}
Error		29.66%	8.95%	5.75%

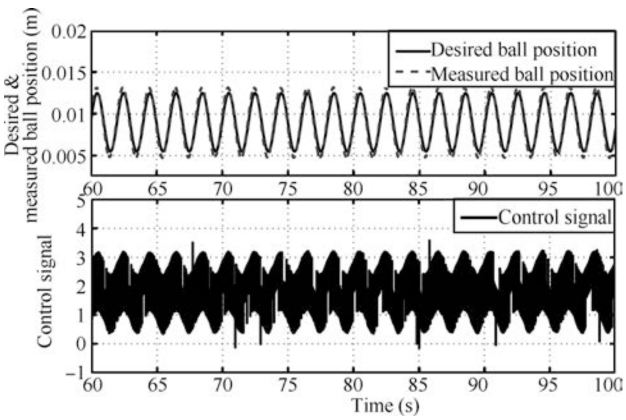

Fig. 17. (a) Controlled output result of MLS using a PID controller (b) Control signal of PID controller.

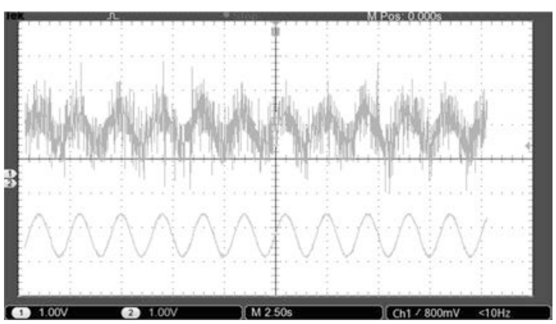

Fig. 18. Experimental PID controller output and object's trajectory captured on DSO.

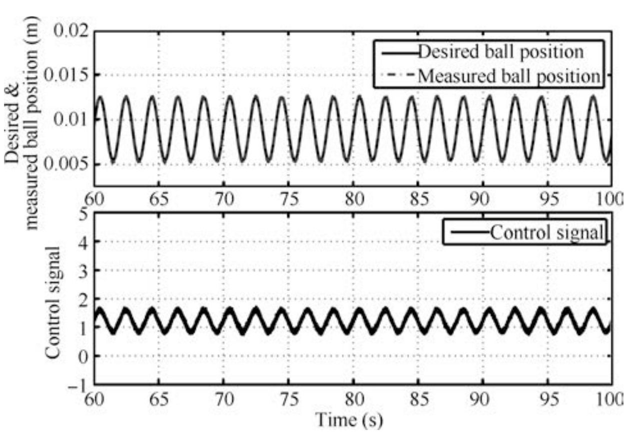

Fig. 19. (a) Controlled output result of MLS using a FO-PID controller (b) Control signal of FO-PID controller.

From the data presented in Table IV it is observed that FO-PID controller has improved the position accuracy of MLS compared to PD or PID controllers in real time implementation. Also, the percentage error is least for FO-PID controller.

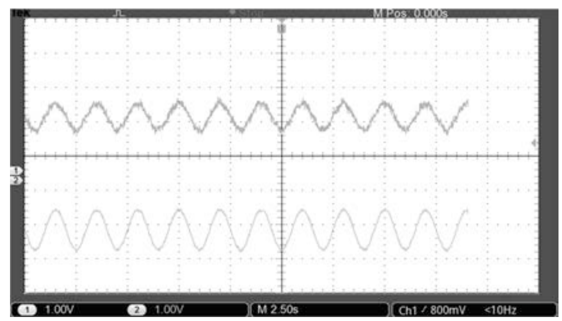

Fig. 20. Experimental FO-PID controller output and object's trajectory captured on DSO.

Table V
CONTROL EFFORT ANALYSIS OF DIFFERENT CONTROLLERS IN REAL TIME IMPLEMENTATION

Performance Indices		**Controllers** PD	PID	FO-PID
IAE	Error Signal	51.97	14.56	12.79
	Control Signal	208	181	151.5
ITAE	Error Signal	609	455.7	425.5
	Control Signal	900.6	797.9	602.5
ISE	Error Signal	28.38	4.978	2.488
	Control Signal	832.6	647.2	347.2

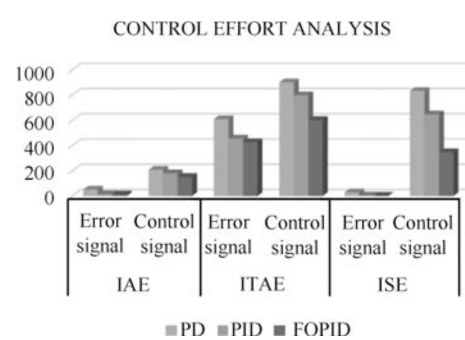

Fig. 21. Control effort analysis.

The control effort required by PD, PID, and FO-PID controllers is calculated using IAE (Integral Absolute Error), ITAE, and ISE (Integral Square Error). The analysis has been carried out for a period of $100s$ and is tabulated in Table V. Fig.21 represents the control effort analysis in pictorial form.

The error signal is maximum in the case of PD controller and least in the case of FO-PID controller. The control signal also follows the same pattern and is least in case of FO-PID controller, leading to inference that the control effort in terms of power required by the FO-PID controller to maintain the ball position is least amongst the three controllers.

From the analysis, it infers that PID controller is better than PD controller through performance characteristic. FO-PID controller shows slight improvement over PID controller, but the effort required is appreciably less for the same improvement. Thus proving superiority of FO-PID over integer order controllers.

4) Disturbance Injection Analysis of Controllers: The effect of disturbance is studied by injecting step input to MLS and effect of increased load is studied by introducing another metallic ball in levitation system as shown in Fig.22. The step is applied after interval of $25s$ on initiation of the input while another ball is introduced manually after $35s$. The measured and desired ball positions using a PD controller are presented in Fig.23(a) and the control signal of a controller is shown in Fig.23(b). PD controller output and object's trajectory as captured on DSO is presented in Fig.24.

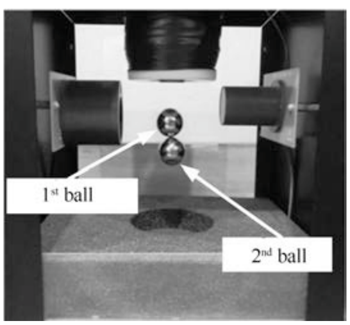

Fig. 22. Levitation of two metallic balls.

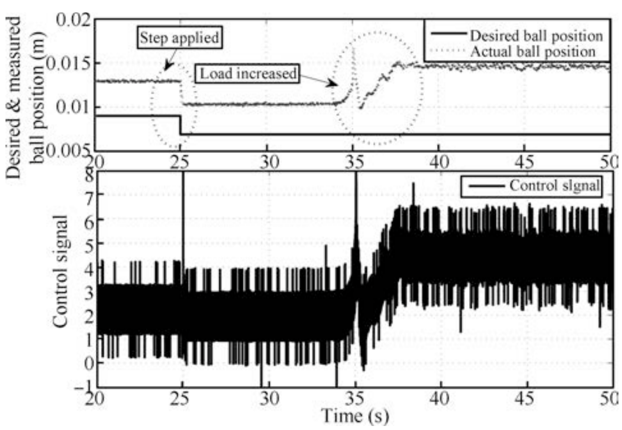

Fig. 23. (a) Controlled output result of MLS using a PD controller (b) Control signal of PD controller.

The instant of step applied in input signal and the instant of the addition of extra load are demonstrated by circles marked on figures. Overshoot is observed at the instant of step and after introducing second ball in levitation system.

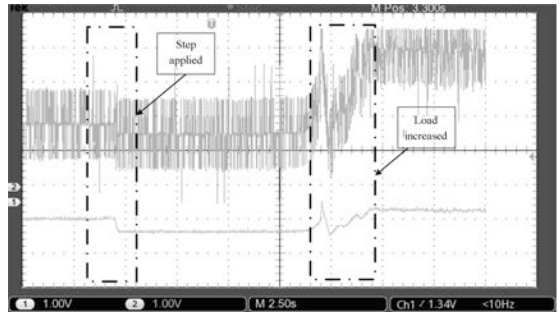

Fig. 24. Experimental PD controller output and object's trajectory captured on DSO.

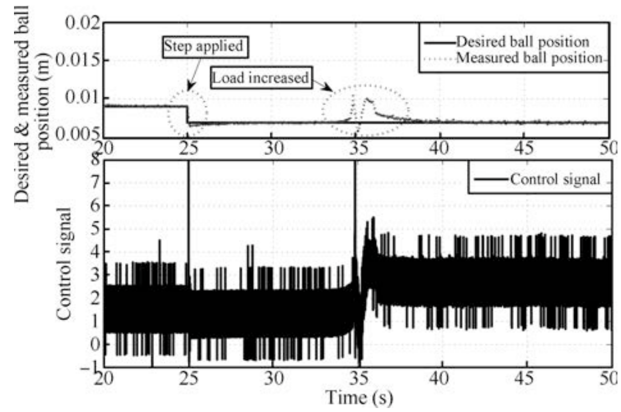

Fig. 25. (a) Controlled output result of MLS using a PID controller (b) Control signal of PID controller.

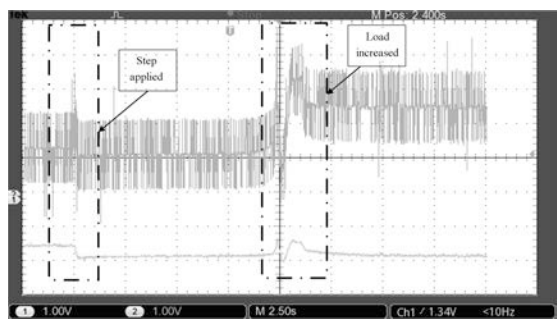

Fig. 26. Experimental PID controller output and object's trajectory captured on DSO.

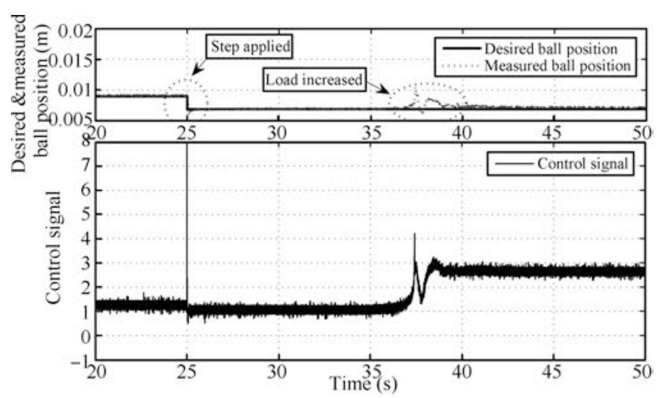

Fig. 27. (a) Controlled output result of MLS using a FO-PID controller (b) Control signal of FO-PID controller.

The deviation in ball position is higher as load is increased and greater amount of effort (power consumption, as indicated by high switching fluctuations in the voltage graph) is required by controller to achieve desired ball position.

Similar analysis for PID and FO-PID controllers is presented in Fig.25 - Fig.28. These figures lead to inference that in case of PID controller, the deviation in ball position is high and greater amount of effort is required by controller to achieve ball position as compared to FO-PID controller. Comparison shows that FO-PID controller requires lesser effort to levitate the object and effect of disturbance is less as compared to PD or PID controllers.

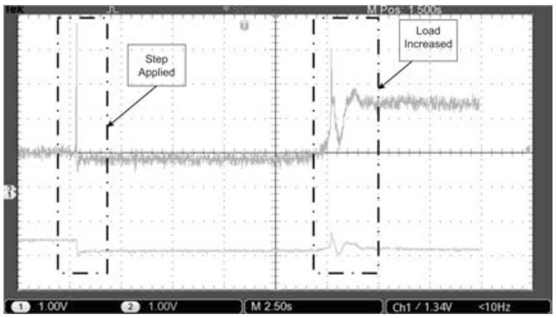

Fig. 28. Experimental FO-PID controller output and object's trajectory captured on DSO.

V. Conclusion

In this paper, digital FO-PID controller is applied on MLS to improve the positional accuracy and control effort. A new discrete optimal pole-zero approximation method is proposed for realization of controller. This method provides the optimal number of pole-zero pairs to maintain the phase value within the tolerance, of around 1^o. dPSO method is used for tuning the parameters of controller. The performance analysis for integer and fractional order controllers have been carried out in both simulation and experimentation. The results show that a better control over position accuracy with lesser efforts (over conventional methods) can be achieved. In practical terms, this efficiency improvement translates to better fuel efficiency. This paper provides a basis for evaluating the utility of fractional order control to improve the performance of power conversion systems and precision robotic applications.

Table VI
PARAMETERS OF THE MLS

Symbol	**Parameters**	**Values**
i	Input Current in the Coil	$[0-3]$A
u	Input Voltage	$[0-5]$V
m	Mass of the Steel Sphere	20×10^{-3} kg
k	Magnetic Constant	8.54×10^{-5} kg
k_1	Input Conductance	$0.3971/\Omega$
g	Gravitational Acceleration	$9.81m/s^2$

References

[1] C. M. Lin, M. H. Lin, and C. W. Chen, "SoPC-based adaptive PID control system design for magnetic levitation system," *IEEE Systems Journal*, Vol. 5, No. 2, pp. 278–287, June 2011. doi: 10.1109/JSYST.2011.2134530

[2] H. K. Chiang, C. A. Chen, and M. Y. Li, "Integral variable-structure grey control for magnetic levitation system," *IEE Proc. Electric Power Applications*, Vol. 153, No. 6, pp. 809–814, November 2006. doi: 10.1049/ip-epa:20060056

[3] Z. J. Yang, K. Kunitoshi, S. Kanae, and K. Wada, "Adaptive robust output-feedback control of a magnetic levitation system by K-filter approach," *IEEE Trans. on Industrial Electronics*, Vol. 55, No. 1, pp. 390–399, January 2008. doi: 10.1109/TIE.2007.896488

[4] R. Morales, V. Feliu, and H. Sira-Ramrez, "Nonlinear control for magnetic levitation systems based on fast online algebraic identification of the input gain," *IEEE Trans. on Control Systems Technology*, Vol. 19, No. 4, pp. 757–771, July 2011. doi: 10.1109/TCST.2010.2057511

[5] C. M. Lin, Y. L. Liu, and H. Y. Li, "SoPC-based function-link cerebellar model articulation control system design for magnetic ball levitation systems," *IEEE Trans. on Industrial Electronics*, Vol. 61, No. 8, pp. 4265–4273, August 2014. doi: 10.1109/TIE.2013.2288201

[6] A. El Hajjaji and M. Ouladsine, "Modeling and nonlinear control of magnetic levitation systems," *IEEE Trans. on Industrial Electronics*, Vol. 48, No. 4, pp. 831–838, August 2001. doi: 10.1109/41.937416

[7] R. C. Kluever, C. A. Kluever, *Dynamic Systems: Modeling, Simulation, and Control*, 1st Edition, John Wiley and Sons, April 2015.

[8] G. F. Franklin, J. D. Powell, and A. Emami-Naeini, *Feedback Control of Dynamic Systems*, 3rd Edition, Addison-Wesley, Reading, MA, 1994.

[9] T. H. Wong, "Design of a magnetic levitation control system - An undergraduate project," *IEEE Trans. on Education*, Vol. 29, No. 4, pp. 196–200, November 1986. doi: 10.1109/TE.1986.5570565

[10] R. Sinha and M. L. Nagurka, "Analog and labview-based control of a maglev system with NI-ELVIS," *ASME International Mechanical Engineering Congress and Exposition*, Orlando, Florida, USA, pp. 741–746, November 2005.

[11] S. Saha, S. Das, R. Ghosh, B. Goswami, R. Balasubramanian, A. K. Chandra, A. Gupta, "Design of a fractional order phase shaper for iso-damped control of a PHWR under step-back condition," *IEEE Trans. on Nuclear Science*, Vol. 57, No.3, pp. 1602–1612, June 2010. doi: 10.1109/TNS.2010.2047405

[12] S. Das, S. Das, and A. Gupta, "Fractional order modeling of a PHWR under step-back condition and control of its global power with a robust controller," *IEEE Trans. on Nuclear Science*, Vol. 58, No. 5, pp. 2431–2441, October 2011. doi: 10.1109/TNS.2011.2164422

[13] S. Saha, S. Das, R. Ghosh, B. Goswami, R. Balasubramanian, A. K. Chandra, S. Das, A. Gupta, "Fractional order phase shaper design with Bode integral for iso-damped control system," *ISA Trans.*, Vol. 49, No. 2, pp. 196–206, April 2010. doi:10.1016/j.isatra.2009.12.001

[14] S. Das, "Fuel efficient nuclear reactor control," *International Conference on Nuclear Engineering*, Beijing, China, May 16-20, 2005.

[15] K. J. Astrom and T. Hagglund, *PID Controllers: Theory, Design and Tuning*, Instrument Society of America, North Carolina, 1995.

[16] I. Podlubny, *Fractional Differential Equations*, Academic Press, New York, 1999.

[17] S. Das, (a) *Functional Fractional Calculus for System Identification and Controls*, Springer Science and Business Media, 2007, doi: 10.1007/978-3-540-72703-3; and (b) *Functional Fractional Calculus*, Springer Science and Business Media, 2011. doi: 10.1007/978-3-642-20545-3

[18] I. Podlubny, "Fractional-order systems and $PI^{\lambda}D^{\mu}$ controllers," *IEEE Trans. on Automatic Control*, Vol. 44, No. 1, pp. 208–214, January 1999. doi: 10.1109/9.739144

[19] A. Charef, H. H. Sun, Y. Y. Tsao, and B. Onaral, "Fractal system as represented by singularity function," *IEEE Trans. on Automatic Control*, Vol. 37, No. 9, pp. 14651470, September 1992. doi: 10.1109/9.159595

[20] A. Oustaloup, F. Levron, B. Mathiew, and F. M. Nanot, "Frequency-band complex noninteger differentiator: characterization and synthesis," *IEEE Trans. on Circuits and Systems I: Fundamental Theory and Applications*, Vol. 47, No. 1, pp. 25–39, January 2000. doi: 10.1109/81.817385

[21] Feedback Instruments Ltd., *Magnetic levitation control experiments, manual: 33-942S Ed01 122006*, Feedback Part No. 1160–33942S.

[22] R. Pintelon and J. Schoukens, *System Identification: A Frequency Domain Approach*, Wiley-IEEE Pres, ISBN 978-0-470-64037-1, 2012.

[23] C. Yeroglu and N. Tan, "Note on fractional-order proportional-integral-differential controller design," *IET Control Theory and Applications*, Vol. 5, No. 17, pp. 19781989, November 2011. doi: 10.1049/iet-cta.2010.0746

[24] D. Valerio and J. Sa da Costa, "Introduction to single-input, single-output fractional control," *IET Control Theory and Applications*, Vol. 5, No. 8, pp. 10331057, May 2011. doi: 10.1049/iet-cta.2010.0332

[25] D. Chen, Y. Q. Chen, and D. Xue, "Digital fractional order Savitzky-Golay differentiator," *IEEE Trans. on Circuits And Systems II: Express Briefs*, Vol. 58, No. 11, pp. 758–762, November 2011. doi: 10.1109/TCSII.2011.2168022

[26] M. O. Efe, "Fractional order systems in industrial automation-a survey," *IEEE Trans. on Industrial Informatics*, Vol. 7, No. 4, pp. 582–591, November 2011. doi: 10.1109/TII.2011.2166775

[27] J. A. T. Machado, "Discrete-time fractional-order controllers," *Fractional calculus and Applied Analysis*, Vol. 4, No. 1, pp. 47–66, January 2001.

[28] A. S. Dhabale, R. Dive, M. V. Aware, and S. Das, "A new method for getting rational approximation for fractional order differintegrals," *Asian Journal of Control*, Vol. 17, No. 6, pp. 21432152, November 2015. doi: 10.1002/asjc.1148

[29] Y. Q. Chen and K. L. Moore, "Discretization schemes for fractional-order differentiators and integrators," *IEEE Trans. on Circuits and Systems I: Fundamental Theory and Applications*, Vol. 49, No. 3, pp. 363–367, March 2002. doi: 10.1109/81.989172

[30] I. Pan and S. Das, *Gain and Order Scheduling for Fractional Order Controllers*, Intelligent Fractional Order Systems and Control, Springer Berlin Heidelberg, pp. 147157, 2013. doi: 10.1007/978-3-642-31549-7

[31] I. Petras, "Fractional order feedback control of a DC motor," *Journal of Electrical Engineering*, Vol. 60, No. 3, pp. 117128, March 2009.

[32] S. Cuoghi and L. Ntogramatzidis, "Direct and exact methods for the synthesis of discrete-time proportional-integral-derivative controllers," *IET Control Theory and Applications*, Vol. 7, No. 18, pp. 21642171, December 2013. doi: 10.1049/iet-cta.2013.0064

[33] Y. Q. Chen, I. Petras, and D. Xue, "Fractional order control-a tutorial," *American Control Conference*, St. Louis, MO, USA, June 10-12, pp. 1397–1411, 2009. doi: 10.1109/ACC.2009.5160719

[34] Y. Jin, Y. Q. Chen, and D. Xue, "Time-constant robust analysis of a fractional order [proportional derivative] controller," *IET Control Theory and Applications*, Vol. 5, No. 1, pp. 164172, January 2011. doi: 10.1049/iet-cta.2009.0543

[35] C. A. Monje, B. M. Vinagre, V. Feliu, and Y. Q. Chen, "Tuning and auto-tuning of fractional order controllers for industry applications," *Control Engineering Practice*, Vol. 16, No. 7, pp. 798812, July 2008. doi: 10.1016/j.conengprac.2007.08.006

[36] J. Zhong and L. Li, "Tuning fractional-order controllers for a solid-core magnetic bearing system," *IEEE Trans. on Control Systems Technology*, Vol. 23, No. 4, pp. 1648–1656, July 2015. doi: 10.1109/TCST.2014.2382642

[37] F. Padula and A. Visioli, "Optimal tuning rules for proportional-integral derivative and fractional-order proportional-integral-derivative controllers for integral and unstable processes," *IET Control Theory and Applications*, Vol. 6, No. 6, pp. 776786, April 2012. doi: 10.1049/iet-cta.2011.0419

[38] S. Das, S. Saha, S. Das, and A. Gupta, "On the selection of tuning methodology of FOPID controllers for the control of higher order processes," *ISA Transactions*, Vol. 50, No. 3, pp. 376–388, July 2011. doi: 10.1016/j.isatra.2011.02.003

[39] S. Das, I. Pan, S. Das, and A. Gupta, "A novel fractional order fuzzy PID controller and its optimal time domain tuning based on integral performance indices," *Engineering Applications of Artificial Intelligence*, Vol. 25, No. 2, pp. 430–442, March 2012. doi: 10.1016/j.engappai.2011.10.004

[40] S. Das, I. Pan, S. Das, and A. Gupta, "Improved model reduction and tuning of fractional-order $PI^{\lambda}D^{\mu}$ controllers for analytical rule extraction with genetic programming," *ISA Transactions*, Vol. 51, No. 2, pp. 237–261, March 2012. doi: 10.1016/j.isatra.2011.10.004

[41] S. Das, I. Pan, K. Halder, S. Das, and A. Gupta, "LQR based improved discrete PID controller design via optimum selection of weighting matrices using fractional order integral performance index," *Applied Mathematical Modelling*, Vol. 37, No. 6, pp. 4253–4268, March 2013. doi: 10.1016/j.apm.2012.09.022

[42] S. Das, I. Pan, and S. Das, "Performance comparison of optimal fractional order hybrid fuzzy PID controllers for handling oscillatory fractional order processes with dead time," *ISA Transactions*, Vol. 52, No. 4, pp. 550–566, July 2013. doi: 10.1016/j.isatra.2013.03.004

[43] S. Das, I. Pan, S. Das, and A. Gupta, "Master-slave chaos synchronization via optimal fractional order $PI^{\lambda}D^{\mu}$ controller with bacterial foraging algorithm," *Nonlinear Dynamics*, Vol. 69, No. 4, pp. 2193–2206, September 2012. doi: 10.1007/s11071-012-0419-x

[44] S. Saha, S. Das, S. Das, and A. Gupta, "A conformal mapping based fractional order approach for sub-optimal tuning of PID controllers with guaranteed dominant pole placement," *Communications in Nonlinear Science and Numerical Simulation*, Vol. 17, No. 9, pp. 3628–3642, September 2012. doi: doi:10.1016/j.cnsns.2012.01.007

[45] S. Das, I. Pan, K. Halder, S. Das, and A. Gupta, "Impact of fractional order integral performance indices in LQR based PID controller design via optimum selection of weighting matrices," *IEEE International Conference on Computer Communication and Informatics*, Coimbatore, India, Jan. 1012, pp. 1–6, 2012. doi: 10.1109/ICCCI.2012.6158892

[46] S. Das, I. Pan, S. Das, and A. Gupta, "Genetic algorithm based improved sub-optimal model reduction in nyquist plane for optimal tuning rule extraction of PID and $PI^{\lambda}D^{\mu}$ controllers via genetic programming," *IEEE International Conference on Process Automation, Control and Computing*, July 20, pp. 1–6, 2011. doi: 10.1109/PACC.2011.5978962

[47] A. Rajasekhar, S. Das, and A. Abraham, "Fractional order PID controller design for speed control of chopper fed DC motor drive using artificial bee colony algorithm," *IEEE World Congress on Nature and Biologically Inspired Computing*, August 12, pp. 269–266, 2013. doi: 10.1109/NaBIC.2013.6617873

[48] R. Song and Z. Chen, "Design of PID controller for maglev system based on an improved PSO with mixed inertia weight," *Journal of Networks*, Vol. 9, No. 6 , pp. 1509–1517, January 2014. doi: 10.4304/jnw.9.6.1509-1517

[49] A. Q. Badar, B. S. Umre, and A. S. Junghare, "Reactive power control using dynamic particle swarm optimization for real power loss minimization," *International Journal of Electrical Power and Energy Systems*, Vol. 41, No. 1, pp. 133136, Octomber 2012. doi: 10.1016/j.ijepes.2012.03.030

Amit S. Chopade (S'16) received the B.E. degree from Nagpur University, India, in 2012. Currently, he is working as Junior Research Fellow on BRNS Research Project "Development of Industrial Fractional Order PID Controller" at Visvesvaraya National Institute of Technology, Nagpur, India.

His research interests include electrical drives, energy efficient systems, and applications of fractional order controllers.

Swapnil W. Khubalkar (S'15) received the B.E. and M.Tech degree from Nagpur University, India, in 2010 and 2012, respectively. Currently he is working toward Ph.D. in the area of fractional order controllers at Visvesvaraya National Institute of Technology, Nagpur, India.

His research interests include electrical drives, controls, and applications of fractional order controllers.

Anjali S. Junghare received the B.E. and M.Tech degree from Visvesvaraya Regional College of Engineering (VRCE), Nagpur, India, in 1981 and 1985, respectively. She received the Ph.D. degree from VRCE in 2007. She is currently an associate professor in the Department of Electrical Engineering, Visvesvaraya National Institute of Technology, Nagpur, India. She has 13 years of industrial experience and 19 years of academic experience.

Her research areas are control system, fractional order controllers, fuzzy Logic and its applications.

Mohan V. Aware (M'08, SM'14) received the B.E. degree in Electrical Engineering from College of Engineering, Amravati, India, in 1980, the M.Tech degree from the Indian Institute of Technology, Bombay, in 1982 and the Ph.D. degree for research work on "Direct Torque Controlled Induction Motor Drives" from Nagpur University, India, in 2002. From 1982 to 1989, he was a Design Officer with Crompton Greaves Ltd., Nasik, India. From 1989 to 1991, he was a Development Engineer with Nippon Denro India pvt. Ltd. During 2001-2002, he was a Research fellow with Electrical Engineering Department, Hong Kong Polytechnic University, Hong Kong. Presently, he is a Professor in Electrical Engineering Department, Visvesvaraya National Institute of Technology, Nagpur, India.

His research areas are electrical drives, distributed generation with energy storage and power electronics. He has published more than 150 technical papers in different journals and conferences.

Shantanu Das works as a Scientist Bhabha Atomic Research Centre(BARC), India. He graduated in Electrical Engineering and Electronics Engineering, from BITS Pilani and thereafter working as scientist at BARC, since 1984, in the area of Nuclear Reactor Control and Safety. He is doing development on Fractional Calculus since about 1998, in order to understand natural laws and to engineer for betterment in controls, signal processing and systems identification. Since 2004, he is working on development of meta-material science to understand exotic properties of electro magnetism and to manipulate electromagnetic flow for usage is electronics systems, and also in application of microwave power for material processing. He is Honorary Senior Research Professor at Department of Physics, Jadavpur University, Adjunct Professor at DIAT Pune, and under UGC Visiting Fellow at Department of Applied Mathematics, Calcutta University. He has several publications and patents on all these topics.

Optimal Nonlinear System Identification Using Fractional Delay Second-Order Volterra System

Manjeet Kumar, Apoorva Aggarwal, Tarun Rawat and Harish Parthasarathy

Abstract*—The aim of this work is to design a fractional delay second order Volterra filter that takes a discrete time sequence as input and its output is as close as possible to the output of a given nonlinear unknown system which may have higher degree nonlinearities in the least square sense. The basic reason for such a design is that rather than including higher than second degree nonlinearities in the designed system, we use the fractional delay degrees of freedom to approximate the given system. The advantage is in terms of obtaining a better approximation of the given nonlinear system than is possible by using only integer delays (since we are giving more degrees of freedom via the fractional delays) and simultaneously it does not require to incorporate higher degree nonlinearities than two. This work hinges around the fact that if the input signal is a decimated version of another signal by a factor of M, then fractional delays can be regarded as delays by integers less than M. Using the well known formula for calculating the discrete time Fourier transform (DTFT) of a decimated signal, we then arrive at an expression for the DTFT of the output of a fractional delay system in terms of the unknown first and second order Volterra system coefficients and the fractional delays. The final energy function to be minimized is the norm square of the difference between the DTFT of the given output and the DTFT of the output of the fractional delay system. Minimization over the filter coefficients is a linear problem and thus the final problem is to minimize a highly nonlinear function of the fractional delays which is accomplished using search techniques like the gradient-search and nature inspired optimization algorithms. The effectiveness of the proposed method is demonstrated using two nonlinear benchmark systems tested with five different input signals. The accuracy of the stated models using the globally convergent metaheuristic, cuckoo-search algorithm (CSA) are observed to be superior when compared with other techniques such as real-coded genetic algorithm (RGA), particle swarm optimization (PSO) and gradient-search (GS) methods. Finally, statistical analysis affirms the potential of the proposed designs for its successful implementation.

***Index Terms*—Fractional delay, second-order Volterra system, gradient-search method, stochastic search algorithm, mean square error**

I. INTRODUCTION

THE modeling of unknown systems is of significant importance in different fields of engineering[1]. Various linear systems have been utilized owing to the simplicity in solving the system identification problems and in developing different signal processing techniques[2−8]. Such linear systems have been extensively applied with the comprehensive mathematical analysis and simplified simulations. However, most of the practical systems exhibit nonlinear behaviour due to which the estimation using linear systems is not accurate. To state some, in estimating the saturation-type nonlinear systems[9], development of nonlinear behaviour due to brake sequel conditions in automotive industry[10], identification of nonlinear dynamical structures[11], using linear models can often give corrupt results. The application of nonlinear systems have been extensively researched by practitioners in various science and engineering fields such as in communication engineering, signal processing, biomedical engineering and system identification[12]. Some typical applications[13] in communication systems include amplifier nonlinearities, nonlinear satellite channel, compensation of nonlinearities, equalization of nonlinear channels, blind identification, nonlinearities in orthogonal frequency division multiplexing systems and digital magnetic recording. In speech and image processing, the nonlinear systems are employed for the compensation of loudspeaker nonlinearities, in adaptive quadratic filters, nonlinear echoes cancelation and many more.

In the past, much research has been carried out for estimating practical systems using a variety of nonlinear systems based on different models. These nonlinear models and functions include Volterra and Wiener series[14,15], Hammerstein model[16], Walsh functions[17], Kautz models[18], Laguerre transform[19], Uryson model[20] and neural networks[21] etc. The aforementioned models have been substantially implemented in nonlinear system identification problems. Conventionally, the modeling of unknown systems was practiced using the gradient based search methods. Based on the successful implementation of metaheuristic algorithms in the system identification problems, the trend has been shifted towards the use of these algorithms. In [14], Chang efficiently utilized the improved particle swarm optimization algorithm for the different memory size Volterra filter models of nonlinear discrete-time systems. The implementation of the gravitational search algorithm for the nonlinear and linear system identification problem was proposed by Rashedi et al. in [22]. Gotmare et al. applied the CSA for the improvement of nonlinear system identification of adaptive Hammerstein model[16].

The above referred techniques implemented the concept of integer delays to obtain a nonlinear system with significantly accurate estimations. In this paper, we propose to model a highly nonlinear system with quadratic, cubic and even higher order nonlinearities in the presence of noise using a fractional

This article has been accepted for publication in a future issue of this journal, but has not been fully edited. Content may change prior to final publication.

This article was recommended by Associate Editor Antonio Visioli.

M. Kumar, A. Aggarwal, T. Rawat and H. Parthasarathy are with the Department of Electronics and Communication Engineering Division, Netaji Subhas Institute of Technology, Sector-3, Dwarka, New Delhi 110078, India (e-mail: manjeetchhillar@gmail.com, 16.apoorva@gmail.com, tarundsp@gmail.com, harisignal@yahoo.com).

Digital Object Identifier 10.1109/JAS.2016.7510184

delay second order Volterra nonlinear system. The input-output equation for such an approximating system is the usual relation for a system involving an FIR linear system and an FIR second order Volterra system but with fractional delays. Both the continuous time and the discrete time models have been addressed. The fractional delay Volterra system is an LIP (Linear in parameters) model as far as the filter coefficients are concerned, but it is an NLIP (nonlinear in the parameters) model as far as the fractional delays are concerned. Thus, using the standard least squares algorithm, the first and second order filter coefficient estimates from input-output data can be obtained using standard orthogonal projection theory, but with the orthogonal projection being a highly nonlinear function of the fractional delays. By substituting this expression for the filter coefficient estimation into the original least squares energy function, we obtain an energy function that is a nonlinear function of the time delays but not involving the filter coefficients. Then, a search algorithm is used to minimize this energy function w.r.t. the fractional delays and hence obtain good estimates for the latter. The computation has been carried out entirely in the frequency domain because time delays appear as exponentials which multiplies with the Fourier transform of the signals. These exponentials can be represented as steering vectors which depend on the fractional time delays and elegant expressions for the energy function in terms of these steering vectors can be derived. If however, we work in the time domain, then the fractional delays appear inside the time argument of the signals involved and hence optimization algorithms are impossible to carry out. For practical implementation using MATLAB the signals must be discrete time and we have formulated this discrete time version by representing the input signal as a decimated version of the original input by an integer factor of $M > 1$ and the fractional delays by integers in the range $0, 1, \ldots, M-1$. The simulation results show that it is possible to approximate complicated nonlinear systems like the ratio of two nonlinear Volterra systems using this second order system involving fractional delays. The advantage of the proposed approach is that no extra filter coefficient energy is required. Indeed, fractional delays do not change the signal energy, they merely shift the signal and superpose. Here, we identify the parameters of a fractional delay second-order Volterra system from input data. This model gives a more accurate system identification with fewer filter coefficients, especially for nonlinear systems like multipath systems with interaction between the different paths shown in Fig. 1. Further, the gradient-search (GS) and stochastic-search approaches are employed to obtain a close approximation of the unknown nonlinear systems. The optimization algorithms utilized are, real-coded genetic algorithm (RGA), particle swarm optimization (PSO) and cuckoo-search algorithm (CSA). The results and analysis presented, demonstrate high accuracy using the proposed design methods.

The paper is organized in 6 sections. Following the literature survey in Section I, the nonlinear system identification problem is modeled as a second order Volterra system using fractional delays in Section II. Section III presents the gradient-search optimization technique articulated for the Volterra system identification problem. A brief overview of stochastic algorithms for the formulated problem is discussed in Section IV. In Section V, two design examples are illustrated and analyzed for different input signals. Finally, Section VI concludes the paper.

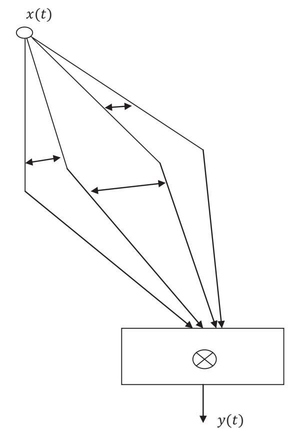

Fig. 1. Multipath system with interaction between the different paths.

II. Volterra System Modeling using Fractional Delay

Suppose $y_d(t)$ is the desired nonlinear system output and it is well approximated using a third order Volterra system with p integer delays, given by

$$\begin{aligned} y(t) &= \sum_{k=0}^{p} h(k)x(t-k\Delta) \\ &\quad + \sum_{k,m=0}^{p} g(k,m)x(t-k\Delta)x(t-m\Delta) \\ &\quad + \sum_{k,m,r=0}^{p} f(k,m,r)x(t-k\Delta)x(t-m\Delta)x(t-r\Delta) \end{aligned} \tag{1}$$

where, $x(t)$, $y(t)$ are the input and corresponding output of the Volterra system, $\{h(k)\}$ are the first order kernels of the linear system response with integer delays, $k\Delta$ and $\{g(k,m)\}$ are the second order kernels associated with the nonlinear system response with integer delays, $k\Delta, m\Delta$ and $\{f(k,m,r)\}$ are the third order kernels associated with the nonlinear system response with integer delays, $k\Delta, m\Delta$ and $r\Delta$.

To implement this filter, we require $\mathcal{O}(p^3)$ multiplications and further, the right hand side of the above expression is modeled as

$$M_0\sum_{k=0}^{p}|h(k)| + M_0^2\sum_{k,m=0}^{p}|g(k,m)| + M_0^3\sum_{k,m,r=0}^{p}|f(k,m,r)| \tag{2}$$

where, $M_0 = \max_t |x(t)|$.

In this system identification problem, the aim is to estimate the filter coefficients of a second order Volterra system modeled using the fractional delays, such that it matches the response of an unknown system with higher order nonlinearities. In Fig. 2, this concept is demonstrated by applying the gradient-search and stochastic optimization algorithms. The Volterra system mathematically models the linear and nonlinear combinations of its input signal using the infinite

Volterra series expansion in the form of convolution integrals. The second order Volterra system can be expressed as [23]

$$y(t) = h(0) + \sum_{k=1}^{p} h(k)x(t-\tau_k) + \sum_{k,m=0}^{p} g(k,m)x(t-\tau_k)x(t-\tau_m) \quad (3)$$

where, $h(0)$ is the constant kernel, $\{h(k)\}$ are the first order kernels of the linear system response with fractional delays, τ_k and $\{g(k,m)\}$ are the second order kernels associated with the nonlinear system response with fractional delays, τ_m.

Here, τ_k is varied in addition to the $\{h(k)\}$ and $\{g(k,m)\}$, to get an equally good output match, with $\mathcal{O}(p^2)$ multiplications. The right hand side of eq. (3) is modeled as

$$M_0 \sum_{k=0}^{p} |h(k)| + M_0^2 \sum_{k,m=0}^{p} |g(k,m)| \quad (4)$$

which is likely to be much smaller than eq. (2). Thus, by spending less energy and fewer multiplications, we are able to obtain nearly the same output error.

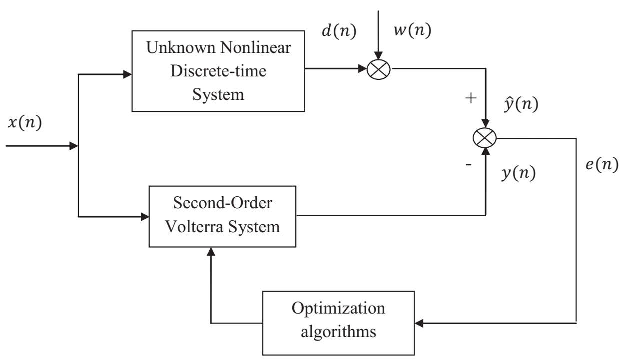

Fig. 2. Volterra System Modeling of nonlinear system using gradient search, RGA, PSO and CSA.

The objective is to optimize the parameters, $\{\tau_k\}$, $\{h(k)\}$ and $\{g(k,m)\}$, such that $\tau_k \in [k\Delta, (k+1)\Delta)$, $0 \le k,\, m \le p$ and

$$\begin{aligned}\xi(\mathbf{h},\mathbf{g},\tau) &= \int_0^{\mathrm{T}} \left(y_d(t) - y(t)\right)^2 \mathrm{d}t \\ &= \int_0^{\mathrm{T}} \left(y_d(t) - \sum_{k=1}^{p} h(k)x(t-\tau_k) \right. \\ &\quad \left. - \sum_{k,m=0}^{p} g(k,m)x(t-\tau_k)x(t-\tau_m) \right)^2 \mathrm{d}t \end{aligned} \quad (5)$$

is minimum. Here, $y_d(t)$ is the desired output. Let $\tau = \{\tau_k\}_{k=0}^{p}$, $\mathbf{h} = \{h(k)\}_{k=0}^{p}$, $\mathbf{g} = \mathrm{vec}(g(k,m))$ and

$$\zeta(t,\tau) = \begin{bmatrix} x(t-\tau_1) \\ x(t-\tau_2) \\ \vdots \\ x(t-\tau_p) \end{bmatrix} \quad (6)$$

then,

$$\xi(\mathbf{h},\mathbf{g},\tau) = \int_0^{\mathrm{T}} (y(t) - \mathbf{h}^{\mathrm{T}}\zeta(t,\tau) - \mathbf{g}^{\mathrm{T}}(\zeta(t,\tau)\otimes\zeta(t,\tau)))^2 \mathrm{d}t \quad (7)$$

where $\zeta(t,\tau)\otimes\zeta(t,\tau) = \mathrm{vec}(x(t-\tau_\alpha)x(t-\tau_\beta))$, $1 \le \alpha, \beta \le p$. The optimal equations are

$$\frac{\partial\xi}{\partial\mathbf{h}} = 0,\ \frac{\partial\xi}{\partial\mathbf{g}} = 0,\ \frac{\partial\xi}{\partial\tau} = 0 \quad (8)$$

Calculating the first two terms, we get

$$\int_0^{\mathrm{T}} \zeta(t,\tau)y(t)\mathrm{d}t = \left(\int_0^{\mathrm{T}} \zeta(t,\tau)\zeta(t,\tau)^{\mathrm{T}}\mathrm{d}t\right)\mathbf{h} + \left(\int_0^{\mathrm{T}} \zeta(t,\tau)(\zeta(t,\tau)\otimes\zeta(t,\tau))\mathrm{d}t\right)\mathbf{g} \quad (9)$$

Calculating the third term, we obtain

$$\begin{aligned}&\int_0^{\mathrm{T}} (\zeta(t,\tau)\otimes\zeta(t,\tau))y(t)\mathrm{d}t \\ &= \left(\int_0^{\mathrm{T}} (\zeta(t,\tau)\otimes\zeta(t,\tau))(\zeta(t,\tau))^{\mathrm{T}}\mathrm{d}t\right)\mathbf{h} \\ &+ \left(\int_0^{\mathrm{T}} (\zeta(t,\tau)\otimes\zeta(t,\tau))(\zeta(t,\tau)\otimes\zeta(t,\tau))^{\mathrm{T}}\mathrm{d}t\right)\mathbf{g}\end{aligned} \quad (10)$$

Defining the nonlinear filter vector

$$\mathbf{k} = \begin{bmatrix} \mathbf{h} \\ \mathbf{g} \end{bmatrix} \in R^{p+p^2} \quad (11)$$

and the $(p+p^2)\times(p+p^2)$ matrix is given by eq. (12). Also define

$$\mathbf{b}(\tau) = \begin{bmatrix} \int_0^{\mathrm{T}} \zeta(t,\tau)y(t)\mathrm{d}t \\ \int_0^{\mathrm{T}} (\zeta(t,\tau)\otimes\zeta(t,\tau))y(t)\mathrm{d}t \end{bmatrix} \in R^{p+p^2} \quad (13)$$

Then, the optimal equations for $\mathbf{k} = [\mathbf{h}^{\mathrm{T}}, \mathbf{g}^{\mathrm{T}}]^{\mathrm{T}}$ are solved as

$$\hat{\mathbf{k}}(\tau) = \mathbf{A}(\tau)^{-1}\mathbf{b}(\tau) = \begin{bmatrix} \hat{\mathbf{h}}(\tau) \\ \hat{\mathbf{g}}(\tau) \end{bmatrix} \quad (14)$$

Further, τ is extended as

$$\hat{\tau} = \arg\min_{\tau} \xi(\hat{\mathbf{h}}(\tau), \hat{\mathbf{g}}(\tau), \tau) \quad (15)$$

$$= \arg\min_{\tau} \xi(\hat{\mathbf{k}}(\tau), \tau) \quad (16)$$

Now

$$\xi(\hat{\mathbf{k}}(\tau),\tau) = \left[\int_0^{\mathrm{T}} y_d^2(t)\mathrm{d}t - \hat{\mathbf{k}}(\tau)^{\mathrm{T}}\mathbf{b}(\tau)\right] \quad (17)$$

$$= [\sigma_y^2 - \mathbf{b}(\tau)^{\mathrm{T}}\mathbf{A}(\tau)\mathbf{b}(\tau)] \quad (18)$$

So the optimal fractional delays are

$$\hat{\tau} = \arg\min_{\tau} \mathbf{b}(\tau)^{\mathrm{T}}\mathbf{A}(\tau)\mathbf{b}(\tau) \quad (19)$$

The proposed method can be applied to better equalization of nonlinear channels with random delays, for better forecasting of system and better system identification. Less power loss is there since loss depends on the number of coefficients and

$$\mathbf{A}(\tau)=\left[\begin{array}{cc}\int_0^{\mathrm{T}}\zeta(t,\tau)\zeta(t,\tau)^{\mathrm{T}}\mathrm{d}t & \int_0^{\mathrm{T}}\zeta(t,\tau)(\zeta(t,\tau)\otimes\zeta(t,\tau))\mathrm{d}t\\ \int_0^{\mathrm{T}}(\zeta(t,\tau)\otimes\zeta(t,\tau))(\zeta(t,\tau))^{\mathrm{T}}\mathrm{d}t & \int_0^{\mathrm{T}}(\zeta(t,\tau)\otimes\zeta(t,\tau))(\zeta(t,\tau)\otimes\zeta(t,\tau))^{\mathrm{T}}\mathrm{d}t\end{array}\right] \tag{12}$$

not on the delay given to each one. Moreover, the Volterra fractional delay system can be made adaptive, resulting in better adaptive noise cancelation, when the noise is generated from nonlinearities with delays like hysteresis. The optimal values of these fractional delays and Volterra kernels of first and second order are computed using the gradient-search and metaheuristic algorithms, described in the following section.

III. Gradient Search Method

This section focusses on the implementation of the gradient-search method to approximate the response of the unknown nonlinear system. This optimization is carried out using a gradient descent approach explained as follows.

$$\zeta(t,\tau)=\left(\int_R X(\omega)e^{j\omega(t-\tau_k)}\mathrm{d}\omega\right)_{k=1}^{p} \tag{20}$$

where, $X(\omega)$ is the DTFT of input signal $x(t)$ and $R\in(0,T)$. Now,

$$\begin{aligned}&\zeta(t,\tau)\otimes\zeta(t,\tau)\\ =&\mathrm{vec}\Bigg(\int_R X(\omega_1)X(\omega_2)\\ &\times e^{j(\omega_1+\omega_2)t}e^{j(\omega_1\tau_k+\omega_2\tau_m)}\mathrm{d}\omega_1\mathrm{d}\omega_2\Bigg)_{k,m=0}^{p}\end{aligned} \tag{21}$$

Substituting eqs. (20) and (21) in eq. (13), we get (22) at the top of next page. The derivative of $\mathbf{b}(\tau)$ in eq. (22) w.r.t. the fractional delays, τ_k is expressed as (23) at the top of next page, where

$$\mathbf{e}_k=\begin{bmatrix}0\\0\\ \vdots\\0\\1(\mathrm{k}^{th}\mathrm{row})\\0\\ \vdots\\0\end{bmatrix} \tag{24}$$

and $\frac{\partial\mathbf{A}(\tau)}{\partial\tau_k}$ can be calculated using eq. (20), we get

$$\begin{aligned}\frac{\partial\zeta(t,\tau)}{\partial\tau_k}&=\frac{\partial}{\partial\tau_k}\left(\int X(\omega)e^{j\omega(t-\tau_m)}\mathrm{d}\omega\right)_{m=0}^{p}\\ &=\left(-j\int\omega X(\omega)e^{j\omega(t-\tau_k)}\mathrm{d}\omega\right)\mathbf{e}_k\end{aligned} \tag{25}$$

$$\frac{\partial\mathbf{A}(\tau)}{\partial\tau_k}=\begin{bmatrix}a_{11}&a_{12}\\a_{21}&a_{22}\end{bmatrix} \tag{26}$$

where

$$a_{11}=\int_0^{\mathrm{T}}\left(\frac{\partial\zeta(t,\tau)}{\partial\tau_k}\zeta(t,\tau)^{\mathrm{T}})+\zeta(t,\tau)\left(\frac{\partial\zeta(t,\tau)}{\partial\tau_k}\right)^{\mathrm{T}}\right)\mathrm{d}t$$

$$\begin{aligned}a_{12}=\int_0^{\mathrm{T}}&\Bigg(\frac{\partial\zeta(t,\tau)}{\partial\tau_k}\Big(\zeta(t,\tau)\otimes\zeta(t,\tau)\Big)^{\mathrm{T}}\\ &+\zeta(t,\tau)\left(\frac{\partial\zeta(t,\tau)}{\partial\tau_k}\otimes\zeta(t,\tau)\right)^{\mathrm{T}}\\ &+\zeta(t,\tau)\left(\zeta(t,\tau)\otimes\frac{\partial\zeta(t,\tau)}{\partial\tau_k}\right)^{\mathrm{T}}\Bigg)\mathrm{d}t\end{aligned}$$

$$\begin{aligned}a_{21}=\int_0^{\mathrm{T}}&\Bigg(\left(\frac{\partial\zeta(t,\tau)}{\partial\tau_k}\otimes\zeta(t,\tau)\right)\Big(\zeta(t,\tau)\Big)^{\mathrm{T}}\\ &+\left(\zeta(t,\tau)\otimes\frac{\partial\zeta(t,\tau)}{\partial\tau_k}\right)\Big(\zeta(t,\tau)\Big)^{\mathrm{T}}\\ &+\Big(\zeta(t,\tau)\otimes\zeta(t,\tau)\Big)\left(\frac{\partial\zeta(t,\tau)}{\partial\tau_k}\right)^{\mathrm{T}}\Bigg)\mathrm{d}t\end{aligned}$$

$$\begin{aligned}a_{22}=\int_0^{\mathrm{T}}&\Bigg(\left(\frac{\partial\zeta(t,\tau)}{\partial\tau_k}\otimes\zeta(t,\tau)\right)(\zeta(t,\tau)\otimes\zeta(t,\tau))^{\mathrm{T}}\\ &+\left(\zeta(t,\tau)\otimes\frac{\partial\zeta(t,\tau)}{\partial\tau_k}\right)(\zeta(t,\tau)\otimes\zeta(t,\tau))^{\mathrm{T}}\\ &+(\zeta(t,\tau)\otimes\zeta(t,\tau))\left(\frac{\partial\zeta(t,\tau)}{\partial\tau_k}\otimes\zeta(t,\tau)\right)^{\mathrm{T}}\\ &+(\zeta(t,\tau)\otimes\zeta(t,\tau))\left(\zeta(t,\tau)\otimes\frac{\partial\zeta(t,\tau)}{\partial\tau_k}\right)^{\mathrm{T}}\Bigg)\mathrm{d}t\end{aligned}$$

Now,

$$F(\tau)=\mathbf{b}(\tau)^{\mathrm{T}}\mathbf{A}(\tau)^{-1}\mathbf{b}(\tau) \tag{27}$$

The designed system can be formulated using the above equations with

$$\tau_k[m+1]=\tau_k[m]-\mu\frac{\partial}{\partial\tau_k[m]}\left(\mathbf{b}(\tau[m])^{\mathrm{T}}\mathbf{A}(\tau[m])^{-1}\mathbf{b}(\tau[m])\right) \tag{28}$$

Eq. (28) updates the gradient-search algorithm for the fractional delay values.

IV. Stochastic Search Algorithms

The stochastic search algorithms are proven to produce optimal solutions to the complex problems in a reasonably practical time. These algorithms are characterized as heuristic, adaptive and learning with which they produce effective optimizations. Genetic algorithm, particle swarm optimization and cuckoo-search algorithm are population based, since they use a set of strings, particles and host nest, respectively to obtain the solution which are globally optimal. Further, these algorithms are briefly reviewed in this section.

$$\mathbf{b}(\tau) = \begin{bmatrix} \left(\int X(\omega)\overline{Y(\omega)}e^{-j\omega\tau_k}\mathrm{d}\omega\right)_{k=0}^{p} \\ \mathrm{vec}\left(\int X(\omega_1)X(\omega_2)\overline{Y(\omega_1+\omega_2)}e^{-j(\omega_1\tau_k+\omega_2\tau_m)}\mathrm{d}\omega_1\mathrm{d}\omega_2\right)_{k,m=0}^{p} \end{bmatrix} \tag{22}$$

$$\frac{\partial\mathbf{b}(\tau)}{\partial\tau_{\mathbf{k}}} = \begin{bmatrix} \left(-j\int \omega X(\omega)\overline{Y(\omega)}e^{-j\omega\tau_k}\mathrm{d}\omega\right)\mathbf{e}_k \\ \left(-j\int \omega_2 X(\omega_1)X(\omega_2)\overline{Y(\omega_1+\omega_2)}e^{-j(\omega_1\tau_m)}\mathrm{d}\omega_1\mathrm{d}\omega_2\right)_{m=0}^{p}\otimes\mathbf{e}_k \\ +\mathbf{e}_k\otimes\left(-j\int \omega_2 X(\omega_1)X(\omega_2)\overline{Y(\omega_1+\omega_2)}e^{-j(\omega_1\tau_m)}\mathrm{d}\omega_1\mathrm{d}\omega_2\right)_{m=0}^{p} \end{bmatrix} \tag{23}$$

A. Real-Coded Genetic Algorithm

The basic concept of GA was introduced by Holland in 1975[24] and it is an adaptive population based optimization method. This bio-inspired technique is based on the evolutionary ideas of natural selection and genetics, wherein a set of coefficient chromosomes is selected and encoded as binary strings. To avoid the precision problems, the final local tuning potential of a binary coded GA is improved with the use of RGA. Using real values, the natural form of the strings is maintained, thus, avoiding the coding and decoding processes. A considerable increase in the speed of operation, efficiency and precision in the results can be observed. RGA is universally employed to obtain the set of optimal solutions[25]. The algorithm undergoes three main processes after randomly generating the initial population. The selection process chooses better individual genotype chromosome depending on computing the fitness of each individual and produce a new generation of offspring chromosomes. The use of tournament operator allows a competition amongst the chromosomes on the grounds of their fitness values, where winners are selected with better fitness values. The crossover process is responsible for combining two chromosomes to produce new generations in search of a better fitness. A heuristic crossover operator aims towards determining the direction towards a better solution. Finally, the mutation process makes random changes to incorporate diversity in the results for achieving the global solution. The adaptive feasible mutation generates random variations adaptively with respect to the last successful or unsuccessful generation. The implementation steps of GA for the nonlinear system modeling using second order Volterra system model are adopted from [26].

B. Particle-Swarm Optimization

The social behavior of certain animals within a team such as fish schooling, insect swarming and bird flocking is transformed into an artificial swarm and is mathematically modeled as the PSO algorithm. It is a robust, population-based stochastic search technique which is suitable for non-differentiable and multiple objective functions. It was developed in 1995[27], and is successfully being applied to many engineering applications. In this algorithm, each particle acts as agent and is a potential solution. It is characterized by its position in the solution space and velocity with which it moves towards the optimal solution evaluated by the best fitness value. At every iteration, each particle is attracted towards the position of the current global best location. The velocity of the ith particle in the current iteration (let l), is adapted by evaluating the sum of three terms: the global best position vector, $gbest$, its personal best value, $pbest$ and the particle's present velocity, v^l. This new velocity vector is determined by the following formula considering the initial velocity, $v_i^{l=0} = 0$.

$$\begin{aligned} v_i^{l+1} =& W * v_i^l + \alpha C_1[gbest^l - x_i^l] \\ &+ \beta C_2[pbest_i^l - x_i^l] \end{aligned} \tag{29}$$

where W is the inertia weight parameter that controls the tradeoff between $gbest$ and $pbest$ of the swarm. Its value is set less than one. C_1, C_2 are the learning parameters that indicates the relative attraction towards $gbest$ and $pbest$ and α, β are random numbers ranging between $[0, 1]$. Also, the new position, x_i^{l+1} of the ith particle is updated by using

$$x_i^{l+1} = x_i^l + v_i^{l+1} \tag{30}$$

v_i can be bounded with the range $[v_{min}, v_{max}]$. On calculation of the new position, the particle flies to that location and ultimately at the final iteration, the global best solution becomes the optimal solution searched by PSO. The implementation steps of PSO for the nonlinear system modeling using second order Volterra system model are adopted from [28].

C. Cuckoo-Search Algorithm

CSA is a mathematical conceptualization which simulates the breeding strategy of the cuckoo birds. It was developed in 2009 by Yang and Deb[29]. It is based on the unique parasitic behaviour of some cuckoo bird species in combination with the Lévy flight. These bird species reproduce and lay their eggs in the nests of other birds. The host birds sometimes belligerently throw away the foreign eggs to increase the probability of hatching their own eggs. Whereas, some host birds simply abandon their nests and build a new nest at a new location. In CSA, each cuckoo egg in the host's nest symbolizes to a potential solution of the design problem. Each solution is characterized by its fitness value. The objective of CSA is to exchange a low fitness value solution with a better solution. In the process of generating a new solution, the concept of random walk performed by Lévy flights is applied. In this, the next step of the random walk is based on the current location (solution) and the transition probability to the next location.

In order to simplify the algorithm, it is governed by three guiding rules[29]. (i) Each bird is allowed to lay only one egg at once, which is randomly placed among the host bird's nests. (ii) The nest with the high quality eggs (solutions with high fitness values) will be imparted over to the next generation. (iii) A predetermined number of host nests are available, in which the probability of identification of alien eggs by host birds is also fixed ($P_a \in [0, 1]$). In instance of discovery, the host bird can either throw the alien egg or abandon the nest.

While generating a new solution, the Lévy flight is performed, represented in eq. (31). It is a Markov chain in which the next step depends on the current location and the transition probability.

$$\mathbf{a}_{l+1} = \mathbf{a}_l + \delta \oplus \text{Lévy}(\lambda) \tag{31}$$

where $\mathbf{a}_l$ is the solution vector which is the location of current solution at iteration, l, δ ($\delta > 0$) is the step size that determines the distance of the random walk. If δ is too big, then $\mathbf{a}_{l+1}$ will be too far away from $\mathbf{a}_l$. Similarly, if δ is too small, then $\mathbf{a}_{l+1}$ will be very close to $\mathbf{a}_l$ to be of any importance. Lévy(λ) is adopted from the Lévy distribution with an infinite variance and infinite mean[29].

The steps involved in the optimization algorithm utilizing the strategy of cuckoo birds for the process of evolving their generations along with their parasitic behavior are as follows.

Step 1: Initialize the maximum number of iterations (N) and randomly generate an initial population of n_c host nests, $\mathbf{a}_l$.

Step 2: Compute the fitness value, say E_l, of randomly generated host nest, $\mathbf{a}_l$.

Step 3: Generate a new nest using the Lévy flights given in eq. (31) and compute the fitness value, say E_{l+1}, of the new nests.

Step 4: Compare the two fitness values. For a minimization problem, if $E_l > E_{l+1}$, the initial host nests $\mathbf{a}_l$ are replaced by new nests, $\mathbf{a}_{l+1}$, generated by Lévy flights.

Step 5: Abandon a fraction of worst nests depending on the probability parameter p_a and build new nests, $\mathbf{a}_n$ using the random flights.

Step 6: Calculate the fitness of all the new nests and update the best nest, $\mathbf{a}_b$ of the generation until the current iteration. Compare it with the fitness value of the nest of next iteration and update the best nest.

Step 7: Repeat Steps 2-6 till the maximum number of iterations has reached. The best solution, $\mathbf{a}_b$ gives the optimal solution to the problem.

V. Simulation and Analysis

In this section, the discrete time nonlinear system identification problem is formulated and the simulated results have been presented. In order to implement the above formulated continuous time Volterra system using MATLAB, the discrete time signals are incorporated, by decimating the original input with integer factor of $M > 1$ and the fractional delays by integers in the range $0, 1, \cdots, M-1$.

A. Fractional delay system in discrete time

Given an input signal $x[n] = z[Mn]$. It is delayed by a fraction of r/M, where r is an integer in $0, 1, \cdots, M-1$, given by $x[n-r/M] = z[Mn-r]$. Let r_k be an integer of the form $(Mk + s_k)$ where $s_k \in 0, 1, \cdots, M-1$, $k = 1, 2, \cdots, p$. The output generated by passing the input signal $x[n]$ through a second order Volterra filter with fractional delays of $r_1, \cdots, r_p$ is given by

$$\begin{aligned}
y[n] = h[0] &+ \sum_{k=1}^{p} h[k]x[n - r_k/M] \\
&+ \sum_{k,m=0}^{p} g[k,m]x[n - r_k/M]x[n - r_m/M] \\
= h[0] &+ \sum_{k} h[k]z[Mn - r_k] \\
&+ \sum_{k,m} g[k,m]z[Mn - r_k]z[Mn - r_m]
\end{aligned} \tag{32}$$

Considering a noisy signal, eq. (32) is an approximate relation. Now, the aim is to determine the coefficients $h[k]$, $g[k, m]$ and the integers $r_1, \cdots, r_p$ such that the difference between the left hand side and right hand side of eq. (32) has minimum error energy. The Fourier transform (DTFT) of $z[Mn - r]$ is given by

$$\begin{aligned}
&\text{DTFT}\{z[Mn - r]\} = \\
&\quad M^{-1} \sum_{l=0}^{M-1} e^{(-jr(\omega - 2\pi l)/M)} Z\left(\frac{\omega - 2\pi l}{M}\right)
\end{aligned} \tag{33}$$

The Fourier transform of $y_1[n] = \sum_k h[k]z[Mn - r_k]$ in eq. (32) is

$$Y_1(\omega) = M^{-1} \sum_{k,l} h[k]e^{(-j(\omega - 2\pi l)r_k/M)} Z\left(\frac{\omega - 2\pi l}{M}\right) \tag{34}$$

where, k ranges over $1, 2, \cdots, p$ and l ranges over $0, 1, \cdots, M - 1$. The Fourier transform of $y_2[n] = \sum_{k,m} g[k,m]z[Mn - r_k]z[Mn - r_m]$ in eq. (32) is given by

$$\begin{aligned}
Y_2(\omega) = M^{-1} &\sum_{k,m,l} g[k,m] \int_{-\pi}^{\pi} e^{(-j(\omega_1 r_k + ((\omega - 2\pi l)/M - \omega_1) r_m))} \\
&\times Z(\omega_1) Z\left(\frac{\omega - \omega_1 - 2l\pi}{M}\right) \mathrm{d}\omega_1
\end{aligned} \tag{35}$$

Let Ω be a discrete set of frequencies in $[-\pi, \pi]$ which are equispaced. For each integer, r, a column vector of size equal to the cardinality of Ω is defined by

$$\hat{e}(r) = (e^{(-j\omega r/M)})_{\omega \in \Omega} \tag{36}$$

Further the diagonal matrix is defined as

$$D_Z[\alpha] = M^{-1} \times \text{diag}\left[Z\left(\frac{\omega - \alpha}{M}\right), \omega \in \Omega\right] \tag{37}$$

Assume that the inter-frequency spacing of Ω is Δ. Then we have

$$\begin{aligned}
Y_1 =& (Y_1(\omega))_{\omega \in \Omega} \\
=& \sum_{k,l} h[k]e^{(j2\pi l r_k/M)} D_Z[2\pi l] D(r_k) \hat{e}(r_k)
\end{aligned} \tag{38}$$

where

$$D(r) = \text{diag}\left[e^{(-j\omega r/M)} : \omega \in \Omega\right] \tag{39}$$

$$Y_2 = (Y_2(\omega))_{\omega\in\Omega} = \Delta \times \sum_{k,m,l,\omega_1} g[k,m]e^{(-j\omega_1(r_k-r_m))} \times Z(\omega_1)e^{(j2\pi l r_m/M)}D_Z(\omega_1+2l\pi)\hat{e}(r_m) \quad (40)$$

Considering the vectors

$$Q[k,m|\mathbf{r}] = \Delta \times \sum_{l,\omega_1} e^{(-j\omega_1(r_k-r_m))} \times Z(\omega_1)e^{(j2\pi l r_m/M)}D_Z(\omega_1+2l\pi)\hat{e}(r_m) \quad (41)$$

and

$$P[k|\mathbf{r}] = \sum_l e^{(j2\pi l r_k/M)}D_Z(2\pi l)D(r_k)\hat{e}(r_k) \quad (42)$$

where

$$\mathbf{r} = (r_m)_{m=0}^p$$

Then,

$$Y_1 = \sum_k h[k]P[k|\mathbf{r}]$$
$$Y_2 = \sum_{k,m} g[k,m]Q[k,m|\mathbf{r}] \quad (43)$$

Further, in terms of the matrices

$$P[\mathbf{r}] = \mathrm{Col}[P[k|\mathbf{r}] : k = 1,2,\cdots,p]$$
$$Q[\mathbf{r}] = [Q[k,m|\mathbf{r}] : k,m = 1,2,\cdots,p] \quad (44)$$

Thus,

$$Y \approx Y_1 + Y_2 = P[\mathbf{r}]h + Q[\mathbf{r}]g \quad (45)$$

Here,

$$h = (h[k]) \in R^p, g = \mathrm{vec}(g[k,m]) \in R^{p^2} \quad (46)$$

$h, g, \mathbf{r}$ are estimated by minimizing

$$E[h,g,\mathbf{r}] = \| Y - P[\mathbf{r}]h - Q[\mathbf{r}]g \|^2 \quad (47)$$

Now, writing

$$\begin{pmatrix} h \\ g \end{pmatrix} = q \in R^{p^2+p} \quad (48)$$

and

$$[P[\mathbf{r}]|Q[\mathbf{r}]] = S[\mathbf{r}] \quad (49)$$

gives

$$E[q,\mathbf{r}] = \| Y - S[\mathbf{r}]q \|^2 \quad (50)$$

Eq. (50) has to be minimized w.r.t q, $\mathbf{r}$. Firstly, minimizing E w.r.t. q gives

$$\hat{q}(\mathbf{r}) = (S[\mathbf{r}]^{\mathrm{T}}S[\mathbf{r}])^{-1}S[\mathbf{r}]^{\mathrm{T}}Y \quad (51)$$

Substituting eq. (51) into the expression for E gives

$$E[\mathbf{r}] = E[\hat{q}(\mathbf{r}),\mathbf{r}] = \| Y \|^2 - \| P_{S[\mathbf{r}]}Y \|^2 \quad (52)$$

Minimizing this w.r.t. $\mathbf{r}$ is equivalent to maximizing

$$F(\mathbf{r}) = \| P_{S[\mathbf{r}]}Y \|^2 \quad (53)$$

w.r.t $\mathbf{r}$. Here, $P_{S[\mathbf{r}]}$ is the orthogonal projection onto $\mathcal{R}(S[\mathbf{r}])$:

$$P_{S[\mathbf{r}]} = S[\mathbf{r}](S[\mathbf{r}]^{\mathrm{T}}S[\mathbf{r}])^{-1}S[\mathbf{r}]^{\mathrm{T}} \quad (54)$$

The above result has been simulated using the MATLAB software and the results are illustrated in the next subsection.

TABLE I
CONTROL PARAMETERS FOR FILTER DESIGN.

Parameters	Symbol	RGA	PSO	CSA
Population Size	n_g, n_p, n_c	55	55	25
Max. Iteration Cycle	N	200	200	200
Tolerance		10^{-6}	10^{-6}	10^{-6}
Limits of System Coefficients		-10,+10	-10,+10	-10,+10
Selection	Tournament	Size: 4	-	-
Crossover Rate, Ratio	Heuristic	0.8, 1.2	-	-
Mutation rate	Adaptive feasible	0.01	-	-
Learning Parameters	C_1, C_2	-	2, 2	-
Particle Velocity	v_{min}, v_{max}	-	0.01, 1	-
Inertia Weight	W	-	0.4	-
Discovering Rate of alien eggs	P_a	-	-	0.25

B. Nonlinear System Modeling Examples

Extensive simulations have been conducted with two nonlinear system examples to evaluate the performance of the proposed method based on second order Volterra system using fractional delay. The unknown nonlinear system and a second order Volterra system are tested with five different input signals. The results obtained are presented in terms of the comparison between the actual system output and the estimated output using gradient search, RGA, PSO and CSA. Mean square error (MSE), accuracy and statistical data are investigated in order to demonstrate the effectiveness of the proposed nonlinear system modeling method. The fitness function is minimized such that the output of the estimated Volterra system closely approximates the actual nonlinear system output. The mean square error objective function is defined as

$$E = \frac{1}{M}\sum_{n=1}^{M}(\hat{y}[n] - y[n])^2 \quad (55)$$

where $\hat{y}[n]$ and $y[n]$ are the response of the actual nonlinear system and the second order Volterra system, respectively, M is the number of samples utilized to compute the fitness function. The two examples are expressed below.

1) Example 1: A standard nonlinear model is considered to carry out the simulations as utilized by Chang in [14]. This system is input with the discrete-time signal, $x[n]$ and the system output is given as

$$d[n] = \frac{0.3d^2[n-1] + 0.8x[n-1] + 0.6d[n-2]}{1 + x^2[n-1] + d^2[n-1]} \quad (56)$$

The eq. (56) is considered as the actual output which is approximated with the discrete-time output of the second-order Volterra system, $y[n]$ given in eq. (32). Table 1 summarizes the control parameters of the stochastic algorithms to perform the system identification task. Several simulation runs have been performed with different initial conditions in order to obtain an accurate approximation to the nonlinear system under consideration.

Computations are performed with the Volterra kernel size, $p = 5$ and with following five different discrete-time input signals, (i) sinusoidal signal, $x[n] = 0.8\sin(\frac{\pi}{9}n)$, (ii) noisy sinusoidal signal, $x[n] = 0.8\sin(\frac{\pi}{9}n) + w[n]$, (iii) square input, $x = 0.4 \times square(n)$, (iv) noisy square input, $x =$

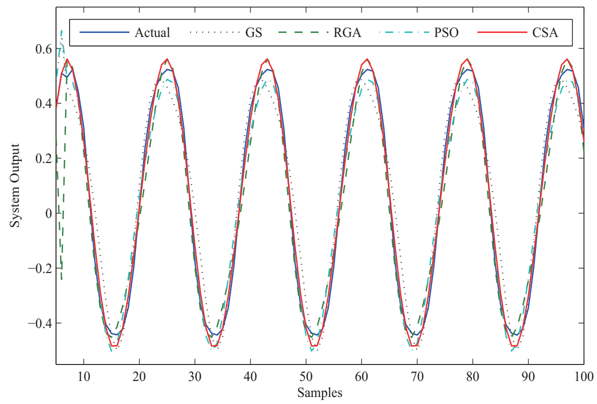

Fig. 3. Comparison of actual nonlinear system output with second order fractional delay Volterra system model output using gradient search, RGA, PSO and CSA for sinusoidal input signal $x(n) = 0.8\sin(\frac{\pi}{9}n)$ in example 1.

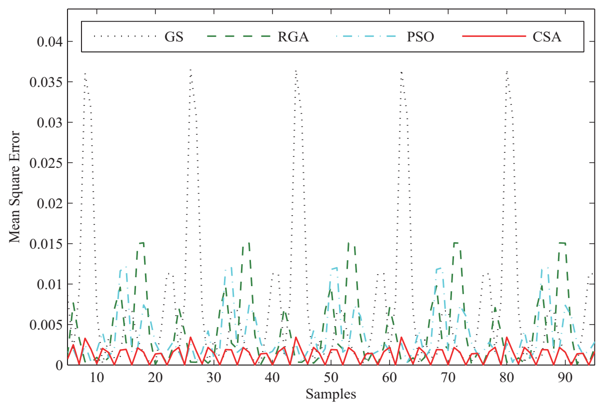

Fig. 4. Comparison of MSE for second order fractional delay Volterra system model output using gradient search, RGA, PSO and CSA for sinusoidal input signal $x(n) = 0.8\sin(\frac{\pi}{9}n)$ in example 1.

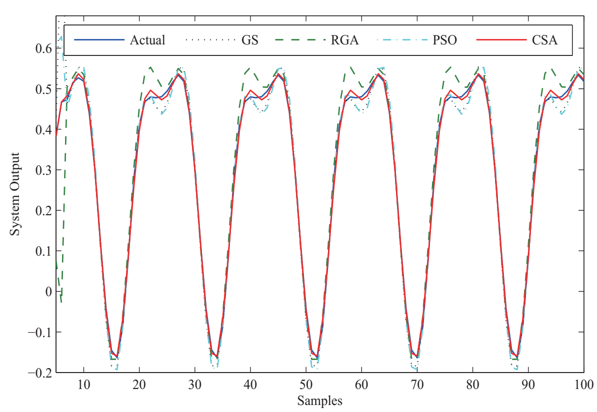

Fig. 5. Comparison of actual nonlinear system output with second order fractional delay Volterra system model output using gradient search, RGA, PSO and CSA for noisy sinusoidal input signal $x(n) = 0.8\sin(\frac{\pi}{9}n) + w(n)$ in example 1.

TABLE II
KERNEL PARAMETERS OF SECOND ORDER FRACTIONAL DELAY VOLTERRA SYSTEM MODEL USING GRADIENT SEARCH, RGA, PSO AND CSA BASED METHODS FOR SINUSOIDAL INPUT SIGNAL $x(n) = 0.8\sin(\frac{\pi}{9}n)$ FOR EXAMPLE 1.

Kernel Parameters	Gradient search	RGA	PSO	CSA
$h(0)$	4.7819	-2.6580	-0.2483	-1.1851
$h(1)$	6.9289	7.0705	0.9464	0.3521
$h(2)$	-1.6173	-6.4367	-0.6477	0.3159
$h(3)$	-7.6525	0.3392	-0.1653	-0.2498
$h(4)$	-0.4248	-3.5871	0.3371	-0.1913
$h(5)$	6.3502	5.5849	0.4426	0.6771
$g(0,0)$	-2.6945	10.0000	-0.2351	-0.2155
$g(0,1)$	-8.0000	-6.5660	0.5631	2.7324
$g(0,2)$	7.4322	0.3116	-1.4216	-0.1614
$g(0,3)$	1.7955	0.4281	0.3063	0.5090
$g(0,4)$	6.2381	-0.3697	-0.9874	-3.9133
$g(1,1)$	-6.6592	-6.8174	-0.3265	-1.5858
$g(1,2)$	-0.4924	9.3514	1.5749	0.5226
$g(1,3)$	-1.4650	-0.3788	0.1068	1.5532
$g(1,4)$	-4.5295	-4.4736	-1.0289	1.0851
$g(2,2)$	7.9095	-2.0326	1.0759	0.9137
$g(2,3)$	-7.3655	-2.9788	-1.0691	-0.5968
$g(2,4)$	-6.1501	-0.4481	0.3015	0.1160
$g(3,3)$	7.7976	9.8700	0.3764	-0.9234
$g(3,4)$	1.9988	-0.0004	1.2163	0.8949
$g(4,4)$	-7.6527	0.0220	-0.8601	1.0284

TABLE III
KERNEL PARAMETERS OF SECOND ORDER FRACTIONAL DELAY VOLTERRA SYSTEM MODEL USING GRADIENT SEARCH, RGA, PSO AND CSA BASED METHODS FOR NOISY SINUSOIDAL INPUT SIGNAL $x(n) = 0.8\sin(\frac{\pi}{9}n) + w(n)$ FOR EXAMPLE 1.

Kernel Parameters	Gradient search	RGA	PSO	CSA
$h(0)$	-0.0517	-0.2039	-0.0371	0.6549
$h(1)$	2.7845	-1.6059	0.7056	-2.6148
$h(2)$	-2.3396	1.3792	0.2225	0.2798
$h(3)$	0.0679	-0.7032	0.4377	2.8849
$h(4)$	1.2805	0.0966	-1.1508	1.5909
$h(5)$	0.3900	-1.0010	1.6167	-2.9161
$g(0,0)$	-1.3171	1.7034	0.6819	-0.4359
$g(0,1)$	-0.0356	0.8047	-0.4647	0.8494
$g(0,2)$	-0.2043	0.0536	-0.3457	1.9477
$g(0,3)$	-0.5186	2.8425	0.0924	-2.9480
$g(0,4)$	1.7869	0.1401	0.0518	1.6660
$g(1,1)$	0.3328	-0.9125	-0.8096	2.1944
$g(1,2)$	1.4369	-2.3005	-1.1969	-2.5532
$g(1,3)$	2.1203	-2.4689	-1.0682	0.9425
$g(1,4)$	-2.7382	-1.5798	1.9820	-0.9348
$g(2,2)$	-0.2732	1.5571	1.6017	-2.8826
$g(2,3)$	-3.4732	-0.8132	1.3062	0.1963
$g(2,4)$	-0.3665	2.1578	-2.5803	0.0648
$g(3,3)$	1.1350	0.7772	0.5590	0.7749
$g(3,4)$	0.8235	-1.1588	-1.3976	4.0653
$g(4,4)$	0.0337	1.9707	0.5623	-2.7554

$0.4\times square(n)+w[n]$ and (v) random input signal. The noise factor, $w[n]$ is taken to be 0.5. Fig. 3 shows the comparison of the actual system output by simulating eq. (56) with the sinusoidal input signal and the estimated signal using gradient-search, RGA, PSO and CSA. The mean square error between the actual and estimated system output with sinusoidal input signal is depicted in Fig. 4 for gradient-search, RGA, PSO and CSA. The Volterra system coefficients, $h(k)$ and $g(k,m)$ with kernel memory size, $p = 5$, optimized using aforementioned algorithms are listed in Table II. The mean value of MSE with

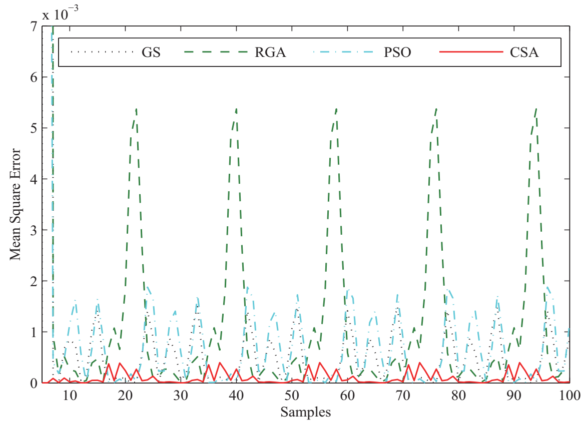

Fig. 6. Comparison of MSE for second order fractional delay Volterra system model output using gradient search, RGA, PSO and CSA for noisy sinusoidal input signal $x(n) = 0.8\sin(\frac{\pi}{9}n) + w(n)$ in example 1.

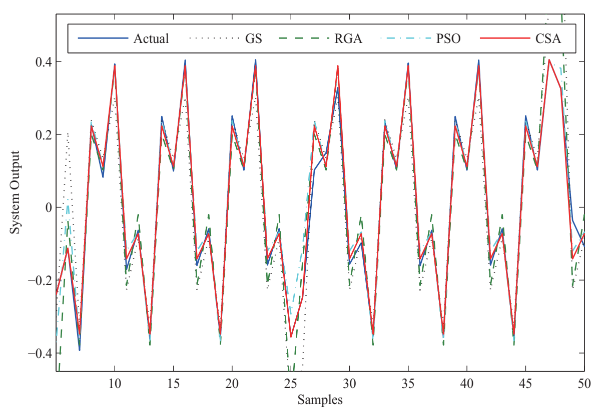

Fig. 7. Comparison of actual nonlinear system output with second order fractional delay Volterra system model output using gradient search, RGA, PSO and CSA for square input signal in example 1.

a sinusoidal signal using gradient-search, RGA, PSO and CSA is observed to be 0.0028, 0.0036, 0.0016, and 8.6450×10^{-4}, respectively. Based on the observations of MSE values and the graphical comparison in Figs. 3 and 4, it is inferred that CSA gives a better approximation to the nonlinear system coefficients. The performance of the employed methodologies is sequenced as, CSA $>$ PSO $>$ GS $>$ RGA. The comparison of output response of the system when tested with noisy sinusoidal signal is demonstrated in Fig. 5. The MSE obtained when the system is subjected to noisy sinusoidal signal using gradient-search, RGA, PSO and CSA is shown in Fig. 6. Table III indicates the kernel parameters of Volterra system with noisy sinusoidal input signal. The mean MSE values obtained are 0.0013, 0.0020, 9.5133×10^{-4} and 5.3905×10^{-4}, respectively, with gradient-search, RGA, PSO and CSA when the system is tested with noisy sinusoidal input signal. Thus, a better approximation to the nonlinear system coefficients is achieved with CSA and optimization techniques can be arranged according to the performance as, CSA $>$ PSO $>$ GS $>$ RGA.

TABLE IV
KERNEL PARAMETERS OF SECOND ORDER FRACTIONAL DELAY VOLTERRA SYSTEM MODEL USING GRADIENT SEARCH, RGA, PSO AND CSA BASED METHODS FOR SQUARE INPUT SIGNAL FOR EXAMPLE 1.

Kernel Parameters	Gradient search	RGA	PSO	CSA
$h(0)$	0.2427	-0.0773	-0.3601	-0.3919
$h(1)$	0.3044	0.2828	-0.0349	0.0153
$h(2)$	1.1082	0.7179	0.5309	0.5852
$h(3)$	-0.1549	-0.1826	-0.1097	-0.1126
$h(4)$	0.5619	0.6813	0.3180	0.3600
$h(5)$	0.4230	-0.0164	-0.1591	-0.1024
$g(0,0)$	0.1047	1.2752	0.1685	0.5475
$g(0,1)$	0.1606	0.4552	0.6614	0.6311
$g(0,2)$	0.2924	0.3694	-0.0932	-0.5869
$g(0,3)$	0.7192	0.1017	0.2101	0.4265
$g(0,4)$	1.1304	0.7404	0.6378	0.4574
$g(1,1)$	0.1574	-0.0658	0.7991	0.0763
$g(1,2)$	0.5883	0.5414	0.9405	0.5744
$g(1,3)$	-0.0925	0.5049	-0.0661	-0.0203
$g(1,4)$	0.3228	0.1119	0.0264	0.0726
$g(2,2)$	0.9729	-1.0543	0.6691	1.4622
$g(2,3)$	-0.4436	0.4137	0.5556	0.0912
$g(2,4)$	1.2680	0.3468	0.4035	-0.0375
$g(3,3)$	-0.5785	0.0981	0.1056	-0.1419
$g(3,4)$	0.2559	0.9561	0.6068	0.4822
$g(4,4)$	-0.4156	0.3841	0.3029	0.5164

TABLE V
KERNEL PARAMETERS OF SECOND ORDER FRACTIONAL DELAY VOLTERRA SYSTEM MODEL USING GRADIENT SEARCH, RGA, PSO AND CSA BASED METHODS FOR NOISY SQUARE INPUT SIGNAL FOR EXAMPLE 1.

Kernel Parameters	Gradient search	RGA	PSO	CSA
$h(0)$	0.5125	-0.1586	-0.0891	0.4181
$h(1)$	0.5834	-0.6495	0.4696	0.6257
$h(2)$	-0.4553	1.8403	-0.5114	-0.1225
$h(3)$	-0.9315	0.9366	-0.1402	-0.1988
$h(4)$	-0.4992	-0.5597	0.2433	-0.9789
$h(5)$	0.6559	-0.5733	0.0443	-0.1059
$g(0,0)$	-0.4693	0.4794	0.1119	-0.6883
$g(0,1)$	-0.6476	-0.4107	-0.1892	0.3784
$g(0,2)$	-0.7153	-0.0229	0.0493	-0.2357
$g(0,3)$	1.5708	1.0239	-0.4435	-0.0758
$g(0,4)$	-0.5353	0.7520	-0.5391	0.0521
$g(1,1)$	1.0706	-0.5719	0.9744	-2.6585×10^{-4}
$g(1,2)$	0.7109	-0.6802	-0.4078	0.6443
$g(1,3)$	-1.0828	-0.1425	-0.0566	-0.1139
$g(1,4)$	0.1929	0.0527	0.2139	-0.2014
$g(2,2)$	0.7066	-0.5288	0.4387	-0.2642
$g(2,3)$	0.9443	-0.3442	0.0375	0.3473
$g(2,4)$	-0.6769	0.0722	-0.3825	0.0691
$g(3,3)$	-0.3896	0.5909	0.2997	0.9077
$g(3,4)$	0.5375	0.6186	-0.3601	0.2017
$g(4,4)$	-0.5179	0.2909	0.4694	0.0131

Fig. 7 shows the comparison of the actual system output with square input signal and the estimated signal using gradient-search, RGA, PSO and CSA. Fig. 8 depicts the MSE observed when the system is tested with square input signal using gradient-search, RGA, PSO and CSA. The kernel parameters of Volterra system with squared input are reported in Table IV. The mean value of MSE noticed with gradient-search, RGA, PSO and CSA is 0.0042, 0.0026, 8.7709×10^{-4} and 5.4547×10^{-4}, respectively when squared signal is applied at the input of the system. From the graphical results and numerical values of MSE, one can conclude that CSA provides

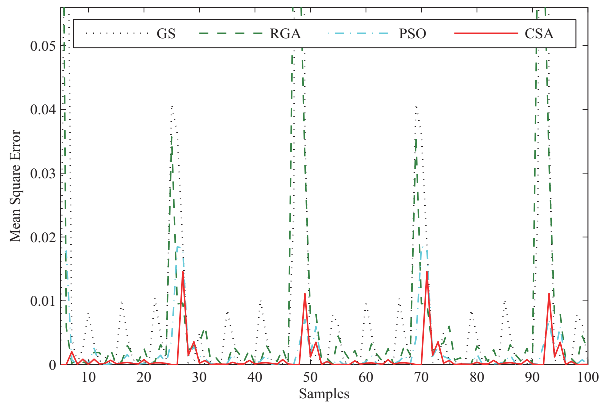

Fig. 8. Comparison of MSE for second order fractional delay Volterra system model output using gradient search, RGA, PSO and CSA for square input signal in example 1.

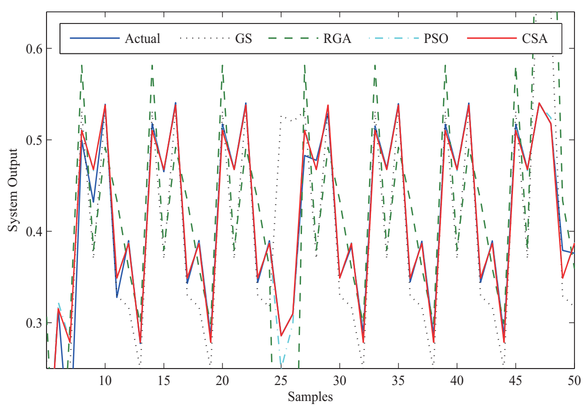

Fig. 9. Comparison of actual nonlinear system output with second order fractional delay Volterra system model output using gradient search, RGA, PSO and CSA for noisy square input signal in example 1.

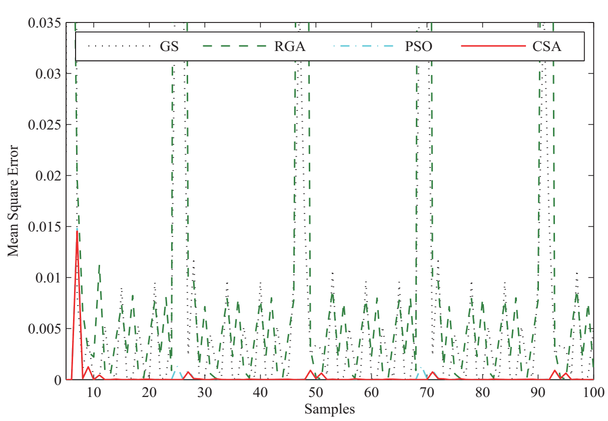

Fig. 10. Comparison of MSE for second order fractional delay Volterra system model output using gradient search, RGA, PSO and CSA for noisy square input signal in example 1.

a good approximation to the nonlinear fractional delay second order Volterra system coefficients compared to other applied

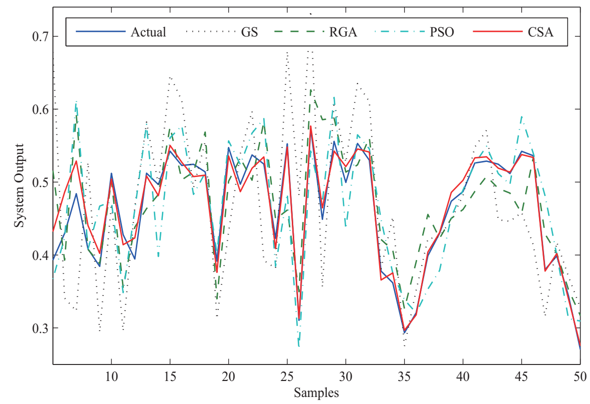

Fig. 11. Comparison of actual nonlinear system output with second order fractional delay Volterra system model output using gradient search, RGA, PSO and CSA for the random input signal in example 1.

TABLE VI
KERNEL PARAMETERS OF SECOND ORDER FRACTIONAL DELAY VOLTERRA SYSTEM MODEL USING GRADIENT SEARCH, RGA, PSO AND CSA BASED METHODS FOR RANDOM INPUT SIGNAL FOR EXAMPLE 1.

Kernel Parameters	Gradient search	RGA	PSO	CSA
$h(0)$	0.2872	0.3162	0.1696	0.2202
$h(1)$	0.0922	0.0613	0.3087	0.0095
$h(2)$	0.1827	0.5617	0.1116	0.5814
$h(3)$	-0.2102	-0.4402	0.0351	-0.0396
$h(4)$	0.0715	0.1864	0.4296	0.3219
$h(5)$	0.2372	0.0375	0.1394	0.0298
$g(0,0)$	0.0045	0.0853	-0.0468	0.0147
$g(0,1)$	0.0971	-0.1805	-6.4717×10^{-5}	-0.0171
$g(0,2)$	0.6207	0.0495	-0.3325	-0.0077
$g(0,3)$	0.0275	-0.2599	-0.2727	-0.0041
$g(0,4)$	-0.8997	0.0516	0.1541	-0.0085
$g(1,1)$	0.2362	-0.2754	-0.1177	-0.3871
$g(1,2)$	-0.4174	0.1923	0.2645	0.0192
$g(1,3)$	0.2129	-0.1189	-0.0345	-0.0073
$g(1,4)$	-0.1775	-0.0659	0.1635	0.0210
$g(2,2)$	-0.1632	0.0866	-0.0579	0.0247
$g(2,3)$	-0.1397	0.0479	0.1556	-0.0484
$g(2,4)$	0.7185	0.3258	-0.1632	0.0172
$g(3,3)$	-0.2123	0.2361	-0.0389	-0.1671
$g(3,4)$	0.3809	-0.2795	-0.3564	-0.0522
$g(4,4)$	-0.2813	-0.0921	-0.0363	-0.0268

optimization algorithms. The performance of these algorithms is arranged as, CSA $>$ PSO $>$ GS $>$ RGA. Fig. 9 exhibits the comparison of output response of the system analyzed with noisy square input using gradient-search, RGA, PSO and CSA. The MSE remarked for the system under consideration when examined with noisy square input is shown in Fig. 10. Table V summarizes the kernel parameters of Volterra system with noisy square input signal. The MSE values for second order fractional delay Volterra system with gradient-search, RGA, PSO and CSA are 0.0033, 0.0057, 6.0527×10^{-4} and 5.9464×10^{-4}, respectively. Based on these MSE values, it can be finally deduced that nonlinear system identification with the second order Volterra system using CSA surpasses the other employed optimization methods. The performance can be ranked as CSA $>$ PSO $>$ RGA $>$ GS. The comparison of output response of the system with random signal using

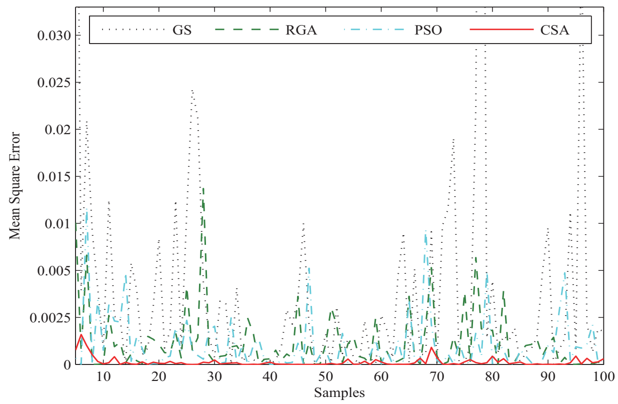

Fig. 12. Comparison of MSE for second order fractional delay Volterra system model output using gradient search, RGA, PSO and CSA for the random input signal in example 1.

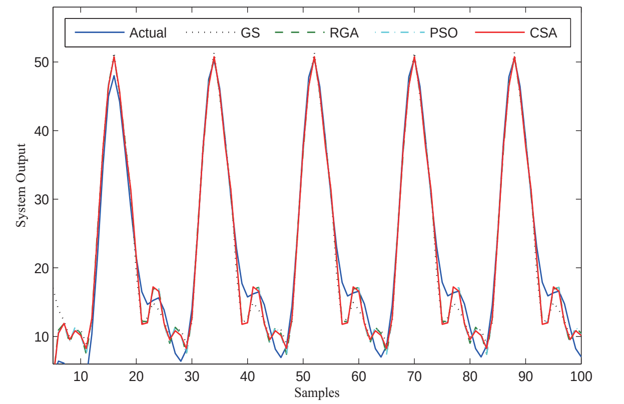

Fig. 13. Comparison of actual nonlinear system output with second order fractional delay Volterra system model output using gradient search, RGA, PSO and CSA for sinusoidal input signal $x(n) = 0.8\sin(\frac{\pi}{9}n)$ in example 2.

gradient-search, RGA, PSO and CSA is demonstrated in Fig. 11. The observed values of MSE and kernel parameters of Volterra system with random signal are exhibited in Fig. 12 and Table VI, respectively. The mean MSE values obtained are 0.0027, 8.5199×10^{-4}, 7.7135×10^{-4} and 1.9658×10^{-4}, respectively, with gradient-search, RGA, PSO and CSA when the system is tested with random signal. It can be concluded from the aforementioned results that the CSA based nonlinear system identification outperforms all other reported algorithms in terms of MSE. The order of the algorithm based on its performance is given as CSA > PSO > RGA > GS.

Furthermore, the statistical analysis in terms of maximum, minimum, mean, variance and standard deviation of the MSE is performed to evaluate the performance of the proposed method. Table VII shows the comparative numerical values of different characteristics like maximum, minimum, mean, variance and standard deviation of mean square error of the proposed second order fractional delay Volterra system for different input signals using gradient-search, RGA, PSO and CSA algorithms. This analysis provides a detailed comparison amongst the performance of estimated Volterra systems employing all four optimization techniques. It is observed that the MSE value obtained with CSA is lower as compared to other algorithms with all input signals. From Figs. 3-12 and statistically analyzed results from Table VII, it is evident that with all input signals, the proposed nonlinear system modeling method based on fractional delay second order Volterra system produced minimum MSE compared to that of the gradient-search, RGA and PSO. Finally, it can be concluded that CSA based second order fractional delay Volterra system identification method gives superior results compared to other reported algorithms with all the input signals.

2) Example 2: In this example, the mathematical model of heat exchanger used in [14] is considered. The system can be expressed as

$$w[n] = x[n] - 1.3228x^2[n] + 0.7671x^3[n] - 2.1755x^4[n] \quad (57)$$

$$d[n] = 1.608d[n-1] - 0.6385d[n-2] - 6.5306w[n-1] + 5.5652w[n-2] \quad (58)$$

where $x[n]$ be the input to the system, $w[n]$ is the static nonlinearity and $d[n]$ be the output of the system.

In order to evaluate the performance of this system Volterra kernel size is selected as $p = 5$ and the input to the system is tested with five different input signals. Fig. 13 shows the comparison of actual output and the estimated output using gradient-search, RGA, PSO and CSA, when the sinusoidal input signal is applied. The Volterra system coefficients obtained with sinusoidal input using gradient-search, RGA, PSO and CSA are listed in Table VIII. The MSE error noticed with sinusoidal input is exhibited in Fig. 14. The mean MSE values obtained are 0.0220, 0.0155, 0.0154 and 0.0151, respectively, with gradient-search, RGA, PSO and CSA, when the system

TABLE VIII
KERNEL PARAMETERS OF SECOND ORDER FRACTIONAL DELAY VOLTERRA SYSTEM MODEL USING GRADIENT SEARCH, RGA, PSO AND CSA BASED METHODS FOR SINUSOIDAL INPUT SIGNAL $x(n) = 0.8\sin(\frac{\pi}{9}n)$ FOR EXAMPLE 2.

Kernel Parameters	Gradient search	RGA	PSO	CSA
$h(0)$	9.4709	16.2089	16.6626	14.4537
$h(1)$	-0.6698	25.5888	25.1569	19.6381
$h(2)$	-19.3316	11.4107	13.3984	15.6001
$h(3)$	8.6093	-11.0001	-11.9957	-14.5285
$h(4)$	-5.0777	43.6126	44.6720	42.9363
$h(5)$	-4.6264	13.3334	14.0811	11.2961
$g(0,0)$	-9.7089	5.2952	4.6671	1.2645
$g(0,1)$	15.3888	7.2002	7.6748	8.8481
$g(0,2)$	4.2497	-0.2573	4.3471	0.6401
$g(0,3)$	9.2702	-6.0859	-6.9853	-10.2706
$g(0,4)$	4.8762	-6.8910	-10.3297	-10.0909
$g(1,1)$	-3.8765	-0.6058	-2.8362	4.3473
$g(1,2)$	-16.4299	0.7216	-0.0073	-2.2931
$g(1,3)$	-17.3760	-3.6154	-1.2420	-6.1239
$g(1,4)$	-0.6727	-46.8916	-47.5947	-47.6447
$g(2,2)$	-0.4807	16.0521	15.5387	15.1564
$g(2,3)$	35.0206	28.9075	29.4013	31.9329
$g(2,4)$	-2.0420	-19.8110	-20.3997	-18.8809
$g(3,3)$	-10.0147	27.3951	28.3579	30.8179
$g(3,4)$	-15.3354	-17.4811	-17.5201	-22.3759
$g(4,4)$	11.2373	19.7659	19.8043	19.8045

TABLE VII
STATISTICAL COMPARISON OF MEAN SQUARE ERROR FOR THE IDENTIFICATION OF NONLINEAR SYSTEM WITH DIFFERENT INPUT SIGNAL USING GRADIENT SEARCH, RGA, PSO AND CSA BASED METHODS FOR EXAMPLE 1.

Input Signal	Algorithm	Mean Square Error (MSE)				
		Max	Min	Mean	Variance	Standard Deviation
$x(n) = 0.8\sin(\frac{\pi}{9}n)$	GS	0.0446	4.8916×10^{-5}	0.0028	2.8003×10^{-5}	0.0053
	RGA	0.1788	8.6341×10^{-6}	0.0036	3.4486×10^{-4}	0.0186
	PSO	0.0446	2.0815×10^{-5}	0.0016	2.1110×10^{-5}	0.0046
	CSA	0.0446	1.3196×10^{-9}	8.6450×10^{-4}	2.0281×10^{-5}	0.0045
$x(n) = 0.8\sin(\frac{\pi}{9}n) + w(n)$	GS	0.0623	5.0772×10^{-7}	0.0013	6.4219×10^{-5}	0.0080
	RGA	0.0787	2.4005×10^{-6}	0.0020	9.5760×10^{-5}	0.0098
	PSO	0.0494	1.9535×10^{-8}	9.5133×10^{-4}	2.7945×10^{-5}	0.0053
	CSA	0.0494	2.1471×10^{-11}	5.3905×10^{-4}	2.5107×10^{-5}	0.0050
$x(n) = 0.4\text{square}(n)$	GS	0.0945	1.3653×10^{-7}	0.0042	1.9755×10^{-4}	0.0141
	RGA	0.0409	1.2848×10^{-9}	0.0026	4.2058×10^{-5}	0.0065
	PSO	0.0242	6.8875×10^{-7}	8.7709×10^{-4}	7.6877×10^{-6}	0.0028
	CSA	0.0242	1.0647×10^{-16}	5.4547×10^{-4}	6.5939×10^{-6}	0.0026
$x(n) = 0.4\text{square}(n) + w(n)$	GS	0.0836	9.3438×10^{-7}	0.0033	1.0524×10^{-4}	0.0103
	RGA	0.0615	7.7230×10^{-6}	0.0057	1.7510×10^{-4}	0.0132
	PSO	0.0504	2.4164×10^{-8}	6.0527×10^{-4}	2.6298×10^{-5}	0.0051
	CSA	0.0504	5.7384×10^{-13}	5.9464×10^{-4}	2.6299×10^{-5}	0.0051
$x(n) = \text{rand}(n)$	GS	0.0341	4.6628×10^{-10}	0.0027	2.3409×10^{-5}	0.0048
	RGA	0.0110	1.1880×10^{-7}	8.5199×10^{-4}	2.2017×10^{-6}	0.0015
	PSO	0.0110	2.9739×10^{-9}	7.7135×10^{-4}	2.0691×10^{-6}	0.0014
	CSA	0.0110	3.9740×10^{-8}	1.9658×10^{-4}	1.2529×10^{-6}	0.0011

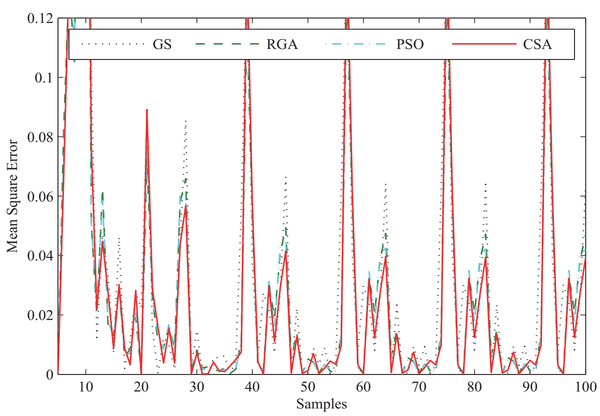

Fig. 14. Comparison of MSE for second order fractional delay Volterra system model output using gradient search, RGA, PSO and CSA for sinusoidal input signal $x(n) = 0.8\sin(\frac{\pi}{9}n)$ in example 2.

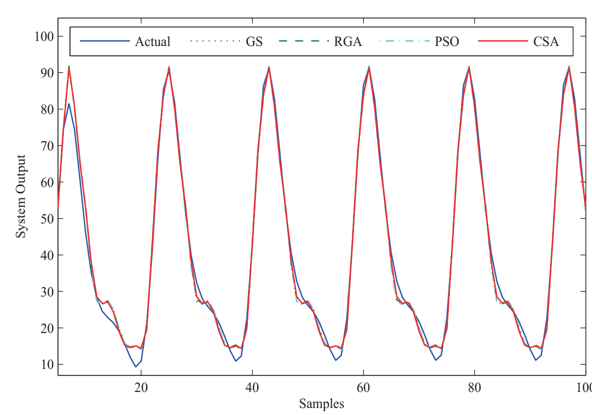

Fig. 15. Comparison of actual nonlinear system output with second order fractional delay Volterra system model output using gradient search, RGA, PSO and CSA for noisy sinusoidal input signal $x(n) = 0.8\sin(\frac{\pi}{9}n) + w(n)$ in example 2.

is tested with sinusoidal input. Based on the observations of MSE values and the graphical comparison in Figs. 13 and 14, it is inferred that CSA gives a better approximation to the nonlinear system coefficients. The performance of the employed methodologies is sequenced as, CSA $>$ PSO $>$ RGA $>$ GS.

The comparison of output response of the system when tested with noisy sinusoidal signal is demonstrated in Fig. 15. The MSE obtained when the system is subjected to noisy sinusoidal signal using gradient-search, RGA, PSO and CSA is shown in Fig. 16. Table IX lists the kernel parameters of Volterra system with noisy sinusoidal input signal. The mean value of MSE with noisy sinusoidal signal using gradient-search, RGA, PSO and CSA is observed to be 0.0154, 0.0158, 0.0154, and 0.0137, respectively. Thus, a better approximation to the nonlinear system coefficients is achieved with CSA and optimization techniques can be arranged according to the performance as, CSA $>$ PSO $=$ GS $>$ RGA.

The kernel parameters of Volterra system with squared input are reported in Table X. Fig. 17 shows the comparison of the actual system output with square input signal and the

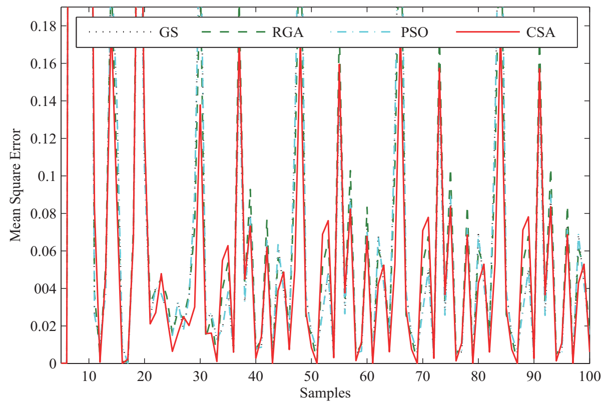

Fig. 16. Comparison of MSE for second order fractional delay Volterra system model output using gradient search, RGA, PSO and CSA for noisy sinusoidal input signal $x(n) = 0.8\sin(\frac{\pi}{9}n) + w(n)$ in example 2.

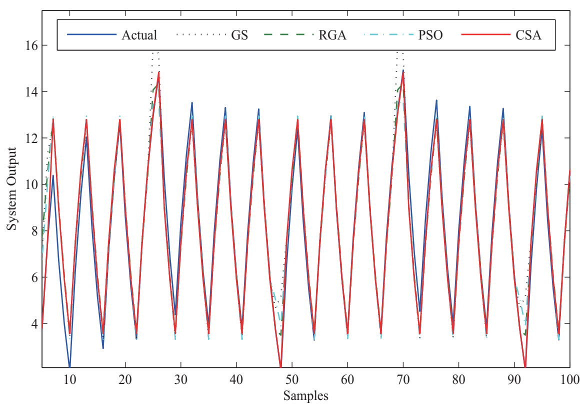

Fig. 17. Comparison of actual nonlinear system output with second order fractional delay Volterra system model output using gradient search, RGA, PSO and CSA for square input signal in example 2.

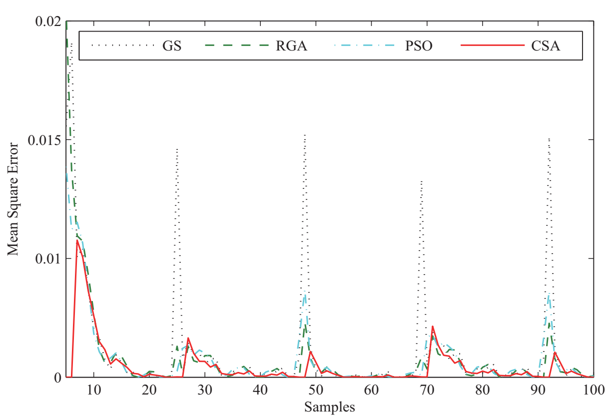

Fig. 18. Comparison of MSE for second order fractional delay Volterra system model output using gradient search, RGA, PSO and CSA for square input signal in example 2.

estimated signal using gradient-search, RGA, PSO and CSA.

TABLE IX
KERNEL PARAMETERS OF SECOND ORDER FRACTIONAL DELAY VOLTERRA SYSTEM MODEL USING GRADIENT SEARCH, RGA, PSO AND CSA BASED METHODS FOR NOISY SINUSOIDAL INPUT SIGNAL $x(n) = 0.8\sin(\frac{\pi}{9}n) + w(n)$ FOR EXAMPLE 2.

Kernel Parameters	Gradient search	RGA	PSO	CSA
$h(0)$	19.7175	19.9878	19.7175	19.6256
$h(1)$	2.5659	2.0529	2.5659	3.4482
$h(2)$	-24.1582	-23.6178	-24.1582	-26.4619
$h(3)$	-2.0403	-0.4954	-2.0403	-0.3887
$h(4)$	19.9393	20.0624	19.9393	23.4229
$h(5)$	-7.6989	-7.4160	-7.6989	-10.5589
$g(0,0)$	-7.0703	-7.2762	-7.0703	-6.6456
$g(0,1)$	11.4793	12.0153	11.4793	10.4377
$g(0,2)$	1.4172	2.3618	1.4172	1.6714
$g(0,3)$	-1.8849	-0.4439	-1.8849	-0.8707
$g(0,4)$	1.5957	0.1224	1.5957	0.9816
$g(1,1)$	-3.3497	-4.2333	-3.3497	-3.1366
$g(1,2)$	-5.7131	-6.3393	-5.7131	-5.6986
$g(1,3)$	0.4449	-1.0819	0.4449	1.1859
$g(1,4)$	4.8335	6.2813	4.8335	4.3979
$g(2,2)$	-2.1866	-1.1669	-2.1866	-1.8611
$g(2,3)$	6.8904	7.1536	6.8904	4.9551
$g(2,4)$	-1.2842	-1.4654	-1.2842	-1.7116
$g(3,3)$	2.6831	2.7344	2.6831	3.8625
$g(3,4)$	-10.9289	-11.3184	-10.9289	-9.3152
$g(4,4)$	7.6593	7.9471	7.6593	6.4721

TABLE X
KERNEL PARAMETERS OF SECOND ORDER FRACTIONAL DELAY VOLTERRA SYSTEM MODEL USING GRADIENT SEARCH, RGA, PSO AND CSA BASED METHODS FOR SQUARE INPUT SIGNAL FOR EXAMPLE 2.

Kernel Parameters	Gradient search	RGA	PSO	CSA
$h(0)$	5.3951	3.8427	5.2620	-1.4383
$h(1)$	6.6501	1.0145	1.2080	1.8399
$h(2)$	4.5466	-2.4147	-2.3915	-3.0599
$h(3)$	4.7278	0.5306	-1.4995	-0.6803
$h(4)$	5.1116	-0.8780	1.8397	5.3169
$h(5)$	7.1848	-1.2398	1.5111	6.1945
$g(0,0)$	3.4676	1.8247	-0.8796	3.7098
$g(0,1)$	8.5345	1.1147	2.1813	0.6935
$g(0,2)$	4.6133	2.4419	0.5851	-0.5799
$g(0,3)$	0.9336	-1.4757	0.4633	-0.0428
$g(0,4)$	8.2602	0.3734	0.4705	-0.4795
$g(1,1)$	6.7420	3.0117	0.9524	5.2397
$g(1,2)$	3.4231	0.6770	1.5778	4.5719
$g(1,3)$	5.9950	2.9727	0.6525	1.9149
$g(1,4)$	4.2657	-0.8576	1.3171	-5.3846
$g(2,2)$	6.8185	4.0588	1.4162	1.2048
$g(2,3)$	2.3524	3.0529	3.6863	7.1106
$g(2,4)$	6.0669	0.1657	-1.3885	-3.1878
$g(3,3)$	10.1462	0.9998	4.1036	5.8609
$g(3,4)$	3.8599	2.8173	2.1098	8.6596
$g(4,4)$	3.4468	-1.8829	1.6816	15.5536

Fig. 18 depicts the MSE observed when the system is tested with square input signal. The mean value of MSE noticed with gradient-search, RGA, PSO and CSA is 0.0023, 0.0016, 0.0016 and 8.9512×10^{-4}, respectively when squared signal is applied at the input of the system. From the graphical results and numerical values of MSE, one can conclude that CSA provides a good approximation to the nonlinear fractional delay second order Volterra system coefficients compared to other applied optimization algorithms. The performance of these algorithms is arranged as, CSA $>$ PSO $=$ RGA $>$ GS.

Table XI summarizes the kernel parameters of Volterra

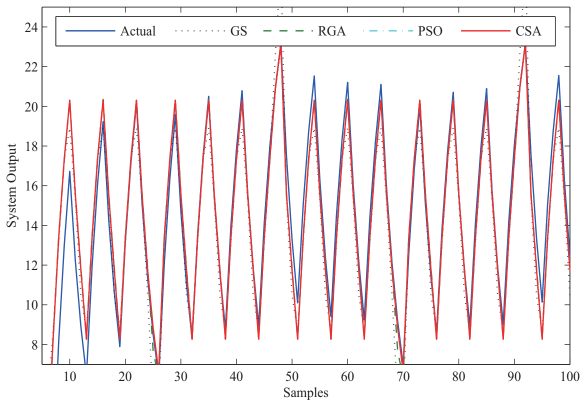

Fig. 19. Comparison of actual nonlinear system output with second order fractional delay Volterra system model output using gradient search, RGA, PSO and CSA for noisy square input signal in example 2.

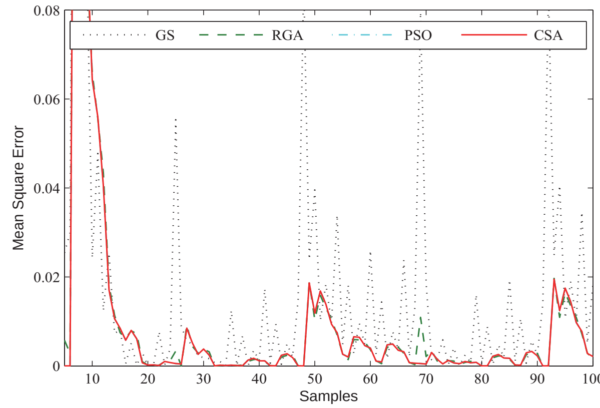

Fig. 20. Comparison of MSE for second order fractional delay Volterra system model output using gradient search, RGA, PSO and CSA for noisy square input signal in example 2.

TABLE XI
KERNEL PARAMETERS OF SECOND ORDER FRACTIONAL DELAY VOLTERRA SYSTEM MODEL USING GRADIENT SEARCH, RGA, PSO AND CSA BASED METHODS FOR NOISY SQUARE INPUT SIGNAL FOR EXAMPLE 2.

Kernel Parameters	Gradient search	RGA	PSO	CSA
$h(0)$	2.0734	2.0628	6.1067	3.5476
$h(1)$	1.2933	-0.4618	4.7040	-0.7788
$h(2)$	1.3408	1.0626	2.0808	-2.4513
$h(3)$	3.3256	-0.0636	2.7889	0.0166
$h(4)$	0.0297	0.2113	6.8997	0.8947
$h(5)$	1.8156	1.5619	4.4455	-1.2868
$g(0,0)$	3.4476	2.6711	3.7141	1.8125
$g(0,1)$	4.0397	-0.8521	3.0184	0.1079
$g(0,2)$	-1.3687	-1.2592	1.6243	-0.4851
$g(0,3)$	-1.3194	-0.4355	-2.9203	-1.7564
$g(0,4)$	1.1708	-2.5746	0.7713	-3.0847
$g(1,1)$	5.1978	8.6357	5.4871	3.6384
$g(1,2)$	5.3892	1.6294	3.9281	2.8376
$g(1,3)$	0.0668	-1.2428	3.6944	1.6550
$g(1,4)$	1.6461	-0.8980	-3.9143	-3.6949
$g(2,2)$	3.4492	3.1523	1.0847	1.3733
$g(2,3)$	3.5700	4.9677	6.3690	3.5562
$g(2,4)$	0.9387	-4.7134	-0.9484	-1.3355
$g(3,3)$	2.6421	0.4263	3.3774	0.7597
$g(3,4)$	2.3118	3.6257	6.6161	2.9279
$g(4,4)$	4.4797	6.1514	5.4867	3.3231

TABLE XII
KERNEL PARAMETERS OF SECOND ORDER FRACTIONAL DELAY VOLTERRA SYSTEM MODEL USING GRADIENT SEARCH, RGA, PSO AND CSA BASED METHODS FOR RANDOM INPUT SIGNAL FOR EXAMPLE 2.

Kernel Parameters	Gradient search	RGA	PSO	CSA
$h(0)$	1.0418	1.1669	1.1405	1.1775
$h(1)$	0.2133	-0.5722	0.1031	-0.2277
$h(2)$	-7.4315	-7.5149	-6.8923	-7.5111
$h(3)$	-4.4032	-4.4664	-4.3393	-4.4983
$h(4)$	-2.5474	-2.5632	-2.9064	-2.7099
$h(5)$	-0.0057	-0.6688	-1.5127	-1.3608
$g(0,0)$	-0.0514	-1.1548	-0.3505	-0.6698
$g(0,1)$	-0.1563	0.5335	-0.2269	-0.3422
$g(0,2)$	2.6338	2.7008	2.5176	2.5249
$g(0,3)$	0.7263	1.2250	0.8140	0.8262
$g(0,4)$	2.1507	1.7291	1.6591	1.5885
$g(1,1)$	-1.5875	-1.5097	-0.7013	-1.4393
$g(1,2)$	0.6341	-0.3207	-0.3789	-0.3649
$g(1,3)$	1.7894	1.6511	1.4016	1.3383
$g(1,4)$	2.2614	1.6739	0.8213	1.2354
$g(2,2)$	0.1802	0.2774	0.3187	0.1962
$g(2,3)$	-0.7735	-1.1470	-0.6745	-0.8926
$g(2,4)$	1.4143	1.2553	1.4124	1.2015
$g(3,3)$	0.9802	1.0123	0.5143	0.8377
$g(3,4)$	-0.7264	-0.3468	-0.1677	-0.7615
$g(4,4)$	2.6381	1.9273	0.9942	1.2558

system with noisy square input signal. The comparison of output response of the system analyzed with noisy square input using gradient-search, RGA, PSO and CSA is demonstrated in Fig. 19. The MSE remarked for the system under consideration when examined with noisy square input is shown in Fig. 20. The MSE values for second order fractional delay Volterra system with gradient-search, RGA, PSO and CSA are 0.0068, 0.0040, 0.0039 and 0.0039, respectively. Based on these MSE values, it can be finally deduced that nonlinear system identification with the second order Volterra system using CSA surpass the other employed optimization methods. The performance can be ranked as CSA $=$ PSO $>$ RGA $>$ GS. The comparison of output response of the system with random signal using gradient-search, RGA, PSO and CSA is depicted in Fig. 21. The noted values of MSE with random signal is exhibited in Fig. 22 and Table XII lists the kernel parameters of Volterra system with random input. The mean MSE values obtained are 0.0023, 0.0023, 0.0023 and 0.0022, respectively. It can be concluded from the aforementioned results that the CSA based nonlinear system identification outperforms all other reported algorithm in terms of MSE. The order of the algorithm based on its performance is given as CSA $>$ PSO $=$ RGA $=$ GS. Table XII shows the comparative numerical values of different characteristics like maximum, minimum, mean, variance and standard deviation of mean square error of proposed second order Volterra system using fractional delay for five different input signals using gradient-search, RGA, PSO and CSA algorithms. It is observed that the MSE value observed with CSA is lower as compared to other algorithms with all input signals. From Figs. 13-22 and statistically analyzed results from Table XIII, it is evident that

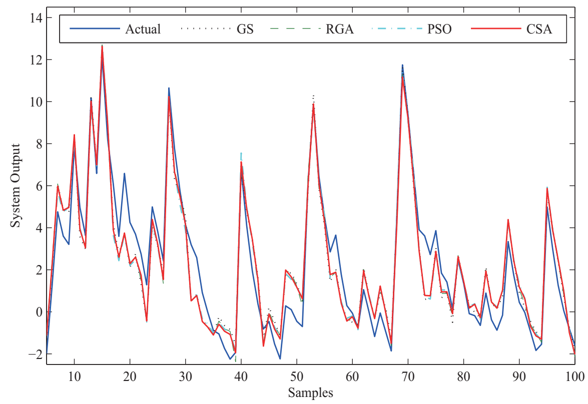

Fig. 21. Comparison of actual nonlinear system output with second order fractional delay Volterra system model output using gradient search, RGA, PSO and CSA for random input signal in example 2.

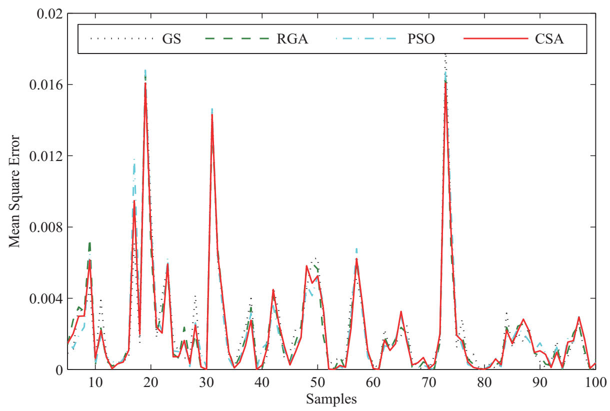

Fig. 22. Comparison of MSE for second order fractional delay Volterra system model output using gradient search, RGA, PSO and CSA for the random input signal in example 2.

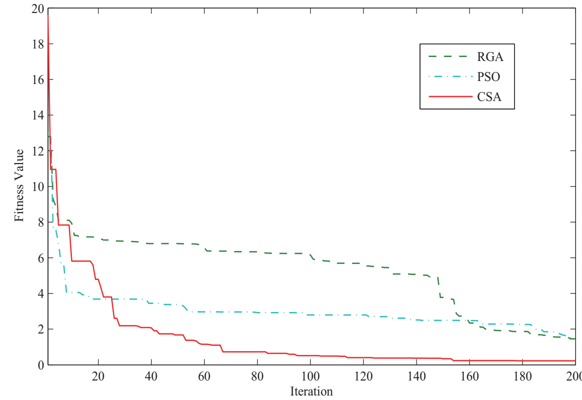

Fig. 23. Convergence profile for RGA, PSO and CSA for nonlinear system identification using second order fractional delay Volterra system model in example 1.

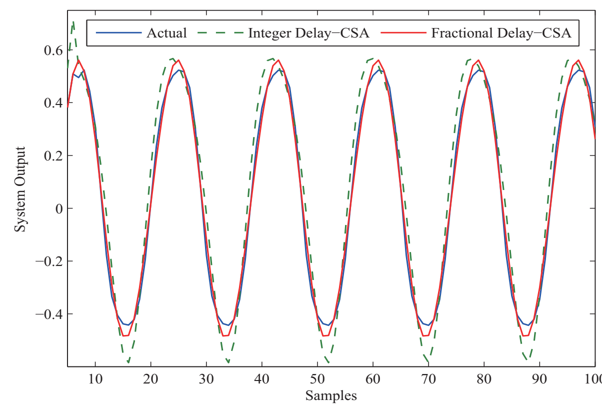

Fig. 24. Comparison of third order integer delay Volterra system output with second order fractional delay Volterra system model output using CSA for sinusoidal input signal in example 1.

with all input signals, the proposed nonlinear system modeling method based on fractional delay second order Volterra system produced minimum MSE compared to that of the gradient-search, RGA and PSO. Finally, it can be concluded that CSA based second order fractional delay Volterra system identification method gives superior results compared to other reported algorithms with all the input signals. In order to demonstrate the effectiveness of the proposed method in terms of convergence rate, Fig. 23 shows the convergence of MSE obtained, for example 1 tested with sinusoidal input. Similar plots have also been obtained for the example 1 and 2 with different input signals which are not shown here.

C. Comparative Analysis

1) Comparison with a Third Order Integer Delay Volterra System: The superiority of the proposed Volterra system identification method is demonstrated by comparing the results with a nonlinear Volterra system using an integer delay. Fig. 24 shows the comparison of approximated output of proposed second order fractional delay Volterra system in example 1, eq. (56) with the output of a third order integer delay Volterra system when both the systems are subjected to the sinusoidal input signal. From the visual analysis of Fig. 24, it can be inferred that a better approximation of the nonlinear unknown system is achieved using the proposed second order fractional delay Volterra system to its integer counterpart of third order. The mean values of MSE for integer and fractional delay system are obtained to be 3.2914×10^{-3} and 8.6450×10^{-4}. Thus, the introduction of fractional delay in the Volterra system identification technique leads to a better approximation with the involvement of less number of multipliers (due to order reduction) and low energy consumption in comparison to the integer delay systems. Similar graphical results are obtained for example 1 and example 2 with different input signals, which are not reported here.

2) Comparison with the Existing Techniques: The comparison of the proposed second order fractional delay Volterra system with the other reported nonlinear system modeling method has been presented in Table XIV. The observations are made on the MSE values of the existing methodologies

TABLE XIII
STATISTICAL COMPARISON OF MEAN SQUARE ERROR FOR THE IDENTIFICATION OF NONLINEAR SYSTEM WITH DIFFERENT INPUT SIGNAL USING GRADIENT SEARCH, RGA, PSO AND CSA BASED METHODS FOR EXAMPLE 2.

Input Signal	Algorithm	Mean Square Error (MSE)				
		Max	Min	Mean	Variance	Standard Deviation
$x(n) = 0.8\sin(\frac{\pi}{9}n)$	GS	0.3326	2.9491×10^{-6}	0.0220	0.0020	0.0443
	RGA	0.1787	6.3511×10^{-5}	0.0155	7.7422×10^{-4}	0.0278
	PSO	0.1815	5.0935×10^{-5}	0.0154	7.7765×10^{-4}	0.0279
	CSA	0.1605	2.0301×10^{-8}	0.0151	7.4953×10^{-4}	0.0274
$x(n) = 0.8\sin(\frac{\pi}{9}n) + w(n)$	GS	0.2117	1.3487×10^{-5}	0.0154	7.4549×10^{-4}	0.0273
	RGA	0.2129	8.0414×10^{-7}	0.0158	7.4020×10^{-4}	0.0272
	PSO	0.2117	1.3487×10^{-5}	0.0154	7.4549×10^{-4}	0.0273
	CSA	0.1947	5.4686×10^{-8}	0.0137	6.0762×10^{-4}	0.0246
$x(n) = 0.4\text{square}(n)$	GS	0.0282	6.2620×10^{-7}	0.0023	2.7538×10^{-5}	0.0052
	RGA	0.0311	3.3186×10^{-8}	0.0016	1.6176×10^{-5}	0.0040
	PSO	0.0177	2.5478×10^{-7}	0.0016	8.8820×10^{-6}	0.0030
	CSA	0.0115	4.8790×10^{-14}	8.9512×10^{-4}	3.4831×10^{-6}	0.0019
$x(n) = 0.4\text{square}(n) + w(n)$	GS	0.0975	5.2938×10^{-6}	0.0068	1.6614×10^{-4}	0.0129
	RGA	0.0880	1.8202×10^{-9}	0.0040	1.3367×10^{-4}	0.0116
	PSO	0.0865	1.0412×10^{-14}	0.0039	1.3078×10^{-4}	0.0114
	CSA	0.0865	3.7582×10^{-11}	0.0039	1.3078×10^{-4}	0.0114
$x(n) = \text{rand}(n)$	GS	0.0184	2.3431×10^{-6}	0.0023	1.0509×10^{-5}	0.0032
	RGA	0.0166	6.7229×10^{-7}	0.0023	9.7658×10^{-6}	0.0031
	PSO	0.0168	7.0138×10^{-8}	0.0023	1.0681×10^{-5}	0.0033
	CSA	0.0161	1.5406×10^{-9}	0.0022	9.6443×10^{-6}	0.0031

TABLE XIV
COMPARISON OF THE PROPOSED FRACTIONAL DELAY BASED NONLINEAR SYSTEM IDENTIFICATION WITH OTHER REPORTED METHODS.

Method	Example	Algorithm	Input signal	Memory size (p)	MSE
Rashedi et al. [22]	Example 1	GSA	White noise sequence $x(k)$ + noise $\eta(k) \in [-0.001, 0.001]$	-	3.91×10^{-7}
		GSA	White noise sequence $x(k)$ + noise $\eta(k) \in [-0.01, 0.01]$	-	4.23×10^{-5}
Chang [14]	Example 1	IPSO	$x(n) = 0.8\cos(\frac{\pi}{9}n)$	5	0.00929002
		IPSO	$x(n) = 0.8\cos(\frac{\pi}{9}n)$	8	0.00491307
		IPSO	$x(n) = rand(n)$	5	0.00556229
		IPSO	$x(n) = rand(n)$	8	0.00260959
Present Study	Example 1	CSA	$x(n) = 0.8\sin(\frac{\pi}{9}n)$	5	8.6450×10^{-4}
		CSA	$x(n) = 0.8\sin(\frac{\pi}{9}n) + w(n)$	5	5.3905×10^{-4}
		CSA	$x(n) = 0.4\text{square}(n)$	5	5.4547×10^{-4}
		CSA	$x(n) = 0.4\text{square}(n) + w(n)$	5	5.9464×10^{-4}
		CSA	$x(n) = \text{rand}(n)$	5	1.9658×10^{-4}
	Example 2	CSA	$x(n) = 0.8\sin(\frac{\pi}{9}n)$	5	7.4953×10^{-4}
		CSA	$x(n) = 0.8\sin(\frac{\pi}{9}n) + w(n)$	5	0.0137
		CSA	$x(n) = 0.4\text{square}(n)$	5	8.9512×10^{-4}
		CSA	$x(n) = 0.4\text{square}(n) + w(n)$	5	0.0039
		CSA	$x(n) = \text{rand}(n)$	5	0.0022

for nonlinear system identification problem.

VI. CONCLUSION

The objective of this work is to design an efficient method for nonlinear system approximation with the use of fractional delays. The novelty is that in implementing the fractional order delays, the higher order nonlinearities are estimated using a low order Volterra model with higher accuracy by using adept optimization methodologies. A discrete model of the estimation problem is formulated in order to simulate the proposed method in MATLAB. The Gradient-search method is developed for the system identification problem and optimizing the Volterra system parameters. To further optimize the system coefficients, different stochastic algorithms are applied. Two design examples are presented using nonlinear benchmark models with five different input signals and close approximations of the unknown system are analyzed in figures and tables, comparing the proposed gradient-search, RGA, PSO and CSA techniques. The statistical analysis of the estimated results is portrayed by computing the mean, variance and standard deviation of the computed error while performing multiple simulations. The accuracy in results is achieved with the globally convergent and widely applied metaheuristic optimization, CSA. A comparison between the various optimization technique is made. It can be concluded that the proposed method incorporating the fractional delay systems, delivers an effective approximation to an unknown nonlinear system modeled using a second order Volterra function.

REFERENCES

[1] Widrow B, Strearns S D. *Adaptive signal processing*. NJ, Prentice-Hall: Englewood Cliffs, 1985

[2] Panda G, Pradhan P M, Majhi B. IIR system identification using cat swarm optimization. *Expert Systems with Applications*, 2011, **38**(10): 12671-12683

[3] Majhi B, Panda G, Choubey A. Efficient scheme of pole-zero system identification using particle swarm optimization technique. In *Proc. IEEE Congress on Evolutionary Computation*, 2008, 446-451

[4] Saha S K, Kar R, Mandal D, Ghoshal S P. Harmony search algorithm for infinite impulse response system identification. *Computers & Electrical Engineering*, 2014, **40**(4): 1265-1285

[5] Patwardhan AP, Patidar R, George NV. On a cuckoo search optimization approach towards feedback system identification. *Digital Signal Processing*, 2014, **32**: 156-163

[6] Upadhyay P, Kar R, Mandal D, Ghoshal S P. Craziness based particle swarm optimization algorithm for IIR system identification problem. *International Journal of Electronics and Communications*, 2014, **68**(5): 369-378

[7] Upadhyay P, Kar R, Mandal D, Ghoshal S P, Mukherjee V. A novel design method for optimal IIR system identification using opposition based harmony search algorithm. *Journal of the Franklin Institute*, 2014, **351**(5): 2454-2488

[8] Jiang S, Wang Y, Ji Z. A new design method for adaptive IIR system identification using hybrid particle swarm optimization and gravitational search algorithm. *Nonlinear Dynamics*, 2015, **79**(4): 2553-2576

[9] Mathews V J. Adaptive polynomial filters. *IEEE Signal Processing Magazine*, 1991, **8**: 10-26

[10] Rhee S H, Tsang P H S, Yen S W. Friction-induced noise and vibrations of disc brakes. *Wear*, 1989, **133**: 39-45

[11] Kerschen G, Worden K, Vakakis A F, Golinval J C. Past, present and future of nonlinear system identification in structural dynamics. *Mechanical Systems and Signal Processing*, 2006, **20**(3): 505-592

[12] Nelles O. *Nonlinear System Identification: From Classical Approaches to Neural Networks and Fuzzy Models*. Springer, 2001

[13] Giannakis G B, Serpedin E. A bibliography on nonlinear system identification. *Signal Processing*, 2001, **81**: 533-580

[14] Chang W D. Volterra filter modeling of nonlinear discrete-time system using improved particle swarm optimization. *Digital Signal Processing*, 2012, **22**: 1056-1062

[15] Boyd S, Chua L O. Fading memory and the problem of approximating nonlinear operators with Volterra series. *IEEE Transactions on Circuits and Systems*, 1985, **32**(11): 1150-1161

[16] Gotmare A, Patidar R, George N V. Nonlinear system identification using a cuckoo search optimized adaptive Hammerstein model. *Expert Systems with Applications*, 2015, **42**: 2538-2546

[17] Sloss B G, Blyth W F. A Walsh function method for a non-linear Volterra integral equation. *Journal of the Franklin Institute*, 2003, **340**(1): 25-41

[18] Wahlberg B O. System identification using Kautz models. *IEEE Transactions on Automatic Control*, 1994, **39**(6): 1276-1282

[19] Aadaleesan P, Miglan N, Sharma R, Saha P. Nonlinear system identification using Wiener type Laguerre avelet network model. *Chemical Engineering Science*, 2008, **63**(15): 3932-3941

[20] Gallman P G. An iterative method for the identification of nonlinear systems using a Uryson model. *IEEE Transactions on Automatic Control*, 1975, **20**(6): 771-775

[21] Narendra K S, Parthasarathy K. Identification and control of dynamical systems using neural networks. *IEEE Transactions on Neural Networks*, 1990, **1**(1): 4-27

[22] Rashedi E, Hossien N P, Saeid S. Filter modeling using gravitational search algorithm. *Engineering Applications of Artificial Intelligence*, 2011, **24**(1): 117-122

[23] Volterra V. *Theory of functionals and of integral and integrodifferential equations*. Dover, New York, 2005

[24] Holland JH. *Adaptation in Natural and Artificial Systems*. University of Michigan Press, Ann Arbor, 1975

[25] Aggarwal A, Rawat T K, Kumar M, Upadhyay D K. Optimal design of FIR high pass filter based on L_1 error approximation using real coded genetic algorithm. *Engineeing Science and Technology, an International Journal*, 2015, **18**(4): 594-602

[26] Kumar M, Rawat T K. Optimal design of FIR fractional order differentiator using cuckoo search algorithm. *Expert Systems with Applications*, 2015, **42**(7): 3433-3449

[27] Kennedy J, Eberhart R. Particle Swarm Optimization. In *Proceedings of IEEE International Conference on Neural Network*, 1995, **4**: 1942-1948

[28] Kumar M, Rawat T K. Optimal Fractional Delay-IIR Filter Design Using Cuckoo Search Algorithm. *ISA Transactions*, 2015, **59**: 39-54

[29] Yang X S, Deb S. Cuckoo search via Lévy flights. In *Proceedings of World Congress on Nature and Biologically Inspired Computing, IEEE Publications*, USA, 2009, 210-214

Manjeet Kumar graduated from Kurukshetra University, Haryana with B.Tech in Electronics & Communication Engineering in 2008. He received his M.Tech from Ambedkar Institute of Technology, GGSIPU, Delhi in 2011. He is currently pursuing Ph.D. in the area of optimal design of fractional order digital filter from Netaji Subhas Institute of Technology, University of Delhi. His research interests include digital signal processing, fractional calculus, filter design and optimization, fractional order differentiator and fractional delay filter.

Apoorva Aggarwal graduated from GGSIPU, Delhi with B.Tech in Electrical & Electronic Engineering in 2011. She received her M.Tech from GGSIPU, Delhi in 2013. She is currently pursuing Ph.D. in the area of optimal design of digital filters from Netaji Subhas Institute of Technology, University of Delhi. Her research interests include filter design and optimization, digital signal processing, nature-inspired metaheuristic optimization techniques, digital electronics and innovative projects.

Tarun Rawat received his M.Tech and Ph.D. from NSIT, University of Delhi in 2003 and 2010, respectively. Presently, he is attached with NSIT, Delhi, India, as Assistant Professor in the Department of Electronics and Communication Engineering. He has published more than 30 research papers in international journals and two books: Signal and System, Digital Signal Processing in Oxford University Press. His research interests include VLSI signal processing, digital signal processing, statistical signal processing and filter optimization via nature-inspired computational techniques.

Harish Parthasarathy received B.Tech. in 1990 (from Indian Institute of Technology Kanpur, India) and Ph.D. (from Indian Institute of Technology Delhi, India) in 1994, both in Electrical Engineering. He worked as Assistant Professor during 1994-1997 at Indian Institute of Tehnology Bombay in Electrical Engineering Department and during 1997-1998 at Indian Institute of Technology Kanpur in Electrical Engineering Department. He worked as Application Engineer at ST MicroElectronics, Delhi, during 1998-2000 before joining Netaji Subhas Institute of Technology, New Delhi, in 2000, where he worked as Assistant Professor till June 2007. Since July 2007, he has been working as Professor in the Division of Electronics and Communication Engineering at Netaji Subhas Institute of Technology, New Delhi. His teaching and research interests are in the areas of circuits and systems, signal processing, stochastic nonlinear filters, electromagnetics and group representations and he has published 40 papers in various international journals of repute.

Fractional-Order Control for a Novel Chaotic System without Equilibrium

Shu-Yi Shao and Mou Chen *Member, IEEE,*

***Abstract*—The control problem is discussed for a chaotic system without equilibrium in this paper. On the basis of the linear mathematical model of the two-wheeled self-balancing robot, a novel chaotic system which has no equilibrium is proposed. The basic dynamical properties of this new system are studied via Lyapunov exponents and Poincaré map. To further demonstrate the physical realizability of the presented novel chaotic system, a chaotic circuit is designed. By using fractional-order operators, a controller is designed based on the state-feedback method. According to the Gronwall inequality, Laplace transform and Mittag-Leffler function, a new control scheme is explored for the whole closed-loop system. Under the developed control scheme, the state variables of the closed-loop system are controlled to stabilize them to zero. Finally, the numerical simulation results of the chaotic system with equilibrium and without equilibrium illustrate the effectiveness of the proposed control scheme.**

***Index Terms*—Chaotic system, Circuit implementation, Fractional-order, Stabilization.**

I. INTRODUCTION

FROM From the simplified equation of convection rolls in the equations of the atmosphere, the first three-dimensional chaotic system was derived by Lorenz in 1963[1]. With the development and applying of chaos theory, a number of chaotic systems, hyperchaotic systems, fractional-order chaotic systems and fractional-order hyperchaotic systems have been proposed, such as Rössler chaotic system[2], Liu chaotic system[3], hyperchaotic Chen system[4], hyperchaotic Lü system[5], fractional-order financial system[6], fractional-order Lotka-Volterra equation[7], fractional-order hyperchaos Lorenz system[8], a modified four-dimensional fractional order hyperchaotic system[9] and so on. The above mentioned chaotic systems have equilibrium. In addition, there are a number of chaotic systems without equilibrium which have been studied by [10-13]. As a result, chaos control became one of the important issues for chaotic systems. Due to great potential application in electrical engineering, information processing and secure communication, it is important to investigate new control methods for chaotic systems.

Over the past few decades, chaos control and chaos synchronization have received much attention and many important results have been reported. In the early 1990s, the synchronization of chaotic systems was achieved by Pecora and Carroll[14,15], which was a trailblazing result, and the result promoted the development of chaos control and chaos synchronization[16,17]. In recent years, different chaos control and chaos synchronization strategies have been developed for chaotic systems. The sliding mode control method was applied to chaos control[18,19] and chaos synchronization[20]. In [21], the feedback control method and the adaptive control method were used to realize chaos control for the energy resource chaotic system. The chaos control problems were investigated for Lorenz system, Chen system and Lü system based on backstepping design method in [22]. By using adaptive control method, the problems of chaos control[23,24] and chaotic synchronization[25] were studied for chaotic systems. The neural adaptive control method was developed for a class of chaotic systems with uncertain dynamics, input and output constraints in [26]. In [27], on the basis of impulsive control method, the problems of the stabilization and synchronization were explored for Lorenz systems. The synchronization problem was resolved for a class of chaotic systems by using a fractional-order observer-based method and the synchronization was applied to secure communication in [28]. In [29], the synchronization was studied for fractional-order systems based on the output feedback sliding mode control method. A new synchronization strategy was presented for two fractional-order systems and the synchronization was applied in image encryption in [30]. The above literature works focused on chaos control and chaos synchronization in practical chaotic systems with equilibrium points. However, the control of chaotic systems without equilibrium has rarely been investigated[13]. Meanwhile, for most of the above mentioned works, fractional-order controllers have rarely been used to realize the chaos control of integer-order chaotic systems, although some important results on the fractional-order controllers have been proposed for various systems[31−33]. In [31], a well-known fractional-order controller was presented. In [32], the concept of a fractional-order $PI^{\lambda}D^{\mu}$ controller was proposed and the fractional-order controller included fractional order integrator and fractional-order differentiator. In [33], on the basis of the Lyapunov stability theory, a novel fractional-order controller was given, and fractional-order chaotic and hyperchaotic systems were controlled by the proposed fractional-order controller. The fractional-order controllers are effective to control systems, which have been proved in the mentioned works. Therefore, it is valuable to further explore the chaos control of integer-order chaotic systems without equilibrium by using fractional-order controllers.

Inspired by the above discussions, the objective of this paper

This article has been accepted for publication in a future issue of this journal, but has not been fully edited. Content may change prior to final publication.

This work is supported by National Natural Science Foundation of China (61573184), Jiangsu Natural Science Foundation of China (SBK20130033), Six Talents Peak Project of Jiangsu Province (2012-XXRJ-010) and Fundamental Research Funds for the Central Universities (NE2016101). Recommended by Associate Editor Antonio Visioli.

Shu-Yi Shao and Mou Chen are with the College of Automation Engineering, Nanjing University of Aeronautics and Astronautics, Nanjing 211106, China (e-mail: shaosy@163.com, chenmou@nuaa.edu.cn).

Digital Object Identifier 10.1109/JAS.2016.7510124

is to design an efficient fractional-order controller and the stability is realized for the closed-loop system. A novel chaotic system without equilibrium is proposed based on the model of two-wheeled self-balancing robot. Meanwhile, the presented new system is used to verify the effectiveness of the proposed control scheme.

The organization of the paper is as follows. Section II details the problem formulation. A novel chaotic system is proposed and the chaotic system circuit is designed in Section III. Section IV presents the fractional-order controller based on the state-feedback method. The numerical simulation studies are presented to demonstrate the effectiveness of the developed control method in Section V, followed by some concluding remarks in Section VI.

II. Problem Statement and Preliminaries

In this paper, a novel chaotic system will be proposed by only considering the straight line position x_r and the pitch angle θ_p of the two-wheeled self-balancing robot of Googol Technology as shown in Fig. 1. A mathematical model related to the two-wheeled self-balancing robot of Googol Technology was established in [34]. The linear mathematical model for x_r and θ_p of the two-wheeled self-balancing robot of Googol Technology is described in the form

$$\begin{bmatrix} \dot{x}_r \\ \ddot{x}_r \\ \dot{\theta}_p \\ \ddot{\theta}_p \end{bmatrix} = \begin{bmatrix} 0 & 1 & 0 & 0 \\ 0 & 0 & -23.6701 & 0 \\ 0 & 0 & 0 & 1 \\ 0 & 0 & 124.5128 & 0 \end{bmatrix} \begin{bmatrix} x_r \\ \dot{x}_r \\ \theta_p \\ \dot{\theta}_p \end{bmatrix} + \begin{bmatrix} 0 \\ 4.5974 \\ 0 \\ -19.0414 \end{bmatrix} C_\theta \tag{1}$$

where C_θ denotes the pitch torque.

Fig. 1. Two-wheeled self-balancing robot of Googol Technology.

In order to transform the linear mathematical model into a chaotic system, we consider C_θ as a nonlinear term $\Phi(x_r, \dot{x}_r, \dot{\theta}_p, \ddot{\theta}_p)$, which will be given in next section.

Considering the nonlinear function $\Phi(x_r, \dot{x}_r, \dot{\theta}_p, \ddot{\theta}_p)$ and the control input u, (1) can be described as

$$\begin{bmatrix} \dot{x}_r \\ \ddot{x}_r \\ \dot{\theta}_p \\ \ddot{\theta}_p \end{bmatrix} = \begin{bmatrix} 0 & 1 & 0 & 0 \\ 0 & 0 & -23.6701 & 0 \\ 0 & 0 & 0 & 1 \\ 0 & 0 & 124.5128 & 0 \end{bmatrix} \begin{bmatrix} x_r \\ \dot{x}_r \\ \theta_p \\ \dot{\theta}_p \end{bmatrix} + \begin{bmatrix} 0 \\ 4.5974 \\ 0 \\ -19.0414 \end{bmatrix} \Phi(x_r, \dot{x}_r, \dot{\theta}_p, \ddot{\theta}_p) + u \tag{2}$$

where the control input $u = [u_1, u_2, u_3, u_4]^{\mathrm{T}}$.

This paper aims at constructing a novel chaotic system without equilibrium and developing a fractional-order control scheme, so that the stabilization of the whole closed-loop system is realized based on the designed control strategy. Under designed fractional-order controller, the state variables of the closed-loop system will be asymptotically stable. To develop the fractional-order control scheme, we firstly introduce the following definitions and lemmas:

Definition 1[35]**.** The Caputo fractional derivative operator, which is one of the most widely used fractional derivative operators, is defined for the function $f(t)$ as follows :

$$D^\alpha f(t) = \frac{1}{\Gamma(m-\alpha)} \int_{t_0}^{t} \frac{f^{(m)}(\tau)}{(t-\tau)^{\alpha-m+1}} \mathrm{d}\tau, \tag{3}$$

where α is the fractional order and $m-1 < \alpha < m$, $m = [\alpha]+1$, $[\alpha]$ denotes the integer part of α, and $\Gamma(\cdot)$ is gamma function, which is defined as $\Gamma(m-\alpha) = \int_0^\infty t^{m-\alpha-1} e^{-t} \mathrm{d}t$. The main advantage of (3) is that Caputo derivative of a constant is equal to zero. Particularly, when $0 < \alpha \leq 1$, we have $\mathcal{L}\{D^\alpha f(t)\} = s^\alpha F(s) - s^{\alpha-1} f(0)$. The Laplace transform of fractional integral at $t_0 = 0$ has the following form:

$$\mathcal{L}\left\{D^{-\alpha} f(t)\right\} = s^{-\alpha}\mathcal{L}\{f(t)\} = s^{-\alpha} F(s), \quad (\alpha > 0), \tag{4}$$

where t and s are the variables in the time domain and Laplace domain, respectively. $F(s) = \mathcal{L}(f(t))$ and $\mathcal{L}(\cdot)$ stands for the Laplace transform.

In this paper, the fractional-order controller will be described by using Caputo definition with lower limit of integral $t_0 = 0$ and the order $1 < \alpha < 2$. Furthermore, there have been some important control schemes proposed for fractional-order systems by using different fractional calculus. In [36-38], Mittag-Leffler stability theorems have been proposed for fractional-order systems. The stability theorem was developed for fractional differential system with Riemann-Liouville derivative in [39-41].

Definition 2[42]**.** The Mittag-Leffler function with two parameters is defined as

$$E_{\alpha_1,\beta_1}(z) = \sum_{k=0}^{\infty} \frac{z^k}{\Gamma(k\alpha_1 + \beta_1)}, \tag{5}$$

where $\alpha_1 > 0$, $\beta_1 > 0$, z denotes the set of complex numbers. When $\beta_1 = 1$, the Mittag-Leffler function can be written as

$$E_{\alpha_1,1}(z) = E_{\alpha_1}(z) = \sum_{k=0}^{\infty} \frac{z^k}{\Gamma(k\alpha_1 + 1)}, \tag{6}$$

The Laplace transform of Mittag-Leffler function is given by

$$\begin{cases} \mathcal{L}\left\{t^{\beta_1-1}E_{\alpha_1,\beta_1}(-\lambda t^{\alpha_1})\right\} = \frac{s^{\alpha_1-\beta_1}}{s^{\alpha_1}+\lambda}, \Re(s) > |\lambda|^{\frac{1}{\alpha_1}}, \\ \mathcal{L}\left\{E_{\alpha_1,1}(-\lambda t^{\alpha_1})\right\} = \frac{s^{\alpha_1}}{s(s^{\alpha_1}+\lambda)}. \end{cases} \tag{7}$$

where $\Re(s)$ stands for the real part of s and $\lambda \in R$.

Lemma 1[43]**.** For the the Mittag-Leffler function $E_{\alpha_3,\beta_3}(A_0 t^{\alpha_3})$, if $1 < \alpha_3 < 2$, then, for $\beta_3 = 1$, 2 or α_3, one has

$$\|E_{\alpha_3,\beta_3}(A_0 t^{\alpha_3})\| \leq \left\| e^{A_0 t^{\alpha_3}} \right\|, \ \ t \geq 0. \tag{8}$$

Moreover, if A_0 is a stable matrix, we have

$$\left\| e^{A_0 t^{\alpha_3}} \right\| \leq M e^{-\eta t}, \ \ t \geq 0, \tag{9}$$

where $M \geq 1$, $-\eta(\eta > 0)$ is the largest eigenvalue of the matrix A_0, $\|\cdot\|$ denotes any vector or induced matrix norm.

Lemma 2[44,45]**(Gronwall-Bellman lemma).** Assume that the function $h(t)$ satisfies

$$h(t) \leq \int_0^t p(\tau)h(\tau)\mathrm{d}\tau + b(t), \tag{10}$$

with $p(\tau)$ and $b(t)$ being known real functions. Then, we obtain

$$h(t) \leq \int_0^t p(\tau)h(\tau)e^{\int_\tau^t p(\upsilon)\mathrm{d}\upsilon}\mathrm{d}\tau + b(t). \tag{11}$$

If $b(t)$ is differentiable, we have

$$h(t) \leq b(0)e^{\int_0^t p(\tau)\mathrm{d}\tau} + \int_0^t \dot{b}(\tau)e^{\int_\tau^t p(\upsilon)\mathrm{d}\upsilon}\mathrm{d}\tau. \tag{12}$$

In particular, if $b(t)$ is a constant, one has

$$h(t) \leq b(0)e^{\int_0^t p(\tau)\mathrm{d}\tau}. \tag{13}$$

III. Design of Chaotic System and Circuit Implementation

In this section, a novel chaotic system without equilibrium is constructed based on the linear mathematical model (1) of the two-wheeled self-balancing robot. For this case, the proposed novel chaotic system can be regarded as an open-loop system of the system (2). Furthermore, the chaotic circuit is designed to show the physical realizability of the proposed chaotic system.

A. A Novel Chaotic System

From (2), the novel chaotic system is described as follows:

$$\begin{aligned} \dot{x}_1 &= x_2 \\ \dot{x}_2 &= -23.6701x_3 + 4.5974\Phi(x) \\ \dot{x}_3 &= x_4 \\ \dot{x}_4 &= 124.5128x_3 - 19.0414\Phi(x) \end{aligned} \tag{14}$$

where $x = [x_1, x_2, x_3, x_4]^{\mathrm{T}}$ is the state vector of the nonlinear system with $x_1 = x_r$, $x_2 = \dot{x}_r$, $x_3 = \theta_p$ and $x_4 = \dot{\theta}_p$. The nonlinear function $\Phi(x)$ is given by

$$\Phi(x) = \kappa_1(x_2 + x_4 + x_1 x_3) + \kappa_2 \tag{15}$$

where κ_1 and κ_2 are constants. When $\kappa_1 = 10$ and $\kappa_2 = 0.5$, we obtain the Lyapunov exponents $\lambda_{L_1} = 0.0177$, $\lambda_{L_2} = 0$, $\lambda_{L_3} = -0.0148$ and $\lambda_{L_4} = -143.8384$ by using the initial conditions $x_{10} = x_{20} = x_{30} = x_{40} = 0.1$ based on the numerical method of [46]. Obviously, the system (14) is a chaotic system because $\lambda_{L_1} > 0$, $\lambda_{L_2} = 0$, $\lambda_{L_3} < 0$ and $\lambda_{L_4} < 0$. On the basis of the system (14) and the mentioned parameter values, some simulation results are further presented as shown in Fig. 2. In addition, to further reflect the properties of chaos, a Poincaré map is shown in Fig. 3.

In order to solve the equilibrium of system (14), we have $\dot{x}_1 = 0$, $\dot{x}_2 = 0$, $\dot{x}_3 = 0$ and $\dot{x}_4 = 0$, that is

$$\begin{aligned} x_2 &= 0 \\ -23.6701x_3 + 4.5974\Phi(x) &= 0 \\ x_4 &= 0 \\ 124.5128x_3 - 19.0414\Phi(x) &= 0 \end{aligned} \tag{16}$$

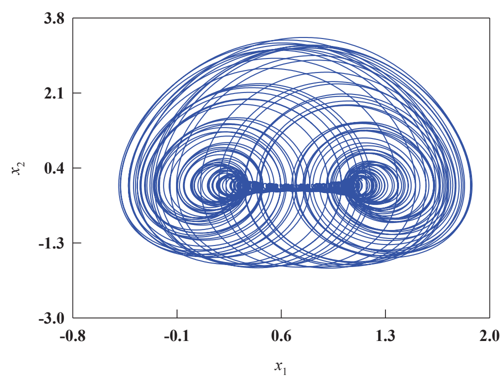

(a)

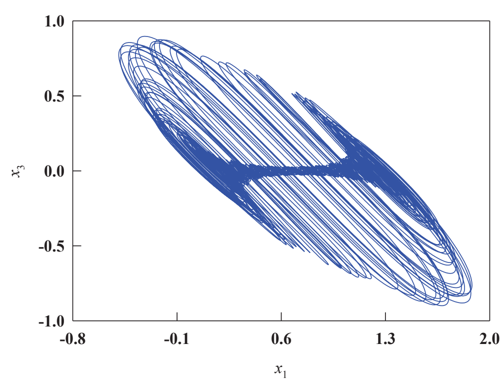

(b)

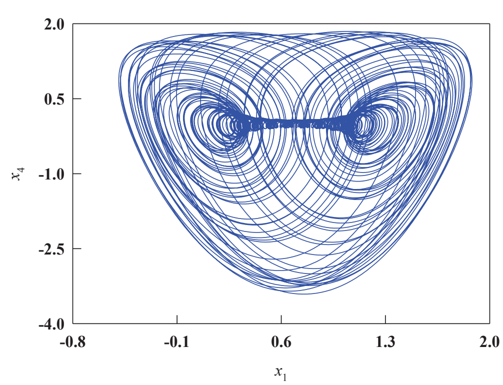

(c)

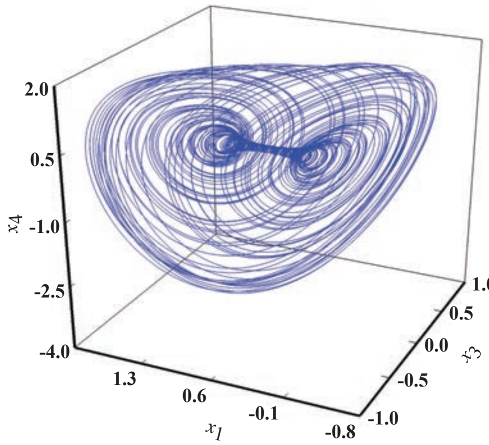

(d)

Fig. 2. Chaotic behaviors of the novel chaotic system (a) $x_1 - x_2$ plane, (b) $x_1 - x_3$ plane, (c) $x_1 - x_4$ plane, (c) $x_3 - x_1 - x_4$ space.

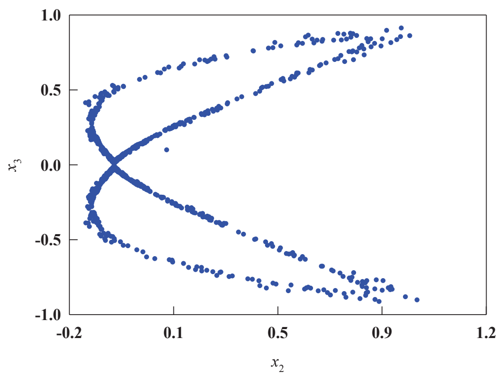

Fig. 3. Poincaré map in the $x_2 - x_3$ plane.

According to (16), we obtain that there is no equilibrium in system (14). Furthermore, we ensure that the system (14) is dissipative with the following exponential contraction rate:

$$\frac{\mathrm{d}V}{\mathrm{d}t} = e^{-144.44t} \tag{17}$$

with

$$\begin{aligned} \nabla V &= \frac{\partial \dot{x}_1}{\partial x_1} + \frac{\partial \dot{x}_2}{\partial x_2} + \frac{\partial \dot{x}_3}{\partial x_3} + \frac{\partial \dot{x}_4}{\partial x_4} \\ &= -144.44 < 0 \end{aligned} \tag{18}$$

B. Circuit Implementation

To further illustrate the physical realizability of the proposed novel chaotic system (14), the system circuit is designed. By using the resistors, the capacitors and the operational amplifiers TL082, the designed circuit of the chaotic system is shown in Fig. 4. According to Fig. 4, the circuit system of the chaotic system is described as

$$\begin{aligned} \dot{x}_1 &= \frac{R_{12}}{C_1 R_{11} R_{13}} x_2 \\ \dot{x}_2 &= -\frac{1}{C_2 R_{28}} x_3 + \frac{R_{22}}{C_2 R_{23} R_{21}} x_2 + \frac{R_{26}}{C_2 R_{25} R_{27}} x_1 x_3 \\ &\quad + \frac{R_{210}}{C_2 R_{29} R_{211}} x_4 + V_1 \frac{1}{C_2 R_{24}} \\ \dot{x}_3 &= \frac{R_{32}}{C_3 R_{31} R_{33}} x_4 \\ \dot{x}_4 &= \frac{R_{42}}{C_4 R_{41} R_{44}} x_3 - \frac{1}{C_4 R_{46}} x_2 - \frac{1}{C_4 R_{45}} x_1 x_3 \\ &\quad - \frac{1}{C_4 R_{47}} x_4 - V_2 \frac{1}{C_4 R_{43}} \end{aligned} \tag{19}$$

By comparing (14) with (19), all resistance values R_{11}, R_{12}, R_{21}, R_{22}, R_{25}, R_{26}, R_{29}, R_{210}, R_{31}, R_{32}, R_{41} and R_{42} are $10\,K\Omega$, R_{13} and R_{33} are $1\,M\Omega$, R_{23}, R_{27} and R_{211} are $21.7514\,K\Omega$, R_{45}, R_{46} and R_{47} are $5.251715\,K\Omega$, R_{28} is $42.2474\,K\Omega$, R_{44} is $8.031303\,K\Omega$, R_{24} is $435.02849\,K\Omega$ and R_{43} is $105.0343\,K\Omega$. The voltage values $V_1 = 1\,V$ and $V_2 = -1\,V$. In order to speed up the circuit response time, we make a time scale transformation by multiplying a factor of 100 on the right hand side of (14), the capacitance values C_1, C_2, C_3 and C_4 are $10\,nF$. In Fig. 4, $U_{Ai}(i = 1, 2, \cdots, 10)$ are operational amplifiers, A is a unity gain multiplier.

From the designed circuit of chaotic system (14), the circuit experimental phase portraits are presented in Fig. 5. Comparing Fig. 2 and Fig. 5, we observe that there exists consistency between numerical simulations and circuit experimental simulations, the circuit simulation results prove the physical realizability of the proposed novel chaotic system (14).

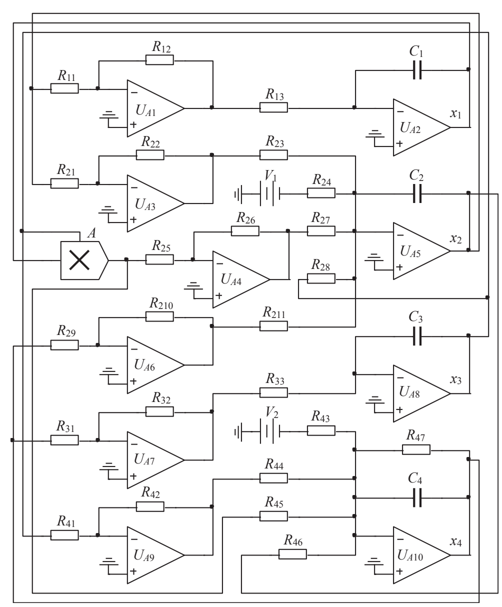

Fig. 3. Circuit of the novel chaotic system (14).

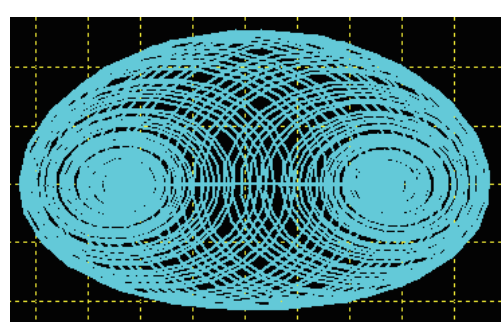

(a)

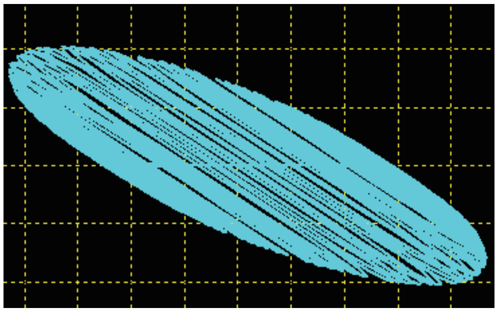

(b)

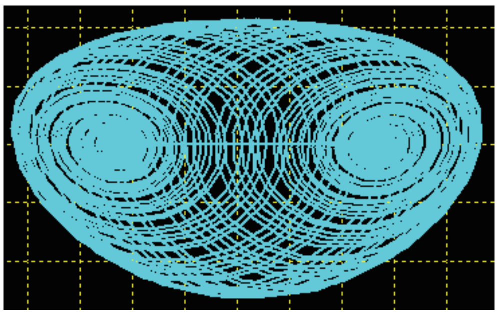

(c)

Fig. 5. Chaotic behaviors of the chaotic circuit (a) $x_1 - x_2$ plane, (b) $x_1 - x_3$ plane, (c) $x_1 - x_4$ plane.

IV. Design of Fractional-order Controller and Stability Analysis

In this section, the control scheme will be proposed for the whole closed-loop system including the constructed chaotic system (14) and the designed fractional-order controller. The goal is to guarantee the stabilization of the closed-loop system under the proposed fractional-order controller.

From (14), the chaotic system can be rewritten as

$$\dot{x} = Ax + q(x) + \bar{q} \tag{20}$$

where $x = [x_1, x_2, x_3, x_4]^{\mathrm{T}}$ is the state vector,

$$A = \begin{bmatrix} 0 & 1 & 0 & 0 \\ 0 & 45.974 & -23.6701 & 45.974 \\ 0 & 0 & 0 & 1 \\ 0 & -190.414 & 124.5128 & -190.414 \end{bmatrix}$$
$$q(x) = \begin{bmatrix} 0 \\ 45.974x_1x_3 \\ 0 \\ -190.414x_1x_3 \end{bmatrix}$$
$$\bar{q} = \begin{bmatrix} 0 \\ 2.2987 \\ 0 \\ -9.5207 \end{bmatrix}.$$

According to the chaotic system (14) and considering the control input u, the corresponding system has the following form:

$$\dot{x} = Ax + q(x) + \bar{q} + u \tag{21}$$

where $u = [u_1, u_2, u_3, u_4]^{\mathrm{T}}$ is the designed fractional-order control input.

Based on the state-feedback control method, the controller u is defined as

$$u = -Ax - \bar{q} + KD^{1-\alpha}x. \tag{22}$$

where $K = \mathrm{diag}(k_1, k_2, \cdots, k_n)$ is a design control gain matrix and the fractional order satisfies $1 < \alpha < 2$.

According to (21) and (22), one has

$$\dot{x} = q(x) + KD^{1-\alpha}x. \tag{23}$$

To render the stabilization of the system (21) under the proposed controller (22), the following assumption is required:

Assumption 1. Nonlinear function $q(x)$ satisfies $q(0) = 0$ and $\lim_{\|x\|\to 0}\|q(x)\|/\|x\| = 0$.

The fractional-order controller based control scheme for the closed-loop system (23) can be summarized in the following theorem.

Theorem 1. For the closed-loop system (23), the fractional-order controller is designed based on (22). Then, the state variables of the closed-loop system (23) are asymptotically stabilized to zero when the zero is a stable equilibrium point of the closed-loop system (23), under the conditions of $\lim_{\|x\|\to 0}\|q(x)\|/\|x\| = 0$, the fractional order α: $1 < \alpha < 2$, and the design matrix K satisfies $\eta = -\max\{\mathrm{Re}\lambda(K)\} > 1$, where $\lambda(K)$ denotes the eigenvalues of K and $M \geq 1$.

Proof. By taking the Laplace transform on system (23), we have

$$sX(s) - x(0) = \mathcal{L}(q(x(t))) + Ks^{1-\alpha}X(s), \tag{24}$$

where $X(s)$ is the Laplace transform of $x(t)$, $x(0)$ is the initial condition of (17) and $1 < \alpha < 2$.

Let us multiply both sides of (24) by s^{α}, it yields

$$s^{\alpha+1}X(s) - s^{\alpha}x(0) = s^{\alpha}\mathcal{L}(q(x(t))) + KsX(s). \tag{25}$$

From (25), one has

$$X(s) = s^{\alpha-1}(Is^{\alpha} - K)^{-1}(x(0) + \mathcal{L}(q(x(t)))), \tag{26}$$

where I denotes the 4×4 identity matrix.

Taking the Laplace inverse transform on (26), one obtains

$$\begin{aligned} x(t) \quad &= \quad E_{\alpha,1}(Kt^{\alpha})x(0) \\ &\quad + \int_0^t E_{\alpha,1}(K(t-\varphi)^{\alpha})q(x(\varphi))\mathrm{d}\varphi. \end{aligned} \tag{27}$$

On the basis of Lemma 1, since K is a stable matrix, $-\eta = \max(\mathrm{Re}\lambda(K))(\eta > 0)$, $M \geq 1$ and $1 < \alpha < 2$, (27) can be written as

$$\|x(t)\| \leq Me^{-\eta t}\|x(0)\| + \int_0^t Me^{-\eta(t-\varphi)}\|q(x(\varphi))\|\,\mathrm{d}\varphi. \tag{28}$$

Multiplying by $e^{\eta t}$ on both sides of (28), it yields

$$e^{\eta t}\|x(t)\| \leq M\|x(0)\| + \int_0^t Me^{\eta\varphi}\|q(x(\varphi))\|\,\mathrm{d}\varphi. \tag{29}$$

According to Assumption 1 and the properties of $\lim_{\|x\|\to 0}\|q(x)\|/\|x\| = 0$[43,47], there exists a constant $\delta > 0$, such that

$$\|q(x)\| \leq \frac{1}{M}\|x\|\, as\, \|x\| < \delta. \tag{30}$$

Substituting (30) into (29), one has

$$e^{\eta t}\left\|x(t)\right\| \leq M\left\|x(0)\right\| + \int_0^t e^{\eta\varphi}\left\|x(\varphi)\right\| \mathrm{d}\varphi. \tag{31}$$

Based on Lemma 2, $b(t) = M\left\|x(0)\right\|$, $p(\varphi) = 1$ and $h(t) = e^{\eta t}\left\|x(t)\right\|$, we have

$$e^{\eta t}\left\|x(t)\right\| \leq M\left\|x(0)\right\| e^t. \tag{32}$$

Inequality (32) is equivalent to

$$\left\|x(t)\right\| \leq \frac{M\left\|x(0)\right\|}{e^{(\eta-1)t}}. \tag{33}$$

When $\eta = -\max\left\{\mathrm{Re}\lambda(K)\right\} > 1$, $t \to \infty$, $\left\|x(t)\right\|$ asymptotically tends to zero, which implies the closed-loop system (23) is asymptotically stable if zero is a stable equilibrium point. This concludes the proof.

V. Numerical Simulation

In this section, in order to illustrate and verify the effectiveness of the proposed control scheme, the closed-loop system (23) is analyzed. Furthermore, we use the proposed control scheme to stabilize the chaotic systems with equilibrium such as Chen system[48], Genesio's system[49], and hyperchaotic Lorenz system[50].

A. Novel chaotic system

Combining the novel chaotic system (14) and the designed controller (22), we have

$$\begin{aligned} \dot{x}_1 &= k_1 D^{1-\alpha} x_1 \\ \dot{x}_2 &= 45.974 x_1 x_3 + k_2 D^{1-\alpha} x_2 \\ \dot{x}_3 &= k_3 D^{1-\alpha} x_3 \\ \dot{x}_4 &= -190.414 x_1 x_3 + k_4 D^{1-\alpha} x_4 \end{aligned} \tag{34}$$

The equilibrium of system (34) is obtained by solving $\dot{x}_1 = 0$, $\dot{x}_2 = 0$, $\dot{x}_3 = 0$ and $\dot{x}_4 = 0$, that is

$$\begin{aligned} k_1 D^{1-\alpha} x_1 &= 0 \\ 45.974 x_1 x_3 + k_2 D^{1-\alpha} x_2 &= 0 \\ k_3 D^{1-\alpha} x_3 &= 0 \\ -190.414 x_1 x_3 + k_4 D^{1-\alpha} x_4 &= 0 \end{aligned} \tag{35}$$

According to (35), we obtain that $O = (0,0,0,0)$ is the equilibrium of the system (34). Furthermore, when the design parameters k_1, k_2, k_3 and k_4 satisfy $k_1 < 0$, $k_2 < 0$, $k_3 < 0$ and $k_4 < 0$, we can guarantee that the equilibrium $O = (0,0,0,0)$ is a stable equilibrium based on the stability analysis method of the equilibrium[51].

From (34), we have

$$\begin{aligned} \lim_{\|x\|\to 0} \frac{\|q(x)\|}{\|x\|} &= \lim_{\|x\|\to 0} \frac{\sqrt{38371 x_1^2 x_3^2}}{\sqrt{x_1^2+x_2^2+x_3^2+x_4^2}} \\ &\leq \lim_{\|x\|\to 0} \frac{\sqrt{38371 x_1^2 x_3^2}}{\sqrt{x_3^2}} \\ &= \lim_{\|x\|\to 0} 195.8854\left|x_1\right| = 0 \end{aligned} \tag{36}$$

which implies that $q(x)$ satisfies Assumption 1. On the basis of Theorem 1 and pole placement technique, the feedback control gain matrix and the order α are chosen as

$$K = \mathrm{diag}(-10,-10,-10,-10), \quad \alpha = 1.6 \tag{37}$$

From the above discussion, we have $\left\|e^{Kt^\alpha}\right\| \leq e^{-10t}$, $M = 1$ and $\eta = -\max\left\{\mathrm{Re}\lambda(K)\right\} = 10 > 1$, which satisfy Theorem 1. The simulation results are shown in Fig. 6 and Fig. 7. According to the numerical simulation results, the closed-loop system (34) is asymptotically stable, which implies that the proposed control scheme works effectively.

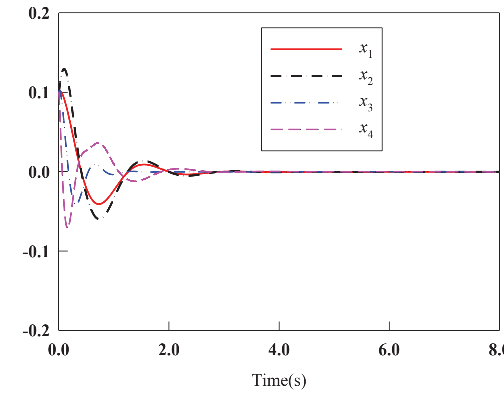

Fig. 6. Numerical simulation results of the system (34).

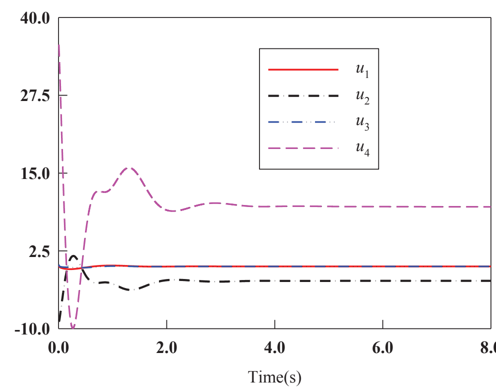

Fig. 7. Control inputs.

B. Chaotic systems with equilibrium

In order to further illustrate the effectiveness of the developed control scheme in this paper, we use the proposed control scheme (22) to control Chen system[48], Genesio's system[49], and hyperchaotic Lorenz system[50]. We firstly analyze the following dynamical model of Chen system[48]:

$$\begin{aligned} \dot{x}_1 &= 35(x_2 - x_1) \\ \dot{x}_2 &= -7x_1 - x_1 x_3 + 28 x_2 \\ \dot{x}_3 &= x_1 x_2 - 3x_3 \end{aligned} \tag{38}$$

From (22), the control input u is designed for the Chen system as follows:

$$\begin{aligned} u_1 &= -35(x_2 - x_1) + k_1 D^{1-\alpha} x_1 \\ u_2 &= 7x_1 - 28x_2 + k_2 D^{1-\alpha} x_2 \\ u_3 &= 3x_3 + k_3 D^{1-\alpha} x_3 \end{aligned} \tag{39}$$

Invoking (38), we have

$$\lim_{\|x\|\to 0} \frac{\sqrt{x_1^2 x_2^2 + x_1^2 x_3^2}}{\sqrt{x_1^2 + x_2^2 + x_3^2}} \le \lim_{\|x\|\to 0} |x_1| = 0 \tag{40}$$

where $x = [x_1, x_2, x_3]^{\mathrm{T}}$.

According to (40), the nonlinear function in (38) can satisfy the Assumption 1. Therefore, the Chen system (38) can be stabilized to zero by choosing appropriate parameters k_1, k_2 and k_3.

The Genesio's system is written by

$$\begin{aligned} \dot{x}_1 &= x_2 \\ \dot{x}_2 &= x_3 \\ \dot{x}_3 &= -6x_1 - 2.92x_2 - 1.2x_3 + x_1^2 \end{aligned} \tag{41}$$

To control the Genesio's system (41), the control input u can be designed based on (22) as

$$\begin{aligned} u_1 &= -x_2 + k_1 D^{1-\alpha} x_1 \\ u_2 &= -x_3 + k_2 D^{1-\alpha} x_2 \\ u_3 &= 6x_1 + 2.92x_2 + 1.2x_3 + k_3 D^{1-\alpha} x_3 \end{aligned} \tag{42}$$

From (41), we obtain

$$\lim_{\|x\|\to 0} \frac{\sqrt{x_1^4}}{\sqrt{x_1^2 + x_2^2 + x_3^2}} \le \lim_{\|x\|\to 0} |x_1| = 0 \tag{43}$$

where $x = [x_1, x_2, x_3]^{\mathrm{T}}$.

The nonlinear function in (41) can satisfy the Assumption 1 based on (43). Thus, the Genesio's system (41) can be stabilized to zero under the appropriate parameters k_1, k_2 and k_3.

The hyperchaotic Lorenz system is given as follows:

$$\begin{aligned} \dot{x}_1 &= 10(x_2 - x_1) \\ \dot{x}_2 &= 28x_1 - x_1 x_3 - x_2 \\ \dot{x}_3 &= x_1 x_2 - \frac{8}{3} x_3 \\ \dot{x}_4 &= -x_1 x_3 + 1.2x_4 \end{aligned} \tag{44}$$

Combining the hyperchaotic Lorenz system (44) and the control scheme (22), the control input u is written as

$$\begin{aligned} u_1 &= -10(x_2 - x_1) + k_1 D^{1-\alpha} x_1 \\ u_2 &= -28x_1 + x_2 + k_2 D^{1-\alpha} x_2 \\ u_3 &= \frac{8}{3} x_3 + k_3 D^{1-\alpha} x_3 \\ u_4 &= -1.2x_4 + k_4 D^{1-\alpha} x_4 \end{aligned} \tag{45}$$

According to (44), we have

$$\lim_{\|x\|\to 0} \frac{\sqrt{2x_1^2 x_3^2 + x_1^2 x_2^2}}{\sqrt{x_1^2 + x_2^2 + x_3^2}} \le \lim_{\|x\|\to 0} \sqrt{2x_2^2 + x_3^2} = 0 \tag{46}$$

where $x = [x_1, x_2, x_3, x_4]^{\mathrm{T}}$.

On the basis of (46), the Assumption 1 is satisfied for the nonlinear function in (44). By designing appropriate parameters k_1, k_2, k_3 and k_4, the stabilization of the hyperchaotic Lorenz system (44) can be realized.

According to the above discussion and analysis, we obtain that the Chen system (38), the Genesio's system (41) and the hyperchaotic Lorenz system (44) can be controlled by using the designed control scheme in this paper. For the numerical simulation of the Chen system (38), we choose the control parameters $k_1 = -10$, $k_2 = -10$ and $k_3 = -10$, the initial conditions $x_0 = (3, 2, 3)^{\mathrm{T}}$ and the fractional order $\alpha = 1.6$. For the numerical simulation of the Genesio's system (41), we set the control parameters as $k_1 = -10$, $k_2 = -10$ and $k_3 = -10$, the initial conditions as $x_0 = (-1, -1, 0)^{\mathrm{T}}$ and the fractional order $\alpha = 1.6$. The control parameters are designed as $k_1 = -10$, $k_2 = -10$, $k_3 = -10$ and $k_4 = -10$, the initial conditions are assumed as $x_0 = (0.1, 0.1, 0.1, 0.1)^{\mathrm{T}}$ and the fractional order is chosen as $\alpha = 1.6$ in the numerical simulation of the hyperchaotic Lorenz system (44).

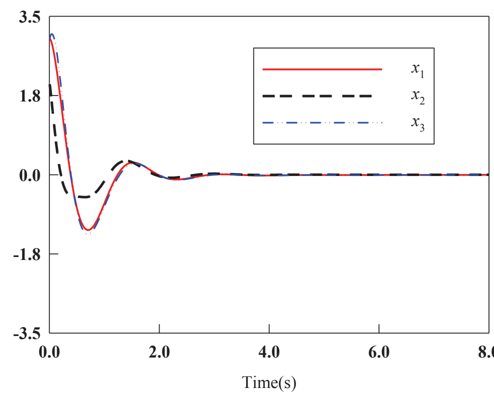

Fig. 8. Stabilization of Chen system (38).

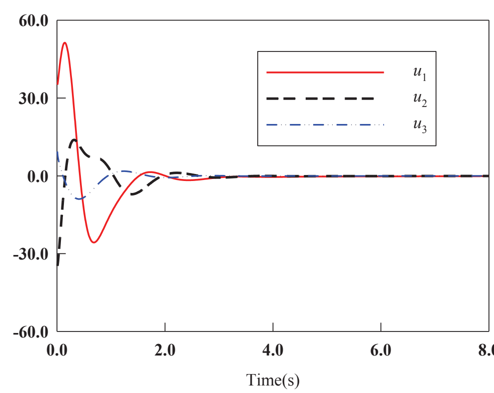

Fig. 9. Control inputs of Chen system (38).

On the basis of the above given simulation conditions, the numerical results are presented in Fig. 8-Fig. 13 for the Chen system (38), the Genesio's system (41), and the hyperchaotic Lorenz system (44). The control result of the Chen system (38) is shown in Fig. 8. It is illustrated that good control performance is obtained under the designed controller (39). Fig. 9 presents the control input (39). The numerical results of the Genesio's system (41) are given in Fig. 10 and Fig. 11. Fig. 10 and Fig. 11 show that the controller (42) can stabilize the Genesio's system (41) well. Finally, Fig. 12 and Fig. 13 show that the fractional-order controller (45) can control all state variables of the hyperchaotic Lorenz system (44) to the origin point. Therefore, all the simulation results show that the fractional-order controller also can control the chaotic and hyperchaotic systems with equilibrium.

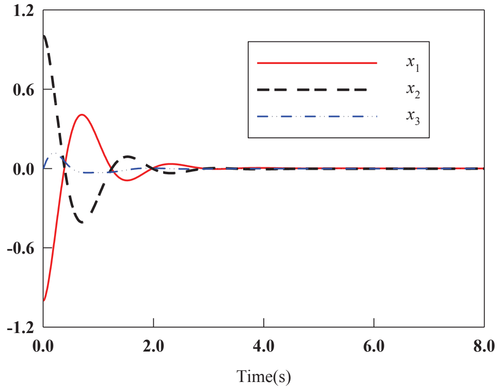

Fig. 10. Stabilization of Genesio's system (41).

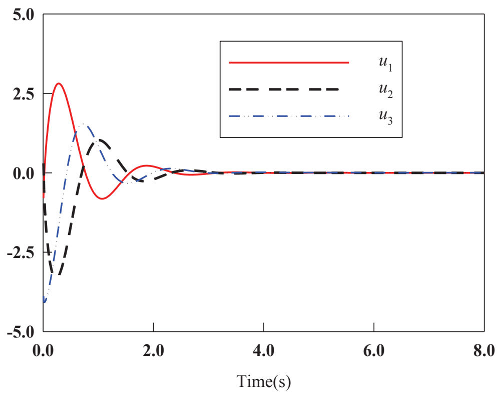

Fig. 11. Control inputs for Genesio's system (41).

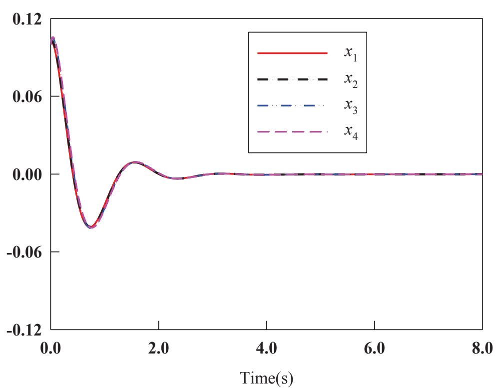

Fig. 12. Stabilization of hyperchaotic Lorenz system (44).

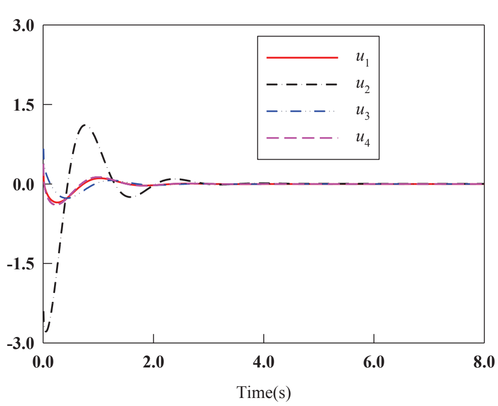

Fig. 13. Control inputs for hyperchaotic Lorenz system (44).

VI. Conclusion

In this paper, a novel chaotic system without equilibrium has been proposed. The Lyapunov exponents and Poincaré map of the proposed chaotic system have been given. Meanwhile, the dissipativeness of the new chaotic system has been illustrated. The chaotic circuit has been designed to demonstrate the physical realizability of the novel chaotic system. In addition, on the basis of the Gronwall inequality, the Laplace transform, the Mittag-Leffler function and the state-feedback method, a stability theorem for a class of closed-loop systems has been given. The designed controller has been developed to realize the stabilization of the closed-loop system. Furthermore, the proposed control scheme has been developed to control the chaotic and hyperchaotic systems with equilibrium, i.e. Chen system, Genesio's system and hyperchaotic Lorenz system. Finally, the numerical simulation results further illustrate the effectiveness of the developed control scheme.

References

[1] Lorenz E N. Deterministic nonperiodic flow. *Journal of the Atmospheric Sciences*, 1963, **20**(2): 130-141

[2] Rössler O E. An equation for continuous chaos. *Physics Letters A*, 1976, **57**(5): 397-398

[3] Liu C X, Liu T, Liu L, Liu K. A new chaotic attractor. *Chaos, Solitons & Fractals*, 2004, **22**(5): 1031-1038

[4] Li Y X, Tang W K S, Chen G R. Generating hyperchaos via state feedback control. *International Journal of Bifurcation and Chaos*, 2005, **15**(10): 3367-3375

[5] Chen A M, Lu J N, Lü J H, Yu S M. Generating hyperchaotic lü attractor via state feedback control. *Physica A: Statistical Mechanics and its Applications*, 2006, **364**: 103-110

[6] Chen W C. Nonlinear dynamics and chaos in a fractional-order financial system. *Chaos, Solitons & Fractals*, 2008, **36**(5): 1305-1314

[7] Das S, Gupta P K. A mathematical model on fractional lotka–volterra equations. *Journal of Theoretical Biology*, 2011, **277**(1): 1-6

[8] Wang X Y, Song J M. Synchronization of the fractional order hyperchaos lorenz systems with activation feedback control. *Communications in Nonlinear Science and Numerical Simulation*, 2009, **14**(8): 3351-3357

[9] Liu L, Liang D L, Liu C X. Nonlinear state-observer control for projective synchronization of a fractional-order hyperchaotic system. *Nonlinear Dynamics*, 2012, **69**(4): 1929-1939

[10] Jafari S, Sprott J C, Gohammad S M R H. Elementary quadratic chaotic flows with no equilibria. *Physics Letters A*, 2013, **377**(9): 699-702

[11] Pham V T, Volos C, Jafari S, Wei Z C, Wang X. Constructing a novel no-equilibrium chaotic system. *International Journal of Bifurcation and Chaos*, 2014, **24**(5): 1450073

[12] Wang X, Chen G R. Constructing a chaotic system with any number of equilibria. *Nonlinear Dynamics*, 2013, **71**(3): 429-436

[13] Pham V T, Rahma F, Frasca M, Fortuna L. Dynamics and synchronization of a novel hyperchaotic system without equilibrium. *International Journal of Bifurcation and Chaos*, 2014, **24**(6): 1450087

[14] Pecora L M, Carroll T L. Synchronization in chaotic systems. *Physical review letters*, 1990, **64**(8): 821-824

[15] Carroll T L, Pecora L M. Synchronizing chaotic circuits. *IEEE Transactions on Circuits and Systems*, 1991, **38**(4): 453-456

[16] Chen G R, Yu X H. *Chaos control: theory and applications*. New York: Springer, 2003.

[17] Miranda J M G. *Synchronization and control of chaos: an introduction for scientists and engineers*. London: Imperial College Press, 2004.

[18] Yang S K, Chen C L, Yau H T. Control of chaos in lorenz system. *Chaos, Solitons & Fractals*, 2002, **13**(4): 767-780

[19] Nazzal J M, Natsheh A N. Chaos control using sliding-mode theory. *Chaos, Solitons & Fractals*, 2007, **33**(2): 695-702

[20] Cai N, Jing Y W, Zhang S Y. Modified projective synchronization of chaotic systems with disturbances via active sliding mode control. *Communications in Nonlinear Science and Numerical Simulation*, 2010, **15**(6): 1613-1620

[21] Sun M, Tian L X, Jiang S M, Xu J. Feedback control and adaptive control of the energy resource chaotic system. *Chaos, Solitons & Fractals*, 2007, **32**(5): 1725-1734

[22] Yassen M T. Chaos control of chaotic dynamical systems using backstepping design. *Chaos, Solitons & Fractals*, 2006, **27**(2): 537-548
[23] Hua C C, Guan X P, Shi P. Adaptive feedback control for a class of chaotic systems. *Chaos, Solitons & Fractals*, 2005, **23**(3): 757-765
[24] Luo R Z, Zeng Y H. The adaptive control of unknown chaotic systems with external disturbance via a single input. *Nonlinear Dynamics*, 2015, **80**(1): 989-998
[25] Aghababa M P, Hashtarkhani B J. Synchronization of unknown uncertain chaotic systems via adaptive control method. *Journal of Computational and Nonlinear Dynamics*, 2015, **10**(5): 051004
[26] Gao S G, Dong H R, Ning B. Neural adaptive control of uncertain chaotic systems with input and output saturation. *Nonlinear Dynamics*, 2015, **80**(1): 375-385
[27] Xie W X, Wen C Y, Li Z G. Impulsive control for the stabilization and synchronization of lorenz systems. *Physics Letters A*, 2000, **275**(1): 67-72
[28] Doye I N, Voos H, Darouach M. Observer-based approach for fractional-order chaotic synchronization and secure communication. *IEEE Journal on Emerging and Selected Topics in Circuits and Systems*, 2013, **3**(3): 442-450
[29] Deng L W, Song S M. Synchronization of fractional order hyperchaotic systems based on output feedback sliding mode control. *Acta Automatica Sinica*, 2014, **40**(11): 2420-2427
[30] Xu Y, Wang H, Li Y G, Pei B. Image encryption based on synchronization of fractional chaotic systems. *Communications in Nonlinear Science and Numerical Simulation*, 2014, **19**(10): 3735-3744
[31] Oustaloup A, Sabatier J, Lanusse P. From fractal robustness to the CRONE control. *Fractional Calculus and Applied Analysis*, 1999, **2**(1): 1-30
[32] Podlubny I. Fractional-order systems and $PI^{\lambda}D^{\mu}$-controller. *IEEE Transactions on Automatic Control*, 1999, **44**(1): 208-214
[33] Li T Z, Yu W, Luo M K. Control of fractional chaotic and hyperchaotic systems based on a fractional order controller. *Chinese Physics B*, 2014, **23**(8): 80501
[34] Son N N, Anh H P H. Adaptive backstepping self-balancing control of a two-wheel electric scooter. *International Journal of Advanced Robotic Systems*, 2014, doi: 10.5772/59100
[35] Podlubny I. *Fractional Differential Equations*. London: Academic Press, 1999.
[36] Li Y, Chen Y Q, Podlubny I. Mittag-leffler stability of fractional order nonlinear dynamic systems. *Automatica*, 2009, **45**(8): 1965-1969
[37] Sadati S J, Baleanu D, Ranjbar A, Ghaderi R, Abdeljawad T. Mittag-leffler stability theorem for fractional nonlinear systems with delay. *Abstract and Applied Analysis*, 2010, **2010**: Article ID 108651
[38] Liu S, Li X Y, Jiang W, Zhou X F. Mittag-leffler stability of nonlinear fractional neutral singular systems. *Communications in Nonlinear Science and Numerical Simulation*, 2012, **17**(10): 3961-3966
[39] Qian D L, Li C P, Agarwal R P, Wong P J Y. Stability analysis of fractional differential system with Riemann-Liouville derivative. *Mathematical and Computer Modelling*, 2010, **52**(5): 862-874.
[40] Zhang F R, Li C P. Stability analysis of fractional differential systems with order lying in (1, 2). *Advances in Difference Equations*, 2011, **2011**: Article ID 213485
[41] Qin Z Q, Wu R C, Lu Y F. Stability analysis of fractional-order systems with the Riemann-Liouville derivative. *Systems Science & Control Engineering*, 2014, **2**(1): 727-731
[42] Kilbas A K, Srivastava H M, Trujillo J J. *Theory and applications of fractional differential equations*. New York: Elsevier, 2006.
[43] Chen L P, He Y G, Chai Y, Wu R C. New results on stability and stabilization of a class of nonlinear fractional-order systems. *Nonlinear Dynamics*, 2014, **75**(4): 633-641
[44] Ye H P, Gao J M, Ding Y S. A generalized Gronwall inequality and its application to a fractional differential equation. *Journal of Mathematical Analysis and Applications*, 2007, **328**(2): 1075-1081
[45] Wu Z B, Zou Y Z. Global fractional-order projective dynamical systems. *Communications in Nonlinear Science and Numerical Simulation*, 2014, **19**(8): 2811-2819
[46] Yu S M. *Chaotic Systems and Chaotic Circuits: Principle, Design and its Application in Communications*. Xi'an: Xidian University press, 2011.
[47] Wen X J, Wu Z M, Lu J G. Stability analysis of a class of nonlinear fractional-order systems. *IEEE Transactions on Circuits and Systems II: Express Briefs*, 2008, **55**(11): 1178-1182
[48] Hua C C, Guan X P. Adaptive control for chaotic systems. *Chaos, Solitons & Fractals*, 2004, **22**(1): 55-60
[49] Liu L P, Han Z Z, Li W L. Global sliding mode control and application in chaotic systems. *Nonlinear Dynamics*, 2009, **56**(1): 193-198
[50] Jia Q. Hyperchaos generated from the lorenz chaotic system and its control. *Physics Letters A*, 2007, **366**(3): 217-222
[51] Petráš I. *Fractional-Order Nonlinear Systems: Modeling, Analysis and Simulation*. Beijing: Higher Education Press, 2011.

Shu-Yi Shao received the M.S. degree in Control Theory and Control Engineering from Nanjing Normal University, Nanjing, China, in 2014. He is currently working toward the PH.D. degree with major in Control Theory and Control Engineering from College of Automation Engineering, Nanjing University of Aeronautics and Astronautics, Nanjing, China. His research interests include fractional-order nonlinear system control and applications of chaos synchronization.

Mou Chen received the B.S. degree in Material Science and Engineering in 1998 and the M.S. and Ph.D. degrees in Automatic Control Engineering from the Nanjing University of Aeronautics and Astronautics (NUAA), Nanjing, China, in 1998 and 2004, respectively.

He is currently a Full Professor in the College of Automation Engineering at NUAA. He was an Academic Visitor in the Department of Aeronautical and Automotive Engineering at Loughborough University, U.K., from November 2007 to February 2008. From June 2008 to September 2009, he was a Research Fellow in the Department of Electrical and Computer Engineering at the National University of Singapore. He was a Senior Academic Visitor in the School of Electrical and Electronic Engineering at the University of Adelaide, Australia, from May 2014 to November 2014.

His research interests include nonlinear system control, intelligent control, and flight control.

Fuzzy Adaptive Control of a Fractional Order Chaotic System with Unknown Control Gain Sign Using a Fractional Order Nussbaum Gain

Khatir Khettab, Samir Ladaci, *Member, IEEE*, and Yassine Bensafia

***Abstract*—In this paper we propose an improved fuzzy adaptive control strategy, for a class of nonlinear chaotic fractional order (SISO) systems with unknown control gain sign. The online control algorithm uses fuzzy logic sets for the identification of the fractional order chaotic system, whereas the lack of a priori knowledge on the control directions is solved by introducing a fractional order Nussbaum gain. Based on Lyapunov stability theorem, stability analysis is performed for the proposed control method for an acceptable synchronization error level. In this work, the Grünwald-Letnikov method is used for numerical approximation of the fractional order systems. A simulation example is given to illustrate the effectiveness of the proposed control scheme.**

***Index Terms*—Adaptive fuzzy control, nonlinear fractional order systems, fractional order Nussbaum function, chaos synchronization, Lyapunov stability.**

I. Introduction

FHERE order chaotic systems are gathering an important research effort because of their powerful properties and potential applications in secure communication and control processing. Many mathematical models have been developed in literature such as the fractional-order Chua system[1], the fractional-order Duffing system[2], the fractional-order Lü system and the fractional order Chen system[3]. Since the work of Deng and Li[4] who investigated the synchronization problem of fractional order chaotic Lü systems, many studies were focused on the control and synchronization of fractional order chaos[5−6].

This article has been accepted for publication in a future issue of this journal, but has not been fully edited. Content may change prior to final publication.

This work was supported by the Algerian Ministry of Higher Education and Scientific Research (MESRS) for CNEPRU Research Project No. A01L08UN210120110001. Recommended by Associate Editor Dingyü Xue.

Khatir Khettab is with University of Mohamed Boudiaf, Electrical Engineering Department, 28000 M'sila, Algeria, and also with University of Skikda, Electrical Engineering Department, 21000 Skikda, Algeria (e-mail: zoubirhh@yahoo.fr).

Samir Ladaci is with the National Polytechnic School of Constantine, EEA Department, B.P. 75 A, Ali Mendjli, 25000 Constantine, Algeria, and also with SP-Lab Laboratory, Department of Electronics, Mentouri University, Route de Ain Elbey, Constantine, 25000, Algeria. (e-mail: samir_ladaci@yahoo.fr).

Yassine Bensafia is with University of Bouira, Electrical Engineering Department, 10000 Bouira, Algeria (e-mail: bensafiay@yahoo.fr).

Digital Object Identifier 10.1109/JAS.2016.7510169

In this paper we are concerned by fractional adaptive control of nonlinear fractional order systems using Fuzzy logic identification technique. Fractional adaptive systems have been largely investigated for a decade as they showed an improved behavior comparatively to classical adaptive control for partially unknown plants [7−10].

Based on the universal approximation theorem, adaptive fuzzy control systems present an effective control solution for a large class of nonlinear systems[11]. The adaptive controller is synthesized from a collection of fuzzy IF-THEN rules and the parameters of the membership functions characterizing the linguistic terms in the IF-THEN rules change according to some adaptive law for the purpose of controlling a plant to track a reference trajectory[12−13].

A particular class of such nonlinear plants pose the challenging control problem with unknown control directions[15]. The Nussbaum function approach was introduced in the 1980's[16]. This technique was used for adaptive control of first-order nonlinear systems in[17]. Later, many studies of adaptive control schemes with Nussbaum function were successfully carried out for different classes of nonlinear systems[18−20].

The main contribution of this study is the introduction of a Nussbaum function in the fuzzy adaptive control scheme for nonlinear fractional systems with unknown control gain sign. Stability analysis of the proposed adaptive fuzzy control system is performed using Lyapunov stability theory. Moreover, the influence of the approximation error and external disturbance on the tracking error can be attenuated to an arbitrarily prescribed level via the proposed design technique. The fuzzy adaptive control design with Nussbaum function is applied for nonlinear fractional order chaotic systems with a large uncertainty or unknown variation in plant parameters and structures. The Grünwald-Letnikov technique is used for the numerical approximation of the fractional order chaotic system[21].

This paper is organized as follows: in Section II, basic definitions and preliminaries for fractional order systems are presented with the numerical approximation technique. A description of the Nussbaum-type function is given in Section III. Section IV presents the fuzzy adaptive control scheme with unknown control direction for uncertain fractional order chaotic systems in the presence of uncertainty.

The proposed control system stability proof is detailed in Section V. In Section VI, application of the proposed method on fractional order chaotic Duffing systems is investigated. Finally, the simulation results and conclusion are presented in Section VII.

II. Basics of fractional order systems

A. Fractional Derivatives and Integrals

The mathematical definition of fractional derivatives and integrals has been the subject of several descriptions. The three most frequently used definitions for the general fractional differ-integral are: the Grünwald-Letnikov (GL) definition, the Riemann-Liouville (RL) and the Caputo definition[9],[21]. The Riemann-Liouville (RL) definition of the fractional order integral is given by:

$$ {}_{a}^{RL}D_t^{-\mu} f(t) = \frac{1}{\Gamma(\mu)} \int_a^t (t-\tau)^{\mu-1} f(\tau) d(\tau), \tag{1}$$

while the definition of fractional order derivatives is

$$\begin{aligned} {}_{a}^{RL}D_t^{\mu} f(t) &= \frac{d}{dt}\left[{}_{a}^{RL}D_t^{-(1-\mu)} f(t)\right], \qquad (2)\\ &= \frac{1}{\Gamma(1-\mu)} \frac{d}{dt} \int_a^t (t-\tau)^{-\mu} f(\tau) d(\tau), \end{aligned}$$

where

$$\Gamma(x) = \int_0^\infty y^{x-1} e^{-y} dy, \tag{3}$$

where $\Gamma(.)$ is the Euler's Gamma function, a and t are the limits of the operation, and μ is the number identifying the fractional order. In this paper, μ is assumed to be a real number that satisfies the restriction $0 < \mu < 1$. Also, it is assumed that $a = 0$. The following convention is used: ${}_aD_t^\mu \equiv D^\mu$.

B. Numerical Approximation Method

Many different approaches have been proposed to model fractional order systems. The numerical simulation of such systems depends on the way to approximate the fractional derivative operator. The most common approach used in the fractional order chaotic systems literature is an improved version of the Adams-Bashforth-Moulton method based on predictor-correctors[22−23]. However, we will use in this work a simpler approach consisting of the fractional order derivative operator discretization according to the Grünwald-Letnikov method. This method is very simple to use and has approximately the same order of accuracy as the predictor-corrector method, even if the simulation requires, for each step the computation of sums of increasing dimension with time.

The Grünwald-Letnikov fractional order derivative definition is expressed as:

$$ {}_{a}^{GL}D_t^{-\mu} = \lim_{h\to 0} \frac{1}{h^\mu} \sum_{j=0}^{\left[\frac{t-a}{h}\right]} (-1)^j \begin{pmatrix} \mu \\ j \end{pmatrix} f(t-jh), \tag{4}$$

where $\left[\frac{t-a}{h}\right]$ indicates the integer part and $(-1)^j \begin{pmatrix} \mu \\ j \end{pmatrix}$ are binomial coefficients $c_j^{(\mu)}$, $(j = 0, 1, \ldots)$.

The calculation of these coefficients is done by a formula of following recurrence:

$$c_0^{(\mu)} = 1;\ c_j^{(\mu)} = \left(1 - \frac{1+\mu}{j}\right) c_{j-1}^{(\mu)}.$$

The general numerical solution of the fractional differential equation,

$$ {}_{a}^{GL}D_t^{-\mu} = f\left(y(t)\right), \tag{5}$$

can be expressed as follows:

$$y(t_k) = f\left(y(t_k), t_k\right) h^\mu - \sum_{j=0}^{k} c_j^{(\mu)} y(t_{k-j}). \tag{6}$$

This approximation of the fractional derivative within the meaning of Grünwald-Letnikov is on the one hand equivalent to the definition of Riemman-Liouville for a broad class of functions[24], and on the other hand, it is well adapted to the definition of Caputo (Adams method) because it requires only the initial conditions and has a clear physical direction.

III. Nussbaum-type gain

Definition 1: A function $N(\zeta)$ is called a Nussbaum-type function if it has the following properties[14],[25−27]:

$$\lim_{s\to\infty} \sup \frac{1}{s} \int_0^s N(\zeta) d\zeta = +\infty, \tag{7}$$

$$\lim_{s\to\infty} \inf \frac{1}{s} \int_0^s N(\zeta) d\zeta = -\infty. \tag{8}$$

The continuous functions $N_1(\zeta) = \zeta^2 \cos(\zeta)$, $N_2(\zeta) = \zeta \cos(\sqrt{|\zeta|})$, $N_3(\zeta) = \cos(\frac{\pi}{2}\zeta) e^{\zeta^2}$ and $N_4(\zeta) = \ln(\zeta + 1) \cos(\sqrt{\ln(\zeta+1)})$ are Nussbaum functions.
For example the continuous function $N_1(\zeta) = \zeta^2 \cos(\zeta)$, is positive at interval $(2\pi n, 2\pi n + \frac{\pi}{2})$ and negative at the interval $(2\pi n + \frac{\pi}{2}, 2\pi n + \frac{3\pi}{2})$, where n is an integer. And we have,

$$\frac{1}{2\pi n + \frac{\pi}{2}} \int_0^{2\pi n + \frac{\pi}{2}} N_1(\zeta) d\zeta = +\infty,$$

$$\frac{1}{2\pi n + \frac{3\pi}{2}} \int_0^{2\pi n + \frac{3\pi}{2}} N_1(\zeta) d\zeta = -\infty.$$

The following lemma[28] is used in the stability analysis.

Lemma 1: Consider the following fractional-order system,

$$D^\alpha y(t) = -a y(t) + b. \tag{9}$$

then there exists a constant $t_0 > 0$ such that for all $t \in (t_0, \infty)$,

$$\|y(t)\| \le \frac{2b}{a}, \tag{10}$$

where $y(t)$ is the state variable, and a, b are two positive constants.

The proof of Lemma 1 can be found in[28].
A Nussbaum function will be used in future work, to estimate the control direction.

IV. Problem Statement

Consider a fractional order SISO nonlinear dynamic system of the form:

$$\begin{cases} x_1^{(q_1)} = x_2, \\ \vdots, \\ x_{n-1}^{(q_{n-1})} = x_n, \\ x_n^{(q_n)} = f(\underline{x},t) + g(\underline{x},t)u + d(t), \\ y = x_1, \end{cases} \tag{11}$$

where,
$\underline{x} = [x_1, x_2, ..., x_n]^{\mathrm{T}} = [x, x^{(q)}, x^{(2q)}, ..., x^{((n-1)q)}]^{\mathrm{T}} \in \mathbf{R}^n$ is the system's state vector, $u \in \mathbf{R}$ is the control input and $y \in \mathbf{R}$ is the output, with the initial conditions : $u(0) = 0$ and $y(0) = 0$.
The initial conditions are set to zero to avoid the lack of robustness for Nussbaum type adaptive controllers as proved by Georgiou and Smith[29],
If $q_1 = q_2 = ... = q_n = q$ the above system is called a commensurate order system. Then an equivalent form of the above system is described as :

$$\begin{cases} x^{(nq)} = f(\underline{x},t) + g(\underline{x},t)u + d(t), \\ y = x_1, \end{cases} \tag{12}$$

where $f(\underline{x},t)$ and $g(\underline{x},t)$ are unknown but bounded nonlinear functions which express system dynamics and $d(t)$ is the external bounded disturbance. The control objective is to force the system output $\underline{y}$ to follow a given bounded reference signal $\underline{y}_d$, under the constraint that all signals involved must be bounded.
The reference signal vector $\underline{y}_d$ and the tracking error vector $\underline{e}$ are defined as,

$$\begin{aligned} \underline{y}_d &= [y_d,\, y_d^{(q)},\, y_d^{(2q)},\, ...,\, y_d^{((n-1)q)}]^{\mathrm{T}} \in \mathbf{R}^n, \\ \underline{e} &= \underline{y}_d - \underline{y} = [e,\, e^{(q)},\, ...,\, e^{((n-1)q)}]^{\mathrm{T}} \in \mathbf{R}^n, \\ e^{(iq)} &= y_d^{(iq)} - y^{(iq)}. \end{aligned}$$

Let $\underline{k} = [k_1,\, k_2,\, ...,\, k_n]^{\mathrm{T}} \in \mathbf{R}^n$ be chosen such that the stability condition $|\arg(eig(A))| > q\pi/2$ is met, where $0 < q < 1$ and $eig(A)$ represents the eigenvalues of the system state matrix.

i) Let us first suppose that the functions $f(\underline{x},t)$ and $g(\underline{x},t)$ are known and the system is free of external disturbance (i.e. $d(t) = 0$).
The following assumptions are considered[19−20],

Assumption 1: The control gain $g(\underline{x},t)$ is not zero and of known sign. It is also strictly positive or strictly negative.

Assumption 2: The external disturbance is bounded: $|d(t)| \le D$ with D an unknown positive constant.

Then the control law of the certainty equivalent controller is obtained as[30],

$$u^* = \frac{1}{g(\underline{x},t)}\left(-f(\underline{x},t) + y_d^{(nq)} + k^T e\right), \tag{13}$$

where

$$\begin{aligned} \underline{y}_d &= [y_d,\, y_d^{(q)},\, y_d^{(2q)},\, ...,\, y_d^{((n-1)q)}]^{\mathrm{T}} \in \mathbf{R}^n, \\ \underline{e} &= \underline{y}_d - \underline{y} = [e,\, e^{(q)},\, ...,\, e^{((n-1)q)}]^{\mathrm{T}} \in \mathbf{R}^n, \\ e^{(iq)} &= y_d^{(iq)} - y^{(iq)}, \end{aligned}$$

is the tracking error vector.
Substituting (13) into (12), we have:

$$e^{nq} = k_n e^{(n-1)q} + \cdots + k_1 e = 0, \tag{14}$$

which is the main objective of control, $\lim_{t\to\infty} e(t) = 0$.

ii) However, $f(\underline{x},t)$ and $g(\underline{x},t)$ are unknown and external disturbance $d(t) \neq 0$, the ideal control effort (13) cannot be implemented; this problem was solved by the control strategy proposed previously by the use of fuzzy systems to approximate unknown functions[13]. In this case, we consider the following assumptions[19−20]:

Assumption 3: The state vector x is not measurable, except the system output y.

Assumption 4: The reference trajectory $y_d(t)$ and its derivatives up to order (nq) are known, continuous and bounded.

Assumption 5: The control gain $g(\underline{x},t)$ is not zero and of unknown sign.

Remark 1: In Assumption 5, and contrary to the previous case, the sign of $g(\underline{x},t)$ need not to be known, as the *Nussbaum* technique will estimate the control gain sign.

From Definition 1, one knows that Nussbaum functions should have infinite gains and infinite switching frequencies. Subsequently to this part, the Nussbaum function

$$N(\zeta) = \zeta^2\cos(\zeta),$$

will be used for the control of nonlinear chaotic systems.
By substituting (13) into (12) we obtain the closed loop control system in the state space domain as follows:

$$\begin{aligned} \underline{x}^{(nq)} &= A\underline{x} + B[f(\underline{x}) + g(\underline{x})u], \\ y &= c^T\underline{x}, \end{aligned} \tag{15}$$

where

$$A = \begin{bmatrix} 0 & 1 & 0 & 0 & \cdots & 0 & 0 \\ 0 & 0 & 1 & 0 & \cdots & 0 & 0 \\ \vdots & \vdots & \vdots & \vdots & \ddots & \vdots & \vdots \\ 0 & 0 & 0 & 0 & \cdots & 0 & 1 \\ -k_1 & -k_2 & -k_3 & -k_4 & \cdots & -k_{(n-1)} & -k_n \end{bmatrix},$$

$$B = \begin{bmatrix} 0 \\ 0 \\ \vdots \\ 0 \\ 1 \end{bmatrix} \text{ and, } \quad c = \begin{bmatrix} 1 \\ 0 \\ \vdots \\ 0 \\ 0 \end{bmatrix}.$$

By using the relation $y_d^{(q)} = Ay_d + By_d^{(nq)}$ the following equation (16) is obtained:

$$\begin{aligned} \underline{e}^{(q)} &= A\underline{e} + B[f(\underline{x}) + g(\underline{x})u^* - y_d^{(nq)}], \\ e &= c^T\underline{e}. \end{aligned} \tag{16}$$

In what follows, a fuzzy adaptive control will be designed to stabilize the system (11) or the equivalent system (16).
Replacing $f(\underline{x})$ by the fuzzy system $f(\underline{x},\theta_f)$ which is specified as:

$$f(\underline{x},\theta_f) = \theta_f^T\xi(\underline{x}). \tag{17}$$

Here the fuzzy basis function $\xi(\underline{x})$ depends on the fuzzy membership functions and is supposed to be fixed, while θ_f is the adjusted by adaptive laws based on a Lyapunov stability criterion.

Using (17), (16) can be rewritten as following:

$$\begin{aligned} \underline{e}^{(q)} &= A\underline{e}+B[\xi^T(\underline{x})\theta_f+g(\underline{x})u^*-y_d^{(nq)}], \\ e &= c^T\underline{e}. \end{aligned} \tag{18}$$

The optimal parameter estimation vector θ_f^* is defined by:

$$\theta_f^*=\arg\min_{\theta_f\in\Omega_f}\left[\sup_{x\in\Omega_x}|f(\underline{x}\mid\theta_f)-f(\underline{x},t)|\right]. \tag{19}$$

with $\phi_f=\theta_f-\theta_f^*$ and Ω_f,Ω_x are constraints sets for θ_f and x respectively, and are defined as:

$$\begin{aligned} \Omega_f &= \{\theta_f \mid \ |\theta_f|\le M_f\}, \\ \Omega_x &= \{x \mid \ |x|\le M_x\}, \end{aligned} \tag{20}$$

where M_f and M_x are positive constants.

The following theorem is proposed to show the control performance of the closed loop system.

Theorem 1: Considering system (12), and the fuzzy adaptive control law proposed with fractional Nussbaum function is given as follows:

$$u^*=N(\zeta)\left[k^T\underline{e}+\theta_f^T\xi(\underline{x})-y_d^{nq}\right], \tag{21}$$

where $N(\zeta)=\zeta^2\cos(\zeta)$ and,

$$\zeta^{(q)}=\underline{e}^TPB\left[k^T\underline{e}+r_1\theta^T\xi(\underline{x})-y_d^{(nq)}\right], \tag{22}$$

and the fractional adaptive law for the vector θ is chosen as following:

$$\theta^{(q)}=-r_1\theta+r_1\underline{e}^TPB\xi(\underline{x}), \tag{23}$$

where r_1 is a positive constant, and $P=P^T>0$ is a positive definite matrix, also there is a positive definite symmetric matrix $Q=Q^T$ satisfying the following Lyapunov equation:

$$A_cP+PA_c^T+PBB^TP=-Q.$$

We choose $A_c=A-B\underline{k}^T$ is Hurwitz. So all signals in the closed loop system are bounded and the tracking error converges to a bounded compact set defined by $\Omega=\{e_1,|e_1|\le a_1\}$, where a_1 is a positive constant.

V. Stability Analysis

The Lyapunov function is chosen as

$$V=\frac{1}{2}\underline{e}^TP\underline{e}+\frac{1}{2r_1}\phi_f^T\phi_f. \tag{24}$$

The derivative of (24) with respect to time verifies[31−32]:

$$V^{(q)}(t)\le\frac{1}{2}(\underline{e}^{(q)})^TP\underline{e}+\frac{1}{2}\underline{e}^T(t)P\underline{e}^{(q)}(t)+\frac{1}{r_1}\phi_f^T\phi_f^{(q)}. \tag{25}$$

By substituting (18) into (25), we obtain:

$$\begin{aligned} V^{(q)}(t)\le{}&\frac{1}{2}\underline{e}^T\left(PA+A^TP\right)\underline{e}+\frac{1}{r_1}\phi_f^T\phi_f^{(q)} \\ &+\underline{e}^TPB\left[\xi(\underline{x})\theta_f^T+gu^*-y_d^{(nq)}\right]. \end{aligned} \tag{26}$$

By using (21) and (22), (26) becomes:

$$\begin{aligned} V^{(q)}(t)\le{}&\frac{1}{2}\underline{e}^T\left(PA+A^TP\right)\underline{e}+\frac{1}{r_1}\phi_f^T\phi_f^{(q)} \\ &+\underline{e}^TPB\left[\xi(\underline{x})\theta_f^T+gu^*-y_d^{(nq)}\right]-\underline{e}PB\theta_f^T\xi(\underline{x}) \\ \le{}&\frac{1}{2}\underline{e}^T\left(PA+A^TP\right)\underline{e}+\phi_f^T\left[\frac{1}{r_1}\phi_f^{(q)}-\underline{e}^TPB\xi(\underline{x})\right] \\ &+\underline{e}^TPB\left[\xi(\underline{x})\theta_f^T-y_d^{(nq)}\right]+\underline{e}^TPBgN(\zeta)\left(k^T\underline{e}\right. \\ &\left.+\xi(\underline{x})\theta_f^T-y_d^{(nq)}\right) \\ \le{}&\frac{1}{2}\underline{e}^T\left(PA_c+A_c^TP\right)\underline{e}+\phi_f^T\left[\frac{1}{r_1}\phi_f^{(q)}-\underline{e}^TPB\xi(\underline{x})\right] \\ &+\left[gN(\zeta)+1\right]\zeta^{(q)}. \end{aligned} \tag{27}$$

Using (23), the following inequality is obtained

$$\begin{aligned} \phi_f^T\left[\frac{1}{r_1}\phi_f^{(q)}-\underline{e}^TPB\xi(\underline{x})\right]&=-\phi_f^T\theta=-\phi_f^T\phi_f-\phi_f^T\theta_f^* \\ &\le-\frac{1}{2}\phi_f^T\phi_f+\frac{1}{2}\left\|\theta_f^*\right\|^2. \end{aligned} \tag{28}$$

And thus (Young inequality),

$$\underline{e}^TPB\le\frac{1}{2}\underline{e}^TPBB^TP\underline{e}+\frac{1}{2}b^2, \tag{29}$$

where b is a positive constant.

By Substituting (28) and (29) into (27), the following inequality is obtained:

$$\begin{aligned} V^{(q)}(t)\le{}&\frac{1}{2}\underline{e}^T\left(PA_c+A_c^TP\right)\underline{e}+\frac{1}{2}\underline{e}^TPBB^TP\underline{e} \\ &+\frac{1}{2}b^2-\frac{1}{2}\phi_f^T\phi_f+\frac{1}{2}\left\|\theta_f^*\right\|^2+\left[gN(\zeta)+1\right]\zeta^{(q)} \\ \le{}&-\frac{1}{2}\underline{e}^TQ\underline{e}+\frac{1}{2}b^2-\frac{1}{2}\phi_f^T\phi_f+\frac{1}{2}\left\|\theta_f^*\right\|^2 \\ &+\left[gN(\zeta)+1\right]\zeta^{(q)} \end{aligned} \tag{30}$$

where $\mu=\lambda_{min}(QP^{-1},r_1)$ and $\beta=\left\|\theta_f^*\right\|^2+\frac{1}{2}b^2$.

The inequality (30) can be expressed as:

$$V^{(q)}\le-\mu V+\omega, \tag{31}$$

where $\omega=\beta+\left[gN(\zeta)+1\right]\zeta^{(q)}$.

Then depending on the sign of ω two cases arise:

1) If $\omega\le 0$ then we have $V^{(q)}\le 0$ and the uniform continuity of the fractional order derivative (3) allows to apply Barbalats lemma[33]. Hence, $V(t)$ is bounded and e and θ_f are also bounded.
2) If $\omega>0$ then according to Lemma 1, we have

$$\|V(t)\|\le\frac{2\omega}{\mu}. \tag{32}$$

which yields that

$$\|e(t)\| \leq 2\sqrt{\frac{\omega}{\mu\lambda_{min}(P)}}.$$

This means that $\|e(t)\|$ can be made arbitrarily small, and θ_f is bounded. From (21), u is bounded. Then all the signals in the closed loop system are bounded.

The diagram of the proposed control is given in Fig. 1.

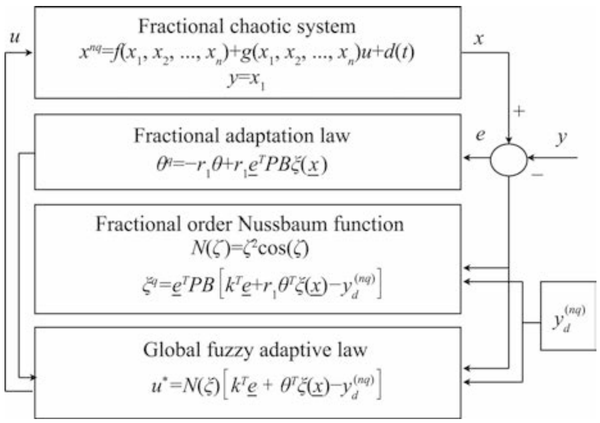

Fig. 1. Global block diagram of the proposed fuzzy adaptive control with unknown control sign gain.

VI. Simulation results

To illustrate the performance of the proposed control approach, we consider two fractional order chaotic systems of Duffing as follows [34],

The first one is a reference system:

$$\begin{aligned} D^q y_{d1} &= y_{d2}, \\ D^q y_{d2} &= 1.2\, y_{d1} - y_{d2} - y_{d1}^2 + 0.5\cos(t). \end{aligned} \tag{33}$$

The second is the response system (to be controlled):

$$\begin{aligned} D^q y_1 &= y_2, \\ D^q y_2 &= y_1 - 1.8\, y_2 - y_1^2 + 0.9\cos(t) + u(t) + d(t). \end{aligned} \tag{34}$$

Initial conditions are selected as follows:
$y_d(0) = [0, 0]^{\mathrm{T}}$ and $y(0) = [1, -1]^{\mathrm{T}}$.
We consider in this case the fractional order value $q = 0.98$, with the external disturbance $d(t) = 0.1\sin(t)$.

The other design constants are set as:
$k_1 = k_2 = 1$, $r_1 = 200$, $\rho = 0.05$, $h = 0.01$ and $T_{sim} = 40\ s$.

The main objective is to control our response system to track the reference system output with consideration that the functions $f(\underline{x}, t)$ and $g(\underline{x}, t)$ are completely unknown.

Fig. 2 shows the phase plane without the studied control systems.

Results & Discussion:

- According to the Fig. 4, the trajectories of the responses converge accurately to the reference trajectories, even in the presence of external disturbances.
- One can remark the vibrations in the beginning of Fig. 4(b) and Fig. 4(c). This transitory phase is necessary for converge of the system model estimated parameters. They depend mainly on the arbitrary choice of initial conditions.

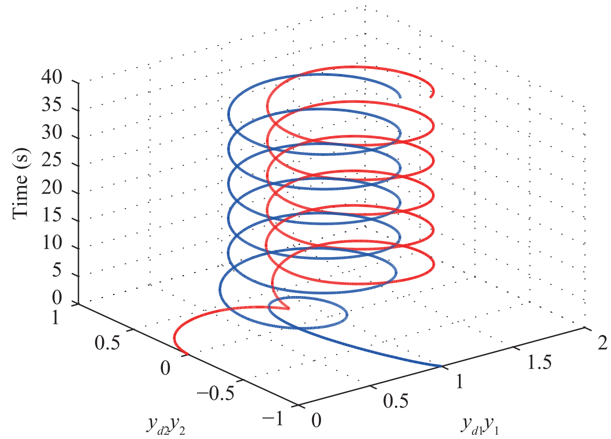

Fig. 2. Phase portrait of Duffing chaotic systems (without control action).

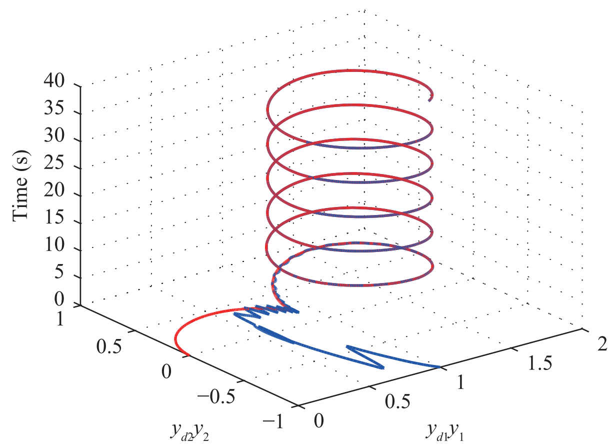

Fig. 3. Synchronization performance of Duffing chaotic drive and response systems.

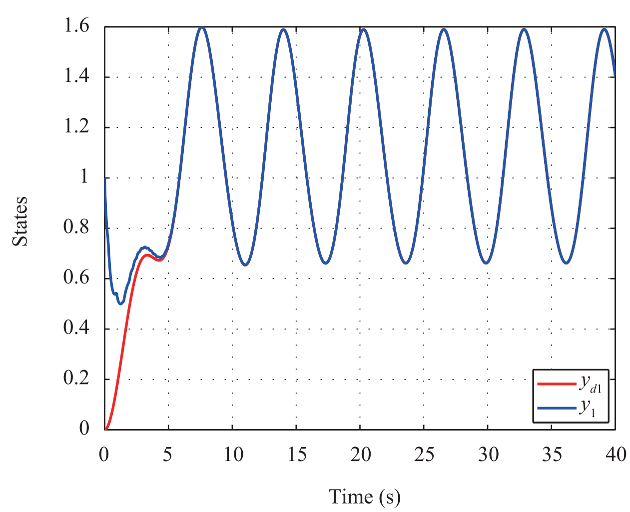

Fig. 4. (a) Trajectories of the states of systems y_1 and y_{d1}.

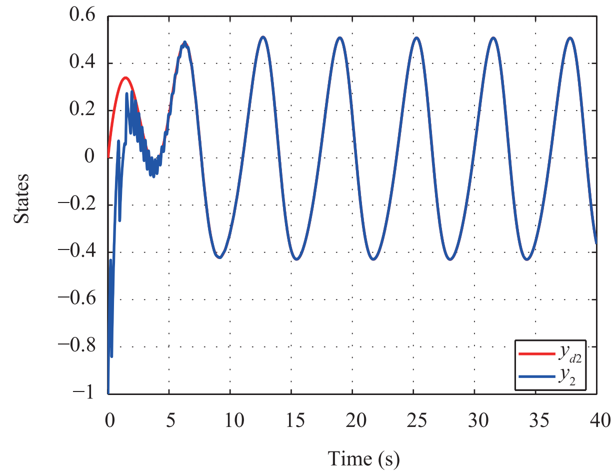

Fig. 4. (b) Trajectories of the states of systems y_2 and y_{d2}.

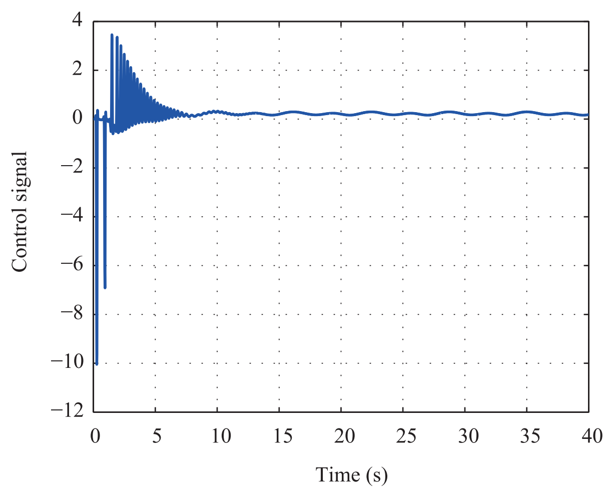

Fig. 4. (c) Control signal $u(t)$.

- Fig. 5 shows that the errors are bounded and converge asymptotically to zero.
- From Fig. 6 and Fig. 7 one can remark that the adopted settings and the function of Nussbaum which estimates the sign of control gain are always bounded.

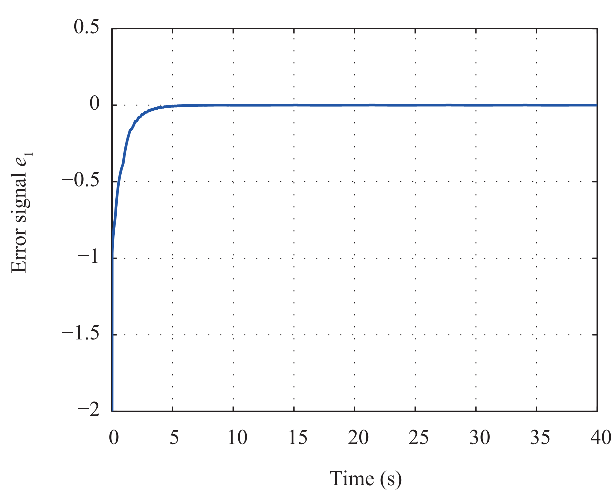

Fig. 5. (d) The error signal $e_1 = y_1 - y_{d1}$.

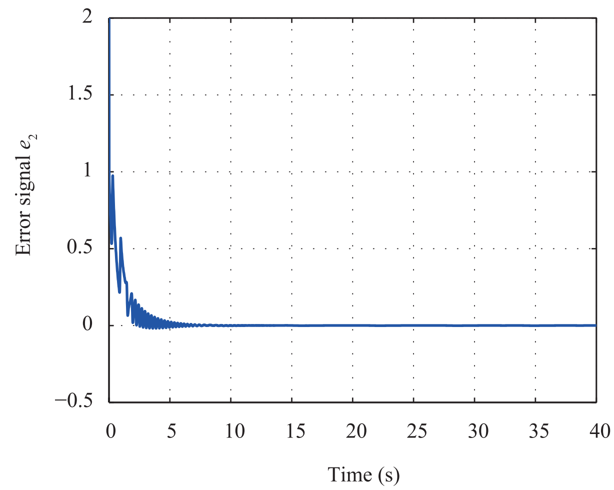

Fig. 5. (e) The error signal $e_2 = y_2 - y_{d2}$.

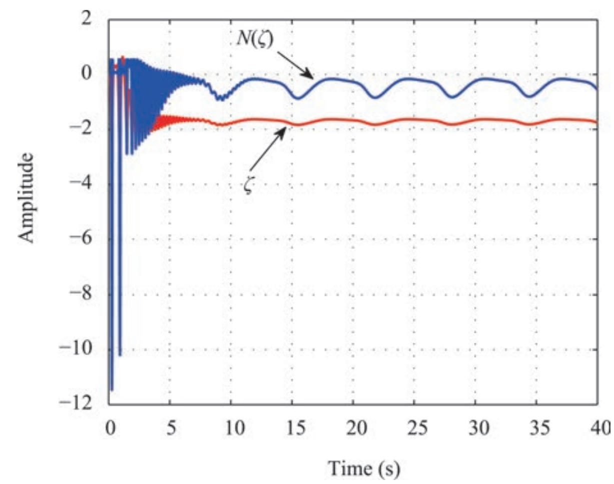

Fig. 6. Nussbaum function $N(\zeta)$ and its variation $\zeta(t)$.

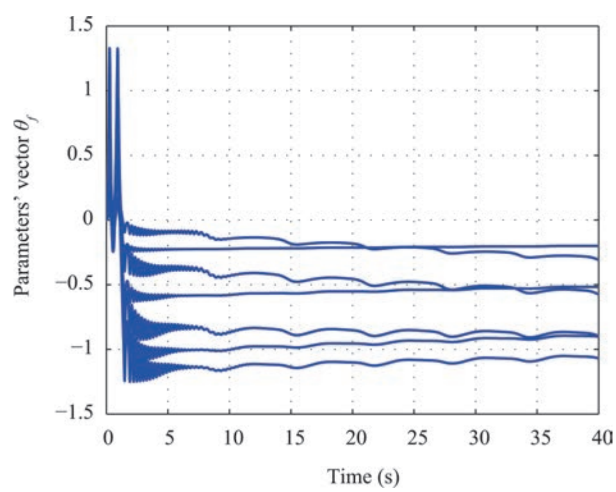

Fig. 7. Optimal parameters vector $\theta_f(t)$.

VII. CONCLUSION

In this work, a fuzzy adaptive control scheme is proposed for a class of nonlinear fractional order SISO systems with unknown control gain sign. The fuzzy systems were used to approximate online the unknown dynamics including all nonlinearities of the system. The numerical approximation of the fractional order systems is realized by means of the Grünwald-Letnikov method.

The main contribution of this paper is to introduce the technique of fractional order Nussbaum-type function to estimate the control gain sign for the fractional chaotic system. The developed controller guarantees the boundedness of all the signals in the closed-loop and the tracking error convergence. Simulation results show the good tracking performance of the proposed fuzzy adaptive control method.

REFERENCES

[1] Petráš I. A note on the fractional-order Chua's system. *Chaos, Solitons and Fractals*, 2008, **38**(1): 140−147.

[2] Gao X, Yu J. Chaos in the fractional order periodically forced complex Duffing's oscillators. *Chaos, Solitons and Fractals*, 2005, **26**: 1125−1133.

[3] Rabah K, Ladaci S, Lashab M. Stabilization of Fractional Chen Chaotic System by Linear Feedback Control. In: Proceedings of the 3rd International Conference on Control, Engineering & Information Technology, CEIT'2015, Tlemcen, Algeria. IEEE, 25−27 May 2015.

[4] Deng W H, Li C P. Chaos synchronization of the fractional Lü system. *Physica A*, 2005, **353**(1): 61−72.

[5] Lin T-L, Kuo C-H. H^{∞} synchronization of uncertain fractional order chaotic systems: Adaptive fuzzy approach. *ISA Transactions*, 2011, **50**: 548−556.

[6] Rabah K, Ladaci S, Lashab M. State Feedback with Fractional $PI^{\lambda}D^{\mu}$ Control Structure for Genesio-Tesi Chaos Stabilization. In: Proceedings of the 15th IEEE International Conference on Sciences and Techniques of Automatic control & computer engineering, STA'2015, Monastir, Tunisia. IEEE, 21−23 December 2015. 328−333.

[7] Ladaci S, Charef A. On fractional adaptive control. *Nonlinear Dynamics*, 2006, **43**(4): 365−378.

[8] Ladaci S, Loiseau J J, Charef A. Adaptive Internal Model Control with Fractional Order Parameter. *International Journal of Adaptive Control and Signal Processing*, 2010, **24**: 944−960.

[9] Ladaci S, Khettab K. Fractional Order Multiple Model Adaptive Control. *International Journal of Automation & Systems Engineering*, 2012, **6**(2): 110−122.

[10] Li Y, Chen Y-Q, Cao Y. Fractional Order Universal Adaptive Stabilization. In: Proceedings of the 3rd IFAC workshop on fractional differentiation and its applications, Ankara, Turkey, 5−7 November 2008.

[11] Wang L X. *Adaptive fuzzy systems and control: design and stability analysis*. Englewood Cliffs, NJ: Prentice-Hall, 1994.

[12] Wang L X. Stable adaptive fuzzy control of nonlinear systems. *IEEE Transactions on Fuzzy Systems*, 1993, **1**: 146−155.

[13] Khettab K, Bensafia Y, Ladaci S. Robust Adaptive Fuzzy control for a Class of Uncertain nonlinear Fractional Systems. In: Proceedings of the Second International Conference on Electrical Engineering and Control Applications, ICEECA 2014, Constantine, Algeria, November 2014.

[14] Nussbaum R D. Some remarks on the conjecture in parameter adaptive control. *Systems & Control Letters*, 1983, **3**(5): 243−246.

[15] Ye X D, Jiang J P. Adaptive nonlinear design without a priori knowledge of control directions. *IEEE Transactions on Automatic Control*, 1998, **43**(11): 1617−1621.

[16] Willems J C, Byrnes C I. Global adaptive stabilization in the absence of information on the sign of the high frequency gain. *Lecture Notes in Control and Information Sciences*, Berlin, Springer-Verlag, 1984, **62**: 49−57.

[17] Martesson B. Remarks on adaptive stabilization of first order nonlinear systems. *Systems and Control Letters*, 1990, **14**(1): 1−7.

[18] Zhang Y, Wen C Y, Soh Y C. Adaptive backstepping control design for systems with unknown high-frequency gain. *IEEE Transactions on Automatic Control*, 2000, **45**(12): 2350−2354.

[19] Liu Y-J, Wang Z-F. Adaptive fuzzy controller design of nonlinear systems with unknown gain sign. *Nonlinear Dynamics*, 2009, **58**: 687−695.

[20] Boulkroune A, M'saad M. On the design of observer-based fuzzy adaptive controller for nonlinear systems with unknown control gain sign. *Fuzzy Sets and Systems*, 2012, **201**: 71−85.

[21] Oldham K B, Spanier J. *The Fractional Calculus*. New York: Academic Press, 1974.

[22] Diethelm K, Ford N J, Freed A D. A predictor-corrector approach for the numerical solution of fractional differential equations. *Nonlinear Dynamics*, 2002, **29**: 3−22.

[23] Bensafia Y, Ladaci S, Khettab K. Using a fractionalized integrator for control performance enhancement *International Journal of Innovative Computing, Information and Control*, 2015, **11**(6): 2013−2028.

[24] Caponetto R, Dongola G, Fortina L, Petráš I. Fractional Order Systems: Modeling and control application. *World Scientific Series on Nonlinear Science Series A*, 2010, **72**: 62−65.

[25] Nechadi E, Harmas M N, Essounbouli N, Hamzaoui A. Adaptive Fuzzy Sliding Mode Power System Stabilizer Using Nussbaum Gain. *International Journal of Automation and Computing*, 2013, **10**(4): 281−287.

[26] Ge S S, Yang C, Lee T H. Adaptive robust control of a class of nonlinear strict-feedback discrete-time systems with unknown control directions. *Systems & Control Letters*, 2008, **57**(11): 888−895.

[27] Ge S S, Wang J. Robust adaptive tracking for time-varying uncertain nonlinear systems with unknown control coefficients. *IEEE Transactions on Automatic Control*, 2003, **48**(8): 1463−1469.

[28] Li L, Sun Y. Adaptive Fuzzy Control for Nonlinear Fractional-Order Uncertain Systems with Unknown Uncertainties and External Disturbance. *Entropy*, 2015, **17**: 5580−5592.

[29] Georgiou T T, Smith M C. Robustness Analysis of Nonlinear Feedback Systems: An Input-Output Approach. *Transactions on Automatic Control*, 1997, **42**(9): 1200−1221.

[30] Tsung C L, Chi W, Han L L. Observer-based indirect adaptive fuzzy-neural tracking control for nonlinear SISO systems using VSS and H^{∞} approaches. *Fuzzy Sets and Systems*, 2004, **143**: 211−232.

[31] Aguila-Camacho N, Duarte-Mermoud M A, Gallegos J A. Lyapunov functions for fractional order systems. *Communications in Nonlinear Science and Numerical Simulation*, 2014, **19**: 2951−2957.

[32] Duarte-Mermoud M A, Aguila-Camacho N, Gallegos J A, Castro-Linares R. Using general quadratic Lyapunov functions to prove Lyapunov uniform stability for fractional order systems. *Communications in Nonlinear Science and Numerical Simulation*, 2015, **22**(1-3): 650−659.

[33] Gallegos J A, Duarte-Mermoud M A, Aguila-Camacho N, Castro-Linares R. On fractional extensions of Barbalat Lemma. *Systems & Control Letters*, 2015, **84**: 7−12.

[34] Tsung C L, Balas V E. Fractional Order Chaotic System Tracking Design Based on Adaptive Hybrid Intelligent Control. In: Proceedings of the IEEE International Conference on Fuzzy Systems, Taipei, Taiwan, June 2011.

Khatir Khettab graduated from Ferhat Abbes University of Sétif (UFAS), Algeria, in 2001. He received the M. Sc. degree from UFAS in 2005, Algeria. He is currently working toward the Ph.D. degree in Automatic Control, at Skikda University, Algeria. He is an assistant professor at the Mohamed Boudiaf University of M'sila, Algeria. His research interests include robotics and automation, especially the fractional systems control, chaos synchronization and fractional adaptive intelligent control.

Samir Ladaci received the State Engineer degree in Automatics in 1995 from the National Polytechnic School of Algiers and the Magister degree in Industrial Automation from Annaba University, Algeria in 1999. He obtained his Science Doctorate and Habilitation degrees from the Department of Electronics, Mentouri University of Constantine, Algeria, in 2007 and 2009 respectively. He was a visiting researcher at IRCCyN, CNRS Nantes, France from 2006 to 2008, and has many collaboration projects with different research teams in France, Tunisia and Italy. From 2001 to 2013 he worked at the Department of Electrical Engineering at Skikda University, Algeria, as an Associate Professor. And since 2013 he joined the National Polytechnic School of Constantine, where he is a full Professor. He is also the Head of Control research team at the SP-Lab Laboratory, University of Mentouri Constantine since 2014. He has more than seventy papers in journals and international conferences, and supervises many PhD theses. His current research interests include Fractional order Systems and Control, Fractional Adaptive Control, Robust Control, Systems Identification and Nonlinear control systems. Corresponding author of this paper.

Yassine Bensafia was born in Béjaia, Algeria, in 1978. He received the Engineering and Magister degrees in Electrical Engineering from the Béjaia University, in 2003 and in 2006, respectively. Recently, he obtained his Science Doctorate in Automatic Control from the Department of Electrical Engineering, University of the 20th August 1955 of Skikda, Algeria. Since 2015, he joined the University of Bouira as an assistant professor. His research interests include Fractional systems control, Adaptive control, Robust control.

DOA Estimation Based on Sparse Representation of the Fractional Lower Order Statistics in Impulsive Noise

Sen Li, Rongxi He, *Member, IEEE*, Bin Lin, *Member, IEEE*, Fei Sun

***Abstract*—This paper is mainly to deal with the problem of direction of arrival (DOA) estimations of multiple narrow-band sources impinging on a uniform linear array under impulsive noise environments. By modeling the impulsive noise as -stable distribution, new methods which combine the sparse signal representation technique and fractional lower order statistics theory are proposed. In the new algorithms, the fractional lower order statistics vectors of the array output signal are sparsely represented on an overcomplete basis and the DOAs can be effectively estimated by searching the sparsest coefficients. To enhance the robustness performance of the proposed algorithms, the improved algorithms are advanced by eliminating the fractional lower order statistics of the noise from the fractional lower order statistics vector of the array output through a linear transformation. Simulation results are shown to demonstrate the effectiveness of the proposed methods for a wide range of highly impulsive environments.**

***Index Terms*—α-stable distribution, direction of arrival, impulsive noise, sparse representation, fractional lower-order statistics.**

I. Introduction

DIRECTION of arrival (DOA) estimation of multiple emitting sources is an important issue in array processing and has various applications in military, radar, sonar, wireless communications and source localization[1−2]. A large number of solutions have been proposed to solve this problem during the past years. Usually, these solutions can be categorized into three groups: time-delay based methods, beamforming methods and signal subspace methods. However, majority of DOA estimation algorithms are developed under certain assumptions: the source signal needs to be statistically stationary and uncorrelated, the number of snapshots is sufficient, and the signal-noise ratio (SNR) is moderately high. Practically, these conditions are barely satisfied, thus these methods achieve the limited estimation accuracy. In order to increase the DOA estimation accuracy, the well-known subspace-based method of multiple signal classification (MUSIC) algorithm and estimation method of signal parameters via rotational invariance techniques (ESPRIT) have been widely used due to its high estimation accuracy but at the price of the high complexity.

Recently, sparse representation technique of signal has been applied in many areas, such as image processing, wireless channel estimation and biomedical signal processing, which also provides a new idea for DOA estimation based on the fact that the number of sources is in general much smaller than the number of potential source points when implementing the array processing algorithms. Several DOA estimation methods based on sparse representation have been proposed in the literature[3−16]. In [3-4], a whiten sparse covariance-based representation model is first presented for source parameter estimation by applying the global matched filter (GMF). In [5] the most representative sparse recovery algorithm for DOA estimation (l_1-SVD) was proposed, which can effectively estimate DOA with single measurement. By using singular value decomposition (SVD) of received data matrix, it not only can work in multiple measurements case but also can reduce the computational complexity. Although the l_1-norm minimization is a convex problem and the global minima can be guaranteed easily, its weakness is their undemocratic penalization for larger coefficients, which results in the degradation of signal recovery performance. To conquer this problem, the iterative reweighted l_1 minimization was designed[6−7], where the large weights could be used to discourage nonzero entries in the recovered signals. To improve the convergence rate and better estimation accuracy of the $l_{2,1}$-norm minimization approach, Wei et al. develop a novel greedy block coordinate descent (GBCD) algorithm by using a greedy strategy for choosing descent directions[8]. In [9], a mixed $l_{2,0}$-norm based joint sparse approximation technique is introduced into DOA estimation where the l_0 norm constraint is approached by a set of convex functions, and a method called JLZA-DOA is proposed. Algorithms in [5-9] address the DOA estimation problem by directly representing the array output in time domain with an overcomplete basis from the array response vector.

To make use of the second order statistics of the array output, a sparse iterative covariance-based estimation (SPICE) approach for array signal processing by the minimization of a covariance matrix fitting criterion and can be used in both single and multiple measurements cases was proposed in [10]. Another method called l_1-SRACV in [11] was also proposed for DOA estimation by using the array covariance matrix

This article has been accepted for publication in a future issue of this journal, but has not been fully edited. Content may change prior to final publication.

This work was supported in part by the National Natural Science Foundation of China (61301228, 61371091), the Fundamental Research Funds for the Central Universities (3132014212). Recommended by Associate Editor YangQuan Chen.

Sen Li, Rongxi He (corresponding author), Bin Lin,and Fei Sun are with the Department of Information Science and Technology, Dalian Maritime University, Dalian 116026, China (e-mails: listen@dlmu.edu.cn; hrx@dlmu.edu.cn; binlin@dlmu.edu.cn; sunfei@dlmu.edu.cn).

Digital Object Identifier 10.1109/JAS.2016.7510187

sparse representation and exhibit some merits of increased resolution. Because of recovering a joint-sparse inverse problem form multiple measurement vectors, the l_1-SRACV algorithm suffers from a high computational cost. Then a new DOA estimation method was proposed in [12-13] which based on the combination of the Khatri-Rao product and sparse representation to estimate the DOAs of signals by recovering a sparse covariance vector of only a single measurement vector, thereby implying lower computational complexity than the l_1-SRACV algorithm. The authors of Literature [14] firstly transform the multiple measurement vectors problem to the virtual single measurement vector (VSMV) problem in sparse signal representation framework, and then exploit a surrogate truncated l_1 function to approximate l_0-norm, and successively demonstrate how the nonconvex minimization problem can be treated by the difference of convex functions decomposition and the iterative approach. The study of [15] demonstrates how the multiple parameters can be exactly obtained by solving a weighted 'group lasso' problem in second-order statistics using a cross-dipole array. In [16], the DOA estimation of the wideband signal has been studied by the sparse representation of the covariance matrix.

All the above mentioned sparse representation based DOA estimation algorithms assume that the ambient noise is Gaussian distributed. However, the noise in practice often exhibits non-Gaussian properties, sometimes accompanied by strong impulsiveness[17]. For example, atmospheric noise (thunderstroms), car ignitions, microwave ovens, office equipments, and other types of naturally occurring or man-made signal sources can result in aggregating noise components that may exhibit high amplitudes for small time intervals. Under investigation, it is found that α-stable distribution ($0 < \alpha \leq 2$) is a suitable noise model to describe this type of noise[18]. It can be considered as the greatest potential distribution to characterize various impulsive noises as different characteristic exponent parameter is selected.

An important characteristic of the α-stable distribution is that only moments of order less than α exist. Therefore the performance of the DOA estimation algorithms based on second order statistics of the array out will severely degrade in the presence of the α-stable non-Gaussian noise. One way to alleviate this problem is to introduce new covariance estimates. Authors in [19] proposed new subspace DOA estimation methods based on fractional lower order moments (FLOM) matrices, namely FLOM_MUSIC. However, it is limited in range of $2 \geq \alpha \geq 1$. Authors in [20] introduce a new subspace algorithm based on the phased fractional lower order moment (PFLOM), namely PFLOM_MUSIC, which it is applicable for $0 < \alpha \leq 2$. In [21], a subspace-augmented MUSIC technique for recovering the joint sparse support of a signal ensemble corrupted by additive impulsive noise is introduced. In order to mitigate the performance degradation of the DOA estimation methods based on the sparse representation of the second order statistics of the array output, the new algorithms are proposed in this paper by using the sparse representation of the fractional lower order statistics vector of the array output. To enhance the robustness performance of the proposed algorithms, the improved algorithms are advanced by eliminating the fractional lower order statistics of the noise from the fractional lower order statistics vector of the array output through a linear transformation. Computer simulation experiments are presented to illustrate the performance superiority of the proposed methods over the DOA estimation method based on the sparse representation of the second order statistics of the array output under α-stable noise environments.

II. α-Stable Distribution

The α-stable distribution's probability density function does not have closed form. It can be conveniently described by its characteristic function as

$$\phi(t) = e^{\{jat - \gamma|t|^{\alpha}[1 + j\beta \operatorname{sgn}(t)\varpi(t,\alpha)]\}} \tag{1}$$

where $\varpi(t,\alpha) = \tan\frac{\pi\alpha}{2}$, if $\alpha \neq 1$; $\varpi(t,\alpha) = \frac{2}{\pi}\log|t|$, if $\alpha = 1$, and $\operatorname{sgn}(t)$ is $|t|$ if $t \neq 0$ and 0 if $t = 0$. α is the characteristic exponent, it controls the thickness of the tail in the distribution and is restricted in $0 < \alpha \leq 2$. γ is the dispersion parameter and is similar to the variance of the Gaussian distribution. β is the symmetry parameter. If $\beta = 0$, the distribution is symmetric and the observation is referred to as the SαS (symmetry α-stable) distribution. a is the location parameter. When $\alpha = 2$ and $\beta = 0$, the α-stable distribution becomes a Gaussian distribution. The tails of stable distribution with characteristic exponent $0 < \alpha < 2$ are significantly thicker than that of the Gaussian distribution and the smaller α, the thicker the tails. An important difference between the Gaussian and the α-stable distribution ($0 < \alpha < 2$) is that only moments of order less than α exist for the α-stable distribution. As the non-existence of the second order statistics of α-stable distribution when the characteristic exponent is restricted in $0 < \alpha < 2$, the second order statistics, such as correlation and covariance, does not make sense. Therefore, the fractional lower order statistics (FLOS) has been defined[18], such as the fraction lower order moment (FLOM) in [19] and the phased fractional lower order moment (PFLOM) in [20].

III. DOA Estimation Based on Sparse Representation of Second Order Statistics Vector

Consider the case of K narrow far-field signals $s_1(t)$, $s_2(t)$, $\ldots$, $s_K(t)$ with different DOA θ_1, θ_2, $\ldots$, θ_K arriving at a uniform linear array (ULA) with M sensors in presence of additive noise $n_1(t)$, $n_2(t)$, $\ldots$, $n_M(t)$. Assume that the noise is i.i.d random variable and is not correlated with signals. The received signal vector is given by

$$X(t) = A(\theta)S(t) + N(t) \tag{2}$$

where

$$\begin{aligned}
X_{M\times1}(t) &= [x_1(t), x_2(t), \ldots, x_M(t)]^{\mathrm{T}}, \\
A_{M\times K}(\theta) &= [\mathbf{a}(\theta_1), \mathbf{a}(\theta_2), \ldots, \mathbf{a}(\theta_K)] \\
S_{K\times1}(t) &= [s_1(t), s_2(t), \ldots, s_K(t)]^{\mathrm{T}}, \\
N_{M\times1}(t) &= [n_1(t), n_2(t), \ldots, n_M(t)]^{\mathrm{T}},
\end{aligned}$$

where $x_m(t)$, $m = 1, 2, \ldots, M$ is the output of the mth array element, $\mathbf{a}(\theta_n)$, $n = 1, 2, \ldots, K$ are the steering vector can be expressed as

$$\mathbf{a}(\theta_n) = \left[1,\ e^{-j\frac{2\pi}{\lambda}d\sin\theta_n},\ \ldots,\ e^{-j\frac{2\pi}{\lambda}(M-1)d\sin\theta_n}\right]^{\mathrm{T}} \quad (3)$$

where λ is the carrier wavelength of the signal, d is the intersensor spacing.

Assume the noise in (2) is zero-mean Gaussian white noise with the power of σ_n^2, the second order statistics covariance matrix of the array out can be expressed as

$$R = E(X(t)X^H(t)) = A(\theta)R_sA^H(\theta) + \sigma_n^2 I_M \quad (4)$$

where the source covariance matrix $R_s = E(s(t)s^H(t)) = diag(\sigma_s)$ is diagonal with source signal power vector $\sigma_s = [\sigma_1^2, \ldots, \sigma_K^2]^{\mathrm{T}}$ and I_M denotes the $M \times M$ identity matrix. σ_i^2, $i = 1, \ldots, K$ is the source signal power.

Applying the vectorization operator on equation (4), we have[22]

$$y = \mathrm{vect}(R) = B(\theta)\sigma_s + \sigma_n^2\mathrm{vect}(I_M), \quad (5)$$

$$B(\theta) = [a^*(\theta_1) \otimes a(\theta_1), \ldots, a^*(\theta_K) \otimes a(\theta_K)] \quad (6)$$

where $\otimes$ denote Kronecker product . It is interesting to see that in (5) ,similar to (2), can be taken as the array output of single snapshot where $B(\theta)$, σ_s and $\mathrm{vect}(I_M)$ are the virtual manifold matrix with its dimension $M^2 \times K$, equivalent source vector, and equivalent noise vector, respectively. The new signal vector y can be sparsely represented in a redundant basis. Define a set $\hat{\theta} = [\hat{\theta_1}, \hat{\theta_1}, \ldots, \hat{\theta_Q}]$, which denotes potential source location of interest and assume that the true DOAs are exactly on this set. The number of the potential source locations Q should be much greater than the number of actual sources K and the number of virtual array sensors M^2. Define the overcomplete basis $B(\hat{\theta}) = [a^*(\hat{\theta}_1) \otimes a(\hat{\theta}_1), \ldots, a^*(\hat{\theta}_Q) \otimes a(\hat{\theta}_Q)]$ and the signal power vector $\nu = [\nu_1, \nu_2, \ldots, \nu_Q]$ where $a^*(\hat{\theta}_i) \otimes a(\hat{\theta}_i)$ denotes the steering vector of the virtual array and the elements of vector ν have K nonzeros, that is, $\nu_j = \sigma_i^2$ if $\hat{\theta}_j = \theta_i$, $i = 1, \ldots, K$. As a result, y can be rewritten as the following form

$$y = B(\hat{\theta})\nu + \sigma_n^2\mathrm{vect}(I_M) \quad (7)$$

Hence the DOA estimation can be reduced to the detection of the nonzero elements of ν. In practice, the unknown y is estimated from the N snapshots, let $\hat{y}$ be the estimation of y, then $\hat{y} = \mathrm{vect}(\hat{R})$, where $\hat{R} = \frac{1}{N}\sum_{t=1}^{N} X(t)X^H(t)$. Define Δy as the estimation error, then $\Delta y = \hat{y} - y$. Let $\hat{nu}$ be the estimate of ν, the DOA estimation problem can be further converted into the following convex optimization problem[12]:

$$\min \|\mu\|_1, \quad s.t.\ \|\hat{y} - B(\hat{\theta})\hat{\nu} - \sigma_n^2\mathrm{vect}(I_M)\|_2 \le \varepsilon \quad (8)$$

ε is a parameter which means how much of the error we wish to allow and plays an important role in the algorithm performance. It can be known that the error Δy satisfies asymptotically normal (AsN) distribution[23],

$$\Delta y = \hat{y} - y = \mathrm{vect}(\hat{R} - R) \sim \mathrm{AsN}\left(0_{M^2,1}, \frac{1}{N}R^T \otimes R\right) \quad (9)$$

Define the weighted matrix $W^{-\frac{1}{2}} = \sqrt{N}R^{-\frac{T}{2}} \otimes R^{-\frac{1}{2}}$, then

$$W^{-\frac{1}{2}}\Delta y \sim \mathrm{AsN}\left(0_{M^2,1}, I_{M^2}\right) \quad (10)$$

Then from (7), we can further get

$$\left\|W^{-\frac{1}{2}}\left[\hat{y} - B(\hat{\theta})\hat{\nu} - \sigma_n^2\mathrm{vect}(I_M)\right]\right\|_2^2 \sim \mathrm{As}\chi^2(M^2) \quad (11)$$

where $\mathrm{As}\chi^2(M^2)$ is the asymptotic chi-square distribution with M^2 degrees of freedom. Therefore, the parameter ε should be introduced such that

$$\left\|W^{-\frac{1}{2}}\left[\hat{y} - B(\hat{\theta})\hat{\nu} - \sigma_n^2\mathrm{vect}(I_M)\right]\right\|_2^2 \le \varepsilon^2$$

with a high probability pc, that is $\varepsilon = \sqrt{\chi^2_{pc}(M^2)}$. Let $\hat{W}^{-\frac{1}{2}} = \sqrt{N}\hat{R}^{-\frac{T}{2}} \otimes \hat{R}^{-\frac{1}{2}}$ be the estimate of the weighted matrix $W^{-\frac{1}{2}}$ and $\hat{\sigma}_n^2$ be the estimate of σ_n^2 by the average of $M-K$ smallest eigenvalue of the eigenvalue decomposition (EVD) of the estimate covariance matrix $\hat{R}$, then the statistically robust and tractable formula for DOA estimation can be reduced as follows

$$\min \|\hat{\nu}\|_1,\ s.t.\ \left\|\hat{W}^{-\frac{1}{2}}\left[\hat{y} - B(\hat{\theta})\hat{\nu} - \hat{\sigma}_n^2\mathrm{vect}(I_M)\right]\right\|_2 \le \varepsilon \quad (12)$$

This DOA estimation algorithm based on the sparse representation of the second order statistics covariance vector can be namely as SS_SOSCV algorithm.

IV. DOA Estimation Based on Sparse Representation of Fractional Lower Order Statistics Vector

When the noise in (2) is α-stable impulsive noise with a characteristic exponent $0 < \alpha < 2$, the performance of the SS_SOSCV algorithm will degrade since the covariance matrix is not defined for $0 < \alpha < 2$. In this case, introducing a modified covariance matrix instead of the covariance matrix can alleviate the problem. In this paper, we introduce two DOA estimation methods based on sparse representation of fractional lower order statistics vector, and the improved algorithms which can enhance the robustness of the proposed algorithms are further studied.

A. SS_FLOMV Algorithm

The fractional lower order moment (FLOM) matrix C which is suitable for α-stable distribution noise environments can be used to replace the covariance matrix R in (4). The (i,k) element of matrix C can be defined as:

$$C_{i,k} = E\{x_i(t)|x_k(t)|^{p-2}x_k^*(t)\} \quad (13)$$

where p is the order of the moments. Setting $p = 2$ reduces (13) to an appropriate covariance matrix under the condition of Gaussianity. However, as we deviate from this condition p should be set to a lower value and it must satisfy the inequality $1 < p < \alpha \le 2$ so that $C_{i,k}$ is bounded. It can be proved that the FLOM matrix C can be expressed as[19]

$$C = A(\theta)\Lambda_s A(\theta)^H + \xi I_M \quad (14)$$

where the diagonal matrix $\Lambda_s = diag(\gamma_s)$ can be interpreted as the FLOM matrix of the source signals and ξ can be interpreted as the FLOM of the α-stable additive noise level. $\gamma_s = [\gamma_1, \ldots, \gamma_K]^{\mathrm{T}}$, γ_i, $i = 1, \ldots, K$ is the fractional lower order power of the signals. Applying the vectorization operator on (14), we have

$$y_{FLOM} = \text{vect}(C) = B(\theta)\gamma_s + \xi\text{vect}(I_M) \tag{15}$$

The vector y_{FLOM} can be sparsely represented in the overcomplete basis $B(\hat{\theta})$ as the following form

$$y_{FLOM} = B(\hat{\theta})\nu_{FLOM} + \xi\text{vect}(I_M) \tag{16}$$

As with the SS_SOSCV algorithm, the DOA estimation can be resolved by the following convex optimization problem:

$$\begin{gathered}\min \|\hat{\nu}_{FLOM}\|_1 \\ s.t.\ \left\|\hat{W}_{FLOM}^{-\frac{1}{2}}\left[\hat{y}_{FLOM} - B(\hat{\theta})\hat{\nu}_{FLOM} - \hat{\xi}\text{vect}(I_M)\right]\right\|_2 \le \varepsilon\end{gathered} \tag{17}$$

where the weighted matrix $\hat{W}_{FLOM}^{-\frac{1}{2}}$ can be defined as

$$\hat{W}_{FLOM}^{-\frac{1}{2}} = \sqrt{N}\hat{C}^{-\frac{T}{2}} \otimes \hat{C}^{-\frac{1}{2}} \tag{18}$$

$\hat{C}$ is the estimate of the FLOM matrix C and the (i,k) element of matrix $\hat{C}$ can be defined as

$$\hat{C}_{i,k} = \frac{1}{N}\sum_{t=1}^{N}\left\{x_i(t)|x_k(t)|^{p-2}x_k^*(t)\right\} \tag{19}$$

$\hat{\nu}_{FLOM}$ and $\hat{y}_{FLOM}$ are the estimation of ν_{FLOM} and y_{FLOM}, $\hat{\xi}$ is the estimation of ξ by the average of $M-K$ smallest eigenvalue of the EVD of the matrix $\hat{C}$. This DOA estimation method based on the sparse representation of the FLOM vector can be namely as SS_FLOMV algorithm.

B. SS_PFLOMV Algorithm

Form the FLOM definition, it can be seen that it is limited in range of $2 \ge \alpha > 1$, so the SS_FLOMV algorithm is not applicable under the α-stable noise with characteristic exponent $0 < \alpha \le 1$. In [20] a new class of robust bounded covariance matrices based on phased fraction lower order moment (PFLOM) which is applicable for $0 < \alpha \le 2$ was used. The (i,k) element of PFLOM matrix Γ can be defined as

$$\Gamma_{i,k} = E\left\{x_i^{\langle b\rangle}(t)x_k^{\langle -b\rangle}(t)\right\},\ 0 < b < \alpha/2 \tag{20}$$

where the PFLOM operation on a complex number z is

$$z^{\langle b\rangle} = \begin{cases}\frac{|z|^{b+1}}{z^*}, & z \ne 0\\ 0, & z = 0\end{cases} \tag{21}$$

and the conjugate of the bth PFLOM of z as $z^{-\langle b\rangle} = (z^*)^{\langle b\rangle} = (z^{\langle b\rangle})^*$. It can be proved that the matrix Γ can be expressed as[20]

$$\Gamma = A(\theta)\Phi_s A(\theta)^H + \kappa I_M \tag{22}$$

where the diagonal matrix $\Phi_s = diag(\varphi_s)$ can be interpreted as the PFLOM matrix of the source signals and κ can be interpreted as the PFLOM of the α-stable additive noise level. $\varphi_s = [\varphi_1, \ldots, \varphi_K]^{\mathrm{T}}$, $\varphi_i,\ i = 1, \ldots, K$ is the phased fractional lower order power of the signals. Applying the vectorization operator on (22) and then sparse representation in the overcomplete basis $B(\hat{\theta})$, we can have

$$y_{FLOM} = \text{vect}(\Gamma) = B(\theta)\varphi_s + \kappa\text{vect}(I_M) \tag{23}$$

$$y_{PFLOM} = B(\theta)\nu_{PFLOM} + \kappa\text{vect}(I_M) \tag{24}$$

Likewise, the DOAs can be estimated by solving the following optimization problem

$$\begin{gathered}\min \|\hat{\nu}_{PFLOM}\|_1 \\ s.t.\ \left\|\hat{W}_{PFLOM}^{-\frac{1}{2}}\left[\hat{y}_{PFLOM} - B(\hat{\theta})\hat{\nu}_{PFLOM} - \hat{\kappa}\text{vect}(I_M)\right]\right\|_2 \le \varepsilon\end{gathered} \tag{25}$$

where the weighted matrix $\hat{W}_{PFLOM}^{-\frac{1}{2}}$ can be defined as

$$\hat{W}_{PFLOM}^{-\frac{1}{2}} = \sqrt{N}\hat{\Gamma}^{-\frac{T}{2}} \otimes \hat{\Gamma}^{-\frac{1}{2}} \tag{26}$$

$\hat{\Gamma}$ is the estimation of the PFLOM matrix Γ and the (i,k) element of matrix $\hat{\Gamma}$ can be defined as

$$\hat{\Gamma}_{i,k} = \frac{1}{N}\sum_{t=1}^{N}\left\{x_i^{\langle b\rangle}(t)x_k^{\langle -b\rangle}(t)\right\} \tag{27}$$

$\hat{\nu}_{PFLOM}$ and $\hat{y}_{PFLOM}$ are the estimation of ν_{PFLOM} and y_{PFLOM}, $\hat{\kappa}$ is the estimation of κ by the average of $M-K$ smallest eigenvalue of the EVD of the matrix $\hat{\Gamma}$. This DOA estimation method based on the sparse representation of the PFLOM vector can be namely as SS_PFLOMV algorithm.

C. Improved Algorithms

The equation (16) and (24) can be unified expressed as

$$y_{FLOS} = B(\hat{\theta})\nu_{FLOS} + (\xi|\kappa)\text{vect}(I_M) \tag{28}$$

Notice that the vector $(\xi|\kappa)\text{vect}(I_M)$ has only M nonzero elements, then these elements of y_{FLOS} corresponding to these positions of nonzero elements in $(\xi|\kappa)\text{vect}(I_M)$ can be removed and the rest $M(M-1)$ entries of y_{FLOS} corresponding to these positions of zeros elements in $(\xi|\kappa)\text{vect}(I_M)$ can be preserved. Mathematically, this operation can be formulated as

$$\begin{aligned}y_{IFLOS} &= \mathbf{J}y_{FLOS}\\ &= \mathbf{J}\left\{B(\hat{\theta})\nu_{FLOS} + (\xi|\kappa)\text{vect}(I_M)\right\}\\ &= \mathbf{D}(\hat{\theta})\nu_{FLOS}\end{aligned} \tag{29}$$

where, $\mathbf{J}$ is a $M(M-1) \times M^2$ selecting matrix and can be represented as

$$\mathbf{J}^{\mathrm{T}} = [\mathbf{J}_1, \mathbf{J}_2, \ldots, \mathbf{J}_{M-1}] \tag{30}$$

where

$$\begin{gathered}\mathbf{J}_m = [\mathbf{e}_{(m-1)(M+1)+2}, \mathbf{e}_{(m-1)(M+1)+3}, \ldots, \mathbf{e}_{m(M+1)}] \in \mathbf{R}^{M^2 \times M},\\ m = 1, \ldots, M-1\end{gathered} \tag{31}$$

$\mathbf{e}_i$ $(i = (m-1)(M+1)+2, \ldots, m(M+1))$ is an $M^2 \times 1$ column vector with 1 at the ith position and 0 elsewhere. $\mathbf{D}(\hat{\theta}) = \mathbf{J}B(\hat{\theta}) \in C^{M(M-1)\times Q}$ is the new steering matrix. This elimination operation avoids the estimation of the fractional lower order statistics of the impulsive noise and further reduces the effect of the impulsive noise. Hence the DOAs estimation can be obtained by the following minimization

$$\min \|\nu_{FLOS}\|_1,\ s.t.\ \left\|y_{IFLOS} - \mathbf{D}(\hat{\theta})\nu_{FLOS}\right\|_2 < \varepsilon_I \tag{32}$$

Let $\hat{y}_{IFLOS}$ be the estimation of y_{IFLOS} and $\Delta y_{IFLOS} = \hat{y}_{IFLOS} - y_{IFLOS}$ is the estimation error, we can get $\Delta y_{IFLOS} = \mathbf{J}\Delta y_{FLOS}$. From (9), we can further get that Δy_{IFLOS} satisfies

$$\Delta y_{IFLOS} \sim \mathrm{AsN}\Big(0_{M(M-1),1}, \frac{1}{N} J\big((C|\Gamma)^{\mathrm{T}} \otimes (C|\Gamma)\big) J^{\mathrm{T}}\Big) \tag{33}$$

Define the weighted matrix $\hat{W}_{IFLOS}^{-\frac{1}{2}}$ as

$$\hat{W}_{IFLOS}^{-\frac{1}{2}} = \sqrt{N} J^{-\frac{1}{2}} \big((C|\Gamma)^{-\frac{T}{2}} \otimes (C|\Gamma)^{-\frac{1}{2}}\big) J^{-\frac{T}{2}} \tag{34}$$

and its estimation as $\hat{W}_{IFLOS}^{-\frac{1}{2}}$, then

$$W_{IFLOS}^{-\frac{1}{2}} \Delta y_{IFLOS} \sim \mathrm{AsN}\Big(0_{M(M-1),1}, I_{M(M-1),1}\Big) \tag{35}$$

$$\Big\| W_{IFLOS}^{-\frac{1}{2}} \Big[\hat{y}_{IFLOS} - \mathbf{D}(\hat{\theta})\hat{\nu}_{FLOS}\Big] \Big\|_2^2 \sim \mathrm{As}\chi^2[M(M-1)] \tag{36}$$

Therefore, a parameter ε_I should be selected such that $\Big\| W_{IFLOS}^{-\frac{1}{2}} \Big[\hat{y}_{IFLOS} - \mathbf{D}(\hat{\theta})\hat{\nu}_{FLOS}\Big] \Big\|_2^2 \leq \varepsilon_I^2$ with a high probability pc, that is $\varepsilon_I = \sqrt{\chi_{pc}^2(M(M-1))}$. Likewise, the DOAs can be estimated by solving the following optimization problem:

$$\begin{aligned} &\min \|\hat{\nu}_{FLOS}\|_1 \\ &s.t. \ \Big\| \hat{W}_{IFLOS}^{-\frac{1}{2}} \big[\hat{y}_{IFLOS} - \mathbf{D}(\hat{\theta})\hat{\nu}_{FLOS}\big] \Big\|_2 \leq \varepsilon_I \end{aligned} \tag{37}$$

The DOA estimation methods based on (37) by using the FLOM matrix C and the PFLOM matrix Γ can be namely as SS_IFLOMV and SS_IPFLOMV, respectively.

D. Algorithm Computational Costs and Steps

The main computational costs of the SS_FLOMV or SS_PFLOMV algorithms include the calculation of the FLOM matrix C or the PFLOM matrix Γ, the EVD of the matrix C or Γ to estimate the parameter ξ and κ, and solving the optimization problem of (17) and (25), require $O(NM^2)$, $O(M^3)$ and $O(Q^3)$, respectively. As the SS_IFLOMV and SS_IPFLOMV algorithms don't need to estimate the parameter ξ and κ, so their computational costs are slighter lower than those of the SS_FLOMV and SS_PFLOMV algorithm. But the computational costs of these four algorithms are higher than those of subspace-based FLOM_MUSIC and PFLOM_MUSIC algorithms, where the main complexity of these two algorithms are in calculating the array covariance matrix R and its EVD.

From the above analysis, the SS_FLOMV and SS_PFLOMV algorithms' steps can be summarized as following:

Step 1: Obtain the FLOM estimate matrix $\hat{C}$ or the PFLOM estimate matrix $\hat{\Gamma}$ using the array received data by equation (19) or (27). Then apply the vectorization operator on them to get the vector $\hat{y}_{FLOM}$ and $\hat{y}_{PFLOM}$.

Step 2: Get the estimation of the parameter $\hat{\xi}$ or $\hat{\kappa}$ by the average of $M-K$ smallest eigenvalue of the EVD of the matrix $\hat{C}$ or $\hat{\Gamma}$.

Step 3: Calculate the weighted matrix $\hat{W}_{FLOM}^{-\frac{1}{2}}$ or $\hat{W}_{PFLOM}^{-\frac{1}{2}}$ by equation (18) and (26).

Step 4: Solve the convex optimization problem of (17) or (25) to get the estimation of the vector $\hat{\nu}_{FLOM}$ or $\hat{\nu}_{PFLOM}$.

Step 5: Estimate the DOAs according the location of nonzero elements in the vector $\hat{\nu}_{FLOM}$ or $\hat{\nu}_{PFLOM}$.

The SS_IFLOMV and SS_IPFLOMV algorithms' steps are similar to that of SS_FLOMV and SS_PFLOMV algorithms except that step 2 is applying the elimination operation (29) on the vector $\hat{y}_{FLOS}$ to get the vector $\hat{y}_{IFLOS}$.

V. Simulation Results

In this section, a series of numerical experiments under different conditions are conducted to compare the performance of the proposed SS_FLOMV, SS_PFLOMV, SS_IFLOMV and SS_IPFLOMV algorithms with that of the FLOM_MUSIC, PFLOM_MUSIC and SS_SOSCV methods. Throughout this section, the convex optimization problem of (12), (17), (25) and (37) are resolved by using the software package CVX[24], the probability pc in the proposed algorithms is set as 0.999. A $M = 8$ element ULA with an intersensors pacing of half a wavelength is used. The direction grid is set to have 181 points sampled form $-90°$ to $90°$ with $1°$ intervals. Two performance criteria are used to assess the performance of the algorithms. The first one is the probability of resolution. The DOAs are considered to be resolved within $1°$ estimate error. 2000 independent Monte Carlo experiments are performed, the experiment number that DOAs can be resolved is denoted as N_{ok}, then the probability of resolution is defined as $N_{ok}/2000$. In the case of DOAs can be resolved, set $\overline{\theta}_i(n)$, $i = 1, 2, \ldots, K$ as the estimation of θ_i for the nth Monte Carlo experiment, the average mean square error (RMSE) of the DOAs estimation is defined as:

$$RMSE = \frac{1}{N_{ok}} \sum_{n=1}^{N_{ok}} \sqrt{\frac{1}{K} \sum_{i=1}^{K} \Big(\bar{\theta}_i(n) - \theta_i(n)\Big)^2} \tag{38}$$

As the characteristic of the α-stable distribution makes the use of the standard SNR meaningless, a new SNR measure, generalized signal-to-noise ratio (GSNR), is defined as[18]:

$$\mathrm{GSNR} = 10 \log_{10} \frac{\sigma_s^2}{\gamma} \tag{39}$$

where σ_s is the variance of the signal, γ is the dispersion parameter of the α-stable noise.

Example 1. Three sources impinging on array from $-50°$, $0°$ and $50°$ under the condition of α stable distribution noise with characteristic exponent $\alpha = 1.5$ are considered. The GSNR is 10dB and the number of snapshots is fixed at 100. Fig. 1 to Fig. 7 are the normalized spatial spectrum of FLOM_MUSIC, PFLOM_MUSIC, SS_SOSCV, SS_FLOMV, SS_PFLOMV, SS_IFLOMV and SS_IPFLOMV algorithm, respectively. It can be seen that sparse representation based methods have the higher resolution than that of the subspace based methods, that is the normalized spatial spectrum in Fig. 3-Fig. 7 are sharper than that in Fig. 1-Fig. 2. In these sparse representation based methods, the SS_FLOMV and SS_PFLOMV methods proposed in this paper have a better spatial spectrum performance than that of SS_SOSCV algorithm. And the improved SS_IFLOMV and SS_IPFLOMV algorithms have the best spatial spectrum performance.

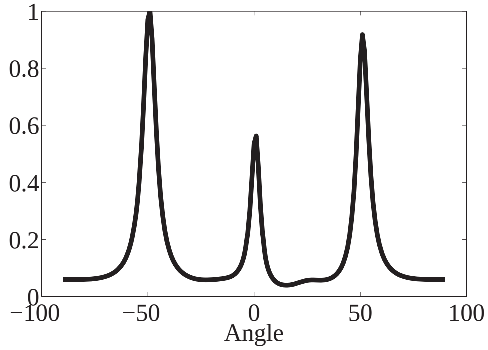

Fig. 1. Normalized Spatial spectrum of FLOM_MUSIC algorithm.

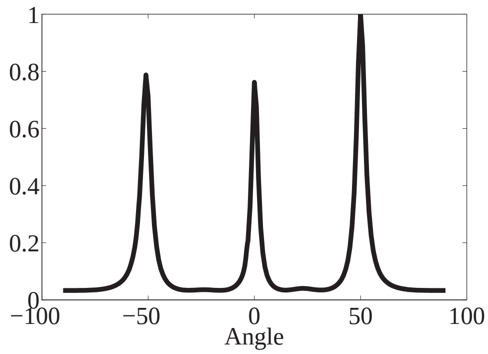

Fig. 2. Normalized Spatial spectrum of PFLOM_MUSIC algorithm.

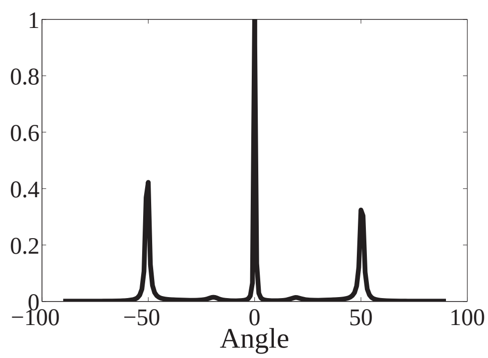

Fig. 3. Normalized Spatial spectrum of SS_SOSCV algorithm.

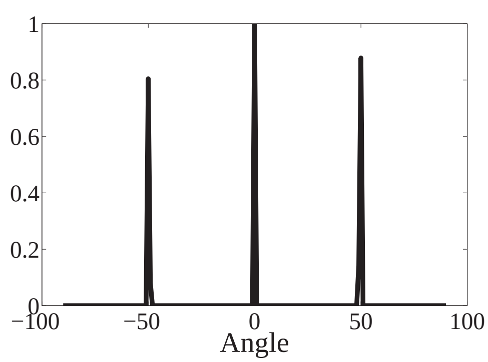

Fig. 4. Normalized Spatial spectrum of SS_FLOMV algorithm.

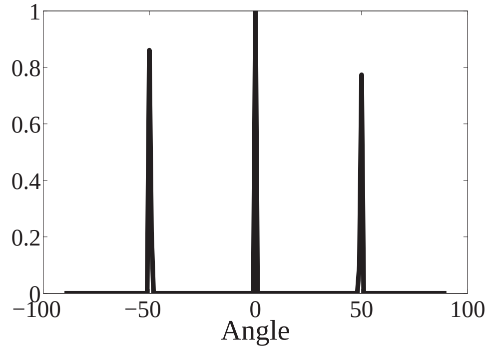

Fig. 5. Normalized Spatial spectrum of SS_PFLOMV algorithm.

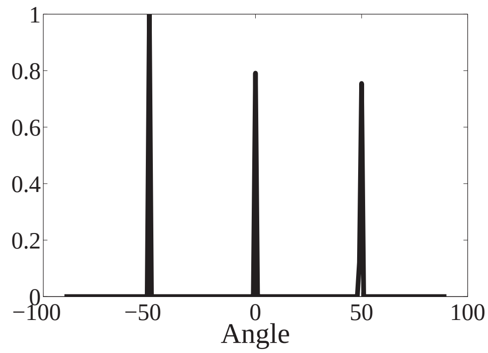

Fig. 6. Normalized Spatial spectrum of SS_IFLOMV algorithm.

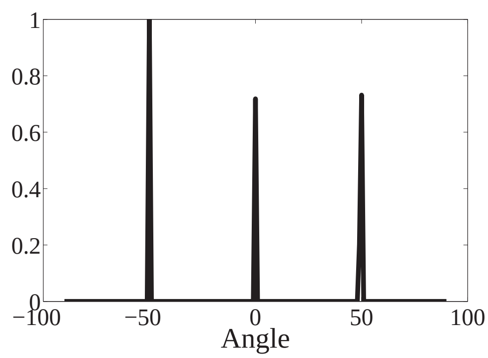

Fig. 7. Normalized Spatial spectrum of SS_IPFLOMV algorithm.

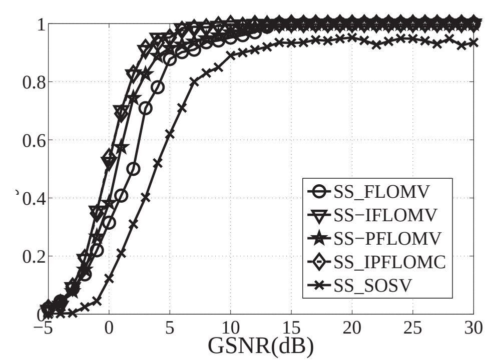

Fig. 8. Probability of resolution versus GSNR.

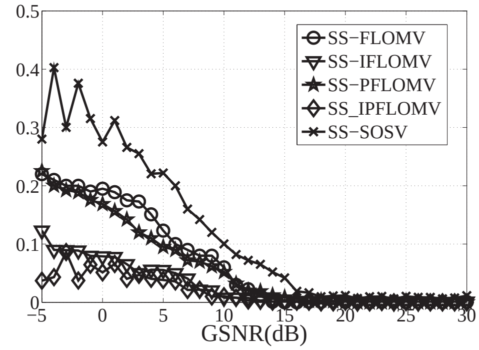

Fig. 9. RMSE of DOA estimation versus GSNR.

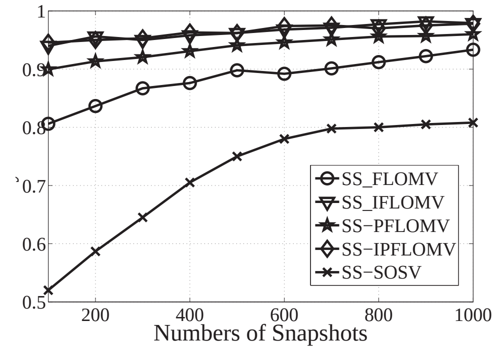

Fig. 10. Probability of resolution versus number of snapshots.

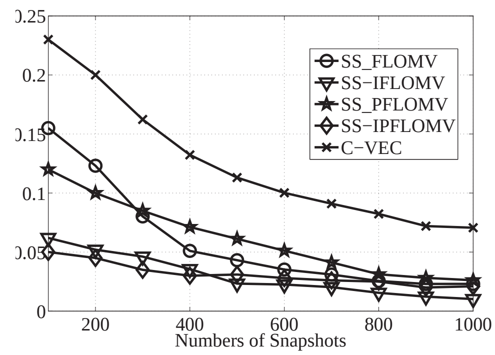

Fig. 11. RMSE versus number of snapshots.

Example 2. Three sources impinging on array from $-50°$, $0°$ and $50°$ under the condition of α stable distribution noise with characteristic exponent $\alpha = 1.5$ are considered, the number of snapshots is fixed at 100. Fig. 8 and Fig. 9 show the comparison of the probability of resolution and the RMSE with the increase of GSNR between the proposed methods and the SS_SOSCV method, respectively. It can be seen that the probability of resolution and RMSE performance of all methods improve with the increased GSNR. However, the performance of the proposed methods which are based on the sparse representation of the fractional lower order statistics vector are much better than that of second order statistics based methods. At the same time, the SS_IFLOMV and SS_IPFLOMV methods have a better performance than the SS_FLOMV and SS_PFLOMV methods, since the effects of the noise on the algorithms are further reduced by the linear transform on the fractional lower order statistics vector of the array output. It also can be seen that the performance of the methods which are based on the sparse representation of the PFLOM vector are slightly better than that of the methods which are based on the sparse representation of the FLOM vector.

Example 3. Three sources impinging on array from $-50°$, $0°$ and $50°$ under the condition of α stable distribution noise with characteristic exponent $\alpha = 1.5$ are considered under the condition of GSNR=4dB. Fig. 10 and Fig. 11 show the simulated performance of five algorithms versus the number of snapshots. It can be seen from Fig. 10 that the proposed SS_IFLOMV and SS_IPFLOMV algorithms have the similar probability of resolution performance, and are better than that of the SS_PFLOMV and SS_FLOMV, the SS_SOSCV method has the worst probability of resolution performance compared with the other algorithms. It can be seen from Fig. 11 that the RMSEs of the proposed algorithms decrease monotonically with the number of snapshots, the proposed SS_IFLOMV and SS_IPFLOMV algorithms show a more satisfactory performance than the SS_FLOMV and SS_PFLOMV algorithms, especially when the snapshot is smaller than 400.

Example 4. In this example, the performance of the proposed algorithms versus the characteristic exponent α of the noise is assessed. The other simulation conditions are similar to the example 1 except that the GSNR is set at 10dB. Firstly, the situation that the characteristic exponent varying from $\alpha = 1$ to $\alpha = 2$ is considered. The probability of resolution and RMSE performance of the five methods are displayed in Fig. 12 and Fig. 13. It can be seen from these figures that the results are similar to those of before mentioned examples. As expected, the resolution capability improves and the RMSE decreases with increased characteristic exponent and the performance of the FLOS based methods outperform the SOS based methods. The performance of the SS_IFLOMV and SS_IPFLOMV algorithms outperforms the SS_FLOMV and SS_PFLOMV algorithms, and at the same time the performance of the PFLOM vector based methods outperforms the FLOM vector based methods.

Although the FLOM and PFLOM have the good performance in suppressing the α-stable impulsive noise, they are applicable for different impulsive environment. The FLOM is limited in range of $2 \geq \alpha > 1$ and the PFLOM is applicable for $0 < \alpha \leq 2$. In other words, although FLOM can be calculated by the average in practice, there is no definition for FLOM in theory for $0 < \alpha \leq 1$. So, it can be predicted that the performance of the SS_FLOMV algorithm is inferior to that of the SS_PFLOMV algorithm, even the SS_FLOMV algorithm will does not work, when the characteristic exponent of the impulsive noise is in the range of $0 < \alpha \leq 1$. To verify this, Fig. 14 and Fig. 15 show the simulated performance of the SS_FLOMV and SS_PFLOMV algorithm under the condition of $0.1 \leq \alpha \leq 1$. It can be seen that the probability of resolution of the SS_FLOMV algorithm is zero, that is it does not work, when $0.1 < \alpha \leq 0.6$. So at this time the RMSE of the SS_FLOMV algorithm also does not exist. However, the

SS_PFLOMV algorithm maintains a stable lower probability of resolution and has a fluctuating RMSE when $0.1 < \alpha \leq 0.6$. And the performance of SS_FLOMV algorithm is much lower than that of SS_PFLOMV algorithm when $0.6 < \alpha \leq 1$.

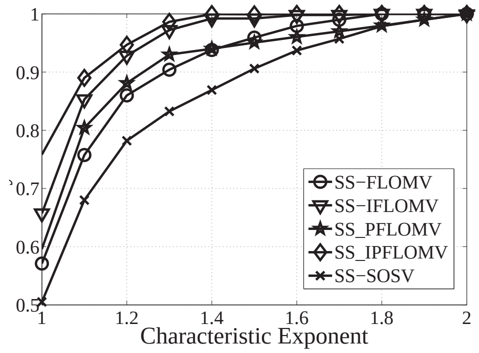

Fig. 12. Probability of resolution versus characteristic exponent α.

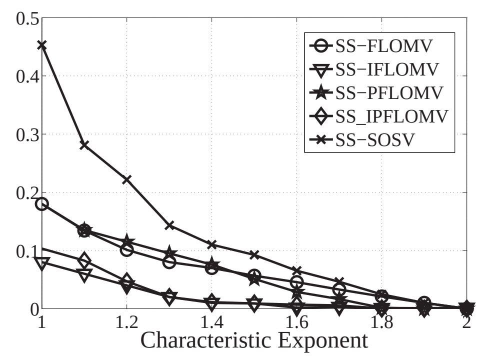

Fig. 13. RMSE versus characteristic exponent α.

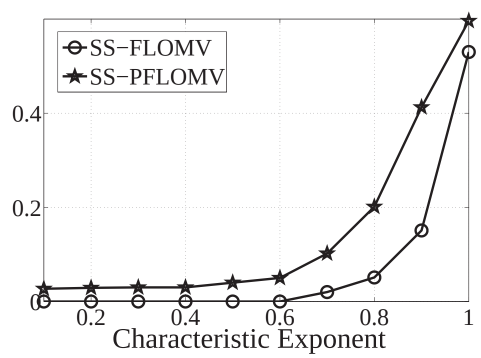

Fig. 14. Probability of resolution versus characteristic exponent α when $\alpha \leq 1$.

VI. Conclusion

The new methods based on sparse representation of the fractional lower order statistics vector are proposed for DOAs estimation under α-stable distribution impulsive noise environments. To enhance the performance of the proposed algorithms, the improved algorithms are advanced by a linear transformation on the fractional lower order statistics vector of the array output. Simulation results are shown to demonstrate the effectiveness of the proposed methods for a wide range of highly impulsive environments.

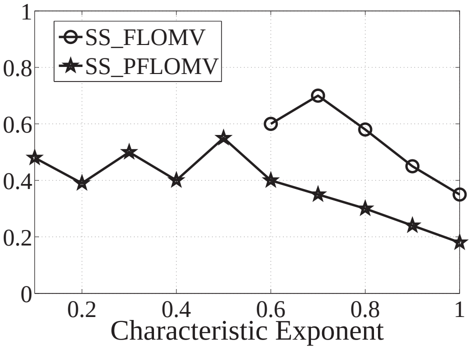

Fig. 15. RMSE versus characteristic exponent α when $\alpha \leq 1$.

References

[1] So H C. Source localization: Algorithms and analysis. *Handbook of Position Location: Theory, Practice and Advances*, Zekavat R and Michael Buehrer R, Eds. New York, NY, USA: Wiley-IEEE Press, 2011.

[2] Krim H , Viberg M. Two decades of array signal processing research: The parametric approach. *IEEE Signal Processing Magazine*, 1996, **13**(4): 67-94

[3] Fuchs J. On the use of the globe matched filter for DOA estimation in the presence of correlated waveform. In: Proceedings of the 42ndAsilomar Conference on Signals, Systems and Computers, Pacific Grove, CA, 2008, pp. 269-273

[4] Fuchs J. Identification of real sinusoids in noise, the global matched filter approach. In: Proceeding of the 15th IFCA symposium on System Identification, Saint-Malo, France, 2009, pp. 1127-1132

[5] Malioutov D, Cetin M, and Willsk A S. A sparse signal reconstruction perspective for source localization with sensor array. *IEEE Transactions on Signal Processing*, 2005, **53**(8): 3010-3022

[6] Xu X, Wei X, Ye Z. DOA estimation based on sparse signal recovery utilizing weighted l_1-norm penalty. *IEEE Signal Processing Letter*, 2012, **19**(3): 155C158

[7] Hu N, Ye Z, Xu D, Cao S. A sparse recovery algorithm for DOA estimation using weighted subspace ?tting. *Signal Processing*, 2012, **92**(10): 2566C2570

[8] Wei X, Yuan Y, Ling Q. DOA estimation using a greedy block coordinate descent algorithm. *IEEE Transaction on Signal Processing*, 2012, **60**(12): 6382C6394

[9] Hyder M M , Mahata K. Direction of arrival estimation using a mixed $L_{2,0}$ norm approximation. *IEEE Transaction on Signal Processing*, 2010, **58**(9): 4646-4655

[10] Stocia P, Prabhu B, Li J. SPICE: a sparse covariance-based estimation method for array processing. *IEEE Transaction on Signal Processing*, 2011, **59**(2): 629-638

[11] Yin J H, Chen T. Direction-of-arrival estimation using a sparse representation of array covariance vectors. *IEEE Transactions on Signal Processing*, 2011, **59**(9): 4489-4493

[12] He Z Q, Liu Q H, Jin L N, Ouyang S. Low complexity method for DOA estimation using array covariance matrix sparse representation. *Electronics Letters*, 2013, **49**(3): 228-230

[13] He Z Q, Shi Z P, Huang L. Covariance sparsity-aware DOA estimation for nonuniform noise. *Digital Signal Processing*, 2014, **28**(5): 75-81

[14] Tian Y, Sun X Y, Zhao S S. DOA and power estimation using a sparse representation of second order statistics vector and l_0-norm approximation. *Signal Processing*, 2014, **105**(12): 98-108

[15] Tian Y, Sun X Y , Zhao S S. Sparse-reconstruction-based direction of arrival, polarisation and power estimation using a cross-dipole array. *IET Radar, Sonar & Navigation*, 2015, **9**(7): 727C731

[16] Sha Z H, Liu Z M, Huang Z T, Zhou Y Y. Covariance-Based Direction-of-Arrival Estimation of Wideband Coherent Chirp Signals via Sparse Representation. *Sensors*, 2013, **13**(9): 11490C11497

[17] Mahmood A. PSK communication with passband additive symmetric α-stable noise. *IEEE Transactions on Communications*, 2012, **60**(12): 2990-3000

[18] Nikias C L, Shao M. *Signal processing with Alpha-stable distributions and applications*. New York, NY, USA: Wiely, 1995.
[19] Liu T H, Mendel J M. A subspace-based direction finding algorithm using fractional lower order statistics. *IEEE Transactions on Signal Processing*, 2001, **49**(8): 1605-1613
[20] Belkacemi H, Marcos S. Robust subspace-based algorithms for joint angle/Doppler estimation innon-Gaussian clutter. *Signal Processing*, 2007, **87**(7): 1547-1558
[21] Tzagkarakis G, Tsakalides P, Starck J L. Covariate-based subspace-augmented MUSIC for joint sparse support. *Signal Processing*, 2013, **93**(5): 1365-1373
[22] Ma W K, Hsieh T H, Chi C Y. Direction-of-arrival estimation of quasi-stationary signals with less sensors than sources and unkown spatial noise covariance: a Khatri-Rao subspace approach. *IEEE Transactions on Signal Processing*, 2010, **58**(4): 2168-2180
[23] Ottersten B, Stocia P, Roy R. Covariance matching estimation techniques for array signal processing application. *Digital Signal Processing*, 1998, **18**(7): 185-210
[24] Grant M, Boyd S, Ye Y. *CVX: Matlab Software for Disciplined Convex Programming*. CVX Research, Inc., 2008.

Sen Li received the B.S. degree in microelectronics from Liao Ning University, Shenyang, China, in 1996, M.S. degree in Information and Communication engineering from Dalian Maritime University, Dalian, China in 1999 and the Ph.D. degree in Information and Signal Processing from Dalian University of Technology, Dalian, China in 2011. In 2013, she held a postdoctoral position with the Department of Electrical and Computer Engineering, Concordia University, Montreal, Canada. She is currently an Associate Professor with the Department of Information Science and Technology, Dalian Maritime University. Her research interests include spectral estimation, array signal processing, communication signal processing, statistics and adaptive signal processing and non-Gaussian signal processing.

Rongxi He received his B.S. and M.S. degrees from Dalian Maritime University in 1992 and 1995, and his Ph. D. degree from University of Electronic Science and Technology of China in 2002. He is currently a Professor with the Department of Information Science and Technology, Dalian Maritime University. His research interests include wireless communication and networks. He is senior member of China Computer Federation (CCF), and a member of IEEE.

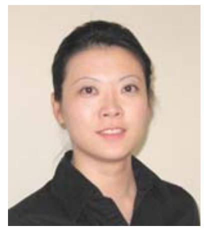

Bin Lin received the B.Sc. degree in computer communications and the M.Sc. degree in computer science from Dalian Maritime University, Dalian, China, in 1999 and 2003, respectively, and the Ph.D. degree in electrical and computer engineering from the University of Waterloo, Waterloo, ON, Canada, in 2009. In 2009, she held a postdoctoral position with the Department of Electrical and Computer Engineering, University of Waterloo. She is currently a Professor with the Department of Information Science and Technology, Dalian Maritime University. Her research interests include wireless communications, wireless/optical network integration, network dimensioning and optimization, location problems, resource allocation, artificial intelligence, pattern recognition, artificial neural networks, and marine remote sensing.

PLACE PHOTO HERE

Fei Sun no information is provided, please contact with the author.

Relationship Between Integer Order Systems and Fractional Order Systems and Its Two Applications

Xuefeng Zhang

***Abstract*—Existence of periodic solutions and stability of fractional order dynamic systems are two important and difficult issues in fractional order systems (FOS) field. In this paper, the relationship between integer order systems (IOS) and fractional order systems is discussed. A new proof method based on the above involved relationship for the non existence of periodic solutions of rational fractional order linear time invariant systems is derived. Rational fractional order linear time invariant autonomous system is proved to be equivalent to an integer order linear time invariant non-autonomous system. It is further proved that stability of a fractional order linear time invariant autonomous system is equivalent to the stability of another corresponding integer order linear time invariant autonomous system. The examples and state figures are given to illustrate the effects of conclusion derived.**

***Index Terms*—Existence, equivalence, periodic solutions, rational fractional order systems, stability.**

I. Introduction

THE concept of fractional differentiation appeared first in a famous correspondence between L' Hopital and Leibniz, in 1695. Fractional calculus has had a 300 years old history, the development of fractional calculus theory is a matter of almost exclusive interest for few mathematicians and theoretical physicists. In recent years, researchers have noticed that the description of some phenomena is more accurate when the fractional derivative is introduced. Many practical control system models can be described by fractional differential equations. It is worth mentioning that many physical phenomena having memory and genetic characteristics can be described by modeling as fractional order systems. Fractional order systems have attracted much attention. In what concerns automatic control, T. T. Hartley and C. F. Lorenzo [1] studied the fractional order algorithms for the control of dynamic systems. Podlubny [2] proposed a generalization of the PID controller, namely the PI$^{\lambda}$D$^{\mu}$ controller, involving an integrator of order λ and a differentiator of order μ. L. Yan and Y. Q. Chen [3] propose the definition of Mittag-Leffler stability and introduce the fractional Lyapunov direct method. Fractional comparison principle is introduced and the application of Riemann-Liouville fractional order systems is extended by using Caputo fractional order systems. C.P Li and F.R. Zhang [4] give a survey on the stability of fractional differential equations based on analytical methods.

This article has been accepted for publication in a future issue of this journal, but has not been fully edited. Content may change prior to final publication.

This article was recommended by Associate Editor Dingyu Xue.

X. F. Zhang is with the School of Sciences, Northeastern University, Shenyang, 110004, China (e-mail: fushun-info@163.com).

Digital Object Identifier 10.1109/JAS.2016.7510205

Fractional-order differential operators present unique and intriguing peculiarities, not supported by their integer-order counterpart, which raise exciting challenges and opportunities related to the development of control and estimation methodologies involving fractional order dynamics. In recent years, most of papers are devoted to the solvability of the linear fractional equation in terms of a special function and to problems of analyticity in the complex domain. Fractional system and its control has become one of the most popular topics in control theory [5]−[8]. The number of applications where fractional calculus has been used rapidly grows. These mathematical phenomena allow to describe a real object more accurately than the classical integer-order methods [9]−[12]. Paper [10] gives the non existence of periodic solutions in fractional order systems with Mellin transform. But for singular fractional order systems, the Mellin transform method is invalid because of singularity of systems.

In this paper, we will show that rational fractional order linear time invariant autonomous system is equivalent to an integer order linear time invariant non-autonomous system but cannot be equivalent to any integer order linear time invariant autonomous system with any system parameters. The nonexistence of periodic solutions of fractional order dynamic systems are proved by means of contradiction method. Stability of a fractional order linear time invariant autonomous system is equivalent to the stability of another corresponding integer order linear time invariant autonomous system. The examples and state figures are given to illustrate the effects of the conclusions derived. The conclusions provided in the paper can be easily extended to singular fractional order linear time invariant systems.

II. Preliminaries

Let us denote by $\mathbb{Z}^+$ the set of positive integer numbers, $\mathbb{C}$ the set of complex numbers, $\mathbb{R}^{n\times n}$ the set of $n\times n$ dimension real numbers. We denote the real part of complex number α by Re(α).

Caputo derivative has been often used in fractional order systems since it has the practical initial states like that of integer order systems.

Definition 1: The Caputo fractional order derivative with order α of function $x(t)$ is defined as

$$ {}_0^C D_t^{\alpha} x(t) = \frac{1}{\Gamma(n-\alpha)} \int_0^t (t-\tau)^{n-\alpha-1} x^{(n)}(\tau) d\tau $$

where $n-1<\alpha<n\in\mathbb{Z}^+, \Gamma$ is well-known Euler Gamma function.

Definition 2: The Riemann-Liouville derivative of fractional order α of function $x(t)$ is defined as

$$ {}_0^{RL}D_t^{\alpha}x(t)=\frac{1}{\Gamma(n-\alpha)}(\frac{d}{dt})^n\int_0^t(t-\tau)^{n-\alpha-1}x(\tau)d\tau $$

where $n-1<\alpha<n\in\mathbb{Z}^+$.

Definition 3: The Grunwald-Letnikov derivative of fractional order α of function $x(t)$ is defined as

$$ {}_0^{GL}D_t^{\alpha}x(t)=\lim_{h\to 0}h^{-\alpha}\sum_{r=0}^{(t-\alpha)/h}(-1)^rC_{\alpha}^rx(t-rh) $$

where $n-1<\alpha<n\in\mathbb{Z}^+$.

Definition 4: The Mittag-Leffler function is defined as

$$ E_{\alpha}(t)=\sum_{k=0}^{\infty}\frac{t^k}{\Gamma(k\alpha+1)} $$

where $\text{Re}(\alpha)>0,t\in\mathbb{C}$. The two-parameter Mittag-Leffler function is defined as

$$ E_{\alpha,\beta}(t)=\sum_{k=0}^{\infty}\frac{t^k}{\Gamma(k\alpha+\beta)} $$

where $\text{Re}(\alpha)>0,\beta,t\in\mathbb{C}$.

Property 1: The Laplace transform of Caputo derivative of function $x(t)$ is

$$ L({}_0^{C}D_t^{\alpha}x(t))=s^{\alpha}X(s)-\sum_{k=0}^{n-1}s^{\alpha-k-1}x^k(0), $$

where $X(s)=L[x](s),n-1<\alpha<n\in\mathbb{Z}^+$.

Property 2: If let $\alpha\in(0,\infty)\setminus\mathbb{N}$. Then, we have

$$ {}_0^{RL}D_t^{\alpha}x(t)={}_0^{GL}D_t^{\alpha}x(t)={}_0^{C}D_t^{\alpha}x(t)+\sum_{i=0}^{n-1}\frac{x^{(i)}(0)}{\Gamma(i-\alpha+1)}t^{i-\alpha} $$

where $n-1<\alpha<n\in\mathbb{Z}^+$.

Lemma 1: The Laplace transform of $t_+^{\alpha-1}/\Gamma(\alpha)$ is:

$$ L(\frac{t_+^{\alpha-1}}{\Gamma(\alpha)})=s^{-\alpha} $$

and

$$ t_+^{\alpha-1}=\begin{cases}t^{\alpha-1}, & t>0\\ 0, & t\le 0.\end{cases} $$

Lemma 2: The Laplace transform of $\frac{e^{-at}}{\sqrt{b-a}}\text{erf}(\sqrt{(b-a)t})$ is:

$$ L(\frac{e^{-at}}{\sqrt{b-a}}\text{erf}(\sqrt{(b-a)t}))=\frac{1}{\sqrt{s+b}(s+a)} $$

where $\text{erf}(t)$ is the error function for each element of t, $\text{erf}(t)=\frac{2}{\sqrt{\pi}}\int_0^te^{-\tau^2}d\tau$.

Lemma 3: The Laplace transform of $\frac{1}{\sqrt{\pi t}}-\frac{2}{\sqrt{\pi}}\text{daw}(\sqrt{t})$ is:

$$ L(\frac{1}{\sqrt{\pi t}}-\frac{2}{\sqrt{\pi}}\text{daw}(\sqrt{t}))=\frac{\sqrt{s}}{s+1} $$

where $\text{daw}(t)$ is Dawson function for each element of t, $\text{daw}(t)=e^{-t^2}\int_0^te^{\tau^2}d\tau$.

Lemma 4: The Laplace transform of $A\cos(\omega t)$ is:

$$ L(A\cos(\omega t))=\frac{As}{s^2+\omega^2}. $$

Lemma 5: The Laplace transform of $t^{\beta-1}E_{\alpha,\beta}(-\omega t^{\alpha})$ is:

$$ L(t^{\beta-1}E_{\alpha,\beta}(-\omega t^{\alpha}))=\frac{s^{\alpha-\beta}}{s^{\alpha}+\omega}. $$

Lemma 6: The Laplace transform of n order derivative $f^n(t)$ is:

$$ L(f^{(n)}(t))=s^nF(s)-\sum_{i=0}^{n-1}s^{n-1-i}f^{(i)}(0). $$

III. Main Results

A. Equivalence Between FOS and IOS

Integer order linear time invariant (LTI) systems have been developed quite maturely. Fractional order LTI system is a subsystem of dynamic control system and is less discussed due to its difficulty. In order to obtain the better control cost index, the control components and devices with fractional order properties are needed to be introduced. Algorithms in measurement technology sometimes process the fractional order characteristics. Some control plants are more difficult to be modeled than integer order systems. By the above reason, fractional order dynamic control systems are essential to be introduced. From Fig. 1, we can see that state figures of $\dot{x}(t)=tx(t)$, and those of $D^{\alpha}x(t)=x(t),\alpha=0.2,0.4,\cdots,1$, are similar to each other, but they are not identically coincided with each other. An obvious question is whether there exists an integer order LTI System (1) equivalent to a fractional order LTI System (2) with any appropriate parameters or be equivalent to a fractional order LTV System (3) with any appropriate parameters or not. It is an important problem for the reason that if the answer is 'yes' the fractional order systems can be regarded as a part of integer order systems and if the answer is 'no' the fractional order systems cannot be ignored so that the research of FOS is magnificently innovative. From the theorems in Section III, it is found that the answer is negative. It can hold only if the state is zero solution. Actually, System (1) is equivalent to System (4) in some cases. In the following subsection, we can have that if $\alpha=1/2$, System (4) reduces to System (5).

$$ D^{\alpha}x(t)=Ax(t) \tag{1} $$

$$ \dot{x}(t)=A_1x(t) \tag{2} $$

$$ \dot{x}(t)=A_2(t)x(t) \tag{3} $$

$$ \dot{x}(t)=\frac{A}{\Gamma(\alpha)}\int_0^t(t-\tau)^{\alpha-1}x'(\tau)d\tau+\frac{Ax(0)t_+^{\alpha-1}}{\Gamma(\alpha)} \tag{4} $$

$$ \dot{x}(t)=A^2x(t)+\frac{Ax(0)t_+^{-\frac{1}{2}}}{\Gamma(\frac{1}{2})}. \tag{5} $$

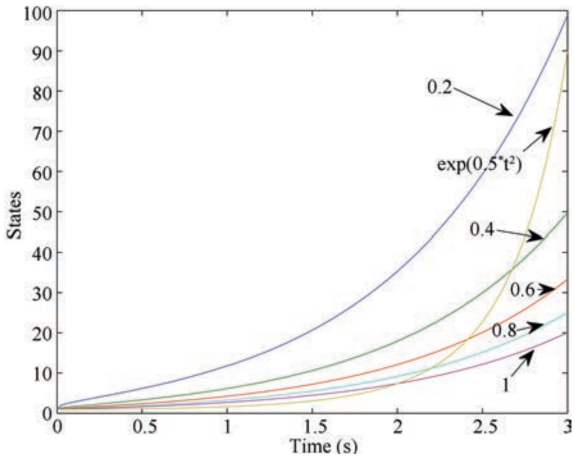

Fig. 1. Plot of states of $\dot{x}(t) = tx(t)$ and $D^\alpha x(t) = x(t)$.

From the discussion on relationship between FOS and IOS in the above subsection, it is easy to introduce its two applications i.e., non existence of periodic solutions for FOS and stability between FOS and IOS.

B. Non Existence of Periodic Solutions for FOS

Theorem 1: While $\alpha = 1/2$, System (1) is equivalent to (5).

Proof: Using Laplace transform for System (1), taking into account the Caputos definition for the fractional-order derivatives in (2), and applying Property 1 in the case that $0 < \alpha < 1$, it yields that

$$s^\alpha X(s) - s^{\alpha-1}x(0) = AX(s).$$

Pre- and post-multiplying above equation by $s^{1-\alpha}$, it follows that

$$\begin{aligned} sX(s) - x(0) =& As^{1-\alpha}X(s) \\ =& A(s^{1-\alpha}X(s) - s^{-\alpha}x(0)) + As^{-\alpha}x(0). \end{aligned}$$

By Lemma 1 and taking inverse Laplace transform in above equation, we have (4).

When $\alpha = 1/2$, we have System (5). If we denote $B = Ax(0), u(t) = t_+^{-\frac{1}{2}}/\Gamma(\frac{1}{2})$, then (5) changes as (6)

$$\dot{x}(t) = A^2x(t) + Bu(t). \tag{6}$$

When $\alpha = p/q, p, q \in \mathbb{Z}^+$, System (1) can be proved to be equivalent to (7).

$$\begin{aligned} x^{(p)}(t) =& A^q x(t) + \sum_{i=1}^{q-1} A^{q-i} \frac{t_+^{-\frac{ip}{q}}}{\Gamma(1-\frac{ip}{q})} x(0) \\ &+ \sum_{i=1}^{p-1} \delta^{(p-1-i)}(t) x^{(i)}(0) \end{aligned} \tag{7}$$

where δ is the unit pulse function.

Theorem 2: While $\alpha = p/q$, System (1) is equivalent to (7).

Proof: Using Laplace transform in (1), taking into account the Caputos definition for the fractional-order derivatives in (2), and applying Property 1 in the case that $0 < \alpha < 1$, we have that

$$s^\alpha X(s) - s^{\alpha-1}x(0) = AX(s)$$

i.e.,

$$s^{\frac{p}{q}}X(s) - s^{p/q-1}x(0) = AX(s).$$

Pre- and post-multiplying above equation by $s^{p/q}$, it follows that

$$\begin{aligned} & s^{\frac{2p}{q}}X(s) - s^{\frac{2p}{q}-1}x(0) \\ &= As^{\frac{p}{q}}X(s) = A(s^{\frac{p}{q}}X(s) - s^{\frac{p}{q}-1}x(0)) + As^{\frac{p}{q}-1}x(0) \\ &= A^2X(s) + As^{\frac{p}{q}-1}x(0). \end{aligned}$$

Keeping on pre- and post-multiplying above equation by $s^{\frac{p}{q}}$ till q times, it follows that

$$s^pX(s) - s^{p-1}x(0) = A^qX(s) + \sum_{i=1}^{q-1} A^{q-i}s^{\frac{ip}{q}-1}x(0)$$

i.e.,

$$\begin{aligned} & s^pX(s) - \textstyle\sum_{i=0}^{p-1} s^{p-1-i}x^{(i)}(0) \\ &= A^qX(s) + \textstyle\sum_{i=1}^{q-1} A^{q-i}s^{\frac{ip}{q}-1}x(0) - \sum_{i=1}^{p-1} s^{p-1-i}x^{(i)}(0). \end{aligned}$$

By Lemma 1 and Property 1 and taking inverse Laplace transform in above equation, we have (7).

Theorem 3: Linear time invariant fractional system (1) with order $0 < \alpha < 1, \alpha = p/q, p, q \in \mathbb{Z}^+$ has no periodic solution.

Proof: By contradiction, suppose linear time invariant fractional system (1) has a periodic solution $x(t)$. For $T-$periodic function $x(t+T) = x(t)$, from

$$\frac{d}{dt}x(t+T) = \frac{d}{d(t+T)}x(t+T)\frac{d}{dt}(t+T) = x'(t+T)$$

it is easy to see that $x^{(k)}(t+T) = x^{(k)}(t)$. From Theorem 2, we know that (1) is equivalent to (7). If we denote

$$\begin{aligned} & f(t) = x^{(p)}(t) - A^qx(t) \\ & g(t) = \textstyle\sum_{i=1}^{q-1} A^{q-i}\frac{t_+^{-\frac{i}{q}}}{\Gamma(1-\frac{i}{q})}x(0) + \sum_{i=1}^{p-1}\delta^{(p-1-i)}x^{(i)}(0) \end{aligned}$$

then $f(t) = g(t)$. However, $f(t)$ is periodic function but $g(t)$ is a non-periodic function. So, there does not exist any periodic solution for System (1). ■

Remark 1: From Theorem 2, we know that there does not exist any integer order LTI System (2) be equivalent to a fractional order LTI System (7) with any appropriate parameters. It means the properties of fractional order LTI systems may be different from those of integer order LTI systems. It can attract researchers to explore the distinct properties of fractional order LTI systems.

Remark 2: Theorem 3 gives a concise and effective proof that there does not exist periodic solutions for fractional order LTI System (7).

Remark 3: With the equivalence between the integer order LTI System (7) and the fractional order LTI System (1), we succeed in finding a new research approach of discussing the difficult fractional order LTI System (1). However, relative to System (1), it is easy and there exists extensive results to discuss the integer order LTI System (7). For example, we can further discuss the stability and robust stability of fractional order LTI System (1) in the future.

Remark 4: From Theorem 3, we can see that only if α is an integer, it follows $g(t) = 0$. This means only if α is an integer, it is possible for System (1) to satisfy periodic solutions.

C. Stabilities Between FOS and IOS

Lemma 7: [12] System (1) is asymptotically stable if and only if there exist two matrices $X, Y \in \mathbb{R}^{n\times n}$, such that

$$\begin{bmatrix} X & Y \\ -Y & X \end{bmatrix} > 0$$
$$aAX + bAY + aXA^T - bYA^T < 0$$

where $a = \sin(\alpha\pi/2), b = \cos(\alpha\pi/2)$.

Lemma 8: [12] System (1) is asymptotically stable if and only if there exist two matrices $X, Y \in \mathbb{R}^{n\times n}$, such that

$$\begin{bmatrix} X & Y \\ -Y & X \end{bmatrix} > 0, \quad \begin{bmatrix} \Pi_1 & \Pi_2 \\ -\Pi_2 & \Pi_1 \end{bmatrix} < 0$$

where

$$\Pi_1 = aAX + bAY + aXA^T - bYA^T$$
$$\Pi_2 = aAY - bAX + bXA^T + aYA^T$$

and a, b are the same as those in Lemma 7.

Lemma 9: [12] A complex matrix $X \in \mathbb{C}^{n\times n}$ satisfies $X < 0$ if and only if

$$\begin{bmatrix} \mathrm{Re}(X) & \mathrm{Im}(Y) \\ -\mathrm{Im}(Y) & \mathrm{Re}(X) \end{bmatrix} < 0. \tag{8}$$

Consider the following specific complex integer order linear time invariant system

$$\dot{x}(t) = (a + jb)A^T x(t) \tag{9}$$

where system matrix $A \in \mathbb{R}^{n\times n}$, j is the imaginary unit.

Using Lyapunov theory of integer order systems and Lemmas 7 and 8, it is easy to obtain the following equivalence stability criterion.

Theorem 4: Fractional order system (1) is asymptotically stable if and only if integer order system (9) is asymptotically stable.

Proof For the specific complex integer order LTI system (9), we choose the quadratic Lyapunov candidate function as

$$V(x(t)) = x^T(t)(X + jY)x(t)$$

where $X + jY > 0$. Then, differentiating $V(x(t))$ with respect to time t along to the solution of (9), we obtain

$$\begin{aligned}\dot{V} &= x^T(t)[(a - jb)A(X + jY) + (X + jY)(a + jb)A^T]x(t)\\ &= x^T(t)(\Pi_1 + j\Pi_2)x(t) < 0.\end{aligned}$$

Using Lyapunov theory of complex integer order systems and considering (8) in Lemma 9, this completes the proof.

IV. Numerical Examples

Example 1: Consider integer order System (2) with parameters as follows:

$$A_1 = \begin{bmatrix} 0 & 1 \\ -1 & 0 \end{bmatrix}, \quad x(0) = \begin{bmatrix} 1 \\ 1 \end{bmatrix}$$

from Fig. 2, we can see that the solutions are periodic. But if we consider System (1) with the same above parameters and $\alpha = 1/2$, then by Laplace transform for System (1) we have

$$s^{\frac{1}{2}}X_1(s) - X_2(s) = s^{-\frac{1}{2}}$$
$$s^{\frac{1}{2}}X_2(s) + X_1(s) = s^{-\frac{1}{2}}.$$

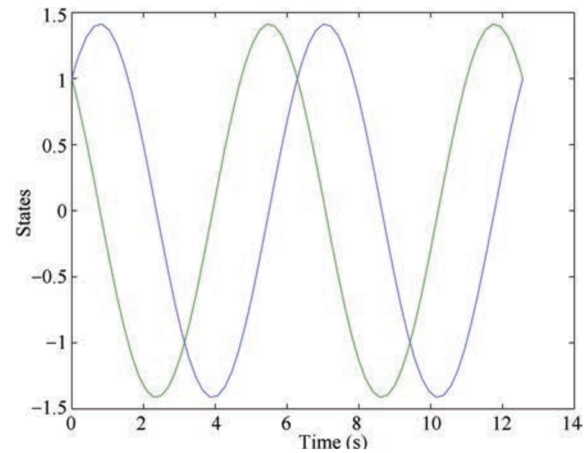

Fig. 2. State curves of IOS in Example 1.

It is easy to obtain the solutions of the above equations as follows:

$$X_1(s) = \frac{s^{-\frac{1}{2}+1}}{s+1}, \quad X_2(s) = \frac{s^{\frac{1}{2}}+1}{s+1} - s^{\frac{1}{2}}.$$

Consider Lemma 1 and 3, and take the inverse Laplace transform for $X_1(s)$ and $X_2(s)$, it follows that:

$$x_1(t) = e^{-t} + \tfrac{2}{\sqrt{\pi}}\mathrm{daw}(\sqrt{t})$$
$$x_2(t) = e^{-t} + \tfrac{1}{\sqrt{\pi t}} - \tfrac{2}{\sqrt{\pi}}\mathrm{daw}(\sqrt{t}) - \tfrac{t^{-\frac{1}{2}}}{\Gamma(\frac{1}{2})}.$$

With Lemma 5, it also follows that:

$$x_1(t) = e^{-t} + t^{\frac{1}{2}}E_{1,\frac{3}{2}}(-t)$$

$$x_2(t) = e^{-t} - t^{\frac{1}{2}}E_{1,\frac{1}{2}}(-t) - \frac{t^{-\frac{1}{2}}}{\Gamma(\frac{1}{2})}.$$

It is easy to see from Fig. 3 that the state curves of fractional order System (1) with parameter $\alpha = 1/2$ do not possess periodic dynamic orbits.

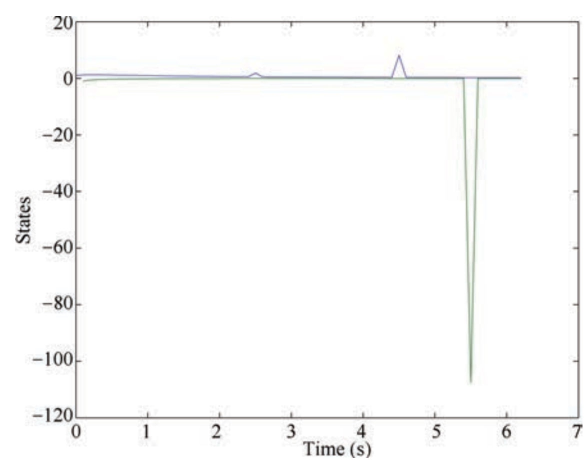

Fig. 3. State curves of FOS in Example 1.

Example 2: By Theorem 2, for $\alpha = 1/3$, we have that System (1) is equivalent to

$$\dot{x}(t) = x(t) + \frac{t_+^{-\frac{1}{3}}}{\Gamma(1-\frac{1}{3})}x(0) + \frac{t_+^{-\frac{2}{3}}}{\Gamma(1-\frac{2}{3})}x(0).$$

From Fig. 4, we can see the state curves of fractional order System (1) with parameter $\alpha = 1/3$ are completely identical to the corresponding state curves of integer order System (7).

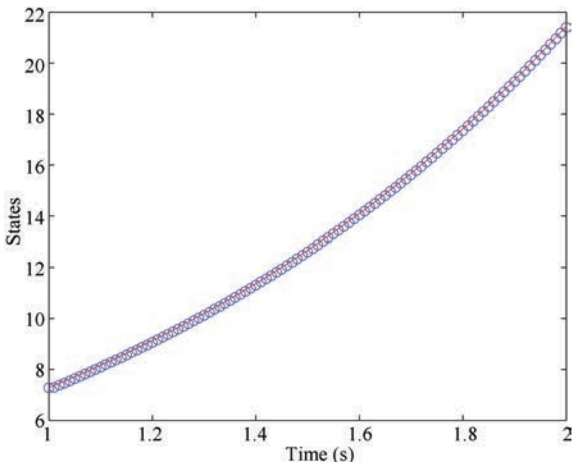

Fig. 4. State curves of FOS in Example 2.

V. CONCLUSIONS

Many systems exhibit the fractional phenomena, such as motions in complex media or environments, random walk of bacteria in fractal substance, etc. These models can be obtained by solving modified fractional order systems. In this paper, we discuss the relationship between rational fractional order systems and integer order systems and conclude that the two kind of systems cannot be substituted for each other. The criteria of nonexistence of periodic solution of fractional order systems are addressed. The proof approach is based on the properties of Laplace transform of fractional order systems. Stability of a fractional order linear time invariant autonomous system is equivalent to the stability of another corresponding integer order linear time invariant autonomous system. Some numerical examples are given to verify the feasibility of results presented. The methods provided in the paper can be extended to singular fractional order linear time invariant systems in the future.

REFERENCES

[1] Hartley T T, Lorenzo C F. Dynamics and control of initialized fractional-order systems. *Nonlinear Dynamics*, 2002, **29**(1−4): 201−233

[2] Podlubny I. Fractional-order systems and PI$^{\lambda}$D$^{\mu}$-controllers. *IEEE Transactions on Automatic Control*, 1999, **44**(1): 208−214

[3] Li Y, Chen Y Q, Podlubny I. Mittag-Leffler stability of fractional order nonlinear dynamic systems. *Automatica*, 2009, **45**(8): 1965−1969

[4] Li C P, Zhang F R. A survey on the stability of fractional differential equations. *The European Physical Journal Special Topics*, 2011, **193**(1): 27−47

[5] Liao Z, Peng C, Li W, Wang Y. Robust stability analysis for a class of fractional order systems with uncertain parameters. *Journal of the Franklin Institute*, 2011, **348**(6): 1101−1113

[6] Li C P, Deng W H. Remarks on fractional derivatives. *Applied Mathematics and Computation*, 2007, **187**(2): 777−784

[7] Haubold H J, Mathai A M, Saxena R K. Mittag-Leffler functions and their applications. *Journal of Applied Mathematics*, 2011, **2011**: Article ID 298628

[8] Erdélyi A. *Tables of Integral Transforms*. New York: McGraw-Hill, 1954.

[9] Sabatier J, Moze M, Farges C. LMI stability conditions for fractional order systems. *Computers & Mathematics with Applications*, 2010, **59**(5): 1594−1609

[10] Kaslik E, Sivasundaram S. Non-existence of periodic solutions in fractional-order dynamical systems and a remarkable difference between integer and fractional-order derivatives of periodic functions. *Nonlinear Analysis: Real World Applications*, 2012, **13**(3): 1489−1497

[11] Bagley R L, Calico R A. Fractional order state equations for the control of viscoelastically damped structures. *Journal of Guidance, Control, and Dynamics*, 1991, **14**(2): 304−311

[12] Zhang X F, Chen Y Q. D-stability based LMI criteria of stability and stabilization for fractional order systems. In: Proceedings of the ASME 2015 International Design Engineering Technical Conferences & Computers and Information in Engineering Conference. Boston, USA: ASME, 2015.

Xuefeng Zhang is currently with the School of Sciences, Northeastern University, Shenyang, China. His research interests include fractional order control systems and singular systems. He received the B.Sc. degree in applied mathematics in 1989 and the M.S. degree in control theory and control engineering in 2004 and the Ph.D. degree in control theory and control engineering in 2008 from Northeastern University, China.

Dynamics of the Fractional-order Lorenz System Based on Adomian Decomposition Method and Its DSP Implementation

Shaobo He, Kehui Sun, and Huihai Wang

***Abstract*—Dynamics and digital circuit implementation of the fractional-order Lorenz system are investigated by employing Adomian decomposition method (ADM). Dynamics of the fractional-order Lorenz system with derivative order and parameter varying is analyzed by means of Lyapunov exponents (LEs), bifurcation diagram, chaos diagram and phase diagram. Results show that the fractional-order Lorenz system has rich dynamical behavior and it is a potential model for application. It is also found that the minimum order is affected by numerical algorithm and time step size. Finally, the fractional-order system is implemented on DSP digital circuit. Phase diagrams generated by the DSP are consistent with that generated by simulation.**

***Index Terms*—fractional calculus, Lorenz system, Adomian decomposition method, dynamics, DSP implementation.**

I. INTRODUCTION

IN recent years, the application of fractional calculus to chaotic system has become a hot topic [1], and researchers begin to investigate dynamics and applications of the fractional-order chaotic systems [2,3].

The fractional-order Lorenz system with a new set of parameters is firstly analyzed by Grigorenko I et.al [4], and they reported that the system can generate chaos when the total order is 2.91 by a numerical method they derived. Unfortunately, an error was found in the derived numerical method, thus the result in this paper was not reliable [5]. More recently, Jia H Y et al. [6] analyzed dynamics of this system with order q=0.7, 0.8 and 0.9 and implemented it in analog circuit by employing frequency domain method (FDM) [7]. However, whether this method accurately reflects chaotic characteristics in fractional-order chaotic system was questioned in [8-10]. Another method for solving fractional-order chaotic systems is the Adams-Bashforth-Moulton algorithm (ABM) [11]. It can be used to analyze dynamics with continuous derivative order [12], and some researches of the fractional-order chaos are based on this algorithm [13, 14]. But the calculation speed of this algorithm is very slow, and it consumes too many computer resources [15]. Meanwhile, Adomian decomposition method (ADM)[16] is employed to obtain numerical solution of the fractional-order chaotic system for its high precision and fast speed of convergence [17-19]. For instance, the fractional-order Chen system is investigated by Cafagna D et.al [19] by applying ADM, and the results show that it is a good method for solving the fractional-order chaotic systems. In addition, based on ADM, Lyapunov exponents (LEs) of the fractional-order system are calculated [20]. Furthermore, circuit design is essential for application of fractional-order chaotic systems. Although analog circuit implementation is widely reported by researchers [6], digital circuit realization of the fractional-order chaotic system has better flexibility and repeatability [21]. So, we focus on dynamics of the fractional-order Lorenz system and its DSP implementation by employing ADM in this paper.

The structure of the paper is as follows. In Sec.II, characteristics of the ADM are presented and the numerical solution of fractional-order Lorenz system is obtained. In Sec.III, dynamics of the fractional-order Lorenz system is investigated. In Sec.IV, the fractional-order Lorenz system is realized by employing DSP technology. Finally, we summarize the conclusions.

This article has been accepted for publication in a future issue of this journal, but has not been fully edited. Content may change prior to final publication.

This work was supported by the National Natural Science Foundation of China (Nos. 61161006 and 61573383). Recommended by Associate Editor Dingyü Xue.

S. He, K. Sun and H. Wang are with School of Physics and Electronics, Central South University, China (e-mail: heshaobo_123@163.com;kehui@csu.edu.cn;wanghuihai_csu@csu.edu.cn).

K. Sun is also with School of Physics Science and Technology, Xinjiang University, China.

Digital Object Identifier 10.1109/JAS.2016.7510133

II. NUMERICAL SOLUTION FOR THE FRACTIONAL-ORDER LORENZ SYSTEM

A. Advantages of Adomian decomposition method

We choose ADM to solve the fractional-order chaotic system since it has some advantages over the following aspects comparing with other standard numerical methods.

i) ADM can get more exact solution of the fractional-order system as it preserves the system nonlinearities. The precision of FDM is within 2dB or 3dB, and a satisfying approximation of the actual system can be obtained within the desired frequency band. But a large error is illustrated at the high and low frequency band [10, 23]. The truncation error of ABM is $O(h^p)$, p=min(2,1+q). It is acceptable, but it is not as effective as ADM [15].

ii) ADM obtains chaos with much lower order. Taking fractional-order Chen system as an example, the minimum order by ADM is 0.24 [19], and this value represents the lowest order reported in literatures. However, the minimum order of this system by ABM is 2.64 [8], and it is difficult for FDM to obtain the minimum order of a fractional-order chaotic system.

iii) ADM provides a potential iterative approach for digital circuit implementation of the fractional-order chaotic system.

ABM is not suitable for practical application of fractional-order chaotic system since it needs more and more time and memory space for computation as time goes on [15]. FDM is the theoretical basis for the fractional-order chaotic systems implemented in analog circuit.

B. Description of Adomian decomposition method

For a given fractional-order chaotic system with form of $D_{t_0}^q \mathbf{x}(t)$=$f(\mathbf{x}(t))$+$\mathbf{g}(t)$, where $\mathbf{x}(t)$=[$x_1(t)$, $x_2(t)$, ..., $x_n(t)$] is the state variable, $\mathbf{g}(t) = [g_1(t), g_2(t), ..., g_n(t)]$ is the constant in the system, and $D_{t_0}^q$ is the Caputo fractional derivative operator [17]. So it can be divided into three parts as the form

$$D_{t_0}^q \mathbf{x}(t) = L\mathbf{x}(t) + N\mathbf{x}(t) + \mathbf{g}(t), \tag{1}$$

where $m \in N$, $m-1 < q \leq m$. $L\mathbf{x}(t)$ and $N\mathbf{x}(t)$ are the linear and nonlinear terms of the fractional differential equations respectively. Here, let $J_{t_0}^q$ is the inverse operator of $D_{t_0}^q$, thus we have [17].

$$\mathbf{x} = J_{t_0}^q L\mathbf{x} + J_{t_0}^q N\mathbf{x} + J_{t_0}^q \mathbf{g} + \Phi, \tag{2}$$

where $\Phi = \sum_{k=0}^{m-1} \mathbf{b}_k (t-t_0)^k/k!$, $\mathbf{x}^{(k)}(t_0^+) = \mathbf{b}_k, k = 0, \cdots, m-1$, and it involves the initial condition. By applying the recursive relation [17]

$$\begin{cases} \mathbf{x}^0 = J_{t_0}^q \mathbf{g} + \Phi \\ \mathbf{x}^1 = J_{t_0}^q L\mathbf{x}^0 + J_{t_0}^q \mathbf{A}^0(\mathbf{x}^0) \\ \mathbf{x}^2 = J_{t_0}^q L\mathbf{x}^1 + J_{t_0}^q \mathbf{A}^1(\mathbf{x}^0, \mathbf{x}^1) \\ \cdots \\ \mathbf{x}^i = J_{t_0}^q L\mathbf{x}^{i-1} + J_{t_0}^q \mathbf{A}^{i-1}(\mathbf{x}^0, \mathbf{x}^1, \cdots, \mathbf{x}^{i-1}) \\ \cdots \end{cases}, \tag{3}$$

the analytical solution of the fractional-order system is presented as

$$\mathbf{x}(t) = \sum\nolimits_{i=0}^{\infty} \mathbf{x}^i, \tag{4}$$

where $i = 1, 2, ..., \infty$, and the nonlinear terms of the fractional differential equations $N\mathbf{x}(t)$ are evaluated by [22]

$$N\mathbf{x} = \sum_{i=0}^{\infty} \mathbf{A}^i(\mathbf{x}^0, \mathbf{x}^1, \cdots, \mathbf{x}^i), \tag{5}$$

$$\begin{cases} A_j^i = \frac{1}{i!}\left[\frac{d^i}{d\lambda^i} N(v_j^i(\lambda))\right]_{\lambda=0} \\ v_j^i(\lambda) = \sum\limits_{k=0}^{i} (\lambda)^k x_j^k \end{cases}. \tag{6}$$

Because ADM converges very fast [17-19], we choose $i = 6$ for the approximate solution in this paper. To discretize Eq.(4), a time interval $[t_0, t]$ is divided into subintervals $[t_n, t_{n+1}]$, where $h = t_{n+1} - t_n$. So, the solution of the fractional-order Lorenz system is expressed as

$$\mathbf{x}(t_n) = \sum\nolimits_{i=0}^{6} \mathbf{x}^i(t_{n-1}) = F(\mathbf{x}(t_{n-1})). \tag{7}$$

Then we can obtain the discrete iterative form $\mathbf{x}(t_{n+1}) = F(\mathbf{x}(t_n))$, which is denoted as $\mathbf{x}(n+1) = F(\mathbf{x}(n))$ for general cases.

C. Solution of the fractional-order Lorenz system

The fractional-order chaotic Lorenz system is presented by [4, 6] as

$$\begin{cases} D_{t0}^q x_1 = a(x_2 - x_1) \\ D_{t0}^q x_2 = cx_1 - x_1x_3 + dx_2 \\ D_{t0}^q x_3 = x_1x_2 - bx_3 \end{cases}, \tag{8}$$

where a, b, c, and d are system parameters, and q is the derivative order. As the same with [4] and [6], we investigate dynamics and digital circuit realization of this system by fixing $a = 40$, $b = 3$, $c = 10$, and varying d and q. By applying ADM, the numerical solution of the fractional-order Lorenz system is denoted by

$$\begin{cases} x_1(n+1) = \sum_{j=0}^{6} \kappa_1^j h^{jq}/\Gamma(jq+1) \\ x_2(n+1) = \sum_{j=0}^{6} \kappa_2^j h^{jq}/\Gamma(jq+1) \\ x_3(n+1) = \sum_{j=0}^{6} \kappa_3^j h^{jq}/\Gamma(jq+1) \end{cases}. \tag{9}$$

where h is the integration step-size, $\Gamma(\cdot)$ is the Gamma function, and $\kappa_i^j(\cdot)$ are defined as

$$\kappa_1^0 = x_1(n), \kappa_2^0 = x_2(n), \kappa_3^0 = x_3(n), \tag{10}$$

$$\begin{cases} \kappa_1^1 = a(\kappa_2^0 - \kappa_1^0) \\ \kappa_2^1 = c\kappa_1^0 + d\kappa_2^0 - \kappa_1^0\kappa_3^0 \\ \kappa_3^1 = -b\kappa_3^0 + \kappa_1^0\kappa_2^0 \end{cases}, \tag{11}$$

$$\begin{cases} \kappa_1^2 = a(\kappa_2^1 - \kappa_1^1) \\ \kappa_2^2 = c\kappa_1^1 + d\kappa_2^1 - \kappa_1^0\kappa_3^1 - \kappa_1^1\kappa_3^0 \\ \kappa_3^2 = \kappa_1^1\kappa_2^0 + \kappa_1^0\kappa_2^1 - b\kappa_3^1 \end{cases}, \tag{12}$$

$$\begin{cases} \kappa_1^3 = a(\kappa_2^0 - \kappa_1^0) \\ \kappa_2^3 = c\kappa_1^2 + d\kappa_2^2 - \kappa_1^0\kappa_3^2 - \\ \qquad \kappa_1^1\kappa_3^1\frac{\Gamma(2q+1)}{\Gamma^2(q+1)} - \kappa_1^2\kappa_3^0 \\ \kappa_3^3 = \kappa_1^0\kappa_2^2 + \kappa_1^1\kappa_2^1\frac{\Gamma(2q+1)}{\Gamma^2(q+1)} + \\ \qquad \kappa_1^2\kappa_2^0 - b\kappa_3^2 \end{cases}, \tag{13}$$

$$\begin{cases} \kappa_1^4 = a(\kappa_2^3 - \kappa_1^3) \\ \kappa_2^4 = c\kappa_1^3 + d\kappa_2^3 - \kappa_1^0\kappa_3^3 - \kappa_1^3\kappa_3^0 - \\ \qquad (\kappa_1^2\kappa_3^1 + \kappa_1^1\kappa_3^2)\frac{\Gamma(3q+1)}{\Gamma(q+1)\Gamma(2q+1)} \\ \kappa_3^4 = \kappa_1^0\kappa_2^3 + \kappa_1^3\kappa_2^0 + b\kappa_3^3 + \\ \qquad (\kappa_1^2\kappa_2^1 + \kappa_1^1\kappa_2^2)\frac{\Gamma(3q+1)}{\Gamma(q+1)\Gamma(2q+1)} \end{cases}, \tag{14}$$

$$\begin{cases} \kappa_1^5 = a(\kappa_2^4 - \kappa_1^4) \\ \kappa_2^5 = c\kappa_1^4 + d\kappa_2^4 - \kappa_1^0\kappa_3^4 - \\ \qquad (\kappa_1^3\kappa_3^1 + \kappa_1^1\kappa_3^3)\frac{\Gamma(4q+1)}{\Gamma(q+1)\Gamma(3q+1)} - \\ \qquad \kappa_1^2\kappa_3^2\frac{\Gamma(4q+1)}{\Gamma^2(2q+1)} - \kappa_1^4\kappa_3^0 \\ \kappa_3^5 = \kappa_1^0\kappa_2^4 + (\kappa_1^3\kappa_2^1 + \kappa_1^1\kappa_2^3)\frac{\Gamma(4q+1)}{\Gamma(q+1)\Gamma(3q+1)} \\ \qquad + \kappa_1^2\kappa_2^2\frac{\Gamma(4q+1)}{\Gamma^2(2q+1)} + \kappa_1^4\kappa_2^0 - b\kappa_3^4 \end{cases}, \tag{15}$$

$$\begin{cases} \kappa_1^6 = a(\kappa_2^5 - \kappa_1^5) \\ \kappa_2^6 = c\kappa_1^5 + d\kappa_2^5 - \kappa_1^0\kappa_3^5 - \\ \qquad (\kappa_1^1\kappa_3^4 + \kappa_1^4\kappa_3^1)\frac{\Gamma(5q+1)}{\Gamma(q+1)\Gamma(4q+1)} - \\ \qquad (\kappa_1^2\kappa_3^3 + \kappa_1^3\kappa_3^2)\frac{\Gamma(5q+1)}{\Gamma(2q+1)\Gamma(3q+1)} - \kappa_1^5\kappa_3^0 \\ \kappa_3^6 = \kappa_1^0\kappa_2^5 + \kappa_1^5\kappa_2^0 - b\kappa_3^5 + \\ \qquad (\kappa_1^1\kappa_2^4 + \kappa_1^4\kappa_2^1)\frac{\Gamma(5q+1)}{\Gamma(q+1)\Gamma(4q+1)} + \\ \qquad (\kappa_1^2\kappa_2^3 + \kappa_1^3\kappa_2^2)\frac{\Gamma(5q+1)}{\Gamma(2q+1)\Gamma(3q+1)} \end{cases}, \tag{16}$$

According to Eq.(9), the chaotic sequences of the fractional-order Lorenz system are obtained with appropriate initial values. Meanwhile, Eq.(9) provides a necessary iterative approach for DSP implementation of the fractional-order Lorenz system.

III. Chaotic dynamics of the fractional-order Lorenz system

A. Design of Lyapunov exponents calculation algorithm

The Lyapunov exponents are calculated based on Jacobian matrix obtained from Eqs. (9)-(16) and QR decomposition method [20]. The QR decomposition method is shown as

$$\begin{aligned} qr(\mathbf{J}_N\mathbf{J}_{N-1}\cdots\mathbf{J}_1) &= qr\left(\mathbf{J}_N\mathbf{J}_{N-1}\cdots\mathbf{J}_2(\mathbf{J}_1\mathbf{Q}_0)\right) \\ &= qr\left(\mathbf{J}_N\mathbf{J}_{N-1}\cdots\mathbf{J}_3(\mathbf{J}_2\mathbf{Q}_1)\right)\mathbf{R}_1\ , \\ &= \mathbf{Q}_N\mathbf{R}_N\cdots\mathbf{R}_2\mathbf{R}_1 \end{aligned} \tag{17}$$

where $qr(\cdot)$ is the QR decomposition function, $\mathbf{J}$ is the Jacobian matrix of Eq.(9). The Lyapunov exponents are obtained as

$$\lambda_k = \frac{1}{Nh}\sum_{i=1}^{N}\ln|R_i(k,k)|, \tag{18}$$

where k=1, 2, 3, and N is the iteration times. The flow chart for LEs calculation is shown in Fig.1. Before calculating LEs, parameters, time step size h and number of iterations N should be confirmed. The Jacobian matrix is obtained according to Eq.(9) by applying mathematical software Matlab. LEs are calculated based on the QR decomposition method as illustrated in Eqs. (17) and (18).

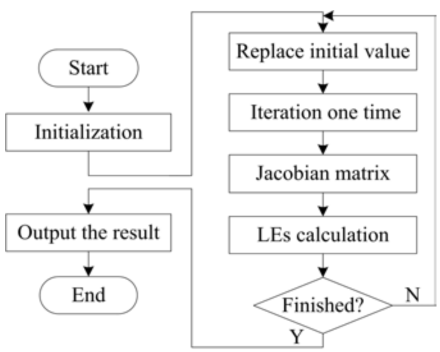

Fig. 1. Flow diagram for LEs calculation algorithm.

B. Dynamics with varying parameters

In this section, dynamics in the fractional-order Lorenz system with varying system parameter d and derivative order q are investigated. Parameter fixed dynamical analysis method and chaos diagram are used. Here, we set N=20000 and h=0.01. Three cases are investigated.

i) Fix $d = 25$, and vary derivative order q from 0.75 to 1 with step size of 0.0005. The bifurcation diagram and LEs are shown in Fig.2. It shows that the system generates chaos for $0.813 \leq q < 1$ except some periodic windows. Thus the minimum total order for fractional-order Lorenz system to generate chaos is 2.439 and the corresponding phase diagram is shown in Fig.3. In addition, the maximum Lyapunov exponent illustrates a decreasing trend as order q increasing.

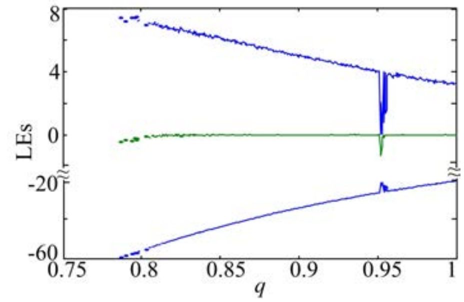

(a) LEs

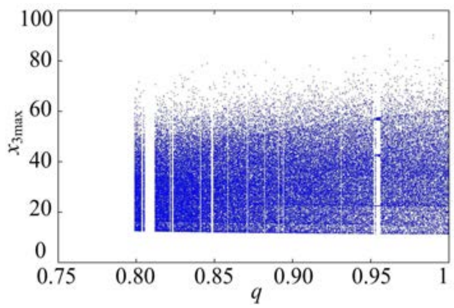

(b) Bifurcation diagram

Fig. 2. Dynamics of the fractional-order Lorenz system with $d = 25$ and q varying

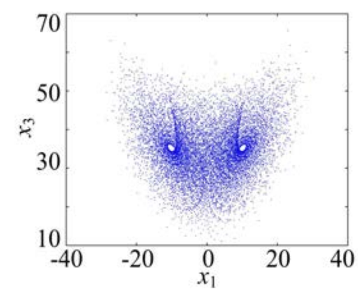

Fig. 3. Phase diagram of the fractional-order Lorenz system with $d = 25$ and $q = 0.813$.

ii) Fix $q = 0.96$ and vary d from 0 to 38 with step size of 0.1. When d decreases from 38, the system presents periodical states until it enters into chaos at $d = 32.1$ by the period-doubling bifurcation as shown in Fig. 4(a). Chaos covers most of the range $d \in [9.8, 32.1]$ with several small periodic widows, such as $d \in [14.5, 16.3] \cup [21.1, 21.5]$. Finally, the system becomes convergent at $d = 9.8$ by a tangent bifurcation. To observe dynamics better, phase diagrams are presented in Fig.5. When d=15, 21.5 and 37, the system is periodic, and the system is chaotic when $d = 20$. It shows that the system presents different states with different values of parameter d.

iii) Vary q from 0.75 to 1 with step size of 0.0025 and vary d from 0 to 38 with step size of 0.38 simultaneously. The maximum Lyapunov exponent based chaos diagram in

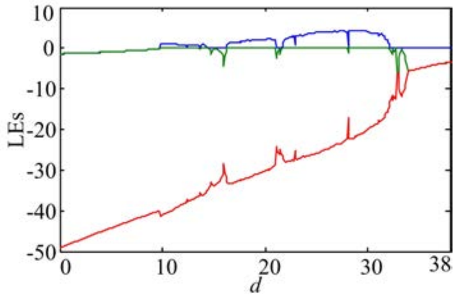

(a) LEs

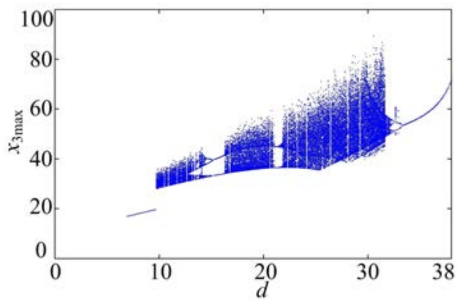

(b) Bifurcation diagram

Fig. 4. Dynamics of the fractional-order Lorenz system with $q = 0.96$ and d varying

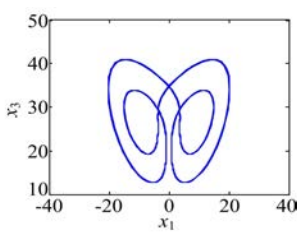

(a) d=15

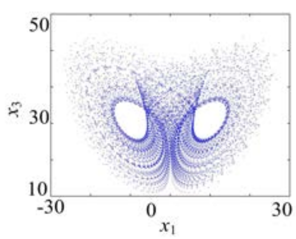

(b) d=20

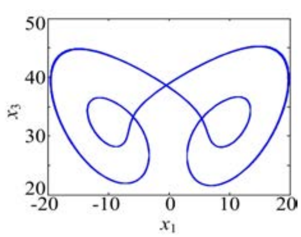

(c) d=21.5

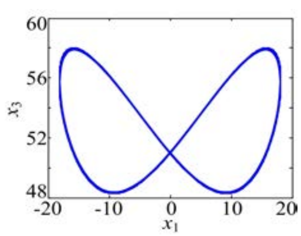

(d) d=37

Fig. 5. Phase diagrams of the fractional-order Lorenz system with $q = 0.96$ and d varying

this $q-d$ parameter plane is illustrated in Fig.6. In this figure, we only plot the case when the maximum Lyapunov exponent is larger than zero. According to Fig.6, chaos exists in the range of $d \in [10, 32]$. A high complexity region is observed within $d \in [25, 30]$ and $q \in [0.8, 0.97]$, which is favorable for practical application. So, the fractional-order Lorenz system is a good model for real application. It shows that the chaos diagram provides a parameter selection basis for fractional-order chaotic Lorenz system in practical application.

Compared with bifurcation analysis results based on FDM

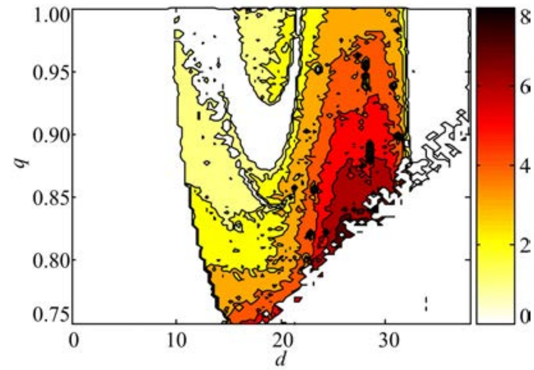

Fig. 6. Maximum Lyapunov exponent based chaos diagram.

as shown in [6], results based on ADM are more detailed and accurate. It also shows that we can analyze dynamics of the system with q varying continuously, but it is difficult for FDM to do so.

C. Discussion about the minimum order

Obviously, the minimum order for chaos is different for different system parameter. But it is also different when the numerical solution algorithm or time step size h is different. Thus these two aspects are discussed as follows.

i) Compared with other approaches, chaotic system has a much lower order if it is solved by ADM algorithm. The equilibrium point of this system is (0, 0, 0) and ($\pm\sqrt{b(c+d)}$, $\pm\sqrt{b(c+d)}$, $c+d$). When $d = 25$, the eigenvalues at (0, 0, 0) are λ_1=-45.6608, λ_2=30.6608, λ_3=-3.0000, and the eigenvalues at $(\pm\sqrt{105}, \pm\sqrt{105}, 35)$ are λ_1=-25.2415, λ_2=3.6207+17.8795i and λ_3=3.6207-17.8795i. According to the stability theory as proposed in Refs. [8] and [9], the lowest order q to generate chaos is $q = 0.8726$. It is not difficult to find out that ABM satisfies this result. However, FDM and ADM do not. According to [6], when $q = 0.7$, the system has rich dynamics and chaos still exists by applying FDM. According to Fig.2, the minimum order of the system is $q = 0.813$ by applying ADM. Actually, the stability theory from [25] is proposed to analyze fractional-order linear systems. For fractional-order nonlinear systems, Li L X et al. [26] proved that the stability theory does not always work when the specified matrix $J(X)$ is time-varying. We believe that it is more complex to analyze stability of fractional-order nonlinear system. Besides, although FDM and ADM do not satisfy the stability theory as presented in [8] and [9], they are widely used and accepted by researchers [7, 15-21]. In addition, it shows in [27] that different results of a fractional-order system may be achieved when simulations are performed based on different numerical methods. Since FDM and ADM can obtain chaos at a much lower order, they extend the parameter space of fractional-order chaotic systems.

ii) The effect of time step h should be further investigated. As for ADM, when h=0.01, the lowest order to generate chaos is q=0.813. We also find that the lowest order decreases with the decrease of the time step size h. As shown in Fig.7, when

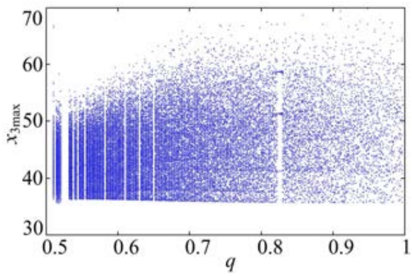

(a) h=0.001

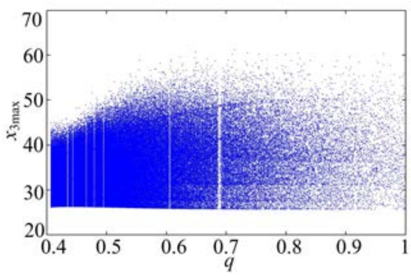

(b) $h = 0.0001$

Fig. 7. Bifurcation diagrams of the fractional-order Lorenz system under different h

h=0.001, the lowest order is q=0.505, and the lowest order is q=0.402 for h=0.0001. The system generates chaos with lower order when time step h is smaller, but more memory and computing resources are needed. It is not good for real application of the system. We think $h = 0.01$ is a suitable choice for general cases. However, the reason why the lowest order decreases with the decrease of time h needs further study.

According to the discussion above, when a minimum order for chaos generation of a fractional-order chaotic system is presented, the certain set of parameters, numerical algorithm and time step size should also be specified.

IV. Digital circuit implementation

In this section, the digital circuit of the fractional-order Lorenz system is designed, and the numerical solution applied in DSP board is presented as Eqs.(9)-(16). Hardware block diagram of the digital circuit is shown in Fig.8. The floating-point DSP TMS320F28335 produced by TI is chosen. A 16-bit dual-channel D/A converter DAC8552 is used to convert time series generated by DSP. An oscilloscope is used to capture figures randomly. The flow diagram is presented in Fig.9. Firstly, the DSP is initialized, then the initial values, including h, q, $\mathbf{x}_0$, parameters and iteration number are confirmed. In this step, all $\Gamma(\cdot)$ and h^{nq} are computed and saved before iterative computation to improve the iteration speed. When the data is popped out, the data should be processed before D/A conversion. There are two steps in data processing. At first, a big enough data is added to make sure the data is larger than zero. Then, the data is rescaled and truncated to adapt data width of the DAC8552. It should be pointed out that the iterative computation is not affected by data processing with pushing and popping operation. If the iteration is not finished, the initial value should be replaced before the next iteration.

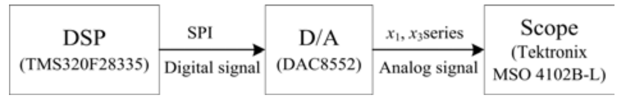

Fig. 8. Hardware block diagram of DSP implementation

Here, the initial value is $\mathbf{x}_0 = [1, 2, 3]$. Setting $q = 0.8130$, $d = 25$, the phase diagram is shown in Fig. 10(a). The corresponding Matlab simulation result is illustrated in Fig.3. Setting $q = 0.96$, $d = 15$, the phase diagram is shown in Fig. 10(b), and its corresponding Matlab simulation result is presented in Fig.5(a). Setting $q = 0.96$ and varying d (d=20 and d=37), the phase diagrams are shown in Figs. 10(c) and (d). It can be seen that they consist of phase diagrams as shown in Fig.5(b) and Fig.5(d). It shows that the fractional-order Lorenz system is implemented in the DSP successfully. It lays a hardware foundation for the applications of the fractional-order Lorenz chaotic system.

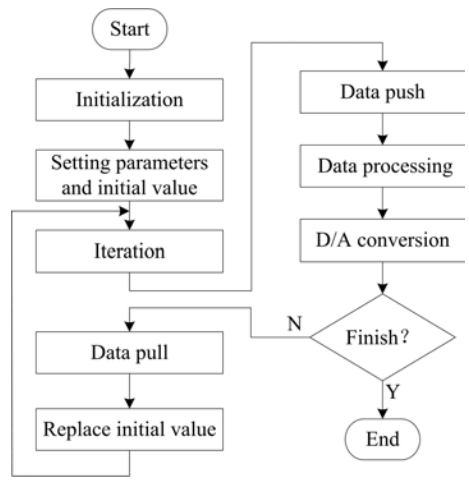

Fig. 9. Flow diagram for DSP implementation of the fractional-order Lorenz system.

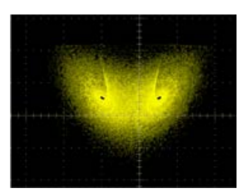

(a) q=0.8130 and d=25

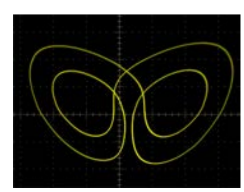

(b) q=0.96 and d=15

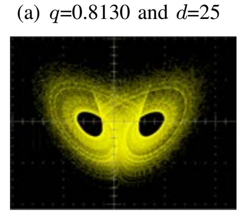

(c) q=0.96 and d=20

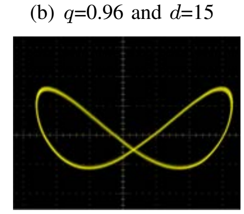

(d) q=0.96 and d=37

Fig. 10. Phase diagrams of the fractional-order Lorenz system recorded by the oscilloscope

V. Conclusions

In this paper, based on ADM algorithm, we investigated the dynamics of fractional-order Lorenz system again. It shows that the fractional-order Lorenz system has rich dynamical characteristics. The system is more complex for smaller derivative order q, and the maximum Lyapunov exponent decreases with the increase of q. The lowest order for chaos generation is different according to different numerical algorithms. The fractional-order Lorenz system has a much lower order for chaos if it is solved by ADM algorithm. Meanwhile, the lowest order for chaos is smaller when the time step size h is smaller. Finally, the system is implemented in the digital circuit by employing DSP technology, and phase diagrams generated by the DSP device are consistent with the simulation results. Our further work will focus on real applications of the fractional-order Lorenz system.

Acknowledgements

The authors would like to thank the editor and the referees for their carefully reading of this manuscript and for their valuable suggestions.

References

[1] Chen F, Xia L, Guo D, et al. A fractional-order multi-scroll chaotic system [J]. *J. Inf. Comput. Sci*, 2013, **10**(4): 1203∼1211.

[2] Wang Z, Huang X, Li Y X. A new image encryption algorithm based on the fractional-order hyperchaotic Lorenz system [J]. *Chin. Phys. B*, 2013, **22** (1): 010504.

[3] Zhe G, Liao X Z. A stability criterion for linear fractional order systems in frequency domain [J]. *Acta Automat. Sin.*, 2011, **37**(11): 1387∼1394.

[4] Grigorenko I, Grigorenko E. Chaotic dynamics of the fractional Lorenz system [J]. *Phys. Rev. Lett.*, 2003, **91**(3): 034101.

[5] Grigorenko I, Grigorenko E. Erratum: chaotic dynamics of the fractional Lorenz system [Phys. Rev. Lett. 91 , 034101 (2003)] [J]. *Phys. Rev. Lett*, 2006, **96**(19): 199902.

[6] Jia H Y, Chen Z Q, Xue W. Analysis and circuit implementation for the fractional-order Lorenz system [J]. *Acta Phys. Sin.*, 2013, **62**(14): 140503.

[7] Charef A, Sun H H, Tsao Y Y, et al. Fractal system as represented by singularity function [J]. *IEEE Trans. Auto. Cont.*, 1992, **37**(9): 1465∼1470.

[8] Tavazoei M S, Haeri M. Unreliability of frequency-domain approximation in recognizing chaos in fractional-order systems [J]. *IET Signal Proce.*, 2007, **1**(4): 171∼181.

[9] Tavazoei M S, Haeri M. Limitations of frequency domain approximation for detecting chaos in fractional order systems [J]. *Nonl. Anal.*, 2008, **69**(4):1299∼1320.

[10] Wang M, Sun G H, Wei Y L. Limitations of frequency domain approximation in the calculation of fractional order chaotic systems [J]. *J. Herbin, Instit. Tech.*, 2011, **43**(5): 8∼12.

[11] Sun H H, Abdelwahab A A, Onaral B. Linear approximation of transfer function with a pole of fractional power [J]. *IEEE Trans. Auto. Cont.*, 1984, **29**(5): 441∼444.

[12] Sun K H, Wang X, Sprott J C. Bifurcations and chaos in fractional-order simplified Lorenz system [J]. *Inter. J. Bifur. Chaos*, 2010, **20**(4): 1209∼1219.

[13] Wang Y, Sun K H, He S B, et al. Dynamics of fractional-order sinusoidally forced simplified Lorenz system and its synchronization [J]. *Eur. Phys. J. Special Topic*, 2014, **223**(8): 1591∼1600.

[14] Li R H, Chen W S. Lyapunov-based fractional-order controller design to synchronize a class of fractional-order chaotic systems [J]. *Nonl. Dyn.*, 2014, **76**(1): 785∼795.

[15] He S B, Sun K H, Wang H H. Solving of fractional-order chaotic system based on Adomian decomposition algorithm and its complexity analyses [J]. *Acta Phys. Sin.*, 2014, **63**(3): 030502.

[16] Adomian G. A review of the decomposition method and some recent results for nonlinear equations [J]. *Math. Comp. Model.*, 1990, **13**(7): 17∼43.

[17] Daftardar-Gejji V, Jafari H. An iterative method for solving nonlinear functional equations [J]. *J. Math. Anal. Appl.*, 2006, **316**(2): 753∼763.

[18] He S B, Sun K H, Wang H H. Complexity Analysis and DSP Implementation of the Fractional-Order Lorenz Hyperchaotic System [J]. *Entropy*, 2015, **17**(12): 8299∼8311.

[19] Cafagna D, Grassi G. Bifurcation and chaos in the fractional-order Chen system via a time-domain approach [J]. *Int. J. Bifur. Chaos*, 2008, **18**(7): 1845∼1863.

[20] Caponetto R, Fazzino S. An application of Adomian decomposition for analysis of fractional-order chaotic systems [J]. *Inter. J. Bifur. Chaos*, 2013, **23**(3): 1350050.

[21] Wang H H, Sun K H, He S B. Dynamic analysis and implementation of a digital signal processor of a fractional-order Lorenz-Stenflo system based on the Adomian decomposition method [J]. *Phys. Scr.*, 2015, **90**(1): 015206

[22] Cherruault Y, Adomian G. Decomposition methods: a new proof of convergence [J]. *Math. Comp. Model.*, 1993, **18**(12): 103∼106.

[23] Xue D, Zhao C N, Chen Y Q. A modified approximation method of fractional order system. **In: Proceedings of** the 2006 IEEE International Conference on Mechatronics and Automation. Luoyang China: IEEE, 2006: 1043∼1048.

[24] Abbaoui K, Cherruault Y. Convergence of Adomian's method applied to differential equations [J]. *Comp. Math. Appl.*, 1994, **28**(5): 103∼109.

[25] Matignon D. Stability results for fractional differential equations with applications to control processing [J]. *Comp. Eng. Sys. Appl.*, 1997, **2**(3): 963∼968.

[26] Li L X, Peng H M, Luo Q, et.al. Problem and analysis of stability decidable theory for a class of fractional order nonlinear system [J]. *Acta Phys. Sin.*, 2013, **62**(2): 020502.

[27] Tavazoei M S, Haeri M. A proof for non existence of periodic solutions in time invariant fractional order systems [J]. *Automatica*, 2009, **45**(8): 1886∼1890.

Shaobo He Ph. D. candidate at the School of Physics and Electronics, Central South University, China. He received his Bachelor and Master degree from Central South University, China, in 2010 and 2013, respectively. His research interests include chaotic secure communication and complexity analysis of chaotic systems.

Kehui Sun Professor at the School of Physics and Electronics, Central South University. He received his Bachelor, Master and Ph. D. degree from Central South University in 1991, 1998 and 2005, respectively. His research interests include nonlinear circuits design and dynamical analysis of chaotic systems. Corresponding author of this paper.

Huihai Wang Ph. D. candidate and lecturer at the School of Physics and Electronics, Central South University. He received his Bachelor and Master degree from Central South University in 2001 and 2004, respectively. His research interests include signal processing and dynamical analysis of nonlinear systems.

Discrete Fractional Order Chaotic Systems Synchronization Based on the Variable Structure Control with a New Discrete Reaching-law

Lilian Huang, Longlong Wang, and Donghai Shi

Abstract—**In this paper, we directly derive a new discrete state space expression of the fractional order chaotic system based on the fractional order Grnwald-Letnikow(G-L) definition and design a variable structure controller with a new faster reaching-law. The new reaching-law has the advantages of weakening the high frequency shake. Firstly, the condition of the discrete sliding mode surface is demonstrated. Then a multi-parametric function for sliding mode surface is constructed for weakening the high frequency shake through improving the Gao discrete reaching-law. Finally, the newly designed variable structure controller is applied to realize the synchronization of two different order discrete fractional chaotic systems. The simulation results show that the designed controller in this paper is effective, as it can achieve the synchronization of the discrete fractional order chaotic systems with external disturbances. Theoretical analysis and simulation results prove the effectiveness and robustness of this control method.**

Index Terms—**Discrete fractional order chaotic system, Different order system, Sliding mode control, Discrete reaching-law, Chaos synchronization.**

I. Introduction

RECENTLY the fractional calculus is applied widely in image processing neural network, signal processing, robust control and so on[1], because it can more accurately describe the actual dynamic characteristics of the physical system. Through researching on fractional calculus, many researchers generally accepted that fractional order calculus is a generalization of the integer calculus[2], and they also believed that the fractional calculus had many new characteristics of the systematic memory, the dynamic system and so on. The fractional calculus' relationship with the chaos and the fractal theory deeply attracted researchers because new chaotic phenomenon was found in fractional order nonlinear systems[3].

The chaotic synchronization has a great potential of application in the subject field[4−5] of communication, information science, medicine, biological engineering and so on. There are many methods about chaotic synchronization, for example linear feedback control[6], coupled synchronization[7], adaptive synchronization, sliding mode control[8]. The research on chaotic synchronization is usually aiming for the same structure systems[9] with different initial values or known parameters[10] or fractional order hyper chaos system[11]. As far as the synchronization of discrete fractional order chaotic systems[12], many researchers had developed some methods. Liao et al[13] realized the synchronization of Henon map by using sliding-mode control. Hu[14] proposed tracking control and predicted synchronization control on discrete chaotic system. Majidabad et al[15] designed the algorithm of fast synchronization and zero steady-steady error fast synchronization and so on. On the other side, A.Dzielinski[16] proposed the expression of the discrete fractional order state space system. D. Sierociuk[17] obtained some results including the controllability of discrete fractional order state space system and adaptive feedback control. J. A. Tenreiro[18] designed a discrete fractional order controller which could be applied to the linear and nonlinear systems in the time domain. Yao[19] put forward another form of discrete fractional order chaotic system and realized synchronous control, and Gong[20] came up with a different form of expression on discrete fractional order chaotic systems. In all the above, the form of discrete fractional order chaotic systems is obtained indirectly by different discrete methods. In this paper, we derive directly a new discrete state space expression of the fractional order chaotic system based on the fractional order Grünwald-Letnikow[21] definition. We can obtain the scope of the order using bifurcation diagram when the system is chaotic. Then based on the state space analysis method, the synchronization control problem is researched for different structural discrete fractional order chaotic systems by sliding mode control theory.

Based on the fractional order definition of Grünwald-Letnikow, the paper directly derives a new discrete state space expression of the fractional order chaotic system Then the paper designed a new kind of discrete sliding mode controller through improving the Gao's discrete reaching-law. The structure of controller designed is simple and easy to select. For two different structures of discrete fractional order chaotic systems with different dimensions, we can achieve synchronization using the new controller. Simulation results show that two fractional order chaotic systems with different dimensions can still realize synchronization when the driven system has

This article has been accepted for publication in a future issue of this journal, but has not been fully edited. Content may change prior to final publication.

This research is funded by National Natural Science Foundation of China (60772025, 61306142) and Natural Science Foundation of Heilongjiang Province (F201220). Recommended by Associate Editor Antonio Visioli.

L. Huang is professor in College of Information and Communication Engineering, Harbin Engineering University, Harbin 150001, China (e-mail: lilian_huang@163.com).

L. Wang and D. Shi are postgraduate in College of Information and Communication Engineering, Harbin Engineering University, China (e-mail: 495473324|526611481@qq.com)

Digital Object Identifier 10.1109/JAS.2016.7510016

disturbance, which proved the controller's effectiveness and feasibility.

II. Discrete Fractional Grünwald-Letnikow (G-L) Definition

The discrete fractional order G-L expression is as following:

$$\nabla^{\alpha}x(k)=\sum_{j=0}^{k}(-1)^{j}\left(\begin{array}{c}\alpha\\ j\end{array}\right)x(k-j)$$
$$\left(\begin{array}{c}\alpha\\ j\end{array}\right)=\begin{cases}1, & j=0\\ \dfrac{\alpha(\alpha-1)\cdots(\alpha-j+1)}{j!} & j>0\end{cases}\tag{1}$$

where $\left(\begin{array}{c}\alpha\\ j\end{array}\right)$ is binomial coefficient, α is the order of discrete equations, $\alpha\in R$.

Considering the general nonlinear discrete systems, the expression for general nonlinear discrete systems is

$$x(k+1)=f(x(k))\tag{2}$$

Consider the first order integer discrete difference equation as below:

$$\nabla^{1}=x(k+1)-x(k)=f(x(k))-x(k)\tag{3}$$

We generalize the above align toαorder differential align as follows:

$$\nabla^{\alpha}(x(k+1))=f(x(k))-x(k)\tag{4}$$

From the expression (1), we can get

$$\nabla^{\alpha}x(k+1)=$$
$$x(k+1)-\alpha x(k)+\sum_{j=2}^{k+1}(-1)^{j}\left(\begin{array}{c}\alpha\\ \beta\end{array}\right)x(k-j+1)\tag{5}$$

For formula (5), introducing a new parameter m and let $m=j-1$, so $j=m+1$, and obtaining another formula:

$$\begin{aligned}\nabla^{\alpha}x(k+1)&=x(k+1)-\alpha x(k)\\&\quad+\sum_{m=1}^{k}(-1)^{m+1}\left(\begin{array}{c}\alpha\\ m+1\end{array}\right)x(k-m)\\&=x(k+1)-\alpha x(k)+\sum_{m=1}^{k}M_{m}x(k-m)\end{aligned}\tag{6}$$

where $M_{m}=(-1)^{m+1}\left(\begin{array}{c}\alpha\\ m+1\end{array}\right)m\in N$.

The general form of discrete fractional order aligns could be obtained from (4) and (6):

$$x(k+1)=f(x(k))+(\alpha-1)x(k)+\sum_{m=1}^{k}M_{m}x(k-m)\tag{7}$$

where $\sum\limits_{m=1}^{k}M_{m}x(k-m)$ is the memory term for align, and it indicates that the value of a certain point is not only related to the function of the point, but also with the previous function value And the farther away from the point, the less influence on that point value The memory term can be replaced by truncation function that is, the above form (7) can be written as follows.

$$x(k+1)=f(x(k))+(\alpha-1)x(k)+\sum_{m=1}^{L}M_{m}x(k-m)\tag{8}$$

where L is the length of the memory, usually $L=20$

For general discrete proportional fractional order system, the state space expression can be written:

$$\left[\begin{array}{c}\nabla^{\alpha}x_{1}(k+1)\\ \nabla^{\alpha}x_{2}(k+1)\\ \vdots\\ \nabla^{\alpha}x_{n}(k+1)\end{array}\right]=\left[\begin{array}{c}f_{1}(x(k))-x_{1}(k)\\ f_{2}(x(k))-x_{2}(k)\\ \vdots\\ f_{n}(x(k))-x_{n}(k)\end{array}\right]\tag{9}$$

where ∇^{α} represents fractional differential factor of system, α is the order of the fraction. The ∇^{α} can be rewritten based on the discrete fractional G-L definition:

$$\left[\begin{array}{c}x_{1}(k+1)\\ x_{2}(k+1)\\ \vdots\\ x_{n}(k+1)\end{array}\right]=$$
$$\left[\begin{array}{c}f_{1}(x(k))+(\alpha-1)x_{1}(k)+\sum\limits_{m=1}^{L}M_{m}x_{1}(k-m)\\ f_{2}(x(k))+(\alpha-1)x_{2}(k)+\sum\limits_{m=1}^{L}M_{m}x_{2}(k-m)\\ \vdots\\ f_{n}(x(k))+(\alpha-1)x_{n}(k)+\sum\limits_{m=1}^{L}M_{m}x_{n}(k-m)\end{array}\right]\tag{10}$$

III. The Synchronization of Discrete Fractional Order Chaotic Systems Based on Sliding Mode Variable Structure Control

A. The design of the new discrete sliding mode reaching law

Selecting the following and regarding as the sliding-mode surface.

$$s(k)=Be(k)\tag{11}$$

where B is an invertible matrix. When the system is in sliding mode, it needs to satisfy the following conditions:

$$s_{i}(k)\rightarrow 0\tag{12}$$

The basic principles of discrete and continuous sliding modes are nearly same, and they have two stages from the initial state to the stable state, also called two modes. The first stage is a reaching process and the second stage is sliding state, but they also have some differences. Based on the discrete sliding mode variable structure, in order to get the better of discrete sliding mode, firstly select a discrete sliding surface, so that the system has good dynamic characteristics. Secondly, for satisfying reaching condition, design a controller based on the reaching law. So the controller can make the system converge to the discrete sliding mode surface from any point in finite time.

The classic Gao's discrete reaching law is as following:

$$s(k+1) - s(k) = -\varepsilon s(k) - \beta \operatorname{sgn}(s(k)) \tag{13}$$

where ε is the reaching speed, β indicates the reaching speed index. The reaching condition of Gao′s reaching law is that the dynamics of system once moves across the switching surface, the subsequent movements are from the other side of the switching surface and then the dynamics keeps on it. This can ensure strong robustness of sliding mode control, but it also leads to the phenomenon of high frequency chattering. In order to weaken the high frequency chattering, we propose a new reaching-law by considering the two aspects.

The improved discrete reaching-law is shown below.

$$s(k+1) - s(k) = -\beta(s(k)) \operatorname{sgn}(s(k)) \tag{14}$$

where β is a function that can be designed as following:

$\beta(s(k)) = \beta + \gamma |s(k)| + \gamma |s(k)| \operatorname{sgn}(|s(k)| - \delta)$ where $0 < \beta < \delta$, $0 < \gamma < 1/2$

According to the existing conditions for the discrete sliding surface, we illustrate the rationality of the new reaching law from two aspects as follows.

1) Since $s(k+1) - s(k) = -\beta(s(k)) \operatorname{sgn}(s(k))$

Then $(s(k+1) - s(k)) \operatorname{sgn}(s(k)) = -\beta(s(k)) \operatorname{sgn}^2(s(k)) = -\beta(s(k))$

And $\beta(s(k)) = \beta + \gamma |s(k)| + \gamma |s(k)| \operatorname{sgn}(|s(k)| - \delta)$, $0 < \beta < \delta$, $0 < \gamma < 1/2$

So $\beta(s(k)) > 0$, therefore $(s(k+1) - s(k)) \operatorname{sgn}(s(k)) < 0$

2) Since $s(k+1) - s(k) + 2s(k) = -\beta(s(k)) \operatorname{sgn}(s(k)) + 2s(k)$

$$\begin{aligned}
&(s(k+1) + s(k)) \operatorname{sgn}(s(k)) \\
&= -\beta(s(k)) \operatorname{sgn}^2(s(k)) + 2s(k) \operatorname{sgn}(s(k)) \\
&= -\beta(s(k)) \operatorname{sgn}^2(s(k)) + 2|s(k)| \\
&= -\beta(s(k)) + 2|s(k)|
\end{aligned}$$

Now compare $\beta(s(k))_{max}$ and $2|s(k)|$. When $|s(k)| > \delta$, $\beta(s(k))$is the max value $\beta(s(k))_{max} = \beta + 2\gamma |s(k)|$, so $\beta < \delta < |s(k)|$ that is $\beta + 2\gamma |s(k)| < |s(k)| + 2\gamma |s(k)|$. Because $\gamma < 1/2$ then $\beta(s(k))_{max} < 2|s(k)|$ so $(s(k+1) + s(k)) \operatorname{sgn}(s(k)) > 0$.

From (1) and (2), we can get:

$$\begin{aligned}
(s(k+1) - s(k)) \operatorname{sgn}(s(k)) < 0 \\
(s(k+1) + s(k)) \operatorname{sgn}(s(k)) > 0
\end{aligned}$$

That is $|s(k+1)| < |s(k)|$. So the discrete sliding mode surface exists under the control of new reaching-law.

In the new reaching-law, β is the function of $s(k)$. By setting the expression of β, it contains the parameters of the reaching-law speed and reaching speed index. In the process of approaching the discrete sliding surface, the parameter δ determines the reaching rate. After reaching the sliding surface, the system will be stable in the neighborhood of sliding surface, at this time β determines reaching speed index.

B. The synchronization of discrete fractional order chaotic systems

Consider the following two discrete fractional order chaotic systems, as the drive system and response system, respectively:

$$\nabla^\alpha X(k+1) = f(X(k)) - X(k) \tag{15}$$

$$\nabla^\alpha Y(k+1) = g(Y(k)) - Y(k) + U(k) \tag{16}$$

where ∇^α is fractional order differential factor, $\alpha \in R$. Based on the discrete fractional G-L definition, the differential factor is expanded as follows.

$$\begin{aligned}
X(k+1) &= f(X(k)) + (\alpha - 1)X(k) + \sum_{m=1}^{L} M_m X(k-m) \\
&= R_f(X(k)) + (\alpha - 1)X(k)
\end{aligned} \tag{17}$$

$$\begin{aligned}
Y(k+1) &= g(Y(k)) + (\alpha - 1)Y(k) \\
&\quad + \sum_{m=1}^{L} M_m Y(k-m) + U(k) \\
&= R_g(Y(k)) + (\alpha - 1)Y(k) + U(k)
\end{aligned} \tag{18}$$

where $R_f(X(k))$ is the function of $f(X(k))$ and $\sum_{m=1}^{L} M_m X(k-m)$, also the same as $R_g(Y(k)) \sum_{m=1}^{L} M_m X(k-m)$ and $\sum_{m=1}^{L} M_m Y(k-m)$ are the memory terms for drive system and response system. $X(k) \in R^m$ and $Y(k) \in R^n$ are the state variables of drive system and response system, respectively. α is the order value of systems. $U(k)$ is the controller for the response system to be designed.

The purpose of designing controller $U(k)$ is to guarantee the synchronization of the drive-response system and to have strong robustness, i.e. $\lim_{k\to\infty} \|e(k)\| = 0$ where$e(k)$ is the generalized synchronization state error, and $e(k) = Y(k) - CX(k)$, $e(k) = (e_1(k), e_2(k), ...e_n(k))^{\mathrm{T}}$, $C \in R^{n\times m}$, so the state error dynamic system can be written:

$$\begin{aligned}
e(k+1) &= Y(k+1) - CX(k+1) \\
&= R_g(Y(k)) - CR_f(X(k)) + U(k)
\end{aligned} \tag{19}$$

C. Controller design

Theorem: To achieve the synchronization of system (17) and (18), the following controller is designed.

$$U(k) = U_0 + CR_f(X(k)) - R_g(Y(k)) + Y(k) - CX(k)$$

where $U_0 = [u_1, u_2, \cdots, u_n]$, $u_i = -\sum_{j=0}^{n} a_{ij}(\beta(s_i(k)) \operatorname{sgn}(s_i(k)))$, $A = B^{-1}\beta(s_i(k)) = \beta + \gamma |s_i(k)| + \gamma |s_i(k)| \operatorname{sgn}(|s_i(k)| - \delta)$, $s_i(k) = \sum_{j=1}^{n} b_{ij} e_j(k)$, $|B| \neq 0$.

Proof: Choosing Lyapunov function as follows:

$$
\begin{aligned}
v(k) &= (s(k))^{\mathrm{T}} s(k) \\
\Delta v(k) &= v(k+1) - v(k) \\
&= (s(k+1))^{\mathrm{T}} s(k+1) - s(k)^{\mathrm{T}} s(k) \\
&= (-\beta(s(k))\mathrm{sgn}(s(k)) + s(k))^{\mathrm{T}}(-\beta(s(k))\mathrm{sgn}(s(k)) \\
&\quad + s(k)) - (s(k))^{\mathrm{T}} s(k) \\
&= (-\beta(s(k))\mathrm{sgn}(s(k)))^{\mathrm{T}}(-\beta(s(k))\mathrm{sgn}(s(k))) \\
&\quad + (-\beta(s(k))\mathrm{sgn}(s(k)))^{\mathrm{T}} s(k) \\
&\quad + s(k)^{\mathrm{T}}(-\beta(s(k))\mathrm{sgn}(s(k))) \\
&\quad + (s(k))^{\mathrm{T}} s(k) - (s(k))^{\mathrm{T}} s(k)
\end{aligned}
$$

Since $-\beta(s(k))\mathrm{sgn}(s(k))$ and $s(k)$ are all column vectors.

So $(-\beta(s(k))\mathrm{sgn}(s(k)))^{\mathrm{T}} s(k) = s(k)^{\mathrm{T}}(-\beta(s(k))\cdot \mathrm{sgn}(s(k)))$ is constant. Then

$$
\begin{aligned}
\Delta v(k) =& (-\beta(s(k))\mathrm{sgn}(s(k)))^{\mathrm{T}}(-\beta(s(k))\mathrm{sgn}(s(k))) \\
&+ 2(-\beta(s(k))\mathrm{sgn}(s(k)))^{\mathrm{T}} s(k) \\
=& (-\beta(s(k))\mathrm{sgn}(s(k)))^{\mathrm{T}}(-\beta(s(k))\mathrm{sgn}(s(k)) + 2s(k))
\end{aligned}
$$

Now assuming that $\beta(s(k))\mathrm{sgn}(s(k)) = (m_1, m_2, \cdots, m_n)^T$, $2s(k) = (n_1, n_2, \cdots, n_n)^T$

So

$$
\begin{aligned}
\Delta v(k) &= (m_1, m_2, \cdots, m_n)(m_1 - n_1, m_2 - n_2, \cdots, m_n - n_n)^T \\
&= (m_1^2 - m_1 n_1) + (m_2^2 - m_2 n_2) + \cdots + (m_n^2 - m_n n_n)
\end{aligned}
$$

Otherwise $\beta(s(k))_{\max} < 2\,|s(k)|$,

So $\beta(s(k))\mathrm{sgn}(s(k)) < 2\,|s(k)|\,\mathrm{sgn}(s(k)) = 2s(k)$ that is $m_i < n_i, i = 1, 2, \cdots, n$

it is easy to obtain:

$$\Delta v(k) < 0$$

According to Lyapunov stability theory, the original Lyapunov function is positive definite $v(k) > 0$ and its first derivative is negative definite $\Delta v(k) < 0$ then the error system $e(k)$ converges to zero. So the expression (17) and (18) achieve synchronization finally.

IV. SIMULATION

A. Case 1: The dimension of drive system is bigger than that of the response system

The generalized discrete Henon chaotic system as drive system is,

$$
\begin{cases}
x_1(k+1) = ax_3(k) \\
x_2(k+1) = bx_1(k) + ax_3(k) \\
x_3(k+1) = 1 + x_2(k) - cx_3^2(k)
\end{cases}
\tag{20}
$$

According to the above, the fractional order of this system is:

$$
\begin{cases}
\nabla^{\alpha} x_1(k+1) = ax_3(k) - x_1(k) \\
\nabla^{\alpha} x_2(k+1) = bx_1(k) + ax_3(k) - x_2(k) \\
\nabla^{\alpha} x_3(k+1) = 1 + x_2(k) - cx_3^2(k) - x_3(k)
\end{cases}
\tag{21}
$$

From the above the equation, every differential align contains fractional differential factor ∇^{α} and α is the order, which would be set to make the system be chaotic. By using the definition of G-L, the ∇^{α} can be expanded to get the driving system as follows:

$$
\begin{cases}
x_1(k+1) = ax_3(k) + (\alpha - 1)x_1(k) + \sum\limits_{m=1}^{L} M_m x_1(k-m) \\
\qquad = f_1(x(k)) + \Delta f(x(k)) \\
x_2(k+1) = bx_1(k) + ax_3(k) + (\alpha - 1)x_2(k) \\
\qquad + \sum\limits_{m=1}^{L} M_m x_2(k-m) \\
\qquad = f_2(x(k)) \\
x_3(k+1) = 1 + x_2(k) - cx_3^2(k) + (\alpha - 1)x_3(k) \\
\qquad + \sum\limits_{m=1}^{L} M_m x_3(k-m) \\
\qquad = f_3(x(k))
\end{cases}
\tag{22}
$$

where a, b, c are the parameters of drive system, $\Delta f(x(k))$ indicates external disturbance. The bifurcation diagram of the system can be obtained when selecting the parameter $a = 0.358$, $b = 1.3$, $c = 1.07$ and the initial value is $(0.45, 0.3, 0.4)$.

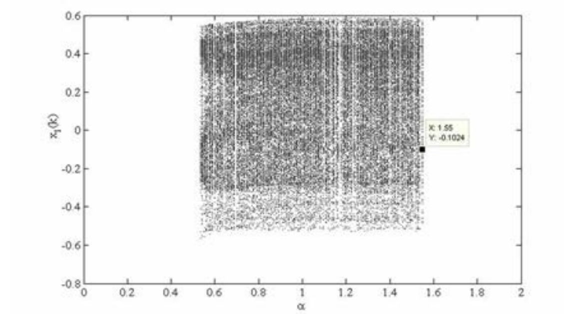

Fig. 1. Bifurcation diagram of generalized discrete fractional Henon chaotic system

From the Fig.(1), the drive system is chaotic when $0.534 < \alpha < 1.55$. In this simulation we choose $\alpha = 0.8$.

Selecting the discrete map Ikeda [22] as the response system is,

$$
\begin{cases}
y_1(k+1) = a' + b'(y_1(k)\cos(\theta) - y_2(k)\sin(\theta)) \\
y_2(k+1) = b'(y_1(k)\sin(\theta) - y_2(k)\cos(\theta))
\end{cases}
\tag{23}
$$

where $\theta = y_1^2(k) + y_2^2(k), a', b'$ are the parameters of the system. We can obtain its fractional order expression from above.

$$
\begin{cases}
\nabla^{\alpha} y_1(k+1) = a' + b'(y_1(k)\cos(\theta) - y_2(k)\sin(\theta)) - y_1(k) \\
\nabla^{\alpha} y_2(k+1) = b'(y_1(k)\sin(\theta) - y_2(k)\cos(\theta)) - y_2(k)
\end{cases}
\tag{24}
$$

By using the definition of G-L, the ∇^{α} can be simplified. Then the above expression can be rewritten as following:

$$
\begin{cases}
y_1(k+1) = a' + b'(y_1(k)\cos(\theta) - y_2(k)\sin(\theta)) \\
\qquad + (\alpha - 1)y_1(k) + \sum\limits_{m=1}^{L} M_m y_1(k-m) + u_1(k) \\
\qquad = g_1(y(k)) + u_1(k) \\
y_2(k+1) = b'(y_1(k)\sin(\theta) - y_2(k)\cos(\theta)) \\
\qquad + (\alpha - 1)y_2(k) + \sum\limits_{m=1}^{L} M_m y_2(k-m) + u_2(k) \\
\qquad = g_2(y(k)) + u_2(k)
\end{cases}
\tag{25}
$$

$u_1(k)$, $u_2(k)$ are the controllers for response system. Selecting transfer matrix $C = \begin{bmatrix} 1 & 0 & 0 \\ 0 & 1 & 1 \end{bmatrix}$ the state error dynamic system $e(k) = y(k) - Cx(k)$ can be rewritten:

$$\begin{cases} e_1(k) = y_1(k) - x_1(k) \\ e_2(k) = y_2(k) - (x_2(k) + x_3(k)) \end{cases} \tag{26}$$

From the details in subsection **(3.3)** $U(k)$ can be designed as following:

$$U(k) = \begin{bmatrix} u_{01}(k) + f_1(x(k)) - g_1(y(k)) + y_1(k) - x_1(k) \\ u_{02}(k) + f_2(x(k)) + f_3(x(k)) - g_2(y(k)) \\ +y_2(k) - (x_2(k) + x_3(k)) \end{bmatrix} \tag{27}$$

where $u_{0i}(k), i = 1, 2$ is

$$\begin{cases} u_{01}(k) = -a_{11}\beta(s_1(k))\mathrm{sgn}(s_1(k)) - a_{12}\beta(s_2(k))\mathrm{sgn}(s_2(k)) \\ u_{02}(k) = -a_{21}\beta(s_1(k))\mathrm{sgn}(s_1(k)) - a_{22}\beta(s_2(k))\mathrm{sgn}(s_2(k)) \end{cases} \tag{28}$$

where $\beta(s_i(k)) = \beta + \gamma\,|s_i(k)| + \gamma\,|s_i(k)|\,\mathrm{sgn}(|s_i(k)| - \delta)$, the sliding surface is chosen as below:

$$\begin{cases} s_1(k) = b_{11}e_1(k) + b_{12}(e_1(k) + e_2(k)) \\ s_2(k) = b_{21}e_1(k) + b_{22}(e_1(k) + e_2(k)) \end{cases} \tag{29}$$

The matrix A and B meet the conditions of $A = B^{-1}$ based on the **Theorem.** The parameters of the drive system are $a = 0.358$, $b = 1.3$, $c = 1.07$, $\alpha = 0.8$ and its initial value is $(0.45, 0.3, 0.4)$. The parameters of the response system are $a' = 1.5$, $b' = 0.2$, $\alpha = 0.8$ and its initial value is $(0.9, 0.2)$. The parameters of the sliding surface are $(0.7, 2.4)(0.2, 3.6)$ Selecting the controller's parameters $\beta = 0.04$, $\gamma = 0.4$, $\delta = 0.8$. Assuming that the external disturbance $\Delta f(x(k)) = 0.01\sin(0.04k\pi)$. The result of simulation is shown in Fig.(2).

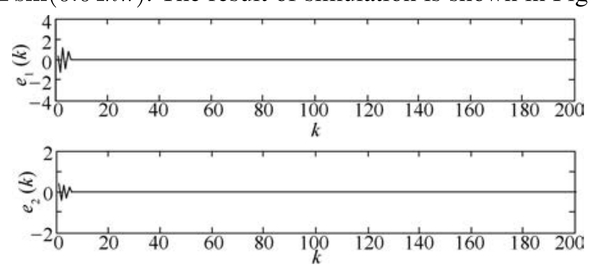

Fig. 2. Synchronization error curves

B. Case 2: The dimension of the drive system is smaller than that of the response system

Selecting the discrete Henon map as drive system is,

$$\begin{cases} x_1(k+1) = 1 - ax_1^2(k) + x_2(k) + \Delta f(x(k)) \\ x_2(k+1) = bx_1(k) \end{cases} \tag{30}$$

where $\Delta f(x(k))$ is an external disturbing perturbations. The fractional order of drive system is below:

$$\begin{cases} x_1(k+1) = 1 - ax_1^2(k) + x_2(k) + (\alpha - 1)x_1(k) \\ \qquad\qquad + \sum\limits_{m=1}^{L} M_m x_1(k-m) \\ \qquad = f_1(x(k)) + \Delta f(x(k)) \\ x_2(k+1) = bx_1(k) + (\alpha - 1)x_2(k) + \sum\limits_{m=1}^{L} M_m x_2(k-m) \\ \qquad = f_2(x(k)) \end{cases} \tag{31}$$

Selecting the parameters of system $a = 1.4$, $b = 0.3$ and its initial value is $(0.5, 0.2)$. The Bifurcation diagram of drive system can be obtained without the external disturbance.

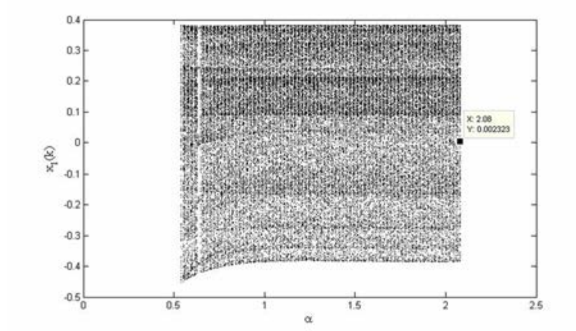

Fig. 3. Bifurcation diagram of discrete fractional Henon chaotic system

The drive system is chaotic when $0.54 < \alpha < 2.08$ from the Fig.(3). The generalized discrete Henon chaotic system as response system is:

$$\begin{cases} y_1(k+1) = a'y_3(k) + (\alpha - 1)y_1(k) \\ \qquad + \sum\limits_{m=1}^{L} M_m y_1(k-m) + u_1(k) \\ \qquad = g_1(y(k)) + u_1(k) \\ y_2(k+1) = b'y_1(k) + a'y_3(k) + (\alpha - 1)y_2(k) \\ \qquad + \sum\limits_{m=1}^{L} M_m y_2(k-m) + u_2(k) \\ \qquad = g_2(y(k)) + u_2(k) \\ y_3(k+1) = 1 + y_2(k) - c'y_3^2(k) + (\alpha - 1)y_3(k) \\ \qquad + \sum\limits_{m=1}^{L} M_m y_3(k-m) + u_3(k) \\ \qquad = g_3(y(k)) + u_3(k) \end{cases} \tag{32}$$

From the content of (**4.1**), the response system is chaotic when $0.534 < \alpha < 1.55$. Selecting transfer matrix $C = \begin{bmatrix} 1 & 0 \\ 0 & 1 \\ 1 & 1 \end{bmatrix}$, so the state error dynamic system $e(k) = y(k) - Cx(k)$ can be rewritten:

$$\begin{cases} e_1(k) = y_1(k) - x_1(k) \\ e_2(k) = y_2(k) - x_2(k) \\ e_3(k) = y_3(k) - (x_1(k) + x_2(k)) \end{cases} \tag{33}$$

The controller of $U(k)$ is designed as following:

$$U(k) = \begin{bmatrix} u_{01}(k) + f_1(x(k)) - g_1(y(k)) + y_1(k) - x_1(k) \\ u_{02}(k) + f_2(x(k)) - g_2(y(k)) + y_2(k) - x_2(k) \\ u_{03}(k) + f_2(x(k)) + f_1(x(k)) - g_2(y(k)) \\ +y_2(k) - (x_1(k) + x_2(k)) \end{bmatrix} \tag{34}$$

The $u_{0i}(k)$, $i = 1, 2, 3$ is,

$$\begin{cases} u_{01}(k) = a_{11}\beta(s_1(k)) + a_{12}\beta(s_2(k)) + a_{13}\beta(s_3(k)) \\ u_{02}(k) = a_{21}\beta(s_2(k)) + a_{22}\beta(s_2(k)) + a_{23}\beta(s_3(k)) \\ u_{03}(k) = a_{31}\beta(s_1(k)) + a_{32}\beta(s_2(k)) + a_{33}\beta(s_3(k)) \end{cases} \tag{35}$$

where $\beta(s_i(k)) = \beta + \gamma\,|s_i(k)| + \gamma\,|s_i(k)|\,\mathrm{sgn}(|s_i(k)| - \delta)$ the sliding surface is chosen as below:

$$\begin{cases} s_1(k) = b_{11}e_1(k) + b_{12}e_2(k) + b_{13}e_3(k) \\ s_2(k) = b_{21}e_1(k) + b_{22}e_2(k) + b_{23}e_3(k) \\ s_3(k) = b_{31}e_1(k) + b_{32}e_2(k) + b_{33}e_3(k) \end{cases} \tag{36}$$

The matrix A and B meet the conditions of $A = B^{-1}$ based on the **Theorem** and selecting the parameters of the drive system $a = 1.5$, $b = 0.2$, $\alpha = 0.8$, and its initial value is $(1.2, 0.8)$. The parameters of response system are $a' = 0.358b' = 1.3$, $c' = 1.07$, $\alpha = 0.8$, and its initial value is $(0.1, 0.2, 0.1)$. The parameters of the sliding surface will be $(0.2, 1.1, 2.4)$, $(0.8, 0.3, 3.6)$, $(0.1, 0.8, 3.9)$. The length of the memory $L = 20$. Setting the parameters of controller$\beta = 0.02$, $\delta = 0.8$,$\gamma = 0.3$ Assuming that the drive system of external disturbance is $\Delta f(x(k)) = 0.05\sin(0.4k\pi)$. The result of simulation is shown in Fig.(4).

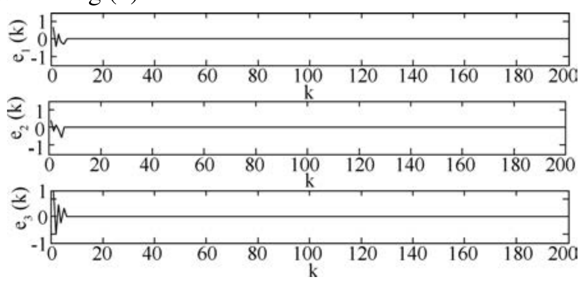

Fig. 4. Synchronization error curves

The simulation results show that the synchronization state error converges to the origin asymptotically in finite time and stabilize the origin eventually with external disturbance. The results demonstrate that the different dimensional structure discrete fractional order chaotic systems achieved synchronization under the action of designed controller.

V. Conclusions

In this paper, a new general state space expression of discrete fractional order chaotic system is obtained based on the fractional order definition of Grünwald-Letnikow. A new discrete sliding mode reaching-law control strategy which has the advantage of weakening the high frequency chatting is proposed by improving the Gao's discrete reaching-law. Based on a novel strategy, a new controller is designed, which would guarantee the different dimensional structure discrete fractional order chaotic systems achieving synchronization. When the systems are with external disturbances, they can still achieve the synchronization of the discrete fractional order chaotic systems. Simulation results verify the effectiveness of the proposed methods and demonstrate the rationality of the designed controller.

References

[1] Zhu C X, Zou Y. Summary of research on fractional-order control. *Control and Decision*, 2009, **24**(2): 161∼169

[2] Podlubny, I. Fractional differential aligns: an introduction to fractional derivatives, fractional differential aligns, to methods of their solution and some of their applications. *Academic press*, 1998, Vol. **198**

[3] Huang Li-Lian, Qi Xue. The synchronization of fractional order chaotic systems with different orders based on adaptive sliding mode control. *Acta Physica Sinica*, 2013, **62**(8): 61∼67

[4] Li L X, Peng H P, Lu H B, Guan X P. Control and synchronization of Henon chaotic system. *Acta Physica Sinica* , 2001, **50**(4): 629∼632

[5] Liu F C, Liang X M. A fast algorithm for generalized predictive control and synchronization of Henon chaotic systems. *Acta Physica Sinica*, 2005, **54**(10): 4585∼4589

[6] Wen S H, Wang Z, Liu F C. A fast algorithm for adaptive generalized predictive control of Hnon chaotic systems. *Acta Physica Sinica*, 2009, **58**(6): 3754∼3758 (in Chinese)

[7] Han Min, Xu Mei-Ling, Ren Wei-Jie. Research on multivariate chaotic time series prediction using mRSM model. *Acta Automatica Sinica*, 2014, **40**(5): 822∼829

[8] Deng Li-Wei, Song Shen-Min. Synchronization of Fractional Order Hyperchaotic Systems Based on Output Feedback Sliding Mode Control. *Acta Automatica Sinica* , 2014, **40**(11): 2421∼2427

[9] Liu Fu-Cai, Wang Juan, Peng Hai-Peng. Predictive control and synchronization of Henon chaotic system. *Acta Physica Sinica.* 2002, **51**(9): 1954∼1959 (in Chinese)

[10] Sun Biao, Sun Xiu-xia, Chen Lin, Xue Jian-ping. Algorithm of discrete-time sliding mode control based on power-function. *Control and Decision*, 2011, **26**(2): 285∼288

[11] Zhang Y, Zhang J, Chen Z. A Survey of Research on Variable Structure Control of Discrete-Time System. *Information and Control*, 2003, **32**(2): 136∼141

[12] Peng G, Jiang Y, Chen F. Generalized projective synchronization of fractional order chaotic systems. *Statistical Mechanics and its Applications*, 2008, **387**(14): 3738∼3746

[13] Liao X, Gao Z, Huang H. Synchronization control of fractional-order discrete-time chaotic systems, *Control Conference (ECC), 2013 European. IEEE*, **2013**: 2214∼2219

[14] Hu T. Discrete Chaos in Fractional Henon Map. *Applied Mathematics*, 2014, **5**(15): 2243

[15] Majidabad S S, Shandiz H T. Discrete-time Terminal Sliding Mode Control of Chaotic Lorenz System. *Journal of Control and Systems Engineering*, 2013, **1**(1): 1

[16] Dzielińki A, Sierociuk D. Stability of discrete fractional order state-space systems. *Journal of Vibration and Control*, 2008, **14**(9): 1543∼1556

[17] Sierociuk D, Dzielinski A. Estimation and control of discrete fractional order states-space systems. *Photonics Applications in Astronomy, Communications*, 2006.

[18] Machado J A T. Discrete-time fractional-order controllers. *Fractional Calculus and Applied Analysis*, 2001, **4**(1): 47∼66

[19] Yao M, Qi D, Zhao G. On control of discrete-time chaotic systems based on Lyapunov exponents. *Control and Decision*, 2002, **17**(2): 171∼174

[20] Lihua G. Correlatively Coupled Synchronization of Discrete Mapping Chaotic Systems. *Journal-university of Electronic Science and Technology of China*, 2004, **33**(2): 214∼217

[21] Trzasko W. Reachability and controllability of positive fractional discrete-time systems with delay. *Journal of Automation Mobile Robotics and Intelligent Systems*, 2008, **2**: 43∼47

[22] Kuznetsov A P, Savin A V, Savin D V. On some properties of nearly conservative dynamics of Ikeda map and its relation with the conservative case. *Physica A: Statistical Mechanics and its Applications*, 2008, **387**(7): 1464∼1474

Lilian Hung received the Ph.D. degree in Navigation, Guidance and Control from Harbin Institute of Technology, Harbin, China, in 2005. She is currently professor in College of Information and Communication Engineering, Harbin Engineering University.

Her research interests include nonlinear systems theory, the generalized synchronization of chaotic system and its application, Fractional order chaotic systems synchronization control.

Longlong Wang received bachelor degree in Communication Engineering from the Zaozhuang University, Shandong, China, in 2013. As a postgraduate, he studied in Harbin Engineering University in Information and Communication Engineering department from 2014. His primary areas of research are discrete fractional order chaotic systems and its synchronization control.

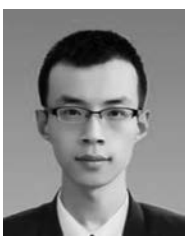

Donghai Shi received bachelor degree in Communication Engineering from the Ludong University, Shandong, China, in 2013. As a postgraduate, he studied in Harbin EngineeringUniversity in Information and Communication Engineering department from 2014. His primaryareas of research are dislocation synchronization and complex chaotic system.

The Multi-scale Method for Solving Nonlinear Time Space Fractional Partial Differential Equations

Hossein Aminikhah, Mahdieh Tahmasebi, and Mahmoud Mohammadi Roozbahani

***Abstract*—In this paper, we present a new algorithm to solve a kind of nonlinear time space-fractional partial differential equations on a finite domain. The method is based on B-spline wavelets approximations, some of these functions are reshaped to satisfy on boundary conditions exactly. The Adams fractional method is used to reduce the problem to a system of equations. By multi-scale method this system is divided into some smaller systems which have less computations. We get an approximated solution which is more accurate on some subdomains by combining the solutions of these systems. Illustrative examples are included to demonstrate the validity and applicability of our proposed technique, also the stability of the method is discussed.**

***Index Terms*—Adams fractional method, B-spline wavelets, multi-scale method, nonlinear fractional partial differential equations.**

I. Introduction

IN the last few decades fractional differential equations have found applications in several different disciplines of science and technology including physics, biology, engineering [1]−[3], viscoelasticity [4], finance [5]−[7], hydrology [8]−[13], and control systems [14]. Several numerical methods are proposed to solve these equations such as the finite difference methods [15]−[20], Laplace transformation method [21], [22], Fourier transformation method [23], [24], the Adomian decomposition method [25], variational iteration method [26] and multi-scale methods [27]−[32]. Also Aminikhah *et al.* handled multiscaling collocation method to solve linear Fractional Partial Differential Equations (FPDE) [33]. They combined Adams fractional method and the multi-scale techniques to solve the linear fractional partial differential equations. This paper continues this line of approach. We intend to consider a kind of the nonlinear time-space FDE with Robin condition boundary,

$$D_t^{\beta} u(x,t) = \sum_{k=1}^{S} f_k(x)\, D_x^{\alpha_k} u(x,t)\, D_x^{\beta_k} u(x,t)$$
$$\begin{cases} u(x,0) = g(x) \\ c_1 u(0,t) + c_2 u_x(0,t) = c_3 \\ c_4 u(n,t) + c_5 u_x(n,t) = c_6 \end{cases} \tag{1}$$

where $x \in \Omega = [0,m]$, $0 \le t \le T$, and $f_k(x)$ are bounded functions on Ω and the operator D_x^{α}, (D_t^{β}) is caputo space time fractional derivative of order $\alpha_k(\beta)$ defined by [2]

$$D_x^{\alpha} u(x,t) = \begin{cases} \frac{\partial^{\alpha}}{\partial \tau^{\alpha}} u(x,t), & \alpha = m \in \mathbb{N} \cup \{0\} \\ \frac{1}{\Gamma(m-\alpha)} \int\limits_0^x (x-\tau)^{m-\alpha} \frac{\partial^m}{\partial \tau^m} u(\tau,t)\, d\tau & \\ \qquad m-1 < \alpha < m \end{cases} \tag{2}$$

$$D_t^{\beta} u(x,t) = \begin{cases} \frac{\partial^{\beta}}{\partial \tau^{\beta}} u(x,t), & \beta = p \in \mathbb{N} \cup \{0\} \\ \frac{1}{\Gamma(p-\beta)} \int\limits_0^t (t-\tau)^{p-\beta} \frac{\partial^p}{\partial \tau^p} u(x,\tau)\, d\tau & \\ \qquad p-1 < \beta < p. \end{cases} \tag{3}$$

First, we present the differential operator in matrix form by using collocation method. Second, we need a time stepping scheme to convert FPDE to an implicit linear system. Finally, by dividing the domain Ω into several smaller subdomains, the system can be divided into smaller systems, then each of them will have different resolution and less computation than the primary system. Then by combining the solutions of these systems, we derive an approximation of the true solution with less computation.

The paper is organized as follows: In section II the basic definitions and required properties of the wavelet are briefly mentioned. In the next two sections we provided essential tools for constructing our method. In section III the fractional derivative matrix was approximated by collocation method. In section IV the wavelets and scaling functions were reshaped to satisfy the boundary conditions, so the approximated solution will be exact in the boundary points. In section V we employ the fractional Adams method for time discretization FPDE then describe how to construct a system by operational matrices where introduced in previous sections, finally by multi-resolution method in some subdomains this system divides to some smaller systems which involve less computation. In section VI, the stability of the method is investigated. In section VII numerical examples are given to demonstrate the validity of the proposed method.

II. Preliminaries and Notations

In this work we will use the wavelets whose scaling functions are cubic B-splines

$$\phi(x) = B_3(x) = \frac{1}{6} \sum_{k=0}^{4} \begin{pmatrix} 4 \\ k \end{pmatrix} (-1)^k (x-k)_+^3 \tag{4}$$

where

$$x_+^n = \begin{cases} x^n & x > 0 \\ 0 & x \le 0. \end{cases}$$

This article has been accepted for publication in a future issue of this journal, but has not been fully edited. Content may change prior to final publication.

Recommended by Associate Editor Dingyü Xue.

H. Aminikhah and M. M. Roozbahani are with the Department of Applied Mathematics, University of Guilan, Rasht 41938-19141, Iran (e-mail: aminikhah@guilan.ac.ir; mahmoudroozbahani@gmail.com).

M. Tahmasebi is with the Department of Applied Mathematics, Faculty of Mathematical Sciences, Tarbiat Modares University, Tehran 14115-137, Iran (e-mail: tahmasebi@modares.ac.ir).

Digital Object Identifier 10.1109/JAS.2016.7510058

The best way to understand wavelets is through a multi-resolution analysis.

Definition 1: (Multi-resolution Analysis) A multi-resolution analysis of $L_2(\mathbb{R})$ with inner product $\langle .,. \rangle$, is defined as a sequence of closed subspaces $V_j \subset L_2(\mathbb{R})$, $j \in \mathbb{Z}$ with the following properties

1) $\cdots \subset V_1 \subset V_0 \subset V_{-1} \subset \cdots$.

2) $\underset{j\in\mathbb{Z}}{\cup} V_j$ is dense in $L_2(\mathbb{R})$ and $\underset{j\in\mathbb{Z}}{\cap} V_j = \emptyset$.

3) If $f(x) \in V_0$ then $f\left(2^{-j}x\right) \in V_j$.

4) If $f(x) \in V_0$ then $f\left(2^{-j}x - k\right) \in V_j$.

5) $\phi(x-k)$, $k \in \mathbb{Z}$ is a Riesz basis in V_0. As a consequence of Definition 1, V_j is spanned by $\phi_{j,k}(x) = 2^{-j/2}\phi\left(2^{-j}x-k\right)$. One may construct wavelets by first completing the spaces V_j to the space V_{j-1} by means of a space W_j, i.e., $V_{j-1} = V_j \oplus W_j$. From the inclusion $V_0 \subset V_{-1}$ we have the important identity, called scaling equation of the form

$$\phi(t) = \sqrt{2}\sum_k h_k \phi(2x-k) \tag{5}$$

where $h_k = \frac{\sqrt{2}}{2^4}\begin{pmatrix} 4 \\ k \end{pmatrix}, 0 \le k \le 4$.

Also from $W_0 \subset V_{-1}$ we have

$$\psi(t) = \sqrt{2}\sum_k g_k \phi(2x-k). \tag{6}$$

For more details refer to [34]−[37].

The dual cubic B-spline bases involve another multi-resolution analysis of $L_2(\mathbb{R})$, it is usually denoted by $\left\{\widetilde{V}_j\right\}$. The dual scaling function $\widetilde{\phi}$ is biorthogonal to ϕ in the following sense

$$\left\langle \phi_{j,k}, \tilde{\phi}_{l,m}\right\rangle = \delta_{j,l}\delta_{k,m}, for\ all\ j,k,l,m \in \mathbb{Z}.$$

$\widetilde{\phi}(x-k)$, $k \in \mathbb{Z}$ produces a Riesz basis for the space $\widetilde{V}_0$. The dual wavelet $\widetilde{\psi}$ is constructed by taking linear combinations of the dual scaling functions

$$\widetilde{\psi}(x) = \sqrt{2}\sum_k \widetilde{g}_k \widetilde{\phi}(2x-k). \tag{7}$$

Also from $\widetilde{V}_0 \subset \widetilde{V}_{-1}$ we have

$$\widetilde{\phi}(x) = \sqrt{2}\sum_k \widetilde{h}_k \widetilde{\phi}(2x-k) \tag{8}$$

where $\widetilde{g}_k = (-1)^k h_{1-k}$ and $\widetilde{h}_k = (-1)^k g_{1-k}$. The function $\tilde{\psi} \in L_2(\mathbb{R})$ is biorthogonal to ψ.

$$\left\langle \psi_{j,k}, \tilde{\psi}_{l,m}\right\rangle = \delta_{j,l}\delta_{k,m}, \text{for all j, k, l, m} \in \mathbb{Z}.$$

Designing biorthogonal wavelets allows more freedom than orthogonal wavelets. One of them is the possibility of constructing symmetric wavelet functions.

Any function of V_j can be represented by finite series of cubic B-splines. Let $f_{|V_j}$ denote the projection $f \in L_2(\mathbb{R})$ onto V_j. We can obtain the cubic B-spline expansion of $f_{|V_j}$ as

$$f_{|\ V_{j-1}}(x) = \sum_{i=0}^{2N} a_{j-1,\,i}\phi_{j-1,\,i}(x) \tag{9}$$

where $a_{j-1,\,i} = \left\langle f, \tilde{\phi}_{j-1,\,i}\right\rangle$ $N = m2^{-j}$. Note that the cubic B-splines have compact support, so this property guarantees that in the bounded domain $\Omega = [0,m]$ the sum only contains finite nonzero terms. We have $V_{j-1} = V_j \oplus W_j$, this means that $f_{|\ V_{j-1}}$ can also be represented by the expansion

$$\begin{aligned} f_{|\ V_j \oplus W_j}(x) &= \sum_{i=0}^{N} a_{j\,i}\phi_{j\,i}(x) + \sum_{i=0}^{N-1} b_{j\,i}\psi_{j\,i}(x) \\ &= \begin{bmatrix} a \\ b \end{bmatrix} [\Phi\ \Psi] \end{aligned} \tag{10}$$

where $a^T = [a_{j0}, a_{j1}, \ldots, a_{j\,N}]$, $b^T = [b_{j0}, b_{j1}, \ldots, b_{j\,N-1}]$, $b_{j\,i} = \langle f, \widetilde{\psi}_{j\ i}\rangle$, $a_{ji} = \langle f, \widetilde{\phi}_{j\,i}\rangle$, $\Phi = [\phi_{j0}, \phi_{j1}, \ldots, \phi_{j\,N}]$ and $\Psi = [\psi_{j0}, \psi_{j1}, \ldots, \psi_{j\,N-1}]$.

The vector $F = \begin{bmatrix} a \\ b \end{bmatrix}$ is called "the vector form of f in $V_j \oplus W_j$". Let, Λ be the subdomainn of Ω then some member of the vector F is assigned to Λ. We represent restricted F to subdomain Λ by $F_\Lambda = \begin{bmatrix} a_\Lambda \\ b_\Lambda \end{bmatrix}$.

Definition 2: (the Fast Wavelet Transform) FWT converts the scaling function coefficients in space V_j to scaling function and wavelet function coefficients in space $V_j \oplus W_j$. From (7) and (8) and biorthogonal property of wavelets we have:

$$a_{j,k} = \sum_i \tilde{h}_i a_{j-1,2k+i} \text{and} b_{j,k} = \sum_i \tilde{g}_i a_{j-1,2k+i}. \tag{11}$$

The fast wavelet transform embodied by these two equations, and indeed FWT maps $\overrightarrow{a_{j-1}}$ onto $\overrightarrow{a_j}$ and $\overrightarrow{b_j}$, $FWT\left[\overrightarrow{a_{j-1}}\right] = \begin{bmatrix} \overrightarrow{a_j} \\ \overrightarrow{b_j} \end{bmatrix}$.

The inverse fast wavelet transform recursively uses the formula

$$a_{j-1,k} = \sum_n h_{k-2n}\, a_{j,n} + \sum_l g_{k-2l}\, b_{j,l}\,. \tag{12}$$

Equation (12) is constructed from (9) and (10) biorthogonal property of wavelets. We obtain IFWT by using (12) as $IFWT\begin{bmatrix} \overrightarrow{a_j} \\ \overrightarrow{b_j} \end{bmatrix} = \left[\overrightarrow{a_{j-1}}\right]$.

III. Matrix Approximations

In the following we need operational matrix M^α to approximate D_x^α on V_j where $0 \le \alpha \le 2$. Producing M^α takes a number of steps, starting with the construction of the matrix P_j which is a square matrix that converts the vector form of f in V_j into the actual values of f at some points:

$$P_j F = \overline{F} \tag{13}$$

where $P_j = [\phi_{j\,k}(x_i)]_{k,\,i}$, $F = [a_{j\,0}, a_{j\,1}, \ldots, a_{j\,N}]^T$, $\overline{F} = [\phi_{j\,0}(x_0), \phi_{j\,1}(x_1), \ldots, \phi_{j\,N}(x_N)]$, $f(x) = \sum_{k=0}^{N} a_{jk}\phi_{jk}(x)$, $x_i = i\,2^j$, for $0 \le i \le N = m2^{-j}$.

Next, we construct the matrix P_j^α which converts the vector form of $D_x^\alpha f$ in V_j into the actual values of $D_x^\alpha f$ at some points:

$$P_j^\alpha F = \overline{F}^\alpha \tag{14}$$

where $P_j^{\alpha} = [D_x^\alpha \phi_{j\,k}(x_i)]_{k,\,i}$, $\overline{F}^\alpha = [D_x^\alpha \phi_{j\,0}(x_0),\, D_x^\alpha \phi_{j\,1}(x_1), \dots,\, D_x^\alpha \phi_{j\,N}(x_N)]$, $x_i = i\,2^j$, for $0 \le i \le N = m2^{-j}$.

$$M^\alpha = FWT \times (P_{j-1})^{-1} \times P_j^\alpha \times IFWT. \tag{15}$$

In the below, we illustrate the function of the fractional derivative matrix.

$$\begin{array}{lll}
V_j \oplus W_j : \sum\limits_k a_{jk}\phi_{jk} + \sum\limits_k d_{jk}\psi_{jk}, & & \sum\limits_k b_{j-1k}\phi_{jk} + \sum\limits_k c_{j-1k}\psi_{jk} \\
\quad IFWT \ \downarrow & & \quad FWT \ \uparrow \\
V_{j-1} : \sum\limits_k a_{j-1,k}\phi_{j-1,k} & & \sum\limits_k b_{j-1,k}\phi_{j-1,k} \\
\quad P_j^\alpha \searrow & \sum\limits_k a_{j-1,k} D_x^\alpha \phi_{j-1,k}(x_i) & \nearrow (P_j)^{-1}
\end{array}$$

One further requirement is the multiplication by the space independent function $g(x)$. We create the linear operator G to approximate the multiplication

$$FWT \times (P_j)^{-1} \times G \times P_j \times IFWT$$

G is a diagonal matrix with the values of function g in $x_k = k2^j, 0 \le k \le N$.

IV. Boundary Conditions

The basic idea for constructing the boundary wavelets and boundary scaling functions can be described as follows, for the case where $\Omega = [0, m]$. Firstly we take all wavelets and scaling functions that are located near the boundary, we are thus constructing the specific linear combinations of these functions that satisfy the fixed non zero boundary conditions (I). We separate the function u into two functions.

$$u(x,t) = v(x,t) + B(x) \tag{16}$$

where the function v satisfies the zero boundary conditions

$$\begin{cases} v(x,0) = g(x) - B(x) \\ c_1 v(0,t) + c_2 v_x(0,t) = 0 \\ c_4 v(n,t) + c_5 v_x(n,t) = 0 \end{cases}$$

and

$$\begin{cases} c_1 B(0) + c_2 B'(0) = c_3 \\ c_4 B(n) + c_5 B'(n) = c_6. \end{cases}$$

Now, we only reshape wavelets at $x = 0$, the construction of other scaling functions and wavelets at the boundary is nearly same as this. We let ψ denote the combination of the wavelets in V_j which their support contains $x = 0$.

$$\psi(x) = a\psi_{j,-1}(x) + b\psi_{j,0}(x) + c\psi_{j,+1}(x). \tag{17}$$

Here ψ must satisfy the boundary conditions

$$c_1\psi(0) + c_2\psi'(0) = 0. \tag{18}$$

On the other hand we need to represent $\sum\limits_{k=1}^{S} f_k(x) D_x^{\alpha_k}\psi(x)$ $D_x^{\beta_k}\psi(x)$ with the reshaped wavelet $\psi(x)$ which satisfies the boundary condition so we must have

$$\begin{aligned} &c_1 \sum_{k=1}^{S} f_k(0) D_x^{\alpha_k}\psi(0) D_x^{\beta_k}\psi(0) \\ &\quad + c_2 \frac{\partial}{\partial x}_{|x=0} \sum_{k=1}^{S} f_k(x) D_x^{\alpha_k}\psi(x) D_x^{\beta_k}\psi(x) = 0. \end{aligned} \tag{19}$$

So a nonlinear system is obtained from (18) and (19), and we get the coefficients a, b and d from solving this system.

V. The Proposed Method

We consider the fractional Adams method for solving FPDE (1). This method was first studied by Diethelm, Ford and Freed [38]. Their method for solving (20) is as follows:

$$D^\beta y(t) = f(t, y(t)), \quad y(0) = y_0; 0 < \beta < 1 \tag{20}$$

$$\begin{aligned} y_{n+1} = \ & y_0 \\ & + \frac{h^\beta}{\Gamma(\beta+2)} \sum_{k=0}^{n} c_{k,n+1} f(t_k, y_k) \\ & + \frac{h^\beta}{\Gamma(\beta+2)} c_{n+1,n+1} f\left(t_{n+1}, y_{n+1}^P\right) \end{aligned} \tag{21}$$

where

$$c_{k,n+1} = \begin{cases} n^{\beta+1} - (n-\beta)(n+1)^\beta, & k = 0 \\ (n-k+2)^{\beta+1} + (n-k)^{\beta+1} - 2(n-k+1)^{\beta+1} & \\ & 1 \le k \le n \\ 1, & k = n+1 \end{cases}$$

and $h = T/N$, $\{t_k = kh\ ,\ k = 0, 1, .., N\}$, $y_k \approx y(t_k)$.

Also we can show $0 < c_{k,n+1} \le 2$ for all $0 \le k \le n+1$ and $0 < \beta < 1$.

The predictor y_{n+1}^P is determined by

$$y_{n+1}^P = y_0 + \frac{h^\beta}{\Gamma(\beta+1)} \sum_{k=0}^{n} b_{k,\,n+1} f(t_k\,, y_k)$$

where $b_{k,\,n+1} = (n+1-k)^\beta - (n-k)^\beta$.

So the approximate solution for the time space-fractional (1) by using the fractional Adam's method would be

$$\begin{aligned} u(x, t_{n+1}) = \ & u(x, t_0) \\ & + \frac{h^\beta}{\Gamma(\beta+2)} \sum_{k=0}^{n} c_{k,n+1} (Nu(x, t_k)) \\ & + \frac{h^\beta}{\Gamma(\beta+2)} Nu^P(x, t_{n+1}) \end{aligned} \tag{22}$$

where $N(u(x,t)) = \sum\limits_{i=1}^{S} f_i(x) D_x^{\alpha_i} u(x,t) D_x^{\beta_i} u(x,t)$ and $u^P(x, t_{n+1}) = u(x, t_0) + \frac{h^\beta}{\Gamma(\beta+1)} \sum\limits_{k=0}^{n} b_{k,\,n+1} N(u(x, t_k))$.

Now we can take the space V_{j-1} to approximate the solution of (22). If we consider $\begin{bmatrix} a^k \\ b^k \end{bmatrix}$ as a vector form of $u(x, t_k)$

in V_{j-1}, then from (22) and the definition of M^{α} from (15) we have

$$\begin{aligned}\begin{bmatrix} a^{n+1} \\ b^{n+1} \end{bmatrix} = \begin{bmatrix} a^{0} \\ b^{0} \end{bmatrix} & + \frac{h^{\beta}}{\Gamma(\beta+2)} \left\{ \sum_{k=0}^{n} c_{k,n+1} \sum_{r=1}^{S} F_r \right. \\ & \times \operatorname{diag}\left(M^{\alpha_r} \begin{bmatrix} a^{k} \\ b^{k} \end{bmatrix} \right) M^{\beta_r} \begin{bmatrix} a^{k} \\ b^{k} \end{bmatrix} \\ & + \sum_{r=1}^{S} F_r \operatorname{diag}\left(M^{\alpha_r} \begin{bmatrix} a^{P} \\ b^{P} \end{bmatrix} \right) \\ & \left. \times M^{\beta_r} \begin{bmatrix} a^{n+1} \\ b^{n+1} \end{bmatrix} \right\} \end{aligned} \tag{23}$$

where

$$\begin{aligned}\begin{bmatrix} a^{P} \\ b^{P} \end{bmatrix} = \begin{bmatrix} a^{0} \\ b^{0} \end{bmatrix} + \frac{h^{\beta}}{\Gamma(\beta+1)} \sum_{k=0}^{n} b_{k,n+1} \sum_{r=1}^{S} F_r \\ \times \operatorname{diag}\left(M^{\alpha_r} \begin{bmatrix} a^{k} \\ b^{k} \end{bmatrix} \right) M^{\beta_r} \begin{bmatrix} a^{k} \\ b^{k} \end{bmatrix} \end{aligned} \tag{24}$$

also we can write as a system:

$$\left(I - \frac{h^{\beta}}{\Gamma(\beta+2)} M \right) \begin{bmatrix} a^{n+1} \\ b^{n+1} \end{bmatrix} = \begin{bmatrix} \overline{a_n} \\ \overline{b_n} \end{bmatrix} \tag{25}$$

where

$$\begin{aligned} M = & \sum_{r=1}^{S} F_r \operatorname{diag}\left(M^{\alpha_r} \begin{bmatrix} a^{P} \\ b^{P} \end{bmatrix} \right) M^{\beta_r}, \\ \begin{bmatrix} \overline{a_n} \\ \overline{b_n} \end{bmatrix} = & \begin{bmatrix} a^{0} \\ b^{0} \end{bmatrix} + \frac{h^{\beta}}{\Gamma(\beta+2)} \sum_{k=0}^{n} c_{k,n+1} \sum_{r=1}^{S} F_r \\ & \times \operatorname{diag}\left(M^{\alpha_r} \begin{bmatrix} a^{k} \\ b^{k} \end{bmatrix} \right) M^{\beta_r} \begin{bmatrix} a^{k} \\ b^{k} \end{bmatrix}. \end{aligned} \tag{26}$$

Solving system in the Finer space V_{j-1} produces more accurate solution, But if the system becomes larger then calculations are also increased. To increase the accuracy of solution in some places of domain Ω and to avoid increase of our calculations we use the multiscaling method. This means that once we solve the system in a space V_j and domain Ω that we call large scale system. Once again we solve the system in a Finer space V_{j-1} and subdomain Λ that we call small scale system. Combination of these two systems provides suitable accuracy and less calculations than the solutions of the system achieved in the space V_{j-1} on domain Ω. If we want to get a more accurate solution in a subdomain Λ, we need to do the following process (we can do this process for several subdomains). In the beginning we consider the matrix M in the space V_{j-1}, since in the first step we will not be using all of M so The elements of M will have to be broken up, into a block decomposition of the form

$$M = \begin{bmatrix} A & B \\ C & D \end{bmatrix}.$$

We only consider the block A which operates as operator N in the space V_j over all domain Ω. Then using time stepping scheme (22) we find an approximation for a^{n+1} which we will call a_{Λ}^{Tm}

$$\left(I - \frac{h^{\beta}}{\Gamma(\beta+2)} A \right) a^{Tm} = \overline{a_n}. \tag{27}$$

The small-scale system is expressed in terms of a matrix M_{Λ} of the form

$$M_{\Lambda} = \begin{bmatrix} A_{\Lambda} & B_{\Lambda} \\ C_{\Lambda} & D_{\Lambda} \end{bmatrix}$$

where A_{Λ}, B_{Λ}, C_{Λ} and D_{Λ}, are composed of the elements from A, B, C and D that are related to Λ. We have the time step solved at the large-scale resolution V_j on all Ω. What we want now is to solve the system on Λ at the small scale resolution V_{j-1}. However, a^{n} and the newly calculated a_{Λ}^{Tm} have to be included. So, we take the components of $\overline{a_n}$ and a_{Λ}^{Tm} that are in Λ, a_{Λ}^{n} and a_{Λ}^{Tm}. These are used in the system. Next, we are looking for vector correction a^{Cr} where $a^{n+1} = a^{Tm} + a^{Cr}$. Now, what we want is to solve the system on Λ at the small scale resolution V_{j-1}.

Consider the fractional Adam's method for this case

$$\left(I - \frac{h^{\beta}}{\Gamma(\beta+2)} \begin{bmatrix} A & B \\ C & D \end{bmatrix} \right)_{\Lambda} \begin{bmatrix} a^{n+1} \\ b^{n+1} \end{bmatrix}_{\Lambda} = \begin{bmatrix} \overline{a_n} \\ \overline{b_n} \end{bmatrix}_{\Lambda}. \tag{28}$$

Since $a_{\Lambda}^{n+1} = a_{\Lambda}^{Tm} + a_{\Lambda}^{Cr}$ thus

$$\begin{aligned} \left(I - \tfrac{h^{\beta}}{\Gamma(\beta+2)} \begin{bmatrix} A & B \\ C & D \end{bmatrix} \right)_{\Lambda} \left(\begin{bmatrix} a^{Cr} \\ b^{n+1} \end{bmatrix}_{\Lambda} + \begin{bmatrix} a^{Tm} \\ 0 \end{bmatrix}_{\Lambda} \right) \\ = \begin{bmatrix} \overline{a_n} \\ \overline{b_n} \end{bmatrix}_{\Lambda} \end{aligned} \tag{29}$$

then

$$\begin{aligned} \left(I - \frac{h^{\beta}}{\Gamma(\beta+2)} \begin{bmatrix} A & B \\ C & D \end{bmatrix} \right)_{\Lambda} \begin{bmatrix} a^{C_r} \\ b^{n+1} \end{bmatrix}_{\Lambda} \\ = \begin{bmatrix} 0 \\ \widetilde{b_n} + \frac{h^{\beta}}{\Gamma(\beta+2)} C\, a^{Tm} \end{bmatrix}_{\Lambda}. \end{aligned} \tag{30}$$

We get $\begin{bmatrix} a^{n+1} \\ b^{n+1} \end{bmatrix}_{\Lambda}$ by solving the above system.

The last step is to construct the vector $\begin{bmatrix} a^{n+1} \\ b^{n+1} \end{bmatrix}_{\Omega}$ from vectors $\begin{bmatrix} a^{Tm} \\ 0 \end{bmatrix}_{\Omega}$ and $\begin{bmatrix} a^{n+1} \\ b^{n+1} \end{bmatrix}_{\Lambda}$. In the subdomain Λ the vector $\begin{bmatrix} a^{n+1} \\ b^{n+1} \end{bmatrix}_{\Lambda}$ is a better approximate solution than the vector $\begin{bmatrix} a^{Tm} \\ 0 \end{bmatrix}_{\Lambda}$ for the system (25). So to increase the accuracy of the approximated vector $\begin{bmatrix} a^{Tm} \\ 0 \end{bmatrix}_{\Omega}$ we must replace elements of $\begin{bmatrix} a^{Tm} \\ 0 \end{bmatrix}_{\Omega}$ by the elements of $\begin{bmatrix} a^{n+1} \\ b^{n+1} \end{bmatrix}_{\Lambda}$, the only ones that are related to subdomain Λ.

$$\begin{bmatrix} a^{Tm} \\ \\ \rule{1cm}{0.4pt} \\ \\ 0 \end{bmatrix} = \begin{bmatrix} a_1^{Tm} \\ \vdots \\ a_\Lambda^{Tm} \\ \vdots \\ a_N^{Tm} \\ \rule{1cm}{0.4pt} \\ 0 \\ \vdots \\ 0_\Lambda \\ \vdots \\ 0 \end{bmatrix} \begin{matrix} \longleftrightarrow \\ \\ and \\ \\ \longleftrightarrow \end{matrix} \begin{bmatrix} a_\Lambda^{n+1} \\ \\ \\ \\ b_\Lambda^{n+1} \end{bmatrix}$$

$$\begin{bmatrix} a_\Lambda^{n+1} \\ \\ \\ \\ b_\Lambda^{n+1} \end{bmatrix} \overset{REPLACE}{\longrightarrow} \begin{bmatrix} a_1^{Tm} \\ \vdots \\ a_\Lambda^{Tm} \\ \vdots \\ a_N^{Tm} \\ \rule{1cm}{0.4pt} \\ 0 \\ \vdots \\ 0_\Lambda \\ \vdots \\ 0 \end{bmatrix} \equiv \begin{bmatrix} a^{n+1} \\ \\ \rule{1cm}{0.4pt} \\ \\ b^{n+1} \end{bmatrix}.$$

Now, we present the algorithm of the proposed method. In this algorithm j, h and g are resolution level, time step and initial function respectively. If the vector $a = [a_0, a_2, \ldots, a_N]^T$ be the vector form of a function in V_j then we suppose the restricted vector a_Λ is $[a_r, \ldots, a_{s+1}]^T$.

Algorithm 1 Proposed Method

Step 1: $v \leftarrow [g_0, g_1, \ldots, g_{2N}]$ where $N = m2^{-j}$ and $g_k = g\left(k2^j\right), \quad k = 0, \ldots, 2N.$

Step 2: $\begin{bmatrix} a \\ b \end{bmatrix} \leftarrow FWT \times P_j^{-1} \times v.$

Step 3: Constructing matrix M by using (17).

Step 4: Blocking the matrix $M = \begin{bmatrix} A & B \\ C & D \end{bmatrix}$ where $A \leftarrow M(1:N+1, 1:N+1)$, $B \leftarrow M(1:N+1, N+1:2N+1)$ and so on for C, D.

Step 5: $M_\Lambda = \begin{bmatrix} A_\Lambda & B_\Lambda \\ C_\Lambda & D_\Lambda \end{bmatrix}$ Limiting M to subdomain Λ, where $A_\Lambda \leftarrow A(r:s+1, r:s+1)$, $B_\Lambda \leftarrow B(r:s+1, r:s)$ and so on for C_Λ and D_Λ.

Step 6: for $n = 0$ to k.

Step 7: $\begin{bmatrix} a_n \\ b_n \end{bmatrix} \leftarrow \begin{bmatrix} a \\ b \end{bmatrix}.$

Step 8: $a_\Lambda \leftarrow a(r:s+1), \; b_\Lambda \leftarrow b(r:s).$

Step 9: Solve the system (25) to get vector a^{Tm}.

Step 10: $a_\Lambda^{Tm} \leftarrow a^{Tm}(r:s+1).$

Step 11: Solve the system (28) to get vector $\begin{bmatrix} a_\Lambda^{Cr} \\ b_\Lambda \end{bmatrix}$.

Step 12: $a_\Lambda \leftarrow a_\Lambda^{Cr} + a_\Lambda^{Tm}.$

Step 13: $a^{Tm}(r:s+1) \leftarrow a_\Lambda, \; b(r:s) \leftarrow b_\Lambda, \; v \leftarrow \begin{bmatrix} a^{Tm} \\ b \end{bmatrix}.$

Step 14: end for.

VI. Stability

In order to show stability of the approximate solution, we recall discrete Gronwall lemma.

Lemma 1: (Discrete Gronwall Lemma) If $\{y_k\}$, $\{f_k\}$ and $\{g_k\}$ are nonnegative sequences and

$$y_n \leq f_n + \sum_{0 \leq k \leq n} g_k y_k, \quad \text{for } n \geq 0 \tag{31}$$

then

$$y_n \leq f_n + \sum_{0 \leq k \leq n} f_k g_k \exp\left(\sum_{k \leq i \leq n} g_i\right), \quad for\ n \geq 0. \tag{32}$$

If, in addition, $\{f_k\}$ is nondecreasing then

$$y_n \leq f_n \exp\left(\sum_{0 \leq i \leq n} g_i\right), \quad for\ n \geq 0. \tag{33}$$

Theorem 1: The approximation scheme (23) is stable.

Proof: Let $u_n = [u(x_0, t_n), u(x_1, t_n), \ldots, u(x_{2N}, t_n)]$ denote the exact solution and $\widetilde{U}_n$ denote approximate solution of it. From approximation scheme (23) and $\widetilde{U}_n = P_j \times IFWT \begin{bmatrix} a^n \\ b^n \end{bmatrix}$ we have

$$\begin{aligned} \widetilde{U}_{n+1} = \; & \widetilde{U}_0 \\ & + \frac{h^\beta}{\Gamma(\beta+2)} \Bigg\{ \sum_{k=0}^{n} c_{k,n+1} \sum_{r=1}^{S} F_r M^{\alpha_r} \\ & + \operatorname{diag}\left(FWT \times P_j^{-1} \times \widetilde{U}_k\right) M^{\beta_r} \\ & \times FWT \times P_j^{-1} \times \widetilde{U}_k + \sum_{r=1}^{S} F_r M^{\alpha_r} \\ & \times \operatorname{diag}\left(FWT \times P_j^{-1} \times \widetilde{U}_{n+1}^P\right) \\ & \times M^{\beta_r} FWT \times P_j^{-1} \times \widetilde{U}_{n+1} \Bigg\} \end{aligned} \tag{34}$$

where

$$\begin{aligned} \widetilde{U}_{n+1}^P = \; & \widetilde{U}_0^P \\ & + \tfrac{h^\beta}{\Gamma(\beta+1)} \left\{ \textstyle\sum_{k=0}^{n} b_{k,n+1} \sum_{r=1}^{S} F_r M^{\alpha_r} \right. \\ & \times \operatorname{diag}\left(FWT \times P_j^{-1} \times \widetilde{U}_k\right) \\ & \times M^{\beta_r} FWT \times P_j^{-1} \times \widetilde{U}_k \end{aligned}$$

and $b_{k,\,n+1} = (n+1-k)^\beta - (n-k)^\beta$.

There is no loss of generality in assuming that u_n and its approximation are bounded in the domain $\left\|\widetilde{U}_n\right\| \leq M^*$. Also we can choose h enough small that makes

$$\frac{h^\beta}{\Gamma(\beta+2)} \sum_{r=1}^{S} \|F_r\| \|M^{\alpha_r}\| \|FWT\| \left\|P_j^{-1}\right\| M^* \left\|M^{\beta_r}\right\| \|FWT\| \left\|P_j^{-1}\right\| \leq \frac{1}{2} < 1 \tag{35}$$

this guarantees nonsingularity of the matrix

$$I-\frac{h^\beta}{\Gamma(\beta+2)} \sum_{r=1}^{S} F_r \times M^{\alpha_r} \times \operatorname{diag}\left(FWT \times P_j^{-1} \times \widetilde{U}_{n+1}^P\right) \times M^{\beta_r} \times FWT \times P_j^{-1}. \tag{36}$$

Then we have

$$\begin{aligned}\widetilde{U}_{n+1} = &\Big(I - \frac{h^\beta}{\Gamma(\beta+2)} \sum_{r=1}^{S} F_r \times M^{\alpha_r} \\ &\times \operatorname{diag}\left(FWT \times P_j^{-1} \times \widetilde{U}_{n+1}^P\right) \\ &\times M^{\beta_r} \times FWT \times P_j^{-1}\Big)^{-1} \widetilde{U}_0 \\ &+ \frac{h^\beta}{\Gamma(\beta+2)} \Big(I - \frac{h^\beta}{\Gamma(\beta+2)} \sum_{r=1}^{S} F_r \times M^{\alpha_r} \\ &\times \operatorname{diag}\left(FWT \times P_j^{-1} \times \widetilde{U}_{n+1}^P\right) \times M^{\beta_r} \\ &\times FWT \times P_j^{-1}\Big)^{-1} \\ &\times \Big\{\sum_{k=0}^{n} c_{k,n+1} \sum_{r=1}^{S} F_r \times M^{\alpha_r} \\ &\times \operatorname{diag}\left(FWT \times P_j^{-1} \times \widetilde{U}_k\right) \times M^{\beta_r} \\ &\times FWT \times P_j^{-1} \widetilde{U}_k\Big\}.\end{aligned} \tag{37}$$

Next using the fact that

$$\left\|\left(I - \frac{h^\beta}{\Gamma(\beta+2)} \sum_{r=1}^{S} F_r \times M^{\alpha_r} \times \operatorname{diag}\left(FWT \times P_j^{-1} \times \widetilde{U}_{n+1}^P\right) \times M^{\beta_r} \times FWT \times P_j^{-1}\right)^{-1}\right\| \leq \frac{1}{1-\left\|\frac{h^\beta}{\Gamma(\beta+2)} \sum_{r=1}^{S} F_r \times M^{\alpha_r} \times diag\left(FWT \times P_j^{-1} \times \widetilde{U}_{n+1}^P\right) \times M^{\beta_r} \times FWT \times P_j^{-1}\right\|} \leq 2. \tag{38}$$

Therefore, equation (37) yields

$$\left\|\widetilde{U}_{n+1}\right\| \leq 2\left\|\widetilde{U}_0\right\| + \frac{\left(\frac{T}{N}\right)^\beta}{\Gamma(\beta+2)} \sum_{k=0}^{n} c_{k,n+1} \left\|\widetilde{U}_k\right\|. \tag{39}$$

By applying Gronwall's inequality, we obtain

$$\left\|\widetilde{U}_{n+1}\right\| \leq 2\left\|\widetilde{U}_0\right\| \exp\left(\frac{T^\beta}{\Gamma(\beta+2)} \sum_{k=0}^{n} \frac{c_{k,n+1}}{N^\beta}\right) \tag{40}$$

since $\frac{c_{k,n+1}}{N^\beta} = \frac{(n-k+2)^{\beta+1}}{N^\beta} + \frac{(n-k)^{\beta+1}}{N^\beta} - 2\frac{(n-k+1)^{\beta+1}}{N^\beta} \leq \frac{2}{N}$ is bounded and increasing function with respect to β so we have

$$\left\|\widetilde{U}_{n+1}\right\| \leq 2\left\|\widetilde{U}_0\right\| \exp\left(\frac{2T^\beta}{\Gamma(\beta+2)}\right) \tag{41}$$

this completes the proof of stability. ■

VII. Numerical Example

In this section we implement the presented method to solve two examples, and also we compare the exact solution with the approximate solution.

Example 1: We consider the following nonlinear time space fractional Burger equation:

$$D_t^\alpha u = -u D_x^\beta u + \nu u_{xx}$$

with the initial condition and boundary condition

$$\begin{cases} u(x,0) = \coth(5x-10), & 0 < x < 4 \\ u(0,t) = u(4,t) = 0, & 0 \leq t \leq 1. \end{cases}$$

For comparison, this example was solved numerically in different levels of resolutions. The Table I, II show the convergence when j decreases, also the Fig. 1 shows in different times the approximated results satisfy the boundary conditions exactly.

Example 2: We consider the following fractional nonlinear Klein-Gordon differential equation:

$$D_t^\beta u = u_{xx} - u + u^3$$

with initial condition and boundary condition are as follows:

$$\begin{cases} u(x,0) = \cos(x), & 1 < x < 7 \\ u(1,t) = u(7,t) = 0, & 0 \leq t \leq 1. \end{cases}$$

The example was solved by the presented multi-scale method with V_{-4} on Ω and V_{-5} on Λ. The Table III shows that the accuracy can be improved by enlarging subdomain.

TABLE I The Errors are the Difference Between the V_j Results and the V_{j-1} Results (V_j/V_{j-1}) with $h = 0.01$ at $t = 0.5$

(a) error $\alpha=0.9,\ \beta=0.8$				(b) error $\alpha=0.7,\ \beta=0.8$			
x	V_{-3}/V_{-4}	V_{-4}/V_{-5}	V_{-5}/V_{-6}	x	V_{-3}/V_{-4}	V_{-4}/V_{-5}	V_{-5}/V_{-6}
1	4.86851E-5	1.20725E-5	3.01086E-6	1	3.87951E-5	9.5696E-6	2.38312E-6
1.5	-6.27884E-5	-1.78008E-5	-4.54069E-6	1.5	-3.15994E-5	-8.706E-6	-2.21822E-6
2	-0.00048152	-0.000117335	-2.86878E-5	2	-7.38939E-5	-2.2020E-5	-5.64321E-6
2.5	0.003519481	0.000616091	0.000135349	2.5	-0.000228084	-9.5180E-5	-2.53185E-5
3	0.000154392	4.97541E-5	1.25426E-5	3	0.004762792	-0.0008628	-0.00039248
3.5	7.77682E-6	1.98912E-6	4.99819E-7	3.5	-3.36494E-5	1.52567E-5	4.19946E-6

TABLE II THE ERRORS ARE THE DIFFERENCE BETWEEN THE V_j RESULTS AND THE V_{j-1} RESULTS (V_j/V_{j-1}) WITH $h = 0.01$ AT $t = 0.5$

(a) error $\alpha = 0.9,\ \beta = 0.8$				(b) error $\alpha = 0.7,\ \beta = 0.8$			
x	V_{-6}/V_{-7}	V_{-7}/V_{-8}	$solution on V_{-8}$	x	V_{-6}/V_{-7}	V_{-7}/V_{-8}	$solution on V_{-8}$
1	7.52109E-7	1.87972E-7	0.01563038	1	5.95109E-7	1.48723E-7	0.017861225
1.5	-1.13743E-6	-2.84176E-7	0.126210355	1.5	-5.56031E-7	-1.38975E-7	0.08964552
2	-7.09146E-6	-1.76352E-6	0.428300053	2	-1.41355E-6	-3.52853E-7	0.225663084
2.5	3.2228E-5	7.92191E-6	0.471766274	2.5	-6.38202E-6	-1.59423E-6	0.388315038
3	3.13962E-6	7.8496E-7	0.020295168	3	-0.00011126	-2.87553E-5	0.250095232
3.5	1.25102E-7	3.12235E-8	0.001442839	3.5	1.07135E-6	2.69138E-7	0.002252919

TABLE III THE ERRORS ARE THE DIFFERENCE BETWEEN THE MULTI-SCALE RESULTS AND THE RESULTS OBTAINED USING V_{-5}, WITH $h = 0.01$ AT $t = 0.5$

x	$error \Lambda = [3\ 5]$	$error \Lambda = [4\ 6]$	$solution\ on V_{-5}$
1.25	-0.000132	-7.99128E-5	-0.022484
2.25	-0.0003292	**-2.97362E-6**	-0.0542849
3.25	**1.60129E-6**	**1.22943E-6**	0.0224848
4.25	**3.87375E-6**	**2.97362E-6**	0.0542849
5.25	-0.0001361	**-1.22943E-6**	-0.0224848
6.25	-0.00032	-0.00019	-0.05428

The points in the subdomain Λ are dislayed by bold font

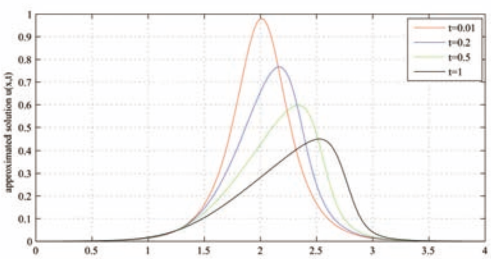

Fig. 1. This figure is the approximated solution of the presented method in different times with $\alpha = 0.9$, $h = 0.01$, $\beta = 0.8$.

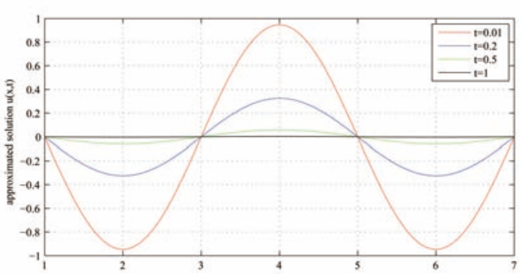

Fig. 2. This figure is the approximated solution of the presented method in different times with $\alpha = 0.9$, $h = 0.01$.

VIII. RESULTS

In this work a practical approach for solving nonlinear time space fractional partial differential equation is presented. Multi scaling method via wavelets is used to increase resolution in some locations, furthermore the computations are reduced because of the compact support of wavelets, also wavelets are employed in such a way that satisfy the boundary conditions exactly.

REFERENCES

[1] Li X X. Numerical solution of fractional differential equations using cubic B-spline wavelet collocation method. *Communications in Nonlinear Science and Numerical Simulation*, 2012, **17**(10): 3934−3946

[2] Miller K S, Ross B. *An Introduction to the Fractional Calculus and Fractional Differential Equations*. New York: John Wiley and Sons, 1993.

[3] Podlubny I. *Fractional Differential Equations*. San Diego, CA: Academic Press, 1999.

[4] Li X K, Han X H, Wang X P. Numerical modeling of viscoelastic flows using equal low-order finite elements. *Computer Methods in Applied Mechanics and Engineering*, 2010, **199**(9−12): 570−581

[5] Gorenflo R, Mainardi F, Scalas E, Raberto M. Fractional calculus and continuous-time finance. III: the diffusion limit. *Mathematical Finance*. Konstanz, Germany: Birkhäuser, 2001. 171−180

[6] Raberto M, Scalas E, Mainardi F. Waiting-times and returns in high-frequency financial data: an empirical study. *Physica A: Statistical Mechanics and its Applications*, 2002, **314**(1−4): 749−755

[7] Sabatelli L, Keating S, Dudley J, Richmond P. Waiting time distributions in financial markets. *The European Physical Journal B - Condensed Matter and Complex Systems*, 2002, **27**(2): 273−275

[8] Baeumer B, Benson D A, Meerschaert M M, Wheatcraft S W. Subordinated advection-dispersion equation for contaminant transport. *Water Resources Research*, 2001, **37**(6): 1543−1550

[9] Benson D A, Schumer R, Meerschaert M M, Wheatcraft S W. Fractional dispersion, Lévy motions, and the MADE tracer tests. *Transport in Porous Media*, 2001, **42**(1): 211−240

[10] Benson D A, Wheatcraft S W, Meerschaert M M. Application of a fractional advection-dispersion equation. *Water Resources Research*, 2000, **36**(6): 1403−1412

[11] Benson D A, Wheatcraft S W, Meerschaert M M. The fractional-order governing equation of Lévy motion. *Water Resources Research*, 2000, **36**(6): 1413−1424

[12] Schumer R, Benson D A, Meerschaert M M, Baeumer B. Multiscaling fractional advection-dispersion equations and their solutions. *Water Resources Research*, 2003, **39**(1): 1022

[13] Tadjeran C, Benson D, Meerschaert M M. Fractional radial flow and its application to field data. *Water Resources Research*, to be published

[14] Machado J A T. Discrete-time fractional-order controllers. *Fractional Calculus & Applied Analysis*, 2001, **4**(1): 47−66

[15] Fix G J, Roof J P. Least squares finite element solution of a fractional order two-point boundary value problem. *Computers & Mathematics with Applications*, 2004, **48**(7−8): 1017−1033

[16] Shen S, Liu F, Anh V, Turner I. The fundamental solution and numerical solution of the Riesz fractional advection-dispersion equation. *IMA Journal of Applied Mathematics*, 2008, **73**(6): 850−872

[17] Meerschaert M M, Tadjeran C. Finite difference approximations for fractional advection dispersion flow equations. *Journal of Computational and Applied Mathematics*, 2004, **172**(1): 65−77

[18] Richtmyer R D, Morton K W. *Difference Methods for Initial-Value Problems* (Second edition). Malabar, Florida: Krieger Publishing, 1994.

[19] Li C P, Zeng F H. *Numerical Methods for Fractional Calculus*. New York: Chapman and Hall, 2015.

[20] Guo B L, Pu X K, Huang F H. *Fractional Partial Differential Equations and their Numerical Solutions*. Singapore: World Scientific Publishing Co., 2015.

[21] Luchko Y F, Srivastava H M. The exact solution of certain differential equations of fractional order by using operational calculus. *Computers and Mathematics with Applications*, 1995, **29**(8): 73−85

[22] Samko S G, Kilbas A A, Marichev O I. *Fractional Integrals and Derivatives: Theory and Applications*. Switzerland: Gordon and Breach Science Publishers, 1993.

[23] Kilbas A A, Srivastava H M, Trujillo J J. *Theory and Applications of Fractional Differential Equations*. Amsterdam: Elsevier, 2006.

[24] Odibat Z M, Momani S. Application of variational iteration method to nonlinear differential equations of fractional order. *International Journal of Nonlinear Sciences and Numerical Simulation*, 2006, **7**(1): 27−34

[25] Momani S, Odibat Z. Numerical comparison of methods for solving linear differential equations of fractional order. *Chaos, Solitons & Fractals*, 2007, **31**(5): 1248−1255

[26] Momani S. Non-perturbative analytical solutions of the space- and time-fractional Burgers equations. *Chaos, Solitons & Fractals*, 2006, **28**(4): 930−937

[27] Dahmen W, Kurdila A, Oswald P. *Multiscale Wavelet Methods for Partial Differential Equations, Volume 6*. San Diego: Academic Press, 1997.

[28] McLaren D A. Sequential and Localized Implicit Wavelet based Solvers for Stiff Partial Differential Equations [Ph. D. dissertation], University of Ottawa, Ottawa, ON, 2012

[29] Hesthaven J S, Jameson L M. A wavelet optimized adaptive multi-domain method. *Journal of Computational Physics*, 1998, **145**(1): 280−296

[30] Mehra M, Kevlahan N K R. An adaptive multilevel wavelet solver for elliptic equations on an optimal spherical geodesic grid. *SIAM Journal on Scientific Computing*, 2008, **30**(6): 3073−3086

[31] Müller S, Stiriba Y. A multilevel finite volume method with multiscale-based grid adaptation for steady compressible flows. *Journal of Computational and Applied Mathematics*, 2009, **277**(2): 223−233

[32] Vasilyev O V, Paolucci S. A dynamically adaptive multilevel wavelet collocation method for solving partial differential equations in a finite domain. *Journal of Computational Physics*, 1996, **125**(2): 498−512

[33] Aminikhah H, Tahmasebi M, Roozbahani M M. Numerical solution for the time space-fractional partial differential equation by using wavelet multi-scale method. *U. P. B Scientific Bulletin-Series A-Applied Mathematics and Physics*, to be published

[34] Blatter C. *Wavelets: A Primer*. Naticks, Massachusetts: A K Peters/CRC Press, 2002.

[35] Goswami J C, Chan A K. *Fundamentals of Wavelets: Theory, Algorithms, and Applications*. New York: John Wiley and Sons, 1999.

[36] Mallat S. *A Wavelet Tour of Signal Processing* (Second edition). New York: Academic Press, 1999.

[37] Sweldens W. The Construction and Application of Wavelets in Numerical Analysis [Ph. D. dissertation], KU Leuven, Leuven, 1995

[38] Diethelm K, Ford N J, Freed A D. Detailed error analysis for a fractional Adams method. *Numerical Algorithms*, 2004, **36**(1): 31−52

Hossein Aminikhah was born in Iran, in 1979. He received a Ph. D. degree in Applied Mathematics (Numerical Analysis) from the University of Guilan, Rasht, Iran, in 2008, where he is currently Associate Professor in the Department of Applied Mathematics. His research interests include numerical methods for functional differential equations and numerical linear algebra.

Mahdieh Tahmasebi was born in Tehran, Iran, in 1980. She received her B. Sc. in Applied Mathematics from Shahid Beheshti University. She finished her M. Sc. and Ph. D. in Sharif University of Technology in Pure Mathematics. She is a member of Applied Mathematics Department of Tarbiat Modares University as an assistant professor from 2012 to now. Her research interests includes stochastic differential equation, Malliavin calculus, stochastic modelling, stochastic control theory, mathematical finance and numerical solution of SDEs.

Mahmoud Mohammadi Roozbahani is now a Ph. D. degree student in the Applied Mathematics Department of the University of Guilan. His interests and research areas include numerical analysis.

Decentralized Adaptive Strategies for Synchronization of Fractional-Order Complex Networks

Quan Xu, Shengxian Zhuang, Yingfeng Zeng, and Jian Xiao

***Abstract*—This paper focuses on synchronization of fractional-order complex dynamical networks with decentralized adaptive coupling. Based on local information among neighboring nodes, two fractional-order decentralized adaptive strategies are designed to tune all or only a small fraction of the coupling gains respectively. By constructing quadratic Lyapunov functions and utilizing fractional inequality techniques, Mittag-Leffler function, and Laplace transform, two sufficient conditions are derived for reaching network synchronization by using the proposed adaptive laws. Finally, two numerical examples are given to verify the theoretical results.**

***Index Terms*—Decentralized adaptive control, synchronization, fractional-order complex networks, quadratic Lyapunov functions.**

I. Introduction

It is well known that numerous natural and man-made systems can be modeled as complex dynamical networks. Examples include social networks, food webs, epidemic spreading networks, biological networks, scientific citation networks, Internet networks, World Wide Web, electric power grids, and so on[1−3]. In recent years, extensive efforts have been made to understand and study the topology and dynamics of complex networks. Specifically, as a typical collective behavior of complex networks, synchronization has received increasing attention due to its potential applications in many real scenarios[4−5]. So far, many systematic results on different synchronization patterns, such as complete synchronization, lag synchronization, generalized synchronization, cluster synchronization, etc., have been obtained for many kinds of complex networks, see [6-16] and relevant references therein.

To our best knowledge, the results on synchronization mainly concentrated on integer-order complex networks. Nevertheless, it has been recognized that the real objects are generally fractional and fractional calculus allows us to describe and model a real object more accurately than the classical integer-order methods. Not surprisingly, dynamics and control of fractional-order systems has attracted increasing attention from various fields[17−23]. Particularly, synchronization in fractional-order complex networks[24−26] has currently become an interesting and open problem. From a control perspective, the aim here is to find some appropriate controllers such that the controlled fractional-order network is synchronized.

Among them, adaptive control technique has been widely used to synchronize complex networks. In [27-29], many kinds of adaptive strategies were designed to adjust the gains of feedback controllers. Note that, in diffusively coupled networks, nodes are coupled with states difference $x_i - x_j$. This means that a state feedback controller is added to every node. Thus, a network could be synchronized by designing suitable coupling gains among the network nodes. Mathematically, these coupling gains are described by the non-null elements of the weighted time-varying adjacency matrix $G(t)$. Recently, some decentralized adaptive strategies have been used to tune the coupling gains so as to achieve synchronization in complex networks, see [30-34]. Moreover, decentralized adaptive strategies are introduced only to a small fraction of coupling gains[35]. Compared with the centralized adaptive strategies developed in [36,37], the coupling gains are adapted based on local information exchanged among neighboring nodes. However, the synchronization of fractional-order complex networks with decentralized adaptive coupling has never been investigated elsewhere. Therefore, it is important and interesting to study the synchronization of fractional-order complex networks by using the fractional-order decentralized adaptive strategies.

As is known to all, Lyapunov direct method is a standard tool to derive the synchronization criteria for integer-order complex networks. Despite much effort, the Lyapunov-based results about synchronization of integer-order complex networks cannot be directly extended to the fractional-order cases. The main difficulty lies in calculating the fractional derivative of a composite Lyapunov function. For more details about this, one can refer the existing literatures [38,39], in which there were several issues regarding calculation of the fractional derivative of a composite Lyapunov function.

Quite recently, Aguila-Camacho *et al*[40] and Duarte-Mermoud *et al*[41] introduce two lemmas for estimating the Caputo fractional derivative of a quadratic function. Thus,

This article has been accepted for publication in a future issue of this journal, but has not been fully edited. Content may change prior to final publication.

This work was supported by the National Natural Science Foundation of China (51177137), Scientific Research Foundation of the Education Department of Sichuan Province (16ZB0163), and in part by the China Scholarship Council. Recommended by Associate Editor YangQuan Chen.

Quan Xu is with the School of Electrical Engineering, Southwest Jiaotong University, Chengdu 610031, China, and also with School of Technology, Xihua University, Chengdu 610039, China (e-mail: quanxnjd@sina.com).

Shengxian Zhuang, Yingfeng Zeng, Jian Xiao are with the School of Electrical Engineering, Southwest Jiaotong University, Chengdu 610031, China (e-mail: zhuangsx@sina.com; zyf9999999@163.com; jxiao@home.swjtu.edu.cn).

Digital Object Identifier 10.1109/JAS.2016.7510142

one can analyze the stability for fractional-order uncoupled systems and coupled networks by using quadratic Lyapunov functions like classic Lyapunov direct method. But the conditions of fractional Lyapunov direct method[42,43] are relatively conservative and rigorous. As the extensions of Lyapunov direct method, LaSalle's invariance principle, Barbalat's Lemma and other mathematical techniques can be used to solve the adaptive stability problem of integer-order nonlinear systems. However, these tools cannot be directly used in the fractional order case. Thus, additional tools need to be developed, in order to prove the errors convergence in the fractional order case. In this paper, by utilizing Lyapunov functional method combined with fractional inequality techniques, Mittag-Leffler function, and Laplace transform, we study the decentralized adaptive synchronization in fractional-order networks with diffusive coupling.

The remaining of this paper is organized as follows. In Section II, some necessary preliminaries and the model of fractional-order complex networks are given. The main results of this paper are given in Section III. In Section IV, two numerical examples are provided to validate the theoretical results. Finally, some conclusions are presented in Section V.

II. Model description and preliminaries

A. Fractional Calculus and Properties

Definition 1. The Riemann-Liouville fractional integral with $0<\alpha<1$ is given by

$$\mathrm{I}_t^\alpha f(t)=\frac{1}{\Gamma(\alpha)}\int_{t_0}^{t}(t-\tau)^{\alpha-1}f(\tau)\mathrm{d}\tau, \tag{1}$$

where $t\geq t_0,\ f(t)$ is an arbitrary integrable function I_t^α is the fractional integral operator, $\Gamma(\cdot)$ is the gamma function $\Gamma(\alpha)=\int_0^\infty t^{\alpha-1}\exp(-t)\mathrm{d}t$, and $\exp(\cdot)$ is exponential function.

In this paper, we consider the Caputo definition for fractional derivative, which is most popular in engineering applications because of its advantages[17].

Definition 2. The Caputo fractional derivative with fractional-order $0<\alpha<1$ can be expressed as

$$\mathrm{D}_t^\alpha f(t)=\frac{1}{\Gamma(1-\alpha)}\int_{t_0}^{t}(t-\tau)^{-\alpha}\dot{f}(\tau)\mathrm{d}\tau, \tag{2}$$

where $t\geq t_0$, D_t^α is the Caputo fractional derivative operator. In the following, unless otherwise stated, we consider $\alpha\in(0,1)$.

Moreover, the Laplace transform of Caputo fractional derivative is

$$\mathcal{L}\left\{\mathrm{D}_t^\alpha f(t)\right\}=s^\alpha F(s)-s^{\alpha-1}f(t_0), \tag{3}$$

where $\alpha\in(0,1)$, s denotes the variable in Laplace domain, $\mathcal{L}\{\cdot\}$ is the Laplace transform operator, $F(s)$ is the Laplace transform of $f(t)$ and $f(t_0)$ is the initial value.

Let us pay attention to the following properties of the fractional derivatives[17], which are most commonly used in applications.

Property 1.

$$\mathrm{D}_t^\alpha(ax(t)+by(t))=a\mathrm{D}_t^\alpha x(t)+b\mathrm{D}_t^\alpha y(t). \tag{4}$$

Property 2.

$$\mathrm{I}_t^\alpha\mathrm{D}_t^\alpha f(t)=f(t)-f(t_0),\ \ \forall\, t\geq t_0,\ 0<\alpha<1. \tag{5}$$

Property 3. The Caputo fractional derivative of a constant function is always zero.

Definition 3[42,43]. The Mittag-Leffler function with one parameter and two parameters can be defined as

$$\begin{aligned}E_\alpha(z)&=\sum_{n=0}^{\infty}\frac{z^n}{\Gamma(n\alpha+1)},\\ E_{\alpha,\beta}(z)&=\sum_{n=0}^{\infty}\frac{z^n}{\Gamma(n\alpha+\beta)},\end{aligned} \tag{6}$$

where $z\in\mathbb{C},\alpha>0,\beta>0$. Note that $E_{\alpha,1}(z)=E_\alpha(z)$, $E_{1,1}(z)=\exp^z$.

The Laplace transform of Mittag-Leffler function with two parameters can be written as

$$\mathcal{L}\left\{t^{\beta-1}E_{\alpha,\beta}(-kt^\alpha)\right\}=\frac{s^{\alpha-\beta}}{s^\alpha+k},\quad \Re(s)>\mid k\mid^{\frac{1}{\alpha}}, \tag{7}$$

where $t\geq 0$, $\Re(s)$ is the real part of s, $k\in\mathbb{R}$.

A new property for Caputo derivative can be stated in Lemma 1, which can facilitate estimating the fractional derivative of a common quadratic Lyapunov function.

Lemma 1[41]. Let $x(t)\in\mathbb{R}^n$ be a vector of derivable functions. Then, the following inequality holds

$$\mathrm{D}_t^\alpha(x^{\mathrm{T}}(t)Px(t))\leq 2x^{\mathrm{T}}(t)P\mathrm{D}_t^\alpha x(t), \tag{8}$$

where $\alpha\in(0,1]$, $t\geq t_0$ and $P\in\mathbb{R}^{n\times n}$ is a constant, symmetric and positive definite matrix.

B. Network model

Consider a fractional-order complex dynamical network consisting of N identical nodes, which is described by

$$\mathrm{D}_t^\alpha x_i(t)=f(t,x_i(t))+c\sum_{j=1}^{N}G_{ij}(t)Ax_j(t),\quad i=1,2,\cdots,N, \tag{9}$$

where $0<\alpha<1$, $x_i=(x_{i1},x_{i2},...,x_{in})\in\mathbb{R}^n$ is the pseudo-state vector of node i, $f:\mathbb{R}^+\times\mathbb{R}^n\to\mathbb{R}^n$ is a nonlinear vector field, $c>0$ is the coupling strength, $A=\mathrm{diag}(\rho_1,\rho_2,\cdots,\rho_\mathrm{n})\in\mathbb{R}^{\mathrm{n}\times\mathrm{n}}$ is a positive definite inner coupling matrix, $G(t)=(G_{ij}(t))_{N\times N}$ is the time-varying diffusive coupling matrix representing the topological structure of an undirected network. If there is an edge between node i and j at time t, then $G_{ij}(t)=G_{ji}(t)>0$; otherwise $G_{ij}(t)=G_{ji}(t)=0$ $(i\neq j)$, and the diagonal elements of $G(t)$ are defined by

$$G_{ii}=-\sum_{j=1,j\neq i}^{N}G_{ij},\ i=1,2,\cdots,N.$$

Throughout this paper, only connected networks are considered, and $G_{ij}(t),i,j\in\{1,2,\cdots,N\}$ has the same meaning.

Definition 4. The complex network (9) is said to achieve synchronization in the sense that

$$\lim_{t\to\infty}\left\|x_i(t)-\frac{1}{N}\sum_{j=1}^{N}x_j(t)\right\|_2=0,\ i=1,2,\cdots,N, \tag{10}$$

Let $\bar{x}=\frac{1}{N}\sum_{j=1}^{N}x_j$. Then, we get

$$\begin{aligned}\mathrm{D}_t^{\alpha}\bar{x}(t)&=\frac{1}{N}\sum_{j=1}^{N}\mathrm{D}_t^{\alpha}x_j(t)\\&=\frac{1}{N}\sum_{j=1}^{N}\left[f(t,x_j(t))+c\sum_{k=1}^{N}G_{jk}(t)Ax_k(t)\right]\\&=\frac{1}{N}\sum_{j=1}^{N}f(t,x_j(t))+\frac{c}{N}\sum_{i=1}^{N}\sum_{j=1}^{N}G_{ij}(t)Ax_j(t)\\&=\frac{1}{N}\sum_{j=1}^{N}f(t,x_j(t)).\end{aligned} \tag{11}$$

Note that $\frac{c}{N}\sum_{i=1}^{N}\sum_{j=1}^{N}G_{ij}(t)Ax_j(t)=0$ can be obtained from $G_{ij}=G_{ji}$, $G_{ii}=-\sum_{j=1,j\neq i}^{N}G_{ij}$.

Defining$e_i(t)=x_i(t)-\bar{x}(t)$, then the error dynamical network is described as follows:

$$\begin{aligned}\mathrm{D}_t^{\alpha}e_i(t)=&f(t,x_i(t))-\frac{1}{N}\sum_{j=1}^{N}f(t,x_j(t))\\&+c\sum_{j=1}^{N}G_{ij}(t)Ae_j(t),\ i=1,2,\cdots,N.\end{aligned} \tag{12}$$

Assumption 1. The nonlinear function $f(t,x)$ is said to be Lipschitz if there exists a nonnegative constant ε such that $(x-y)^{\mathrm{T}}(f(t,x)-f(t,y))\leq\varepsilon(x-y)^{\mathrm{T}}(x-y)$.

Lemma 2[31]. Let $G=(G_{ij})_{N\times N}$ is a real symmetric and irreducible matrix with

$$G_{ij}=G_{ji}\geq 0(i\neq j),G_{ii}=-\sum_{j=1,j\neq i}^{N}G_{ij}$$

Then,
(1) The eigenvalues of G satisfy

$$\begin{aligned}&0=\lambda_1(G)>\lambda_2(G)\geq\cdots\geq\lambda_N(G),\\&\lambda_2(G)=\max_{x^{\mathrm{T}}1_N=0,x\neq 0}\frac{x^{\mathrm{T}}Gx}{x^{\mathrm{T}}x}.\end{aligned}$$

(2) For any $\eta=(\eta_1,\eta_2,\cdots,\eta_N)^{\mathrm{T}}\in\mathbb{R}^N$

$$\eta^{\mathrm{T}}G\eta=-\frac{1}{2}\sum_{i=1}^{N}\sum_{j=1}^{N}G_{ij}(\eta_i-\eta_j)^2.$$

III. Main results

In this section, two fractional-order decentralized adaptive laws to tune the coupling gains among network nodes are proposed. By utilizing the proposed adaptive strategies, two sufficient conditions are derived to synchronize the proposed fractional-order complex networks.

A. Fractional-order decentralized adaptive strategy for the synchronization

Theorem 1. Suppose that Assumption 1 holds. Then, the network (9) is synchronized under the following fractional-order decentralized adaptive strategy:

$$\begin{aligned}&\mathrm{D}_t^{\alpha}G_{ij}(t)=\gamma_{ij}(x_i(t)-x_j(t))^{\mathrm{T}}A(x_i(t)-x_j(t)),\\&G_{ij}(0)=G_{ji}(0)>0,\end{aligned} \tag{13}$$

$(i,j)\in E$, where E is the set of undirected edges, $\gamma_{ij}=\gamma_{ji}$ are positive constants.

Proof. Construct the Lyapunov functional candidate for system (12) as

$$V_1(t)=\frac{1}{2}\sum_{i=1}^{N}e_i^{\mathrm{T}}(t)e_i(t)+\sum_{i=1}^{N}\sum_{j\in N_i}\frac{c}{4\gamma_{ij}}(G_{ij}(t)-h_{ij})^2, \tag{14}$$

where $h_{ij}=h_{ji}(i\neq j)$ are nonnegative constants, and $h_{ij}=0$ if and only if $G_{ij}(t)=0$.

Applying Lemma 1, the fractional derivative of V_1 along the trajectories of system (12) gives

$$\begin{aligned}\mathrm{D}_{\mathrm{t}}^{\alpha}V_1\leq&\sum_{i=1}^{N}e_i^{\mathrm{T}}(t)\mathrm{D}^{\alpha}e_i(t)\\&+\sum_{i=1}^{N}\sum_{j\in N_i}\frac{c}{2\gamma_{ij}}(G_{ij}(t)-h_{ij})\mathrm{D}^{\alpha}(G_{ij}(t)-h_{ij})\\=&\sum_{i=1}^{N}e_i^{\mathrm{T}}(t)\left[f(t,x_i(t))-\frac{1}{N}\sum_{j=1}^{N}f(t,x_j(t))\right]\\&+c\sum_{i=1}^{N}\sum_{j=1}^{N}e_i^{\mathrm{T}}(t)G_{ij}(t)Ae_j(t)\\&+\sum_{i=1}^{N}\sum_{j\in N_i}\frac{c}{2\gamma_{ij}}(G_{ij}(t)-h_{ij})\mathrm{D}^{\alpha}G_{ij}(t)\\=&\sum_{i=1}^{N}e_i^{\mathrm{T}}(t)\left[f(t,x_i(t))-\frac{1}{N}\sum_{j=1}^{N}f(t,x_j(t))\right]\\&+c\sum_{i=1}^{N}\sum_{j=1}^{N}e_i^{\mathrm{T}}(t)G_{ij}(t)Ae_j(t)\\&+\sum_{i=1}^{N}\sum_{j\in N_i}\frac{c}{2}(G_{ij}(t)-h_{ij})(x_i-x_j)^{\mathrm{T}}A(x_i-x_j)\\=&\sum_{i=1}^{N}e_i^{\mathrm{T}}(t)\left[f(t,x_i(t))-f(t,\ \bar{x})\right]\\&+\sum_{i=1}^{N}e_i^{\mathrm{T}}(t)\left[f(t,\ \bar{x})-\frac{1}{N}\sum_{j=1}^{N}f(t,x_j(t))\right]\\&+c\sum_{i=1}^{N}\sum_{j=1}^{N}e_i^{\mathrm{T}}(t)G_{ij}(t)Ae_j(t)\\&+\sum_{i=1}^{N}\sum_{j\in N_i}\frac{c}{2}(G_{ij}(t)-h_{ij})(e_i-e_j)^{\mathrm{T}}A(e_i-e_j),\end{aligned} \tag{15}$$

Since $\sum_{i=1}^{N} e_i^{\mathrm{T}}(t) = 0$, we have

$$\sum_{i=1}^{N} e_i^{\mathrm{T}}(t) \left[f(t,\ \bar{x}) - \frac{1}{N}\sum_{j=1}^{N} f(t, x_j(t)) \right] = 0. \quad (16)$$

According to Assumption 1, we can obtain

$$\sum_{i=1}^{N} e_i^{\mathrm{T}}(t) \left[f(t, x_i(t)) - f(t, \bar{x}) \right] \le \varepsilon \sum_{i=1}^{N} e_i^{\mathrm{T}}(t) e_i(t). \quad (17)$$

Let $H = (h_{ij})_{N\times N}$, where $h_{ii} = -\sum_{j=1, j\ne i}^{N} h_{ij}$. From Lemma 2, we can easily obtain

$$\begin{aligned}\sum_{i=1}^{N}\sum_{j\in N_i} &(G_{ij}(t) - h_{ij})(e_i(t) - e_j(t))^{\mathrm{T}} A (e_i(t) - e_j(t)) \\ &= -2\sum_{i=1}^{N}\sum_{j=1}^{N} (G_{ij}(t) - h_{ij}) e_i^{\mathrm{T}}(t) A e_j(t). \quad (18)\end{aligned}$$

Combining (15), (16), (17) and (18), we have

$$\begin{aligned}\mathrm{D}_t^{\alpha} V_1 \le& \varepsilon \sum_{i=1}^{N} e_i^{\mathrm{T}}(t) e_i(t) + c\sum_{i=1}^{N}\sum_{j=1}^{N} e_i^{\mathrm{T}}(t) G_{ij}(t) A e_j(t) \\ &- c\sum_{i=1}^{N}\sum_{j=1}^{N} (G_{ij}(t) - h_{ij}) e_i^{\mathrm{T}}(t) A e_j(t) \\ \le& \varepsilon \sum_{i=1}^{N} e_i^{\mathrm{T}}(t) e_i(t) + c\sum_{i=1}^{N}\sum_{j=1}^{N} h_{ij} e_i^{\mathrm{T}}(t) A e_j(t) \\ =& e^{\mathrm{T}}(t) \left[\varepsilon (I_N \otimes I_n) + c(H \otimes A) \right] e(t), \quad (19)\end{aligned}$$

where $e(t) = (e_1^{\mathrm{T}}(t), e_2^{\mathrm{T}}(t), \cdots, e_N^{\mathrm{T}}(t))^{\mathrm{T}} \in R^{nN}$.

Let $\Lambda = \mathrm{diag}(\lambda_1(H), \lambda_2(H), \cdots, \lambda_N(H))$ be the diagonal matrix associated with H, that is, there exists a unitary matrix $\Phi = (\phi_1, \phi_2, \cdots, \phi_N)$ such that $\Phi^{\mathrm{T}} H \Phi = \Lambda$. Let $y(t) = (y_1^{\mathrm{T}}, y_2^{\mathrm{T}}, \cdots, y_N^{\mathrm{T}})^{\mathrm{T}} = (\Phi^{\mathrm{T}} \otimes I_n) e(t)$. Since $\phi_1 = \frac{1}{\sqrt{N}}(1, 1, \cdots, 1)^{\mathrm{T}}$, one has $y_1(t) = (\phi_1^{\mathrm{T}} \otimes I_n) e(t) = 0$. Then, it follows from (19) that

$$\begin{aligned}\mathrm{D}_t^{\alpha} V_1 \le& \varepsilon e^{\mathrm{T}}(t)(I_N \otimes I_n) e(t) \\ &+ c e^{\mathrm{T}}(t)(\Phi \otimes I_n)(\Lambda \otimes A)(\Phi^{\mathrm{T}} \otimes I_n) e(t) \\ =& e^{\mathrm{T}}(t) \left[\varepsilon (I_N \otimes I_n) \right] e(t) + c y^{\mathrm{T}}(t)(\Lambda \otimes A) y(t). \quad (20)\end{aligned}$$

According to the definition of matrix H, one can easily verify that matrix H satisfies the conditions of Lemma 2. Then, by Lemma 2 and since A is positive, we get

$$y^{\mathrm{T}}(t)(\Lambda \otimes A) y(t) \le \lambda_2(H) y^{\mathrm{T}}(t)(I_N \otimes A) y(t). \quad (21)$$

From (20) and (21), it follows that

$$\begin{aligned}\mathrm{D}_t^{\alpha} V_1 \le& \varepsilon e^{\mathrm{T}}(t)(I_N \otimes I_n) e(t) \\ &+ c\lambda_2(H) y^{\mathrm{T}}(t)(I_N \otimes A) y(t) \\ =& \varepsilon e^{\mathrm{T}}(t)(I_N \otimes I_n) e(t) \\ &+ c\lambda_2(H) e^{\mathrm{T}}(t)(\Phi \otimes I_n)(I_N \otimes A)(\Phi^{\mathrm{T}} \otimes I_n) e(t) \\ =& e^{\mathrm{T}}(t) \left[\varepsilon (I_N \otimes I_n) + c\lambda_2(H)(I_N \otimes A) \right] e(t). \quad (22)\end{aligned}$$

Thus, for a given overall coupling strength c, one can choose h_{ij} sufficiently large such that

$$\varepsilon (I_N \otimes I_n) + c\lambda_2(H)(I_N \otimes A) + 1 < 0. \quad (23)$$

Then, it follows from (22) and (23) that

$$\mathrm{D}_t^{\alpha} V_1(t) \le -e^{\mathrm{T}}(t) e(t). \quad (24)$$

There exists a function $m(t) \ge 0$ such that

$$\mathrm{D}_t^{\alpha} V_1(t) + m(t) = -e^{\mathrm{T}}(t) e(t). \quad (25)$$

Applying Laplace transform operator $\mathcal{L}\{\cdot\}$ to (25), we have

$$\mathrm{s}^{\alpha} V_1(\mathrm{s}) - \mathrm{s}^{\alpha-1} V_1(0) + M(s) = -E(s), \quad (26)$$

where the nonnegative constant $V_1(0)$ is the initial value of $V_1(t)$, $V_1(s)$, $M(s)$, and $E(s)$ are the Laplace transforms of $V_1(t)$, $m(t)$, and $e^{\mathrm{T}}(t)e(t)$ respectively.

Since $V_1(t) \ge \frac{1}{2}\sum_{i=1}^{N} e_i^{\mathrm{T}}(t) e_i(t) = \frac{1}{2} e^{\mathrm{T}}(t) e(t)$, there exists a function $n(t) \ge 0$ such that

$$V_1(t) = \frac{1}{2} e^{\mathrm{T}}(t) e(t) + n(t). \quad (27)$$

Applying Laplace transform operator $\mathcal{L}\{\cdot\}$ to (27), we have

$$V_1(\mathrm{s}) = \frac{1}{2} E(s) + N(s), \quad (28)$$

where $N(s)$ is the Laplace transform of $n(t)$.

Combining (26) and (28), we can easily obtain

$$\begin{aligned}E(s) =& \frac{2\mathrm{s}^{\alpha-1}}{\mathrm{s}^{\alpha}+2} V_1(0) - \frac{2\mathrm{s}^{\alpha}}{\mathrm{s}^{\alpha}+2} N(s) \\ &- \frac{2}{\mathrm{s}^{\alpha}+2} M(s), \quad (29)\end{aligned}$$

Taking the Laplace inverse transform of (29), it gives

$$\begin{aligned}e^{\mathrm{T}}(t) e(t) =& 2V_1(0) E_{\alpha}(-2t^{\alpha}) - 2n(t) * t^{-1} E_{\alpha,0}(-2t^{\alpha}) \\ &- 2m(t) * t^{\alpha-1} E_{\alpha,\alpha}(-2t^{\alpha}). \quad (30)\end{aligned}$$

where $*$ stands the convolution operator.

Since $t^{-1}, t^{\alpha-1}, E_{\alpha,0}(-2t^{\alpha})$, and $E_{\alpha,\alpha}(-2t^{\alpha})$ are nonnegative functions, it follows from (30) that

$$e^{\mathrm{T}}(t) e(t) \le 2V_1(0) E_{\alpha}(-2t^{\alpha}). \quad (31)$$

Moreover, we should also note the fact that, for $0 < \alpha < 1$ and $k > 0$, $E_{\alpha}(-kt^{\alpha})$ is completely monotonic and decreases much faster than the exponential function $\exp^{-kt}$(see [42]). Therefore, we can conclude from inequality (31) that $\lim_{t\to+\infty} e^{\mathrm{T}}(t) e(t) = 0$, that is, $\lim_{t\to+\infty} \|e(t)\|_2 = 0$. It means that the network (9) is synchronized under the adaptive law (13). The convergence of error vector implies, from (13) and from the fact that A is positive definite, $\lim\limits_{t\to+\infty} \mathrm{D}_t^{\alpha} G_{ij}(t) = 0$. According to Property 3, one can conclude that $G_{ij}(t)((i,j) \in E)$ converges to a finite constant. The proof is completed. ■

Remark 1. In recent years, many kinds of adaptive strategies were designed to adjust the gains of feedback controllers, see [27-29] and relevant references therein. Actually, a diffusively coupled network could be synchronized by designing suitable coupling gains among the network nodes. As a natural extension of the existing network models and control methods, a new fractional-order complex dynamical network with time-varying diffusive coupling is proposed, and then the fractional-order decentralized adaptive strategy to tune the coupling gains between the network nodes is designed based on the local mismatch between neighboring nodes. To our knowledge, this is the first paper to consider the synchronization of fractional-order complex dynamical networks with adaptive coupling. Fortunately, this challenging problem has been solved by fractional Lyapunov functional method combined with Mittag-Leffler function, Laplace transform, and fractional inequality techniques.

Remark 2. From (13), we have $\mathrm{D}_t^{\alpha} G_{ij}(t) \geq 0$. However, one cannot conclude that $G_{ij}(t)$ is monotonously non-decreasing for $0<\alpha<1$. To state the reason, we assume $x(t) \in C^1[t_0, +\infty)$ and satisfies

$$\mathrm{D}_t^{\alpha} x(t) = f(t,x) \geq 0,\ 0<\alpha<1. \tag{32}$$

$\forall t_0 \leq t_2 < t_1 < +\infty$, integrating both sides of (32) from t_0 to t_1 and t_0 to t_2 respectively, it follows from Definition 1 and Property 2 that

$$x(t_1)-x(t_0)= \frac{1}{\Gamma(\alpha)}\int_{t_0}^{t_1}\frac{f(\tau,x(\tau))}{(t_1-\tau)^{1-\alpha}}\mathrm{d}\tau. \tag{33}$$

$$x(t_2)-x(t_0)= \frac{1}{\Gamma(\alpha)}\int_{t_0}^{t_2}\frac{f(\tau,x(\tau))}{(t_2-\tau)^{1-\alpha}}\mathrm{d}\tau. \tag{34}$$

Subtracting (34) from (33), we have

$$\begin{aligned}
x(t_1)-x(t_2)= &\frac{1}{\Gamma(\alpha)}\int_{t_0}^{t_1}\frac{f(\tau,x(\tau))}{(t_1-\tau)^{1-\alpha}}\mathrm{d}\tau \\
&-\frac{1}{\Gamma(\alpha)}\int_{t_0}^{t_2}\frac{f(\tau,x(\tau))}{(t_2-\tau)^{1-\alpha}}\mathrm{d}\tau \\
=& \frac{1}{\Gamma(\alpha)}\int_{t_0}^{t_2}\frac{f(\tau,x(\tau))}{(t_1-\tau)^{1-\alpha}}\mathrm{d}\tau + \frac{1}{\Gamma(\alpha)}\int_{t_2}^{t_1}\frac{f(\tau,x(\tau))}{(t_1-\tau)^{1-\alpha}}\mathrm{d}\tau \\
&-\frac{1}{\Gamma(\alpha)}\int_{t_0}^{t_2}\frac{f(\tau,x(\tau))}{(t_2-\tau)^{1-\alpha}}\mathrm{d}\tau \\
=& \frac{1}{\Gamma(\alpha)}\int_{t_0}^{t_2}\left[\frac{f(\tau,x(\tau))}{(t_1-\tau)^{1-\alpha}}-\frac{f(\tau,x(\tau))}{(t_2-\tau)^{1-\alpha}}\right]\mathrm{d}\tau \\
&+\frac{1}{\Gamma(\alpha)}\int_{t_2}^{t_1}\frac{f(\tau,x(\tau))}{(t_1-\tau)^{1-\alpha}}\mathrm{d}\tau,
\end{aligned} \tag{35}$$

where $\frac{1}{(t_1-\tau)^{1-\alpha}} - \frac{1}{(t_2-\tau)^{1-\alpha}} < 0$ for $0<\alpha<1$. Thus, as can be seen from (35), one cannot establish the sign of $x(t_1)-x(t_2)$, which is closely related to α. Obviously, this analysis result is not consistent with that of integer-order case. It should be noted that our numerical results for coupling gains can be theoretically interpreted by the analysis result in this remark.

B. Fractional-order decentralized adaptive pinning strategy for the synchronization

In Theorem 1, all the coupling gains are adjusted according to the adaptive law (13). Here, only a small fraction of the coupling gains is updated to reach synchronization.

Let $\tilde{E}$ be a subset of E. Assume that network (9) is connected through the pinning edges $\tilde{E}$.

Here, we define

$$L_{ij}=\begin{cases} G_{ij}(0), & \text{if } (i,j)\in E-\tilde{E} \\ -\sum_{j=1,j\neq i}^{N} G_{ij}(0), & \text{if } i=j \\ 0, & \text{otherwise} \end{cases} \tag{36}$$

Theorem 2. Suppose that Assumption 1 holds. Then, the network (9) is synchronized under the following fractional-order decentralized adaptive pinning strategy:

$$\begin{aligned} &\mathrm{D}_t^{\alpha} G_{ij}(t) = \gamma_{ij}(x_i(t)-x_j(t))^{\mathrm{T}} A (x_i(t)-x_j(t)), \\ &G_{ij}(0)=G_{ji}(0)>0,\ (i,j)\in\tilde{E}, \end{aligned} \tag{37}$$

where $\gamma_{ij}=\gamma_{ji}$ are positive constants.

Proof. Consider the following Lyapunov functional candidate for system (12)

$$V_2(t)=\frac{1}{2}\sum_{i=1}^{N} e_i^{\mathrm{T}}(t)e_i(t) + \sum_{i=1}^{N}\sum_{(i,j)\in\tilde{E}} \frac{c}{4\gamma_{ij}}(G_{ij}(t)-\tilde{h}_{ij})^2, \tag{38}$$

where $\tilde{h}_{ij}$ is defined as

$$\begin{aligned} &\tilde{h}_{ij}=\tilde{h}_{ji}>0, && \text{if } (i,j)\in\tilde{E}, \\ &\tilde{h}_{ij}=0 (i\neq j), && \text{otherwise}. \end{aligned} \tag{39}$$

Let $\tilde{H}=(\tilde{h}_{ij})_{N\times N}$, $\tilde{h}_{ii}=-\sum_{j=1,j\neq i}^{N}\tilde{h}_{ij}$. Now, we calculate the fractional derivative of V_2 along the trajectories of system (12)

$$\begin{aligned}
\mathrm{D}_t^{\alpha} V_2 \leq& \sum_{i=1}^{N}\sum_{(i,j)\in\tilde{E}}\frac{c}{2\gamma_{ij}}\big(G_{ij}(t)-\tilde{h}_{ij}\big)\mathrm{D}^{\alpha}\big(G_{ij}(t)-\tilde{h}_{ij}\big) \\
&+\sum_{i=1}^{N} e_i^{\mathrm{T}}(t)\mathrm{D}^{\alpha} e_i(t) \\
=&\sum_{i=1}^{N} e_i^{\mathrm{T}}(t)\Bigg[f(t,x_i(t))-f(t,\bar{x})+f(t,\bar{x}) \\
&-\frac{1}{N}\sum_{j=1}^{N} f(t,x_j(t)) + c\sum_{j=1}^{N} G_{ij}(t)Ae_j(t)\Bigg] \\
&+\sum_{i=1}^{N}\sum_{(i,j)\in\tilde{E}}\frac{c}{2}(G_{ij}(t)-\tilde{h}_{ij})(e_i(t)-e_j(t))^{\mathrm{T}} \\
&\times A(e_i(t)-e_j(t)) \\
&\leq \varepsilon\sum_{i=1}^{N} e_i^{\mathrm{T}}(t)e_i(t) + c\sum_{i=1}^{N}\sum_{j=1}^{N} L_{ij}e_i^{\mathrm{T}}(t)Ae_j(t) \\
&+c\sum_{i=1}^{N}\sum_{j=1}^{N}\tilde{h}_{ij}e_i^{\mathrm{T}}(t)Ae_j(t) \\
=&e^{\mathrm{T}}(t)\big[\varepsilon(I_N\otimes I_n)+c(L\otimes A)+c(\tilde{H}\otimes A)\big]e(t),
\end{aligned} \tag{40}$$

where $e(t)=(e_1^{\mathrm{T}}(t), e_2^{\mathrm{T}}(t),\cdots,e_N^{\mathrm{T}}(t))^{\mathrm{T}}$, $L=(L_{ij})_{N\times N}$, $\tilde{H}=(\tilde{H}_{ij})_{N\times N}$. Then, following similar steps as in the proof of Theorem 1, we can complete the proof. ■

IV. Numerical examples

In this section, two numerical examples are given to validate the above obtained theoretical results. Here, the predictor-corrector method studied in [44] is utilized to solve the differential equations of the fractional-order systems. In the following examples, the simulation step-size is chosen as h=0.01.

Example 1. Consider a diffusively coupled scale-free[1] network with 50 nodes, where each node is a fractional-order non-autonomous parametrically excited Duffing oscillator described by

$$\begin{aligned}&\mathrm{D}_t^{\alpha}x_1 = x_2,\\ &\mathrm{D}_t^{\alpha}x_2 = (1+\mu\sin(\omega t))x_1 - \gamma x_2 - x_1^3.\end{aligned}\tag{41}$$

When $\mu = 0.5$, $\omega = 1$, $\gamma = 0.2$, $\alpha = 0.975$, system (41) has a chaotic attractor as shown in Fig.1.

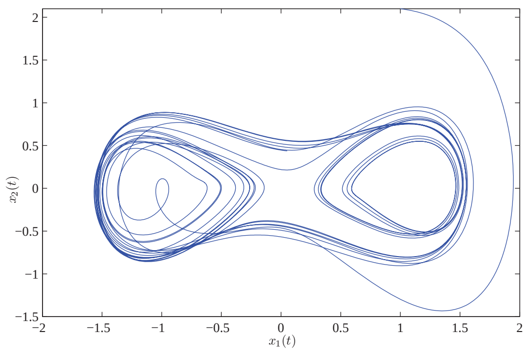

Fig. 1. (color online) Chaotic attractor of system (41) with $\mu = 0.5$, $\omega = 1$, $\gamma = 0.2$, $\alpha = 0.975$ and $(x_1(0), x_2(0)) = (1.0,\ 2.1)$

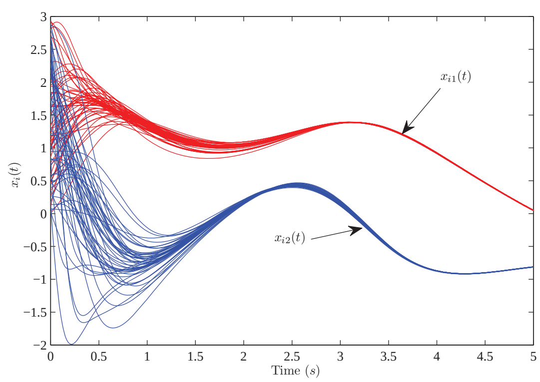

Fig. 2. (color online) Time evolutions of $x_i = (x_{i1}, x_{i2})^{\mathrm{T}}, i = 1, 2, \cdots, 50$

For simplicity and without losing generality, we take $c = 1$, $A = \mathrm{diag}(1, 1, 1)$. For connected nodes i and j, $G_{ij}(0) = G_{ji}(0)$ are chosen randomly in $(0,\ 1)$ and $\gamma_{ij} = \gamma_{ji} = 1$, $\forall (i, j) \in E$. The initial states x_i are chosen randomly in $(0,\ 3)$. Therefore, all the conditions of Theorem 1 are satisfied, and the network synchronization is asymptotically achieved. As shown in Figs.2 and 3, the simulation results agree well with the theoretical analysis.

Example 2. Consider a diffusively coupled complex network with 10 nodes, where each node is a fractional-order Arneodo's system described by

$$\begin{aligned}&\mathrm{D}_t^{\alpha}x_1 = x_2,\\ &\mathrm{D}_t^{\alpha}x_2 = x_3\\ &\mathrm{D}_t^{\alpha}x_3 = \beta_1 x_1 - \beta_2 x_2 - \beta_3 x_3 + \beta_4 x_1^3.\end{aligned}\tag{42}$$

When $\beta_1 = 5.5$, $\beta_2 = 3.5$, $\beta_3 = 0.4$, $\beta_4 = -1$, and $\alpha = 0.9$, system (42) is chaotic[45]. We take $c = 1$,

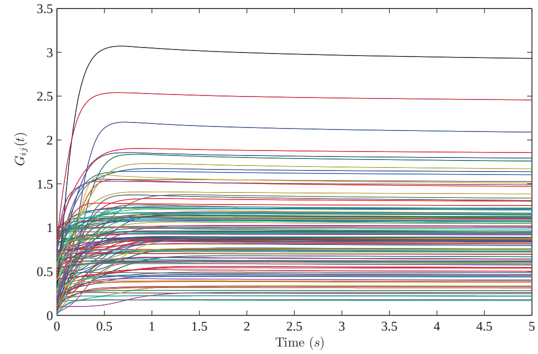

Fig. 3. (color online) Adaptive coupling gains $G_{ij}(t),\ (i, j) \in E$

$A = \mathrm{diag}(1, 1, 1)$. The initial coupling matrix is chosen as

$$\mathrm{G}(0) = \begin{bmatrix} -3.8 & 0.8 & 0.6 & 0.3 & 0 & 0.3 & 0.6 & 0.7 & 0.5 & 0\\ 0.8 & -2.5 & 0.2 & 0 & 0.4 & 0 & 0 & 0.2 & 0.2 & 0.7\\ 0.6 & 0.2 & -1.8 & 0.4 & 0 & 0.5 & 0.1 & 0 & 0 & 0\\ 0.3 & 0 & 0.4 & -0.8 & 0.1 & 0 & 0 & 0 & 0 & 0\\ 0 & 0.4 & 0 & 0.1 & -0.6 & 0 & 0 & 0 & 0 & 0.1\\ 0.3 & 0 & 0.5 & 0 & 0 & -1.1 & 0.3 & 0 & 0 & 0\\ 0.6 & 0 & 0.1 & 0 & 0 & 0.3 & -1.2 & 0 & 0.2 & 0\\ 0.7 & 0.2 & 0 & 0 & 0 & 0 & 0 & -0.9 & 0 & 0\\ 0.5 & 0.2 & 0 & 0 & 0 & 0 & 0.2 & 0 & -0.9 & 0\\ 0 & 0.7 & 0 & 0 & 0.1 & 0 & 0 & 0 & 0 & -0.8 \end{bmatrix}$$

Here, we select a fraction of coupling gains in the network. Choose $\gamma_{12} = \gamma_{21} = 0.5$, $\gamma_{13} = \gamma_{31} = 0.6$, $\gamma_{17} = \gamma_{71} = 0.7$, $\gamma_{18} = \gamma_{81} = 0.8$, $\gamma_{19} = \gamma_{91} = 0.9$, $\gamma_{25} = \gamma_{52} = 0.5$, $\gamma_{2,10} = \gamma_{10,2} = 0.6$, $\gamma_{36} = \gamma_{63} = 0.7$, $\gamma_{34} = \gamma_{43} = 0.8$. The initial states x_i are chosen randomly in $(0,\ 2)$. According to Theorem 2, the network synchronization is asymptotically achieved. The simulation results depicted in Figs.4 and 5 agree well with the theoretical analysis. As can be seen from Figs.3 and 5, the adaptive coupling gains are not monotonously non-decreasing, which further validates our theoretical analysis in Remark 2.

V. Conclusions

In this paper, two fractional-order decentralized adaptive strategies have been proposed to tune the coupling gains between network nodes. Based on the proposed adaptive coupling strategies, two sufficient conditions have been derived for synchronization of fractional-order complex networks. In the proofs of the theorems, an inequality has been used to estimate the fractional-order derivative of a quadratic Lyapunov function. Thus, we can investigate the synchronization for

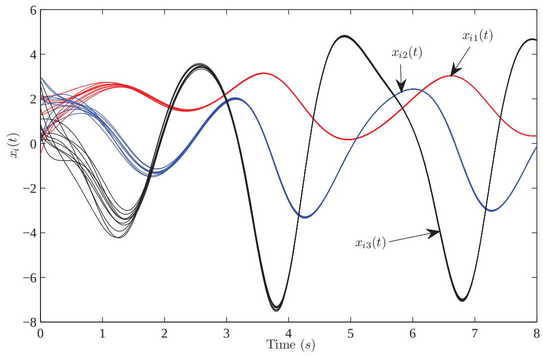

Fig. 4. (color online) Time evolutions of $x_i = (x_{i1}, x_{i2}, x_{i3})^{\mathrm{T}}$, $i = 1, 2, \cdots, 10$.

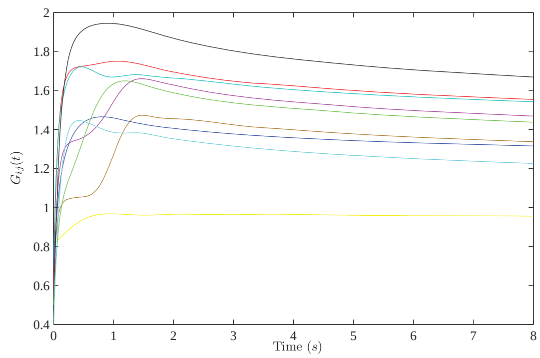

Fig. 5. (color online) Adaptive coupling gains $G_{ij}(t), (i, j) \in \tilde{E}$.

fractional-order complex networks like integer-order complex networks. Numerical examples have been given to validate the theoretical results. The obtained results show that the adaptive coupling gains are not monotonously non-decreasing even though $\mathrm{D}_t^{\alpha} G_{ij}(t) \geq 0$. This counter-intuitive conclusion also implies that the fractional-order system has additional attractive feature over the integer-order system.

REFERENCES

[1] Barabsi A L, Albert R. Emergence of Scaling in Random Networks. *Science*, 1999, **286**(5439): 509-512.

[2] Strogatz S H. Exploring complex networks. *Nature*, 2001, **410**: 268-276

[3] Wang X, Chen G R. Complex networks: small-world, scale-free and beyond. *IEEE Circuits and Systems Magazine*, 2003, **3**(1): 6-20

[4] Motter A E, Myers S A, Anghel M, Nishikawa T. Spontaneous synchrony in power-grid networks. *Nature Physics*, 2013, **9**: 191-197

[5] Tang Y, Qian F, Gao H, Kurths J. Synchronization in complex networks and its application-A survey of recent advances and challenges. *Annual Reviews in Control*, 2014, **38**(2): 184-198

[6] Arenas A, Diaz-Guilera A, Kurths J, Moreno Y, Zhou C. Synchronization in complex networks. *Physics Reports*, 2008, **469**(3): 93-153

[7] Song Q, Cao J. On pinning synchronization of directed and undirected complex dynamical networks. *IEEE Transactions on Circuits and Systems I*, 2010, **57**(3): 672-680

[8] Lee T H, Park J H, Jung H Y, Lee S M, Kwon O M. Synchronization of a delayed complex dynamical network with free coupling matrix. Nonlinear Dynamics, 2012, **69**(3): 1081-1090

[9] Ji P, Peron T K, Menck P J, Rodrigues F A, Kurths J. Cluster explosive synchronization in complex networks. *Physical Review Letters*, 2013, **110**: 218701

[10] Lu R, Yu W, Lu J, Xue A. Synchronization on complex networks of networks. *IEEE Transactions on Neural Networks and Learning Systems*, 2014, **25**(11): 2110-2118

[11] Lu J, Zhong J, Tang Y, Huang T, Cao J, Kurths J. Synchronization in output-coupled temporal Boolean networks. *Scientific Reports*, 2014, **4**: 6292

[12] Wang J L, Wu H N. Adaptive output synchronization of complex delayed dynamical networks with output coupling. *Neurocomputing*, 2014, **142**(22): 174-181

[13] Wu Z G, Shi P, Su H, Chu J. Sampled-data exponential synchronization of complex dynamical networks with time-varying coupling delay. *IEEE Transactions on Neural Networks and Learning Systems*, 2013, **24**(8): 1177-1187

[14] Park J H, Lee T H. Synchronization of complex dynamical networks with discontinuous coupling signals. *Nonlinear Dynamics*, 2015, **79**(2): 1353-1362

[15] Wang J L, Wu H N, Huang T. Passivity-based synchronization of a class of complex dynamical networks with time-varying delay. *Automatica*, 2015, **56**: 105-112

[16] DeLellis P, Bernardo M, Liuzza D. Convergence and synchronization in heterogeneous networks of smooth and piecewise smooth systems. *Automatica*, 2015, **56**: 1-11

[17] Kilbas A, Srivastava H, Trujillo J. *Theory and Applications of Fractional Differential Equations*. Elsevier, 2006.

[18] Li C P, Zhang F R. A survey on the stability of fractional differential equations. *The European Physical Journal Special Topics*, 2011, **193**(1): 27-47

[19] Zeng C, Chen Y Q, Yang Q. Almost sure and moment stability properties of fractional order Black-Scholes model. *Fractional Calculus and Applied Analysis*, 2013, **16**(2): 317-331

[20] Lu J G, Chen Y Q, Chai Y, Wu R. Stability and stabilization of fractional-order linear systems with convex polytopic uncertainties. *Fractional Calculus and Applied Analysis*, 2013, **16**(1): 142-157

[21] Hu J B, Lu G P, Zhang S B, Zhao L D. Lyapunov stability theorem about fractional system without and with delay. *Communications in Nonlinear Science and Numerical Simulation*, 2015, **20**(3): 905-913

[22] Yin C, Chen Y Q, Zhou S. Fractional-order sliding mode based extremum seeking control of a class of nonlinear systems. *Automatica*, 2014, **50**(12): 3173-3181

[23] Hu J B, Zhao L D. Stability theorem and control of fractional systems. *Acta Physica Sinica*, 2013, **62**(24): 240504(in Chinese)

[24] Wang F, Yang Y, Hu M. Projective cluster synchronization of fractional-order coupled-delay complex network via adaptive pinning control. *Physica A*, 2015, **434**: 134-143

[25] Wang J, Zeng C. Synchronization of fractional-order linear complex networks. *ISA Transactions*, 2015, **55**: 129-134

[26] Wang Y, Li T. Synchronization of fractional order complex dynamical networks. *Physica A*, 2015, **428**: 1-12

[27] Guo X, Li J. A new synchronization algorithm for delayed complex dynamical networks via adaptive control approach. *Communications in Nonlinear Science and Numerical Simulation*, 2012, **17**(11): 4395-4403

[28] Chai Y , Chen L, Wu R, Sun J. Adaptive pinning synchronization in fractional-order complex dynamical networks. *Physica A*, 2012, **391**(22): 5476-5758

[29] Si G, Sun Z, Zhang H, Zhang Y. Parameter estimation and topology identification of uncertain fractional order complex networks. *Communications in Nonlinear Science and Numerical Simulation*, 2012, **17**(12): 5158-5171

[30] Delellis P, di Bernardo M, Garofalo F. Novel decentralized adaptive strategies for the synchronization of complex networks. *Automatica*, 2009, **45**(5): 1312-1318

[31] Yu W, DeLellis P, Chen G, diBernardo M, Kurths J. Distributed adaptive control of synchronization in complex networks. *IEEE Transactions on Automatic Control*, 2012, **57**(8): 2153-2158

[32] Wang J L, Wu H N. Synchronization and adaptive control of an array of linearly coupled reaction-diffusion neural networks with hybrid coupling. *IEEE Transactions on Cybernetics*, 2014, **44**(8): 1350-1361

[33] Wang J L, Wu H N, Guo L. Novel Adaptive Strategies for Synchronization of Linearly Coupled Neural Networks with Reaction-Diffusion Terms. *IEEE Transactions on Neural Networks and Learning Systems*, 2014, **25**(2): 429-440

[34] Wang J L, Wu H N, Huang T, Ren SY. Passivity and synchronization of linearly coupled reaction-diffusion neural networks with adaptive coupling. *IEEE Transactions on Cybernetics*, 2015, **45**(9): 1942-1952

[35] Turci L F R, DeLellis P, Macau E E N, Bernardo M. Adaptive pinning control: A review of the fully decentralized strategy and its extensions. *The European Physical Journal Special Topics*, 2014, **223**: 2649-2664

[36] Chen T, Liu X, Lu W. Pinning Complex Networks by a Single Controller. *IEEE Transactions on Circuits and Systems I*, 2007, **54**(6): 1317-1326

[37] Wu W, Zhou W, Chen T. Cluster synchronization of linearly coupled complex networks under pinning control. *IEEE Transactions on Circuits and Systems I*, 2009, **56**(4): 829-839

[38] Chen D, Zhang R, Liu X, Ma X. Fractional order Lyapunov stability theorem and its applications in synchronization of complex dynamical networks. *Communications in Nonlinear Science and Numerical Simulation*, 2014, **19**: 4105-4121

[39] Aguila-Camacho N, Duarte-Mermoud M A. Comments on "Fractional order Lyapunov stability theorem and its applications in synchronization of complex dynamical networks". *Communications in Nonlinear Science and Numerical Simulation*, 2015, *25*(1-3): 145-148

[40] Aguila-Camacho N, Duarte-Mermoud M A, Gallegos J. Lyapunov functions for fractional order systems. *Communications in Nonlinear Science and Numerical Simulation*, 2014, **19**: 2951-2957

[41] Duarte-Mermoud MA, Aguila-Camacho N, Gallegos JA, Castro-Linares R. Using general quadratic Lyapunov functions to prove Lyapunov uniform stability for fractional order systems. *Communications in Nonlinear Science and Numerical Simulation*, 2015, **22**: 650-659

[42] Li Y, Chen Y, Podlubny I. Stability of fractional-order nonlinear dynamic systems: Lyapunov direct method and generalized Mittag Leffler stability. *Computers and Mathematics with Applications*, 2010, **59**: 1810-1821

[43] Li Y, Chen Y, Podlubny I. Mittag-Leffler stability of fractional order nonlinear dynamic systems. *Automatica*, 2009, **45**(8): 1965-1969

[44] Diethelm K, Ford N J, Freed A D. A predictor-corrector approach for the numerical solution of fractional differential equations. *Nonlinear Dynamics*, 2002, **29**: 3-22

[45] Ma T D, Jiang W B, Fu J, Chai Y, Chen L P, Xue F Z. Adaptive synchronization of a class of fractional-order chaotic systems. *Acta Physica Sinica*, 2012, **61**(16): 160506(in Chinese)

Quan Xu graduated from Xihua University, China, 2006. He received the M.Sc. degree from Xihua University, China, in 2009. He is currently a Lecturer with Xihua University, and he is also working towards the Ph.D. degree at the School of Electrical Engineering, Southwest Jiaotong University, China. His research interests include nonlinear control, fractional-order systems, stability theory, complex networks. He serves as a reviewer for several journals.

Shengxian Zhuang was born in Hunan, China, in 1964. He received his M.Sc. degree from Southwest Jiaotong University, and Ph.D. degree from University of Electronics and Technology of China, in 1991 and 1999 respectively. He has been a Professor of Electrical Engineering at the Southwest Jiaotong University since 2003. His research interests include nonlinear control, stability theory and power electronics.

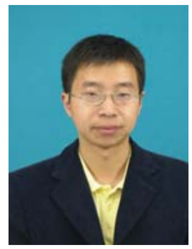

Yingfeng Zeng graduated from Xihua University, 2001. He received his M.Sc. degree from Xihua University, in 2009. He is working towards the Ph.D. degree at the School of Electrical Engineering, Southwest Jiaotong University, China. His research interest covers the controllability and stability of complex networks.

Jian Xiao graduated from Hunan University, 1979. He received his M.Sc. degree from Hunan University, and Ph.D. degree from Southwest Jiaotong University, in 1982 and 1989 respectively. He has been a Professor of Electrical Engineering at the Southwest Jiaotong University since 1994. His research interests include robust control, fuzzy systems and power electronics.

Robust Finite-time Synchronization of Non-Identical Fractional-order Hyperchaotic Systems and its Application in Secure Communication

Hadi Delavari and Milad Mohadeszadeh

Abstract—**This paper proposes a novel adaptive sliding mode control (SMC) method for synchronization of non-identical fractional-order (FO) chaotic and hyper-chaotic systems. Under the existence of system uncertainties and external disturbances, finite-time synchronization between two FO chaotic and hyperchaotic systems is achieved by introducing a novel adaptive sliding mode controller (ASMC). Here in this paper, a fractional sliding surface is proposed. A stability criterion for FO nonlinear dynamic systems is introduced. Sufficient conditions to guarantee stable synchronization are given in the sense of the Lyapunov stability theorem. To tackle the uncertainties and external disturbances, appropriate adaptation laws are introduced. Particle Swarm Optimization (PSO) is used for estimating the controller parameters. Finally, finite-time synchronization of the FO chaotic and hyper-chaotic systems is applied to secure communication.**

Index Terms—**Adaptive sliding mode control, chaos synchronization, fractional order, hyper-chaotic system, Lyapunov theorem, secure communication**

I. Introduction

CHAOTIC behavior is a prevalent phenomenon appearing in nonlinear systems. Chaotic systems have received more attention in the literature during the last three decades. A chaotic system is a nonlinear deterministic system that has complex and unpredictable behavior.

Fractional calculus is a mathematical topic more than three centuries old, but its application to physics and engineering fields have attracted more attention only in recent years[1−3]. This happens because it has been recently found that several physical phenomena can be more adequately described by fractional differential equations rather than integer-order models[4], and it has been found that many FO systems can show complex dynamical behavior such as chaos. The advantages of the FO systems are that there are more degrees of freedom in the model. Also memory is included in FO systems. Many systems in interdisciplinary fields, such as viscoelastic materials[5] and micro-electromechanical systems[6] can be described using fractional calculus methods.

Recently many researchers have recognized that many complex systems, such as FO Lorenz system[7], FO Chen system[8] and FO Arnodo-Coullet system[9], can be described using fractional integrals and derivatives.

Since Pecora and Carroll[10] established a chaos synchronization scheme for two identical chaotic systems with different initial conditions, chaos synchronization has attracted a great attention. The chaotic synchronization occurs whenever the state trajectories of the slave system track the state trajectories of the master system in a given finite-time[11,12]. Chaos synchronization is a contemporary topic in nonlinear science because of its broad and considerable applications in secure communication, automatic control, neural networks and etc.[13−15].

Due to the existence of chaos in real practical systems and many applications in physics and engineering fields, control and synchronization of FO chaotic systems have attracted many researchers attention in the past few years[16−23]. In [24], an active sliding mode approach for synchronization of FO chaotic system is proposed. The FO Novel and Chen hyper-chaotic systems are proposed for synchronization in [25], where the states of the FO hyper-chaotic Novel system are used to control the states of the FO hyper-chaotic Chen system. Several methods have been proposed to achieve chaos synchronization such as adaptive feedback control, adaptive impulsive control, sliding mode control, active control, backstepping design and optimal control[26−36].

Most of the published papers focus on asymptotic stability which leads to infinite-time synchronization, but in practical applications, finite-time synchronization is more valuable than infinite-time synchronization. Also, most of the researches are related to synchronization between two chaotic systems without uncertainty or two identical chaotic systems, but in a real control system, due to the limitations of physical devices and the effect of interference (such as noise, temperature, etc.), uncertainties are unavoidable.

Motivated by the above discussion, a novel adaptive sliding mode control approach for synchronization of a class of new FO chaotic system and a FO hyper-chaotic system is proposed. In our contribution we pursue five main research aims. First, the proposed approach is very simple and easily realized experimentally for secure communication. Second, the proposed controller can be applied for a width range of systems and is more suitable for engineering applications. Third, finite-time convergence to zero and stability of the proposed method are analytically proved, which contains new ideas. Fourth, a fractional sliding surface is presented and stability of the proposed surface is proved. Fifth, the upper

This article has been accepted for publication in a future issue of this journal, but has not been fully edited. Content may change prior to final publication.

Recommended by Associate Editor YangQuan Chen.

H. Delavari and M. Mohadeszadeh are with the Electrical Engineering Department, Hamedan University of Technology, Hamedan, CO 65155 Iran (email: delavari@hut.ac.ir).

Digital Object Identifier 10.1109/JAS.2016.7510145

bound of the system uncertainties and external disturbances are estimated using Lyapunov stability theorem.

The rest of this paper is organized as follows. First, the fractional calculus and the fractional systems stability theory are briefly introduced. Then, the system description and problem statement are given. After that, the design strategy of the proposed ASMC is presented. Then, the simulations for synchronization of non-identical FO chaotic and hyperchaotic systems are done and the application of the proposed synchronization scheme is studied in secure communication. Finally, concluding remarks are addressed.

II. Derivative and Stability Theorem on FO System

The Caputo fractional derivative of order α of m order continuous function $f(t)$ with respect to t is defined by

$$ {}_{t_0}^{C}D_t^{\alpha} f(t) = I^{m-\alpha} f^{(m)}(t), \quad \alpha > 0 \tag{1}$$

where m is the smallest integer number, larger than , and I^{β} is the Riemann-Liouville integral operator of order β which is described as follows

$$ {}_{t_0}I_t^{\beta} f(t) = \frac{1}{\Gamma(\beta)} \int_{t_0}^{t} \frac{f(\tau)}{(t-\tau)^{1-\beta}} \mathrm{d}\tau, \quad \beta > 0 \tag{2}$$

In (2), $\Gamma(\cdot)$ is the Gamma function which is given by

$$ \Gamma(\beta) = \int_0^{\infty} t^{\beta-1} e^{-t} \mathrm{d}t \tag{3}$$

The numerical simulation of a fractional differential equation is not as simple as that of an ordinary differential equation. Recently, many approaches have been investigated for solving nonlinear FO differential equations. Throughout this paper, we choose the fractional Adams-Bashforth-Moulton method as a representative numerical scheme[37,38]. In order to explain this method, the following differential equation is considered

$$ \begin{cases} D_t^{\alpha} y(t) = r(t, y(t)),\ 0 \le t \le T, \\ y^{(k)}(0) = y_0^{(k)},\ k = 0, 1, \cdots, m-1. \end{cases} \tag{4}$$

The differential equation (4) is equivalent to Volterra integral equation which is as follows

$$ y(t) = \sum_{k=0}^{\lceil \alpha \rceil - 1} y_0^{(k)} \frac{t^k}{k!} + \frac{1}{\Gamma(\alpha)} \int_0^t (t-s)^{\alpha-1} r(s, y(s)) \mathrm{d}s. \tag{5}$$

Now, set $h = T/N$, $t_n = nh$, $n = 0, 1, \cdots, N$. The integral equation can be discretized as

$$ \begin{aligned} y_h(t_{n+1}) = &\sum_{k=0}^{\lceil \alpha \rceil - 1} y_0^{(k)} \frac{t^k}{k!} + \frac{h^{\alpha}}{\Gamma(\alpha+2)} r\left(t_{n+1}, y_h^p(t_{n+1})\right) \\ &+ \frac{h^{\alpha}}{\Gamma(\alpha+2)} \sum_{j=0}^{n} a_{j,n+1} r(t_j, y_h(t_j)) \end{aligned} \tag{6}$$

where

$$ y_h^p(t_{n+1}) = \sum_{k=0}^{\lceil \alpha \rceil - 1} y_0^{(k)} \frac{t^k}{k!} + \frac{1}{\Gamma(\alpha)} \sum_{j=0}^{n} b_{j,n+1} r(t_j, y_h(t_j)) \tag{7}$$

and

$$ a_{j,n+1} = \begin{cases} n^{\alpha+1} - (n-\alpha)(n+1)^{\alpha}, & j = 0 \\ (n-j+2)^{\alpha+1} + (n-j)^{\alpha+1} - 2(n-j+1)^{\alpha+1}, & \\ & 1 \le j \le n \\ 1, & j = n+1 \end{cases} \tag{8}$$

$$ b_{j,n+1} = \frac{h^{\alpha}}{\alpha} \left((n+1-j)^{\alpha} - (n-j)^{\alpha}\right) \tag{9}$$

The error of this approximation is described as follows

$$ \max_{j=0,1,\cdots,N} |y(t_j) - y_h(t_j)| = O(h^p) $$

where $p = \min(2, 1+\alpha)$.

In this paper, the operator D^{α} is generally called the "Caputo differential operator of order α".

Remark 1. In this paper, let us define $\|f(t)\| = \sqrt{f_1(t)^2 + f_2(t)^2 + \cdots + f_n(t)^2}$, and $\|f(t)\|_1 = |f_1(t)| + |f_2(t)| + \cdots + |f_n(t)|$, where $f(t) = (f_1(t), f_2(t), \cdots, f_n(t))^{\mathrm{T}}$ is a vector of continuous functions.

Property 1. For the Caputo derivative, we have[1,39]

$$ {}_{t_0}^{C}D_t^{1-\alpha}\left({}_{t_0}^{C}D_t^{\alpha} f(t)\right) = {}_{t_0}^{C} D_t^{1} = \dot{f}(t) \tag{10}$$

Property 2. For the Caputo derivative, the following equality holds[1,39]

$$ {}_{t_0}^{C}D_t^{\alpha_1}\left({}_{t_0}^{C}D_t^{-\alpha_2} f(t)\right) = {}_{t_0}^{C} D_t^{\alpha_1-\alpha_2} f(t) \tag{11}$$

where $\alpha_1 \ge \alpha_2 \ge 0$.

Property 3. For the Caputo derivative, if $f(t) \in C^1[0, T]$ for some $T > 0$, then we have[39]

$$ \begin{aligned} &{}_{t_0}^{C}D_t^{\alpha_1}\,{}_{t_0}^{C}D_t^{\alpha_2} f(t) = {}_{t_0}^{C} D_t^{\alpha_2}\,{}_{t_0}^{C}D_t^{\alpha_1} f(t) = {}_{t_0}^{C} D_t^{\alpha_1+\alpha_2} f(t), \\ &t \in [0, T] \end{aligned} \tag{12}$$

where $\alpha_1,\ \alpha_2 \in R^{+}$ and $\alpha_1 + \alpha_2 \le 1$.

III. FO Chaotic System Description

Consider a general form of nonlinear master and slave systems as follows. The master system is

$$ D^{\alpha} X = f(X) + \Delta f(X) + d(X) \tag{13}$$

where $\alpha \in (0, 1]$ is the FO operator, $X \in R^n$ is the state vector of the master system, $f(X) \in R^n$ is the continuous nonlinear vector functions of the master system, $\Delta f(X) \in R^n$ and $d(X) \in R^n$ are the system uncertainties and external disturbances of the master system, respectively. And the slave system is

$$ D^{\alpha} Y = g(Y) + \Delta g(Y) + d(Y) + u(t) \tag{14}$$

where $Y \in R^n$ is the state vector of the slave system, $g(Y) \in R^n$ is the continuous nonlinear vector functions of the slave system, $\Delta g(Y) \in R^n$ and $d(Y) \in R^n$ are the system uncertainties and external disturbances of the slave system, respectively. Also, $u(t) \in R^n$ is the vector of control inputs.

The tracking error can be defined as

$$ e(t) = Y(t) - X(t) \tag{15}$$

By subtracting (13) from (14), the error dynamics are obtained as

$$D^{\alpha}e(t) = (g(Y) + \Delta g(Y) + d(Y)) - (f(X) + \Delta f(X) + d(X)) + u(t)$$

Then one can conclude that

$$D^{\alpha}e_i(t) = (g_i(Y) + \Delta g_i(Y) + d_i(Y)) - (f_i(X) + \Delta f_i(X) + d_i(X)) + u_i(t), \quad i = 1, 2, \cdots, n \tag{16}$$

Chaos synchronization problem can be defined as follows; Design an appropriate robust sliding mode controller for the slave system (14) whose its state trajectories track the state trajectories of the master system (13) in finite-time.

In this paper it will be proved that for any defined master system (13) and slave system (14) with system uncertainties and external disturbances, a suitable control input $u(t)$ is derived such that the finite-time stability of the resulting error dynamics by (16) can be obtained in the sense of

$$\lim_{t\to T} \|e(t)\| = 0, \ \|e(t)\| = 0 \text{ for } t > T \tag{17}$$

Assumption 1. It is assumed that the system uncertainties $\Delta f(X)$, $\Delta g(Y)$ and external disturbances $d(X)$, $d(Y)$ are bounded by

$$\begin{array}{ll} \|\Delta f(X)\|_1 \le \tau_1, & \|\Delta g(Y)\|_1 \le \tau_2, \\ \|d(X)\|_1 \le \varphi_1, & \|d(Y)\|_1 \le \varphi_2, \end{array} \tag{18}$$

Then one can conclude that

$$\|\Delta g(Y) - \Delta f(X)\|_1 < \gamma, \ \|d(Y) - d(X)\|_1 < \delta$$

Therefore we have

$$\begin{array}{l} |(\Delta g_i(Y) - \Delta f_i(X))| < \gamma_i, \ i = 1, 2, \cdots, n \\ |(d_i(Y) - d_i(X))| < \delta_i, \ i = 1, 2, \cdots, n \end{array} \tag{19}$$

where τ_1, τ_2, φ_1, φ_2, γ and δ are positive constants; then, γ_i, $i = 1, 2, \cdots, n$ and δ_i, $i = 1, 2, \cdots, n$ are positive constants. Also $|\cdot|$ is absolute value.

IV. Robust Adaptive Sliding Mode Control

A. Design of FO Sliding Surface

Design of a sliding mode control law may be divided into two phases: First, choosing an adequate FO sliding surface to achieve the control objective. Second, designing a discontinuous control law which forces the system trajectories to reach the sliding surface in a finite-time. We used the following FO sliding surface

$$\sigma_i(t) = a_i D^{\alpha-1}(e_i(t)), \ i = 1, 2, \cdots, n \tag{20}$$

where a_i is a positive constant. Then we have

$$D^{\alpha}\sigma_i(t) = a_i D^{2\alpha-1}(e_i(t)) \tag{21}$$

When the FO system (16) operates in the sliding mode, the derivative of the sliding surface must satisfy $\dot{\sigma}_i(t) = 0$[40].

This step concerns the design of control scheme for steering the system (16) in finite-time onto the sliding surface (20). The task is not trivial due to, both, the presence of the unknown disturbance and the FO nature of the system dynamics[41]. Taking the integer-order derivative of (20) yields

$$\dot{\sigma}_i(t) = a_i D^{\alpha}(e_i(t)), \ i = 1, 2, \cdots, n \tag{22}$$

By substituting (16) into (22), we have

$$\dot{\sigma}_i(t) = a_i\Big((g_i(Y) + \Delta g_i(Y) + d_i(Y)) - (f_i(X) + \Delta f_i(X) + d_i(X)) + u_i(t)\Big), \quad i = 1, 2, \cdots, n \tag{23}$$

The finite-time stability of system (23) with the control law (25) is proven by Lyapunov analysis in Theorem 1.

B. Design of Robust Control Scheme

After establishing a suitable fractional sliding surface (20), the sliding mode controller is designed in a way so that the system trajectories drive onto the sliding mode $\sigma_i(t) = 0$, in finite-time.

Using (23) and $\dot{\sigma}_i(t) = 0$, the equivalent control law can be derived as follows

$$u_{eq_i}(t) = (f_i(X) - g_i(Y))$$

In order to improve the robustness against uncertainties, we design the reaching control law, which drives the system trajectories onto the sliding surface $\sigma_i(t) = 0$.

$$u_{r_i}(t) = -\Big(k_i\sigma_i(t) + (\omega_i + \gamma_i + \delta_i)\mathrm{sgn}(\sigma_i(t))\Big) \tag{24}$$

where

$$\mathrm{sgn}(\sigma_i(t)) = \begin{cases} +1, & \sigma_i(t) > 0 \\ 0, & \sigma_i(t) = 0 \\ -1, & \sigma_i(t) < 0 \end{cases}$$

k_i, ω_i are positive switching gains.

Finally, the control input law can be obtained as follows

$$u_i(t) = (f_i(X) - g_i(Y)) - \Big(k_i\sigma_i(t) + (\omega_i + \gamma_i + \delta_i)\mathrm{sgn}(\sigma_i(t))\Big) \tag{25}$$

C. Stability Analysis

In this section, Lyapunov theorem is used to analyze the stability of the system. The basic philosophy of Lyapunovs direct method is the mathematical extension of a principal physical observation: If all of the energy of a mechanical (or electrical) system is continuously reduced, then the system, that may be linear or nonlinear, must move to an equilibrium point at last. Thus, the stability of a system by examining the variation of a single Lyapunov function can be analyzed[42].

Theorem 1. If the uncertain FO system (16) is controlled by the control input (25), then the system trajectories will converge to the sliding surface $\sigma_i(t) = 0$ in a finite-time t_i.

Proof. Selecting a positive Lyapunov function candidate $v_i(t) = \frac{1}{2}\sigma_i^2(t)$ and taking its time derivative, results

$$\dot{v}_i(t) = \sigma_i(t)\Big(a_i D^{\alpha}(e_i(t))\Big) \tag{26}$$

Inserting (16) in (26), results

$$\dot{v}_i(t) = a_i\sigma_i(t)\Big((g_i(Y) + \Delta g_i(Y) + d_i(Y))$$

$$-\left(f_i(X)+\Delta f_i(X)+d_i(X)\right)+u_i(t)\Big) \tag{27}$$

By substituting (25) into (27) and using Assumption 1, then

$$\begin{aligned}\dot{v}_i(t) \leq & a_i\sigma_i(t)(|\Delta g_i(Y)-\Delta f_i(X)|+|d_i(Y)-d_i(X)|) \\ & -a_i\sigma_i(t)\Big(k_i\sigma_i(t)+(\omega_i+\gamma_i+\delta_i)\text{sgn}(\sigma_i(t))\Big)\end{aligned} \tag{28}$$

Hence the above inequality can be written as

$$\dot{v}_i(t) \leq -(2a_ik_iv_i(t)+\sqrt{2}a_i\omega_iv_i(t)^{0.5}) \tag{29}$$

Multiplying both sides of (29) by $v_i(t)^{-0.5}$, results

$$v_i(t)^{-0.5}\dot{v}_i(t)+2a_ik_iv_i(t)^{0.5} \leq -\sqrt{2}a_i\omega_i \tag{30}$$

Multiplying (30) by $(1/2)e^{a_ik_it}$ and then integrating at both sides from zero to t, one obtains

$$\begin{aligned}v_i(t)^{0.5} \leq & \Big((\sqrt{2}/2)(\omega_i/k_i)+v_i(0)^{0.5}\Big)e^{-a_ik_it} \\ & -(\sqrt{2}/2)(w_i/k_i)\end{aligned} \tag{31}$$

then one can get

$$t \leq (1/a_ik_i)\ln\left(1+\sqrt{2}(k_i/\omega_i)v_i(0)^{0.5}\right) \tag{32}$$

Hence, the proof is achieved. i.e., according to the inequality (31), the state trajectories of the error system (16) will converge to $\sigma_i(t)=0$ in a finite-time

$$t_i=(1/a_ik_i)\ln\left(1+(k_i/\omega_i)|\sigma_i(0)|\right)$$

D. Adaptation Law Synthesis

In the previous sections, it has been shown knowing the bounds of system uncertainties and external disturbances is vital to guarantee the system stability. However, in practice it is not convenient to determine these bounds precisely. In what follows, we develop an adaptation laws to overcome this problem. In order to estimate the unknown controller parameters, appropriate update laws are derived as follow:

$$\dot{\widehat{k}}_i=\mu_i\sigma_i(t)^2, \dot{\widehat{\omega}}_i=\rho_i|\sigma_i(t)|, \dot{\widehat{\gamma}}_i=\kappa_i|\sigma_i(t)|, \dot{\widehat{\delta}}_i=\xi_i|\sigma_i(t)| \tag{33}$$

Theorem 2. If the chaotic system of this paper is controlled by the discontinuous control law (25) with the adaptation laws (33), then the system trajectories will converge to the sliding surface $\sigma_i(t)=0$.

Proof. Consider the Lyapunov function candidate as

$$\begin{aligned}v_i(t)= & \frac{1}{2}\sigma_i(t)^2+\frac{1}{2}\Big(\mu_i^{-1}\widetilde{k}_i^2+\rho_i^{-1}\widetilde{\omega}_i^2 \\ & +\kappa_i^{-1}\widetilde{\gamma}_i^2+\xi_i^{-1}\widetilde{\delta}_i^2\Big),\ i=1,2,\cdots,n\end{aligned} \tag{34}$$

where $\widetilde{k}_i=k_i-\widehat{k}_i$, $\widetilde{\omega}_i=\omega_i-\widehat{\omega}_i$, $\widetilde{\gamma}_i=\gamma_i-\widehat{\gamma}_i$, and $\widetilde{\delta}_i=\delta_i-\widehat{\delta}_i$. In this case, k_i, ω_i, γ_i, and δ_i are the actual values of $\widehat{k}_i$, $\widehat{\omega}_i$, $\widehat{\gamma}_i$, and $\widehat{\delta}_i$, respectively. Also μ_i, ρ_i, κ_i and ξ_i are rates of adaptation. Taking derivative of both sides of (34) with respect to time, yields

$$\begin{aligned}\dot{v}_i(t)= & \sigma_i(t)\dot{\sigma}_i(t)-\mu_i^{-1}\widetilde{k}_i(\dot{\widehat{k}}_i)-\rho_i^{-1}\widetilde{\omega}_i(\dot{\widehat{\omega}}_i) \\ & -\kappa_i^{-1}\widetilde{\gamma}_i(\dot{\widehat{\gamma}}_i)-\xi_i^{-1}\widetilde{\delta}_i(\dot{\widehat{\delta}}_i)\end{aligned} \tag{35}$$

Using Property 1 and then inserting (21) in (35), one obtains

$$\begin{aligned}\dot{v}_i(t)= & \sigma_i(t)D^{1-\alpha}\Big(a_iD^{2\alpha-1}(e_i(t))\Big)-\mu_i^{-1}\widetilde{k}_i(\dot{\widehat{k}}_i) \\ & -\rho_i^{-1}\widetilde{\omega}_i(\dot{\widehat{\omega}}_i)-\kappa_i^{-1}\widetilde{\gamma}_i(\dot{\widehat{\gamma}}_i)-\xi_i^{-1}\widetilde{\delta}_i(\dot{\widehat{\delta}}_i)\end{aligned} \tag{36}$$

Using Properties 2 and 3, one gets

$$\begin{aligned}\dot{v}_i(t)= & a_i\sigma_i(t)D^{\alpha}(e_i(t))-\mu_i^{-1}\widetilde{k}_i(\dot{\widehat{k}}_i) \\ & -\rho_i^{-1}\widetilde{\omega}_i(\dot{\widehat{\omega}}_i)-\kappa_i^{-1}\widetilde{\gamma}_i(\dot{\widehat{\gamma}}_i)-\xi_i^{-1}\widetilde{\delta}_i(\dot{\widehat{\delta}}_i)\end{aligned} \tag{37}$$

Substituting (16) into (37) and using Assumption 1, we have

$$\begin{aligned}&\dot{v}_i(t) \leq (\gamma_i+\delta_i)|\sigma_i(t)|+\sigma_i(t)(g_i(Y)-f_i(X)+u_i(t)) \\ &-\mu_i^{-1}\widetilde{k}_i(\dot{\widehat{k}}_i)-\rho_i^{-1}\widetilde{\omega}_i(\dot{\widehat{\omega}}_i)-\kappa_i^{-1}\widetilde{\gamma}_i(\dot{\widehat{\gamma}}_i)-\xi_i^{-1}\widetilde{\delta}_i(\dot{\widehat{\delta}}_i)\end{aligned} \tag{38}$$

By assuming that the parameters of the controller (25) are unknown, then

$$\begin{aligned}&\dot{v}_i(t) \leq -\widehat{k}_i|\sigma_i(t)|^2-\widehat{\omega}_i|\sigma_i(t)|+(\widetilde{\gamma}_i+\widetilde{\delta}_i)|\sigma_i(t)| \\ &-\mu_i^{-1}\widetilde{k}_i(\dot{\widehat{k}}_i)-\rho_i^{-1}\widetilde{\omega}_i(\dot{\widehat{\omega}}_i)-\kappa_i^{-1}\widetilde{\gamma}_i(\dot{\widehat{\gamma}}_i)-\xi_i^{-1}\widetilde{\delta}_i(\dot{\widehat{\delta}}_i)\end{aligned} \tag{39}$$

Introducing the adaptation laws (33) in (39), will lead to

$$\dot{v}_i(t) \leq -k_i|\sigma_i(t)|^2-\omega_i|\sigma_i(t)| \tag{40}$$

Hence, the motion on the sliding surface is asymptotically stable. Therefore, the output can track the desired reference.

E. Particle Swarm Optimization (PSO)

In this section, the parameters of the ASMC are estimated using PSO algorithm. There are a lot of optimal techniques for optimization. One of the simple approaches for optimization is PSO. PSO was introduced by Kennedy and Eberhart[43], and is useful for continuous space. PSO algorithm imitates the behavior of birds and others like fishes for searching the best solution in the space. PSO has been found to be robust in solving problems featuring nonlinearity, multiple optima, and high dimensionality through adaptation, which is derived from the social-psychological theory. In this technique, every particle can be illustrated by two vectors[44]. These vectors are position vector and velocity vector that can be updated with this algorithm to get the best parameters of the controller. The PSO algorithm, at each time step, changes the speed of each particle moving towards its *pBest* and *gBest* locations. Speed is weighted by random terms, with separate random numbers being generated for acceleration toward *pBest* and *gBest* locations, respectively.

Our aim is to have low tracking error; hence the following cost function (Mean Squared Error) is used

$$MSE=\frac{1}{N}\sum_{i=0}^{N}\Big(e_k(i)\Big)^2 \tag{41}$$

where, $e_k(i)$ is the kth error state variable. N is the length of every error state variable.

The procedure for implementing PSO algorithm for estimating the controller parameters is given by the following steps:

i Initialize a (population) of particles with random positions and velocities in the n-dimensional problem space using a uniform probability distribution function;

ii For each particle in swarm, evaluate its fitness value;

iii Compare each particles fitness evaluation with the current particles *pBest*. If current value is better than *pBest*, set its *pBest* value to the current value and the *pBest* location to the current location in n-dimensional space;

iv Compare the fitness evaluation with the populations overall previous best. If current value is better than *gBest*, then reset *gBest* to the current particles array index and value;

v During this process, the position vector and velocity vector of each particle are updated to tend the best position as follows:

$$\begin{aligned} V_i(t+1) =& wV_i(t) + c_1\mathrm{rand}(0,1)(pBest_i(t) - X_i(t)) \\ &+ c_2\mathrm{rand}(0,1)(gBest_i(t) - X_i(t)) \\ X_i(t+1) =& X_i(t) + V_i(t+1) \end{aligned} \tag{42}$$

where $i = 1, 2, \cdots, n$ is the particles index, t is the time (iteration or generation).

In this case, the position and speed vectors are with dimensions d. c_1 and c_2 are acceleration coefficients, w is the inertia weight. In (42), $pBest_i$ is the position with the best fitness found by the ith particle, and $gBest_i$ is the best fitness position in neighborhood.

V. Applications and Numerical Experiments

In this section, an illustrative example is presented to show the feasibility and applicability of the proposed nonsingular sliding mode approach and to confirm the theoretical results. In this example, numerical simulation for two non-identical FO chaotic and FO hyper-chaotic systems is presented. Fourth-order Runge-Kutta method is used with a step time of 0.001 in order to solve the FO differentials.

A. Synchronization of Non-Identical FO Chaotic and FO Hyper-chaotic Systems

In this section, numerical simulations are presented to validate the robustness and effectiveness of the proposed ASMC, when the controller parameters are estimated by PSO algorithm. These values are obtained in order to minimize the synchronization errors. The FO chaotic system[45] as master system drives the FO hyper-chaotic system[46] as slave system.

The master system is

$$\underbrace{\begin{bmatrix} D^\alpha x_1 \\ D^\alpha x_2 \\ D^\alpha x_3 \\ D^\alpha x_4 \end{bmatrix}}_{D^\alpha X} = \underbrace{\begin{bmatrix} 5(x_2 - x_1) + x_4 \\ -x_1x_3 \\ -90 + x_1x_2 \\ -10x_1 \end{bmatrix}}_{f(X)} + \underbrace{\begin{bmatrix} 0.2\cos(x_2) \\ 0.3\cos(x_1) \\ 0.25\sin(x_4) \\ 0.35\sin(x_3) \end{bmatrix}}_{\Delta f(X)} + \underbrace{\begin{bmatrix} 0.3\cos(t) \\ 0.25\sin(t) \\ 0.3\cos(t) \\ 0.2\cos(t) \end{bmatrix}}_{d(X)} \tag{43}$$

and the slave system is

$$\underbrace{\begin{bmatrix} D^\alpha y_1 \\ D^\alpha y_2 \\ D^\alpha y_3 \\ D^\alpha y_4 \end{bmatrix}}_{D^\alpha Y} = \underbrace{\begin{bmatrix} 10(y_2 - y_1) \\ 40y_1 + y_1y_3 + 2y_4 \\ -2y_1^2 - 2y_2^2 - 2.5y_3 \\ -5y_2 \end{bmatrix}}_{g(Y)} + \underbrace{\begin{bmatrix} 0.3\sin(y_2) \\ 0.25\cos(y_3) \\ 0.25\cos(y_1) \\ 0.2\sin(y_2) \end{bmatrix}}_{\Delta g(X)} + \underbrace{\begin{bmatrix} 0.25\cos(t) \\ 0.3\sin(t) \\ 0.3\sin(t) \\ 0.3\cos(t) \end{bmatrix}}_{d(Y)} + \underbrace{\begin{bmatrix} u_1(t) \\ u_2(t) \\ u_3(t) \\ u_4(t) \end{bmatrix}}_{u(t)} \tag{44}$$

The FO operator (α) is set to 0.95 to ensure the existence of chaos for the system. Assume, the initial states of the master and slave systems are selected as $(x_1(0), x_2(0), x_3(0), x_4(0))^{\mathrm{T}} = (2.5, 0.5, 1, 0.5)^{\mathrm{T}}$ and $(y_1(0), y_2(0), y_3(0), y_4(0))^{\mathrm{T}} = (4, 2.5, 3.5, 3)^{\mathrm{T}}$, respectively. μ_i, ρ_i, κ_i and ξ_i are rates of adaptation which are supposed to be 5, 3, 5 and 2 for $(i = 1, \cdots, 4)$, respectively. The control input suffers high chattering. In order to reduce this drawback of the controller we have used the saturation function instead of the sign function. The time responses of the synchronized states are depicted in Fig. 1. Fig. 2 shows the synchronization errors between two FO chaotic and hyper-chaotic systems. The time response of $\widehat{k}_i$ and $\widehat{\omega}_i$ for $(i = 1, \cdots, 4)$ are depicted in Fig. 3. Besides, the time response of $\widehat{\gamma}_i$ and $\widehat{\delta}_i$ for $(i = 1, \cdots, 4)$ are depicted in Fig. 4. In Table. 1, the controller parameters are depicted before optimization and after that.

PSO parameters are set as follow:

Population size$= 20$, *Iterations*$= 40$, $c_1 = 2.0$, $c_2 = 2.0$, *weighting factor*$= 1$, *Inertia weight*$= 0.999$.

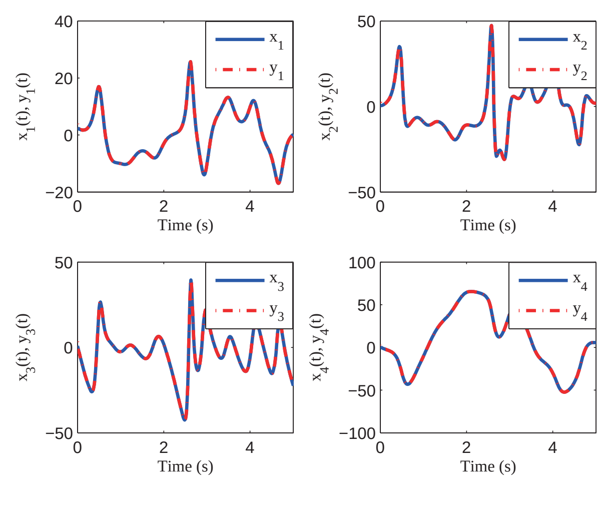

Fig. 1. Time response of signals for master system and slave system.

VI. A Secure Communication Scheme

A secure communication system involves the development of a signal that contains the information which is to remain undetectable by others within a carrier signal. In this section, a popular application of chaotic synchronization in the area

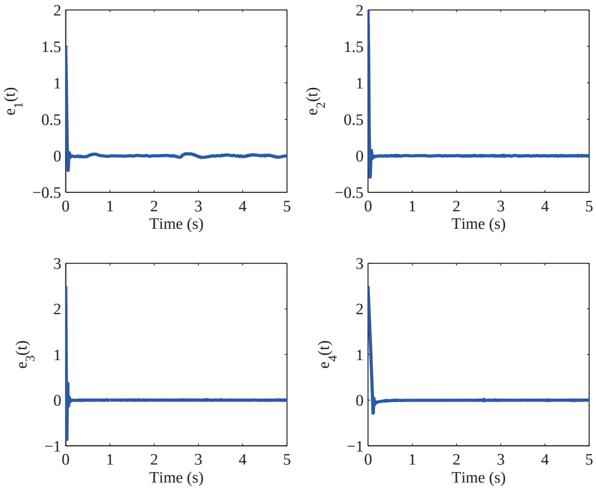

Fig. 2. Time response of the synchronization errors between two non-identical FO chaotic and hyper-chaotic systems.

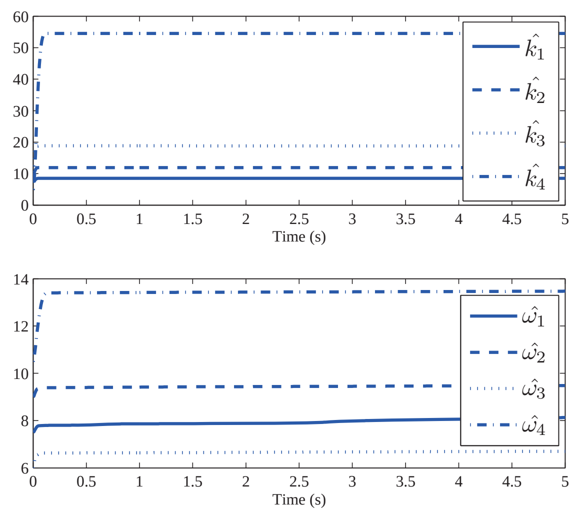

Fig. 3. Time response of the controller parameters.

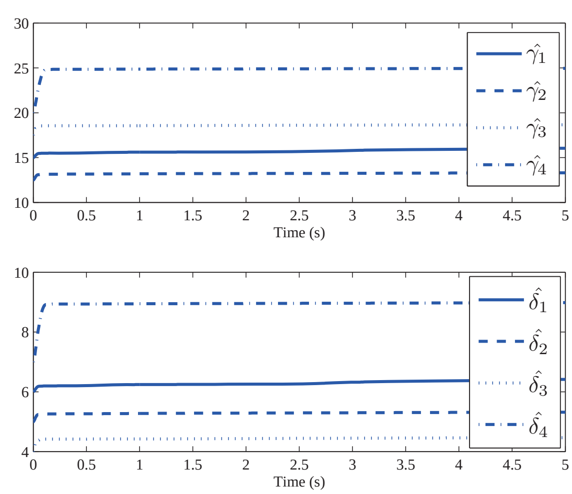

Fig. 4. Time response of the controller parameters.

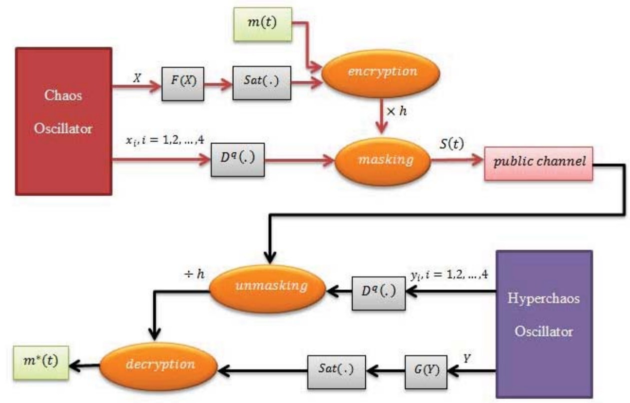

Fig. 5. The secure communication scheme based on the synchronization of FO chaotic and hyper-chaotic systems.

TABLE I
CONTROLLER PARAMETERS BEFORE AND AFTER OPTIMIZATION AND THE COST FUNCTION VALUES

	a_1	a_2	a_3	a_4	Cost
Before optimization	5.0000	6.0000	3.5000	7.5000	8.8959
After optimization	3.5728	4.0087	9.7267	8.1469	7.7656

of secure communications is presented. The useful signal has been modulated two times to improve the security of the system, encrypted by secret key firstly and masked secondly by the FO derivative of chaos variable. Fig. 5 depicts a sketch designed for our communication scheme.

In the transmitter, two chaotic variables of the chaos oscillator are employed to construct a function $F(X)$ which is used to generate secret key $k(t)$. The secret key $k(t)$ is added to the proposed useful signal $m(t)$ in order to encrypt the useful signal. The encrypted useful signal is masked by the FO derivative of chaos variable x_i. Then, the encrypted and masked useful signal is transmitted to the receiver through public channel. In the receiver, first the received signal is unmasked by the FO derivative of hyperchaos variable y_i. Then, the unmasked signal is decrypted by the secret key $k^*(t)$. It is impossible to extract the useful signal $m(t)$ from the transmitted signal $S(t)$ without the dynamics of X. Therefore, when the control signal (25) is designed in the receiver, then the synchronization between chaos oscillator and hyper-chaos oscillator will be obtained and X will converge to Y in finite-time.

The simulation results above are based on discrete useful signal. In the transmitter, the nonlinear function $F(X) = (x_2x_4)^2$ is transmitted through the saturation function to generate the secret key. The FO of the chaos state variable x_3 is used to mask the encrypted message. Demodulation process is inverse operation to modulation. So $G(Y) = (y_2y_4)^2$ and the FO of hyper-chaos variable y_3 is used to unmask the received signal. The notation $D^q(\cdot)$ denotes the FO derivative, where the FO is selected as $q = 0.5$. Also, h is a small constant which is supposed to be 3. By using a small constant h, the security of the transmitted signal in a public channel can be increased.

The useful signal $m(t)$ is shown in Fig. 6-a; chaotic signal

$S(t)$ which is transmitted to the receiver is illustrated in Fig. 6-b; the comparison between demodulated useful signal $m^*(t)$ and sent useful signal $m(t)$ is shown in Fig. 6-c. As a result of the simulation, demodulated signal and useful signal can quickly implement synchronization as a short transient. The error between the demodulated signal and the useful signal is depicted in Fig. 6-d.

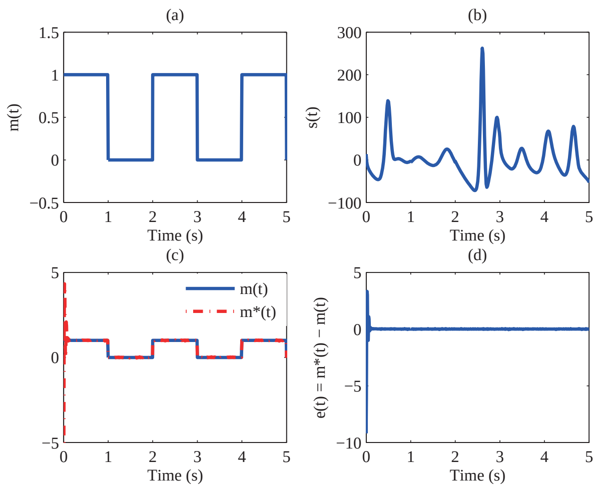

Fig. 6. Simulation results of the proposed secure communication scheme using finite-time synchronization of FO chaotic and hyper-chaotic systems.

VII. Conclusion

In this paper, the proposed novel sliding mode controller is shown to be robust against high uncertainties and variation of the parameters. Suitable adaptive laws are proposed to tackle the unknown parameters and PSO algorithm is used in this paper for optimization of the controller parameters. Finally, the proposed scheme is applied in secure communication. The simulation results show that the synchronization time is very short and the recovered signal is close to the useful signal and it can realize secret communication successfully, having strong security and practicability.

References

[1] Podlubny I. *Fractional differential equations*. Academic Press, New York, 1999

[2] Uchaikin V. *Fractional derivatives for physicists and engineers*. Nonlinear physical science. Springer, Berlin, 2013

[3] Baleanu D, Machado J A T, Luo A C J. *Fractional dynamics and control*. Springer, New York, 2012

[4] Hilfer R. *Applications of fractional calculus in physics*. World Scientific, Singapore, 2000

[5] Wilkie K P, Drapaca C S, Sivaloganathan S. A nonlinear viscoelastic fractional derivative model of infant hydrocephalus. *Applied Mathematics and Computation*, 2011, **217**(21): 8693-8704

[6] Tusset A M, Balthazar J M, Bassinello D G, Pontes Jr. B R, Palacios Felix J L. Statements on chaos control designs, including a fractional-order dynamical system, applied to a MEMS comb-drive actuator. *Nonlinear Dynamics*, 2012, **69**(4): 1837-1857

[7] Yang Q, Zeng C. Chaos in fractional conjugate Lorenz system and its scaling attractors. *Communications in Nonlinear Science and Numerical Simulation*, 2010, **15**(12): 4041-4051

[8] Lu J G, Chen G. A note on the fractional-order Chen system. *Chaos, Solitons & Fractals*, 2006, **27**(3): 685-688

[9] Delavari H, Senejohnny D M, Baleanu D. Sliding observer for synchronization of fractional-order chaotic systems with mismatched parameter. *Central European Journal of Physics*, 2012, **10**(5): 1095-1101

[10] Pecora L M, Carroll T L. Synchronization in chaotic systems. *Physical Review Letters*, 1990, **64**(8): 821-824

[11] Aghababa M P, Aghababa H P. A general nonlinear adaptive control scheme for finite-time synchronization of chaotic systems with uncertain parameters and nonlinear inputs. *Nonlinear Dynamics*, 2012, **69**(4): 1903-1914

[12] Faieghi M R, Delavari H, Baleanu D. A note on stability of sliding mode dynamics in suppression of fractional-order chaotic systems. *Computers and Mathematics with Applications*, 2013, **66**(5): 832-837

[13] Zhang L F, An X L, Zhang J G. A new chaos synchronization scheme and its application to secure communications. *Nonlinear Dynamics*, 2013, **73**(1): 705-722

[14] Dasgupta T, Paralt P, Bhattacharya S. Fractional order sliding mode control based chaos synchronization and secure communication. *Int. Conference on Computer Communication and Informatics*, 2015, pp. 8-10

[15] Sheikhan M, Shahnazi R, Garoucy S. Synchronization of general chaotic systems using neural controllers with application to secure communication. *Neural Computing and Applications*, 2013, **22**(2): 361-373

[16] Faieghi M R, Delavari H, Baleanu D. A note on stability of sliding mode dynamics in suppression of fractional-order chaotic systems. *Computers & Mathematics with Applications*, 2013, **66**(5): 832-837

[17] Wu X J, Wang H, Lu H. Modified generalized projective synchronization of a new fractional-order hyper-chaotic system and its application to secure communication. *Nonlinear Analysis: Real World Applications*, 2012, **13**(3): 1441-1450

[18] Ma T, Guo D, Xi Q. Adaptive synchronization for a class of uncertain fractional order chaotic systems with random perturbations: Theory and experiment. *Control and Decision Conference (CCDC), 27th Chinese*, 2015, pp. 1309-1314

[19] Mohadeszadeh M, Delavari H. Synchronization of fractional-order hyper-chaotic systems based on a new adaptive sliding mode control. *International Journal of Dynamics and Control*, 2015, doi: 10.1007/s40435-015-0177Cy

[20] Faieghi M R, Delavari H, Baleanu D. Control of an uncertain fractional-order Liu system via fuzzy fractional-order sliding mode control. *Journal of Vibration and Control*, 2012, **18**(9): 1366-1374

[21] Liao X. Active disturbance rejection control for synchronization of different fractional-order chaotic systems. *Intelligent Control and Automation (WCICA), 2014 11th World Congress on*, 2014, pp. 2699-2704

[22] Zhang F, Chen G, Li C, Kurths J. Chaos synchronization in fractional differential systems. *Philosophical Transactions of the Royal Society A*, 371, 2013.

[23] Aghababa M P. Robust finite-time stabilization of fractional-order chaotic systems based on fractional Lyapunov stability theory. *Journal of Computational and Nonlinear Dynamics*, 2012, **7**: p.021010

[24] Tavazoei, M S, Haeri, M. Synchronization of chaotic fractional-order systems via active sliding mode controller. *Physica A*, 2008, **387**(1): 57-70

[25] Matouk A E, Elsadany A A. Achieving synchronization between the fractional-order hyper-chaotic Novel and Chen systems via a new nonlinear control technique. *Applied Mathematics Letters*, 2014, **29**(1): 30-35

[26] Vincent U E, Guo R. Finite-time synchronization for a class of chaotic and hyper-chaotic systems via adaptive feedback controller. *Physics Letters A*, 2011, **375**(24): 2322-2326

[27] Xi H, Yu S, Zhang R, Xu L. Adaptive impulsive synchronization for a class of fractional-order chaotic and hyper-chaotic systems. *International Journal for Light and Electron Optics*, 2014, **125**(9): 2036-2040

[28] Yan J J, Hung M L, Chiang T Y, Yang Y S. Robust synchronization of chaotic systems via adaptive sliding mode control. *Physics Letters A*, 2006, **356**(3): 220-225

[29] Mohadeszadeh M, Delavari H. Synchronization of uncertain fractional-order hyper chaotic systems via a novel adaptive interval type-2 fuzzy active sliding mode controller. *International Journal of Dynamics and Control*, 2015, doi: 10.1007/s40435C015C0207C9

[30] Das S, Srivastava M, Leung A Y T. Hybrid phase synchronization between identical and non-identical three-dimensional chaotic systems using the active control method. *Nonlinear Dynamics*, 2013, **73**(4): 2261-2272

[31] Runzi L, Yinglan W, Shucheng D. Combination synchronization of three classic chaotic systems using active backstepping design. *Chaos*, 2011, doi: 10.1063/1.3655366

[32] Hung M L, Lin J S, Yan J J, Liao T L. Optimal PID control design for synchronization of delayed discrete chaotic systems. *Chaos, Solitons & Fractals*, 2008, **35**(4): 781-785

[33] Behinfaraz R, Badamchizadeh M A. Synchronization of different fractional-ordered chaotic systems using optimized active control. *Modeling, Simulation, and Applied Optimization (ICMSAO), 2015 6th International Conference on*, 2015

[34] Faieghi M R, Kuntanapreeda S, Delavari H, Baleanu D. Robust stabilization of fractional-order chaotic systems with linear controllers: LMICbased sufficient conditions. *Journal of Vibration and Control*, 2014, **20**(7): 1042-1051

[35] Senejohnny D M, Delavari H. Active sliding observer scheme based fractional chaos synchronization. *Communications in Nonlinear Science and Numerical Simulation*, 2012, **17**(11): 4373-4383

[36] N'Doye I, Voos H, Darouach M. Observer-based approach for fractional-order chaotic synchronization and secure communication. *IEEE Journal on Emerging and Selected Topics in Circuits and Systems*, 2013, **3**(3): 442-450

[37] Diethelm K, Ford N J, Freed A D. A predictor-corrector approach for the numerical solution of fractional differential equations. *Nonlinear Dynamics*, 2002, **29**(1): 3-22

[38] Diethelm K, Ford N J, Freed A D. Detailed error analysis for a fractional Adams method. *Numerical Algorithms*, 2004, **36**(1): 31-52

[39] Li C, Deng W. Remarks on fractional derivatives. *Applied Mathematics and Computation*, 2007, **187**(2): 777-784

[40] Utkin V I. *Sliding modes in control optimization*. Springer Verlag, 1992, pp. 66-73

[41] Pisano A, Rade Rapaić M, D. Jeličić Z, Usai E. Sliding mode control approaches to the robust regulation of linear multivariable fractional-order dynamics. *International Journal of Robust and Nonlinear Control*, 2010, **20**(18): 2045-2056

[42] Slotine J J E, Li W. *Applied nonlinear control*. Prentice Hall, USA, 1991

[43] Kennedy J, Eberhart R. Particle swarm optimization. *Proceedings of the Fourth IEEE International Conference on Neural Networks*, 4: 1942, pp. 1948-1995

[44] Eberhart R, Kennedy J. A new optimizer using particle swarm theory. In: *IEEE 6th international symposium on micro machine and human science*, 1995, pp. 39-43

[45] Li H, Liao X, Luo M. A novel non-equilibrium fractional-order chaotic system and its complete synchronization by circuit implementation. *Nonlinear Dynamics*, 2012, **68**(1): 137-149

[46] Zhu D, Liu L, Liu C, Pang X, Yan B. Adaptive projective synchronization of a novel fractional-order hyper-chaotic system. *Proceedings of the 2014 9th IEEE Conference on Industrial Electronics and Applications*, 2014, pp. 814-818

Hadi Delavari received the Ph.D. degree, M. Sc. degree and B.Sc. degree in control engineering in 2011, 2006 and 2004, respectively. Since 2008, he has been with the Department of Electrical Engineering, Hamedan University of Technology. His research interests include nonlinear control theory and applications, fractional order control, chaos control, robotic and etc.

Milad Mohadeszadeh graduated from Islamic Azad University of Mashhad (IAUM), Iran, in 2012. He received the M. Sc. degree from Hamedan University of Technology (HUT), Iran, in 2015. His research interests include control and synchronization of fractional-order chaotic systems, stability criterions of fractional-order systems and chaotic secure communication.

An Implementation of Haar Wavelet Based Method for Numerical Treatment of Time-fractional Schrödinger and Coupled Schrödinger Systems

Najeeb Alam Khan, Tooba Hameed

***Abstract*—The objective of this paper is to solve the time-fractional Schrödinger and coupled Schrödinger differential equations (TFSE) with appropriate initial conditions by using the Haar wavelet approximation. For the most part, this endeavor is made to enlarge the pertinence of the Haar wavelet method to solve a coupled system of time-fractional partial differential equations. As a general rule, piecewise constant approximation of a function at different resolutions is presentational characteristic of Haar wavelet method through which it converts the differential equation into the Sylvester equation that can be further simplified easily. Study of the (TFSE) is theoretical and experimental research and it also helps in the development of automation science, physics, and engineering as well. Illustratively, several test problems are discussed to draw an effective conclusion, supported by the graphical and tabulated results of included examples, to reveal the proficiency and adaptability of the method.**

***Index Terms*—Fractional calculus, haar wavelets, operational matrix, wavelets.**

I. INTRODUCTION

IN recent decades, fractional calculus (calculus of integrals and derivatives of any arbitrary real order) has attained appreciable fame and importance due to its manifest uses in apparently diverse and outspread fields of science. Certainly, it provides potentially helpful tools for solving integral and differential equations and many other problems of mathematical physics. The fractional differential equations have become crucial research field essentially due to their immense range of utilization in engineering, fluid mechanics, physics, chemistry, biology, viscoelasticity etc. Numerous mathematicians and physicists have been studying the properties of fractional calculus [1], [2] and have established several methods for accurate analytical and numerical solutions of fractional differential equations, such as the variational iteration method [3], differential transform method [4], homotopy analysis method [5], Jacobi spectral tau and collocation method [6]−[8], Laplace transform method [9], homotopy perturbation method [10], Adomian decomposition method [8], [9], high-order finite element methods [13] and many others [14], [19]. The scope and distinct aspects of fractional calculus have been written by many authors in Refs [20]−[22].

In the past few years, there has been an extensive attraction in employing the spectral method (see [23]−[25]) for numerically solving the copious type of differential and integral equations. The spectral methods have an exponential quota of convergence and high level of efficiency. Spectral methods are to express the approximate solution of the problem in term of a finite sum of certain basis functions and then selection of coefficients in order to reduce the difference between the exact and approximate solutions as much as possible. The spectral collocation method is a distinct type of spectral methods, that is more relevant and extensively used to solve most of differential equations [26].

For the reason of the distinctive attributes of wavelet theory in representing continuous functions in the form of discontinuous functions [27], its applications as a mathematical tool is widely expanding nowadays. Besides image processing and signal decomposition it is also used to assess many other mathematical problems, such as differential and integral equations. Wavelets comprise the incremental conception between two consecutive levels of resolution, called multi-resolution. The first component of multi-resolution analysis is vector spaces. For each vector space, another vector space of higher resolution is found and this continues until the final image or signal is executed. The basis of each of these vector spaces acts as the scaling function for the wavelets. Each vector space having an orthogonal component and a basis function is said to be the wavelet [28].

Up till now, a number of wavelet families have been presented by different authors, but among all Haar wavelet are considered to be the easiest wavelets family. Haar wavelet was introduced in 1910 by Hungarian mathematician Alfred Haar. These wavelets are obtained from Daubechies wavelets of order 1, which consist of piecewise constant functions on the real axis that can take only three values, -1, 0 and 1. Here we are using collocation method, by increasing the level of resolution, collocation points are also increasing and level of accuracy too. Haar wavelet collocation method is extensively used due to its constructive ability of being smooth, fast, convenient and being computationally attractive [29]. In addition, it has the competency to reduce the computations for solving differential equations by converting them into some system of algebraic equations. The main advantages of

This article has been accepted for publication in a future issue of this journal, but has not been fully edited. Content may change prior to final publication.

This article was recommended by Associate Editor Antonio Visioli.

Najeeb Alam Khan is with the Department of Mathematics, University of Karachi, Karachi-75270, Pakistan. (e-mail: njbalam@yahoo.com; tooba-hameed@hotmail.com).

Digital Object Identifier 10.1109/JAS.2016.7510193

the proposed algorithm are, its simple application and no residual or product operational matrix is required. The method is well addressed in [22], [29]−[32].

The time-fractional Schrödinger equation (T-FSE) differs from the standard Schrödinger equation. The first-order time derivative is replaced by a fractional derivative, it makes the problem overall in time. It describes, how the quantum state (physical situation) of a quantum system changes with time, soliton dispersion, deep water waves, molecular orbital theory and the potential energy of a hydrogen-like atom (fractional 'Bohr atom'). The aim of this work is to explore the numerical solutions of the time-fractional Schrödinger equations by using Haar wavelet method. Due to the large number of applications of the Schrödinger equation in different aspects of quantum mechanics and engineering, many attempts have been exercised on analytical and numerical methods to calculate the approximate solution of (T-FSE). Some of them are studied [6], [10], [18], [33]−[36], and enumerated here for better perception of the presented analysis. Also, the existence and uniqueness of solutions of fractional Schrödinger equation have been proved by multiple authors [35], [37], [38].

II. Preliminaries

In this section, some notations and properties of fractional calculus, the basis of Haar function approximation for partial differential equation and solution of Haar by multi-resolution analysis are given that will help us in exploring the main theme of the paper.

A. Riemann-Liouville Differential and Integral Operator

Assume $\nu > 0$, $m = \lceil \nu \rceil$ and $f(x,t) \in C^m([0,1] \times [0,1])$ then the partial Caputo fractional derivative of $f(x,t)$ with respect to t is defined as

$$\frac{\partial^\nu}{\partial t^\nu} f(x,t) = \begin{cases} I_t^{m-\nu} \frac{\partial^m}{\partial t^m} f(x,t) \\ \frac{\partial^m}{\partial t^m} f(x,t) \end{cases} \tag{1}$$

where I_t^ν is the Riemann-Liouville fractional integral, given as

$$\begin{aligned} I_t^\nu f(t) &= \frac{1}{\Gamma(\nu)} \int_0^t (t-\varphi)^{\nu-1} f(\varphi) d\varphi \\ I_t^0 f(t) &= f(t) \end{aligned} \tag{2}$$

we use the notation D_t^ν in replacement of $\frac{\partial^\nu}{\partial t^\nu}$for the Caputo fractional derivative. The Caputo fractional derivative of order $\nu > 0$ for $f(t) = t^\alpha$ is given as

$$D_t^\nu f(t) = \begin{cases} \frac{\Gamma(\alpha+1)}{\Gamma(\alpha-\nu+1)} t^{\alpha-\nu}, m > \alpha \geq m-1, \\ 0 \text{ if } \alpha \in \{0,1,2,...,m-1\} \end{cases} \tag{3}$$

In the following, some main computational properties and relations of fractional integral and differential operators are defined as

$$\begin{aligned} & i) I_t^\alpha I_t^\beta f(t) = I_t^{\alpha+\beta} f(t) = I_t^\beta I_t^\alpha f(t) \\ & ii) \frac{\partial^\beta}{\partial t^\beta} I_t^\alpha f(x,t) = I_t^{\alpha-\beta} f(x,t) \\ & iii) \frac{\partial^\alpha}{\partial t^\alpha} f(x,t) = f(x,t) - \sum_{k=0}^{n-1} \frac{t^k}{k!} \frac{\partial^k f(x,t) \mid_{t=0}}{\partial t^k} \\ & = f(x,t) + \sum_{k=0}^{n-1} \zeta_k(x) t^k \end{aligned} \tag{4}$$

where,$\zeta_k(x) = -\frac{1}{k!} \frac{\partial^k f(x,t)|_{t=0}}{\partial t^k}$. For more details see [1].

B. Haar wavelets and function approximation

Basis of Haar wavelets is obtained with a multi-resolution of piecewise constant functions. Let the interval $x \in [0,1)$ be divided into $2m$ subintervals of equal length, where $m = 2^j$ and J is maximal level of resolution. Next, two parameters are introduced, $j = 0,1,2,\ldots,J$ and $k = 0,1,2, ldots, m-1$, such that the wavelet number i satisfies the relation $i = k+m+1$. The ith Haar wavelet can be determined as

$$h_i(x) = \begin{cases} 1, x \in [\vartheta_1, \vartheta_2) \\ -1, x \in [\vartheta_2, \vartheta_3) \\ 0, \text{ elsewhere} \end{cases} \tag{5}$$

where $\vartheta_1 = \frac{k}{m}, \vartheta_2 = \frac{k+0.5}{m}, \vartheta_3 = \frac{k+1}{m}$

For the case $i = 1$, corresponding scaling function can be defined as:

$$h_1 = \begin{cases} 1, x \in [\vartheta_1, \vartheta_3) \\ 0, \text{ elsewhere} \end{cases} \tag{6}$$

Here, we consider the wavelet-collocation method, therefore collocation points are generated by using,

$$x_l = \frac{l-0.5}{2m}, \ l = 1,2,3, ldots, 2m \tag{7}$$

The Haar system forms an orthonormal basis for the Hilbert space $f(t) \in L_2(0,1)$. We may consider the inner product expansion of $f(t) \in L_2([0,1))$ in Haar series [31] as:

$$f(t) \approx \langle f, \varphi \rangle \varphi(t) + \sum_{j=0}^{J-1} \sum_{i=0}^{2^j-1} \langle f, h_{j,k} \rangle h_{j,k}(t) = C^T H(t) \tag{8}$$

where, C is 1×2^J coefficient vector and $H(t) = [h_0(t), h_1(t), ldots, h_{m-1}(t)]^T$. Also, a function of two variables can be expanded by Haar wavelets [32] as:

$$u(x,t) \approx \sum_{i=0}^{m-1} \sum_{j=0}^{m-1} u_{i,j} h_i(x) h_j(t) = H^T(x).U.H(t) \tag{9}$$

where, U is $2^J \times 2^J$ coefficient matrix calculated by the inner product $u_{i,j} = \langle h_i(x), \langle u(x,t), h_j \rangle \rangle$ The operational matrix of fractional integration of Haar function is needed to solve PDE of fractional order. A more rigorous derivation for the generalized block pulse operational matrices is proposed in [39]. The block pulse function forms a complete set of orthogonal functions which is defined in interval $[a, b)$ as

$$\psi_i(t) = \begin{cases} 1, & \frac{i-1}{m} b \leq t < \frac{i}{m} b \\ 0 & \text{elsewhere} \end{cases} \quad (10)$$

for $i = 1, 2, ldots, m$ It is known that any absolutely integrable function $f(t)$ on $[a, b)$, can be expanded in block pulse functions as

$$f(t) \cong F^T \psi_{(m)}(t) \quad (11)$$

so that the mean square error of approximation is minimized. Here, $F^T = [f_1, f_2, f_3, ldots, f_m]$ and $\psi^T_{(m)}(t) = [\psi_1(t), \psi_2(t), \psi_3(t), ldots, \psi_m(t)]$. where,

$$f_i = \frac{m}{b} \int_a^b f(t)\psi_i(t)dt = \frac{m}{b} \int_{(i-1)b/m}^{(i/m)b} f(t)\psi_i(t)dt \quad (12)$$

The Riemann-Liouville fractional integral is simplified and expanded in block pulse functions to yield the generalized block pulse operational matrix F^ν as

$$(I^\nu \psi_m)(t) = F^\nu \psi_m(t) \quad (13)$$

where

$$F^\nu = (\frac{b}{m})^\nu \frac{1}{\Gamma(\nu+2)} \begin{pmatrix} 1 & \xi_2 & \xi_3 & \dots & \xi_m \\ 0 & 1 & \xi_2 & \dots & \xi_{m-1} \\ 0 & 0 & 1 & \dots & \xi_{m-2} \\ \vdots & \vdots & \vdots & \ddots & \vdots \\ 0 & 0 & 0 & 0 & 1 \end{pmatrix}$$

with $\xi_1 = 1$, $\xi_p = p^{\nu+1} - 2(p-1)^{\nu+1} + (p-2)^{\nu+1}$ $(p = 2, 3, 4, ldots, m - i + 1)$ For further details see refs. [39]. The Haar functions are piecewise constant, so it may be expanded into an $m-$term block pulse functions (BPF) as

$$H_m(t) = H_{m\times m}\psi_m(t) \quad (14)$$

In [31] Haar wavelets operational matrix of fractional order integration is derived by

$$(I^\nu H_m)(t) \approx P^\nu H_m(t) \quad (15)$$

where P^ν is $m \times m$ order Haar wavelets operational matrix of fractional order integration. Substituting Eq.(2) in Eq.(14) we get

$$\begin{aligned}(I^\nu H_m)(t) &\approx (I^\nu H_{m\times m}\psi_m)(t) = H_{m\times m}(I^\nu \psi_m)(t) \\ &\approx H_{m\times m} F^\nu \psi_m(t) \quad (16)\end{aligned}$$

From Eq.(15) and Eq.(16), it can be written as:

$$P^\nu H_m(t) = H_{m\times m} F^\nu \quad (17)$$

Therefore, P^ν can be obtained as

$$P^\nu = H.F^\nu.H^{-1} \quad (18)$$

C. Multi Resolution Analysis (MRA)

Any space V can be constructed using a basis function $h(2^m t)$ as:

$$V_m = span\{h(2^m t - n)\}_{n,m\in Z}$$

$h(t)$ is called scaling function, also known as 'Father function'. The chain of subspaces $ldots V_{-2}, V_{-1}, V_0, V_1, V_2 ldots$ with the following axioms is called multi-resolution analysis (MRA) [28].

$$i)\{\overline{\bigcup V_m}\}_{m\in Z} = L_2(R)$$

$$ii)\{\bigcap V_m\}_{m\in Z} = \{0\}$$

$iii)$There exists $h(t)$such that,$V_0 = span\{h(t-n)\}_{n\in Z}$

$iv)\{h(t-n)\}_{n\in Z}$is an orthogonal set.

$v)$If$f(t) \in V_m$ then $f(2^{-m}t) \in V_0,\ \forall\ m \in Z)$

$vi)$If$f(t) \in V_0$ then $f(t-n) \in V_0,\ \forall\ n \in Z)$ (19)

Under the given axioms, there exists a $\psi(.) \in L_2(R)$, such that $\{\psi(2^m t - n)\}_{m,n\in Z}$ spans $L_2(R)$. The wavelet function $\psi(.)$ is also called 'Mother wavelet'.

Convergence of the method

Let $\frac{\partial^3 u(x,t)}{\partial t \partial x^2}$ and $\frac{\partial^3 v(x,t)}{\partial t \partial x^2}$ are continuous and bounded functions on $(0, 1) \times (0, 1)$, then $\exists M_1, M_2 > 0, \forall x, t \in (0, 1) \times (0, 1)$

$$|\frac{\partial^3 u(x,t)}{\partial t \partial x^2}| \leq M_1 \text{and } |\frac{\partial^3 v(x,t)}{\partial t \partial x^2}| \leq M_2 \quad (20)$$

Let $u_m(x, t)$ and $v_m(x, t)$ are the following approximations of $u(x, t)$ and $v(x, t)$,

$$\begin{aligned} u_m(x,t) &\approx \sum_{i=0}^{m-1}\sum_{j=0}^{m-1} u_{ij} h_i(x) h_j(t) \text{ and} \\ v_m(x,t) &\approx \sum_{i=0}^{m-1}\sum_{j=0}^{m-1} v_{ij} h_i(x) h_j(t) \quad (21)\end{aligned}$$

then we have

$$\begin{aligned} u(x,t) - u_m(x,t) &= \sum_{i=m}^{\infty}\sum_{j=m}^{\infty} u_{ij} h_i(x) h_j(t) \\ &= \sum_{i=2^{p+1}}^{\infty}\sum_{j=2^{p+1}}^{\infty} u_{ij} h_i(x) h_j(t) \text{ and} \\ v(x,t) - v_m(x,t) &= \sum_{i=m}^{\infty}\sum_{j=m}^{\infty} v_{ij} h_i(x) h_j(t) \\ &= \sum_{i=2^{p+1}}^{\infty}\sum_{j=2^{p+1}}^{\infty} v_{ij} h_i(x) h_j(t) \quad (22)\end{aligned}$$

Theorem 1: Let the functions $u_m(x,t)$ and $v_m(x,t)$ obtained by using Haar wavelets are the approximation of $u(x,t)$ and $v(x,t)$ then we have the errors bounded as following

$$\|u(x,t)-u_m(x,t)\|_E \leq \frac{M_1}{\sqrt{3}m^3} \text{ and } \\ \|v(x,t)-v_m(x,t)\|_E \leq \frac{M_2}{\sqrt{3}m^3} \tag{23}$$

where

$$\|u(x,t)\|_E = (\int_0^1\int_0^1 u^2(x,t)dxdt)^{1/2} \text{ and } \\ \|v(x,t)\|_E = (\int_0^1\int_0^1 v^2(x,t)dxdt)^{1/2} \tag{24}$$

See proof in [32].

III. The Schrödinger equations

A. The time-fractional Schrödinger equation

The time-fractional Schrödinger equation (T-FSE) has the following form

$$i\frac{\partial^\nu \phi(x,t)}{\partial t^\nu} + \lambda\frac{\partial^2\phi(x,t)}{\partial x^2} + \eta \mid \phi \mid^2 \phi + \mu(x)\phi = q(x,t), \\ 0 < x,t \leq 1 \tag{25}$$

with initial conditions $\phi(x,0) = f(x), \phi(0,t) = g(t)$, $\phi^{'}(0,t) = h(t)$
where $0 < \nu \leq 1, \lambda$ and η are real constants, $\mu(x)$ is the trapping potential and $\phi(x,t), f(x), g(t), h(t)$ and $q(x,t)$ are complex functions. We can express complex functions $\phi(x,t), f(x), g(t), h(t)$ and $q(x,t)$ into their respective real and imaginary parts as

$$\begin{aligned} \phi(x,t) &= u(x,t) + iv(x,t) \\ \mu(x) &= \mu_1(x) + i\mu_2 \\ f(x) &= f_1(x) + if_2(x) \\ g(t) &= g_1(t) + ig_2(t) \\ h(t) &= h_1(t) + ih_2(t) \\ q(x,t) &= q_1(x,t) + iq_2(x,t) \end{aligned} \tag{26}$$

Substituting Eq. (26) into Eq. (25) and collecting real and imaginary parts, then Eq. (25) can be written as coupled time-fractional nonlinear partial differential equations as:

$$-\frac{\partial^\nu v(x,t)}{\partial t^\nu} + \lambda\frac{\partial^2 u(x,t)}{\partial x^2} + \eta(u^2+v^2)u + \mu_1(x) \\ u(x,t) - q_1(x,t) = 0 \\ \frac{\partial^\nu u(x,t)}{\partial t^\nu} + \lambda\frac{\partial^2 v(x,t)}{\partial x^2} + \eta(u^2+v^2)v + \mu_2(x) \\ v(x,t) - q_2(x,t) = 0 \tag{27}$$

with initial conditions

$$u(x,0) = f_1(x), v(x,0) = f_2(x), u(0,t) = g_1(t), \\ v(0,t) = g_2(t), u^{'}(0,t) = h_1(t), v^{'}(0,t) = h_2(t) \tag{28}$$

B. The time-fractional coupled Schrödinger system

The time-fractional coupled Schrödinger system (T-FCSS) has the following form

$$i\frac{\partial^\nu \phi(x,t)}{\partial t^\nu} + i\frac{\partial^2\phi(x,t)}{\partial x^2} + \frac{\partial^2\phi(x,t)}{\partial x^2} + \lambda_1(\mid\phi\mid^2 + \mid\psi\mid^2) \\ \phi(x,t) + \alpha_1(x)\phi(x,t) + \beta_1\psi(x,t) - f_1(x,t) = 0 \\ i\frac{\partial^\nu \psi(x,t)}{\partial t^\nu} + i\frac{\partial^2\psi(x,t)}{\partial x^2} + \frac{\partial^2\psi(x,t)}{\partial x^2} + \lambda_2(\mid\phi\mid^2 + \mid\psi\mid^2) \\ \psi(x,t) + \alpha_2(x)\phi(x,t) + \beta_2\psi(x,t) - f_2(x,t) = 0 \tag{29}$$

with initial conditions

$$\phi(x,0) = f_3(x), \phi(0,t) = g_3(t), \phi^{'}(0,t) = h_3(t), \\ \psi(x,0) = f_4(x), \psi(0,t) = g_4(t), \psi^{'}(0,t) = h_4(t) \tag{30}$$

where $0 < \nu \leq 1, \lambda_1, \lambda_2, \alpha_1, \alpha_2, \beta_1$ andβ_2 are real constants and $\phi(x,t), \psi(x,t), f_3(x), f_4(t), g_3(t), g_4(t), h_3(t), h_4(t)$, $q_1(x,t)$ and $q_2(x,t)$ are complex functions. We can express complex functions into their respective real and imaginary parts as

$$\phi(x,t) = u(x,t) + iv(x,t),\ \psi(x,t) = r(x,t) + is(x,t) \\ f_3(x) = f_5(x) + if_6(x),\ f_4(x) = f_7(x) + if_8(x) \\ g_3(t) = g_5(t) + ig_6(t),\ g_4(t) = g_7(t) + ig_8(t) \\ h_3(t) = h_5(t) + ih_6(t),\ h_4(t) = h_7(t) + ih_8(t) \\ q_3(x,t) = q_5(x,t) + iq_6(x,t),\ q_4(x,t) = q_7(x,t) + iq_8(x,t) \tag{31}$$

Substituting Eq. (31) into Eq. (29) and equating real and imaginary parts we get the system of two coupled time-fractional nonlinear partial differential equations.

$$-\frac{\partial^\nu v(x,t)}{\partial t^\nu} - \frac{\partial v(x,t)}{\partial x} + \frac{\partial^2 u(x,t)}{\partial x^2} + \lambda_1(u^2+v^2+r^2+s^2) \\ u(x,t) + \alpha_1 u(x,t) + \beta_1 r(x,t) - q_3(x,t) = 0 \\ \frac{\partial^\nu u(x,t)}{\partial t^\nu} + \frac{\partial u(x,t)}{\partial x} + \frac{\partial^2 v(x,t)}{\partial x^2} + \lambda_1(u^2+v^2+r^2+s^2) \\ v(x,t) + \alpha_1 v(x,t) + \beta_1 s(x,t) - q_4(x,t) = 0 \\ -\frac{\partial^\nu s(x,t)}{\partial t^\nu} + \frac{\partial s(x,t)}{\partial x} + \frac{\partial^2 r(x,t)}{\partial x^2} + \lambda_2(u^2+v^2+r^2+s^2) \\ r(x,t) + \alpha_2 u(x,t) + \beta_2 r(x,t) - q_5(x,t) = 0 \\ \frac{\partial^\nu r(x,t)}{\partial t^\nu} - \frac{\partial r(x,t)}{\partial x} + \frac{\partial^2 s(x,t)}{\partial x^2} + \lambda_2(u^2+v^2+r^2+s^2) \\ s(x,t) + \alpha_2 v(x,t) + \beta_2 s(x,t) - q_6(x,t) = 0 \tag{32}$$

IV. The proposed method

A. For time-fractional Schrödinger equation

Any arbitrary function $u(x,t) \in L_2([0,1)\times[0,1))$ and $v(x,t) \in L_2([0,1)\times[0,1))$, can be expanded into Haar series [32] as:

$$\dot{u}^{''}(x,t) = \sum_{i=1}^{2m}\sum_{j=1}^{2m} u_{ij}h_i(x)h_j(t) \\ \dot{v}^{''}(x,t) = \sum_{i=1}^{2m}\sum_{j=1}^{2m} v_{ij}h_i(x)h_j(t) \tag{33}$$

where $2M \times 2M$ Haar coefficient matrix of u_{ij} and v_{ij} in Eq. (33) can be written as:

$$\begin{aligned} \dot{\boldsymbol{U}}^{''} &= H^T(x).U.H(t) \\ \dot{\boldsymbol{V}}^{''} &= H^T(x).V.H(t) \end{aligned} \tag{34}$$

Let dots and primes in Eq. (33) represent differentiation with respect to t and x, respectively. By integrating Eq. (34) with respect to t from 0 to t, we get

$$\begin{aligned} \boldsymbol{U}^{''} &= H^T(x).U.P^1.H(t) + u^{''}(x,0) \\ \boldsymbol{V}^{''} &= H^T(x).V.P^1.H(t) + v^{''}(x,0) \end{aligned} \tag{35}$$

on integrating Eq. (35) twice with respect to x from 0 to x, then we get

$$\begin{aligned} \boldsymbol{U}^{'} &= H^T(x).[P^1]^T.U.P^1.H(t) + u^{'}(x,0) - u^{'}(0,0) + u^{'}(0,t) \\ \boldsymbol{V}^{'} &= H^T(x).[P^1]^T.V.P^1.H(t) + v^{'}(x,0) - v^{'}(0,0) + v^{'}(0,t) \end{aligned} \tag{36}$$

and then

$$\begin{aligned} \boldsymbol{U} &= H^T(x).[P^2]^T.U.P^1.H(t) + u(x,0) - u(0,0) - xu^{'}(0,0) + xu^{'}(0,t) + u(0,t) \\ \boldsymbol{V} &= H^T(x).[P^2]^T.V.P^1.H(t) + v(x,0) - v(0,0) - xv^{'}(0,0) + xv^{'}(0,t) + v(0,t) \end{aligned} \tag{37}$$

Applying differential operator D_t^{ν} on both sides of Eq. (37) and using property (ii) of Eq. (4)

$$\begin{aligned} D_t^{\nu}\boldsymbol{U} &= H^T(x).[P^2]^T.U.P^{1-\nu}.H(t) + xD_t^{\nu}u^{'}(0,t) + D_t^{\nu}u(0,t) \\ D_t^{\nu}\boldsymbol{V} &= H^T(x).[P^2]^T.V.P^{1-\nu}.H(t) + xD_t^{\nu}v^{'}(0,t) + D_t^{\nu}v(0,t) \end{aligned} \tag{38}$$

Substitution of Eqs. (35), (37) and (38) into Eq. (27) may lead to coupled system of time-fractional differential equations. This system will have some unknown functions $u^{''}(x,0), u^{'}(x,0), u^{'}(0,0), u(0,0), D_t^{\nu}u^{'}(0,t), D_t^{\nu}u(0,t)$, $v^{''}(x,0), v^{'}(x,0), v^{'}(0,0), v(0,0), D_t^{\nu}v^{'}(0,t)$, and $D_t^{\nu}v(0,t)$. With the help of initial conditions all these functions are calculated. We solve Eq. (27) for unknown Haar coefficients by using collocation method. Finally, for Haar solution of T-FSE, we substitute values of Haar coefficients in Eq. (37).

B. For time-fractional coupled Schrödinger system

Now, we approximate $u(x,t), v(x,t), r(x,t)$ and $s(x,t)$, by the Haar series [32] as:

$$\begin{aligned} \dot{u}^{''}(x,t) &= \sum_{i=1}^{2m}\sum_{j=1}^{2m} u_{ij}h_i(x)h_j(t) \\ \dot{v}^{''}(x,t) &= \sum_{i=1}^{2m}\sum_{j=1}^{2m} v_{ij}h_i(x)h_j(t) \\ \dot{r}^{''}(x,t) &= \sum_{i=1}^{2m}\sum_{j=1}^{2m} r_{ij}h_i(x)h_j(t) \\ \dot{s}^{''}(x,t) &= \sum_{i=1}^{2m}\sum_{j=1}^{2m} s_{ij}h_i(x)h_j(t) \end{aligned} \tag{39}$$

Matrix form of Eq. (39) can be written as:

$$\begin{aligned} \dot{\boldsymbol{U}}^{''} &= H^T(x).U.H(t) \\ \dot{\boldsymbol{V}}^{''} &= H^T(x).V.H(t) \\ \dot{\boldsymbol{R}}^{''} &= H^T(x).R.H(t) \\ \dot{\boldsymbol{S}}^{''} &= H^T(x).S.H(t) \end{aligned} \tag{40}$$

Let dots and primes in Eq. (40) represent differentiation with respect to t and x, respectively. By integrating Eq. (40) with respect to t from 0 to t, we get

$$\begin{aligned} \boldsymbol{U}^{''} &= H^T(x).U.P^1.H(t) + u^{''}(x,0) \\ \boldsymbol{V}^{''} &= H^T(x).V.P^1.H(t) + v^{''}(x,0) \\ \boldsymbol{R}^{''} &= H^T(x).R.P^1.H(t) + r^{''}(x,0) \\ \boldsymbol{S}^{''} &= H^T(x).S.P^1.H(t) + s^{''}(x,0) \end{aligned} \tag{41}$$

on integrating Eq. (41) twice with respect to x from 0 to x, once we get

$$\begin{aligned} \boldsymbol{U}^{'} &= H^T(x).[P^1]^T.U.P^1.H(t) + u^{'}(x,0) - u^{'}(0,0) + u^{'}(0,t) \\ \boldsymbol{V}^{'} &= H^T(x).[P^1]^T.V.P^1.H(t) + v^{'}(x,0) - v^{'}(0,0) + v^{'}(0,t) \\ \boldsymbol{R}^{'} &= H^T(x).[P^1]^T.R.P^1.H(t) + r^{'}(x,0) - r^{'}(0,0) + r^{'}(0,t) \\ \boldsymbol{S}^{'} &= H^T(x).[P^1]^T.S.P^1.H(t) + s^{'}(x,0) - s^{'}(0,0) + s^{'}(0,t) \end{aligned} \tag{42}$$

and

$$\begin{aligned} \boldsymbol{U} &= H^T(x).[P^2]^T.U.P^1.H(t) + u(x,0) - u(0,0) - xu^{'}(0,0) + xu^{'}(0,t) + u(0,t) \\ \boldsymbol{V} &= H^T(x).[P^2]^T.V.P^1.H(t) + v(x,0) - v(0,0) - xv^{'}(0,0) + xv^{'}(0,t) + v(0,t) \\ \boldsymbol{R} &= H^T(x).[P^2]^T.R.P^1.H(t) + r(x,0) - r(0,0) - xr^{'}(0,0) + xr^{'}(0,t) + r(0,t) \\ \boldsymbol{S} &= H^T(x).[P^2]^T.S.P^1.H(t) + s(x,0) - s(0,0) - xs^{'}(0,0) + xs^{'}(0,t) + s(0,t) \end{aligned} \tag{43}$$

Applying differential operator D_t^{ν} on both sides of Eq. (43) and using property (ii) of Eq. (4)

$$\begin{aligned} D_t^{\nu}\boldsymbol{U} &= H^T(x).[P^2]^T.U.P^{1-\nu}.H(t) + xD_t^{\nu}u^{'}(0,t) + D_t^{\nu}u(0,t) \\ D_t^{\nu}\boldsymbol{V} &= H^T(x).[P^2]^T.V.P^{1-\nu}.H(t) + xD_t^{\nu}v^{'}(0,t) + D_t^{\nu}v(0,t) \\ D_t^{\nu}\boldsymbol{R} &= H^T(x).[P^2]^T.R.P^{1-\nu}.H(t) + xD_t^{\nu}r^{'}(0,t) + D_t^{\nu}r(0,t) \\ D_t^{\nu}\boldsymbol{S} &= H^T(x).[P^2]^T.S.P^{1-\nu}.H(t) + xD_t^{\nu}s^{'}(0,t) + D_t^{\nu}s(0,t) \end{aligned} \tag{44}$$

Substitution of Eqs. (41), (42), (43) and (44) into Eq. (32) may lead to the two coupled systems of time-fractional differential equations. This system has some unknown functions. With the help of initial conditions all these functions are calculated. We solve system of Eq. (32) for unknown Haar coefficients by using collocation method. Finally, for Haar solution of time-fractional coupled Schrödinger system (T-FCSS), we substitute values of Haar coefficients in Eq. (43).

V. Numerical Problems

In this section, four test problems are taken to test the efficiency and accuracy of the proposed scheme. The computations associated with the problems were executed using *Mathematica 10*.

Problem 1: Consider the linear T-FSE which is also found in [6] with

$$\lambda = 1, \eta = 0, \mu(x) = 0 \text{ and } q(x,t) = (\frac{2it^{2-\nu}}{\Gamma(3-\nu)} - t^2)e^{ix} \quad (45)$$

Subjected to initial conditions

$$\phi(x,0) = 0, \phi(0,t) = t^2, \phi^{'}(0,t) = it^2 \quad (46)$$

the exact solution for $\nu = 1$ is

$$\phi(x,t) = t^2 e^{ix} \quad (47)$$

Substitute Eq. (45) in Eq. (25) the determined coupled system of equations is

$$-\frac{\partial^\nu v(x,t)}{\partial t^\nu} + \frac{\partial^2 u(x,t)}{\partial x^2} - (t^2 \cos x + \frac{2t^{2-\nu} \sin x}{\Gamma(3-\nu)}) = 0$$
$$\frac{\partial^\nu u(x,t)}{\partial t^\nu} + \frac{\partial^2 v(x,t)}{\partial x^2} - (t^2 \sin x - \frac{2t^{2-\nu} \cos x}{\Gamma(3-\nu)}) = 0 \quad (48)$$

By using the method given in Section IV A, Eq. (48) can be written as

$$-H^T(x).[P^2]^T.V.P^{1-\nu}.H(t) + H^T(x).U.P^1.H(t) + \frac{\Gamma(\nu+1)xt^{2-\nu}}{\Gamma(2-\nu+1)} - (t^2 \cos x + \frac{2t^{2-\nu} \sin x}{\Gamma(3-\nu)}) = 0$$
$$H^T(x).[P^2]^T.U.P^{1-\nu}.H(t) + H^T(x).V.P^1.H(t) + \frac{\Gamma(\nu+1)t^{2-\nu}}{\Gamma(2-\nu+1)} - t^2 \sin x + \frac{2t^{2-\nu} \cos x}{\Gamma(3-\nu)}) = 0 \quad (49)$$

Towards the approximate solution, we first collocate Eq. (49) at points

$$x_i = \frac{i-0.5}{2m}, \; t_j = \frac{j-0.5}{2m} \quad (50)$$

Eq. (49) $\Rightarrow$

$$-H^T(x_i).[P^2]^T.V.P^{1-\nu}.H(t_j) + H^T(x_i).U.P^1.H(t_j) + \frac{\Gamma(\nu+1)x_i t_j^{2-\nu}}{\Gamma(2-\nu+1)} - (t_j^2 \cos x_i + \frac{2t_j^{2-\nu} \sin x_i}{\Gamma(3-\nu)}) = 0$$
$$H^T(x_i).[P^2]^T.U.P^{1-\nu}.H(t_j) + H^T(x_i).V.P^1.H(t_j) + \frac{\Gamma(\nu+1)t_j^{2-\nu}}{\Gamma(2-\nu+1)} - t_j^2 \sin x_i + \frac{2t_j^{2-\nu} \cos x_i}{\Gamma(3-\nu)}) = 0 \quad (51)$$

Eq. (51) generates two systems of $2M$ algebraic equations of Haar coefficients. The values of Haar coefficients are obtained from system of Eq. (51) by using Newton's iterative method. With the help of these coefficients, Haar solutions are attained from Eq. (37). Comparison of the Haar solutions by Homotopy analysis method in [5] is shown in Table I with different values of ν.

TABLE I
COMPARISON BETWEEN HAAR SOLUTIONS ($J = 1, m = 4$) AND HAM [5] OF PROBLEM 1

t	x	$\nu = 0.1$ HWCM	$\nu = 0.1$ HAM[5]	$\nu = 0.3$ HWCM	$\nu = 0.3$ HAM[5]	$\nu = 0.5$ HWCM	$\nu = 0.5$ HAM[5]
0.125	0.125	0.015584	0.015729	0.015588	0.018166	0.015602	0.032192
	0.375	0.140258	0.140320	0.140277	0.126725	0.140322	0.18097
	0.625	0.389603	0.391911	0.389639	0.331403	0.389698	0.417840
	0.875	0.763621	0.773331	0.763678	0.642092	0.763759	0.735157
0.375	0.125	0.015639	0.014928	0.015909	0.015876	0.016599	0.029901
	0.375	0.140697	0.137242	0.142257	0.117591	0.144873	0.171424
	0.625	0.390743	0.387923	0.394153	0.321101	0.398660	0.407056
	0.875	0.765763	0.770778	0.771532	0.639027	0.778130	0.736778
0.625	0.125	0.015881	0.014367	0.017251	0.013413	0.020637	0.026391
	0.375	0.142657	0.135328	0.150692	0.110280	0.164111	0.159805
	0.625	0.395831	0.385461	0.413348	0.315020	0.436643	0.396412
	0.875	0.775363	0.768819	0.805018	0.639973	0.839202	0.740576
0.875	0.125	0.016431	0.014212	0.020145	0.011454	0.028487	0.022180
	0.375	0.147236	0.135101	0.169643	0.107096	0.205320	0.148820
	0.625	0.407697	0.385159	0.456638	0.314912	0.519962	0.388621
	0.875	0.797810	0.767939	0.880970	0.644682	0.974802	0.745598

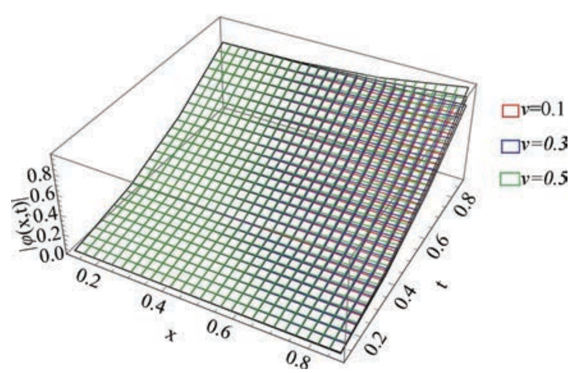

Fig. 1. Haar solutions of Problem 1 at $\nu = 0.1, 0.3, 0.5$

Problem 2: Consider a nonlinear cubic form of T-FSE [6] with

$$\lambda = 1, \eta = 1, \mu(x) = 0 \text{ and}$$
$$q(x,t) = (-\frac{2t^{2-\nu}}{\Gamma(3-\nu)} + (-4\pi^2 t^2 + t^6)i)e^{-2\pi ix} \quad (52)$$

and initial conditions

$$\phi(x,0) = 0, \phi(0,t) = it^2, \phi^{'}(0,t) = 2\pi t^2 \quad (53)$$

with exact solution for $\nu = 1$ is

$$\phi(x,t) = t^2 ie^{-2\pi ix} \quad (54)$$

Substitute Eq. (52) in Eq. (25) the determine coupled system of equations is

$$-\frac{\partial^{\nu}v(x,t)}{\partial t^{\nu}}+\frac{\partial^{2}u(x,t)}{\partial x^{2}}+(u^{2}+v^{2})u-((t^{6}-4\pi^{2}t^{2})\sin 2\pi x-\frac{2t^{3-\nu}}{\Gamma(3-\nu)}\cos 2\pi x)=0 \tag{55}$$

$$\frac{\partial^{\nu}u(x,t)}{\partial t^{\nu}}+\frac{\partial^{2}v(x,t)}{\partial x^{2}}+(u^{2}+v^{2})v-((t^{6}-4\pi^{2}t^{2})\cos 2\pi x+\frac{2t^{3-\nu}}{\Gamma(3-\nu)}\sin 2\pi x)=0 \tag{56}$$

On following the method described in Section IV A, we have

$$\begin{gathered}-H^{T}(x).[P^{2}]^{T}.V.P^{1-\nu}.H(t)+H^{T}(x).U.P^{1}.H(t)+ \\ ((H^{T}(x).[P^{2}]^{T}.U.P^{1}.H(t)+2\pi t^{2}x)^{2}+ \\ (H^{T}(x).[P^{2}]^{T}.V.P^{1}.H(t)+t^{2})^{2}).(H^{T}(x).[P^{2}]^{T}.U.P^{1}.H(t)+ \\ 2\pi t^{2}x)+\frac{\Gamma(3)}{\Gamma(3-\nu)}t^{2-\nu}-((t^{6}-4\pi^{2}t^{2})\sin 2\pi x- \\ \frac{2t^{3-\nu}}{\Gamma(3-\nu)}\cos 2\pi x)=0, \\ H^{T}(x).[P^{2}]^{T}.U.P^{1-\nu}.H(t)+H^{T}(x).V.P^{1}.H(t)+ \\ ((H^{T}(x).[P^{2}]^{T}.U.P^{1}.H(t)+2\pi t^{2}x)^{2}+ \\ (H^{T}(x).[P^{2}]^{T}.V.P^{1}.H(t)+t^{2})^{2}).(H^{T}(x).[P^{2}]^{T}.V.P^{1}.H(t)+ \\ t^{2})+\frac{2\pi\Gamma(3)}{\Gamma(3-\nu)}xt^{2-\nu}-((t^{6}-4\pi^{2}t^{2})\cos 2\pi x+ \\ \frac{2t^{3-\nu}}{\Gamma(3-\nu)}\sin 2\pi x)=0\end{gathered} \tag{57}$$

For approximate solution of Eq. (56), putting collocation points of Eq. (50) in above equations generates two systems of $2M$ non linear algebraic equations of Haar coefficients. The values of Haar coefficients are obtained by using Newton's iterative method and then with the help of these coefficients Haar solutions are attained from Eq. (37). The Haar solutions comparisone with the method in [5] for the different values of ν is shown in Table II.

Problem 3: Consider T-FSE with trapping potential [6] for

$\lambda=1,\eta=1,\mu(x)=\cos^{2}x$ and

$$q(x,t)=(i\frac{6t^{3-\nu}}{\Gamma(4-\nu)}-\frac{1}{4}t^{3}+t^{9}+t^{3}\cos^{2}x)e^{\frac{ix}{2}} \tag{58}$$

Subjected to initial conditions

$$\phi(x,0)=0,\phi(0,t)=t,\phi^{'}(0,t)=i\frac{t^{3}}{2} \tag{59}$$

with exact solution for $\nu=1$ is

$$\phi(x,t)=t^{3}e^{\frac{ix}{2}} \tag{60}$$

TABLE II

COMPARISON BETWEEN HAAR SOLUTIONS ($J=1,m=4$) AND HAM [5] OF PROBLEM 2

t	x	$\nu=0.1$ HWCM	$\nu=0.1$ HAM[5]	$\nu=0.5$ HWCM	$\nu=0.5$ HAM[5]	$\nu=0.9$ HWCM	$\nu=0.9$ HAM[5]
0.125	0.125	0.013539	0.013276	0.013578	0.006316	0.013768	0.002593
	0.375	0.121912	0.132538	0.121985	0.097840	0.122023	0.062856
	0.625	0.339272	0.385008	0.339565	0.347687	0.340151	0.276693
	0.875	0.668433	0.770812	0.668861	0.793325	0.669170	0.730876
0.375	0.125	0.010136	0.013277	0.012634	0.006316	0.020531	0.002593
	0.375	0.087449	0.132538	0.091611	0.097839	0.097166	0.062855
	0.625	0.235941	0.385008	0.240394	0.347687	0.248868	0.276693
	0.875	0.450485	0.770812	0.449529	0.793327	0.445334	0.730872
0.625	0.125	0.016209	0.013277	0.018019	0.006316	0.037906	0.002600
	0.375	0.144228	0.132538	0.142259	0.097840	0.133228	0.062856
	0.625	0.391331	0.385008	0.383766	0.347687	0.379218	0.276693
	0.875	0.723229	0.770812	0.709533	0.793325	0.681230	0.730876
0.875	0.125	0.016724	0.013276	0.011634	0.006316	0.064282	0.002600
	0.375	0.161766	0.132538	0.166036	0.097840	0.180905	0.062856
	0.625	0.448134	0.385008	0.430220	0.347687	0.413375	0.276693
	0.875	0.856867	0.770812	0.860240	0.793327	0.847833	0.730872

Determine the coupled system of equations by substituting Eq. (57) in Eq. (25). Next, following the method illustrated in Section IV A, by following same steps of *problem 1* Haar solutions are attained. The obtained Haar solutions are compared with the Homotopy analysis method [5] and at different values of ν are shown in Table III.

TABLE III

COMPARISON BETWEEN HAAR SOLUTIONS ($J=1,m=4$) AND HAM [5] OF PROBLEM 3

t	x	$\nu=0.1$ HWCM	$\nu=0.1$ HAM[5]	$\nu=0.3$ HWCM	$\nu=0.3$ HAM[5]	$\nu=0.5$ HWCM	$\nu=0.5$ HAM [5]
0.125	0.125	0.002666	0.001164	0.005127	0.001923	0.009737	0.003186
	0.375	0.064478	0.032624	0.099565	0.043939	0.151781	0.100635
	0.625	0.283647	0.155864	0.395466	0.219652	0.544319	0.438394
	0.875	0.752604	0.482083	0.981003	0.706422	1.262370	1.267630
0.375	0.125	0.002335	0.001064	0.004453	0.001859	0.008360	0.002993
	0.375	0.056487	0.029282	0.086504	0.040986	0.130392	0.082892
	0.625	0.248554	0.138363	0.343701	0.159805	0.467832	0.388469
	0.875	0.660306	0.425678	0.853338	0.297603	1.085680	1.080400
0.625	0.125	0.001737	0.000940	0.003234	0.001782	0.005880	0.002751
	0.375	0.042093	0.025192	0.062894	0.046640	0.091797	0.073477
	0.625	0.185563	0.117006	0.250376	0.240900	0.330180	0.329875
	0.875	0.498019	0.355007	0.625716	0.854561	0.769576	0.869481
0.875	0.125	0.000973	0.000833	0.001714	0.001823	0.002981	0.002530
	0.375	0.023635	0.021729	0.033100	0.051878	0.045350	0.065040
	0.625	0.105052	0.098823	0.131553	0.315074	0.158672	0.279519
	0.875	0.299206	0.291128	0.337855	0.257690	0.368943	0.300179

Problem 4: Take into consideration non-linear T-FCSS [35] for

$$\lambda_1 = 2, \lambda_2 = 4, \alpha_1 = \alpha_2 = 1, \beta_1 = 1 \text{ and } \beta_2 = -1$$
$$q_1(x,t) = -\frac{2t^{2-\nu}}{\Gamma(3-\nu)}\sin x + 4t^6\cos x + i(\frac{2t^{2-\nu}}{\Gamma(3-\nu)}\cos x + 4t^6\sin x) \text{ and} q_2(x,t) = -\frac{2t^{2-\nu}}{\Gamma(3-\nu)}\sin x + 8t^6\cos x + i(\frac{2t^{2-\nu}}{\Gamma(3-\nu)}\cos x + 8t^6\sin x) \quad (61)$$

with initial conditions

$$\begin{aligned}\phi(x,0) &= \psi(x,0) = 0,\\ \phi(0,t) &= \psi(0,t) = t,\\ \phi'(0,t) &= \psi'(0,t) = it^2\end{aligned} \quad (62)$$

and with exact solution for these values of λ, α, β and $\nu = 1$ is

$$\phi(x,t) = \psi(x,t) = t^2 e^{ix}, \quad (63)$$

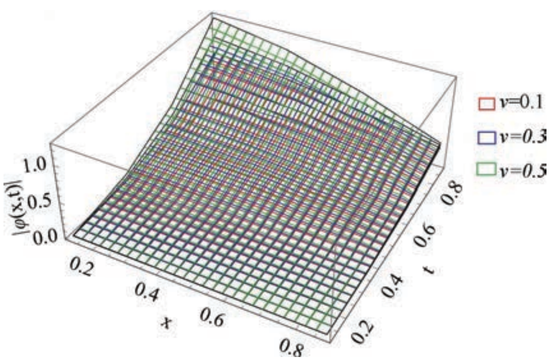

Fig. 2. Haar solutions of Problem 3 at $\nu = 0.1, 0.3, 0.5$

Determine the coupled system of two equations by substituting Eq. (60) in Eq. (29) as

$$\begin{aligned}&-\frac{\partial^\nu v(x,t)}{\partial t^\nu} - \frac{\partial v(x,t)}{\partial x} + \frac{\partial^2 u(x,t)}{\partial x^2} + 2(u^2+v^2+r^2+s^2)\\ &u(x,t) + u(x,t) + r(x,t) + \frac{2t^{2-\nu}}{\Gamma(3-\nu)}\sin x + 4t^6\cos x = 0,\\ &\frac{\partial^\nu u(x,t)}{\partial t^\nu} + \frac{\partial u(x,t)}{\partial x} + \frac{\partial^2 v(x,t)}{\partial x^2} + 2(u^2+v^2+r^2+s^2)\\ &v(x,t) + v(x,t) + s(x,t) - (\frac{2t^{2-\nu}}{\Gamma(3-\nu)}\cos x + 4t^6\sin x) = 0,\\ &-\frac{\partial^\nu s(x,t)}{\partial t^\nu} + \frac{\partial s(x,t)}{\partial x} + \frac{\partial^2 r(x,t)}{\partial x^2} + 2(u^2+v^2+r^2+s^2)\\ &r(x,t) + u(x,t) - r(x,t) + \frac{2t^{2-\nu}}{\Gamma(3-\nu)}\sin x + 8t^6\cos x = 0,\\ &\frac{\partial^\nu r(x,t)}{\partial t^\nu} - \frac{\partial r(x,t)}{\partial x} + \frac{\partial^2 s(x,t)}{\partial x^2} + 2(u^2+v^2+r^2+s^2)\\ &s(x,t) + v(x,t) - s(x,t) - (\frac{2t^{2-\nu}}{\Gamma(3-\nu)}\cos x + 8t^6\sin x) = 0\end{aligned} \quad (64)$$

Next, following the method illustrated in Section IV B, we have

$$\begin{aligned}&-(H^T(x).[P^2]^T.V.P^{1-\nu}.H(t) + \frac{\Gamma(\nu+1)}{\Gamma(2-\nu+1)}xt^{2-\nu}) -\\ &H^T(x).[P^1]^T.V.P^1.H(t) + H^T(x).U.P^1.H(t) + \boldsymbol{U} +\\ &2(\boldsymbol{U}^2 + \boldsymbol{V}^2 + \boldsymbol{R}^2 + \boldsymbol{S}^2)\boldsymbol{U} + \boldsymbol{R} + \frac{2t^{2-\nu}}{\Gamma(3-\nu)}\sin x +\\ &4t^6\cos x = 0,\end{aligned} \quad (65)$$

$$\begin{aligned}&H^T(x).[P^2]^T.U.P^{1-\nu}.H(t) + \frac{\Gamma(\nu+1)}{\Gamma(2-\nu+1)}xt^{2-\nu} +\\ &H^T(x).[P^1]^T.U.P^1.H(t) + H^T(x).V.P^1.H(t) + \boldsymbol{V} +\\ &2(\boldsymbol{U}^2 + \boldsymbol{V}^2 + \boldsymbol{R}^2 + \boldsymbol{S}^2)\boldsymbol{V} + \boldsymbol{S} - (\frac{2t^{2-\nu}}{\Gamma(3-\nu)}\cos x +\\ &4t^6\sin x) = 0,\\ &-(H^T(x).[P^2]^T.S.P^{1-\nu}.H(t) + \frac{\Gamma(\nu+1)}{\Gamma(2-\nu+1)}xt^{2-\nu}) +\\ &H^T(x).[P^1]^T.S.P^1.H(t) + H^T(x).R.P^1.H(t) + \boldsymbol{U} +\\ &4(\boldsymbol{U}^2 + \boldsymbol{V}^2 + \boldsymbol{R}^2 + \boldsymbol{S}^2)\boldsymbol{R} - \boldsymbol{R} + \frac{2t^{2-\nu}}{\Gamma(3-\nu)}\sin x +\\ &8t^6\cos x = 0,\\ &(H^T(x).[P^2]^T.R.P^{1-\nu}.H(t) + \frac{\Gamma(\nu+1)}{\Gamma(2-\nu+1)}xt^{2-\nu}) -\\ &H^T(x).[P^1]^T.R.P^1.H(t) + H^T(x).S.P^1.H(t) + \boldsymbol{V} +\\ &4(\boldsymbol{U}^2 + \boldsymbol{V}^2 + \boldsymbol{R}^2 + \boldsymbol{S}^2)\boldsymbol{S} - \boldsymbol{S} - (\frac{2t^{2-\nu}}{\Gamma(3-\nu)}\cos x + 8t^6\sin x) = 0\end{aligned} \quad (66)$$

where $\boldsymbol{U} = H^T(x).[P^2]^T.U.P^1.H(t) + t^2$,
$\boldsymbol{V} = H^T(x).[P^2]^T.V.P^1.H(t) + xt^2$,
$\boldsymbol{R} = H^T(x).[P^2]^T.R.P^1.H(t) + t^2$ and
$\boldsymbol{S} = H^T(x).[P^2]^T.S.P^1.H(t) + xt^2$

TABLE IV
COMPARISON BETWEEN HAAR SOLUTIONS ($J = 1, m = 4, \nu = 0.1$) AND HAM [5] OF PROBLEM 4

t	x	$\mid \phi(x,t) \mid$		$\mid \psi(x,t) \mid$	
		HWCM	**HAM** [5]	**HWCM**	**HAM** [5]
0.125	0.125	0.015383	0.014440	0.0153167	0.004286
	0.375	0.138501	0.128015	0.137928	0.038537
	0.625	0.385851	0.365216	0.384604	0.143183
	0.875	0.763499	0.949120	0.763355	0.811326
0.375	0.125	0.013949	0.014439	0.013495	0.004286
	0.375	0.125927	0.128015	0.121958	0.038536
	0.625	0.357238	0.365216	0.348492	0.143183
	0.875	0.747914	0.949120	0.746334	0.811326
0.625	0.125	0.011086	0.014440	0.009704	0.004285
	0.375	0.100695	0.128015	0.088716	0.038536
	0.625	0.297240	0.365216	0.272767	0.143183
	0.875	0.697857	0.949120	0.706649	0.811326
0.875	0.125	0.008487	0.014440	0.004160	0.004286
	0.375	0.077508	0.128015	0.040194	0.038537
	0.625	0.236292	0.365216	0.163674	0.143183
	0.875	0.634398	0.949120	0.664360	0.811326

Using Eq. (50), the values of Haar coefficients are obtained and finally with the help of these coefficients Haar solutions are attained from Eq. (43). The Haar solutions are compared with the method in [5] with $\nu = 0.1$ and results are shown in Table IV, and for $\nu = 0.5$ and $\nu = 0.9$ in Table V and Table VI, respectively.

TABLE V
COMPARISON BETWEEN HAAR SOLUTIONS ($J = 1, m = 4, \nu = 0.5$) AND HAM [5] OF PROBLEM 4

t	x	$\mid \phi(x,t) \mid$		$\mid \psi(x,t) \mid$	
		HWCM	**HAM** [5]	**HWCM**	**HAM** [5]
0.125	0.125	0.015386	0.015609	0.015323	0.008203
	0.375	0.138522	0.139708	0.137974	0.074131
	0.625	0.385897	0.376762	0.384668	0.225031
	0.875	0.763618	0.919085	0.763415	0.811099
0.375	0.125	0.013951	0.015608	0.013522	0.008203
	0.375	0.125873	0.139708	0.122165	0.074132
	0.625	0.357309	0.376762	0.348789	0.225031
	0.875	0.748433	0.919085	0.746600	0.811099
0.625	0.125	0.011025	0.015609	0.009723	0.008203
	0.375	0.100259	0.139708	0.088875	0.074132
	0.625	0.296585	0.376762	0.272878	0.225031
	0.875	0.696443	0.919085	0.705993	0.811099
0.875	0.125	0.008579	0.015609	0.004118	0.008202
	0.375	0.079810	0.139708	0.040065	0.074131
	0.625	0.235819	0.376762	0.162549	0.225031
	0.875	0.623663	0.919085	0.660364	0.811099

TABLE VI
COMPARISON BETWEEN HAAR SOLUTIONS ($J = 1, m = 4, \nu = 0.9$) AND HAM [5] OF PROBLEM 4

t	x	$\mid \phi(x,t) \mid$		$\mid \psi(x,t) \mid$	
		HWCM	**HAM** [5]	**HWCM**	**HAM** [5]
0.125	0.125	0.015395	0.013101	0.015357	0.013101
	0.375	0.138552	0.117724	0.138256	0.118102
	0.625	0.385995	0.322206	0.384873	0.336649
	0.875	0.763808	0.631637	0.763550	0.834047
0.375	0.125	0.013964	0.013101	0.013688	0.013101
	0.375	0.125649	0.117724	0.123396	0.118102
	0.625	0.357809	0.322206	0.349879	0.336649
	0.875	0.749377	0.631637	0.747267	0.834047
0.625	0.125	0.010878	0.013101	0.009803	0.013101
	0.375	0.099177	0.117725	0.089536	0.118102
	0.625	0.296418	0.322206	0.273663	0.336649
	0.875	0.694211	0.631637	0.701977	0.834047
0.875	0.125	0.008446	0.013101	0.003678	0.013101
	0.375	0.085571	0.117725	0.040710	0.118102
	0.625	0.231591	0.322206	0.157683	0.336649
	0.875	0.604013	0.631637	0.640823	0.834047

VI. CONCLUSION

In this paper, we extended the capability of the Haar wavelet collocation method (HWCM) for the solution of time-fractional coupled system of partial differential equations. The main advantage of HWCM is the ability to achieve a good solution and rapid convergence with small number of collocation points. The presence of maximum zeros in the Haar matrices reduces the number of unknown wavelet coefficients that is to be determined, which as a result diminishes the computation time as well. The scheme is tested on some examples of time fractional Schrödinger equations. The presented procedure may very well be extended to solve two dimensional Schrödinger equation and other similar nonlinear problems of partial differential equations of fractional order. The problem discussed here is just for showing the applicability of the proposed computational technique to handle the complex system of differential equation in fractional-order problems in a straight forward way. Also, the Haar wavelet method proves to be capable to efficiently handle the nonlinearity of partial differential equations of fractional order. The main advantages of the proposed algorithm are, its simple application and no requirement of residual or product operational matrix. Numerical solutions for different order of fractional time derivative by Haar wavelet are shown in Tables and Figures. The increasing values of ν show that the solutions are valuable in understanding their respective exact solutions for $\nu = 1$. Comparisons between our approximate solutions of the problems with their actual solutions and with the approximate solutions achieved by a homotopy analysis method [5] confirm the validity and accuracy of our scheme.

REFERENCES

[1] K. Diethelm, The analysis of fractional differential equations, Springer-Verlag, Berlin, 2010.

[2] I. Podlubny, Fractional Differential equations. Academic Press San Diego, 1999.

[3] M. G. Sakar, F. Erdogan, and A. Yldrm, Variational iteration method for the time-fractional Fornberg-Whitham equation, *Computers and Mathematics with Applications*, 2012, **63**(9): 1382-1388.

[4] J. Liu and G. Hou, Numerical solutions of the space- and time-fractional coupled Burgers equations by generalized differential transform method, *Applied Mathematics and Computation*, 2011, **217**(16): 7001-7008.

[5] N. A. Khan, M. Jamil, and A. Ara, Approximate Solutions to Time-Fractional Schrödinger Equation via Homotopy Analysis Method, *ISRN Mathematical Physics*, 2012, Article ID 197068http://dx.doi.org/10.5402/2012/197068.

[6] A. H. Bhrawy, E. H. Doha, S. S. Ezz-Eldien, and R. A. Van Gorder, A new Jacobi spectral collocation method for solving 1+1 fractional Schrödinger equations and fractional coupled Schrödinger systems, *THE EUROPEAN PHYSICAL JOURNAL PLUS*, 2014 **129**:(260) DOI 10.1140/epjp/i2014-14260-6.

[7] A. H. Bhrawy and M. A. Zaky, A method based on the Jacobi tau approximation for solving multi-term time-space fractional partial differential equations, *Journal of Computational Physics*, 2015, **281**: 876-895.

[8] A. Bhrawy and M. Zaky, A fractional-order Jacobi Tau method for a class of time-fractional PDEs with variable coefficients, *Maththematical Methods in the Applied Sciences*, 2015, DOI: 10.1002/mma.3600.

[9] Z. J. Fu, W. Chen, and H. T. Yang, Boundary particle method for Laplace transformed time fractional diffusion equations, *Journal of Computational Physics*, 2013, **235**: 52-66.

[10] H. Aminikhah, A. R. Sheikhani, and H. Rezazadeh, An Efficient Method for Time-Fractional Coupled Schrödinger System, *International Journal of Partial Differential Equations*, 2014, Article ID 137470: http://dx.doi.org/10.1155/2014/137470.

[11] V. Daftardar-Gejji and a. Babakhani, Analysis of a system of fractional differential equations, *Journal of Mathematical Analysis and Applications*, **293**, 2004, :511-522.

[12] V. Daftardar-Gejji and H. Jafari, Adomian decomposition: A tool for solving a system of fractional differential equations, *Journal of Mathematical Analysis and Application*, 2005 **301**: 508-518.

[13] Y. Jiang and J. Ma, High-order finite element methods for time-fractional partial differential equations, *Journal of Computational and Applied Mathematics*, 2011, **235**(11): 3285-3290.

[14] Y. Hu, Y. Luo, and Z. Lu, Analytical solution of the linear fractional differential equation by Adomian decomposition method, *Journal of Computational and Applied Mathematics*, 2008, **215**(1): 220-229.

[15] Z. Odibat and S. Momani, Numerical methods for nonlinear partial differential equations of fractional order, *Applied Mathematical Modelling*, 2008,**32**(1): 28-39.

[16] A. K. Gupta and S. Saha Ray, Wavelet Methods for Solving Fractional Order Differential Equations, *Mathematical Problems in Engineering*, 2014, **2014**. Article ID 140453, doi:10.1155/2014/140453

[17] A. Setia and Y. Liu, Solution of linear fractional Fredholm integro-differential equation by using second kind Chebyshev wavelet, *11th International Conference on Information Technology (ITNG2014), Las Vegas, USA, April 7-9*, 2014, Las Vegas, USA.

[18] A. H. Bhrawy, M. M. Tharwat, and A. Yildirim, A new formula for fractional integrals of Chebyshev polynomials: Application for solving multi-term fractional differential equations, *Applied Mathematical Modelling*, 2013 **37**(6): 4245-4252.

[19] A. Setia, Y. Liu, A.S. Vatsala, Numerical solution of fredholm-volterra fractional integro-differential equations with nonlocal boundary conditions, *Journal of Fractional Calculus and Applications*, 2014, **5**(2): 155-165.

[20] N. Laskin, Fractional quantum mechanics, *The American Physical Society*, 2000, **62**(3): 3135-3145.

[21] M. Rehman and R. A. Khan, Existence and uniqueness of solutions for multi-point boundary value problems for fractional differential equations, *Applied Mathematics Letters*, 2010, **23**(9): 1038-1044.

[22] M. U. Rehman and R. A. Khan, Numerical solutions to initial and boundary value problems for linear fractional partial differential equations, *Applied Mathematical Modelling*, 2013, **37**(7): 5233-5244.

[23] J. Shen, T. Tang, Mathematics Monoqraph Series: Spectral and High-Order Methods, SCIENCE PRESS Beijjng.

[24] A. H. Bhrawy, T. M. Taha, and J. A. T. Machado, A review of operational matrices and spectral techniques for fractional calculus, *Nonlinear Dynamics*, 2015, DOI 10.1007/s11071-015-2087-0.

[25] E. H. Doha, A. H. Bhrawy, and S. S. Ezz-Eldien, A new Jacobi operational matrix: An application for solving fractional differential equations, *Applied Mathematical Modelling*, 2012, **36**(10): 4931-4943.

[26] A. H. Bhrawy and M. A. Zaky, Numerical simulation for two-dimensional variable-order fractional nonlinear cable equation, *Nonlinear Dynamics*., 2015, **80**(1-2): 101-116.

[27] Mallat Stephane G., A Theory for Multiresolution Signal Decomposition: The Wavelet Representation,*Pattern Analysis and Machine Intelligence, IEEE Transactions on*, 1989, **7**(9): 674-693.

[28] S. Mallat, A Wavelet Tour of Signal Processing A wavelet tour of signal processing, *Academic press*.

[29] Ü. Lepik, Solving PDEs with the aid of two-dimensional Haar wavelets, *Computers and Mathematics with Applications*, 2011, **61**(7): 1873-1879.

[30] S. Islam, I. Aziz and B. Šarler, The numerical solution of second-order boundary-value problems by collocation method with the Haar wavelets, *Mathematical and Computer Modelling*, 2010, **52**(9-10):1577-1590.

[31] Y. Li and W. Zhao, Haar wavelet operational matrix of fractional order integration and its applications in solving the fractional order differential equations, *Applied Mathematics and Computation*, 2010, **216**(8): 2276-2285.

[32] L. Wang, Y. Ma, and Z. Meng, Haar wavelet method for solving fractional partial differential equations numerically, *Applied Mathematics and Computation*, 2014, **227**: 66-76.

[33] A. Mohebbi, M. Abbaszadeh, and M. Dehghan, The use of a meshless technique based on collocation and radial basis functions for solving the time fractional nonlinear Schrödinger equation arising in quantum mechanics, *Engineering Analysis with Boundary Elements*, 2013, **37**(2): 475-485.

[34] D. Wang, A. Xiao, and W. Yang, Crank-Nicolson difference scheme for the coupled nonlinear Schrödinger equations with the Riesz space fractional derivative, *Journal of Computational Physics*, 2013, **242**: 670-681.

[35] L. Wei, X. Zhang, S. Kumar, and A. Yildirim, A numerical study based on an implicit fully discrete local discontinuous Galerkin method for the time-fractional coupled Schrödinger system, 2012, *Computers and Mathematics with Applications*, **64**(8): 2603-2615.

[36] A. H. Bhrawy and M. A. Abdelkawy, A fully spectral collocation approximation for multi-dimensional fractional Schrödinger equations, *Journal of Computational Physics*, 2015, **294**: 462-483.

[37] X. Guo and M. Xu, Some physical applications of fractional Schrödinger equation, *Journal of Mathematical Physics*, 2006, **47** Article ID 082104, doi: 10.1063/1.2235026.

[38] Y. Wei, Some Solutions to the Fractional and Relativistic Schrödinger Equations, *International Journal of Theoretical and Mathematical Physics*, 2015, **5**(5): 87-111.

[39] W. Chi-hsu, On the Generalization Operational Matrices and Operational, *The Franklin Institute*, 1983, **315**(2): 91-102.

Najeeb Alam Khan obtained the Ph. D. degree from University of Karachi in 2013. He is the assistant professor in the Department of Mathematics, University of Karachi. His research interest include the areas of Nonlinear system, Numerical methods, Approximate analytical methods, Fluid Mechanics, differential equations of applied mathematics, fractional calculus, fractional differential equation and theoretical analysis. He has published more than 75 refereed journal papers.

Tooba Hameed is a research scholar. Her research interest include Numerical methods, fractional calculus and differential equation.

Asymptotic Magnitude Bode Plots of Fractional-Order Transfer Functions

Ameya Anil Kesarkar, *Member, IEEE,* and N. Selvaganesan, *Senior Member, IEEE*

***Abstract*—Development of asymptotic magnitude Bode plots for integer-order transfer functions is a well-established topic in the control theory. However, construction of such plots for the fractional-order transfer functions has not received much attention in the existing literature. In the present paper, we investigate in this direction and derive the procedures for sketching asymptotic magnitude Bode plots for some of the popular fractional-order controllers such as PI^{α}, $[PI]^{\alpha}$, PD^{β}, $[PD]^{\beta}$, and $PI^{\alpha}D^{\beta}$. In addition, we deduce these plots for general fractional commensurate-order transfer functions as well. As applications of this work, we illustrate (i) the analysis of the designed fractional-control loop and (ii) the identification of fractional-order transfer function from a given plot.**

***Index Terms*—Asymptotic magnitude bode, commensurate-Order, fractional-Order.**

I. Introduction

Bode plot [1], [2] plays an important role in the control theory for graphically visualizing the frequency behavior of a transfer function. Generally, software tools such as MATLAB, SCILAB, etc. are used for obtaining an accurate Bode plot as it involves significant amount of computational efforts. However, one can sketch a good straight-line approximation of the exact Bode plot known as asymptotic Bode plot [3], [4] by doing a few simple calculations.

Asymptotic Bode plots are useful for quick manual analysis of a designed control system with a reasonable degree of accuracy [5]. They are also important for understanding the role of each parameter of the given transfer function in deciding the shape of its Bode response [6]. This knowledge, in particular about the controller structures is very important to a design engineer for manually tuning the control system. The procedures to sketch asymptotic Bode plots of *integer-order* transfer functions are well-established in the existing theory [3] [4].

Fractional calculus [7] generalizes the notion of *integer-order* transfer functions to arbitrary orders, which leads to the existence of *fractional-order* transfer functions [8]−[10]. The control theory finds application of fractional calculus in the form of fractional-order controllers such as PI^{α}, $[PI]^{\alpha}$, PD^{β}, $[PD]^{\beta}$, $PI^{\alpha}D^{\beta}$, etc. which have *fractional-order* transfer functions [9]−[11].

For a given fractional-order transfer function, one may consider its integer-order approximation to sketch its asymptotic Bode plot using existing procedures for integer-order transfer functions. However, the development of asymptotic Bode plots of fractional-order transfer functions in their original irrational-form has not received much attention in the literature. In [11], [12], only a brief mention is found about such plots in the context of fractional-order lead compensator. Therefore, it is important to formulate and analytically justify development of asymptotic plots for general fractional-order transfer functions, which is undoubtedly lacking in the existing literature. In the current paper, we obtain asymptotic magnitude Bode plots of: a) PI^{α}, $[PI]^{\alpha}$, PD^{β}, $[PD]^{\beta}$, $PI^{\alpha}D^{\beta}$ controllers and b) general fractional commensurate-order transfer functions. The contributions of our paper are summarized as follows:

1) To define basic fractional-order terms and develop their individual asymptotic magnitude Bode plots.
2) To utilize above plots for developing asymptotic magnitude Bode plots of:
   a) Fractional-order controllers such as PI^{α}, $[PI]^{\alpha}$, PD^{β}, $[PD]^{\beta}$, $PI^{\alpha}D^{\beta}$.
   b) General fractional commensurate-order transfer functions.
3) To illustrate the applications of these plots for:
   a) Performance analysis of designed fractional-order control loop.
   b) Identifying fractional-order transfer function from given asymptotic magnitude plot.

II. Asymptotic Magnitude Bode Plots of Basic Terms

We introduce a few basic fractional-order terms given in Table I, where K, a, a_1, $a_2 \in \mathbb{R}$ and $\alpha, \beta \in \mathbb{R}_{>0}$.

First, we explain the development of asymptotic magnitude Bode plots for terms namely, constant gain, fractional zero, and fractional double-term pole. Later, such plots are obtained for the remaining terms.

A. Constant Gain

It is easy to see that for the constant gain transfer function $T(s) = K$, the magnitude $|T(j\omega)|_{dB} = 20log_{10}|K|$, $\forall\omega$. Therefore, to draw magnitude Bode plot of constant gain, one just has to sketch a horizontal line at $20log_{10}|K|$. In Bode

This article has been accepted for publication in a future issue of this journal, but has not been fully edited. Content may change prior to final publication.

This article was recommended by Associate Editor Dingyü Xue.

Ameya Anil Kesarkar (Corresponding Author) is with Space Applications Centre (SAC), Indian Space Research Organization (ISRO), Ahmedabad, Gujarat, India. (email: ameyakesarkar27@gmail.com)

N. Selvaganesan is with the Department of Avionics, Indian Institute of Space Science and Technology (IIST), Thiruvananthapuram, Kerala, India. (email: n_selvag@iist.ac.in)

Digital Object Identifier 10.1109/JAS.2016.7510196

plot, x-axis represents frequency (ω) in rad/s on a logarithmic scale and y-axis represents magnitude in dB on a linear scale.

TABLE I
BASIC FRACTIONAL-ORDER TERMS

TERM DESCRIPTION	TRANSFER FUNCTION ($T(s)$)
CONSTANT GAIN	K
FRACTIONAL ZERO	$s^\alpha + a$
FRACTIONAL POLE	$\frac{1}{s^\alpha + a}$
FRACTIONAL ZERO AT ORIGIN	s^α
FRACTIONAL POLE AT ORIGIN	$\frac{1}{s^\alpha}$
FRACTIONAL [ZERO]	$(s+a)^\alpha$
FRACTIONAL [POLE]	$\frac{1}{(s+a)^\alpha}$
FRACTIONAL DOUBLE-TERM ZERO	$s^{\alpha+\beta} + a_1 s^\alpha + a_2$
FRACTIONAL DOUBLE-TERM POLE	$\frac{1}{s^{\alpha+\beta}+a_1 s^\alpha + a_2}$

B. Fractional Zero

The transfer function of fractional zero is given by:

$$T(s) = (s)^\alpha + a$$

Substituting $s = j\omega$ (where, $\omega \in \mathbb{R}_{\geq 0}$) results into:

$$T(j\omega) = (j\omega)^\alpha + a$$

Therefore, the magnitude in dB is given by,

$$|T(j\omega)|_{dB} = 20log_{10}\left(a^2 + \omega^{2\alpha} + 2a\omega^\alpha cos\left(\frac{\pi\alpha}{2}\right)\right)^{\frac{1}{2}}$$

In the sum $\left(a^2 + \omega^{2\alpha} + 2a\omega^\alpha cos\left(\frac{\pi\alpha}{2}\right)\right)$, the term a^2 dominates at lower frequencies whereas the term $\omega^{2\alpha}$ dominates at higher frequencies. For the intended approximation, we choose the corner frequency (or break frequency) ω_{cr} such that these terms are equal, that is, $a^2 = \omega^{2\alpha}|_{\omega=\omega_{cr}}$. From which, one obtains the corner frequency, $\omega_{cr} = |a|^{\frac{1}{\alpha}}$. Thus, the following approximation of the magnitude is obtained:

1) For $\omega \leq \omega_{cr}$, $|T(j\omega)|_{dB} = 20log_{10}\left(a^2\right)^{\frac{1}{2}} = 20log_{10}|a|$.
2) For $\omega > \omega_{cr}$, $|T(j\omega)|_{dB} = 20log_{10}\left(\omega^{2\alpha}\right)^{\frac{1}{2}} = 20\alpha log_{10}\omega$.

Based on the above discussion, we lay down the following procedure to construct the asymptotic magnitude plot for $(s^\alpha + a)$ shown in Fig. 1:

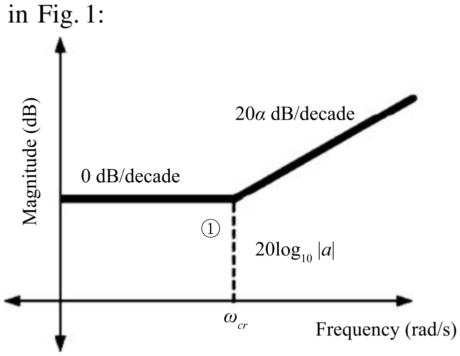

Fig. 1. Asymptotic Magnitude Bode Plot for Fractional Zero.

Procedure:

1) Compute the corner frequency $\omega_{cr} = |a|^{\frac{1}{\alpha}}$ and locate point ① at magnitude $20log_{10}|a|$.
2) Draw a line with slope 0 dB/decade for $\omega \leq \omega_{cr}$, and a line with slope 20α dB/decade for $\omega > \omega_{cr}$ as shown in Fig. 1.

Comparison with Real Magnitude Bode Plot:

1) At this point, let us compare the asymptotic magnitude Bode plot with the real magnitude Bode plot for the *Fractional Zero* term $(s^\alpha + a)$. For this purpose, let the numerical values be: $\alpha = 0.9, a = 2$.[1]
2) Fig. 2 shows the real as well as asymptotic magnitude Bode plots for the fractional zero term, $(s^{0.9} + 2)$.
3) As seen from Fig. 2, the asymptotic plot follows the real plot quite closely, thereby confirming the correctness of our asymptotic formulation.

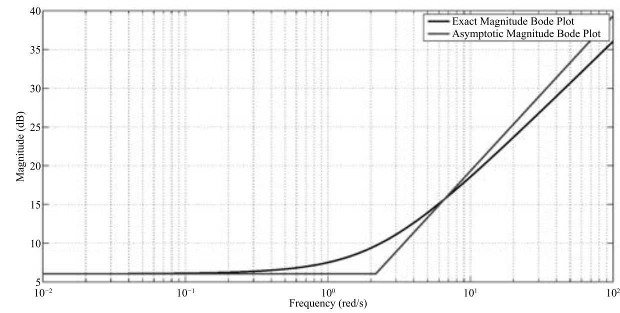

Fig. 2. Real and Asymptotic Magnitude Bode Plot for $(s^{0.9} + 2)$

C. Fractional Double-Term Pole

The transfer function of fractional double-term pole is given by $T(s) = \frac{1}{(s^{\alpha+\beta}+a_1 s^\alpha + a_2)}$. Substituting $s = j\omega$ (where, $\omega \in \mathbb{R}_{\geq 0}$) leads to:

$$T(j\omega) = \frac{1}{(j\omega)^{\alpha+\beta} + a_1(j\omega)^\alpha + a_2}$$

The decibel magnitude of $T(j\omega)$ is given by,

$$|T(j\omega)|_{dB} = -20log_{10}\Big(\omega^{2(\alpha+\beta)} + a_1^2\omega^\alpha + a_2^2 + 2a_1\omega^{2\alpha+\beta}cos\left(\frac{\pi\beta}{2}\right) + 2a_2\omega^{\alpha+\beta}cos\left(\frac{\pi(\alpha+\beta)}{2}\right) + 2a_1a_2\omega^\alpha cos\left(\frac{\pi\alpha}{2}\right)\Big)^{\frac{1}{2}}$$

In the sum $\left(\omega^{2(\alpha+\beta)} + a_1^2\omega^\alpha + a_2^2 + 2a_1\omega^{2\alpha+\beta}cos\left(\frac{\pi\beta}{2}\right) + 2a_2\omega^{\alpha+\beta}cos\left(\frac{\pi(\alpha+\beta)}{2}\right) + 2a_1a_2\omega^\alpha cos\left(\frac{\pi\alpha}{2}\right)\right)$, the term a_2^2 dominates at lower frequencies whereas the term $\omega^{2(\alpha+\beta)}$ dominates at higher frequencies. For the approximation purpose, the corner frequency ω_{cr} is chosen such that the dominant terms are equal,

$$a_2^2 = [\omega^{2(\alpha+\beta)}]_{\omega=\omega_{cr}}$$

Therefore, one gets the corner frequency,

$$\omega_{cr} = |a_2|^{\frac{1}{(\alpha+\beta)}}$$

Hence, the following magnitude approximation is obtained:

1) For $\omega \leq \omega_{cr}$:

$$|T(j\omega)|_{dB} = -20log_{10}|a_2|$$

[1]Although only one numerical example has been illustrated here, one may consider different sets of parameter values for the numerical confirmation.

2) For $\omega > \omega_{cr}$:

$$|T(j\omega)|_{dB} = -20log_{10}|\omega^{(\alpha+\beta)}| = -20(\alpha+\beta)log_{10}\omega$$

From the discussion above, following procedure is stated to sketch asymptotic magnitude Bode plot for fractional double-term pole $\frac{1}{(s^{\alpha+\beta}+a_1 s^{\alpha}+a_2)}$ shown in Fig. 3:

Procedure:

1) Compute the corner frequency $\omega_{cr} = |a_2|^{\frac{1}{(\alpha+\beta)}}$ and locate point ① at magnitude $-20log_{10}|a_2|$.

2) Draw a line with slope 0 dB/decade for $\omega \leq \omega_{cr}$, and a line with slope $-20(\alpha+\beta)$ dB/decade for $\omega > \omega_{cr}$ as shown in Fig. 3.

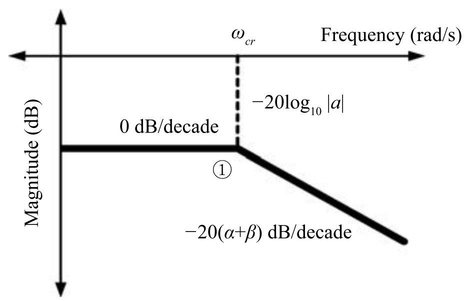

Fig. 3. Asymptotic Magnitude Bode Plot for Fractional double-term Pole.

Comparison with Real Magnitude Bode Plot:

1) Let us consider a numerical example of finding the magnitude Bode plot of the *Fractional Double-Term Pole* term, with the parameters: $\alpha = 0.5, \beta = 0.9, a_1 = 2, a_2 = 3$.

2) Fig. 4 shows the real as well as asymptotic magnitude Bode plots for fractional double-term pole, $\frac{1}{(s^{(0.5+0.9)}+2s^{0.5}+3)}$.

As seen from Fig. 4, the asymptotic plot follows the real plot quite closely, thereby confirming the correctness of our formulation.

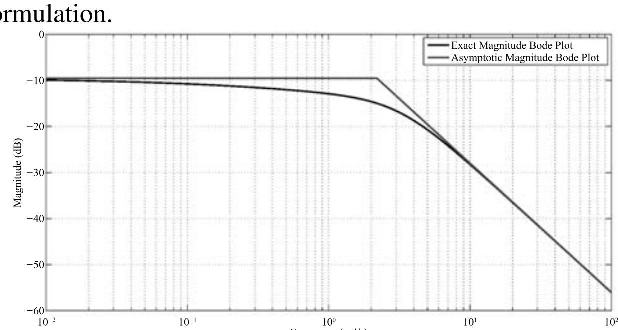

Fig. 4. Real and Asymptotic Magnitude Bode Plot for $\frac{1}{(s^{(0.5+0.9)}+2s^{0.5}+3)}$

Similarly, one can obtain such plots for terms: $\frac{1}{s^{\alpha}+a}$, s^{α}, $\frac{1}{s^{\alpha}}$, $(s+a)^{\alpha}$, $\frac{1}{(s+a)^{\alpha}}$, and $s^{\alpha+\beta} + a_1 s^{\alpha} + a_2$. The results are summarized in Tables II and III. Also, in each case, the comparison is made between the real and asymptotic plots using suitable examples. It can be seen from the Tables II and III that for the numerical cases under consideration, the asymptotic and real Bode plots are quite close to each other.[2]

[2]As seen from Table II, in case of fractional zero at origin (s^{α}) the asymptotic and real plots 'coincide' (as the magnitude with both, the real and asymptotic formulation, turns out to be: $20\alpha log_{10} w$). Therefore, for the numerical example, the plots overlap each other. The same is also true in case of fractional pole at origin ($\frac{1}{s^{\alpha}}$).

Remark 1: It can be observed in Tables II and III that since the transfer functions of fractional zero and fractional pole are reciprocal to each other, their magnitude plots are mirror images of each other with respect to ω-axis. This is also true for pairs such as fractional pole and zero at origin, fractional [pole] and [zero], fractional double-term pole and zero.

D. Asymptotic Magnitude Bode Plots for Fractional-Order Controllers

In the present subsection, the asymptotic magnitude Bode plots of basic fractional-order terms are used to obtain such plots for fractional-order controllers, PI^{α}, $[PI]^{\alpha}$, PD^{β}, $[PD]^{\beta}$, and $PI^{\alpha}D^{\beta}$.

Let us consider PI^{α} controller which has the transfer function:

$$C(s) = K_p\left(1+\frac{K_i}{s^{\alpha}}\right) = (K_p)\left(s^{\alpha}+K_i\right)\left(\frac{1}{s^{\alpha}}\right) \quad (1)$$

As observed in (1), PI^{α} is expressed as a product of transfer functions of constant gain, fractional zero and fractional pole at origin. Therefore, the asymptotic magnitude Bode plot of PI^{α} can be obtained by *adding* such plots of its constituent elements as shown in Table IV. Similarly, one can develop the asymptotic magnitude Bode plots for $[PI]^{\alpha}$, PD^{β}, $[PD]^{\beta}$, and $PI^{\alpha}D^{\beta}$ controllers as summarized in Table V.

Remark 2: The asymptotic magnitude Bode plots of fractional-order controllers are obtained from those of basic fractional-order terms. Therefore, we do not pursue the comparison between asymptotic and real magnitude Bode plots for the fractional-order controllers exclusively. Nevertheless, in Section IV, a numerical example is considered to demonstrate the analysis of fractional control loop using the asymptotic formulation, wherein the real and asymptotic plots have been compared.

III. ASYMPTOTIC MAGNITUDE BODE PLOTS FOR GENERAL FRACTIONAL COMMENSURATE-ORDER TRANSFER FUNCTIONS

Let us consider a general fractional-order transfer function,

$$\frac{Y(s)}{U(s)} = \frac{b_m s^{\beta_m} + b_{m-1}s^{\beta_{m-1}} + ... + b_0 s^{\beta_0}}{a_n s^{\alpha_n} + a_{n-1}s^{\alpha_{n-1}} + ... + a_0 s^{\alpha_0}} \quad (2)$$

The transfer function (2) represents a *commensurate*-order system, if there exists a greatest common divisor $q \in \mathbb{R}$ such that $\alpha_i = qe_i(i = 0, 1, 2, \ldots, n), \beta_k = qf_k(k = 0, 1, 2, \ldots, m); e_i, f_k \in \mathbb{Z}$. Here, q is called the commensurate order, which can be rational or irrational. Therefore,

$$T(s) := \frac{Y(s)}{U(s)} = \frac{P(s^q)}{Q(s^q)}$$

where, $P(.), Q(.)$ are polynomial functions. If $p = s^q$, then,

$$T(p) = \frac{P(p)}{Q(p)} \quad (3)$$

On factorization, (3) can be expressed as follows[3]:

[3]This is because any polynomial with real coefficients has either real roots or complex roots in pairs. The real roots lead to terms of the form $(p + c_i), (p+g_k)$ and complex roots in pairs lead to terms such as $(d_j p^2 + e_j p + f_j), (h_l p^2 + o_l p + q_l)$.

TABLE II
ASYMPTOTIC MAGNITUDE BODE PLOTS FOR REMAINING BASIC FRACTIONAL-ORDER TERMS

Term & Corner Frequency	**Asymptotic Magnitude Bode Plot**	**Numerical Example**
Fractional Pole, $\frac{1}{s^{\alpha}+a}$ $\omega_{cr}=\lvert a\rvert^{\frac{1}{\alpha}}$ (For Numerical Example, α=0.9,a=2)	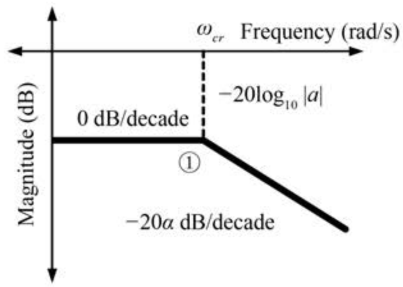	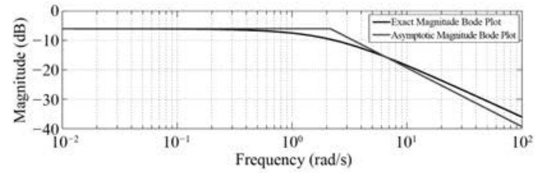
Fractional Zero at Origin,s^{α} (For Numerical Example, α=0.9)	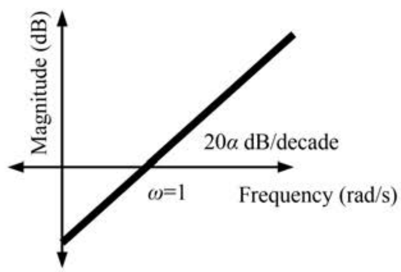	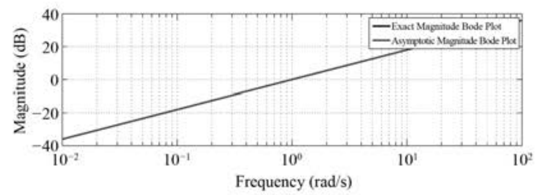
Fractional Zero at Origin, $\frac{1}{s^{\alpha}}$ (For Numerical Example, α=0.9)	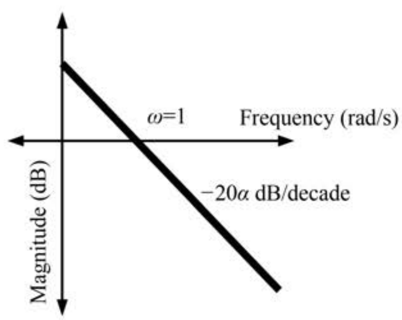	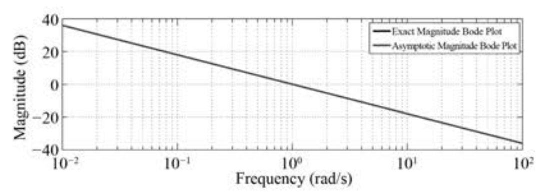

$$T(p)=\frac{\prod_{i=0}^{m_1}(p+c_i)\prod_{j=0}^{m_2}(d_jp^2+e_jp+f_j)}{\prod_{k=0}^{m_3}(p+g_k)\prod_{l=0}^{m_4}(h_lp^2+o_lp+z_l)}$$

where c_i $(i=0,1,\ldots m_1)$, d_j,e_j,f_j $(j=0,1,\ldots m_2)$, g_k $(k=0,1,\ldots m_3)$, h_l,o_l,z_l $(l=0,1,\ldots m_4)$ are real constants. m_1,m_2,m_3,m_4 are positive integers.

Now, by re-substituting $p=s^q$, one gets,

$$T(s)=\frac{\prod_{i=0}^{l_1}(s^q+c_i)\prod_{j=0}^{l_2}(d_js^{2q}+e_js^q+f_j)}{\prod_{k=0}^{l_3}(s^q+g_i)\prod_{l=0}^{l_4}(h_ls^{2q}+o_ls^q+z_l)} \quad (4)$$

It is seen that (4) is composed of fractional zeros, fractional poles, fractional double-term zeros and fractional double-term poles. Hence, one can construct asymptotic Bode plots of $T(s)$ by adding such plots of their constituent terms similar to the PI^{α} case explained in Table IV.

IV. APPLICATIONS OF ASYMPTOTIC MAGNITUDE BODE PLOTS

In this section, we demonstrate two applications of asymptotic magnitude Bode formulations, 1) Analysis of fractional control loop and 2) Identification of fractional-order transfer function from asymptotic magnitude plot.

A. Analysis of Fractional Control Loop

Let us suppose that we have tuned a $[PD]^{\beta}$ controller for a type-1 motion plant of the form $\frac{K}{s(Ts+1)}$ to meet required gain crossover frequency (ω_{gc}), phase margin (ϕ_m), and isodamping property [13] by following the methodology given in [14]. The numerical values are: $K=1,T=0.4,\omega_{gc}=10$ $rad/s,\phi_m=70°$. The plant ($G(s)$) and designed controller ($C(s)$) are as follows:

TABLE III
ASYMPTOTIC MAGNITUDE BODE PLOTS FOR REMAINING BASIC FRACTIONAL-ORDER TERMS

Term & Corner Frequency	Asymptotic Magnitude Bode Plot	Numerical Example
Fractional [Zero], $(s+a)^{\alpha}$ $\omega_{cr}=\lvert a\rvert$ (For Numerical Example, $\alpha=0.9, a=2$)	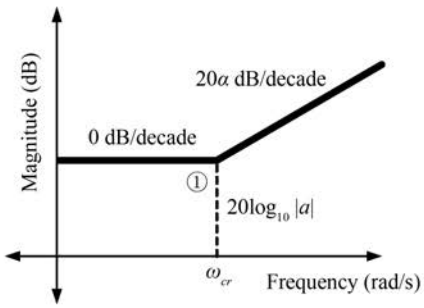	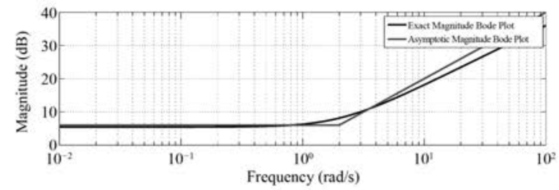
Fractional [Pole], $\frac{1}{(s+a)^{\alpha}}$ $\omega_{cr}=\lvert a\rvert$ (For Numerical Example, $\alpha=0.9, a=2$)	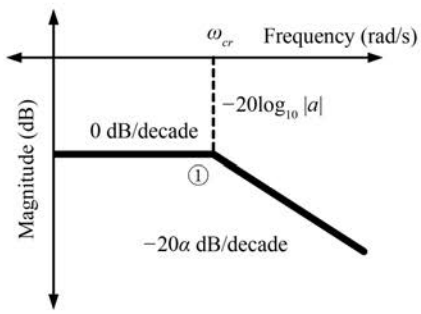	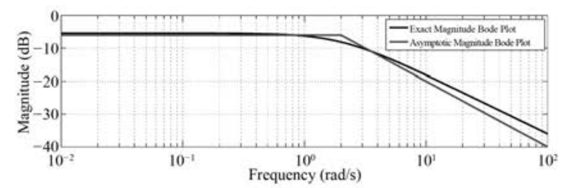
Fractional Double-Term Zero, $(s^{\alpha+\beta}+a_1 s^{\alpha}+a_2)$ $\omega_{cr}=\lvert a_2\rvert^{\frac{1}{(\alpha+\beta)}}$ (For Numerical Example, $\alpha=0.9, \beta=0.9, a_1=2, a_2=3$)	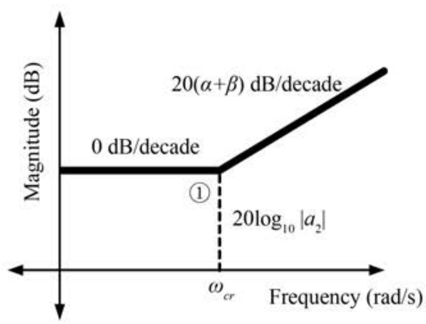	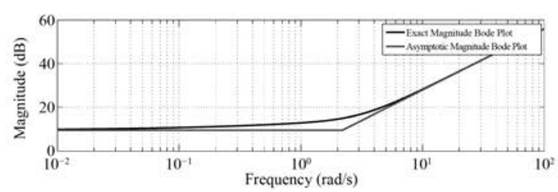

$$
\begin{aligned}
G(s) &= \frac{1}{s(0.4s+1)}, C(s) = 16.7780(1+0.2992s)^{0.7826} \\
\therefore L(s) & \\
&= C(s)G(s) = 16.7780(1+0.2992s)^{0.7826}\frac{1}{s(0.4s+1)} \\
&= (16.3143)\left(s+\frac{1}{0.2992}\right)^{0.7826}\left(\frac{1}{s^1}\right)\frac{1}{(s^1+2.5)}
\end{aligned} \tag{5}
$$

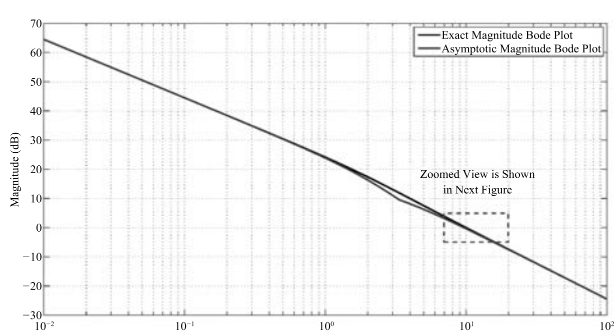

Fig. 5. Application of Asymptotic Magnitude Plot for Loop Analysis.

Our focus is to illustrate the usefulness of earlier formulations for analyzing magnitude Bode characteristics of the designed loop transfer function $L(s)$. More precisely, we intend to verify the gain crossover frequency met by $L(s)$. From (5), it can be seen that $L(s)$ is composed of basic terms defined in Section II. One can draw their individual asymptotic plots and add them to get the plot for $L(s)$. Fig. 5 presents exact and asymptotic magnitude bode plots for $L(s)$.

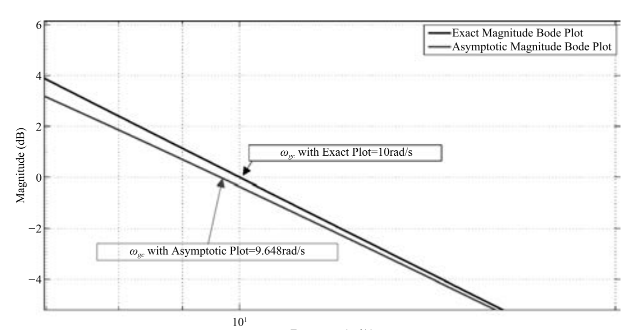

Fig. 6. Identification of Fractional-Order transfer function from Asymptotic Magnitude Bode Plot

TABLE IV
ASYMPTOTIC MAGNITUDE BODE PLOT FOR PI^α CONTROLLER

Term	Asymptotic Magnitude Bode Plot
Constant Gain, K_p	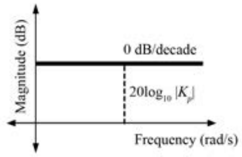
Fractional Zero, $s^\alpha+K_i$ $\omega_{cr}=\lvert K_i\rvert^{\frac{1}{\alpha}}$	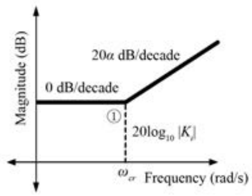
Fractional Pole at Origin, $\frac{1}{s^\alpha}$	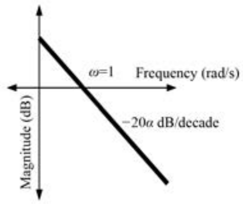
On adding the above plots, one gets:	
PI^α Controller $=K_p(1+\frac{K_i}{s^\alpha})$ $=(K_p)(s^\alpha+K_i)(\frac{1}{s^\alpha})$ $\omega_{cr}=\lvert K_p\rvert^{\frac{1}{\alpha}}$	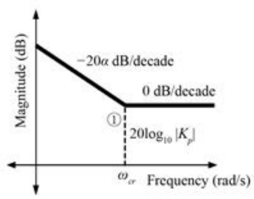

TABLE V
ASYMPTOTIC MAGNITUDE BODE PLOTS FOR OTHER FRACTIONAL-ORDER CONTROLLERS

Controller	Asymptotic Magnitude Bode Plot
$[PI]^\alpha$ $=K_p(1+\frac{K_i}{s})^\alpha$ $=K_p(s+K_i)^\alpha(\frac{1}{s^\alpha})$ $\omega_{cr}=\lvert K_i\rvert$	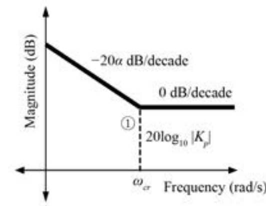
PD^β $=K_p(1+K_d s^\beta)$ $=K_pK_d(s^\beta+\frac{1}{K_d})$ $\omega_{cr}=\lvert\frac{1}{K_d}\rvert^{\frac{1}{\beta}}$	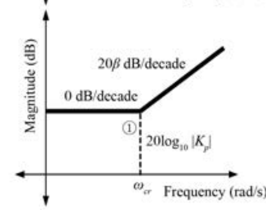
PD^β $=K_p(1+K_d s)^\beta$ $=K_pK_d^\beta(s+\frac{1}{K_d})^\beta$ $\omega_{cr}=\lvert\frac{1}{K_d}\rvert$	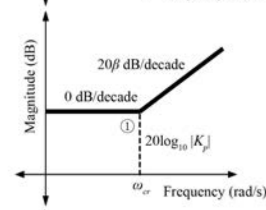
$PI^\alpha D^\beta$ $=K_p(1+\frac{K_i}{s^\alpha}+K_d s^\beta)$ $=K_pK_d(s^{\alpha+\beta}+\frac{s^\alpha}{K_d}+\frac{K_i}{K_d})\frac{1}{s^\alpha}$ $\omega_{cr}=\lvert\frac{K_i}{K_d}\rvert^{\frac{1}{(\alpha+\beta)}}$	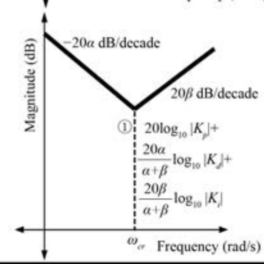

The zoomed view of a selected portion of Fig. 5 is shown in Fig. 6. From Fig. 6, it is seen that the ω_{gc} values with asymptotic and exact magnitude Bode plots (9.648 and 10 rad/s, respectively) are quite close to each other. This confirms the correctness of our formulations.

B. Identification of Fractional-Order Transfer Function

Let us consider a general asymptotic magnitude Bode plot as shown in Fig. 7 (Where, $a_1, a_2, \ldots a_n \in \mathbb{R}_{>0}, b_1, b_2, \ldots b_{n+1} \in \mathbb{R}$). It is desired to identify the fractional-order transfer function corresponding to the asymptotic magnitude Bode plot in Fig. 7. It must be noted that in Fig. 7, the straight-line approximations assume any arbitrary slope. (In integer-order transfer function case, such slopes are always integer multiples of 20.)

Prior to identification, it is essential to consider the asymptotic magnitude Bode plots of following composite terms:

1) ks^α (where, $k, \alpha \in \mathbb{R}$)

ks^α is composed of constant gain k and the term s^α. Based on the value of α, there are following possible cases:

a) $\alpha > 0$: In such case, s^α is fractional zero at origin. Asymptotic magnitude Bode plot of ks^α obtained from its constituent terms is shown in Fig. 8. Figure is sketched for $|k| > 1$. One can also sketch the corresponding one for $|k| < 1$.

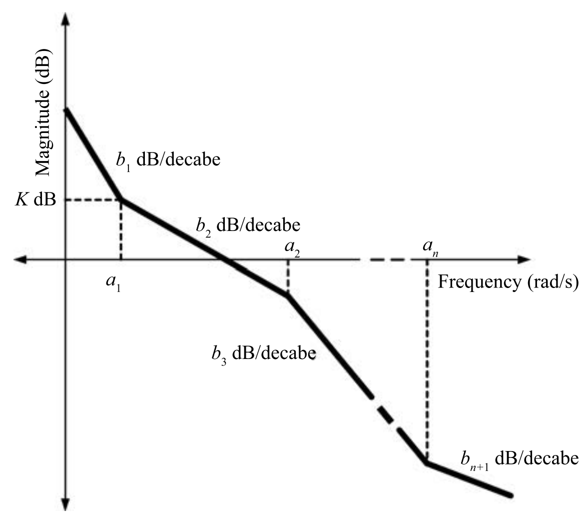

Fig. 7. Identification of Fractional-Order transfer function from Asymptotic Magnitude Bode Plot

b) $\alpha < 0$: In this case, s^α represents fractional pole at origin. Fig. 9 shows the asymptotic magnitude Bode plot for ks^α.

c) $\alpha = 0$: For this case, ks^α reduces to k. The discussion for asymptotic magnitude plot for such a term was made in Section II-A.

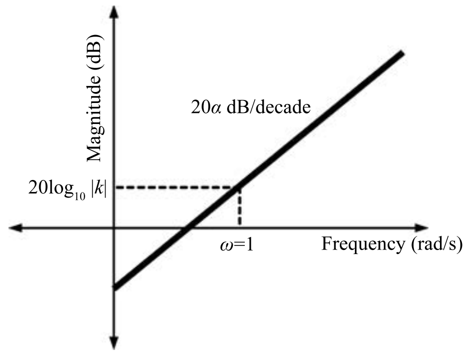

Fig. 8. Asymptotic Magnitude Bode Plot for ks^{α} when $\alpha < 0$.

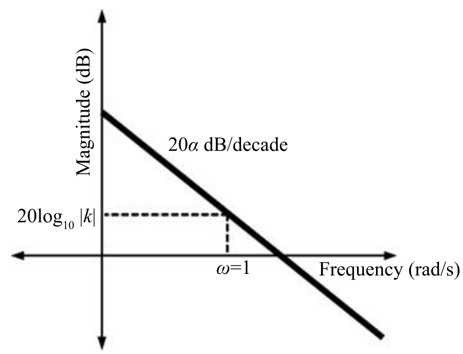

Fig. 9. Asymptotic Magnitude Bode Plot for $\frac{(s+a)^{\alpha}}{a^{\alpha}}$ when $\alpha > 0$.

Remark: It can be inferred from the above asymptotic plots that the term ks^{α} is identified when a line of given slope offset by a known magnitude is observed.

2) $\frac{(s+a)^{\alpha}}{a^{\alpha}}$ (where, $a \in \mathbb{R}$, $\alpha \in R_{\neq 0}$)

$\frac{(s+a)^{\alpha}}{a^{\alpha}}$ is composed of constant gain $\frac{1}{a^{\alpha}}$ and the term $(s+a)^{\alpha}$. When $\alpha > 0$, $(s+a)^{\alpha}$ represents fractional [zero]. For such case, the asymptotic magnitude plot of $\frac{(s+a)^{\alpha}}{a^{\alpha}}$ obtained from its constituent elements is as shown in Fig. 10.

On the other hand, for $\alpha < 0$, $(s+a)^{\alpha}$ represents fractional [pole]. Therefore, the asymptotic magnitude plot of $\frac{(s+a)^{\alpha}}{a^{\alpha}}$ in this case takes the shape as shown in Fig. 11.

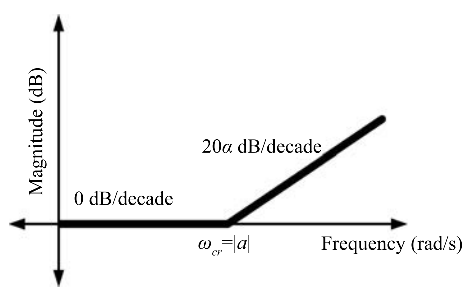

Fig. 10. Asymptotic Magnitude Bode Plot for $\frac{(s+a)^{\alpha}}{a^{\alpha}}$ when $\alpha > 0$.

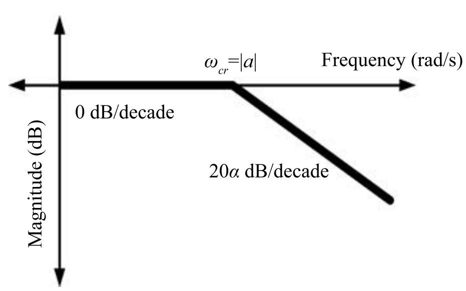

Fig. 10. Asymptotic Magnitude Bode Plot for $\frac{(s+a)^{\alpha}}{a^{\alpha}}$ when $\alpha < 0$.

Remark: It can be observed from Figs. 10 and 11 that,

1) $\frac{(s+a)^{\alpha}}{a^{\alpha}}$ with $\alpha > 0$ is identified when there is an 'increase' in slope at given corner frequency.

2) $\frac{(s+a)^{\alpha}}{a^{\alpha}}$ with $\alpha < 0$ is identified when there is a 'decrease' in slope at given corner frequency.

Based on above discussion, we identify the fractional-order transfer function from the asymptotic magnitude Bode plot given in Fig. 7 as follows:

1) From Fig. 7, it is seen that for the frequency range from 0 to a_1, the plot is a line with slope b_1 dB/decade. Recalling Remark 3, we identify the corresponding term as ks^{α} with $\alpha = \frac{b_1}{20}$ (Since, $20\alpha = b_1$). The constant k is obtained as follows:

From Fig. 7, $20log_{10}|ks^{\alpha}|_{s=ja_1} = K$.

Therefore, $|k| = \frac{10^{\frac{K}{20}}}{a_1^{\alpha}} \implies k = \pm \frac{10^{\frac{K}{20}}}{a_1^{\frac{b_1}{20}}}$.

2) At corner frequency a_1, there is an observed increase of slope from b_1 to b_2. From Remark 4, this corresponds to the term $\frac{(s+a)^{\alpha}}{a^{\alpha}}$ with $\alpha = \frac{b_2 - b_1}{20}$, $a = a_1$ (since, $b_2 > b_1$, $\alpha > 0$). Similarly, at corner frequency a_2, there is an observed decrease of slope from b_2 to b_3. From Remark 4, we get the corresponding term as $\frac{(s+a)^{\alpha}}{a^{\alpha}}$ with $\alpha = \frac{b_3 - b_2}{20}$, $a = a_2$ (since, $b_3 < b_2$, $\alpha < 0$). One can similarly obtain the terms for observed change in slopes at $a_3, a_4, \ldots, a_n$.

3) The individual identified terms are multiplied to get the complete transfer function $T(s)$ for the asymptotic magnitude plot given in Fig. 7 as follows:

$$T(s) = \pm \left(\frac{10^{\frac{K}{20}} s^{\frac{b_1}{20}}}{a_1^{\frac{b_1}{20}}} \right) \left(\frac{(s + a_1)^{\frac{b_2 - b_1}{20}}}{a_1^{\frac{b_2 - b_1}{20}}} \right) \left(\frac{(s + a_2)^{\frac{b_3 - b_2}{20}}}{a_2^{\frac{b_3 - b_2}{20}}} \right) \cdots \left(\frac{(s + a_n)^{\frac{b_{n+1} - b_n}{20}}}{a_n^{\frac{b_{n+1} - b_n}{20}}} \right)$$

It is important to note that the above general case considers asymptotic magnitude Bode plots containing lines with arbitrary slopes. Therefore, it also includes the integer-order transfer function cases when slopes are integer multiples of 20.

V. Conclusion

In this paper, we presented the construction of asymptotic magnitude Bode plots for popular fractional-order controllers such as PI^{α}, $[PI]^{\alpha}$, PD^{β}, $[PD]^{\beta}$, and $PI^{\alpha}D^{\beta}$. The plots were also developed for general fractional commensurate-order transfer functions. The applicability of this work to quickly analyze the performance of designed control system containing fractional-order elements was demonstrated with the help of a numerical example. We also showed the usefulness of our formulation in identifying fractional-order transfer function from the given asymptotic magnitude Bode plot. Development of asymptotic phase Bode plots for fractional-order transfer functions can be an another interesting direction to this work.

References

[1] H. W. Bode, "Relations between attenuation and phase in feedback amplifier design," *Bell Syst. Tech. J.*, vol. 19, no. 3, pp. 421−454, July. 1940.

[2] H. W. Bode, *Network Analysis and Feedback Amplifier Design*. New York: Van Nostrand, 1945.

[3] R. C. Dorf and R. H. Bishop, *Modern Control Systems*. 12th ed. Upper Saddle River, NJ: Pearson, 2011.

[4] B. C. Kuo, *Automatic Control Systems*. Englewood Cliffs: Prentice Hall PTR, 1981.

[5] J. J. Distefano, A. J. Stubberud, and I. J. Williams, *Schaum's Outline of Feedback and Control Systems*. New York, NY: McGraw-Hill Professional, 1997.

[6] D. Gajdošík and K. Žáková, "Bode plots in maxima computer algebra system," in *Proc. 18th Int. Conf. Process Control*, Tatranská Lomnica, Slovakia, 2011, pp. 352−355.

[7] K. B. Oldham and J. Spanier, *The fractional calculus: theory and applications of differentiation and integration to arbitrary order*. New York: Academic Press, 1974.

[8] I. Podlubny, "Fractional-order systems and $PI^{\lambda} D^{\mu}$-controllers," *IEEE Trans. Autom. Control*, vol. 44, no. 1, pp. 208−214, Jan. 1999.

[9] Y. Q. Chen, I. Petras, and D. Y. Xue, "Fractional order control-a tutorial," in *American Control Conf.*, St. Louis, MO, USA, 2009, pp. 1397−1411.

[10] D. Y. Xue, Y. Q. Chen, and D. P. Atherton, *Linear Feedback Control-Analysis and Design with MATLAB*. Philadelphia, Pennsylvania, USA: SIAM, 2007.

[11] C. A. Monje, A. J. Calderón, B. M. Vinagre, and V. Feliu, "The fractional order lead compensator," in *Proc. 2nd IEEE Int. Conf. Computational Cybernetics*, Vienna, 2004, pp. 347−352.

[12] C. A. Monje, Y. Q. Chen, B. M. Vinagre, D. Y. Xue, and V. Feliu, *Fractional-Order Systems and Controls: Fundamentals and Applications*. London: Springer, 2010.

[13] Y. Q. Chen, C. H. Hu, and K. L. Moore, "Relay feedback tuning of robust PID controllers with iso-damping property," in *Proc. 42nd IEEE Conf. Decision and Control*, Maui, HI, 2003, pp. 2180−2185.

[14] Y. Luo and Y. Q. Chen, "Fractional-order [proportional derivative] controller for robust motion control: tuning procedure and validation," in *American Control Conf., 2009. ACC09,* St. Louis, MO, USA, 2009, pp. 1412−1417.

Ameya Anil Kesarkar Ameya Anil Kesarkar was born in Mumbai, India in 1986. He received his Bachelor of Engineering (B. E.) degree in Electronics from University of Mumbai, Maharashtra, India in 2007, Master of Technology (M.Tech.) degree in Control and Automation from Indian Institute of Technology Delhi (IITD), Delhi, India in 2009, and Ph. D. degree from Indian Institute of Space Science and Technology (IIST), Kerala, India in 2015. Currently, he is working in microwave remote sensors area in Space Applications Centre (SAC), Indian Space Research Organization (ISRO), Ahmedabad, Gujarat, India. He has 6 international journal papers and 5 conference papers to his credit. His research interests include classical control, fractional calculus, fractional-order control, numerical optimization, nonlinear dynamics, and microwave remote sensing.

N. Selvaganesan N. Selvaganesan received his B.E. in Electrical and Electronic Engineering, M. E. in Control Systems and Ph. D. in System Identification and Adaptive Control from Mepco Schlenk Engineering College-Sivakasi, PSG College of Technology-Coimbatore and MIT Campus, Anna University, India in the year 1997, 2000, and 2005 respectively. He has more than 16 years of research and teaching experience. Currently, he is working as an Associate Professor and Head of Department of Avionics in Indian Institute of Space Science and Technology, Trivandrum, India. He has 26 international journal papers and 36 conference papers to his credit. He has been involved in many editorial activities / reviews in various international Journals / conferences. His areas of interest include system identification, fault diagnosis, model reduction, converters, power filter control design and fractional order control.

Stability analysis of a class of nonlinear fractional differential systems with Riemann-Liouville derivative

Ruoxun Zhang, Shiping Yang, Shiwen Feng

Abstract—**This paper investigates the stability of n-dimensional nonlinear fractional differential systems with Riemann-Liouville derivative. By using the Mittag-Leffler function, Laplace transform and the Gronwall-Bellman lemma, one sufficient condition is attained for the asymptotical stability of a class of nonlinear fractional differential systems whose order lies in (0, 2). According to this theory, if the nonlinear term satisfies some conditions, then the stability condition for nonlinear fractional differential systems is the same as the ones for corresponding linear systems. Several examples are provided to illustrate the applications of our result.**

Index Terms—**Stability, Nonlinear fractional differential system, Riemann-Liouville derivative**

I. Introduction

IN this paper, we consider the stability of n-dimensional nonlinear fractional differential systems with Riemann-Liouville derivative:

$$ {}_0^{RL}D_t^{\alpha}x(t) = Ax(t) + f(x(t)) \tag{1}$$

where $0 < \alpha < 2$, $x(t) \in \mathbf{R}^{n\times 1}$is the state vector, ${}_0^{RL}D_t^{\alpha}x(t)$denotes Riemann-Liouville's fractional derivative with the lower limit 0 for the function $x(t)$, $A \in \mathbf{R}^{n\times n}$is the constant parameter matrix and$f(x(t)) \in \mathbf{R}^{n\times 1}$is a nonlinear function vector.

In the last 30 years, fractional calculus has attracted attention of many mathematicians, physicists and engineers. Significant contributions have been made to both the theory and applications of fractional differential equations (see [1] and references there in). Also, fractional differential equations have recently been proved to be valuable tools in modeling of many physical phenomena in various ?elds of science and engineering.

Recently, the stability of fractional differential systems has attracted increasing interest due to its importance in control theory. In 1996, Matignon [2] firstly studied the stability of linear fractional differential systems. Since then, many researchers have studied further on the stability of linear fractional differential systems $[3-5]$. The stability analysis of nonlinear fractional differential systems is much more difficult and only a few available. For example, Li et al. investigated the Mittag-Leffler stability of fractional order nonlinear dynamic systems [6] and proposed Lyapunov direct method to check stability of fractional order nonlinear dynamic systems [7]. Wen et al. [8] and Zhou et al [9] considered the stability of nonlinear fractional differential systems. In [10], Zhang et al proposed a single state adaptive-feedback controller for stabilization of three-dimensional fractional-order chaotic systems. Based on the theory of Linear Matrix Inequality (LMI), Faieghi et al [11] proposed a simple controller for stabilization of a class of fractional-order chaotic systems. Wang et al. present the Ulam -Hyers stability for fractional Langevin equations [12], and Ulam- Hyers-Mittag-Lef?er stability for fractional delay differential equations [13]. The methods which they proposed for stability of a class of fractional differential equations provide us with a very useful method for studying Hyers–Ulam stable system. That is, one does not have to reach the exact solution. What is required is to get a function which satis?es a suitable approximation inequality.

Note that these papers on the stability of the fractional differential systems mainly concentrated on fractional orderαlying in (0, 1). Recently, in Ref [14], Zhang et al considered the stability of nonlinear fractional differential systems with Caputo derivative whose order lies in (0, 2). In this paper, we study the stability of the nonlinear fractional differential systems with Riemann-Liouville derivative whose order lies in (0, 2). By using the Mittag-Leffler function, Laplace transform and the Gronwall-Bellman lemma, a stability theorem is proven theoretically. The stability conditions have no restriction on the norm of the linear parameter matrix A. The paper is outlined as follows. In section II, some definitions and lemmas are introduced. In section III, the stability of a class of nonlinear fractional differential systems with commensurate order $0 < \alpha < 2$ is investigated. The simulation and conclusions are included in section IV and V, respectively.

II. PRELIMINARIES

Definition 2.1 [15]**.** The Riemann-Liouville derivative with $\alpha$of function $x(t)$ is defined as follows

$$ {}_{t_0}^{RL}D_t^{\alpha}x(t) = \frac{1}{\Gamma(n-\alpha)}\frac{d^n}{dt^n}\int_{t_0}^{t}\frac{x(\tau)}{(t-\tau)^{\alpha-n+1}}\mathrm{d}\tau, \quad (n-1 \le \alpha < n) \tag{2}$$

This article has been accepted for publication in a future issue of this journal, but has not been fully edited. Content may change prior to final publication.

This article was recommended by Associate Editor Antonio Visioli.

Ruoxun Zhang and Shiwen Feng are with the College of Teacher Education, Xingtai University, Xingtai 054001, China (email: xtzhrx@126.com, xtxyfsw@126.com)

Shiping Yang is with the College of Physics and Information Engineering, Hebei Normal University, Shijiazhuang 050016,China (email: yangship@mail.hebtu.edu.cn)

Digital Object Identifier 10.1109/JAS.2016.7510199

The Laplace transform of the Riemann-Liouville fractional derivative ${}_{t_0}^{RL}D_t^{\alpha}x(t)$ is

$$\int_0^{\infty} e^{-st}{}_{t_0}^{RL}D_t^{\alpha}x(t)\mathrm{d}t = s^{\alpha}X(t) - \sum_{k=0}^{n-1} s^k[D^{\alpha-k-1}x(t)]_{t=t_0} \tag{3}$$

Definition 2.2 [15]**.** The two-parameter Mittag- Leffler function is defined as

$$E_{\alpha,\,\beta}(z) = \sum_{k=0}^{\infty} \frac{z^k}{\Gamma(\alpha k+\beta)}\,,\ (Re\alpha > 0,\ \beta \in C, z \in C). \tag{4}$$

The Laplace transform of Mittag-Leffler function can be found to be

$$\int_0^{\infty} e^{-st}t^{\alpha k-\beta-1}E_{\alpha,\beta}^{(k)}(\pm at^{\alpha})\mathrm{d}t = \frac{k!s^{\alpha-\beta}}{(s^{\alpha}\mp a)^{k+1}},\ (R(s) > |a|^{\frac{1}{n}}). \tag{5}$$

Definition 2.3 [16]**.** By analogy with *Definition* 2.2, for $A \in C^{n\times n}$, a matrix Mittag-Leffler function is defined as: $E_{\alpha,\beta}(A) = \sum\limits_{k=0}^{\infty} \frac{A^k}{\Gamma(\alpha k+\beta)}, \quad (\beta \in C, R(\alpha) > 0)$

Lemma 2.1 [8]**.** If $A \in C^{n\times n},\ 0 < \alpha < 2,\ \beta$ is an arbitrary real number, μ is such that $\frac{\pi\alpha}{2} < \mu < \min\{\pi, \pi\alpha\}$ and $C_1$is a real constant, then

$$||E_{\alpha,\beta}(A)|| \le \frac{C_1}{1+||A||}, \tag{6}$$

where $\mu \le \arg(\lambda(A)) \le \pi,\ \lambda(A)$ denotes the eigenvalues of matrix A and $||\cdot||$denotes the l_2-norm.

Lemma 2.2 [17]**.** (Gronwall-Bellman lemma) If

$$\varphi(t) \le h(t) + \int_{t_0}^{t} g(\tau)\varphi(\tau)\mathrm{d}\tau, \quad t_0 \le t \le t_1. \tag{7}$$

where $g(t),\ h(t)$ and $\varphi(t)$ are continuous on $[t_0,\, t_1]$, $t_1 \to \infty$, $t_0 \le t \le t_1$ and $g(t) \ge 0$. Then $\varphi(t)$ satisfies

$$\phi(t) \le h(t) + \int_{t_0}^{t} h(\tau)g(\tau)\exp[\int_{\tau}^{t} g(s)\mathrm{d}s]\mathrm{d}\tau. \tag{8}$$

In addition, if $h(t)$ is nondecreasing, then

$$\phi(t) \le h(t)\exp[\int_{t_0}^{t} g(s)\mathrm{d}s]\mathrm{d}\tau. \tag{9}$$

III. Stability Theory of N-Dimensional Nonlinear Fractional Differential Systems

In this section, based on the definition and lemma in section 2, we present the stability theorem for a class of nonlinear fractional differential systems such as system (1).

Theorem 1. Consider the system (1). Let $\lambda_i(A)$ $(i = 1, 2, \cdots, n)$be the eigenvalues of matrix A. If

1) $|\arg(\lambda_i(A))| > \alpha\pi/2$;
2) The nonlinear function $f(x(t))$satisfies

$$\lim_{||x(t)||\to 0} \frac{||f(x(t))||}{||x(t)||} = 0. \tag{10}$$

Then the zero solution of (1) is locally asymptotically stable.

Proof. a) The case $0 < \alpha < 1$

In this case, the initial condition is

$${}_0^{RL}D_t^{\alpha-1}x(t)|_{t=0} = x_0 \tag{11}$$

Taking Laplace transform of (1), we have

$$X(s) = (Is^{\alpha} - A)^{-1}(x_0 + L[f(x(t))]) \tag{12}$$

where I is an $n \times n$ identity matrix.

Then taking inverse Laplace transform for (12), it yields

$$x(t) = x_0t^{\alpha-1}E_{\alpha,\alpha}(At^{\alpha}) + \int_0^t (t-\tau)^{\alpha-1}E_{\alpha,\alpha}(A(t-\tau)^{\alpha})f(x(\tau))\mathrm{d}\tau \tag{13}$$

By the condition (10), there exist $C_0 > 0$ and $\delta > 0$, such that

$$||f(x(t))|| < \frac{\alpha||A||}{2C_0}||x(t)||\mathrm{as}||x(t)|| < \delta \tag{14}$$

From (14) and Lemma 2.1 , (13) gives

$$\begin{aligned}||x(t)|| \le{}& \frac{C_0||x_0||t^{\alpha-1}}{1+||At^{\alpha}||} + \int_0^t \frac{||(t-\tau)^{\alpha-1}||C_0}{1+||A(t-\tau)^{\alpha}||}\frac{\alpha||A||}{2C_0}||x(\tau)||\mathrm{d}\tau = \\ & \frac{C_0||x_0||t^{\alpha-1}}{1+||A||t^{\alpha}} + \int_0^t \frac{\alpha||A||(t-\tau)^{\alpha-1}}{2(1+||A||(t-\tau)^{\alpha})}||x(\tau)||\mathrm{d}\tau\end{aligned}$$

According to Lemma 2.2, we obtain

$$\begin{aligned}||x(t)|| \le{}& \frac{C_0||x_0||t^{\alpha-1}}{1+||A||t^{\alpha}} + \int_0^t \frac{C_0||x_0||\tau^{\alpha-1}}{1+||A||\tau^{\alpha}} \\ & \times \frac{\alpha||A||(t-\tau)^{\alpha-1}}{2(1+||A||(t-\tau)^{\alpha})} \\ & \exp\Big(\int_{\tau}^{t} \frac{\alpha||A||(t-s)^{\alpha-1}}{2(1+||A||(t-s)^{\alpha})}\mathrm{d}s\Big)\mathrm{d}\tau \\ &= \frac{C_0||x_0||}{t^{1-\alpha}+||A||t} \\ & + \int_0^t \frac{\alpha C_0||x_0||\tau^{\alpha-1}||A||(t-\tau)^{\alpha-1}}{2(1+||A||\tau^{\alpha})(1+||A||(t-\tau)^{\alpha})^{0.5}}\mathrm{d}\tau \\ &\le \frac{C_0||x_0||}{t^{1-\alpha}+||A||t} \\ & + \int_0^t \frac{\alpha C_0||x_0||\tau^{\alpha-1}||A||(t-\tau)^{\alpha-1}}{2(1+||A||\tau^{\alpha})^{0.5}(1+||A||(t-\tau)^{\alpha})^{0.5}}\mathrm{d}\tau \\ &\le \frac{C_0||x_0||}{t^{1-\alpha}+||A||t} \\ & + 0.5\alpha C_0||x_0||\int_0^t \tau^{0.5\alpha-1}(t-\tau)^{0.5\alpha-1}\mathrm{d}\tau \\ &\le \frac{C_1||x_0||}{t^{1-\alpha}+||A||t} \\ & + 0.5\alpha C_0||x_0||\frac{\Gamma(0.5\alpha)\Gamma(0.5\alpha)}{\Gamma(\alpha)}t^{\alpha-1} \to 0 \\ & \text{as } t \to \infty.\end{aligned}$$

So, the zero solution of (1) is locally asymptotically stable.

2) The case $1 < \alpha < 2$

In this case, the initial condition is

$$ {}_0^{RL}D_t^{\alpha-k}x(t)|_{t=0} = x_{k-1},\ (k = 1,\ 2) \tag{15}$$

We can get the solution of (1) with the initial condition (15) by using the Laplace transform and Laplace inverse transform:

$$\begin{aligned} x(t) &= x_0 t^{\alpha-1}E_{\alpha,\alpha}(At^\alpha) + t^{\alpha-2}\,x_1 E_{\alpha,\alpha-1}(At^\alpha) \\ &\quad + \int_0^t (t-\tau)^{\alpha-1}E_{\alpha,\alpha}(A(t-\tau)^\alpha)f(x(\tau))\mathrm{d}\tau \end{aligned} \tag{16}$$

By the condition (10), there exist $C_0 > 0$ and $\delta > 0$, such that

$$ ||f(x(t))|| < \frac{(\alpha-1)||A||}{2C_0}||x(t)||\mathrm{as}||x(t)|| < \delta. \tag{17}$$

From (17) and Lemma 2.1 , (16) gives

$$\begin{aligned} ||x(t)|| &\le \frac{C_0||x_0||t^{\alpha-1}}{1+||At^\alpha||} + \frac{C_1||x_1||t^{\alpha-2}}{1+||At^\alpha||} \\ &\quad + \int_0^t \frac{||(t-\tau)^{\alpha-1}||C_0}{1+||A(t-\tau)^\alpha||}\frac{(\alpha-1)||A||}{2C_0}||x(\tau)||\mathrm{d}\tau \\ &= \frac{C_0||x_0||t^{\alpha-1}}{1+||A||t^\alpha} + \frac{C_1||x_1||t^{\alpha-2}}{1+||A||t^\alpha} \\ &\quad + \int_0^t \frac{||(t-\tau)^{\alpha-1}||}{1+||A||(t-\tau)^\alpha}\frac{(\alpha-1)||A||}{2}||x(\tau)||\mathrm{d}\tau \end{aligned} \tag{18}$$

where $C_1 \quad > 0$. According to Lemma 2.2, we obtain

$$\begin{aligned} ||x(t)| &\le \frac{C_0||x_0||\tau^{\alpha-1}}{1+||A||\tau^\alpha} + \\ &\quad \frac{C_1||x_1||\tau^{\alpha-2}}{1+||A||\tau^\alpha} + \int_0^t \Big(\frac{C_0||x_0||\tau^{\alpha-1}}{1+||A||\tau^\alpha} \\ &\quad + \frac{C_1||x_1||\tau^{\alpha-2}}{1+||A||\tau^\alpha}\Big)\frac{(\alpha-1)||A||(t-\tau)^{\alpha-1}}{2(1+||A||(t-\tau)^\alpha)} \\ &\quad \times \exp\Big(\int_\tau^t \frac{(\alpha-1)||A||(t-s)^{\alpha-1}}{2(1+||A||(t-s)^\alpha)}\mathrm{d}s\Big)\mathrm{d}\tau \\ &= \frac{C_0||x_0||t^{\alpha-1}}{1+||A||t^\alpha} + \frac{C_1||x_1||t^{\alpha-2}}{1+||A||t^\alpha} \\ &\quad + \int_0^t \Big(\frac{C_0||x_0||t^{\alpha-1}}{1+||A||t^\alpha} + \frac{C_1||x_1||t^{\alpha-2}}{1+||A||t^\alpha}\Big) \\ &\quad \times \frac{(\alpha-1)||A||(t-\tau)^{\alpha-1}}{2(1+||A||(t-\tau)^\alpha)^{1-\frac{\alpha-1}{2\alpha}}}\mathrm{d}\tau \\ &\le \frac{C_0||x_0||t^{\alpha-1}}{1+||A||t^\alpha} + \frac{C_1||x_1||t^{\alpha-2}}{1+||A||t^\alpha} \\ &\quad + \int_0^t \frac{C_0||x_0||\tau^{\alpha-1}}{(1+||A||\tau^\alpha)^{0.75}} \\ &\quad \times \frac{(\alpha-1)||A||(t-\tau)^{\alpha-1}}{2(1+||A||(t-\tau)^\alpha)^{1-\frac{\alpha-1}{2\alpha}}}\mathrm{d}\tau \\ &\quad + \int_0^t \frac{C_1||x_1||\tau^{\alpha-2}}{(1+||A||\tau^\alpha)^{\frac{\alpha-1}{2\alpha}}} \\ &\quad \times \frac{(\alpha-1)||A||(t-\tau)^{\alpha-1}}{2(1+||A||(t-\tau)^\alpha)^{1-\frac{\alpha-1}{2\alpha}}}\mathrm{d}\tau \\ &\le \frac{C_0||x_0||t^{\alpha-1}}{1+||A||t^\alpha} + \frac{C_1||x_1||t^{\alpha-2}}{1+||A||t^\alpha} \\ &\quad + \frac{(\alpha-1)C_0||x_0||}{2||A||^{0.25+1/(2\alpha)}}\int_0^t \tau^{0.25\alpha-1}(t-\tau)^{0.5\alpha-1.5}\mathrm{d}\tau \\ &\quad + \frac{(\alpha-1)C_1||x_1||}{2}\int_0^t \tau^{0.5\alpha-1.5}(t-\tau)^{0.5\alpha-1.5}\mathrm{d}\tau \\ &\le \frac{C_0||x_0||}{||A||t} + \frac{C_1||x_1||}{||A||t^2} \\ &\quad + \frac{(\alpha-1)C_0||x_0||}{2||A||^{0.25+1/(2\alpha)}}\frac{\Gamma(0.25\alpha)\Gamma(0.5\alpha-0.5)}{\Gamma(0.75\alpha-0.5)t^{0.75(2-\alpha)}} \\ &\quad + \frac{(\alpha-1)C_1||x_1||}{2}\frac{\Gamma(0.5\alpha)\Gamma(0.5\alpha-0.5)}{\Gamma(\alpha-0.5)t^{2-\alpha}} \\ &\quad \to 0\ as\ t \to \infty. \end{aligned} \tag{19}$$

So, the zero solution of (1) is locally asymptotically stable.

Remark 1. The nonlinear term of many fractional order chaotic systems satisfy (12). For example, fractional-order Lorenz system [17], fractional-order Chen system [18], fractional-order Lü system [19], fractional-order Liu system [20], fractional-order Arneodo system [21], fractional-order Chua system [22] and fractional-order hyperchaotic Chen system [23] etc. So, Theorem 1 can be applicable to control chaos in a large class of generalized fractional-order chaotic or hyperchaotic systems via a linear feedback controller. See Example 3 in Section 4.

Remark 2. Theorem 1 provides us with a simple procedure for determining the stability of the fractional order nonlinear systems with Caputo derivative with order $0 < \alpha < 2$. If the nonlinear term $f(x(t))$satisfies Eq.(10), then one does not have to reach the exact solution. What is required is to calculate the eigenvalues of the matrix A, and test their arguments. If $|\arg(\lambda_i(A))| > \alpha\pi/2$for all i, we conclude that the origin is asymptotically stable.

IV. Three Illustrative Examples

The following illustrative examples are provided to show the effectiveness of the stability theorem. When numerically solving fractional differential equations, we adopt the method introduced in [24].

Example 1. Consider the nonlinear fractional differential systems

$$\begin{aligned} {}_0^{RL}D_t^{\alpha}x_1 &= x_1 + x_2 + x_3 + x_2x_3 \\ {}_0^{RL}D_t^{\alpha}x_2 &= -x_1 + x_2 - x_3 + x_2^2 \\ {}_0^{RL}D_t^{\alpha}x_3 &= x_1x_2 - x_3 \end{aligned} \tag{20}$$

System (20) can be rewritten as (1), in which

$$A = \begin{pmatrix} 1 & 1 & 1 \\ -1 & 1 & -1 \\ 0 & 0 & -1 \end{pmatrix}, \quad f(x(t)) = \begin{pmatrix} x_2x_3 \\ x_2^2 \\ x_1x_2 \end{pmatrix} \tag{21}$$

Obviously, it is easy to verify that

$$\begin{aligned} \lim_{||x(t)||\to 0} \frac{||f(x(t)||}{||x(t)||} &= \lim_{||x(t)||\to 0} \frac{\sqrt{(x_2x_3)^2 + x_2^4 + (x_1x_2)^2}}{\sqrt{x_1^2 + x_2^2 + x_3^2}} \\ &\le \lim_{||x(t)||\to 0} \frac{\sqrt{(x_2x_3)^2 + x_2^4 + (x_1x_2)^2}}{\sqrt{x_2^2}} \\ &\le \lim_{||x(t)||\to 0} \sqrt{x_3^2 + x_2^2 + x_1^2} = 0, \end{aligned}$$

which implies that $f(x(t)$ satisfies Condition (2) in Theorem 1. By using simple calculation, the eigenvalues

of A are $\lambda_{1,2} = 1 \pm i$ and $\lambda_3 = -1$. According to Theorem 1, if $\alpha < 0.5$, the zero solution of (20) is asymptotically stable. Simulation results are displayed in Figs. 1–3. Fig. 1 and Fig. 2 show the zero solution of system (20) is asymptotically stable with $\alpha = 0.4$ and $\alpha = 0.49$, respectively. Fig. 3 shows the zero solution of the system (20) is unstable with $\alpha = 0.5$.

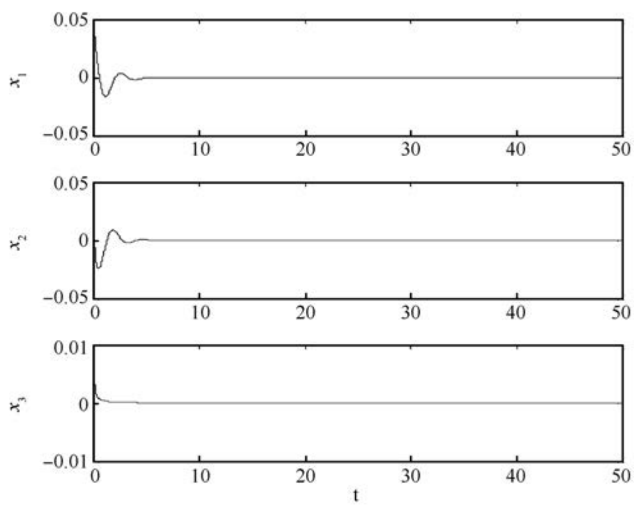

Fig. 1. System (20) is asymptotically stable with $\alpha = 0.4$

Example 2. Consider the nonlinear fractional differential systems

$$\begin{aligned} {}_0^{RL}D_t^{\alpha}x_1 &= -x_1 + x_2x_3 \\ {}_0^{RL}D_t^{\alpha}x_2 &= x_3 \\ {}_0^{RL}D_t^{\alpha}x_3 &= x_1 - x_2 - x_3 - x_1x_2 \end{aligned} \tag{22}$$

System (22) can be rewritten as (1), in which

$$A = \begin{pmatrix} -1 & 0 & 0 \\ 0 & 0 & 1 \\ 1 & -1 & -1 \end{pmatrix}, \quad f(x(t)) = \begin{pmatrix} x_2x_3 \\ 0 \\ -x_1x_2 \end{pmatrix} \tag{23}$$

Obviously, it is easy to verify that $\lim_{||x(t)||\to 0} \frac{||f(x(t)||}{||x(t)||} = 0$, which implies that $f(x(t)$ satisfies Condition (2) in Theorem 1. By using simple calculation, the eigenvalues of A are $\lambda_{1,2} = -1/2 \pm \sqrt{3}i/2$ and $\lambda_3 = -1$. According to Theorem 1, if $\alpha < 4/3$, the zero solution of (22) is asymptotically stable. Simulation results are displayed in Figs. 4–7. Figs.4–6 show the zero solution of the system (22) is asymptotically stable with $\alpha = 1.1 \alpha = 1.3$ and $\alpha = 1.33$, respectively. Fig. 7 shows the zero solution of the system (22) is not stable with $\alpha = 1.34$.

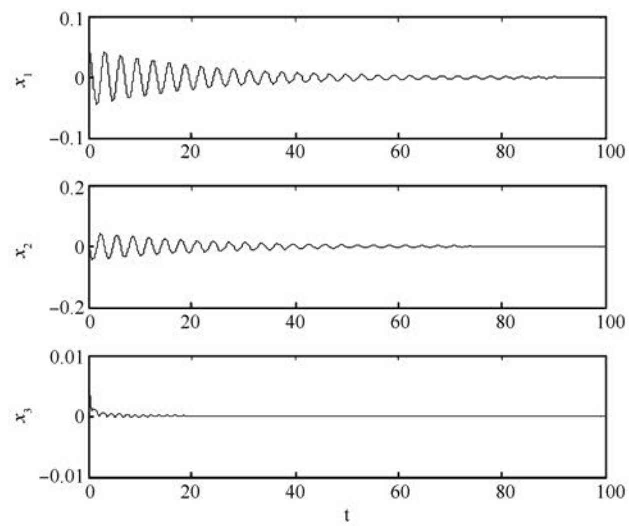

Fig. 2. System (20) is asymptotically stable with $\alpha = 0.49$

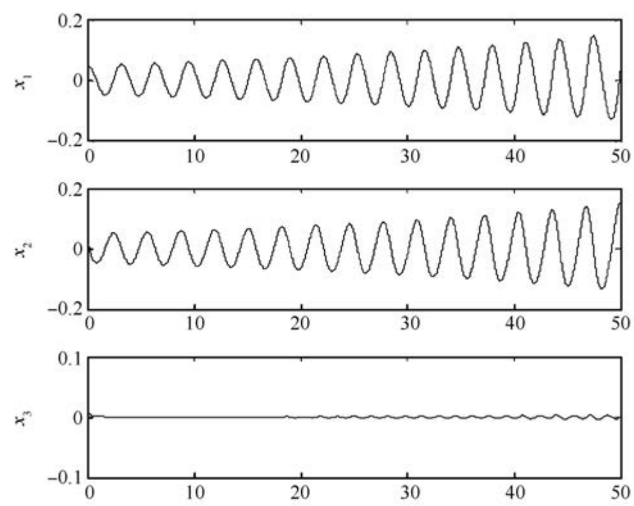

Fig. 3. System (20) is unstable with $\alpha = 0.50$

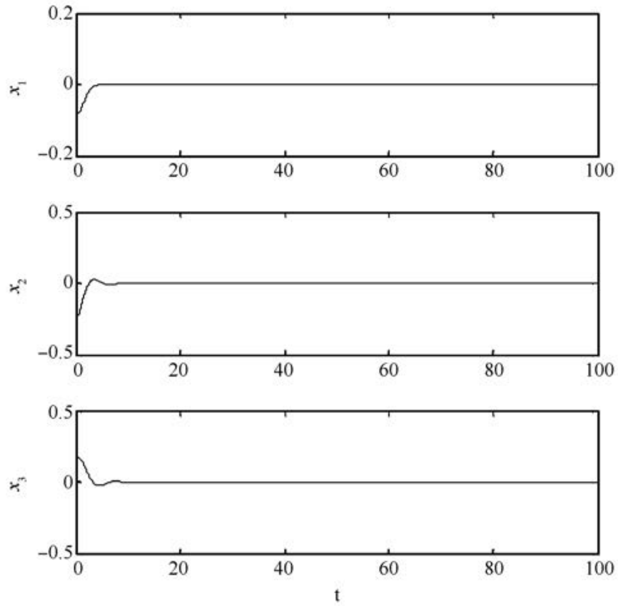

Fig. 4. System (22) is asymptotically stable with $\alpha = 1.1$

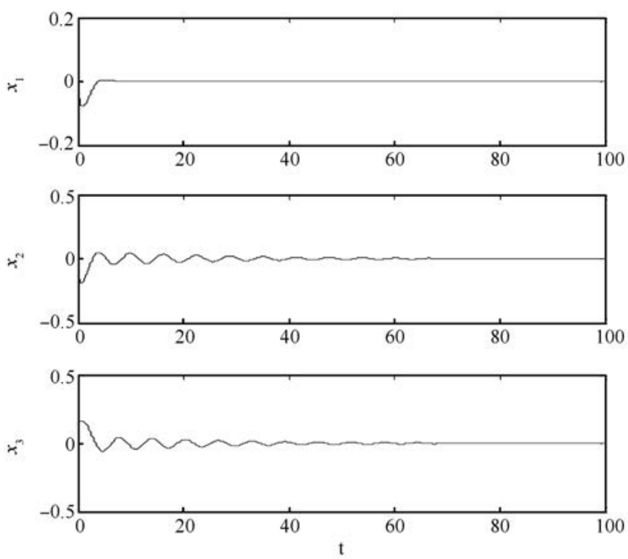

Fig. 5. System (22) is asymptotically stable with $\alpha = 1.30$

Example 3. The fractional-order hyperchaotic Chen system can be written as

$$\begin{aligned}
{}_0^{RL}D_t^{\alpha}x_1 &= a(x_2 - x_1) + x_4 \\
{}_0^{RL}D_t^{\alpha}x_2 &= dx_1 + cx_2 - x_1x_3 \\
{}_0^{RL}D_t^{\alpha}x_3 &= x_1x_2 - bx_3 \\
{}_0^{RL}D_t^{\alpha}x_4 &= x_2x_3 + rx_4
\end{aligned} \tag{24}$$

where a, b, c,d and r are five parameters. When $a = 35,\ b = 3,\ c = 12,\ d = 7, r = 0.3$ and $\alpha = 1.1$ system (24) displays a chaotic attractor, as shown in Fig. 8.

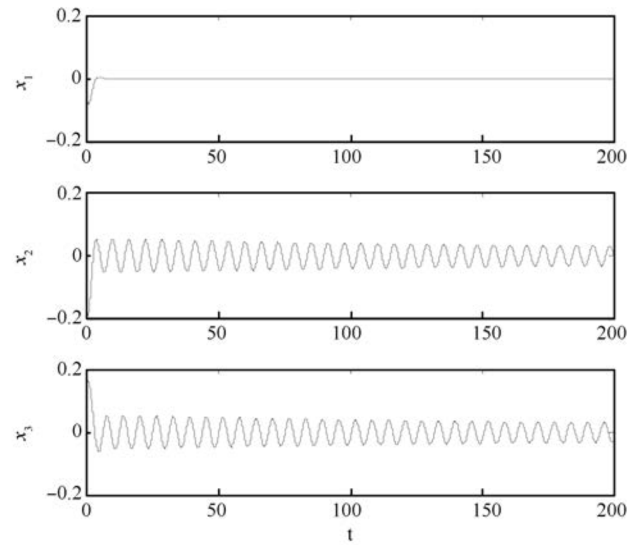

Fig. 6. System (22) is asymptotically stable with $\alpha = 1.33$

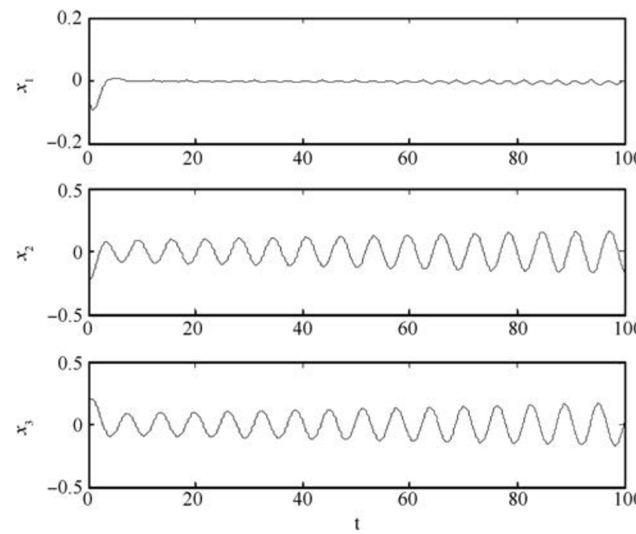

Fig. 7. System (22) is not stable with $\alpha = 1.34$

System (24) can be rewritten as a controlled system:

$$\begin{aligned}
{}_0^{RL}D_t^{\alpha}x_1 &= a(x_2 - x_1) + x_4 \\
{}_0^{RL}D_t^{\alpha}x_2 &= dx_1 + cx_2 - x_1x_3 + u_1 \\
{}_0^{RL}D_t^{\alpha}x_3 &= x_1x_2 - bx_3 \\
{}_0^{RL}D_t^{\alpha}x_4 &= x_2x_3 + rx_4 + u_2
\end{aligned}$$

When $\alpha = 1.1,\ a = 35,\ \ b = 3,\ c = 12,\ d = 7, r = 0.3$, we select the linear state feedback controller $u_1 = -22x_2$, $u_2 = -x_4$. Then, the two conditions of Theorem 1 are satisfied well. It concludes that the zero solution of the controlled system is asymptotically stable. The results of simulation are shown in Fig. 9, while the feedback is activated at time$t$ =10 s.

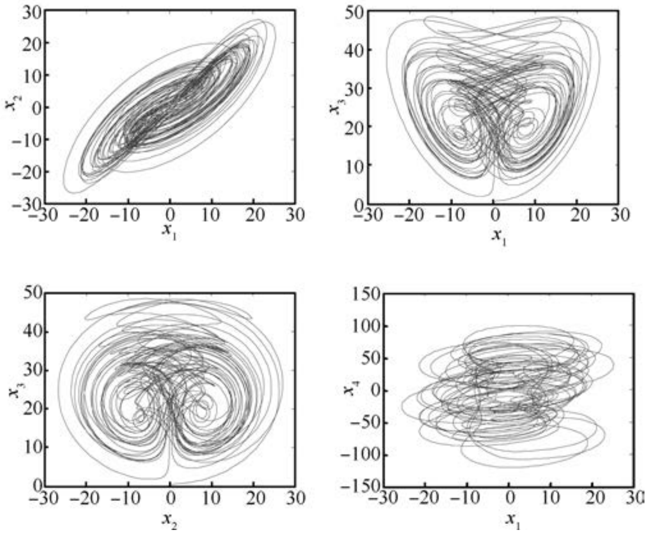

Fig. 8. Attractor of fractional order hyperchaotic Chen system with order $\alpha = 1.1$ $(a = 35,\ b = 3,\ c = 12,\ d = 7, r = 0.3)$

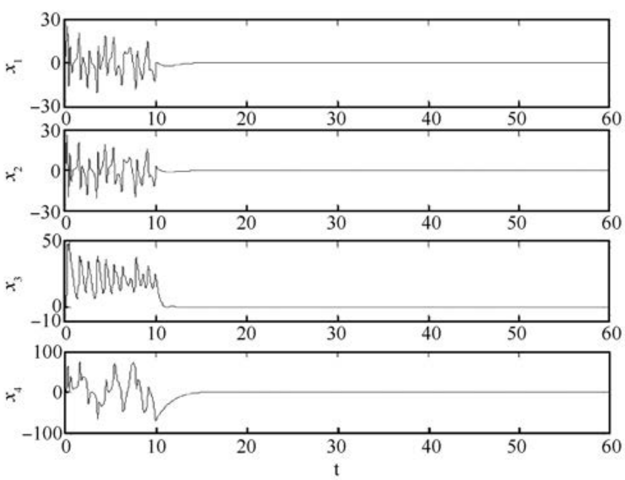

Fig. 9. Asymptotical stabilization of fractional order hyperchaotic Chen system with order $\alpha = 1.1$

V. Conclusions

In this paper, we have studied the local asymptotic stability of the zero solution of n-dimensional nonlinear fractional differential systems with with Riemann-Liouville derivative. The results are obtained in terms of the Mittag-Leffler function, Laplace transform and the Gronwall-Bellman lemma. Compare of the current results with the results in Ref.[14] shows that the stability condition of Riemann-Liouville fractional differential system is same as that for Caputo fractional differential systems. Three numerical examples are given to demonstrate the effectiveness of the proposed approach.

VI. Acknowledgement

This work was supported by the Natural Science Foundation of Hebei Province, China (No. A2015108010 and No.A2015205161), the science research project of Hebei higher education institutions, China (No.z2012021).

References

[1] Machado J T, Kiryakova V, Mainardi F. Recent history of fractional calculus. Commun Nonlinear Sci Numer Simul, 2011,**16**:1140–1153.

[2] Matignon D. Stability results for fractional di?erential equations with applications to control processing, in Proceedings of the IMACS-SMC, 1996, **2**: 963–968.

[3] Deng W, Li C, Guo Q. Analysis of fractional differential equations with multi-orders, Fractals, 2007,**15**:173–182.

[4] Deng W, Li C, Lü J. Stability analysis of linear fractional di?erential system with multiple time delays, Nonlinear Dynamics, 2007, **48**: 409–416.

[5] Moze M, Sabatier J, Oustaloup A. LMI characterization of fractional systems stability, in Advances in Fractional Calculus, pp. 419–434, Springer, Dordrecht, The Netherlands, 2007.

[6] Li Y, Chen Y . Podlubny I. Mittag–Leffler stability of fractional order nonlinear dynamic systems, Automatica, 2009, **45:** 1965-1969

[7] Li Y, Chen Y. Podlubny I. Stability of fractional-order nonlinear dynamic systems: Lyapunov direct method and generalized Mittag–Leffler stability, Computers & Mathematics with Applications, 2010, **59**: 1810-1821.

[8] Wen X, Wu Z, Lu J. Stability analysis of a class of nonlinear fractional-order systems, IEEE Transactions on Circuits and Systems II, 2008, **55**: 1178–1182.

[9] Zhou X, Hu L, Liu S, Jiang W, Stability criterion for a class of nonlinear fractional differential system, Appl. Math. Lett., 2014, **28**: 25-29.

[10] Zhang R, Yang S. Stabilization of fractional-order chaotic system via a single state adaptive-feedback controller, Nonlinear Dyn. 2012,**68**: 45-51.

[11] Faieghi M, Kuntanapreeda S, Delavari H, Baleanu D. LMI-based stabilization of a class of fractional-order chaotic systems, Nonlinear Dyn. 2013,**72**: 301-309.

[12] Wang J, Li X. Ulam–Hyers stability of fractional Langevin equations. Applied Mathematics and Computation, 2015, **258**: 72-83

[13] Wang J, Zhang Y. Ulam-Hyers- Mittag-Leffler stability of fractional-order delay differential equations. Optimization, 2014, **63**(8): 1181-1190.

[14] Zhang R, Tian G, Yang S, Cao H. Stability analysis of a class of fractional order nonlinear systems with order lying in (0, 2). ISA transactions, 2015, **56**: 102-110.

[15] Kilbas A, Srivastava H, Trujillo J. Theory and Applications of Fractional Differential Equations, vol. 204 of North-Holland Mathematics Studies, Elsevier Science, Amsterdam, The Netherlands, 2006.

[16] Corduneanu C. Principles of Di?erential and Integral Equations, Allyn and Bacon, Boston, Mass, USA, 1971.

[17] Grigorenko I, Grigorenko E, Chaotic dynamics of the fractional Lorenz system. Phys. Rev. Lett. 2003, **91**: 034101.

[18] Li C, Chen G. Chaos in the fractional order Chen system and its control. Chaos Solitons Fractals, 2004,**22**:549-554.

[19] Lu J. Chaotic dynamics of the fractional- order Lu system and its synchronization. Phys. Lett. A 2006, **354**:305–311.

[20] Wang X, Wang M. Dynamic analysis of the fractional-order Liu system and its synchronization. Chaos, 2007, **17**: 033106.

[21] Lu J. Chaotic dynamics and synchronization of fractional-order Arneado's systems. Chaos Solitons Fractals , 2005, **26**:1125–1133.

[22] Hartly T, Lorenzo C. Qammer, H.K.: Chaos in a fractional order Chua's system. IEEE Trans. CAS: I 1995, **42**: 485- 490.

[23] Hegazi A, Matouk A. Dynamical behaviors and synchronization in the fractional order hyperchaotic Chen system, Appl. Math. Lett., 2011, **284**:1938-1944.

[24] Wang F, Yang Y, Hu M. Asymptotic stability of delayed fractional-order neural networks with impulsive effects. Neurocomputing, 2015, **154**: 239– 244

Ruoxun Zhang received the B.S., M.S. and Ph.D. degrees in Physics and Information Engineering all from Hebei Normal University, Shijiazhuang, China, in 1990, 2008 and 2012 respectively. He is currently an associate professor at Xingtai University. His current research interests include control and synchronization of fractional-order chaotic systems, neural networks, adaptive control theory. E-mail: xtzhrx@126.com

Shiping Yang received the B.S. degree in Physics Department from Beijing Normal University, Beijing, China, in 1982, and the M.S. degree in Institute of Physics from Chinese Academy of Sciences, Beijing, China, in 1988. He is currently a professor and a doctoral adviser at Hebei Normal University. His current research interests include fractional-order nonlinear dynamic systems, chaos, neural networks, control theory. E-mail: yangship@mail.hebtu.edu.cn,

Shiwen Feng received the B.S. degree in Computer Science from Hebei Normal University, Shijiazhuang, China, in 1992, and the M.S. degree in Information Science and Technology from East China Normal University, Shanghai, China, in 2009. He is currently an associate professor at Xingtai University. His current research interests include information processing, chaos, neural networks, control theory. E-mail: xtxyfsw@126.com

Research on the Higher-order Logic Formalization of Fractance Element

Shanshan Li, Chunna Zhao, *Member, IEEE,* Yong Guan, *Member, IEEE,* Zhiping Shi, *Member, IEEE CAA,* Xiaojuan Li, *Member, IEEE,* Rui Wang, *Member, IEEE,* and Qianying Zhang

***Abstract*—Fractance element reflects the fractional order behavior of circuits, which can show the characteristics of the actual circuits. Higher-order logic theorem proving is based on the rigorous and correct mathematical theories. It becomes more and more important in the verifications of high-reliability systems. Fractance element is formalized using the proof of higher-order logic theorem in this paper. Firstly, the formalized model of fractional calculus which is based on Caputo definition is established in higher-order logic theorem proof tool. Then some properties of fractional calculus are proved, including the zero order property, the fractional differential of a constant and the consistency of fractional calculus and integer order calculus. Finally, fractance element and fractional differential circuit constituted by fractance element are formally analyzed. These formalizations demonstrate the effectiveness of the formal method in the analysis of fractance element.**

***Index Terms*—Fractional Calculus, Caputo Definition, Theorem Proving, Fractance Element, Fractional Differential Circuit.**

I. Introduction

FRACTANCE element is a component with fractional order impedance. It can accomplish the function of fractional calculus for signal. Fractance element is different from the impedance, capacitive reactance or inductive reactance. It can show the characteristics between capacitance and inductance [1]. Fractance circuit refers to the circuit which includes fractance elements. Components in the circuits are often considered to be a resistance, capacitance, or inductance which is with integer order. However, due to the materials or other reasons, the components in actual circuits do not show these desirable characteristics. Actually, they present the characteristics between these ideal characteristics. Ignoring these facts will lead to inaccurate modeling. In addition, accuracy problems will emerge if we adjust the circuits according to the misconception that the components present ideal characteristics. Fractional calculus is the theoretical basis of fractance element and fractance circuit. It can be used to effectively describe the dynamic process of some systems which cannot be accurately described by integer order calculus [2]. Now, fractional calculus is widely used in hyperchaotic system [3], viscoelastic system [4], anomalous diffusion, fluid dynamics [5], image processing [6], signal processing, seismic analysis, control of robot [7], electric power transmission line [8], fuzzy control [9] and other fields. Studies have shown that the models using fractional calculus can better and more accurately describe the characteristics of actual systems [10].

The current phase of research on fractance element and fractance circuit is concerned with their realization. For instance, the realizations of fractance element and fractance circuit are discussed in references $[11-13]$. In reference [11], the fractional order operator is realized by using the finite inertia and the cascade of proportional differential circuit. Reference[12] presents an implementation of variable order analog circuit by using operational transconductance amplifier. Besides, the realization of fractional analog circuit by using the method of binomial expansion is given in reference[13]. A wide variety of implementation schemes have been proposed and these schemes have also been obtained in some applications. However, few studies have focused on the analysis of the fractance element and fractance circuit. For the analysis of fractance element and fractance circuit, the traditional methods include paper-and-pencil based proofs, analog simulation and computer algebra system. The results of these methods cannot achieve 100% rate of precision because of the cumbersome process, approximation errors, difficulty in building environment for application of these methods and that the algorithms for symbolic computation have not been verified. Formal methods can avoid these precision problems. Model checking and theorem proving are two commonly used formal methods. Considering the characteristics of fractional calculus, we use theorem proving to formally analyze the fractance element and fractance circuit. Theorem proving formalizes the systems and their properties into mathematical models, and then converts the mathematical models into logical models. It logically estimates the correctness of systems. Theorem proving is the strictest and most standardized method so far and the credibility of conclusion is also the highest. The theorem proof tool we use is HOL4. HOL system is one of the theorem prover and it is developed by Cambridge University. HOL4 is the fourth edition of HOL system and it is the newest edition. It is implemented basing on the meta-language. Meta-language is an interactive programming language and it is efficient and

This article has been accepted for publication in a future issue of this journal, but has not been fully edited. Content may change prior to final publication.

This work was supported by the International S&T Cooperation Program of China (2010DFB10930, 2011DFG13000); the National Natural Science Foundation of China (60873006, 61070049, 61170304, 61104035, 61174145, 61201378); the Beijing Natural Science Foundation, Beijing Outstanding Talents Project, and the S&R Key Program of BMEC (4122017, KZ201210028036, KM201010028021, 2012D005016000011). Recommended by Associate Editor YangQuan Chen.

Shanshan Li, Chunna Zhao, Yong Guan, Zhiping Shi, Xiaojuan Li, Rui Wang, and Qianying Zhang are with the Capital Normal University. (email: shanshan_xiong@126.com, chunnazhao@163.com, guanyong@cnu.enu.cn, shizp@cnu.edu.cn, lixjxxxy@263.net, rwang04@gmail.com, zsjzqy@gmail.com)

Digital Object Identifier 10.1109/JAS.2016.7510208

strict. Now, HOL4 is widely used in the validation of software and hardware, and has obtained welcome results. Besides, HOL4 has a rich theorem library, including Boolean algebra, collection, Gauge integral, complex number and so on. The more theorems HOL4 has, the stronger the deduction ability is. Because a proof in the HOL4 system is constructed by repeatedly applying inference rules to axioms or to previously proved theorems.

As mentioned above, fractional calculus is the theoretical basis of fractance element, so we should formalize fractional calculus before the formal analysis of fractance element. On FMCAD2011, Umair and Osman [14] have formalized the Gamma function and the Riemann-Liouville definition of fractional calculus and formally verified some properties of them. And then they analyzed the fractional order behaviors of capacitance and differentiator. Their work pioneered the use of formal method for the analysis of fractional order systems. Shi Likun [15] has formalized the Grunwald-Letnikov definition of fractional calculus and formally analyzed the fractional order FC component and fractional position servo system in HOL4. In this paper, for the purpose of perfecting the definitions and properties of fractional calculus in HOL4, and improving the modelling and deduction ability of HOL4, we firstly establish the higher-order logic model of fractional calculus which is based on Caputo definition, and then formally verify some related basic properties of it. The formalization of theorem is known as the goal in HOL4 and we will use the existed definitions and theorems in HOL4 to prove the goal. It will illustrate the correctness of the theorem if the goal has been verified. We form these verified properties into separate theorems, so these definitions and theorems can be used directly by other users. At last, in order to illustrate the consistency of fractional calculus and integer order calculus and the validity of theorem proving method for the analysis of fractional order systems, we use the formalizations to formally analyze the fractance element and fractional differential circuit.

The rest of the paper is organized as follows: we present the formalizations of basic theories in Section 2, including the formalization of fractional calculus which is based on Caputo definition, and the verifications of some related basic properties. These basic properties include zero order property, the fractional differential of a constant and the consistency of fractional calculus and integer order calculus. In Section 3, the formalizations of these basic theories are applied to analyze fractance element and fractional differential circuit. The relationship of fractance element and ideal components, as well as the unification of fractional differential circuit and integer differential circuit are proved here. Section 4 concludes the paper.

II. Formalizations of Basic Theories

A. Caputo Definition of Fractional Calculus

The origin of fractional calculus can be traced back to more than 300 years. Fractional calculus is based on the definition of integer order calculus. It extends the order of integer order calculus from integer to non-integer. It can be used to describe actual systems more accurately. Grunwald-Letnikov, Riemann-Liouville and Caputo definition are the three commonly used definitions of fractional calculus. These three definitions have different characteristics. Grunwald-Letnikov definition is suitable for numerical computation while Riemann-Liouville definition which is defined in the form of differential-integral can make the mathematical analysis of fractional calculus become easier. Caputo definition can facilitate the modeling of actual problems and compact the Laplace transform of fractional calculus. The solution of fractional calculus equation is also given in the form of Caputo definition. In addition, Caputo definition is more able to reflect the feature that fractional calculus is the expansion of integer order calculus. Therefore, Caputo definition is more widely used in the modeling of actual problems [16].

These three definitions are defined from different perspectives. Riemann-Liouville definition and Caputo definition are the improvement of Grunwald-Letnikov definition. These three definitions can achieve unification under certain conditions. When the initial value is 0, the Grunwald-Letnikov definition and Caputo definition are equivalent. And the Riemann-Liouville definition and Caputo definition are equivalent when the original function $f(t)$ is $(\lfloor v \rfloor + 1)^{th}$ order derivable and all of the derivatives are 0, where v is the fractional order and the operator $\lfloor v \rfloor$ returns the biggest integer which is not greater than v.

In this paper, we research on the Caputo definition. The mathematical expression of fractional calculus based on Caputo definition is shown in Formula(1) [17].

$$ {}_a^C D_t^v f(t) = \frac{1}{\Gamma(m-v)} \int_a^t \frac{f^{(m)}(x)}{(t-x)^{v-m+1}} \,\mathrm{d}x. \quad m = \lfloor v \rfloor + 1 \tag{1} $$

where ${}_a^C D_t^v$ is the operator of fractional calculus with order v, lower limit a and upper limit t. Formula(1) is the unified expression of fractional differential and integral. When the order v is a positive value, Formula(1) means fractional differential and it means fractional integral when v is a negative value. The letter C on the top left corner of the operator is the abbreviation of Caputo. It indicates that Formula(1) is defined by Caputo definition, so that we can distinguish it from other definitions. Γ represents Gamma function[17] and its definition is as below.

$$ \Gamma(z) = \int_0^\infty e^{-t} t^{z-1} \,\mathrm{d}t \tag{2} $$

where the real part of z is greater than 0. Gamma function is the most commonly used basic function of fractional calculus. It extends the factorial from a natural number to a real number. Gamma function is also known as generalized factorial.

When modeling and verifying fractance element in HOL4, the formal model of fractional calculus based on Caputo definition is needed. We firstly establish the formal model of fractional calculus based on Caputo definition in HOL4.

Definition 1. Fractional Calculus based on Caputo Definition

$\forall f\ v\ a\ t. frac\_c\ f\ v\ a\ t\ =\ if\ (v = 0)\ then\ f\ t$
$\quad else$
$\lim(\lambda n.1/Gamma\ (\&(flr\ v) + 1 - v) * (integral(a, t - 1/2\ pow\ n)(\lambda x.(((t-x)\ rpow\ (\&(flr\ v) + 1 - v - 1)) * (n\_order\_deriv(flr\ v + 1) f\ x)))))$

Definition 1 is formalized basing on the real library[18], transcendental function library and integer order integral library[19] which have been already formalized in HOL4. The operator $frac\_c$ represents the Caputo definition of fractional calculus. f is the initial function of type $(real- > real)$. v is a real number which indicates the order of fractional calculus. t and a are the upper and lower limit, respectively. $Gamma$ represents Gamma function which has been formalized in reference[14]. $(flr\ v)$ is the formalization of $\lfloor v \rfloor$. $integral(a, t-1/2\ pow\ n)$ represents integral with lower limit a and upper limit $(t - 1/2\ pow\ n)$ where pow is a power function with natural exponent.

Formula(1) is a definite integral with variable upper limit. The formalization of variable upper limit is a difficulty for our work. The function $integral(a, b) f$ in HOL4 only represents integral with lower limit a and upper limit b, where a and b are both constant. The variable upper limit should be reconstructed according to the existing definitions and theorems in HOL4. We solve this problem by nesting the integral into the limitation. Taking the existing definitions and theorems into account, we construct formula $(t - \frac{1}{2^n})$ and take the limit of it as $\lim_{n\to+\infty}(t - \frac{1}{2^n})$. The variable upper limit t will be expressed when $\frac{1}{2^n}$ becomes very close to 0 as n becomes very large. Here we use $lim(\lambda n.t - 1/2\ pow\ n)$ to formalize the variable upper limit t in HOL4. $lim(\lambda n.f)$ computes the limit of f when n tends to infinity and it is a function in sequence library [20].

Caputo definition has certain requirements for the original function. As can be seen from Formula(1), it firstly requires the original function $f(x)$ is m^{th} order derivable. Moreover, the product of $f^{(m)}(x)$ and $\frac{1}{(t-v)^{v-m+1}}$ should be integrable. Besides, in practical applications of fractional calculus such as fractance element, their parameters are always based on time so that we can analyze the systems from one moment to the next moment. So, the upper limit and lower limit which is based on time here should satisfy the condition that the upper limit should be greater than lower limit. Furthermore, we stipulate Formula(1) is limited because a limitation is used to denote the variable upper limit in the formalization of Caputo definition. These existent conditions of Caputo definition are formalized as follows:

Definition 2. Existent Conditions
$\forall f\ v\ a\ t\ n\ l.frac\_c\_exists\ f\ v\ a\ t\ n\ l\ =\ (\forall m.m <= (flr\ v{+}1) ==> (\lambda t.n\_order\_deriv\ m\ f\ t)\ differentiable\ t)$
$\wedge\ (\forall v.integrable(a, t - 1/2\ pow\ n)(\lambda x.(((t-x)\ rpow$
$(\&(flr\ v){+}1{-}v{-}1)) * (n\_order\_deriv(flr\ v{+}1)\ f\ x)))) \wedge$
$a <= t - 1/2\ pow\ n \wedge (\lambda n.1/Gamma\ (\&(flr\ v) + 1 - v) *$
$(integral(a, t - 1/2\ pow\ n)(\lambda x.(((t-x)\ rpow\ (\&(flr\ v) +$
$1 - v - 1)) * (n\_order\_deriv(flr\ v + 1)\ f\ x))))) - - > l)$

Only the above conditions are met, the Caputo definition and its formalization are existent. When using operator ${}^{C}_{a}D^{v}_{t}$, we always assume that these existent conditions are established. The formalization of these conditions can be utilized to be the antecedent when proving the subsequent properties of fractional calculus.

B. Zero Order Property

If function $f(t)$ satisfies the existent conditions of Caputo definition and the order of fractional calculus is 0, the fractional calculus of $f(t)$ will return the original function. The property is shown in Formula(3).

$$ {}^{C}_{a}D^{0}_{t}f(t) = f(t) \tag{3} $$

The formal verification of this property in HOL4 is given in the following theorem.

Theorem 1. Zero Order Property
$\forall f\ v\ a\ t\ n.$
$frac\_c\_exists\ f\ v\ a\ t\ n\ l ==> (frac\_c\ f\ 0\ a\ t = f\ t)$
where $frac\_c$ and $frac\_c\_exists$ have been formalized in Definition 1 and Definition
2. A special case that the order is 0 has been considered in Definition 1, so the proof of Theorem 1 is relatively simple. There are two proving methods in HOL4 system, including forward proof and goal oriented proof. The second method is more commonly used. In this paper, we use the method of goal oriented proof. This method uses the tactic of HOL4, and the existing conditions, definitions and theorems to divide the original goal into one or more relatively simple sub-goals. Then we only have to prove these sub-goals. And the original goal will be proved when all the sub-goals are proved. In the proof of Theorem 1, the combination of tactic $REPEAT$ and tactic GEN_TAC is used to remove all of the universal quantifiers firstly. And then the proof is completed by using Definition 1 to rewrite the current goal.

C. Fractional Differential of a Constant

$$ {}^{C}_{a}D^{v}_{t}C = \begin{cases} C, & v = 0 \\ 0, & v > 0 \end{cases} \tag{4} $$

Caputo definition is commonly used in engineering applications. This is partly because the fractional differential of a constant under Caputo definition is bounded, as shown in Formula(4), while it is unbounded under other definitions. For example, under Riemann-Liouville definition, the fractional differential of a constant C is expressed as ${}^{RL}_{a}D^{v}_{t}C = \frac{Ct^{-v}}{\Gamma(1-v)}$, which will be bounded unless the starting point t tends to ∞. However, it is impossible to set the starting point to $-\infty$ when analyzing the transient process. Hence, Caputo definition is more appropriate in engineering applications[21]. The formal verification of this special property in HOL4 is given in Theorem 2.

Theorem 2. Fractional Differential of a Constant
$\forall f : real- > real\ c : real\ v : real\ a\ t.$
$(\forall a\ t\ n\ l.frac\_c\_exists\ f\ v\ a\ t\ n\ l) \wedge (0 <= v) ==>$
$(frac\_c\ (\lambda t.c)\ v\ a\ t = if\ (v = 0)\ then\ c\ else\ 0)$

The integer order derivative of a constant is included in the verification of Theorem 2. In order to simplify the verification process and facilitate the formal verification of other verification, here we firstly verify the integer order derivative of a constant and form it as a separate lemma.

Lemma 1. Integer Order Derivative of Constant c
$\forall m\ c.(0 < m) ==> (n\_order\_deriv\ m\ (\lambda x.c)\ t = 0)$

Lemma 1 verifies that the m^{th} order derivative of constant c is 0. This result is consistent with the mathematical result. The variable m in Lemma 1 is a positive integer and it has infinite possibilities. For such goal, we generally use mathematical induction method to prove it. The proof of Lemma 1 is finished by using mathematical induction method twice. We firstly make an induction on m and then divide the goal into two cases whose precondition is $(0 < 0)$ and $(0 < m + 1)$, respectively. As we all know, the premise condition $(0 < 0)$ is not established. The inference rule of HOL4 is that any conclusion can be deduced by the impossible precondition. Here we use the tactic $FULL\_SIMP\_TAC$ to complete the proof of the first case. In the proof of the second case, we firstly verify that the $(m+1)^{th}$ order derivative of c is equal to the m^{th} order derivative of the derivative of c, and then prove that the derivative of c is equal to 0. Finally, the proof of the second case can be done by doing a mathematical induction on m again. Hence Lemma 1 is proved.

Theorem 2 is implemented with statement $if \cdots then \cdots else \cdots$ because it has two cases. One case is that the differential order is 0 and the other one is that the differential order is greater than 0. We firstly proceed with Theorem 2 by separating the goal into two sub-goals using tactic $COND\_CASES\_TAC$.

The first sub-goal describes that the fractional differential of a constant returns the constant itself when the differential order is 0. We finish the proof of the first sub-goal by using an assumption and Theorem 1 to rewrite the goal.

For the case that the differential order is greater than 0, we firstly use tactic $COND\_CASES\_TAC$ to divide the present goal into two sub-goals:

$C = 0$

and

$lim(\lambda n.1/Gamma\ (\&flr\ v + 1 - v) * integral(a, t - 1/2\ pow\ n)(\lambda x.(t - x)\ rpow\ (flr\ v + 1 - v - 1) * n\_order\_deriv\ (flr\ v + 1)\ (\lambda t.C)\ x)) = 0.$

For the sub-goal $C = 0$, C is an arbitrary constant so we cannot say that C must equal to 0. But there is a contradiction between $(v \neq 0)$ and $(v = 0)$ in the assumption. According to the inference rule of HOL4, we apply tactic $FULL\_SIMP\_TAC$ to deduce sub-goal $C = 0$. In the proof of the second sub-goal, we firstly establish a new sub-goal:

$\forall n\ c\ x.n\_order\_deriv\ (flr\ v + 1)\ (\lambda t.c)\ x = 0$

It can be seen that the new sub-goal is the conclusion in Lemma 1. We can directly apply Lemma 1 to prove the above sub-goal as long as we can prove that the order $(flr\ v + 1)$ is greater than 0. It is difficult to prove $(0 < flr\ v + 1)$. Here, the assumption is used to deduce that v is greater than 0 firstly. Secondly, we prove that $(flr\ v)$ is equal to or greater than zero by using theorems NUM_FLOOR_LE2 and $REAL\_LT\_IMP\_LE$. Thirdly, it can be naturally proved that $(flrv + 1)$ is greater than 0 by using the combination of theorem $GSYM\ ADD1$ and tactic $REWRITE\_TAC$ as well as theorem $LESS\_EQ\_IMP\_LESS\_SUC$ and tactic $FULL\_SIMP\_TAC$. Now that Lemma 1 can be used to deduce the above sub-goal. Then the proved sub-goal can be applied to simplify the original goal. Now, the second sub-goal of Theorem 2 is simplified to:

$lim(\lambda n.1/Gamma\ (\&flr\ v + 1 - v) * integral(a, t - 1/2\ pow\ n)(\lambda x.(t - x)\ rpow\ (\&flr\ v + 1 - v - 1) * 0)) = 0$

Then the item $integral(a, t - 1/2\ pow\ n)(\lambda x.(t - x)\ rpow\ (\&flr\ v + 1 - v - 1) * 0))$ is simplified to $(integral(a, t - 1/2\ pow\ n)(\lambda x.0))$ by using theorem $REAL\_MUL\_RZERO$. Next, we prove that $(lim(\lambda n.1/Gamma\ (\&flr\ v + 1 - v) * 0))$ is equal to $(lim(\lambda n.0))$. With this, the second sub-goal of Theorem 2 is simplified to:

$$lim(\lambda n.0) = 0$$

Finally, the formal verification of Theorem 2 is done by using the definition lim, theorem $INTEGRAL\_CONST$ and theorem SEQ_CONST.

D. Integer Order Differential is the Special Case of Fractional Differential

Fractional differential is the generalized form of integer order differential and integer order differential is the special case of fractional differential. When the order m is a positive integer and the initial condition is 0, fractional differential is consistent with integer order differential. Theorem 3 is the formal verification of this property. Lemma 2 and Lemma 3 are the required lemmas in the verification of Theorem 3. We also prove these two lemmas separately.

Theorem 3. Integer Order Differential is the Special Case of Fractional Differential
$\forall f\ m\ n\ t.(0 <= m \wedge (\forall t\ n.frac\_c\_exists\ f\ (\&m)\ a\ t\ n\ l) \wedge ((n\_order\_deriv\ m\ f\ a) = 0)) ==> (frac\_c\ f\ (\&m)\ a\ t = n\_order\_deriv\ m\ f\ t)$

Lemma 2. The Derivative of nth Order Derivative is (n+1)th Order Derivative
$\forall m\ f\ t.(\forall m.m <= n + 1 ==> (\lambda t.n\_order\_deriv\ m\ f\ t)\ differentiable\ t) ==> ((\lambda t.n\_order\_deriv\ n\ f\ t)\ diffl\ (n\_order\_deriv\ (n + 1)\ f\ t))\ (t)$

Lemma 3. Newton Leibniz Formula
$\forall (f : real- > real)\ (f' : real- > real)\ a : real\ b : real.\ a <= b \wedge (\forall t.a <= t \wedge t <= b ==> (f\ diffl\ f'\ t)\ t) ==> (integral(a, b)\ f' = f\ b - f\ a)$

Lemma 2 shows that equation $\frac{df^n(t)}{dt} = f^{n+1}(t)$ will be tenable if function $f(t)$ is $(n+1)^{th}$ order derivable. Lemma 3 verifies that the integral of function f' in interval [a,b] equals to the difference value between the value of function f at upper limit and the value of function f at lower limit, where f is the original function of f'. Proofs of these two lemmas are challenging for us. The key is to transform the goal flexibly. When proving Lemma 2, we are unable to do a further conversion of the goal until we change our way of thinking. The precondition of Lemma 2 is that function f is m^{th} order derivable for every m which meets condition $(m \leq n+2)$. Taking the definition of m^{th} order derivative into account, we convert the precondition to that f' is m^{th} order derivative for every m which meets condition $(m \leq n + 1)$, where f' is the derived function of f. This conversion enables the proof to be applied with the definition of m^{th} order derivative, and then we can overcome the difficulty. Analogously, in the proof of Lemma 3, we need to prove a sub-goal $(n\_order\_deriv\ 1\ f\ x = deriv\ f\ x)$

which is also unable to do further transformation under the existing theorems. Here, if the number 1 is replaced with $(SUC\ 0)$ which means $(0+1)$, it will be possible for us to use the definition of m^{th} order derivative to rewrite the sub-goal and then finish the proof.

In Theorem 3, the antecedent (0≤m) limits that Formula(1) just indicates fractional differential. $(n\_order\_deriv\ m\ f\ a = 0)$ denotes that the initial condition of fractional calculus is 0. HOL4 is a rigorous tool for logical verification and error will occur if the type is not consistent. Here, the order m is a natural number of type num while the order defined in $frac\_c$ needs to be the type of $real$. So we should introduce operator & to map the natural number m to its corresponding real number of type $real$ here. Only in this way, we can avoid the error of type inconsistency.

The formal verification of Theorem 3 is relatively complex. We firstly simplify Theorem 3 to two sub-goals by using Definition 1 and tactic RW_TAC:

$f\ t = n\_order\_deriv\ m\ f\ t$
$----------0.\exists t\ n.frac\_c\_exists\ f\ (\&m)\ a\ t\ n\ l$
$1.n\_order\_deriv\ m\ f\ a = 0$
$2.\&m = 0$

and

$lim(\lambda n.$
$1/Gamma\ (\&flr(\&m)+1-\&m)*$
$integral(a,t-1/2\ pow\ n)$
$(\lambda x.$
$(t-x)\ rpow\ (\&flr\ (\&m)+1-\&m-1)*$
$n\_order\_deriv\ (flr\ (\&m)+1)\ f\ x)) =$
$n\_order\_deriv\ m\ f\ t$
$----------0.\exists t\ n.frac\_c\_exists\ f\ (\&m)\ a\ t\ n\ l$
$1.n\_order\_deriv\ m\ f\ a = 0$
$2.\&m <> 0$

What should be mentioned here is that the statements under imaginary line are the assumptions which are the known conditions of the goal. For the first sub-goal, we firstly prove $(m=0)$ by using theorem $GSYM\ REAL\_INJ$ and the known conditions. Then the proof of the first sub-goal can be done by utilizing the definition $n\_order\_deriv\_def$. In the proof of the second sub-goal, we firstly deduce another condition (0≤&m) from the known condition (&m<>0) by applying the statement $(ASSUM\_LIST(fn\ thl\ => ASSUME\_TAC(REWRITE\_RULE[REAL\_LT\_NZ]$ $(el\ 3\ (rev\ thl)))))$ to the current goal. Here, $ASSUM\_LIST(fn\ thl)$ represents the operation on the assumption list, $ASSUME\_TAC$ and $REWRITE\_RULE$ are the tactics of HOL4, $REAL\_LT\_NZ$ is a theorem and $(el\ 3\ (rev\ thl))$ is a positioning statement. Next, we establish a new sub-goal:

$\forall n\ x.(\&(flr((\&(m:num)):real):num):real) = \&m$
And the above new sub-goal can be verified by using theorem $REAL\_IN$ and NUM_FLOOR_EQNS. Then we utilize the proved sub-goal to simplify the initial goal to:

$lim(\lambda n.1/Gamma\ (\&m+1-\&m)*integral(a,t-1/2\ pow\ n)(\lambda x.(t-x)\ rpow\ (\&m+1-\&m-1)*n\_order\_deriv\ (flr\ (\&m)+1)\ f\ x)) = n\_order\_deriv\ m\ f\ t$

The next step is to simplify $(flr\ (\&m))$ to m by using theorem $REAL\_INJ$. Then we use theorem $REAL\_ADD\_SUB$ and $REAL\_SUB\_REFL$ to prove that $(\&m+1-\&m-1)$ is equal to 0. Next, the sub-goal $(\forall n\ x.(t-x)\ rpow\ 0*n\_order\_deriv\ (m+1)\ f\ x = n\_order\_deriv\ (m+1)\ f\ x)$ is verified and used to simplify the second sub-goal of Theorem 3 to: $lim(\lambda n.1/Gamma(1)*integral(a,t-1/2\ pow\ n)(\lambda x.n\_order\_deriv\ (m+1)\ f\ x)) = n\_order\_deriv\ m\ f\ t$

The property of Gamma function $GAMMA\_1\_EQUAL\_1$ which has been verified in reference [14] is used here to verify that $(Gamma\ 1)$ is equal to 1. Finally, we accomplish the proof of Theorem 3 by using Lemma 2, Lemma 3, the known conditions and the definition and properties of limit function.

Establishing sub-goal is needed in the proving process many times. But when we use the proved sub-goal to rewrite the goal, it fails. For instance, when proving goal $(lim(\lambda n.1/Gamma(1)*integral\ (a,t-1/2\ pow\ n)\ (\lambda x.(t-x)\ rpow\ 0*n\_order\_deriv\ (m+1)\ f\ x)) = n\_order\_deriv\ m\ f\ t)$, we establish a sub-goal $((t-x)\ rpow\ 0*n\_order\_deriv\ (m+1)\ f\ x = n\_order\_deriv\ (m+1)\ f\ x)$ and then prove it. The types of variables in the sub-goal are completely consistent with the types in initial goal, but it fails when we use the sub-goal to simplify the initial goal. This is because (λn) in the initial goal has the implication of arbitrary n. We overcome this problem by adding (λn) to the sub-goal when we established it.

E. Integer Order Integral is the Special Case of Fractional Integral

Similarly, when the order of fractional calculus is a negative integer m, the fractional integral ${}_a^C D_t^m$ is the same as the mth order integral of integer order calculus. When the order of fractional calculus is -1, there is Formula(5).

$$ {}_a^C D_t^{-1} f(x) = \int_a^t f(x)\mathrm{d}x \tag{5}$$

We formally verify Formula(5) in HOL4 as follows:

Theorem 4. First Order Integral is the Special Case of Fractional Integral
$\forall f\ a\ t.FLR\_NEG\_1 \wedge FLR\_NEG\_0 ==> (frac\_c\ f\ (-\&(1:num))\ a\ t = lim(\lambda n.integral(a,t-1/2\ pow\ n)\ f))$

Definition of FLR_NEG_1 and FLR_NEG_0 are respectively shown as follows:
$FLR\_NEG\_1 = (\&flr\ (-\&(1:num)) = -1)$
$FLR\_NEG\_0 = (flr\ (-\&(1:num))+1:num = 0:num)$

The first definition indicates that -1 is round off to -1. The second definition demonstrates that the result of the rounding off of -1 plus 1 is 0. When proving Theorem 4, we firstly use Definition 1 to rewrite the goal and then utilize tactic $COND\_CASES\_TAC$ to divide the goal into two sub-goals:

$ft = lim(\lambda n.integral\ (a,t-1/2\ pow\ n)\ f)$

and

$lim(\lambda n.1/Gamma\ (\&flr\ (-1)+1--1)*integral(a,t-1/2\ pow\ n)(\lambda x.(t-x)\ rpow\ (\&flr\ (-1)+1--1-1)*n\_order\_deriv\ (flr\ (-1)+1)\ f\ x)) = lim(\lambda n.integral\ (a,t-1/2\ pow\ n)\ f)$

According to the inference rules of HOL4, the first sub-goal can be deduced by the contradictory assumptions. For the second sub-goal, we firstly use theorem $REAL\_SUB\_RNEG$ to simplify $(1 - -1)$ to $(1 + 1)$. Then we utilize the above two definitions and some laws of computing to simplify the current goal. Finally, the definition of m^{th} order derivative and theorem ETA_THM are used to realize the proof.

Proofs of properties not only ensure the correctness of the formalization of fractional calculus based on Caputo definition, but also reduce the interventions of user when formally analyze the fractional order systems. The formalizations of fractional calculus and its properties are the keys to formally analyze fractional order systems. The work in this section provides the bases to the formal analysis of fractance element and fractional differential circuit.

III. Formalization of Fractance Element

The actual circuits tend to show the fractional order behavior. For example, the modeling and analysis of traditional capacitance is always based on the integer order differential theory. However, with the development of nonlinear theory and fractal differential geometry theory, the researchers found that the traditional capacitance which is based on integer order calculus is just the idealization of the actual model. Actually, the ideal capacitance does not exist in practice. This is mainly because that the electrolyte materials which make up the capacitance show the fractal dimension characteristic. In fact, the capacitance presents the fractional characteristics on the physical property. The integer order differential and integral circuit which respectively show the behaviors of high and low pass, are also the results of the idealized processing of real circuit. Fractance element and fractional differential circuit can describe the fractional order behaviors of circuits. We will use fractional calculus to model them. Then the relationship of fractance element and ideal elements as well as the unification of fractional differential circuit and integer differential circuit are verified. The purpose is to illustrate that fractional calculus is the extension of integer order calculus and the real systems can be described more comprehensively by using fractional calculus. Meanwhile, the correctness of the above formalizations and the effectiveness of theorem proving method in the analysis of fractional order systems are also demonstrated here.

Any lumped parameter element can be described by mathematical model and physical model. Fractance element is no exception. In this section, we will give the circuit symbol graph and mathematical expression of fractance element, and then formally analyze it and fractional differential circuit which is the simplest circuit composed by fractance element.

Fractance element is a two-port element and it can be represented by symbol F. The circuit symbol graph of it is given in Fig.1.

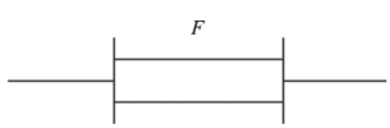

Fig. 1. Fractance Element

In the complex frequency domain, the impedance of fractance element is shown as $Z(S) = kS^v$, where k is a constant coefficient and v is the order of fractance element. In reference [1], when the order v is greater than 0, fractance element which has the form of $Z(S) = kS^{-v}$ is called fractional capacitance and it is called fractional inductance when it is in the form of $Z(S) = kS^v$. The voltage and current of fractance element satisfy Ohm's law and the relationship of them is given in Formula (6).

$$i(t) = kD^v[v(t)] \tag{6}$$

As can be seen from Formula (6), the current of fractance element is the v^{th} order calculus of voltage and v is a real number. Due to the arbitrariness of order v, the definition of fractance element is broader than common components and the function of fractance element is also more powerful. Definition 3 is the formalization of fractance element in HOL4.

Definition 3. Fractance Element
$\forall k\ v\_t\ v\ t. i\_t\ k\ v\_t\ v\ t = k * frac\_c\ v\_t\ v\ 0\ t$
where i_t and v_t are the current and voltage of fractance element at moment t, respectively. k is the constant coefficient and $frac\_c$ is the formalization of fractional calculus based on Caputo definition which is given in Definition 1.

According to the circuit analysis theory, the current flowing through the resistance R is $i(t) = \frac{v(t)}{R}$, while the current flowing through the capacitance C is $i(t) = C\frac{dv(t)}{dt}$ and the current flowing through the inductance L is $i(t) = \frac{\int_0^t v(\tau)d\tau}{L}$. Introducing the concept of fractance element, the resistance can be understood as the case where the order of fractance element is 0, and the capacitance can be understood as the case where the order is 1 and the inductance can be understood as the case where the order is -1. Therefore, there are connections between the fractance element and the traditional resistance, inductance and capacitance. The traditional components are three ideal models of actual components. Fractance element can better describe the performance of practical elements in the circuit. Based on Definition 3, we will use the formalizations in Section 2 to formally verify the relationship between fractance element and the three ideal components. The formal verifications of these three relationships using higher-order logic are shown below.

Theorem 5. Relationship between Fractance Element and Resistance
$\forall k\ v\_t\ t.(v = 0 : real) ==> (i\_t\ k\ v\_t\ v\ t = k * v\_t\ t)$

Theorem 6. Relationship between Fractance Element and Capacitance
$\forall k\ v\_t\ t.(v = \&(1 : num)) \wedge (\forall v\ t\ n\ l\ a.$
$frac\_c\_exists\ v\_t\ v\ a\ t\ n\ l) \wedge (n\_order\_deriv\ 1\ v\_t\ 0 =$
$0) ==> (i\_t\ k\ v\_t\ v\ t = k * deriv\ v\_t\ t)$

Theorem 7. Relationship between Fractance Element and Inductance
$\forall k\ v\_t\ t.(v = -\&(1 : num)) \wedge FLR\_NEG\_1 \wedge$
$FLR\_NEG\_0 ==> (i\_t\ k\ v\_t\ v\ t = k *$
$lim(\lambda n.integral(0, t - 1/2\ pow\ n)\ v\_t))$

Theorem 5 verifies that the fractance element exhibits the behavior of a resistance for $v = 0$. Here, the relationship between the flowing current and voltage is expressed as

$i(t) = kv(t)$ in time domain, where k equals to $\frac{1}{R}$ and R is the value of resistance. The proof of Theorem 5 is completed by using Definition 3 and Theorem 1 to rewrite the goal and make a further calculation. Theorem 6 proves that fractance element displays the characteristic of ideal capacitance for $v = 1$. At this time, the relationship between the flowing current and voltage is expressed as $i(t) = k\frac{dv(t)}{dt}$, where k means the value of capacitance. The formal verification of Theorem 6 is based on Theorem 3. Theorem 7 deduces that fractance element will behave as an ideal inductance if $v = -1$. The connection between the flowing current and voltage is expressed as $i(t) = k\int_0^t v(\tau)d\tau$, where k equals to $\frac{1}{L}$ and L is the value of inductance. Theorem 4 is utilized in this proof.

The fractional differential circuit is a kind of fractance circuit and it is composed of fractance element. It outputs the fractional differential of input signal and its amplitude frequency characteristic is a high pass filter. In terms of fractional order controller, initial implementation of fractional differential circuit[22] makes a foundation for the universal application of fractional order controllers in the field of information science[23]. Fig.2 is a fractional differential circuit with power source Vi, resistance R and fractance element F which is realized by fractional capacitance. Based on the formalization of fractance element, the formal modeling and verification of fractional differential circuit will be performed next.

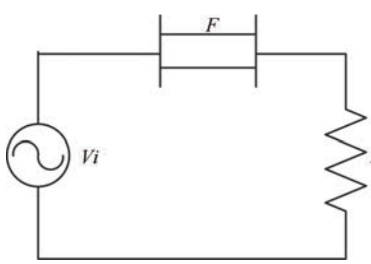

Fig. 2. Fractional Differential Circuit

The output voltage of fractional differential circuit in Fig.2 is the voltage across the resistance R and the input voltage is the voltage of power source. The relationship between the output voltage and the input voltage is inferred as:

$$v_o(t) = RCD^v v_i(t) \qquad (v > 0) \tag{7}$$

where $v_o(t)$ is the output voltage and $D^v v_i(t)$ returns the v^{th} order calculus of input voltage $v_i(t)$. The condition of Formula(7) limits the operator $D^v v_i(t)$ as the expression of fractional differential. The order v is the same as the order of fractance element. The formalization of fractional differential circuit in HOL4 is given in Definition 4.

Definition 4. Fractional Differential Circuit
$\forall R\ C\ vi\_t\ v\ t.vo\_D\_t\ R\ C\ vi\_t\ v\ t = R * C * frac\_c\ vi\_t\ v\ 0\ t\ R\ C\ vi\_t\ v\ t.vo\_D\_t\ R\ C\ vi\_t\ v\ t = R * C * frac\_c\ vi\_t\ v\ 0\ t$
where vo_D_t and vi_t indicate the output voltage and the input voltage of the circuit at moment t. vo_D_t and vi_t are both type of $(real- > real)$ here. R, C, v and t represent resistance, capacitance, differential order and the upper limit. If the order v equals to 1, Definition 4 will represent a first order differential circuit. For the first order differential circuit, the output response just reflects the rate of input change. So the output response of first order differential circuit is 0 if a constant signal is applied at the input. This is because the rate of change for constant signal is 0. The following is the verification of this property in HOL4 using the already verified definition and properties in Section 2.

$(v = 1) \wedge (\exists a\ t\ n\ l.frac\_c\_exists\ (\lambda t.v\_0 : real)\ v\ a\ t\ n\ l)$
$==> (vo\_D\_t\ R\ C\ (\lambda t.v\_0 : real)\ v\ t = 0)$

The precondition $(v = 1)$ guarantees that the order of fractional differential circuit is 1. Under this condition, fractional differential circuit will behave as first order differential circuit of integer order calculus. The second precondition $(frac\_c\_exists\ (\lambda x.v\_0\ :\ real)\ v\ a\ x\ n\ l)$ ensures the existence of fractional calculus which is based on Caputo definition for function v_0 . Under these two preconditions, it can be gradually verified that the output response of this fractional differential circuit is 0 when the constant signal v_0 is the input. The availability of already verified property of fractional calculus in Section 2 let us to achieve the simple sub-goal.

The fractional order differentiator has been formalized in reference[12]. It formally verified the output response of fractional order differentiator when unit step signal is applied at the input and the order is between 0 and 1. A lot of work has been done in [12], which is very significant and gives us much inspiration. However, the formal verification of fractional order differentiator did not take the order of integer 1 into account. In other words, they have not considered the unification of fractional differential and integer order differential. In this paper, we take the differential order of integer 1 into account, and use the Caputo definition to verify the output response of the fractional differential circuit with constant signal v_0 as input. The fractional differential circuit will behave as first order differential circuit if the order is integer 1. According to the property of Riemann-Liouville definition of fractional calculus, the output response of first order differential circuit is RCv_0t^{-1} when constant signal v_0 is applied at the input. This result is in contradiction with the result that the output response of first order differential circuit only reflects the rate of input change. As analyzed above, the result using Caputo definition in this paper is consistent with the fact. The formal result not only verifies the consistency of fractional first order differential circuit and integer first order differential circuit, which besides achieving uniformity in fractional differential and integer order differential, but also correctly deduces the output response of first order differential circuit with constant signal as the input.

Due to the completeness of theorem proving, the results are accurate and complete. Besides, the results in this paper are consistent with the theoretical results, which illustrate the correctness of the formalizations of fractional calculus, as well as the validity of the analysis of fractance element using theorem proving.

IV. Conclusion

Theorem proving, as a formal method, formalizes the specifications and designs of systems to the logic models. The validation process is intuitional and rigorous. Besides, its self-prove function can ensure the correctness of formalization. Based on theorem proof tool HOL4, we completed the formalized analysis of fractance element and fractional differential circuit which is made up of fractance element. Caputo definition of fractional calculus and some properties of it are the theoretical bases of the formal analysis of fractance element and fractional differential circuit. Therefore, their formalization is a significant work presented in this paper. These works factually lay good foundations for the formal analysis of circuits fractional order behaviors. Meanwhile, the formal analysis of fractance elements and fractional differential circuit also shows the effectiveness, practicality and correctness of the formalizations of fractional calculus theorems. The formalization of fractional calculus based on Caputo definition in this paper, completes the definition of fractional calculus in HOL4 and provides more choices for the formal analysis of fractional order systems. In addition, the formal analysis of fractance element not only enriches the studies of fractance element, but also provides a way to the analysis of fractance element. The next step will be taken to verify the other properties of fractional calculus based on Caputo definition, to lay a solid foundation for the complete analysis of fractance element and fractional differential circuit.

References

[1] hou Ji-Liu, Pu Yi-Fei, Liao Ke. *Fractional Calculus's Principle and its Application in Signal Analysis and Processing*. Beijing:Science Press, 2006. 151–154

[2] Zhang YZ. Study on Fractional-order Calculus and its Applications [Ph.D.dissertation], Northeastern University, China, 2008

[3] Deng Li-Wei, Song Shen-Min. Synchronization of fractional order hyperchaotic systems based on output feedback sliding mode control. *Acta Automatica Sinica*, 2014, **40**(11):2420–2427

[4] Liao Guangkai, Long Zhilin, Xu Fu, et al. Investigation on the viscoelastic behavior of an fe-base bulk amorphous alloys based on the fractional order rheological model. *Acta Physica Sinica*, 2015, **64**(13): 136101–136101

[5] Mehdi Dalir. Applications of fractional calculus. *Applied Mathematical Sciences*, 2010, **4**(21): 1021–1032

[6] Huang Guo, Xu Li, Pu Yi-Fei. Summary of research on image processing using fractional calculus. *Application Research of Computers*, 2012, **29**(2):414–426

[7] Zafer BINGUL, Oguzhan KARAHAN. Fractional PID controllers tuned by evolutionary algorithms for robot trajectory control. *Turkish Journal of Electrical Engineering & Computer Sciences*, 2012, **20**(Sup.1), 1123–1136

[8] Yan Li-Mei, Zhu Yu-Song, Xu Jian-Jun, et al. Transmission lines modeling method based on fractional order calculus theory. *Transactions of China Electrotechnical Society*, 2014, **29**(9):260–268

[9] Cao Jun-Yi, Liang Jin, Cao Bing-Gang. Fuzzy fractional order controller based on fractional calculus. *Journal of Xi'an Jiao Tong University*, 2005, **39**(11):1246–1253

[10] Krishnan Balachandran, Venkatesan Govindaraj, Luis Rodrłguez-Germ, et al. Stabilizability of fractional dynamical systems. *Fractional Calculus & Applied Analysis*, 2014, **17**(2):511–531

[11] Zhang Song. Implementation of electric circuit for changeable order-changeable fractional resistance. *Communication Technology*, 2010,**43**(10):164–166

[12] Zhou Ji-Liu, Yuan Xiao, Liao Ke, et al. One Method to realize alterable order analog fractance circuits . *Journal of Sichuan University (Engineering Science Edition)*, 2007, **39**(3):141–144

[13] Ren Yi, Yuan Xiao. Implementation of fractional-order analog fractance circuit using binomial expansion. *Journal of Sichuan University (Natural Science Edition)*, 2008,**45**(5):1100–1104

[14] Umair Siddique, Osman Hasan. Formal analysis of fractional order systems in HOL. *Formal Methods in Computer-Aided Design*, 2011.163–170

[15] Shi LK. The Formal Analysis of Fractional Systems based on Grunwald-Letnikov Definition using Higher-order Logic[Master dissertation], Capital Normal University, China, 2014

[16] Zivorad Tomovski, Roberto Garra. Analytic solutions of fractional integro-differential equations of volterra type with variable coefficients. *Fractional Calculus & Applied Analysis*, 2014, **17**(1):38–60

[17] Zhao Chun-Na, Li Ying-Shun, Lu Tao. *The Analysis and Design of Fractional Systems*. Beijing: National Defence Industry Press, 2010.13–20

[18] Harrison J. *Theorem Proving with the Real Numbers*. Berlin:Springer-Verlag, 1998

[19] Gu Wei-Qing, Shi Zhi-Ping, Guan Yong, et al. Formalization of gauge integration theory in HOL4, *Computer Science*,2013, **40**(2):191–194

[20] Zhao Gang, Zhao Chun-Na, Guan Yong, et al. Formalization of laplace transform calculus in HOL4. *Micro Computer System*, 2014, **35**(9):2178–2181

[21] Mohammad Saleh Tavazoei. Time response analysis of fractional-order control systems:a survey on recent results. *Fractional Calculus & Applied Analysis*, 2014, **17**(2):440–461

[22] M.Nakagava, K.Sorimachi. Basic characteristics of a fractance device. *IEICE TRANSACTIONS on Fundamentals of Electronics, Communications and Computer Sciences*, 1992, **E75-A**(12):1814–1819

[23] Wang Ji-Feng. *The Analysis of Control Performance for Fractional-order Systems*. Beijing: Electronic Industry Press, 2010.13–14

LI Shanshan is currently a graduate student in Capital Normal University. She received her bachelor degree from Minzu University of China in 2013. Her research interests cover formal verification and fractional calculus.
e-mail:shanshan_xiong@126.com

ZHAO Chunna graduated from Northeastern University in 2006 and received the Ph.D degree. She is currently an associate professor in Capital Normal University. Her research interests include formal verification and the modeling and control of fractional order system.
e-mail:chunnazhao@163.com
corresponding author

LI Xiaojuan graduated from China Agricultural University in 1999 and received the Ph.D degree. She is currently a professor in Capital Normal University. Her research interests cover formal verification and the computer network.
e-mail:lixj@cnu.edu.cn

GUAN Yong graduated from China University of Mining and Technology in 2004 and received the Ph.D degree. He is currently a professor in Capital Normal University. His research interests cover formal verification, robot and the embedded system with high reliability.
e-mail:guanyong@cnu.edu.cn

WANG Rui graduated from Tsinghua University in 2012 and received the Ph.D degree. She is currently a teacher in Capital Normal University. Her research interests include formal verification and the verification of robot safety.
e-mail:rwang04@cnu.edu.cn

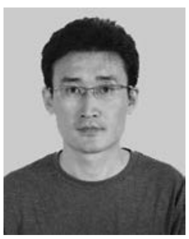

SHI Zhiping graduated from Institute of Computing Technology, Chinese Academy of Sciences in 2005 and received the Ph.D degree. He is currently an associate researcher in Capital Normal University. His research interests include formal verification and artificial intelligence.
e-mail:shizp@cnu.edu.cn

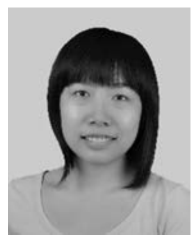

ZHANG Qianying graduated from University of Chinese Academy of Sciences in 2015 and received the Ph.D degree. She is currently a teacher in Capital Normal University. Her research interests include real-time operating system and formal verification.
e-mail:zsjzqy@gmail.com

Containment Control of Fractional Order Multi-Agent Systems with Time Delays

Hongyong Yang, Fuyong Wang and Fujun Han

Abstract—**In complex environments, many distributed multi-agent systems are described with the fractional-order dynamics. In this paper, containment control of fractional-order multi-agent systems with multiple leader agents are studied. Firstly, the collaborative control of fractional-order multi-agent systems (FOMAS) with multiple leaders is analyzed in a directed network without delays. Then, by using Laplace transform and frequency domain theorem, containment consensus of networked FOMAS with time delays is investigated in an undirected network, and a critical value of delays is obtained to ensure the containment consensus of FOMAS. Finally, numerical simulations are shown to verify the results.**

Index Terms—**containment control, multi-agent systems, fractional-order, time delays.**

I. Introduction

RESENTLY, with the rapid development of network and communication technology, the distributed coordination for networked systems has been studied deeply ([1−5]). Cooperative control of multi-agent systems has become a hot topic in the fields of automation, mathematics, computer science, etc ([6−10]). It has been applied in both military and civilian sectors, such as the formation control of mobile robots, the cooperative control of unmanned spacecraft, the attitude adjustment and position of satellite, and the scheduling of smart power grid systems, etc. As a kind of distributed cooperative control problems of multi-agent systems with multiple leaders, containment control regulates followers eventually converge to a target area (convex hull formed by the leaders) by designing a control protocol, which has been paid much more attention in recent years ([11−13]).

In the complex practical environments, many distributed systems cannot be illustrated with the integer-order dynamics and can only be characterized with the fractional-order dynamics ([14−16]). For example, flocking movement and food searching by means of the individual secretions, exploring of submarines and underwater robots in the seabed with a massive number of microorganisms and viscous substances, working of unmanned aerial vehicles in the complex space environment ([17−18]). Cao and Ren have studied the coordination of multi-agent systems with fractional order ([19−20]), and obtained the relationship between the number of individuals and the order in the stable fractional system. Yang et.al. have studied the distributed coordination of fractional order multi-agent systems with communication delays ([21−22]). Motivated by the broad application of coordination algorithms in FOMAS, the containment control of distributed fractional-order systems will be studied in this paper.

For containment control problems, the current research works are mainly focused on integer-order systems ([11−13,23−26]). In [11], containment control problem for first-order multi-agent systems with the undirected connected topology is investigated, and the effectiveness of control strategy is proven by using partial differential equation method. In [12], second-order multi-agent systems with multiple leaders are investigated, the containment control of multi-agent systems with multiple stationary leaders can be achieved in arbitrary dimensions. In [13], two asymptotic containment controls of continuous-time systems and discrete-time systems are proposed for the multi-agent systems with dynamic leaders, and the constraint condition for control gain and sampling period are given. Considering factors such as external disturbance and parameter uncertainty in [23], the attitude containment control problem of nonlinear systems are studied in a directed network. The impulsive containment control for second-order multi-agent systems with multiple leaders is studied in [25−26], where all followers are regulated to access the dynamic convex hull formed by the dynamic leaders.

When agents transfer information by means of sensors or other communication devices in coordinated network, communication delays have a great impact on the behaviors of the agents. Now, the influences of communication delays on multi-agent systems have also been paid more attentions ([2,7−10]) where these research activities on the coordination problem are mainly concentrated on integer-order multi-agent systems. In [24], containment control problem of multi-agent systems with time delays is studied in fixed topology, and two cases of multiple dynamic leaders and multiple stationary leaders are discussed, respectively. As far as we know, few researches have been done on the containment consensus of fractional order multi-agent systems with time delays.

In this paper, the containment control algorithms for multi-agent systems with fractional dynamics are presented, and the containment consensus of distributed FOMAS with communication delays is studied under directed connected topologies. The main innovation of this paper is that the distributed containment control of fractional order multi-agent systems with multiple leaders and communication delays is studied for the first time. The research presented in this paper is different from Reference[21], where consensus of FOMAS without lea-

This article has been accepted for publication in a future issue of this journal, but has not been fully edited. Content may change prior to final publication.

This article was recommended by Associate Editor Feng Zhu.

Hongyong Yang , Fuyong Wang and Fujun Han are with the Department of Information and Electrical Engineering, Ludong University, Yantai, 264025, China (E-mail: hyyang@ldu.edu.cn; yhy9919@sina.com; fswang@yeah.net).

Digital Object Identifier 10.1109/JAS.2016.7510211

der[21] is much easier than containment control of FOMAS with multiple leaders in this paper. The rest of the paper is organized as follows. In Section 2, we recall some basic definitions about fractional calculus. In Section 3, some preliminaries about graph theory are shown, and fractional order coordination model of multi-agent systems is presented. Containment control of fractional coordination algorithm for multi-agent systems with communication delay is studied in Section 4. In Section 5, numerical simulations are used to verify the theoretical analysis. Conclusions are finally drawn in Section 6.

II. Fractional Calculus

Fractional calculus has played an important role in modern science. There are two fractional operators used widely: Caputo and Riemann-Liouville (R-L) fractional operators. In physical systems, Caputo fractional order operator is more practical than R-L fractional order operator because R-L operator has initial value problems. Therefore, in this paper we will apply Caputo fractional order operator to describe the system dynamics and analyze the stability of proposed FOMAS algorithms. Generally, Caputo operator includes Caputo fractional integral and Caputo fractional derivative. Caputo fractional integral is defined as

$$ {}_{t_0}^{C}D_t^{-p}f(t)=\frac{1}{\Gamma(p)}\int_{t_0}^{t}\frac{f(\theta)}{(t-\theta)^{1-p}}\mathrm{d}\theta, $$

where the integral order $p\in(0,1]$, $\Gamma(.)$ is the Gamma function, and t_0 is a real number. Based on the Caputo fractional integral, for a nonnegative real number α, Caputo fractional derivative is defined as

$$ {}_{t_0}^{C}D_t^{\alpha}f(t)={}_{t_0}^{C}D_t^{-p}\left[\frac{\mathrm{d}^{[\alpha]+1}}{\mathrm{d}t^{[\alpha]+1}}f(t)\right], \tag{1} $$

where $p=[\alpha]+1-\alpha\in(0,1]$ and $[\alpha]$ is the integral part of α. If α is an integer, then $p=1$ and the Caputo fractional derivative is equivalent to the integer-order derivative. In this paper, we will use a simple notation $f^{(\alpha)}$ to replace ${}_{t_0}^{C}D_t^{\alpha}f(t)$. Let $\mathcal{L}()$ denote the Laplace transform of a function, the Laplace transform of Caputo derivative is shown as

$$ \mathcal{L}(f^{(\alpha)})=s^{\alpha}F(s)-\sum_{k=1}^{[\alpha]+1}s^{\alpha-1}f^{(k-1)}(0), \tag{2} $$

where $F(s)=\mathcal{L}(f^{(\alpha)})=\int_{0-}^{\infty}e^{-st}f(t)dt$ is the Laplace transform of function $f(t)$, $f^{(k)}(0)=\lim_{\xi\to 0-}f^{(k)}(\xi)$ and $f^{(0)}=f(0)=\lim_{\xi\to 0-}f(\xi)$.

III. Problem Statement

Assume that n autonomous agents constitute a network topology graph $\mathcal{G}=\{V,E,A\}$, in which $V=\{v_1,v_2,...,v_n\}$ represents a set of n nodes, and its edges set is $E\subseteq V\times V$. $I=\{1,2,...,n\}$ is the node indexes set, $A=[a_{ij}]\in\mathbf{R}^{n\times n}$ is an adjacency matrix with elements $a_{ij}\geq 0$. An edge of the diagraph $\mathcal{G}$ is denoted by $e_{ij}=(v_i,v_j)\in E$. Let the adjacency element $a_{ij}>0$ when $e_{ij}\in E$, otherwise, $a_{ij}=0$. The neighbors' set of node i is denoted by $N_i=\{j\in I: a_{ij}>0\}$.

Let $\mathcal{G}$ be a weighted graph without self-loops, i.e., $a_{ii}=0$, and matrix $D=\mathrm{diag}\{d_1,d_2,...,d_n\}$ be the diagonal matrix with the diagonal elements $d_i=\sum_{j=1}^{n}a_{ij}$ representing the out-degree of the i-th agent. $L=D-A$ is the Laplacian matrix of the weighted digraph $\mathcal{G}$. For two nodes i and k, there is index set $\{k_1,k_2,...k_l\}$ satisfying $a_{ik_1}>0$, $a_{k_1k_2}>0$, ..., $a_{k_lk}>0$, then there is an information transmission linked path between node i and k, also we say node i can transfer the information to node k. If node i can find a path to reach any node of the graph, then node i is globally reachable from every other node in the digraph.

Lemma 1[3]**.** 0 is a simple eigenvalue of Laplacian matrix L, and $X_0=C[1,1,...,1]^{\mathrm{T}}$ is corresponding right eigenvector, i.e., $LX_0=0$, if and only if the digraph $\mathcal{G}=(V,E,A)$ has a globally reachable node.

Lemma 2[9]**.** Matrix $L+B$ is a positive definite matrix, where L is a Laplacian matrix of the digraph $\mathcal{G}=(V,E,A)$ with a globally reachable node, and $B=\mathrm{diag}\{b_1,...,b_n\}$ with $b_i\geq 0$ and at least there is one element $b_i>0$.

Definition 1. The convex hull of a finite set of points $x_1,...,x_m$ denoted by $Co\{x_1,...,x_m\}$, is the minimal convex set containing all points $x_i,\ i=1,...,m$. More specifically, $Co\{x_1,...,x_m\}=\{\sum_{i=1}^{m}\nu_i x_i|\nu_i>0,\sum_{i=1}^{m}\nu_i=1\}$.

Recently, Fractional order systems have been widely applied in various science fields, such as physics, hydrodynamics, biophysics, aerodynamics, signal processing and modern control. The theories of fractional order equations are studied deeply, and the relationship between the fractional order and the number of agents to ensure coordination has been presented in [19]. Assume that Caputo fractional derivative is used to indicate the dynamics of multi-agent systems in the complex environments, the fractional order dynamical equations are defined as:

$$ x_i^{(\alpha)}(t)=u_i(t), i=1,...,n, \tag{3} $$

where $x_i(t)\in R$ and $u_i(t)\in R$ represent the i-th agent's state and control input respectively, $x_i^{(\alpha)}$ represents the $\alpha(\alpha\in(0,1])$ order Caputo derivative. Assume the following control protocols are used in FOMAS:

$$ u_i(t)=-\gamma\sum_{k\in N_i}a_{ik}[x_i(t)-x_k(t)], i\in I. \tag{4} $$

where a_{ik} represents the (i,k) elements of adjacency matrix A, $\gamma>0$ is control gain, N_i represents the neighbors collection of the i-th agent.

Suppose the multi-agent systems consisting of n_1 following agents and n_2 leader agents in this paper, where $n_1+n_2=n$. Then, the control protocols of the multi-agent systems can be rewritten as

$$ u_i(t)=\begin{cases} -\gamma\sum_{k\in N_i}a_{ik}[x_i(t)-x_k(t)], i=1,2,...,n_1; \\ 0, i=n_1+1,...,n. \end{cases} \tag{5} $$

The systems(3-5) can be rewritten as

$$ X^{(\alpha)}(t)=-\gamma\begin{pmatrix} L_1 & L_2 \\ 0 & 0 \end{pmatrix}X(t), \tag{6} $$

where $X(t) = [X_1(t), X_2(t)]^{\mathrm{T}}$, $X_1(t) = [x_1(t), x_2(t), ..., x_{n_1}(t)]^{\mathrm{T}}$, $X_2(t) = [x_{n_1+1}(t), ..., x_n(t)]^{\mathrm{T}}$, $L_1 \in \mathbf{R}^{n_1 \times n_1}$, $L_2 \in \mathbf{R}^{n_1 \times n_2}$. $X_1(t)$ is the set of the followers, and $X_2(t)$ is the set of the leaders.

Remark 1. Matrix $L_1 = (l_{ik}) \in \mathbf{R}^{n_1 \times n_1}$ satisfying

$$l_{ik} = \begin{cases} d_i - a_{ii}, i = k, \\ -a_{ik},\ i \neq k. \end{cases}$$

Matrix $L_2 = (l_{ik}) \in \mathbf{R}^{n_1 \times n_2}$ satisfying

$$l_{ik} = -a_{ik}, i = 1, 2, ..., n_1; k = n_1 + 1, ..., n.$$

Assume the collection formed by leaders is regarded as a virtual node, if one follower agent can connect to some leader, then the follower is connected to the virtual node.

Definition 2. The containment control is realized for the system (3) under certain control input (5), if the position states of the followers are asymptotically converged to the convex hull formed by the leaders.

Assumption 1. For any one follower, there is a directed connected path to the virtual node formed by leaders.

Lemma 3. With Assumption 1, matrix L_1 is positive definite, and $-L_1^{-1}L_2$ is a non-negative matrix whose entries sum in every row equals to 1.

Proof. From Lemma 2, matrix L_1 is positive definite matrix. Let $L_1 = dI_{n_1} - Q$ where d is a positive number which is large enough and matrix Q is a non-negative matrix. it has

$$\begin{aligned} L_1^{-1} &= (dI_{n_1} - Q)^{-1} \\ &= d^{-1}(I_{n_1} + d^{-1}Q + (d^{-1}Q)^2 + ...). \end{aligned}$$

Then, we obtain $-L_1^{-1}L_2$ is a non-negative matrix.

From Lemma 1, Laplacian matrix L will be satisfied with $LX_0 = 0$, where $X_0 = [1, 1, ..., 1]^{\mathrm{T}} \in \mathbf{R}^{n \times 1}$. Then we have

$$L_1X_{01} + L_2X_{02} = 0,$$

where $X_{01} = [1, 1, ..., 1]^{\mathrm{T}} \in \mathbf{R}^{n_1 \times 1}$ and $X_{02} = [1, 1, ..., 1]^{\mathrm{T}} \in \mathbf{R}^{n_2 \times 1}$. Since L_1 is a positive definite matrix from Assumption 1 and Lemma 2, it has

$$X_{01} = -L_1^{-1}L_2X_{02}.$$

Therefore, $-L_1^{-1}L_2$ is a stochastic matrix with entries sum in every row equaling to 1.

Theorem 1. Consider a directed dynamic system of n_1 followers and n_2 leaders with dynamics (3), whose dynamic topologies are satisfied with Assumption 1. Then the containment control is realized for the FOMAS under certain control protocol (5).

Proof. Based on the system (6), we have

$$\begin{aligned} &X_1^{(\alpha)}(t) = -\gamma(L_1X_1(t) + L_2X_2(t)), \\ &X_2^{(\alpha)}(t) = 0. \end{aligned} \tag{7}$$

Let $\bar{X}_1(t) = X_1(t) + L_1^{-1}L_2X_2(t)$, system (7) can be rewritten as

$$\begin{aligned} &\bar{X}_1^{(\alpha)}(t) = -\gamma L_1\bar{X}_1(t), \\ &X_2^{(\alpha)}(t) = 0. \end{aligned} \tag{8}$$

It is known that the fractional differential system (8) is asymptotically stable iff $\|arg(spec(L_1))\| > \alpha\pi/2$. Since L_1 is positive definite matrix, $\alpha \in (0, 1]$, we obtain $\lim_{t\to\infty} \bar{X}_1(t) = 0$, i.e.

$$\lim_{t\to\infty} X_1(t) = -L_1^{-1}L_2X_2(t).$$

Since matrix $-L_1^{-1}L_2$ is stochastic matrix, the states of the followers are asymptotically converged to the convex hull formed by the leaders with Definition 1. Then, based on Definition 2, the containment control is realized for the system (3) with the control protocol (5).

Remark 2. If FOMAS of n agents and $n_2 = 1$ leaders with dynamics (3), the containment control result in Theorem 1 will become the consensus of multi-agent systems with one leader.

Remark 3. If the fractional order $\alpha = 1$ in FOMAS, the containment control result in Theorem 1 will become that of multi-agent systems with integer-order dynamics[1].

IV. Containment control of FOMAS with time delays

In this section, we assume that there are communication delays in the dynamical systems, and containment control of the fractional-order agent systems with communication delays will be studied. Under the influence of communication delays, we can get the following algorithm:

$$x_i^{(\alpha)}(t) = u_i(t - \tau), i = 1, ..., n, \tag{9}$$

where τ is the communication delay of agent i. Through a simple change we can obtain

$$\begin{aligned} &X_1^{(\alpha)}(t) = -\gamma(L_1X_1(t - \tau) + L_2X_2(t - \tau)), \\ &X_2^{(\alpha)}(t) = 0. \end{aligned} \tag{10}$$

Let $\bar{X}_1(t) = X_1(t) + L_1^{-1}L_2X_2(t)$, system (10) can be rewritten as

$$\begin{aligned} &\bar{X}_1^{(\alpha)}(t) = -\gamma L_1\bar{X}_1(t - \tau), \\ &X_2^{(\alpha)}(t) = 0. \end{aligned} \tag{11}$$

Theorem 2. Suppose that multi-agent systems are composed of n independent agents with n_1 followers and n_2 leaders, whose connection network topology is undirected with Assumption 1. Then fractional-order multi-agent system (10) with time delays can asymptotically reach containment control, if

$$\tau < \frac{(2 - \alpha)\pi}{2(\bar{\lambda}\gamma)^{1/\alpha}}, \tag{12}$$

where $\bar{\lambda} = \max\{\lambda_i, i \in I\}$, λ_i is the eigenvalues of matrix L_1.

Proof. By applying Laplace transformation to system(11), we can obtain the characteristic equation of the system

$$\det(s^\alpha I_n + \gamma e^{-\tau s}L_1) = 0.$$

Since the Laplacian matrix L_1 is symmetrical positive definite, there is an orthogonal matrix P satisfying $L_1 = P\Lambda P^{-1}$, where $\Lambda = \mathrm{diag}\{\lambda_1, ..., \lambda_n\}$ with $\lambda_i > 0$. Therefore, the root of the characteristic equation is satisfied with $s \neq 0$.

When $s \neq 0$, let $F(s) = \det(I_n + \gamma s^{-\alpha}e^{-\tau s}L_1)$, we will prove that all solutions of $F(s) = 0$ have negative real parts. Let $G(s) = \gamma s^{-\alpha} e^{-\tau s} L_1$, according to the generalized Nyquist criterion, if for $s = j\omega$, where j is complex number unit, point $-1 + j0$ is not surrounded by the Nyquist curve of $G(j\omega)$'s eigenvalues, then all zero points of $F(s)$ have negative real parts. Let $s = j\omega$, we can get

$$G(j\omega) = \omega^{-\alpha} e^{-j(\omega\tau+\alpha\pi/2)} \gamma L_1, \tag{13}$$

We have the eigenvalues of $G(j\omega)$

$$\begin{aligned}|\lambda I_{n_1} - G(j\omega)| &= |\lambda I_{n_1} - (\omega^{-\alpha} e^{-j(\omega\tau+\alpha\pi/2)} \gamma L_1)| \\ &= \Pi_{i=1}^{n_1} (\lambda - \gamma \lambda_i \omega^{-\alpha} e^{-j(\omega\tau+\alpha\pi/2)}),\end{aligned}$$

where λ_i is the eigenvalues of L_1. When $\omega = (2-\alpha)\pi/(2\tau)$ the Nyquist curve of $G(j\omega)$'s eigenvalues will cross the left of the real axis. If

$$\tau < \min\{\frac{(2-\alpha)\pi}{2(\lambda_i\gamma)^{1/\alpha}}, i = 1, 2, ...n_1\},$$

the point $-1 + j0$ is not surrounded by the Nyquist curve of $G(j\omega)$'s eigenvalues. Since fractional order $\alpha \in (0, 1]$, we obtain

$$\tau < (2-\alpha)\pi/(2(\bar{\lambda}\gamma)^{1/\alpha}),$$

where $\bar{\lambda} = \max\{\lambda_i, i \in I\}$, the fractional-order multi-agent system (11) with time delays can asymptotically reach containment control.

Corollary 1. Suppose multi-agent systems are composed of n independent agents with $n_2 = 1$ leader, whose connection network topology is directed and symmetrical with Assumption 1. Then FOMAS (10) with time delays can asymptotically follow the tracks of the leader, if

$$\tau < \frac{(2-\alpha)\pi}{2(\lambda_{\max}\gamma)^{1/\alpha}}, \tag{14}$$

where λ_{max} is the max eigenvalue of matrix L_1.

Corollary 2. Suppose multi-agent systems are composed of n independent agents with n_1 followers and n_2 leaders, whose connection network topology is directed and symmetrical with Assumption 1. Then fractional order multi-agent system (10) with time delays can asymptotically reach consensus with $\alpha = 1$, if

$$2\gamma\tau < \pi/\lambda_{\max}, \tag{15}$$

where $\lambda_{\max}$ is the max eigenvalue of matrix L_1.

Remark 4. If the fractional order $\alpha = 1$ in FOMAS, the containment control result in Theorem 2 will become that of delayed multi-agent systems with integer-order dynamics.

Remark 5. The consensus result in Corollary 2 for $\gamma = 1$ is in accord with that of delayed multi-agent systems with integer-order dynamics in [2].

V. SIMULATIONS

Consider the dynamic topology with 5 followers and 3 leaders (illustrated as A1, A2, A3) shown in Fig. 1, where the connection weights of each edge is 1. Suppose the fractional order of the multi-agent system $\alpha = 0.9$.

From the communication topology of FOMAS, the system matrix can be obtained,

$$L_1 = \begin{bmatrix} 3 & -1 & 0 & 0 & -1 \\ -1 & 2 & 0 & 0 & 0 \\ 0 & 0 & 2 & -1 & 0 \\ 0 & 0 & -1 & 3 & -1 \\ -1 & 0 & 0 & -1 & 3 \end{bmatrix} \tag{16}$$

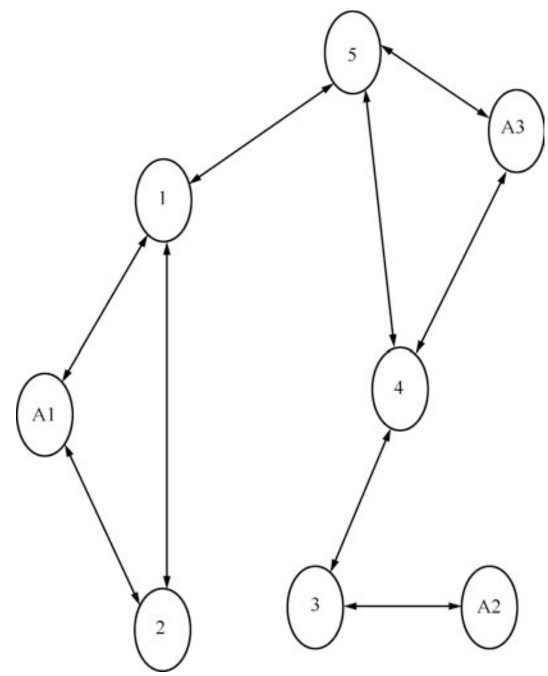

Fig. 1. Network topology of multi-agent systems.

Assume that the control parameter of system is taken $\gamma = 1.0$. The initial positions of followers are taken as $x_1(0) = (1, 1)$, $x_2(0) = (1, 2)$, $x_3(0) = (2, 1)$, $x_4(0) = (2, 3)$, $x_5(0) = (3, 2)$, respectively. The initial positions of leaders are taken as $A_1(0) = (4, 4)$, $A_2(0) = (4, 6)$, $A_3(0) = (6, 4)$. Fig. 2 shows the state trajectories of FOMAS without time delays, where the followers have converged into the convex hull formed by the leaders.

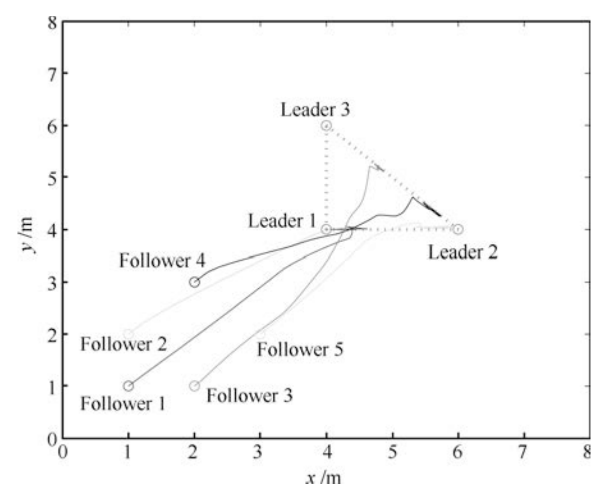

Fig. 2. Moving track of FOMAS without communication delays.

Next, we will verify the results of FOMAS with time delays. The maximum eigenvalue of L_1 is 4.618. According to the constraints of Theorem 2 in this paper, the allowed upper bound of the delays is 0.3157. Let $\tau(t) = 0.20$ is the time delay of multi-agent systems. The initial parameters in the experiments are same as the simulation without time delays. Fig. 3 shows the state trajectories of FOMAS with time delays, where the followers have converged into the convex hull formed by the leaders.

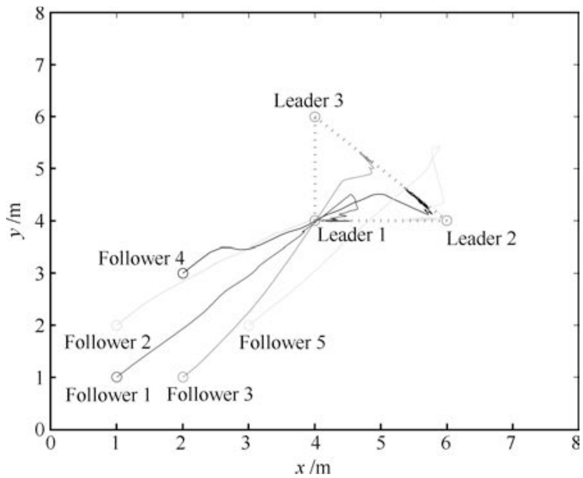

Fig. 3. Moving track of FOMAS with communication delay $\tau = 0.20$.

Then, we will enlarge the time delays in FOMAS. Let $\tau(t) = 0.30$ is the time delay of multi-agent systems in the experiments. Fig. 4 shows the running trajectories of FOMAS. The followers can asymptotically converge to the dynamic region formed by three leaders, i.e., the containment control of fractional-order multi-agent systems with time delays can be achieved.

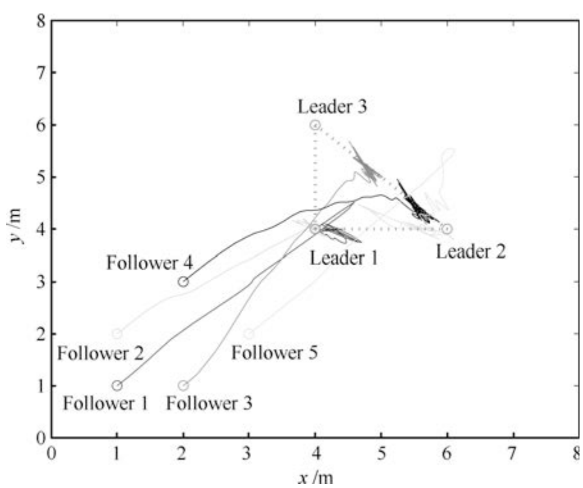

Fig. 4. Moving track of FOMAS with communication delay $\tau = 0.30$.

VI. CONCLUSION

This paper studies containment control of fractional multi-agent systems with communication time delays. Containment consensus of multi-agent systems with directed network topology is studied. By applying the stability theory of frequency domain, FOMAS with delay is analyzed, and the relationship between the control gain of multi-agent systems and the upper bound of time delays is derived. Suppose the orders of the fractional dynamical systems are all 1, the extended conclusion in this paper is the same with ordinary integer order systems. The containment control of fractional order multi-agent systems with dynamical topologies and linear time-varying (LTV) systems will be investigated in the future works.

ACKNOWLEDGEMENTS

The authors would like to thank the review experts. This research is supported by the National Natural Science Foundation of China (under grant 61273152, 61202111, 61304052, 51407088), the Science Foundation of Education Office of Shandong Province of China (under grant ZR2011FM07, BS2015DX018).

REFERENCES

[1] Jadbabaie A, Lin J, Morse A S. Coordination of groups of mobile autonomous agents using nearest neighbor rules. *IEEE Transactions on Automatic Control*, 2003, **48**(6): 988-1001

[2] Olfati-Saber R, Murray R M. Consensus problems in networks of agents with switching topology and time-delays. *IEEE Transactions on Automatic Control*, 2004, **49**(9): 1520-1533

[3] Ren W, Beard R W, Atkins E M. Information consensus in multivehicle cooperative control: Collective group behavior through local interaction. *IEEE Control Systems Magazine*, 2007, **27**(2): 71-82

[4] Li S, Du H, Lin X. Finite-time consensus algorithm for multi-agent with double-integrator dynamics. *Automatica*, 2011, **47**(8): 1706-1712

[5] Chen F, Chen Z Q, Xiang L, Liu Z, Yuan Z. Reaching a consensus via pinning control. *Automatica*, 2009, **45**(5): 1215-1220

[6] Yang H Y, Zhang Z, Zhang S. Consensus of Second-Order Multi-Agent Systems with Exogenous Disturbances. *International Journal of Robust and Nonlinear Control*, 2011, **21**(9): 945-956

[7] Lin P, Jia Y M. Consensus of second-order discrete-time multi-agent systems with nonuniform time-delays and dynamically changing topologies. *Automatica*, 2009, **45**(9): 2154-2158

[8] Yu J, Wang L. Group consensus in multi-agent systems with switching topologies and communication delays. *Systems & Control Letters*, 2010, **59**(6): 340-348

[9] Tian Y P, Liu C. Consensus of multi-agent systems with diverse input and communication delays. *IEEE Transactions on Automatic Control*, 2008, **53**(9): 2122-2128

[10] Yang H Y, Zhu X, Zhang S. Consensus of second-order delayed multi-agent systems with leader-following. *European Journal of Control*, 2010, **16**(2): 188-199

[11] Ji M, Ferrari-Trecate G, Egerstedt M, Buffa A. Containment control in mobile networks. *IEEE Transactions on Automatic Control*, 2008, **53**(8): 1972-1975

[12] Liu H, Xie G, Wang L. Necessary and Sufficient Conditions for Containment Control of Networked Multi-agent Systems. *Automatica*, 2012, **48**(7): 1415-1422

[13] Meng Z, Ren W, You Z. Distributed finite-time attitude containment control for multiple rigid bodies. *Automatica*, 2010, **46**(12):2092-2099

[14] Podlubny I. *Fractional differential equations*. San Diego, CA: Academic Press, 1999.

[15] Li Y, Chen Y Q, Podlubny I. Stability of fractional-order nonlinear dynamic systems: Lyapunov direct method and generalized Mitta-Leffler stability. *Computers and Mathematics with Applications*, 2009, **24**(6): 1429-1468

[16] Chen Y Q, Ahn H, Podlubny I. Robust stability check of fractional order linear time invariant systems with interval uncertainties. *Signal Processing*, 2006, **86**(10): 2611-2618

[17] Ren W, Cao Y. *Distributed coordination of multi-agent networks*, Springer-Verlag, London, 2011.

[18] Lu J, Chen Y Q. Stability and stabilization of fractional-order linear systems with convex polytopic uncertainties. *Fract. Calc. Appl. Anal.*, 2013, **16**(1) 142-157

[19] Cao Y, Li Y, Ren W, Chen Y Q. Distributed coordination of networked fractional-order systems. *IEEE Transactions on Systems, Man, and Cybernetics, Part B: Cybernetics*, 2010, **40**(2): 362-370

[20] Cao Y, Ren W. Distributed coordination for fractional-order systems: dynamic interaction and absolute/relative damping. *Systems* & *Control Letters*, 2010, **43**(3-4): 233-240

[21] Yang H Y, Zhu X, Cao K. Distributed coordination of fractional order multi-agent systems with communication delays. *Fract. Calc. Appl. Anal.*, 2014, **17**(1): 23-37; DOI: 10.2478/s13540-014-0153-9

[22] Yang H Y, Guo L, Zhang Y, Yao X. Movement consensus of complex fractional-order multi-agent systems. *Acta Automatica Sinica*, 2014, **40**(3): 489-496

[23] Cao Y, Stuart D, Ren W, Meng Z. Distributed containment control for multiple autonomous vehicles with double-integrator dynamics: algorithms and experiments, *IEEE Trans. Control Syst. Technol*, 2011, **19**(4): 929-938

[24] Liu K, Xie G, Wang L. Containment control for second-order multi-agent systems with time-varying delays. *Systems* & *Control Letters*, 2014, **67**, 24-31

[25] Li J, Guan Z, Liao R, et al. Impulsive containment control for second-order networked multi-agent systems with sampled information. *Nonlinear Analysis: Hybrid Systems*, 2014, **12**, 93-103

[26] Liu J, Zhou J. Distributed impulsive containment control for second-order multi-agent systems with multiple leaders, *Journal of Vibration and Control*, 2014, September **11**, DOI: 10.1177/1077546314547377

Hong-yong Yang Professor. He received his Ph. D. degree in control theory and control engineering from Southeast University in 2005. He is a professor in School of Information and Electrical Engineering, Ludong University. His research interest covers complex network, multi-agent systems, Intelligence control. He is the corresponding author of this paper, e-mail: hyyang@yeah.net; hyyang@ldu.edu.cn.

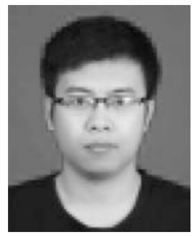

Fu-yong Wang He received his bachelor's degree from Ludong university in 2013. Now, he is a graduate student in computer application technology in Ludong university. His research field is a complex network, multi-agent formation control, etc.

Fu-jun Han Associate Professor. He received his Ph.D. degree in Precision Instruments and Machinery from Beijing University of Aeronautics and Astronautics in 2009. He is an associate professor in School of Information and Electrical Engineering, Ludong University. His main research direction is Control theory and control engineering.

Using Fractional Order Method to Generalize Strengthening Buffer Operator and Weakening Buffer Operator

Lifeng Wu, Sifeng Liu, *Senior Member, IEEE*, and Yingjie Yang, *Senior Member, IEEE*

***Abstract*—To reveal the relationship between the weakening buffer operator and strengthening buffer operator, the traditional integer order buffer operator is extended to fractional order one. Fractional order buffer operator not only can generalize the weakening buffer operator and the strengthening buffer operator, but also realize tiny adjustment of buffer effect. The effectiveness of grey model (GM(1,1)) with the fractional order buffer operator is validated by six cases.**

***Index Terms*—Fractional order, grey system theory, strengthening buffer operator, weakening buffer operator.**

I. Introduction

DUE to the growing demand for reliable small sample statistics, small sample prediction is of great importance topic. Over the years, many scholars have carried out vigorous programs[1−4]. Among these programs, it is reported that the forecasting performance of grey model is better than many conventional methods with incomplete or insufficient data[4−6]. Grey system theory is developed by Deng[7]. As the primary forecasting method of grey system theory, GM(1,1) has been applied in many fields[4−7]. However, GM(1,1) is suitable for the stable time series, how to predict the non-stationary series is a difficult problem which deserves to be researched.

For non-stationary time series prediction problem, the theory on how to select model would lose its validity. That is not the problem of selecting better model; instead, when a system is severely affected by shock, the available data of the past cannot truthfully reflect the law of the system. Under the circumstances, buffer operator of grey system theory[7] has been successfully used in many fields to overcome the above difficulties[8−13], it combines quantitative and judgmental forecast (qualitative analysis). Many kinds of buffer operators have been proposed simultaneously[14−18], how to choose a suitable kind of buffer operator is very important in practice. In this paper, many kinds of buffer operators are unified and generalized based on fractional order method.

The rest of this paper is organized as follows. Section II is a compendium of grey buffer operator. In Section III, the inherent relationship between weakening buffer operator and strengthening buffer operator based on fractional order method is revealed. In Section IV, real examples for fractional order buffer operator are discussed. Some conclusions of this study are provided in the final section.

This article has been accepted for publication in a future issue of this journal, but has not been fully edited. Content may change prior to final publication.

This work was supported by Social Science Foundation of China Ministry of Education (15YJA630017), The Leverhulme Trust International Network (IN-2014-020), National Natural Science Foundation of China (71401051), Zhejiang Provincial Natural Science Foundation Project (LY14G010005) and Cultural and artistic scientific research project of Hebei Province (HBWY2014-Y-C031). Recommended by Associate Editor YangQuan Chen.

Lifeng Wu is with the College of Economics and Management, Hebei University of Engineering, Handan 056038, China (e-mail: wlf6666@126.com).

Sifeng Liu is with the Centre for Computational Intelligence, DMU, Leicester, LE1 9BH, U.K and the Institute for Grey System Studies, NUAA, Nanjing 210016, China (e-mail: sifeng.liu@dmu.ac.uk; sfliu@nuaa.edu.cn).

Yingjie Yang is with the Centre for Computational Intelligence, De Montfort University, Leicester, LE1 9BH, UK (e-mail: yyang@dmu.ac.uk).

Digital Object Identifier 10.1109/JAS.2016.7510214

II. Weakening Buffer Operator and Strengthening Buffer Operator

Assume that $X=\{x(1),x(2),\dots,x(n)\}$ is the true behavior sequence of a system, the observed behavior sequence of the system is $Y=\{x(1)+\epsilon_1,x(2)+\epsilon_2,\dots,x(n)+\epsilon_n\}$, where $(\epsilon_1,\epsilon_2,\dots,\epsilon_n)$ is a term for the shocking disturbance. To correctly discover and recognize the true behavior sequence X of the system from the shock-disturbed sequence Y, one first has to go over the hurdle $(\epsilon_1,\epsilon_2,\dots,\epsilon_n)$ (That is to say that cleaning up the disturbance). If we directly use the severely impacted data Y to construct model and to make predictions, then our prediction is likely to fail, because what the model described was not the true situation X of the underlying system.

The wide existence of severely shocked systems often causes quantitative predictions disagree with the outcomes of intuitive qualitative analysis. Hence, seeking an equilibrium between qualitative analysis and quantitative predictions by eliminating these disturbances is an important task in order to discover the true situation of the system. Grey buffer operator proposed by Liu can address the problem, its definition is as follows.

Definition 1[7]**.** Assume that raw data sequence is $X=\{x(1),x(2),\dots,x(n)\}$. If $\forall k=2,3,\dots,n$, $x(k)-x(k-1)>0$, then X is called as a monotonic increasing sequence. If $\forall k=2,3,\dots,n$, $x(k)-x(k-1)<0$, then X is called as a monotonic decreasing sequence. If there are $k,k'\in\{k=2,3,\dots,n\}$ such that $x(k)-x(k-1)>0$, $x(k')-x(k'-1)<0$, then X is defined as a random vibrating or fluctuating sequence. If $M=\max\{x(k)|k=1,2,\dots,n\}$ and $m=\min\{x(k)|k=1,2,\dots,n\}$, then $M-m$ is called as the amplitude of the sequence X.

Lemma 1[7]**.** $X=\{x(1), x(2), \dots, x(n)\}$ is a monotonic increasing sequence. Then, $XD=\{x(1)d, x(2)d, \dots, x(n)d\}$

is a weakening buffer operator(WBO), iff $x(k)d \geq x(k)$, $k = 1,2,\ldots,n$; $XD = \{x(1)d,\ x(2)d,\ \ldots,\ x(n)d\}$ is a strengthening buffer operator(SBO), iff $x(k)d \leq x(k)$, $k = 1,2,\ldots,n$.

Lemma 2[7]**.** Assume that $X = \{x(1),\ x(2),\ \ldots,\ x(n)\}$ is a monotonic decreasing sequence. Then, $XD = \{x(1)d,\ x(2)d,\ \ldots,\ x(n)d\}$ is a WBO, iff $x(k)d \leq x(k)$, $k = 1,2,\ldots,n$; $XD = \{x(1)d, x(2)d, \ldots, x(n)d\}$ is a SBO, iff $x(k)d \geq x(k)$, $k = 1,2,\ldots,n$.

Lemma 3[7]**.** Assume that $X = \{x(1), x(2), \ldots, x(n)\}$ is a fluctuating sequence, $XD = \{x(1)d, x(2)d, \ldots, x(n)d\}$ is a WBO, iff $\max\{x(k)|k = 1,2,\ldots,n\} \geq \max\{x(k)d|k = 1,2,\ldots,n\}$ and $\min\{x(k)|k = 1,2,\ldots,n\} \leq \min\{x(k)d| k = 1,2,\ldots,n\}$; $XD = \{x(1)d,\ x(2)d,\ \ldots,\ x(n)d\}$ is a SBO, iff $\max\{x(k)|k = 1,2,\ldots,n\} \leq \max\{x(k)d|k = 1,2,\ldots,n\}$ and $\min\{x(k)|k = 1,2,\ldots,n\} \geq \min\{x(k)d|k = 1,2,\ldots,n\}$.

Definition 2[7]**.** Assume that raw data sequence is $X = \{x(1), x(2), \ldots, x(n)\}$, $XD = \{x(1)d, x(2)d, \ldots, x(n)d\}$, where

$$x(k)d = \frac{x(k) + x(k+1) + \ldots + x(n)}{n-k+1}, \tag{1}$$

D is a first order WBO no matter whether X is monotonic decreasing, increasing, or vibrating. If $XD^2 = XDD = \{x(1)dd, x(2)dd, \ldots, x(n)dd\}$, D^2 is a second order WBO. Similarity, D^3 is a third order WBO.

If

$$x(k)d = \frac{x(1) + x(2) + \ldots + x(k-1) + kx(k)}{2k-1}, \tag{2}$$

then D is a first order SBO when sequence X is either monotonic decreasing or increasing. If $XD^2 = XDD = \{x(1)dd, x(2)dd, \ldots, x(n)dd\}$, D^2 is a second order SBO. Similarity, D^3 is a third order SBO.

$x^{(0)}(k)d = x^{(0)}(k)$ of WBO is consistent with the results of above studies, that is they all suggested that more emphasis should be placed on the most recent and most relevant information.

III. The Relationship Between WBO and SBO

Due to traditional weakening buffer operators cannot tune the effect intensity to a small extent, which leads to problems that the buffer effect may be too strong or too weak. Considering this situation, and like the fractional-order systems[19−21], fractional weakening buffer operator is constructed. Then (1) can be expressed by

$$\begin{aligned} XD =& \{x(1)d, x(2)d, \ldots, x(n)d\} \\ =& [x(1), x(2), \ldots, x(n)] \begin{bmatrix} \frac{1}{n} & 0 & \ldots & 0 \\ \frac{1}{n} & \frac{1}{n-1} & \ldots & 0 \\ \vdots & \vdots & \ddots & \vdots \\ \frac{1}{n} & \frac{1}{n-1} & \ldots & 1 \end{bmatrix} \end{aligned}$$

then second order WBO can be expressed by

$$XD^2 = [x(1), x(2), \ldots, x(n)] \begin{bmatrix} \frac{1}{n} & 0 & \ldots & 0 \\ \frac{1}{n} & \frac{1}{n-1} & \ldots & 0 \\ \vdots & \vdots & \ddots & \vdots \\ \frac{1}{n} & \frac{1}{n-1} & \ldots & 1 \end{bmatrix}^2$$

Similarly, $\frac{p}{q}(\frac{p}{q} \in R^+)$ order WBO is

$$XD^{\frac{p}{q}} = [x(1), x(2), \ldots, x(n)] \begin{bmatrix} \frac{1}{n} & 0 & \ldots & 0 \\ \frac{1}{n} & \frac{1}{n-1} & \ldots & 0 \\ \vdots & \vdots & \ddots & \vdots \\ \frac{1}{n} & \frac{1}{n-1} & \ldots & 1 \end{bmatrix}^{\frac{p}{q}}$$

Theorem 1. For original data $X = [x(1), x(2), \ldots, x(n)]$, $-\frac{p}{q}(\frac{p}{q} \in R^+)$ order WBO from (1) is the $\frac{p}{q}$ order SBO.

Proof. Set

$$\begin{bmatrix} \frac{1}{n} & 0 & \ldots & 0 \\ \frac{1}{n} & \frac{1}{n-1} & \ldots & 0 \\ \vdots & \vdots & \ddots & \vdots \\ \frac{1}{n} & \frac{1}{n-1} & \ldots & 1 \end{bmatrix} = A,$$

since $-\frac{p}{q}(\frac{p}{q} \in R^+)$ order WBO is

$$\begin{aligned} XD^{-\frac{p}{q}} =& X \begin{bmatrix} \frac{1}{n} & 0 & \ldots & 0 \\ \frac{1}{n} & \frac{1}{n-1} & \ldots & 0 \\ \vdots & \vdots & \ddots & \vdots \\ \frac{1}{n} & \frac{1}{n-1} & \ldots & 1 \end{bmatrix}^{-\frac{p}{q}} \\ =& XA^{-\frac{p}{q}} \\ =& X \begin{bmatrix} n & 0 & 0 & \ldots & 0 \\ -(n-1) & n-1 & 0 & \ldots & 0 \\ 0 & -(n-2) & n-2 & \ldots & 0 \\ \vdots & \vdots & \vdots & \ddots & \vdots \\ 0 & 0 & 0 & \ldots & 1 \end{bmatrix}^{\frac{p}{q}} \end{aligned}$$

The result of $XA^{\frac{p}{q}}$ is a vector. When each component of $XA^{\frac{p}{q}}$ is not less than the corresponding component of X, we can write as $XA^{\frac{p}{q}} \geq X$. If sequence X is either monotonically decreasing or increasing, because $XA^{\frac{p}{q}} \geq X$ and A is an invertible matrix, we have $XA^{\frac{p}{q}}A^{-\frac{p}{q}} \geq XA^{-\frac{p}{q}}$, that is $X \geq XA^{-\frac{p}{q}}$. So $-\frac{p}{q}$ order WBO is the $\frac{p}{q}$ order SBO when sequence X is either monotonically decreasing or increasing.

If sequence $X = [x(1), x(2), \ldots, x(n)]$ is a fluctuating sequence, $x(l) = \max\{x(k)|k = 1,2,\ldots,n\}$, $x(h) = \min\{ x(k)|k = 1,2,\ldots,n\}$, because $[x(l), x(l), \ldots, x(l)]A^{\frac{p}{q}} \geq [x(l), x(l), \ldots, x(l)]$ and A is an invertible matrix, we have $[x(l), x(l), \ldots, x(l)]A^{\frac{p}{q}}A^{-\frac{p}{q}} \geq [x(l), x(l), \ldots, x(l)]A^{-\frac{p}{q}}$, that is $[x(l), x(l), \ldots, x(l)] \geq [x(l), x(l), \ldots, x(l)]A^{-\frac{p}{q}}$; Similarly, we have $[x(h), x(h), \ldots, x(h)] \leq [x(h), x(h), \ldots, x(h)]A^{-\frac{p}{q}}$. So $-\frac{p}{q}$ order WBO is the $\frac{p}{q}$ order SBO when sequence X is a fluctuating sequence.

So $-\frac{p}{q}$ $(\frac{p}{q} \in R^+)$ order WBO from (1) is the $\frac{p}{q}$ order SBO. ■

Corollary 1. For original data $X = [x(1), x(2), \ldots, x(n)]$, $-\frac{p}{q}(\frac{p}{q} \in R^+)$ order SBO from (2) is the $\frac{p}{q}$ order WBO.

Corollary 2. For original data $X = [x(1), x(2), \ldots, x(n)]$, if nonnegative matrix B satisfies $XB^{-\frac{p}{q}}$ $(\frac{p}{q} \in R^+) > 0$ and $XD^{-\frac{p}{q}} = XB^{-\frac{p}{q}}$ is SBO (WBO), then $XD^{\frac{p}{q}} = XB^{\frac{p}{q}}$ is WBO (SBO).

The procedures of GM(1,1) model with $\frac{p}{q}$ order WBO ($\frac{p}{q}$WGM(1,1)) are more complex than the traditional GM(1,1), because more work must be done before forecasting. The procedures can be summarized as follows:

Step 1: Given a raw data sequence $X^{(0)} = \{x^{(0)}(1), x^{(0)}(2), \ldots, x^{(0)}(n)\}$, $\frac{p}{q}$ order WBO sequence is $X^{(0)}D^{\frac{p}{q}} = \{x^{(0)}(1)d^{\frac{p}{q}}, x^{(0)}(2)d^{\frac{p}{q}}, \ldots, x^{(0)}(n)d^{\frac{p}{q}}\}$.

Step 2: Sequence $\{x^{(0)}(1)d^{\frac{p}{q}}, x^{(0)}(2)d^{\frac{p}{q}}, \ldots, x^{(0)}(n)d^{\frac{p}{q}}\}$ is used to establish GM(1,1), accumulated generating operator $x^{(1)}(k)d^{\frac{p}{q}} = \sum_{i=1}^{k} x^{(0)}(i)d^{\frac{p}{q}}$, $k = 1, 2, \ldots, n$.

Step 3: The parameter a and b can be obtained by

$$\begin{bmatrix} \hat{a} \\ \hat{b} \end{bmatrix} = (A^T A)^{-1} A^T Y$$

where

$$Y = \begin{bmatrix} x^{(0)}(2)d^{\frac{p}{q}} \\ x^{(0)}(3)d^{\frac{p}{q}} \\ \vdots \\ x^{(0)}(n)d^{\frac{p}{q}} \end{bmatrix},\ A = \begin{bmatrix} -\frac{x^{(1)}(1)d^{\frac{p}{q}} + x^{(1)}(2)d^{\frac{p}{q}}}{2} & 1 \\ -\frac{x^{(1)}(2)d^{\frac{p}{q}} + x^{(1)}(3)d^{\frac{p}{q}}}{2} & 1 \\ \vdots & \vdots \\ -\frac{x^{(1)}(n-1)d^{\frac{p}{q}} + x^{(1)}(n)d^{\frac{p}{q}}}{2} & 1 \end{bmatrix}$$

Step 4: After substituting $\hat{a}$ and $\hat{b}$ into $\hat{x}^{(0)}(k+1) = \hat{x}^{(1)}(k+1) - \hat{x}^{(1)}(k) = [x^{(0)}(1) - \frac{\hat{b}}{\hat{a}}](1 - e^{\hat{a}})e^{-\hat{a}k}$ $(k = 1, 2, \ldots, n-1)$, we can make prediction $x^{(0)}(n+1), x^{(0)}(n+2), \ldots$.

Step 5: If the predicted value $x^{(0)}(n+1), x^{(0)}(n+2), \ldots$ is not consistent with the result of qualitative analysis, then change the order number $\frac{p}{q}$. (If we want to pay more attention to the recent data, the order number $\frac{p}{q}$ must be the larger one. If we want to pay more attention to the old data, the order number $\frac{p}{q}$ must be the smaller one. Because the strengthening buffer operator reflects the priority of old data[22]).

Step 6: Repeat Step 1-5 until the predicted values $x^{(0)}(n+1), x^{(0)}(n+2), \ldots$ are consistent with the result of qualitative analysis.

IV. Experimentation results

To test the proposed model, mean absolute percentage error ($\text{MAPE} = 100\% \times \frac{1}{n}\sum_{k=1}^{n}\left|\frac{x^{(0)}(k) - \hat{x}^{(0)}(k)}{x^{(0)}(k)}\right|$) is used to evaluate the precision.

Case 1. Energy consumption forecasting in China[23]

The data from 1998 to 2005 ($X^{(0)} = \{13.22, 13.38, 13.86, 14.32, 15.18, 17.50, 20.32, 22.47\}$) are used to establish different GM(1,1) models with different WBO, and the data from 2006 to 2007 are used to determine the optimal order of WBO. The results are shown in Table I.

As can be seen from Table I, 0.1WGM(1,1) is the best model among the above models in out-of sample data. So 0.1WGM(1,1) is used to predict the data from 2008 to 2009. The results are listed in Table II. As can be seen from Table II, 0.1WGM(1,1) yielded the lowest MAPE in out-of-sample data. This implies that 0.1WGM(1,1) can improve the prediction precision.

TABLE II
THE RESULTS OF TWO GREY MODELS

Year	Actual value	0.1WGM(1,1)	The result of Reference[23]
2008	29.10	28.86	28.59
2009	31.00	31.41	31.23
MAPE		0.98	1.26

Case 2. Electricity consumption per capita forecasting in China[24]

The data from 2000 to 2005 ($X^{(0)} = \{132.4, 144.6, 156.3, 173.7, 190.2, 216.7\}$) are used to obtain different GM(1,1) models with different WBO, and the data of 2006 is predicted by these models. The results are shown in Table III.

As can be seen from Table III, both WGM(1,1) models are better than the best result of Reference[23], as a conclusion, fractional order WBO has a perfect forecasting capability.

Case 3. The qualified discharge rate of industrial wastewater forecasting in Jiangxi in China[17]

The data from 2000 to 2005 ($X^{(0)} = \{68.63, 75.9, 77.59, 83.06, 88.66, 92.13\}$) are used to construct two GM(1,1) models with WBO, and the data from 2006 to 2007 are predicted by these models. The results are shown in Table IV.

As can be seen from Table IV, the WGM(1,1) model is better than the best result of Reference[17], so fractional order WBO can improve the prediction accuracy of conventional GM(1,1) model.

TABLE IV
THE FITTED VALUES AND MAPE OF TWO GREY MODELS

Year	Actual value	GM(1,1)	WGM(1,1)
2006	93.23	93.4	93.95
2007	93.89	94.5	95.77
MAPE		0.42	1.75

Case 4. The electricity consumption forecasting in Vietnam[25]

The data from 2000 to 2003 ($X^{(0)} = \{1927, 2214, 2586, 2996\}$, unit: KTOE) are used to construct four models with WBO, and the data from 2004 to 2007 are predicted by these models. The results are shown in Table V.

As can be seen from Table V, the WGM(1,1) model is better than the best result of Reference[17], so fractional order WBO can improve the prediction accuracy of conventional GM(1,1) model.

Case 5. The logistics demand forecasting in Jiangsu[26]

The data from 2005 to 2008 are used to construct three grey models with WBO, and the data from 2009 are predicted by these models. The results are shown in Table VI.

As can be seen from Table VI, the WGM(1,1) model is better than the traditional grey model, so fractional order WBO can improve the prediction accuracy of conventional GM(1,1).

TABLE VI
THE FITTED VALUES AND MAPE OF THREE GREY MODELS

Year	Actual value	GM(1,1)[26]	1WGM(1,1)	0.5WGM(1,1)
2009	5154.46	5330	5008	5138
MAPE		3.41	2.84	0.32

Case 6: The energy production forecasting in China[27]

The 1985-1989 data are used for model building, while the 1990-1995 data are used as an ex-post testing data set. The

TABLE I
THE RESULTS OF DIFFERENT GREY MODELS

Year	Actual value	0.3WGM(1,1)	0.1WGM(1,1)	The best result of Reference[23]
2006	24.63	23.95	24.05	27.95
2007	26.56	25.97	26.34	26.16
MAPE		2.43	1.55	2.12

TABLE III
THE FITTED VALUES AND MAPE OF DIFFERENT GREY MODELS

Year	Actual value	-0.6WGM(1,1)	-0.7WGM(1,1)	The best result of Reference[24]
2006	249.4	248.3	250.8	241.21
MAPE		0.44	0.56	3.28

TABLE V
THE FITTED VALUES AND MAPE OF FOUR GREY MODELS

Year	Actual value	GM(1,1)	AGM(1,1)[25]	1WGM(1,1)	0.1WGM(1,1)
2004	3437	3477	3334	3215	3439
2005	3967	4042	3807	3452	3953
2006	4630	4699	4347	3706	4544
2007	5256	5462	4963	3979	5224
MAPE		2.12	4.68	15.92	0.72

results given by the GM(1,1) model and 1.5WGM(1,1) as well as the observed values are shown in Table VII.

TABLE VII
THE FITTED VALUES AND MAPE OF TWO GREY MODELS

Year	Actual value	GM(1,1)[27]	1.5WGM(1,1)
1990	103922	106069	103407
1991	104844	111296	105320
1992	107265	116781	107270
1993	111059	122536	109255
1994	118729	128574	111277
1995	129034	134910	113337
MAPE		6.71	3.50

Table VII shows that the 1.5WGM(1,1) model is better for forecasting the energy production in China. The forecasted values are more precise than the GM(1,1) model, for data sequence with large random fluctuation.

V. Conclusion

Let us now return to the name of the fractional calculus. The fractional calculus is a name for the theory of integrals and derivatives of arbitrary order. which unifies and generalizes the notions of integer-order differential and integral. Similarly, fractional order WBO unifies and generalizes the notions of WBO and SBO. As can be seen from Table II-VII, GM(1,1) with the fractional order buffer operator can predict the development trend of the system accurately.

Six real cases were seen to obtain good results, however, the order $\frac{p}{q}$ may be not optimal. In this paper, the order $\frac{p}{q}$ is chosen from more computational experiments. In future studies, it is suggested that the particle swarm algorithm should be used to determine the optimal order.

References

[1] Brannas K. Prediction and control for a time-series count data model. *International Journal of Forecasting*, 1995, **11**(2): 263-270

[2] Pfeffermann D. Small area estimation-new developments and directions. *International Statistical Review*, 2002, **70**(1): 125-143

[3] Tao C, Wei S. Multi-source data fusion based small sample prediction of gear random reliability. *Journal of Mechanical Science and Technology*, 2012, **26**(8): 2547-2555

[4] Choi T M, Hiu C L, Ng S F, Yu Y. Color trend forecasting of fashionable products with very few historical data. *IEEE Transactions on Systems, Man and Cybernetics-part C: Applications and Reviews*, 2012, **42**(6): 1003-1010

[5] Liu J, Xiao X X, Guo J H, Mao S H. Error and its upper bound estimation between the solutions of GM(1,1) grey forecasting models. *Applied Mathematics and Computation*, 2014, **246**: 648-660

[6] Wu L F, Liu S F, Yao L G, Yan S L, Liu D L. Grey system model with the fractional order accumulation. *Communications in Nonlinear Science and Numerical Simulation*, 2013, **18**(7): 1775-1785

[7] Chen C I, Huang S J. The necessary and sufficient condition for GM(1,1) grey prediction model. *Applied Mathematics and Computation*, 2013, **219**(11): 6152-6162

[8] Li W, Xie H. Geometrical variable weights buffer GM(1,1) model and its application in forecasting of China's energy consumption. *Journal of Applied Mathematics*, 2014, **131432**: 1-6

[9] Liao R J, Bian J P, Yang L J, Grzybowski S, Wang Y Y, Li J. Forecasting dissolved gases content in power transformer oil based on weakening buffer operator and least square support vector machine-Markov. *IET Generation, Transmission & Distribution*, 2012, **6**(2): 142-151

[10] Zhu J M, Zhai D T, Huang Z W. Fracture healing stress prediction based on weakening buffer operator and GM(1,1) equal-dimension-new-information model. *Chinese Journal of Biomedical Engineering*, 2012, **31**(2): 268-275

[11] Guo C L, Xu X X, Gong Z W. Co-integration analysis between GDP and meteorological catastrophic factors of Nanjing city based on the buffer operator. *Natural Hazards*, 2014, **71**(2): 1091-1105

[12] Wang D P, Wang B W. Medium and long term load forecasting based on variable weights buffer grey model. *Power System Technology*, 2013, **37**(1): 167-171

[13] Cheng K, Cheng L, Huang Y. The water quality prediction based on the gray model and curve fitting. *Journal of Information and Computational Science*, 2013, **10**(8): 2329-2335

[14] Gao Y, Zhou D Q, Liu C C, Zhang L. Constructing methods of new buffer operators with variable weights and their inner link. *System Engineering Theory & Practice*, 2013, **33**(2): 489-497

[15] Dai W Z, Su Y. New strengthening buffer operators and their applications based on prior use of new information. *Acta Automatica Sinica*, 2012, **38**(8): 1329-1334

[16] Li D M, Li X. Research on a new weakening buffer operator of investment forecasting for constructing digital libraries. *Journal of Nanjing Institute of Technology*, 2012, **10**(4): 48-51

[17] Wang Z X, Dang Y G, Liu S F. A sort of power weaken buffer operators and its properties. *Control and Decision*, 2012, **27**(10): 1482-1488

[18] Hu X L, Wu Z P, Han R. Analysis on the strengthening buffer operator based on the strictly monotone function. *International Journal of Applied Physics and Mathematics*, 2013, **3**(2): 132-136

[19] Sabatier J, Farges C, Trigeassou J C. A stability test for non-commensurate fractional order systems. *Systems & Control Letters*, 2013, **62**(9): 739-746

[20] Wu Y. Discretization of fractional order diffeerentiator over Paley-Wiener space. *Applied Mathematics and Computation*, 2014, **247**: 162-168

[21] Abbas S, Benchohra M, Rivero M, Trujillo J J. Existence and stability results for nonlinear fractional order Riemann-Liouville Volterra-Staieltjes quadratic integral equations. *Applied Mathematics and Computation*, 2014, **247**: 319-328

[22] Wu L F, Liu S F, Yao L G. Distinguishing method of buffer operators whether meet the principle of new information priority. *System Engineering Theory & Practice*, 2015, **35**(4): 991-996

[23] Li X M, Dang Y G, Wang Z X. Harmonic buffer operators with variable weights and effect strength comparison. *System Engineering Theory & Practice*, 2012, **32**(11): 2486-2492

[24] Cui L Z, Liu S F, Wu Z P. New strengthening buffer operators and their applications. *System Engineering Theory & Practice*, 2010, **30**(3): 484-489

[25] Li D C, Chang C J, Chen C C, Chen W C. Forecasting short-term electricity consumption using the adaptive grey-based approach-An Asian case. *Omega*, 2012, **40**(6): 767-773

[26] Tian G, Li N, Liu S F. Grey forecast of logistics demand based on parameter optimization model. *East China Economic Management*, 2011, **25**(6): 155-157

[27] Pi D, Liu J, Qin X. A grey prediction approach to forecasting energy demand in China. *Energy Sources, Part A: Recovery, Utilization, and Environmental Effects*, 2010, **32**(16): 1517-1528

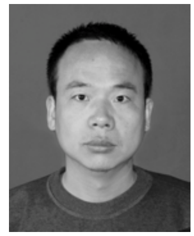

Lifeng Wu received the M. Sc. degree in Science from Wenzhou University, Wenzhou, China, and the Ph. D degree in Management Science and Engineering from Nanjing University of Aeronautics and Astronautics, Nanjing, China, in 2010 and 2015, respectively. He is currently a lecturer in the College of Economics and Management, Hebei University of Engineering, Handan, China. He has published 35 papers on grey systems and their applications. His current research interests focus on the grey system modeling. He is also a member of the Grey Systems Society of China.

Sifeng Liu (SM'08) received the B. Sc. degree in Mathematics from Henan University, Kaifeng, China, in 1981, the M. S. degree in Economics and the Ph. D degree in Systems Engineering from Huazhong University of Science and Technology, Wuhan, China, in 1986 and 1998, respectively. He spent 22 years with Henan Agricultural University, Henan, China, in various roles including the Head of Department, Deputy Director, and a Full Professor. He joined the Nanjing University of Aeronautics and Astronautics, Nanjing, China, in 2000, as a Distinguished Professor and led the College of Economics and Management from 2001 until 2012. He is also the Founding Director of the Institute for Grey Systems Studies, the Founding Chair of the IEEE SMC Technical Committee on Grey Systems, the President of the Grey Systems Society of China, the Founding Editor-in-Chief of the Grey Systems Theory and Application (Emerald), and the Editor-in-Chief of the Journal of Grey Systems (Research Information). He has over 600 research publications of which about 300 have been published in international journals.

Dr. Liu is an Honorary Fellow of the World Organization of Systems and Cybernetics. Sifeng Liu is a research professor of Centre for Computational Intelligence, De Montfort University for the project of Marie Curie International Incoming Fellowships (FP7-PEOPLE-2013-IIF) of the 7th Research Framework Programme of the European Commission.

Yingjie Yang (SM'13) received the B. Sc., M. Sc. and Ph. D. degrees in Engineering from Northeastern University, Shenyang, China, in 1987, 1990, and 1994, respectively. He was awarded his PhD degree in Computer Science at Loughborough University, Loughborough, U.K., in 2008.

He is currently a professor in computational intelligence in the School of Computer Science and Informatics at De Montfort University, Leicester, U.K. He has published over 100 papers on grey systems, fuzzy sets, rough sets, neural networks and their applications to civil engineering, transportation and environmental engineering. His research interests include the representation and modelling of various uncertainties and the application of computational intelligence to engineering problems.

Dr. Yang is a senior member of IEEE Systems, Man and Cybernetics Society, a co-chair of IEEE SMC Technical Committee on Grey Systems and a member of Rail Research UK Association.

Paper Download Links

1. Fudong Ge, YangQuan Chen, Chunhai Kou. Cyber-physical systems as general distributed parameter systems: three types of fractional order models and emerging research opportunities. IEEE/CAA Journal of Automatica Sinica, 2015, 2(4): 353-357

http://ieeexplore.ieee.org/stamp/stamp.jsp?tp=&arnumber=7296529 (Local PDF)

2. Bruce J. West, Malgorzata Turalska. The Fractional Landau Model. *IEEE/CAA Journal of Automatica Sinica*, 2016, 3(3), 257-260

http://ieeexplore.ieee.org/stamp/stamp.jsp?tp=&arnumber=7508800 (Local PDF)

3. Kecai Cao, YangQuan Chen, Daniel Stuart. A Fractional Micro-Macro Model for Crowds of Pedestrians Based on Fractional Mean Field Games. *IEEE/CAA Journal of Automatica Sinica*, 2016, 3(3), 261-270

http://ieeexplore.ieee.org/stamp/stamp.jsp?tp=&arnumber=7508801 (Local PDF)

4. Jiacai Huang, YangQuan Chen, Haibin Li, Xinxin Shi. Fractional Order Modeling of Human Operator Behavior with Second Order Controlled Plant and Experiment Research. *IEEE/CAA Journal of Automatica Sinica*, 2016, 3(3), 271-280

http://ieeexplore.ieee.org/stamp/stamp.jsp?tp=&arnumber=7508802 (Local PDF)

5. Yan Ma, Xiuwen Zhou, Bingsi Li, Hong Chen. Fractional Modeling and SOC Estimation of Lithium-ion Battery. IEEE/CAA Journal of Automatica Sinica, 2016, 3(3), 281-287

http://ieeexplore.ieee.org/stamp/stamp.jsp?tp=&arnumber=7508803 (Local PDF)

6. Bingsan Chen, Chunyu Li, Benjamin Wilson, Yijian Huang. Fractional Modeling and Analysis of Coupled MR Damping System. IEEE/CAA Journal of Automatica Sinica, 2016, 3(3), 288-294

http://ieeexplore.ieee.org/stamp/stamp.jsp?tp=&arnumber=7508804 (Local PDF)

7. Xiaojuan Chen, Jun Zhang, Tiedong Ma. Parameter estimation and topology identification of uncertain general fractional-order complex dynamical networks with time delay. IEEE/CAA Journal of Automatica Sinica, 2016, 3(3): 295-303

http://ieeexplore.ieee.org/stamp/stamp.jsp?tp=&arnumber=7508805 (Local PDF)

8. Cuihong Wang, Huanhuan Li, YangQuan Chen. $H\infty$ Output Feedback Control of Linear Time-invariant Fractional-order Systems over Finite Frequency Range. IEEE/CAA Journal of Automatica Sinica, 2016, 3(3), 304-310

http://ieeexplore.ieee.org/stamp/stamp.jsp?tp=&arnumber=7508806 (Local PDF)

9. Kai Chen, Junguo Lu, Chuang Li. The Ellipsoidal Invariant Set of Fractional Order Systems Subject to Actuator Saturation: The Convex Combination Form. IEEE/CAA Journal of Automatica Sinica, 2016, 3(3), 311-319

http://ieeexplore.ieee.org/stamp/stamp.jsp?tp=&arnumber=7508807 (Local PDF)

10. Mojtaba Naderi Soorki, Mohammad Saleh Tavazoei. Constrained Swarm Stabilization of Fractional Order Linear Time Invariant Swarm Systems. IEEE/CAA Journal of Automatica Sinica, 2016, 3(3), 320-331

http://ieeexplore.ieee.org/stamp/stamp.jsp?tp=&arnumber=7508808 (Local PDF)

11. Norelys Aguila-Camacho, Manuel A. Duarte-Mermoud. Improving the Control Energy in Model Reference Adaptive Controllers Using Fractional Adaptive Laws. IEEE/CAA Journal of Automatica Sinica, 2016, 3(3), 332-337

http://ieeexplore.ieee.org/stamp/stamp.jsp?tp=&arnumber=7508809 (Local PDF)

12. Arturo Rojas-Moreno. An Approach to Design MIMO FO Controllers for Unstable Nonlinear Plants. IEEE/CAA Journal of Automatica Sinica, 2016, 3(3), 338-344
http://ieeexplore.ieee.org/stamp/stamp.jsp?tp=&arnumber=7508810 (Local PDF)

13. T. Sathiyaraj, P. Balasubramaniam. Controllability of Fractional Order Stochastic Differential Inclusions with Fractional Brownian Motion in Finite Dimensional Space. IEEE/CAA Journal of Automatica Sinica, 2016, 3(4), 400-410
http://ieeexplore.ieee.org/stamp/stamp.jsp?tp=&arnumber=7589487 (Local PDF)

14. Baris Baykant Alagoz. A Note on Robust Stability Analysis of Fractional Order Interval Systems by Minimum Argument Vertex and Edge Polynomials. IEEE/CAA Journal of Automatica Sinica, 2016, 3(4), 411-421
http://ieeexplore.ieee.org/stamp/stamp.jsp?tp=&arnumber=7589488 (Local PDF)

15. Mohammad Saleh Tavazoei. Criteria for Response Monotonicity Preserving in Approximation of Fractional Order Systems. IEEE/CAA Journal of Automatica Sinica, 2016, 3(4), 422-429
http://ieeexplore.ieee.org/stamp/stamp.jsp?tp=&arnumber=7589489 (Local PDF)

16. Hua Chen, Yang Quan Chen. Fractional-order Generalized Principle of Self-support (FOGPSS) in Control System Design. IEEE/CAA Journal of Automatica Sinica, 2016, 3(4), 430-441
http://ieeexplore.ieee.org/stamp/stamp.jsp?tp=&arnumber=7589490 (Local PDF)

17. Songsong Cheng, Shengguo Wang, Yiheng Wei, Qing Liang, Yong Wang. Study on Four Disturbance Observers for FO-LTI Systems. IEEE/CAA Journal of Automatica Sinica, 2016, 3(4), 442-450
http://ieeexplore.ieee.org/stamp/stamp.jsp?tp=&arnumber=7589491 (Local PDF)

18. Fabrizio Padula, Antonio Visioli. Set-point Filter Design for a Two-degree-of-freedom Fractional Control System. IEEE/CAA Journal of Automatica Sinica, 2016, 3(4), 451-462
http://ieeexplore.ieee.org/stamp/stamp.jsp?tp=&arnumber=7589492 (Local PDF)

19. Zhuoyun Nie, Qingguo Wang, Ruijuan Liu, Yonghong Lan. Identification and PID Control for a Class of Delay Fractional-order Systems. IEEE/CAA Journal of Automatica Sinica, 2016, 3(4), 463-476
http://ieeexplore.ieee.org/stamp/stamp.jsp?tp=&arnumber=7589653 (Local PDF)

20. Changchun Hua, Tong Zhang, Yafeng Li, Xinping Guan. Robust Output Feedback Control for Fractional Order Nonlinear Systems with Time-varying Delays. IEEE/CAA Journal of Automatica Sinica, 2016, 3(4), 477-482
http://ieeexplore.ieee.org/stamp/stamp.jsp?tp=&arnumber=7589654 (Local PDF)

21. Yige Zhao, Yuzhen Wang, Haitao Li. State Feedback Control for a Class of Fractional Order Nonlinear Systems. IEEE/CAA Journal of Automatica Sinica, 2016, null(4), 483-488
http://ieeexplore.ieee.org/stamp/stamp.jsp?tp=&arnumber=7589656 (Local PDF)

22. P. Lino, G. Maione, S. Stasi, F. Padula, and A. Visioli, "Synthesis of fractional-order PI controllers and fractional-order filters for industrial electrical drives," IEEE/CAA Journal of Automatica Sinica, vol. 4, no. 1, pp. 58-69, Jan. 2017.
http://ieeexplore.ieee.org/stamp/stamp.jsp?tp=&arnumber=7815552 (Local PDF)

23. J. X. Liu, T. B. Zhao, and Y. Q. Chen, "Maximum power point tracking with fractional order high pass filter for proton exchange membrane fuel cell," IEEE/CAA Journal of Automatica Sinica, vol. 4, no. 1, pp. 70-79, Jan. 2017
http://ieeexplore.ieee.org/stamp/stamp.jsp?tp=&arnumber=7815553 (Local PDF)

24. D. Tavares, R. Almeida, and D. F. M. Torres, “Constrained fractional variational problems of variable order,” IEEE/CAA Journal of Automatica Sinica, vol. 4, no. 1, pp. 80-88, Jan. 2017.
http://ieeexplore.ieee.org/stamp/stamp.jsp?tp=&arnumber=7815554 (Local PDF)

25. Q. Xue and H. B. Duan, “Robust attitude control for reusable launch vehicles based on fractional calculus and pigeon-inspired optimization,” IEEE/CAA Journal of Automatic Sinica, vol. 4, no. 1, pp. 89-97, Jan. 2017.
http://ieeexplore.ieee.org/stamp/stamp.jsp?tp=&arnumber=7815555 (Local PDF)

26. V. S. Krishnasamy, S. Mashayekhi, and M. Razzaghi, “Numerical solutions of fractional differential equations by using fractional Taylor basis,” IEEE/CAA Journal of Automatica Sinica, vol. 4, no. 1, pp. 98-106, Jan. 2017.
http://ieeexplore.ieee.org/stamp/stamp.jsp?tp=&arnumber=7815556 (Local PDF)

27. W. J. Gu, Y. G. Yu, and W. Hu, “Artificial bee colony algorithmbased parameter estimation of fractional-order chaotic system with time delay,” IEEE/CAA Journal of Automatica Sinica, vol. 4, no. 1, pp. 107-113, Jan. 2017.
http://ieeexplore.ieee.org/stamp/stamp.jsp?tp=&arnumber=7815557 (Local PDF)

28. S. Das and V. K. Yadav, “Stability analysis, chaos control of fractional order Vallis and El-Nino systems and their synchronization,” IEEE/CAA Journal of Automatica Sinica, vol. 4, no. 1, pp. 114-124, Jan. 2017.
http://ieeexplore.ieee.org/stamp/stamp.jsp?tp=&arnumber=7815558 (Local PDF)

29. A. Bekir, O. Guner, and A. Cevikel, “The exp-function method for some time-fractional differential equations,” IEEE/CAA Journal of Automatica Sinica, vol. 4, no. 2, pp. 315-321, Apr. 2017.
http://ieeexplore.ieee.org/stamp/stamp.jsp?tp=&arnumber=7739896 (Local PDF)

30. Y. Zhao, Y. Li, F. Y. Zhou, Z. K. Zhou, and Y. Q. Chen, “An iterative learning approach to identify fractional order KiBaM model,” IEEE/CAA Journal of Automatica Sinica, vol. 4, no. 2, pp. 322-331, Apr. 2017.
http://ieeexplore.ieee.org/stamp/stamp.jsp?tp=&arnumber=7833249&tag=1 (Local PDF)

31. W. Y. Ma, Y. J. Wu, and C. P. Li, “Pinning synchronization between two general fractional complex dynamical networks with external disturbances,” IEEE/CAA Journal of Automatica Sinica, vol. 4, no. 2, pp. 332-339, Apr. 2017.
http://ieeexplore.ieee.org/stamp/stamp.jsp?tp=&arnumber=7783960 (Local PDF)

32. M. J. Lazo, D. F. M. Torres, “Variational calculus with conformable fractional derivatives,” IEEE/CAA Journal of Automatica Sinica, vol. 4, no. 2, pp. 340-352, Apr. 2017.
http://ieeexplore.ieee.org/stamp/stamp.jsp?tp=&arnumber=7739894 (Local PDF)

33. J. H. Wang, L. Y. Qiao, Y. Q. Ye, and Y. Q. Chen, “Fractional envelope analysis for rolling element bearing weak fault feature extraction,” IEEE/CAA Journal of Automatica Sinica, vol. 4, no. 2, pp. 353-360, Apr. 2017.
http://ieeexplore.ieee.org/stamp/stamp.jsp?tp=&arnumber=7739893 (Local PDF)

34. M. Xiao, G. P. Jiang, J. D. Cao, and W. X. Zheng, “Local bifurcation analysis of a delayed fractional-order dynamic model of dual congestion control algorithms”, IEEE/CAA Journal of Automatica Sinica, vol. 4, no. 2, pp. 361-369, Apr. 2017.
http://ieeexplore.ieee.org/stamp/stamp.jsp?tp=&arnumber=7739001 (Local PDF)

The remaining papers (online):

35. Y. Yang, and D. Y. Xue, “Modified grey model predictor design using optimal fractional-order accumulation calculus,” IEEE/CAA Journal of Automatica Sinica, pp. 1-10, 2017. DOI:

10.1109/JAS.2017.7510355.
http://ieeexplore.ieee.org/stamp/stamp.jsp?tp=&arnumber=7833248 (Local PDF)

36. J. B. Long, H. B. Wang, P. Li and H. S. Fan, “Applications of Fractional Lower Order Time-Frequency Representation to Machine Bearing Fault Diagnosis”, IEEE/CAA Journal of Automatica Sinica, pp. 1-17, 2017. DOI: 10.1109/JAS.2016.7510190
http://ieeexplore.ieee.org/stamp/stamp.jsp?tp=&arnumber=7783955 (Local PDF)

37. J. M. Wei, Y. A. Hu, and M. M. Sun, “An exploration on adaptive iterative learning control for a class of commensurate high-order uncertain nonlinear fractional order systems,” IEEE/CAA Journal of Automatica Sinica, pp. 1–10, 2017. DOI: 10.1109/JAS.2017.7510361
http://ieeexplore.ieee.org/stamp/stamp.jsp?tp=&arnumber=7833250 (Local PDF)

38. Amit S. Chopade, Swapnil W. Khubalkar, A. S. Junghare, M. V. Aware, and Shantanu Das, “ Design and Implementation of Digital Fractional Order PID Controller using Optimal Pole-Zero Approximation Method for Magnetic Levitation System”, IEEE/CAA Journal of Automatica Sinica, pp. 1–12, 2017. DOI: 10.1109/JAS.2016.7510181
http://ieeexplore.ieee.org/stamp/stamp.jsp?tp=&arnumber=7783935 (Local PDF)

39. Manjeet Kumar, Apoorva Aggarwal, Tarun Rawat and Harish Parthasarathy, “Optimal Nonlinear System Identification Using Fractional Delay Second-Order Volterra System”, IEEE/CAA Journal of Automatica Sinica, pp. 1–17, 2017. DOI: 10.1109/JAS.2016.751018
http://ieeexplore.ieee.org/stamp/stamp.jsp?tp=&arnumber=7783953 (Local PDF)

40. S. Y. Shao and M. Chen. “Fractional-Order Control for a Novel Chaotic System without Equilibrium”, IEEE/CAA Journal of Automatica Sinica, pp. 1–9, 2017. DOI: 10.1109/JAS.2016.7510124
http://ieeexplore.ieee.org/stamp/stamp.jsp?tp=&arnumber=7738995 (Local PDF)

41. Khatir Khettab, Samir Ladaci, and Yassine Bensafia, “Fuzzy Adaptive Control of a Fractional Order Chaotic System with Unknown Control Gain Sign Using a Fractional Order Nussbaum Gain”, IEEE/CAA Journal of Automatica Sinica, pp. 1–8, 2017. DOI: 10.1109/JAS.2016.7510169
http://ieeexplore.ieee.org/stamp/stamp.jsp?tp=&arnumber=7739895 (Local PDF)

42. Sen Li, Rongxi He, Bin Lin, Fei Sun, “DOA Estimation Based on Sparse Representation of the Fractional Lower Order Statistics in Impulsive Noise”, IEEE/CAA Journal of Automatica Sinica, pp. 1–9, 2017. DOI: 10.1109/JAS.2016.7510187
http://ieeexplore.ieee.org/stamp/stamp.jsp?tp=&arnumber=7783954 (Local PDF)

43. Xuefeng Zhang, “Relationship Between Integer Order Systems and Fractional Order Systems and Its Two Applications”, IEEE/CAA Journal of Automatica Sinica, pp. 1–9, 2017. DOI: 10.1109/JAS.2016.7510205
http://ieeexplore.ieee.org/stamp/stamp.jsp?tp=&arnumber=7783961 (Local PDF)

44. Shaobo He, Kehui Sun, and Huihai Wang, “Dynamics of the Fractional-order Lorenz System Based on Adomian Decomposition Method and Its DSP Implementation”, IEEE/CAA Journal of Automatica Sinica, pp. 1–6, 2017. DOI: 10.1109/JAS.2016.7510133
http://ieeexplore.ieee.org/stamp/stamp.jsp?tp=&arnumber=7738993 (Local PDF)

45. Lilian Huang, Longlong Wang, and Donghai Shi, “Discrete Fractional Order Chaotic Systems Synchronization Based on the Variable Structure Control with a New Discrete Reaching-law”, IEEE/CAA Journal of Automatica Sinica, pp. 1–7, 2017. DOI: 10.1109/JAS.2016. 7510016
http://ieeexplore.ieee.org/stamp/stamp.jsp?tp=&arnumber=7739000 (Local PDF)

46. Hossein Aminikhah, Mahdieh Tahmasebi, and Mahmoud Mohammadi Roozbahani, “The Multi-scale Method for Solving Nonlinear Time Space Fractional Partial Differential Equations”,

IEEE/CAA Journal of Automatica Sinica, pp. 1–8, 2017. DOI: 10.1109/JAS.2016.7510058
http://ieeexplore.ieee.org/stamp/stamp.jsp?tp=&arnumber=7739889 (Local PDF)

47. Quan Xu, Shengxian Zhuang, Yingfeng Zeng, and Jian Xiao, "Decentralized Adaptive Strategies for Synchronization of Fractional-Order Complex Networks", IEEE/CAA Journal of Automatica Sinica, pp. 1–8, 2017. DOI: 10.1109/JAS.2016. 7510142
http://ieeexplore.ieee.org/stamp/stamp.jsp?tp=&arnumber=7739890 (Local PDF)

48. Hadi Delavari and Milad Mohadeszadeh, "Robust Finite-time Synchronization of Non-Identical Fractional-order Hyperchaotic Systems and its Application in Secure Communication", IEEE/CAA Journal of Automatica Sinica, pp. 1–8, 2017. DOI: 10.1109/JAS.2016. 7510145
http://ieeexplore.ieee.org/stamp/stamp.jsp?tp=&arnumber=7739891 (Local PDF)

49. Najeeb Alam Khan, Tooba Hameed, "An Implementation of Haar Wavelet Based Method for Numerical Treatment of Time-fractional Schrodinger and Coupled Schrodinger Systems", IEEE/CAA Journal of Automatica Sinica, pp. 1–10, 2017. DOI: 10.1109/JAS.2016. 7510193
http://ieeexplore.ieee.org/stamp/stamp.jsp?tp=&arnumber=7783957 (Local PDF)

50. Ameya Anil Kesarkar, and N. Selvaganesan, "Asymptotic Magnitude Bode Plots of Fractional-Order Transfer Functions", IEEE/CAA Journal of Automatica Sinica, pp. 1–8, 2017. DOI: 10.1109/JAS.2016.7510196
http://ieeexplore.ieee.org/stamp/stamp.jsp?tp=&arnumber=7783958 (Local PDF)

51. Ruoxun Zhang, Shiping Yang, Shiwen Feng, "Stability analysis of a class of nonlinear fractional differential systems with Riemann-Liouville derivative", IEEE/CAA Journal of Automatica Sinica, pp. 1–7, 2017. DOI: 10.1109/ JAS.2016.7510199
http://ieeexplore.ieee.org/stamp/stamp.jsp?tp=&arnumber=7783959 (Local PDF)

52. Shanshan Li, Chunna Zhao, Yong Guan, Zhiping Shi, Xiaojuan Li, Rui Wang, and Qianying Zhang, "Research on the Higher-order Logic Formalization of Fractance Element", IEEE/CAA Journal of Automatica Sinica, pp. 1–9, 2017. DOI: 10.1109/ JAS.2016.7510208
http://ieeexplore.ieee.org/stamp/stamp.jsp?tp=&arnumber=7783962 (Local PDF)

53. Hongyong Yang, Fuyong Wang and Fujun Han, "Containment Control of Fractional Order Multi-Agent Systems with Time Delays", IEEE/CAA Journal of Automatica Sinica, pp. 1–6, 2017. DOI: 10.1109/ JAS.2016. 7510211
http://ieeexplore.ieee.org/stamp/stamp.jsp?tp=&arnumber=7783963 (Local PDF)

54. Lifeng Wu, Sifeng Liu , and Yingjie Yang, "Using Fractional Order Method to Generalize Strengthening Buffer Operator and Weakening Buffer Operator", IEEE/CAA Journal of Automatica Sinica, pp. 1–5, 2017. DOI: 10.1109/ JAS.2016. 7510214
http://ieeexplore.ieee.org/stamp/stamp.jsp?tp=&arnumber=7783964 (Local PDF)